

INTERNATIONAL JOURNAL OF MODERN ENGINEERING RESEARCH (IJMER)

ISSN : 2249-6645



Volume 2 - Issue 6

Web : www.ijmer.com
Email : ijmer.editor@gmail.com

International Journal of Modern Engineering Research (IJMER)

Editorial Board

Executive Managing Editor

Prof. Shiv Kumar Sharma
India

Editorial Board Member

Dr. Jerry Van
Department of Mechanical, USA

Dr. George Dyrud
Research centre dy. Director of Civil Engineering, New Zealand

Dr. Masoud Esfal
R& D of Chemical Engineering, Australia

Dr. Nouby Mahdy Ghazaly
Minia University, Egypt

Dr. Stanley John
Department of Textile Engineering, United Kingdom

Dr. Valfitaf Rasoul
Professor and HOD of Electromechanical, Russian

Dr. Mohammed Ali Hussain
HOD, Sri Sai Madhavi Institute of Science & Technology, India

Dr. Manko dora
Associate professor of Computer Engineering, Poland

Dr. Ahmed Nabih Zaki Rashed
Menoufia University, Egypt

Ms. Amani Tahat
Ph.D physics Technical University of Catalonia-Spain

Associate Editor Member
Dr. Mohd Nazri Ismail
University of Kuala Lumpur (UniKL), Malaysia

Dr. Kamaljit I. Lakhtaria
Sir Padmapat Singhania University, Udaipur

Dr. Rajesh Shrivastava
Prof. & Head Mathematics & computer Deptt. Govt. Science & commerce College Benazir. M.P

Dr. Asoke Nath
Executive Director, St. Xavier's College, West Bengal, India

Prof. T. Venkat Narayana Rao
Head, CSE, HITAM Hyderabad

Dr. N. Balasubramanian
Ph. D (Chemical Engg), IIT Madras

Jasvinder Singh Sadana
M. TECH, USIT/GGSIPU, India

Dr. Bharat Raj Singh

Associate Director, SMS Institute of Technology, Lucknow

DR. RAVINDER RATHEE

C. R. P, Rohtak, Haryana

Dr. S. Rajendran

Research Supervisor, Corrosion Research Centre Department of Chemistry, GTN Arts College, Dindigul

Mohd Abdul Ahad

Department of Computer Science, Faculty of Management and Information Technology, Jamia Hamdad, New Delhi

Kunjal Mankad

Institute of Science & Technology for Advanced Studies & Research (ISTAR)

NILANJAN DEY

JIS College of Engineering, Kalyani, West Bengal

Dr. Hawz Nwayu

Victoria Global University, UK

Prof. Plewin Amin

Crewe and Alsager College of Higher Education, UK

Dr. (Mrs.) Annifer Zalic

London Guildhall University, London

Dr. (Mrs.) Malin Askiy

Victoria University of Manchester

Dr. ABSALOM

Sixth form College, England

Dr. Nimrod Nivek

London Guildhall University, London

Equilibrium and Kinetics of Adsorption of Cationic Dyes by STISHOVITE Clay – TiO₂ Nanocomposite

Venkateswaran Vinayagam¹, Priya Thangaraju²

¹Sree Saraswathi Thyagaraja College (Autonomous), Bharathiar University, Pollachi, Tamilnadu, India.

²PG & Research Department of Chemistry Erode Arts & Science College (Autonomous), Erode, Bharathiar University, Tamilnadu, India.

Abstract: In this study an attempt has been made to study the feasibility of removal of methyl violet using Stishovite-TiO₂ nanocomposite as an adsorbent. The commercially available Stishovite and TiO₂ are stirred with alcohol, dried and used. Batch adsorption experiments have been conducted under various operating parameters like initial dye concentration, contact time, adsorbent dose, p^H and temperature. The equilibrium data fitted well with the Langmuir and Freundlich isotherms. From these the adsorption efficiency, adsorption energy, adsorption capacity, intensity of adsorption and dimensionless separation factor all are calculated. The experimental data fitted very well with pseudo second order kinetic model and Elcovich model suggesting chemisorption which is substantiated by desorption studies.

Keywords: adsorption isotherm, methyl violet, kinetics, Stishovite-TiO₂ nanocomposite, desorption

I. Introduction

Various methods like coagulation, oxidation, electrochemical, ion-exchange, biodegradation and ultra-filtration have been applied to overcome the excessive discharges of colourants from petrochemical, textile, leather-making, pharmaceutical as well as food and beverage industries. All these are not comparable to adsorption technique in term of efficiency, operating cost, process flexibility and ease of operation (Shi and Li, 2007; Fathima, 2008; Shen, 2006; Ahmad, 2006; Raghu and Ahmed Basha, 2007; Walker and Weatherley, 2000). Further all these techniques were found to be inefficient and incompetent because of the fairly high solubility and stability of the dyes towards light, oxidizing agents and aerobic digestion. A comprehensive survey indicates that adsorption technique was the most appropriate and efficient one (Ruthven, 1984; Suzuki, 1993).

The objective of the present study was to explore the feasibility of the removal of methyl violet using the nanocomposites prepared from Stishovite clay and TiO₂ as adsorbent.

II. Materials and Methods

Stishovite (3g) was allowed to swell in 15ml of water-free alcohol and stirred for 2 hours at 25°C to get a uniform suspension. At the same time, the titanium dioxide was dispersed into water-free alcohol. The diluted titanium dioxide was then added slowly by dropping it into the suspension of Stishovite and stirred for further 5 hours at 25°C. Then 5ml alcohol mixed with 0.2ml deionized water was added slowly and stirring continued for another 5 hours at 25°C. The suspension was then kept over night for 10 hours at room temperature and the precipitate obtained was carefully dehydrated in a vacuum oven for 6 hours at 80°C to a loose dry powder. A stock solution (1000mg/L) of dye was prepared using doubly distilled water. Various dye solutions with different initial concentrations were prepared by diluting the stock dye solution. The adsorbate used in this study is methyl violet.

2.1. Characterization of Adsorbent

Physico-chemical characteristics of the adsorbents were studied as per the standard testing methods (Waranusantigul, 2003). Fig.1, 2 shows the XRD pattern of pure Stishovite clay and that of Stishovite-TiO₂ nanocomposite respectively. The peaks at 28° (Fig. 1) and at 30° (Fig. 2) confirm the presence of Stishovite-TiO₂ phase in the nanocomposite. The surface morphology of the adsorbent was visualized via scanning electron microscopy (SEM). The diameter of the composite range was 50 µm.

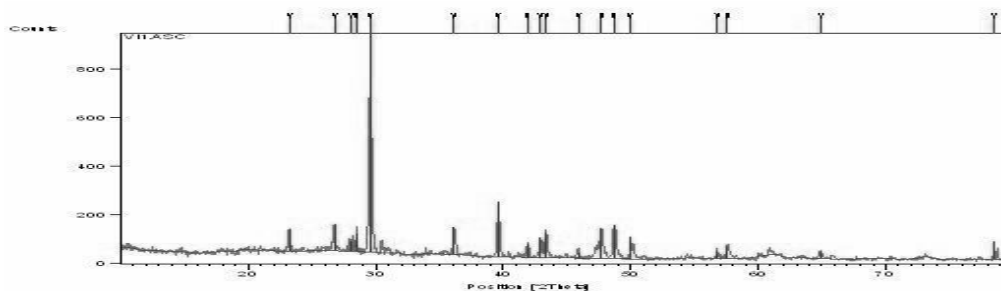
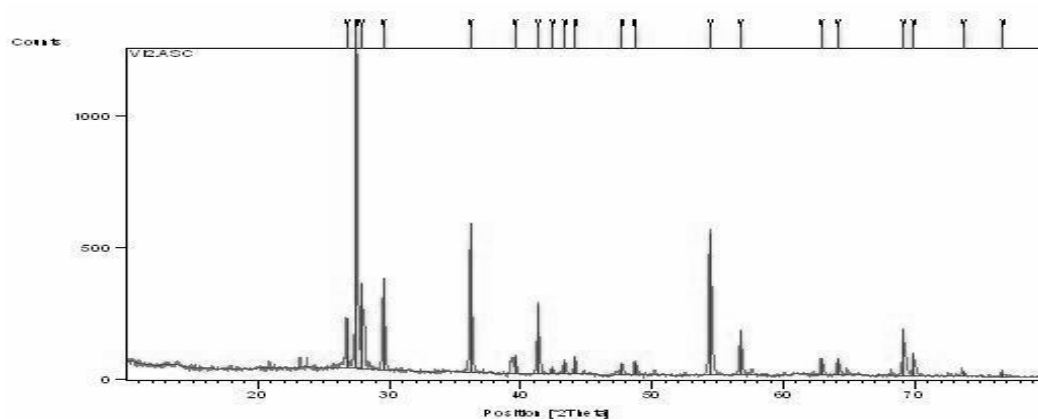


Fig. 1. XRD analysis of STISHOVITE

Fig. 2. XRD



analysis of STISHOVITE-TiO₂ COMPOSITE

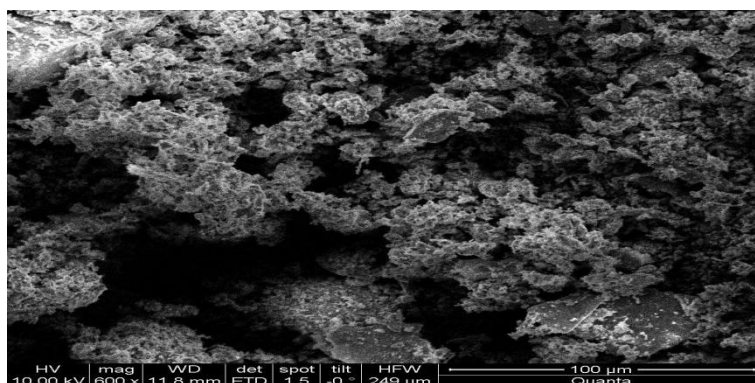


Fig. 3.SEM of STISHOVITE

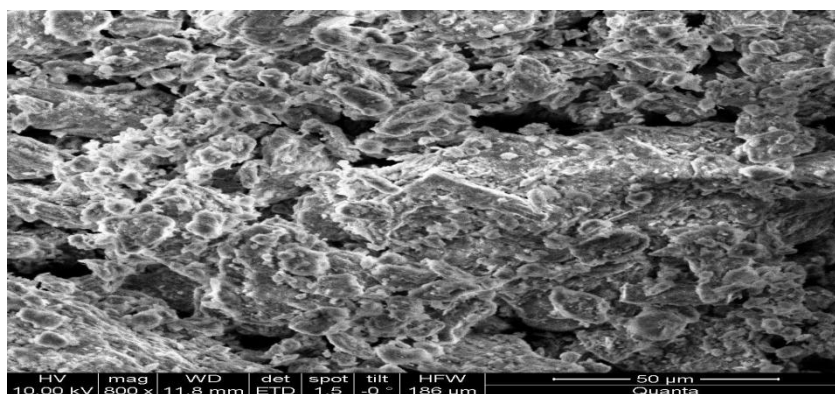


Fig. 4. SEM of STISHOVITE – TiO₂ COMPOSITE

IR Spectroscopy:

Stishovite Clay : Si-O-Si = 1011 cm⁻¹, Si-O-Ti = 872 cm⁻¹, Ti-O-Si = 872 cm⁻¹,

Ti-O-Ti = 1633 cm⁻¹

Stishovite + TiO₂ NC : Si-O-Si = 1014 cm⁻¹, Si-O-Ti = 873 cm⁻¹, Ti-O-Si = 873 cm⁻¹,

Ti-O-Ti = 1796 cm⁻¹

III. Batch adsorption experiments

Entire batch mode experiments were carried out in the temperature range 303K to 311K by taking 50ml of the respective dye solution and known amount of the adsorbent in a 100ml conical flask. The flasks were agitated for pre-

determined time intervals in a thermostat attached with a shaker at the desired temperature. The adsorbent and adsorbate were separated by filtration. Studies on the effects of agitation time, p^H , initial dye concentration, adsorbent dose and temperature were carried out by using known amount of adsorbent and 50ml of dye solution of different concentrations. Dye solution (50ml) with different amounts of adsorbent was taken to study the effect of adsorbent dosage on the removal of dyes.

IV. Results and Discussion

4.1. Effect of agitation time and initial dye concentration

The effect of initial dye concentration and contact time for the removal of methyl violet is shown in Fig.5. For this study 50ml of 10 to 40 mg/L of dye solution was agitated with 100mg of adsorbent. The extent of removal of dye was faster in initial stages, then showed decreasing pattern and finally became constant showing the attainment of equilibrium. The extent of removal was found to be 88%. The curves obtained are single and smooth, indicating monolayer coverage on the adsorbent surface.

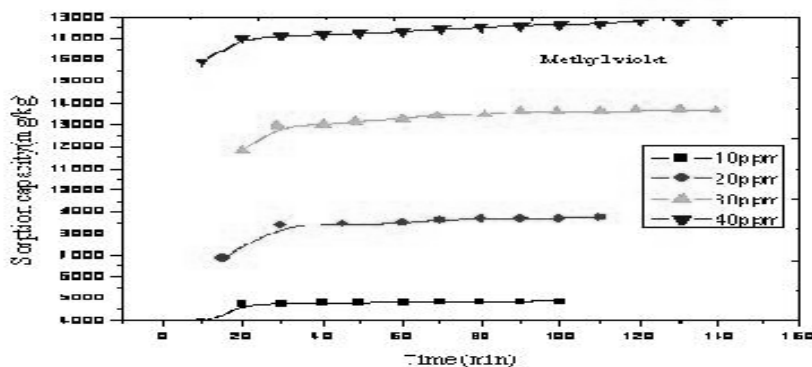


Fig. 5. Effect of initial dye concentration

4.2. Effect of adsorbent dosage on adsorption process

The effect of adsorbent dosage on basic dye removal was studied by keeping all other experimental conditions constant except that of adsorption dosage. The amount adsorbed per unit mass of the adsorbent decreased with increase in adsorbent concentration (Fig.6). The decrease in unit adsorption with increasing dose of adsorbent may basically be due to the fact that adsorption sites remaining unsaturated during the adsorption process.

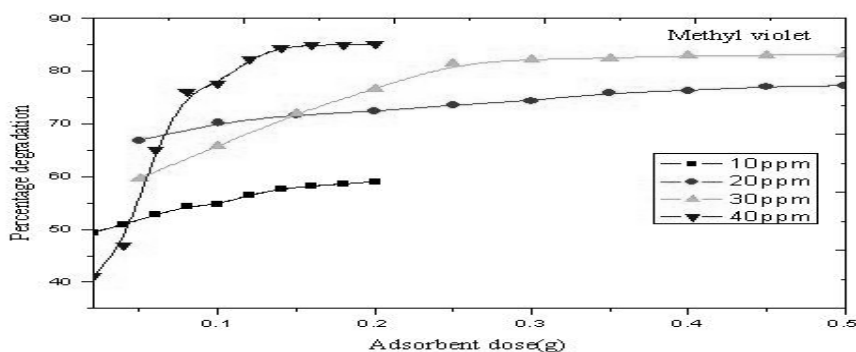


Fig 6. Effect of adsorbent dosage

4.3. Effect of p^H

Adsorption experiments were carried out at various p^H values ranging from 6 to 11 maintaining the required p^H by adding necessary amount of dilute hydrochloric acid and sodium hydroxide solutions. A p^H meter calibrated with 4.0 and 9.0 buffers were used. Fig.7 indicates that maximum dye removal had occurred in basic medium. It was observed that as the p^H increases the sorption capacity also increases. The p^H_{zpc} for the nanocomposite was determined as 8.0.

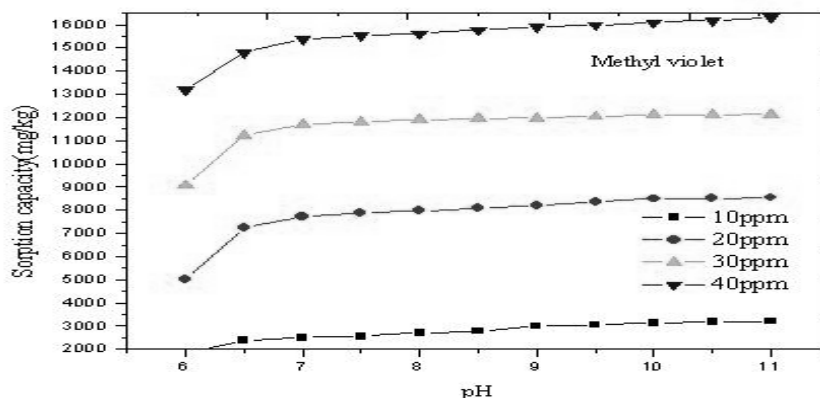


Fig. 7. Effect of p^H

4.4. Effect of temperature

Temperature has an important effect on the adsorption process. Fig.8 shows effect of different temperature on the removal of methyl violet by the nanocomposite. The amount of basic dye adsorbed increases with increasing temperature from 303K to 311K indicating the adsorption process to be endothermic. This may be due to the fact that as the temperature increases, rate of diffusion of adsorbate molecules across the external boundary layer and internal pores of adsorbent particle increase.

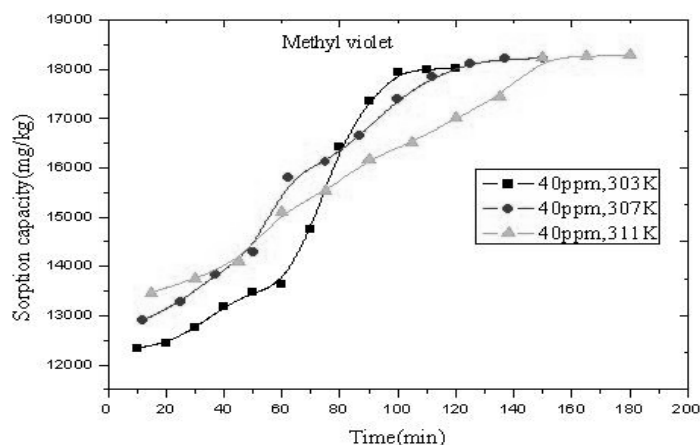


Fig. 8. Effect of temperature

4.5. Adsorption isotherm

The relationship between the amount of dye adsorbed and its equilibrium concentration was analysed using Langmuir and Freundlich isotherms.

4.5.1. Langmuir isotherm

The Langmuir adsorption isotherm which assumes that adsorption takes place at specific homogeneous sites within the adsorbent has been used successfully for many systems that involve monolayer adsorptions. The linearized Langmuir equation (Eq.1):

$$C_e / q_e = 1/bq_0 + C_e / q_0 \quad (1)$$

Where C_e is the equilibrium concentration of the adsorbate (mg/L), q_e is the amount of dye adsorbed per unit mass of adsorbent (mg/L) and q_0 and b are Langmuir constants related to adsorption capacity and adsorption rate respectively. As required by equation (1) plotting C_e/q_e against C_e gave a straight line, indicating that the adsorption of basic dyes on the nanocomposite follow the Langmuir isotherm. The Langmuir constants b and q_0 were evaluated, from the slope and intercept of the graph.

The essential characteristics of the Langmuir isotherm can be expressed in terms of a dimensionless equilibrium parameter R_L which is defined by,

$$R_L = 1/(1 + bC_0) \quad (2)$$

Where, C_0 is the highest initial solute concentration, 'b' the Langmuir adsorption constant (L/mg).

If the value of R is less than one then it indicates favourable adsorption. The R_L values shown in Table 1 all are less than one indicating the applicability of Langmuir isotherm to this adsorption process.

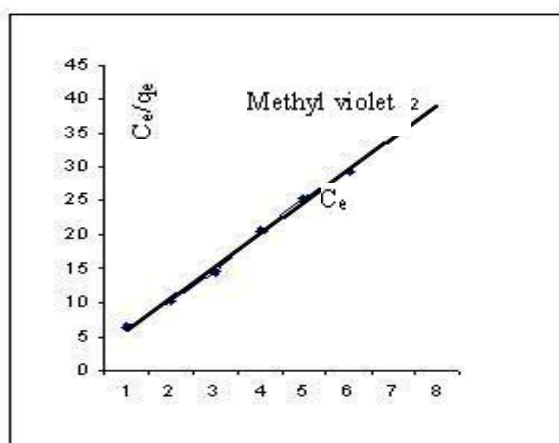


Fig.9: Plot of Langmuir adsorption isotherm

Table 1. The values of Langmuir constant Q^0 and b in addition to R_L

Concentration of dye(mg/L)	Methyl violet			
	R_L	b	Q^0 mg/g	R^2
20	0.9939			
40	0.9879			
60	0.9819	0.000306	57.208	0.9962
80	0.9761			
100	0.9703			
120	0.9645			

4.5.2. Freundlich Model

The Freundlich isotherm, an empirical relationship used to describe heterogeneous systems can be expressed in its logarithmic form (Eq.3):

$$\log q_e = \log K_f + 1/n \log C_e \quad (3)$$

Where K_f and $1/n$ are Freundlich constants related to adsorption capacity and adsorption intensity of the sorbent respectively. q_e is the amount adsorbed at equilibrium (mg/g); C_e is the equilibrium concentration of the adsorbate. The values of K_f and $1/n$ calculated from the intercept and slope respectively are recorded in Table 2. The plot of $\log q_e$ versus $\log C_e$ gave a straight line (Fig.10) with good regression coefficient indicating that the adsorption of methyl violet follows the Freundlich isotherm.

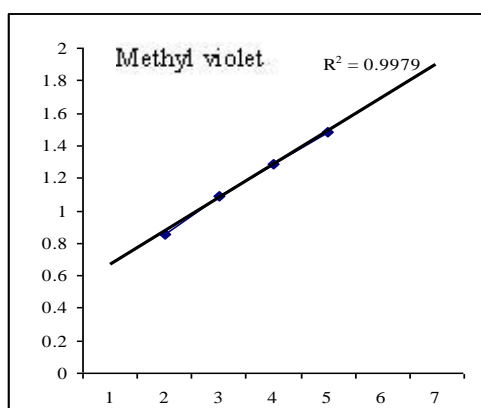


Fig.10: Plot of Freundlich adsorption isotherm

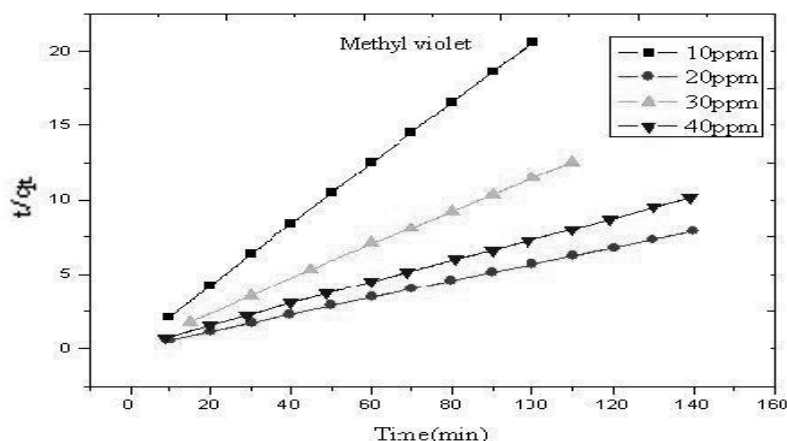


Table 2 .The values of Freundlich constant K_f and n

Dye	K_f L/mg	n mg/g	R^2
Methyl violet	10.9647	2.0000	0.9979

4.6. Kinetics of adsorption

In order to investigate the mechanism of adsorption of methyl violet by the nanocomposite the following three kinetic models were considered.

4.6.1. Pseudo first order kinetic model

The integrated linear form of this model proposed by Lagergren (Eq.4):

$$\log(q_e - q_t) = \log q_e - (k_1 / 2.303) t \quad (4)$$

Where q_e is the amount of dye adsorbed at equilibrium (mg/g), and q_t is the amount of dye adsorbed (mg/g) at time t , k_1 is the first order rate constant (min^{-1}) and t is time (m). Hence a linear trace is expected between the two parameters $\log(q_e - q_t)$ and t , provided the adsorption follows first order kinetics. It is observed that the data does not fit in to first order equation.

4.6.2. Pseudo second order kinetics

The adsorption may also be described by pseudo second order kinetic model. The linearised form of the pseudo second order model (Eq.5):

$$t/q_t = 1/k_2 q_e^2 + 1/q_e \times t \quad (5)$$

Where k_2 is the second order rate constant (g/mg min). A plot of t/q_t vs t should be linear if the adsorption follows second order. q_e and k_2 can be calculated from the slope and intercept of the plot. Methyl violet obeys the pseudo order kinetics.

4.7. Elovich kinetic model

The Elovich equation is mainly applicable for chemisorption processes involving heterogeneous adsorbing surfaces. The Elovich model in its integrated form can be

$$Q_t = (1/b) \ln(ab) + (1/b) \ln t \quad (6)$$

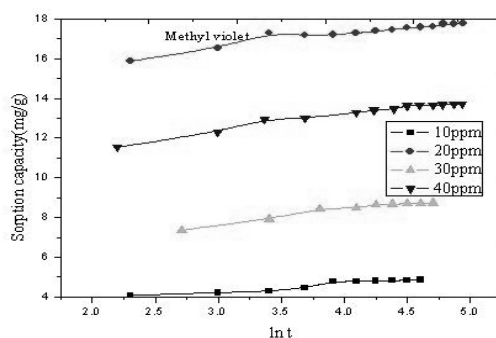


Fig.12: Elkovich kinetic model

Where 'a' is the initial adsorption rate (mg/g min) and 'b' is related to the extent of surface coverage and the activation energy for chemisorptions (g/mg). A plot of q_t vs $\ln t$ is a straight line, as expected, with a slope of $1/b$ and an intercept $\log 1/b \ln(ab)$ with good correlation coefficients confirming the chemisorptive nature of adsorption.

4.8. Thermodynamic of Adsorption

Thermodynamic parameters like ΔH^0 and ΔS^0 were evaluated using Van't Hoff's equation:

$$\ln K_c = \Delta S^0 / R - \Delta H^0 / RT \quad (8)$$

Where K_c is the Langmuir equilibrium constant, ΔH^0 and ΔS^0 , are the standard enthalpy and entropy changes of adsorption respectively and their values are calculated from the slopes and intercepts respectively of the linear plot of $\ln K_c$ vs $1/T$. The free energy change for the adsorption process ΔG^0 (kJ/mol) is derived (Eq.9):

$$\Delta G^0 = \Delta H^0 - T\Delta S^0 \quad (9)$$

Negative free energy change and positive entropy change of adsorption (Table 3) indicate that the adsorption process is favourable and spontaneous in nature. The endothermic nature of adsorption is confirmed by the positive ΔH^0 value.

Table 3: Thermodynamic parameters for adsorption of methyl violet on Stishovite-TiO₂ NC

Dyes	$-\Delta G^0$ kJ/mol			ΔS^0 kJ/mol	ΔH^0 kJ/mol
	303K	307K	311K		
Methyl violet	1.631	1.652	1.673	5.320	19.745

V. Desorption studies

Desorption studies with acetic acid revealed that the regeneration of adsorbent was not satisfactory, which confirms the chemisorptive nature of adsorption.

VI. Conclusion

The present investigation showed that Stishovite-TiO₂ nanocomposite can be used as adsorbent for removal of methyl violet. The amount of dye adsorbed varied with initial dye concentration, adsorbent dose, p^H and temperature. Removal of methyl violet by nanocomposite obeyed both Langmuir and Freundlich isotherms. The adsorption process followed pseudo second order kinetics. This has been further supported by Elkovich chemisorptive kinetic model. Desorption studies reveals that no satisfactory desorption taking place confirming chemisorptive nature of adsorption. Evaluation of thermodynamic parameters showed the process as endothermic and spontaneous.

References

- [1] Shi, B.G.Li, (2007), Removal of direct dyes by coagulation: The performance polymeric aluminium species. *Journal of Hazardous Materials*, 143 (1-2): 567-574.
- [2] Fathima, N.N. (2008), Dye house wastewater treatment through advanced oxidation process using Cu-exchanged Y zeolite: A heterogenous catalytic approach. *Chemosphere* 70(6):1146-1151.
- [3] Shen, Z. M. (2006), Methods to improve electrochemical treatment effect of dye wastewater. *Journal of Hazardous Materials*, 131(1-3): 90-97.
- [4] Ahmad, (2006), Micellar-enhancement ultra filtration for removal of reactive dyes from an aqueous solution. *Desalination*, 191(1-3):153-161.
- [5] Raghu, S. and C.Ahmed Basha, (2007), Chemical or electrochemical techniques, followed by ion exchange for recycle of textile dye wastewater. *Journal of Hazardous Materials*, 149(2):324-330.
- [6] Walker, G.M. and L.R.Weatherley, (2000), Biodegradation and biosorption of acid anthraquinone dye. *Environmental Pollution*, 108(2):219-223.
- [7] Ruthven, D.M. (1984), Principles of Adsorption and Desorption Processes, John Willey and Sons, New York.
- [8] Suzuki. 1993, *Fundamentals of Adsorption IV*, Kodansha, Tokyo.
- [9] M.Ittal, (2008) Removal and recovery of hazardous triphenylamine dye, Methyl Violet through adsorption over granulated waste materials, *Journal of Hazardous Materials*, 150:364-375.
- [10] Lillie, R.D. and H.J.Conn, (1977), Biological Stains: *A Handbook on the Nature and Uses of the Dyes Employed in the Biological laboratory*, Williams & Wilkins, Baltimore.
- [11] Waranusantigul.P, (2003), Kinetics of basic dyes biosorption by giant duckweed, *Environ Pollu.*, 125, 385-392.

Face Detection System on Ada boost Algorithm Using Haar Classifiers

M. Gopi Krishna, A. Srinivasulu, Prof (Dr.) T.K.Basak

^{1,2}Department of Electronics (E.C.E), Vaagdevi Institute of Tech & Science, Peddasettipalli(Village), Proddatur(M.D), Kadapa(Dist), Andhra Pradesh A.P, India.

³Dean (R&D), JIS College of Engineering, Kalyani, W.B.

ABSTRACT: This paper presents an architecture for face detection based system on AdaBoost algorithm using Haar features. We describe here design techniques including image scaling, integral image generation, pipelined processing as well as classifier, and parallel processing multiple classifiers to accelerate the processing speed of the face detection system. Also we discuss the optimization of the proposed architecture which can be scalable for configurable devices with variable resources. The proposed architecture for face detection has been designed using Verilog HDL and implemented in Modelsim. Its performance has been measured and compared with an equivalent hardware implementation. We show about 35 time's increase of system performance over the equivalent hardware implementation.

Keywords: AdaBoost; architecture; face detection; Haar classifier; image processing; real-time.

I. INTRODUCTION

Face detection in image sequence has been an active research area in the computer vision field in recent years due to its potential applications such as monitoring and surveillance [1], human computer interfaces [2], smart rooms [3], intelligent robots [4], and biomedical image analysis [5]. Face detection is based on identifying and locating a human face in images regardless of size, position, and condition. Numerous approaches have been proposed for face detection in images. Simple features such as color, motion, and texture are used for the face detection in early researches. However, these methods break down easily because of the complexity of the real world.

Face detection proposed by Viola and Jones [6] is most popular among the face detection approaches based on statistic methods. This face detection is a variant of the AdaBoost algorithm which achieves rapid and robust face detection. They proposed a face detection framework based on the AdaBoost learning algorithm using Haar features. Therefore, this constitutes a bottleneck to the application of face detection in real time.

The main contribution of our work, described in this paper, is design and implementation of a physically feasible hardware system to accelerate the processing speed of the operations required for real-time face detection. Therefore, this work has resulted in the development of a real-time face detection system employing an FPGA implemented system designed by Verilog HDL. Its performance has been measured and compared with an equivalent software implementation.

This paper is organized as follows: In Section II, we explain the face detection algorithm. In Section III, we describe the architecture, designed with Verilog HDL, of a face detection system using block diagrams. In Section IV, we show the implementation of the real-time face detection

system in an FPGA and measure the corresponding performance. Finally, we conclude in Section V.

II. FACE DETECTION ALGORITHM

The face detection algorithm proposed by Viola and Jones is used as the basis of our design. The face detection algorithm looks for specific Haar features of a human face. When one of these features is found, the algorithm allows the face candidate to pass to the next stage of detection. A face candidate is a rectangular section of the original image called a sub-window. Generally these sub-windows have a fixed size (typically 24×24 pixels).

This sub-window is often scaled in order to obtain a variety of different size faces. The algorithm scans the entire image with this window and denotes each respective section a face candidate [6].

A. Integral Image

The integral image is defined as the summation of the pixel values of the original image. The value at any location (x, y) of the integral image is the sum of the image's pixels above and to the left of location (x, y). "Fig. 1" illustrates the integral image generation.

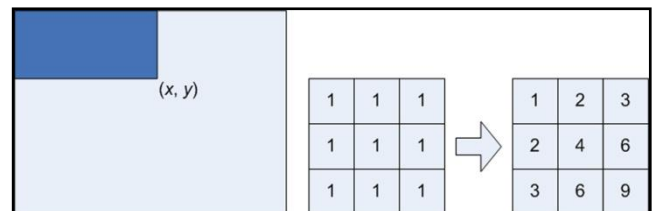


Figure 1. Integral image generation. The shaded region represents the sum of the pixels up to position (x, y) of the image. It shows a 3×3 image and its integral image representation.

B. Haar Features

Haar features are composed of either two or three rectangles. Face candidates are scanned and searched for Haar features of the current stage. The weight and size of each feature and the features themselves are generated using a machine learning algorithm from AdaBoost [6][7]. The weights are constants generated by the learning algorithm. There are a variety of forms of features as seen below in "Fig. 2".



Figure 2. Examples of Haar features. Areas of white and black regions are multiplied by their respective weights and then summed in order to get the Haar feature value.

Each Haar feature has a value that is calculated by taking the area of each rectangle, multiplying each by their respective weights, and then summing the results. The area of each rectangle is easily found using the integral image. The coordinate of the any corner of a rectangle can be used to get the sum of all the pixels above and to the left of that location using the integral image. By using each corner of a rectangle, the area can be computed quickly as denoted by "Fig. 3". Since $L1$ is subtracted off twice it must be added back on to get the correct area of the rectangle. The area of the rectangle R , denoted as the rectangle integral, can be computed as follows using the locations of the integral image: $L4-L3-L2+L1$.

C. Haar Feature Classifier

A Haar feature classifier uses the rectangle integral to calculate the value of a feature. The Haar feature classifier multiplies the weight of each rectangle by its area and the results are added together. Several Haar feature classifiers compose a stage. A stage comparator sums all the Haar feature classifier results in a stage and compares this summation with a stage threshold.

The threshold is also a constant obtained from the AdaBoost algorithm. Each stage does not have a set number of Haar features. Depending on the parameters of the training data individual stages can have a varying number of Haar features. For example, Viola and Jones' data set used 2 features in the first stage and 10 in the second. All together they used a total of 38 stages and 6060 features [6]. Our data set is based on the OpenCV data set which used 22 stages and 2135 features in total.

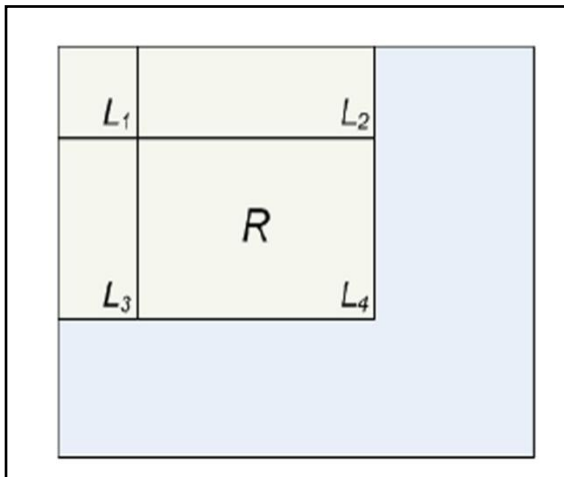


Figure 3. Calculating the area of a rectangle R is done using the corner of the rectangle: $L4-L3-L2+L1$.

D. Cascade

The Viola and Jones face detection algorithm eliminates face candidates quickly using a cascade of stages. The cascade eliminates candidates by making stricter requirements in each stage with later stages being much more difficult for a candidate to pass. Candidates exit the cascade if they pass all stages or fail any stage. A face is detected if a candidate passes all stages. This process is shown in "Fig. 4".

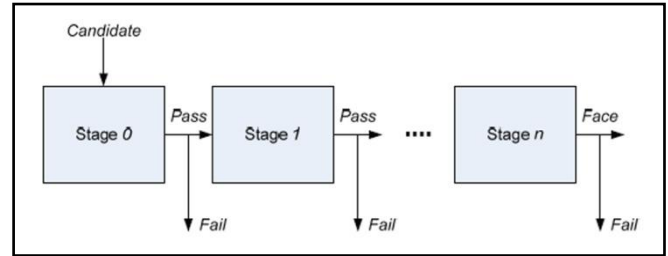


Figure 4. Cascade of stages. Candidate must pass all stages in the cascade to be concluded as a face.

III. IMPLEMENTATION

A. System Overview

We proposed architecture for a real-time face detection system. "Fig. 5" shows the overview of the proposed architecture for face detection. It consists of five modules: variant pose, illumination condition, Facial Expression, Occlusion, Uncontrolled Background, display. Face Detection systems are not only detected faces on uniform environment. In reality, Peoples are always located on complex background with different texture and object. These 'thing' are the major factors to affect the performance of face detection system

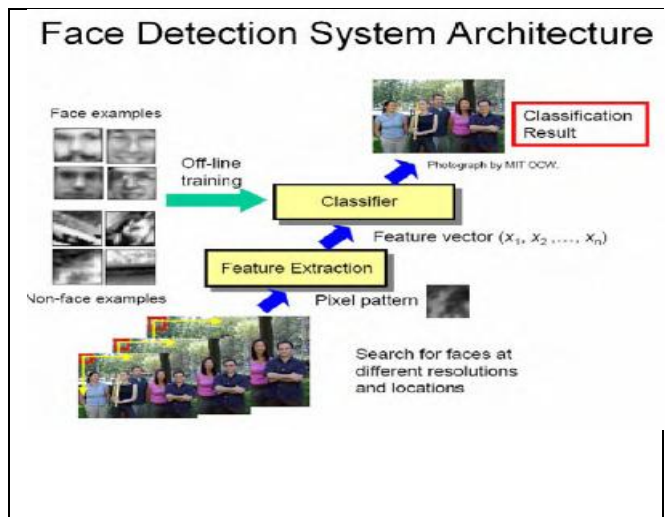


Figure 5. Block diagram of proposed face detection system.

B. Architecture for Face Detection

1) Variant Pose

Variant pose is occurred because of peoples not always orient to camera.

The image sync signal and the color image data are transferred from the image interface module. The image cropper crops the images based on the sync signals. These image data and sync signals are used in all of the modules of the face detection system.

2) Illuminatin Condition

Different lighting and the quality of camera directly affect the quality of face. Sometimes it can be varied greater than facial expression and occlusion.

3) Facial Expression

Different expression in the face is presented different information to the machine. Face is non-rigid objects which are changed by different expression.

The integral image generation requires substantial computation. A general purpose computer of Von Neumann

architecture has to access image memory at least width×height times to get the value of each pixel when it processes an image with width×height pixels. For the incoming pixel where the coordinate is (x, y), the image line buffer controller

4) Occlusion

Face detection not only deals with different faces, however, it need deal with any optional object. E.g. Hairstyle, sunglasses are the example of occlusion in face detection. For global feature, occlusion is one of major difficulty factor in face detection..

C. Integral Image

For the incoming pixel where the coordinate is (x, y), the image line buffer controller performs operations such as in “(1)”, where n is the image window row size, p(x, y) is the incoming pixel value, and L(x, y) represents each pixel in the image line buffer.

$$L(x, y - k) = L(x, y - (k - 1)), \text{ where } 1 \leq k \leq n - 2 \quad (1)$$

$$L(x, y - k) = p(x, y), \text{ where } k = 0$$

The image window buffer stores pixel values moving from the image line buffer and its controller generates control signals for moving and storing the pixel values. Since pixels of an image window buffer are stored in registers, it is possible to access all pixels in the image window buffer simultaneously to generate the integral image window.

$$I(i - k, j) = I(i - (k - 1), j), \text{ where } 1 \leq k \leq m - 1 \quad (2)$$

$$I(i, j - l) = L(x, y - (l - 1)), \text{ where } 1 \leq l \leq n - 1$$

$$I(i - k, j - l) = p(i, j) = p(x, y), \text{ where } k = l = 0,$$

$$\text{when } k + l = n - 1, 1 \leq k \leq n - 1, 0 \leq l \leq n - 2, m = 2n,$$

$$I(i - k, j - l) = I(i - (k - 1), j - l) + I(i - (k - 1), j - (l + 1))$$

For the incoming pixel with coordinate (x, y), the image window buffer controller performs operation as in “(2)” where n and m are the row and column size of the image window buffer, respectively. p(i, j) is the incoming pixel value in the image window buffer; p(x, y) is the incoming pixel value; I(i, j) represents each of the pixels in the image window buffer; and L(x, y) represents each of the pixels in the image line buffer.

$$II(s - u, t - v) = II(s - u, t - v) + I(i - k, j - l) - I(i - (2n - 1), j - l) \quad (3)$$

where $0 \leq u \leq n - 1, 0 \leq v \leq n - 1, n - 1 \leq k \leq 2n - 2, 0 \leq l \leq n - 1$

Since pixels of an integral image window buffer are stored in registers, it is possible to access all integral pixels in the integral image window buffer simultaneously to perform the Haar feature classification. For incoming pixel with coordinate (i, j), the integral image window buffer controller performs operation as in “(3)”

“Fig. 6” shows all of the actions in the proposed architecture to generate the integral image. For every image from the frame grabber module, the integral image window buffer is calculated to perform the feature classification using the integral image.

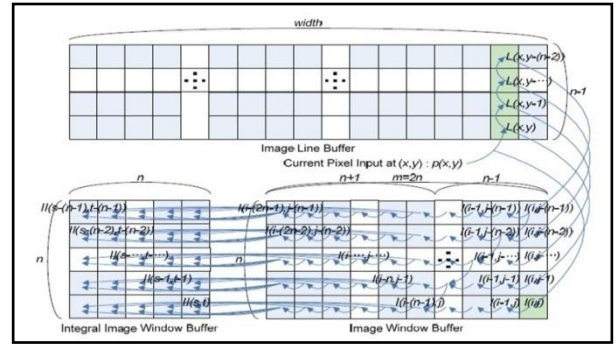


Figure 6. Architecture for generating integral image window.

A Haar classifier consists of two or three rectangles and their weight values, feature threshold value, and left and right values. Each rectangle presents four points using the coordinates (x, y) of most left and up point, width w, and height h as shown in “Fig. 7”.

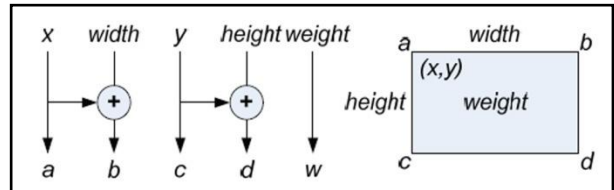


Figure 7. Rectangle calculation of Haar feature classifier.

The integral pixel value of each rectangle can be calculated using these points from the integral image window buffer as shown in “Fig. 8”.

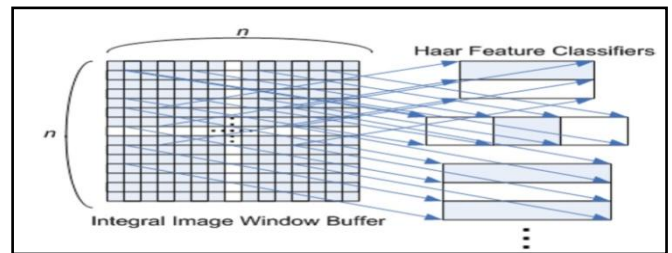


Figure 8. Simultaneous access to integral image window in order to calculate integral image of Haar feature classifiers.

Four points of the rectangles of the Haar feature classifier are calculated by the method as shown in “Fig. 7”. The integral image values of Haar classifier are obtained from the integral image window buffer as shown in “Fig. 8”. Integral image value of each rectangle multiplies with its weight. The summation of all integral image values multiplied by their weight is the result of one Haar feature classifier.

Display

In the display module, the Digital Visual Interface (DVI) specification is applied to display the image sequence to the LCD monitor through a DVI transmitter in the DVI interface module. This module generates the sync signals and image data for the DVI transmitter using the image signals and image data from the other modules.

D. Implementation

The proposed architecture for face detection has been designed using Verilog HDL and implemented in

MODEL-SIM Altera 6.3. We use the Haar feature training data from OpenCV to detect the frontal human faces based on the Viola and Jones algorithm. This Haar feature training data are trained by frontal faces whose size are 20x20, that includes a total of 22 stages, 2135 Haar classifiers, and 4630 Haar features.

1. Preprocessing

"System input is color images which included images of human faces or not, output is the human faces which is extracted from original images. In order to get the better result of detection, pre-processing is essential. In this section, pre-processing is addressed with giving detail description

2. Gray scale Conversion

For getting to reduce the information of images, image should be done a converting to grayscale. Each color images (RGB images) are composed of 3 channels to present red, green and blue components in RGB space. Below is the example to giving the general ideal of the RGB color image.

1. Given example images (R1,G1,B1),...,(Rn,Gn,Bn) where R, G, B are the value of red, green and blue respectively and 'n' is total number of pixel in given image.

3. The new grayscale images has pixel from G1,...,Gn, where using formula is as follows: $0.21R + 0.71G + 0.07B = G$. Unlike averages method, this form is considering the ratio because of human perception.

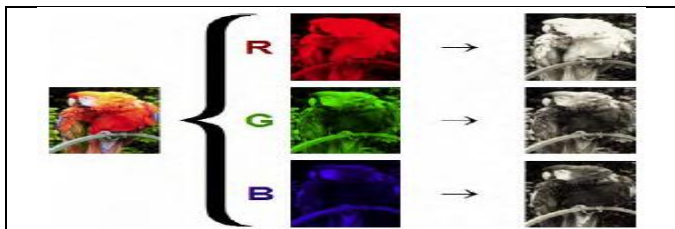
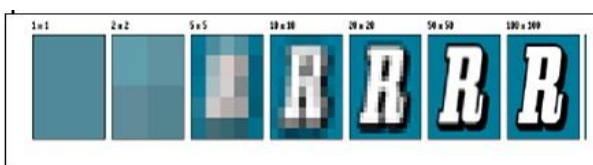


Figure 9 : RGB to Gray Scale Conversion
Image resizing

Images are synthesized by numerous of pixel which is the small unit in the image. Also, images are the 2-dimensional matrix pattern, every pixel in the images is represented something information.

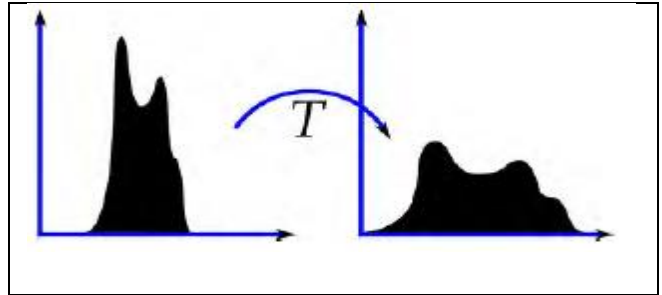
For example, '0' is white and '255' is black in gray scale images. Because there are a lot of information to deal with.

The top-left side of each image is the resolution of each one. Left-side's image is the original. Image has 3000 pixels in width and 2000 pixels in height which means it has $3000 \times 2000 = 6,000,000$ pixels or 6 megapixels. If the image has been resized into 1000 pixels in width and 600 pixels in height, image only has 0.6 megapixels. At least system only uses 1/10 timing to handle it.



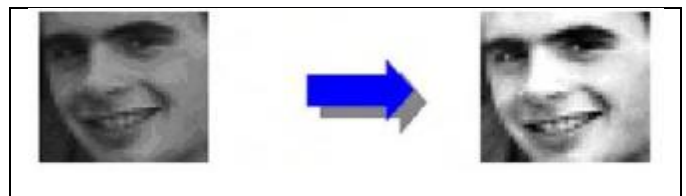
3. Histogram Equalization

Histogram equalization is a statistical method of images processing. It works as a statistical histogram of color distribution of the average scattered in the histogram, so that the distribution of a histogram graph homogenization.



The ideal is present as a follows: The change of the histogram after perform histogram equalization. In the above chart, the shape of graph has been widened which is the meaning of average scattered in the histogram.

This method usually increases the contrast of the input images.[34] In face detection system, The left-hand side of below images is resized grayscale images. Other is output images after proceed the processing of histogram equalization. You will see very significant results.



Example of the process of histogram equalization

Algorithms of Histogram equalization:

1. Grayscale images has X_n pixels with i represent a value of gray level in each pixel. The following chart is represent the relationship between probability of occurrence and the value of each pixel:

Chart of Probability Density Function (PDF) And

$$\sum_{i=0}^{255} p(x_i) = 1$$

P_x is being histogram of images and normalized to [0,1]

2. Let us define the cumulative distribution function as follows:

$$F(x) = \sum_{i=0}^x p(x_i) \quad x = 0, 1, 2, \dots, 255$$

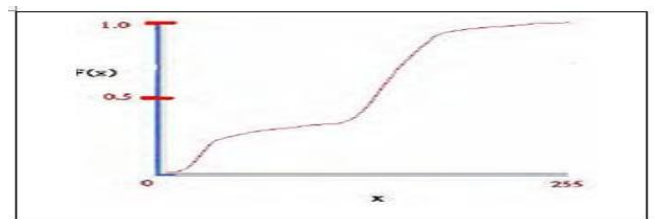


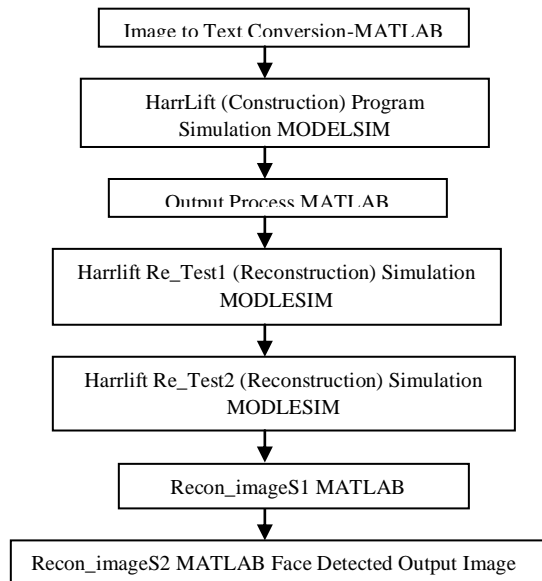
Chart of Cumulative distribution function

4. Minimum and maximum value are found and applied into following equation to find out the histogram equalization of each pixel:

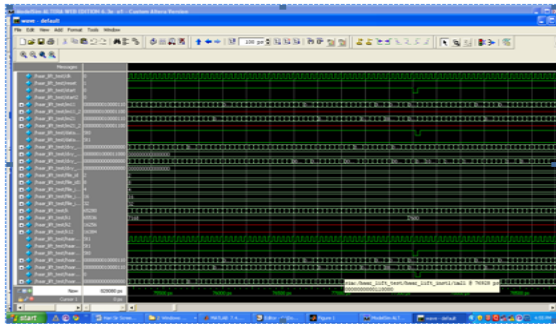
$$h(v) = \text{round} \left(\frac{cdf(v) - cdf_{min}}{(M \times N) - cdf_{min}} \times (L - 1) \right)$$

Where cdf_{\min} is the minimum value of CDF, M is the width of image and N is the height of image. L represent a large value of grey level, = 25

SIMULATION FLOW



WAVE FORMS IN MODELSIM



IV. EXPERIMENTS/RESULTS

A high frame processing rate and low latency are important for many applications that must provide quick decisions based on events in the scene. We measure the performance of the proposed architecture for the face detection system. Face detection system when it is applied to a camera, which produces images consisting of 640×480 pixels at 60 frames per second.



Figure 9. Experimental result of face detection system

V. CONCLUSION

We present face detection based on the AdaBoost algorithm using Haar features. In our architecture, the scaling image technique is used instead of the scaling sub-window, and the integral image window is generated instead of the integral image contains whole image during one clock cycle.

The Haar classifier is designed using a pipelined scheme, and the triple classifier which three single classifiers processed in parallel is adopted to accelerate the processing speed of the face detection system. Also we discussed the optimization of the proposed architecture which can be scalable for configurable devices with variable resources.

Finally, the proposed architecture is implemented on a Modelsim Altera 6.3 and its performance is measured and compared with an equivalent hardware implementation. We show about 35 time's increase of system performance over the equivalent software implementation. We plan to implement more classifiers to improve our design.

When the proposed face detection system is used in a system which requires face detection, only a small percentage of the system resources are allocated for face detection. The remainder of the resources can be assigned to pre-processing stage or to high level tasks such as recognition and reasoning. We have demonstrated that this face detection, combined with other technologies, can produce effective and powerful applications.

REFERENCES

- [1] Z. Guo, H. Liu, Q. Wang and J. Yang, "A Fast Algorithm of Face Detection for Driver Monitoring," In Proceedings of the Sixth International Conference on Intelligent Systems Design and Applications, vol. 2, pp.267 - 271, 2006.
- [2] M. Yang, N. Ahuja, "Face Detection and Gesture Recognition for Human-Computer Interaction," The International Series in Video Computing, vol.1, Springer, 2001.
- [3] Z. Zhang, G. Potamianos, M. Liu, T. Huang, "Robust Multi- View Multi-Camera Face Detection inside Smart Rooms Using Spatio-Temporal Dynamic Programming," International Conference on Automatic Face and Gesture Recognition, pp.407-412, 2006.
- [4] W. Yun; D. Kim; H. Yoon, "Fast Group Verification System for Intelligent Robot Service," IEEE Transactions on Consumer Electronics, vol.53, no.4, pp.1731-1735, Nov. 2007.
- [5] V. Ayala-Ramirez, R. E. Sanchez-Yanez and F. J. Montecillo-Puente "On the Application of Robotic Vision Methods to Biomedical Image Analysis," IFMBE Proceedings of Latin American Congress on Biomedical Engineering, pp.1160-1162, 2007.
- [6] P. Viola and M. Jones, "Robust real-time object detection," International Journal of Computer Vision, 57(2), 137-154, 2004.

On rg-Separation Axioms

S. Balasubramanian¹ C. Sandhya² and M.D.S. Saikumar³

¹Department of Mathematics, Govt. Arts College (A), Karur – 639 005, Tamilnadu

² Department of Mathematics, C.S.R. Sarma College, Ongole – 523 001, Andhraparaksh

³ Department of Mathematics, Krishnaveni Degree College, Narasaraopet – 522 601, Andhraparaksh

Abstract: In this paper we define almost rg-normality and mild rg-normality, continue the study of further properties of rg-normality. We show that these three axioms are regular open hereditary. Also define the class of almost rg-irresolute mappings and show that rg-normality is invariant under almost rg-irresolute M-rg-open continuous surjection.

AMS Subject Classification: 54D15, 54D10.

Key words and Phrases: rg-open, almost normal, mildly normal, M-rg-closed, M-rg-open, rc-continuous.

I. Introduction:

In 1967, A. Wilansky has introduced the concept of US spaces. In 1968, C.E. Aull studied some separation axioms between the T_1 and T_2 spaces, namely, S_1 and S_2 . Next, in 1982, S.P. Arya et al have introduced and studied the concept of semi-US spaces and also they made study of s-convergence, sequentially semi-closed sets, sequentially s-compact notions. G.B. Navlagi studied P-Normal Almost-P-Normal, Mildly-P-Normal and Pre-US spaces. Recently S. Balasubramanian and P.Aruna Swathi Vyjayanthi studied ν -Normal Almost- ν -Normal, Mildly- ν -Normal and ν -US spaces. Inspired with these we introduce rg-Normal Almost- rg-Normal, Mildly- rg-Normal, rg-US, rg- S_1 and rg- S_2 . Also we examine rg-convergence, sequentially rg-compact, sequentially rg-continuous maps, and sequentially sub rg-continuous maps in the context of these new concepts. All notions and symbols which are not defined in this paper may be found in the appropriate references. Throughout the paper X and Y denote Topological spaces on which no separation axioms are assumed explicitly stated.

II. Preliminaries:

Definition 2.1: $A \subseteq X$ is called g-closed[resp: rg-closed] if $\text{cl}A \subseteq U$ [resp: $\text{scl}(A) \subseteq U$] whenever $A \subseteq U$ and U is open[resp: semi-open] in X .

Definition 2.2: A space X is said to be

- (i) $T_1(T_2)$ if for $x \neq y$ in X , there exist (disjoint) open sets U, V in X such that $x \in U$ and $y \in V$.
- (ii) weakly Hausdorff if each point of X is the intersection of regular closed sets of X .
- (iii) Normal [resp: mildly normal] if for any pair of disjoint [resp: regular-closed] closed sets F_1 and F_2 , there exist disjoint open sets U and V such that $F_1 \subseteq U$ and $F_2 \subseteq V$.
- (iv) almost normal if for each closed set A and each regular closed set B such that $A \cap B = \emptyset$, there exist disjoint open sets U and V such that $A \subseteq U$ and $B \subseteq V$.
- (v) weakly regular if for each pair consisting of a regular closed set A and a point x such that $A \cap \{x\} = \emptyset$, there exist disjoint open sets U and V such that $x \in U$ and $A \subseteq V$.
- (vi) A subset A of a space X is S-closed relative to X if every cover of A by semi-open sets of X has a finite subfamily whose closures cover A .
- (vii) R_0 if for any point x and a closed set F with $x \notin F$ in X , there exists a open set G containing F but not x .
- (viii) R_1 iff for $x, y \in X$ with $\text{cl}\{x\} \neq \text{cl}\{y\}$, there exist disjoint open sets U and V such that $\text{cl}\{x\} \subseteq U, \text{cl}\{y\} \subseteq V$.
- (ix) US-space if every convergent sequence has exactly one limit point to which it converges. (x) pre-US space if every pre-convergent sequence has exactly one limit point to which it converges.
- (xi) pre- S_1 if it is pre-US and every sequence pre-converges with subsequence of pre-side points.
- (xii) pre- S_2 if it is pre-US and every sequence in X pre-converges which has no pre-side point.
- (xiii) is weakly countable compact if every infinite subset of X has a limit point in X .
- (xiv) Baire space if for any countable collection of closed sets with empty interior in X , their union also has empty interior in

Definition 2.3: Let $A \subseteq X$. Then a point x is said to be a

- (i) limit point of A if each open set containing x contains some point y of A such that $x \neq y$.
- (ii) T_0 -limit point of A if each open set containing x contains some point y of A such that $\text{cl}\{x\} \neq \text{cl}\{y\}$, or equivalently, such that they are topologically distinct.
- (iii) pre- T_0 -limit point of A if each open set containing x contains some point y of A such that $\text{pcl}\{x\} \neq \text{pcl}\{y\}$, or equivalently, such that they are topologically distinct.

Note 1: Recall that two points are topologically distinguishable or distinct if there exists an open set containing one of the points but not the other; equivalently if they have disjoint closures. In fact, the T_0 -axiom is precisely to ensure that any two distinct points are topologically distinct.

Example 1: Let $X = \{a, b, c, d\}$ and $\tau = \{\{a\}, \{b, c\}, \{a, b, c\}, X, \phi\}$. Then b and c are the limit points but not the T_0 -limit points of the set $\{b, c\}$. Further d is a T_0 -limit point of $\{b, c\}$.

Example 2: Let $X = (0, 1)$ and $\tau = \{\phi, X, \text{ and } U_n = (0, 1 - 1/n), n = 2, 3, 4, \dots\}$. Then every point of X is a limit point of X . Every point of $X \sim U_2$ is a T_0 -limit point of X , but no point of U_2 is a T_0 -limit point of X .

Definition 2.4: A set A together with all its T_0 -limit points will be denoted by $T_0\text{-cl}A$.

Note 2: i. Every T_0 -limit point of a set A is a limit point of the set but converse is not true.
 ii. In T_0 -space both are same.

Note 3: R_0 -axiom is weaker than T_1 -axiom. It is independent of the T_0 -axiom. However $T_1 = R_0 + T_0$

Note 4: Every countable compact space is weakly countable compact but converse is not true in general. However, a T_1 -space is weakly countable compact iff it is countable compact.

Definition 3.01: In X , a point x is said to be a $rg\text{-}T_0$ -limit point of A if each rg -open set containing x contains some point y of A such that $rgcl\{x\} \neq rgcl\{y\}$, or equivalently; such that they are topologically distinct with respect to rg -open sets.

III. Example

Let $X = \{a, b, c\}$ and $\tau = \{\phi, \{b\}, \{a, b\}, \{b, c\}, X\}$. For $A = \{a, b\}$, a is $rg\text{-}T_0$ -limit point.

Definition 3.02: A set A together with all its $rg\text{-}T_0$ -limit points is denoted by $T_0\text{-}rgcl(A)$

Lemma 3.01: If x is a $rg\text{-}T_0$ -limit point of a set A then x is rg -limit point of A .

Lemma 3.02: If X is rgT_0 [resp: rT_0]-space then every $rg\text{-}T_0$ -limit point and every rg -limit point are equivalent.

Theorem 3.03: For $x \neq y \in X$,

- (i) X is a $rg\text{-}T_0$ -limit point of $\{y\}$ iff $x \notin rgcl\{y\}$ and $y \in rgcl\{x\}$.
- (ii) X is not a $rg\text{-}T_0$ -limit point of $\{y\}$ iff either $x \in rgcl\{y\}$ or $rgcl\{x\} = rgcl\{y\}$.
- (iii) X is not a $rg\text{-}T_0$ -limit point of $\{y\}$ iff either $x \in rgcl\{y\}$ or $y \in rgcl\{x\}$.

Corollary 3.04:

- (i) If x is a $rg\text{-}T_0$ -limit point of $\{y\}$, then y cannot be a rg -limit point of $\{x\}$.
- (ii) If $rgcl\{x\} = rgcl\{y\}$, then neither x is a $rg\text{-}T_0$ -limit point of $\{y\}$ nor y is a $rg\text{-}T_0$ -limit point of $\{x\}$.
- (iii) If a singleton set A has no $rg\text{-}T_0$ -limit point in X , then $rgclA = rgcl\{x\}$ for all $x \in rgclA$.

Lemma 3.05: In X , if x is a rg -limit point of a set A , then in each of the following cases x becomes $rg\text{-}T_0$ -limit point of A ($\{x\} \neq A$).

- (i) $rgcl\{x\} \neq rgcl\{y\}$ for $y \in A, x \neq y$.
- (ii) $rgcl\{x\} = \{x\}$
- (iii) X is a $rg\text{-}T_0$ -space.
- (iv) $A \sim \{x\}$ is rg -open

IV. $rg\text{-}T_0$ AND $rg\text{-}R_i$ AXIOMS, $i = 0, 1$:

In view of Lemma 3.5(iii), $rg\text{-}T_0$ -axiom implies the equivalence of the concept of limit point with that of $rg\text{-}T_0$ -limit point of the set. But for the converse, if $x \in rgcl\{y\}$ then $rgcl\{x\} \neq rgcl\{y\}$ in general, but if x is a $rg\text{-}T_0$ -limit point of $\{y\}$, then $rgcl\{x\} = rgcl\{y\}$

Lemma 4.01: In X , a limit point x of $\{y\}$ is a $rg\text{-}T_0$ -limit point of $\{y\}$ iff $rgcl\{x\} \neq rgcl\{y\}$.

This lemma leads to characterize the equivalence of $rg\text{-}T_0$ -limit point and rg -limit point of a set as $rg\text{-}T_0$ -axiom.

Theorem 4.02: The following conditions are equivalent:

- (i) X is a $rg\text{-}T_0$ space
- (ii) Every rg -limit point of a set A is a $rg\text{-}T_0$ -limit point of A
- (iii) Every r -limit point of a singleton set $\{x\}$ is a $rg\text{-}T_0$ -limit point of $\{x\}$

(iv) For any x, y in X , $x \neq y$ if $x \in \text{rgcl}\{y\}$, then x is a rg-T_0 -limit point of $\{y\}$

Note 5: In a rg-T_0 -space X , if every point of X is a r-limit point, then every point is rg-T_0 -limit point. But if each point is a rg-T_0 -limit point of X it is not necessarily a rg-T_0 -space

Theorem 4.03: The following conditions are equivalent:

- (i) X is a rg-R_0 space
- (ii) For any x, y in X , if $x \in \text{rgcl}\{y\}$, then x is not a rg-T_0 -limit point of $\{y\}$
- (iii) A point rg-closure set has no rg-T_0 -limit point in X
- (iv) A singleton set has no rg-T_0 -limit point in X .

Theorem 4.04: In a rg-R_0 space X , a point x is rg-T_0 -limit point of A iff every rg-open set containing x contains infinitely many points of A with each of which x is topologically distinct

Theorem 4.05: X is rg-R_0 space iff a set A of the form $A = \cup \text{rgcl}\{x_i, i=1 \text{ to } n\}$ a finite union of point closure sets has no rg-T_0 -limit point.

Corollary 4.06: The following conditions are equivalent:

- (i) X is a rR_0 space
- (ii) For any x, y in X , if $x \in \text{rgcl}\{y\}$, then x is not a rg-T_0 -limit point of $\{y\}$
- (iii) A point rg-closure set has no rg-T_0 -limit point in X
- (iv) A singleton set has no rg-T_0 -limit point in X .

Corollary 4.07: In an rR_0 -space X ,

- (i) If a point x is rg-T_0 -[resp: rT_0 -] limit point of a set then every rg-open set containing x contains infinitely many points of A with each of which x is topologically distinct.
- (ii) If $A = \cup \text{rgcl}\{x_i, i=1 \text{ to } n\}$ a finite union of point closure sets has no rg-T_0 -limit point.
- (iii) If $X = \cup \text{rgcl}\{x_i, i=1 \text{ to } n\}$ then X has no rg-T_0 -limit point.

Various characteristic properties of rg-T_0 -limit points studied so far is enlisted in the following theorem.

Theorem 4.08: In a rg-R_0 -space, we have the following:

- (i) A singleton set has no rg-T_0 -limit point in X .
- (ii) A finite set has no rg-T_0 -limit point in X .
- (iii) A point rg-closure set has no rg-T_0 -limit point in X
- (iv) A finite union point rg-closure sets have no rg-T_0 -limit point in X .
- (v) For $x, y \in X$, $x \in \text{rgcl}\{y\}$ iff $x = y$.
- (vi) $x \neq y \in X$, iff neither x is rg-T_0 -limit point of $\{y\}$ nor y is rg-T_0 -limit point of $\{x\}$
- (vii) For any $x, y \in X$, $x \neq y$ iff $\text{rgcl}\{x\} \cap \text{rgcl}\{y\} = \emptyset$.
- (viii) Any point $x \in X$ is a rg-T_0 -limit point of a set A in X iff every rg-open set containing x contains infinitely many points of A with each which x is topologically distinct.

Theorem 4.09: X is rg-R_1 iff for any rg-open set U in X and points x, y such that $x \in X \sim U$, $y \in U$, there exists a rg-open set V in X such that $y \in V \subset U$, $x \notin V$.

Lemma 4.10: In rg-R_1 space X , if x is a rg-T_0 -limit point of X , then for any non empty rg-open set U , there exists a non empty rg-open set V such that $V \subset U$, $x \notin \text{rgcl}(V)$.

Lemma 4.11: In a rg-regular space X , if x is a rg-T_0 -limit point of X , then for any non empty rg-open set U , there exists a non empty rg-open set V such that $\text{rgcl}(V) \subset U$, $x \notin \text{rgcl}(V)$.

Corollary 4.12: In a regular space X , If x is a rg-T_0 -[resp: T_0 -] limit point of X , then for any $U \neq \emptyset \in \text{RGO}(X)$, there exists a non empty rg-open set V such that $\text{rgcl}(V) \subset U$, $x \notin \text{rgcl}(V)$.

Theorem 4.13: If X is a rg-compact rg-R_1 -space, then X is a Baire Space.

Proof: Routine

Corollary 4.14: If X is a compact rg-R_1 -space, then X is a Baire Space.

Corollary 4.15: Let X be a rg-compact rg-R_1 -space. If $\{A_n\}$ is a countable collection of rg-closed sets in X , each A_n having non-empty rg-interior in X , then there is a point of X which is not in any of the A_n .

Corollary 4.16: Let X be a rg -compact R_1 -space. If $\{A_n\}$ is a countable collection of rg -closed sets in X , each A_n having non-empty rg -interior in X , then there is a point of X which is not in any of the A_n .

Theorem 4.17: Let X be a non empty compact rg - R_1 -space. If every point of X is a rg - T_0 -limit point of X then X is uncountable.

Proof: Since X is non empty and every point is a rg - T_0 -limit point of X , X must be infinite. If X is countable, we construct a sequence of rg -open sets $\{V_n\}$ in X as follows:

Let $X = V_1$, then for x_1 is a rg - T_0 -limit point of X , we can choose a non empty rg -open set V_2 in X such that $V_2 \subset V_1$ and $x_1 \notin rgclV_2$. Next for x_2 and non empty rg -open set V_2 , we can choose a non empty rg -open set V_3 in X such that $V_3 \subset V_2$ and $x_2 \notin rgclV_3$. Continuing this process for each x_n and a non empty rg -open set V_n , we can choose a non empty rg -open set V_{n+1} in X such that $V_{n+1} \subset V_n$ and $x_n \notin rgclV_{n+1}$.

Now consider the nested sequence of rg -closed sets $rgclV_1 \supset rgclV_2 \supset rgclV_3 \supset \dots \supset rgclV_n \supset \dots$. Since X is rg -compact and $\{rgclV_n\}$ the sequence of rg -closed sets satisfies finite intersection property. By Cantors intersection theorem, there exists an x in X such that $x \in rgclV_n$. Further $x \in X$ and $x \in V_1$, which is not equal to any of the points of X . Hence X is uncountable.

Corollary 4.18: Let X be a non empty rg -compact rg - R_1 -space. If every point of X is a rg - T_0 -limit point of X then X is uncountable

V. rg - T_0 -IDENTIFICATION SPACES AND rg -SEPARATION AXIOMS

Definition 5.01: Let \mathfrak{R} be the equivalence relation on X defined by $x\mathfrak{R}y$ iff $rgcl\{x\} = rgcl\{y\}$

Problem 5.02: show that $x\mathfrak{R}y$ iff $rgcl\{x\} = rgcl\{y\}$ is an equivalence relation

Definition 5.03: $(X_0, Q(X_0))$ is called the rg - T_0 -identification space of (X, τ) , where X_0 is the set of equivalence classes of \mathfrak{R} and $Q(X_0)$ is the decomposition topology on X_0 .

Let $P_X: (X, \tau) \rightarrow (X_0, Q(X_0))$ denote the natural map

Lemma 5.04: If $x \in X$ and $A \subset X$, then $x \in rgclA$ iff every rg -open set containing x intersects A .

Theorem 5.05: The natural map $P_X: (X, \tau) \rightarrow (X_0, Q(X_0))$ is closed, open and $P_X^{-1}(P_X(O)) = O$ for all $O \in PO(X, \tau)$ and $(X_0, Q(X_0))$ is rg - T_0

Proof: Let $O \in PO(X, \tau)$ and $C \in P_X(O)$. Then there exists $x \in O$ such that $P_X(x) = C$. If $y \in C$, then $rgcl\{y\} = rgcl\{x\}$, which implies $y \in O$. Since $\tau \subset PO(X, \tau)$, then $P_X^{-1}(P_X(U)) = U$ for all $U \in \tau$, which implies P_X is closed and open.

Let $G, H \in X_0$ such that $G \neq H$; let $x \in G$ and $y \in H$. Then $rgcl\{x\} \neq rgcl\{y\}$, which implies $x \notin rgcl\{y\}$ or $y \notin rgcl\{x\}$, say $x \notin rgcl\{y\}$. Since P_X is continuous and open, then $G \in A = P_X\{X \sim rgcl\{y\}\} \notin PO(X_0, Q(X_0))$ and $H \notin A$

Theorem 5.06: The following are equivalent:

(i) X is rgR_0 (ii) $X_0 = \{rgcl\{x\}: x \in X\}$ and (iii) $(X_0, Q(X_0))$ is rgT_1

Proof: (i) \Rightarrow (ii) Let $x \in C \in X_0$. If $y \in C$, then $y \in rgcl\{y\} = rgcl\{x\}$, which implies $C \in rgcl\{x\}$. If $y \in rgcl\{x\}$, then $x \in rgcl\{y\}$, since, otherwise, $x \in X \sim rgcl\{y\} \in PO(X, \tau)$ which implies $rgcl\{x\} \subset X \sim rgcl\{y\}$, which is a contradiction. Thus, if $y \in rgcl\{x\}$, then $x \in rgcl\{y\}$, which implies $rgcl\{y\} = rgcl\{x\}$ and $y \in C$. Hence $X_0 = \{rgcl\{x\}: x \in X\}$

(ii) \Rightarrow (iii) Let $A \neq B \in X_0$. Then there exists $x, y \in X$ such that $A = rgcl\{x\}$; $B = rgcl\{y\}$, and $rgcl\{x\} \cap rgcl\{y\} = \emptyset$. Then $A \in C = P_X\{X \sim rgcl\{y\}\} \in PO(X_0, Q(X_0))$ and $B \notin C$. Thus $(X_0, Q(X_0))$ is rg - T_1

(iii) \Rightarrow (i) Let $x \in U \in RGO(X)$. Let $y \notin U$ and $C_x, C_y \in X_0$ containing x and y respectively. Then $x \notin rgcl\{y\}$, implies $C_x \neq C_y$ and there exists rg -open set A such that $C_x \in A$ and $C_y \notin A$. Since P_X is continuous and open, then $y \in B = P_X^{-1}(A) \in x \in RGO(X)$ and $x \notin B$, which implies $y \notin rgcl\{x\}$. Thus $rgcl\{x\} \subset U$. This is true for all $rgcl\{x\}$ implies $\bigcap rgcl\{x\} \subset U$. Hence X is rg - R_0

Theorem 5.07: (X, τ) is rg - R_1 iff $(X_0, Q(X_0))$ is rg - T_2

The proof is straight forward using theorems 5.05 and 5.06 and is omitted

Theorem 5.08: X is rg - T_i ; $i = 0, 1, 2$. iff there exists a rg -continuous, almost-open, 1-1 function from X into a rg - T_i space; $i = 0, 1, 2$. respectively.

Theorem 5.09: If f is rg -continuous, rg -open, and $x, y \in X$ such that $rgcl\{x\} = rgcl\{y\}$, then $rgcl\{f(x)\} = rgcl\{f(y)\}$.

Theorem 5.10: The following are equivalent

(i) X is rg - T_0

(ii) Elements of X_0 are singleton sets and

(iii) There exists a rg -continuous, rg -open, 1-1 function $f: X \rightarrow Y$, where Y is rg - T_0

Proof: (i) is equivalent to (ii) and (i) \Rightarrow (iii) are straight forward and is omitted.

(iii) \Rightarrow (i) Let $x, y \in X$ such that $f(x) \neq f(y)$, which implies $rgcl\{f(x)\} \neq rgcl\{f(y)\}$. Then by theorem 5.09, $rgcl\{x\} \neq rgcl\{y\}$. Hence (X, τ) is $rg-T_0$

Corollary 5.11: X is $rg-T_i$; $i = 1, 2$ iff X is $rg-T_{i-1}$; $i = 1, 2$, respectively, and there exists a rg -continuous, rg -open, $1-1$ function $f: X$ into a $rg-T_0$ space.

Definition 5.04: f is point- rg -closure $1-1$ iff for $x, y \in X$ such that $rgcl\{x\} \neq rgcl\{y\}$, $rgcl\{f(x)\} \neq rgcl\{f(y)\}$.

Theorem 5.12: (i) If $f: X \rightarrow Y$ is point- rg -closure $1-1$ and (X, τ) is $rg-T_0$, then f is $1-1$

(ii) If $f: X \rightarrow Y$, where X and Y are $rg-T_0$ then f is point- rg -closure $1-1$ iff f is $1-1$

The following result can be obtained by combining results for $rg-T_0$ -identification spaces, rg -induced functions and $rg-T_i$ spaces; $i = 1, 2$.

Theorem 5.13: X is $rg-R_i$; $i = 0, 1$ iff there exists a rg -continuous, almost-open point- rg -closure $1-1$ function $f: (X, \tau)$ into a $rg-R_i$ space; $i = 0, 1$ respectively.

VI. rg -Normal; Almost rg -normal and Mildly rg -normal spaces

Definition 6.1: A space X is said to be rg -normal if for any pair of disjoint closed sets F_1 and F_2 , there exist disjoint rg -open sets U and V such that $F_1 \subset U$ and $F_2 \subset V$.

Example 4: Let $X = \{a, b, c\}$ and $\tau = \{\emptyset, \{a\}, \{b, c\}, X\}$. Then X is rg -normal.

Example 5: Let $X = \{a, b, c, d\}$ and $\tau = \{\emptyset, \{b, d\}, \{a, b, d\}, \{b, c, d\}, X\}$. Then X is rg -normal and is not normal.

Example 6: Let $X = \{a, b, c, d\}$ with $\tau = \{\emptyset, \{a\}, \{b\}, \{d\}, \{a, b\}, \{a, d\}, \{b, d\}, \{a, b, c\}, \{a, b, d\}, X\}$ is rg -normal, normal and almost normal.

We have the following characterization of rg -normality.

Theorem 6.1: For a space X the following are equivalent:

- (i) X is rg -normal.
 - (ii) For every pair of open sets U and V whose union is X , there exist rg -closed sets A and B such that $A \subset U$, $B \subset V$ and $A \cup B = X$.
 - (iii) For every closed set F and every open set G containing F , there exists a rg -open set U such that $F \subset U \subset rgcl(U) \subset G$.
- Proof:** (i) \Rightarrow (ii): Let U and V be a pair of open sets in a rg -normal space X such that $X = U \cup V$. Then $X - U$, $X - V$ are disjoint closed sets. Since X is rg -normal there exist disjoint rg -open sets U_1 and V_1 such that $X - U \subset U_1$ and $X - V \subset V_1$. Let $A = X - U_1$, $B = X - V_1$. Then A and B are rg -closed sets such that $A \subset U$, $B \subset V$ and $A \cup B = X$.
- (ii) \Rightarrow (iii): Let F be a closed set and G be an open set containing F . Then $X - F$ and G are open sets whose union is X . Then by (b), there exist rg -closed sets W_1 and W_2 such that $W_1 \subset X - F$ and $W_2 \subset G$ and $W_1 \cup W_2 = X$. Then $F \subset X - W_1$, $X - G \subset X - W_2$ and $(X - W_1) \cap (X - W_2) = \emptyset$. Let $U = X - W_1$ and $V = X - W_2$. Then U and V are disjoint rg -open sets such that $F \subset U \subset X - V \subset G$. As $X - V$ is rg -closed set, we have $rgcl(U) \subset X - V$ and $F \subset U \subset rgcl(U) \subset G$.
- (iii) \Rightarrow (i): Let F_1 and F_2 be any two disjoint closed sets of X . Put $G = X - F_2$, then $F_1 \cap G = \emptyset$. $F_1 \subset G$ where G is an open set. Then by (c), there exists a rg -open set U of X such that $F_1 \subset U \subset rgcl(U) \subset G$. It follows that $F_2 \subset X - rgcl(U) = V$, say, then V is rg -open and $U \cap V = \emptyset$. Hence F_1 and F_2 are separated by rg -open sets U and V . Therefore X is rg -normal.

Theorem 6.2: A regular open subspace of a rg -normal space is rg -normal.

Definition 6.2: A function $f: X \rightarrow Y$ is said to be almost- rg -irresolute if for each x in X and each rg -neighborhood V of $f(x)$, $rgcl(f^{-1}(V))$ is a rg -neighborhood of x .

Clearly every rg -irresolute map is almost rg -irresolute.

The Proof of the following lemma is straightforward and hence omitted.

Lemma 6.1: f is almost rg -irresolute iff $f^{-1}(V) \subset rg-int(rgcl(f^{-1}(V)))$ for every $V \in RGO(Y)$.

Lemma 6.2: f is almost rg -irresolute iff $f(rgcl(U)) \subset rgcl(f(U))$ for every $U \in RGO(X)$.

Proof: Let $U \in RGO(X)$. If $y \notin rgcl(f(U))$. Then there exists $V \in RGO(y)$ such that $V \cap f(U) = \emptyset$. Hence $f^{-1}(V) \cap U = \emptyset$. Since $U \in RGO(X)$, we have $rg-int(rgcl(f^{-1}(V))) \cap rgcl(U) = \emptyset$. By lemma 6.1, $f^{-1}(V) \cap rgcl(U) = \emptyset$ and hence $V \cap f(rgcl(U)) = \emptyset$. This implies that $y \notin f(rgcl(U))$.

Conversely, if $V \in RGO(Y)$, then $W = X - rgcl(f^{-1}(V)) \in RGO(X)$. By hypothesis, $f(rgcl(W)) \subset rgcl(f(W))$ and hence $X - rgcl(rgcl(f^{-1}(V))) = rgcl(W) \subset f^{-1}(rgcl(f(W))) \subset f^{-1}(rgcl[f(X - f^{-1}(V))]) \subset f^{-1}[rgcl(Y - V)] = f^{-1}(Y - V) = X - f^{-1}(V)$. Therefore $f^{-1}(V) \subset rgcl(rgcl(f^{-1}(V)))$. By lemma 6.1, f is almost rg-irresolute.

Theorem 6.3: If f is M-rg-open continuous almost rg-irresolute, X is rg-normal, then Y is rg-normal.

Proof: Let A be a closed subset of Y and B be an open set containing A . Then by continuity of f , $f^{-1}(A)$ is closed and $f^{-1}(B)$ is an open set of X such that $f^{-1}(A) \subset f^{-1}(B)$. As X is rg-normal, there exists a rg-open set U in X such that $f^{-1}(A) \subset U \subset rgcl(U) \subset f^{-1}(B)$. Then $f(f^{-1}(A)) \subset f(U) \subset f(rgcl(U)) \subset f(f^{-1}(B))$. Since f is M-rg-open almost rg-irresolute surjection, we obtain $A \subset f(U) \subset rgcl(f(U)) \subset B$. Then again by Theorem 6.1 the space Y is rg-normal.

Lemma 6.3: A mapping f is M-rg-closed iff for each subset B in Y and for each rg-open set U in X containing $f^{-1}(B)$, there exists a rg-open set V containing B such that $f^{-1}(V) \subset U$.

Theorem 6.4: If f is M-rg-closed continuous, X is rg-normal space, then Y is rg-normal.

Proof of the theorem is routine and hence omitted.

Theorem 6.5: If f is an M-rg-closed map from a weakly Hausdorff rg-normal space X onto a space Y such that $f^{-1}(y)$ is S-closed relative to X for each $y \in Y$, then Y is rg- T_2 .

Proof: Let $y_1 \neq y_2 \in Y$. Since X is weakly Hausdorff, $f^{-1}(y_1)$ and $f^{-1}(y_2)$ are disjoint closed subsets of X by lemma 2.2 [12.]. As X is rg-normal, there exist disjoint $V_i \in RGO(X, f^{-1}(y_i))$ for $i = 1, 2$. Since f is M-rg-closed, there exist disjoint $U_i \in RGO(Y, y_i)$ and $f^{-1}(U_i) \subset V_i$ for $i = 1, 2$. Hence Y is rg- T_2 .

Theorem 6.6: For a space X we have the following:

- (a) If X is normal then for any disjoint closed sets A and B , there exist disjoint rg-open sets U, V such that $A \subset U$ and $B \subset V$;
- (b) If X is normal then for any closed set A and any open set V containing A , there exists an rg-open set U of X such that $A \subset U \subset rgcl(U) \subset V$.

Definition 6.2: X is said to be almost rg-normal if for each closed set A and each regular closed set B with $A \cap B = \emptyset$, there exist disjoint $U, V \in RGO(X)$ such that $A \subset U$ and $B \subset V$.

Clearly, every rg-normal space is almost rg-normal, but not conversely in general.

Example 7: Let $X = \{a, b, c\}$ and $\tau = \{\emptyset, \{a\}, \{a, b\}, \{a, c\}, X\}$. Then X is almost rg-normal and rg-normal.

Theorem 6.7: For a space X the following statements are equivalent:

- (i) X is almost rg-normal
- (ii) For every pair of sets U and V , one of which is open and the other is regular open whose union is X , there exist rg-closed sets G and H such that $G \subset U$, $H \subset V$ and $G \cup H = X$.
- (iii) For every closed set A and every regular open set B containing A , there is a rg-open set V such that $A \subset V \subset rgcl(V) \subset B$.

Proof: (i) \Rightarrow (ii) Let $U \in \tau$ and $V \in RO(X)$ such that $U \cup V = X$. Then $(X - U)$ is closed set and $(X - V)$ is regular closed set with $(X - U) \cap (X - V) = \emptyset$. By almost rg-normality of X , there exist disjoint rg-open sets U_1 and V_1 such that $X - U \subset U_1$ and $X - V \subset V_1$. Let $G = X - U_1$ and $H = X - V_1$. Then G and H are rg-closed sets such that $G \subset U$, $H \subset V$ and $G \cup H = X$.

(ii) \Rightarrow (iii) and (iii) \Rightarrow (i) are obvious.

One can prove that almost rg-normality is also regular open hereditary.

Almost rg-normality does not imply almost rg-regularity in general. However, we observe that every almost rg-normal rg- R_0 space is almost rg-regular.

Theorem 6.8: Every almost regular, rg-compact space X is almost rg-normal.

Recall that a function $f: X \rightarrow Y$ is called rc-continuous if inverse image of regular closed set is regular closed.

Theorem 6.9: If f is continuous M-rg-open rc-continuous and almost rg-irresolute surjection from an almost rg-normal space X onto a space Y , then Y is almost rg-normal.

Definition 6.3: X is said to be mildly rg-normal if for every pair of disjoint regular closed sets F_1 and F_2 of X , there exist disjoint rg-open sets U and V such that $F_1 \subset U$ and $F_2 \subset V$.

Example 8: Let $X = \{a, b, c, d\}$ with $\tau = \{\emptyset, \{a\}, \{b\}, \{d\}, \{a, b\}, \{a, d\}, \{b, d\}, \{a, b, c\}, \{a, b, d\}, X\}$ is Mildly rg-normal.

Theorem 6.10: For a space X the following are equivalent.

- (i) X is mildly rg -normal.
- (ii) For every pair of regular open sets U and V whose union is X , there exist rg -closed sets G and H such that $G \subset U$, $H \subset V$ and $G \cup H = X$.
- (iii) For any regular closed set A and every regular open set B containing A , there exists a rg -open set U such that $A \subset U \subset rgcl(U) \subset B$.
- (iv) For every pair of disjoint regular closed sets, there exist rg -open sets U and V such that $A \subset U$, $B \subset V$ and $rgcl(U) \cap rgcl(V) = \emptyset$.

Proof: This theorem may be proved by using the arguments similar to those of Theorem 6.7.

Also, we observe that mild rg -normality is regular open hereditary.

Definition 6.4: A space X is weakly rg -regular if for each point x and a regular open set U containing $\{x\}$, there is a rg -open set V such that $x \in V \subset clV \subset U$.

Example 9: Let $X = \{a, b, c\}$ and $\tau = \{\emptyset, \{b\}, \{a, b\}, \{b, c\}, X\}$. Then X is weakly rg -regular.

Example 10: Let $X = \{a, b, c\}$ and $\tau = \{\emptyset, \{a\}, \{b\}, \{a, b\}, X\}$. Then X is not weakly rg -regular.

Theorem 6.11: If $f: X \rightarrow Y$ is an M - rg -open rc -continuous and almost rg -irresolute function from a mildly rg -normal space X onto a space Y , then Y is mildly rg -normal.

Proof: Let A be a regular closed set and B be a regular open set containing A . Then by rc -continuity of f , $f^{-1}(A)$ is a regular closed set contained in the regular open set $f^{-1}(B)$. Since X is mildly rg -normal, there exists a rg -open set V such that $f^{-1}(A) \subset V \subset rgcl(V) \subset f^{-1}(B)$ by Theorem 6.10. As f is M - rg -open and almost rg -irresolute surjection, $f(V) \in RGO(Y)$ and $A \subset f(V) \subset rgcl(f(V)) \subset B$. Hence Y is mildly rg -normal.

Theorem 6.12: If $f: X \rightarrow Y$ is rc -continuous, M - rg -closed map and X is mildly rg -normal space, then Y is mildly rg -normal.

VII. rg -US spaces:

Definition 7.1: A point y is said to be a

- (i) rg -cluster point of sequence $\langle x_n \rangle$ iff $\langle x_n \rangle$ is frequently in every rg -open set containing x . The set of all rg -cluster points of $\langle x_n \rangle$ will be denoted by $rg-cl(x_n)$.
- (ii) rg -side point of a sequence $\langle x_n \rangle$ if y is a rg -cluster point of $\langle x_n \rangle$ but no subsequence of $\langle x_n \rangle$ rg -converges to y .

Definition 7.2: A sequence $\langle x_n \rangle$ is said to be rg -converges to a point x of X , written as $\langle x_n \rangle \rightarrow^{rg} x$ if $\langle x_n \rangle$ is eventually in every rg -open set containing x .

Clearly, if a sequence $\langle x_n \rangle$ r -converges to a point x of X , then $\langle x_n \rangle$ rg -converges to x .

Definition 7.3: A subset F is said to be

- (i) sequentially rg -closed if every sequence in F rg -converges to a point in F .
- (ii) sequentially rg -compact if every sequence in F has a subsequence which rg -converges to a point in F .

Definition 7.4: X is said to be

- (i) rg -US if every sequence $\langle x_n \rangle$ in X rg -converges to a unique point.
- (ii) rg - S_1 if it is rg -US and every sequence $\langle x_n \rangle$ rg -converges with subsequence of $\langle x_n \rangle$ rg -side points.
- (iii) rg - S_2 if it is rg -US and every sequence $\langle x_n \rangle$ in X rg -converges which has no rg -side point.

Definition 7.5: A function f is said to be sequentially rg -continuous at $x \in X$ if $f(x_n) \rightarrow^{rg} f(x)$ whenever $\langle x_n \rangle \rightarrow^{rg} x$. If f is sequentially rg -continuous at all $x \in X$, then f is said to be sequentially rg -continuous.

Theorem 7.1: We have the following:

- (i) Every rg - T_2 space is rg -US.
- (ii) Every rg -US space is rg - T_1 .
- (iii) X is rg -US iff the diagonal set is a sequentially rg -closed subset of $X \times X$.
- (iv) X is rg - T_2 iff it is both rg - R_1 and rg -US.
- (v) Every regular open subset of a rg -US space is rg -US.
- (vi) Product of arbitrary family of rg -US spaces is rg -US.
- (vii) Every rg - S_2 space is rg - S_1 and every rg - S_1 space is rg -US.

Theorem 7.2: In a rg -US space every sequentially rg -compact set is sequentially rg -closed.

Proof: Let X be rg -US space. Let Y be a sequentially rg -compact subset of X . Let $\langle x_n \rangle$ be a sequence in Y . Suppose that $\langle x_n \rangle$ rg -converges to a point in $X-Y$. Let $\langle x_{np} \rangle$ be subsequence of $\langle x_n \rangle$ that rg -converges to a point $y \in Y$ since Y is sequentially rg -compact. Also, let a subsequence $\langle x_{np} \rangle$ of $\langle x_n \rangle$ rg -converge to $x \in X-Y$. Since $\langle x_{np} \rangle$ is a sequence in the rg -US space X , $x = y$. Thus, Y is sequentially rg -closed set.

Theorem 7.3: If f and g are sequentially rg -continuous and Y is rg -US, then the set $A = \{x \mid f(x) = g(x)\}$ is sequentially rg -closed.

Proof: Let Y be rg -US. If there is a sequence $\langle x_n \rangle$ in A rg -converging to $x \in X$. Since f and g are sequentially rg -continuous, $f(x_n) \rightarrow^{rg} f(x)$ and $g(x_n) \rightarrow^{rg} g(x)$. Hence $f(x) = g(x)$ and $x \in A$. Therefore, A is sequentially rg -closed.

VIII. Sequentially sub- rg -continuity:

Definition 8.1: A function f is said to be

- (i) sequentially nearly rg -continuous if for each point $x \in X$ and each sequence $\langle x_n \rangle \rightarrow^{rg} x$ in X , there exists a subsequence $\langle x_{n_k} \rangle$ of $\langle x_n \rangle$ such that $\langle f(x_{n_k}) \rangle \rightarrow^{rg} f(x)$.
- (ii) sequentially sub- rg -continuous if for each point $x \in X$ and each sequence $\langle x_n \rangle \rightarrow^{rg} x$ in X , there exists a subsequence $\langle x_{n_k} \rangle$ of $\langle x_n \rangle$ and a point $y \in Y$ such that $\langle f(x_{n_k}) \rangle \rightarrow^{rg} y$.
- (iii) sequentially rg -compact preserving if $f(K)$ is sequentially rg -compact in Y for every sequentially rg -compact set K of X .

Lemma 8.1: Every function f is sequentially sub- rg -continuous if Y is a sequentially rg -compact.

Proof: Let $\langle x_n \rangle \rightarrow^{rg} x$ in X . Since Y is sequentially rg -compact, there exists a subsequence $\{f(x_{n_k})\}$ of $\{f(x_n)\}$ rg -converging to a point $y \in Y$. Hence f is sequentially sub- rg -continuous.

Theorem 8.1: Every sequentially nearly rg -continuous function is sequentially rg -compact preserving.

Proof: Assume f is sequentially nearly rg -continuous and K any sequentially rg -compact subset of X . Let $\langle y_n \rangle$ be any sequence in $f(K)$. Then for each positive integer n , there exists a point $x_n \in K$ such that $f(x_n) = y_n$. Since $\langle x_n \rangle$ is a sequence in the sequentially rg -compact set K , there exists a subsequence $\langle x_{n_k} \rangle$ of $\langle x_n \rangle$ rg -converging to a point $x \in K$. By hypothesis, f is sequentially nearly rg -continuous and hence there exists a subsequence $\langle x_{j_i} \rangle$ of $\langle x_{n_k} \rangle$ such that $f(x_{j_i}) \rightarrow^{rg} f(x)$. Thus, there exists a subsequence $\langle y_{j_i} \rangle$ of $\langle y_n \rangle$ rg -converging to $f(x) \in f(K)$. This shows that $f(K)$ is sequentially rg -compact set in Y .

Theorem 8.2: Every sequentially s -continuous function is sequentially rg -continuous.

Proof: Let f be a sequentially s -continuous and $\langle x_n \rangle \rightarrow^s x \in X$. Then $\langle x_n \rangle \rightarrow^{rg} x$. Since f is sequentially s -continuous, $f(x_n) \rightarrow^s f(x)$. But we know that $\langle x_n \rangle \rightarrow^s x$ implies $\langle x_n \rangle \rightarrow^{rg} x$ and hence $f(x_n) \rightarrow^{rg} f(x)$ implies f is sequentially rg -continuous.

Theorem 8.3: Every sequentially rg -compact preserving function is sequentially sub- rg -continuous.

Proof: Suppose f is a sequentially rg -compact preserving function. Let x be any point of X and $\langle x_n \rangle$ any sequence in X rg -converging to x . We shall denote the set $\{x_n \mid n = 1, 2, 3, \dots\}$ by A and $K = A \cup \{x\}$. Then K is sequentially rg -compact since $(x_n) \rightarrow^{rg} x$. By hypothesis, f is sequentially rg -compact preserving and hence $f(K)$ is a sequentially rg -compact set of Y . Since $\{f(x_n)\}$ is a sequence in $f(K)$, there exists a subsequence $\{f(x_{n_k})\}$ of $\{f(x_n)\}$ rg -converging to a point $y \in f(K)$. This implies that f is sequentially sub- rg -continuous.

Theorem 8.4: A function $f: X \rightarrow Y$ is sequentially rg -compact preserving iff $f|_K: K \rightarrow f(K)$ is sequentially sub- rg -continuous for each sequentially rg -compact subset K of X .

Proof: Suppose f is a sequentially rg -compact preserving function. Then $f(K)$ is sequentially rg -compact set in Y for each sequentially rg -compact set K of X . Therefore, by Lemma 8.1 above, $f|_K: K \rightarrow f(K)$ is sequentially rg -continuous function. Conversely, let K be any sequentially rg -compact set of X . Let $\langle y_n \rangle$ be any sequence in $f(K)$. Then for each positive integer n , there exists a point $x_n \in K$ such that $f(x_n) = y_n$. Since $\langle x_n \rangle$ is a sequence in the sequentially rg -compact set K , there exists a subsequence $\langle x_{n_k} \rangle$ of $\langle x_n \rangle$ rg -converging to a point $x \in K$. By hypothesis, $f|_K: K \rightarrow f(K)$ is sequentially sub- rg -continuous and hence there exists a subsequence $\langle y_{n_k} \rangle$ of $\langle y_n \rangle$ rg -converging to a point $y \in f(K)$. This implies that $f(K)$ is sequentially rg -compact set in Y . Thus, f is sequentially rg -compact preserving function.

The following corollary gives a sufficient condition for a sequentially sub- rg -continuous function to be sequentially rg -compact preserving.

Corollary 8.1: If f is sequentially sub- rg -continuous and $f(K)$ is sequentially rg -closed set in Y for each sequentially rg -compact set K of X , then f is sequentially rg -compact preserving function.

IX. Acknowledgments:

The authors would like to thank the referees for their critical comments and suggestions for the development of this paper.

References:

- [1.] S.P. Arya and M.P. Bhamini, A note on semi-US spaces, Ranchi Uni. Math. J. Vol. 13 (1982), 60-68.
- [2.] S.Arya and T.Nour, Characterizations of s -normal spaces, I.J.P.A.M., 21(1990), 717-719.
- [3.] Ashish Kar and P.Bhattacharyya, Some weak separation axioms, Bull. Cal. Math. Soc., 82(1990) 415-422.
- [4.] C.E. Aull, Sequences in topological spaces, Comm. Math. (1968), 329-36.

- [5.] S. Balasubramanian and P. Aruna Swathi Vyjayanthi, On v -separation axioms Inter. J. Math. Archive, Vol 2, No. 8(2011) 1464-1473.
- [6.] S. Balasubramanian and M. Lakshmi Sarada, gpr -separation axioms, Bull. Kerala Math. Association, Vol 8. No.1 (2011)157 – 173.
- [7.] Chawalit Boonpak-Generalized continuous functions from any topological space into product, Naresuan University journal (2003)11(2)93-98.
- [8.] H.F. Cullen, Unique sequential limits, Boll. UMI, 20 (1965) 123-127.
- [9.] Charles Dorsett, semi- T_1 , semi- T_2 and semi- R_1 spaces, Ann. Soc. Sci. Bruxelles, 92 (1978) 143-158.
- [10.] K.K. Dube and B.L. namdeo, T_0 -Limit point of a set and its implications, J.Tripura Math. Soc, Vol.9 (2007)85-96.
- [11.] W.Dunham, $T_{1/2}$ Spaces, Kyungpook Math. J.17 (1977), 161-169.
- [12.] G.L.Garg and D.Sivaraj, presemiclosed mappings, Periodica Math.Hung., 19(2)(1988) ,97-106.
- [13.] S. R. Malghan and G. B. Navalagi, Almost- p -regular, p -completely regular and almost $-p$ -completely regular spaces, Bull. Math. Soc. Sci. Math., R.S.R. Tome 34(82),nr.4 (1990),317-326.
- [14.] S. N. Maheshwari and R. Prasad, Some new separation axioms, Ann. Soc. Sci., Bruxelles, 89 (1975), 395-402.
- [15.] G.B.Navalagi, Further properties of preseparation axioms, (Unpublished)
- [16.] G. B. Navalagi, P-Normal Almost-P-Normal, Mildly-P-Normal, Topology Atlas.
- [17.] G. B. Navalagi, Pre-US Spaces, Topology Atlas.
- [18.] T.Noiri, Almost continuity and some separation axioms, Glasnik Mat.,9(29)(1974),131-135.
- [19.] T. Noiri, Sequentially subcontinuous functions, Accad. Naz. Dei. Lincei. Estratto dei. Rendiconti. Della Classe di Sci. Fis. Mat. Nat. Series. VIII, Vol. LVIII, fase. 3 (1975), 370-376.
- [20.] Norman Levine, Semi-open sets and semi continuity in topological spaces, Amer.Math. Monthly, 70(1963), 36-41.
- [21.] Norman Levine, Generalized closed sets in topology, Rend. Circ. Mat. Palermo, 19(2)(1970), 89-96.3-21.
- [22.] Paul and Bhattacharyya, On p -normal spaces, Soochow Jour.Math.,Vol.21. No.3,(1995),273-289
- [23.] V.K.Sharma, generalized separation axioms, Acta Cienceia Indica
- [24.] V.K.Sharma, semigeneralized separation axioms, Acta Cienceia Indica
- [25.] M. K. Singal and S. P. Arya, On almost normal and almost completely regular spaces, Glasnik Mat.,5(25)(1970),141-152.
- [19.] M. K. Singal and A. R. Singal, Mildly normal spaces, Kyungpook Math. J., 13(1)(1973)27-31.
- [26.] P. Sundaram and K.Balachandran, Generalized continuous mappings in topological Spaces, Bull. Fukuoka Univ.Ed.PartIII, 42(1993),1
- [27.] T. Thompson , S-closed spaces, Proc. Amer. Math. Soc., 60(1976)335-338.
- [28.] A. Wilansky, Between T_1 and T_2 , Amer. Math. Monthly. 74 (1967), 261-266.

The Role of Mobile and Remote Sensing Satellites in Disaster Management

Mehdi Mari, Amir kabir

Department of Electrical Engineering, University of technology, Tehran, Iran

Abstract: Disaster management aim is human casualty decreasing in natural events such as earth quack, flood, thunderstorms and As well as in air crashes, accidents and.... In this paper we use mobile satellite services (MSS) and remote sensing satellites to provide this purpose. Mobile satellites contains 3 type of satellites; LEO, MEO and GEO. Remote sensing satellites are two categories: optical and microwave. In first section the introduction is presented, section two and three are about mobile satellites and remote sensing satellites, section four analyzes data and finally conclusion will be presented.

Key words: disaster management, mobile satellite, remote sensing.

I. Introduction

Unpredictable events are happened at anytime and anywhere. These events can be manage consciously whereas we have been the least damages and casualty. In this paper we use iDirect [1] idea to disaster management. There are 3 phases: preparedness, response, recovery and reconstruction. Preparedness phase is fast action in damaged area, response phase is search and rescue operation that takes place within several weeks, recovery phase is make temporary centers to aid victims or local people and reconstruction phase is help to develop and reconstruct the area to get normal conditions. Several problems should be considered in using satellites such as flexibility, scalability, fast deployment, portability, easy installation, mobility, industrialized equipment, bandwidth management, and security. Figure 1 shows satellites connections.

We use communication satellites for make connections among people and send different files; the main use of this is in telemedicine. Also we use remote sensing satellites to take photos from damaged area then extract data from them, finally analyze and compare data before and after event.

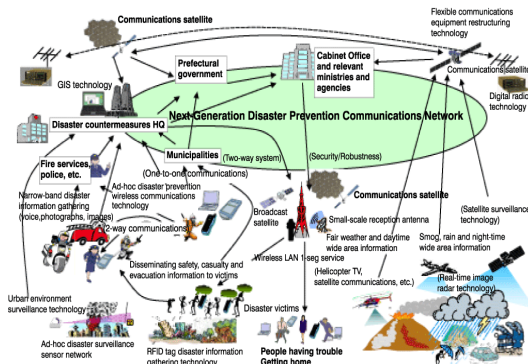


Fig.1: satellites connections [2]

Several research have been done such as satellite image analysis for disaster management [3], a satellite core network

system for disaster recovery [4], small satellite utilization for disaster management [5], ASTER satellite for disaster management [6], rapid image product from satellite for disaster management [7] and satellite-enabled ehealth in disaster management [8].

II. Mobile satellite services

The mobile satellites have been launched since 1980. Because they have mobile ground station, they are called mobile satellites. They are used in several industries amongst disaster management to communicate data.

2-1. whole shape

The mobile satellite network includes 3 segments: user segment, ground segment and space segment. It is illustrates in figure 2.

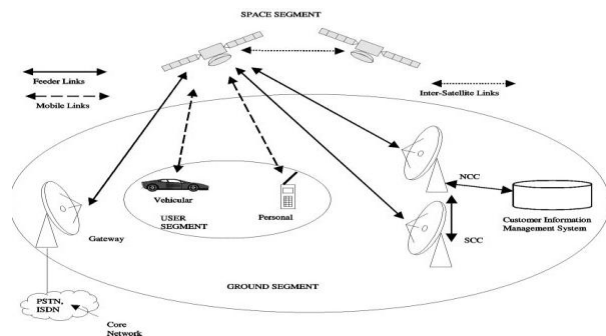
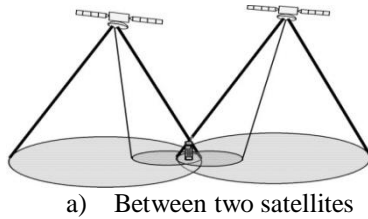


Fig.2. whole shape [9]

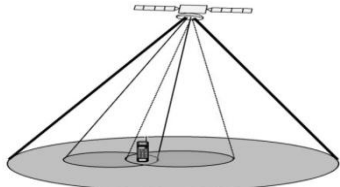
User segment is mobile node that can be a device to send telemedicine or any other data in damaged area. Ground segment contains 3 sections: gateway which is fixed node and provides local networks, network control center which manages network and satellite control center which controls satellite performance. Space segment makes connection between users and gateways.

2-2. Network performance

There are 2 approaches here: integration and mobility management. Integration refers to different generation of mobile telecommunication and mobility management refers to place management and handover. In place management, satellite provides a condition for users to roam within coverage areas. In hand over phase, mobile users change their communication link between two satellites or transponders as mention in figure 3 because of received strength signal (RSS) or quality of service decreasing.



a) Between two satellites



b) Between two transponders
Fig.3: users roaming [9]

2-3.Channel characteristics

For mobile channel [9]:

Ground mobile channel: it contains 3 components such as direct wave, diffuses components and ground reflections.

Aerial mobile channel: it is more complicated and refers to aircrafts. In this case direct waves are obstructed and the body of aircraft cause to signal multipath, also the Doppler effect should be considered.

Marin mobile channel: in this case the reflections from sea surface should be considered.

For fixed channel [9]:

Troposphere: refers to atmosphere conditions.

Ionosphere: refers to frequencies over 10GHz.

III. Remote sensingsatellites

Using remote sensing data especially satellite photographs enable us to extract data before and after events and compare with each other, these pictures have been taken by use of different electromagnetic spectrums. Then we can manage disasters after they happen.

3-1.Optical remote sensing

Opticalremote sensing satellites work in infrared and visible wavelength. The main process to get image data is as figure 4.

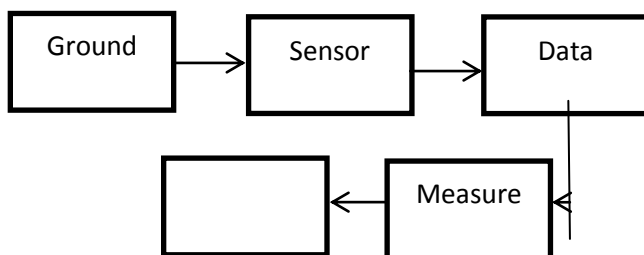


Fig.4: process to get image

Sun radiation is the main source of energy and its radiation above atmosphere is nearly equal to black body temperature (is an ideal radiator that emits all energy

incident). Before sun radiation reach earth surface, it should get through atmosphere. Small part of radiation is absorbedby atmosphere windows or scatter in this area but large part of the radiation will reach earth surface.Finally there are two types of reflection from earth surface that based on shape and material of surface: diffuse and specular. The energy incident from earth surface will return to sensors of satellite to configure pictures. All process is illustrated in figure 5.

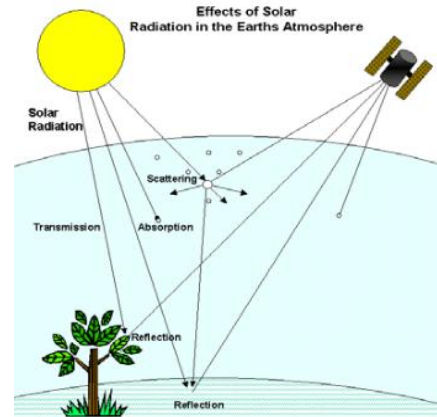


Fig.5: Sun radiation [10]

The amount of energy above Zero K measure by sensors of satellite as two ways: internal temperature and emissivity that is the radiation of an object at a given temperature relative to radiation of a blackbody at the same temperature. The radiation can be measured by Stefan-Boltzmann's law, Wien's Radiation's law, Rayliegh-Jean's law and Plank's law.

2-2. Microwave remote sensing

There are two types of microwave remote sensing: active and passive. Passive remote sensing responds to microwave energy that are reflected or emitted from surface of objects and active remote sensing suppliesits own source of illumination (radar).

As mentioned in optical remote sensing the amount of radiation emitted by an object in is determined by internal temperature and emissivity, Also this amount is applied by passive remote sensing. In passive remote sensing the emitted energy is sensed by radiometers and scanners.

Active remote sensing is divided to two parts: imaging (radar) and non-imaging (altimeters and scatter meters). For imaging remote sensing the most important parameters for both satellite and target are wavelength or frequency, polarization, look angle, look direction, resolution, surface roughness, complex dielectric, slop angle and orientation as well as it is divided to two type: real aperture radar and synthetic aperture radar, the difference between them is their beam width. Figure 6 shows performance of imaging remote sensing.Azimuth is thedirection on the ground parallel to the motion of sensor and range is the directionin which the signal is transmitted.

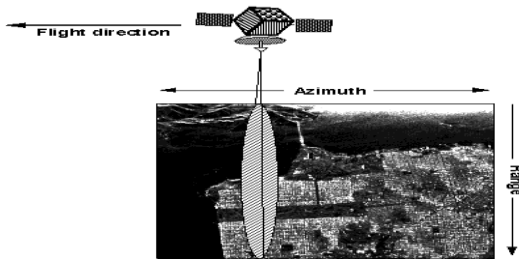


Fig.6: Imaging remote sensing [11]

IV. Data analysis

After explanation of mobile satellite and remote sensing satellite in previous sections, in this section the given data by this satellites and their application will be discussed. Figure 7 illustrate an area in Indonesia before and after earth quake. These received data from optical remote sensing satellite enable local officials to better identify the area then evaluate the finance and human casualty as well as all damages. Eventually, try to reconstruct the area as soon as possible.



a) Before earth quake



b) After earth quake

Fig.7: Earth quake in Indonesia [12]

In figure 8, the data received by optical remote sensing satellite illustrate a serious damage in farm lands of Manitoba, the farm damage is obvious by the white sign. These data that help farmers and related specialist to better evaluate the area and make consequent decisions in future.

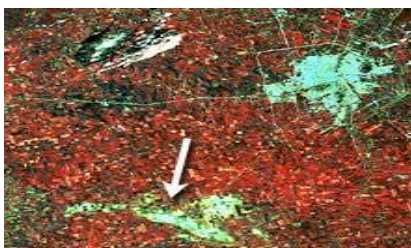


Fig.8: Tornado in Manitoba Figure 9 illustrates a photo before and after hurricane like flood in Haiti. This photo has been

taken by imaging (Radar) remote sensing satellite. The data from this photo can help local officials to better manage crisis and locate damaged areas that has been specified by cream color after disaster.

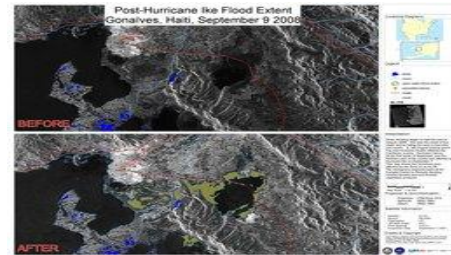


Fig.9: Before and after hurricane in Haiti [13]

Figures 10 to 12 show interpret the disaster, send telemedicine data and communicate with each other in disaster time. Mobile satellites can provide these communications at this time and help related officials to better manage disaster and other people to inform that.



Fig.10: Emergency management [12]



Fig.11: Mobile communication [12]

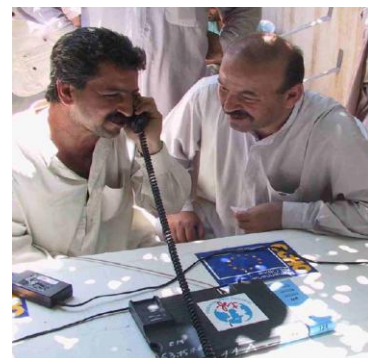


Fig.12: Communication within disaster hours [12]

V. Conclusion

As reviewed in this paper, the phases of disaster management based on iDirect method [1] was discussed and we summarize it in a figure 13 by using the method which has been stated in esoa [12] then the performance of mobile and remote sensing satellites were explained.

We should consider to relation between performance of satellites and access data. As mentioned before mobile satellites provide communication and send data at and after disaster time but remote sensing satellite provide an images to compare before and after disaster. We should use the procedures, types, designs, information and ... about satellites and combine them to extract data from images.

This field of study has great extent as well as is expandable and can be related with other fields to interpret results from images.

Because of unpredictable nature of disasters, we should more focus on this field to prevent human and environments damages and finally provide a secure world.



Fig.12: Disaster management phases [12]

Reference

- [1] <http://www.idirect.net/> "Satellite Solution for Emergency Relief and Disaster Recovery Management", May.2009.
- [2] "MIC Communication News", Vol.18, No.5, June.2007.
- [3] T.Kemper, T.Reidlinger, R.Kiefl and H.Mehl, "Satellite Image Analysis for Disaster and Crisis-management Support", IEEE Transaction on Geoscience and Remote Sensing", June.2007, pp.1520-1528.
- [4] Yong-Min Lee, Bon-Jun Ku and Do-SeobAhn, "A Satellite Core Network System for Emergency Management and Disaster Recovery", Int'l conf. on Information and Communication Technology Convergence, Nov.2010, pp.549-552.
- [5] Dr.OzlemAlbayrak, "Small Satellite Utilization for Disaster Management Information Systems".
- [6] K.A, Duda and M.Abrams, " ASTERSatellite Observation for International Disaster Management", Proc. of the IEEE, 2012, pp.1-14.
- [7] Trisirisatayawong, T.Jongrujanan, C.Fraser, "Rapid Image Product Generation from High-resolutionSatellite Imagery Disaster Management", Proc.IEEEInt'l, Geoscience and Remote Sensing Symposium, July.2005.
- [8] Kontoyiannis, E.Charalambos, G.Vrouchos and A.Mamantopoulos, "Satellite-enabled ehealthApplication in Disaster Management-experience from a Readiness Exercise, Int'l Conf. on Computers in Cardiology", Sep.2008, pp.1005-1008.
- [9] Ray.E.Shariff, Y.Fun.Hu, "Mobile Satellite Communication Networks", John Wiley & Sons Ltd, 2001.
- [10] Carmen Gonzalez Sanpedro, "Optical and Remote Sensing Applied to Agricultural Areas in Europe", Departament de Física de la Terra iTermodinàmica, Oct.2008.
- [11] AhadTavakoli, "Remote Sensing Course", Department of Electrical Engineering, Amirkabir University of Technology.
- [12] [http:// www.esoa.net/](http://www.esoa.net/) NihatOktay, "The Roles of Satellite in Effective Disaster Management", July.2008.
- [13] <http://www.disastercharter.org/>

A new structure in Tandem Solar Cells

J. Fariborz¹, S. Mirzakuchaki²

^{1, 2} (Department of Electrical Engineering, Iran University of Science and Technology, Iran.

ABSTRACT : In this paper, we introduce a new structure for AlGaAs/GaAs Tandem Solar Cells as AlGaAs/InSb/GaAs. In typical structures, cells build on top of each other from higher to lower energy band gaps, respectively with tunnel junctions between them. Therefore, high energy photons are absorbed in upper layers and lower energy photons in bottom layers. Tunnel junctions guarantee low ohmic resistance. Due to its low ohmic resistance, a thin layer of InSb is proposed here to replace the tunnel junctions. Some disadvantages such as light absorption in these narrow band gap layers and lattice mismatch are present but very low ohmic loss with typical doping, and wide range of short circuit currents that we can choose for these cells are major advantages achieved.

Keywords: AlGaAs/GaAs, InSb, MBE, Tandem Solar Cells, Tunnel Junction

I. INTRODUCTION

Using Tandem solar cells is one of the methods for achieving high efficiency in transforming solar energy into electricity [1]-[8]. Solar cells made from III-V semiconductors can be arranged in a cascade architecture which increases their efficiency [9]-[14]. A tunnel diode structure is thus normally used [9],[10],[12],[13],[14].

The optical and electrical losses of these diodes must be as low as possible in order not to affect the increased efficiency of the cells. A small thickness of cascaded layers and large rates of I_p/V_p can lower the optical and electrical losses, respectively [12],[15].

On the other hand, in the process of tunnel diode production, high density of dopants will result in crystal defects and light absorption. Also unwanted diffusion of impurity atoms may occur when subsequent layers are grown [12].

InSb has a very small band gap resulting in such a large number of intrinsic carriers that diodes built with InSb do not act properly at room temperature unless they are designed under special conditions [16]. These diodes are appropriate at cryogenic temperature and their PN junction has a very small resistance at room temperature. In the case of producing a triple junction cell, GaInP/GaAs/Ge structure seems appropriate [11]. Ge can be used as a suitable substrate in this formation. Ge has the advantage of providing a PN junction at normal working temperature while its lattice constant matches well with GaAs. InSb is not a good choice as a substrate in such structures and would not work properly because it does not play any role in energy production and also due to its large mismatch will cause many defects in the formation of the upper crystal lattice.

In this research, the first step is considering a double junction Tandem solar cell with AlGaAs/GaAs structure whose efficiency was 28% [12] and simulating its energy bands structure. Then considering the limitation of current density related to the tunnel diode used in this structure, it was replaced with an InSb diode. Finally, this

New Formation was simulated. The results are explained in detail in the following sections.

II. OVERALL VIEW OF THE DESIGN

Fig. 1 illustrates the structure of a tandem AlGaAs/GaAs double junction solar cell. The GaAs tunnel diode with a 30 nm thickness provides electrical connection Between AlGaAs and GaAs cells. In order to lower the effect of the p-type region impurities diffusion, C is applied instead of Zn. However in the thermal process of AlGaAs cell production, Current- Voltage behavior of this tunnel diode becomes more non-ideal and current density peak decreases [12]. This fact is shown in Fig. 2.

Previous works on the MBE growth of a PN junction with InSb and corresponding simulations have shown that at 300°K when a small reverse or forward bias is applied, a considerable current density would be achieved. Having noticed these results, the idea of using such a diode instead of a tunnel diode in Tandem solar cells was formed.

In order not to change the overall structure and to compare the results more precisely, the thickness of layers is kept unchanged. The AlGaAs layers with large amount of Al which helps to reduce the undesired diffusion of impurities are used. In addition to different semiconductor types and doping densities, the mentioned diode was applied in a different direction. Since in the typical structure and near zero volts, tunnel diode permeates current in both directions, P⁺ layer is placed above P layer of GaAs cell. So PN⁺ is not formed in this point and would not obstruct photo current flow of the solar cell.

Electrode	
p ⁺ -GaAs	MgF ₂ /ZnS antireflective coating
p-Al _{0.35} Ga _{0.65} As	10 ¹⁹ cm ⁻³ 0.04 μm
p-Al _{0.35} Ga _{0.65} As	10 ¹⁸ cm ⁻³ 0.07 μm
p ⁺ -Al _{0.35} Ga _{0.65} As	10 ¹⁹ cm ⁻³ 0.3 μm
n ⁻ -Al _{0.35} Ga _{0.65} As	10 ¹⁶ cm ⁻³ 0.5 μm
n-Al _{0.35} Ga _{0.65} As	10 ¹⁷ cm ⁻³ 0.1 μm
n ⁺ -GaAs	0.02 μm
p ⁺ -GaAs	0.01 μm
p-Al _{0.35} Ga _{0.65} As	10 ¹⁹ cm ⁻³ 0.1 μm
p-GaAs	10 ¹⁹ cm ⁻³ 0.5 μm
n-GaAs	10 ¹⁹ cm ⁻³ 3.5 μm
n-Al _{0.35} Ga _{0.65} As	10 ¹⁷ cm ⁻³ 0.1 μm
n-GaAs	10 ¹⁷ cm ⁻³ 1 μm
	n-GaAs substrate
	Electrode

Fig. 1. A double junction AlGaAs/GaAs tandem solar cell with 28% efficiency

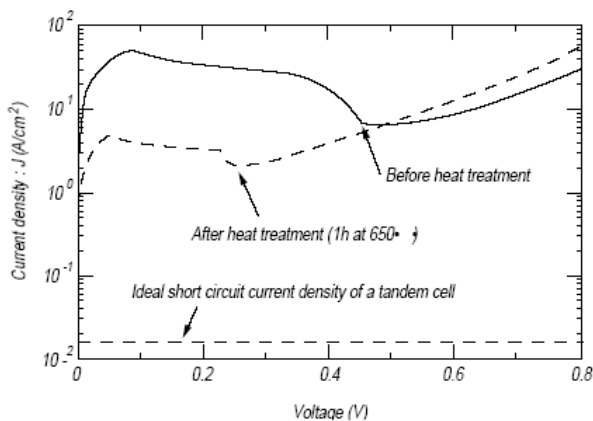


Fig. 2. GaAs tunnel junction I-V characteristics after and before heat treatment

The N^+ region of the tunnel diode is placed under the AlGaAs N layer so P^+N diode is not formed in this point, therefore there will be no problem in solar cell function during light absorption and photo current generation. In fact this is the main advantage in using tunnel diode in Tandem structures.

In our studied structure (Fig. 3), a diode is applied in such a form that the whole design is similar to a Tandem triple junction. Thus if the optical flow was generated in this sector, however slightly, it would not be in the opposite direction to the current in the other sections and would not decrease the solar cell's V_{oc} . Also, no section of this junction forms a diode at room temperature and therefore it doesn't block the photo current.

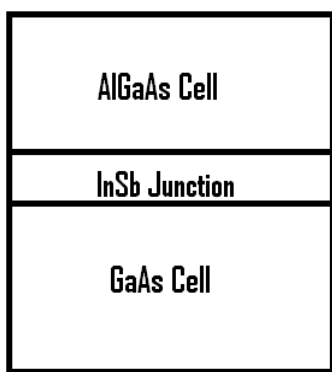
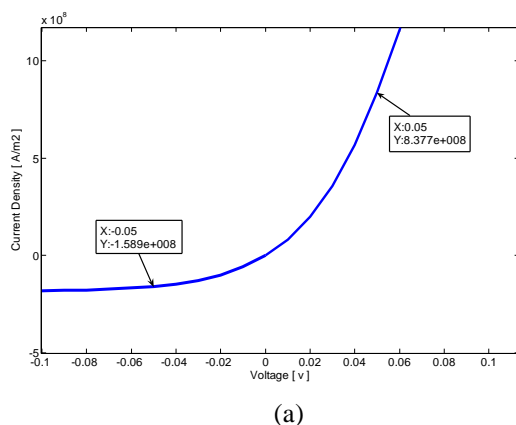


Fig. 3. New structure for tandem solar cell



(a)

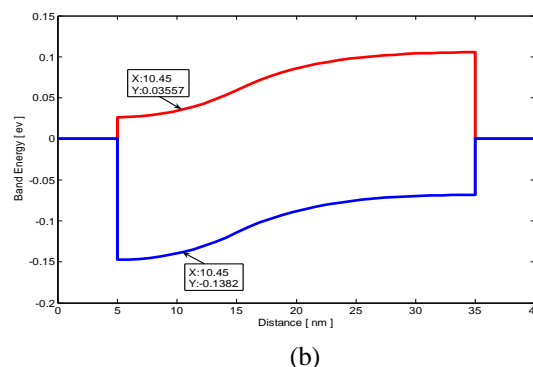


Fig. 4. (a) I-V characteristic and (b) band diagram of InSb PN Junction at 300°K

Another major advantage here is that there is no need to use very high density of impurities, unlike what is required in the tunnel diode.

Thus the undesired effect of impurity diffusion during the process of producing other sections and thermal procedures is reduced. Fig. 4-a shows part of the current-voltage characteristic obtained from simulating InSb PN junction at 300 degrees Kelvin.

Layer thickness of N and P are 10^{nm} and 20^{nm} respectively. The density of impurities is considered to be $10^{18}/cm^3$ in both sections. Impurities used for the P region are Be atoms with an acceptor band 26^{mev} higher than valance band. For the N region, donor atoms with a donor band very close to conduction band are considered. The energy band structure of the junction is illustrated in Fig. 4-b. As can be seen in this figure, the band gap of InSb has a small value of 170^{mev} at room temperature. Fig. 2 shows that even at best condition, which is before heat treatment process, the current density peak of GaAs tunnel diode doesn't reach $100 A/cm^2$. The peak current density is obtained for a voltage of 0.1 V. This value is greater than $15000 A/cm^2$ for InSb junction at 0.05 volt reverse bias (Fig. 4-a).

It is predicted that in case of an InSb junction instead of a tunnel diode, the results of V_{oc} and subsequently the performance will be better. In order to examine this issue, solar cells of section (I) were simulated. First the GaAs cell which is the lower section of the discussed structure, was analyzed. Energy bands and current-voltage characteristics of this diode were obtained by numerical solution of Poisson equation with Newton's method using Simba-2 model for electrons and holes mobility and ignoring quantum effects. Results are observed in Fig. 5-a and Fig. 5-b.

However, the diode in Fig. 5 is not a simple GaAs diode and according to necessities of production is in DH form [12]. Conduction threshold was obtained at about 1.25 V from Fig. 5-b. As can be seen, the results are well consistent with both theory and practice. Simulation for the upper cell -AlGaAs diode- was also done and it's results can be seen in Fig. 6. This time, the conduction threshold obtained from Fig. 6-b is about 1.5 volts.

Since the simulation of tunnel diodes requires consideration of quantum effects and electron's tunneling, which is very time consuming and complex, in the conventional method of calculating the efficiency of tandem solar cells, the effect of all parts are added together and then

a few tenths of volts is subtracted from the total amount of V_{oc} in order to include the tunnel junction voltage drop. Here, we have only simulated the energy band structure in the tandem solar cell shown in Fig. 1. The result of simulation and the magnified portion of the tunnel junction can be seen in Fig. 7.

Fig. 8 shows the maximum displacement in a crystal lattice of the cell of Fig. 1. We already know that AlGaAs and GaAs crystalline lattices, even for the greatest amount of Al, present a good lattice match. So not much displacement and strain in the lattice would be observed. The maximum displacement is about 0.012 \AA which agrees with the theory [18].

Certainly in practice, a lot of parameters make the final result different from what was ideally anticipated by the theory. For example, V_{oc} of the GaAs cell in Fig. 1, which is made alone, is equal to 1.047 volts in practice [12]. This value is measured to be 2.420 volts for Tandem cell. Both of these values are rather smaller than what was calculated theoretically from the simulation results.

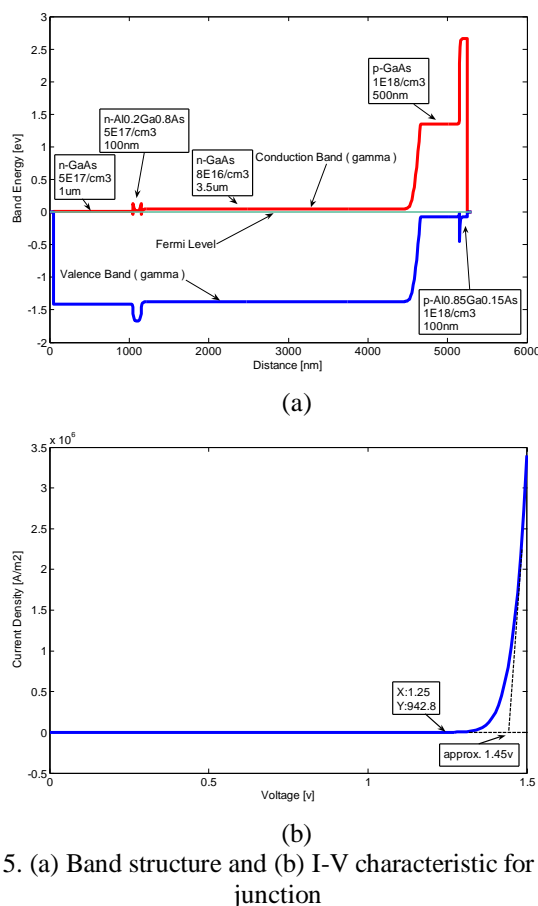


Fig. 5. (a) Band structure and (b) I-V characteristic for GaAs junction

Finally, the new AlGaAs/InSb/GaAs structure was completely simulated. Since there is no tunnel connection, we can use classical calculations for current-voltage behavior. Simulation results for the energy band structure are shown in Fig. 9. One of the noteworthy points in this regard is the modified form of the energy band in the crystal lattice of InSb caused by the exerted strain. As it is clearly shown in Fig. 9-b, the energy gap in this case has increased to about 370 meV .

On the other hand, energy band related to GaAs and AlGaAs diodes are modified because of the stress exerted on that region and rather above the InSb layer which

is shown in Fig. 9-b. Maximum displacement in the crystal lattice is shown in Fig. 10.

As we expected, this value in the new structure was far higher than the previous structure. Finally current-voltage characteristic of the new structure was calculated by simulation with the results shown in Fig. 11.

The theoretical results show that V_{oc} of this structure must be about 3.4 volts. However, due to manufacturing limitations, of course in practice the open circuit voltage would be somewhat less. Anyway, this structure is expected to have a high efficiency.

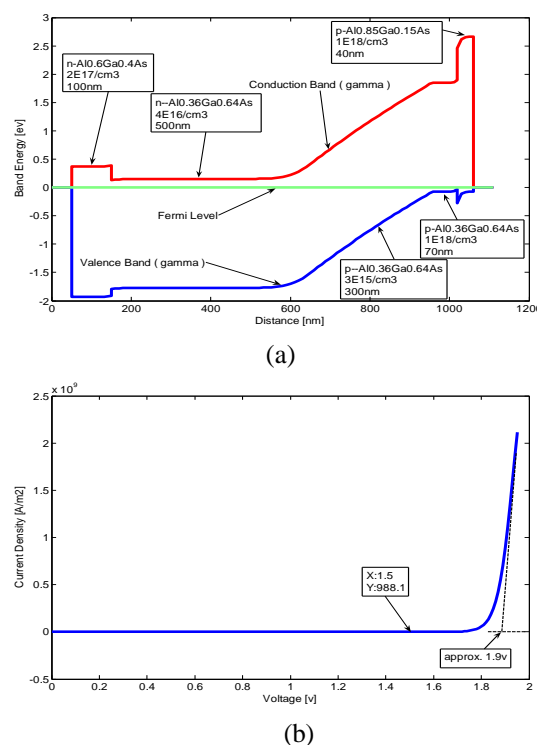


Fig. 6. (a) Band structure and (b) I-V characteristic for AlGaAs junction

III. CONCLUSION

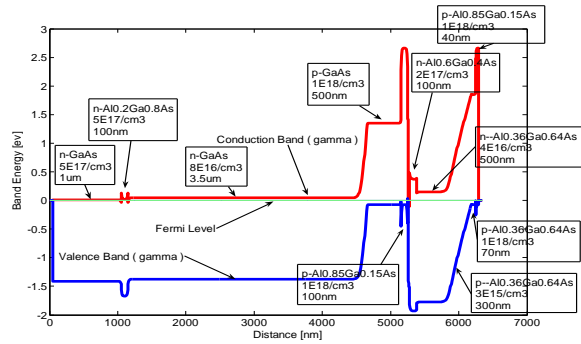
The new structure proposed for the Tandem-type solar cells can greatly benefit the market of solar energy. Cells made from III-V semiconductors are advancing rapidly but in comparison with silicon and polymer solar cells, they are more expensive. So today they are used in more demanding applications such as satellites.

However, the proposed idea was initiated by studying the characteristics of InSb layers grown by MBE in previous works and observing their ability to produce high ranges of current. By using InSb layers instead of tunnel diode in Tandem cells a new structure was invented and the simulation results confirmed its appropriate performance.

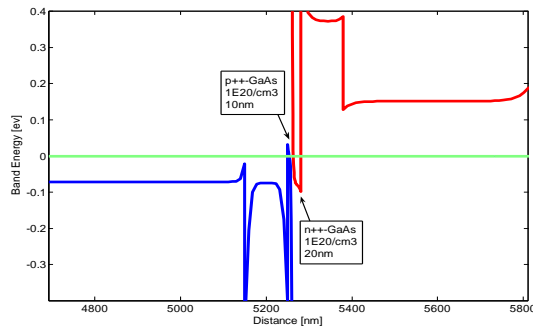
This structure has some deficiencies such as: light absorption in InSb region, formation of crystal flaws due to unmatched lattice constant of InSb with GaAs and AlGaAs, and also the possibility of damaging the InSb lattice in the case of growing AlGaAs at high temperatures. Of course, first and second cases can be effectively moderated by choosing a thin layer of InSb.

On the other hand, if the layers are grown at low temperature or smaller rate, the third problem will also be solved. Low growth rate in MBE will result in improvement

of the crystalline structure. Other growing methods such as MOVPE can also be effective in this case.



(a)



(b)

Fig. 7. (a) Band structure of tandem solar cell shown in Fig. 1 and (b) magnified portion of the tunnel junction

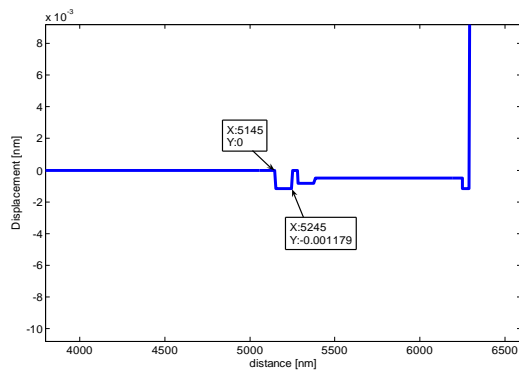
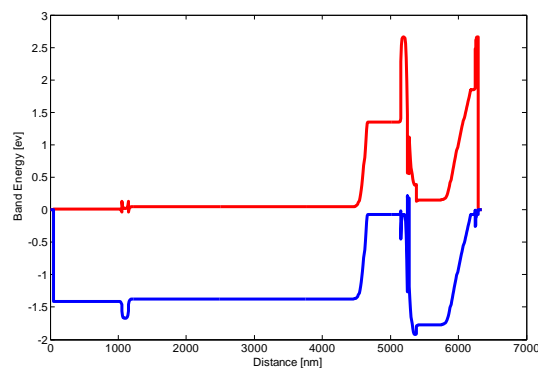
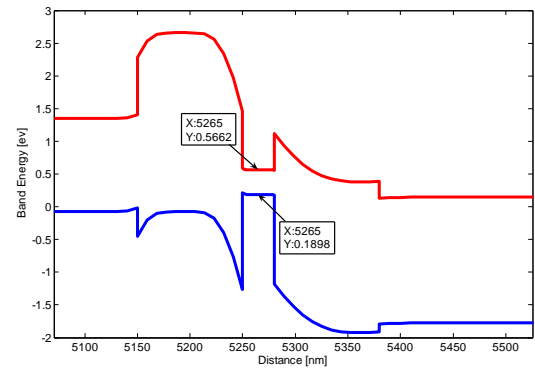


Fig. 8. Maximum displacement in crystalline lattice of tandem solar cell of Fig. 1



(a)



(b)

Fig. 9. (a) Band structure of new tandem cell and (b) magnified portion of the InSb junction

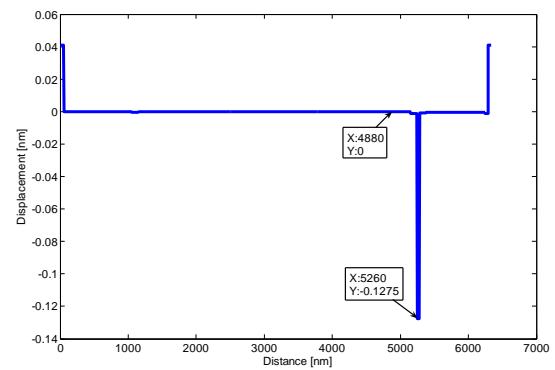


Fig. 10. Maximum displacement in crystalline lattice of new structure

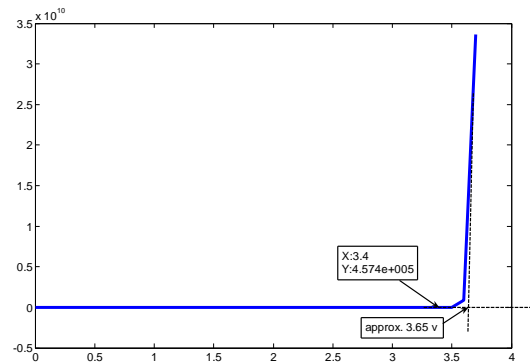


Fig. 11. I-V characteristic of new structured tandem solar cell

REFERENCES

- [1] C.H. Henry, Limiting efficiencies of ideal single and multiple energy gap terrestrial solar cells, *J. Appl. Phys.* 51(8) (1980) p.4494
- [2] Mae-Wan Ho, Peter Bunyard, Peter Saunders, Elizabeth Bravo, Rhea Gala, Which Energy?, 2006 *Institute of Science in Society Energy Report (ISIS 2006)*
- [3] NAGASAKI SHIPYARD & MACHINERY WORKS, Microcrystalline High-Efficiency Tandem Solar Cell to Begin Production, *Mitsubishi Heavy Industries, Ltd. Technical Review Vol. 44 No. 4 (Dec. 2007)*

- [4] Green, et al., Nanostructured Silicon-Based Tandem Solar Cells, *GCEP Technical Report 2006*
- [5] Arvind Shah, J. Meier, E. Vallat-Sauvain, C. Droz, U. Kroll, N. Wyrsh, J. Guillet, U. Graf, Microcrystalline silicon and micromorph tandem solar cells, *Thin Solid Films* 403-404, 179-187, 2002
- [6] J. Meier a, S. Dubail, R. Platz, P. Torres, U. Kroll, J.A. Anna Selvan, N. Pellaton Vaucher, Ch. Hof, D. Fischer, H. Keppner, R. Flickiger, A. Shah, V. Shklover, K.-D. Ufert, Towards high-efficiency thin-film silicon solar cells with the micromorph concept, *Elsevier Science, Solar Energy Materials and Solar Cells* 49 (1997) 35-44
- [7] Serap GÜNEŞ, Niyazi Serdar SARIÇİFTÇİ, An Overview of Organic Solar Cells, *Journal of Engineering and Natural Sciences, Sigma Vol./Cilt* 25 Issue/Sayı 1, 2007
- [8] Armin G. Aberle, Nils-Peter Harder, and Stefan Oelting, Recent Advances in Crystalline Silicon Film and Thin-Film Solar Cell Growth by Ion-Assisted Deposition, *17th European PV Conference*, Munich, Oct. 2001
- [9] F. Dimroth, High-efficiency solar cells from III-V compound Semiconductors, *phys. stat. sol. (c)* 3, No. 3, 373–379 (2006), DOI 10.1002/pssc.200564172
- [10] Masafumi Yamaguchi, Physics and technologies of super-high-efficiency tandem solar cells, *Toyota Technological Institute*, (1999)
- [11] National Center for Photovoltaics, High-Efficiency Concepts and Concentrators, p.1-3 (2005)
- [12] Ken Takahashi, Shigeki Yamada, Tsunehiro Unno, High-efficiency AlGaAs/GaAs Tandem Solar Cells, *Advanced Research Center, Hitachi Cable, Ltd.*, U.D.C. 621.383.51 : 523.9-7: [546.681'62'19 : 546.681'19]
- [13] M. W. Wanlass, S. P. Ahrenkiel, D. S. Albin, J. J. Carapella, A. Duda, K. Emery, J. F. Geisz, K. Jones, Sarah Kurtz, T. Moriarty, and M. J. Romero, Ultra-Thin Triple-Bandgap GaInP/GaAs/GaInAs Monolithic Tandem Solar Cells, *National Renewable Energy Laboratory (NREL)*, NASA/CP—2007-214494
- [14] M. W. Wanlass, J. S. Ward, K. A. Emery, and T. J. Coutts, Monolithic, Two-Terminal $InP/Ga_{0.47}In_{0.53}As$ Tandem Solar cells, *National Renewable Energy Laboratory*, 1993
- [15] John C. Zolper, Jhon F. Klem, Thomas A. Plut, and Chris P. Tigges, GaAsSb-Based Heterojunction Tunnel Diodes For Tandem Solar Cell Interconnects, *Sandia National Laboratories*, Albuquerque, NM 87185-0603
- [16] Tim Ashley, Ian. M. Baker, Theresa M. Burker, David T. Dutton, John A. Haigh, Leslie G. Hipwood, Richard Jefferies, Andrew D. Johnson, Peter Knowles, J. Chris Little, InSb focal plane arrays grown by molecular beam epitaxy, DOI: 10.1117/12.391753, *Proceedings Vol. 4028 Infrared Detectors and Focal Plane Arrays VI*, Eustace L. Dereniak; Robert E. Sampson, Editors, pp.398-403, Date: 17 July 2000
- [17] M. Mohammadkhani, J. Fariborz, and A. Mohades Kassai, Growth and Characterization of p-type InSb on n-type (111) and (110) InSb Substrates Using Molecular Beam Epitaxy, *Journal of Applied Sciences*, 2010, ISSN 1812-5654
- [18] H.C. Casey Jr., M.B. Panish, Heterostructure Lasers, *Academic Press* New York (1978)

Authors' information



Jamshid Fariborz received the BS in 1988 and the MS in 1993 in Electrical Engineering from the Iran University of Science and Technology, He has been a faculty member of the College of Electrical Engineering at the Iran University of Science and Technology, Tehran, since 1995.



Sattar Mirzakuchaki received the BS in Electrical Engineering from the University of Mississippi in 1989, and the MS and PhD in Electrical Engineering from the University of Missouri-Columbia, in 1991 and 1996, respectively. He has been a faculty member of the College of Electrical Engineering at the Iran University of Science and Technology, Tehran, since 1996. His current research interests include characterization of semiconductor devices and design of VLSI circuits. Dr. Mirzakuchaki is a member of IEEE and IET (formerly IEE) and a Chartered Engineer.

Smart Connect Using Cellular Technology

Ms. Priyanka V. Kampasi, Prof. Y.C. Kulkarni,

^{1,2}Bharati Vidyapeeth's College of Engineering/IT, Pune, India

ABSTRACT: Technical developments in computer hardware and software make it possible to introduce automation into virtually all aspects of human-machine systems. Automation has made Software applications much more efficient to use. This paper proposes that automation can be applied to desktop sharing in which a system can operate automatically anywhere in the world using GSM technology & VIRTUAL LAN concept.

The proposed system will be used to make the purpose of data access simpler, keeping in mind the needs of the IT industries. Through this system, automated desktop sharing can be implemented with effective cause. Today's desktop conferencing and groupware software often assume a serial work model in which information (pictures, documents, and presentations) are prepared by one person and then disseminated to others for comments, revision, or review. However, many types of collaborative work are much more parallel, with many people viewing, updating, and adding information concurrently across cross-platform display sharing between Mac OS, Windows, and UNIX operating systems. The current EMSL Televiewer prototype supports display sharing of application windows, screen regions, and desktops. This system proposes enhancements to the EMSL Televiewer that will provide collaborative annotations over the display, shared mouse cursors, pointer, high performance data compression, and session recording capabilities. When completed, the EMSL Televiewer will provide researchers and the scientific community a powerful tool that can by itself open up many new avenues for collaboration and will fit well with other tools to provide a comprehensive collaborative environment.

Keywords: Cell Phone, Desktop Sharing, Encryption, GSM, Microcontroller.

I. INTRODUCTION

The concept of Desktop Sharing has revolutionized the work of IT professionals immensely. While sitting at home or while roaming, an IT professional can work on his office computer anytime. The Computer system in the office can be accessed by the employee anywhere. Yes, of Course there are security considerations that must be met. That is, the authenticity of the person requesting access to the workplace computer. Earlier even though a person could remotely access his/her office computer but still he/she required a desktop computer or a laptop. The Goal of designing this application is for the benefit of industry people by allowing them multi-sharing of the computer screen for their assignments through cellular technology like a Cell Phone. It requires a PC with a modem setup. The computer/laptop contains important data or information. This information can be accessed by the user anywhere anytime through her mobile phone. The Cell Phone must be Internet enabled. When a request is send by the cell phone to the respective modem which is received using the GSM

system, it shall respond back by sending an acknowledgment message asking password so as to confirm that an authentic user has made the request.

As soon as the correct password is received as a response to the request, the system shall generate 4-digit conformation code for establishing the connectivity. As soon as the system is connected, the data transfer can take place. For providing security to the data transmission, SHA-1 algorithm is used.

The system is basically focused for those people who travel around the globe and need to be consistently connected to their workplace or home at the same time. The proposed system has a great potential and it will benefit the masses for a long time.

Everybody these days possesses a Mobile Phone. As it is small in size and portable, it become a smarter choice for accessing the remote desktop than a PC or a laptop. This paper proposes the use of Mobile Phones (equipped with Internet features) by the IT professionals to access their office computers after proper authentication check.

The overall system will require hardware components like a Modem, Microcontroller, Microprocessor and a USB Port to accomplish this task. For secure transmission of data between the cellular device and the PC, encryption algorithm (SHA 1) will be used.

Apart from this if ROBOT APIs are used then we can use our Mobile phone as a remote control for switching on or off the lights, adjusting the thermostat of our AC. It could also be used for indicating the temperature in high temperature zones like Nuclear Reactors.

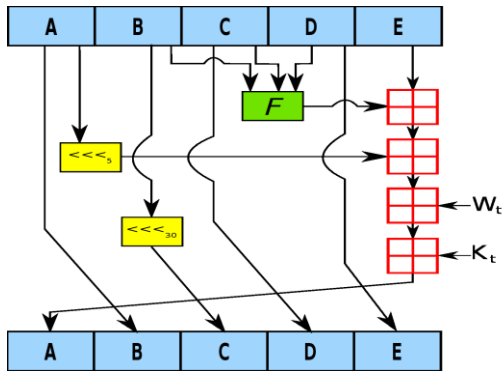
The whole application is divided into modules according to their functionalities. The output of one module is input for the next module. Intended Audience and Reading Suggestions This document is intended for the persons in the following categories Students doing Graduation in Computers. Internal and External guide. Most of the industries need it for their project development.

II. The SHA-1 hash function

SHA-1 produces a 160-bit message digest based on principles similar to those used by Ronald L. Rivest of MIT in the design of the MD4 and MD5 message digest algorithms, but has a more conservative design. The original specification of the algorithm was published in 1993 as the *Secure Hash Standard*, FIPS PUB 180, by US government standards agency NIST (National Institute of Standards and Technology). This version is now often referred to as *SHA-0*. It was withdrawn by NSA shortly after publication and was superseded by the revised version, published in 1995 in FIPS PUB 180-1 and commonly referred to as *SHA-1*.

SHA-1 differs from SHA-0 only by a single bitwise rotation in the message schedule of its compression function; this was done, according to NSA, to correct a flaw in the original algorithm which reduced its cryptographic security. However, NSA did not provide any further explanation or identify the flaw that was corrected.

Weaknesses have subsequently been reported in both SHA and SHA-1. SHA-1 appears to provide greater resistance to attacks, supporting the NSA's assertion that the change increased the security.



One iteration within the SHA-1 compression function:
A, B, C, D and E are 32-bit words of the state;
F is a nonlinear function that varies;
n denotes a left bit rotation by n places;
n varies for each operation;
Wt is the expanded message word of round t;
Kt is the round constant of round t;
Denotes addition modulo 232

III. LITRATURE SURVEY

Desktop sharing commonly refers to a remote frame buffer technology. Desktop sharing allows a user to send screen data to be drawn elsewhere and receive input remotely. Its applications vary from remote system administration to accessing virtual machines. There has been much research concerning the use of desktop sharing as a platform for collaboration. A few useful features appear in several papers.

The BASS Application Sharing System established the idea of applying a secondary protocol to re-encode video and stream it separately from the frame buffer for any video playing on the screen. Additionally the sharing system supports per-application sharing by removing all non-application specific information from the remote frame buffer. In one system researchers enhanced the Virtual Network Computing (VNC) protocol by adding an additional layer of authentication to allow for view-only or normal interactivity connections.

Systems that support multicast (multiple people only seeing one screen) tend to use the Binary Floor Control Protocol to determine controllability of the screen at any one point in time. There are also other papers of interest that cover non-desktop sharing collaboration. For example, research on remote pair programming, where two users work on the same code at the same time using shared cursors and synchronized codebases, differs from desktop sharing because both users are still seeing different desktops. Instead of actually visualizing the other collaborator's desktop, a user of the Sangam tool has a synchronized view and cursor with the other collaborators. This approach works well in very specialized environments such as programming Integrated Development

Environments (IDEs) but lacks usability in more general scenarios. Unfortunately no hard research has been done on the efficacy of the technique but it is important to remember that desktop sharing is just one facet of collaboration technology.

Help desk is a generic name typically associated with an end-user support center. Prior to the creation of a dedicated help desk, end-users often resorted to contacting a friend or colleague for assistance. Today's savvy technology managers realize that it is critical to transform outdated "help desks," which rely primarily on telephone communications, into efficiently managed "service desks" that efficiently and economically accommodate multiple forms of interaction - from voice and data to email and instant messaging. They also understand that by transitioning to self-assist and remote incident resolution they can reduce service desk operational costs by half, while dramatically improving the quality of service provided.

Although the telephone is the preferred method of seeking support, end-users can encounter frustration when calling the help desk. End-users often lack confidence that they will be able to adequately describe the issue they are experiencing or fear embarrassment for their lack of application and or computer knowledge and skills. This can lead to confusion and misinterpretation for the support specialist as they attempt to resolve the issue. Concern over a language barrier is a potential drawback of phone support as well. The end-user may become frustrated and abandoned the call before their issue is resolved if they're unable to understand a support specialist due to a thick accent.

In order to overcome such problem, the Help Desk can capture the customers desktop and solve the problem themselves.

3. SYSTEM ARCHITECTURE

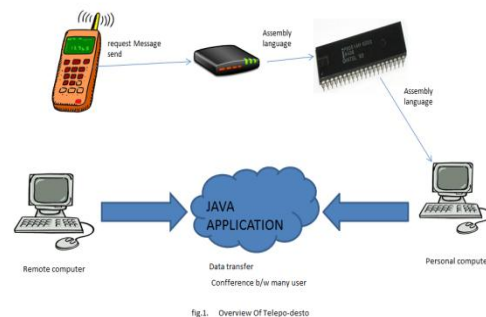


Fig. 1,

A user has to send an SMS by the cell phone to the home server. It will be received through hardware modules like modem, microcontroller and a microprocessor. The system responds back by sending an acknowledgment message asking user to prove his /her authenticity.

Incase of authentic password reception, the system generates a onetime password for the user to establish the connectivity. As soon as the system is connected, the data transfer can take place. For providing security to the data transmission, a very powerful encryption algorithm is used.

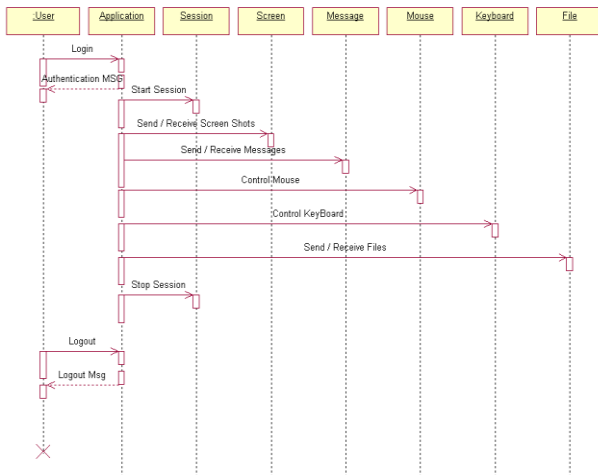


Fig. 2, Sequence Diagram

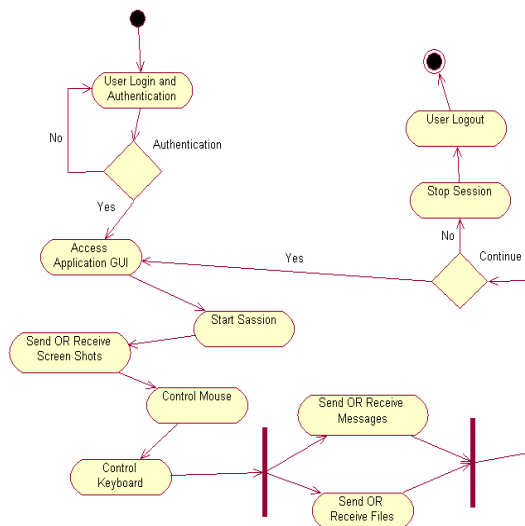


Fig. 3, Use case diagram

IV. ADVANTAGES

- 4.1 Anyone can access data from a PC anywhere and anytime by simply sending an SMS.
- 4.2 It saves money by lowering your monthly utility bills.
- 4.3 Easy to operate and use as Mobile Phones are extensively used.
- 4.4 Has negligible portability issues as Cell Phones easily fit in pockets.

V. DISADVANTAGES

- 5.1 The energy required to run the devices .This problem can be removed by using solar technology to run the system.
- 5.2 Installation will need expertise person the local resident will face a problem in installation.
- 5.3 There is maintenance of this system is required as this is a new technology and have potential risks. Regular checkup of the security and other critical operations are necessary for such new technology.

VI. CONCLUSION

In conclusion, we feel that the proposed system has a great potential in revolutionizing the concept of Desktop Sharing. As Mobile phones are small in size and easily portable, they become a smarter choice for accessing the remote desktop than a PC or a laptop. They can be easily carried and handled by their users. They are a smarter means of working on Remote Systems than a traditional desktop computer or a laptop. Also a cell phone can become a remote control for its users in switching on or off the light bulbs or also act as an indicator showing temperature readings in high temperature zones.

REFERENCES

- [1] Two Factor Authentication Using Mobile Phones Fadi Aloul,Syed Zahidi, Wassim El-Hajj
- [2] Towards Ubiquitous Computing via Secure Desktop Service Pan-Lung Tsai, Student Member,IEEE, and Chin-Laung Lei, Member , IEEE
- [3] A Herzberg, "Payments and Banking with Mobile Personal Devices", Communications of the ACM, 46(5), 53-59, May 2008
- [4] J. Brainard, A. Juels, R. L. Rivest, "Fourth Factor Authentication": ACM CCS, 168-179,2010
- [5] National Institute on Standards and Technology Computer Security Resource Center, NIST's Policy on Hash Functions, March 29, 2009.
- [6] Niels Ferguson, Bruce Schneier, and Tadayoshi Kohno, Cryptography Engineering ([http:// www.schneier.com/ book-ce. html](http://www.schneier.com/book-ce.html)), John Wiley & Sons, 2010.
- [7] A. Josang and G. Sanderud, "Security in Mobile Communications: Challenges and Opportunities" in Proc. Of the Australian information security workshop condence on sACSW frontiers, 43-48, 2003.

Elastic Properties of RCC under Flexural Loading

S. K. Kulkarni¹, M. R. Shiyekar², B. Wagh³

¹(Department of Civil Engineering, Sinhgad College of Engineering, Pune/ Pune University, India

^{2,3}(Department of Civil Engineering, Pune University, India

ABSTRACT : In structural analysis, especially in indeterminate structures, it becomes essential to know material and geometrical properties of members. The codal provisions recommend elastic properties of concrete and steel and these are fairly accurate enough. The stress-strain curve for concrete cylinder or a cube specimen is plotted. The slope of this curve is modulus of elasticity of plain concrete. Another method of determining modulus of elasticity of concrete is by flexural test of a beam specimen. The modulus of elasticity most commonly used for concrete is secant modulus. The modulus of elasticity of steel is obtained by performing a tension test of steel bar. While performing analysis by any software for high rise building, cross area of plain concrete is taken into consideration whereas effects of reinforcement bars and concrete confined by stirrups are neglected. Present aim of study is to determine elastic properties of reinforced cement concrete material. Two important stiffness properties such as AE and EI play important role in analysis of high rise RCC building idealized as plane frame. The experimental program consists of testing of beams (model size 150 x 150 x 700 mm) with percentage of reinforcement varying from 0.54 to 1.21%.

Keywords: indeterminate structures, stiffness properties.

I. Introduction

In order to design an RC structural element, it is important to gain a general overview of reinforced concrete structures and an understanding of the basic material properties. It is also important to get acquainted with the basic concepts relating to performance criteria in reinforced concrete design. The aim of structural design is to design a structure so that it fulfils three criteria namely safety in terms of strength, stability and structural integrity; adequate serviceability in terms of stiffness, durability, deformation and economy. The behaviour of section at various stages of loading can be studied in two parts i.e. initial un-cracked phase and the ultimate condition at collapse.

For a simply supported beam subjected to gradually increasing load, the applied moment at any section is less than cracking moment M_{cr} and the maximum tensile stress f_{ct} in the concrete is less than its flexural tensile strength f_{cr} . This phase is called the un-cracked phase. In this case, the entire section is effective in resisting the moment. The un-cracked phase reaches its limit when the applied moment M becomes equal to the cracking moment M_{cr} . In the stress-strain curve, uncracked phase falls within the initial linear portion.

As the applied moment exceeds M_{cr} , the maximum tensile stress in concrete exceeds the flexural tensile strength of Concrete and the propagation of crack enhances. The cracks get developed in the bottom fibers of the beam. As

the load increases, the cracks get widened and propagate towards the neutral axis. The cracked portion of the concrete becomes ineffective in resisting tensile stress. Hence, the effective concrete section is reduced. For further increment in the applied moment, strain in tension steel increases which results in an upward shift of the neutral axis and ultimately there is an increase in curvature and collapse occurs.

II. Current Codal Provisions in IS: 456-2000 [1]

For the analysis purpose, modular ratio concept makes it possible to transform the composite section into an equivalent homogeneous section made up entirely of one material. The use of transformed section concept may be limited in determining the neutral axis as the centroidal axis of the transformed section. The stress can be computed in transformed section by applying the flexure formula. In this case the second moment of area I_g of the transformed section has to be considered.

Applying the concept of transformed section, the area of tension reinforcement steel A_{st} is transformed into equivalent concrete area as $m A_{st}$. This transformation is valid in reinforced concrete not only for flexural members but also for members subjected to axial forces.

The long-term effects of creep and shrinkage of concrete and non-linearity at high stresses result in much larger compressive strains in the compression steel. Hence the Code recommends that the transformed area of the compression steel A_{sc} can be taken as $1.5m A_{sc}$ rather than $m A_{sc}$. While considering the area of concrete under compression in the transformed section, net area A_c i.e. gross area A_g minus A_{sc} making allowance for the concrete area displaced by the steel area should be considered.

Considering the current practice of RC design, it is necessary to carry out one more cycle of analysis and design. IS Code specifies E value for plain concrete and not for the composite reinforced concrete. Second cycle of analysis can be done with available design from the first cycle. In this second cycle, as steel area is known for both beam and column, it becomes important to make the use of this steel area in defining effective area of cross section as well as effective moment of inertia considering the amount of steel. Then there exists two parts in the analysis i.e. pre-cracking and post-cracking of RC members. For this, one should know the material and geometrical properties such as E , A and I for RCC section. This may also vary for pre-cracking and post-cracking conditions. The effect of the reinforcement ratio was considered in a model which was used to estimate the effective moment of inertia of reinforced concrete beams [2]. A parametric study was also carried out to determine effective stiffness of concrete and beams [3]. Further, a procedure was developed analytically for moment-curvature behavior of beams [4]. Effect of material properties was studied on behavior of over-reinforced concrete beams [5]. From all these studies, it was observed that effective modulus of elasticity and effective

moments of inertia of RC sections are not addressed much in the literature.

III. Rationale and Significance of the Study

In structural analysis, especially in indeterminate structures, it becomes essential to know material and geometrical properties of members. The IS codal provisions recommend elastic properties of concrete and steel and these are fairly accurate enough. These elastic properties are known independently for concrete and steel. But reinforced concrete is a composite material containing steel and concrete. While performing analysis by any software for high rise building, cross area of plain concrete is taken into consideration whereas effects of reinforcement bars and concrete confined by stirrups are neglected. Present aim of study is to determine elastic properties of reinforced cement concrete material. Two important stiffness properties such as AE and EI play important role in analysis of high rise RCC building idealized as plane frame. It is also hoped that knowing exact material and geometrical properties, analysis may become more accurate and economical design can be achieved. The proposed experimental program consists of testing of beams (model size 150 x 150 x 700 mm) with percentage of reinforcement varying from 0.5 to 1.2%. The experimental results have been verified by using 3D finite element techniques. The present paper reviews critically codal provisions of Indian as well as other international codes such as ACI, BS, Australian and Canadian codes.

IV. Shortcomings of the traditional method of RC design

In pre-cracked state, area of concrete below neutral axis is to be considered. Hence value of I_g is known. In post-cracked state, area of concrete below neutral axis is to be ignored. If the cracks developed below neutral axis are within acceptable limits i.e. hairline cracks, then this area should not be ignored. But if these cracks are wider and deeper, then question arises to what limit for depth and width of cracks is to be considered. Another problem is concerned with E value of RCC. In conventional design, we take into account E value of plain concrete given by code.

Beam section is considered to be safe if ultimate moment of resistance M_{ur} is greater than or equal to the factored moment M_u . The ductile failure is accepted to be desirable. The excessive cover to the reinforcement causes cracks at the early stages of loading. In over-reinforced sections, the strength requirement may be satisfied but not the ductility requirement. The ductility requirement may be partly satisfied in case of mild steel, even if x_u slightly exceeds $x_{u,max}$.

V. Experimental program

In the present study, experimental investigation of the RCC models under flexural loadings was carried out. Possible combinations of reinforcement for flexure test for M_{20} and M_{25} grade of concrete are shown in Table 1 and Table 2 respectively. Model size 150x150x700mm is used as per IS 516:1959 (Reaffirmed 1999) Methods of Tests for Strength of Concrete [6].

For each combination, 3 models are tested and average results are presented.

TABLE 1 Combinations of reinforcement for flexure test (M_{20})

Model No.	Diameter (mm)	No of Bars	Ast (sq.mm)	pt (%)
1	-	-	0.00	0.00
2	8	2	100.53	0.54
3	8 + 6	2 + 1	128.81	0.60
4	8	3	150.79	0.80
5	10	2	157.08	0.84

TABLE 2 Combinations of reinforcement for flexure test (M_{25})

Model No.	Diameter (mm)	No of Bars	Ast (sq.mm)	pt (%)
1	-	-	0.00	0.00
2	8	2	100.53	0.54
3	8 + 6	2 + 1	128.81	0.60
4	8	3	150.79	0.80
5	10	2	157.08	0.84



Fig. 1: Typical Beam Specimen Showing First Crack During Loading



Fig. 2: Typical Beam Specimen Showing Crack at Failure



Fig. 3: Typical Beam Specimen Showing Shear Crack at Failure

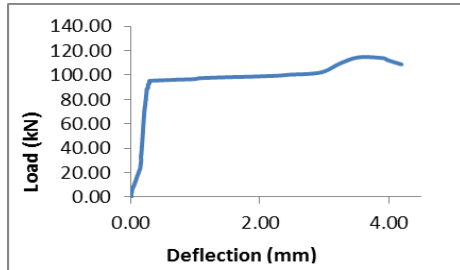


Fig.4 Typical Load Deflection Curve for Model 4 (M_{20})

VI. Experimental Results

For a beam subjected to two-point loading the deflection formula is given in equation (1)

$$\delta = \left(\frac{5}{384} \right) \times \left(\frac{wl^4}{EI} \right) + \left(\frac{23}{648} \right) \left(\frac{Wl^3}{EI} \right) \quad (1)$$

where w is self-weight of beam in N/mm and W is half the load at failure in N

TABLE 3 Percentage of Steel and Corresponding E and f_{cr} values of RCC for M_{20}

Model No	Percentage of Reinforcement	Modulus of Elasticity (N/mm^2)	
		M20	M25
1	0.00	24066.81	25994.86
2	0.54	28288.60	29161.02
3	0.69	28453.85	29502.47
4	0.80	31013.40	29716.23
5	0.84	32478.33	31438.35
6	1.21	-	35510.70

VII. Analytical Investigation

The realistic and practical modeling of steel and surrounded concrete is one of the most challenging problems in structural analysis. Such a modeling is unavoidable in studying structural behavior. The grades of concrete selected in the present study are M_{20} and M_{25} . For concrete, the element used is SOLID65. The element is defined by eight nodes having three degrees of freedom at each node i.e. translation in x , y , and z directions. This element is a highly non-linear element and specifically used for materials like concrete and it takes into account cracking in three orthogonal directions due to tension, compression and plastic deformation. Strain ratio between the concrete and steel is supposed to be equal assuming perfect bond, therefore it is accepted that there is a unique adherence between the concrete and steel [7]. Hence there is no element defined between concrete and steel.

For the main reinforcement and stirrups, LINK8 spar element with three degrees of freedom at each node is used. It considers the parameters like plasticity, creep, swelling, stress stiffening and large deflection.

It was observed that the region of load and the supports are facing a problem of stress concentration. Hence in order to arrest this problem, the supports and loading region are modeled with a steel block. The element used for this is SOLID45 with three degrees of freedom (u , v , w) at each node. This element is treated as a linear element which handles plasticity, creep, bulge, stress stiffening and big deflection [8].

7.1 Load step and load increment

For the prediction of non-linear behaviour, the total load was divided into series of load increments or load steps as required by Newton-Raphson method. The number of load steps, minimum and maximum step sizes was determined after number of trials [9]. For each load increment, the crack depth in the section was observed. By considering only the effective area of cross-section and tension reinforcement, effective moment of inertia was determined. This value of moment of inertia was used for calculation of modulus of elasticity of RCC section. Fig. 5 and 6 show variation of modulus of elasticity of each model for various crack depths for M_{20} and M_{25} grades of concrete respectively.

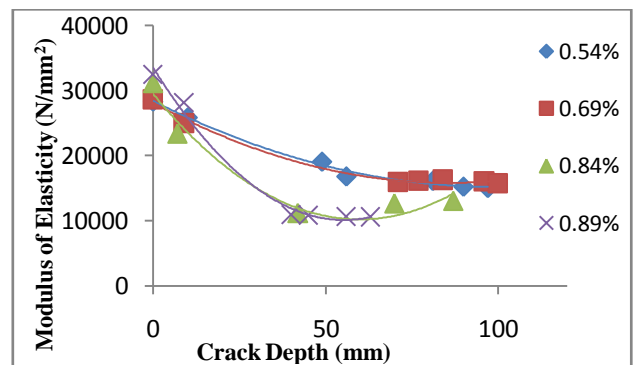


Fig. 5 Modulus of Elasticity vs Crack Depth for M_{20} grade of Concrete

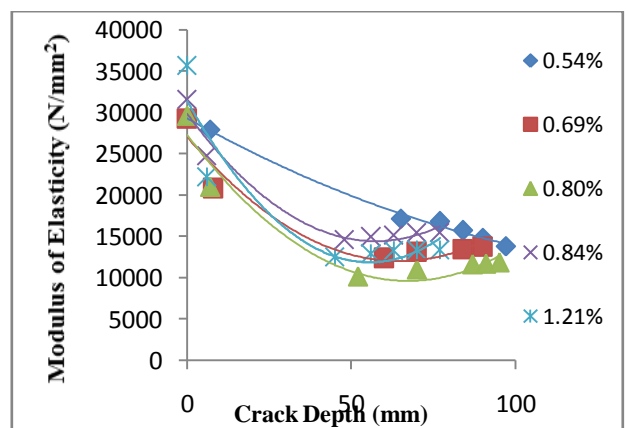


Fig. 6 Modulus of Elasticity vs Crack Depth for M_{20} grade of Concrete

VIII. Observations

8.1 M₂₀ Grade

- For $A_{st} = 0.54$ to 0.69% E reduction variation is almost identical as crack depth increases. E remains constant from crack depth 50mm onwards.
- More drop of E for $A_{st} = 0.84\%$. E remains same almost from 40mm crack depth.
- E remains same for $A_{st} = 0.89\%$ after crack depth of 40mm.
- $E = 18000 \text{ N/mm}^2$ for $A_{st} = 0.54$ to 0.69% and $E = 12000 \text{ N/mm}^2$ for $A_{st} = 0.84$ and 0.89% after crack depth of 40mm.

8.2 M₂₅ Grade

- E lies in the range of $12000 - 17000 \text{ N/mm}^2$ for $A_{st} = 0.69\%$
- E for A_{st} beyond 0.69% is as follows- 17000 N/mm^2 for $A_{st} = 0.84\%$, 12000 N/mm^2 for $A_{st} = 0.80\%$ and 13000 N/mm^2 for $A_{st} = 1.21\%$

IX. Conclusions

- For both grades of concrete, 120mm is the effective depth of section to be considered for calculation of modulus of elasticity.
- For no crack depth in the section, modulus of elasticity increases with increase in percentage of reinforcement for both the grades.
- Equation for effective moment of inertia of the RC section can be proposed. Equation of I_{eff} given in IS: 456-2000 is for plain section which neglects tension reinforcement.
- Also in the same equation of I_{eff} given in IS: 456-2000, the code remains silent about moment of inertia of cracked section I_r .

X. Acknowledgements

The experiments were carried out under the research project funded by BCUD. The authors are very much thankful to BCUD for the financial support. The authors also acknowledge the support of SCOE team for conducting experiments in the laboratory.

References

- IS:456-2000, *Plain and Reinforced Concrete- Code of Practice (Fourth Revision)* (Bureau of Indian Standards, New Delhi, July 2000)
- Al-Shaikh A H, Al-Zaid RZ 1993 Effect of reinforcement ratio on the effective moment of inertia of reinforced concrete beams. *ACI Structural Journal* 90: 144-149.
- Khuntia M, Ghosh S K 2004 Flexural stiffness of reinforced concrete columns and beams: Analytical approach. *ACI Journal of Structures* 101(3): 364-374.
- Shrikant M, Kumar G R, Giri S 2007 Moment curvature of reinforced concrete beams using various confinement models and experimental validation. *Asian Journal of Civil Engineering (Building and Housing)* 8(3): 247-265.
- Siddique M A, Rouf M A 2006 Effect of material properties on behavior of over-reinforced concrete

beams. *Asian Journal of Civil Engineering (Building and Housing)* 7(2): 195-204.

- IS 516:1959 (Reaffirmed 1999) *Methods of Tests for Strength of Concrete* (Bureau of Indian Standards, New Delhi, 1999)
- Alper B, (2010) *Scientific Research and Essays*, 5(6), 533-544.
- ANSYS-12, ANSYS User's Manual, ANSYS, USA.
- Vasudevan G and Kothandaraman S, (2011) *Int J Civil & StrEng* 2(1), 98-111.

Bearing Life Improvement of Centrifugal Blowers by Vibration Analysis

B. A. Kardile,
Associate Member, IEI,

Abstract: This study work is proposed to carry out vibration analysis of heavy duty centrifugal Blowers & bearing failure analysis. The life of bearing can be improved by carrying corrective actions on blower & modifying its accessories like Plumber block to prevent bearing failure. The proposed work is planned in following phases Preparation of measuring instrument for data collection (PRUFTECK VIBROEXPERT METER) Collection of data from various locations on blower surfaces in different directions. Data analysis is done on the basis of spectral plot, amplitude against frequencies with the help of prufteck vibroexpert meter. In comparison of vibration spectral with experimental actions are carried out under the vibration severity standard, the chart results of rectification will be compared with spectral plot & corrective action. The results will be compared with initial condition & condition monitoring schedule is prepared for avoiding premature failure of equipment. Standard schedule for maintaining basic condition of variables of equipment like as CBM /TBM will be planned to avoid premature failure of the bearing.

Index Terms: Blower Vibration Data Collection, Spectral plot analysis, analysis of bearing structure, Corrective actions on equipment,, Comparison of results & Standardize the method

I. INTRODUCTION

The Report Contents

- 1] Blower readings with Vibro-meter
- 2] Blower problem Diagnosis
- 3] Bearing & Plumber block analysis
- 4] Bearing failure analysis
- 5] Bearing with Wavy leaf spring analysis

Scope: This Report contains fault diagnosis with the analysis and recommendations for corrective actions. These all are supported by spectrum plots for each point of the equipment identified as being deviated. A color coding system is employed, as per ISO standard which make it easy to understand the criticality of the fault and how quickly it needs to be investigated & rectified.

Measurement: An overall vibration reading of displacement & velocity are measured in micron & mm/sec respectively, A RMS values are used to determine general mechanical and electrical fault within rotating machinery.

Equipment Used: PRUFTECHNIK VIBXPERT DUAL CHANNEL ANALYZER



Fig-1. Structure of Centrifugal Blower

II. BLOWER STRUCTURAL ANALYSIS

Machine vibration has several categories of causes that we have discovered after so many repairs, but it is useful now to review them to gain more confidence in the diagnosis. The actual structure of blower shown in Fig 1.

The Major categories of diagnoses are –

- Design defects
- Manufacturing defects
- Operational stresses
- Maintenance actions
- Aging

Design defects are mostly structural related with active resonances built-in because of improper sizing and proportioning of the parts statically, the structure seems good, but it remains dynamically weak. This is not discovered until the machine is energized and brought up to the required speed. This is more common than it should be, but the designers are not well equipped to predict or test for natural frequencies. In addition, the owners' foundation or base has a significant effect on natural frequencies, which the designer has little control over. Hence, resonances are best detected during startup testing and corrected on-site with strategic stiffeners added. Manufacturing defects are built-in during the casting, machining, heat-treating, and assembly processes. They are latent defects that may show up in the first 24-hours of running, or they may not be obvious during the run-in period, appearing years later. The machine does not survive to a normal life expectancy as vibration may or may not be present.

An example is residual stresses in a shaft that gradually distorts the shaft over a period of years. Manufacturing defects are difficult to control, impossible to predict, and elusive to fix. The best strategy to deal with both design defects and manufacturing defects is to insist on start up vibration testing with limits of acceptability in accordance.

Here in Table1 we have tabulated velocity & shock pulse readings on plumber block at drive end & non drive end in axial, horizontal & vertical direction at threshold .The Colour coding is used to classify vibration severity as per ISO 10816, as good, satisfactory, unsatisfactory & unacceptable from green to red mark indicates alarming zone. This experiment conducted on 110 Kw capacity blowers with Prufteck Vibroexpert Meter.

Table1.Velocity & shock pulse reading with alarm code

RAJAJ AUTO LIMITED / CHAKRAKAR PANT SHOP / PETROL TANK LINE PRIMER COAT EXHAUST FAN / FAN										
Measurement	Value	Unit	Threshold	Level	Color	Code	%			
Non Drive Horizontal	101 Overall velocity -800 (rms)	mm/s	2.30	2.5	Green	N	24			
	106 Shock pulse m. -120 (dBrms)	mm/s	2.5	2.5	Green	N				
Non Drive Vertical	101 Overall velocity -800 (rms)	mm/s	2.30	4.50	Green	P	17			
	106 Shock pulse m. -120 (dBrms)	mm/s	2.5	2.5	Green	N				
Non Drive Axial	101 Overall velocity -800 (rms)	mm/s	2.30	1.5	Green	W	19			
	106 Shock pulse m. -120 (dBrms)	mm/s	2.5	2.5	Green	N				
Drive Horizontal	101 Overall velocity -800 (rms)	mm/s	2.30	2.5	Green	N				
	106 Shock pulse m. -120 (dBrms)	mm/s	2.5	2.5	Green	N				
Drive Vertical	101 Overall velocity -800 (rms)	mm/s	2.30	4.50	Green	P	49			
	106 Shock pulse m. -120 (dBrms)	mm/s	2.5	2.5	Green	N				
Drive Axial	101 Overall velocity -800 (rms)	mm/s	2.30	1.5	Green	N				
	106 Shock pulse m. -120 (dBrms)	mm/s	2.5	2.5	Green	N				
RAJAJ AUTO LIMITED / CHAKRAKAR PANT SHOP / PETROL TANK LINE PRIMER COAT EXHAUST FAN / MOTOR										
Measurement	Value	Unit	Threshold	Level	Color	Code	%			
Non Drive Horizontal	101 Overall velocity -800 (rms)	mm/s	2.30	2.5	Green	N				
	106 Shock pulse m. -120 (dBrms)	mm/s	2.5	2.5	Green	N				
Non Drive Vertical	101 Overall velocity -800 (rms)	mm/s	2.30	4.50	Green	P	6			
	106 Shock pulse m. -120 (dBrms)	mm/s	2.5	2.5	Green	N				
Non Drive Axial	101 Overall velocity -800 (rms)	mm/s	2.30	1.5	Green	N				
	106 Shock pulse m. -120 (dBrms)	mm/s	2.5	2.5	Green	N				
Drive Horizontal	101 Overall velocity -800 (rms)	mm/s	2.30	2.5	Green	N				
	106 Shock pulse m. -120 (dBrms)	mm/s	2.5	2.5	Green	N				
Drive Vertical	101 Overall velocity -800 (rms)	mm/s	2.30	4.50	Green	P	18			
	106 Shock pulse m. -120 (dBrms)	mm/s	2.5	2.5	Green	N				
Drive Axial	101 Overall velocity -800 (rms)	mm/s	2.30	1.5	Green	N				
	106 Shock pulse m. -120 (dBrms)	mm/s	2.5	2.5	Green	N				

The analysis of the data indicates that the excessive operational stresses on blower are developed due to material buildup or erosion, which changes the balance condition, or thermal expansion that changes component alignment. Both of these cause high dynamic loads at the bearings which lead to accelerated wear out. These defects are easily detected with periodic vibration measurements and there are well established methods to correct them on site. Our maintenance actions, or interactions, are the most common cause of blower failure. It is well known in the repair business that a blower machine never goes back together the same way. Some of this is due to rough handling, but some is simply the fact that field repair is less controlled than the original factory build. The field environment is darker, dirtier, and less precise tooling is available to control fits and alignments. The repair is usually rushed by management. It is surprisingly difficult to install a bearing into aluminium housing in the field and not get it crooked. The first question to ask in vibration analysis is "What recent maintenance activity has occurred on this machine?" other maintenance activities that affect on blower vibration are-

- Excessive localized heating, like welding on a shaft
- Too high belt tension
- Shaft, or bearing, misalignment
- Substandard replacement parts
- Coupling, or other component, binding
- Lack of lubrication
- Loose hardware
- Replacing hardware with different weights that Affects on balance
- Re-assembling hardware in different orientations (also affect on balance)
- Hammering on a bearing
- Unclean, or burred, precision machine surfaces

Aging effects are only be detected with long term vibration monitoring. The two dominant aging effects are residual stress relaxation and softening of structural joints. The residual stresses left behind in machine components are always relieve themselves over time. This process is accelerated at higher temperature of shaft, being long and slender component, are particularly vulnerable to bowing. The symptoms are an increase in 1x RPM balance condition and beating up of the bearings. Bearing replacements do not restore the original smooth running condition, and mass balancing is unsuccessful, until the shaft is replaced.

All joints soften over time, and joints are the weak links in any structure. These are the prominent symptom of lowering of the natural frequencies of the machine. This has usually first detected with high vibration when the lowest natural frequency drops down into the operating speed range of the machine.

III. BALANCING & ALIGNING METHOD

This is well known that blower vibration related problems are corrected in place. The corrective methods are well experienced undergoing the trouble shooting of the blower problem in depth. These are listed here to close this discussion.

- Disassembly, visual inspection, cleaning, and re-assembly fix some elusive problems without knowing

- Bearing replacement
- Identifying other bad parts and replacing them
- Mass balancing
- Alignment
- Lubrication is just greasing noisy bearings to Quiet them, but changing the lubrication schedule Extent their lives
- Structural stiffening to raise natural frequencies.
- Mass loading and stiffening reduces any Measured vibration

If blower has lower motion, it may increase local stresses at the bearings resulting in faster bearing wear. This is to be used only as a last resort when nothing else works and measured motion must be lowered.

The Fig-2 gives the velocity (mm/sec) trend of 110kw blower from Dec-2007 to June-2012 with alarming zone

Vibration Monitoring Trend-
ABS Line : Top Coat Booth Exhaust Blower

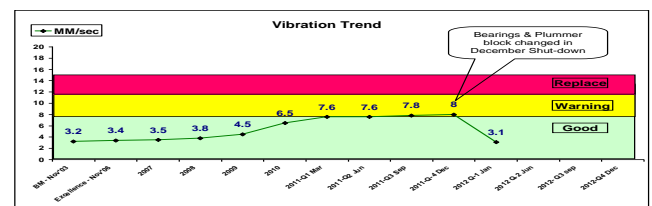


Fig-2.Vibration monitoring trend for exhaust blower
110 Kw capacities

Finally, a few blowers are still generating excessive vibration, the cause has not been discovered nor corrected, and they have not shaken themselves apart yet. Some blowers are just rough characters and it is neither necessary nor desirable to retrain them. As long as the vibration amplitude remains stable, it is safe to continue to operate at elevated levels, thus avoiding repair cost and downtime. Regular vibration monitoring has allowed machines to operate longer into the wear out cycle without fear of failure.

IV. FFT SPECTRUM

The prufteck vibroexpert meter is the simplest, and least expensive, is an overall meter. It provides not only frequency information, but also overall amplitudes for the analysis of data. It is useful for trending or comparison measurements on similar machines, but for diagnosing problems on machines, it is best left turned off. The other two major vibration instruments are tuneable filters and FFT (Fast Fourier Transform) analyzers. Analyzer is a misnomer because analysis is a human function. An electronic "analyzer" does not analyze. It only measures and display electrical signals. The electrical signals from accelerometers and velocity transducers are very small AC voltages, typically millivolts. Hence, the tuneable filters and FFT instruments are nothing more than fancy AC voltmeters with a frequency display axis. Any of these two major vibration measuring instruments, from any manufacturer, can be used effectively to diagnose machine vibrations. No specific instrument or manufacturer has a unique connection to a higher intelligence. As it's FFT spectrum is shown in Fig-3

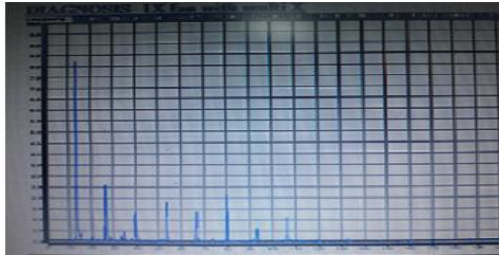


Fig- 3. FFT Spectrum for blower vibration

However, some are an order of magnitude or two more complicated to use by design. The instrument in use is the least significant factor in diagnosis. The instrument operator and the methods employed are the most significant.

The fundamental method of using a vibration instrument is to conduct a survey of the entire blower system; driver, driven, and any intermediary machines such as gearboxes & pulleys of belt drive.



Fig- 4. Frequency versus time graph for exhaust Blower 110 Kw capacity

The spectrum shown in Fig-4 implies that the displacement varies with outer race wear in Axial, vertical, horizontal direction as rotor moves under centrifugal forces. Which lifts the shaft from impeller side causes reducing amplitude the displacement for non drive end to drive end.

The velocity of vibration depends upon the shaft speed, type of bearing, type of drive supporting distance of the shaft within the bearing & cantilever of the shaft along with the pulley end. The bearing condition can be detected by vibrating parameters trend and the life of bearing can be increased by taking corrective action to prevent extreme condition of the equipment. The bearing & shaft assembly is shown in Fig-5

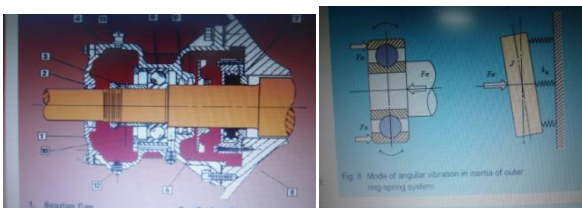


Fig- 5. Bearing assembly & Bearing load of exhaust Blower

4. MATHS & EQUATIONS

- 1) Ball Pass Frequency for the outer race
= No of Roller x Shaft Speed x 0.4
- 2) Ball Pass Frequency for the inner race
= No of rollers x Shaft Speed x 0.6
- 3) Ball pass frequency train race
= Shaft Speed X 0.3

4) Bearing life in Revolutions

$$L = (C/W)^{10/3} \times 10^6$$

C= Basic Load Carrying Capacity

$$C = W (L/100)$$

L= 60 X N X LH, Where LH in Hours

W= Equivalent Dynamic Load

L= Life in Revolutions

5) Heat calculation

a) Heat generated due to friction

$$Q_g = \mu \cdot W \cdot V \text{ Watt}$$

μ = Coefficient of friction

W= Load on bearing in N=P x A

V= Speed of journal in RPM

b) Heat dissipated.

$$Q_d = C \cdot A (T_b - T_a) \text{ in Watt}$$

C= Heat dissipation coefficient

A= Projected area of bearing in m²

T_b= Temperature of bearing surface °C

T_a= Temperature of surrounding air °C

$$T_b - T_a = 1/2 (T_o - T_a)$$

c) Heat conveyed by the oil

$$Q_t = M \cdot S \cdot T \text{ in Watt}$$

M= Mass of oil

S= Specific heat of oil 1840-2100 J/kg°C

T= Temperature difference between outlet & inlet

6) Grease quantity inside bearing

$$G_g = 0.005 \times D \times B$$

G_g=Gram of grease

D=Bearing dia in mm

B= Bearing width

7) Coefficient of friction for bearing is expressed as

$$\mu = \phi [ZN/P, d/c, l/d]$$

$$\mu = 33/10^8 [ZN/P] [d/c] + k$$

μ = Coefficient of friction

ϕ =Functional relationship

Z=Absolute viscosity of lubricant in kg/m-s

N=Speed of journal in RPM

P=Bearing pressure=load/area

d=Diameter of journal

l=Length of bearing

c=Diametral clearance

k=Factor of correction for end leakage

ZN/P=Bearing characteristic number, dimensionless number, helps to predict bearing performance called Bearing modulus

V. BEARING FAILURE ANALYSIS

The dampening of the bearing inside the plumber block can be absorbed by providing Wavy leaf spring of adequate stiffness which can prevent the transmission of vibrating wave from inner race to outer race through roller by sharing the load as shown in Fig-6. Which minimize the shock impulse influence directly on bearing & plumber block cause the life improvement for certain hour.

A step change in amplitude is symptomatic of an unstable bearing. Examination of the bearings and their supports is in order as soon as practical. A drop in frequency is bad news. It indicates structural softening such as cracks or joint loosening. Slow changes in amplitude from cold to hot running conditions are related to alignment of the shafts.



Fig- 6.Bearing with Roller condition & wavy leaf spring

A fourth judgement criterion is operational condition. The load level has a dramatic effect on vibration levels, especially electrical machines such as generators. It is usually assumed in analysis that the machine has no operational problem.

The taper roller bearings are used for heavy duty centrifugal blower mounted with on sleeve with lock nut & washer inside plumber block. Taper roller bearings are designed for carrying radial load. This bearing are specified with 5 digit number as 32224 K C3, 32226 K C3, K suffix is attached for taper roller bearing only & C3 is attached for bearing clearance, as bearing clearance varies from C1 to C5 for high temperature & high RPM. Material used for taper roller bearing are babbit metal, bronze, cast iron & silver.

Bearing clearance is provided for the purpose of adjust thermal expansion, deflection of rollers & provide film thickness in lubrication. This clearance is kept 90 to 120 μm before mounting & expected to reduce by 30 % in assembly, if it increases than this the bearing is to be replaced.



Fig-7.Assembly of taper roller bearing on shaft sleeve
With lock nut

The bearing manufacturers are SKF, NTP, FAG & KEYDON. The duplicity in the bearing are easily identified by its finishing standard & clearance value. The clearance is measured with filler gauge & dial gauge, if measured closer to the bearing assembly with dial gauge. Bearing assembly with shaft sleeve & lock nut is shown in Fig-7

The taper roller bearings for heavy duty blowers are fitted by heating the oil upto 120°C with induction coil or flame. Lubrication life of this bearing is depend on load, RPM, bearing ID/OD, Width, & bearing mounting method is expressed in equation 6.

These sliding contact bearing should have following properties

- 1) Compressive & fatigue strength
- 2) Confirmability
- 3) Embeddability
- 4) Bondability
- 5) Corrosion resistance
- 6) Higher thermal conductivity & lower expansion

The bearing failure analysis requires following information as

- 1) Date of mounting & type of bearing
- 2) Load type, temperature & RPM
- 3) M/c & bearing surrounding
- 4) M/c precision/accuracy
- 5) Frequency of failure

- 6) Total hours of working
- 7) Lubrication standard & frequency
- 8) Condition of bearing & lubricant after removal

VI. CONCLUSION

The vibration analysis of the heavy duty centrifugal blower gives the results as

The bearing life the rotating parts depends upon

- 1) The bearing characteristic number, ZN/P
- 2) Running condition-Temperature & RPM under Which the machine runs
- 3) Bearing load condition as static & dynamic load Carrying capacity
- 4) Clearance between roller & outer race
- 5) Heat dissipation capacity of the plumber block & Other accessories
- 6) Lubrication frequency & standard of lubricant

Generally the vibration parameters as displacement & velocity are depends upon the bearing wear of outer race because of roller hits on surface of the race at high temperature

VII. ACKNOWLEDGEMENT

The author would like to thanks the Institution of Engineers (India) for permission to publish the paper. The author gratefully thanks to Bajaj Auto Ltd, Pune to provide platform for the experiment & Dr.D.Y.Patil College of Engineering, Pune for inspiring the subject choosen.

REFERENCES

- [1] Analysis Guide for Machine Designers, journals of white paper, 2008.
- [2] Analytical Diagnostic Approach & Innovative Impeller Design
By Bruno Schiavello & Gian Carlo cicatalli, 2006.
- [3] Vibration Transmission through Rolling Element-
by T.C Lim &
R.Sing 1990, 139(2)
- [4] Rolling Bearing Analysis by T.A.Harris, New York: John wiley, 1966.
- [5] Study of Vibration Characteristic of Bearing, by O. Gustafson,
SKF Report, AL62 L005, 1962.
- [6] Standards for Vibration Monitoring & Analysis
by J.Michael,
Robichaud, P.Eng.2005.
- [7] Maedel, Jr, P. Vibration Standards and Test Codes, Shock and
Vibration Handbook 5th Edition (Cyril Harris, editor), McGraw Hill Publishing Co. (2001)

BIOGRAPHIES

Mr.Balasaheb a Kardile AMIE (Mech, ST-438760-6), ME (Design), Engineer, Bajaj Auto Ltd, Pune, A 2/3 wheeler Mfg Group.



Enhancement of Power Quality by UPQC Device in SCIG Wind Farm to Weak Grid Connection

Laxman Rao¹, Hari Krishna²

1(P.G Student, MIST, Sathupally, Khammam Dist, and A.P)

2 (Assoc. Professor & HOD of EEE, MIST, Sathupally, Khammam Dist, and A.P)

ABSTRACT : In the last years, the wind power generation incorporated into standard grids has been increased significantly. This situation forced the revision of grid connection code requirements, to guarantee the reliability in systems with high wind power penetration. These strategies were implemented using a Unified Power Quality Compensator (UPQC). A model of wind farm with induction generators connected to a weak grid system, including a detailed UPQC compensator was developed on simulation software. In case of wind farms based on SCIG directly connected to the grid, is necessary to employ the last alternative. Custom power devices technology (CUPS) result very use full for this kind of application. A customized internal control scheme of the UPQC device was developed to regulate the voltage in the WF terminals, and to mitigate voltage fluctuations at grid side. The internal control strategy is based on the management of active and reactive power in the series and shunt converters of the UPQC, and the exchange of power between converters through UPQC DC-Link. This approach increases the compensation capability of the UPQC with respect to other custom strategies that use reactive power only. Simulations results show the effectiveness of the proposed compensation strategy for the enhancement of Power Quality and Wind Farm stability.

Keywords: Unified Power Quality Compensator (UPQC), Squirrel Cage Induction Generators (SCIG), Power Quality, Wind Farm, Voltage Fluctuations.

I. INTRODUCTION

The location of generation facilities for wind energy is determined by wind energy resource availability, often far from high voltage (HV) power transmission grids and major consumption centers [1]. In case of facilities with medium power ratings, the WF is connected through medium voltage (MV) distribution head-lines. A situation commonly found in such scheme is that the power generated is comparable to the transport power capacity of the power grid to which the WF is connected, also known as weak grid connection. The main feature of this type of

Connections are the increased voltage regulation sensitivity to changes in load [2]. So, the system's ability to regulate voltage at the point of common coupling (PCC) to the electrical system is a key factor for the successful operation of the WF. Also, is well known that given the random nature of wind resources, the WF generates fluctuating electric power. These fluctuations have a negative impact on stability and power quality in electric power systems. [3] Moreover, in exploitation of wind resources, turbines employing squirrel cage induction generators (SCIG) have been used since the beginnings. The operation of SCIG

demands re-active power, usually provided from the mains and/or by local generation in capacitor banks [4], [5]. In the event that changes occur in its mechanical speed, ie due to wind disturbances, so will the WF active (reactive) power injected(demanded) into the power grid, leading to variations of WF terminal voltage because of system impedance. These power disturbances propagate into the power system, and can produce a phenomenon known as "flicker", which consists of fluctuations in the illumination level caused by voltage variations. Also, the normal operation of WF is impaired due to such disturbances. In particular for the case of "weak grids", the impact is even greater. In order to reduce the voltage fluctuations that may cause "flicker", and improve WF terminal voltage regulation, several solutions have been posed. The most common one is to upgrade the power grid, increasing the short circuit power level at the point of common coupling PCC, thus reducing the impact of power fluctuations and voltage regulation problems [5]. In recent years, the technological development of high power electronics devices has led to implementation of electronic equipment suited for electric power systems, with fast response compared to the line frequency. These active compensators allow great flexibility in: a) controlling the power flow in transmission systems using Flexible AC Transmission

System (FACTS) devices, and b) enhancing the power quality in distribution systems employing Custom Power System (CUPS) devices [6] [9]. The use of these active compensators to improve integration of wind energy in weak grids is the approach adopted in this work.

In this paper we propose and analyze a compensation strategy using an UPQC, for the case of SCIG-based WF, connected to a weak distribution power grid. This system is taken from a real case [7].

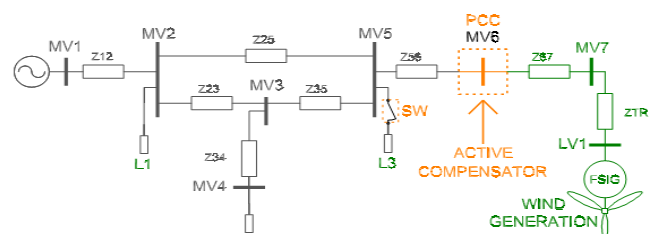


Fig. 1 Study Case Power System

The UPQC is controlled to regulate the WF terminal voltage, and to mitigate voltage fluctuations at the point of common coupling (PCC), caused by system load changes and pulsating WF generated power, respectively.

The voltage regulation at WF terminal is conducted using the UPQC series converter, by voltage injection "in phase" with PCC voltage. On the other hand, the shunt

converter is used to filter the WF generated power to prevent voltage fluctuations, requiring active and reactive power handling capability. The sharing of active power between converters is managed through the common DC link. Simulations were carried out to demonstrate the effectiveness of the proposed compensation approach.

II. UNIFIED POWER QUALITY COMPENSATOR

A. UPQC:

The UPQC is utilized for simultaneous compensation of the load current and the voltage disturbance at the source side. Normally the UPQC has two voltage source inverters of three-phase four-wire or three-phase three-wire configuration. One inverter, called the series inverter is connected through transformers between the source and the common connection point. The other inverter, called the shunt inverter is connected in parallel through the transformers. The series inverter operates as a voltage source, while the shunt inverter operates as a current source. The UPQC has compensation capabilities for the harmonic current, the reactive power compensation, the voltage disturbances, and the power flow control. However, it has no compensation capability for voltage interruption because no energy is stored.

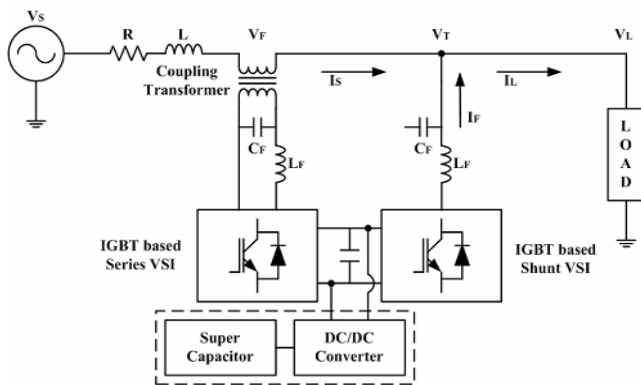


Fig. 2 UPQC system interconnected with energy storage

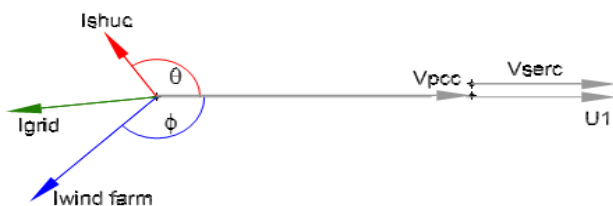


Fig. 3 Phasor diagram of UPQC

B. UPQC control strategy:

The UPQC serial converter is controlled to maintain the WF terminal voltage at nominal value (see U1 bus-bar in Fig.4), thus compensating the PCC voltage variations. In this way, the voltage disturbances coming from the grid cannot spread to the WF facilities. As a side effect, this control action may increase the low voltage ride-through (LVRT) capability in the occurrence of voltage sags in the WF terminals. Fig.5 shows a block diagram of the series converter controller. The injected voltage is obtained subtracting the PCC voltage from the reference voltage, and is phase aligned with the PCC voltage (see Fig.3). On the

other hand, the shunt converter of UPQC is used to filter the active and reactive power pulsations generated by the WF. Thus, the power injected into the grid from the WF compensator set will be free from pulsations, which are the origin of voltage fluctuation that can propagate into the system. This task is achieved by appropriate electrical currents injection in PCC. Also, the regulation of the DC bus voltage has been assigned to this converter. Fig. 4 shows a block diagram of the shunt converter controller. This controller generates both voltages commands $Ed_shu(t)^*$ and $Eq_shu(t)^*$ based on power fluctuations ΔP and ΔQ , respectively. Such deviations are calculated subtracting the mean power from the instantaneous power measured in PCC. The mean values of active and reactive power are obtained by low-pass filtering, and the bandwidth of such filters are chosen so that the power fluctuation components selected for compensation, fall into the flicker band as stated in IEC61000-4-15 standard. In turn, $Ed_shu(t)^*$ also contains the control action for the DC-bus voltage loop. This control loop will not interact with the fluctuating power compensation, because its components are lower in frequency than the flicker-band.

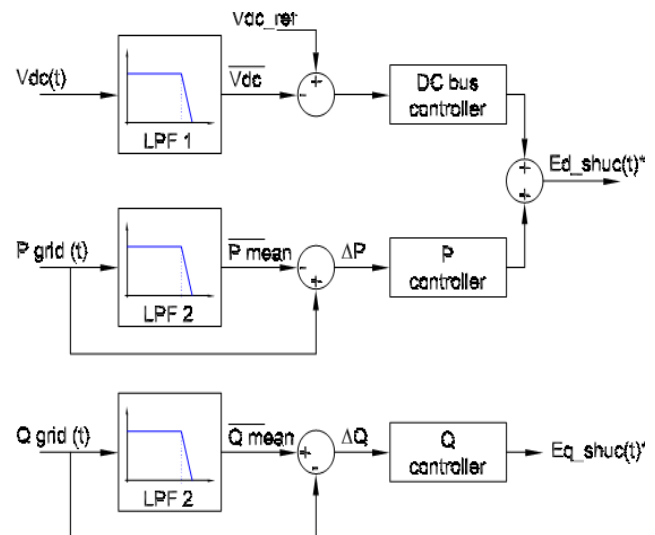


Fig. 4 Shunt compensator controller

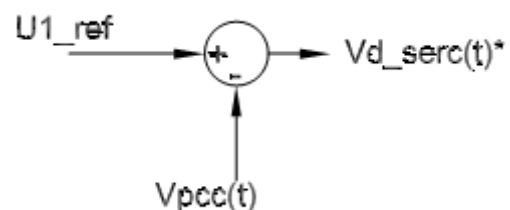


Fig. 5 Series Compensator Controller

In summary, in the proposed strategy the UPQC can be seen as a "power buffer", leveling the power injected into the power system grid. The Fig.6 illustrates a conceptual diagram of this mode of operation. It must be remarked that the absence of an external DC source in the UPQC bus, forces to maintain zero-average power in the storage element installed in that bus. This is accomplished by a proper design of DC voltage controller. Also, it is necessary to note that the proposed strategy can-not be implemented using other CUPS devices like D-Statcom or

DVR. The power buffer concept may be implemented using a D-Statcom, but not using a DVR. On the other and, voltage regulation during relatively large disturbances, cannot be easily coped using reactive power only from D-Statcom; in this case, a DVR device is more suitable.

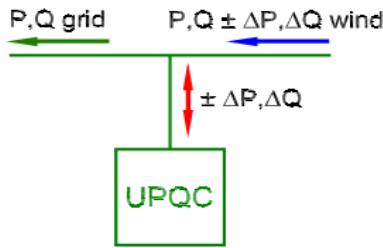


Fig. 6 Power Buffer Control

III. SIMULATION RESULTS AND DISCUSSION

The model of the power system scheme illustrated in Fig. 1, including the controllers with the control strategy detailed in section III, was implemented using Matlab/Simulink software. Numerical simulations were performed to determine and then compensate voltage fluctuation due to wind power variation, and voltage regulation problems due to a sudden load connection. The simulation was conducted with the following chronology:

- at $t = 0.0''$ the simulation starts with the series converter and the DC-bus voltage controllers in operation.
- at $t = 0.5''$ the tower shadow effect starts;
- at $t = 3.0''$ Q and P control loops (see Fig. 4) are enabled;
- at $t = 6.0''$ L3 load is connected.
- at $t = 6.0''$ L3 load is disconnected

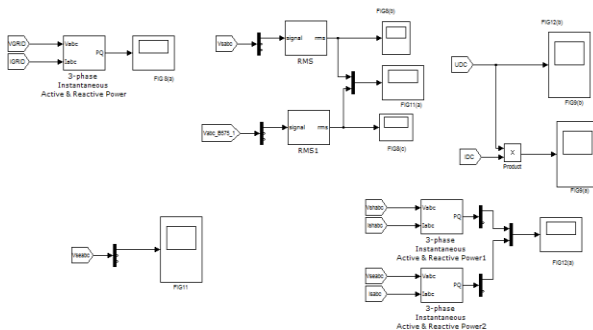


Fig. 7 Simulink diagram for UPQC Sub system

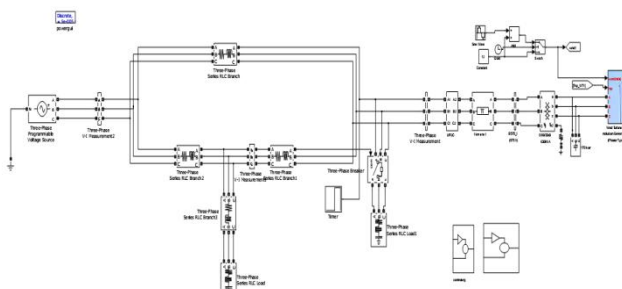


Fig. 8 Main Simulink diagram for UPFC

At $t = 0.5''$ begins the cyclical power pulsation produced by the tower shadow effect. As was mentioned, the tower shadow produces variation in torque, and hence in the active and reactive WF generated power. For nominal wind

speed condition, the power fluctuation frequency is $f = 3.4$ Hz, and the amplitude of the resulting voltage variation at PCC, expressed as a percentage is 1.50%. This voltage fluctuation is seen in middle curve of Fig. 9 & Fig. 10 for $0.5 < t < 3$.

The fluctuation value is higher than the maximum allowed by the IEC61000-4-15 standard. This means that even in normal operation, the WF impacts negatively on the System Power Quality. At $t = 3.0''$ the active and reactive power pulsations are attenuated because the P and Q controllers come into action. The amplitude of the PCC voltage fluctuation is reduced from its original value of 1.6% (without compensation) to this new value 0.18% (with compensation). The pulsation of active power and voltage at the UPQC DC-side, are shown in Fig. 9

As can be observed in the upper curve, the series converter requires negligible power to operate, while the shunt converter demands a high instantaneous power level from the capacitor when compensating active power fluctuation. Compensation of reactive powers has no influence on the DC side power.

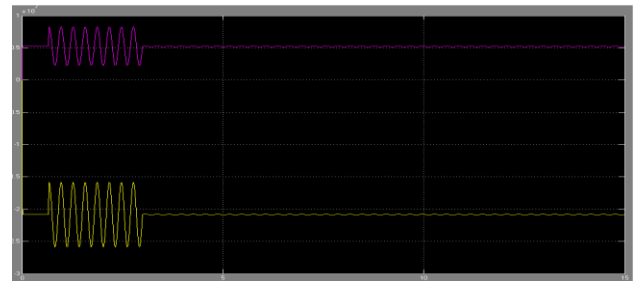


Fig. 9 active and reactive power demand at power grid side

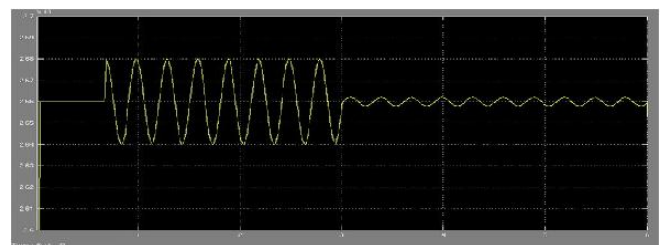


Fig. 10 PCC voltage

The DC-bus has voltage level limitations in accordance with the VSI's operational characteristics. As the fluctuating active power is handled by the capacitor, its value needs to be selected so that the "ripple" in the DC voltage is kept within a narrow range.

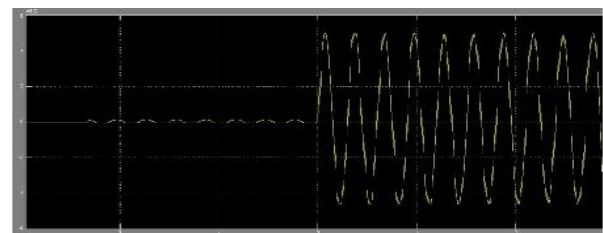


Fig. 11 Power of the capacitor in the DC-Bus

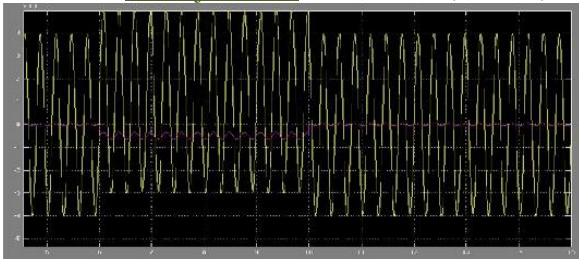


Fig. 12 Shunt and Series Active Power

In the upper curve of Fig.11 and Fig. 12 is seen shunt and series converter active power behavior. The mean power injected (absorbed) by series converter is absorbed (injected) by shunt converter, because of DC voltage regulation loop action (Fig.9). So, the step in series converter active power is the same but opposite sign, that shunt converter power. Fig.12 also shows DC-bus voltage, and is clearly seen the VDC control action

IV. CONCLUSION

In this paper, a new compensation strategy implemented using an UPQC type compensator was presented, to connect SCIG based wind farms to weak distribution power grid. The proposed compensation scheme enhances the system power quality, exploiting fully DC-bus energy storage and active power sharing between UPQC converters, features not present in DVR and D-Statcom compensators. The simulation results show a good performance in the rejection of power fluctuation due to "tower shadow effect" and the regulation of voltage due to a sudden load connection. So, the effectiveness of the proposed compensation approach is demonstrated in the study case. In future work, performance comparison between different compensator types will be made.

REFERENCES

- [1] M.P. Pålsson, K. Uhlen, J.O.G. Tande. "Large-scale Wind Power Integration and Voltage Stability Limits in Regional Networks"; IEEE 2002. p.p. 762–769
- [2] P. Ledesma, J. Usaola, J.L. Rodriguez "Transient stability of a fixed speed wind farm" Renewable Energy 28, 2003 pp.1341–1355
- [3] P. Rosas "Dynamic influences of wind power on the power system". Technical report RISØR-1408. Ørsted Institute. March 2003.
- [4] R.C. Dugan, M.F. McGranahan, S. Santoso, H.W. Beaty "Electrical Power Systems Quality" 2nd Edition McGraw-Hill, 2002. ISBN 0-07- 138622-X
- [5] P. Kundur "Power System Stability and Control" McGraw-Hill, 1994. ISBN 0-07-035958-X
- [6] N. G. Hingorani y L. Gyugyi. "Understanding FACTS". IEEE Press; 2000.
- [7] Z. Saad-Saoud, M.L. Lisboa, J.B. Ekanayake, N. Jenkins and G. Strbac "Application of STATCOM's to wind farms" IEE Proc. Gen. Trans. Distrib. vol. 145, No. 5; Sept. 1998
- [8] T. Burton, D. Sharpe, N. Jenkins, E. Bossanyi "Wind Energy Handbook" John Wiley & Sons, 2001. ISBN 0-471-48997-2.
- [9] A. Ghosh, G. Ledwich "Power Quality Enhancement Using Custom Power Devices" Kluwer Academic Publisher, 2002. ISBN 1-4020-7180- 9

- [10] C. Schauder, H. Mehta "Vector analysis and control of advanced static VAR compensators" IEE PROCEEDINGS-C, Vol.140, No.4, July 1993.
- [11] E.M. Sasso, G.G. Sotelo, A.A. Ferreira, E.H. Watanabe, M. Aredes, P.G. Barbosa, "Investigação dos Modelos de Circuitos de Sincronismo Trifásicos Baseados na Teoria das Potências Real e Imaginária Instantâneas (p-PLL e q-PLL)", In: Proc. (CDROM) of the CBA 2002 – XIV Congresso Brasileiro de Automática, pp. 480-485, Natal RN, Brasil, 1-4, Sep. 2002
- [12] International Electrotechnical Commission "INTERNATIONAL STANDARD IEC 61000-4-15: Electromagnetic compatibility (EMC) Part 4: Testing and measurement techniques Section 15: Flickermeter Functional and design specifications." Edition 1.1 2003
- [13] H. Akagi, E. H. Watanabe, M. Aredes "Instantaneous power theory and applications to power conditioning", John Wiley & Sons, 2007. ISBN 978-0-470-10761-4.

Investigating the Effect of Pounding on Seismic Response of Isolated Structures

Saeed Hedayat

Department of Civil Engineerin, uneversity of guilan, Rasht, Iran

Abstract: Some investigations have been conducted on pounding phenomenon in fixed base buildings and results showed that most sever damages are pertaining to adjacent buildings with different (unequal) heights or different structural systems [1,3]. But few investigations have been carried out for poundings of isolated buildings. In a case study about Fire Command and Control (FCC) building in Los Angeles which collided with its adjacent structure during Northridge earthquake, it was shown that peak ground acceleration in pounding direction increased from 0.22 g to 0.35 g while in other direction, in which no pounding occurred, the ground acceleration reduced from 0.18 g to 0.07 g which demonstrates good performance of seismic isolation when a pounding occurs.

Key words: seismic isolation, pounding, earthquake, seismic gap

I. introduction:

In recent years, there has been a growing demand for both reducing structural and non-structural damages and preventing any failure in performance and protection of equipments and costly sensitive components of buildings during earthquake. Seismic isolation as a new approach in design and one of practical methods for reduction of seismic damages has grown considerably during the last two decades [1-6]. In the most common method of seismic isolation, by insertion of flexible abutments at foundation level of building, the system time period increases to a value more than predominant earthquake energy containing time periods. Therefore, since the isolated structure has lower fundamental frequency than both frequency of fixed base buildings and predominant frequencies of ground motions, in the first vibrational mode of isolated building displacement s only occur at isolation level and abutments and superstructure approximately remains rigid and consequently acceleration of the floor reduces considerably. Hence, seismic isolation is considered as an appropriate approach for reducing damages of internal non-structural components [4]. Nevertheless, one of practical limitations in implementation of isolation is required seismic gap around the structure to accommodate large displacements at isolation level. In some cases of seismic isolations, this provided gap at isolation level is not sufficient during earthquake event. Therefore, there is possibility that the isolated structure collide with adjacent structure during one strong earthquake [3-5].

II. Modeling:

The isolated building has been modeled as a shear model with masses lumped at the floors level and it has been assumed that superstructure remains within elastic limit [1, 3, 4], because one purpose of seismic isolation is preventing non-elastic displacements in the structure. Damping and elastic forces of isolation level depend on isolation system characteristics which are modeled linearly in this study. Pounding has also been modeled by introducing k_{imp} and c_{imp} which are used for calculating both elastic and damping forces of impact (figure 1). Damping (c_{imp}) was introduced for modeling dissipated energy during the impact. The point of impact is assumed exactly at base mass level and isolation level diaphragm. Effects of interactions between soil and structure are ignored [1-5]. Also since energy dissipation mechanism of the isolated building is not uniformly distributed and it considerably differs from isolation system to superstructure, damping is considered to be non-classic. Damping matrix \underline{C} for the isolated building is calculated by assembling (اسمیل کردن) the provided damping by isolation system c_{iso} and damping matrix c_{sup} which is corresponding to superstructure damping [1, 3].

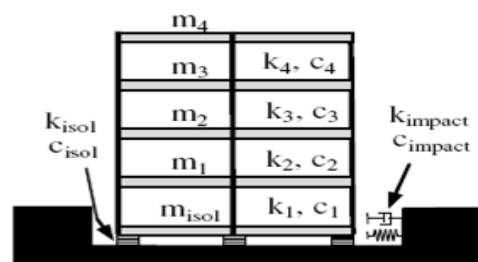


Figure 1. The isolated building, seismic gap [3].

In order to demonstrate effects of pounding on structure behavior, one four-story building was considered under below conditions:

- Fixed base
- Isolated without impact
- Isolated with 15 cm seismic gap at isolation level (about 15% less than required amount)

The fixed base building has four stories, each has mass and stiffness of 500 tons and 1000 MN/m, respectively. Its time period is also equal to 0.4 sec. In the case of isolated building, the mass of each floor is the same as the fixed base building and only one additional rigid diaphragm with mass of 500 tons is considered at isolation level. Time period and effective stiffness of isolators in this case are 1.44 sec and 50 MN/m, respectively. Classical Rayleigh damping has been used for the fixed base building whereas non-classical damping has been considered for the isolated building. The fixed base building damping ratio is considered to be 5%. Superstructure and isolation system damping ratios for energy dissipation are equal to $\xi_{sup} = 5\%$ و $\xi_{iso} = 15\%$. In the case of pounding, impact damping coefficient and impact stiffness coefficient are equal to $c_{imp} = 2000 \text{ MNs/m}$ and $k_{imp} = 2500 \text{ KN/mm}$. Impact stiffness coefficient is obtained using finite element methods and by analysis of the impact between concrete wall (دال) of isolation level and concrete wall of adjacent structure having height of 2.5 m and thickness of 25 cm. [1, 3]. Then for all above cases, one dynamic analysis was performed using 1994 Northridge earthquake, as a known strong earthquake, record. Maximum displacement of isolation level under this earthquake was obtained to be $U_{max}^{iso} = 179 \text{ mm}$ which shows assuming 15 cm gap around the structure an impact with isolation level wall occurs. Also the results showed that for the case of poundings interstory displacements, floor shear forces and floor accelerations increase considerably.

Below table lists the obtained results from analysis of this structure.

Table 1. Maximum response values of the fixed base building and the isolated building in case of pounding and no pounding, under Northridge earthquake.

	Fixed base building	Isolated building (without impact)	Isolated building (with impact)
Time period (sec.)	0.4	1.44	1.44
Peak interstory displacement (mm)	20	7	12
peak floor acceleration (/s ²)	13.67	4.14	9.85
peak base shear force (MN)	20.3	8.9	12.2

Based on obtained results, absolute floor acceleration under Northridge earthquake remarkably is influenced by impact and its value for the isolated building is about two times more than the value in the case of no impact and it is almost the same as absolute floor acceleration in the fixed base building. According to the fact that one of main purposes of seismic isolation is reduction of floor acceleration and consequently protection of internal equipments, the results show that when an impact occurs, the performance of seismic isolation significantly reduces. Effect of some parameters on behavior of the isolated building during pounding was also investigated and the results are discussed in the following sections.

III. Effect of isolation system softness (horizontal stiffness)

In order to investigate effect of isolation system softness, time period of four-story isolated building was varied in the range of 1.0-4.0 sec and each system was analyzed under Northridge earthquake and with gap widths of 15 cm, 20 cm, 30 cm and ∞ (without impact). Figures 2 and 3 demonstrate results of these analyses for maximum floor displacement (drift), maximum floor acceleration and maximum base shear force.

The maximum floor acceleration and maximum base shear force for the fixed base building with time period of 0.4 sec are equal to 13.7 m/s^2 ($2.3 \times \text{PGA}$) and 20.3 MN, respectively. This value of maximum base shear force is almost the same as weight of the structure (24.5 MN). According to the results, it can be concluded that pounding of an isolated structure can increase the floor acceleration and reach it to a value several times more than PGA (peak ground acceleration) and increase the structure response to the values experienced in the case of fixed base or even more. This can be very destructive for components of the structure. The results showed that in some cases, peak floor acceleration can be experienced despite larger gap sizes.

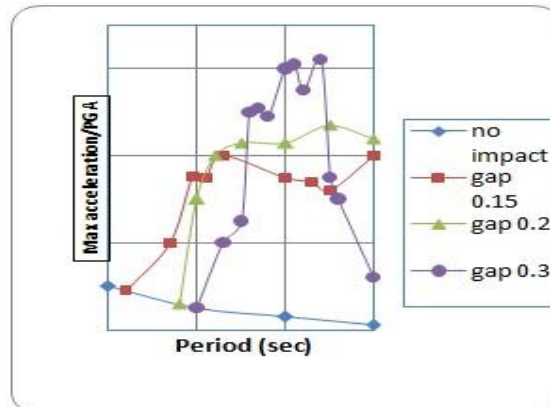


Figure 2. Variation of maximum floor acceleration Versus time period [3].

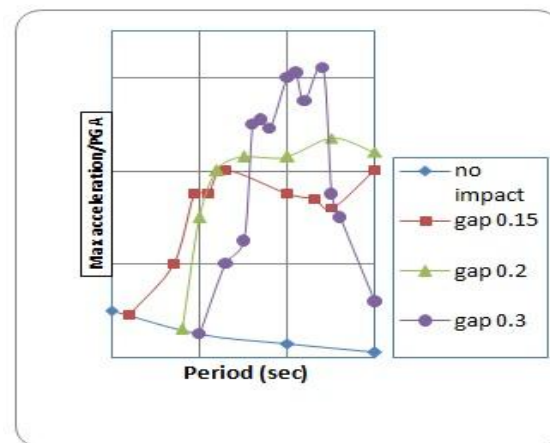


Figure 3. Variation of maximum relative displacement versus time period [3].

IV. Effect of superstructure stiffness

In this section the effect of superstructure stiffness on the isolated building response during impact is investigated. For this aim, flexibility of the studied four-story building is varied and the responses are studied for four different seismic gap sizes of 10 cm, 13 cm, 16 cm and ∞ using Northridge earthquake record (Figures 4,5 and 6). The results are presented in below figure for maximum interstory displacement, maximum floor acceleration and maximum base shear. The results of maximum acceleration and maximum floor shear are normalized with respect to PGA and weight of the structure, respectively and normalized responses are presented as a function of ratio of superstructure stiffness to isolation system stiffness. The results indicate that with increasing superstructure flexibility, interstory displacements increase remarkably but a minor increase occurs in floor acceleration. It is obvious that increasing interstory displacements is very important for damages of structural and non-structural components and they should be controlled. In this study it was found that interstory displacement and floor acceleration reduce as seismic gap around the structure becomes larger.

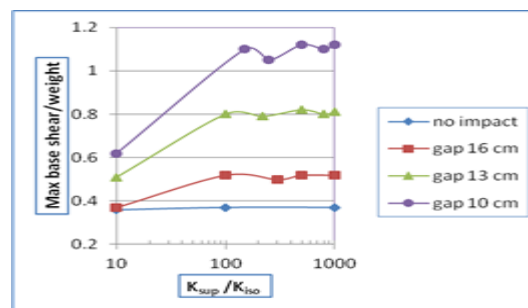


Figure 4. variation of relative displacement versus changes in superstructure stiffness.

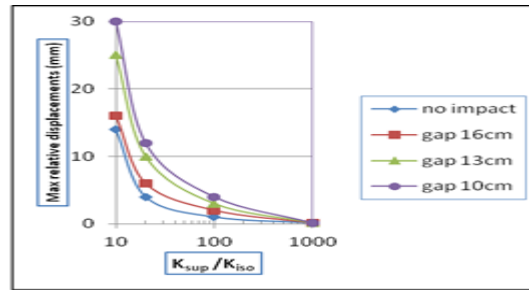


Figure 5. Variation of acceleration versus changes in superstructure stiffness

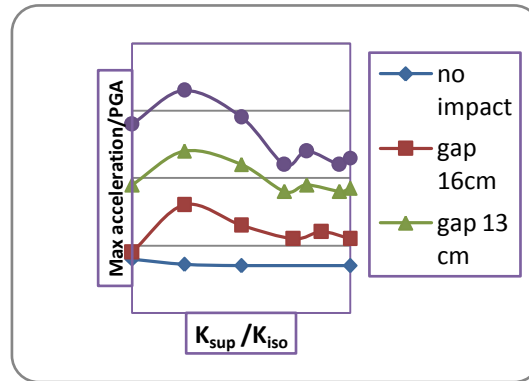


Figure 6. Variation of base shear versus changes in superstructure stiffness.

V. Effect of damping:

Recent researches have shown that employing supplemental damping devices such as viscous dampers can reduce relative displacement of base level in the isolated building under strong ground motions and earthquake near fault [6]. Hence, in order to investigate the effect of damping on reduction of destructive effects of impact, some analyses were conducted. For this aim, the isolated building was analyzed using different earthquake records and the results showed that relative displacement of isolation level reduces as damping ratio increases (figure 7). Consequently, the possibility of pounding with adjacent structure is reduced. It was also found that impact velocity reduces with increasing damping ratio (figure 8). Therefore, employing supplemental damping devices at isolation level can be useful for reducing destructive effects of pounding. But anyway increasing damping has some limitations because it leads to an increase in both interstory displacement and absolute floor acceleration.

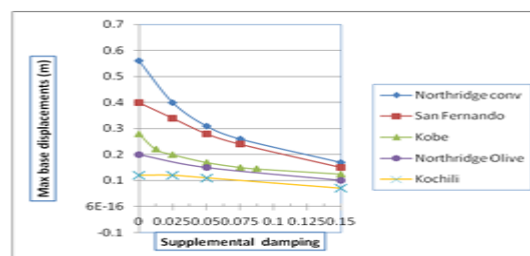


Figure 7. Variation of maximum base displacement versus changes in damping [1].

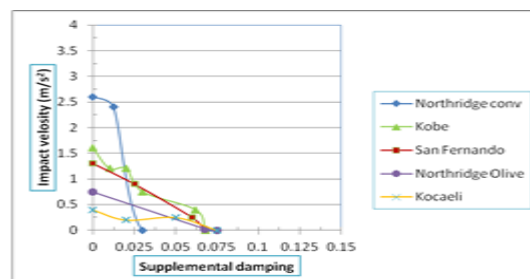


Figure 8. Variation of maximum impact acceleration versus damping [1].

In order to reduce destructive effects of pounding on the isolated building behavior, sudden changes of stiffness can also be avoided by insertion of flexible materials with damping properties, such as bumpers, at certain points at isolation level expected to experience impact. In this way, sudden increases in acceleration due to sudden impact to some extent can be prevented. For this aim, the studied four-story building was studied under below conditions using Northridge earthquake record to determine advantages of using bumpers:

- a) A seismic gap equal to 10 cm without using bumper
- b) A seismic gap equal to 10 cm with using a 5 cm thick bumper
- c) A seismic gap equal to 15 cm
- d) Base condition

Interstory displacements, floor acceleration, inertia and elastic forces are listed in below table. The results indicate that employing bumper at isolation level have positive effects on the structure behavior. It also must be mentioned that using damping devices (bumper) always does not lead to improvement of structure response. For example in the case where pounding may occur slightly, insertion of such devices may cause structure response to increase.

Table 2. Response values of the structure for different conditions of seismic gap with and without employing bumper at isolation level [3].

	(a)	(b)	(c)	(d)
Interstory displacement (mm)	18.6	11.5	12.2	17.9
Maximum floor acceleration (PGA)	3.28	1.17	1.66	2.31
Maximum inertia force (MN)	9.7	3.47	4.9	6.8
Maximum elastic forces (MN)	18.6	11.5	12.2	20.3
Maximum impact force (MN)	13.3	5.2	5.6	-

VI. Conclusion:

In this paper, it was tried to indicate destructive effects of pounding on isolated structures behavior relying on pervious researches and effects of some parameters on structure behavior were also investigated. The results showed that performance of seismic isolation may reduce significantly under the influence of pounding phenomenon. This phenomenon leads to an increase in acceleration and intersory displacements as well as excites higher modes of deformation of isolated building and causes the superstructure to behave no longer like a “rigid body”. Therefore, taking into account the possibility of pounding in seismically isolated structures which experience large displacements is essential. Also it should be tried prevent pounding phenomenon specially in softer isolation systems because it immensely reduces performance of isolated building and in some cases floor accelerations become much higher than those for the fixed base building while the main purposes of seismic isolation are reducing floor acceleration and protecting internal components of structure. In order to reduce the intensity of pounding, it is also recommended to employ impact reducing devices such as bumper and flexible materials at isolation level. This leads to prevention of sudden changes in stiffness as well as reduction of destructive effects of impact.

Choosing the Best Probabilistic Model for Estimating Seismic Demand in Steel Moment Frames

Saeed Hedayat¹, Omolbanin Arasheh Khoshbin²

¹Department of Civil Engineerin, uneversity of guilan, Rasht, Iran

²Department of Civil Engineering, Lashtenesha-Zibakenar Branch, Islamic Azad University, Lashtenesha, Iran

Abstract: Provided that fundamental components of an quake demand, capacity and limiting conditions, to be reasonably determined. The great crash due to uncertainty and the structural response to that exists. It should be said that estimation of seismic demand of structures has become a major challenge. The reason is that the seismic demand using a probabilistic framework is possible. A method commonly known by the name of probabilistic seismic demand. The main core of probabilistic seismic analysis of the fundamental components of modern design method is based on the model of probabilistic seismic demand. The main task of selecting an appropriate model is establishing a mathematical relationship between seismic demand parameters and ground motion severity index is the seismic demand cause a significant increase in the accuracy of estimated. Such pre a field, selected the best model for probabilistic seismic steel moment resisting frames based on such factors as for applicability, effectiveness, efficiency and adequacy will be main in this research. The main task of selecting an appropriate model to establish a mathematical relationship between the intensity of ground motion index and parameter of seismic demand and can cause a dramatic increase in accuracy of seismic demand estimate. With such a background, choosing the best model for probabilistic seismic demand about steel moment resisting frames based on factors such as practicality, effectiveness, efficiency and efficiency is carried out. The main objective of this research in this selection, is the use of a fully methods in statistical calculations, which are very powerful tool in the simultaneous bayesian modeling of the accident, and caused the results obtained to be reliable and practical. In this paper, out of the models of probabilistic seismic demand with a single severity index, with a combined severity index, and with two single severity indexes, the best model is selected. The results show that the model's current estimates seismic demand, in terms of first-mode spectral acceleration. Frames with different levels of accuracy and precision are not identical in tall frames lose their accuracy in tall buildings. Also, due to the problems on the model being applied is a combination of indicators It seems that the best model is the model can be found with two single severity index. Based on these results, the model is a linear combination of spectral accelerations of first and second modes.

Keywords: Probabilistic models for seismic demand, steel moment frame, demand estimation, performance-based design

I. Introduction

Estimating seismic demand is one of the main components of a new method for performance-based design. In this way, a reasonable estimate of the parameters of the seismic demand is generally chosen to represent a structural displacement response that is nonlinear behavior of structures. It is inevitable for comparison with the amount of the performance-based design framework [1]. But the biggest challenge in estimating seismic demands is uncertainty in the quantity and frequency of accidents. This source of uncertainty can be of two types, namely uncertainty in earthquake ground motions (such as earthquake magnitude, distance, etc.) as well as uncertainties in the nonlinear behavior of structures (such as hard, plasticity, nonlinear functions, etc.). So it is natural that the uncertainty is required to perform the estimation due to the accident, using a probabilistic framework. Probabilistic seismic demand analysis is applied to such a framework [2]. The usual method for creating such a framework is based on removing the uncertainty of seismic behavior of structures with uncertainties by using a parameter called severity index (Intensity Measure), [3]. Various studies have shown that the first-mode spectral acceleration, spectral acceleration, especially, SA1, can be an appropriate severity index [4]. Severity index is a parameter that on the one hand cans the risk level of the earthquake, and on the other hand it could be indicative of the level of seismic risk at different levels of performance, it was connected to the seismic demand parameters. So in this way, the problem of estimating seismic demand turns into two separate issues, seismology, and the other one structural. If the seismic demand parameter is the maximum relative displacement between classes and selected to be shown with DR IM, severity index mark is displayed, the seismic demand estimation problem can be solved as follows [2]:

$$P[DR > x] = \int P[DR > x | IM = y] \cdot dH_{IM}(y) \quad (1)$$

In this expression, HIM (y) means annual incidence of IM parameters exceed a certain value, or in other words the curve y parameter of the differential severity index that has been used at point y. This is generally calculated by probabilistic seismic hazard analysis method that this paper does not focus on it; there are several references [4]. An important component of this relationship, the term P [DR > x | IM = y] means the probability that the seismic demand parameter exceeds a certain value of the parameter x if y is interpreted to be of equal intensity.

In essence, it is the task of linking parameters of indices and parameters of seismic demand that is responsible for the distribution and is calculated assuming a normal distribution of data and the use of a probabilistic model. The core of the estimation of seismic demand, the demand for seismic probabilistic model (Probabilistic Seismic Demand Model) or PSDM is short. PSDM is a general mathematical relation of the parameters of the different functional levels of seismic demand parameters.

The probabilistic relationship between the mean and the standard deviation is a functional level, although the standard deviations are generally considered to be constant.

In fact, this short article also demonstrates the role of a probabilistic model for estimating seismic demand. Therefore, the present study was done in order to choose the best model for probabilistic seismic demand for structural steel bending of the frame. The seismic demand parameter is the maximum relative displacement between classes, based on various studies, it is more suitable for describing the behavior of a response of steel moment frames, especially in the overall structure in collapse mode.

II. Generic frames used for modeling of steel moment frames

One of the main goals of this paper is to obtain results that can be generalized for all of steel moment frames. To this end, the general frame concept is used to model structures [5]. In this research, the nonlinear behavior of the users is applied using rotational springs (stiffness and resistance to decay) at the foot of the beams and columns Peak-Oriented Modeling and model for showing the behavior of the hysteresis loop (Hysteresis Curve) as well as to consider a cycle of decline by the model of Ibarra et al. In this paper the general frame of five classes 3, 6, 9, 12 and 15 floors are being used on the cover of the first mode period equal to one-tenth of their classes, respectively, 3/0, 6/0 9 / 0, 2/1 and 5/1 second. The next two legal costs, charges the same for all classes, high and during the opening of classes they are respectively 12 and 24 feet. The latest software version is OPENSEES. The software is extremely powerful nonlinear analysis of structures, has been helping.

III. Selecting accelerators suitable for nonlinear dynamic analysis

In this study, 80 of the theoretical value based on the standard terms of magnitude and distance Bin Strategy are selected and divided into four groups of 20 were classified as follows [6].

- A long, long distance (LMLR) Features: 6.5 <MW <7.0 30 Km <R <60 Km
- A very short distance (LMSR) Features: 6.5 <MW <7.0 30 Km <R <60 Km
- A low, long distance (SMLR) Features: 5.8 <MW <6.5 30 Km <R <60 Km
- A small, short distance (SMSR) Features: 5.8 <MW <6.5 13 Km <R <30 Km

IV. Analysis of nonlinear dynamical accelerator

Unknown parameters in a model of probabilistic seismic demand should be estimated according to the results of nonlinear dynamic analysis. Dynamic multiplier analysis is the best format for the analysis [7]. In this analysis, using a scale factor which can be larger or smaller than a parameter of theoretical intensity, gradually from a very low level to high level, which is the cause of severe nonlinear behavior of structures be to scale.

In this paper, in order to create a complete database, which can be a basis for estimating the unknown parameters of the probability models used in seismic applications, enabling dynamic analysis of structural models under the three main uses 80 theoretical introduction to the [8]. As an example of the results of the dynamic analysis enhancer for frames 3 and 15 in Figure (1) is observed. It should be noted that in order to avoid being crowded figure, only the results of the theoretical group of 20 is seen instead of 80 theoretical LMLR. This is shown in Fig.

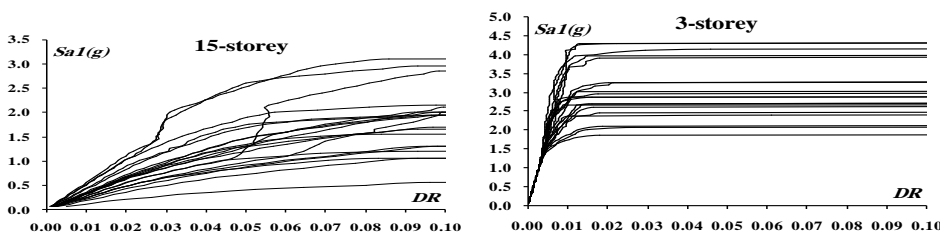


Figure 1 - Results of the dynamic analysis of accelerator in frames 3 and 15 floors LMLR

V. Evaluating the precision of probabilistic models of seismic demand

The main objective of this study was to select the best model probabilistic seismic demand for steel moment frames. To do this, different models for each of these frames is defined in terms of adequacy, efficiency and applicability. The SD model which in fact is accurate in estimating seismic demands can be a very good criterion for judging its main objective is to estimate the standard deviation using Bayesian statistics. The adequacy of the model can be attributed to the constant SD and SD to the low efficiency of the model is defined. Models defined in this study, three groups according to their severity index used in the model with a single severity index, a model with a combination of indicators and models are divided into two single severity index.

VI. Model with a single intensity index

The easiest way to build a probabilistic model of seismic demand is using a four-parameter peak ground acceleration (PGA) and spectral acceleration at the first mode, second and third order vibration with SA1, SA2 and SA3, as an indicator of severity. In this way, the four models of probabilistic seismic demand can be derived as follows:

Model No01: $\ln(DR) = a \cdot \ln(PGA) + w + \sigma \cdot \varepsilon$

Model No02: $\ln(\text{DR}) = a.\ln(\text{SA1}) + w + \sigma.\varepsilon$

Model No03: $\ln(\text{DR}) = a.\ln(\text{SA2}) + w + \sigma.\varepsilon$

Model No04: $\ln(\text{DR}) = a.\ln(\text{SA3}) + w + \sigma.\varepsilon$

However, in order to select the best model, it is necessary to use Bayesian statistics; the standard deviation of the four models, the model covers a number of different classes of σ to be estimated. Figure (2), standard deviation estimates for the four models No01 to No04 frame model is shown separately.

What is clear from Figure (2) concluded that the standard deviation of models is largely dependent on the number of classes. In other words, the accuracy of these models and the number of classes are different and it's not a good sign because it indicates this model is inadequate. Although the seismic demand model based on first-mode spectral acceleration estimates in short time frames 3 and 6 class, the best model, and the accuracy is quite good and efficient model is considered. But with increasing numbers of classes of frames, standard deviations, and also increases the accuracy of the model loses its effectiveness, so that the frames 9, 12 and 15 floors, the model is considered inefficient.

Notable is that the frame 15 floors, this model is the weakest model, based on the seismic demand model No03 second mode spectral acceleration estimates, accurate models, but the three-story model frame, the model is the weakest. Perhaps the only adequate model among the four models, Model No01 maximum ground acceleration based on the seismic demand estimates. But the problem is that the standard deviation is high because the model is inefficient.

Applying the case of the four models, so there is no need to talk, because all they do in terms of feasibility analysis and probabilistic seismic hazard calculations simply because they are in the best position possible, and fully functional.

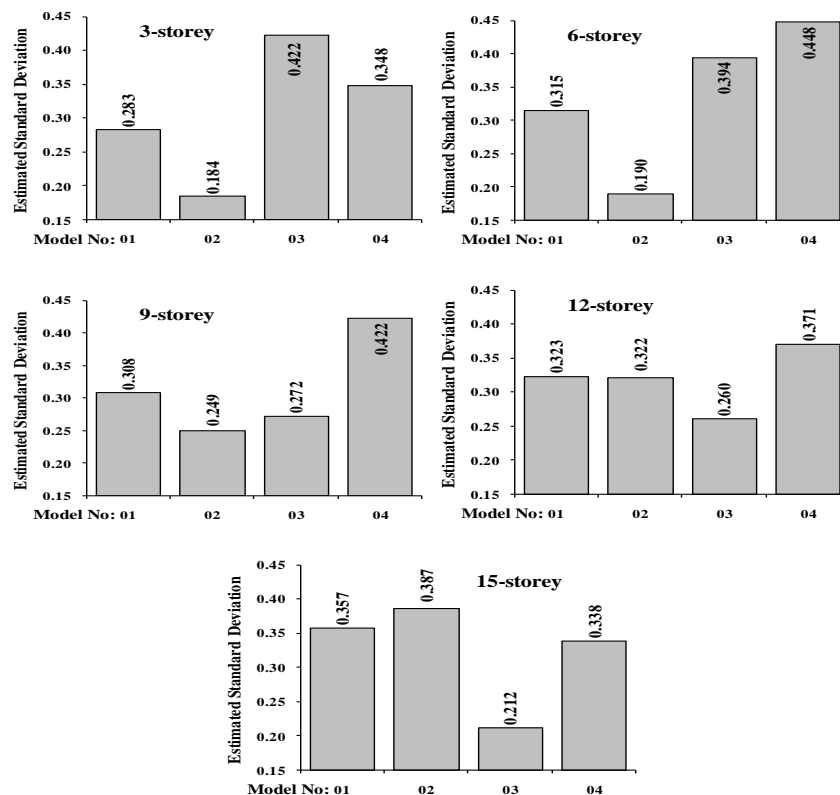


Figure 2 - Standard deviation of the estimated probabilistic models with a single severity index

In general, and as a result it should be stated that although the four models built in this area, they are simple and functional, but should be viewed with suspicion in their performance and efficiency.

In other words, none of the models can be a single severity index as the best model for all frames with different classes recommended. It seems that the use of such models in estimating seismic demand to prevent a selective effect on the model results for different structures of the different models used.

VII. Model with a combination of indicators

This section will attempt to use a combination of parameters, optimum probabilistic model is constructed. In order to use the four parameters PGA, SA1, SA2 and SA3, thirteen combined severity index is defined as IM used to be made of 13 different models as follows.

Model No05: $\ln(\text{DR}) = a.\ln\left(\frac{SA1 + PGA}{2}\right) + w + \sigma.\varepsilon$

Model No06: $\ln(\text{DR}) = a.\ln\left(\frac{SA1 + SA2}{2}\right) + w + \sigma.\varepsilon$

Model No07: $\ln(\text{DR}) = a.\ln\left(\frac{SA1 + SA3}{2}\right) + w + \sigma.\varepsilon$

Model No08: $\ln(\text{DR}) = a.\ln(\sqrt{SA1.PGA}) + w + \sigma.\varepsilon$

Model No09: $\ln(\text{DR}) = a.\ln(\sqrt{SA1.SA2}) + w + \sigma.\varepsilon$

Model No10: $\ln(\text{DR}) = a.\ln(\sqrt{SA1.SA3}) + w + \sigma.\varepsilon$

Model No11: $\ln(\text{DR}) = a.\ln(\sqrt{SA1^2 + PGA^2}) + w + \sigma.\varepsilon$

Model No12: $\ln(\text{DR}) = a.\ln(\sqrt{SA1^2 + SA2^2}) + w + \sigma.\varepsilon$

Model No13: $\ln(\text{DR}) = a.\ln(\sqrt{SA1^2 + SA3^2}) + w + \sigma.\varepsilon$

No05 to No13 SD models are estimated using Bayesian statistics, in the form (3) has shown, it can be about the performance and efficiency of these models has commented.

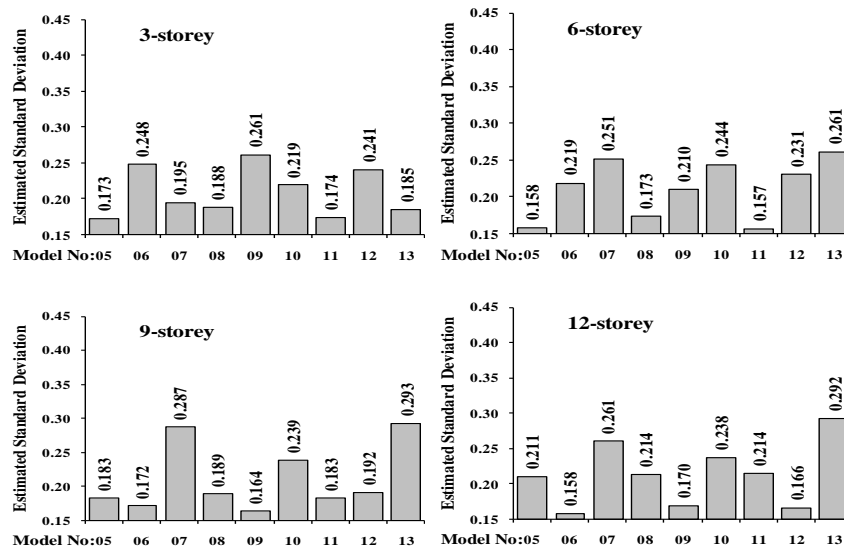


Figure 3 - Standard deviation of the estimated probabilistic models with a combination of indicators

The significant point is that the results can be seen in general SD model built in the previous section, this model is less. These models can also be argued that the standard deviation is relatively independent of the number of classes. Although this may partly reflects the efficiency of models, but it still seems to be one of the models to be recommended as an ideal model. In fact, as is known, none of these models to estimate demand at various heights is not appropriate for all legal fees.

In other words, the optimal models in short time frames within frames Rank high with good models are different. The main problem with this model is being applied. The particular combination of parameters used in the model causes they use a lot of problems associated with the performance-based design framework, because the common practice for determining seismic hazard curves using probabilistic seismic hazard analysis exists. Also, you can see that in this model, a very poor indicator of the high degree of accuracy is being exhausted. An obvious example of such a story, three-story frame model No06 spectral acceleration mode in which the first mode spectral acceleration has reduced accuracy.

In an overall assessment, using a combination of indicators can increase the efficiency and adequacy of the model is a probabilistic seismic demand and maybe even good enough to be a model. But before using such a model, two points

should be considered in the first place to define the composition of the index parameter is used to ensure the efficiency and adequacy of the model for all frames. Second, the severity index is defined for a relationship, lowering the production of specific probabilistic seismic hazard analysis to be used in the application and satisfies these criteria extremely well crafted.

VIII. Model with two single intensity index

In this section we build a probabilistic model for seismic intensity using a single index is used. With the four parameters, PGA, SA1, SA2 and SA3, six models can be defined as follows:

Model No14: $\ln(DR) = a.\ln(SA1) + b.\ln(PGA) + w + \sigma.\varepsilon$

Model No15: $\ln(DR) = a.\ln(SA1) + b.\ln(SA2) + w + \sigma.\varepsilon$

Model No16: $\ln(DR) = a.\ln(SA1) + b.\ln(SA3) + w + \sigma.\varepsilon$

Model No17: $\ln(DR) = a.\ln(PGA) + b.\ln(SA2) + w + \sigma.\varepsilon$

Model No18: $\ln(DR) = a.\ln(PGA) + b.\ln(SA3) + w + \sigma.\varepsilon$

Model No19: $\ln(DR) = a.\ln(SA2) + b.\ln(SA3) + w + \sigma.\varepsilon$

The estimated standard deviation of the model using Bayesian statistics in the form of (4) is on display. This means the Model No15, which is a linear combination of the first and second mode spectral acceleration and standard deviations of the different frameworks, both in terms of efficiency and adequacy of the condition is quite good. The big advantage of this model is able to accurately estimate both its severity index is the seismic demand.

The problem is that the standard deviation and accuracy, it is always constant and satisfactory. SD model, compared with the models introduced in the previous section is very good and it can be concluded that the accuracy is unparalleled in the estimation of seismic demand. It should be noted that the application of these models requires further evaluation. The practical problem is the same as the previous section, the possible lack of probabilistic seismic hazard analysis criteria in their intensity, but the use of these models, the models that are in an index, the calculation is more difficult and require more time to volume for their calculations.

But the problem is not caused by the use of the framework design and performance estimation of seismic demand, is impossible.

However, considering all aspects can be probabilistic model No15 as a model for optimal seismic steel moment frames for seismic demand estimation presented with a number of different classes [9].

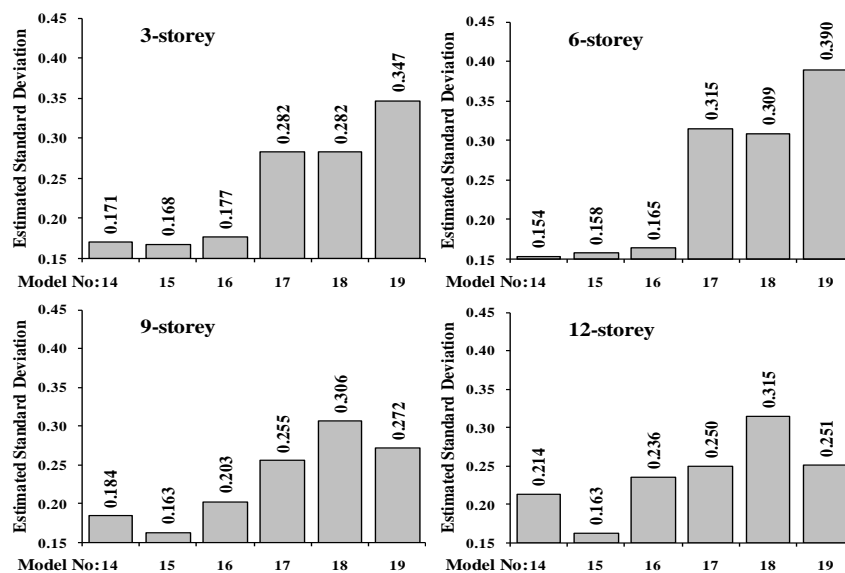


Figure 4 - SD estimated probabilistic models with two single severity index

IX. Conclusions

In this paper, the best model of probabilistic seismic demand for steel moment frames using Bayesian statistics is selected. Given the importance of estimating seismic demand, such a model can have an important role in the performance based design.

All results obtained in this study are summarized in the table below and can be based on their conclusion that the current model, the estimation of the seismic demand model with first-mode spectral acceleration, high efficiency is not required and the total finest model with a linear combination of the first and second mode spectral acceleration is introduced.

Table 1 - Summary of results from the various models of probabilistic seismic demand Probabilistic seismic demand model with a single parameter Severity Index

Some frames in model performance is acceptable, but in others a very low efficiency. Adequacy of the model is generally acceptable, except perhaps the models that have low efficiency.

Application model, the probabilistic analysis of seismic hazard in terms of practicality and ease of calculation, it is in the best position possible.

General recommendation to use this model as the model is unique in design framework based on function is not recommended. If such models are to be used to estimate the demand for each frame is used to define a model of its own.

Probabilistic seismic demand models with a combination of indicator parameters if you select the right combination of model performance indicators can be acceptable. Adequacy of the model is acceptable.

Applicability of the model of computation is not difficult, but impossible to use it, usually within a seismic hazard analysis.

Overall recommendation - a good combination of indicators, selection, and use within the context of the problem of probabilistic seismic demand is high, given that the performance is satisfactory enough can be a good model.

Probabilistic seismic demand models of the two parameters of a single Model performance are acceptable. Adequacy of the model is acceptable.

Application model, the probabilistic seismic hazard analysis may be no problem, but the volume is very high and many components calculations for estimating seismic demand needs.

General recommendation if the volume of computation and time consuming if they use this model to be adopted model is very suitable and acceptable.

Resources

1. Cornell, C., Jalayer, F., Hamburger, R., and Foutch, D., (2002) "The probabilistic basis for the 2000 SAC/FEMA steel moment frame guidelines," *Journal of Structural Engineering (ASCE)*, **128**, pp 526–533.
2. Luco, N., (2002), "*Probabilistic seismic demand analysis, SMRF connection fractures, and near source effects*," Ph.D. Dissertation, Department of Civil and Environmental Engineering, Stanford University, Stanford, CA, 260 pp.
3. Shome, N., (1999), "*Probabilistic seismic demand analysis of nonlinear structures*," Ph.D. Dissertation, Department of Civil and Environmental Engineering, Stanford University, Stanford, CA, 260 pp.
4. Mahdavi Adeli, M., Banazadeh, M., Deylami, A. (2010), "A Bayesian Approach to Probabilistic Seismic Demand Analysis of Steel Moment-Resisting Frames," *Proceedings of the 9th US National and 10th Canadian conf. on earthquake engineering*, Canada, Toronto, paper ID 368.
5. Luco, N., Mori, Y., Funahashi, Y. and Nakashima, M., (2003), "Evaluation of predictors of non-linear seismic demands using 'fishbone' models of SMRF buildings," *Earthquake Engineering and Structural Dynamics*, **32**, pp 2267-2288.
6. Medina, R. and Krawinkler, H., (2003), "Evaluation of drift demands for the seismic performance assessment of frames," *Journal of Structural Engineering*, **131**, pp 1003-1013.
7. Vamvatsikos, D. and Cornell, C., (2002) "Incremental dynamic analysis," *Earthquake Engineering & Structural Dynamic*, **31**, pp 491-514.
8. Mahdavi Adeli, M., Alinia, M., Deylami, A. and Banazadeh, M. (2011) "The comparison of probabilistic seismic demand models estimated through the incremental dynamic analysis and the use of scaled ground motion records," *ASIAN JOURNAL OF CIVIL ENGINEERING (BUILDING AND HOUSING)*, **12**, pp 319-335.
9. Banazadeh, M., Deylami, A. and Mahdavi Adeli, M., (2011), "Using Bayesian Statistics to Evaluate the Accuracy of Probabilistic Seismic Demand Models," *Proc. Of the 6th International Conference of Seismology and Earthquake Engineering*, Tehran, Iran.

Seismic Behavior of Two Layers of Drum And Up To the Mouth of the Mouth Depth Changes

Omolbanin Arasheh Khoshbin¹, Saeed Hedayat²

¹Department of Civil Engineering, Lashtenesha-Zibakenar Branch, Islamic Azad University, Lashtenesha, Iran

²Department of Civil Engineerin, uneversity of guilan, Rasht, Iran

Abstract: In this study Space structures widely used in large openings are covered. Space lattice structures are more used than the similar ones. Shape and position of these families are common to both cask layers. Dynamic and seismic behavior of these structures has increased considerably in recent years. It was thought that long structures are vulnerable to earthquakes. However, the events of the Kobe at 1995 earth quake and ... Showed that although these structures are safer than conventional structures, but it should not be considered as absolutely safe. Among the notable studies on anti-seismic behavior of these space structures we can point out to works of Japanese researchers [1] Ishikawa, Kato and Sadeghi [2] and [3].

Keywords: industrial technology building, concrete construction, tunnel format, capabilities and limitations

I. Introduction

casks with two types of different angle of deflection to span ratio of (0.2,0.3,0.4), which are designed only for dead and live loads, have been selected. Treatment of the two- layer casks due to anchor point and horizontal components of displacement, the earthquake, the non-linear material and geometric nonlinear analysis was conducted and for this purpose all the finite element analyses have been done by the software of ANSYS [4].

II. Shape and characteristics of casks

Several layers casks with the square on square tashe and with deflection to opening rates of (0.2,0.3,0.4) considered that spans were over 34 meters and the height of (13.6, 6.8, 10.2) meter. Figure 1 shows an example of the cask. Cask fitting joint. And the angle of deflection was various for each cask type. The first type is called A and the support structures located on either side of the top layer. The first type is called A and the support structures located on either side of the low layer. Bilayer structures in cask Formian [5] Tashh transduction was then performed to determine the exact coordinates of the points above, and elements. The results of the structural geometry (Geometry only) for software defined as "Mechanical Desktop" and then SAP 2000 software for design and for nonlinear dynamic analysis software of ANSYS have been transferred. Every structure has been defined with abbreviation symptoms based on deflection to opening. The first letter (B) is the first letter of (Barrel Vaults). The second letter indicates the anglesituation, The first number is the ratio of deflection to span (H / S) is the percentage. And the second number represents the span depth ratio (D / S). Right letter of H shows earthquake force in the horizontal direction H (Horizontal).

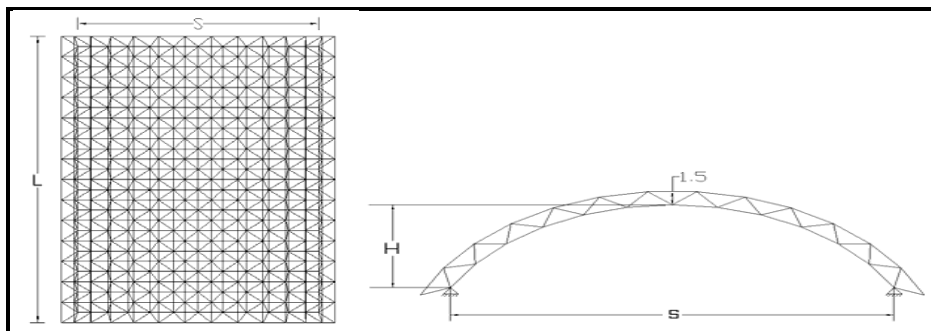


Fig1: casks characteristic

III. Static analysis for structural design

Structural geometry and sections in the initial selection, proper design requires Members to be able to construct an adequate safety factor to handle the loads. Resistance of structural members must be more than the maximum stresses induced by external loads and other factors. Used elements are of hollow tubes.

The designation, based on steel structures design codes (the tenth topic of the National Building Regulations) took place. The slimness of all members are considered by cask of 100. Loaded cask in the sixth topic of regulations for snow loads for arc roofs is as the two followings:

1 - symmetric loading 2 - asymmetric loading

Dead load: load weight and coating facility and space structure together is $50\text{kg} / \text{m}^2$ and a concentrated load is applied on all the nodes above.

After loading, the models were analyzed and designed in 2000 SAP and crossings of each of the models obtained. Steel Building characteristics seen in the tables used in the analysis are as follows:

E (Young's modulus) 2.1×10^{11} (N / m²):

v (Poisson's ratio): 0.3

P (mass per unit volume of material): 7850 (kg / m³)

σ_y (flow stress): 2.4×10^8 (N / m²)

After designing and obtaining the whole weights sections, each section and weight of models in Table 1 as the ratio of the weight of steel used in models up to the mouth of the mouth depth of 0.2 to 0.4 and by the ratio of 0.007353 and 0.02941, the aforementioned models are all chosen terms.

According to this table, the following results were obtained:

1 - On the rise to span ratio (0.2,0.3,0.4), the largest structural steel is used in the chorus: first base A then B happens.

2 - deflection the mouth to increase steel consumption increases with increasing depth to span ratio is reduced by this amount.

IV. Modal Analysis and its Application in Structure Analysis

The first model has a static analysis and we get it's cross sections and then the program of ANSYS using element 180 Link sections devoted to modeling and modal analysis is performed. Due to the force of the earthquake in X enters the surfing output modal analysis must consider the output of the X ...

To obtain the frequency and the second mass participation factor of together and the greatest rate of participation was considered their frequencies.

For the structural damping ratio = 0.02 ξ space considered

In formula (1) are replaced by the same formulas of Rayleigh and Rayleigh coefficients are obtained.

(1)

$$\beta = \xi \frac{2}{f_i + f_j}$$

$$\alpha = \xi \frac{2f_i f_j}{f_i + f_j}$$

Table 1 - Weight of steel used in models up to the mouth of the mouth depth of 0.2 to 0.4 Vbansbt 0.007353 and 0.02941

Model Name	Total steel used (kg)	Total steel used in each square meters (kg/m ²)
BA-0.2-0.007353	42558.16	33.37
BB-0.2-0.007353	9302.42	7.29
BA-0.2-0.0220	18154.29	14.23
BB-0.2-0.0220	16098.21	12.62
BA-0.2-0.03676	15128.04	11.86
BB-0.2-0.03676	13237.57	10.38
BA-0.2-0.05882	13965.22	10.95
BB-0.2-0.05882	11259.83	8.83
BA-0.3-0.007353	66972.29	47.35
BB-0.3-0.007353	57260.56	40.48
BA-0.3-0.0220	21592.63	15.26
BB-0.3-0.0220	18831.32	13.31
BA-0.3-0.03676	17831.26	12.60
BB-0.3-0.03676	15682.66	11.08
BA-0.3-0.05882	15628.42	11.04
BB-0.3-0.05882	12627.09	8.92
BA-0.4-0.007353	132273.31	84.39
BB-0.4-0.007353	111421.5	71.08
BA-0.4-0.0220	27789.94	17.72
BB-0.4-0.0220	25212.43	16.08
BA-0.4-0.03676	21918.26	13.98
BB-0.4-0.03676	19538.27	12.46
BA-0.4-0.05882	20264.55	12.92
BB-0.4-0.05882	16674.91	10.63

Results concerning the eigenvalues (period comparison) in different support conditions and with increased deflection to depth and span to mouth of the casks: (H / S)

Results concerning the eigenvalues (period comparison) in different support conditions and with increased deflection and depth to span the mouth of the cask: (H / S)

Modal analysis of this model is that the following would be the first mode is the most effective one. For the models with the rich depth of the mouth and the mouth of different support conditions can be compared with each other. All conditions except the rich depth of the mouth and the mouth and support conditions are considered equal. Due to a Figures

(10-2) observed that the models with support requirements of A than the models of B, with equal deflection to mouth and depth to mouth have greater period.

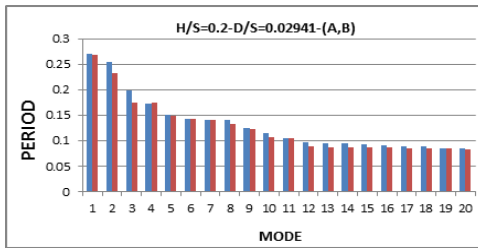


Fig3. Mode period diagram for B{-0.2-0.02941}

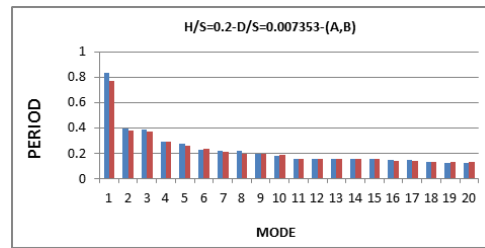


Fig2. Mode period diagram for B{A,B}-0.2-0.0

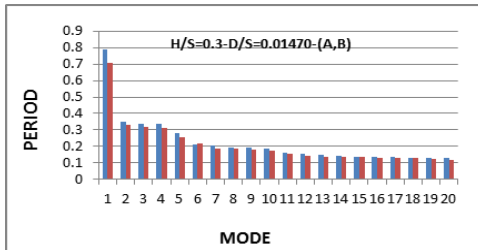


Fig5. Mode period diagram for 01470

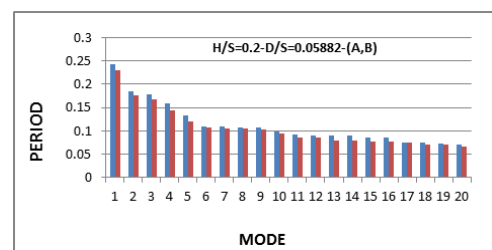


Fig4. Mode period diagram for (B{A,B}-0.2-0.05882)

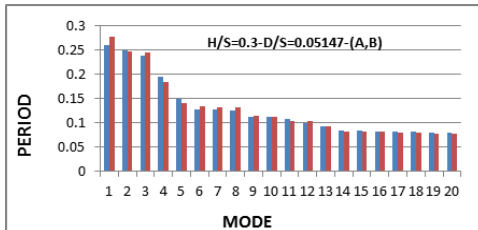


Fig7. Mode period diagram for B{A,B}-0.3-0.05147

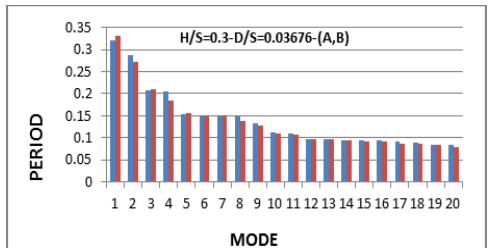


Fig6. Mode period diagram for (B{A,B}-0.3-0.03676)

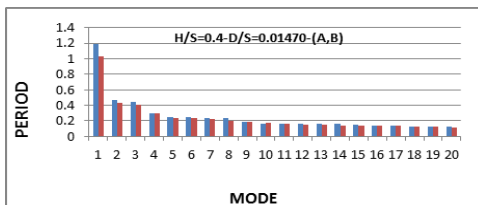


Fig9. Mode period diagram for B{A,B}-0.4-0.04411

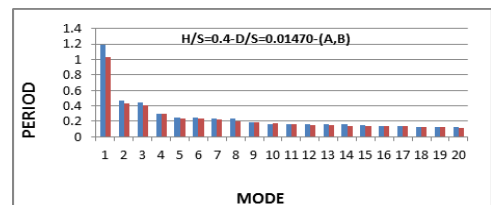


Fig8. Mode period diagram for (B{A,B}-0.4-0.01470)

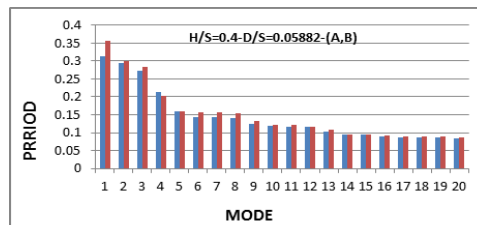


Fig10. Mode period diagram for (B{A,B}-0.4-0.05882)

According to the figures(, 13-11) for models with different depths of the mouth to mouth depth increase structural period increases..

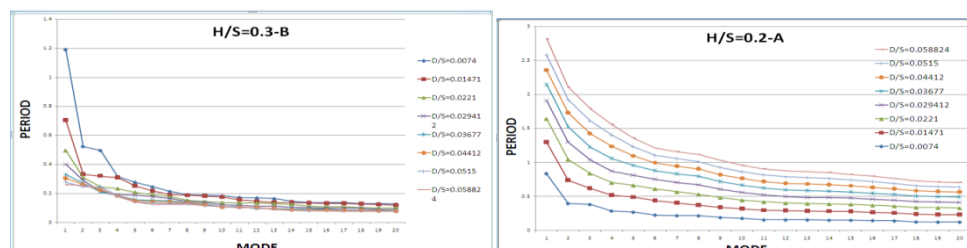


Fig12: Structural comparison period to increase the depth of the mouth (the mouth up to 0.3)

Figure 11 - Comparison of time-frequency structures to increase the depth of the mouth (the mouth up to 0.2)

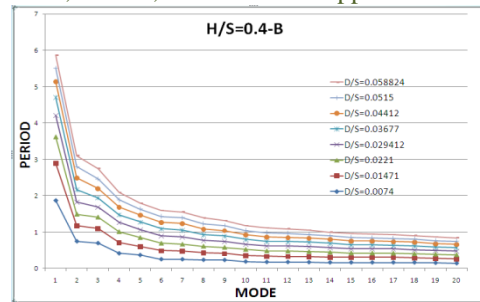


Figure 13 - Comparison of the structure with increasing depth in the opening period (rise to span ratio of 0.4)

Forms (14) and (15) with the support of BA and BB shows the period time of “ Deflection to span” by increasing this ratio, The period increases with increasing depth to span ratio of period decreases.

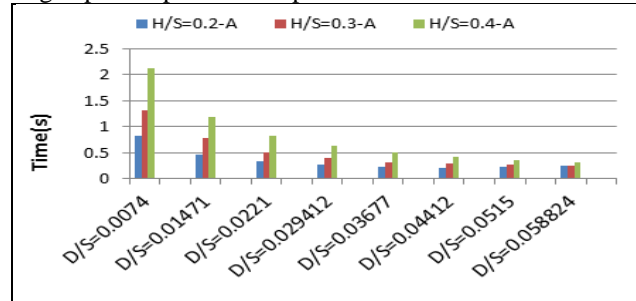


Fig14. Period diagram in depth to mouths of 058824 to 007352, The ratio of rise to span the fulcrum A

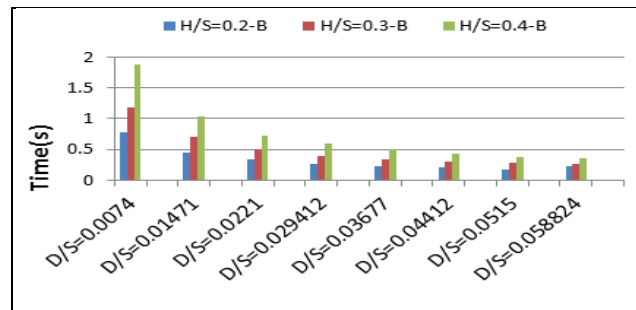


Fig15.Period diagram in depth to mouths of 058824 to 007353 the ratio of rise to span the fulcrum B

Rayleigh coefficients α and β in the calculation of dynamic analysis, f_j and f_i , respectively, first and second frequency components are dominant. To obtain the first and second frequencies, the mass participation factor and mode compared with large mass participation factors are considered, the effective mass for each mode models for mass participation factor V between the fortieth mode is the fifth mode.

V. Analyzings for of the dynamic analysis

In this case earthquakes in the database, under the theoretical due to the large selection of PGA has been used. Table (2) information about the selected earthquakes in the seismic analysis, it has been seen.

Table 2 - Earthquake theoretical information TABAS

Earthquake	TABAS , Iran 1978/09/16	TABA ,Iran 1978/09/16 (V)
Record/component	TABAS /TAB-TR	TABAS/TAB-UP
HP(Hz)	0/05	0/05
LP(Hz)	null	null
PGA(g)	0/852	0/688
PGV(cm/s)	121/4	Mar-98
PGD(cm)	94/58	76/37

The defining feature of nonlinear geometry and nonlinear material for dynamic analysis in ANSYS Azalmanhay MASS21 and COMBIN39 used. Membership models, structures Fzakar desired coefficients wasting 100 addressed and values thinness of the formula (2) and Figure (16) by Mr. Kato and Ishikawa obtained have been used.

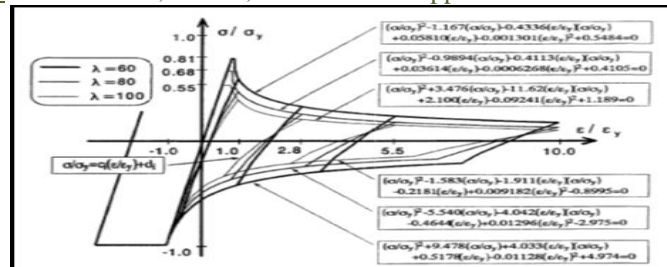


Figure 16 - Graph coefficients are thin 60-80-100 by Mr. Ishikawa and Kato

(2)post-buckling formula for weight loss: 100

$$\left(\frac{\sigma}{\sigma_y}\right)^2 + 3.476 \left(\frac{\sigma}{\sigma_y}\right) - 11.62 \left(\frac{\epsilon}{\epsilon_y}\right) \left(\frac{\sigma}{\sigma_y}\right) + 2.10 \left(\frac{\epsilon}{\epsilon_y}\right)^2 - .09241 \left(\frac{\epsilon}{\epsilon_y}\right)^2 + 1.189 = 0$$

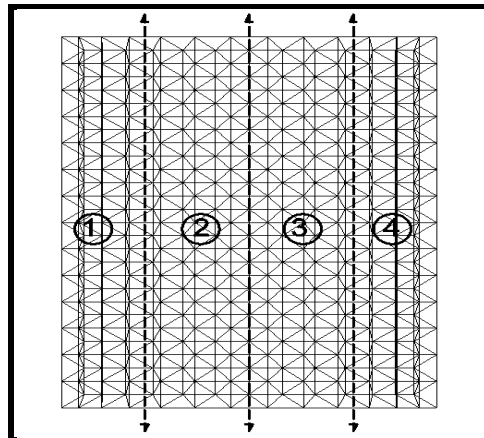


Figure 17 - cask divided into four equal regions

Because the structures go into non-linear phase during earthquakes (member) therefore geometrically nonlinear behavior for structures and materials have been applied. The post-buckling curves after slimmness of 100 were defined for this model. These models for 19.5 seconds were applied to the quake of (TABAS) Iran. Placed in the horizontal direction H and the seismic behavior of the casks have been studied., some of the results are shown in Table (3)

Number of Buckled members	First buckling zone	First buckling time(s)	The greatest nodal displacement in y direction	The greatest nodal displacement in x direction	Model
-	-	-	.04048	0	BA-.2-.007353
.	Top	4.52	.03801	.03092	BB-.2-.02941
4-1	Top-jan	4.8	.02145	.01895	BA-.3-.03176
-	-	-	.001985	.002467	BB-.3-.0220
4	Jan	1.74	0	1.82	BA-.4-.2941
14	jan	7.89	.05821	.02357	BB-.4-.007351

The BB-0.4-0.02941 with a fuller analysis model is investigated. This model can be used to analyze the seismic TABAS. As of the form (18) View node created for this model to be the biggest shift in the direction of (x) the amount of node 276 m 0.02357 and Also, the form (19) observed that the largest shift in the positive direction for the model node (Y) the number of nodes is 231 m 0.05821 times the amount of Tabas earthquake. Forms (20) and (21) local buckling of members which have been with the show, In the first buckling in the second layer of jan has happened.

And first-time of buckling is 7.89 seconds. Then, by passing time, In District members of top layer and in district 2, members of jan layer, and in district three, members of jan layer and in district four, members of the top layer go buckling. Finally, for the first time and last time buckling 14 members in jan layer, and in last buckling time, 18 members in the layer above and 2 members in low layer and 42 members in the jan layer have gone buckling. Now we investigate the buckling behavior of buckled member with slimmness of 100.

Figure (23) shows that, a, b, respectively, have been the biggest change for Model BB-0.4-0.02941 buckling length member show. And these points on the graph where the buckling shapes (22) are corresponding.

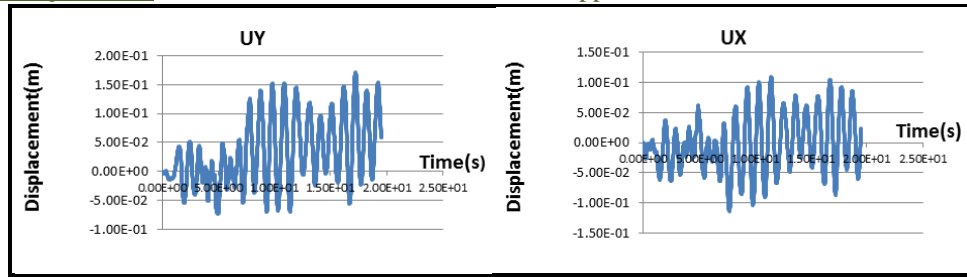
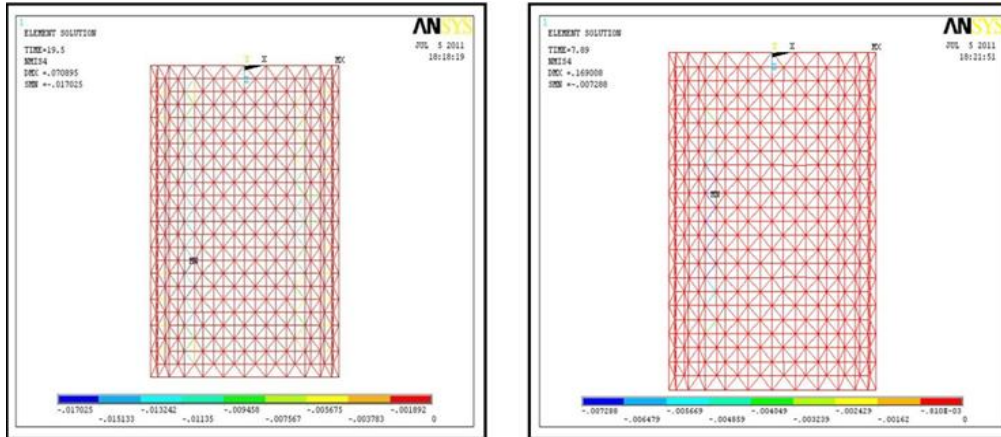


Fig.19. Chart shift - time for Y to model **BB-0.4-0.02941**



The BB-0.4-0.02941 Figure 21 - The last time the buckling model BB-0.4-0.02941

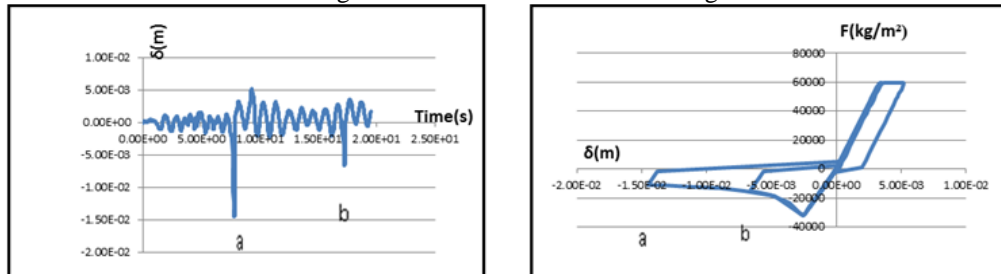


Figure 22 - Graph to model the buckling member of BB-0.4-0.02941 Figure 23 - Change Over Chart (Member) - Time for Model BB-0.4-0.02941

VI. Conclusion

- 1 - The time of the first buckling doesn't differ a lot, and is between 4 to 5 seconds in most of the models.
- 2 -It seems that the best supporting situations based on structural stability is first A and then B and the best deflection to mouth proportion is 0.2
- 3 - With the increasing of deflection to mouth in constant depths displacement of the structure is greater than the potential structural failure occurs and the buckling of the top layer is Jan.
- 4 - With the increase in the ratio of depth to span in constant and variable rates of deflection to mouth, the number of members buckling will be variable.
- 5 - Buckling earliest times in structure is for model of BA-0.4-0.02441 equal to 1.74
 And the last Buckling times in structure is for model of BB-0.4-0.007353 equal to 7.89
- 6 - Increasing deflection to mouth, in earthquake of TABAS (IRAN) time of the first buckling reduced extreme cask with a rich mouth $H/S = 0.2$. Members buckling get very least, and in many cases no buckling in them does not happen if for cask with a deflection to mouth of $H/S = 0.4$, the buckling members will increase a lot and members get buckling in majority of times.

REFERENCES

- [1] Ishikawa, K. and Kato, S., Dynamic Buckling Behaviour of Single and Double Layer Latticed Domes due to Vertical Earthquake Motions, Park, G.A.R. ed., SpaceStructures 4: Proceedings of the Fourth International Conference of Space Structures, Vol. 1, Thomas Telford, 1993, pp. 466-475.
- [2] Sadeghi, A., "Horizontal Earthquake Loading and Linear/Nonlinear Seismic Behaviour of Double Layer Barrel Vaults", International Journal of Space Structures, Vol. 19, No 1, 2004.
- [3] Sadeghi, A., "Vertical effects of earthquakes on the double layer barrel vaults", J. of Space Structures, Vol. 19, No.2, 2004.
- [4] Ansys Theory Reference, 1 7.7, Spectrum Analysis.
- [5] Nooshin, H., "Course on Space Structures, Kerman, Iran, May 2003

Studies of Hydrogeochemical in Groundwater Quality around Chakghat Area, Rewa District, Madhya Pradesh, India

¹A.K.Tripathi, ²U.K.Mishra, ³Ajay Mishra, ⁴Saras Tiwari and ⁵Parul Dubey

¹Principal, Shriyut College Gangeo Rewa-486111, Madhya Pradesh India

²Department of Geology Govt. P.G. College Satna -485001, Madhya Pradesh India

^{3,5}Department of Geology, Govt. P.G. College Rewa-486001, Madhya Pradesh India

⁴Department of Chemistry, I.V. P.G. College Jawa Rewa-486223, Madhya Pradesh India

Abstract : The area is drained by a fourth order Tons river and its tributaries having dendritic to subparallel drainage pattern. The paper deals with studies of hydrogeochemical in groundwater around Chakghat area, Rewa district, Madhya Pradesh. Geologically, the area is occupied by Upper Rewa sandstone of Rewa Group; Ganurgarh shale and Bhandar limestone formations of Bhandar Group, Vindhyan Supergroup. Total of twenty five groundwater samples collected in post monsoon season of 2011 and were analysed to see their suitability for drinking and irrigation purposes. The water samples from Karstic limestone and shaly aquifers are moderately hard to very hard in nature. The higher amount of total dissolved solids in a few samples is due to impervious nature of shale aquifer. The concentration of fluoride in a few samples exceed maximum permissible limit (1.5mg/l) due to fluoride mineral associated with Bhandar limestone aquifer. The study reveals that groundwater samples is more or less within prescribed limits as per World Health Organisation (WHO) and Indian Standard Institute (ISI) for drinking purpose. As per Chadha's scheme of classification, the groundwater of the study area is Ca-Mg-HCO₃ and Ca-Mg-SO₄-Cl type. The calculated sodium adsorption ratio values suggest excellent quality for irrigation. The other parameters such as percent sodium, Kelley's ratio, Permeability index and Residual sodium carbonate suggest that the groundwater of the study area is suitable for irrigation purpose. The samples plotted on U.S. salinity diagram indicate that groundwater of the region is medium to high saline and low alkaline in nature.

Keywords: Groundwater Quality, Chakghat, Rewa, Madhya Pradesh, India

I. Introduction

Groundwater is a most vital natural resources required for drinking and irrigation. The quality of groundwater is largely controlled by discharge-recharge pattern, nature of host and associated rocks as well as contaminated activities. Moreover, the nature and amount of dissolved species in natural water is strongly influenced by mineralogy and solubility of rock forming minerals (Raymahasay, 1996). The quality of groundwater is function of various parameters which determines its suitability for drinking purposes (WHO 1984; Trivedy and Goel 1986; ISI 1991; APHA 1998). In the present study, an attempt has been made to interpret the drinking and irrigation water quality of groundwater around Chakghat area, Rewa District, Madhya Pradesh (Fig.1).

The study area is drained by Tons river and its tributaries and bounded by latitude 24°30' to 24°45' N and longitude 81° 00' to 81°25' E covering an area of about 900 km². The climate is semi arid to humid type and average rainfall of the area is about 1000 mm however in the year 2011 it was recorded 550 mm. The temperature in summer months goes up to 46°C while as low as 3°C during peak winter month. The relative humidity of about 75 percentage.

II. Geology and Hydrogeology

The study area is part of northern extension of Vindhyan Sedimentary Basin; one of the thickest sedimentary basin of India. The main rock types are Govindgarh Sandstone of Rewa Group, Ganurgarh Shale and Bhandar Limestone of Bhandar Group, Vindhyan Supergroup. The sandstone is red and purple in colour, hard and compact, fine to medium grained and quartzitic in nature. The Ganurgarh Shale is buff to purple, thinly laminated and well bedded. The Bhandar Limestone is main litho-unit occupying about seventy percent of the study area is massive to karstified, light to dark grey in colour. Limestone is stromatolitic and non-stromatolitic types. The stromatolitic type shows well bedded branching and non-branching columns. Locally bioherms and biostromes are well developed (Tiwari and Dubey, 2005). The non-stromatolitic are generally well bedded, light pink, light grey to dark grey in colour. Both limestones have been affected by silicification in the form of nodular cherts (Dubey et.al., 2009).

Hydrogeologically, the area lies in Precambrian sedimentary province (Karanth, 1987). Due to high silica cementation in sandstone, the primary porosity is low whereas secondary porosity in the form of joints, fractures form the source of groundwater. The groundwater occurs in confined and semi-confined conditions. The various karstifications-Rillen, Rinnen and Kluft Karrair developed in the study area are potential source of groundwater.

III. Methodology

A total of twenty five groundwater samples from bore well have been collected during post-monsoon season of 2011. The pH and electrical conductivity of the water samples were measured in the field using portable water analysis kit. The cations and anions of the groundwater samples were analysed using standard methods (Ramteke and Moghe, 1986, Trivedi and Goel, 1986, APHA 1998, Mishra et al. 2012; Tripathi et al. 2012). Total dissolved solids (TDS) was calculated by multiplying 0.6 HCO₃ plus other cations and anions.

IV. Result and Discussion

Drinking water Quality

As evident from geochemical analyses of ground water samples presented in table-1, the pH is in range of 7.5 to 8.9 indicating alkaline nature of groundwater. The higher pH values observed in certain samples suggest that carbon dioxide, carbonate-bicarbonate equilibrium is affected more due to change in physico-chemical conditions (Karanth, 1987; Tiwari et al. 2009). Groundwater with pH above maximum desirable limit can affect the mucous membrane. A most of the groundwater samples possess higher electrical conductance indicate that the groundwater was in contact with impervious shale and enough time to react with mineral constituent which added into the groundwater. The total dissolved solids lie between 478.28 mg/l to 1151.80 mg/l; in which most of the samples exceed desirable limit. Water with TDS up to 1000 mg/l is considered to be suitable for drinking (Pophare and Dewalkar, 2007). The higher amount of TDS may cause gastrointestinal irritation in human body. The total hardness of groundwater samples ranges from 299.02 mg/l to 671.68 mg/l. A thirteen samples exceed the maximum permissible limit of hardness as per WHO (1984) and ISI (1991) norms. As per Sawyer and McCarty (1967) classification scheme, the groundwater samples of the study area is very hard in nature may be due to the limestone aquifer which provided the calcium to the groundwater. As a result, the encrustation of carbonate is noticed in water supply pipe lines. The concentration of sulphate varies between 47.4 mg/l to 437.1 mg/l; in which a higher concentration is due to the presence of thin bands of Gypsum ($\text{CaSO}_4 \cdot 2\text{H}_2\text{O}$) associated with shale aquifer. The concentration of fluoride ranges between 0.50 mg/l to 2.50 mg/l. The fluoride concentration greater than 1.5 mg/l may cause dental problem however it was not noticed in the area. The higher concentration of fluorite in few groundwater samples may be due to the presence of fluorapatite [$\text{Ca}_5(\text{PO}_4)_3\text{F}$] mineral in limestone aquifer as reported by Tiwari (2000). As evident from Table1, higher concentration of fluorite is strongly related with pH indicating that higher alkalinity of the water promotes the leaching of F^- and thus affects the concentration of F^- in the groundwater (Saxena and Ahmed, 2001; Madhnure et al. 2007). To ascertain the suitability of groundwater for drinking purpose the geochemical parameters of the study area are compared with the guidelines as recommended by WHO(1984) and ISI (1991) which indicate that groundwater of the study area is more or less suitable for drinking purpose (Table 2). Groundwater samples of the study area have been plotted on Chdha's diagram (1999). In this scheme, the difference in milliequivalent (epm) percent between alkaline earth (calcium + magnesium) expressed as percentage reacting value is plotted on the x-axis and the difference in milliequivalent (epm) percentage between weak acid anions (carbonate +bicarbonate) and strong acid anions (chloride, sulphate and nitrate) is plotted on the y-axis. The milliequivalent percentage difference between alkaline earth and alkalis and between weak acidic anions and strong acidic anions is plotted on one of the four possible sub fields of the diagram. In the present study 12 samples fall in subfield 5 of Ca-Mg- HCO_3 type of water; 13 samples fall in subfield 6 of Ca-Mg- SO_4 - Cl type of water whereas only 1 sample fall in subfield 8 of Na-K- HCO_3 type.

Table 2: Comparison of the quality parameters of groundwater of the study area with WHO and ISI for drinking purpose.

S.No.	Water Quality Parameters	WHO (1984)		ISI (1991)		No. of locations which exceed max. permissible limit (WHO)	Concentration in Study Area	Undesirable Effect Produced Beyond Maximum Allowable Limit
		Max Desirable	Max. Permissible	Max. Desirable	Max. Permissible			
1.	pH	7.0 to 8.5	6.5 to 9.2	6.5 to 8.5	No relaxation	0	6.5 to 8.9	Taste, effects mucus memberane and water supply system.
2.	TH mg/l	100	500	300	600	13	299.02 to 671.68	Encrustation in water supply and adverse effect on domestic use.
3.	TDS mg/l	500	1500	500	1000	0	478.28 to 1151.8	Gastrointestinal irritation.
4.	Ca mg/l	75	200	75	200	0	46.3 to 182.0	Encrustation in water supply, scale formation.
5.	Mg ml/l	30	150	30	100	0	24.3 to 109.8	Encrustation in water supply and adverse effect on domestic use.
6.	Na mg/l	-	200	-	200	0	13.7 to 92.6	--

7.	Cl mg/l	200	600	250	1000	0	38.7 to 208.0	Salty Taste
8.	SO ₄ mg/l	200	400	150	400	2	47.4 to 437.1	Laxative effect.
9.	F mg/l	1	1.5	1	1.5	7	0.50 to 2.50	Dental Problem in children and adults causes Fluorosis

V. Irrigation water quality

The important parameters which determine the irrigation water quality of the study area are discussed below;

Percent Sodium (Na%)

It is an important parameter to classify the groundwater samples for irrigation purpose. It is calculated by the formula proposed by Doneen (1962) as under ;

$$\text{Na\%} = \frac{\text{Na}^+ + \text{K}^+}{\text{Ca}^{++} + \text{Mg}^{++} + \text{Na}^+ + \text{K}^+} \times 100$$

Sodium along with carbonate forms alkaline soil; while sodium with chloride forms saline soil; both of these are not suitable for the growth of plants (Pandian and Shankar, 2007). The quality classification of irrigation water based on the values of sodium percentage as proposed by Wilcox (1955) suggest that the groundwater of study area is good to permissible category (Table. 3).

Electrical Conductivity (EC)

It measures the capacity of substance or solution to conduct electric current. The EC of groundwater increases with the rise in temperature and varies with the amount of TDS. The conductivity in the groundwater samples of the area ranges from 746.1 to 1796.8 $\mu\text{S}/\text{cm}$ at 25°C indicating good category of irrigation water.

Sodium Adsorption Ratio (SAR)

The degree to which the irrigation water tends to enter into cation exchange reaction in soil can be indicated by the sodium adsorption ratio (U.S. Salinity, 1954). Since sodium replaces adsorbed calcium and magnesium in soil, hence it is expressed as ;

$$\text{SAR} = \frac{\text{Na}^+}{\sqrt{(\text{Ca}^{++} + \text{Mg}^{++})/2}} (\text{epm})$$

Excess sodium in groundwater gets adsorbed on soil particles, thus change soil properties and also reduce soil permeability (Ayers and Bronson, 1975). U.S. Salinity Laboratory (1954) proposed to plot SAR against EC for rating irrigation water (Table 3). The sixteen classes in the diagram indicate the extent that the waters can effect the soil in terms of salinity hazard. These classes are : low salinity(C₁), medium (C₂) , high (C₃) and very high salinity (C₄) and similarly sodium hazard as low (S₁), medium (S₂), high (S₃) and very high (S₄). The groundwater samples of the study area fall in C₃S₁ (26 samples) and C₂S₁ (1 sample) categories, hence suitable for irrigation purpose indicate that most of the groundwater samples of the study area are medium to high saline and low sodium hazard zone. Hence high salinity water should be used only in those soils where adequate drainage is available to leach out the excessive water.

As per classification of Wilcox (1955), water with SAR ≤10 is considered as an excellent quality, between 10 to 18 is good; between 18 to 26 is fair and greater than 26 is said to be unsuitable for irrigation purpose in its natural form. As evident from Table 3, most of the groundwater samples having ≤10 SAR; hence excellent for irrigation purpose.

Kelley's Ratio (KR)

It is the ratio of sodium ion to calcium and magnesium ion in epm(Kelley, 1951) and expressed as;

$$\text{K.R.} = \frac{\text{Na}^+}{\text{Ca}^{++} + \text{Mg}^{++}} (\text{epm})$$

The Kelley's Ratio (KR) have been computed for all groundwater samples of the study area and presented in Table 3. In the study area KR ranges from 0.07 to 0.88 indicating that water is suitable for irrigation purpose as the value is less than 1.

Permeability Index (PI)

The classification of irrigation waters has been attempted on the basis of permeability Index, as suggested by Doneen (1962). It is defined as;

$$P.I. = \frac{Na^+ + \sqrt{HCO_3^-}}{Ca^{++} + Mg^{++} + Na^+} \times 100 \text{ (epm)}$$

The groundwater samples of the study area fall in class-I. As per Doneen chart (Domenic and Schwartz, 1990), the groundwater samples of the study area is of good quality for irrigation (Fig. 4). The increased percentage of groundwater samples under class-I is due to dilution subsequent lower values of permeability index.

Magnesium Ratio (MR)

It is expressed as:

$$M.R. = \frac{Mg^+}{Ca^{++} + Mg^{++}} \times 100 \text{ (epm)}$$

(Palliwal, 1972)

If the Magnesium Ratio is greater than 50 percentage it is considered as suitable for irrigation purpose (Palliwal, 1972). In the present study 89 percent samples are good for irrigation whereas 11 percent samples are unsuitable (Table-3).

Corrosivity Ratio (CR)

It is defined as alkaline earth and alkalis and expressed as ;

$$C.R. = \frac{Cl^- / 35.5 + 2 \left(\frac{SO_4^{--}}{96} \right)}{2 \left(\frac{HCO_3^- + CO_3^{--}}{100} \right)}$$

The groundwater with corrosivity ratio < 1 is considered to be safe for transport of water in any type of pipes, whereas >1 indicate corrosive nature and hence not to be transported through metal pipes (Ryner, 1944, Raman, 1985). The calculated values of groundwater samples of the study are presented in Table-3, which suggests that 18 samples are safe whereas 09 samples are corrosive in nature and need non-corrosive pipe for transporting and lifting of groundwater.

Residual Sodium Carbonate (RSC)

It refers to the residual alkalinity and is calculated for irrigation water by the following formula;

$$RSC = (HCO_3^- + CO_3^{--}) - (Ca^{++} + Mg^{++}) \text{ (epm)}$$

The RSC values > 1.25 mg/l are considered as safe for irrigation while those from 1.25 mg/l to 2.5mg/l are marginally suitable for irrigation. If RSC values are > 2.5 the groundwater is unsuitable for irrigation (Eaton, 1950; Richards, 1954).

The RSC values of groundwater samples of the study area ranges from -9.29 to +1.87 mg/l; hence marginally suitable to safe for irrigation purpose.

VI. Conclusion

The results of geochemical analyses of groundwater samples of the study area indicate that water is slightly alkaline in nature due to pH values of more than 7. The calcium ion associated with limestone aquifer and gypsum bands associated with shale aquifer made groundwater samples moderately hard to very hard. The high fluoride concentration in few groundwater samples of the study area may be due to fluorapatite mineral associated with limestone aquifer. In the study area where concentration of fluoride is high; drinking water should be met from surface water or from shallow dugwells and borewells water may be used for other domestic purpose and not for drinking purpose. The higher values of electrical conductance are due to high concentration of ionic constituents in water (Jasrotia and Singh, 2007, Tiwari et.al., 2010). The higher amount of total dissolved solids (TDS) in a few samples is due to impervious nature of shales which provided longer residence to groundwater (Gopalkrishnan, 2006, Pophare and Dewalkar, 2007). Defluoridation techniques and ion exchange technique may be adopted in area where no alternative source is available with community involvement. The Chadha's (1999) diagram indicates that groundwater samples of the area are Ca-Mg-SO₄ – Cl and Ca- Mg-HCO₃ type. The comparison of analysed data with WHO (1984) and ISI (1991) indicate that groundwater samples of the area are more or less suitable for drinking purpose.

The groundwater samples have also been evaluated for their irrigation quality. The plot of Sodium percentage vs electrical conductance of groundwater samples of the study area suggests that majority of samples fall in good to permissible category. The samples plotted in U.S. Salinity diagram fall in medium to high salinity and low sodium hazard zone (C₃S₁); hence a high salinity bearing water samples should be used only in those soils adequate drainage is available to leach out those waters. The area having higher corrosivity ratio (>1) need non-corrosive pipe during water supply. The other parameters such as Kelley's Ratio, Residual sodium carbonate, Magnesium Ratio, Permeability Index suggest that groundwater of the study area are suitable for irrigation purpose.

REFERENCES

- [1] APHA (1998). Standard methods for the examination of water and waste water 20th edition, American Publ. Health Assoc. Washington; pp.10-161.

- [2] Ayers, R.S. and Bronson, R.L. (1975). Guidelines for interpretation of water quality for Agriculture University of California, Extension Mimeographed, 13 p. t
- [3] Chadha, D.K. (1999). A proposed new diagram for geochemical classification of natural waters and interpretation of chemical data. *Hydrogeol. Jour.*, v.7, pp. 431-439.
- [4] Domenico, D.A. and Schwartz, F.W. (1990). *Physical and chemical Hydrogeology*. John Wiley and sons, New York, pp. 410-420.
- [5] Doneen, L.D. (1962). The influence of crop and soil on percolating water. *Proc. 1961 Biennial conference on Groundwater Recharge*, pp.156-163.
- [6] Dubey, D.P., Tiwari, R.N. and Shrivastava, R.K. (2009). Petrography of Chert Nodules from the Bhandar Limestone Formation, Rewa District, Madhya Pradesh, *Gond. Geol. Magz.* v. 24(2), pp. 157-160.
- [7] Eaton, E.M. (1950). Significance of carbonate in irrigation water. *Soil Science*. v.69. pp. 123-133.
- [8] Gopalkrishna, G.S., Harinarayanan, P. and Balasubramanian, A. (2006). Groundwater quality in twin micro-watersheds near Keralapura, Hassan District Karnataka, *Jour. Geol. Soc. India*, v.67, pp.802-808.
- [9] Hegde, G.V. (2006). Evaluation of chemical quality of groundwater in Dharwad District, Karnataka, *Jour. Geol. Soc. India* v.67 pp.47-58.
- [10] ISI (1991). Indian standard specification for drinking water. IS : 10500, Indian Standard Institution, pp. 1-5.
- [11] Jasrotia, A.S. and Singh, R. (2007). Hydrochemistry and groundwater quality around Devak and Rui watershed of Jammu Region, Jammu and Kashmir, *Jour. Geol. Soc. India*, v.69, pp. 1042-1054.
- [12] Karanth, K.R. (1987) *Groundwater Assessment Development and Management* Tata McGraw Hill publishing company Ltd., New Delhi, 725p.
- [13] Kelley, W.P. (1951). *Alkali soils-their formation properties and reclamation*. Reinold Publ. Corp., New York.
- [14] Madhnure, P. Sirsakar, D.Y. Tiwari, A.N., Ranjan, B. and Malpe, D.B. (2007). Occurrence of fluoride in the groundwaters Pandharkawada area, Yawatmal district, Maharashtra, India. *Curr. Sci.* v. 92(5), pp.675-679.
- [15] Mishra, U.K., Tripathi A.K., Tiwari Saras and Mishra Ajay (2012). Assessment of Quality and Pollution Potential of Groundwater around Dabhaura Area, Rewa District, Madhya Pradesh. *Earth Science Research; Canada*. v.1, No.2; pp.249-261 (2012).
- [16] Palliwal, K.V. (1972). *Irrigation with saline water*, ICARI Monograph No.2, New Delhi, 198 p.
- [17] Pandian, K. and Sankar, K. (2007). Hydrochemistry and groundwater quality in the Vaippar river basin, Tamil Nadu. *Jour. Geol. Soc. India*, v.69, pp. 970-982.
- [18] Pophare, A. M. and Dewalkar, M. S. (2007). Groundwater quality in Eastern and Southeastern parts of Rajura Tehsil, Chandrapur District, Maharashtra. *Gond. Geol. Magz. Spec. Vol.* pp.119-126.
- [19] Raman, V. (1985). Impact of corrosion in the conveyance and distribution of water. *Jour. I.W.W.A.*; v. xv(11) pp. 115-121.
- [20] Ramteke, D.S. and Moghe, C.A. (1986). *Manual on water and waste water analysis*. NEERI, Nagpur, 340p.
- [21] Raymahashay, B.C. (1996). *Geochemistry for hydrologists*, CBS Publisher New Delhi; 190p.
- [22] Richards, L.A. (1954). *Diagnosis and improvement of saline and alkali soils*. *Agri. Handbook* 60, U.S. Dept. of Agriculture, Washington. D.C. 160p.
- [23] Ryner, J.W. (1944). A new index for determining amount of calcium carbonate scale formed by water, *Jour. Amer. Water Assoc.* v. 36. pp. 472-486.
- [24] Saxena, V.K. and Ahmed S. (2001). Dissolution of fluoride in groundwater. A water-rock interaction study. *Environ. Ged.* v.40, pp. 1084-1087.
- [25] Sawyer, C.N. and McCarty, P.L. (1967). *Chemistry for sanitary Engineers*, 2nd edition, McGraw Hill, New York, 518 p.
- [26] Singh, D.H. and Lawrence, J.F. (2007). Groundwater quality assessment of shallow aquifer using geographical information system in part of Chennai City, Tamil Nadu. *Jour. Geol. Soc. India*, v.69, pp.1067-1076.
- [27] Tiwari, R.N. (2000). Sedimentological and Geochemical studies of Bhandar Limestone of Vindhyan supergroup, Rewa and Satna District, Madhya Pradesh, unpublished Ph.D. thesis, A.P.S. University Rewa 138 p.
- [28] Tiwari, R.N. and Dubey, D.P. (2005). Stromatolites and depositional environment of Bhandar Limestone, Rewa area, Madhya Pradesh. *Gond. Geol. Magz.* v. 19(1) pp. 131-134.
- [29] Tiwari, R.N. and Singh, A.K. (2010). Groundwater quality and pollution potential of Mahana River Basin, Rewa District, Madhya Pradesh, India, *Proc. International Conference on Hydrology and Watershed*, JN&T Hyderabad, pp. 49-59.
- [30] Tiwari, R.N., Bharti, S.L., Mishra, Umesh (2010) Hydrogeochemical Studies of Groundwater from Odda River Basin, Rewa District, Madhya Pradesh, *Gondwana Geological Magazine, Special v. No. 12*, pp.85-93.
- [31] Tiwari, R.N., Dubey, D.P. and Bharti, S.L. (2009). Hydrogeochemistry and groundwater quality in Beehar River Basin, Rewa district, Madhya Pradesh, India. *Inter. Jour. Earth Eng. Sci.*, v.2(4), pp. 324-330.
- [32] Tripathi, A.K., Mishra U.K., Mishra Ajay and Dubey Parul (2012). Assessment of Groundwater Quality Gurh Tehseel, Rewa District Madhya Pradesh, India *International Journal of Scientific and Engineering Research [IJSER]* v.3, Issue 9, pp.1-12 (2012).
- [33] Trivedy, R.K. and Geol, P. K. (1986). *Chemical and biological methods for waste Pollution studies*. Environmental Publication, Karad, pp. 35-96.
- [34] U.S. Salinity Laboratory Staff (1954). *Diagnosis and improvement of saline and alkali soils*. U.S. Dept. Agriculture Hand book, No. 60, 160p.
- [35] WHO (1984). *Guidelines for drinking water quality v. I Recommendations*. World Health Organization Geneva. 130p.
- [36] Wilcox, L.V. (1955). *Classification and use of irrigation waters*, U.S. Department of Agriculture. Circ. 969, Washington, D.C.

**Table 1 : Geochemical analyses of groundwater samples of the study area
(Except pH and EC, all values are in ppm)**

S.No.	Location	PH	EC	TDS	TH	Na	K	Ca	Mg	F	Cl	SO ₄	HCO ₃
1.	Chandrapur	6.7	1283.0	822.44	546.68	75.06	3.10	108.3	67.3	1.08	66.3	117	640.0
2.	Pahari	8.5	847.0	542.95	530.13	41.20	4.70	123.0	54.30	1.85	53.7	81.2	305.0
3.	Janeh	8.0	915.7	587.01	469.92	69.80	5.20	95.8	56.2	1.38	90.3	102.0	278.3
4.	Sohagi	7.1	1033.1	662.26	582.16	91.70	7.30	89.2	87.6	1.56	58.6	107.3	365.0
5.	Chakghat	7.2	999.3	640.60	671.68	68.50	5.30	88.6	109.8	0.50	163.0	52.5	254.0
6.	Chandi	6.8	1148.9	736.50	410.23	113.00	5.40	69.3	57.8	0.80	78.30	198.3	356.0
7.	Khatiya	7.1	793.9	508.96	464.28	80.70	9.20	127.0	35.8	0.56	57.9	115.0	138.0
8.	Pancha	8.9	900.8	577.47	513.59	74.30	8.40	103.1	62.4	2.01	83.7	51.9	321.1
9.	Sohagi	7.3	858.6	550.38	413.86	33.20	6.70	47.3	72.1	0.78	176.0	85.30	215.00
10.	Barageon	7.5	902.2	578.32	518.33	75.1	7.90	102.7	63.8	1.00	84.2	52.1	319.2
11.	Raipur	7.6	926.0	593.60	591.02	15.70	3.20	118.0	72.2	1.30	45.0	95.2	405.0
12.	Sonauri	6.9	1164.2	746.25	374.13	25.40	15.30	109.8	24.3	1.05	40.2	415.0	192.0
13.	Sonvarsha	6.8	1117.9	716.60	434.15	73.70	2.40	89.2	51.5	1.00	85.7	162.0	418.5
14.	Magee	7.2	860.9	551.87	560.25	52.60	11.20	182.0	25.6	1.40	64.8	47.4	278.0
15.	Satpura	8.3	881.2	564.85	419.99	75.20	4.30	87.8	48.9	1.85	57.3	112.5	295.0
16.	Loni	7.6	758.7	486.37	426.24	72.90	3.20	89.2	49.6	1.00	45.6	115.7	182.0
17.	Chunari	6.8	1199.3	768.77	574.16	92.60	3.70	101.3	78.3	1.20	203.0	78.7	350.0
18.	Malpar	7.2	1290.0	826.90	433.40	74.70	2.60	84.8	54.0	0.70	83.6	278.0	417.5
19.	Antarsuai	8.2	746.1	478.28	299.02	33.80	6.70	75.0	27.2	1.50	55.7	79.0	332.0
20.	Phuthaudha	7.4	1796.8	1151.80	612.37	24.30	3.40	108.5	83.2	1.20	92.1	437.1	670.0
21.	Neebi	8.5	1042.4	668.18	386.41	23.70	18.0	109.3	27.6	2.50	38.7	95.5	585.2
22.	Naribari	8.0	1068.2	684.72	579.62	18.70	4.40	120.0	68.2	1.68	43.8	141.8	475.7
23.	Bharat Nagar	7.4	836.9	536.50	348.84	26.32	3.20	83.4	34.2	0.85	208.0	79.7	168.0
24.	Bagheri	7.2	787.2	504.62	542.28	13.70	4.30	109.0	65.8	0.50	59.2	142.5	182.7
25.	Chunri	6.9	1244.5	797.77	618.71	40.00	1.30	70.2	108.1	0.75	86.1	157.0	557.2

Table-3 Characteristic ratio and indices of ground water samples of the study area.

SN.	Location	Soluble Na%(SSP)	Sodium Adsorption Ratio(SAR)	Permeability Index(PI)	Kelley's Ratio(KR)	Mg Hazard (MR)	Residual Sodium Carbonate(R SC)	Corrosivity Ratio(CR)
1.	Chandrapur	30	1.39	46.2	0.42	38.3	-0.45	0.3
2.	Pahari	21	0.78	32.4	0.23	30.6	-5.60	0.5
3.	Janeh	33	1.38	41.6	0.45	36.9	-4.84	0.8
4.	Sohagi	35	1.64	41.1	0.51	49.5	-5.67	0.5
5.	Chakghat	27	1.14	30.5	0.34	55.3	-9.29	1.0
6.	Chandi	48	2.43	55.8	0.88	45.4	-2.37	0.8
7.	Khatiya	35	1.63	39.2	0.49	21.9	-7.01	1.3
8.	Pancha	33	1.43	40.8	0.45	37.7	-5.01	0.5
9.	Sohagi	25	0.71	34.1	0.27	60.3	-4.77	1.5
10.	Barageon	33	1.42	40.6	0.45	38.3	-5.13	0.5
11.	Raipur	09	0.28	26.1	0.08	37.9	-5.18	0.3
12.	Sonauri	23	0.57	33.6	0.18	18.1	-4.32	2.5
13.	Sonvarsha	35	1.54	48.9	0.52	36.6	-1.83	0.6
14.	Magee	23	0.96	32.8	0.25	12.3	-6.64	0.4
15.	Satpura	36	1.59	46.7	0.55	35.7	-4.43	0.6
16.	Loni	35	1.52	41.9	0.52	35.8	-5.54	1.0
17.	Chunari	34	1.67	41.4	0.51	43.5	-5.75	1.0
18.	Malpar	35	1.56	49.1	0.54	38.9	-1.83	0.9
19.	Antarsuai	28	0.93	51.1	0.33	26.6	-0.53	0.4
20.	Phuthaudha	12	0.43	32.7	0.12	43.4	-1.27	0.8
21.	Neebi	23	0.52	47.2	0.17	20.1	+1.87	0.2
22.	Naribari	11	0.34	29.0	0.09	36.2	-3.80	0.4
23.	Bharat Nagar	20	0.61	34.6	0.22	29.0	-4.22	2.1
24.	Bagheri	09	0.25	20.3	0.07	37.6	-7.85	1.2
25.	Chunri	18	0.70	33.6	0.22	60.6	-3.26	0.5

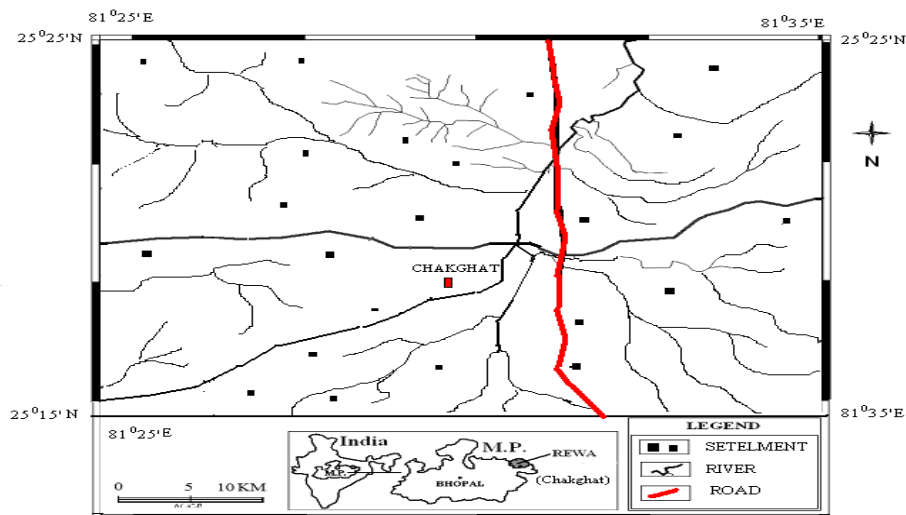


Fig. 1 Location Map of the Study Area.

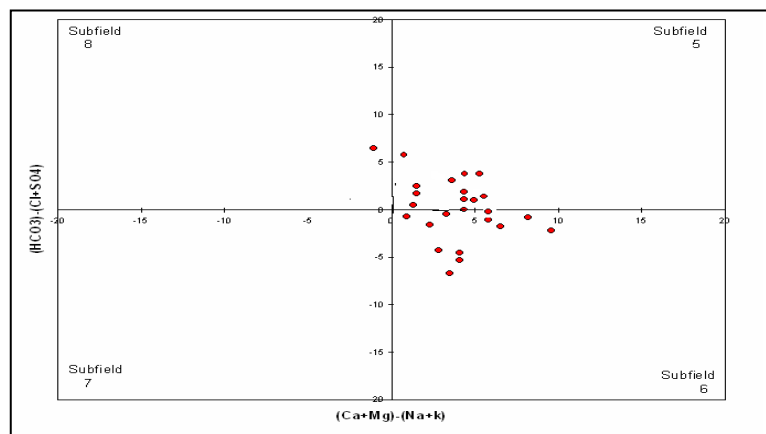


Fig.2: Classification of Groundwater samples as Per Chadha's (1999) Scheme.

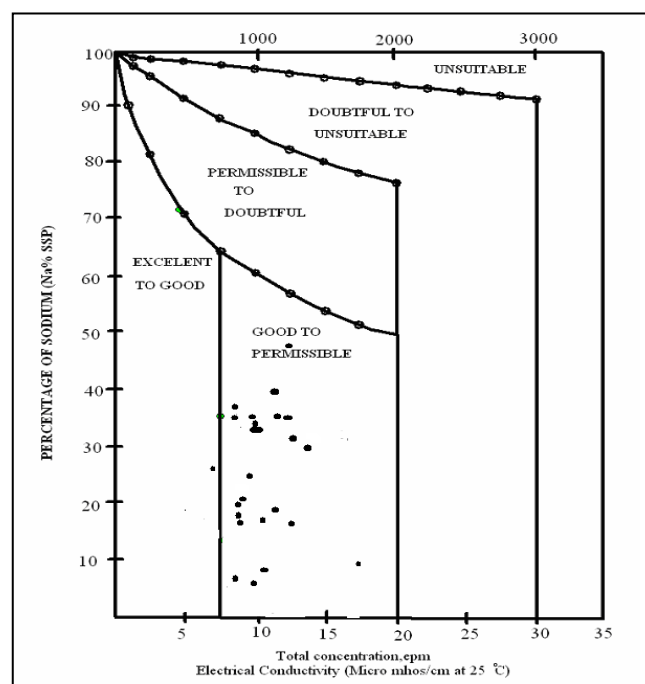


Fig. 3: Plot of Sodium percent vs. Electrical conductivity (after Wilcox 1955).

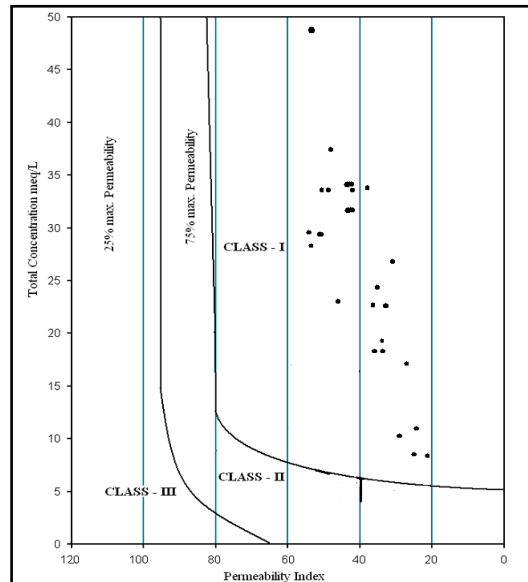


Fig.4: Classification of irrigation water (Doneen, 1962)

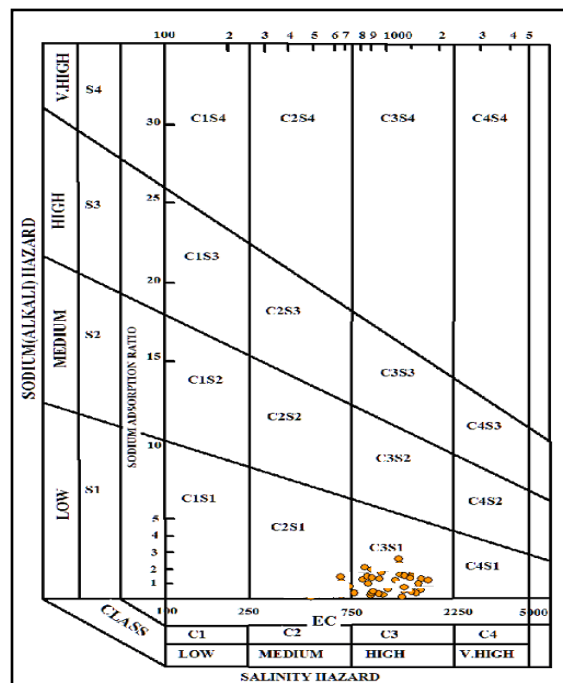


Fig. 5: U.S. Salinity Diagram for classification of irrigation water [after Richards (1954)]

Experimental Investigation & Evaluation of Incorporated Material to Set Their Optimum Re-Order Point

Anand Parashar¹, Pratesh Jayaswal²

Madhav Institute of Technology and Science Gwalior (M.P.) 4754005

Abstract –In a manufacturing company inventory cost is a significant part of expenses. Therefore reordering point (ROP) of the items must be optimum to reduce its carrying cost. In this present work, Investigations have made about the inventory control and R O P in a steel manufacturing plant in India to find the optimum ROP by applying ved and xyz analysis. Mathematical modeling is done with the help of Mat lab software.

Keywords- Re-Order Point (R.O.P.), inventory carrying cost (I.C.C.), VED analysis, XYZ analysis and Mat lab R2011b .

I. INTRODUCTION

In a manufacturing Plant some items are vital from production point of view but inventory cost of these parts is very high. It's not Feasible to keep more safety stock for these kinds of items but unavailability of these items can stop the manufacturing operation of that plant. Now-a-days, business environment is highly uncertain which affects the lead time of the procurement of the items and we have to keep the safety stock of such items. It can include that the company should achieve the balance among the safety stock they have to keep on hand and cost of carrying inventory. In this work an effort has made to find out the optimum value of Re-Order Point (R.O.P).

II. Literature review

A kanban technique attracted many researchers since it was first brought to light by Monden (1983). He originally summarized the Toyota approach for determining the appropriate number of kanbans at a workstation. It is applied recently in supply chain systems to efficiently manage the flow of materials. Rees et al. (1987) extended the Toyota approach to fluctuating product-mix problem by using the next periods forecast demand and the last periods observed lead times. Co and Sharafali (1997) considered the over-planning factor in Toyota's formula for computing the number of kanbans for several production inventory control models.

Altiok and Ranjan (1995) studied a multi-stage pull system that dealt with production inventory system. Martand Telsang (2004) describes the concept of Selective control which means variations in method of control from item to item based on selective basis. The criterion used for the purpose may be cost of the item, criticality, lead-time, consumption, procurement difficulties, or something else. Various classifications are employed to render selective treatment to different types of material, each classification emphasizes on a particular aspect. The ved analysis represents classification of items based on critically. The analysis classifies the items into three groups called Vital, Essential and Desirable. The xyz analysis is based on value of the stock on hand (i.e. inventory investment) items whose inventory values are high are called X items while those whose inventory values are low are called Z items. And Y items are those, which have moderate inventory stocks.

III. DATA COLLECTION

We have visited steel company when the manufacture leaf plate for spring and TMT bar 8mm , 10mm ,12mm, 16mm, 20mm, 25mm diameter. In for inventory they store more than 1000 items in store which are long used for production leaf plate and TMT bar.

Table1; Data Collected from Steel manufacturing plant in India

Name of the Item	Annual Require meant (S)	Ordering Cost in Rs. (Cp)	Unit Cost in Rs. (Cu)	% of Average Inventory Investment (I)	Lead Time (In Days) (LT)	Cons ump ion rate (CR)	Nature of the Item	Source of the supply	Way of the transport rotation
1	200	90	120	1.1904	15	180	Buyer's	Local	Truck
2	1300	60	353	1.2563	15	1279	Buyer's	Local	Train
3	1500	30	400	1.6543	15	1432	commercial	Local	Truck
4	2000	500	543	0.5875	15	1800	commercial	Local	Truck
5	460	25	220	0.0345	15	350	commercial	Local	Train
6	500	10	400	1.8763	15	400	Buyer's	Local	Truck
7	120	20	543	0.0045	15	100	Buyer's	Local	Truck
8	7	90	360	2.7734	21	6	Standard	National	Train
9	1800	120	110	1.8473	15	1650	Buyer's	Local	Truck
10	5	10	190	1.0084	15	4	commercial	Local	Truck
11	4	50	280	0.0765	15	1	Buyer's	Local	Truck

12	13	160	2904	0.1721	18	12	Standard	National	Truck
13	6	16	210	4.7691	15	12	Standard	National	Truck
14	120	75	180	1.8769	15	100	commercial	Foreign	Ship
15	246	37	450	0.3347	15	200	Standard	Local	Truck
16	456	73	200	0.5834	15	400	commercial	Local	Train
17	320	120	620	1.3541	15	260	commercial	Local	Truck
18	650	652	125	0.2541	15	550	commercial	Local	Train
19	15	120	128	0.0806	15	12	commercial	Local	Ship
20	65	10	652	0.9854	15	60	commercial	Local	Truck
21	1200	320	40	0.3654	15	1000	commercial	Local	Train
22	15	40	620	0.0125	15	12	commercial	Local	Train
23	15	15	400	2.7777	15	12	commercial	Local	Train
24	15	35	180	4.1661	15	12	Standard	Local	Train
25	180	40	120	1.1904	18	15	commercial	Local	Truck
26	18	120	4200	1.5625	15	6	Standard	Local	Truck
27	325	25	225	1.1904	20	300	Standard	Local	Truck
28	20	10	250	1.2563	15	10	Standard	National	Truck
29	450	60	500	1.6543	18	420	commercial	National	Truck
30	240	30	625	1.1904	20	5	commercial	Local	truck
31	500	90	451	1.1457	18	420	commercial	Local	Truck
32	800	65	120	0.3547	15	650	commercial	Local	Train
33	1600	255	30	0.3698	20	1200	Buyer's	Local	Truck
34	500	120	80	1.0147	15	150	Buyer's	Local	Train
35	13	70	640	0.8064	20	12	commercial	Local	Truck
36	32	20	45	0.1721	18	12	commercial	Local	Truck
37	1200	110	258	4.7691	15	950	Buyer's	Local	Train
38	300	10	125	1.8769	15	220	commercial	Local	Truck
39	1200	220	520	0.3347	15	960	Buyer's	Local	Truck
40	140	40	120	0.5834	18	120	commercial	National	Train
41	30	10	140	0.2145	18	5	commercial	Local	Truck
42	3000	354	459	0.2541	20	2700	commercial	Local	Truck
43	500	621	1005	0.3698	15	450	commercial	Local	Truck
44	60	25	30	0.1458	20	40	Buyer's	National	Truck
45	5295	140	62	0.3333	15	480	Standard	National	Truck
46	1262	320	1500	0.1851	18	965	commercial	Foreign	Ship
47	32	10	4500	0.1721	15	25	Buyer's	Local	Truck
48	254	39	150	4.7691	15	180	Buyer's	Local	Train
49	125	40	147	1.8769	18	90	Standard	Local	Truck
50	30	15	625	0.3347	20	10	commercial	Local	Train
51	985	90	320	0.5834	15	780	Buyer's	Local	Truck
52	150	160	60	0.0641	15	120	Buyer's	Local	Truck
53	254	60	75	1.8763	20	200	Standard	Local	Train
54	25	15	654	0.0045	18	10	commercial	Local	Truck
55	15	15	250	2.7734	15	10	Buyer's	Local	Truck
56	854	125	500	1.8473	18	720	Buyer's	National	Train
57	680	225	450	1.0084	20	560	commercial	Local	Truck
58	450	135	650	0.0765	15	420	commercial	Local	Truck
59	12	135	262	1.2584	18	1.2	Buyer's	Local	Truck
60	720	1200	7800	2.5	20	680	Standard	National	Truck
61	2	40	20	1.8518	15	1.2	commercial	National	Truck
62	352	420	480	2.5487	15	250	Standard	Foreign	Ship
63	5	10	159	0.1547	18	3	commercial	Local	Truck
64	254	25	320	0.1721	20	180	Buyer's	Local	Train
65	450	60	3520	4.7691	15	360	Buyer's	Local	Truck
66	120	40	258	1.8769	18	90	Standard	Local	Train
67	361	80	652	0.3347	20	250	commercial	Local	Truck
68	900	90	650	0.5834	18	750	Buyer's	Local	Truck
69	771	40	184	1.1904	15	625	Buyer's	Local	Train
70	124	35	450	1.2563	18	120	Standard	Local	Truck
71	254	80	251	1.6543	20	180	commercial	Local	Truck

72	320	40	250	0.2412	15	245	Buyer's	National	Train
73	954	90	500	0.6921	18	780	Buyer's	Local	Truck
74	3000	1200	200	0.4742	20	2565	commercial	Local	Truck
75	140	90	270	1.1904	18	100	Buyer's	Local	Truck
76	150	70	4200	0.25	15	110	commercial	National	Truck
77	265	45	250	1.4653	18	180	Buyer's	National	Truck
78	874	220	500	0.6345	20	650	commercial	Foreign	Ship
79	30	320	2000	0.6097	15	2510	Buyer's	Local	Truck
80	120	25	80	1.8934	18	10	Standard	Local	Train
81	458	65	62	0.5789	20	320	commercial	Local	Truck
82	5741	356	357	1.2676	18	4561	Buyer's	Local	Train
83	850	652	450	1.8763	18	680	Buyer's	Local	Truck
84	954	420	120	0.0045	15	852	Standard	Local	Truck
85	963	120	254	2.7734	18	863	commercial	Local	Train
86	357	120	500	1.8473	20	250	Buyer's	Local	Truck
87	952	90	625	1.0084	15	850	Buyer's	Local	Truck
88	431	80	780	0.0765	18	380	commercial	National	Train
89	940	20	1640	0.2487	20	880	Buyer's	Local	Truck
90	963	80	900	1.4376	18	620	Standard	Local	Truck
91	258	25	5000	0.2623	15	120	commercial	Local	Truck
92	456	50	1541	0.2541	18	400	Buyer's	National	Truck
93	621	80	650	1.0258	20	550	Buyer's	National	Truck
94	120	160	1320	0.4901	15	90	Buyer's	Foreign	Ship
95	900	220	500	0.2777	18	750	commercial	Local	Truck

IV. METHODOLOGY

For this Work we have investigated data from ved analysis and then xyz analysis. By applying both ved and xyz analysis we can find out such items which are very critical and important from research point of view. So, methodology is applied on these 12 items. For finding out the optimum R.O.P. In a manufacturing plant in India shown in table1. On all the items we applied firstly we use the regression modeling with the help of Mat Lab software.

A. VED Analysis

Here we 'V' is consider for 'Vital', 'E' is for 'Essential' and 'D' is for 'Desirable'. The result of this analysis will be helpful in converging our focus on the 'Vital items', for which the level of inventory control required would be tighter than the parts.

For ved analysis we consider following factors, which affects the R.O.P. of items in the plant:

1. Ordering cost(OC) (as per unit)
2. Lead Time (LT)(in Year)
3. Nature Of Item
4. Source Of Supply
5. Way Of Transportation

After finding out the factors which affects the R.O.P., we give them weight age according to their importance for R.O.P. For weight age of factors we draw a table as follows:

Table 2 : factors considered for ved analysis with the plan for weight age & point

S.r NO.	Factors	First Degree	Second Degree	Third Degree
1	Ordering coast(5)	OC<100 (5)	100<OC<1000 (10)	OC>1000 (15)
2	Lead Time(20)	LT <2 (20)	2<LT<4 (40)	LT>4 (60)
3	Nature of item (20)	Buyer's Design (20)	Commercial (40)	Standard (60)
4	Source of Supply (25)	Local (25)	National (50)	Foreign (75)
5	Way of Transportation (30)	Truck (60)	Train (60)	Ship (90)

On the basis of this table we categorized all the items into V or E or D as shown in table 3;

Points	Classification
<150	Desirable(D)
150to 175	Essential(E)
>175	Vital(V)

Table4: Categorization of item into V/E/D

Name of Item	Ordering cost (A)	Lead Time (B)	Nature of Item (C)	Source of Supply(D)	Way of Transportation (G)	Total (A+B+C+D+G)	Category (V/E/D)
1	5	20	20	25	30	100	D
2	5	20	20	25	30	100	D
3	5	20	40	25	30	120	D
4	10	20	40	25	30	125	D
5	5	20	40	25	30	120	D
6	5	20	20	25	30	100	D
7	5	20	20	50	60	175	E
8	5	20	60	50	60	195	V
9	5	20	20	25	60	130	D
10	10	20	40	50	30	145	D
11	5	20	20	25	30	100	D
12	10	40	60	50	30	190	V
13	10	20	60	50	90	220	V
14	5	20	40	50	60	175	V
15	5	20	40	50	30	150	D
16	5	20	40	25	30	120	D
17	10	20	40	25	30	125	D
18	10	20	40	25	60	155	E
19	10	20	40	25	60	190	V
20	10	20	40	25	30	125	D
21	5	40	40	25	60	170	E
22	5	20	40	50	30	120	D
23	5	20	40	50	30	185	V
24	5	20	60	25	60	170	E
25	10	40	40	25	60	175	V
26	10	20	60	25	60	250	V
27	10	20	60	25	60	200	V
28	5	20	40	50	20	135	D
29	5	20	40	50	30	145	D
30	5	20	40	25	60	160	E
31	10	40	40	25	30	145	D
31	15	20	40	50	30	145	D
33	5	20	40	50	30	145	D
34	5	40	40	25	30	140	D
35	5	40	60	75	90	270	V
36	5	40	60	50	60	220	V
37	10	20	60	75	90	250	V
38	5	20	60	25	30	140	D
39	5	20	40	25	30	125	D
40	5	20	40	25	30	120	D
41	5	20	40	25	60	150	E
42	5	20	40	25	60	150	E
43	5	20	60	25	60	170	E
44	5	20	40	50	30	165	E
45	5	20	40	50	30	145	D
46	5	20	90	50	60	225	V
47	5	20	40	50	60	200	V
48	5	20	60	50	30	165	E

49	5	40	60	50	30	175	E
50	5	60	60	50	60	235	V
51	5	40	60	75	60	140	D
52	5	60	60	50	60	235	V
53	5	20	40	50	30	145	D
54	5	20	40	25	30	120	D
55	5	20	40	25	30	125	D
56	10	40	40	25	60	175	E
57	10	40	20	50	30	150	E
58	10	40	40	50	30	170	E
59	15	60	40	50	60	225	V
60	5	40	40	25	60	170	E
61	10	60	40	50	60	215	V
62	5	40	60	25	30	160	E
63	10	20	20	75	90	215	V
64	5	20	40	75	30	170	E
65	10	20	60	50	30	170	E
66	10	20	60	50	30	170	E
67	10	20	40	50	30	150	E
68	5	20	40	50	30	145	D
69	15	20	40	50	30	155	E
70	5	40	40	50	30	165	E
71	10	40	60	25	30	165	E
72	5	40	60	25	30	160	E
73	10	20	60	25	30	145	D
74	10	20	60	50	30	170	E
75	5	20	60	50	60	195	V
76	5	20	60	50	60	195	V
77	5	20	60	50	30	165	E
78	5	20	60	50	30	165	E
79	10	40	60	50	30	190	V
80	5	20	60	25	30	140	D
81	5	20	60	50	30	165	E
82	5	20	60	25	30	140	D
83	5	20	60	25	30	140	D
84	5	20	40	50	60	175	E
85	5	20	40	50	60	175	E
86	5	20	60	50	30	165	E
87	5	20	40	50	60	170	E
88	5	20	40	50	60	170	E
89	5	20	60	50	60	190	V
90	5	20	40	50	30	140	D
91	5	20	20	25	30	95	D
92	5	40	60	25	30	155	E
93	15	40	40	25	30	135	D
94	10	60	40	50	60	210	V
95	5	20	40	25	30	115	D

B. XYZ Analysis

After ved analysis we will switch over to xyz analysis. For this analysis we consider I.C.C. for categorization of items into X or Y or Z. Here we consider X for higher I.C.C., Y for medium I.C.C. and Z for lower I.C.C. as shown in Table .

The following formula of Economic Order Quantity (EOQ) and Inventory carrying Cost (I.C.C.) is used for all 12 items selected for xyz analysis.

$$EOQ = \sqrt{(2S * C_P / C_U * I)}$$

$$I.C.C. = (EOQ/2) * C_U * I$$

Here S = Annual requirements of items (nos.)

C_P = Ordering cost (as per unit)

C_U = Manufacturing cost or Unit cost (Rs. Per Unit)

I = Inventory Investment

Factors considered for xyz analysis and Categorization

Categorization of items into X/Y/Z

Combined result of VED & XYZ

Categorization of items into X/Y/Z

Using the table we made a nine point matrix. In this matrix. We distribute the entire items category into the combination of V/E/D and X/Y/Z

Parameter	Category		
	X	Y	Z
Inventory carrying coast(I.C.C.)	I.C.C.>200	200>I.C.C._>100	I.C.C<100

Sr.NO.	Name of item	V/E/D	Category X/Y/Z
A	8	V	X
B	12	V	Y
C	13	V	X
D	14	V	Z
E	19	V	Z
F	23	V	X
G	25	V	X
H	26	V	X
I	27	V	Z
J	35	V	X
K	36	V	X
L	37	V	Y
M	46	V	Y
N	47	V	Y
O	50	V	X
P	52	V	X
Q	59	V	X
R	61	V	X
S	63	V	X
T	75	V	Y
U	76	V	Y
V	79	V	Z
W	89	V	Y
X	94	V	Z

Nine point matrix

	X	Y	Z
V	a,c,f,g,h,j,k,o,p,q,r,s	b,l,m,n,t,u,w	d,e,i,v,x
E	7,9,21,30,42,43,71,81,87,88,92		
D	1,2,3,4,5,6,31,41,38,39,53,54,73,80,82,90,91,93,95,		

By this table , we find out 12 items a,c,f,g,h,j,k,o,p,q,r,s that comes into category of X and V so these 12 items are very critical from research point of view so we applied methodology on these 12 items only.

C. calculation for Re-order point(R.O.P):

For calculation of R.O.P we consider the following steps for all 12 items

For item a:

Annual consumption = 6 kg

$$EOQ = 3.0045$$

$$\text{Lead time} = 21 \text{ days} = 21/365 = 0.057 \text{ year}$$

As 6 kg consumed in 1 year so as the 3.0045 will consume in 0.50075 year but lead time of the items is 0.057 year so the re-order of items a should be at least 0.057 year before so, appropriate re-order point of items 'a' is $0.50075 - 0.0575 = 0.4432$ year

Some calculation is applied for items c,f,g,h,j,k,o,p,q,r,s

For item c: ROP= 0.2712 year

For item f: ROP= 0.4597 year

For item g: ROP= 0.1986 year

For item h: ROP= 0.1792 year

For item j: ROP= 0.0253 year

For item k: ROP= 0.0639 year

For item o: ROP= 0.2594 year

For item p: ROP= 0.2928 year

For item q: ROP= 0.1482 year

For item r: ROP= 0.9454 year

For item s; ROP= 0.0336 year

D: Modeling of parameters

To generalize the results, the modeling of input parameters (consumption rate, lead time, & unit cost) and re-order point (R.O.P) is done using regression modeling and mat lab software R2011b

The parameters under consideration are

1) Consumption Rate (C.R)

2) Lead time (L.T)

3) Unit cost (U.C)

The re-order point is a function of C.R., L.T., and U.C so we can take R.O.P.as

$$\ln(R.P) = C_1 \ln(C.R) + C_2 \ln(L.T) + C_3 \ln(U.C)$$

Where C_1, C_2, C_3 are constant which are to be determined by regression modeling and using MATLAB software.

The output parameter re-orders point and input parameters are converted from actual absolute values to natural logarithms. For regression analysis the natural logarithms of re-order point is taken as single output parameter [Y] where as natural logarithms of C.R =[X₁]

In (R.P.) = C_1, C_2, C_3 are constants which are to be determined by regressing Modeling and using MATLAB software. The output parameter Re-order point and input parameter are converted from actual absolute valves to natural logarithms. For regression analysis, the natural logarithms of Re-order point is taken as single output parameter[Y] whereas natural logarithms of C.R. = [X₁], DELL

L.T. =[X₂],U.C. =[X₃] has been taken as input parameters $X = [X_1 \ X_2 \ X_3]$.

The following steps were followed and MATLAB is used

1. Consider the output parameter natural logarithms of Re-order point (R.P.) [Y] and input parameter [X].
2. X' = Transpose of [X] was determined.
3. X' Transpose of [X] was multiplied with [X] to get the product $[X' * X]$.
4. The inverse of product $[X' * X] = [X' * X]^{-1}$ was obtained.
5. X' transpose of [X] was multiplied with Re-order point (R.P.) [y] to get for product $[X' * Y]$.

6. Step 4 $[X' * X]^{-1}$ was multiplied with step 5 $[X' * Y]$ to obtained the product of $[X' * X]^{-1}$ and $[X' * Y]$.
7. The final matrices found in the form of :

$$\beta = \begin{bmatrix} \beta_1 \\ \beta_2 \\ \beta_3 \end{bmatrix}$$

Finally, after the completion of program and the values of constants found as follows:

- $C_1 = \beta_1$
- $C_2 = \beta_2$
- $C_3 = \beta_3$

From Regression Modeling we find out the values of ' β ' shown as follows:

$$B = \begin{bmatrix} -0.9474 & 0.2706 & -0.7543 & 5.3323 \end{bmatrix}$$

From this result we get

$$\beta = 5.3323$$

$$\beta = -0.9473$$

$$\beta = 0.2706$$

$$\beta = -0.7543$$

the values of constants obtained are :

$$C_1 \quad \beta = 5.3323$$

$$C_2 \quad \beta = -0.9474$$

$$C_3 \quad \beta = 0.2706$$

$$C_4 \quad \beta = -0.7543$$

Substituting these value then equation of R.O.P becomes

$$R.O.P. = (C.R)^{-0.9474} (U.C)^{0.2706} (L.T)^{-0.7543}$$

V. RESULT

Finally from the R.O.P formula the comparison between actually R.O.P.and calculated R.O.P.by modeling is to be done ,which is shown in below table.

S.No.	Actual Calculation		Calculation by modeling	
	R.O.P	100-R.O.P.	R.O.P	100-R.O.P.
a	0.4432	99.5568	0.3691	99.6309
c	0.2712	99.7288	0.4076	99.5924
f	0.4597	99.5403	0.5392	99.4608
g	0.1986	99.8014	0.1458	99.8542
h	0.1792	99.8208	0.2329	99.7671
j	0.0253	99.9747	0.0218	99.9782
k	0.0639	99.9361	0.0566	99.9434
o	0.2594	99.7406	0.2599	99.7401
p	0.2928	99.7072	0.2206	99.7794
q	0.1482	99.8518	0.1364	99.8636
r	0.0461	99.9539	0.0632	99.9368
s	0.0336	99.9664	0.0386	99.9614

VI. CONCLUSION

The basic aim of this research was to develop a 'Nine point competitive matrix for pull system' which will incorporate XYZ & VED analysis with, Kanban system, so as to optimize the inventory & reducing the number of stock out. In line with that, a competitive matrix has been developed.

Inventory carrying cost is a vital part of economic analysis. It varies with no. of items and its re-order point by mathematically modeling we find out that R.O.P. of every item directly proportional to its consumption rate, lead time , inventory investment and unit cost.

1. MONDEN, 1983 .The Toyota's production system .Industrials engineering and management press, Norcross, GA .

2. Rees, L.P., Philipoom, P.R., Taylor, B.W., Huang, P.Y., 1987. Dynamically adjusting the number of kanbans in a just-in-time production system using estimated values of lead time. IIE Transactions 19(2), 199-207.
3. Co, H.C., Sharafali, M., 1997. Over planning factor in Toyota formula for computing the number of kanban. IIE Transactions 29(5), 409-415.
4. Altioek, T., Ranjan, R., 1995. Multi-stage, pull-type production/inventory system. IIE Transactions 27(2), 190-200. Askin, R.G., Mitwas, M.G. Goldberg, J.B., 1993. Determining the number of kanbans in multiitem just-in-time systems. IIE.
5. Telsang Martand "Industrial Engineering and Production Management", Second Edition, 204.

Power Loss Minimization of Permanent Magnet Synchronous Generator Using Particle Swarm Optimization

Prashant Kumar S. Chinamalli¹, Naveen T. S.², Shankar C. B.³

¹(Electrical Department, Yashoda Technical Campus/Shivaji University, India)

^{2,3}(Electrical & Electronics Department, Acharya Institute of Technology, Bangalore, Vishweshwaraih Technological University, India)

ABSTRACT: Interior Permanent-magnet synchronous generators (IPM) are commonly used for variable-speed wind turbines to produce high efficiency, high reliability, and low-cost wind power generation. An IPM driven by a wind turbine, in which the d -axis and q -axis stator-current components are optimally controlled to achieve the maximum wind power generation and Particle Swarm Optimization (PSO) for loss minimization of the IPMSG. The effect of magnetic saturation, which causes the highly nonlinear characteristics of the IPMSG, has been considered in the control scheme design. The optimal d -axis stator-current command is obtained as a function of the IPMSG rotor speed by solving a constrained nonlinear-optimization problem that minimizes the copper and core losses of the IPMSG. At any wind speed within the operating range, the IPMSG rotor speed is optimally controlled to extract maximum wind power. The PSO technique guides to narrow convergence solution of non-linearity introduced in the model. The proposed control scheme provides the wind generation system with the maximum efficiency and high dynamic performance [1] [2].

Keywords: Permanent magnet synchronous generator, magnetic saturation, loss minimization.

I. INTRODUCTION

Resolving the world's growing demand for energy, for minimizing related impacts on the environment and with increased competition for energy supplies represent some of the greatest technical challenges of the next several decades. Fossil fuels supply more than 80 percent of the world's primary energy but they are finite resources and major contributors to global climate change. The ways and means for their ultimate replacement with clean, affordable and sustainable energy sources at the scale required to power the world are not yet readily available. Turning off the carbon emissions is the first step and many of the solutions which are familiar are windmills, solar panels, nuclear plants etc... All three technologies are part of the energy mix, although each has its issues, including noise from windmills and radioactive waste from nukes. Moreover, existing energy infrastructures around the world are complex and large, where they require enormous capital investment and have operational Life spans of 50 years or more. In windmills (a much older technology) wind energy is used to turn mechanical machinery to do physical work; historically, windmills were used traditionally for grinding grain or spices, pumping water, sawing wood or hammering seeds. The evolution of modern turbines is a remarkable success story of engineering and scientific skill, coupled with a

Strong entrepreneurial spirit. The progress of wind energy around the world in recent years has been

consistently impressive with the main engineering challenge to the wind industry to design an efficient wind turbine to harness energy and turn it into electricity.

The use of permanent-magnet synchronous machines (PMSMs) for wind power generation has received increasing attention in recent years [1]–[6]. The PMSMs can provide high-efficiency and high-reliability power generation, since there is no need for external excitation and no copper losses in the rotor circuits. In addition, the high-power density PMSMs are small in size, which reduces the cost and weight of wind turbines. Furthermore, in the wind generation system equipped with a PMSM and power-electronic converters, the wind turbine can be operated to extract the maximum power from the wind at various wind speeds by adjusting the shaft speed optimally. Therefore, the PMSMs are commonly used for small variable-speed wind turbines to produce high efficiency, high reliability, and low-cost wind power generation.

Energy production and utilization, efficiency is always an important issue, so previously the minimization of the core losses of a PMSM through a suitable design of magnets and slots and the choice of the number of poles. In fact, the efficiency of an IPMSM can be improved not only during the machine design stage but also during the operation stage. By optimally controlling the d -axis component of the stator currents even by optimizing the values with particle swarm optimization, the stator copper and core losses of an IPMSM can be minimized.

II. MODELING OF WIND TURBINE SYSTEM

The basic configuration of an IPMSG driven by a wind turbine is as shown in Fig.1. The IPMSG converts the mechanical power from the wind turbine to ac electrical power, which is then converted to dc power through an IGBT pulse-width modulation (PWM) converter with a dc link to supply the dc load. Control of the IPMSG is achieved by controlling the ac-side voltages of this PWM power converter. By using an additional power inverter, the IPMSG can supply the ac electrical power with constant voltage and frequency to the power grid or ac load.

The mechanical power that the wind turbine extracts from the wind is calculated by

$$P_m = \frac{1}{2} \rho A_r v_w C_p(\lambda, \beta) \quad (1)$$

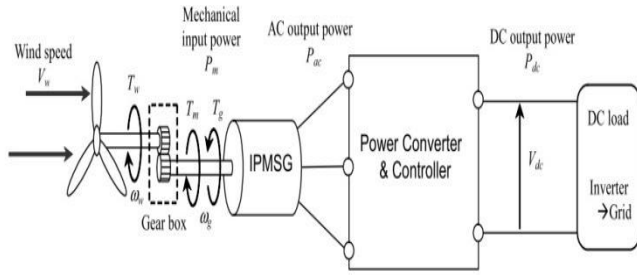


Fig. 1: Wind turbine system using IPMSG [4]

where ρ is the air density in kilograms per cubic meter, $A_r = \pi R^2$ is the area swept by the rotor blades in square meters, R is the wind-turbine rotor radius in meters, v_w is the wind speed in meters per second, and C_p is the power coefficient, which is a function of both tip-speed ratio λ and the blade pitch angle β . The mathematical representation of C_p is given by [4]

$$C_p(\lambda, \beta) = (0.3 - 0.00167\beta) \sin\left(\frac{\pi(\lambda + 0.1)}{10 - 0.3\beta}\right) - 0.000184(\lambda - 3)\beta(2)$$

Where λ is defined by $\omega_r R / v_w$ and ω_r is the wind-turbine rotational speed in radians per second.

The $C_p - \lambda$ curve described by Eqn (2) for the wind turbine is as shown in Fig. 2. In terms of Fig.2 and the definition of λ , at any wind speed within the operating range, there is a unique wind-turbine shaft rotational speed to achieve the maximum power coefficient C_{pmax} . In terms of Eqn (1), when C_p is controlled at the maximum value, the maximum mechanical power is extracted from the wind energy.

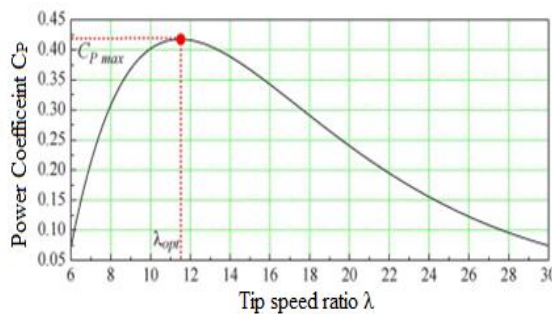


Fig. 2: $C_p - \lambda$ curve of the wind turbine.

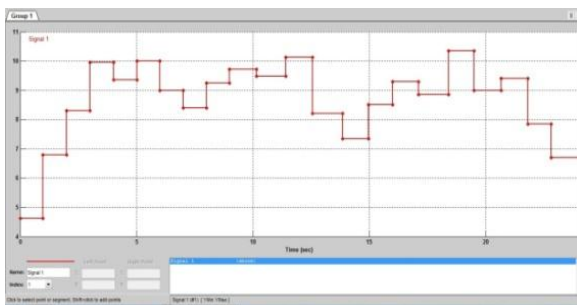


Fig. 3: Wind velocity input by signal builder.

The signal builder block is used to give wind speed as an input to the wind turbine which is as shown in Fig.3.

Wind speed is in the range of 4–11 m/s. The parameters of the wind turbine system as listed in Table. 1.

Table. 1: Parameters of the wind turbine system

Air density	1.08 kg/m ³
Rotor diameter	11 m
Rated wind speed	10 m/s
Rated rotational speed	200 m

III. MODELING OF PERMANENT MAGNET SYNCHRONOUS GENERATOR

Permanent Magnet Synchronous machines (PMSM's) are non-salient pole AC synchronous motors, these synchronous motor drives are suitable for constant speed applications as its speed of operation depends only on the frequency of the stator supply. Synchronous motor with permanent magnet is a choice in kW range for applications like wind turbines, aerospace actuators, electric vehicles etc. The advantages of permanent magnet synchronous motor over the other motors are of higher efficiency, higher torque to inertia ratio and compact in size. The PMSM used here is an Interior Permanent Magnet Synchronous Generator (IPMSG).

3.1 Dynamic Modeling:

The stator consists of three phase winding having spatial displacement from each other. The axis of phase-1 is taken as reference axis for the stationary co-ordinates fixed to the stator. The currents in the winding can have any general variation with respect to time. Assuming that the spatial distribution of mmf produced by each coil is sinusoidal in nature, the stator mmf caused by three phase currents flowing in the three windings can be represented by a single time varying quantity which has got some spatial orientation. The stator current space phasor diagram is shown in Fig. 4. The space vector of stator current can be represented in terms of three phase currents as,

$$i_s^s(t) = i_{s1}(t) + i_{s2}(t)e^{j\gamma} + i_{s3}(t)e^{j2\gamma} \quad (3)$$

where i_{s1} , i_{s2} and i_{s3} are the stator phase currents and γ is the advanced current angle.

The space vector of stator current can also be represented in terms of equivalent two phase (α - β) axis currents as,

$$i_s^s(t) = i_{s\alpha}(t) + ji_{s\beta}(t) \quad (4)$$

As $\gamma = 120^\circ$, the α axis current and β axis currents can be written as,

$$i_{s\alpha}(t) = i_{s1}(t) \cos 0 + i_{s2}(t) \cos 120 + i_{s3}(t) \cos 240 \quad (5)$$

$$i_{s\beta}(t) = i_{s1}(t) \sin 0 + i_{s2}(t) \sin 120 + i_{s3}(t) \sin 240 \quad (6)$$

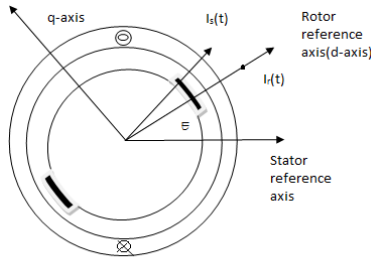


Fig.4: Representations of Co-ordinate Systems

The above equation can be simplified as,

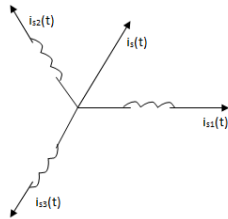


Fig.5: Stator current space phasor

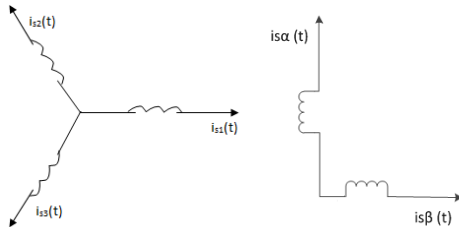


Fig.6: Stator current transformation from three phase to α-β axis.

$$i_{s\alpha}(t) = i_{s1}(t) - \frac{1}{2}i_{s2}(t) - \frac{1}{2}i_{s3}(t) \quad (7)$$

$$i_{s\beta}(t) = \frac{\sqrt{3}}{2}i_{s2}(t) - \frac{\sqrt{3}}{2}i_{s3}(t) \quad (8)$$

For a three phase wire system the condition,

$$i_{s1}(t) + i_{s2}(t) + i_{s3}(t) = 0 \quad (9)$$

holds good for all instants of time. Using this condition in above and (α-β) axis currents can be written as,

$$i_{s\alpha}(t) = \frac{3}{2}i_{s1}(t) \quad (10)$$

$$i_{s\beta}(t) = \frac{\sqrt{3}}{2}i_{s2}(t) - \frac{\sqrt{3}}{2}i_{s3}(t) \quad (11)$$

For the dynamic modeling, first convert the three quantities to two phase quantities i.e. abc to α-β transformation. The general formula can be given as below,

$$X_{\alpha} = \frac{3}{2}X_a \quad (12)$$

$$X_{\beta} = \frac{\sqrt{3}}{2}(X_b - X_c) \quad (13)$$

$$v_{s\alpha} = \frac{3}{2}v_{sa} \quad (14)$$

$$v_{s\beta} = \frac{\sqrt{3}}{2}(v_{sb} - v_{sc}) \quad (15)$$

Similarly the transformation of stator currents and voltages from α-β to d-q co-ordinates is done using the angle ε.

$$v_{sd} = v_{s\alpha} \cos \epsilon + v_{s\beta} \sin \epsilon \quad (16)$$

$$v_{sq} = v_{s\beta} \cos \epsilon - v_{s\alpha} \sin \epsilon \quad (17)$$

where ε is the angle between rotor reference axis and stator reference axis.

The above equations are used in the modeling of transformation of co-ordinates and sources as shown in the below Fig. 7, 8 and 9.

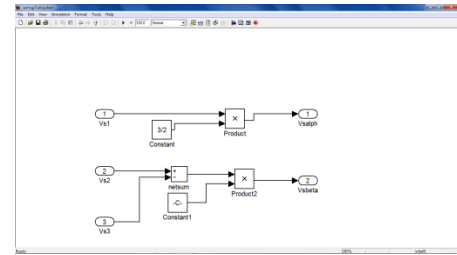


Fig.7: abc to α-β transformation

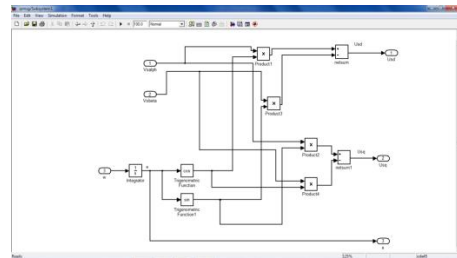


Fig.8: α-β to d-q transformation

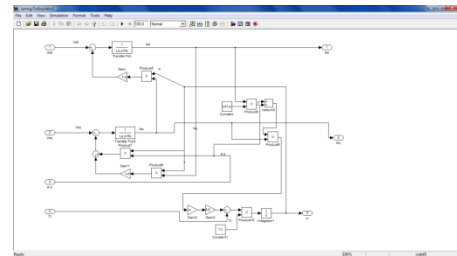


Fig.9: Voltage to Current transformation

3.2 Non-Linearity due to Magnetic Saturation:

Consider a typical Interior PMSG circuit as below in Fig.10. For the IPMSG, burying the magnets inside the rotor introduces saliency into the rotor into the rotor magnet circuit. The d-axis flux passes through a wide region of low-permeability magnets, while the q-axis flux path has a high permeability. Therefore, the IPMSG has a saliency ($L_q > L_d$) and the effect of magnetic saturation along the q-axis is dominant. Interior PMSG is considered with magnetic saturation, i.e. there is a flux linkage between the q-axis inductances so the L_q will be the function of current i_q and d-axis inductance L_d will be considered constant value and they are represented as L_{d1} , $L_q(i_q)$. The dynamic equation of a three-phase IPMSG can be written in the rotor reference frame as.

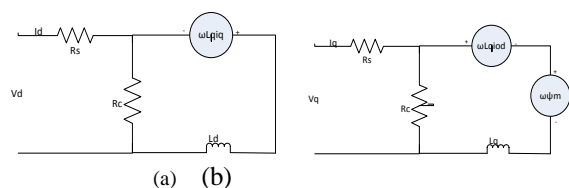


Fig.10. Equivalent circuits of the IPMSG. (a) d-axis equivalent circuit. (b) q-axis equivalent circuit.

$$L_d \frac{di_{od}}{dt} = -R_s i_d + \omega L_q (i_q) i_{oq} + v_d \quad (18)$$

$$L_q (i_q) \frac{di_{oq}}{dt} = -R_s i_q - \omega L_d i_{od} - \omega \psi_m + v_q \quad (19)$$

The electromagnetic torque developed by the machine is given by,

$$T_g = -\frac{3}{4} P_n [\psi_m i_{oq} + (L_d - L_q (i_q)) i_{od} i_{oq}] \quad (20)$$

The following equations help in complete dynamic modeling of IPMSG:

$$v_d = L_d \frac{di_{od}}{dt} + R_s i_d - \omega L_q (i_q) i_{oq} \quad (21)$$

$$v_q = L_q (i_q) \frac{di_{oq}}{dt} + R_s i_q + \omega L_d i_{od} + \omega \psi_m \quad (22)$$

$$J \frac{d\omega}{dt} = T_m - T_g \quad (23)$$

$$\omega = \int \frac{1}{J} (T_m - T_g) dt \quad (24)$$

$$\frac{d\epsilon}{dt} = \left(\frac{P}{2}\right) \omega = \omega_g \quad (25)$$

where ψ_m is the magnet flux linkage, R_s is the stator resistance, P_n is the number of poles, T_m is the input mechanical torque given by $T_m = P_m / \omega_g$, ω_g is the rotor speed, J is the inertia, i_{od} , i_{oq} are initial current values of d-axis and q-axis respectively, L_d is the d-axis inductance and assumed to be constant, and L_q is the q-axis inductance which varies depending on the value of i_q .

The effect of magnetic saturation is considered by modeling L_q as a function of i_q given by [1],

$$L_q = L_{q0} - k |i_q| \quad (26)$$

where k is a positive constant, the parameters of the IPMSG are given in the Table 2.

All the above equations along with parameters specified in Table.2 are used to model interior permanent magnet synchronous generator considering magnetic saturation as shown below in Fig.11.

Table 2. Parameters of IPMSG

R_s	0.1764 Ω
L_d	6.24 mH
L_{q0}	20.5822 mH
ψ_m	0.246 Wb
J	1.2 kg . m ²
P_n	6
k	0.1879 mH/A

Rated power	25 kW
Rated rotor speed	1200 rpm

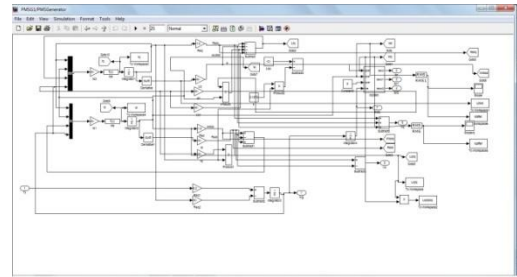


Fig 11. Simulink model of IPMSG

3.3 PWM Generator Side Converter:

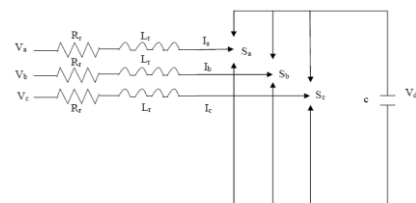


Fig . 12. PWM generator side converter

The pulse width modulation generator side converter consists of IGBT based 3-phase bridge voltage-source converter. The only difference between rectifier and inverter is the definition of power sign. The switching frequency of the converter is assumed to be sufficiently high to make an average analysis valid, which means that the switching ripple should be negligible compared to the averaged values. The generator side converter is shown in Fig. 12. The system equation for generator side converter can be written as:

$$V_a = R_r I_a + L_r \frac{dI_a}{dt} + V_{dc} \cdot \frac{2S_a - S_b - S_c}{3} \quad (27)$$

$$V_b = R_r I_b + L_r \frac{dI_b}{dt} + V_{dc} \cdot \frac{-S_a + 2S_b - S_c}{3} \quad (28)$$

$$V_c = R_r I_c + L_r \frac{dI_c}{dt} + V_{dc} \cdot \frac{-S_a - S_b + 2S_c}{3} \quad (29)$$

where V_a, V_b, V_c are the three phase stator voltage; I_a, I_b, I_c are three phase currents; S_a, S_b, S_c are gate pulses to IGBT and V_{dc} is DC link voltage.

IV. MODELING FOR MAXIMUM WIND POWER GENERATION WITH LOSS MINIMIZATION

4.1 Maximum Wind Power Generation:

By adjusting the wind-turbine shaft speed optimally, the tip speed ratio λ can be controlled at the optimal value to achieve the maximum power coefficient C_{Pmax} regardless of the wind speed. The maximum mechanical power is therefore extracted from the wind energy. At this optimal condition, the optimal IPMSG rotor speed is proportional to the wind speed, given by

$$\omega_{g,opt} = k_{\omega} v_w \quad (30)$$

Where k_{ω} is a constant determined by the wind-turbine characteristics. The generator rotor speed must be a nearer

value to the optimal rotor speed which leads to the extraction of maximum power from wind velocity.

4.2 Minimization of the Copper and Core Losses of IPMSG:

The losses of a PMSG can be decomposed into four components, namely, stator copper loss, core loss, mechanical loss, and stray-load loss. Only the stator copper and core losses are explicitly dependent on and can be controlled by the fundamental components of the stator currents. Therefore, the maximum efficiency condition of the IPMSG is obtained by solving the following nonlinear-optimization problem offline to minimize the total copper and core losses of the IPMSG i.e we have

$$P_{loss} = P_{copper} + P_{core} \quad (31)$$

$$P_{copper} = 1.5 R_s (i_d^2 + i_q^2) \quad (32)$$

$$P_{core} = 1.5 (i_{cd}^2 + i_{cq}^2) R_c (\omega_g) \quad (33)$$

$$= 1.5 \omega^2 \frac{[(L_d i_{od} + \psi_m)^2 + (L_q (i_q) i_{oq})^2]}{R_c (\omega_g)} \quad (34)$$

Where P_{copper} is the copper loss, P_{core} is the core loss [6], and i_{cd} and i_{cq} are the currents at the resistant R_c .

An optimal IPMSG rotor speed calculated by Eqn (30), the solutions of the nonlinear-optimization problem yield the optimal values of i_d and i_q , which minimize the total copper and core losses of the IPMSG. Therefore, at any wind speed, the solutions of Eqn (30) and Eqn (34) provide the desired optimal IPMSG rotor speed, optimal currents i_d and i_q to achieve the maximum wind power extraction, and loss minimization of the IPMSG. Without considering the effect of magnetic saturation (i.e., L_q is constant) and the variation of R_c , Eqn (34) would be a constrained nonlinear quadric optimization problem that can be solved by conventional nonlinear-optimization methods. However, the inclusion of magnetic saturation and variation of R_c results in a complex nonlinear-optimization problem that requires extensive computation effort when using conventional nonlinear optimization methods. In order to achieve this stochastic optimization technique called particle swarm optimization (PSO) [5] is employed to obtain the optimal solution of Eqn (34).

V. PARTICLE SWARM OPTIMIZATION

Particle Swarm Optimization is a population-based stochastic optimization technique. It searches for the optimal solution from a population of moving particles. Each particle represents a potential solution and has a position (vector x_i) and a velocity (vector v_i) in the problem space. Each particle keeps track of its individual best position $x_{i,pbest}$, which is associated with the best fitness it has achieved so far, at any step in the solution. Moreover, the best position among all the particles obtained so far in the swarm is kept track of as x_{gbest} . This information is shared by all particles.

The PSO algorithm is implemented in the following iterative procedure to search for the optimal solution.

- 1) Initialize a population of particles with random positions and velocities of M dimensions in the problem space.
- 2) Define a fitness-measure function to evaluate the performance of each particle.
- 3) Compare each particle's present position x_i with its $x_{i,pbest}$ based on the fitness evaluation. If the current position x_i is better than $x_{i,pbest}$, then set $x_{i,pbest} = x_i$.
- 4) If $x_{i,pbest}$ is updated, then compare each particle's $x_{i,pbest}$ with the swarm best position x_{gbest} based on the fitness evaluation. If $x_{i,pbest}$ is better than x_{gbest} , then set $x_{gbest} = x_{i,pbest}$.
- 5) At iteration k , the velocity of each particle is updated by

$$v_i(k+1) = w \cdot v_i(k) + c_1 \phi_1 (x_{i,pbest}(k) - x_i(k)) + c_2 \phi_2 (x_{gbest}(k) - x_i(k)), i = 1, 2, \dots, N. \quad (35)$$

- 6) Based on the updated velocity, each particle then changes its position by
- 7) Repeat steps (3) to (6) until a criterion, usually a sufficiently good fitness or a maximum number of iterations, is achieved.

The final value of x_{gbest} is regarded as the optimal solution of the problem.

In Eqn (35), c_1 and c_2 are positive constants representing the weighting of the acceleration terms that guide each particle toward the individual best and the swarm best positions, $x_{i,pbest}$ and x_{gbest} , respectively; ϕ_1 and ϕ_2 are uniformly distributed random numbers in $[0, 1]$; w is a positive inertia weight developed to provide better control between exploration and exploitation; N is the number of particles in the swarm. The last two terms in Eqn (12) enable each particle to perform a local search around its individual best position $x_{i,pbest}$ and the swarm best position x_{gbest} . The first term in Eqn (35) enables each particle to perform a global search by exploring a new search space.

Because of many attractive features, e.g., multi-agent search, simple implementation, small computational load, and fast convergence, the PSO algorithm can provide a fast and efficient search for the optimal solution. These features provide PSO with superior performance over other evolutionary computation algorithms (e.g., genetic algorithms) in many applications. In addition, for many complex optimization problems that are difficult to formulate mathematically or to solve by traditional optimization methods, PSO is efficient to find the optimal solution.

The values of the PSO parameters are chosen as:

$$c_1 = c_2 = 2, N = 20 \text{ and } w = 1.4 - (1.4 - 0.4)$$

$*(k/K)$, where k is the iteration number and K is the maximum number of iterations. The PSO algorithm only performs a 1-D search for the optimal value of i_q . The optimal value of i_d is determined by the torque in Eqn (20) and the corresponding optimal value of i_q , where the electrical torque T_g in Eqn (20) is determined by Eqn (30) and the constraint equations of Eqn (34). The fitness-measure function is simply the total copper and core losses P_{loss} of the IPMSG. It is calculated by the first two constraint equations of Eqn (34). By solving the nonlinear-optimization problem in Eqn (34) at various IPMSG rotor speeds, the optimal values of i_d and i_q are obtained as functions of the IPMSG rotor speed ω_g . The relationship between the optimal d -axis and q -axis stator-current

components and the IPMSG rotor speed can be approximated by a fourth-order and a third-order polynomial, respectively, given by

$$i_{d,opt} = K_{d4}\omega_g^4 + K_{d3}\omega_g^3 + K_{d2}\omega_g^2 + K_{d1}\omega_g + K_{d0} \quad (37)$$

$$i_{q,opt} = K_{q3}\omega_g^3 + K_{q2}\omega_g^2 + K_{q1}\omega_g + K_{q0} \quad (38)$$

The coefficients of both polynomials are listed in Table 3. However, it should be pointed out that Eqn (37) and Eqn (38) only provide the optimal operating conditions of the IPMSG for the wind speed below the rated value. When the wind speed exceeds the rated value, the phase current and/or the terminal voltage reach their ceiling values, and therefore, the optimal speed tracking control cannot be applied. Under this condition, the current and voltage limited maximum output control can be applied to control IPMSG.

Table 3. Coefficients of approximating polynomials

Coefficients of $i_{d,opt}$		Coefficients of $i_{q,opt}$	
K_{d4}	1.291×10^{-11}	K_{q3}	7.528×10^{-9}
K_{d3}	-3.523×10^{-8}	K_{q2}	-3.477×10^{-5}
K_{d2}	1.154×10^{-5}	K_{q1}	-1.648×10^{-3}
K_{d1}	-1.348×10^{-2}	K_{q0}	1.263
K_{d0}	-1.589×10^{-2}		

VI. CONTROL OF PMSG

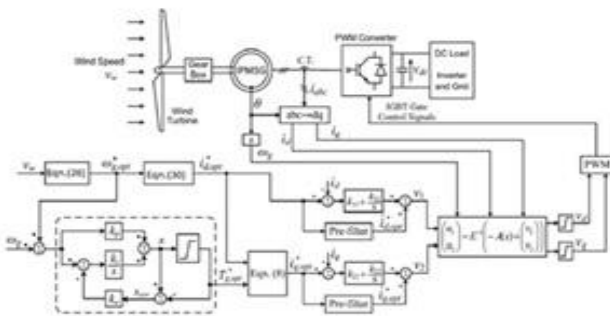


Fig. 13: Control of scheme for the IPMSG

6.1 Optimal IPMSG Rotor-Speed Tracking Control:

Based on the IPMSG motion Eqn (23), a PI-type speed controller is designed to track the optimal rotor speed at any moment, applied for the speed controller, as shown by the dash-line block in Fig. 22. The gain k_a is given by $k_a = 1/k_p$. The output of the speed controller is the optimal torque command $T_{g,opt}^*$ for the IPMSG, which corresponds to the maximum power point for wind power generation. By using this optimal torque command and the optimal d-axis current command from Eqn (37), the solution of Eqn (20) provides the optimal q-axis stator-current command for the inner loop current regulation. In the real application, the values of $i_{q,opt}^*$ can be generated offline over the entire operating range of the IPMSG.

6.2 IOL- Based Non-Linear Current Control:

Instead of approximating a nonlinear system's dynamics locally around some operating point via linearization, the IOL technique transforms the nonlinear system into an equivalent linear system via feedback and nonlinear coordinate transformation. This is a systematic way to globally linearize a part of or all the dynamics of the nonlinear system. In such a scheme, the input-output dynamics are linearized, but the state equations may be only partially linearized. Residual nonlinear dynamics, called internal dynamics, do not depend explicitly on the system input and, thus, are not controlled. If the internal dynamics are trivial or stable at the equilibrium point, then the entire nonlinear system can be stabilized by a standard linear feedback control using the linearized input-output dynamics.

VII. RESULTS

The model of Wind turbine system and IPMSG are previously run for the existing condition of initial values. Later, speed control and current control techniques are introduced for the optimization of rotor speed and current by running Particle Swarm Optimization algorithm. In PSO algorithm the complete model is called through command to get the desired output of Maximum generation and Power loss minimization. All results are taken from the simulation of the modeling in MATLAB 2011b.

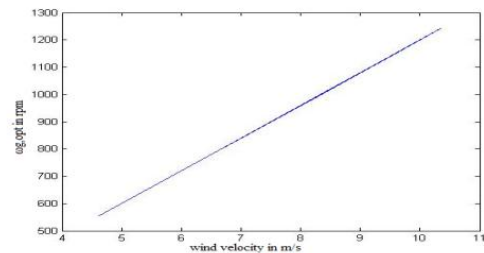


Fig .14. wind velocity Vs $\omega_{g,opt}$

As per the Eqn(30) the $\omega_{g,opt}$ varies linearly with respect to the wind velocity as shown in Fig .14. From this it can be justified that as the wind velocity varies the rotor speed varies optimally in a linear manner.

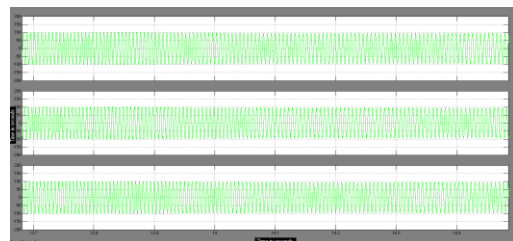


Fig. 15. Three phase stator current

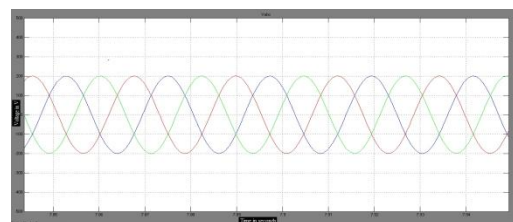


Fig .16. Three stator voltage

Fig. 15 and Fig. 16 show the three-phase controlled stator current and voltage of the IPMSG after PSO. As voltage is 200V and current is 100A so it can be stated that WTG system generates upto 20 Kw power. The simulated result for a dc link current, which is controlled by the rectifier side controller, is as shown in Fig. 17.

For maximum wind power tracking the speed controller is employed, this can be noticed from Fig 18 and Fig 19. Because of the relatively slow response of the WTG mechanical system, during the acceleration of the WTG, the PI-type speed controller is saturated, and the resulting IPMSG electrical-torque command generated by the speed controller remains at its limit value of zero.

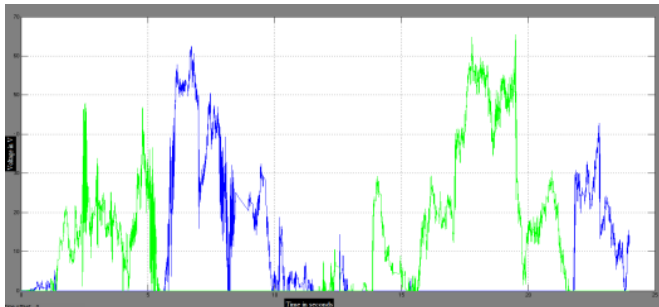


Fig .17. DC link voltage

As a result, the electrical output power and the q -axis stator current of the IPMSG are both regulated at zero during the saturation of the speed controller.

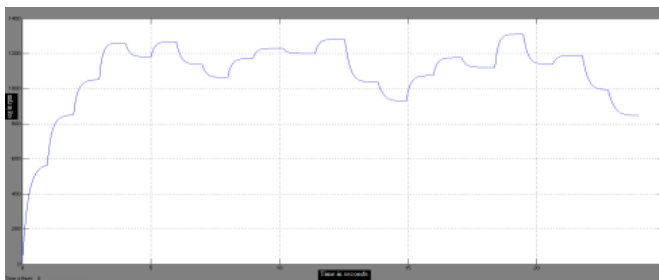


Fig .18. Time Vs ω_g

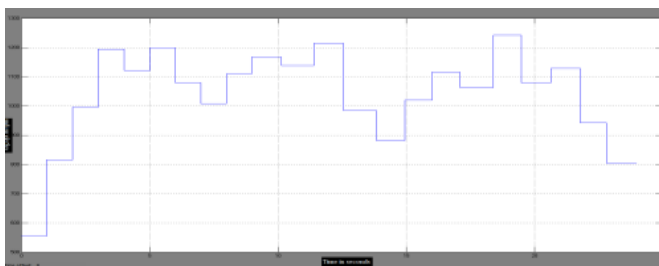


Fig. 19. Time Vs $\omega_{g,opt}$

The optimized results of current of d -axis and q -axis are shown Fig. 20 and Fig. 21. It can be observed that by the optimization the magnetic saturation is nullified.

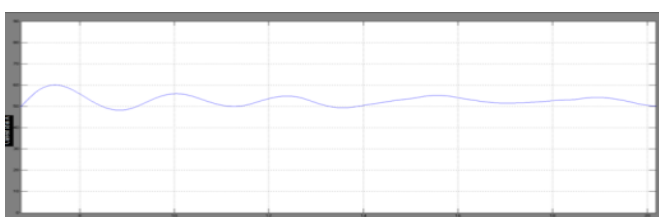


Fig .20. Time Vs I_d , after PSO

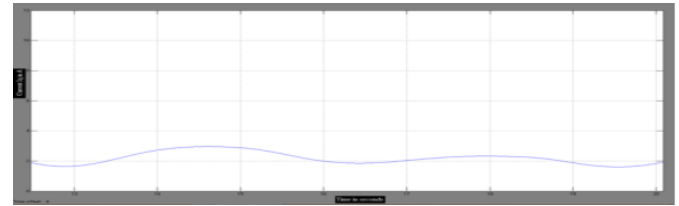


Fig. 21. Time Vs I_q , after PSO

After the PSO algorithm the optimized results of currents are incorporated in Eqn (34), hence there is a minimization in the total power loss as shown in Table 5.

Table .5. Total P_{loss} minimization

Total P_{loss} before PSO	Total P_{loss} after PSO	Total P_{loss} minimization
3.3 kW	2.57 kW	22.12%

VIII. CONCLUSION

Modeling and simulation of a 25kW variable speed wind energy conversion system employing a Maximum Torque per Current control and Particle Swarm Optimization is presented in the paper. PMSGs are commonly used for small variable speed WTG systems. In such systems, by adjusting the shaft speed optimally, the maximum wind power can be extracted at various wind speeds within the operating range. In addition, when using an IPMSG, the stator copper and core losses of the generator can be minimized by optimally controlling the d -axis component of the stator currents. However, to achieve the high performance of the WTG system, magnetic saturation of the IPMSG must be taken into account in the control-system design. Implementation of PSO results in the minimization of total power loss and thus improves the efficiency of the system. This proposed control provides the wind generation system with high dynamic performance and improved power efficiency.

REFERENCES

- [1] T. M. Jahns, G. B. Kliman, and T. W. Neumann, "Interior permanentmagnetsynchronous motors for adjustable-speed drives," *IEEE Trans. Ind. Appl.*, vol. IA-22, no. 4, pp. 738–747, Jul./Aug. 1986.
- [2] E. Muljadi, C. P. Butterfield, and Y. Wang, "Axial-flux modular permanent- magnet generator with a toroidal winding for wind-turbine applications," *IEEE Trans. Ind. Appl.*, vol. 35, no. 4, pp. 831–836, Jul./Aug. 1999.
- [3] S. Grabic, N. Celanovic, and V. A. Katic, "Permanent magnet synchronous generator for wind turbine application," *IEEE Trans. Power Electron.*, vol. 13, no.3, pp. 1136–1142, May 2008.
- [4] S. Morimoto, H. Nakayama, M. Sanada, and Y. Takeda, "Sensorless output maximization control for variable-speed wind generation system using IPMSG," *IEEE Trans. Ind. Appl.*, vol. 41, no. 1, pp. 60–67, Jan./Feb. 2005.
- [5] Y. Shi and R. C. Eberhart, "Empirical study of particle swarm optimization," in *Proc. IEEE Int. Conf. Evol. Comput.*, May 4–9, 1998, pp. 69–73.
- [6] H. Li, Z. Chen, Institute of Energy Technology, Aalborg University, Aalborg East DK-9220, Denmark, "Overview of different wind generator systems and their comparisons". Published in IET Renewable Power Generation Received on 24th January 2007, Revised on 23rd August 2007.

BIOGRAPHY

Prashantkumar.S.Chinamalli born in Shahapur, Karnataka, India on 10th June 1987, received his B.E. degree in Electrical & Electronics Engineering department from Poojya Doddappa Engineering College, Gulbarga in 2010. M.Tech in Power & Energy System from Basaveshwara Engineering Department in 2012. His areas of interest include Power System, Drives and Renewable Energy Sources. He is presently working as Asst. Prof in the Department of Electrical Engineering at Yashoda Technical Campus/Shivaji University, Pune, India.

Naveen T S born in Bangalore, Karnataka, India on 11th Oct 1986, received his B.E. degree in Electrical & Electronics Engineering department from Acharya Institute of Technology, Bangalore in 2008. M.Tech in Power & Energy System from Basaveshwara Engineering Department in 2012. His areas of interest include Power System, Reactive Power management. He is presently working as faculty in the Department of Electrical & Electronics Engineering at Acharya Institute of Technology, Bangalore, India.

Dr. Shankar C B was born in Raichur, Karnataka, India in 1969. He obtained B.E (Electrical & Electronics) and M.E. (Energy systems) degree from Karnataka University Dharwad, Karnataka, India in 1991 and Dec 94 respectively. He got his Ph D from VTU in 2011. His areas of interest include FACTS controllers, optimization techniques and intelligent systems.

He has attended National and International Conferences. He is member of IEEE and presently working as Professor in the Department of Electrical & Electronics Engineering at Acharya Institute of Technology, Bangalore, India.

Influence of chemical admixtures on density and slump loss of concrete

Mr. M K Maroliya.

Assistant professor, Applied Mechanics Dept, Faculty of Technology & Engineering, M. S. University of Baroda, Vadodara,

ABSTRACT: The results of test conducted on concrete in the presence of plasticizers and super plasticizers. The objective was to observe the change in density of concrete & loss of workability under the influence of plasticizers and super plasticizers at various dosages level. The result of the treated mix was compared with the control mix (mix without admixture). Observations were made on solid phases of concrete, to note the variation in density at constant and reduce water cement ratio. From the experience and knowledge gained from this course of study both, plasticizers and super-plasticizers not only improved workability at constant water cement ratio but considerably enhanced the density at reduce water-cement ratio however loss in slump observed.

Key words: slump loss, density, compressive strength, workability.

I. GENERAL INTRODUCTION

All round the globe effort are being made to make concrete a more exact material .and introduction to Admixtures has been one of the most notable contribution to concrete technology.

Today efforts are made not only to improve concrete's compressive strength but also durability. Durability has gained worldwide concern because experts believe that the expenditure in rehabilitation and resurrection of concrete structure in near future going to be equal to the expenditure of new construction. Admixtures are used to change the rheological properties of concrete or mortar to make them suitable for the work at hand, or for economy, or for such other purpose as saving energy.

In many instances e.g. very high strength, resistance to freezing and thawing, for retardation and acceleration of setting time, an admixture may be that only feasible means of achieving the desired result. In other instances, certain desired objectives may be best achieved by changes in composition of proportion of the concrete mix, if doing so result in greater economy than by using an admixture.

Out of different Types of admixtures used, plasticizers and superplasticizers topped the chart. Hence, some effort was made to understand the effect of both plasticizers and superplasticizers in concrete, in a comprehensive manner. Due to certain limitations more stress was laid on understanding the modifications in workability and compressive strength, because a better understanding of their two properties helps us to gauge their effect on other important properties also.

II. EXPERIMENTAL STUDY

Best efforts were made to understand the effects of different types of plasticizers and superplasticizers. A plasticizer – calcium lignosulphate (CLS) and super plasticizers – sulphonated melamine formaldehyde condensate (SMF) and sulphonated naphthalene formaldehyde condensate (SNF) were used to understand their effect on behavior of concrete and highlight the difference between them.

Many times information given by manufactures might appear to be exaggerated. It is quite necessary for a structural engineer to study the quality effects claimed by investigators and manufactures and then quantify the benefits of plasticizers and super plasticizers to produce a novel and economical design of structural units.

The main theme behind conducting the series of experiments was to study the modifications in workability and loss of slump due to the presence of plasticizers and super plasticizers.

The control mix of proportion 1:1.67:3:3.33 by mass, obtained by nominal mix design procedure was used which gives normal workability (55 to 60mm at 0.54 water cement ratio) and M20 grade concrete. Different types of water reducing admixtures at different dosage level were used at constant and reduced water cement ratio. Due to its narrow range plasticizers were used at dosage level of 0.3, 0.45, and 0.6 percent by weight cement. But fir superplasticizers, 05, 0.75, 1.0 percent dosage levels were selected looking to their high range of dosage application slump and slump loss at different dosage levels were also observed at different interval of time

In first step the w/c ration was kept constant and CLS, SNF and SMF were applied at different dosage level to observe the change in workability with the help of slump test. In second step the plasticizers and superplasticizers were applied at the same dosage level as before, but the w/c ration was reduced so as to keep the slump constant.

Once the positive sign of strength gain started to appear, certain quantity of cement was reduced to understand the effect of reduction of cement content on workability and compressive strength. The sole idea behind reducing cement content was to understand the economic benefits of using WRAs. During the course of investigation the effect of WRA s on slump loss was noted.

III. MATERIALS SPECIFICATIONS

- Ordinary Portland cement, 53 Grades conforming to I.S.269-1967.
- River sand ('Goma' sand) passing through is 4.75 mm sieve.
- Dried Basalt crushed stones (Kapchi) with maximum size of 20mm.

Table 1.0 Properties of Plasticizers.

properties	CLS	SMF	SNF
Specific Gravity	1018 ± 0.01	1.22 ± 0.1	1.22 to 1.225 @ 25 °C
Chloride Content	Nil (i.e. less than 0.2%)	Nil	Nil (BS 5075 and IS : 456)
Air entertainment	Less than 2%	Less than 2%	Less than 1%
Self life	12 Months	12 Months	12 Months
Standards	IS: 9103 – 1979	ASTM:C 494	IS: 9103 – 1979, BS: 5.75 -III

IV. MIX PROPORTIONING

Using sand and gravel conforming to IS 383-1979 cubes were casted using mix proportion of 1:1.67:3.33 by weight, which yields M20 grade concrete on 28 days curing. When cement was reduced by 10% the proportion changed to 1:1.86:3.72. With the increase in sand content mix of proportion 1:2.03:3.03 (40% sand of total aggregate) and 1:2.28 : 2.78 (45% sand of total aggregate) was used. Sample were weighted to an accuracy of 50 grams (0.1% of total weight of batch)

V. RESULTS AND DISCUSSION

5.1 EFFECT ON SLUMP LOSS

Maintaining the increased slump is as important as obtaining gain in zero hour slump. Slump test at short intervals were performed to understand the effect of water reducing agent on slump loss. **Table 2.0** shows the comparison of normal concrete with treated concrete.

The most notable observation made was that the rate of slump loss in case of treated concrete was greater than the control mix. With the increased in dosage level not only the slump loss was reported to be higher but the time required to attain zero slump was also increased. Both of the above observations showed pronounced effect with the increased in the dosage level with all type of water reducing admixtures.

The drastic improvement in slump loss was short lived (for few minutes) After first few minutes the slump reduced heavily, at least by 30% to 40% .After this initial period the rate of slump loss was reduced, but was still higher than the control mix.

Result showing the increase in slump at different dosage of water reducing admixtures and after what time the slump equal to zero-hour slump of control concrete was reported is below-

Table 2.0 LOSS OF SLUMP.

WRA type	Dosage level %	Initial slump (mm)	Time after which slump equal to slump of control concrete was reported (min.)
CLS	0.45	117	20
SMF	0.5	163	40
	0.75	175	465
ANF	0.5	179	45
	0.75	190	50

The 60-65 mm slump obtained in case of control mix was obtained even after 20 minutes using CLS and after 40-45 minutes with superplasticizers depending upon the dosage level. With SMF, the time required for zero hour slump increased to 95 and 105 minutes at 0.5 % and 0.75% dosage level compared to 65 minutes in control mix, with SNF the time increased 10 100 and 115 minutes at 0.5% and 0.75% dosage. With CLS the time required for zero slump could be extended from 65 minutes to 90min. From fig.4.29 it can be seen that the slump loss increased in presence of water reducing admixtures and was again higher at higher dosages.

5.2 EFFECT OF DENSITY

Density is a very important parameter as it affects many important properties of concrete including its durability. To understand the effect of water reduction on the density, almost all the cubes were weighed. The weight of the cubes was divided by the volume of moulds used to work out the density. Logically, as the density increases, porosity should reduce giving a durable concrete. All the cubes were weighed after curing to estimate the change in weight after curing. Such observations were noted for control mix and mixes with different water admixtures at different water reducing admixtures as different dosage levels. It was observed that as the water cement ratio was decreased the density of concrete cubes improved. This can be one of the reasons for the increase in the strength of concrete at reduced water cement ratio. For the control mix the average density was reported to be approximately 2700 kg/m³ at water cement ratio 0.54

As the change in density has to do more with the water cement ratio than the type of admixtures, water cement ratio would be taken as a sole variable to explain the change in the density. With the use of water reducing admixtures at the reduced water cement ratio 9with constant slump0, density increased from 2700 to 2745 kg/m³ when the water cement ratio was reduced in the range of 0.42 to 0.44 And when the water cement ration was reduced to 0.4 or less the density improved to 2770 kg/m³ When the cubes were weighed after curing, the weight was reported to be marginally higher. Cubes made from mixes with water cement ratio 0.54 change in the weight was roughly 3.6% When the water cement ratio was reduced to 0.41% 0.44 the change in weight was reduced to 0.8% and at water cement ratio of 0.4 or less the change was low to account (0.12%)

Thus with the decrease in water cement ratio the density increased whilst the change in weight decreased. Once again the use of water reducing admixtures was justified in improving the quality and performance of concrete.

VI. CONCLUSIONS

- Initially the slump loss was very high but the slump of treated concrete at all ages was greater than the control mix. The slump loss was found to be higher for a treated mix than control mix
- The slump loss also increases with the increase in the dosage level.
- At higher dosage signs of segregation and bleeding were noticed, composition needs to adjust the sand content to take care of this problem.
- increase in the dosage level as the water cement ratio required for the given slump decreased, the density of concrete is increased also the percent change in weight of the cubes after curing decreased with reduction in water cement ratio. For maintaining constant slump the reduction in water content for CLS was 5.5% to 14.8%, 20% to 27.7% for SMF and 22.2% to 30.5% for SNF, depending upon the dosage level. There was excessive increase in the compressive strength at reduced water cement ratio.

REFERENCES

- 1) Ram chandran. V. S. *Properties Concrete Mixes and Admixtures*.
- 2) Vance Dodson. *Concrete admixtures .Structural engineering series*. Van Nostrand Reinhold, New York.
- 3) ACI committee 212, *Guide for admixture in concrete*, Journal of American concrete institute Vol.68, No -09 Sept.1971.pp 5-41.
- 4) Banfill P.F.G, *a viscometric study of cement pastes containing Super plasticizers* notes on experimental techniques.
- 5) Kumar V, Roy B.N and A.S.R Sai, *Effect of Super plasticizers on concrete* Indian concrete Journal Vol.68 june1994, pp31-33.
- 6) Litvan G .G, *Air entrainment in presence of Super plasticizers*. Journal of American concrete institute Vol.July-august 1983.pp 326-330.
- 7) Manjrekar S K, *Use of Super plasticizers: Myth sand Reality* .Indian concrete Journal Vol. 68,june 1994 pp317-320.
- 8) Neville, A.M., (1995) "*Properties of concrete*", Pitman, London, 4ème edition, ISBN0-582-23070-5

Stress Analysis of Pulse Detonation Engine Tube

T K Jindal

Assistant Professor PEC University of Technology Chandigarh.

ABSTRACT: *The pulse detonation engine (PDE) has recently emerged as an aerospace propulsion system of the future. In the PDE system, self-sustaining detonation waves propagate in tubes and gases burning behind the detonation front are exhausted backward repeatedly. The PDE system momentum is equal in absolute value to the exhausted gas momentum, but in the opposite direction. The PDE system has high thermal efficiency because of its constant-volume combustion, and it has a simple structure composed of tubes. In this paper we analyze the pulse tube for the pressure build-up during detonation. Axial circumferential and hoop stress are calculated for a selected pipe with respect to temperature for single shot experiments.*

Keywords: *Pulse detonation, deflagration, detonation, thrust stand, hoop stress.*

I. PULSE DETONATION ENGINE

All regular jet engines and most rocket engines operate on the deflagration of fuel, that is, the rapid but subsonic combustion of fuel. The pulse detonation engine is a concept currently in active development to create a jet engine that operates on the supersonic detonation of fuel.

The main difference between a PDE and a traditional pulse jet engine is that the mixture does not undergo subsonic combustion but instead, supersonic detonation. In the PDE, the oxygen and fuel combination process is supersonic, effectively an explosion instead of burning. PDE is considerably more efficient. In the pulse jet engine the combustion pushes a considerable amount of the fuel/air mix (the *charge*) out the rear of the engine before it has had a chance to burn (thus the trail of flame seen on the V-1 flying bomb).

Even while inside the engine the mixture's volume is continually changing, which is an inefficient way to burn fuel. In contrast, the PDE deliberately uses a high-speed combustion process that burns all of the charge while it is still inside the engine at a constant volume to increase the amount of heat produced per unit of fuel above any other engines, although conversion of that energy into thrust would remain inefficient.

The major difficulty with a pulse-detonation engine is starting the detonation. While it is possible to start a detonation directly with a large spark, the amount of energy input is very large and is not practical for an engine. The typical solution is to use a deflagration-to-detonation transition (DDT) that is, start a high-energy deflagration,

and have it accelerate down a tube to the point where it becomes fast enough to become a detonation.

The most widely used is the "Shchelkin spiral", which is designed to create the most useful eddies with the least resistance to the moving fuel/air/exhaust mixture. The eddies lead to the flame separating into multiple fronts, some of which go backwards and collide with other fronts, and then accelerate into fronts ahead of them.

NASA maintains a research program on the PDE, which is aimed at high-speed, about Mach 5, civilian transport systems. However most PDE research is military in nature, as the engine could be used to develop a new generation of high-speed, long-range reconnaissance aircraft that would fly high enough to be out of range of any current anti-aircraft defences, while offering range considerably greater than the SR-71, which required a massive tanker support fleet to use in operation.

II. THE TEST RIG DESIGN

As the research is active at world level to develop a pulse detonation engine, we at PEC University of technology recently entered in the field of research with a sponsored project from DRDO. Initially the test rig was designed for carrying out the single detonation with acetylene and oxygen. The test rig as shown in the figure has a thrust stand on which the experimental pulse detonation system has been installed so that it can slide freely with minimum friction.

The pulse tube was selected from the stainless steel seamless pipes available in the market which were analysed for the strength so that it can sustain the pressure build up during detonation. The pressure developed during C_2H_2 design value was kept as 100 bar. The tube length was kept variable in the form of pieces of the tube joined with the help of flanges. Any number of different lengths can be connected to get the desired length of the pipe. The figure-1 shows the front top and side view of the rig.

III. ANALYSIS OF THE PULSE TUBE STRENGTH

Stainless Steel Grade 304 is the used for the pulse tube. It is austenitic, corrosion resistant steel with excellent *strength*. The selection of the pulse tube was on the basis of the strength and the stresses developed due the pressure build-up due to detonation of the gases. The tube for which the results have been shown has an internal diameter of 48mm and thickness of the pipe is 6mm. The figures below show the arrangement of the pipe and the thrust stand.

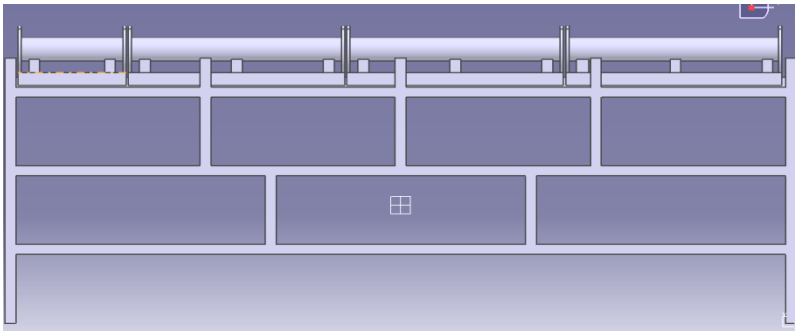
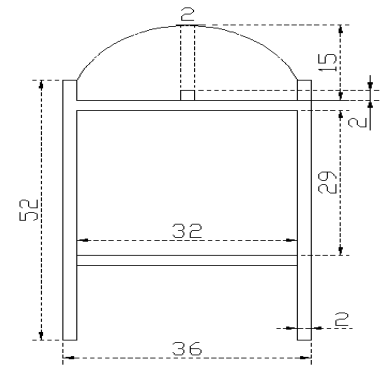


Figure 1 2 View drawing of Test stand (Dimensions in Inches)



3.1 Stress Calculations

While most of the literature is seen on the phenomenon of Pulse detonation the literature on the tube design is hardly available. In the present case the stress has been calculated using the standard expression from the strength of material text books. Longitudinal, circumferential and radial stresses have been calculated for the different pipes which are available in the market. The stress calculations for the selected tube dimensions are being shown here. The analysis can also be done using software like ANSYS etc. The author is of the view in this case simple analysis can serve the purpose, however later on the detailed analysis will be done as the research further progresses.

Longitudinal Stresses in the Detonation Tube.

$$\sigma_l = \frac{P_{in} R_{in}^2}{R_{out}^2 - R_{in}^2} \quad (1)$$

Where

P_{in} The pressure build up in the tube

P_{out} Outside pressure

R_{in} Inner diameter of the pipe

R_{out} Outer diameter of the tube.

σ is the stress developed due pressure build up.

Circumferential Stresses in the Detonation Tube

$$\sigma = \frac{R_{in}^2 P_{in} - R_{out}^2 P_{out} + (P_{in} - P_{out}) R_{in}^2 R_{out}^2 / R^2}{R_{out}^2 - R_{in}^2} \quad (2)$$

Radial Stresses in the Detonation Tube

$$\sigma = \frac{R_{in}^2 P_{in} - R_{out}^2 P_{out} - (P_{in} - P_{out}) R_{in}^2 R_{out}^2 / R^2}{R_{out}^2 - R_{in}^2} \quad (3)$$

The mechanical properties of selected SS304 are as shown in the table 1.

Table-1

Property	Value
Tensile Strength, Ultimate	505 MPa
Tensile Strength, Yield	215 MPa
Modulus of Elasticity	193 - 200 GPa
Poisson's Ratio	0.29
Charpy Impact	325 J
Shear Modulus	86 GPa

IV. RESULTS

The figures 2 below shows the axial/longitudinal stress w.r.t the pressure in the pulse tube. The stress developed varies linearly. The curve shows the stress developed upto 100 bar of pressure. The maximum stress developed at 100 bar is 177X10⁶ N/m². Which is fairly within the limit of 215 MPa?

The yield stress of SS304. Figure 2, 3, and 5 show the variation of stress developed in the tube at different conditions as shown.

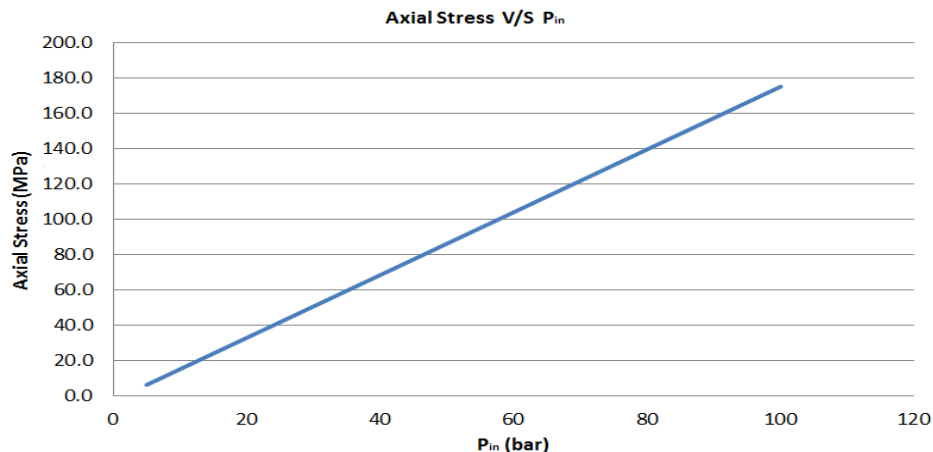


Figure 2 Axial Stress V/S P_{in}

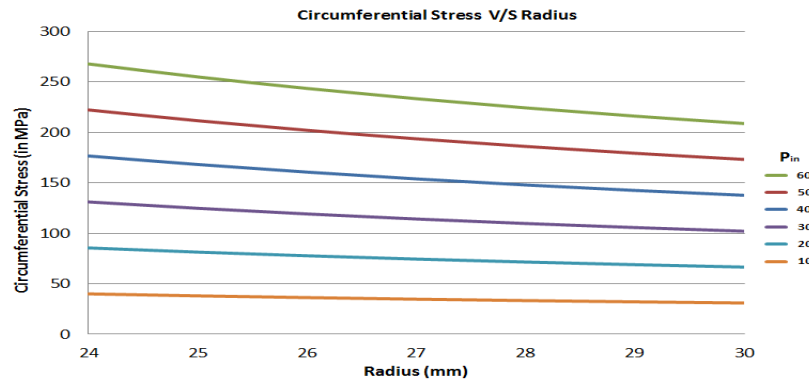


Figure 3- Circumferential stress V/S radius

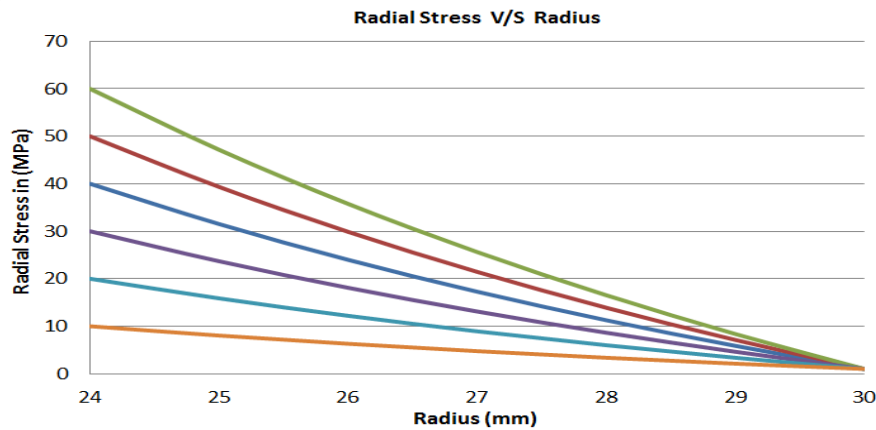


Figure 4-Radial Stress V/S Radius

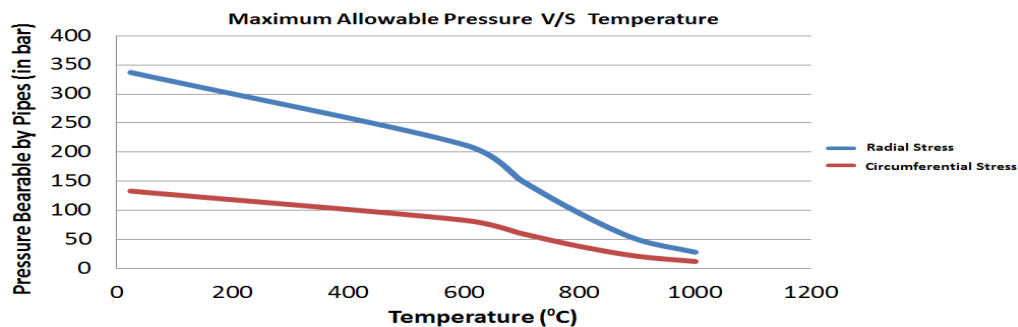


Figure 5- Maximum allowable V/S Temperature of the Detonation Tube

V. Conclusion

From the figures above shown that the pipe selected i.e SS304 with internal diameter of 48 mm and external diameter of 60mm can bear a pressure of 100 bar within the elastic parameter upto 400°C of temperature and hence the testing can be done on the rig till the tube it reaches to a temperature of 400°C. The temperature rise depends upon the number of shots and frequency of shots therefore the safe time and frequency of the testing can be determined w.r.t the temperature of the tube.

REFERENCES

- [1] T. Bussing and G. Pappas, Adroit Systems, Inc., "An Introduction to Pulse Detonation Engines," 32nd Aerospace Sciences Meeting and Exhibit, Reno, NV, AIAA 94-0263 (10-13 January 1994).
- [2] Pulse Detonation Engine Technology: An Overview by Matthew Lam, Daniel Tillie, Timothy Leaver, Brian McFadden.
- [3] S. Eidelman, W. Grossman, N. Gunners and I. Lotti, Science Applications International Corporation, "Progress in Pulsed Detonation Engine Development," 30th AIAA/ASME/SAE/ASEE Joint Propulsion Conference and Exhibit, Indianapolis, IN, AIAA 94- 2721, (June 1994).
- [4] Brady J. Bartosh, "Thrust measurement of a split-path, Valveless pulse detonation engine", Thesis, Naval Postgraduate School, 2007.
- [5] Strength of materials by R K Bansal, Laxmi Publications, Ltd., 01-Jun-2010

Pulse Detonation Engine - A Next Gen Propulsion

T K Jindal

Assistant Professor PEC University of Technology Chandigarh.

Abstract: Pulse detonation technology has the potential to revolutionise both in-atmosphere and space flight. Having an engine capable of running efficiently at Mach 5 will not only allow for faster, more efficient intercontinental travel, but will also change the way spacecrafts are launched. The present paper discusses about the applications of Pulse detonation engines and different possible variants of the engine.

Key words: Pulse detonation, deflagration, detonation, DDT

I. INTRODUCTION

The main differences between the PDE and the conventional internal combustion engine is that in the PDE the combustion chamber is open and no moving parts are used to compress the mixture before ignition and no shaft work is extracted. Instead the compression is an integral part of the detonation, and two of the main advantages of the PDE are the efficiency and simplicity which can be

explained by the fact that the combustion occurs in detonative mode. The efficiency of the cycle can be explained by the high level of pre compression due to the strong shock wave in the detonation. Also, the simplicity of the device is a result of the fact that the shock wave responsible for this compression is an integral part of the detonation. PDE is similar to both the pulse-jet and the ram jet engine as no moving part is present in these engines. But in those two cases the mechanism behind the pre-compression is completely different. For the pulse-jet the pre-compression is a result of momentum effects of the gases, and is a part of the resonance effects of the engine. In the ramjet, pre-compression is obtained through the ram effects as the air is decelerated from supersonic to subsonic.

The major drawback with this concept is that the engine is ineffective for speeds lower than around $M = 2$. The pulse detonation engine works on Humphrey cycle whereas gas turbines work on Brayton cycle. The cycles are as shown in the figure-1.

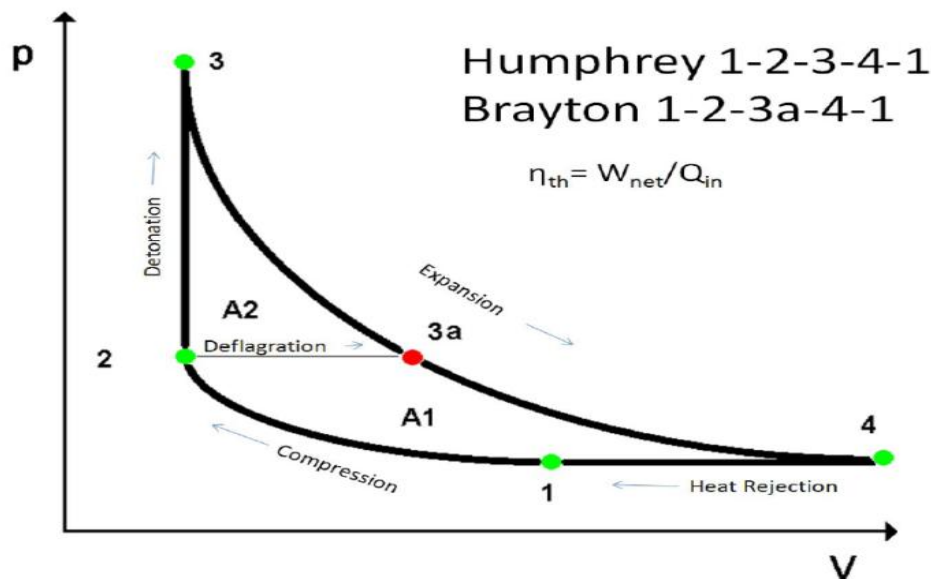


Figure-1 Comparison of Humphrey and Brayton Cycle.

The Humphrey cycle gives more area under the PV curve. Making it more efficient engine as compared to Gas turbine Engines. The frontal area in case of pulse detonation engine will be very small thereby reducing drag to a large extent.

II. APPLICATIONS OF PULSE DETONATION ENGINES

Pulse detonation engine although in the development stage can have following applications.

2.1 Pulse Detonation Applications

The applications of pure PDEs are primarily military, as they are light, easy to manufacture, and have higher performance around Mach 1 than current engine technologies (Marshall Space Flight Center). This makes

them an ideal form of propulsion for missiles, unmanned vehicles, and other small-scale applications (NASA Glenn Research Center 2004). The decrease in efficiency of PDEs at higher Mach numbers, the noise generated by them, and the advantages of using them in a hybrid combination, means that pure PDEs will likely not be used often for large-scale applications (Marshall Space Flight Center 200).

2.2 Hybrid Pulse Detonation Applications

Pulse detonation engines are well-suited for combination with turbofan and turbojet engines. This hybrid combination can be applied not only to produce faster aircraft, but also to make them more efficient and environmentally friendly. In a conventional turbofan engine, air travels into and around the combustion chamber. The air

travelling around the chamber mixes with the exhaust from the combustion chamber to provide the thrust. In a hybrid pulse detonation engine, the bypass air enters pulse detonation tubes that surround the standard combustion chamber as shown in the figure-2. The tubes are then cyclically detonated; one detonates while the others fill with air or are primed with fuel. This combination promises to require simpler engine mechanisms and yield higher thrust with lower fuel consumption (NASA Glenn Research Center 2004; General Electric 2004).

Hybrid pulse detonation engines will allow commercial aircraft to be faster, more efficient, and more environmentally friendly. NASA is projecting that the intercity travel time will reduce significantly by the year 2007, and inter-continental travel time will also reduce significantly by 2022, thanks to this technology. In addition, they suggest that NO_x emissions may decrease by up to 70% and 80% respectively in the same time periods (NASA Glenn Research Center 2004).

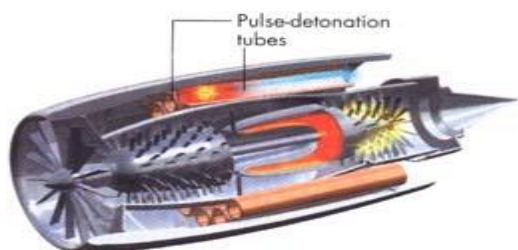


Figure 2: A PDE Hybrid Turbofan (right)

Similarly, hybrid PDEs can also be used in military applications. A large number of modern fighter jets employ afterburner-equipped low-bypass turbofan or turbojet engines. Although this process is an effective solution, it is not a fuel efficient solution. Hybrid PDEs will deliver the same thrust with less fuel consumption.

2.3 Pulse Detonation Rocket Engines (PDREs)

Similar to PDEs, PDREs produce thrust by cyclically detonating propellants within a detonation chamber and exhausting the combustion products through a nozzle. However, unlike PDEs PDREs must carry all of the oxidizer necessary to complete their specific missions onboard, and PDREs may have vacuum start and restart requirements for many applications. PDREs will incorporate propellant storage, feed, and injection system components; one or more detonation chambers ignition systems, detonation chamber/nozzle interface hardware, nozzles, and engine control system components. Similar to PDEs, numerous PDRE configurations may evolve depending upon engineering design solutions adopted to overcome technical challenges.

Once propellants are injected into PDRE detonation chambers, the fast-acting propellant injection valves close to seal the detonation chamber and detonation is initiated. The detonation wave passes through the

detonation chamber at supersonic velocities, igniting the propellants and elevating the upstream pressure to several times (6-12 times) that of the initial fill pressure. Like conventional, steady combustion rocket engines, PRDEs require pressurization of the detonation chamber to obtain high performance. However, due to the high pressure ratios associated with detonation combustion, PDRE detonation chamber fill pressures are much lower than chamber pressures associated with conventional rocket engines.

PDREs can employ a variety of thermodynamic cycles to power turbo pumps, such as gas generator, staged combustion, or expander cycles, or incorporate pressurized feed systems. PDRE operating pressures may be on the order of 100-200 psia, as compared to several hundred psia for conventional open cycle engines and several thousand psia for conventional closed cycle engines.

The multiple-chamber PDRE concept shown in Figure-3 is provided by Pratt & Whitney Aero sciences. This concept includes six detonation chambers coupled to a common feed system and nozzle assembly. Operationally, the detonation chambers are fired in a phased manner allowing the feed system and manifolds to operate in a steady state manner. All of the detonation chamber combustion products are exhausted through the single common nozzle.

Other PDRE configurations are possible. PDRE designs and configurations are influenced by specific mission requirements and engineering solutions adopted to address fundamental technical and operability issues.

2.4 Pulse detonation wave engine

One option for a hypersonic vehicle might be four or six Pulse Detonation Wave Engines (PDWEs), fuelled with liquid methane. As air breathers, these PDWEs could theoretically propel a hypersonic aircraft towards Mach 10 at an altitude in excess of 180,000 feet.

The PDWE works by creating a liquid hydrogen detonation inside a specially designed chamber when the aircraft is traveling beyond the speed of sound [3]. When traveling at such speeds, a thrust wall is created in front of the aircraft. When the detonation takes place, the airplane's thrust wall is pushed forward. This process is continually repeated to propel the aircraft. From the ground the jet stream looks like "donuts-on-a-rope." Not much is known about Pulse Detonation Wave technology, but there have been quite a few reports and sightings of mysterious aircraft using propulsion technology unlike any heard or seen before. One of them is like.....

On February 25, 26, and 27, 1992, there were night-time sightings of an unknown aircraft with a "diamond-pattern" of lights at Beale Air Force Base, which was thought to be the Aurora aircraft. The aircraft had a distinctive engine noise, described as "a very, very low rumble, like air rushing through a big tube." On the night of February 26, what was thought to be a ground test of Aurora's propulsion systems took place. A series of

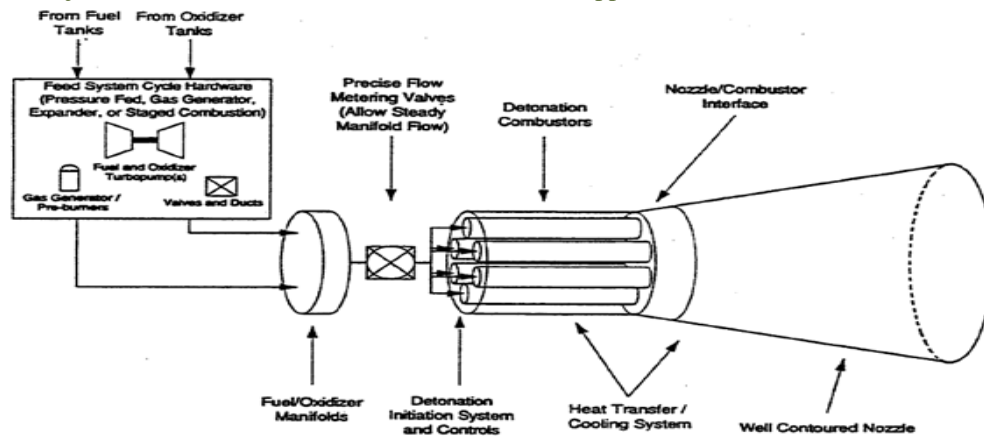


Figure 3 Conceptual Pulse detonation rocket engine

Booms" was heard and described as similar to "artillery fire" and "deep bass notes, not like sonic booms." It was thought these were "light-off" tests of the engines. It was speculated that the aircraft was using Pulse Detonation Wave Engines. The noise and low frequency would, it was said, be consistent with PDWE technology.

III. SPACE FLIGHT APPLICATIONS

While air breathing pulse detonation engines would not be able to operate in space, they may be used to reduce the cost and complexity of launching spacecraft. As PDEs do not require heavy and expensive pumps, they offer a viable alternative to current rocket engines. The decreased weight, along with better fuel consumption, would significantly reduce the cost of launching spacecraft. Using pulse detonation in combination with other propulsion sources could potentially decrease the cost of launching payloads into space.

IV. CONCLUSION

The Pulse detonation is a new technology, though the research started well in 1940. The pulse detonation engines have many advantages over the other engines for propulsive purposes and can be more reliable when developed fully. The main concern is the production of the shocks and noise. The other concern is the frequency of operation and the control of the temperature in the tube which lead to the material concerns. However there have been many excellent demonstrations of the engine all over the world. Pulse detonation engine is being seen as promising next generation propulsion system which will give aircrafts a clean configuration.

REFERNECES

- [1] PULSE DETONATION ENGINE TECHNOLOGY: AN OVERVIEW by Matthew Lam, Daniel Tillie, Timothy Leaver, and Brian McFadden Applied Science 201The University of British Columbia November 26, 2004.
- [2] T. Bussing, J. Hinkey and L. Kaye, Adroit Systems, Inc., "Pulse Detonation Engine Preliminary Design Considerations," 30th AIAA/ASME/SAE/ASEE Joint Propulsion Conference, Indianapolis, IN (27-29 June 1994).
- [3] E. Lynch and R. Eidelman, Rockwell International, "Analysis of the Pulse Detonation Wave Engine," Developments in High-Speed-Vehicle Propulsion Systems, AIAA Progress in Astronautics and Aeronautics, Vol. 165, pp. 473-516 (1996).
- [4] T. Bratkovich, et al., Adroit Systems, Inc., "An Introduction to Pulse Detonation Rocket Engines (PDREs)," 33rd AIAA/ASME/SAE/ASEE Joint Propulsion Conference and Exhibit, Seattle, WA, AIAA 97-2742 (6-9 July 1997),
- [5] Mawid, M.A., Park, T.W., Sekar B. & Arana C. (2003). Application of pulse detonation combustion to turbofan engines. Journal of Engineering for Gas Turbines and Power 125(1). 270-283.

Development of Web-Based Courseware for Van Hiele's Visualization Level

Jaemu Lee¹, Minhee Kim²

¹Department of Computer Education, Busan National University of Education, South Korea

²Ulsan Maekog Elementary school, South Korea

ABSTRACT: This study developed web-based courseware applying van Hiele theory in order to offer different levels of content for figure learning for elementary mathematics students.

In mathematics education, it is difficult to increase educational efficiency by conducting individual learning according to student ability because of the large differences in student levels, in addition to high populations in each classroom. This study provides courseware using van Hiele's visualization levels in order to offer different levels of content. This proposed courseware can improve students' learning achievement by offering differentiated content to learners who need advanced or supplementary learning materials. It also enhances learners' spatial-perception ability by offering various operating activities in figures learning.

Key words: Courseware, E-learning content, Figure learning, Individual learning, van Hiele theory

I. INTRODUCTION

Mathematics, like reading, is an important skill in our everyday lives. Mathematical reasoning is something we all do, from simple counting to complex calculations; however, the ability to use these skills varies greatly and difficulties emerging in childhood can persist through to adulthood. A solid grounding in basic numeracy helps children to succeed in other subject areas in the curriculum and develop more advanced mathematical skills that are essential for higher education and employment [1].

The field of geometrical figures is essential to many parts of mathematics textbooks and is closely related to students' lives. Although it acts as a foundation for abstract visualization, which students find difficult, a proper level of teaching is rarely possible and problems, which are not appropriate to the level of the students, are often assigned [2].

A major drawback of traditional instruction is that many teachers "teach to the middle" [3,4], which means that the needs of a growing number of students go unmet. Traditional instruction has a particularly deleterious effect on students with disabilities who often display diverse cognitive abilities, evidence multiple and varied instructional needs, and perform academically below their same-age classmates [5]. These deficits make students with disabilities especially vulnerable to a one-size-fits-all approach to instruction. The net result is that many of these students perform poorly on standardized tests, and have high dropout rates, low graduation rates, and high percentages of unemployment [6]. One solution is what experts refer to as

Differentiated instruction. Differentiated instruction is the process of "ensuring that what a student learns, how he/she learns it, and how the student demonstrates what he/she has learned is a match for that student's readiness level,

Interests, and preferred mode of learning" [7].

In order to solve such problems, educational resources at various levels were produced according to the cognitive level of students. Even now, however, problems such as excessive numbers of students per class, superior class recognition due to group formation, excessive amounts of work for teachers, problems in the development of supplementary and night educational programs, etc. are occurring; these make the educational process operations for various levels difficult [8].

In this study, various leveled studies applying van Hiele theory are provided. A web-based courseware applying van Hiele theory was developed in order to support different levels of studies in geometrical figure learning for elementary students.

II. VAN HIELE THEORY

In this chapter, we refer van Hiele theory as theoretical background.

1. The Components of the van Hiele Theory

The three components of the van Hiele model are insight, van Hiele thinking level, and studies level [9]. The learner must undergo five levels in their education experience, and if one cannot pass a certain level, that person may not move on to the next.

Insight is the ability to carry on an assignment even in unfamiliar situations and to perform the situational requests proficiently. It also means being able to thoughtfully and consciously find solutions for certain situations.

If students have insight, it means that they know and understand what they are doing, why they are doing it, and when they will do it. In addition, students who have insight have the ability to use their knowledge when solving problems [10].

1.1 The Geometrical Thinking Level of van Hiele Theory Van Hiele theory classifies students' geometrical study thinking levels into the following five categories [11, 12].

The first level is visualization or the holistic level.

It is the basic level and, rather than looking at a geometrical concept through the components or properties, it is seen as a whole. A geometrical shape, when it comes to physical appearance, is identified not through partial characteristics, but through its shape as a whole. Children who are at this level can identify and copy geometrical terms and shapes; but children of this level cannot identify right angles or parallel lines. Thus, when they see a rectangular box, they identify it as being a square shape, and a triangular ruler as a triangle shape, and a delicious pizza as a circular shape. They are able to understand that the shapes are different from one another, but that is about all they are capable of doing.

Although they can identify squares, rectangles,

parallelograms, etc. and other shapes, they are not able to confirm the relationship between the various shapes. In addition, they cannot understand the concept of all squares being rectangles and all rectangles being parallelograms. Children focus on the visual characteristics of the 'geometric' shapes in order to tell them apart.

The second level is the analysis or description level.

In the second level, the classification of geometric concepts begins. Through observation and experimentation, the characteristics of figures are divided. Through these characteristics, the shapes are classified. The fact that figures have parts, and these parts form a geometric figure is identified. Students, however, are not able to make a precise mathematical definition for the figure. In addition, since they do not clearly understand the definition, they are also not able to understand the relationships between the figures' characteristics. Children at this level, for example, recognize that parallelograms have parallel lines and are congruent; however, they merely think that these characteristics are happening at the same time. These children are also not able to identify a quadrangle with congruent parallel lines as a parallelogram. At this level, children can see the similar characteristics of different shapes, but they still are not able to decide upon a 'ranking' among squares, rectangles, and parallelograms.

The third level is the informal deduction level.

Children at this level are able to identify the characteristics within one figure. In addition, they understand the relationships among various geometric figures. This is the point where they move on from an experimental geometry into a formal geometry. Deductive inference can become a concrete proof; and, therefore, children can make inferences about the figure's characteristics; and, not only can they identify that some characteristics can result from other characteristics, but they also have the ability to classify figures through their characteristics. They have, for example, the ability to identify squares as a specialized form of the diamond, and understand the inclusive relationship of quadrangles properly. Once they understands inclusive relationships, not only are they able to understand the definition, but they are also be able to carry out formal arguments. Children at this level, however, cannot understand the importance of deduction as a role in common. Inference is used as an experimental or experiential method. Formal proof may be possible, but the theoretical order that brings about the conclusion is not noticed easily; deductive inference is limited and they need to receive help from teachers or textbooks.

The fourth level is the deduction level.

Students who are at the level of formal deduction are able to understand deduction, which is one of the methods of arranging geometrical figures within the postulates. They can understand the roles and relations of undefined terms, postulates, concept arrangements, postulates and proofs, and identify the deduction systems within geometry. Children at this level are not at the stage of merely demonstrating skills by remembering proof processes, but they can also create them themselves. In addition, they can understand the interrelationships between necessary conditions and sufficient conditions; they can distinguish between their propositions and their roles.

Thus, for the definition "a triangle with two equal sides is

an isosceles triangle," they are able to prove that "the base angles of an isosceles triangle are equal." These students, during the process of propositional deduction, do not understand the necessity of preciseness, nor do they understand the thinking transition relation when going from one deduction to another.

The fifth level is rigor level.

At this level, children are able to understand the necessity of various abstract deductive inferences that are strict and precise; for example, Hilbert's basic geometrical theory. As a result, it is a level where students can grow to understand Euclidean geometry by thinking mathematically in both an abstract and general manner through the specific characteristics of geometry; they can also understand the specific meanings behind it. In addition, they are able to understand the postulate system's characteristics: non-contradiction, independence, and completeness. The fact that "two parallel lines which meet a third straight line result in equal alternative angles" can be proven by 'reduction to absurdity'; and by using these parallel line postulates and sub-organization, they can conclude that "the three angles of a triangle add up to 180°." Children who are at this level exceed the level of high school students and have the ability to study in an academic system. Not only are they be able to compare other systems, but they are also be able to abstractly study various geometries without being provided a concrete shape or diagram. This last level did not receive much interest during the initial research, nor from other researchers as well.

Crowley [9] described some properties of the model. Three are of particular interest to teachers. .

First, students must proceed through the levels in order.

Second, Students move through the levels without skipping any level. Their progress from level to level is more dependent on the content and method of instruction than on age.

Third, for learning to occur, instruction must occur at the level of the student. If instruction is delivered at a higher level than the learner is able to comprehend, the student will have difficulty following the thought processes used.

1.2 Studying Level based on the van Hiele levels

As observed above, it was claimed that there could be no skipping among the thinking levels according to the van Hiele theory, and that things occur in a step by step manner. Students have to pass through one level after another. This progression is not a natural process, however; it is carried out by the support of professionals and organized study programs. According to Crowley [9], the professional support consists of five steps: a quality guidance level, a guided research level, an opinion level, a liberal research level, and a combination level.

2. The Characteristics of the van Hiele Model

If one organizes the characteristics of the study level theory of van Hiele, they are as follows [13].

First, the thinking process is a leveled, discontinuous activity; and therefore, without passing through the low levels, a student cannot move into the higher levels. As a result, for mathematical thinking, all levels must be taken step by step in order for advancement. Thus, without going through the n-1 level, students will not be able to reach the

n level.

Second, not all students pass through each level at the same speed. In addition, the time consumed at each level may be shortened through good guidance, or may even be lengthened because of inappropriate guidance. Advancement from one level to another relies much more on educational content and methods than on age and physical maturity.

Third, in a higher level, the actions that were carried out during lower levels become a subject of classification. Things that had been a method of thinking in the previous level may become a subject of thinking in the next level. In addition, a concept that was understood tacitly in the previous level may be more clearly defined in the next level. The first level is one where you can think of objects around you as figures and shapes. The second level is one where you think of figures and shapes as having a geometric characteristic. The third level is one where the figure's characteristics become a subject of thinking, and the characteristics of the figures are identified through the means of proposition. The fourth level is one where methods become a subject of thinking, and the methods are identified through the means of logic.

Last, at the fifth level, logic itself becomes a subject of research.

The basic premise of the van Hiele theory is an idea that systemizes the experience of mathematical thinking processes. In addition, the method of organizing experiences within a particular level is identified as a new experience. The activity is carried out and these processes are repeated as students move to the next level. Mathematical learning guidance must therefore be able to reinvent these cycles [14].

With respect to geometrical guidance, when children are guided properly, they will increase in level; and, if guided inappropriately, their advancement may be delayed. Thus, the importance of providing children with geometric studies that fit their level and uses the appropriate language and guidance is crucial.

Previous studies have suggested reasonability through the concrete examples regarding the theories of van Hiele and teaching-learning resources that can increase the knowledge level of the learning have been developed. Through these studies, the learners can be provided with individualized figure learning that fits their level. Traditional teaching-learning, however, is being carried out only in offline learning; there has not been enough research on the development of teaching-learning resources that considers the knowledge level of the learners. By keeping pace with the changes happening among new teaching and learning styles, online figure learning applied using van Hiele's theories should be provided for each levels.

III. DEVELOPMENT OF COURSEWARE FOR VISUALIZATION LEVEL

In this chapter, we describe development environments, the courseware interface model, and courseware for visualization levels.

1. Development environments

The major development tool is flash; and, in order to process images and interwork Photoshop and database, the PHP web programming language is used. The developmental direction of this research is as follows.

First, by using the online van Hiele questionnaire, the learner's knowledge skill is accurately diagnosed. Depending on the diagnostic results, leaning that fits the learner's level is ensured within the provided virtual space.

Second, through various games, interest in learning is induced, and motivation is sustained through interaction with the learning system.

Third, the games provided within the virtual space are developed by considering the development of Geometry skills according to van Hiele's theories in order to fit the knowledge level of the learners.

Fourth, game environments that allow learners to personally manipulate shapes are provided in order to increase the spatial sense of the children.

Last, advice that promotes the mindset of the learner should be provided.

2. Developmental of the Courseware Interface

2.1 Log-In of Learners

In the initial screen, the major character visits Figure Land. In order to trigger interest in the learner, this system gives learners a chance to be the main character and sets up a story such that the learner has to bring back several stolen figures.

When those visiting for the first time the learner presses the 'Register' icon, and progresses to the registration screen. When guidelines are followed, an ID and PASSWORD are created, and learner can immediately start learning.

Previously registered learners insert their ID and PASSWORD and press the 'challenge' button. As shown in Fig. 1, once the button is pressed, information about previously learned content is provided. Through this, the learners can discover learning that appropriately suits their level.



Fig. 1 The result of Logging-in

2.2 Main Menu

The main menu screen provides information for the learner. In the major menu, various buttons are provided including buttons for the Room of Abilities Testing where the learner's level is tested, the Room of Strength where learner can learn, the Room of Bravery, the Room of Wisdom, the Spaceship, and the Completion of Studies. In order to trigger motivation in the learners, learners become the actual characters and are able to feel that they are in the midst of an adventure. Fig. 2 illustrates the main screen.

Those who are visiting for the first time have to start in the Room of Abilities Testing so that they can test their levels. Those who have previously visited will start learning in the room that is compatible with their abilities. In order for learners to enter each room, passwords are

needed. By taking the abilities tests, learners can acquire the passwords to rooms that are appropriate to their levels.



Fig. 2 Main Menu

2.3 Diagnosis of the Learner's Level

As shown in Fig. 3, a level test is presented with 20 questions; and, when the presented numbers are clicked, the next question is presented. When the correct answer is clicked, the score increases. The level of the learner is decided depending on this score.

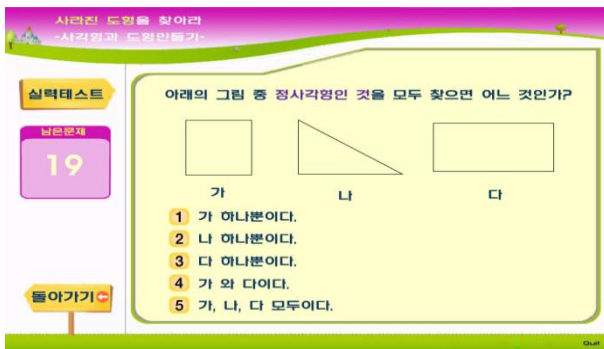


Fig. 3 Level Test

As shown in Fig. 4, depending on the diagnostic test results, passwords that can take learners to the Room of Strength, the Room of Bravery, and the Room of Wisdom can be obtained.

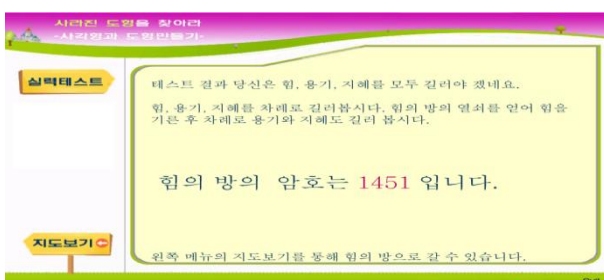


Fig. 4 The result of Level Test

2.4 Figure Learning Games

All the content of figure learning is provided according to the game learning methods for each level and depending upon the learners' levels. When the learning for each level is completed, evaluation is always provided. Depending on the evaluation result, the authority to pass to a higher level of learning is given so that learning for each level can be made appropriately.

3. Courseware for the Visualization Level

We called this room the "Room of Strength". The Room of Strength is formed around four kinds of games. Objects that can be easily seen in our surroundings are used

to observe and manipulate as they are recognized as figures. Explanations for each game are as follows.

As displayed in Fig. 5, 'Find the same Shape' is a game that provides cards with objects that can be seen in the surroundings and the learner must find the same shape. When learners see a notebook, they search for a rectangular shape. If the learners see a mountain or shellfish, they search for a triangular shape. If they see a ball, they will recognize it as a circular shape. Thus, learners are tested on their ability to distinguish between different shapes.



Fig. 5 Find the same Shape Game

As displayed in Fig. 6, 'Capture the Shape' is a game where shapes have to be recognized although the cards have been divided into upper and lower parts and moved from left to right during a short amount of time. In this game, as the shapes pass by, the learners have to guess the shapes. This, then, contributes to helping learners visually recognize various shapes.



Fig. 6 Capture the Shape Game



Fig. 7 Complete the Shapes Game

The game called 'Complete the Shapes' is displayed in Fig. 7, Shapes are given before starting the game, and learners observe the shapes. Once the game starts, the shape disappears and the game is accomplished

when the shape is found. In order to increase learning efficiency, various given pieces are manipulated by the mouse and the learner is able to confirm them visually. Through the replay button, the earlier shapes can be seen according to the learners' desires.

As shown in Fig. 8, 'Find the Hidden Shape' is a game where triangular, rectangular, and circular shapes have to be found in a picture. As learners search for triangular, rectangular, and circular shapes in the game, they will be able to recognize the fact that many of these shapes exist in their surrounding environment as well.



Fig. 8 Find the Hidden Shape Game

Through the games where shapes are found in surrounding objects or by completing shapes using different pieces, learners will be able to visually recognize figures. As their levels increase through each of the games, learners can find the password for the Room of Strength in order to move to a higher level of learning.

IV. CONCLUSION

A web-based courseware applying van Hiele's theory of visualization levels was developed.

In this program, game content that fits the level of awareness of learners regarding shapes is developed so that real-time, individual learning can take place. In addition, graphics and animation stimulate learner interests and motivation, cultivate an appropriate attention span and learning attitude, and provide an interactional, teaching-learning environment between the student and educator. The results of this study are as follows.

First, level learning based on the theories of van Hiele can help enhance effective learning about Geometry as well as increase the level of recognition of shapes. Second, though the adventure-game style of learning, interest in mathematic can be triggered in the learners. Third, diverse learning materials should be introduced when learners are learning shapes, since such learning requires spatial perception skills. By providing various operational activities, learners are able to develop spatial perception skills.

Fourth, mathematics in the 4th grade of elementary school deals with content regarding 'learning about shapes' by levels; so, for learners who need additional deep supplementary lessons, more learning opportunities can be provided.

Last, educators will feel less burdened by having to sacrifice time and effort on developing learning for each level.

This study proposes some of the areas that need improvements as well as some agendas in the educational

field that need to be improved and secured.

First, web courseware and learning models appropriate to each level of mathematics learning should be developed. In addition, proper learning guidance should be developed as well, in order that the two be applied together.

Second, in order for students to learn according to their personal level, development of web courseware for each level is needed in diverse areas beyond figure learning. Third, the authors intend to develop courseware for other levels of van Hiele theory, and need to develop an adaption module to supply a course for learners' differentiated learning at proper levels.

Last, in order to verify the accurate effects of the courseware, it is thought that research on the effects on students is needed.

REFERENCES

- [1] J. W. Adams, Individual differences in mathematical ability: genetic, cognitive and behavioural factors, *Journal of Research in Special Educational Needs*, 7(2), 2007, 97-103.
- [2] E. Halat, In-Service Middle and High School Mathematics Teachers: Geometric Reasoning Stages and Gender. *The Mathematics Educator*, 2008, 8-14.
- [3] M. L. Rock, M. Gregg, E. Ellis and R. A. Gable, REACH: A Framework for Differentiating Classroom Instruction, *Preventing School Failure*, 52(2), 2008, 31-47.
- [4] D. Haager and J. K. Klingner, *Differentiating instruction in inclusive classrooms* (Columbus, OH: Merrill, 2005).
- [5] M. Friend and W. Bursick, *Including students with special needs: A practical guide for classroom teachers* (2nd ed.) (Upper Saddle River, NJ: Allyn & Bacon, 1999).
- [6] D. Lipsky, Are we there yet?, *Learning Disability Quarterly*, 28, 2005, 156-158.
- [7] C. A. Tomlinson, Sharing responsibility for differentiating instruction, *Roper Review*, 26(4), 2004, 188-200.
- [8] H. Unal, E. Jakubowski and D. Corey, D, Differences in learning geometry among high and low spatial ability pre-service mathematics teachers, *International Journal of Mathematical Education in Science and Technology*, 2009, 997-1012.
- [9] M.L. Crowley, The van Hiele Model of the Development of Geometric Thought, Learning and Teaching Geometry, K-12, Mary Montgomery Lindquist(ed), *1987 Yearbook of the National Council of Teachers of Mathematics* (Reston, Va.: National 1987) 1-16.
- [10] P.M. van Hiele, *Structure and insight* (New York, Academic Press, 1986)
- [11] P. van Hiele, *The Child's Thought and Geometry* (Brooklyn, NY: City University of New York, 1985)..
- [12] T. Erdogan, R. Akkaya and S. C. Akkaya, The Effect of the Van Hiele Model Based Instruction on the Creative Thinking Levels of 6th Grade Primary School Students, *Educational Sciences: Theory & Practice*, 9(1), 2009, 181-194.
- [13] M. D. Villiers, Using dynamic geometry to expand mathematics teachers' understanding of proof, *International Journal of Mathematical Education in Science and Technology*, 35(5), 2004, 703-724.
- [14] C. C. Meng, Enhancing students' geometric thinking through phase-based instruction using geometer's sketchpad: A case study, *Journal Pendidikan dan Pendidikan*, 24, 2009, 89-107.

Character Recognition System Based On Android Smart Phone

Soon-kak Kwon¹, Hyun-jun An², Young-hwan Choi,³

Department of Computer Software Engineering, Dongeui University, Korea

ABSTRACT : In this paper, we propose the character recognition method using optical character reader technology for the smart phone application. The camera within Android smart phone captures the document and then the OCR is applied according to language database. As some language is added to the database, the character of the various languages can be easily recognized. From simulation results, we can see the results of tests in English, Korean, Japanese, Chinese recognition.

Keywords: Character recognition, Smart phone, Picture Quality

I. INTRODUCTION

Current OCR (optical character reader) technology [1-6] is widely applied to Zip recognition, product inspection and classification, document recognition, vehicle number recognition, drawings recognition, slips and checks automatically entering. OCR technology in the United States of America was finished in one-stage from starting in the 1950s to early 1970s. In the 1980s, two-stage neural network and VLSI design were progressed. OCR technology of Japan began to develop Zip automatic recognition device in the 1960s. Since 1966, Pattern Information Processing System project became the instrument of development by participating many companies.

On-lain OCR research to recognize at the same time with handwriting was the first attempt in 1959. There are many character recognition system such as mail sorter of Germany's Siemens, auto-inspection system of Japan's NEC, face, fingerprint recognition, document processing system of USA's National Institute of Science and Technology, the field of artificial intelligence, document pattern recognition / analysis, automatic processing of checks, number / word / string recognition of Canada Concordia University.

Most of the character recognition program will be recognized through the input image with a scanner or a digital camera and computer software. There is a problem in the spatial size of the computer and scanner. If you do not have a scanner and a digital camera, a hardware problem occurs. In order to overcome the limitations of computer occupying a large space, character recognition system based on smart phone is proposed. Character recognition software developed by smart phones with an emphasis on mobility and portability, spatial, hardware, financial limitations can be solved. But because the performances of smart phone and computer are different, the speed of massive character recognition is slow. Hardware speeds up the development of smart phones; this issue seems to be resolved as soon as possible. In this paper, the character recognition method is presented by using OCR technology and smart phone.

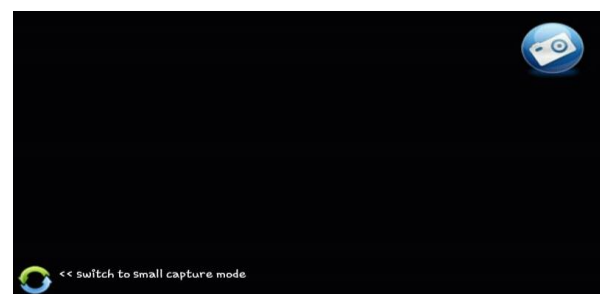
The organization of this paper is as follows. Section II provides the proposed character recognition method. Section III shows the simulation results of the proposed method about recognition rate for various languages. In Section IV, we summarize the main results.

II. PROPOSED CHARACTER RECOGNITION METHOD

In order to create a character recognition system based on Android smart phone, Tesseract-OCR [2] and Mezzofanti were used. Tesseract-OCR 2.03 version supports some languages such as English. From the 3.00 version, the Korean language is supported. It internally utilizes the image processing library called as leptonica. Tesseract-OCR is used in AOSP (Android Open Source Project) and eyes-free project. Mezzofanti is open-source Android Application. It recognizes the characters in the image taken from the camera by using the Tesseract library. The app currently is in version 1.0.3 and uses Tesseract 2.03 version, so it has the disadvantage that does not support many languages recognition. Therefore, we implement Mezzofanti as Tesseract 3.0 version. Tesseract 3.0 is build to NDK and then the source code of the packages associated with the Tesseract is downloaded. Mezzofanti source should be modified. Eclipse or Ant is used to build Mezzofanti.

Mezzofanti application and dictionary and pre-learning data files have to be installed. Mezzofanti for Eclipse or Ant is to build, and installed in Android smart phone. Mezzofanti and Tesseract can add simply a language that is not supported by default; the database only for that language can be easily applied. Proposed system can support full mode and line mode. Full mode is to be recognized for the entire document, and lines mode can be recognized for one line of document. The case of the character misrecognized in results screen can be modified separately; it can increase the recognition rate.

Fig.1 shows the screen shots for the proposed recognition system based on smart phone.



(a) Full mode



(b) Line mode

Fig 1. Screen shots for the proposed recognition system based on smart phone



button : Line mode and Full mode can be changed. In line mode only recognizes the letters inside the white area. Recognizing the character of the white areas, then move on to the results screen.



button : Recognize the letters of the screen.

The recognition result is shown as follows. Fig 2 shows original document with English language. After being captured by smart phone camera, the data is processed by binarization for object segmentation. Then we can see the recognition results on the screen of smart phone as shown in Fig. 4.

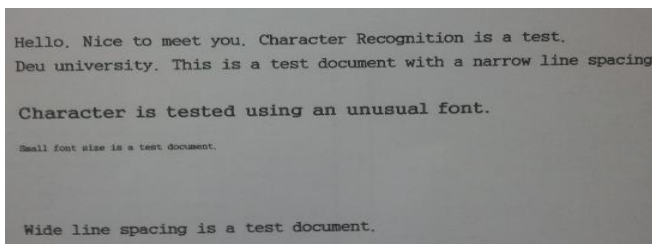


Fig. 2. Example of original document for recognition

Hello. Nice to meet you. Character Recognition is a test.
Deu university. This is a test document with a narrow line spacing.
Character is tested using an unusual font.
Small font size is a test document.

Wide line spacing is a test document.

Fig. 3. Binarization of captured data

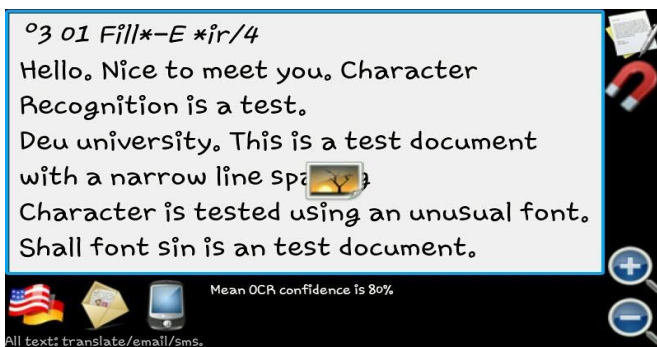


Fig. 4. Screen shot of an example of recognition result

III. SIMULATION RESULTS

For performance of recognition, we simulate the proposed character recognition system to various characters such as English, Korean, Japanese, and Chinese.

We calculate the recognition rate (R) as performance criterion of recognition;

$$R = \frac{\text{Number of correctly recognized character}}{\text{Total number of character}}$$

1) English

English language was recognized relatively high. We can see the recognition rate from the Table I.

Table I. Recognition for English

Document type	Number of characters	Recognition rate
Courier	20	82.7 %
Dark lighting	10	13.1 %
Tilt	7	66.4 %
Special fonts	5	9.3 %
Small font size	5	54.2 %
Wide letter space	14	75.1 %
Narrow letter space	14	51.8 %

Because English is the completion character, this reason seems to affect recognition rates. Result of testing in a dark place is not good. The following test was tilted letters. If we exceed 30 ° inclined angle of characters, the recognition success rate was too low. So, the characters of 10 ° ~ 30 ° were tested. The case of a sentence of less than 30 ° was not recognized satisfactorily but recognized in some degree. Spatial fonts are required according to the shape in the font database. A relatively simple form of the character in the simulation of the character size was accurately recognized, but the case of 'Q, R, G, M' seemed to be difficult to recognize. A broad statement of the characters interval showed good result instead of relatively narrow letter spacing.

2) Korean

Table II shows the recognition rate for Korean language.

Table II. Recognition for Korean

Document type	Number of characters	Recognition rate
Courier	20	65.4 %
Dark lighting	10	5.2 %
Tilt	7	43.1 %
Special fonts	5	4.8 %
Small font size	5	44.2 %
Wide letter space	14	64.7 %
Narrow letter space	14	39.8 %

Test results showed good recognition results. Character recognition rate was high for relatively simple characters consisting of consonants and vowels. Character combination of Consonant + vowel + consonant into 3 pieces showed less recognition rate, depending on the form of the characters. According to the intensity of the light, the results were similar to the English test. Similarly, the slope of the characters beyond 30 ° was difficult to obtain good recognition rate. Some credibility to test unusual fonts could fall. Unusual font standards were vague. Recognition success rate was low. The end of characters are made up of straight lines gave satisfactory recognition results but special fonts were difficult to be recognized. Fonts and characters in order to recognize should be added to the database for each font. The sentence of a wide letter spacing was recognized without difficulty, but for a sentence of between narrow characters, depending on the spacing between the characters, the result was much different. Test showed slightly different

results, depending on the characteristics of each character. The character having the white space to the right of the letters such as “卜, 𠂇” showed some results, but vice versa was somewhat different.

3) Japanese

Table III shows the recognition rate for Japanese language.

Table II. Recognition for Japanese

Document type	Number of characters	Recognition rate
Courier	20	58.8 %
Dark lighting	10	6.2 %
Tilt	7	31.5 %
Special fonts	5	12.1 %
Small font size	5	20.3 %
Wide letter space	14	49.2 %
Narrow letter space	14	35.9 %

The case of Japanese character is also tested under the same conditions such as Korean, English. Testing fonts are Times New Roman, Courier. Japanese forms a completion character as Hiragana and Katakana or a combination character as Kanji. So the recognition rate depends on the combination of recognized characters. Completion characters such as Hiragana and Katakana showed a high recognition rate. However, Chinese characters that are diverse in form had a problem to be recognized. Except in the case of the simple Kanji, Kanji gets complicated higher, recognition rate dropped accordingly. The number of Japanese Kanji was much smaller compared to the comparison of Chinese Kanji. Nevertheless, similar to the appearance of a lot of Kanji, this problem seems to have no other choice. Recognition results showed the same results that are similar to the previous simulation of Korean, English. Chronic problem was still at dark lighting, tilted characters. Specially it was difficult to recognize the Kanji. Simulation according to the font size was also dropped quite a bit from the Kanji recognition. The spacing of letters has yielded good results in relatively, it still seems to recognition success rate varies depending on the form of the Kanji.

4) Chinese

Table IV shows the recognition rate for Chinese language.

Table II. Recognition for Chinese

Document type	Number of characters	Recognition rate
Courier	20	41.4 %
Dark lighting	10	3.8 %
Tilt	7	25.2 %
Special fonts	5	-
Small font size	5	11.3 %
Wide letter space	14	40.0 %
Narrow letter space	14	17.9 %

Recognition Chinese Kanji was tested under the same conditions for other languages. Chinese recognition

test were progressed in Chinese Simplified character based on such as Times New Roman, Courier fonts. Tesseract database was used for Chinese Simplified testing. Chinese character forms of Korean similarly, but the number of combinations of letters surpasses number of characters for each of Korean consonants, vowels. Documents of Courier, wide margins between characters, and simple form were similarly recognized relatively good. Because Kanji is complex, even if successful, the recognition rate was not high.

IV. CONCLUSION

In this paper, character recognition system was implemented by using the Android smart phones. The implementation process of the system was described to recognize the characters in the document using the camera screen.

Photo data taken by a smart phone can be compared with the database of the system, then the characters can be recognized, the recognized character can be created to a text file to take advantage of the as applications of the Internet and pre-retrieval and various strategies Smart phones character recognition system does not need hardware such as a computer or a scanner. Therefore, there are the advantages that the recognition cannot be spatially restricted and simple character recognition is possible.

V. ACKNOWLEDGEMENTS

This work was supported by Dongeui University Foundation Grant (2012AA180). Corresponding author: Soon-kak Kwon

REFERENCES

- [1] J.L. Blue, G.T. Candela, P.J. Grother, R. Chellappa, C.L. Wilson, Evaluation of pattern classifiers for fingerprint and OCR applications, *Pattern Recognition*, 27(4), 1994, 485-501.
- [2] R. Smith, An overview of the Tesseract OCR engine, *Proc. Int. Conf. Document Analysis and Recognition (ICDAR 2007)*, 2007, 629-633.
- [3] M. Seeger, Binarising camera images for OCR, *Proc. Int. Conf. Document Analysis and Recognition*, 2001, 54-58.
- [4] K. Wang, J. A. kangas, Character location in scene images from digital camera, *Pattern Recognition*, 36(10), 2003, 2287-2299.
- [5] C. C. Chang, S. M. Hwang, D. J. Buehrer, A shape recognition scheme based on relative distances of feature points from the centroid. *Pattern Recognition*, 24(11), 1991. 1053-1063.
- [6] T. Bernier, J.-A. Landry, A new method for representing and matching shapes of natural objects. *Pattern Recognition*, 36(8), 2003. 1711-1723.

Enhanced K-Mean Algorithm to Improve Decision Support System Under Uncertain Situations

Ahmed Bahgat El Seddawy¹, Prof. Dr. Turkey Sultan², Dr. Ayman Khedr³

¹ Department of Business Information System, Arab Academy for Science and Technology, Egypt

^{2,3} Department of Information System, Helwan University, Egypt

Abstract: Decision Support System (DSS) is equivalent synonym as management information systems (MIS). Most of imported data are being used in solutions like data mining (DM). Decision supporting systems include also decisions made upon individual data from external sources, management feeling, and various other data sources not included in business intelligence. Successfully supporting managerial decision-making is critically dependent upon the availability of integrated, high quality information organized and presented in a timely and easily understood manner. Data mining have emerged to meet this need. They serve as an integrated repository for internal and external data-intelligence critical to understanding and evaluating the business within its environmental context. With the addition of models, analytic tools, and user interfaces, they have the potential to provide actionable information that supports effective problem and opportunity identification, critical decision-making, and strategy formulation, implementation, and evaluation. The proposed system Investment Data Mining System (IDMS) will support top level management to make a good decision in any time under any uncertain environment and on another hand using enhancing K-mean algorithm.

Keywords: dss, dm, mis, clustering, classification, association rule, k-mean, olap, matlab

I. Introduction

Decision Support System (DSS) is equivalent synonym as management information systems (MIS). Most of imported data are being used in solutions like data mining (DM). Decision supporting systems include also decisions made upon individual data from external sources, management feeling, and various other data sources not included in business intelligence. Successfully supporting managerial decision-making is critically dependent upon the availability of integrated, high quality information organized and presented in a timely and easily understood manner. Data mining have emerged to meet this need. They serve as an integrated repository for internal and external data-intelligence critical to understanding and evaluating the business within its environmental context. With the addition of models, analytic tools, and user interfaces, they have the potential to provide actionable information that supports effective problem and opportunity identification, critical decision-making, and strategy formulation, implementation, and evaluation. The proposed system will support top level management to make a good decision in any time under any uncertain environment [4]. This study aim to investigate the adoption process of decision making under uncertain situations or highly risk environments effecting in decision of investing stoke cash of bank. This applied for two types

of usage investment - direct or indirect - or credit and any sector of investment will be highly or moderate or low risk. And select which one of this sectors risk 'rejected' or un-risk 'accepted' all that under uncertain environments such as; political, economical, marketing, operational, internal policies and natural crises, all that using the contribution of this study enhancing k-mean algorithm to improve the results and comparing results between original algorithm and enhanced algorithm.

The paper is divided into six sections; section two is a background and related work it is divided into two parts, part one is about DSS, part two is about DM including K-m algorithm and enhancing in K-m algorithm. Section three presents the proposed Investing Data Mining System 'IDMS'. Section four presents IDMS experiments, implementations and results using original and enhanced k-m algorithm. Section five presents conclusion and finally section six presents future work.

II. Background and related work

2.1 Decision Support System (DSS)

DSS includes a body of knowledge that describes some aspects of the decision maker's world that specifies how to accomplish various tasks, that indicates what conclusions are valid in different circumstances [4]. The expected benefits of DSS that discovered are higher decision quality, improved communication, cost reduction, increased productivity, time savings, improved customer satisfaction and improved employee satisfaction. DSS is a computer-based system consisting of three main interacting components:

- **A language system:** a mechanism to provide communication between the user and other components of the DSS.
- **A knowledge system:** A repository of problem domain knowledge embodied in DSS as either data or procedures.
- **A problem processing system:** a link between the other two components, containing one or more of the general problem manipulation capabilities required for decision-making.

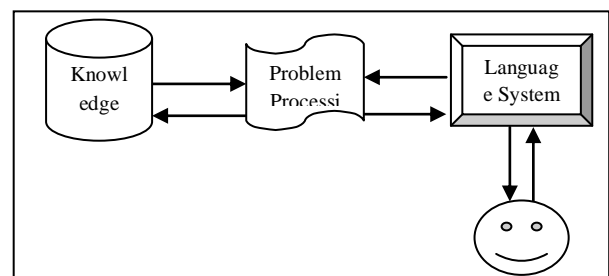


Fig 1: DSS Main Components

After surveying multiple decision support systems, it is concluded that decision support systems are categorized into the following [5]:

- **File drawer systems:** This category of DSS provides access to data items.
- **Data analysis systems:** Those support the manipulation of data by computerized tools tailored to a specific task or by more general tools and operators.
- **Analytical information systems:** Those provide access to a series of decision-oriented databases.
- **Accounting and financial models:** those calculate the consequences of possible actions.
- **Representational models:** those estimate the consequences of actions based on simulation models that include relationships that are causal as well as accounting definitions.
- **Optimization models:** those provide guidelines for actions by generating an optimal solution consistent with a series of constraints.
- **Suggestion models:** those perform the logical processing leading to a specific suggested decision or a fairly structured or well understood task.

This section describes the approaches and techniques mostly used when developing data warehousing systems that data warehousing approaches such as; Online Analytical Processing 'OLAP', Data Mining 'DM' and Artificial Intelligence 'AI'. And in this paper will using DM as approach and technique.

2.2 Data Mining Techniques (DM)

Data mining is the process of analyzing data from different perspectives and summarizing it into useful information [10]. DM techniques are the result of a long process of research and product development [10]. There are several processes for applying DM:

1. Definition of the business objective and expected operational environment.
2. Data selection is required to identify meaningful sample of data.
3. Data transformation that involves data representation in an appropriate format for mining algorithm.
4. Selection and implementation of data mining algorithm depends on the mining objective.
5. Analysis of the discovered outcomes is needed to formulate business outcomes.
6. Representing valuable business outcomes.

DM techniques usually fall into two categories, predictive or descriptive. Predictive DM uses historical data to infer something about future events. Predictive mining tasks use data to build a model to make predictions on unseen future events. Descriptive DM aims to find patterns in the data that provide some information about internal hidden relationships. Descriptive mining tasks characterize the general properties of the data and represent it in a meaningful way. Figure2 shows the classification of DM techniques.

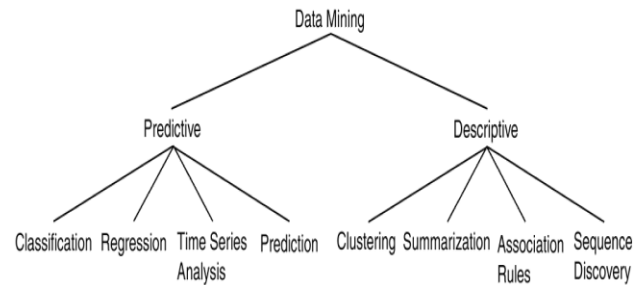


Fig 2: DM Techniques [5]

2.2.1 Clustering Technique

Clustering can be considered the most important learning problem; like every other problem of this kind, it deals with finding a structure in a collection of unlabeled data. A loose definition of clustering could be “the process of organizing objects into groups whose members are similar in some way”.

A cluster is therefore a collection of objects which are “similar” between them while are “dissimilar” to the objects belonging to other clusters as shown in figure 3. [6] Define clustering by saying “Clustering involves identifying a finite set of categories or segments ‘clusters’ to describe the data according to a certain metric. The clusters can be mutually exclusive, hierarchical or overlapping”. [6] Defines clustering as follows: “clustering enables to find specific discriminative factors or attributes for the studied data. Each member of a cluster should be very similar to other members in its cluster and very dissimilar to other clusters. When a new data is introduced, it is classified into the most similar clusters. Techniques for creating clusters include partitioning methods as in k-means algorithm, and hierarchical methods as decision trees, and density-based methods”.

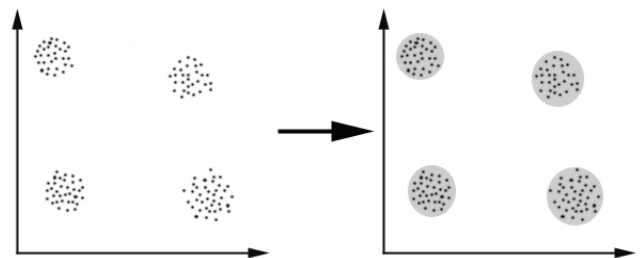


Fig 3: Simple graphical for clustering data [6]

The goal of clustering is [6] to determine the basic grouping in a set of unlabeled data, to find representatives for homogeneous groups which are called “data reduction”, to find ‘natural clusters’ and describe their unknown properties these clusters are called ‘natural’ data types, to find useful and suitable groupings this can be called ‘useful’ data classes’ and to find unusual data objects outlier detection. There are several advantages for the clustering technique use it. Among these advantages are recognizing the number of clusters, grouping similar members together, identifying the discriminate attributes, ranking the discriminate attributes, and recognizing the discriminate

attributes of one cluster and representing them within the business context. A major disadvantage of clustering is that it is suitable for static data but not for dynamic data where its value changes over time or due to any other factor. Another disadvantage is that sometimes the generated clusters may not have a practical meaning. Finally, it is possible not to spot the cluster sometimes as there is no exact idea of what to look for or there is a lack of collected data [7].

2.2.1.1 K-Mean Algorithm

[8] Defines K-means as one of the simplest unsupervised learning algorithms that solve the well known clustering problem. Build to classify or grouping objects based on features into 'k' number of group. K is positive integer number and the grouping is done by mining the sum of squares of distance between data and the corresponding cluster centroid. The cluster centroid is the average point in the multidimensional space defined by the dimensions [9]. There are a lot of applications of the K-mean clustering, range from unsupervised learning of neural network, Pattern recognitions, Classification analysis, Artificial intelligent, image processing, machine vision, etc. In principle, we have several objects and each object have several attributes and we want to classify the objects based on the attributes, then we can apply this algorithm. There are commonly four steps followed for K-mean idea [10];

1. Place K points into the space represented by the objects that are being clustered. These points represent initial group centers.
2. Assign each object to the group that has the closest centered.
3. When all objects have been assigned, recalculate the positions of the K centered.
4. Repeat Steps 2 and 3 until the centered no longer change. This produces a separation of the objects into groups from which the metric to be minimized can be calculated as follows.

$$\sum_{j=1}^k \sum_{i=1}^{n_j} \|x_i^j - c_j\|^2$$

K: number of clusters
nj: number of points in jth cluster
xij: ith point in jth cluster

```

Input:
  D = {t1, t2, ..., tn} // Set of elements
  A // Adjacency matrix showing distance between elements.
  k // Number of desired clusters.
Output:
  K // Set of clusters.
K-Means Algorithm:
  assign initial values for means m1, m2, ..., mk ;
  repeat
    assign each item ti to the cluster which has the closest mean
    calculate new mean for each cluster;
  until convergence criteria is met;
```

Fig 4: Procedures code for k-means algorithm [10]

2.2.1.2 Enhanced K-means 'E_KM'

Before looking to the enhancements that are applied on K-mean algorithm, one should give the impression of pros, cons and problems of k-mean algorithm, then presents the enhanced k-mean algorithm and presents a way for evaluating this enhancement. There are several strengths and weakness shown in table 5.1 (Arthur, 2006).

Table 1: Strengths and weakness of K-men algorithm (Arthur, 2006)

Strengths	Weakness
<ol style="list-style-type: none"> 1. Vectors can flexibly change clusters during the process. 2. Always converges to a local optimum 3. Quite fast for most application 	<ol style="list-style-type: none"> 1. Quality of the output depends on the initial point. 2. Global optimum solution not guaranteed.

There are some problems in k-mean algorithm such as (Arthur, 2006):

1. Non globular clusters (overlapping in data between clusters)
2. Assume wrong number of clusters.
3. Find empty clusters.
4. Bad initialization to centroid point
5. Choosing the number of clusters

The most common measure to evaluate k-men algorithm is Sum of Squared Error 'SSE' with another words called, Sum of Squared Distances 'SSD' (Wenyan Li, 2009).

- For each point, the error is the distance to nearest cluster.
- To get SSE or SSD, we square these error and sum them

$$SSE = \sum_{i=1}^K \sum_{x \in C_i} dist^2(m_i, x)$$

x is a data point in cluster C_i.

m_i is the representative point for cluster C_i.

- There is one way to reduce SSE, is to increase K 'Number of clusters'.
- The good clustering with smaller K can have slower SSE than a poor clustering with higher K.

After investigating the most common algorithms for data clustering, there is enhancement for the most familiar algorithm which called k-means trying to solving some problems of k-mean algorithm. More features will be added to enhanced algorithm such as; change centroid point from random points to center points for data and adding step to avoid empty clusters when visualize data it shows also in steps of algorithm. Figure 5.31 shows the flowchart of enhanced K-men algorithm.

1. Assume number of cluster "K".
2. Calculate 'K' at center points of data set

$H \rightarrow Y \rightarrow \text{Rows}$
 $W \rightarrow X \rightarrow \text{Columns}$
 $\text{Mid } P = (X, Y)$
 $P = (\frac{W}{2}, \frac{H}{2})$ %for every cluster
 Ex,
 $H = 400, W = 30$
 $\text{Mid } P = (\frac{30}{2}, \frac{400}{2}) \quad P = (15, 200) \leftarrow \text{Center point for Cluster}$

Fig 6: Pseudo code of calculating 'k' center point

3. Calculate the distance between a data sample and clusters.
4. Assign a data sample to closest cluster center.
5. Calculate new cluster center.
6. Repeat step 3.4 and 5 until no objects move group.
7. Avoid empty clusters

Loop through each cluster
 If all items inside cluster equal 0 ,
 delete cluster
 Else
 do nothing;

Fig 7: Pseudo code of avoiding empty clusters

8. Perform visualization

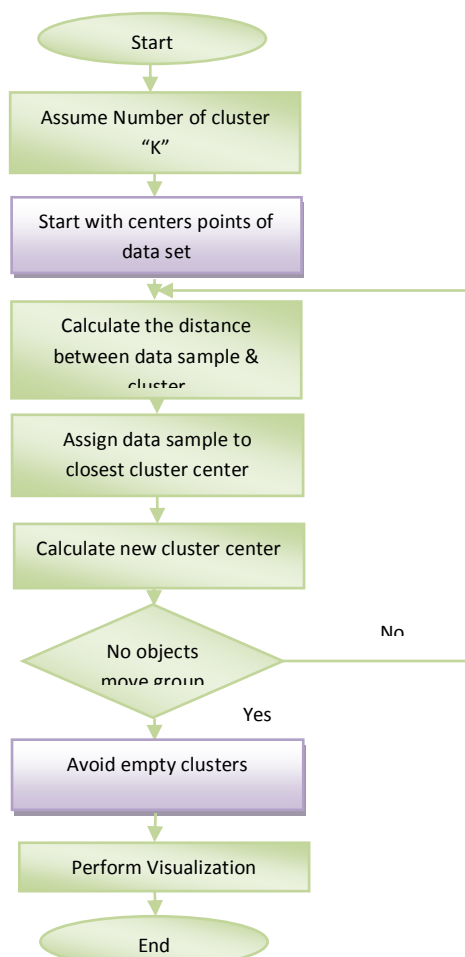


Fig 8: E_K-mean algorithm flowcharts

III. IDMS Implementation

Investment Data Mining System 'IDMS' aims to build a data mining system for investment in the banking sector. IDMS consists of several components; data gathering, preparing data to discover knowledge, data preprocessing, using data mining techniques in sequences steps start with classification data, clustering data especially using K-mean algorithm and enhanced K-mean algorithm to set which best result and then set and run association rules to solve problem, post processing and finally get result and visualize result to create best decision to take a good decision for investment under uncertain situations [18].

3.1 Experiments

3.1.1 Data Collected

The following data is taken from a bank is located in Egypt and has several branches. The bank serves more than 100000 customers per year, contracting with more than 50000 organizations. There are some basics found through interviews such as; explain overall process in bank for usage and resources of cash in bank. IDMS will focus in depth of investment department. All customers and departments data's is stored electronically using SQL database. The database stores values in six fields: Customer name, Customer number or ID, Previous commitments, Paperwork, Type of investment, Sector of the field investment and Previous debt, shown in table 2. The received data is in the form of SQL database converted to excel sheets.

Table 2: Collected Data

Request Date	Request Serial Number	Customer Name	Customer ID	Paperwork	Type of investment	Sector of investment	Previous debt
1-11-2010	1	Ahmed	20123	Ok	Industry	Durable goods	No
5-12-2010	2	Co.	20123	Ok	Securities	Durable goods	No
1-11-2010	3	Samed	20520	Ok	Securities	Cultivation strategies	No
1-11-2010	4	Saaed	20002	Ok	Industry	Import and export	No
1-11-2010	5	Co.	20135	Ok	Agriculture	Cultivation strategies	No
1-11-2010	6	Mohamed	20123	Ok	Industry	Foodstuffs	No
...

Table 3: Format for each field for data

Request Date	Request Serial Number	Customer Name	Customer ID	Paperwork	Type of investment	Sector of the field investment	Previous debt
Date	Number	Text	Number	Text	Text	Text	Text

2010	20520	03	032
2010	73002	01	011
2011	20135	03	031
2012	20033	01	011
...

3.2 Preprocessing

The data collected undergoes four preprocessing steps and the data matrix is reduced from 8 columns to 7 columns. The first step converts data from textual values to numeric ones in order to deal with identification numbers as in table

Table 4: Example of data after converting to numeric sheet

Request Date	Request Serial Number	Customer ID	Paperwork	Type of investment	Sector of investment	Previous debt
2010	1	20123	1	03	032	1
2010	2	20123	1	03	032	1
...

In the second step, the interesting selected attributes are Request data, Customer ID, Type of Investment and Sector of investment as shown in table 5. Elements with values indicate that the type and sector of investment.

Table 5: Example of data after selecting main segments

Request Date	Customer ID	Type of investment	Sector of investment
2010	20123	03	032

IDMS execution done via several techniques started with clustering technique using K-M and enhanced k-mean algorithm, classification technique using ID3 algorithm and association rules technique using apriori algorithm. Next section will discuss the results of execution for first technique clustering.

IV. Clustering Results

4.1 Clustering sectors

First: Original K-mean Algorithm results

Table 6 presents the set of data used in the implementation experiments for training data to set a best result and choosing an effective number of clusters and percentage of data set to apply the technique for the system. These data are divided among 10 clusters representing the different percentage of the set of data used using K-Mean algorithm.

Table 6: Testing data on a 10 clusters model using K-M Algorithm

C 0	C 1	C 2	C 3	C 4	C 5	C 6	C 7	C 8	C 9
Agriculture	Trading	Tourism	Securities	Industry	Petrochemicals	Non	Non	Technologies	Non

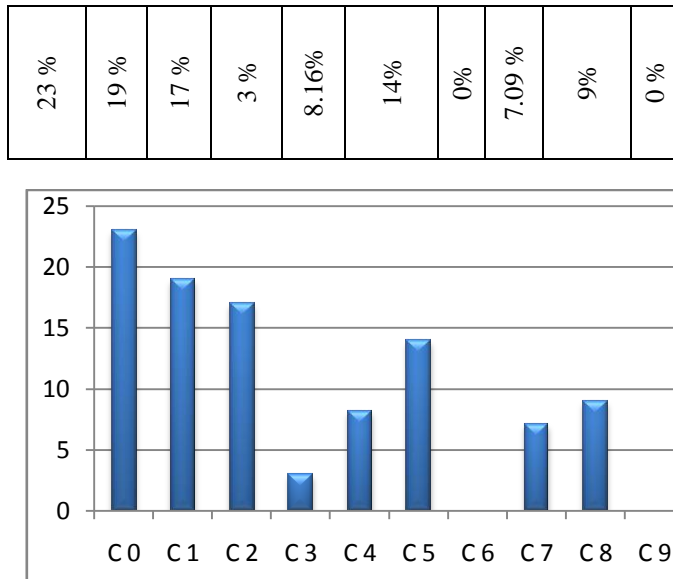


Fig 10 : Distribution percentages of sectors in testing set of data for a 10 cluster model

These graph present clustering of sectors are used in investment sector to find a good usage for cash in bank. The results which are appearing from this algorithm describe the distribution percentage of sectors in testing set of data for 10 clusters by K-M, this enhance consider effect on data results on IDMS.

Second: Enhanced K-mean Algorithm results

After applying enhanced k-mean algorithm to avoid empty clusters and re clustering data more accurate using change center point for 'K', it gives the research more accurate results appear in next section. Table 7 presents the set of data used in the implementation experiments for training data to set a best result and choosing an effective number of clusters and percentage of data set to apply the technique for the system. These data are divided among 7 clusters representing the different percentage of the set of data used using enhanced K-Mean algorithm E_K-M.

Table 7: Testing data on a 7 clusters model using E_K-M Algorithm

C 0	C 1	C 2	C 3	C 4	C 5	C 6
Agriculture	Trading	Tourism	Securities	Industry	Petrochemicals	Technologies
28.57%	4.08%	8.16%	2.04%	8.16%	6.12%	10.20%

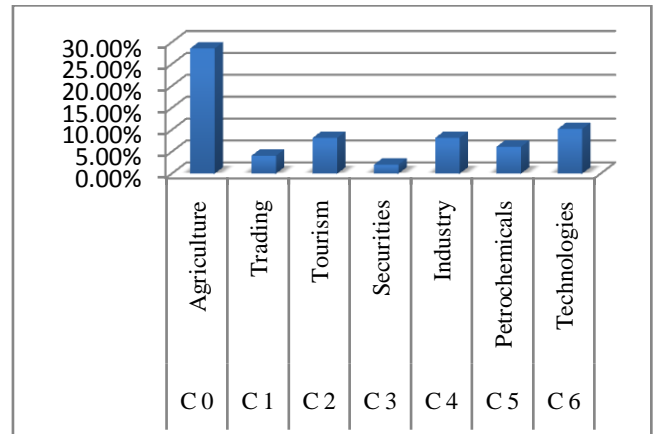


Fig 11: Distribution percentages of sectors in testing set of data for a 10 cluster model

These graph present clustering of sectors are used in investment sector to find a good usage for cash in bank. The results which are appearing from this algorithm describe the distribution percentage of sectors in testing set of data for 7 clusters by E_K-M, this enhance consider effect on data results on IDMS.

4.2 Clustering risks based on sectors using E_K-M

Table 8 presents the set of data used in the implementation experiments for training data to set a best result and choosing an effective number of clusters and percentage of data set to apply the technique for the system. These data are divided among 3 clusters representing the different percentage of the set of data used and how distribute risk of sectors after clustering them to seven clusters using in IDMS.

Table 8: Testing data on a 3 cluster model using E_K-M Algorithm

C 0 Low Risk	C 1 Mid Risk	C 2 High Risk
Agriculture (1) Petrochemicals (6)	Trading (4) Technologies (7) Industry (2)	Tourism (5) Securities (3)
48.57%	40.08%	11.35%

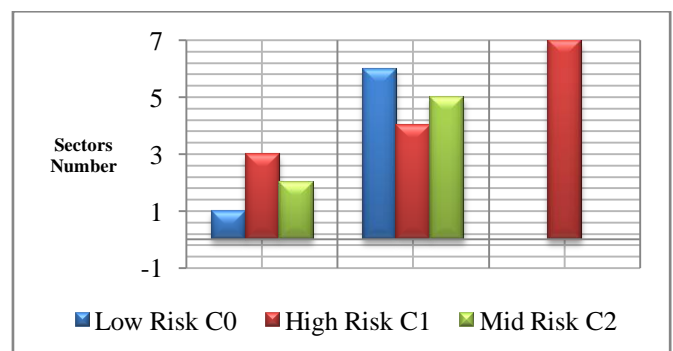


Fig 12: Distribution sectors numbers based on risk level

Figure 12 represent distribution of sectors number based on risk level. Every level of risk has colure such as, red color for high risk to invest in this sector, green color for medium level of risk to invest in this sector and blue color for low risk to invest in this sector.

4.3 Result of Comparison between K-M and E_K-M

There are some similarities and differences between algorithms and their enhancement which describe the utility, efficiency, applicability, accuracy, popularity, flexibility and visualization of the two algorithms. A comparison between the two algorithms is shown in the following table 9.

Based on comparison table finding that, first traditional K-mean algorithm as the size of the data set decreases and the number of clustering increases, the

amount of overlapping elevates and the level of accuracy declines. Second the efficiency is shown in E_K-M and original K-M in two aspects. Time efficiency in original K-M is less than time efficiency in E_K-M because of adding two steps of enhancement, so time will increase and it may be accepted when raise the quality of results. Size efficiency in original K-M is less than space of saving data efficiency in E_K-M because there are steps added to K-M to avoid empty clusters. On the other hand, using the enhanced K-mean algorithm decreases the size of the data set and increases the number of clusters. Accordingly, the amount of overlaps decreases and accuracy increases. Generally, the enhanced K-mean algorithm showed a better performance compared to traditional K-mean algorithm.

Table 9: Comparison between KM and E_K-M algorithms

Approach	K-Mean Algorithm	E_K-mean Algorithm
1. Theory	K-mean start with assume number of clusters, picking 'K' randomly, calculate distance and visualize.	E_K-mean start with assume number of clusters, picking 'K' at center point, calculate distance and avoid empty clusters then visualize.
2. Efficiency (Time and Space)	Time : Less efficient Space : More Efficient	Time : More efficient Space : Less Efficient
3. Applicability	Applicable	Applicable
4. Accuracy	Less accurate	More accurate
5. Popularity	Popular	Under Testing
6. Flexibility	Same level	Same level
7. Visualization data	Use visualization	Use visualization
8. Generalization	Widely used	Limited use
9. Number of cluster	Use small and huge numbers	Use small and huge numbers
10. Type of data source	Use all type of data source	Use all type of data source
11. Size of data source	Huge and small data	Huge and small data

V. Conclusions

This paper represents applying clustering technique by enhancing K-M algorithm for DSS in banking sector especially in investment department under uncertain situations which has been rarely addressed before. IDMS is a new proposed system which is simple, straightforward with low computation needs. The proposed preprocessing component is an aggregation of several known steps. The post processing component is an optional one that eases the interpretation of the investment results. The banking is planning a set of actions in accordance of IDMS outcomes for decision making in investment sector. The investment department in the banking is starting to analyze the approached investment sector, to introduce a good decision under uncertain situation after enhance K-M algorithm to give high accurate and high quality data, that shown in comparison table.

Future work

In next step of this study implementing this proposed approach using classification and association techniques to give full image and best result for high level of management with a good decision and high accurate results.

VI. ACKNOWLEDGMENT

I want to express my deepest gratitude for my professor's supervisors Prof. Dr. Turkey Sultan and Dr. Ayman Khedr for their major help and support through all the phases of research and development.

REFERENCE

- [1] A. Hunter and S. Parsons, "A review of uncertainty handling formalisms", Applications of Uncertainty Formalisms, LNAI 1455, pp.8-37. Springer -Verlag, 1998.
- [2] E. Hernandez and J. Recasens, "A general framework for induction of decision trees under uncertainty", Modelling with Words, LNAI 2873, pp.26-43, Springer-Verlag, 2003.

- [3] M. S. Chen, J. Han, and P. S. Yu. IEEE Trans Knowledge and Data Engineering Data mining. An overview from a database perspective, 8:866-883, 1996.
- [4] U. Fayyad, G. Piatetsky-Shapiro and W. J. Frawley. AAAI/MIT, Press definition of KDD at KDD96. Knowledge Discovery in Databases, 1991.
- [5] Gartner. Evolution of data mining, Gartner Group Advanced Technologies and Applications Research Note, 2/1/95.
- [6] International Conferences on Knowledge Discovery in Databases and Data Mining (KDD'95-98), 1995-1998.
- [7] R.J. Miller and Y. Yang. Association rules over interval data. SIGMOD'97, 452-461, Tucson, Arizona, 1997.
- [8] Zaki, M.J., SPADE An Efficient Algorithm for Mining Frequent Sequences Machine Learning, 42(1) 31-60, 2001.
- [9] Osmar R. Zaïane. "Principles of Knowledge Discovery in Databases - Chapter 8 Data Clustering". & Shantanu Godbole data mining Data mining Workshop 9th November 2003.
- [10] T.Imielinski and H. Mannila. Communications of ACM. A database perspective on knowledge discovery, 39:58-64, 1996.
- [11] BIRCH Zhang, T., Ramakrishnan, R., and Livny, M. SIGMOD '96. BIRCH an efficient data clustering method for very large databases. 1996.
- [12] Pascal Poncelet, Florent Masseglia and Maguelonne Teisseire (Editors). Information Science Reference. Data Mining Patterns New Methods and Applications, ISBN 978 1599041629, October 2007.
- [13] Thearling K, Exchange Applications White Paper, Inc. increasing customer value by integrating data mining and campaign management software, 1998.
- [14] Noah Gans, Spring. Service Operations Management, Vol. 5, No. 2, 2003.
- [15] Joun Mack. IEEE TRANSACTIONS ON PATTERN ANALYSIS AND MACHINE INTELLIGENCE. An Efficient k-Means Clustering Algorithm, Analysis and Implementation, VOL. 24, NO. 7, JULY 2002.
- [16] Andrew Moore and Brian T. Luke. Tutorial Slides, K-means and Hierarchical Clustering and K-Means Clustering, Slide 15, 2003.
- [17] E. Turban, J. E. Aronson, T. Liang, and R. Sharda, Decision Support and Business Intelligence Systems, eighth edition. Prentice Hall, 2007.
- [18] Ahmed El Seddawy, Ayman Khedr, Turkey Sultan, "Adapted Framework for Data Mining Technique to Improve Decision Support System in an Uncertain Situation", International Journal of Data Mining & Knowledge Management Process (IJDMP) Vol.2, No.2, Jun 2012.



Ahmed B. El Seddawy, M.S. degrees in Information System from Arab Academy for Science and Technology in 2009. He now with AAST Egypt Teacher Assisting.

Variant Origin and Course of Ulnar Artery

Dr. Sharadkumar Pralhad Sawant¹, Dr. Shaguphta T. Shaikh², Dr. Rakhi M. More³

^{1, 2, 3} Department of Anatomy, K. J. Somaiya Medical College, Somaiya Ayurvihar, Eastern Express Highway, Sion, Mumbai-400 022.

Abstract: During routine dissection for Ist MBBS students on 65 year old donated embalmed male cadaver in the Department of Anatomy, K.J.Somaiya Medical College, Sion, Mumbai, India, we observed an unusual branch of the brachial artery. The brachial artery terminated in the cubital fossa into radial and common interosseous arteries. The radial artery had normal course and branches. The common interosseous artery was deeper and gave anterior and posterior ulnar recurrent arteries, and terminated into anterior and posterior interosseous arteries. The unusual large branch from the brachial artery was a variant of ulnar artery, arose from the lateral side of the brachial artery, descended on the lateral side upto the cubital fossa and crossed the fossa from lateral to medial, superficial to median nerve. It then descended superficial to the muscles arising from medial epicondyle of the humerus and was covered by the deep fascia of the forearm, pierced the deep fascia proximal to the wrist, crossed the flexor retinaculum, and formed the superficial palmar arch. Throughout its course, this artery gave no branch. There were no associated altered anatomy of the nerves observed in the specimen. The left upper limb of the same cadaver was normal. The photographs of the variations were taken for proper documentation and for ready reference. The embryological basis of the variation is presented.

Key words: Brachial artery, superficial antebrachial artery, superficial brachial artery, superficial ulnar artery, ulnar artery.

I. Introduction:

The brachial artery ends in the cubital fossa by dividing into radial and ulnar arteries. At the elbow, the ulnar artery sinks deeply into the cubital fossa and reaches the medial side of the forearm midway between elbow and wrist. The common interosseous artery is a short branch of the ulnar, passes back to the proximal border of the interosseous membrane and divides into anterior and posterior interosseous arteries. Anterior interosseous artery descends on the anterior aspect of the interosseous membrane with the median nerve's anterior interosseous branch. Median artery, a slender branch from anterior interosseous artery, accompanies and supplies the median nerve. (Williams et al, 1995)

II. Case Report:

During routine dissection for Ist MBBS students on 65 year old donated embalmed male cadaver in the Department of Anatomy, K.J.Somaiya Medical College, Sion, Mumbai, India, we observed an unusual branch of the right brachial artery. The brachial artery terminated in the cubital fossa into radial and common interosseous arteries. The radial artery had normal course and branches. The common interosseous artery was deeper and gave anterior and posterior ulnar recurrent arteries, and terminated into anterior and posterior interosseous arteries. The unusual large branch from the brachial artery was a variant of ulnar artery, arose from the lateral side of the brachial artery, descended on the lateral side upto the cubital fossa and crossed the fossa from lateral to medial, superficial to median nerve. It then descended superficial to the muscles arising from medial epicondyle of the humerus and was covered by the deep fascia of the forearm, pierced the deep fascia proximal to the wrist, crossed the flexor retinaculum, and formed the superficial palmar arch. Throughout its course, this artery gave no branch. There were no associated altered anatomy of the nerves observed in the specimen. The left upper limb of the same cadaver was normal. The photographs of the variations were taken for proper documentation and for ready reference. The photographs were taken for proper documentation.

III. Observations:

The unusual large branch from the brachial artery was a variant of ulnar artery, arose from the lateral side of the brachial artery in the axilla of right upper limb.

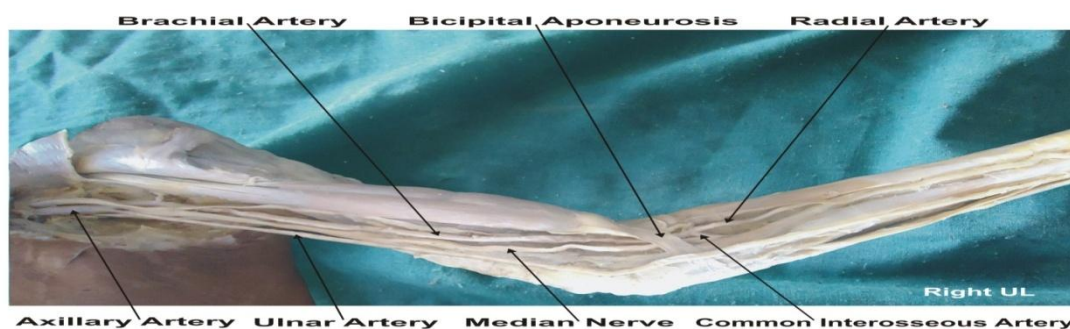


Fig. : The photographic presentation of the unusual origin of the ulnar artery from the brachial artery in the axilla of right upper limb.

IV. Discussion:

The variations in branching pattern of axillary artery are a rule rather than exception (2, 3, 4, 5, 6, 7, 8, 9, 10, 11, 12, 13, 14, 15, 16). Variant branches may arise from the brachial artery (17). Ulnar artery was found to deviate from its usual mode of origin in one in thirteen cases; frequently it sprang from the lower part of the brachial artery; the position of the ulnar artery in the forearm was more frequently altered; in cases of high origin, it invariably descended over the muscles arising from the medial epicondyle of the humerus and was covered by the deep fascia of the forearm (2). The present case of ulnar artery is somewhat similar to the variations presented in Quain's Anatomy (2). If the brachial artery is taken to terminate into radial and ulnar arteries, the embryological basis of the existing ulnar artery and the origin and course of the unusual branch of the brachial artery, replacing the ulnar artery in the present case, is as follows. Primitive axis artery and superficial brachial artery are implicated in the morphogenesis of the arteries of the upper limb (3, 18). The seventh cervical intersegmental artery forms the axis artery of the upper limb and persists in the adult to form the axillary, brachial, and interosseous arteries. Transiently, the median artery arises as a branch of the interosseous artery, begins to regress and remains as a residual artery accompanying the median nerve (18). Radial and ulnar arteries are later additions to the axis artery. An ulnar artery and a median artery are branches of the axis artery (8). A superficial brachial artery is a consistent embryonic vessel, coexisting or not with the brachial artery (19). It has two terminal branches, a lateral that continues as a part of the definitive radial artery (20) and a medial, superficial antebrachial artery, which divides into median and ulnar artery branches, which are the trunks of origin of the median and ulnar arteries. These trunks of deep origin predominate and the superficial arteries regress (8). In the present case, the axis artery had formed the interosseous artery and given the trunks of the median and ulnar arteries. The ulnar branch of the superficial antebrachial artery persists independently, without its usual anastomosis to the branch of the axis artery, as the large lateral branch of the brachial artery and the superficial ulnar artery, which is found in the distal part of the forearm and joins the superficial palmar arch. If the brachial artery is taken to terminate into radial and interosseous arteries, the simpler embryological basis of the interosseous artery and the origin and course of the unusual branch of the brachial artery, replacing the ulnar artery, is the following. It appears probable that the abnormal arrangement results from early obstruction of the ulnar artery below the origin of the interosseous, and the development of a superficial vas aberrans, which replaces the portion of vessel below the obstruction and unites with the brachial. The interosseous artery in such cases of abnormality thus comprises not only the interosseous artery but also the portion of ulnar artery above the obstruction. and, in accordance with this view, the recurrent branches are derived from it (2). The present anomaly is very rare and does not seem to have been reported. This case is of significance. Such an artery may present a superficial pulse and a hazard to venipuncture (21) and lead to intra-arterial injections or ligature instead of the vein in the cubital fossa (22, 23) Variation in the branching pattern of the brachial artery is of significance in cardiac catheterization for angioplasty, pedicle flaps, arterial grafting or brachial pulse.

V. Conclusion:

The knowledge of presence of the unusual origin of the ulnar artery from the brachial artery in the axilla may be clinically important for clinicians, surgeons, orthopaedicians and radiologists performing angiographic studies. Undoubtedly, such variations are important for diagnostic evaluation and surgical management of vascular diseases and injuries. These variations are compared with the earlier data & it is concluded that variations in branching pattern of axillary artery are a rule rather than exception. Therefore both the normal and abnormal anatomy of the region should be well known for accurate diagnostic interpretation and therapeutic intervention.

Competing Interests:

The authors declare that they have no competing interest.

Authors' contributions:

SPS wrote the case report, performed the literature review & obtained the photograph for the study. RMM performed the literature search and assisted with writing the paper. STS conceived the study and helped to draft the manuscript. All authors have read and approved the final version manuscript.

VI. Acknowledgement:

All the authors wish to convey thanks to Dr. Arif A. Faruqui for his valuable support. We are also thankful to Mr. M. Murugan. Authors also acknowledge the immense help received from the scholars whose articles are cited and included in references of this manuscript. The authors are also grateful to authors / editors / publishers of all those articles, journals and books from where the literature for this article has been reviewed and discussed.

References:

1. Williams, P.L.; Bannister, L.H. Berry M.M; Collins, P., Dyson, M. Dussek, J.E., Ferguson, M.W.J.: Gray's Anatomy, In: Cardiovascular system. Gabella, G. Edr. 39th Edn, 2000, Churchill Livingstone, London, Edinburgh pp: 1537-1540.
2. Thane, G. D. Quain's elements of Anatomy. In : Arthrology- Myology-Angiology. 10th Edn; 1892, Longman, Green, and Co. London: 445.
3. Schwyzer, A.G. and DeGaris, C.F : Three diverse patterns of the arteria brachialis superficialis in man, 1935, Anatomical Record 63 : 405- 416.

4. Mc Cormack, L.J. Caldwell, M.D. and Anson, B.J.: Brachial antebrachial arterial patterns, 1953 Surgery Gynecology and Obstetrics 96 : 43-54.
5. Coleman S.S. and Anson, B.J. : Arterial patterns in the hand based upon a study of 650 specimens Surgery Gynecology and Obstetrics, 196, 113 : 409-424.
6. Lippert, H. and Pabst, R: Arterial variations in Man. Bergmann, Munich; 1985, pp. 66-73.
7. Poteat, W.L. : Report of a rare human variation : Absence of the radial artery, 1986, Anatomical Record 214 : 89-95.
8. Rodriguez-Baeza, A. Nebot, J., Ferreira, B., Reina, F, Perez, J., Sanudo, J.R. and Rolg, M. : An anatomical study and ontogenic explanation of 23 cases with variations in the main pattern of the human brachio-antebrachial arteries, 1995, Journal of Anatomy 187 : 473-479.
9. Aharinejad S., Nourani F. and Hollensteiner H. : Rare case of high origin of ulnar artery from the brachial artery, 1997, Clinical Anatomy 10: 253-258.
10. Patnaik, V.V.G., Kalsey, G. and Singla, R.K. : Anomalous course of radial artery and a variant of deep palmar arch: A case report. Journal of the Anatomical Society of India, 2000, 49(1) : 54-57.
11. Patnaik, V.V.G., Kalsey, G. and Singla, R.K. : Superficial palmar arch duplication : A case report. Journal of the Anatomical Society of India, 2000, 49(1) : 63-66.
12. Patnaik, V.V.G., Kalsey, G. and Singla, R.K. : Trifurcation of brachial artery-A case report. Journal of the Anatomical Society of India, 2001, 50(2) : 163-165.
13. Patnaik V.V.G. Kalsey G. and Singla R.K. : Bifurcation of axillary artery in its 3rd part-A case report. Journal of the Anatomical Society of India, 2001, 50(2) : 166-169.
14. Celik, H.H., Germus, G., Aldur, M.M. and Ozcelik, M. : Origin of the radial and ulnar arteries : variation in 81 arteriograms, 2001, Morphologie 85 : 25-27.
15. Clerve, A., Kahn M., Pangilinan, A.J. and Dardik, H. : Absence of the brachial artery : report of a rare human variation and review of upper extremity arterial anomalies, 2001, Journal of Vascular Surgery 33 : 191-194.
16. Suganthi J., Koshy S., Indrasingh I. and Vettivel S. : A very rare absence of radial artery : A case report, 2002, Journal of the Anatomical society of India 51(1) : 61-64.
17. Huber G.C.: Piersol's Human Anatomy. In : The vascular system 9th Edn. 1930, Vol 1, J. B. Lippincott Co. Philadelphia. pp. 767-791.
18. Singer E.: Embryological pattern persisting in the arteries of the arm, 1933, Anatomical Record 55 : 403-409.
19. Tountas, CH.P. And Bergman, R.A. : Anatomic Variations of the upper extremity. Churchill Livingstone, 1993, New York. pp. 196-210.
20. Vancov V.: Une variete extremement complexe des arteres du member superiur chez un foetus humain, 1961, Anatomischer anzeiger 109 : 400-405.
21. Hazlett J.W.: Superficial ulnar artery with reference to accidental intra-arterial injection, 1949, Canadian Medical Association Journal 61 : 289-293.
22. Pabst R. and Lippert H. : Belderseitiges Vorkommen von A. brachialis superficialis, ulnaris superficialis and A. mediana, 1968, Anatomischer Anzeiger 123 : 223-226.
23. Thoma, A. and Young, J.E.M. : The superficial ulnar artery "trap" and the free forearm flap, 1992, Annals of Plastic Surgery 28 : 370-372.



Corresponding author full mailing address : Dr. Sharadkumar Pralhad Sawant, 25/2, Samrat Ashok Nagar Society, Shell Colony Road, Chembur, Mumbai – 400 071, Maharashtra, India.

Variant High Origin of the Posterior Tibial Artery

¹Dr.Sharadkumar Pralhad Sawant, ²Dr.Shaguphta T. Shaikh, ³Dr.Rakhi Milind More

^{1,2,3} Department of Anatomy, K.J.Somaiya Medical College, Somaiya Ayurvihar, Eastern Express Highway, Sion, Mumbai-400 022.

ABSTRACT: During routine dissection for first MBBS students on 65 years donated embalmed male cadaver in the Department of Anatomy, K.J.Somaiya Medical College, we observed the high origin of the posterior tibial artery from the popliteal artery proximal to the popliteus muscle. The posterior tibial artery ran downward on the posterior surface of the popliteus muscle. The anterior peroneotibial trunk distal to the tendinous arch of soleus muscle divides into the anterior tibial and the peroneal arteries. The further course of anterior, posterior tibial and peroneal arteries was normal. The photographs of the variations were taken for proper documentation and ready reference. There were no associated neuromuscular variations found in same specimen. The right lower limb of the same cadaver was normal.

Conclusion: The arthroscopic knee surgery is a convenient and preferred surgical procedure. The knowledge of branching pattern of popliteal artery is important for surgical interventions in the popliteal region in order to minimize the surgical complications due to anatomical variations. Therefore the origin of the posterior tibial artery from the popliteal artery proximal to the popliteus muscle is an important anatomical variation which should be kept in mind by the orthopaedicians doing knee joint surgery and total knee arthroplasty, by the surgeons operating on aneurysms of popliteal artery and by the radiologist performing angiographic study.

Keywords: Popliteal Artery, Anterior Tibial Artery, Popliteus Muscle, Posterior Peroneotibial Trunk, Posterior Tibial Artery, Peroneal Artery, Tendinous Arch of Soleus, Orthopaedicians, Arthroscopic Knee Surgery, Radiologist, Angiographic Study.

I. Introduction:

The popliteal artery is the continuation of the femoral artery. It begins at the level of hiatus magnus and ends at the lower border of popliteal muscle by dividing into anterior tibial and posterior tibial arteries (1). The popliteus muscle is the 'key muscle' of the popliteal region. The popliteal artery may divide proximal to the lower border of popliteal muscle. This is called as 'high division of the popliteal artery'. In high division, the anterior or posterior branch may arise at or above the articular surface of the tibial plateau (2). When the popliteal artery divides anywhere proximal to the lower border of the muscle, it is termed as 'high division of the popliteal artery' (3). The anterior tibial artery runs downwards on the posterior surface of the popliteus muscle and then it enters in to the anterior compartment of the leg through the oval space located at the superior border of the interosseous membrane of the leg. There it travels on the anterior surface of the interosseous membrane along with the deep peroneal nerve (1). The popliteal artery may divide proximal to the popliteus muscle into anterior and posterior tibial arteries. The anterior tibial artery descends downward either anterior or posterior to the popliteus muscle (1). The popliteal artery may terminate distal to the lower border of popliteus muscle which may interfere with the reconstruction surgeries (4). The variations in the branching pattern of the popliteal artery increase the risk of vascular trauma and unnecessary haemorrhage during arthroscopic surgery of knee joint. Preoperative diagnosis of variations in the branching pattern of the popliteal artery may help to avoid excessive unwanted haemorrhage and unnecessary complications during surgery (5). The knowledge of variations in the branching pattern of the limb arteries are important for the success of the arthroscopic surgeries.

II. Case Report:

During routine dissection for first MBBS students on 65 years donated embalmed male cadaver in the Department of Anatomy, K.J.Somaiya Medical College, we observed the origin of the posterior tibial artery from the popliteal artery proximal to the popliteus muscle. The popliteal artery immediately below the adductor hiatus terminated into the posterior tibial artery and anterior peroneotibial trunk. The termination level of the popliteal artery was proximal to the upper border of the popliteus muscle. The posterior tibial artery ran downwards on the posterior surface of the popliteus muscle. It traveled deep to the tendinous arch of soleus muscle to enter into the posterior compartment of leg. The anterior peroneotibial trunk divided in to the anterior tibial and the peroneal arteries. The anterior tibial artery entered in to the anterior compartment of the leg through the oval space located at the superior border of the interosseous membrane of leg. There it traveled downwards on the anterior surface of the interosseous membrane along with the deep peroneal nerve. The rest of the course of anterior, posterior tibial and peroneal arteries was normal. The photographs of the variations were taken for proper documentation and ready reference. There were no associated neuromuscular variations found in same specimen. The right lower limb of the same cadaver was normal.

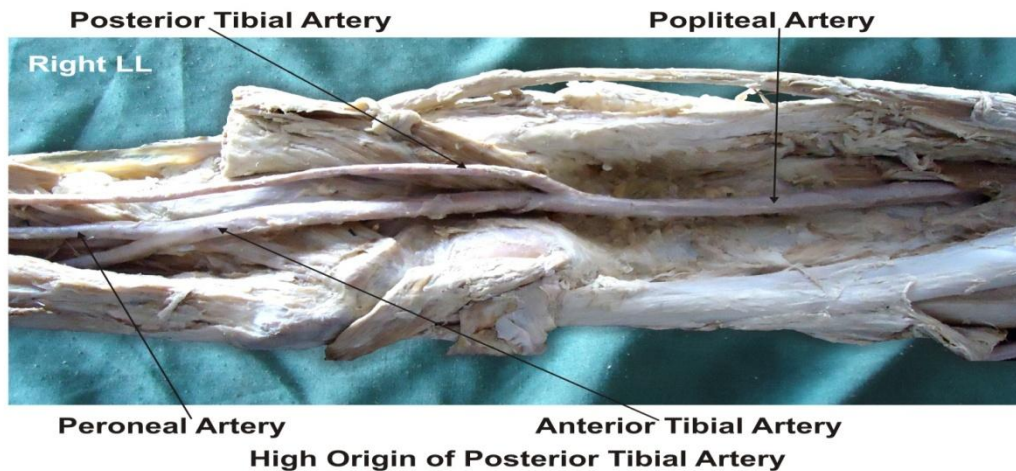


Figure : The photographic presentation of the origin of the right posterior tibial artery from the popliteal artery proximal to the popliteus muscle.

III. Discussion:

The variations in the branching pattern of the popliteal artery are common. The high level termination of the popliteal artery in relation to the upper border of the popliteus muscle was grouped into 3 types by Adachi. In type I the popliteal artery descended on the posterior surface of the popliteus muscle. The popliteal artery divides into the posterior peroneotibial trunk and the anterior tibial artery. The posterior peroneotibial trunk further divides into the peroneal artery and the posterior tibial artery. The diameter of the anterior tibial artery was equal to the popliteal artery or smaller than the posterior peroneotibial trunk. In type II the popliteal artery descended on the posterior surface of the popliteus muscle. It was divided into the posterior tibial artery and the anterior peroneotibial trunk. The diameter of the anterior peroneotibial trunk was observed to be larger. The anterior peroneotibial trunk divided into the peroneal artery and anterior tibial artery at the lower border of the popliteus muscle. In type III the popliteal artery terminated into the anterior tibial artery and posterior peroneotibial trunk at the upper border of the popliteus muscle. The anterior tibial artery ran downward in between the anterior surface of the popliteus muscle and the posterior surface of the tibia. The posterior peroneotibial trunk ran on the posterior surface of the popliteus muscle. The posterior peroneotibial trunk divided into the peroneal artery and posterior tibial artery distal to the tendinous arch of soleus muscle (2). The variation in the termination of popliteal artery observed in the present case is not documented in literature. In the present case the posterior tibial artery originated from the popliteal artery proximal to the popliteus muscle. The diameter of the anterior peroneotibial trunk was observed to be larger. The anterior peroneotibial trunk divided into the peroneal artery and anterior tibial artery at the lower border of the popliteus muscle. But in Adachi's type II, the popliteal artery did not divided proximal to the popliteus muscle. The high origin of anterior tibial artery at or above the level of the articular surface of the tibial plateau is documented in literature (6, 7, 8, 9). Another radiological study of the femoral angiograms on 495 lower extremities was performed to view the tibial arterial anatomy, and found that 7.8% of the cases revealed variations (4). Normally the diameter of the posterior tibial artery is more than the diameter of the peroneal artery, but in present case the diameter of the peroneal artery was more than the diameter of the posterior tibial artery which is similar to the study of Ozgur et al (8). It was reported in previous studies that the course of anterior tibial artery could either be from the anterior or posterior surface of the popliteus muscle (6, 7, 10). The course of anterior tibial artery on the anterior surface of the popliteus muscle was observed in 1-2.1% of the cases (2, 3, 5, 7, 9, 10). The course of anterior tibial artery on the posterior surface of the popliteus muscle was observed in 40% of the cases.

In present case the course of posterior tibial artery on the posterior surface of the popliteus muscle was observed. Clinicians and radiologists have defined a different terminology of the popliteal artery and its main branches in popliteal surgery. The anterior tibial artery was defined as the tibial-fibular trunk as soon as it branched from the popliteal artery (6). The tibial arteries were referred to as anterior or posterior peroneotibial trunk depending upon the origin of the peroneal artery (2). In the present case the peroneal artery arises from the anterior tibial artery and hence the anterior tibial artery is defined as the tibial – fibular trunk.

IV. Conclusion:

The arthroscopic knee surgery is a convenient and preferred surgical procedure. The knowledge of branching pattern of the popliteal artery is important for surgical interventions in the popliteal region in order to minimize the surgical complications due to anatomical variations. Therefore the origin of the posterior tibial artery from the popliteal artery proximal to the popliteus muscle is an important anatomical variation which should be kept in mind by the orthopaedicians doing knee joint surgery and total knee arthroplasty, by the surgeons operating on aneurysms of popliteal artery and by the radiologists performing angiographic study. These variations are compared with the earlier data & it is concluded that variations in branching pattern of the popliteal artery are a rule rather than an exception.

Competing Interests:

The authors declare that they have no competing interest.

Authors' contributions:

SPS wrote the case report, performed the literature review & obtained the photograph for the study. RMM performed the literature search and assisted with writing the paper. STS conceived the study and helped to draft the manuscript. All authors have read and approved the final version manuscript.

V. Acknowledgement:

All the authors wish to convey thanks to Dr. Arif A. Faruqui for his valuable support. We are also thankful to Mr. M. Murugan. Authors also acknowledge the immense help received from the scholars whose articles are cited and included in references of this manuscript. The authors are also grateful to authors / editors / publishers of all those articles, journals and books from where the literature for this article has been reviewed and discussed.

References:

1. Standring S, ed. Gray's Anatomy. 40th Ed., London, Churchill Livingstone. 2008; 1408, 1424.
2. Adachi B. Das Arteriensystem der Japaner, band 2. Kyoto, Kenkyusha. 1928; 198–201.
3. Lippert H, Pabst R. Arterial variations in man: classification and frequency. Munchen, J. F. Bergman Verlag. 1985; 62.
4. Kim D, Orron DE, Skillman JJ. Surgical significance of popliteal arterial variants. A unified angiographic classification. Ann. Surg. 1989; 210: 776–781.
5. Klecker RJ, Winalski CS, Aliabadi P, Minas T. The aberrant anterior tibial artery: magnetic resonance appearance, prevalence, and surgical implications. Am J Sports Med. 2008; 36: 720–727.
6. Day CP, Orme R. Popliteal artery branching patterns -- an angiographic study. Clin Radiol. 2006; 61: 696–699.
7. Kil SW, Jung GS. Anatomical variations of the popliteal artery and its tibial branches: analysis in 1242 extremities. Cardiovasc Intervent Radiol. 2009; 32: 233–240.
8. Ozgur Z, Ucerler H, Aktan Ikiz ZA. Branching patterns of the popliteal artery and its clinical importance. Surg Radiol Anat. 2009; 31: 357–362.
9. Tindall AJ, Shetty AA, James KD, Middleton A, Fernando KW. Prevalence and surgical significance of a high-origin anterior tibial artery. J Orthop Surg (Hong Kong). 2006; 14: 13–16.
10. Trotter M. The level of termination of the popliteal artery in the white and the Negro. Am J Phys Anthropol. 1940; 27: 109–118.



Corresponding author full mailing address: - Dr.Sharadkumar Pralhad Sawant, 25/2, Samrat Ashok Nagar Society, Shell Colony Road, Chembur, Mumbai – 400 071, Maharashtra, India.

Variant Flexor Carpi Ulnaris Muscle and Variant Course of Ulnar Artery in Fore Arm

¹Dr.Sharadkumar Pralhad Sawant, ²Dr.Shaguphta T. Shaikh, ³Dr.Rakhi Milind More

^{1,2,3} Department of Anatomy, K.J.Somaiya Medical College, Somaiya Ayurvihar, Eastern Express Highway, Sion, Mumbai-400 022.

ABSTRACT: During routine dissection, of the right upper limb of a 70 years old donated embalmed male cadaver in the Department of Anatomy, K.J. Somaiya Medical College, Sion, Mumbai, India, we observed a separate humeral and ulnar heads of flexor carpi ulnaris muscle. To recognise Anatomical variations it is necessary to know the normal Anatomy. Normally the flexor carpi ulnaris muscle arises by two heads, humeral and ulnar, connected by a tendinous arch. The humeral head arises from the medial epicondyle via the common flexor tendon. The ulnar head arises from the medial margin of the olecranon process and an aponeurosis attached to the posterior sub cutaneous border of the ulna. The tendon of flexor carpi ulnaris inserted into the hamate and the fifth metacarpal bone through pisohamate and pisometacarpal ligaments. In the present case the ulnar head of flexor carpi ulnaris muscle was more bulky. It separated ulnar nerve and artery. The humeral and ulnar heads were separated from each other by ulnar nerve. These two heads fused with each other just before their insertion, where the ulnar artery came in contact with ulnar nerve. The further course and distribution of ulnar artery and ulnar nerve were normal. The knowledge of such unusual ulnar head separating ulnar artery and ulnar nerve may be clinically important for plastic surgeons doing flap surgeries and for the surgeon dealing with cubital tunnel syndrome.

KEYWORDS: Flexor carpi ulnaris, Ulnar artery, Ulnar Head, Ulnar nerve, Humeral head, plastic surgeons, cubital tunnel syndrome.

I. INTRODUCTION:

Flexor carpi ulnaris muscle is the medial most muscle of the superficial flexor group. It arises by two heads, humeral and ulnar, connected by a tendinous arch. The small humeral head arises from the medial epicondyle via the common flexor tendon. The ulnar head has an extensive origin from the medial margin of the olecranon process and proximal two-thirds of the posterior border of the ulna, an aponeurosis (along with flexor digitorum profundus and extensor carpi ulnaris) and from the intermuscular septum between it and flexor digitorum superficialis. A thick tendon forms along its anterolateral border in its distal half. The tendon is attached to the pisiform, and thence prolonged to the hamate and the fifth metacarpal bone by pisohamate and pisometacarpal ligaments (pisiform is the sesamoid bone developing in the tendon of flexor carpi ulnaris). Acting with the flexor carpi radialis, it flexes the wrist and acting with the extensor carpi ulnaris it adducts the wrist (1). Flexor carpi ulnaris muscle is innervated by the ulnar nerve (C7, C8 and T1). The line between the medial humeral epicondyle and the pisiform, along the anterior palmar margin of the muscle, is used as a reference point for locating the ulnar neurovascular bundle. The ulnar artery reaches the muscle in its middle third, whereas the ulnar nerve is covered by the muscle throughout its entire course running under the tendon in the wrist region. The ulnar artery, the larger of the two terminal branches of the brachial, begins a little below the bend of the elbow, and, passing obliquely downward, reaches the ulnar side of the forearm at a point about midway between the elbow and the wrist. It then runs along the ulnar border to the wrist, crosses the transverse carpal ligament on the radial side of the pisiform bone, and immediately beyond this bone divides into two branches, which enter into the formation of the superficial and deep palmar arches. The ulnar nerve, after descending in the forearm between the flexor digitorum profundus and flexor carpi ulnaris muscles, pierces the deep fascia and enters the wrist through the Guyon's canal. In the distal part of the canal, the ulnar nerve divides into a superficial sensory branch and a deep motor branch, which supplies the hypothenar muscles and then passes across the palm, distributing to other intrinsic hand muscles.

II. MATERIALS AND METHODS:

The right upper limb of a donated embalmed 70 years old male cadaver was dissected during routine dissection in the department of Anatomy at K.J. Somaiya Medical College, Sion, Mumbai. All the superficial flexor muscles were exposed. The humeral and ulnar heads of flexor carpi ulnaris muscle was dissected carefully to observe the arrangement of ulnar artery, ulnar head, ulnar nerve and humeral head. The course of ulnar artery and ulnar nerve were also dissected. The photographs of the variations were taken for proper documentation.

III. RESULTS:

The variation was observed in the forearm of right upper limb. However, the left upper limb was normal. The right forearm showed separate ulnar and humeral heads of flexor carpi ulnaris muscle. The ulnar head of flexor carpi ulnaris muscle separated ulnar artery and nerve. The humeral and ulnar heads were separated from each other by ulnar nerve. The tendons of both the heads of flexor carpi ulnaris fused with each other just before their insertion. The ulnar artery comes in contact with ulnar nerve in the lower part of the forearm near the wrist where the two heads of flexor carpi ulnaris fused with each other. The ulnar artery in the hand takes part in the formation of superficial and deep palmar arches. The ulnar nerve in the hand bifurcates into superficial sensory branch and a deep motor branch. The course and distribution of the terminal branches of both ulnar nerve and ulnar artery were normal.

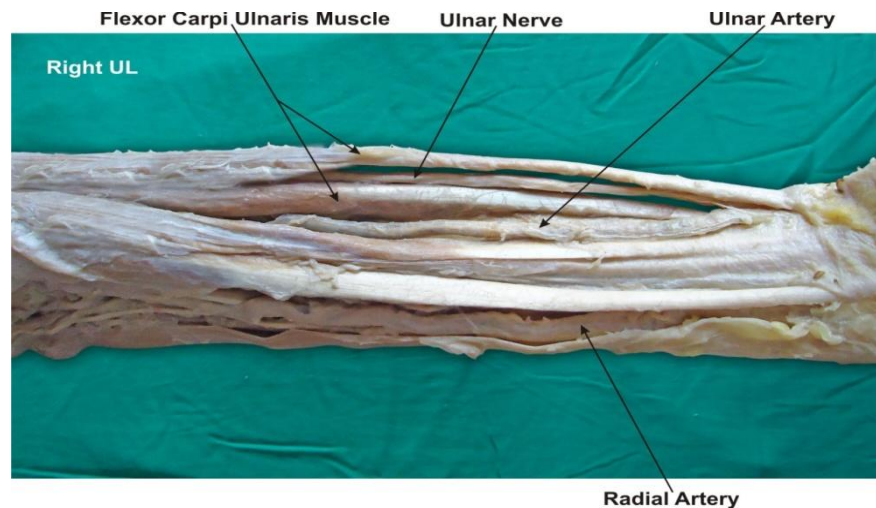


Figure : *Photographic presentation of the right forearm showing separate ulnar and humeral heads of flexor carpi ulnaris muscle. The ulnar artery running in between ulnar and humeral heads of flexor carpi ulnaris muscle.*

IV. DISCUSSION:

The variations of flexor carpi ulnaris muscle have been reported previously by many authors. These variations include: (i) an additional slip of flexor carpi ulnaris (2). (ii) variations in musculotendinous junction of the flexor carpi ulnaris muscle (3), (iii) variant flexor carpi ulnaris causing ulnar nerve compression (4). In the present case the two heads of flexor carpi ulnaris muscle remain separate. The ulnar head separated ulnar artery and nerve. The ulnar nerve runs in between the two heads of the flexor carpi ulnaris muscle in the forearm. Such variation is not yet reported in literature. The flexor carpi ulnaris muscle acts as an anatomical guideline for finding the neurovascular bundle (ulnar nerve, ulnar artery and accompanying venae comitantes), it can be easily palpated in its distal course if the wrist is flexed and adducted. The present variation need to be taken into account when interpreting ultrasound and MR images, as well as during dissection of the ulnar neurovascular bundle when using flexor carpi ulnaris as a guideline. The flexor carpi ulnaris is a useful local muscle flap in the forearm and elbow. It is, however, an important palmar flexor and ulnar deviator of the wrist, and functional loss may arise from the use of this muscle in its entirety. The flexor carpi ulnaris is made up of two distinct neuromuscular compartments. This arrangement allows for splitting of the muscle and the potential use of the larger ulnar compartment as a local muscle flap while maintaining the humeral compartment as an ulnar deviator and palmar flexor of the wrist (5). After multiple efforts to heal an infected nonunion of the proximal ulna, a flexor carpi ulnaris muscle pedicle flap was used to improve blood supply and softtissue coverage at the nonunion site. It was observed that it promoted bone healing and restoration of useful elbow function (6). The course and distribution of ulnar nerve and ulnar artery can assist the surgeon in the diagnosis and effective management of the more common pain syndromes conditions associated with the ulnar aspect of the hand (7). As the two heads of flexor carpi ulnaris muscles were separate the tendinous arch between them was absent. The possibility of entrapment of ulnar nerve in cubital tunnel in such cases is rare.

V. CONCLUSION:

The knowledge of such unusual variations of flexor carpi ulnaris is a must before any operative procedures of the forearm and hand. The ulnar head of flexor carpi ulnaris separating ulnar artery and ulnar nerve seen in present case is important for Anatomists. It may be clinically important for plastic surgeons doing flap surgeries and for the surgeons dealing with cubital tunnel syndrome. Orthopaedicians have used this muscle flap for treating non union of proximal ulna and hence knowledge of this variable head is important.

Competing Interests:

The authors declare that they have no competing interest.

Authors' contributions:

SPS wrote the case report, performed the literature review & obtained the photograph for the study. RMM performed the literature search and assisted with writing the paper. STS conceived the study and helped to draft the manuscript. All authors have read and approved the final version manuscript.

VI. Acknowledgement:

All the authors wish to convey our sincere thanks to Dr. Arif A. Faruqi for his valuable help, support and inspiration. Authors also acknowledge the immense help received from the scholars whose articles are cited and included in references of this manuscript. The authors are also grateful to authors / editors / publishers of all those articles, journals and books from where the literature for this article has been reviewed and discussed.

REFERENCES:

1. Susan, Standring, Gray's Anatomy, 39th Edition Elsevier Churchill Livingstone, 2005. pg: 877.
2. Bergman, R. A.; Thomson, S. A.; Afifi, A. K. & Saadesh, F. A. Compendium of human anatomic variations. Urban & Schwarzenberg, Baltimore – Munich, 13, 1988.
3. Grechenig, W.; Clement, H.; Egner, S.; Tesch, N. P.; Weiglein, A. & Peicha, G. Musculo-tendinous junction of the flexor carpi ulnaris muscle. An anatomical study. Surg. Radiol. Anat., 22:255-60, 2000.
4. Al-Qattan, M. M. & Duerksen, F. A variant of flexor carpi ulnaris causing ulnar nerve compression. J. Anat., 180:189-190, 1992.
5. Lingaraj, K.; Lim, A. Y.; Puhaindran, M. E. & Kumar, P. V. The split flexor carpi ulnaris as a local muscle flap. Clin. Orthop. Relat. Res., 455:262-6, 2007.
6. Meals, R. A. The use of a flexor carpi ulnaris muscle flap in the treatment of an infected nonunion of the proximal ulna. A case report. Clin. Orthop. Relat. Res., 240:168- 72, 1989.
7. Kleinert, H. and Hayes, J. The ulnar tunnel syndrome. Plastic Reconstructive Surgery, 1971, Vol.47, pg. 21-24.



Corresponding author full mailing address: - Dr. Sharadkumar Pralhad Sawant, 25/2,
Samrat Ashok Nagar Society, Shell Colony Road, Chembur, Mumbai – 400 071, Maharashtra, India.

Determination of Optimum Site for Artificial Recharge Aided Geographical Information System (GIS) & Logical Overlay Function (Case Study: Sarpaniran Plain)

Ali Liaghat¹, Karim Hejazi Jahromi², Naeem Shahidi³, Seyed Amir Shamsnia⁴

^{1,4}Department of Water Engineering, Shiraz Branch, Islamic Azad University, Shiraz, Iran.

^{2,3}Post Graduate Student of Water Engineering and Member of young researcher's club, Shiraz Branch, Islamic Azad University, Shiraz, Iran.

ABSTRACT: In dry and semi-dry regions which face lacking of water, using flood is one of the suitable solutions to prevent destruction of agricultural and pasture lands and recharge of ground water aquifers. In this study, flood distribution which is the most common in Iran was examined among various methods of artificial recharge. This study has been performed in Sarpaniran catchment, located in Pasargad in Fars province, considered as one of the important agricultural, industrial and residential centers. In order to flood distribution site selection, slope, surface infiltration, thickness of alluvium (geomorphology), geology (formations) and lands application information layers have been used. Information layers were combined based on intersect logical overlay function with Boolean logic in geographical information system (GIS) and regions suitable for flood distribution were determined. The results of this study show that 2.3 percent of the total area of the district is suitable for flood distribution. In examination of relation between using parameters and suitable places showed that geological factor (formations) is the limiting factor. The results indicate that due to the existence of several properties which are effective in site selection and required analysis with evaluated criteria and their continuous changes, geographical information system is an efficient tool for management and using site data in this field.

KeyWords: Site location, artificial recharge, Flood Distribution, Sarpaniran Catchment, Intersect Logical Overlay Function, Geographical Information System (GIS)

I. INTRODUCTION

Concerning climatic and geographical conditions, a vast area of Iran includes dry and semi-dry regions in a way that 74% of the country has annual rainfall less than 250mm. In fact, due to lack of precipitation, its unbalanced distribution regarding time and place and also inexistence of permanent rivers to provide water requirement in dry and semi-dry regions, exploitation From groundwater resources is the most certain resource for water supply in these regions and done in a vast area (12). Therefore, groundwater resources are considered as economical and social development factors in dry and semi-dry regions (17). Helping the increment of groundwater supplies is one of the useful ways in providing required water of various parts, especially in dry and semi-dry regions and confronting drought crisis.

Recharging ground waters is possible in natural and artificial ways. Physical (natural) recharge of a region is made by water infiltration resulted from precipitations inside the ground, infiltration through river aquifers or through underground flows. Whereas water supply is a main factor of the development of a region and physical supply cannot meet needs, thus artificial recharge has been developed (8,10, 4). Site selection of artificial recharge systems, specially flood distribution, is the fundamental principles of making these systems. Selecting the location based on scientific and natural facts plays the most important role in the stability and application of these systems in the way of realizing relevant objectives (3, 19). To prevent from problems due to the accumulation of sediments and increase of useful life of design and more efficiency of system regarding to the control of flood and achievement of considered objectives, site selection should be precisely made considering return period flood and its mass, size, severity, rainfall distribution, flood quality, soil condition, geology specifications, land slope, depth of groundwater aquifer, ... (12).

In a research for the examination of ground waters potential qualitatively and quantitatively by using GIS and RS, simple and weighted models were used. In this study information layers of the land's shape, geology, faults, waterway, recharge condition map, compaction of materials and soil type were used and finally have determined regions with groundwater potential and also regions suitable for ground waters artificial recharge. Results of this study show that remote sensing (RS) and GIS have high capability for the qualitative and quantitative examination of ground waters and determination of artificial recharge regions (18). In a research the application of Boolean Logic model in geographical information system with the aim of natural resources management in Eshkanan, Lamerd desert region was done. In this study, AND and OR operators of Boolean model have been used and after combining layers and different programs model of natural resources comprehensive management in deserts, suitable areas were recognized and categorized (6).

In another study capability and advantage of geographical information system and remote sensing emphasized as an acceptable solution for decreasing expenses in site selection of suitable regions for artificial recharge of aquifers (9). Using effective information layers in recharge, such as topography, surface infiltration, alluvium thickness, quality of ground water and lands usage with Boolean and Fuzzy models, ground water artificial recharges selection in Shoor desert, in geographical information system and far-distance examination were done. The results has been shown that nearly 5 percent of the studied region is suitable and 19 percent is almost suitable for groundwater artificial recharge (3). In a research using GIS and RS techniques, suitable site selection for artificial recharge of ground water resources of Semnan desert was examined and the results showed that using GIS and RS is an efficient tool for finding place for artificial recharge of ground water (9). In a

study, Geo statistical models for estimation of transferability and site selection of flood distribution maps, using transferability and special capacity data were compared. Their result indicate that Co Kriging method is a suitable method of estimation when correlation coefficient is greater than 0.7(7). Using GIS techniques for determining proper regions for artificial recharge of coastal aquifers in the south of Iran a research was done and the results shown that about 12% of the analyzed region is suitable and 8% is relatively suitable for aquifers artificial recharge (1). In another research capability of artificial recharges of ground waters was addressed by using GIS and economical and environmental aspects (11). Therefore, the aim of this research is studying and determining the most suitable place for artificial recharge designs and places for flood distribution and artificial recharge bed as well as studying the relation between different parts of the earth and suitable regions for ground waters artificial recharge.

II. Materials and Methods

Studying Region: The studying limitation is Sarpaniran plain. This region has been located in the distance of 120km. east-northwards of Shiraz and 12 km. of east-northwards of Saadatshahr in Pasargad, Fars province. Sarpaniran plain is in the limitation of $53^{\circ}09'$ to $53^{\circ}30'$ east longitude and $29^{\circ}52'$ to $30^{\circ}09'$ north latitude. The area of this region is 47288 hectares and around 31663.24 m^3 in a year water harvesting, is considered as an important agricultural, industrial and residential center with about 90% water consumption in agriculture (figure 1).

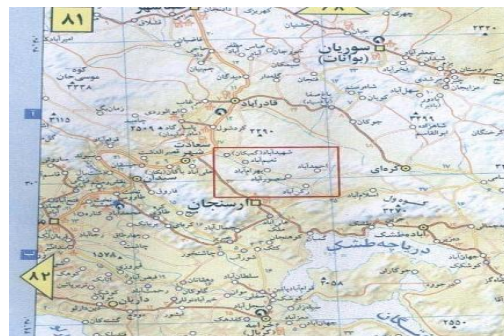


Figure 1: Geographical situation of Studying Region

For physical (natural) and topographic evaluation in the manner of aquifer hydrologic specially temporary water supply due to rainfall and its speed to the out of catchment through river system, Physical specifications of Sarpaniran catchment is observed (table 1).

Physical Specifications	Circle Ratio	Time of Concentration	Form Factor	Gravelius
level	0.34	6.35	0.29	1.69

Table 1: Physical Specifications of Sarpaniran Catchment

For site selection of suitable regions for ground water artificial recharge through flood distribution, evaluating indexes were selected in site selection. In this research 5 parameters (slope, surface infiltration, geomorphology, geology, and lands application) are analyzed and selected among effective factors in site selection of suitable regions for artificial recharge through flood distribution. Flood distribution site selection operation performed by using GIS and logical common method (common logical overlay) in Sarpaniran plain with the area of 47288 hectares and after throwing on four information layers of slope, surface infiltration, geomorphology and geology and suitable sites were identified. Then, corresponded with lands application information layer and those regions where had application limitation separated and the best regions for flood distribution were determined.

Region slope map: To prepare slope map, digital elevation model (dem) was used. In this research elevation contour lines of digital topography maps have been used as a primary data to make digital elevation model. Using digital elevation model, the slope map of catchment plain in GIS environment was prepared based on points' elevation in the earth digital model and their distance from each other, slope map of the region on percent (figure 2). The area and percent of slope of each class has been also presented (table 2).

Table 2: Area and percentage of area of each slope class in Sarpaniran plain

Slope class	Classes range (Percent)	Area (Hectare)	Area (Percent)
apt	0 - 3	11163.4	23.61
inapt	> 3	36117.94	76.39

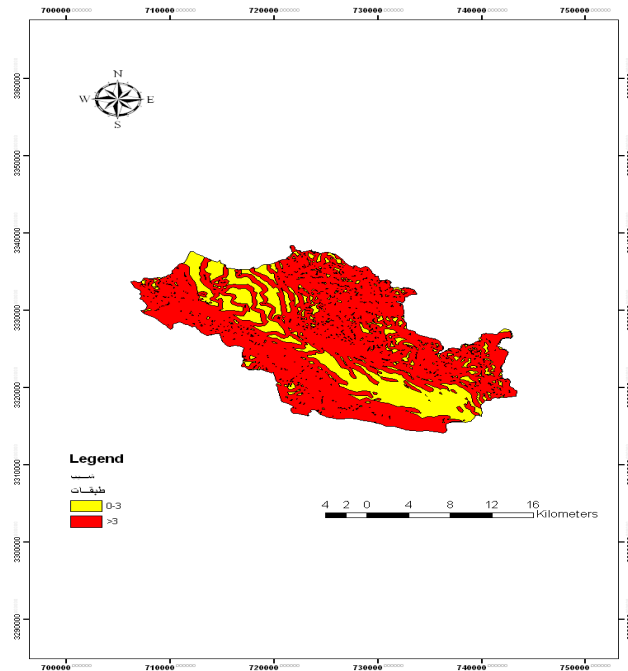


Figure 2: Slope map of Sarpaniran plain

Surface Infiltration Map: To prepare surface infiltration map by field operation, 17 points were selected for measuring the soil penetration (filtration) and double-ring method was used. The best method for variable interpolation is the one which has the least RMS. In this research the best interpolation method is Kriging model of circular type with the RMS equal to 7.876 (table 4). Thus, to convert point map to raster map the same interpolation was used. Surface infiltration map has been shown in figure 3. The extent and percent of area of each infiltration class was presented in table 3.

Table 3: Area and percent of area of each infiltration class

Table 4: RMS results, interpolation methods for preparing surface infiltration map

Interpolation method	RMS	Interpolation method	RMS	Interpolation method	RMS
Inverse Distance Weighting	10.14	Kriging (Gaussian)	8.19	CoKriging (pent spherical)	12.67
Global Polynomial Interpolation	14.47	Kriging (rational quadratic)	8.53	CoKriging (exponential)	12.61
Local Polynomial Interpolation	12.69	Kriging (hole effect)	50.93	CoKriging (Gaussian)	12.67

Infiltration class	Classes range (mm/hr)	Area (Hectare)	Area (Percent)
apt	0 - 25	41490.27	87.74
inapt	> 25	5797.03	12.26

Radial Basis Functions	9.19	Kriging (k - Bessel)	30.57	CoKriging (rational quadratic)	12.58
Kriging (circular)	7.18	Kriging (j - Bessel)	51.45	CoKriging (hole effect)	11.34
Kriging (spherical)	7.98	Kriging (stable)	36.3	CoKriging (k - Bessel)	12.67
Kriging (tetra spherical)	8.04	CoKriging (circular)	12.68	CoKriging (j - Bessel)	11.65
Kirging (pent spherical)	8.08	CoKriging (spherical)	12.67	CoKriging (stable)	12.67
Kriging (exponential)	8.61	CoKriging (tetraspherical)	12.67		

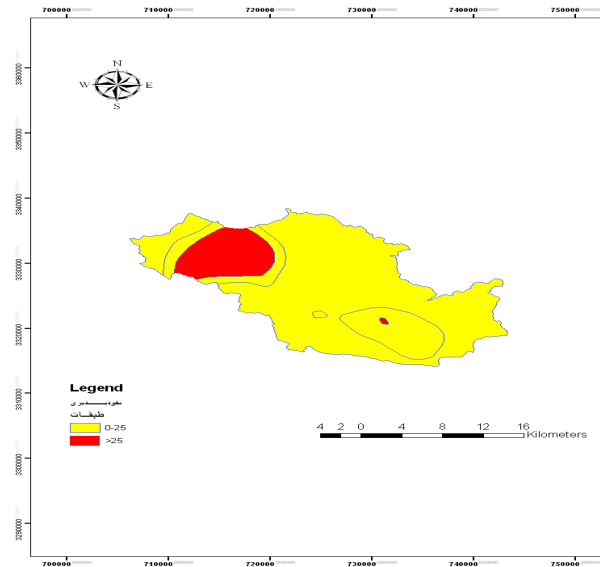


Figure 3: Surface Infiltration Map of Sarpaniran plain

Geomorphology Map: First, in order to provide the alluvium thickness plan concerning the region's area 35 well visited provided by Fars Regional Water Organization in 2010 were used. Next, for preparing raster plan from point plan, Kriging method, Gaussian type with RMS equal to 5.105 was chosen (table 6). Alluvium thickness plan has been shown in figure 4. Area extent and percentage of each alluvium thickness class was presented in table 5 as well.

Table 5- Area and area percentage of each alluvium thickness class

Alluvium thickness class	Classes range (m)	Area (Hectare)	Area (Percent)
apt	0 - 8	29157.79	61.66
inapt	> 8	18130	38.34

Table 6- RMS results, interpolation methods for preparing alluvium thickness plan

Interpolation method	RMS	Interpolation method	RMS	Interpolation method	RMS
Inverse Distance Weighting	6.8	Kriging (Gaussian)	5.1	CoKriging (pent spherical)	5.62
Global Polynomial Interpolation	9.1	Kriging (rational quadratic)	5.98	CoKriging (exponential)	6.02
Local Polynomial Interpolation	5.71	Kriging (hole effect)	6.14	CoKriging (Gaussian)	5.26
Radial Basis Functions	5.12	Kriging (k - Bessel)	5.19	CoKriging (rational quadratic)	5.83
Kriging (circular)	5.63	Kriging (j - Bessel)	6.18	CoKriging (hole effect)	6.54
Kriging (spherical)	5.59	Kriging (stable)	5.22	CoKriging (k - Bessel)	5.24
Kriging (tetraspherical)	5.61	CoKriging (circular)	5.56	CoKriging (j - Bessel)	6.56
Kirging (pent spherical)	5.63	CoKriging (spherical)	5.59	CoKriging (stable)	5.34
Kriging (exponential)	6.1	CoKriging (tetraspherical)	5.6		

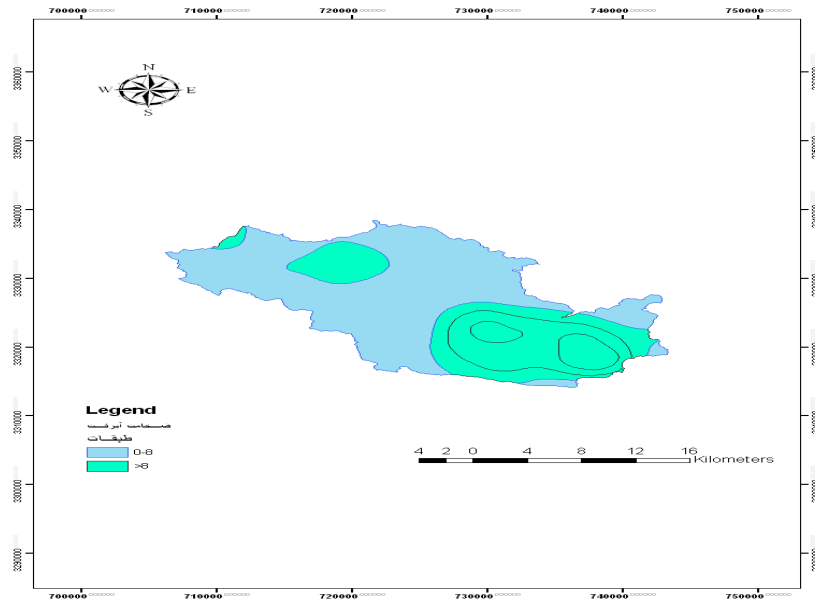


Figure 4- Sarpaniran desert alluvium thickness class.

Lands Usage Plan: In order to produce this information layer, lands usage plan provided by Agricultural Jihad Department of Pasargad, provided for the whole town in 2006 was used. For this purpose, results of combining information layers are used for determining regions suitable for distribution of flood. The resulted plan was overlaid with lands usage plan to separate the regions with usage limitations from areas suitable for flood distribution; because flood distribution operation execution in agricultural lands and other regions with limitation is not possible due to social tensions. Lands usage plan has been shown in Figure 5 and area and percentage of each usage was presented in table 7.

Table7- Area and percentage of pasture and non-pasture usage of Sarpaniran desert

Land class	User	Area (Hectare)	Area (Percent)
apt	Pasture	23011.22	48.66
inapt	non-pasture	24276.04	51.34

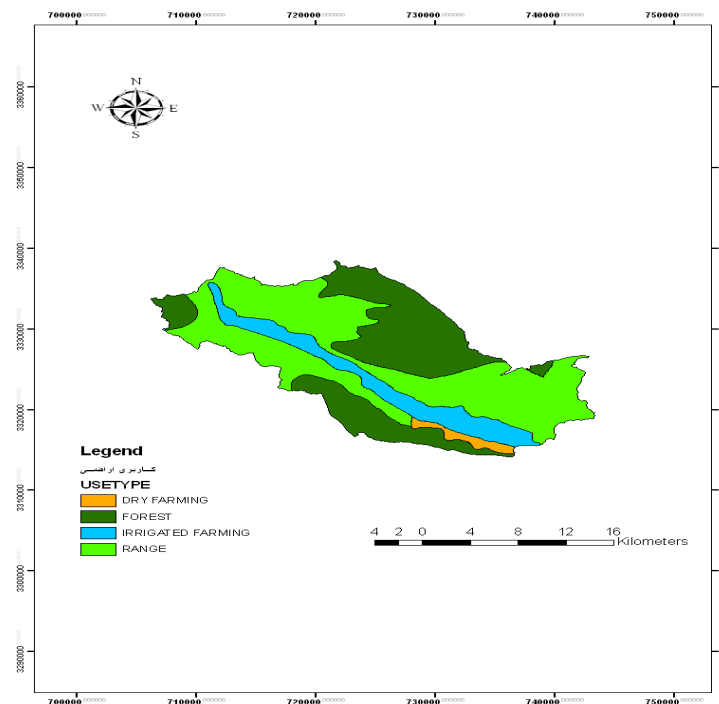


Figure5- Sarpaniran desert lands usage plan

Combining Information Layers & Data Analysis:

Slop basic map, surface infiltration, geological and desert's sediments thickness plans based on logical overlay function, intersect type have been combined in GIS and the output plan resulted from this combination was overlaid once without considering usage layer and once with land usage layer (Fig.6 & 7). Also, Suitable regions for artificial recharge by flood distribution method have been shown in satellite image of the desert in figure 8

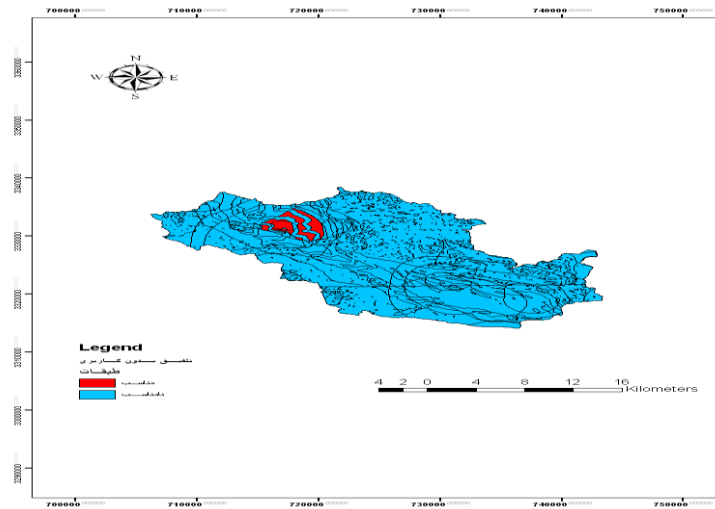


Figure 6- Plan of regions suitable for flood distribution combined without lands usage layer

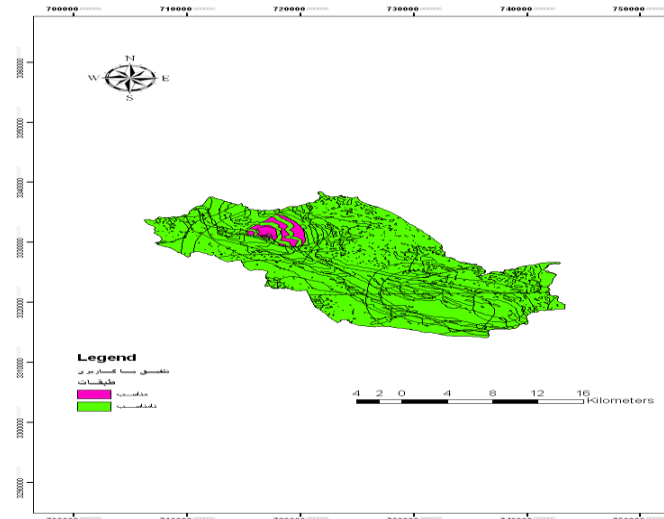


Figure7- Plan of regions suitable for flood distribution combined with lands usage layer

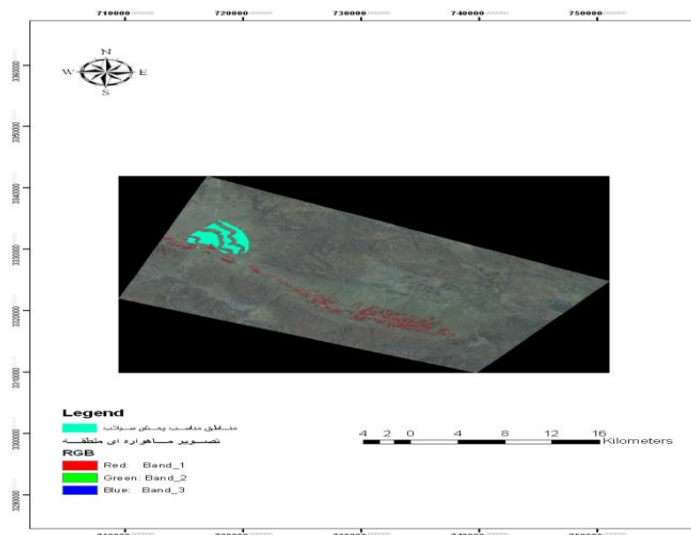


Figure 8- Sites suitable for artificial nourishment with flood distribution method.

then results of relation between layers and sites suitable for flood distribution by omission of selected layers, amount of suitable regions changes and the most important limiting factor in the area was determined. Since slop and usage information layers made the least limitation in the final combining, started to omit other layers one by one and its results was presented in figures 9 to 11.

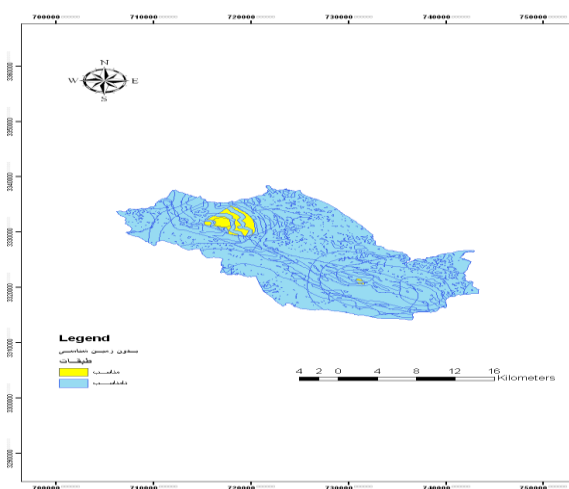


Figure 9- Plan of regions suitable for flood distribution without geological layer

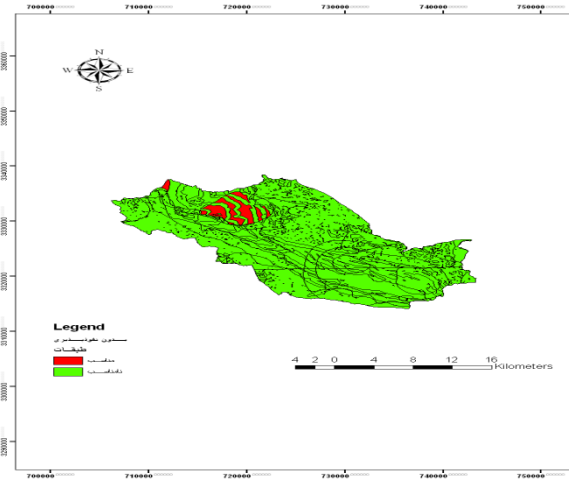


Figure10- Plan of regions suitable for flood distribution without infiltration layer

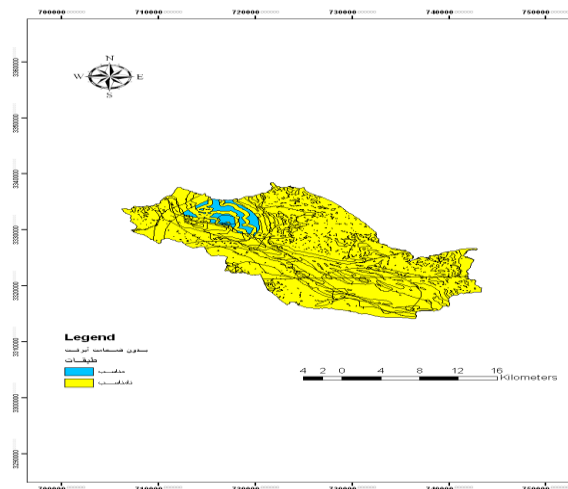


Figure11- Plan of regions suitable for flood distribution without alluvium thickness layer

III. Discussion & Conclusion

Flood distribution site selection studies are of high importance because of being the basis of aquifer and ground floor waters artificial nourishment studies. Since a group of condition (suitable and non-suitable) was used in this study and because the goal is site selection, therefore, logical overlay function, intersect type was used. Flood distribution site selection operation was done by using geographic Information System and logical intersect method in Sarpaniran desert with 47288 hectares area, after lapping 4 information layer of slop, surface infiltration, alluvium thickness and geology and suitable sites were determined. It was then combined with lands usage layer and the regions with usage limitation were separated and the best regions for flood distribution were determined. Geological plan of the region showed that Sarpaniran desert has variety of formation in a way that the most and the least formation area of the desert related to kk formation equal to 33.79 percent and Bakhtiari formation with 0.09 percent form total area of the region. Quaternary formation is the important formation for flood distribution which forms 12.05 percent of the district's area.

The results of this study showed that despite the fact that slop, lands usage and alluvium thickness layers are suitable for artificial recharge in flood distribution method, since quaternary areas form a percentage of the total district and other formations except Bakhtiari Conglomerate formation is not suitable in flood distribution view, it affects infiltration, for executing this operation. So one could say that, geological factors (formations) and surface infiltration are among limiting factors which face such plans with limitation. Ghermezcheshmeh (2000), Al-e-Sheikh (2002), Soltani (2002) and Noori (2003) all have determined suitable sites for flood distribution using geographical information system which correspond with result of this study.

In general, after combining 4 information layers of slop, geology, surface infiltration and alluvium thickness without considering region's land usage based on figure 6 the amount of suitable regions for flood distribution is 1162.03 hectares that forms around 2.46 percent of total of the district, however after combining plan of sites suitable for flood distribution with the region's land usage plan, based on figure 7 amount of suitable regions for flood distribution decreased about 0.2 percent, it means reached an amount equal to 1088.32 hectares that forms 2.3 percent of the district. Thus from the above combination it could be concluded that geological factor is the most limiting layer in determining regions suitable for flood distribution and infiltration and alluvium thickness factors are the next limiting factors. In general, the most important limiting factor in suitable lands class, related to alluvium thickness factor and in non-suitable lands class is related to geological factor.

Resources

- 1- Arasteh, P.D. and S.R. Vahhadj. Simulation of groundwater flow in an artificial recharge system. Proc. 8th International Conference on Water Resour. Manage., Isfahan, Iran, 1997. pp. 79 – 87.
- 2- Asano, Takashi, Artificial recharge of groundwater, California states water resources pp. 69-96.
- 3- Berger. D.L. Ground - water recharge through active sand dunes in northwestern Nevada. Water Resour. Bull. 1992. 28(5) : 959-965
- 4- Ghayoumian, J., Mohseni Saravi, M., Feiznia, S., Nouri, B. and Malekian, A., Application of GIS techniques to determine areas most suitable for artificial groundwater recharge in a coastal aquifer in southern Iran, Journal of Asian Earth Sciences, Volume 30, Issue 2, 2007. PP 364-374.
- 5- Ghermezcheshme, B., and *etal* . Determination of Quaternary deposits of flood-prone areas. Ms C Thesis, (case study : Northeast of Esfahan).2000. pp. 128-131
- 6- Hatefi Ardekani, A.H., and rezaee Rad, N., 2011. GIS and RS techniques for artificial recharge of groundwater resources located in Semnan plain. Seventh National Seminar on Watershed Management Sciences and Engineering.
- 7- Hashemi Tangestani, M., and Raoufat, M.R. Boolean logic models in GIS applications to natural resources management in arid region Ashknan of Fars. Conference Application of remote sensing and geographic information systems of deserts.2000. Pp 6
- 8- Heydarpour, J. Artificial recharge of groundwater aquifers. Iran University Press. 1990. pp 226.
- 9- Jalalvand, A., Kallantari, N. and Keshavarzi, M.R.. Locate suitable sites for artificial recharge of groundwater using remote sensing and GIS. 10th Symposium of Geological Society of Iran. 2006
- 10- Kiaheydari, J. The function of the Flood Plain aquifer recharges Moghar in Isfahan. Master thesis Irrigation and Drainage, College of Agriculture, Isfahan University of Technology.2003.
- 11- Krishnomurthy, J., N. Kumar, V. Jayaraman & M. Manivel. An Approach to Demarcate Ground Water Potential Zones Thorough Remote Sensing and a Geographical Information System, INT. J. Remote Sensing, 17(10). 1998. 1867-1884
- 12- Kousar, A., Artificial recharge of groundwater aquifers in the watershed extension methods. Olive Magazine. Volume 46 & 47. 1985. PP 16-19 & 20-23.
- 13- Mahdian, M.H.. Flooding problem and the need to exploit. First Workshop on management and utilization of water. Soil Conservatoin and Watershed Management Research Institute.1999.
- 14- Noori, B., Designated areas for groundwater supply using remote sensing data and Geographic Information System. Master's thesis. University of Tehran.2003.
- 15- Pedrero, F., Albuquerque, A., Marecos do Monte, A., Cavaleiro, V., Alarcón, A., Application of GIS-based multi-criteria analysis for site selection of aquifer recharge with reclaimed water, Resources, Conservation and Recycling, Volume 56, Issue 1, 2011. PP 105-116
- 16- Ramalingam, M. and Santhakumar, A.R., Case study on artificial recharge using Remote Sensing and GIS. 2004.
- 17- Rezaee, M., and Fakhr bahabadi, M.R., Location of the artificial recharge of groundwater using GIS and remote sensing in the Shurro Plains. 4th Conference of Applied Geology and the Environment. 2008.
- 18- Salajeghe Tazraji, E.A., Dehloran plain hydrological modeling using remote sensing and GIS. Department of Geography, Tarbiat Modares University. 1998.
- 19- Samani, N. and S. Behrooz. Optimal distribution of artificial recharge and its stability. Proc. 8th International Conference on Rainwater Catchment Systems, Tehran, Iran, 1997. pp. 182 - 189 .
- 20- Soltani, M.J., Land evaluation in order to locate areas prone to flooding broadcast operations in a GIS environment. Master's thesis. K.N. Toosi University of Technology. 2002. pp 97.

Tracking Of Multiple Auvs in Two Dimensional Plane

Deepali Chandrakar¹, Bharti Diwani², Dewashri Pansari³

Department of Electrical and Electronics Engineering, DIMAT Raipur
 C.G. Swami Vivekananda Technical University, Raipur, Chhattisgarh, India

ABSTRACT: Formation control using a leader-follower approach is a advancement in AUV technology for control and formation of multiple Autonomous underwater vehicles. This approach leads the other approaches of formation control like behaviour-based method, virtual structural method, artificial potentials as the theoretical formalization and mathematical analysis of these approaches are difficult and consequently it is not easy to guarantee the convergence of the formation to a desired configuration. On the other hand in the leader-follower approach, a robot of the formation, designated as the leader, moves along a predefined trajectory while the other robots, the followers, are to maintain a desired distance and orientation with respect to the leader. Numerical simulations are carried out to illustrate the effectiveness of the proposed formation scheme.

Keywords: Multiple AUV system, Formation control, Kinematics, Dynamics, Leader, Follower.

I. INTRODUCTION

An autonomous underwater vehicle (AUV) is a robot which travels underwater without requiring input from an operator. With the increase in technology and applications of AUV in different areas lots of attentions have been paid to the research on the cooperative control and formation control of multiple autonomous agents, especially on the cooperative control of groups of robots. History says that In 1987, Reynolds introduced a distributed behavioural model for flocks, herds and schools [6] where the three heuristic rules that of flock centring, collision avoidance and velocity matching were also introduced. In [6], each of dynamic agents was considered as a certain particle system whose dynamics can be expressed as a simple second-order linear equation. Furthermore, this kind of dynamic agents (particles) model was used in many of the following researches [4], [10]. Soon It was realized that multiple autonomous agents can be used to carry out more complicated jobs for single agent hard to finish. The recent advances in sensing, communication and computation enable the conduct of cooperative missions.

In many applications, a given task is too complex to be accomplished by a single robot; thus a multi-robot system working cooperatively is required to complete the job. Multi robot systems are more robust as compared to the single-robot systems because a team of robots provides certain amount of redundancy, which is useful when some of the robots malfunction also less time is needed to complete the job e.g. the use of AUVs for offshore operations includes ocean sampling, mapping, minesweeping, ocean floor survey, and oceanographic data collection. Instead of a single specialized expensive AUV, it is beneficial to use comparatively simple and inexpensive AUVs to cooperatively increase the service area.

In this paper the leader-follower formation control can be achieved as the leader AUV has to track the desired trajectory and the follower AUV tries to maintain a desired distance and angle relative to the leader. When all vehicles are in expected positions, the desired formation is established.

II. MODELLING OF AUV'S

To study the motion of marine vehicle 6 degrees of freedom are required since to describe independently the complete position and orientation of the vehicle we require 6 independent coordinates.[8] To describe position and translation motion first three sets of coordinates and their time derivatives are required. While for orientation and rotational motion last three sets of coordinates and their time derivatives are required. Table I shows this DOF.

TABLE I
 NOTATION USED FOR AUV MODELLING

DOF	Motion	Forces	Linear and angular velocity	Position
1	Motion in X-direction(surge)	X	u	X
2	Motion in Y-direction sway)	Y	v	y
3	Motion in Z-direction(heave)	Z	w	z
4	Rotation about X- axis(roll)	K	p	ϕ
5	Rotation about Y- axis(pitch)	M	q	θ
6	Rotation about Z- axis(yaw)	N	r	ψ

To obtain a mathematical model of the AUV, its study can be divided into two sub-categories: Kinematics and Dynamics.

Kinematics deals with bodies at rest or moving with constant velocity whereas dynamics deals with bodies having accelerated motion

III. AUV KINEMATICS AND DYNAMICS

To study the planar motion, we define an inertial frame {I} and a body fixed frame {B}. The origin of {B} frame coincides with the AUV centre of mass (CM) while its axes are along the principal axes of inertia of the vehicle.

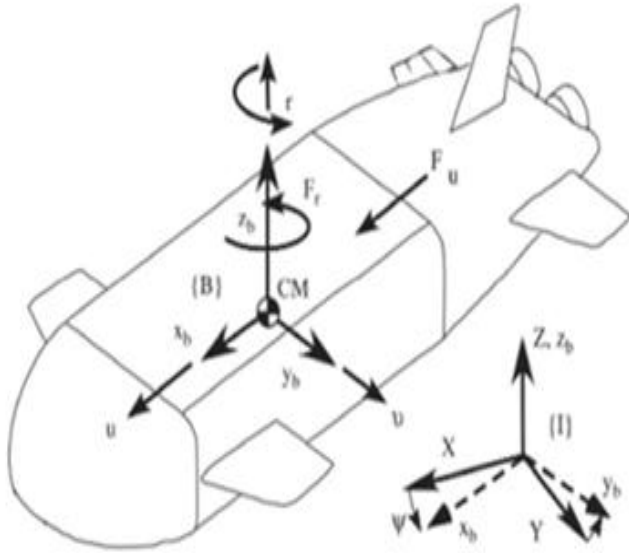


Fig. 1 AUV diagram showing inertial and body fixed frames

X_b is the longitudinal axis, Y_b is the transverse axis, and Z_b is the normal axis. The kinematic equations of motion for an AUV on the horizontal X-Y plane can be written as

$$\begin{bmatrix} \dot{x} \\ \dot{y} \\ \dot{\psi} \end{bmatrix} = \begin{bmatrix} \cos(\Psi) & -\sin(\Psi) & 0 \\ \sin(\Psi) & \cos(\Psi) & 0 \\ 0 & 0 & 1 \end{bmatrix} \begin{bmatrix} u \\ v \\ r \end{bmatrix}$$

(linear) surge (forward) and sway (side) velocities, respectively, defined in the body fixed frame. The orientation of the vehicle is described by angle Ψ measured from the inertial X-axis and r is the yaw (angular) velocity. Assuming that (i) the CM coincides with the centre of buoyancy (CB) (ii) the mass distribution is homogeneous, (iii) the hydrodynamic drag terms of order higher than two are negligible, and (iv) heave, pitch and roll motions can be neglected, the dynamics is expressed by the following differential equations:

$$\dot{u} = \frac{m_{22}}{m_{11}} vr - \frac{X_u}{m_{11}} - \frac{X_u|u|}{m_{11}} + \frac{1}{m_{11}} F_u$$

$$\dot{v} = \frac{m_{11}}{m_{22}} ur - \frac{Y_v}{m_{22}} v - \frac{Y_v|v|}{m_{22}} + \frac{1}{m_{22}} F_v$$

$$\dot{r} = \frac{m_{11}-m_{22}}{m_{33}} uv - \frac{N_r}{m_{33}} r - \frac{N_r|r|}{m_{33}} + \frac{1}{m_{22}} r|r|$$

The variable F_u denotes the control force along the surge motion of the vehicle and variable F_v denotes the control force along the sway motion of the vehicle. Third equation is uncontrolled and the AUV is an underactuated dynamic system. The constants m_{11} and m_{22} are the

combined rigid body and the added mass terms, and m_{33} is the combined rigid body and added moment of inertia about Z_b axis. X_u , $X_{u|u|}$, Y_v , $Y_{v|v|}$, N_r and $N_{r|r|}$ are the linear and quadratic drag terms coefficients.

IV. REFERENCE PATH AND CONTROLLER DESIGN

We choose a reference circular inertial planar trajectory given as follows

$$X_r(t) = 8\sin(0.01t) \text{ m},$$

$$Y_r(t) = 8\cos(0.01t) \text{ m}.$$

From this reference path, we find the error in position (actual position – reference position). This error is then given to proportional derivative controller (PD controller) which generates necessary controlling signals. The output from controller is then feed to system (AUV) which reduces the error in position and thus, AUV tracks the desired trajectory. The reference path for follower AUV is the circle with same frequency but with different radius

V. SIMULATION NUMERICAL DATA'S

Here some numerical data's are considered for simulation

Mass (M)-185 Kg

Rotational mass I_z - 50 kgm²

Added mass X_{ii} - 30 Kg

Added mass Y_v - 80 Kg

Added mass N_r - 30 kgm²

Surge linear drag X_u -70 kg/s

Surge quadratic drag $X_{u|u|}$ - 100 kg/m

Sway linear drag Y_v - 100 kg/s

Sway quadratic drag $Y_{v|v|}$ - 200 kg/m

Yaw linear drag N_r - 50 kgm²/s

Yaw quadratic $N_{r|r|}$ -100 kgm²

Also, $m_{11} = m - X_{ii} = 215$ kg, $m_{22} = m - Y_v = 265$ kg, $m_{33} = m - N_r = 80$ kgm²

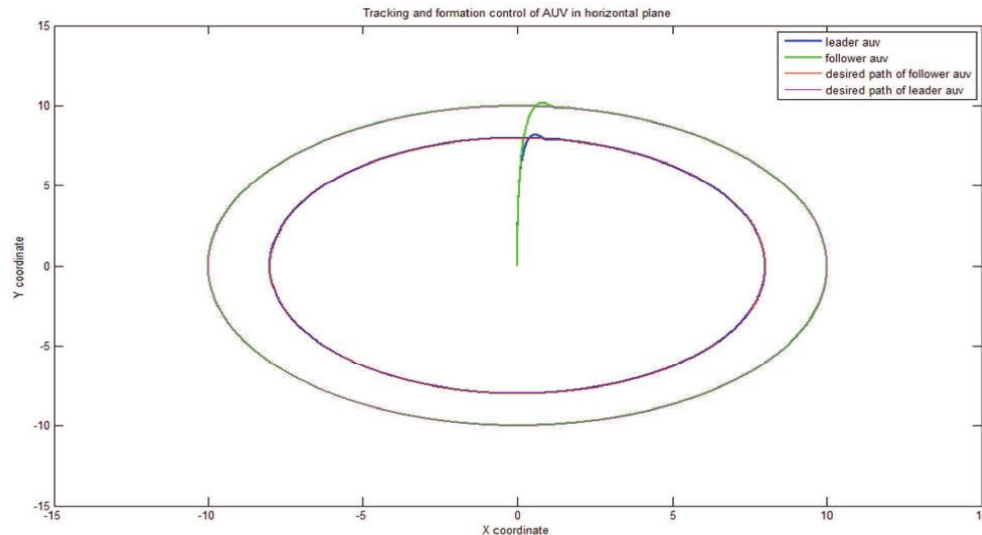


Fig 2. Tracking and formation control of AUVs in horizontal plane

The leader AUV is tracking its desired path which is a circle of radius 8m and also the follower AUV is maintaining a constant distance of 2m from the leader AUV.

VI. CONCLUSIONS

In this paper modelling of AUV is done and kinematics and dynamic equations of motion were obtained. Through simulation of this model we obtain a stable formation scheme for multiple AUV system, Therefore, for the simplification purpose, only formation of the vehicles in horizontal plane not in 3D plane and without obstacle avoidance is considered in this paper. However, from the design procedure presented in this paper, it is not difficult to find that if we add another potential term, which is similar to the one of form, then in future the other issues also can be handled with the proposed formation scheme.

REFERENCES

- [1]. M. Lewis and K.-H. Tan, "High precision formation control of mobile robots using virtual structures," *Autonomous Robots*, vol. 4, pp. 387–403, 1997.
- [2]. Q. Jia and G. Li, "Formation control and obstacle avoidance algorithm of multiple autonomous underwater vehicle(AUVs) based on potential function and behavior rules," in *Proceedings of IEEE International Conference on Automation and Logistics*, Jinan, China, 2007, pp. 569–573.
- [3]. M. Porfiri, D. Roberson, and D. J. Stilwell, "Tracking and formation control of multiple autonomous agents: A two-level consensus approach," *Automatica*, vol. 43, pp. 1318–1328, 2007.
- [4]. E. Fiorelli, N. E. Leonard, P. Bhatta, D. A. Paley, R. Bachmayer, and D. M. Fratantoni, "Multi-AUV control and adaptive sampling in Monterey Bay," *IEEE Journal of Oceanic Engineering*, vol. 31, no. 4, pp. 935–948, 2006.
- [5]. Huizhen Yang and Fumin Zhang, "Geometric Formation Control for Autonomous Underwater Vehicles", 2010 IEEE International Conference on Robotics and Automation Anchorage Convention District May 3-8, 2010, Anchorage, Alaska, USA
- [6]. C. W. Reynolds, "Flocks, herds, and schools: A distributed behavioural model," in *Computer Graphic. (ACM SIGGRAPH'87 Conference Proceeding)*, vol. 21, 1987, pp. 25-34.
- [7]. Fossen, Thor I. "Guidance and Control of Ocean Vehicles". Wiley, New York, 1994
- [8]. Presterio, Timothy. "Verification of a Six-Degree of Freedom Simulation Model of REMUS
- [9]. Burgard, W., Moors, M., Stachniss, C., & Schneider, F. E. (2005). *Coordinated multi-robot exploration. IEEE Transactions on Robotics*, 21(3), 376–386
- [10]. R. O.-Saber and R. M. Murray, "Distributed cooperative control of multiple vehicle formations using structural potential functions," *Proc. Of 15th IFAC World Congress*, Barcelona, Spain, 2002.

The Minimum Cost Forwarding Using MAC Protocol for Wireless Sensor Networks

M.Chithik Raja

Department of Information Technology
Salalah College of Technology
Sultanate of OMAN

ABSTRACT: Many routing protocols have been proposed to facilitate data transport from sensor nodes to a base station; few of these protocols have been formally verified or operationally deployed however. The Minimum Cost Forwarding (MCF) routing protocol in MAC layer, has been proposed. The application of MCF is restricted to networks possessing a single sink node and multiple source nodes. However, it offers several potential advantages for sensor nodes with limited resources. The MCF protocol is the subject of the current study with a view to its implementation in a prototype sensor network. The first phase of the work, and the subject of this paper, is the formal evaluation of the MCF protocol to increase confidence in its correctness and study its ability to handle node failure and other errors. As a result of formal verification using a model checking tool, UPPAAL, we confirm the soundness of the protocol during its initialization and operational phases and we have identified significant weaknesses in the published protocol concerning equal-cost minimum cost paths and node failure. In particular, we identify a flaw in the previously suggested periodic initialization broadcast to reestablish a minimum cost field. Here we present these results and offer improvements to overcome some deficiencies. It is expected that model checking may usefully be applied in the study of other WSN protocols.

I. INTRODUCTION

Sensor networks have been researched and deployed for decades; their wireless extension, however, has witnessed a tremendous upsurge in recent years. This is mainly attributed to the unprecedented operating conditions of wireless sensor networks (WSNs). As of today, a major problem in deploying WSNs is their dependence on limited battery power. A main design criterion is to extend the lifetime of the network without jeopardizing reliable and efficient communications from sensor nodes to other nodes as well as data sinks. A prominent example of today's non-optimized WSN deployment experiences is that the start-up alone costs the network a third of its battery power [1][2]. Optimizing every facet of the communication protocols is therefore vital and imperative. Such stringent design requirements can be met by a plethora of approaches, e.g. using cross-layer design paradigms, collaborative protocols, etc. This has led to copious novel distributed signal processing algorithms, energy-efficient medium access control and fault-tolerant routing protocols, self-organizing and self-healing sensor network mechanisms, reliable data aggregation algorithms, etc. These solutions stipulated first commercial activities as well as standardization approaches, including WOSA [3], KNX [4], IEEE 802.15.4 [5], IETF 6LowPan [6], IETF ROLL [7], etc.

Wireless sensor networks (WSN) consist of small self contained devices with computational, sensing and wireless communication capabilities. When deployed, they allow flexible, powerful, tether-less, automated data monitoring and/or control systems to be created. A sensor network comprises a set of sensor nodes and one or more base stations. The sensors generate, process and forward data via intermediate nodes to the base stations. Anticipated applications include environmental hazard monitoring, forest fire detection, machine instrumentation, etc. SensorNetworking has received considerable attention in recent years and many routing protocols have been proposed to facilitate data transport over such networks. Our current work[4] is based on the Minimum Cost Forwarding (MCF) network routing protocol in MAC layer with the view to its implementation in a prototype sensor network. The first phase of the work, and the subject of this paper, is the formal evaluation of the MCF protocol to increase confidence in its correctness and study its ability to handle node failure and other errors in MAC Protocol. MCF is considered particularly appropriate for sensor networks possessing limited resources since it does not require the storage of routing tables at sensor nodes, it establishes optimal routing paths with few message exchanges and it is scalable and simple to implement. The MCF protocol adopts a so-called *flat* model in which nodes have equal status except for a single base station, i.e. there is no hierarchy amongst the nodes. All message traffic generated at sensor nodes is routed towards a base station by forwarding along minimum cost paths comprising one or more sensor nodes.

The minimal cost path field is established during an initialization phase after which message traffic may commence. We describe in this paper how the MCF routing protocol may be formally modeled as a set of timed automata. The models are amenable to a formal analysis to verify that they possess some well-defined properties. Our aim is to investigate if MCF can successfully establish a minimum cost field and that data generated periodically at sensor nodes is communicated to a base station. Additionally we study the problems of node failure and equal-cost paths which compromise the effectiveness of MCF. Our focus is not merely to restate the MCF protocol but to present a formal verification of its behavior and to identify some of its operational difficulties. The remainder of this paper is organized as follows. In Section II, we describe the operation of the Minimum Cost Forwarding protocol. We present the algorithms used to establish a minimum cost field over a group of sensor nodes and to forward frames generated in sensor nodes to a base station.

II. MAC Protocols

MAC protocols developed for WSNs may be grouped into two main approaches: Scheduled-Based and Contention-Based [15]. Schedule-Based protocols regulate medium access by defining an order or Schedule for nodes to transmit, receive or be inactive. Examples of Schedule-Based protocols include: PEDAMACS, TRAMA and NATP. Power Efficient and Delay Aware Medium Access Protocol (PEDAMACS) [16] however generates overhead traffic needed for synchronizing the nodes and for topology adjustment, Traffic-Adaptive Medium Access Protocol (TRAMA) [15], whose overhead comes from exchanging neighbor and schedule information, and Neighbor Aware Probabilistic Transmission Protocol (NATP) [17], which creates overhead with neighbor information and synchronization beacons. Contention-Based protocols do not require central coordination but they use energy during periods of "Idle listening", which occurs when nodes are listening to the medium and there are no transmissions, thus wasting energy [18]. Sensor MAC (S-MAC) [18] operates in a similar way to 802.11: RTS, CTS and ACK frames are exchanged in order to send data. Additionally, nodes in S-MAC go to sleep and wake up following a schedule given by a SYNC frame. Control frames generate overhead. Timeout MAC (T-MAC) [19] improves on S-MAC energy consumption following the same basic idea: using a schedule for sleeping and waking up. However, T-MAC makes nodes sleep earlier during the schedule if there are no activation events, such as the node needing to send information or hearing activity in the channel. As in S-MAC case, RTS, CTS, ACK and SYNC frames generate overhead. Polastre et al introduced the Berkeley MAC (B-MAC) [20], protocol with no control frame overhead. B-MAC uses a long preamble in data frames and nodes verify the medium periodically, with a period equal to the preamble size. When they are not verifying the medium, nodes go to sleep. However, the preamble itself creates overhead to ensure nodes will check the medium in the proper time. One example results in transmitting 271 bytes for sending 36 bytes of data [20]. Uncertainty Driven MAC (UBMAC) [21] reduces preamble size from B-MAC by estimating clock uncertainty using Rate Adaptive Time Synchronization (RATS). RATS exchanges frames with timestamps between neighbors and computes clock uncertainty within an error boundary, allowing smaller preambles when used over B-MAC. On the other hand, there is a learning phase for the protocol which generates additional overhead besides timestamp frames. Sift [3] is a CSMA type of protocol using a non-uniform probability distribution for selecting the backoff waiting time. S-MAC, B-MAC and 802.11 use Binary Exponential Backoff with uniform probability for selecting the backoff time. Sift has a significantly smaller delay than 802.11 when several sources are sending data in the same zone of the network. The protocol uses RTS, CTS and ACK frames when the packet size is big, but there is no control frame overhead for small packets. However, there is no provision for turning off the radio, so idle listening occurs. To conserve energy many MAC protocols turn off the radio. A routing protocol using any of these MAC protocols must find new routes very frequently, since topology changes not just when nodes die, but also when they are temporarily out of the network due to MAC functionality. Protocols such as GSP do not compute routes, so they may be suitable to work these MAC protocols. However, GSP itself decides when to turn on or off the radio, and to optimize performance, those decisions must agree with the characteristics of the MAC layer. As an example consider using S-MAC or T-MAC with GSP, the Gossip Period must harmonize with the SYNC schedule and all transmissions and sleeping periods must be decided in advance, after considering the Gossip Probability. GSP and Sift do not generate conflicts in changing the radio state but both protocols must exchange state information in order to send a packet, because the radio is on and also the appropriate backoff time has elapsed. Arbitrating the interaction between MAC and Routing protocols adds complexity, additional places where errors may be introduced and the opportunity for hackers to find protocol exploits.

III. Minimum Cost Forwarding Algorithm

Minimum Cost Forwarding Algorithm (MCFA) computes the least cost from each node to the Base Station (BS). If the node is in the shortest path, the node retransmits the data; the same procedure repeats until the packet reaches the BS. Nevertheless, computing and updating the Minimum Cost generates overhead. A Gossiping protocol requires that a node receiving a packet retransmit it with a probability less than 1.0, which improves upon flooding performance because if the packet is not retransmitted, there is one less duplicate in the network. However, sensor nodes using Gossip waste energy receiving a packet if that packet is not retransmitted. The Gossip-based Sleep Protocol (GSP) improves on Gossiping because it drops a packet by not receiving it. If a packet is received it will be retransmitted, so energy spent for receiving is not wasted. GSP divides time in Gossip Periods with fixed duration [4]. At the beginning of each gossip period, every node decides with probability p , the Gossip Probability, to turn off its radio, and with probability $(1-p)$ to turn it on, ready to receive. A node receiving one packet must retransmit it in the following gossip period. All sleeping nodes must wake up in the next gossip period. Figure 1 shows one example of GSP. A node can be in one of three possible states: On Receiving, On Transmitting and Off.

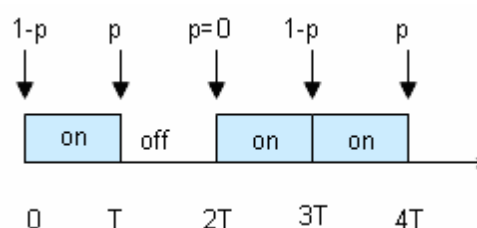


Fig. 1 One node using GSP. Each gossip period has duration T.

A. Initialization Mode

To begin establishing a minimum cost field the base station generates a single advertisement message with a cost of zero:

Begin { *Base Station, INIT protocol* }

Broadcast ADV with node cost 0;

End

A general node, i , sets its minimum cost, L_i , to infinity and waits for *ADV* messages to arrive each containing a cost field, L_m . If the value of the cost field plus the link cost is less than the current minimum cost, the node updates its minimum cost and sets its timer to expire after $_C_{i,m}$. As *ADV* messages with lower costs arrive, the timer may be reset several times before it expires. When the timer finally expires, the node broadcasts its *ADV* message advertising its minimum cost. The backoff time is thus proportional to the minimum cost at a node. Thus, a node will defer its *ADV* broadcast until it has heard the message leading to the minimum cost and make a single broadcast carrying its minimum cost.

Begin { *Node i, INIT protocol* }

$L_i := 1$;

loop

Receive an *ADV* message from node m ;

if ($L_i > L_m + C_{i,m}$)

Reset backoff timer to expire after $_C_{i,m}$;

else

Discard *ADV* message;

End loop

EVENT - backoff timer expires

Broadcast *ADV* with node cost L_i ;

End

This backoff scheme suggested by Ye et al is a means of reducing the overall number of *ADV* broadcasts compared to simply rebroadcasting every *ADV* that is received. Their simulation study showed that by selecting a value of approximately equal to the propagation and software delays, few nodes made broadcast more than once.

B. Operational Mode

Once the cost field has been established, nodes engage in the *OPER* mode protocol. The base station simply consumes *DATA* messages forwarded by nodes:

begin { *Base Station, OPER protocol* }

loop

Read and store *DATA* message;

endloop

end

DATA messages contain the data collected at a sensor node, the original cost and the consumed cost, as depicted in **Figure 2**.



Fig. 2. *DATA* message fields

A general node in *OPER* mode must forward *DATA* messages it receives after checking first that they are from transmitting nodes on a minimum path; messages containing costs greater than the minimum cost are ignored. The consumed cost of the message is computed before it is forwarded. Periodically, a node generates its own sensor *DATA* messages for forwarding.

begin { *Node i, OPER protocol* }

loop

Receive a *DATA* message from node m ;

if ($L_i > O_{Costm}$)

Drop *DATA* message;

else

$CCost := C_{Costm} + C_{i,m}$

if ($L_i = O_{Costm} - C_{Cost}$)

Broadcast *DATA* message ($S_{Datam}, O_{Costm}, C_{Cost}$);

else

Drop *DATA* message;

Endloop

EVENT - sensor data available from instrument

Broadcast DATA message with the local data, OCost = Li and CCost = 0;

End

IV. Scheduled MAC Protocols

Periodic and high-load traffic is most suitably accommodated by means of reservation-based protocols, i.e. those which build a specific schedule. Generally, in the context of WSNs, such protocols are variants of TDMA (Time Division Multiple Access) combined with FDMA (Frequency Division Multiple Access) where different time slots and frequency channels can be used by different nodes. TDMA is attractive because – once the schedule is set up – there are no collisions, no overhearing, and minimized idle listening. In addition, TDMA offers bounded latency, fairness and good throughput in loaded (but not saturated) traffic conditions. The central concern of TDMA type protocols is how to set up and maintain a specific schedule. To this end, three methods are used in the context of WSNs:

Scheduling of communication links: This fairly traditional approach sets up a unique slot dedicated to a specific sender and specific receiver, thereby minimizing idle listening and eliminating collisions and overhearing. Since transmitter and receiver know exactly when to wake up, this is the most energy efficient solution given the schedule is set up and that packets need to be transmitted; however, varying traffic conditions, imprecise clocks and network dynamics require new schedules to be set up which incurs large overheads.

Scheduling of senders: In this approach the slot is specified which is used by the sender which requires all receiving nodes to listen. It hence minimizes idle listening, eliminates collisions and reduces overheads to a certain extent (since any changes at the receiving side remain transparent to the established schedule); however, overhearing remains a problem of such an approach. A node, however, may minimize overhearing further through header filtering, i.e. when the packet is destined to another node, the receiver goes back sleeping during that slot.

Scheduling of receivers: Here, the receiving slots are specified. Overhearing is eliminated, idle listening minimized and overheads are reduced (since network dynamics at the transmitting side are transparent to the schedule). However, collisions between various transmissions can potentially occur if more than one transmitter wishes to reach a specific receiver; suitable contention resolution methods are hence needed. The first two variants of TDMA are suited to periodic, delay sensitive and fairly high-load traffic, the third to periodic and medium-load traffic. Whilst many variants of above protocols exist, such as the beacon-enabled guaranteed time slot transmission during the collision free period of the IEEE 802.15.4 MAC to be exposed in Section 6, we shall discuss the recently emerged Time Synchronized Mesh Protocol (TSMP) [22] to exemplify its functioning. TSMP is TDMA-based and hence requires network-wide synchronization. Access is controlled by means of a tunable amount of timeslots which form a frame. The protocol is designed such that a node can participate in multiple frames at once allowing it to have multiple refresh rates for different tasks. TSMP employs in addition FDMA and frequency hopping, i.e. different links use differing frequency slots and the same link hops during its life time across different frequency slots. This yields high robustness against interference and other channel impairments. A traditional approach to facilitate synchronization is beaconing, where longer frame lengths decrease the refresh rate at which synchronization is performed and hence power consumption and shorter frame lengths conversely invoke the opposite. TSMP does refrain from doing so because it requires long listening windows which consume power. Instead, TSMP nodes maintain a precise sense of time and exchange only offset information with neighbors to ensure alignment. These offset values are exchanged during active periods together with the usual data and acknowledgement packets hence invoking negligible overhead. TSMP nodes are active in three states: 1) sending a packet to a neighbor; 2) listening for a neighbor to talk; and 3) interfacing with an embedded hardware component. The duration of active periods, i.e. the duty cycling is very flexible in TDMA; typical applications require duty cycles of less than 1%. When applied, the sink typically retrieves the list of nodes, their neighbors and their requirements in terms of traffic generation. From this information, it constructs a scheduling table in both time and frequency. When implementing TSMP on IEEE 802.15.4 compatible hardware, 16 frequency channels are available. Exemplified by means of the scheduling table of Fig. 3, the TSMP link establishment and maintenance rules are simple:

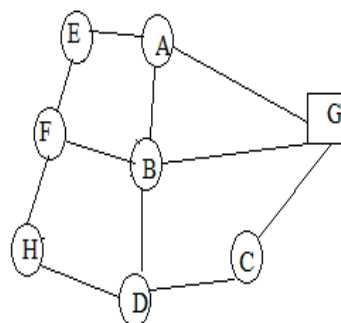


Fig.3.A. connectivity graph.

Ch15									
Ch14	A-G			G-C				E-A	

Ch13						D-H				
Ch12		F-E					B-A			
Ch11					C-D					F-B
Ch10			G-B							
Ch09										
Ch08	E-F					G-A		B-G		
Ch07				D-B						A-E
Ch06					H-F					
Ch05		D-C					C-G			
Ch04									B-D	
Ch03										
Ch02	H-D					B-F				
Ch01			F-H							
Ch00					A-B					

t1 t2 t3 t4 t5 t6 t7 t8 t9 t10

Fig.3B.Possible schedule for given connectivity graph.

Never put two transmissions in the same time/frequency slot; at a given time, a given node should not receive from two neighbors nor have to send to two neighbors. Assuming that slots are 10ms long and node H sends a packet following route $H \rightarrow F \rightarrow B \rightarrow G$, then H send to F in slot $[t5, \text{ch.6}]$, thereafter $F \rightarrow B$ in $[t10, \text{ch.11}]$, then $B \rightarrow G$ at $[t8, \text{ch.8}]$. Latency is hence in this particular case 13 slots (130ms) and in general always guaranteed to be bound by a finite value which depends on the particular design of the time frequency pattern.

V. Distributed Scheduling

By using a local scheme, the drawback of transmitting information to a central node and getting back slots assignment is avoided. SMACS (Self-organizing Medium Access Control for Sensor networks) [28] allows nodes to establish a communication infrastructure between neighboring nodes by defining transmission and reception slots. SMACS is localized and distributed, that is, there is no need for a master node. It contains two phases: neighbor discovery and channel assignment. In SMACS, a channel is assigned to a neighbor if discovered. Each link works on a different channel, i.e. a different frequency randomly chosen from a given set, to reduce collisions. To find its neighbor, a node wakes up and listens for a given time to receive invitation packets. If it does not receive such a packet, it starts inviting others by sending an invitation packet. To save energy, nodes sleep and wake up randomly. There is, however, a non-vanishing probability that two nodes never meet. When a link is formed between two nodes, they establish transmission-reception slots. These slots are used periodically to exchange data between nodes. Outside these slots, nodes sleep to save energy. The advantage of this method is that it is simple to implement, because slots are formed on the fly. The drawbacks are: the energy consumption, the low degree of connectivity of the network, and the difficulty of finding optimal routes. Furthermore, broadcast is not naturally supported since replaced by a series of unicast packets.

VI. Conclusion

In this paper, we explore the problem of the optimal WSN deployment, with an objective of minimizing the network cost with lifetime constraint. We discuss and identify the characteristics of a type of WSN applications and algorithms. The ultimate objectives of the device deployment for such applications are presented and discussed. We refine a deployment problem in a practical and fundamental scenario and its algorithms. We model this problem with the minimum set covering problem. Based on a recursive algorithm, a deterministic deployment strategy is proposed.. Furthermore, no MAC as of today is proven to be highly scalable as well as facilitate network ramp-up and auto organization/configuration/healing. This is particularly of importance, when sensor nodes arrive in a box of several thousands of nodes and are being switched on for deployment. Since this large quantity of nodes are within their one-hop radio neighborhood, any MAC described above will experience serious operational problems. On the deployment side, in the future, less nodes will really be equipped with batteries. It is expected that the majority of the WSN nodes will be relying on power harvesting. This has a profound impact on the MAC design, including its schedules. For instance, if power can be harvested every 24h only, then the MAC protocol needs accordingly be adapted to provide a high activity level during the time the node is energized.

REFERENCES

- [1] D. Yupho and J. Kabara, "The Effect of Physical Topology on Wireless Sensor Network Lifetime," Journal of Networks, vol. 2, September, 2007 2007.
- [2] Q. Jiang and D. Manivannan, "Routing protocols for sensor networks," in Proc. IEEE CCNC, Jan. 2004.
- [3] G. 'Acs, L. Butty'an, and I. Vajda. The security proof of a link-state routing protocol for wireless sensor networks. In Proceedings of the 3rd IEEE Workshop on Wireless and Sensor Networks Security (WSNS 2007), 2007.

- [4] G. 'Acs and L. Butty'an. Secure routing in wireless sensor networks. In Wireless Sensor Network Security (Cryptology and Information Security Series), Eds. J. Lopez and J. Zhou. ISBN: 978-1-58603-813-7, IOS Press, 2008.
- [5] Wood, A. and Stankovic, J. A., (2020) "Denial of Service in Sensor Networks", IEEE Computer, 35(10):54-62, pp. 54-62.
- [6] Intanagonwiwat, C., Govindan, R. & Estrin, D., (2003) "Directed Diffusion for Wireless Sensor Networking", IEEE/ACM Transaction on Networking, VOL. 11, NO. 1.
- [7] Sahaan, I. and Fernandes, L. (2008), "Secure Routing in Wireless Sensor Networks", University of Trento. <http://dit.unitn.it/~fernand/downloads/TWSNSlides.pdf>
- [8] Anthony D. Wood, John A. Stankovic, Gang Zhou, "DEEJAM: Defeating Energy-Efficient Jamming in IEEE 802.15.4-based Wireless Networks," in The 4th Annual IEEE Communications Society Conference on Sensor, Mesh and Ad Hoc Communications and Networks (SECON), San Diego, CA, June 2007.
- [9] Wenliang Du and Jing Deng, "A Pairwise Key Pre-Distribution Scheme for Wireless Sensor Networks," Conference on Computer and Communications Security archive Proceedings of the 10th ACM conference on Computer and communication security table of contents Washington D.C., USA, Pages: 42 – 51, 2011.

About the author



M. Chithik Raja MSc., M.E. (PhD)., He has finished his Master Degree in M.S.S. Wakf Board College at Madurai. Master of Engineering is awarded by Anna University Chennai Affiliation, Tamilnadu. Now He is pursuing his research in Wireless Sensor Network Security and System Architecture. He has written more than 10 Reputed International Journal and Conference Proceedings. He has published 3 International Standard Academic Books. He has more than 11 years of Academic Experience in International level Technological College as well as University. He is fond of conducting workshop and writing Books for Recent Communication Technologies and System Architecture in Wireless sensor Networks..

Performance Analysis of Routing Metrics for Wireless Sensor Networks

Eswar Rao. K,¹ K Naresh Kumar²

(Assistant professor, Aditya Institute of Technology and Management, Andhra Pradesh, India)

ABSTRACT: A wireless sensor network is a heterogeneous network consisting of a large number of tiny low-cost nodes and one or more base stations. Each sensor node comprises sensing, processing, transmission, mobilize, position finding system, and power units. These networks can use in various applications like military, health and commercial. Routing in wireless sensor networks has been an active area of research for many years. Sensor nodes have a limited transmission range, processing, storage capabilities and energy resources are also limited. In wireless sensor networks data is forwarded using multi-hop mechanism. Therefore, a variety of routing metrics has been proposed by various authors in wireless sensor networks for providing routing algorithms with high flexibility in the selection of best path and offering a compromise between throughput, end-to-end delay, and energy consumption. In this paper, we present a detailed survey about existing routing metrics in wireless sensor networks. The routing metrics are also compared based on their essential characteristics and tabulated.

Keywords: WCETT, ETT, ETX, Hopcount, RTT, MIC

I. INTRODUCTION

A wireless sensor network (WSN) is a heterogeneous network consisting of a large number of tiny low-cost nodes (devices) and one or more base stations (sinks). Main purpose of the WSN is to monitor some physical phenomena (e.g., temperature, barometric pressure, light) inside an area of deployment. Nodes are equipped with radio transceiver, processing unit, battery and sensor(s). Nodes are constrained in processing power and energy, whereas the base stations are not severely energy resources. The base station act as gateways between the WSN and other networks such as Internet etc.. The WSN is used in various applications like military, health and commercial. They provide simple and cheap mechanism for monitoring in the specified area. WSNs are frequently deployed to collect sensitive information. WSN can be used to monitor the movements of traffic in a city.

Such a network can be used to determine location of people or vehicles [1]. WSNs can be classified according to several aspects with impact on the security protocol design. One such aspect is the mobility of nodes and the base station. The nodes can be mobile or placed on static positions. The same holds true for the base station. Another consideration is the way the nodes are placed. The nodes can be deployed manually on specific locations following some predefined network topology or randomly deployed in an area, e.g., by dropping from a plane. The number of nodes is also a very important factor number of nodes in a network can range from tens to tens of thousands. Because of limited transmission range, communication between any two devices requires collaborating intermediate forwarding network nodes, i.e. devices act as routers to forward the data. Communication between any two nodes may be

trivially based on simply flooding the entire network. However, more elaborate routing algorithms are essential for the applicability of such wireless networks, since energy has to be conserved in low powered devices and wireless communication always leads to increased energy consumption.

The rest of the paper is organized as section 2: discuss about various routing metrics, section 3: presents a comparison of routing metrics, section 4: concludes the paper.

II. ROUTING METRICS

The existing routing metrics are classified into five categories based on their operation. Topology based, Signal strength based, Active probing based, Mobility aware and Energy aware metrics.

1.1. Topology Based

In this technique the topological information of the network will be considered i.e. the number of neighbors of each node, number of hops and/or paths towards a particular destination. The metrics always consider connectivity information which is available locally by the routing protocol, without requiring additional passive or active measurements. The topology-based metrics do not take into account several variables that have an impact on both the network and application performance, such as the transmit rates of the links are popular due to their simplicity.

Hop count

In this metric, every link counts as one equal unit independent of the quality or other characteristics of the link and very simple technique. The ease of implementation has made hop count the most widely used metric in wired networks and it is the default metric in many wireless sensor networks routing protocols, such as OLSR [2], DSR [3], DSDV [4] and AODV [5]. Fewer hops on the data path produce smaller delay, whether these involve network links or buffers or computational power. The implicit assumption is the existence of error-free links. On the contrary, links in wireless sensor networks cannot be assumed error-free.

1.2. Signal Strength Based Metrics

Signal strength metric has been used as link quality metrics in several routing protocols for wireless sensor networks. The signal strength can be viewed as a good indicator for measuring link quality since a packet can be transferred successfully when the signal strength is more than the threshold value.

1.3. Active Probing Based Metrics

To overcome the drawbacks of topology based metrics various authors have proposed active probing metrics to carry out active measurements and use probe packets to directly estimate those probabilities. Probing

technique had various challenges such as packet sizes of probes in the network should be equal to the data so that what probes measure is as close to the target as possible and probe packets should not give any priority in the network. The probing based metrics have proved promising in the context of wireless sensor networks. They measure directly the quantity of interest, rather than inferring it from indirect measurements, and do not rely on analytical assumptions.

Per-hop Round Trip Time (RTT)

The per-hop Round-Trip Time (RTT) metric is based on the bidirectional delay on a link [6]. In order to measure the RTT, a probe packet is sent periodically to each neighboring node with time stamp. Then each neighbor node returns the probe immediately. This probe response enables the sending node to calculate the RTT value. The path RTT metric is the summation of all links RTT in the route. The RTT metric is dependent on the network traffic. Since it comprises queuing, channel contention, as well as 802.11 MAC retransmission delays.

Per-hop packet pair delay (PktPair)

This delay technique is designed to overcome the problem of distortion of RTT measurements due to queuing delays and it consists periodic transmission of two probe packets with different sizes back-to-back from each node. The neighbor node calculates the inter-probe arrival delay and reports it back to the sender. This metric is less susceptible to self-interference than the RTT metric, but it is not completely immune, as probe packets in multi-hop scenario contend for the wireless channel with data packets. Both the RTT and PktPair metrics measure delay directly, hence they are load-dependent and prone to the self-interference phenomenon. Moreover, the measurement overhead they introduce is $O(n^2)$, where n is the number of nodes.

Expected Transmission Count (ETX)

To overcome drawbacks of RTT and PktPair techniques, authors proposed Expected Transmission Count (ETX) metric which is first routing metric based on active probing measurements designed for wireless sensor networks. ETX estimates the number of transmissions required to send a packet over a link. Minimizing the number of transmissions optimize the overall throughput and energy consumption. Let d_f is the expected forward delivery ratio and d_r is the reverse delivery ratio, Assuming that each attempt to transmit a packet is statistically independent from the precedent attempt, each transmission attempt can be considered a Bernoulli trial and the number of attempts till the packet is successfully received a Geometric variable, the expected number of transmissions is defined as

$$ETX = \frac{1}{d_f \cdot d_r}$$

Expected Transmission Time (ETT), Medium Time Metric (MTM), and Weighted Cumulative Expected Transmission Time (WCETT)

Draves [7] presented the drawbacks of ETX technique such as it prefers heavily congested links to unloaded links, if the link-layer loss rate of congested links is smaller than on the unloaded links. Later he proposed the

Expected Transmission Time (ETT) metric incorporating the throughput into its calculation. Let S be the size of the probing packet and B the measured bandwidth of a link, then the ETT of this link is defined as

$$ETT = ETX * \frac{S}{B}$$

Awerbuch [8] proposed Medium Time Metric (MTM) based on overhead, reliability of the link and size of the packet.

$$\tau(l, p) = \frac{\text{overhead}(l) + \frac{\text{size}(p)}{\text{rate}(l)}}{\text{reliability}(l)}$$

Where overhead is defined as per-packet overhead of the link that includes control frames, back-off, and fixed headers and reliability is denoted as the fraction of packets delivered successfully over the link.

As wireless sensor networks provide multiple non-overlapping channels, they propose an adaptation of the ETT metric accounting for the use of multiple channels, namely the Weighted Cumulative ETT (WCETT). Let k be the total number of channels of a system, the sum of transmission times over all nodes on channel j is defined as:

$$X_j = \sum_{i \text{ uses channel } j} ETT_i, \quad 1 \leq j \leq k$$

As total path throughput will be dominated by the bottleneck channel, they propose to use a weighted average between the maximum value and the sum of all ETTs.

$$WCETT = (1 - \beta) \cdot \sum_{i=1}^n ETT_i + \beta \cdot \max_{1 \leq j \leq k} X_j$$

The main disadvantage of the WCETT metric is that it is not immediately clear if there is an algorithm that can compute the path with the lowest weight in polynomial or less time.

Metric of Interference and Channel switching (MIC)

The Metric of Interference and Channel switching (MIC) [9] considers intra-flow and inter-flow interference problem. The MIC metric of a path p is defined

$$MIC(p) = \frac{1}{N \times \min(ETT)} \sum_{link \in p} IRU_i + \sum_{node \in p} CSC_i$$

where N is the total number of nodes in the network and $\min(ETT)$ is the smallest ETT in the network, which can be estimated based on the lowest transmission rate of the wireless cards. The two components of MIC, Interference-aware Re-source Usage (IRU) and Channel Switching Cost (CSC) are defined as:

$$IRU_i = ETT_i \times N_i$$

$$CSC_i = \begin{cases} w_1 & \text{if } CH(\text{prev}(i)) \neq CH(i) \\ w_2 & \text{if } CH(\text{prev}(i)) = CH(i) \end{cases} \quad 0 \leq w_1 \leq w_2$$

Multi-Channel Routing Metric (MCR)

Kyasanur and Vaidya [10] extend WCETT by considering the cost of changing channels. Let $\text{InterfaceUsage}(i)$ be the fraction of time a switchable

interface spends on transmitting on channel i and let $p_i(j)$ be the probability t used interface is on a different channel when we want to send a packet on channel j . If we assume that the total of the current interface idle time can potentially be used on channel j , we can estimate as $p_i(j)$

$$p_i(j) = \sum_{i,j} \text{InterfaceUsage}(i)$$

Let SwitchingDelay denote the switching latency of an interface. Then, the cost of using channel j is measured as

$$SC(c_i) = p_i(j) * \text{SwitchingDelay}$$

In order to prevent frequent channel switching of the chosen paths, a switching cost is included into the ETT metric, so that the resulting MCR metric becomes

$$MCR = (1 - \beta) \cdot \sum_{i=1}^n (ETT_i + SC(c_i)) + \beta \cdot \max_{1 \leq j \leq K} X_j$$

Modified ETX (mETX) and effective number of transmissions (ENT)

Koksal and Balakrishnan [11] considered the accuracy of loss estimator function. In certain conditions such as links with low average loss rate but high variability, the estimation capacity of the mean statistic is poor. They propose two alternative statistics for the estimation of required number of transmissions over a link.

Modified ETX (mETX), is defined as

$$mETX = \exp(\mu + \frac{1}{2} \sigma^2)$$

where μ is the estimated average packet loss ratio of a link and the variance of this value. Like ETX, mETX is additive over concatenated links.

Effective Number of Transmissions (ENT), is defined as

$$ENT = \exp(\mu + 2\delta\sigma^2)$$

The δ acts as an additional degree of freedom with respect to mETX and the value of δ depends on the number of subsequent retransmissions, which will cause the link layer protocol to give up a transmission attempt.

1.4. Mobility-Aware Metrics

Mobility-aware metrics selects routes with higher expected life-time to minimize the routing overhead related to route changes and their impact on throughput. The metrics largely use signal strength measurements and their rate of variation to infer the stability of links and routes. The path average degree of association stability, as proposed in the context of associativity based routing (ABR) and the affinity metric defined in [12] and reused by the Route-Lifetime Assessment Based Routing (RABR) protocol in [13].

Link associativity ticks and path average degree of association stability

Sensor nodes transmit beacon packets at fixed time intervals and calculate the received number of probs from their neighbors. These values serve as indicators of the actual stability of the link. Low values of associativity ticks imply mobile nodes in high mobility state, whereas high associativity ticks, beyond some threshold value thr_A , are obtained when a mobile node is more stable. The average degree of association stability over route R , A_{ave}^R , is

estimated as a function of the associativity ticks over all links along the route

$$A_{\text{ave}}^R = \frac{1}{n} \sum_{i \in R} 1_{A_i \geq A_{\text{thr}}}$$

Link affinity and path stability

The affinity of a link is related to the received power over that link, its rate of change and a threshold, determining whether the link is broken or not. Each node calculates the strength of the signal received over periodically. The signal strength change rate as the average rate of signal strength change as

$$\Delta P = (P_e(\text{current}) - P_e(\text{previous})) / dt$$

The link affinity is determined by

$$a_e = \begin{cases} \text{high, if } \Delta P_{\text{avg}} > 0 \\ (P_{\text{thr}} - P_e) / \Delta P_{\text{avg}}, \text{ if } \Delta P_{\text{avg}} < 0 \end{cases}$$

The affinity between two nodes A and B is then given by

$$\eta_{AB} = \min[a_{AB}, a_{BA}]$$

The route stability is then given by the minimum of the affinities of all links lying in the route

$$\eta_R = \min_{i \in R} \eta_i$$

The route is selected as long as the estimated value for its stability exceeds the required time to transfer data, whose estimate equals the time required to transmit data over the link capacity C .

Mobility-model driven metrics

Mcdonald and Znati [14] proposed mobility-model driven metric, which defines a probabilistic measure of the availability of links that are subject to link failures caused by node mobility. Each node is characterized by statistical distribution of the mean, variance of the speed of a node and average interval time. Gerharz et al. [15] and Jiang et al. [16] proposed metric based on the estimation of average residual lifetime of a link. However, the weak link in all these studies is the assumption that all nodes have similar mobility characteristics which is not acceptable in wireless sensor networks.

1.5. Energy-Aware Metrics

Energy consumption is an important constraint in wireless sensor networks. Sensors have restricted battery lifetime and are most vulnerable to the energy constraints. In some cases, choosing paths so that the overall delay is minimized may result in overuse of certain nodes in the network and premature exhaustion of their battery. Therefore, energy concerns have to be properly reflected in the definition of routing metrics. The total energy consumed when sending and receiving a packet is influenced by various factors such as the wireless radio propagation environment, interference from simultaneous transmissions, MAC protocol operation, and routing algorithm. The aim objective of energy aware metrics is to minimize overall energy consumption and to maximize the time until the first node runs out of energy.

Minimal Total Power routing (MTPR)

K. Scott [17] proposed Minimal Total Power Routing metric MTPR to minimize the overall energy

consumption. Later Singh [18] formalize this idea. Let $e_{i,j}$ denote the energy consumed for transferring a packet from node i to the neighboring node j . Then, if the packet has to traverse the path p , including nodes n_1, \dots, n_k , the total energy E required for the packet transfer is

$$E = \sum_{i=1}^{k-1} e_{n_i, n_{i+1}}$$

Minimum battery cost routing (MBCR)

In this metric the battery capacity of a node is taken into consideration to balance the energy consumption over all nodes in a network. The "Minimum Battery Cost Routing" (MBCR) [18] is based on the remaining battery capacity of the node. The ratio of battery capacity R_{brc} is defined as

$$R_{brc} = \frac{E_i}{E_{max}} = \frac{\text{Battery remaining capacity}}{\text{Battery full capacity}}$$

Under the assumption that all nodes have the same battery full capacity, a cost value $f_i(E_i)$ is assigned to each node n_i based on its residual battery capacity E_i

$$f_i(E_i) = \frac{1}{E_i}$$

Then the total available battery lifetime along a path p is the sum of the battery capacities of all nodes along the route

$$R_{bcr}^p = \sum_{n_i \in p} f_i(E_i)$$

Out of the full set P of possible paths, the one selected p' features minimum total residual battery capacity

$$p' = \{p \in P \mid R_{bcr}^p > R_{bcr}^q, \forall q \in P\}$$

The aim drawback of MBCR is that the selected route may well feature individual nodes with small remaining battery capacity.

Min-Max Battery Cost Routing (MMBCR)

The Min-Max Battery Cost Routing (MMBCR) metric [19] addresses the drawbacks of MCBR metric in avoiding nodes with very low residual battery capacity along paths with high overall battery capacity. The idea is to select a path, which minimizes the maximum power required at any node in a network. The MMBCR the chosen path must p' fulfill

$$p' = \min_{p \in P} \max_{n_i \in p} f_i(E_i)$$

Conditional max-min battery capacity routing (CMMBCR)

Toh [20] combines the MTPR and MMBCR into one single hybrid routing metric called Conditional Max-Min Battery Capacity Routing (CMMBCR) metric. It searches paths using MTPR, with the restriction that all nodes need to have a remaining percentage battery capacity that exceeds a threshold value γ . If there is no such path then MMBCR is used.

Later Kim [21] compares MTPR, MMBCR and CMMBCR. He presented the overhearing transmissions of some neighboring nodes have a significant impact on the performance of each metric and all behave similarly. In dense networks MTPR allows connections to live longer, whereas in sparse networks it is more important to avoid network partition hence MMBCR performs better.

Maximal residual energy path routing (MREP)

Chang and Tassiulas [22] proposed Maximum Residual Energy Path (MREP) link metric based on the remaining battery capacity and the necessary transmission energy. Let $e_{i,j}$ be the energy consumed to send one packet over the link from node i to node j , E_j the initial battery energy and E'_j the residual energy at node j . Chang and Tassiulas define two metrics for the link i to j . The remaining energy of a node $d_{i,j}$, defined as

$$d_{i,j} = \frac{1}{E_j - e_{i,j}}$$

and the inverse of the residual capacity of a node in terms of packets that can be delivered with the remaining energy

$$d_{i,j} = \frac{e_{i,j}}{E_j}$$

2. Comparison of Routing Metrics

The various metrics are compared based on important parameters and tabulated below table 1.

Table 1: comparison of routing metrics

Metrics	Optimization Objectives	Metric Computation Method	Path Metric Function
Topology based	Minimize delay	Use of locally available information	Summation
Signal strength based	Higher expected route life time	Use of locally available information	Based on routing algorithm
Active probing based	Minimize delay Minimize probability of data delivery	Active probing	Summation
Mobility aware	Higher expected route lifetime	Active probing Metrics piggybacked to route discovery packets	Based on the routing algorithm
Energy aware	Minimize energy consumption	Use of locally available information	Summation

III. CONCLUSION

A wireless sensor network is a heterogeneous network consisting of a large number of tiny low-cost nodes and one or more base stations. These networks can use in various applications like military, health and commercial. Routing in wireless sensor networks has been an active area of research for many years. Sensor nodes have a limited transmission range, processing, storage capabilities and energy resources are also limited. In this paper, we presented a detailed survey about existing routing metrics in wireless sensor networks. The routing metrics are also compared based on their essential characteristics and tabulated. As sensor nodes have limited battery capability energy aware routing metrics are useful.

REFERENCES

- [1] M. Gruteser, G. Schelle, A. Jain, R. Han, and Grunwald, Privacy-aware location sensor networks, 2003
- [2] T. Clausen and P. Jacquet. Optimized link state routing protocol (OLSR). IETF RFC 3626, October 2003; <http://www.ietf.org/rfc/rfc3626.txt>.
- [3] D. Johnson and D. Maltz. Dynamic source routing in ad hoc wireless networks. In T. Imielinski and H. Korth, editors, Mobile Computing, Dordrecht, The Netherlands, 1996. Kluwer Academic Publishers.
- [4] C. Perkins and P. Bhagwat. Highly dynamic destination-sequenced distance-vector routing (dsdv) for mobile computers. In Proceedings of SIGCOMM, October 1994.
- [5] C.E. Perkins and E.M. Royer. Ad hoc on-demand distance vector routing. In Proceedings of the 2nd IEEE Workshop on Mobile Computing Systems and Applications, pp. 90–100, New Orleans, LA, February 1999.
- [6] A. Adya, P. Bahl, J. Padhye, A. Wolman, and L. Zhou. A multi-radio unification protocol for IEEE 802.11 wireless networks. In Proceedings of Broadnets '04, pp. 344 – 354, 2004
- [7] R. Draves, J. Padhye, and B. Zill. Routing in multi-radio, multi-hop wireless mesh networks. In Proceedings of MOBICOM '04, New York, NY, USA, pp. 114–128, 2004.
- [8] B. Awerbuch, D. Holmer, and R. Rubens. The Medium Time Metric: High throughput route selection in multi-rate ad hoc wireless networks. Springer Mobile Networks and Applications, vol. 11, no. 2, pp. 253-266, April 2006.
- [9] Y. Yang, J. Wang, and R. Kravets, Designing routing metrics for mesh networks, Proc. WiMesh, 2005.
- [10] P. Kyasanur and N.H. Vaidya. Routing and link-layer protocols for multi-channel multi-interface ad hoc wireless networks. SIGMOBILE Mob. Comput. Commun., January 2006.
- [11] C. E. Koksal and H. Balakrishnan. Quality aware routing in time-varying wireless networks. in IEEE Journal on Selected Areas of Communication Special Issue on Multi-Hop Wireless Mesh Networks, November 2006.
- [12] K. Paul, S. Bandyopadhyay, A. Mukherjee, and D. Saha. Communication-aware mobile hosts in ad-hoc wireless network. IEEE ICPWC '99. Jaipur, India, February 1999.
- [13] A. Agarwal, A. Ajuja, J.P. Singh, and R. Shorey, Route-lifetime based routing (RABR) protocol for mobile ad-hoc networks. IEEE ICC 2000, New Orleans, LA, United States, June 2000.
- [14] A. McDonald and T. Znati. A path availability model for wireless ad-hoc networks. In Proceedings of the IEEE Wireless Communications and Networking Conference, 1998.
- [15] M. Gerharz, C. de Waal, M. Frank, and P. Martini. Link stability in mobile wireless ad hoc networks. In Proceedings of the 27th Annual IEEE Conference on Local Computer Network, November 2002.
- [16] S. Jiang, D. He, and J. Rao. A prediction-based link availability estimation for mobile ad hoc networks. Proceedings of INFOCOM '01, 2001.
- [17] K. Scott and N. Bambos. Routing and channel assignment for low power transmission in PCS. In ICUPC '96, vol. 2, pp. 498–502, 1996
- [18] J-P. Sheu, C-T. Hu, and C-M. Chao. The Handbook of Ad Hoc Wireless Networks, Chapter Energy-Conserving Grid Routing Protocol in Mobile Ad Hoc Networks. RCR Press LLC, 2003.
- [19] S. Singh, M. Woo, and C. Raghavendra. Power-aware routing in mobile ad hoc networks. In The Fourth Annual ACM/IEEE International Conference on Mobile Computing and Networking, pp. 181–190, 1998.
- [20] C.-K. Toh. Maximum battery life routing to support ubiquitous mobile computing in wireless ad hoc networks. IEEE Communications Magazine, pages 2–11, June 2001.
- [21] D. Kim, J. Garcia-Luna-Aceves, K. Obraczka, J. Cano, and P. Manzonni. Performance analysis of power-aware route selection protocols in mobile ad hoc networks. Proc. IEEE Networks 2002, Atlanta, GA, USA, August 2002
- [22] J. Chang and L. Tassiulas. Maximum lifetime routing in wireless sensor networks. In Proceedings of 37th Annual Allerton Conference on Communication, Control, and Computing, Monticello, IL, September 1999.

The Computational Algorithm for Supported Solutions Set of Linear Diophantine Equations Systems in a Ring of Integer Numbers

Serigiy L. Kryvyi¹, Paweł Dymora², Mirosław Mazurek³

¹(Department of Distributed Systems, Rzeszow University of Technology, Poland)

ABSTRACT: The algorithm for computation of minimal supported set of solutions and base solutions of linear Diophantine equations systems in a ring of integer numbers is proposed. This algorithm is founded on the modified TSS-method.

Keywords: ring of integer numbers, linear Diophantine equations, supported set, supported set of solutions

I. INTRODUCTION

Linear Diophantine equations and also their systems are often present in a wide variety of sciences with heavy usage of computations. In order to solve many different systems these equations are brought to task of integerlinear programming, pattern recognition and mathematical games [2], cryptography [3], unification [4], parallelization of cycles [5], etc. In this case, the sets of parameters of the equations are usually set of integers, residue ring or residue field of any number modulo and sets in which solutions to the equations are found in ring of integers, the set of natural numbers or finite fields and residue rings. Algorithms for finding solutions of linear Diophantine equations system (SLDE) in the set of natural numbers have been described in many publications [6] - [12]. In this work we will focus on analyzes of the computation of SLDE algorithm in a ring of integers. The basis of the proposed algorithm is the TSS method used for the constructing the minimal set of solutions forming a homogeneous system of linear Diophantine equations (HSLDE) on the set of natural numbers [1].

II. PRELIMINARIES

The systems of linear Diophantine equations. The system of linear Diophantine equations in a ring Z is described as follows:

$$S = \begin{cases} L_1(x) = a_{11}x_1 + \dots + a_{1n}x_n = b_1, \\ L_2(x) = a_{21}x_1 + \dots + a_{2n}x_n = b_2, \\ \dots \dots \dots \dots \dots \dots \dots \dots \\ L_q(x) = a_{q1}x_1 + \dots + a_{qn}x_n = b_q, \end{cases} \quad (1)$$

Where: $a_{ij}, b_i, x_i \in Z$, $i = 1, \dots, n$, $j = 1, \dots, q$. Solution to SLDE (1) we will call a vector $c = (c_1, c_2, \dots, c_n)$, which by substitution in $L_i(x)$ for the value x_j , c_j transforms $L_i(c) \equiv b_i$ into identity for all $i = 1, 2, \dots, q$. SLDE is called Homogenous (HSLDE), where all b_i are equal to 0, otherwise the system is called inhomogeneous (ISLDE).

A. 2.1. The TSS method of HSLDE solution

Let's consider HSLDE S presented as (1) and $e_1 = (1, 0, \dots, 0)$, $e_2 = (0, 1, \dots, 0)$, ..., $e_n = (0, \dots, 0, 1)$ which

are unitary vectors of canonical set base Z^n . Let's have M as solutions set for the system S . Since it is homogeneous, than the zero vectors is always valid solution. Such a solution is called trivial and any other non-zero solution of S is called non-trivial. The HSLDE is called contrary, only when the set M is composed exclusively with the trivial solution; otherwise it is called non contrary.

The TSS method and its implementation for linear equations systems in a set of natural numbers have been described in detail in [1]. Let's consider a modification of this method in case of the ring of integer numbers Z .

The case of homogeneous linear Diophantine equation (HLDE). Let's define the HLDE with the following form:

$$L(x) = a_1x_1 + \dots + a_ix_i + \dots + a_nx_n = 0, \quad (2)$$

Where: $a_i, x_i \in Z, i = 1, \dots, n$.

Let's consider a set of canonical base vectors $M = \{e_1, \dots, e_n\}$ and a function $L(x) = a_1x_1 + a_2x_2 + \dots + a_nx_n$ HLDE (2). Without limiting the generality, assume that in the function $L(x)$ the first non-zero coefficient is a_1 and $a_1 > 0$.

Let's build a set of vectors $B = \{e_1 = (-a_2, a_1, 0, \dots, 0), e_2 = (-a_3, 0, a_1, 0, \dots, 0), e_{q-1} = (-a_q, 0, 0, \dots, 0, a_1)\} \cup M_0$ where $M_0 = \{e_r : L(e_r) = 0\}$, $a_j \neq 0$, while, if for some a_i GCD (Great Common Divisor) $(a_i, a_1) \neq 1$, than the coordinates of this vector can be reduced to this GCD. Selected non-zero coefficient a_1 will be called a primary. This way, one can assume, that all vectors in the set B are such, that a_i and a_1 are mutually simple. In other words, set B is constructed by combining the first non-zero coefficient with the last non-zero coefficient, having different signs and being complemented with canonical base vectors, which correspond to zero coefficients HLDE (2). This kind of constructed set is called the TSS set or base set. It is obvious that vectors from the set B are solutions of HLDE (2), and the set B is closed in a respect to summation, subtraction and multiplication by an element from the ring Z .

Lemma 1. Let $x = (c_1, c_2, \dots, c_q)$ - be a some solution of HLDE (2), than, if $x \notin B$, than x can be represented as a nonnegative linear combination in the form:

$$a_1x = c_2e_1 + c_3e_2 + \dots + c_qe_{q-1},$$

where: $e_i \in B, i = 1, \dots, q-1$.

Proof. If $x = (c_1, \dots, c_q) \in M$, than the vector has a following representation:

$$\begin{aligned} a_1x &= c_2e_1 + c_3e_2 + \dots + c_qe_{q-1} = \\ (-c_2a_1 - c_3a_3 - \dots - c_qa_q, c_2a_1, \dots, c_qa_1) &= \\ = (c_1a_1, c_2a_1, \dots, c_qa_1) &= a_1(c_1, c_2, \dots, c_q) \end{aligned}$$

Due to the fact that x is a solution of HLDE (2), i.e.

$$a_1c_1 = -a_2c_2 - a_3c_3 - \dots - a_qc_q.$$

Note, that if a vector e_j from B is a canonical base vector and the j -th coordinate of the vector x is equal to c_j , then in the vector x representation, the vector e_j enters with a coefficient a_1c_j . Lemma proved.

The proved lemma results with the following conclusion.

Conclusion 1. If among the coefficients HLDE is even one coefficient equal 1, then the set B is a base of all HLDE solutions set. Then indeed, the elements of the set B have the form:

$$\begin{aligned} \{e_1 &= (-a_2, 1, 0, \dots, 0), e_2 = \\ &(-a_3, 0, 1, 0, \dots, 0), e_{q-1} = \\ &(-a_q, 0, 0, \dots, 0, 1)\} \cup M_0 \end{aligned}$$

i.e. if in the distribution of any solution x into vectors of the set B the basic coefficient is equal one, then this means, that the set B will be the base.

Example 1. Let's build TSS HLDE

$$L(x) = 3x_1 + y - z + 2u + v = 0$$

The base set or the TSS base of the HLDE has the following form:

$$\begin{aligned} e_1 &= (-1, 3, 0, 0, 0), e_2 = \\ &(1, 0, 3, 0, 0), e_3 = \\ &(-2, 0, 0, 3, 0), e_4 = \\ &(-1, 0, 0, 0, 3) \end{aligned}$$

The solutions LJRD $x_1 = (0, 2, 3, 0, 1), x_2 = (1, 1, 0, -2, 0)$ have the representation $3x_1 = 2e_1 + 3e_2 + e_4, 3x_2 = e_1 - 2e_3$.

All the solutions to any set of HLDE is presented as a set:

$$\begin{aligned} B &= \{e_1 = (1, -3, 0, 0, 0), e_2 = \\ &(0, 1, 1, 0, 0), e_3 = \\ &(0, -2, 0, 1, 0), e_4 = \\ &(0, -1, 0, 0, 1)\} \end{aligned}$$

In this vector's base x_1 and x_2 have the representation:

$$x_1 = 3e_2 + e_4, x_2 = e_1 - 2e_3.$$

The case of homogenous system of linear Diophantine equations. Let's consider the HSLDE:

$$S = \begin{cases} L_1(x) = a_{11}x_1 + \dots + a_{1n}x_n = 0, \\ L_2(x) = a_{21}x_1 + \dots + a_{2n}x_n = 0, \\ \dots \dots \dots \dots \dots \dots \dots \dots \\ L_q(x) = a_{q1}x_1 + \dots + a_{qn}x_n = 0, \end{cases}$$

Where: $a_{ij}, x_i \in \mathbb{Z}, i = 1, \dots, q, j = 1, \dots, n$.

Let's build the base set $B_1 = \{e_1^1, e_2^1, \dots, e_{q-1}^1\}$ for the first equation $L_1(x) = 0$ and let's calculate values $L_2(e_i^1) = b_i$ where $e_i^1 \in B_1, b_i \in \mathbb{Z}$. Then, let's create an equation:

$$b_1y_1 + \dots + b_iy_i + \dots + b_{q-1}y_{q-1} = 0 \quad (4)$$

Then let's build its base set $B_1' = \{s_1, \dots, s_{q-2}\}$. Vectors s_i from B_1' corresponds to solutions vectors $B_2 = \{e_1^2, \dots, e_{q-2}^2\}$ HSLDE $L_1(x) = 0 \wedge L_2(x) = 0$.

Lemma 2. Vectors set B_2 describes the base set of HSLDE $L_1(x) = 0 \wedge L_2(x) = 0$, i.e. any solution x of this system has a representation $kx = l_1e_1^2 + \dots + l_{q-2}e_{q-2}^2$, where: $e_i^2 \in B_2, l_i \in \mathbb{Z}, i = 1, \dots, q-2$.

Proof. Let's have x to be any solution to HSLDE $L_1(x) = 0 \wedge L_2(x) = 0$. Because x is a solution $L_1(x) = 0$, and taking into account lemma 1, x can be represented as:

$$dx = a_1e_1^1 + \dots + a_{q-1}e_{q-1}^1,$$

Where: $e_i^1 \in B_1, a_i \in \mathbb{Z}, i = 1, \dots, q-1$. Then, due to the fact that x is the solution $L_2(x) = 0$ we obtain:

$$L_2(dx) = a_1b_1 + \dots + a_{q-1}b_{q-1} = 0,$$

Where $b_j = L_2(e_j^1), j = 1, \dots, q-1$. Respectively, vector $a = (a_1, \dots, a_{q-1})$ is a solution of HLDE (4) and due to lemma 1 we get:

$$ka = d_1s_1 + \dots + d_{q-2}s_{q-2},$$

Where: $s_i \in B_1', d_i \in \mathbb{Z}, i = 1, \dots, q-2$, and k - is the main coefficient of given HLDE. Thus:

$$kdx = d_1e_1^2 + \dots + d_{q-2}e_{q-2}^2$$

where $e_i^2 \in B_2, i = 1, \dots, q-2$.

The lemma 2 proved.

The following theorem can be proven with a help of mathematical induction, directly from lemma 1 and 2.

Theorem1. TSS HSLDE B_1 (2) is built using the described above manner and it is a base of all solutions set of a given HSLDE.

Example 2. Let's describe the base set of HSLDE:

$$S = \begin{cases} L_1(x) = 3x_1 + x_2 - x_3 + 2x_4 + x_5 = 0, \\ L_2(x) = 2x_1 + 3x_2 + 0x_3 - x_4 + 2x_5 = 0. \end{cases}$$

The base set for the first equation was described in a first example.

$$\begin{aligned} B_1 &= \{e_1^1 = (1, -3, 0, 0, 0), e_2^1 = \\ &(0, 1, 1, 0, 0), e_3^1 = \\ &(0, -2, 0, 1, 0), e_4^1 = \\ &(0, -1, 0, 0, 1)\}. \end{aligned}$$

Values $L_2(x)$ for a given vectors respectively equal to: -7, 3, -7, 1. let's construct the equation $-7y_1 + 3y_2 - 7y_3 - y_4 = 0$ and let's transform the base set of this HLDE:

$$B_1' = \{s_1 = (3, 7, 0, 0), s_2 = (-1, 0, 1, 0), s_3 = (-1, 0, 0, 7)\}.$$

These vectors correspond with TSS vectors (base set):

$$\begin{aligned} B_2 &= \{e_1^2 = (3, -2, 7, 0, 0), e_2^2 = \\ &(-1, 1, 0, 1, 0), e_3^2 = (-1, -4, 0, 0, 7)\}. \end{aligned}$$

If during the construction of the base equation $-7y_1 + 3y_2 - 7y_3 - y_4 = 0$ we perform combining in accordance with the last value (ie. in respect to -1), we will obtain such a base for a set of all solutions of a given HSLDE:

$$\{e_1^2 = (1, 4, 0, 0, 7), e_2^2 = (0, -2, 1, 0, 3), e_3^2 = (0, 5, 0, 1, -7)\}.$$

In regards to conclusion 1, the theorem 1 result can be detailed. Indeed, since the coefficients values in the equation $L_1(x) = a_{11}x_1 + a_{12}x_2 + \dots + a_{1n}x_n = 0$ are mutually simple, it is always possible to have number one among the values $L_1(x)$. Without limiting the generality of considerations we assume that $\text{GCD}(a_{11}, a_{12}, a_{13}) = 1$, i.e. the first three factors are mutually simple in $L_1(x)$. Then there are such numbers d_1, d_2, d_3 , that in vector $y = (d_1, d_2, d_3, 0, \dots, 0)$ values $L_1(y) = 1$. once we obtain this, let's calculate the value $L_1(x)$ for the canonical base vectors. First let's construct a base set B_1 by combining the spare vector y with the other vectors in order to obtain the base set. Let's note now that vectors from B_1 have the form:

$$e'_1 = -a_{11}y + e_1, e'_2 = -a_{12}y + e_2, e'_3 = -a_{13}y + e_3, \\ e'_4 = -a_{14}y + e_4, \dots, e'_n = -a_{1n}y + e_n,$$

where e_i – canonical base vectors; a_{ij} – coefficient in an equation $L_i(x) = 0$.

Vectors e'_i can be presented also in the following form:

$$\begin{aligned} e'_1 &= (-a_{11}d_1 + 1, -a_{11}d_2, -a_{11}d_3, 0, \dots, 0), \\ e'_2 &= (-a_{12}d_1, -a_{12}d_2 + 1, -a_{12}d_3, 0, \dots, 0), \\ e'_3 &= (-a_{13}d_1, -a_{13}d_2, -a_{13}d_3 + 1, 0, \dots, 0), \\ e'_4 &= (-a_{14}d_1, -a_{14}d_2, -a_{14}d_3, 1, \dots, 0), \\ &\dots\dots\dots \\ e'_r &= (-a_{1r}d_1, -a_{1r}d_2, -a_{1r}d_3, 0, \dots, 1). \end{aligned}$$

In this form the following theorem take places.

Theorem 2. TSS HLDE B_1 , is a set base of all solutions for a given HLDE $L_1(x)=0$ and is constructed using the method described above. The complexity of base construction is proportional to the value l^3 , where l - is a maximal number of numbers m and n , n - the number of unknowns in HLDE, and m - the maximum length of the binary representation of HLDE coefficients.

Proof. Having $x = (c_1, c_2, \dots, c_n)$ - is the solution of HLDE $L_1(x) = 0$. Then vector x has the following representation:

$$\begin{aligned} x &= c_1 e'_1 + c_2 e'_2 + c_3 e'_3 + c_4 e'_4 + \dots + c_n e'_n = \\ &= [(-c_1 a_{11} d_1 + c_1 - c_2 a_{12} d_1 - c_3 a_{13} d_1 - c_4 a_{14} d_1 - \dots - c_n a_{1n} d_1], \\ &[c - c_1 a_{11} d_2 - c_2 a_{12} d_2 + c_2 - c_3 a_{13} d_2 - c_4 a_{14} d_2 - \dots - c_n a_{1n} d_2], \\ &[-c_1 a_{11} d_3 - c_2 a_{12} d_3 - c_3 a_{13} d_3 + c_3 - c_4 a_{14} d_3 \\ &\quad - \dots - c_n a_{1n} d_3], c_4, \dots, c_n) = \\ &= (c_1, c_2, c_3, c_4, \dots, c_n) \end{aligned}$$

because $L(x) = a_{11}c_1 + a_{12}c_2 + \dots + a_{1n}c_n = 0$.

The given algorithm complexity is described as a complexity of the extended Euclidean algorithm, defined along with the GCD and linear combination representing this GCD. It is obvious (see [3]), that the complexity is expressed as a value of $O(m \log m)$, where m - is the length of the binary representation of the maximal HLDE coefficient. Algorithm this is used no more than n times and it is measured as a form of $O(mn \log m)$. Building the

base B_1 requires no more than n^3 operations. As a result, the summary measure of the time complexity is described as a value $O(l^3)$, where $l = \max(m, n)$.

The theorem is proved. \square

The above theorem leads to the following conclusion.

Conclusion 2. The time complexity of constructing all solutions base set for the HSLDE with the form (5) is proportional to a value $O(ql^3)$, where: q - is a number of equations HSLDE, and $l = \max(m, n)$.

III. THE TSS METHOD OF ISLDE SOLUTION

Having S be the ISLDE with the form of (1) and $b_q \neq 0$. Executing the free segments eliminations in the first $q-1$ equations, we transform the input ISLDE into the following form:

$$S' = \begin{cases} L'_1(x) = a'_{11}x_1 + \dots + a'_{1n}x_n = 0, \\ L'_2(x) = a'_{21}x_1 + \dots + a'_{2n}x_n = 0, \\ \dots \\ L'_{q-1}(x) = a'_{q-11}x_1 + \dots + a'_{q-1n}x_n = 0, \\ L'_q(x) = a'_{q1}x_1 + \dots + a'_{qn}x_n = b_q. \end{cases} \quad (5)$$

Let's build the HSLDE base solutions set, composed of the first $q-1$ equations of the system (5). Having vectors $\{s_1, \dots, s_k\}$, we specify $L_q(s_j) = a_j, j = 1, \dots, k$. For this values the following theorem is true.

Theorem 3. The ISLDE with the form (1) is consistent only if the ISLDE $a_1y_1 + a_2y_2 + \dots + a_ky_k = b_q$ has at least one solution in the set of integer numbers set.

Proof. If equation $a_1y_1+a_2y_2+...+a_ky_k=b_q$ has solution $(c_1,c_2,...,c_k)$, then it is obvious that vector $s=c_1s_1+c_2s_2+...+c_ks_k$ is a SNLRS solution.

If ISLDE is consistent and $s = (k_1, k_2, \dots, k_n)$ then its solution s is presented in the linear combination form constructed of the first $q-1$ homogenous equations of the system (5), i.e.:

$$S = c_1 s_1 + c_2 s_2 + \dots + c_k s_k.$$

Then $L_q(s) = c_1 a_1 + c_2 a_2 + \dots + c_k s_k = b_q$ should have at least one solution, because s is a solution of ISLDE.

The theorem is proved. \square

It is known that generalized solution of ISLDE has the form

$$y = x + \sum_{i=1}^k a_i x_i, \text{ where: } x - \text{ is a partial solution of ISLDE,}$$

x_i - is a base solution of a given HSLDE, a_i - any integer numbers, and k - is the number of base solutions. In this case, for a comprehensive solution of the ISLDE we should construct its HSLDE base and find one of the ISLDE solutions. Finding such a solution, as a result from the above considerations, is reduced into finding the solution of the equation $a_1 y_1 + a_2 y_2 + \dots + a_k y_k = b_q$. This solution can be found with the use of the least coefficients method.

Example 3. The consistency of the ISLDE should be checked:

$$S = \begin{cases} L_1(x) = 2x_1 - 3x_2 + x_3 + x_4 + 0x_5 = 1, \\ L_2(x) = 3x_1 + x_2 + x_3 + 0x_4 - x_5 = -2. \end{cases}$$

The transformed ISLDE has the following form:

$$S' = \begin{cases} L'_1(x) = 7x_1 - 5x_2 + 3x_3 + 2x_4 - x_5 = 0, \\ L_2(x) = 3x_1 + x_2 + x_3 + 0x_4 - x_5 = -2. \end{cases}$$

The HLDE $L_1(x)' = 0$ base is combined with the vectors (in this case the computation of GCD coefficients is not necessary, because coefficient equals 1):

$$(1, 0, 0, 0, 7), (0, 1, 0, 0, -5), (0, 0, 1, 0, 3), (0, 0, 0, 1, 2).$$

Values $L_2(x)$ for these vectors equals: -4, 6, -2, -2. The greatest common divisor of these values equals 2 and is a divisor of the free member $b_2 = -2$. As a result the ISLDE has a solution, this is it is consistent.

If the system is determined:

$$S' = \begin{cases} L'_1(x) = 7x_1 - 5x_2 + 3x_3 + 2x_4 - x_5 = 0, \\ L_2(x) = 3x_1 + x_2 + x_3 + 0x_4 - x_5 = -3, \end{cases}$$

Therefore it has not solutions in a ring of integer numbers, because $\text{GCD}(-4, 6, -2, -2) = 2$ and doesn't divide the free member -3 and then the equation $-4x + 6y - 2z - 2u = -3$ has no solutions.

In conclusion, we find that the given measurements of the time complexity can be more detailed, if we follow all the details of the processed calculations in the TSS algorithm. In this work it is limited to determining the polynomiality of these algorithms.

IV. THE EXAMPLE USE OF THE ALGORITHM IN THE INTERCONNECTION NETWORK DESIGNING PROCESS

Let's consider the problem of designing the interconnection network with the configuration presented in the Fig. 1.

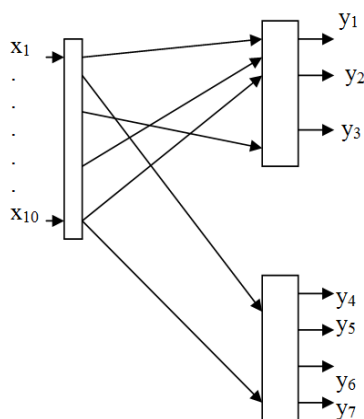


Fig. 1. The designed interconnection network configuration schema.

The designed interconnection network has 10 inputs $x_1 - x_{10}$ and two panels with outputs $y_1 - y_3$ and $y_4 - y_7$ respectively. We should power supply the minimal amount of inputs, in order to satisfy the following conditions: $y_1 = -10$, $y_2 = 20$, $y_3 = -5$, $y_4 = -20$, $y_5 = 50$, $y_6 = -10$, $y_7 = 20$ [V]. To solve this problem we construct the following equations system:

$$\begin{cases} x_1 + x_2 + x_3 + x_9 = -10 \\ x_3 - x_4 + x_5 + x_{10} = 20 \\ x_2 + x_6 - x_7 + x_9 = -5 \\ x_1 + x_3 + x_7 + x_{10} = -20 \\ -x_3 + x_5 + x_6 - x_9 = 20 \\ x_1 - x_4 - x_5 + x_7 + x_8 + x_9 = -10 \\ x_2 + x_3 - x_4 + x_6 + x_7 + x_8 = 20 \end{cases}$$

Such equations system has the following solutions: $x^0 = (0, 80, -50, -35, 5, -45, 0, 0, -40, 30)$. Therefore, we obtain that: $x_1 = 0$, $x_2 = 80$, $x_3 = -50$, $x_4 = -35$, $x_5 = 5$, $x_6 = -45$, $x_7 = 0$, $x_8 = 0$, $x_9 = -40$, $x_{10} = 30$ [V]. This means that inputs x_1, x_7, x_8 may not be connected to any outputs.

The solutions of the homogenous equations system, which corresponds to a given inhomogeneous equations system may be described as follows:

$$\begin{aligned} e &= (-1, 11, -6, 21, -3, -7, -23, 46, -4, 30), \\ s &= (-1, 11, -6, 22, -3, -7, -24, 48, -4, 31), \\ t &= (8, -90, 49, -175, 25, 54, 192, -383, 33, -249), \\ r &= (5, -169, 92, -329, 47, 107, 361, -720, 62, -468). \end{aligned}$$

Using these solutions the interconnection network designer has a choice, because he can select a special variant which suits him best. Thus, the interconnection network designer can use the general solution equation of a given equations system:

$$x = x^0 + ae + bs + ct + dr,$$

Where a, b, c, d are arbitrary integers?

V. CONCLUSION

In this paper we have presented the algorithm for computation the minimal supported set of solutions and base solutions of linear Diophantine equations systems in a ring of integer numbers. Linear Diophantine equations and their systems are often found in a wide variety of sciences which have heavy usage of computations. Solving the Diophantine equations is one of the main issues in computing the data, dependences in algorithm's code especially nested loop programs with memory access which very often occurs in numerical computing. Recently, the Diophantine equations are used to obtain an accurate and predictable computational model in many multi-disciplinary scientific fields especially in bimolecular networks studies.

The most crucial task in such models is to check the model's correctness – model validation problem. In the validation process finding of basic state equations is the most important task which may be checked by existence of integer solutions of Diophantine equations systems. Moreover, one of the motivations of this problem comes from the coding theory which may be implemented in many different fields of cryptography, encryption and users authentication (symmetric-key encryption and public-key cryptosystems) where the nonuniqueness of Diophantine equations solutions is analyzed. Thus, the proposed research is an actual scientific problem.

REFERENCES

- [1] С. Л. Кривый, *Алгоритмы решения систем линейных диофантовых уравнений в целочисленных областях.. Кибернетика и Системный Анализ*, 2006, N 2, pp. 3-17.
- [2] Г. А. Донец, *Решение задачи о сейфена (ОД)-матрицах*, Кибернетика и Системный Анализ, 2002, N1, pp. 98-105.
- [3] А. В. Черемушкин, *Лекции по арифметическим алгоритмам в криптографии*, МЦНМО, 2002, 103 p.
- [4] F. Baader, J. Ziekmann, *Unification theory*, Handbook on Logic in Artificial Intelligence and Logic Programming, Oxford University Press, 1994, pp. 1-85.
- [5] R. Allen, K. Kennedy, *Automatic translation of FORTRAN program to vector form*, ACM Transactions on Programming Languages and systems, 1987, v. 9, N4, pp. 491-542.
- [6] E. Contejan, F. Ajili, *Avoiding slack variables in the solving of linear Diophantine equations and inequations*, Theoretical Corp. Science, 1997, pp. 183 -208.
- [7] L. Pottier, *Minimal solution of linear Diophantine systems: bounds and algorithms*, In Proc. of the Fourth Intern. Conf. on Rewriting Techniques and Applications, Italy, 1991, pp. 162-173.
- [8] E. Domenjoud, *Outils pour la deduction automatique dans les theories associatives-commutatives*, Thesis de Doctoral d'Universite: Universite de Nancy I, 1991.
- [9] M. Clausen, A. Fortenbacher, *Efficient solution of linear Diophantine equations*, J. Symbolic Computation, 1989, N 1,2, pp. 201-216.
- [10] J. F. Romeuf, *A polynomial algorithm for solving systems of two linear Diophantine equations*, TCS, 1990, pp. 329-340.
- [11] M. Filgueiras, A.P. Tomas, *A Fast Method for Finding the Basis of Non-negative Solutions to a Linear Diophantine Equation*, J. Symbolic Computation, 1995, v.19, N2, pp. 507-526.
- [12] H. Comon, *Constraint solving on terms: Automata techniques (Preliminary lecture notes)*, Intern. Summer School on Constraints in Computational Logics: Gif-sur-Yvette, France, September 5-8, 1999, 22 p.

Maintenance Model of Hostel Buildings for Effective Performance and Aesthetics

O.Y.Ojedokun¹, T.O. Odewumi², J.K. Fasola³

(Department of Civil Engineering, the Polytechnic, Ibadan, Nigeria)^{1, 2}

(Plaices Global Concept Limited, Ibadan Nigeria)³

Abstract : Buildings are designed and built to sustain its initial functions and beauty for both the present and future users. Building required maintenance for high performance regardless of whether it meets the sustainability consideration or not. An important segment in the maintenance management system is the identification and analysis of defects in the buildings and the urgency of repair needed. Defect analysis is significance if higher institutions desire to succeed in modeling an efficient maintenance management system for their buildings and engineering services. Thus the aim of this project is to determine, evaluate and categorize the defects in institutional hostel buildings in Nigeria, using the four (4) Hostel buildings of The polytechnic, Ibadan as a case study. Questionnaires were administered on four (4) Hostel buildings of The polytechnic, Ibadan. With 83% response rate, the findings suggest that some defects require maintenance urgently than the others and on the basis of which it is concluded that resources should be directed to the more urgent ones while less urgent ones could be included in the subsequent maintenance programme. The research found that, Toilet and bathroom fittings, faulty electrical systems, faulty door locks, extinguisher, fire alarm, and Smoke Detector were the defects that respondents considered extremely urgent to maintain. The paper concludes by arguing that attention to aesthetics and maintenance management is a strategic issue in the management of buildings.

Keywords: Aesthetics, Defect Analysis, Maintenance, and Maintenance Management

I. INTRODUCTION

Aesthetics and its maintenance have come to be regarded with little concern. Too often, aesthetics is viewed as an "extra" consideration that can only receive attention after the important "functional" requirements have been met and which can always be added on afterwards like a coat of paint. This lack of feeling for the value and essence of beauty leads to an unattractive built environment. For most people, their environment is the built environment. It is built by architects and engineers who are therefore responsible for its aesthetic qualities and maintenance.

Robert Benaim demonstrates that engineers can produce a distinct form of architecture, based on the refinement of their understanding of structural behavior, and on a search for rationality and economy [Robert Benaim, 2000].

If the general public, corporate organizations, governmental authorities and engineers see the potential for structural art and maintenance, then public works in the

Late 20th century can be efficient, economic, and elegant [Billington and David P, 1983]. The cost of aesthetic

Quality is not always higher than the cost of poor design. In any event, attractive projects bring much greater long-term benefits to the public by increasing the development potential of communities. In fact, many designers are shedding the functional style and the modern movement in favor of historic reference and formal shaping of public spaces. An example is the recent trend to build "old style" baseball parks instead of parks with retractable domes and hotels in the outfield of United State of America [Liebenberg, A.C, 1991].

All aesthetic measures must be designed so that they are fully compatible with the project purpose and in no way compromise the safety, integrity or function of the project. For example, it may be appropriate to screen a floodwall with vegetative plantings but it would be inappropriate to plant trees directly on a levee that might endanger its structural integrity or diminish its hydraulic characteristics [Arthur E. Williams, 1991]. Maintenance budgets need to include costs for inspections, replacement of materials or finishes, cleaning and any unforeseen breakdowns or repairs. Budgeting for these items will become more accurate over time if detailed records of maintenance expenditure are kept. Budgets need a simple control system, with regular and frequent reports on actual and committed expenditure [Jan M. Noortwijk and Dan M. Frangopol, 2004].

II. MODELING MAINTENANCE

Maintaining structures in a safe condition during their entire service life has been recognized as a very critical issue worldwide. According to Das (1999) there are two types of maintenance work: preventive maintenance which if it is not done it will cost more at a later stage to keep the structure in a safe condition, and essential maintenance which is required to keep the structure safe. An essential part of modeling maintenance is taking account of the uncertainties in the deterioration and the time of failure. In this paper, a brief overview is given on how to model uncertain deterioration for the purpose of maintenance optimization. Without being complete, a time-dependent deterioration process can be modeled as:

2.1 Failure Rate Function

A lifetime distribution represents the uncertainty in the time to failure of a component or structure. Let the lifetime have a cumulative probability distribution $F(t)$ with probability density function $f(t)$, then the failure rate function is defined as:

$$r(t) = f(t)/F(t) \dots \dots \dots (1) \text{ (Barlow and Proschan, 1965).}$$

2.2 Markov Model

A Markov deterioration model is based on the assumption that the condition of a component can be described in terms of a limited number of condition states. Transition probabilities link the current state with a maintenance action to a future state. Examples of maintenance optimization models based on Markovian deterioration are the Arizona Pavement Management System (Golabi et al., 1982) and the Bridge Management System PONTIS (Golabi and Shepard, 1997).

2.3 Stochastic Process

A convenient way in modeling the uncertainty in time-dependent deterioration is by regarding it as a stochastic process. Gamma processes have been applied to model the following deterioration processes: permanent coastal erosion of dunes (Van Noortwijk and Peerbolte, 2000), crest-level decline of dykes (Speijker et al., 2000), longshore rock transport near berm breakwaters (Van Noortwijk and Van Gelder, 1996), scour-hole development under the block mats of the Eastern-Scheldt barrier (Van Noortwijk and Klatter, 1999), current-induced rock displacement near the rock dumping of the Eastern-Scheldt barrier (Van Noortwijk et al., 1997), loss of steel thickness due to corrosion (Bakker et al., 1999), and corrosion of a hydrogen dryer (Kallen and Van Noortwijk, 2003).

As a basis for optimizing maintenance, the Dutch Ministry of Transport, Public Works and Water Management (Rijkswaterstaat) implemented the age replacement model with discounted cost. This model has been applied for justification and optimization of maintenance measures in the Netherlands (Klatter et al., 2002); detailed information on this model can be found in Van Noortwijk (1998) and Bakker et al. (1999). The criterion of expected discounted cost (net present value) over an unbounded horizon is used for comparing maintenance decisions

III. METHOD OF DATA ANALYSIS

A questionnaire survey approach was used to collect primary data. The questionnaire was divided into three parts. The first part is to give the respondent background information about the project, while the second part focuses on the respondent's profiles. The third section is sub divided into six, to provide feedback on the defects and urgency of repair required as associated with the buildings. The questionnaires were administered on all the 4 Hostels in the Polytechnic, Ibadan. The questionnaire was developed from works of authors including Olanrewaju, A.A. and Kafayah, S.T.(2008), Jones, et al. (2007). Seeley, I.H. (1987), and series of discussions with those concerned with the Polytechnic building maintenance.

Data analysis was performed using two different computer packages: Statistical Package for Social Science and Microsoft Excel to produce descriptive statistics. Descriptive Statistics provide information regarding the distributions of datasets or variables. It measure average (mean, median and mode), spread (variance and standard variation), skewness, kurtosis, maximum and minimum of values. Each of the statistics is require for achieving different objectives.

Measure of central tendency (average) summarizes data in a distribution into a single value or opinion that most

represent the entire datasets, values or scores. In a research, respondents supplied different opinions on a concept or variable addressed to them. Often each of the variables cannot be explained in detail or does not even require to be explained individually. Therefore, a mid-score or value is determined to explain the varying values or opinions. Mean is the average or mid-score of a distribution. It is used to calculate the average of observations. The mean is the most stable of the three measure of average of score. The mean technique is used to calculate the average degree of defects in the buildings. Standard Deviation is to calculate the level of spread of each of the individual value from the mean score. The degree of urgency of each of the defects will be determined by the frequency of the respondents that agreed with each of the defects. For instance, where the mean score falls between 1.0 and 1.5 the defect is considered as not urgent at all. See **Table 1- Table 6** for other distributions.

This cut of point is used, because the lowest possible mean score is 1. However, it was understood, that natural scale originates from zero (0) which in this case is not require. Missing data (i.e. where the respondent refused to tick where applicable or there is multiple entry), could impact negatively on the outcome of the findings, however such effect could be improved during data analysis by either replacing the missing data with the mode or mean of the data. However, in this paper, the missing data will not be treated as such; instead we will prefer to leave the data raw as it were so that the outcomes will not in any way be influenced by the authors. Even though, this tends not to be a problem in the study as nearly all the questions were answered by the respondents.

IV. EXTENT OF DAMAGE/URGENCY OF REPAIR IN THE HOSTEL BUILDINGS

The outcomes on the extent of damage of the different defects are depicted in **Table 1** to **Table 6**. The Tables shows an overview of data obtained, the defects and the extent of damage and urgency of repair. The mean score indicates the degree of damage for each of the defects. The ranking score indicates the defect with the highest degree of damage for each of the defects.

TABLE 1: THE EXTENT OF DAMAGE OF FITTINGS IN HOSTEL ROOMS

DEFECT	GOOD	AVERAGELY DAMAGED	COMPLETELY DAMAGED	NOT APPLICABLE	MEAN	RANKING
Faulty door	1	168	27	4	2.17	9
Damaged window	34	113	42	11	2.15	10
Faulty door locks	32	60	78	30	2.53	7
Damaged roof structure	107	50	10	33	1.84	12
Damaged ceiling	65	40	22	73	2.52	8
Floor tile failure	32	62	62	44	2.59	6
Wall tile failure	24	61	63	52	2.72	3
Faulty bulbs	10	45	94	51	2.93	2
Faulty electrical sockets	0	45	105	50	3.02	1
Damaged Reading Tables	34	43	95	31	2.63	5
Damaged External wall paintings	61	106	12	21	1.96	11
Damaged Internal wall paintings	11	98	43	48	2.64	4

Source: Primary Survey 2012

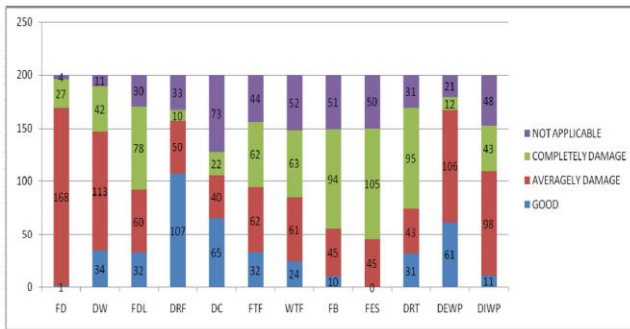


FIGURE 1: COMPONENT BAR CHAT OF EXTENT OF DAMAGE OF FITTINGS IN HOSTEL ROOMS

From **Table 1** and **Fig. 1** above, Faulty electrical sockets were the most extremely rated defect (1) followed by Faulty bulbs (2). While the least considered defect was Damaged roof structure (12) after Damaged External wall paintings (11). In fact, 52.5% of the respondents consider Faulty electrical sockets as completely damage concurrently 47.0% of the respondents considered Faulty bulbs as completely damage. None of the respondent consider electrical socket as good. Although considerable size of the respondent (84.0%) considered Faulty door to be averagely damaged and only 0.5% of the respondent did not, while 56.5% considered Damaged window as averagely damaged. On the other hand, many (47.5%) of the respondent consider Reading Tables as completely damaged.

TABLE 2: THE EXTENT OF DAMAGE OF FITTINGS IN HOSTEL WARDROBES

DEFECT	GOOD	AVERAGELY DAMEGED	COMPLETELY DAMAGED	NOT APPLICABLE	MEAN	RANKING
Faulty door	31	119	31	19	2.19	5
Faulty door locks	21	75	75	29	2.56	2
Damaged Wardrobe Cabinet	32	73	56	39	2.51	4
Damaged External wall paintings	11	65	72	52	2.82	1
Damaged Internal wall paintings	21	87	51	41	2.56	3

Source: Primary Survey 2012

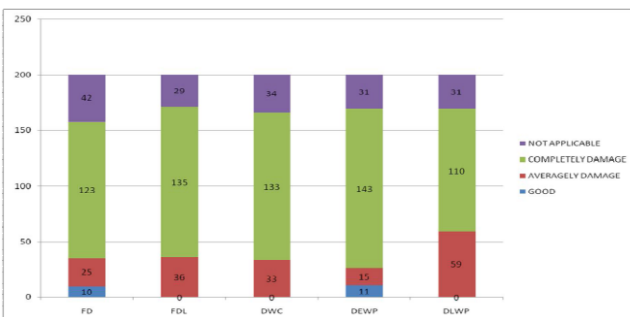


FIGURE 2: COMPONENT BAR CHAT OF EXTENT OF DAMAGE OF FITTINGS IN HOSTEL WARDROBES

From **Table 2** and **Fig. 2** above, Damaged External wall paintings were the most rated defect (1) of the wardrobes, followed by wardrobe door locks (2) while the least most considered defect was Faulty door (5) after Damaged Wardrobe Cabinet (4) and Damaged internal wall paintings of the wardrobes came third with 25.5%

completely damaged . In fact, 36.0% of the respondents consider Damaged External Wall Paintings as completely damage concurrently 37.5% of the respondents considered Faulty door locks as completely damage. Although considerable size of the respondent (84.0%) considered Faulty door to be averagely damaged and only 0.5% of the respondent did not, while the same number of respondent (37.5%) considered Faulty door locks as averagely damaged and completely damaged concurrently.

TABLE 3: THE EXTENT OF DAMAGE OF FITTINGS IN HOSTEL KITCHENETTE

DEFECT	GOOD	AVERAGELY DAMEGED	COMPLETELY DAMAGED	NOT APPLICABLE	MEAN	RANKING
Faulty door	0	33	48	119	3.43	2
Faulty door locks	19	24	61	96	3.17	1
Damaged Kitchen Cabinet	10	32	71	87	3.18	3
Faulty bulbs	10	34	73	83	3.14	5
Faulty electrical sockets	21	12	84	74	3.14	4
Damaged External wall paintings	11	32	83	74	3.10	6
Damaged Internal wall paintings	11	66	82	41	2.7	7

Source: Primary Survey 2012

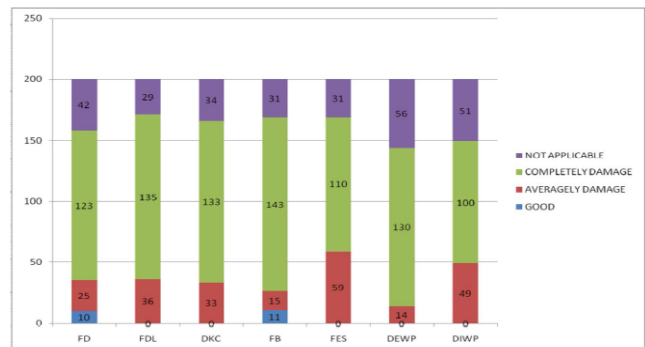


FIGURE 3: COMPONENT BAR CHAT OF EXTENT OF DAMAGE OF FITTINGS IN HOSTEL KITCHENETTE

Table 3 and **Fig. 3** above shows that, Faulty door locks was the most rated defect(1) of the kitchenette followed by Faulty door (2) while the least considered defect was Damaged Internal wall paintings (7) after Damaged External wall paintings (6). While Faulty electrical sockets have the highest value of complete damage as 42.0% of the respondent chose it as completely damaged defect, and Damaged external wall came next with 41.5 defect as considered by the respondent. Although considerable size of the respondent (59.5%) considered Faulty door of the kitchens as not applicable and none of the respondent mark it as good, this high rate of response to both conditions suggest that many of the hostels has no kitchen at all and those that has did not have any of their doors in good condition. While the mean value of all almost all the defects; Faulty door, Faulty door locks, Damaged Kitchen Cabinet, Faulty bulbs, Faulty electrical sockets and Damaged External wall paintings are all at very close range of 3.43, 3.17, 3.18, 3.14, 3.14, and 3.10 respectively, This mean score indicates that degree of damage to all the fixtures and fittings of the kitchen are all almost the same.

TABLE 4: THE EXTENT OF DAMAGE OF FITTINGS IN HOSTEL TOILETS

DEFECT	GOOD	AVERAGELY DAMEGED	COMPLETELY DAMAGED	NOT APPLICABLE	MEAN	RANKING
Faulty door	10	25	123	42	2.98	5
Faulty door locks	0	36	135	29	2.96	7
Clogged water closet	0	33	133	34	3.00	4
Damaged water closet	11	15	143	31	2.97	6
Damaged Flushing System	0	59	110	31	2.86	8
Damaged Wash Hand Basin	0	14	130	56	3.21	1
Damaged Internal wall paintings	0	49	100	51	3.01	3
Floor tile failure	12	56	81	51	2.86	9
Wall tile failure	2	24	115	59	3.16	2

Source: Primary Survey 2012

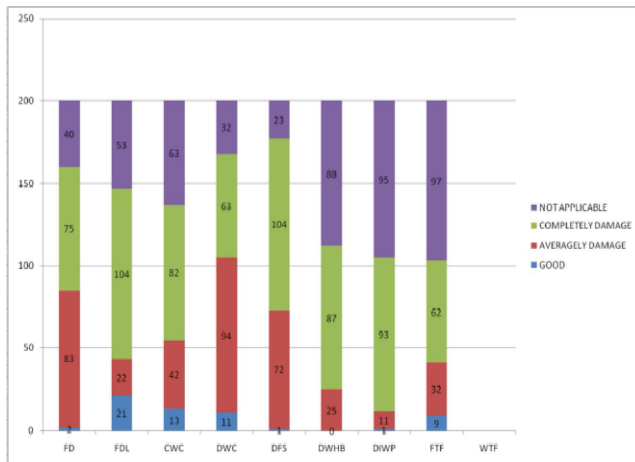


FIGURE 4: COMPONENT BAR CHAT OF EXTENT OF DAMAGE OF FITTINGS IN HOSTEL TOILETS

Table 4 and Fig. 4 above shows that, with the exception of Floor tile failure, all the other fixtures and fittings of the toilet are completely damaged at more than 50% each as the overall responds of the respondent result shows each at: Faulty door (61.5%), Faulty door locks (67.5%), Clogged water closet(66.5%), Damaged water closet(71.5%), Damaged Flushing System(55.0), Damaged Wash Hand Basin(65.0), Damaged Internal wall paintings(50.0%), Wall tile failure(57.5%). Damaged Wash Hand Basin is the extremely rated defect with overall ranking value(1) followed by Wall tile failure (2) while the least considered defect was Floor tile failure(40.5%). While Damaged water closet have the highest value of complete damage as; 71.5% of the respondent chose it as completely damaged defect, and none of Faulty door locks, Clogged water closet, Damaged Flushing System, Damaged Wash Hand Basin, Damaged Internal wall paintings are in good condition.

TABLE 5: THE EXTENT OF DAMAGE OF FITTINGS IN HOSTEL BATHROOMS

DEFECT	GOOD	AVERAGELY DAMEGED	COMPLETELY DAMAGED	NOT APPLICABLE	MEAN	RANKING
Faulty door	1	44	114	41	2.98	3
Faulty door locks	12	23	132	33	2.93	7
Faulty Shower	22	24	124	30	2.81	8
Faulty bulbs	12	24	123	41	2.96	6
Faulty Towel Rail	10	35	104	51	2.98	4
Bad Soup Holder	1	44	93	62	3.08	2
Faulty Floor Drain	1	64	73	62	2.98	5
Faulty Wall Tile	1	48	69	82	3.16	1

Source: Primary Survey 2012

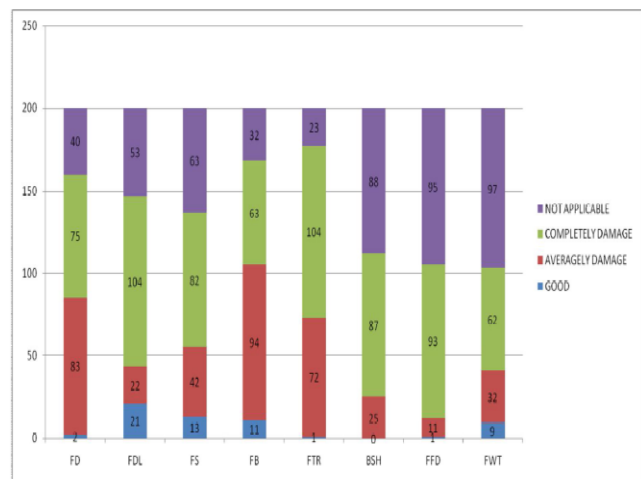


FIGURE 5: COMPONENT BAR CHAT OF EXTENT OF DAMAGE OF FITTINGS IN HOSTEL BATHROOMS

Table 5 and Fig. 5 above shows that, Faulty Wall Tile is the defect with the highest overall ranking(1) followed by Bad Soup Holder (2) while the least most considered defect was Faulty Shower (8) after Faulty door locks (7), and it shows that five of the defect are damaged at more than 50% each as the overall responds of the respondent result shows each at: Faulty door (57.0%), Faulty door locks (66.0%), Faulty Shower (62.0%), Faulty bulbs (61.5%), Faulty Towel Rail (52.0%). While Faulty door locks have the highest value of complete damage; as 66.0% of the respondent chose it as completely damaged defect followed by Faulty Shower (62.0%), and Faulty bulbs (61.5%) of complete damage respectively, and only one of the 200respondents chose Faulty door, Bad Soup Holder, Faulty Floor Drain, and Faulty Wall Tile to be in good condition.

TABLE 6: SUMMARY OF THE EXTENT OF DAMAGES OF FITTINGS IN HOSTELS

DEFECT	GOOD	AVERAGELY DAMEGED	COMPLETELY DAMAGED	NOT APPLICABLE	MEAN	RANKING
Faulty electrical circuit	2	83	75	40	2.76	6
Faulty Stair Rails	21	22	104	53	2.94	5
Faulty Floor Rails	13	42	82	63	2.98	4
Faulty Taps	11	94	63	32	2.58	8
Collapse Drains	1	72	104	23	2.74	7
Faulty Smoke Detector	0	25	87	88	3.32	2
Faulty fire alarm	1	11	93	95	3.41	1
Faulty fire extinguisher	9	32	62	97	3.24	3

Source: Primary Survey 2012

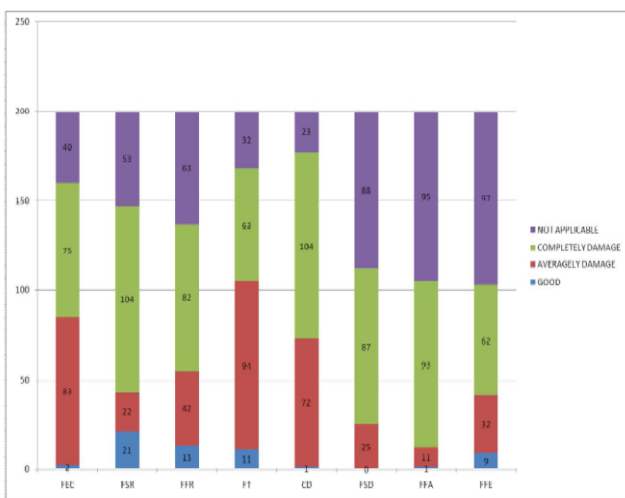


FIGURE 6: COMPONENT BAR CHAT OF SUMMARY OF EXTENT OF DAMAGES OF FITTINGS IN HOSTELS

From Table 6 and Fig. 6 above, Faulty fire alarm was the most rated general defect (1) followed by Faulty Smoke Detector (2) and Faulty fire extinguisher (3) respectively, while the least considered defect was Faulty Taps (8) after Collapse Drains (7). In fact, only 4.5% of the respondents consider Faulty fire extinguisher as good concurrently 0.5% of the respondents considered Faulty fire alarm as good and none of the respondent consider Faulty Smoke Detector as good. Although considerable size of the respondent (47.0%) considered Faulty Taps to be averagely damaged and only 5.5% of the respondent did consider it as good, while 41.5% considered Faulty electrical circuit as averagely damaged. On the other hand, many (52.0%) of the respondent consider Faulty Stair Rails and Collapse Drains as completely damaged.

V. CONCLUSION

This study has been able to identify that 57.0% of the respondents consider Faulty electrical sockets as extremely urgent concurrently 44.5% of the respondents considered Damaged Reading Tables and 43.5% Faulty bulbs as extremely urgent, while a highly considerable size of the respondent (94.0%) considered Faulty door to be very urgent and only 2.0% of the respondent did require for urgent repair, while 60.5% considered Damaged window as very urgent, considerable size of the respondent (39.0%)

considered Faulty door locks to be extremely urgent for the wardrobes and next to it is Damaged Wardrobe Cabinet with extreme urgency of 31.0% concurrently 41.0% of the respondents considered Faulty door locks of the wardrobe as very urgent. However the research shows that 75% of the toilet fittings damage require extreme urgency of repair, responds shows that's 6 of the 9 defect on toilet fixtures and fittings require repair urgency of more than 50% each and the as the overall responds of the respondent result shows each at: extreme urgency of repair for Faulty door (60.0%), Faulty door locks (68.5%), Clogged water closet(64.0%), Damaged water closet(65.0%), Damaged Wash Hand Basin(61.0), Wall tile failure (49.5%). The other 3 defects are also considerably high as shown: Damaged Flushing System (49.5%), Damaged Internal wall paintings (40.5%), and floor tile failure (38.0%), while the bathrooms Faulty Shower require 62.5% urgency of repair. Moreover the result suggests that the Polytechnic Ibadan Hostels either has no fire extinguisher, fire alarm, and Smoke Detector or they are completely damaged as these three items have a very high number of respondents choosing them as not applicable.

Hence it is recommended that for adequate maintenance and prudence, effort should be directed to the above extremely urgent defects then the very urgent and finally to the once that are not very urgent. This is a way to ensure that the ever inadequate fund will be spent judiciously and users' satisfactions can be achieved and maximized accordingly. This model is equally recommended as applicable to other higher institutional Hostels across Nigeria.

REFERENCES

- [1] Arthur E. Williams (1991), Memorandum for Major Subordinate Commands and District Commands, Policy Guidance Letter No. 29, Expenditures on Aesthetics at Civil Works Projects, Pp. 2
- [2] Bakker, J.D., H.J. van der Graaf, and J.M. van Noortwijk (1999). Model of Lifetime-Extending Maintenance, *Proceedings of the 8th International Conference on Structural Faults and Repair, London, United Kingdom*, Edinburgh: Engineering Technics Press.
- [3] Barlow, R.E., and F. Proschan (1965). *Mathematical Theory of Reliability*. New York: John Wiley and Sons.
- [4] Billington and David P. (1983), *The Tower and the Bridge: The New Art of Structural Engineering*, New York: Basic Books, Inc., Pp. 3-15.
- [5] Das, P.C. (1999). Prioritization of bridge maintenance needs, *Case Studies in Optimal Design and Maintenance Planning of Civil Infrastructure Systems*, ASCE, Reston, Virginia, Pp. 26-44.
- [6] Golabi, K., R.B. Kulkarni, and G.B. Way (1982). A state-wise pavement management system. *Interfaces*, 12:5-21.
- [7] Golabi, K., and R. Shepard (1997). Pontis: A system for maintenance optimization and improvement of US bridge networks. *Interfaces*, 27:71-88.
- [8] Jan M. van Noortwijk and Dan M. Frangopol (2003), Deterioration and maintenance models for insuring safety of civil infrastructures at lowest life-cycle cost

- [9] Jones K. and Sharp M. (2007); A New Performance Based Process Model for Built Asset Maintenance Facilities, Vol.25, No. 13/14, pp.525-535.
- [10] Kallen, M.J., and J.M. Van Noortwijk (2003). Inspection and maintenance decisions based on imperfect inspections. In *Proceedings of the European Safety and Reliability Conference, Maastricht, The Netherlands, 2003*.
- [11] Klatter, H.E., J.M. van Noortwijk, and N. Vrisou van Eck (2002). Bridge management in the Netherlands; Prioritisation based on network performance, *First International Conference on Bridge Maintenance, Safety and Management (IABMAS), Barcelona, Spain, 14-17 July 2002*.
- [12] Liebenberg, A.C. (1991), "Aesthetic Evaluation of Bridges," Bridge Aesthetics around the World, Committee on General Structures—Subcommittee on Bridge Aesthetics, Transportation Research Board Washington D.C.: National Research Council, Pp. 1-9.
- [13] Robert Benaim (2000), The Art of Engineering Structures from the Pantheon to the Jubilee Line, Engineering Architecture, Pp. 6
- [14] Seeley I.H. (1987). *Building Maintenance*, 2nd Edition, Houndmills: Macmillan Press Limited, Pp 23 - 25.
- [15] Speijker, L.J.P., J.M. van Noortwijk, M. Kok, and R.M. Cooke, (2000) Optimal maintenance decisions for dikes. *Probability in the Engineering and Informational Sciences*, 14(1):101-121.
- [16] Van Noortwijk, J.M. (1998). Optimal replacement decisions for structures under stochastic deterioration, *Proceedings of the Eighth IFIP WG 7.5 Working Conference on Reliability and Optimization of Structural Systems, Kraków, Poland, University of Michigan, Ann Arbor, 273-280*.
- [17] Van Noortwijk, J.M., and E.B. Peerbolte (2000). Optimal sand nourishment decisions. *Journal of Waterway, Port, Coastal, and Ocean Engineering*, 126(1):30-38.
- [18] Van Noortwijk, J.M., and H.E. Klatter (1999). Optimal inspection decisions for the block mats of the Eastern-Scheldt barrier. *Reliability Engineering and System Safety*, 65(3):203-211.
- [19] Van Noortwijk, J.M., M. Kok, and R.M. Cooke (1997). Optimal maintenance decisions for the sea-bed protection of the Eastern-Scheldt barrier, *Engineering Probabilistic Design and Maintenance for Flood Protection*, Kluwer Academic Publishers, Dordrecht, Pp 25-56.
- [20] Van Noortwijk, J.M., and P.H.A.J.M. Van Gelder (1996). Optimal maintenance decisions for berm breakwaters. *Structural Safety*, 18(4):293-309.
- [21] Olanrewaju A.A. and Kafayah S.T. (2008), The Need to maintain our buildings: Sustainable Development in Proceedings of PSIS Environ, 1st National Seminar on Environment, Development and Sustainability, Sabak Bernam Selangor Malaysia, Pp.1-5.

DC Motor Fed with Double Input Z-Source DC-DC Converter

Santhosh Yamsani¹, Sampath Kumar Boini²

^{1,2}(Department of EEE, Teegala Krishna Reddy Engineering college, JNTU- Hyd, AP, INDIA)

ABSTRACT: This paper proposes a dc motor fed with a double input dc-dc converter based on Z-source converters. In the proposed converter, the input dc voltage can be boosted and also input dc sources can deliver power to the load individually or simultaneously, so combination of a battery with one of the new energy sources such as solar array, wind turbine or fuel cell can be used as input sources. Different states of double input Z-source dc-dc converter are analyzed, steady state operation of converter is explained and modeling of separately excited dc motor is explained in detail. Finally, the simulation results are presented to confirm the theoretical analysis.

Keywords: Z-Source converter; double input; dc-dc converter; dc motor.

I. INTRODUCTION

The renewable energy such as photovoltaic (PV) and wind has created various electric energy sources with different electrical characteristics for the modern power system. In order to combine more than one energy source, such as the solar array, wind turbine, fuel cell (FC) and commercial ac line to get the regulated output voltage, the different topologies of multi input converters (MICs) have been proposed in recent years [1]-[4].

Traditionally, two dc voltage sources are connected to two independent dc-dc power converters to obtain two stable and equivalent output voltages, which are then connected to the dc bus, to provide the electric energy demanded by the load.

Another approach for the double-input dc-dc converter is to put two dc sources in series to form a single voltage source where traditional dc-dc power converters can be used to transfer power to the load. In order to transfer power individually, each dc voltage source needs a controllable switch to provide a bypass short circuit for the input current of the other dc voltage source to deliver electric energy continuously [3], [4].

Another approach is to put PWM converters in parallel with or without electrical isolation using the coupled transformer [5]. Control schemes for these MICs with paralleled dc sources are based on time sharing concept because of the

Clamped Voltage. Because of the voltage amplitude differences between two dc sources, only one of them can be connected to the input terminal of the dc-dc converter and transfer power to the load at a time [3].

The objective of this paper is to propose a dc motor fed with double input dc-dc converter which has the following advantages:

The dc sources can deliver power to the dc motor individually or simultaneously; the multi winding transformer is not needed; the magnitude of the input dc Voltage can be higher or lower than the one with a regulated

Output; minimum switching devices are used in this circuit. The proposed double input dc-dc converter is proper for

Renewable-energy applications and combination of two different sources (such as battery and photovoltaic or fuel cell)

II. CIRCUIT CONFIGURATION AND PRINCIPLE OF OPERATION

A. Z-Source Converters

Z-source converters are modern group of power electronic converters which can overcome problems with traditional converters. The Z-source inverter is a novel topology [6] that overcomes the conceptual and theoretical barriers and limitations of the traditional voltage-source converter and current-source converter. The concept of Z-source was used in direct ac-ac power conversion [7]. Similarly, the concept of Z-source also was extended to dc-dc power conversion [8].

B. Circuit Configuration of Proposed Converter

The schematic circuit diagram of the proposed dc drive fed with double-input Z-source dc-dc converter with two different voltage sources is shown in Fig. 1. It consists of two different input sources, V_{dc1} and V_{dc2} , and four diodes, D1-D4, applied to provide current path in different states. In this paper, permanent connection of input dc sources is considered, so D1 and D2 can be replaced with active switches if it's required to connect and disconnect each of sources to input side of converter frequently. Energy receiver, converter and transmitter sections are situated in the middle side of the converter. This section is a two-port network that consists of a split-inductor L1 and L2 and capacitors C1 and C2 connected in x-shape which is named "Z-network". An active switch, S, is situated in output port of Z-network to control input and output power of converter. The final section of converter is a LC filter beside the load in order to reject output signal ripple.

C. principle Operation of Double Input DC-DC Converter

There are four different operation states with respect to active or inactive states of dc sources. As previously mentioned, both of the input sources can deliver power to the load either individually or simultaneously through the MIC. When only one of the input sources feeds the MIC, it transfers power to the load individually and the MIC will operate as does a PWM converter. Table I summarizes the operation states of the proposed double input dc-dc converter

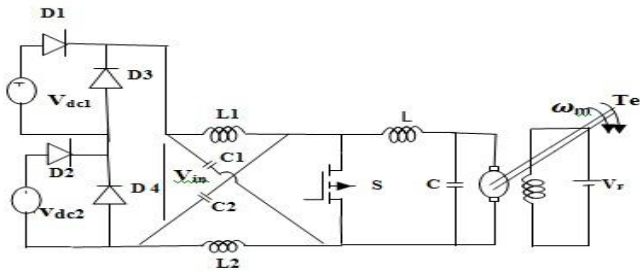


Fig1. DC Motor fed with double input Z-source DC-DC converter

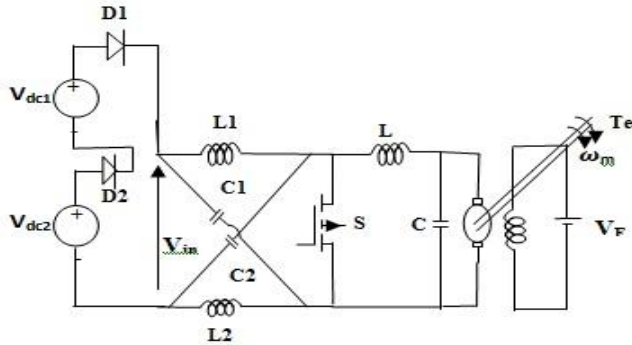


Fig2. Double input DC-DC converter state1 equivalent circuit

1) State 1, both source 1 and source 2 are active

Fig. 2 shows equivalent circuit of this state. When both source1 and source 2 are active, the converter input dc voltage is sum of voltage of two series dc sources, as Fig. 3 and (1) illustrate.

$$V_{in} = V_{dc1} + V_{dc2} \quad (1)$$

In this state, because both two sources are active, D1 and D2 are forward biased and D3 and D4 are reverse biased. Thus, the sources current enters in Z-network through D1 and D2 and after passing load impedance, comes back into sources through negative polarity.

2) State 2, source 1 is active and source 2 is inactive

The equivalent circuit of this state is shown in Fig. 3. In this state, source 1 is active, so only this source provides converter (consequently load) energy. Because of source 1 is active then D1 is forward biased and D3 is reverse biased, so current follows from D1 to Z-network to load.

TABLE I. STATES OF DOUBLE INPUT DC-DC CONVERTER

state	Sources States		Switches States				V_{in}
	V_{dc1}	V_{dc2}	D1	D2	D3	D4	
1	Active	Active	On	On	Off	Off	$V_{dc1} + V_{dc2}$
2	Active	Inactive	On	Off	Off	On	V_{dc1}
3	Inactive	Active	Off	On	On	Off	V_{dc2}
4	Inactive	Inactive	Off	Off	On	On	0

In reverse path from load to the source, current can't pass through source 2 and D2, so D4 is forcedly turned on and

conduct current to source 1. In this state, converter input dc voltage is only provided by source 1, as (2) shows.

$$V_{in} = V_{dc1} \quad (2)$$

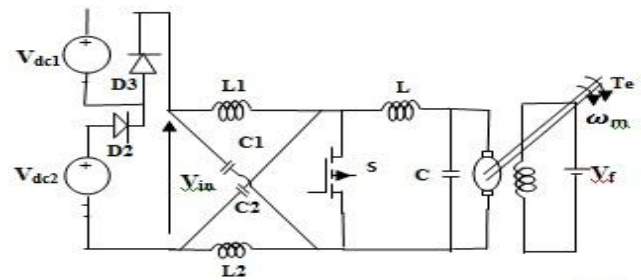


Fig3. Double input DC-DC converter state2 equivalent circuit

3) State 3, source 1 is inactive and source 2 is active

If source 1 is eliminated for each reason and source 2 is active, the converter can operate normally without effect of source 1 elimination. Fig. 5 shows the equivalent circuit for this state. In state 3, it's only source 2 that supplies converter and load. Source2 activation causes forward bias of D2 and reverse bias of D4. Because of source 1 disconnection, current passes through D3 and indeed, current turns it on forcedly to complete current path. In this state, converter input dc voltage is only provided by source 2, as (3) shows.

$$V_{in} = V_{dc2} \quad (3)$$

4) State 4, both source 1 and source 2 are inactive

Basically, this state is only following of one of the previously mentioned three states. Because in this state both dc sources are inactive and disconnected from converter, D1

And D2 are forcedly turned off and consequently, the only existing path for remain current, from previous state, is provided by D3 and D4. Thereupon, in state4 D3 and D4 are turned on. Fig. 6 shows equivalent circuit of this state. Input voltage is zero in this state as shown in (4).

$$V_{in} = 0 \quad (4)$$

Obviously, because both dc sources disconnect from converter, duration of this state is very short and when current descends to zero, whole of converter will be inactive.

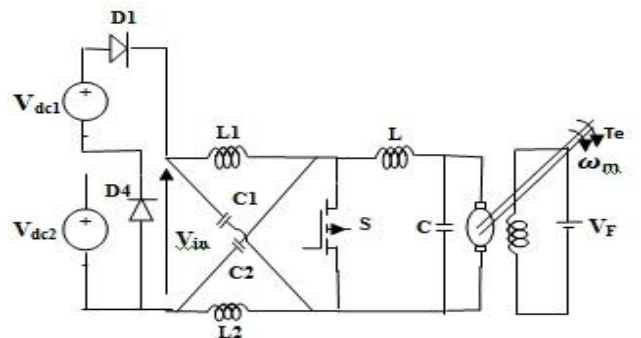


Fig4. Double input DC-DC converter state3 equivalent circuit

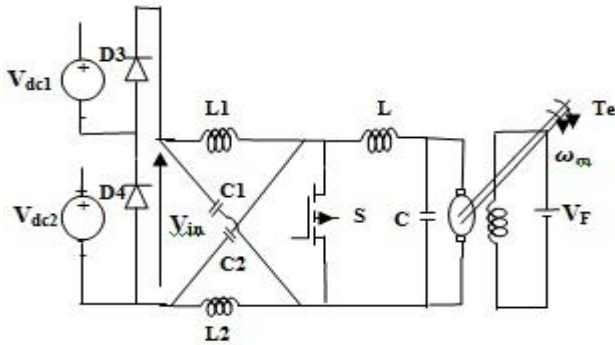


Fig5. Double input DC-DC converter state4 equivalent circuit

III. STEADY STATE ANALYSIS OF DC MOTOR FED WITH DOUBLE INPUT Z-SOURCE DC-DC CONVERTER

All four states of double input Z-source dc-dc converter can be analyzed in similar way, but in this section only first state is analyzed which can be applied to the other states. Fig. 3 is considered as converter circuit for steady state analysis.

Similar to the other Z-source inverter/converter topologies, Z-network of the Z-source dc-dc converter is also symmetrical, that is, the inductors L1 and L2 and capacitors C1 and C2 have the same inductance (L) and capacitance (C), respectively. From the symmetry and the equivalent circuits, the inductor and capacitor voltages have following relations [8]:

$$V_{C1}=V_{C2}=V_C, \quad V_{L1}=V_{L2}=V_L \quad (5)$$

There are two modes in steady state operation of converter circuit. In mode 1 diodes D1 and D2 are turned on and the switch S is turned off. The dc sources charge Z-network capacitors, while Z-network inductors discharge and transfer energy to the load. Converter operating interval in this mode is $(1-D)T$, where D is duty ratio of switch S, and T is switching cycle. Fig. 7 shows equivalent circuit of mode 1. Thus in this interval the following equations are received [8]:

$$V_{in} = V_{dc1} + V_{dc2} \quad (6)$$

$$V_C = V_{in} - V_L \quad (7)$$

$$V_o = V_{in} - 2V_L \quad (8)$$

In mode 2, switch S is turned on and D1 and D2 are turned off. Z-network capacitors discharge, while inductors charge and store energy to release and transfer to the load in the next interval. Converter operating interval in this state is DT. Fig. 8 shows mode 2 equivalent circuit. Following equation expresses this interval equivalent circuit [8]:

$$V_C = V_L, \quad V_o = 0 \quad (9)$$

The average voltage of the inductors over one switching period (T) in steady state should be zero, so (6)-(9) result:

$$V_L = \int V_C \cdot DT + (V_{in} - V_C)(1-D)T \quad (10)$$

Considering (10) equal to zero, results following equation:

$$\frac{V_C}{V_{in}} = \frac{1-D}{1-2D} \quad (11)$$

Similarly, the peak output voltage of converter in a Switching cycle can be expressed as follows:

$$V_L = 2V_C - V_{in} = \frac{V_{in}}{1-2D} \quad (12)$$

The average output voltage can be expressed as:

$$V_o = V_C = \frac{1-D}{1-2D} V_{in} \quad (13)$$

$$V_o = \frac{1-D}{1-2D} (V_{dc1} + V_{dc2}) \quad (14)$$

This output voltage is given as the input to the DC motor.

Modeling of separately excited dc motor

$$V_a(t) = R_a i_a(t) + L_a \frac{di_a(t)}{dt} + e_b(t) \quad (15)$$

$$e_b(t) = K_b \cdot w(t) \quad (16)$$

$$T_m(t) = K_T i_a(t) \quad (17)$$

$$T_m(t) = J_m \cdot \frac{dw(t)}{dt} + B_m \cdot w(t) \quad (18)$$

Where V_a = armature voltage, R_a =armature resistance, L_a =armature inductance, i_a = armature current, e_b =back emf, $w(t)$ =angular speed, T_m =motor torque, J_m =rotor inertia, B_m =viscous friction coefficient, K_T =torque constant and K_b =back emf constant.

Eventually, the transfer function between angular speed and armature voltage at no load is

$$\frac{w(s)}{V(s)} = \frac{K_b}{s^2 J_m L_a + s(B_m L_a + R_a J_m) + (B_m R_a + K_b^2)} \quad (19)$$

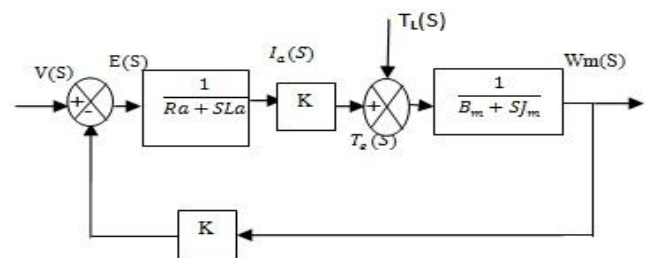


Fig.6 Block diagram of the DC motor

IV. SIMULATION RESULTS

Simulation of double input Z-source dc-dc converter fed dc motor was performed using MATLAB SIMULINK to confirm above analysis. Simulation consists of four sections that each section describes each state of converter. Converter parameters in the simulation were as in Table II.

TABLE II.SIMULATION PARAMETERS

parameter	value
Vdc1	100
Vdc2	40
C1=C2	1000 μ F
C	500 μ F
L1=L2=L	0.5mH
switching frequency	10KHZ
duty ratio	30%
Ra	0.5 $\square \square \Omega$
La	0.01 mH
J_m	0.05kg.m ²
B_m	0.02N.m.s
T _L	10N.m

Double input Z-source dc-dc converter fed dc motor is controlled by PWM duty cycle control. So by adjusting duty cycle, converter output voltage and speed of the dc motor are regulated. As previously mentioned, dc sources can supply converter individually or simultaneously. In this simulation independence of dc sources from each other is shown in four different states.

State 1, both source 1 and source 2 are active For state 1, that both dc sources were active during simulation time, converter produced 244V by 30% duty cycle in boosting mode. Fig. 7 shows converter output voltage. Fig. 8 shows the electromagnetic torque and Fig. 9 shows the angular speed of the motor. Input current passed through D1 and D2 because these switches were forward biased and turned on. D3 and D4 were reverse biased, thus their currents were zero.

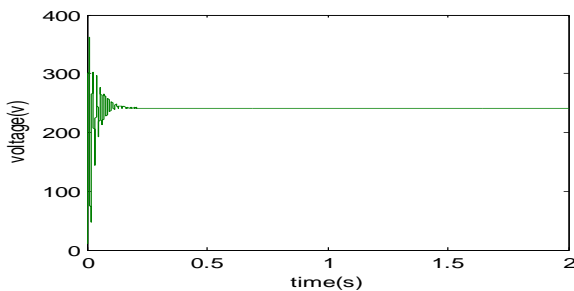


Fig7. Double input DC-DC converter output voltage in state 1

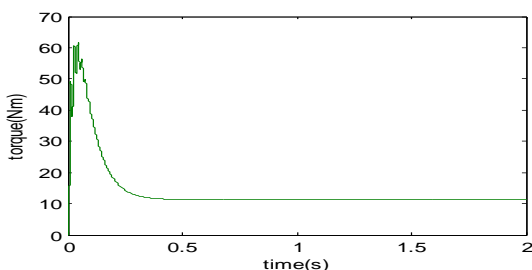


Fig8.electromagnetic torque of the dc motor in state 1

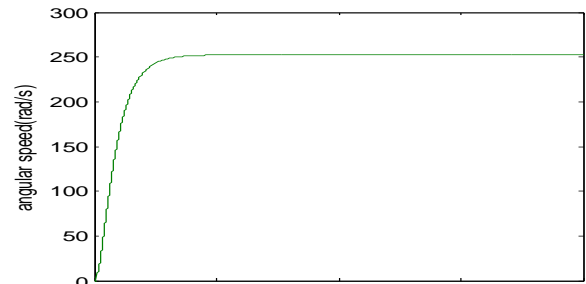


Fig9. Angular speed of the dc motor

State 2, source 1 became inactive

For state 2, that source1 became inactive and disconnected from converter.fig.10 shows output voltage of the converter for state 2. As this figure shows output voltage decreased to 69V which is only source 2 stepped up dc voltage. Thus only source 2 supplied to converter independent of source 1. Simulation time, converter produced 69V by 30% duty cycle in boosting mode. Fig. 10 shows converter output voltage. Fig. 11 shows the electromagnetic torque and Fig. 12 shows the angular speed of the motor. Input current passed through D2 and D3 because these switches were forward biased and turned on. D1 and D4 were reverse biased, thus their currents were zero.

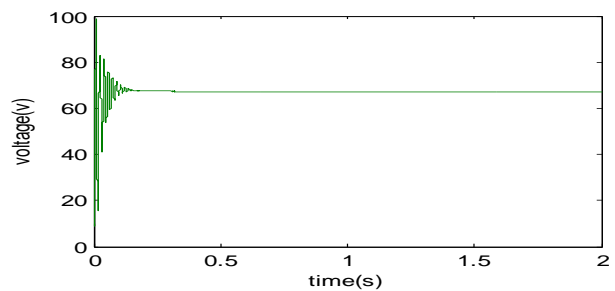


Fig10.converter output voltage in state 2

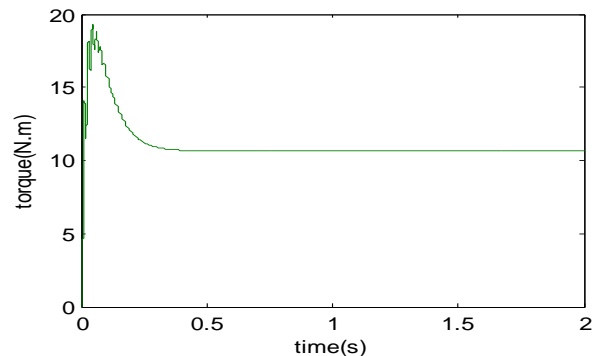


Fig11.electromagnetic torque in state 2

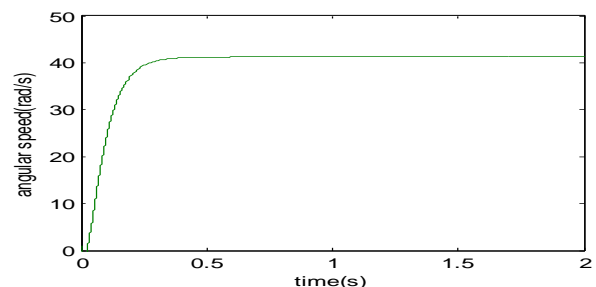


Fig12.angular speed of the dc motor in state

A. State 3, source 2 became inactive

Similar to the state2, in state 3 Source 2 became inactive and disconnected from converter. Fig.13 shows output voltage of the converter for state 3. As this figure shows output voltage decreased to 175V which is only source 1 stepped up dc voltage. Thus only source 1 supplied converter independent of source 2. Simulation time, converter produced 175V by 30% duty cycle in boosting mode. Fig. 13 shows converter output voltage. Fig. 14 shows the electromagnetic torque and Fig. 15 shows the angular speed of the motor. Input current passed through D1 and D4 because these switches were forward biased and turned on. D2 and D3 were reverse biased, thus their currents were zero.

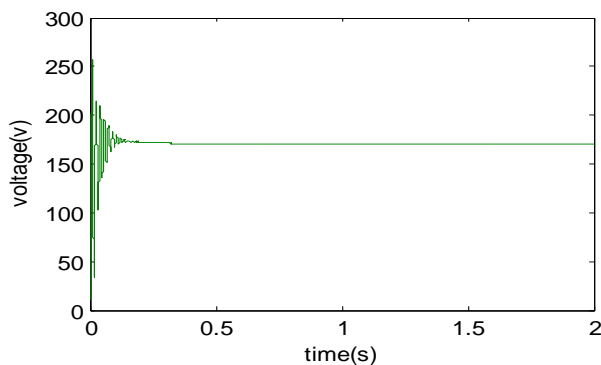


Fig13.converter output voltage in state 3

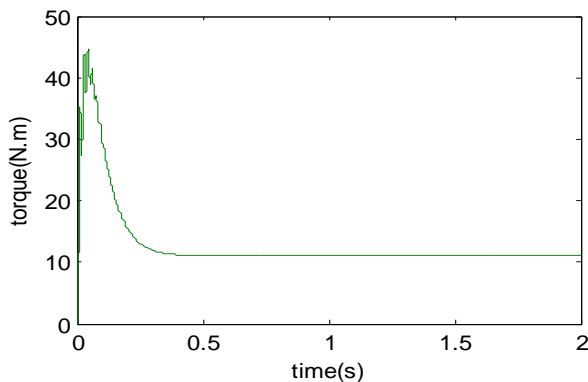


Fig14.electromagnetic torque of the dc motor in state 3

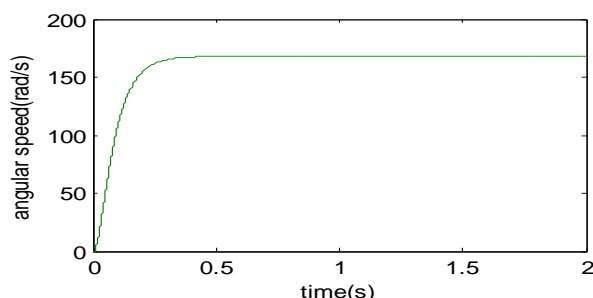


Fig15.angular speed of the dc motor state 3

D. state 4: Both source 1 and source 2 became inactive

This state is not considered as an active operation state, because both dc sources become inactive and indeed, there is not any source to supply converter and load. In this state D1 and D2 were turned off, thereupon converter input current path switched to D3 and D4.

V. CONCLUSION

This paper has proposed a double input Z-source converter fed dc motor. This drive has the advantages of both dc motor and Z-source converter. The system configuration and operation principle have been analyzed in detail. Based on the equivalent circuits, the mathematical model has been established. Simulation results have validated the preferred features as well as the possibility of the proposed drive system.

REFERENCES

- [1] E.Muljadi and H.E.Mckenna, "power quality issues in a hybrid power system," *IEEE Trans. Ind. Appl.*, vol.38, pp.803-809, May/ Jun 2002
- [2] F. Giraud and Z. M. Salameh, "Steady-state performance of a grid connected rooftop hybrid wind-photovoltaic power system with battery storage," *IEEE Trans. Energy Convers.*, vol. 16, no. 1, pp. 1-7, Mar 2001.
- [3] Yaow -Ming Chen, Yuan-Chuan Liu, and Sheng- sien Lin, "Double- Input PWM DC-DC Converter for High-/Low-Voltage Sources," *IEEE Trans. Ind. Electron.*, vol. 53, no. 5, October 2006.
- [4] Yuan-Chuan Liu and Yaow -Ming Chen, "A systematic approach to synthesizing multi-input dc-dc converters" *IEEE Trans. Power Electron.*, vol. 24, no. 1, January 2009.
- [5] H. Matsuo, W. Lin, F. Kurokawa, T. Shigemizu, and N.Watanabe "Characteristics of the multiple-input dc-dc converter," *IEEE Trans. Ind. Electron.*, vol. 51, no. 3, pp. 625-631, Jun 2004.
- [6] F. Z. Peng, "Z-Source inverter," *IEEE Trans. Ind. Appl.*, vol. 39, no.2, pp. 504-510, March/April 2003.
- [7] Xu Peng Fang, Zhao Ming Qian, and Fang Zheng Peng, "Single- phase Z-Source PWM AC-AC Converters," *IEEE Power Electron. Lett.*, vol. 3, no. 4, December 2005.
- [8] Xupeng Fang and Xingquan Ji, "Bidirectional Power Flow Z-Source DC-DC Converter," *IEEE Vehicle Power and Propulsion Conference (VPPC)*, 2008, Harbin, China

Biographies:



Santhosh Yamsani received the B.Tech Degree in EEE from J.N.T.U- Hyderabad, in 2010. He is currently pursuing M.Tech in TKR Engineering College.



Sampath Kumar Boini received the B.Tech Degree in E.E.E from JNTU- Hyderabad in 2005 and the M.Tech Degree from JNTU- Hyderabad in 2007. He is currently working as an associate-Professor in the department of EEE in TKR Engineering College, Hyderabad.

Analysis of Free Space Optical Communication System for Different Atmospheric Conditions & Modulation Techniques

Shalini khare, namrata sahayam

^{1,2} Department of electronics & communication Jabalpur Engineering College, Jabalpur, India

Abstract: The free space optical communication (FSO) is often used for digital communication systems because of its low cost. It is also preferred where the developing the infrastructure is difficult. It also provides the security because of its line of sight nature and very small detectable area, but besides the given advantages it's having serious problem because the performance of FSO is very sensitive to the channel (space) conditions, which changes continuously also the conditions are much complicated then the conditions in RF channels. Hence in this paper an analysis of the FSO communication is presented under scattering, fading & fog conditions with DPSK modulation.

Keywords: Free Space Optical Communication (FSO), Differential Phase Shift Keying (DPSK).

I. Introduction

Free-space optical communication (FSO) is an optical communication technology that use slight propagating in free space to transmit data for telecommunications or computer networking. "Free space" means air, outer space, vacuum, or something similar. This contrasts with using solids such as optical fiber cable or an optical transmission line. The technology is useful where the physical connections are impractical due to high costs or other considerations.

Free-space point-to-point optical links can be implemented using infrared laser light, although low-data-rate communication over short distances is possible using LEDs. Infrared Data Association (IrDA) technology is a very simple form of free-space optical communications. Free Space Optics is additionally used for communications between spacecraft. Maximum range for terrestrial links is in

The order of 2 to 3km [1] but the stability and quality of the link is highly dependent on atmospheric factors such as rain, fog, dust and heat.

Secure free-space optical communications have been proposed using a laser N-slit interferometer where the laser signal takes the form of an interferometric pattern. Any attempt to intercept the signal causes the collapse of the interferometric pattern [2] [3]. This technique has been demonstrated to work over propagation distances of practical interest [4] and in principle; it could be applied over large distances in space [2].

II. Related Work

In free-space optical communication links, atmospheric turbulence causes fluctuations in both the intensity and the Phase of the received light signal, impairing link performance .Xiaoming Zhu at el. [5] describe several communication techniques to mitigate turbulence-induced intensity fluctuations, i.e. signal fading.

They describe the use of maximum-likelihood detection in spatial diversity reception to reduce the diversity gain penalty caused by correlation between the fading at different receivers. In other paper Hennes HENNIGER and Otakar WILFERT [6] gives an overview of the challenges a system designer has to consider while implementing an FSO system. Typical gains and losses along the path from the transmitter through the medium to the receiver are introduced in this paper. This paper also discussed the different modulation and coding techniques for the FSO. Xiaoming Zhu, JosephM. Kahn [7] presented Mitigation of Turbulence-Induced Scintillation Noise in Free-Space Optical Links Using Temporal-Domain Detection Techniques & experimentally demonstrate the effectiveness of these techniques in a 500-m terrestrial link using ON-OFF keying, where MLSD and PSAD yield signal to-noise ratio gains of 2.4 and 1.9 dB, respectively.

Song Gao, Anhong Dang, HongGuo [8] presented a coherent differential phase-shift keying (DPSK) transmission system to improve the receiver sensitivity for wireless optical communications. The error probability expression over atmospheric channels is derived under the assumption of log-normal distributed scintillation, and then the performance of DPSK system is compared with that of a most commonly used on-off keying (OOK) system under the same channel conditions. Theory analysis and numerical results illustrate that with the same bandwidth, DPSK system has a higher sensitivity than OOK, and to a certain extent DPSK format can reduce the impairment from turbulence induced scintillation for its threshold being signal intensity insensitive, and hence, DPSK format is very suitable for atmosphere channels and has a broad prospect in wireless optical communications.

Channel Modeling

A suitable model for simulation of FSO communication channels is presented by S. Sheikh Muhammad & P. Kohldorfer, E. Leitgeb[9] their model is taken here for reference.

2.1 Scintillation Losses

Randomly distributed cells are formed under the influence of thermal turbulence inside the propagation medium; the wave fronts vary causing the focusing and defocusing of the beam. Such fluctuations of the signal are called scintillations. The amplitude and frequency of scintillations depend on the size of the cells compared to the beam diameter [10]. The intensity and the speed of the fluctuations (scintillations frequency) increase with wave frequency. For a plane wave, a low turbulence and a specific receiver, the scintillation variance can be expressed as in equation (1) where λ represent the transmitter wavelength in [nm], l the channel-length in [m] and C_n^2 the refractive index structure parameter in $[m^{-2/3}]$. C_n^2 is

for low turbulence 10^{-16} for moderate turbulence 10^{-14}
 and for high turbulence 10^{-13} [9].

$$a_{scin} = 2\sqrt{23.17\left(\frac{2\pi}{\lambda}10^9\right)^{7/6}c_n^2l^{11/6}} \text{ [dB]} \dots\dots(1)$$

The dependence from C_n^2 is depicted in figure (1). For strong turbulences, a saturation of the variance given by above relationship is observed. The parameter C_n^2 does not have the same value at millimeter waves and at optical waves. Millimeter waves are especially sensitive to humidity fluctuations while in optic, refractive index is a primary function of the temperature.

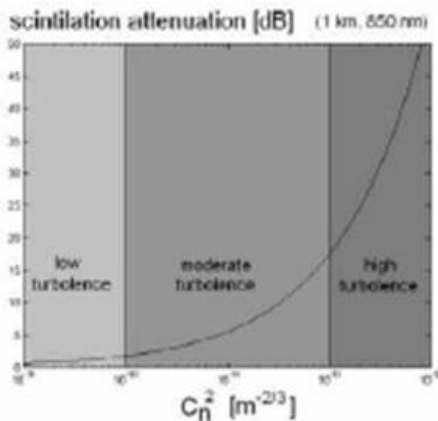


Figure 1: plot for C_n^2 Vs Scintillation Variance[9].

2.2 Fog Attenuation

The theoretical background of fog attenuation for light based on Mie Scattering can be found in [11-13] and is not being dealt with here. Several models exist which allow to calculate specific attenuation for different optical wavelengths based on visibility data. The two most widely used models that we used and implemented in our simulation are the Kruse model and the Kim model. The specific attenuation is calculated in equation (2), with the variables visibility V [km], wavelength λ [nm], visibility reference at wavelength λ_0 [nm] and for transmission of air drops to V % percent of the clear sky; and the results are shown in figure 2. The wavelength dependency in this expression is expressed by q , which is in the Kruse model given by equation (3) and in the Kim model by equation (4).

$$a_{spec} = \frac{10 \log V}{V} \left(\frac{\lambda}{\lambda_0}\right)^{-q} \left[\frac{dB}{km}\right] \dots\dots\dots(2)$$

$$q = \begin{cases} 1.6 & \text{if } V > 50km \\ 1.3 & \text{if } 6km < V < 50km \\ 0.585V^{1/3} & \text{if } V < 6km \end{cases} \dots\dots\dots(3)$$

$$q = \begin{cases} 1.6 & \text{if } V > 50km \\ 1.3 & \text{if } 6km < V < 50km \\ 0.16V + 0.34 & \text{if } 1km < V < 6km \\ V - 0.5 & \text{if } 0.5km < V < 1km \\ 0 & \text{if } V < 0.5km \end{cases} \dots\dots\dots(4)$$

At very high attenuations the Kim model is the better model.

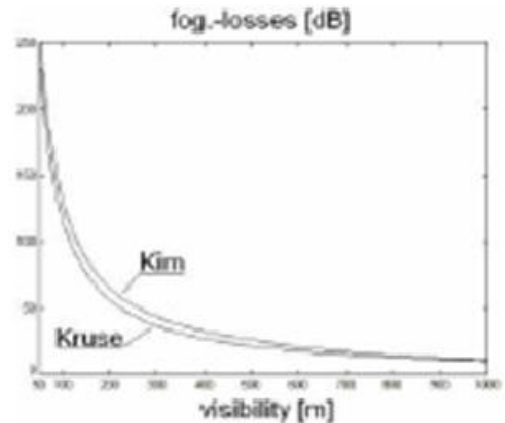


Figure 2: Plot of Visibility Vs Fog attenuation [9]

III. System Architecture

The system architecture of the simulated model contains a DPSK generator formed by the cascading of amplitude and phase modulator & the drive signal of the phase modulator is preceded by a delay-XOR pre-coder to generate the differentially encoded data sequence. Then the channel is formed by performing the noise, scintillation & fading as given by in the section 2.1 & 2.2. Then an asymmetric Mach-Zehnder interferometer (MZI) splits the signal to two paths and recombines these two signals after a path difference corresponding to the symbol duration. A balance receiver follows the interferometer as a multiplier to demodulate the differentially coded signal.

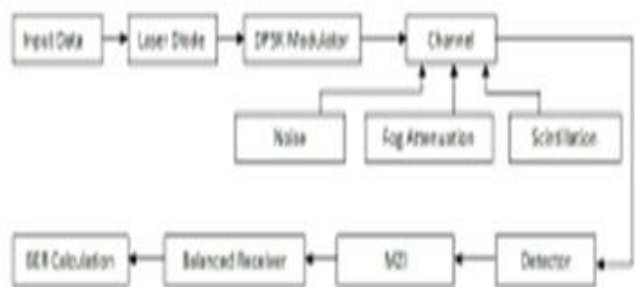


Figure 3: Block Diagram of the simulated model

IV. Simulated Results

The above discussed model is simulated for 650 nm LASER, $q = 1.3$ & $V = 10$, fog visibility 1km to 10km & analyzed for different Modulation techniques OOK, PSK & DPSK with various scintillation indexes.

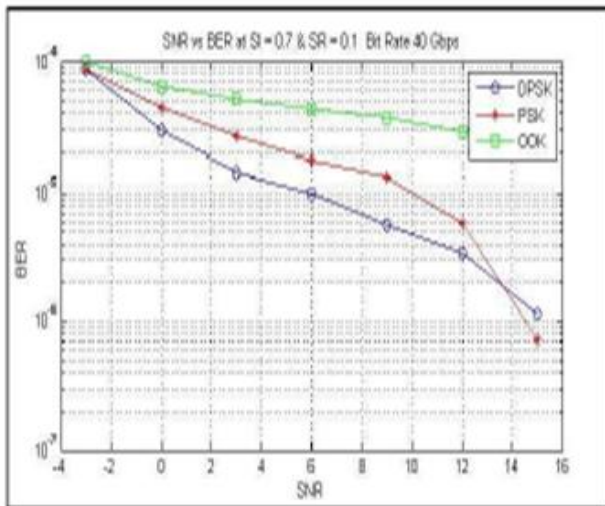


Figure 4: Effect of Scintillation Index on BER for all three modulation techniques. The scintillation rate is maintained constant 0.1 fog visibility is 10 Km and data rate is 40 GB/s. the simulation shows that DPSK has a good performance and the BER remains less than 0.1 for all values of SI (0.1 to 0.7).

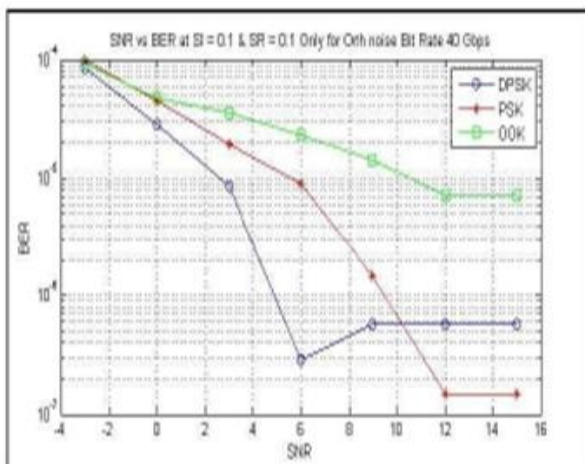


Figure 5: Effect of Additive Noise on BER for all three modulation techniques. The scintillation index and scintillation rate are maintained constant 0.1 fog visibility is 10 Km and data rate is 40 GB/s. the simulation shows that PSK and DPSK behaves similar.

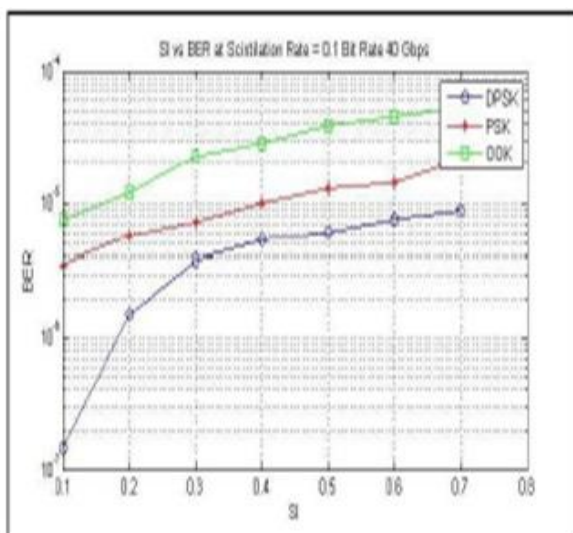


Figure 6: Effect of Additive Noise on BER for all three modulation techniques for higher SI. The scintillation index is maintained constant 0.7 and SR remain 0.1 fog visibility is 10 Km and data rate is 40 GB/s. the simulation shows that in presence of higher additive noise the SI remains ineffective.

5. Conclusion

In this work, we have analyzed the Free Space optical communication System using different modulation techniques and with different channel conditions like Fog & scintillation. The DPSK format has a better performance than OOK & PSK in atmosphere turbulence & Fog conditions for its longer symbol distance and being signal intensity insensitive. It can also be said that an appropriate coding technique will further improve the performance for the wireless optical transmission system.

References

- [1] Tom Garlington, Joel Babbitt and George Long (March 2005). "Analysis of Free Space Optics as Transmission Technology". WP No. AMSEL-IE-TS-05001. U.S. Army Information Systems Engineering Command. p. 3. Archived from the original on June 13, 2007. Retrieved June 28, 2011.
- [2] F. J. Duarte (May 2002). "Secure interferometric communications in free space". *Optics Communications* 205 (4): 313–319. doi:10.1016/S0030-4018(02)01384-6.
- [3] F. J. Duarte (January 2005). "Secure interferometric communications in free space: enhanced sensitivity for propagation in the metre range". *Journal of Optics A: Pure and Applied Optics* 7 (1). doi:10.1088/1464-4258/7/
- [4] F. J. Duarte, T. S. Taylor, A. M. Black, W. E. Davenport, and P. G. Varmette, N-slit interferometer for secure free-space optical communications: 527 m intra interferometric path length, *J. Opt.* 13, 035710 (2011).
- [5] Xiaoming Zhu and Joseph M. Kahn, Fellow, IEEE "Free-Space Optical Communication Through Atmospheric Turbulence Channels", *IEEE TRANSACTIONS ON COMMUNICATIONS*, VOL. 50, NO. 8, AUGUST 2002.
- [6] Hennes HENNIGER & Otakar WILFERT "An Introduction to Free-space Optical Communications", *RADIOENGINEERING*, VOL. 19, NO. 2, JUNE 2010, p203.
- [7] Xiaoming Zhu, Joseph M. Kahn, Fellow, IEEE, and Jin Wang, Student Member, IEEE "Mitigation of Turbulence-Induced Scintillation Noise in Free-Space Optical Links Using Temporal-Domain Detection Techniques", *IEEE PHOTONICS TECHNOLOGY LETTERS*, VOL. 15, NO. 4, APRIL 2003.
- [8] Song Gao, Anhong Dang & Hong Guo "Performance of Wireless Optical Communication Systems Using DPSK Modulation" Feb. 15-18, 2009 ICACT 2009.
- [9] S. Sheikh Muhammad & P. Kohldorfer, E. Leitgeb "Channel Modeling for Terrestrial Free Space Optical Links", *ICTON* 2005.

- [10] R.L. Philips, L.C. Andrews: Laser Beam Propagation through Random Media, in SPIE publications, Washington, 1998.
- [11] F. de Fornel, M. Al Naboulsi, H. Sizun: Fog attenuation prediction for optical and infrared waves, in Journal SPIE, 2003.
- [12] F. de Fornel, M. Gebhart, E. Leitgeb, M. Al Naboulsi, H. Sizun: Availability prediction for free space optic communication systems from local climate visibility data, in Short Term Scientific Report 4. COST 270, 2003.
- [13] E. Korevaar, I.I. Kim, B. McArthur: Comparison of laser beam propagation at 785 nm and 1550 nm in fog and haze for optical wireless communications, in SPIE proceedings, vol. 4124, 2001

Application of Neuro-Fuzzy System to Evaluate Sustainability in Highway Design

Thoedtida Thipparat¹, Thongpoon Thaseepetch²

^{1, 2}(Facility of engineering and architecture, Rajamangala University of Technology, Bangkok, Thailand

ABSTRACT: In this paper, adaptive neuro-fuzzy inference systems (ANFIS), using Sugeno ANFIS is used to evaluate the construction sustainability of highway design projects in Thailand. Input variables include factors associated with geometrics and alignments, earthworks, pavement, drainage, retaining walls, slope protection, landscape and ecology, transportation facilities, transportation maintenance, bridges, sound insulation, tunnels, electrical and mechanical work, and lighting. Finally, on the basis of our analysis, our results hold an important lesson for decision makers who may clearly picture the rules and use the fuzzy neural network approach to promote effective environmental protection to meet the highway district's goals.

Keywords: Sustainability, Highway design, Neuro-fuzzy system, Uncertainty, Evaluation

I. INTRODUCTION

Public awareness of global environmental problems such as global warming and ozone depletion has increased, to become one of the biggest issues for the new millennium, since the concept of sustainable development has attracted public attention as the greatest concern of the late twentieth century. Sustainable development in the construction industry is now an important issue [1]. However, it is lagging behind other sectors because, by its very nature, construction involves manipulation and use of large quantities of natural and man-made materials. Also, the construction and operations of infrastructure are large users of energy. A construction project generates a large amount of pollutants, including noise, air, solid waste and water [2-3]. There are suggestions that the environmental effects of the construction project can be studied under the following headings: (i) energy consumption; (ii) dust and gas emission; (iii) noise distribution; (iv) waste generation; (v) water discharge; (vi) use of water resources; (vii) unnecessary building consumption; (viii) pollution by building materials; (ix) land use; and (x) use of natural resources (Ball, 2002). Environmental impacts of buildings over their entire life cycle process have been recognized as a serious problem [4]. Nevertheless, the construction industry has not been showing very much concern about the environmental issues [5].

The sustainable concepts can be effectively integrated into construction project in the design stage [6]. One of the most importance stage of the life cycle in most green building guidelines and evaluation methods is the design stage [7]. It is important to focus on planning and design services provided by engineering consultants in the initial stages of the life cycle of infrastructure. The sustainable planning and design lead to the good management of the energy and materials required constructing highway, and waste produced by construction.

Considering sustainability early in planning and design will result in high potential reductions in operations' sustainable impacts could be generated [8-10].

As a result, the planning and design stage is a critical stage for the study of ecology, the systematic analysis of resource and energy flows within the anthroposphere, and the realm of man-made or managed resources. The wide variety of materials used in construction work, as well as fuel and electricity used for construction machinery and recycling plants has a significant environmental impact. The risk score is an overall aggregation of construction risks that are usually assessed against different criteria such as safety, functionality, sustainability and environment and characterized by risk ratings such as High, Medium, Low or None. The aggregation process involves a large number of subjective judgments of construction experts, but there is no explicit functional relationship between risk score and risk ratings.

The AASHTO (American Association of State Highway and Transportation Officials) conducted a compendium of practices, procedures, and policies for integrating environmental stewardship into highway construction and maintenance activities for Departments of Transportation (DOT) in many states [11]. It is one of the standards and improvements in environmental processes, practices, and significant environmental items.

Currently, several studies have been done on development of the forecasting models. However, a model used to predict the sustainability of highway design is rarely concerned. The research focus is to investigate the factors affecting sustainability in highway design in Thailand.

The ability of hybrid ANN models in predicting country risk rating was determined [12]. The hybrid ANN models were compared with traditional statistical techniques such as discriminate analysis (DA), logit model, probit model and ordinary neural networks. Their results indicated that hybrid neural networks outperformed all the other models. In order to determine the construction sustainability, mathematical models need to be developed to predict the risk scores of construction project. Adaptive neuro-fuzzy inference systems (ANFIS), using Sugeno ANFIS and logistic regression analysis are two alternative approaches for modelling construction sustainability data. This study compares the modelling mechanisms and performances in modelling construction sustainability data.

This study firstly identified the performance measurement indicator for construction sustainability assessment associated with a construction project. Then the impact of regulatory compliance, auditing activities and resources consumption on construction sustainability were investigated. The study framework is a simple linear model of the relationship between the independent and dependent variables. Sustainability items as the independent variables

consists of 14 groups, namely geometrics and alignments, earthworks, pavement, drainage, retaining walls, slope protection, landscape and ecology, transportation facilities, transportation maintenance, bridges, sound insulation, tunnels, electrical and mechanical work, and lighting. There are 60 input variables. . These input variables used in the measurement of the sustainability are proposed by [13]. Table 1 shows sustainable items for highway design.

Table 1 Sustainable items for highway design (Tsai and Chang, 2012)

Activities	Sustainable items
1. Geometrics and alignments	1.1 Reduction in volume or weight 1.2 Mild curves 1.3 Mild slopes
2. Earthworks	2.1 Earthwork balance 2.2 Minimum excavation and fills 2.3 Topsoil recycling 2.4 Waste reuse
3. Pavement	3.1 Reduction in volume or weight 3.2 Permeable materials 3.3 Recycled materials 3.4 Noise reduction materials 3.5 Fiber materials

Table 1 Sustainable items for highway design (Tsai and Chang, 2012) (con't)

Activities	Sustainable items
4. Drainage	4.1 Runoff reduction 4.2 Vegetated or gravel ditches 4.3 Rainwater catchments 4.4 Infiltration trenches or catch basins 4.5 Sediment ponds 4.6 Regional materials
5. Retaining walls	5.1 Reduction in volume or weight

	5.2 Vegetation 5.3 Grinding stones or soft reinforcing
6. Slope protection	6.1 Vegetation 6.2 Reinforced slopes 6.3 Waste reuse
7. Landscape and ecology	7.1 Avoidance of natural preservation sites 7.2 Embankments or cutting replaced by bridges or tunnels 7.3 Native trees 7.4 Tree transplanting 7.5 Vegetation 7.6 Topsoil recycling 7.7 Culverts for wildlife crossings 7.8 Ecological ponds 7.9 Habitat connectivity 7.10 Biological porous environment 7.11 Reduction in landscaping facilities 7.12 High bridges

Table 1 Sustainable items for highway design (Tsai and Chang, 2012) (con't)

Activities	Sustainable items
8. Transportation facilities	8.1 Reduction in volume or weight 8.2 Multi-function poles
9. Transportation maintenance	9.1 Reduction in path changes
10. Bridges	10.1 Reduction in volume or weight 10.2 Long-span bridges 10.3 Pre-casting techniques 10.4 Temporary bridges for construction 10.5 Hollow railings

	10.6 Reinforced materials
	10.7 High strength concrete
	10.8 Self-compacting concrete
	10.9 Lightweight concrete
	10.10 Steel
11. Sound insulation	11.1 Reduction in volume or weight
	11.2 Landscaping
12. Tunnels	12.1 Reduction in volume or weight
	12.2 Vegetation
	12.3 Reduction in ventilation facilities
	12.4 Waste reuse
	12.5 Fiber materials
13. Electrical and mechanical work	13.1 Reduction in transportation controlling facilities
14. Lighting	14.1 Reduction in lighting equipment
	14.2 Renewable energy
	14.3 Shading board

II. NEURO-FUZZY MODEL

The neuro-fuzzy system attempts to model the uncertainty in the factor assessments, accounting for their qualitative nature. A combination of classic stochastic simulations and fuzzy logic operations on the ANN inputs as a supplement to artificial neural network is employed. Artificial Neural Networks (ANN) has the capability of self-learning, while fuzzy logic inference system (FLIS) is capable of dealing with fuzzy language information and simulating judgment and decision making of the human brain. It is currently the research focus to combine ANN with FLIS to produce fuzzy network system. ANFIS is an example of such a readily available system, which uses ANN to accomplish fuzzification, fuzzy inference and defuzzification of a fuzzy system. ANFIS utilizes ANN's learning mechanisms to draw rules from input and output data pairs. The system possesses not only the function of adaptive learning but also the function of fuzzy information describing and processing, and judgment and decision making. ANFIS is different from ANN in that ANN uses the connection weights to describe a system while ANFIS uses fuzzy language rules from fuzzy inference to describe a system.

The ANFIS approach adopts Gaussian functions (or other membership functions) for fuzzy sets, linear functions for the rule outputs, and Sugeno's inference mechanism [14]. The parameters of the network are the mean and standard deviation of the membership functions (antecedent parameters) and the coefficients of the output linear functions as well (consequent parameters). The ANFIS learning algorithm is then used to obtain these parameters. This learning algorithm is a hybrid algorithm consisting of the gradient descent and the least-squares estimate. Using this hybrid algorithm, the rule parameters are recursively updated until an acceptable level of error is reached. Each iteration includes two passes, forward and backward. In the forward pass, the antecedent parameters are fixed and the consequent parameters are obtained using the linear least-squares estimation. In the backward pass, the consequent parameters are fixed and the error signals propagate backward as well as the antecedent parameters are updated by the gradient descent method. Based on the original ANFIS study [15]; the learning mechanisms should not be applied to determine membership functions in the Sugeno ANFIS, since they convey linguistic and subjective descriptions of possibly ill-defined concepts. Hence, the choice of membership function should depend on the specific types of data.

III. TRAINING ANFIS FOR SUSTAINABILITY EVALUATION

For proving the applicability of the model and illustration, the proposed model was applied in a highway district in Thailand. The first step to apply the model was to construct the decision team. The decision team included head and staffs of highway district, construction consultants, contractors with capital of more than hundred million baht, contractors with capital of less than hundred million baht, and sub-contractors. For training the ANFIS, a questionnaire was designed including 14 activities (60 variables). Fig 2 presents an input-output model for earthworks. The decision team was asked to give a score to them, based on their knowledge about the highway projects in a case study highway district. Then, they rated the highway projects with respect to each criterion in the range of [0, 10] with triangular or trapezoidal membership functions describing the linguistic variables such as the impact of reduction in volume or weight on sustainability, for example: "low", "medium" or "high" (Fig 3). The system was built in the Matlab Fuzzy Toolbox and Simulink environment. A Matlab programme was generated and compiled. The pre-processed input/output matrix which contained all the necessary representative features, was used to train the fuzzy inference system. Fig 4 show membership functions describing the linguistic variables such as the operation performance, for example: "low", "medium" or "high" after training the network. Fig 5 shows the structure of the ANFIS; a Sugeno fuzzy inference system was used in this investigation. From 60 attributes generated by the proposed approach, the decision makers derived 60 completed questions. We used 50 of them for training the ANFIS and the rest (15) for checking and validation of the model. For rule generation, we used subtractive clustering where the range of influence, squash factor, acceptance ratio, and rejection ratio were set at 0.5, 1.25, 0.5 and 0.15,

respectively during the process of subtractive clustering. Rules (clusters) of the trained FIS for earthworks are presented in Fig 6. Because by using subtractive clustering, input space was categorized into 18 clusters. Each input has Gaussian curve built-in membership functions. Fig 7 shows the surface of ANFIS after training. The training error of the ANFIS was ranged from 0.32 to 0.75 after 50 epochs as present in Fig 8. The rate of highway projects with respect to criteria and the output of ANFIS (sustainability level of highway design) have been shown in Table 2.

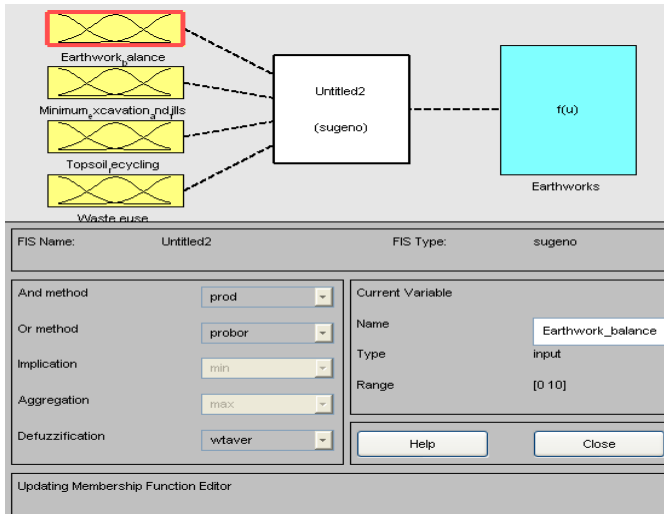


Figure 2 Input-output model for earthworks

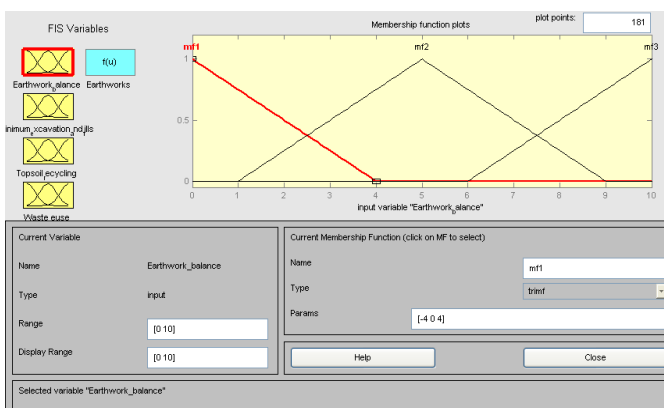


Figure 3 Membership functions of the operation performance (before Training)

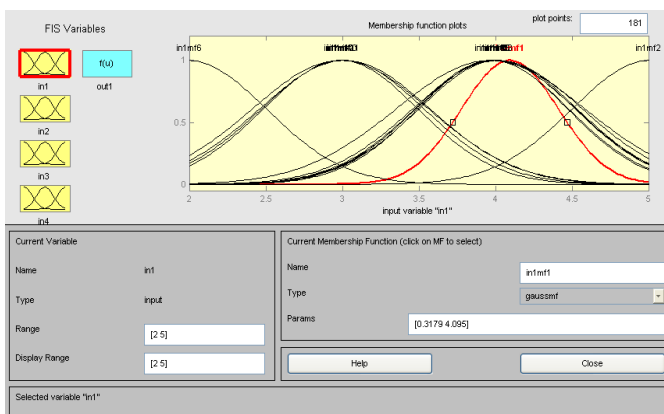


Figure 4 Membership functions of the operation performance (after Training)

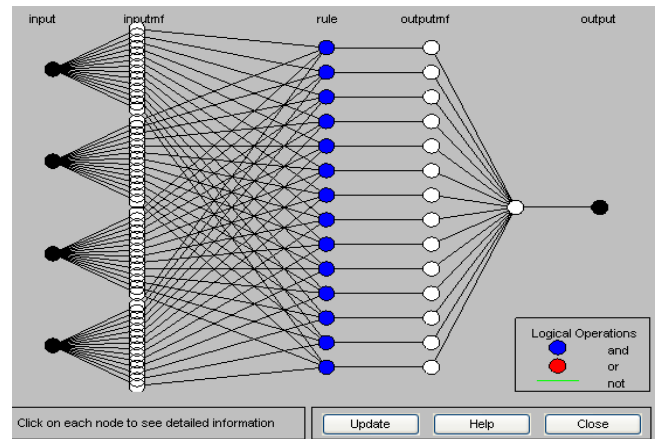


Figure 5 Network of sustainability evaluation by the ANFIS

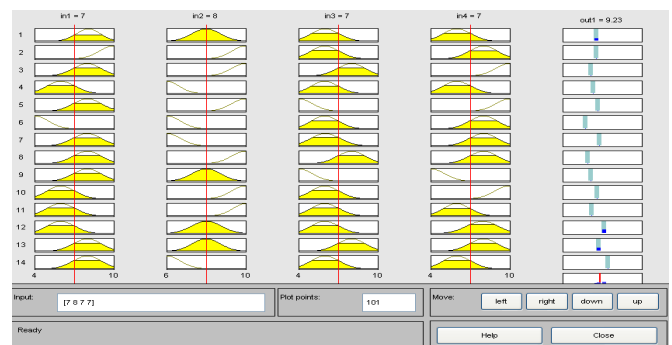


Figure 6 Rules (clusters) of the trained FIS

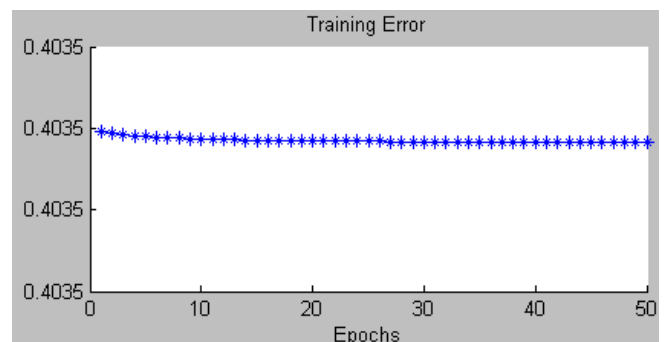


Figure 7 Trained main ANFIS surface: construction sustainability

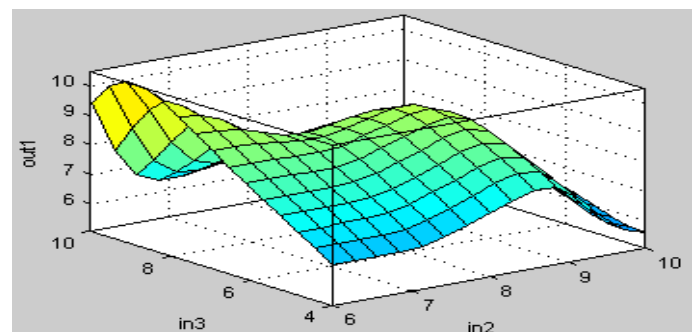


Figure 8 Training error of the ANFIS

Table 2. Inputs (rates of a case study) and output of ANFIS

Activities	Sustainable items	Head and staff of highway district (a case study)	Construction consultants,	Contractors with capital of more than hundred million baht,	Contractors with capital of less than hundred million baht	Sub-contractors
1. Geometrics and alignments	1.1 Reduction in volume or weight	8	10	6	8	6
	1.2 Mild curves	8	10	6	10	6
	1.3 Mild slopes	8	10	8	8	6
2. Earth-works	2.1 Earthwork balance	10	10	8	10	6
	2.2 Minimum excavation and fills	10	10	8	8	4
	2.3 Topsoil recycling	10	10	8	10	8
3. Pavement	3.1 Reduction in volume or weight	8	8	4	10	8
	3.2 Permeable materials	8	8	6	10	6
	3.3 Recycled materials	8	8	10	10	8
4. Drainage	4.1 Erosion reduction	10	8	8	10	8
	4.2 Vegetated or gravel ditches	10	8	10	10	8
	4.3 Rainwater catchments	10	10	6	8	8
5. Retaining walls	5.1 Reduction in volume or weight	10	10	8	8	8
	5.2 Vegetation	10	10	10	10	8
	5.3 Grinding stones or soil reinforcing	8	8	8	8	8
6. Slope protection	6.1 Vegetation	8	8	6	10	8
	6.2 Reinforced slopes	8	8	10	6	6
	6.3 Waste re-use	8	8	10	8	6
7. Landscape and ecology	7.1 Avoidance of natural preservation sites	8	10	10	6	6
	7.2 Embankments or cutting replaced by bridges or tunnels	8	10	10	8	8
	7.3 Native trees	6	10	4	8	6
	7.4 Tree transplanting	8	10	8	8	8
	7.5 Vegetation	8	10	6	8	6
	7.6 Topsoil recycling	10	10	6	10	10
	7.7 Culverts for wildlife crossings	8	10	8	10	6
	7.8 Ecological ponds	8	10	8	8	8
	7.9 Habitat connectivity	6	10	6	8	6
	7.10 Ecological porous environment	8	10	6	8	8

Table 2. Inputs (rates of a case study) and output of ANFIS (con't)

Activities	Sustainable items	Head and staff of highway district (a case study)	Construction consultants,	Contractors with capital of more than hundred million baht,	Contractors with capital of less than hundred million baht	Sub-contractors
7. Landscape and ecology	7.11 Reduction in landscaping facilities	6	8	4	6	4
	7.12 High bridges	8	8	8	8	8
8. Transportation facilities	8.1 Reduction in volume or weight	6	10	4	6	4
	8.2 Multi-function poles	8	10	8	8	8
9. Transportation maintenance	9.1 Reduction in patch change	6	8	4	4	4
	10.1 Reduction in volume or weight	8	8	6	8	8
10. Bridges	10.2 Long-span bridges	6	10	6	8	4
	10.3 Pre-casting techniques	8	10	8	10	10
	10.4 Temporary bridges for construction					
	10.5 Hollow railings	8	10	8	10	10
	10.6 Reinforced materials	6	10	4	4	4
	10.7 High strength concrete	8	10	4	8	6
	10.8 Self-compacting concrete	8	10	8	8	6
	10.9 Light-weight concrete	8	10	8	10	8
	10.10 Reel	8	10	8	8	6
	11.1 Reduction in volume or weight	8	10	8	10	8
11. Sound insulation	11.2 Landscaping	10	10	8	8	6
	12.1 Reduction in volume or weight	10	10	8	10	8
12. Tunnels	12.2 Vegetation	10	10	8	10	6
	12.3 Reduction in ventilation facilities	10	10	8	10	8
	12.4 Waste re-use	10	10	8	10	8
	12.5 Fiber materials	8	10	8	10	8
13. Electrical and mechanical works	13.1 Reduction in transportation communication facilities	8	10	8	10	8
	14.1 Reduction in lighting equipment	10	10	8	8	10
14. Lighting	14.2 Renewable energy	10	10	8	10	8
	14.3 Shading board	10	10	8	10	8
Sustainability level	Expert's opinions	112	105	119	98	84
	ANFIS Model	109	97	115	76	73

IV. CONCLUSION

A major objective of this paper was to present an application of ANFIS, and its performances in modeling a set of construction sustainability data. Considering data obtained from experts based on eighty scenarios, the sustainability level is calculated. Scenarios No. 1 to 50 were used as training cases for both methods. Scenarios No. 51 to 80 were used as test cases to compare performance of the Logistic regression and ANFIS methods. The five scenarios were used to compare the performance of the proposed approach by comparing with the values given by experts in scenarios being tested. The average and standard deviation of the differences between the estimated and the possibility obtained from expert produced by ANFIS are calculated to be 9.91 and 7.89 respectively. The performance of the models developed by ANFIS is summarized in Table 2.

Since it is an important lesson for decision makers aiming to promote effective environmental protection to meet the highway district's goals, the findings present a model of how sustainability for highway design was predicted regarding factors associated with 14 activities. Results present that the ANFIS model enhances sustainability forecasting by using fuzzy rules, which are easy for communication. The ANFIS model can explain the training procedure of outcome and how to simulate the rules for prediction.

REFERENCES

- [1] I. Holton, J. Glass, A.D.F. Price, Managing for sustainability: findings from four company case studies in the UK precast concrete industry, *Journal of Cleaner Production*, 18, 2010 152-160.
- [2] B. Polster, B. Peuportier, I.B. Sommereux, P.D. Pedregal, C. Gobin, Durand, E.: Evaluation of the Environmental Quality of Buildings towards A More Environmentally Conscious Design. *Solar Energy*. 57, 1996, 219–30.
- [3] Y.C.Tse and C. Raymond, The Implementation of EMS in Construction Firms: Case Study in Hong Kong. *Journal of Environmental Assessment Policy and Management*, 3, 2001, 177–94
- [4] R. Morledge, and F. Jackson, Reducing Environmental Pollution Caused by Construction Plant. *Environmental Management and Health*. 12, 2001, 191–206
- [5] R.B. Clements, *Complete guide to ISO 14000* (Prentice Hall: Englewood Cliffs, NJ, 1996).
- [6] National Research Council (NRC) *Improving Engineering Design: Designing for Competitive Advantage*. National Academy Press (Washington, DC, 1999)
- [7] K.R. Bunz, G.P. Henze, D.K.Tiller, Survey of sustainable building design practices in north America, Europe, and Asia, *Journal of Architectural Engineering, ASCE* 12 (1), 2006, 33-62.
- [8] B.C. McLellan, G.D. Corder, D. Giurco, S. Green, Incorporating sustainable development in the design of mineral processing operations review and analysis of current approaches, *Journal of Cleaner Production* 17, 2009, 1414-1425
- [9] C. Cerdan, C. Gazulla, M. Raugei, E. Martinez, P. Fullana-i-Palmer, Proposal for new quantitative eco-design indicators: a first case study, *Journal of Cleaner Production* 17, 2009, 1638-1643.
- [10] J.H. Spangenberg, A. Fuad-Luke, K. Blincoe, Design for sustainability (Dfs): the interface of sustainable production and consumption. *Journal of Cleaner Production* 18, 2010, 1485-1493
- [11] Transportation Research Board (TRB), *Environmental stewardship practices, procedures, and policies for high way construction and maintenance*. NCHRP Report 25e25 (04), (National Cooperative Highway Research Program, prepared by Venner Consulting and Parsons Brinckerhoff, 2004).
- [12] J. Yim, and H. Mitchell, Comparison of country risk models: hybrid neural networks, logit models, discriminant analysis and cluster techniques. *Expert Systems with Applications*. 28(1), 2005, 137–148.
- [13] C.Y. Tsai, A.S. Chang, Framework for developing construction sustainability items: the example of highway design. *Journal of Cleaner Production*, 20, 2012, 127-136
- [14] T. Takagi, and M. Sugeno, Fuzzy Identification of Systems and its Application to Modeling and Control. *IEEE Transactions on Systems Man and Cybernetics*, 5, 1985, 116–132
- [15] J.S.R. Jang, ANFIS: Adaptive- Network based Fuzzy Inference System, *IEEE Trans. IEEE Transactions on Systems Man and Cybernetics*, 23, 1993, 665-685.

A New FSM Watermarking Method to Making Authorship Proof for Intellectual Property of Sequential Circuit Design Using STG

Arunkumar.P, Shangari.B

(Department Of ECE, Anna University, Tamilnadu

(Department Of ECE, Nandha Engineering College, Tamilnadu

ABSTRACT: Finite state machines (FSMs) are mainly used for design an sequential circuits. In this paper, a new FSM watermarking method is introduced to make the authorship information of a designing circuits. To overcome the vulnerability attack and minimize the design error, the Digital watermark bits are seamlessly introduced into the outputs of the existing and free transitions of state transition graph (STG). To offers a high degree of tamper resistance and provides an easy and non invasive copy detection. The assignment of reserved literals is exploited to minimize the overhead of watermarking and make the watermarked FSM fallible upon removal of any pseudo input variable. A direct and convenient detection scheme is also proposed to allow the watermark on the FSM to be publicly detectable. Experimental results an acceptably low overheads with higher tamper resilience and stronger authorship owner proof in comparison with related watermarking schemes for sequential functions. IP providers are in pressing need of a convenient means to track the illegal redistribution of the sold IPs. This method is a great approach to protect a VLSI design against IP infringement has to embedding a signature that can only be uniquely generated by the IP author into the design during the process of its creation.

Keywords: Finite state machine (FSM), intellectual property (IP) protection, IP watermarking and state transition graph (STG).

I. INTRODUCTION

A new dynamic watermarking method is proposed. The watermark is embedded in the state transitions of FSM at the behavioral level. As a FSM design is usually Specified by a STG or other than a behavioral descriptions that can be easily translated into STG, the watermark is embedded into the STG of any size and remains a property of FSM after the watermarked design is synthesized and optimized into circuit net list [6]. The authorship can be directly verified even after the downstream integrated circuit design processes by running the watermarked FSM with a specific code sequence. The proposed watermarking scheme is robust against state reduction attacks. It is different from other transition based embedding methods in that it has lower embedding overhead and has overcome the vulnerability of auxiliary inputs which are inevitably introduced if the embedding capacity is limited, especially for completely specified FSM. The weaknesses of the existing FSM watermarking scheme to be overcome in this paper . There is no easy way to publicly detect the Existence of watermark, once the FSM is integrated into a chip and packaged since the test signals can be traced after the chip is packaged and the scan path provides controlled accesses to all internal states [8]. This paper also proposes

an alternative approach to allow the authorship proof of watermarked FSM to be verified off chip by making it a part of the test kernel. The proposed watermarking scheme thus makes the authorship proof harder to erase and the IP authorship easier to verify.

II. PRINCIPLE

A watermark on a bank note has a different transparency than the rest of the note when a light is shined on it. However, this method is useless in the digital world. Currently there are various techniques for embedding digital watermarks. Basically, they all digitally write desired information directly onto images or audio data in such a manner that the images or audio data are not damaged. Embedding a watermark should not result in a significant increase or reduction in the original data [7]. Digital watermarks are added to images or audio data in such a way that they are invisible or inaudible and unidentifiable by human eye or ear. Furthermore, they can be embedded in content with a variety of file formats. Digital watermarking is the content protection method for the multimedia era. Digital watermarking is applicable to any type of digital content, including still images, animation, and audio data [4]. It is easy to embed watermarks in material that has a comparatively high redundancy level such as color still images, animation, and audio data; however, it is difficult to embed watermarks in material with a low redundancy level, such as black-and-white still images. Solve this problem, we developed a technique for embedding digital watermarks in black and white still images and a software applications.

III. PROPOSED SYSTEM

Dynamic watermarking enables the embedded information to be detected from the output without reverse engineering by running the protected design with a specific code sequence. Dynamic watermarking is typically performed in the state transition graph (STG) of finite state machine (FSM), in the architectural level of digital signal processors or at the design-for-test ability stage[2]. FSM watermarking embeds the signature at a higher (behavioral/RT) level of design abstraction whereas the latter normally embeds the signature after logic synthesis. The authorship can be directly verified even after the downstream integrated circuit design processes by running the watermarked FSM with a specific code sequence. As extracting the STG from a gate level netlist is computationally impractical for large circuits, there are limited options for an attacker to remove or hide the watermark from the watermarked design netlist or netlist obtained by reverse engineering its downstream design. The proposed watermarking scheme is robust against state reduction attacks [5]. It is different from other transition

based embedding methods in that it has lower embedding overhead and has overcome the vulnerability of auxiliary inputs which are inevitably introduced if the embedding capacity is limited, especially for completely specified FSM.

IV. RELATED WORK

A. WATERMARK LIFECYCLE

Depending on the ability of the watermark to withstand normal signal processing operations, digital watermarking can be categorized as robust, fragile and semi-fragile watermarking. Robust watermarks are detectable even after some image processing operations has been performed on the watermarked image such as image scaling, bending, and cropping, and so on. Robust watermarks are mainly used for copyright protection [2]. The implement was designed using similar methods that were used in the implementation of the MD5 hash algorithm which is to be published. Fragile watermarks became invalid even if a slight modification is done to the watermarked image. Fragile watermarks are mainly used for authentication purpose. Semi-fragile watermarks allow some acceptable distortion to the watermarked image [9]. Beyond this acceptance level if any modification is done to the watermarked image, the watermark will not be detected.

B. WATERMARK DETECTION PROCESS

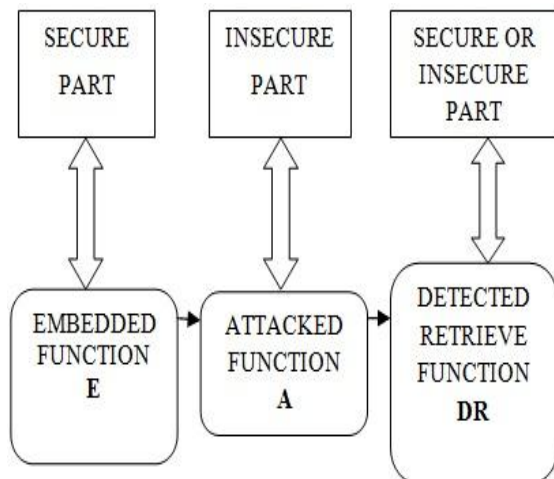


Fig1: Watermark Detecting Procedure

The original input image is not needed at the watermark detector. The watermarked image, the gain factor, and the seed value for creating the watermark are sufficient for the detection Fig.1 Block diagram of the detection process. We use two criteria for detection. A first criterion is similarity comparison result between H and V components for every 8×8 block. Second one is total average similarity measurement for every level [1]. The watermark detection in the DWT domain is implemented. The quotient is available in the register Q , and the remainder in A . The accumulator is implemented as a 14-bit register to accommodate a maximum value of $64 * 256$. The maximum value occurs when each pixel in a $8 * 8$ block assumes the value of pure white pixel gray value.

C. WATERMARK EXTRACT PROCESS

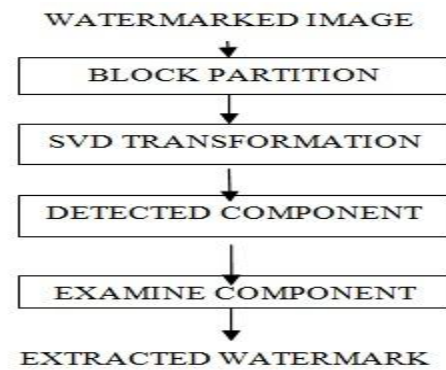


Fig2: Watermark Extracting Procedure

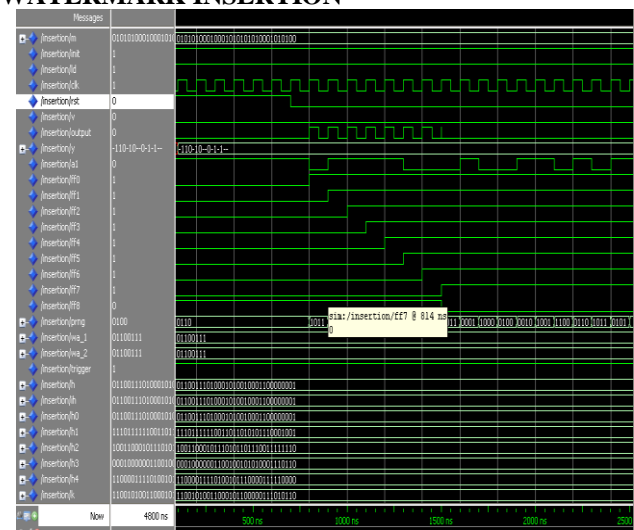
The watermark embedded at a higher level of design abstraction must survive the posterior optimizations so that the same IP distributed at all lower abstraction levels are protected. From the authorship verification perspective, IP watermarking can be classified into static watermarking and dynamic watermarking [3]. In the watermark detection phase, static watermarking requires the downstream design to be reverse engineered to the level where the watermark is embedded to show the additional constraints generated by the author's signature are satisfied. Digital watermarking can be categorized as robust, fragile and semi-fragile watermarking. Robust watermarks are detectable even after some image processing operations has been performed on the watermarked image such as image scaling, bending, and cropping, and so on.

V. APPLICATIONS AND ADVANTAGES

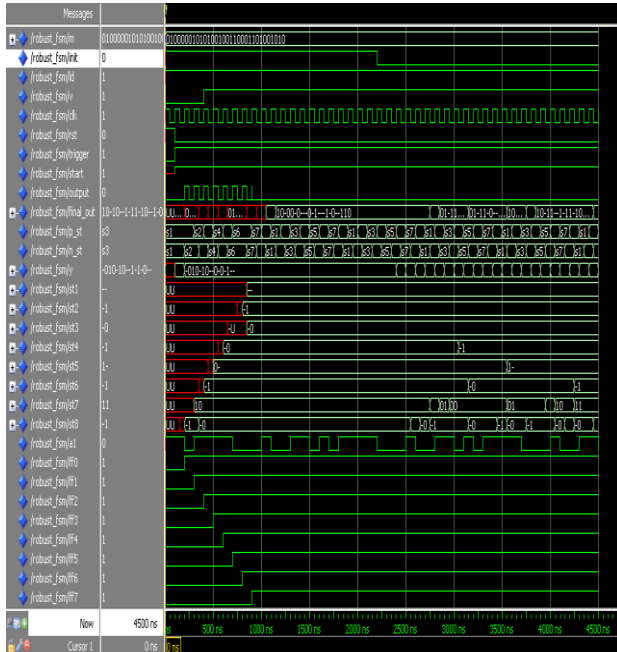
Depending on the ability of the watermark to withstand normal signal processing operations, digital watermarking can be categorized as robust, fragile and semi-fragile watermarking. Robust watermarks are detectable even after some image processing operations has been performed on the watermarked image such as image scaling, bending, and cropping, and so on. Robust watermarks are mainly used for copyright protection.

VI. SOFTWARE IMPLEMENTATION

WATERMARK INSERTION



REFERENCES



VII. CONCLUSION

A new robust dynamic watermarking scheme by embedding the authorship information on the transitions of STG at the behavioral synthesis level. The proposed method offers a high degree of tamper resistance and provides an easy and noninvasive copy detection. The FSM watermark is highly resilient to all conceivable watermark removal attacks. The redundancy in the FSM has been effectively utilized to minimize the embedding overhead. By increasing the length of input code sequence for watermark retrieval and allowing the output compatible transitions to be revisited to embed different watermark bits, the watermarks are more randomly dispersed and better concealed in the existing transitions of FSM. The new approach to the logic state assignments of pseudo input variables also makes it infeasible to attack the watermarked FSM by removing the pseudo inputs[8]. Without compromising the watermark strength, the length of verification code sequence can be adapted to reduce the area overhead of watermarked design to a reasonable bound within a preset number of iterations.

VIII. FUTURE WORK

The copying of digital content without quality loss is not so difficult. Due to this, there are more chances of copying of such digital information. So, there is great need of prohibiting such illegal copyright of digital media. Digital watermarking (DWM) is the powerful solution to this problem. Digital watermarking is nothing but the technology in which there is embedding of various information in digital content which we have to protect from illegal copying. This embedded information to protect the data is embedded as watermark. Beyond the copyright protection, Digital watermarking is having some other applications as fingerprinting, owner identification etc.

- [1] Mangione-Smith.W.H, Mantik.D (Aug 2001) "Intellectual Property Protection Development Working Group, Intellectual Property Protection: Schemes, Alternatives and Discussion", VSI Alliance, white paper, version 1.1. Page.no:25.
- [2] Abdel-Hamid.A.T, Tahar.S, and Aboulhamid.E.M (Jul 2005), "A survey on IP watermarking techniques", in Design Automation for Embedded Systems, vol. 10. Berlin, Germany: Springer-Verlag, Page.no:26 .
- [3] Cui.A, Chang.C.H, and Tahar.S (Sep 2008) "IP watermarking using incremental technology mapping at logic synthesis level", IEEE Trans. Comput.-Aided Design Integr. Circuits Syst., vol. 27, no. 9, Page.no:1.
- [4] Cui.A and Chang.C.H (May 2006) "Stego-signature at logic synthesis level for digital design IP protection", in Proc. IEEE Int. Symp. Circuits Syst., Page.no:37.
- [5] Kahng.A.B, Lach.J, Mangione-Smith.W.H, Mantik.D, Markov.I.L, Wang.H, Potkonjak.M, and Wolfe.G (Oct 2001) "Constraint-based watermarking techniques for design IP protection" , IEEE Trans. Comput.-Aided Design Integr. Circuits Syst., vol. 20, Page.no:34.
- [6] Kim.H.J, Mangione-Smith.W.H and Potkonjak.M (Oct 1998) "Protecting ownership rights of a lossless image coder through hierarchical watermarking", in Proc. Workshop Signal Process. Syst., Page.no:23.
- [7] Rashid.A, Asher.J, Mangione-Smith.W.H, and Potkonjak.M (May 1999) "Hierarchical watermarking for protection of DSP filter cores". in Proc. IEEE Custom Integr. Circuits Conf., Page.no:25.
- [8] Oliveira.A.L (Jun 1999) "Robust techniques for watermarking sequential circuit designs", in Proc. IEEE/ACM Des. Autom.Conf., Page.no:15.
- [9] Torunoglu.I and Charbon.E (Feb 2000) "Watermarking-based copyright protection of sequential functions", IEEE J. Solid-State Circuits, vol. 35., Page.no:3.

Influence of the Powder of Pozzolana on Some properties of the Concrete: Case of the Pozzolana of Djoungo (Cameroon)

Michel Mbessa¹, Emmanuel Cyril Bernard Ndongo², Hippolyte Ntete Nga³, Thomas Tamo Tatietse⁴

^{1,2,3,4}University of Yaoundé I - National Advanced School of Engineering - Department of Civil Engineering- Po Box 8390
Yaoundé, Cameroon. Tél/Fax: (237) 22 22 45 47

ABSTRACT: In this article, it is studied the influence of the pozzolana of Djoungo (ground to less of 80 μ m) on some mechanical characteristics of the concrete. A comparative study is done on the basis of a reference concrete (% of cement) and five other variants distinguished by their percentage in pozzolana as substituting for the Composed Portland Cement class 35 (CPJ 35) Cimencam Factory in Cameroon. The percentages used are: 10, 25, 50, 75 and 90%. The results obtained show that a substitution of less 25% natural pozzolana can be envisaged in the non-carrier structures.

Key-words: characteristic, concrete, compression traction, natural pozzolane, substitution.

I. Introduction

Since more than one decade, the pozzolanicity was the subject of several studies on the much known ultrafine particles notably silica fume, metakaolinite, slag, cristobalite (farsil 10), flying ashes.. It is about the substitution/addition of these ultrafine particles to the cement for the confection of the high performances concrete. The results on the workability, the durability and the mechanical characteristics are more or less satisfactory. The popularization of these concretes is operative on most building sites in Europe [1].

Indeed, the interest of the use of these ultrafine particles in the concrete is the combination of the silica that they contain, with the lime freed by the hydration of the cement in presence of water (pozzolanic reaction) to give hydrated calcium silicates (hcs), real binder contributing considerably to the improvement of the mechanical characteristics of this concrete. The pozzolanicity is the chemical reactivity of the silica with the lime in presence of water at an ambient temperature [1, 3].

From that precedes the idea to think a priori about an improvement of the mechanical characteristics of the concrete by replacing the cement by the pozzolana or adding pozzolana to the cement would not make a doubt anymore. However, the question that one asks is to know its degree of influence on the mechanical properties of the concrete [1].

In Cameroon, research on the pozzolanicity of the local materials has started although late and timidly. The researchers of the Laboratory of Geotechnic and Materials of National Advanced School of Engineering of the University of Yaoundé I bent on the characterization of the pozzolanicity of the materials as : burnt laterite, thermally treated clay from Dibamba, artificial pozzolana from the clay of Etoa (Road Yaoundé - Mfou) [3, 4].

In this work, we studied the influence of the ground pozzolana of Djoungo, on the mechanical characteristics of the concrete.

The tests were led on mortars and concretes with mixed binders (CPJ 35 cement and pozzolana) and with varied percentages of pozzolana, and the results are compared to those of a reference concrete (300 kg CPJ 35 Cement content per cube meter) with a binder/water ratio = 2, following DREUX GORIS method.

II. Materials

The materials used for study are: cement, ground natural pozzolana, sand, gravel and water.

2.1 Cement

The cement used is the composed portland cement CPJ 35 from Cimencam factory in Cameroon. Its characteristics are presented in table 1.

Tableau 1: characteristics of the Composed Portland cement used

Commercial name	CPJ 35 cement		
Color	Gray		
Absolute density	3,1		
Apparent voluminal mass (kg/l)	1,17		
Setting time	3 hours		
Grains diameter	80 μ m		
Specific area	3100		
Real resistance class at 28 days	32 Mpa		
Constitutive elements of cement	clinker	Gypsum	pozzolana
	65%	5%	30%

2.2 Water

The water used is the one produced and distributed by Camerounaise Des Eaux (CDE).

2.3 Aggregates

The 0-5 sand, is extracted from the Sanaga stream of Ebéda (Lékié division in Center Region of Cameroon), apparent density 1,5 and specific weight 2,6.

The 12,5/16 gravel, is from the stone pit quarry of Nkometou (Lékié division and Center region in Cameroon). Its apparent density is 1,7 and its specific weight is 2,6.

3.4 - Natural pozzolana of Djoungo

The pozzolana used is from Djoungo in Littoral Region of Cameroon (Mungo Division). Grey color, it was

finely ground by the mechanical grinder in the Laboratory of Geotechnic and Material of National Advanced School of Engineering of the University of Yaoundé I. The chemical characteristics are presented in table 3, compared to those of the cement.

After sifting with the help of the electric sifter, passersby to the sifter of 80 µm have been retained and kept in waterproof boxes.

Tableau 3: Comparison of the chemical composition of the pozzolana and the CPJ 35 cement.

Chemical composition(%)	CPJ 35	Pozzolanaof Djoungo
SiO ₃	19.5	45.79
Al ₂ O ₃	4.79	11.68
Fe ₂ O ₃	2.74	12.83
MnO	0.04	0.17
MgO	1.26	6.16
CaO	60.42	9.60
Na ₂ O	0.18	3.54
K ₂ O	0.93	1.39
TiO ₂	0.25	2.84
P ₂ O ₅	0.51	0.60
Loss to fire	0.02	0.31
Pozzolana	10	

III. Experimentation

3.1 Test on concrete

3.1.1 Composition of the concrete

The Method used is the one of Dreux - Goris [2] and as hypothesis, the percentage of pozzolana mentioned doesn't take in account the proportion already incorporated in the CPJ 35 cement.

The compositions of the concretes are presented in table 4.

Tableau 4: compositions of the concrete (for one cube meter)

Cte	Ct CPJ 35 (Kg)	Pz		Sd(kg)	Gl (kg)	Wr (kg)
		%	Mass e kg			
Ref.	300	0%	0	780	1170	150
C10	270	10	30	780	1170	150
C25	225	25	75	780	1170	150
C50	150	50	150	780	1170	150
C75	75	75	225	780	1170	150
C90	30	90	270	780	1170	150

Cte: Concrete; **Ct:** Cement; **Sd:** Sand; **Gl:** Gravel and **Wr:** Water

3.1.2 Equivalent composition

Table5: Composition of the concretes for the cylindrical 16x32 cm test-tubes

Cte	Ct CPJ 35 (Kg)	Pz		Sd (kg)	Gl	Wr (kg)
		(%)	M (kg)			
Ref.	7,2	0%	0	19,1	19,1	4,7
C10	6,5	10%	0,72	19,1	19,1	4,7
C25	5,4	25%	1,8	19,1	19,1	4,7
C50	3,6	50%	3,6	19,1	19,1	4,7

C75	1,8	75%	5,4	19,1	19,1	4,7
C90	0,7	90%	6,5	19,1	19,1	4,7
Total	25,137		17,96	19,1	114,5	28,08

Cte: Concrete; **Ct:** Cement; **Sd:** Sand; **Gl:** Gravel and **Wr:** Water

3.1.3 Consistency test

The consistency test was achieved according to the P 18-451 norm [2]. The results of settling to the Abrams cone are presented in table 7.

3.1.4 Compression test on cylindrical 16x32 cm test-tubes

The test was achieved according to NF P 18-406 norm. The results are presented in table 8.

3.2 Tests on mortar

3.2.1 Composition of mortars

The compositions of the six (06) types of mortar are presented in table 6.

Tableau 6: Composition of mortars

Cte	CPJ 35 Ct (Kg)	Pozzolana		Sd (kg)	Wr (kg)
		%	M (kg)		
Ref.	2,70	0%	0,00	8,10	1,35
M10	2,43	10%	0,27	8,10	1,35
M25	2,03	25%	0,68	8,10	1,35
M50	1,35	50%	1,35	8,10	1,35
M75	0,68	75%	2,03	8,10	1,35
M90	0,27	90%	2,43	8,10	1,35
Total	9,450		6,75	48,60	8,10

Cte: Concrete; **Ct:** Cement; **Sd:** Sand; **Gl:** Gravel and **Wr:** Water

3.2.2 Four points bending test on 4x4x16 cm prismatic test-tubes

The test was achieved according to EN 196-1 norm on a machine of 10 KN power and a speed of setting in load 50 N/s.

The test results are presented in table 9.

3.2.3 Compression test on prismatic test-tubes

The compression test on prismatic test-tubes was achieved according to NE P 15-45 norm [2], on the pieces obtained after the four points bending test. The press used was 150 KN power and the speed of setting in load was 2400 N/s.

The results tests are presented in table 10.

IV. Test results

4.1 On the concretes

4.1.1 Setting on the Abrams cone (consistency test results)

Table7: Consistency test results

Concrete	RC	C10	C25	C50	C75	C90
A in cm	3	3,5	2,5	2,5	2,5	2,0

4.1.2 Compression resistances on 16 x 32 cm cylindrical test-tubes

Table8: compression test Results on 16 x 32 cm cylindrical test-tubes

Concrete	compression Resistance (Mpa)
Ref.	13.43 ± 1.3
C10	12.41 ± 0.4
C25	9.77 ± 0.9
C50	5.15 ± 0.0
C75	3.20 ± 0.1
C90	0.96 ± 0.0

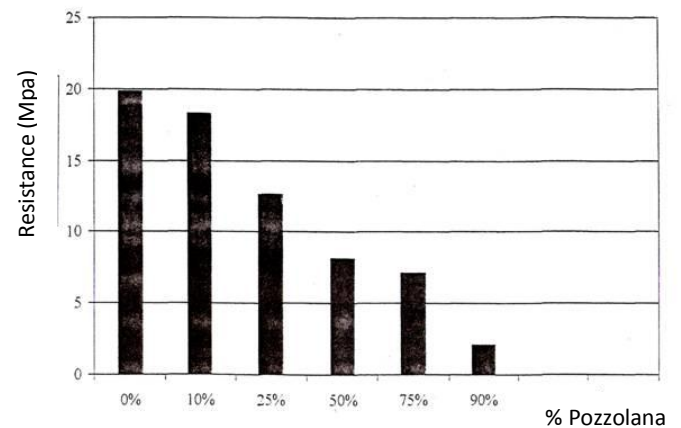


Figure2:strips diagram of thecompression resistances of the prisms according to their percentages in pozzolana.

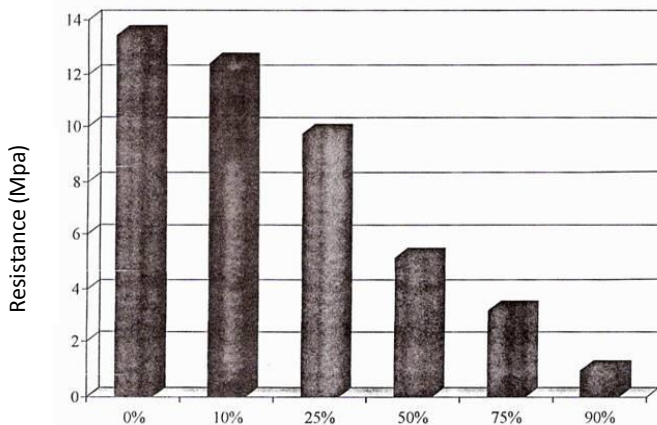


Figure 1:strips diagram of the compression resistances of the cylinders.

4.2 Test on mortars

Table 9: Four point bending test results on 4x4 x 16 cm prismatic test-tubes

Age	Mortars	Bendingresistance (at 28 days)
28 days	Reference	4,36
	M10	4,43
	M25	3,62
	M50	2,37
	M75	1,76
	M90	0,65

Table10:compression test Results on prismatic 4 x 4 x 16 cm test-tubes at 28 days

Mortars	Compression resistance (MPa)
Reference	19.87
M10	18.29
M25	12.62
M50	8.13
M75	7.14
M90	2.14

V. Resultsinterpretation

5.1 Observations on the cool concretes.

- The phenomenon of sweating was the more observed on the B25 concretes, B50, B75 and B90. It is essentially owed to the lack of the fine particles in the mixtures;
- The malleability of the concretes varies from hard for the reference concrete and B10 to very hard for the other concretes;

The presence of a whitish layer on the surface of the test-tubes after removal puts in inscription the insufficiency of the degree of pozzolanicity of the pozzolana used: a good quantity of free lime at the time of the hydration of the cement remained always free.

5.2 Observations on the hardened concretes.

The gray color of the test-tubes for pozzolana content up to 25% is an inheritance of the color and the proportion of the material used;

- The concretes having more than 50% pozzolana content resist less to the wear; they crumble easily to the finger;
- The relative presence of the pores on the pozzolanic concretes puts in inscription the accentuated character of the sweating phenomenon of the concretes evoked above.

5.3 Bending and compression test

The interest of the substitution by the pozzolana for the improvement of the resistances in bending is only observed at 10% of pozzolana. Beyond this value, one moves away more and more the values obtained on the reference concrete.

The gap of resistances obtained on identical test-tubes is not high.

Considering the bending test results (resistances), it is possible to envisage the substitution of the powder of the CPJ 35 cement by the one of the pozzolana of Djoungo in the order of 10 to 25% for works solicited in bending.

The compression tests don't present an increase of the resistance.

Until 25% of substitution, the resistances obtained are all upto:

- * 12.5 Mpa for the 4x4x16 cm prismatic test-tubes;
- * 9.5Mpa for the 16x32 cm cylinders.

This decrease of the compression resistances proves that the pozzolana didn't fully play its role that is at a time granular and pozzolanic [1]. It would be judicious to reinforce the grinding of the pozzolana.

VI. Conclusion

In the framework of the promotion of the use of the local materials in the construction in Cameroon, we studied the substitution of a part of cement by a powder of pouzzolane ground to 80 μm maximal diameters in the composition of the concrete and mortars. The main objective of these works was to analyze the influence of such a substitution on some mechanical properties of the concretes. The results obtained during the bending test show that a weak proportion (lower to 25%) of usual cement powder can be replaced by the one of pozzolana of Djoungo (Cameroon). The analysis of the compression resistance presents some values up to 12.5 Mpa for active substitutions until 25%. An increase of the compression resistance is not observed, what doesn't fill our waiting. The formulation of a concrete with ordinary cement basis, finely ground pozzolana and lime would complete the present research. Such a study would make appear the economic factor in the works of civil engineering and the factor time of drying (90, 180 and 240 days) of the test-tubes in the assessment of the resistances.

Références

- [1] Mbessa M., Rôle des ultrafines dans des bétons industriels à hautes performances. *Editions Universitaires Européennes*, 2011, 172 pages.
- [2] Dreux G., Guide pratique des bétons, *Presses de l'Ecole Nationale des Ponts ET Chaussées*, Paris, 1995.
- [3] Iyambe P., *Réactivité pouzzolanique des matériaux argileux ET étude des ciments de pouzzolane artificielle: cas de l'argile de Dibamba*. Mémoire de fin d'études ingénieur. Ecole Nationale Supérieure Polytechnique, Yaoundé, 1996
- [4] NdiguiBillong. *Investigations sur les propriétés pouzzolaniques de quelques déchets de briques et de tuiles cuites*. Mémoire DEA de chimie inorganique, Université de Yaoundé I, 2000.

Geological and Geotechnical Parameters Controlling Wall Paints Detachment at Selected XXVI Dynasty Tombs, Bahariya Oasis, Egypt

Shehata A. A.¹, G. M. E. Kamh², C.T. Oguchi³, R. A. Rabea⁴, S. S. M. El-Sayed⁵

1- Prof. of Conservation, Dept. of Restoration and Conservation, Faculty of Archaeology, Fayum University, Egypt

2- Prof. of Geoarchaeology, Geology Dept., Faculty of Science, Menoufiya University, Egypt

3- Associated Prof., Geosphere Research Institute, Saitama University, Japan

4- Restoration Authority, Ministry of Antiquities, Atfih, Egypt

5- Restoration Dept., Ministry of Antiquities, Egyptian Antiquities, Egypt

Abstract: Detection and semi-quantification of weathering processes acting on a given archaeological site is more than half way of stone's conservation to survive for longer decades or centuries revealing non-recovered part of nations' history. Bahariya Oasis in the heart of the Western Desert of Egypt has much recently discovered archaeological sites almost related to 26th Dynasty i.e. 2650 YBP. It still requires detailed studies on it regarding several fields of research among those are: weathering processes and intensity on wall paints of these sites.

The main aims of the current study is to find out the impact of bedrock's iron oxide content on wall paints of the structures excavated through it, and to semi-quantify damage category at the two , Badi Eshtar and Bannantiu, tombs under investigation that are related to 26th Dynasty at Bahariya Oasis. Detailed field survey including reporting and measuring weathering features' dimensions as well as air temperature and relative humidity inside and outside these sites in Winter and Summer Seasons have been conducted. Then, laboratory investigations including SEM, XRF, MIP and Ultrasonic waves have been applied on light and dark brown facies at these sites. The net result is moisture condensation inside these tombs particularly in summer as well as micro-pore size distribution, controlled by iron oxide concentration in this bedrock, with the aid of clay content resulted in rock's weathering ranging from Moderate to Very severe damage category at Badi Eshtar Tomb, and from Severe to Very Severe at Bannantiu Tomb.

Urgent controlling air temperature and relative humidity inside such excavations at Bahariya Oasis, and organized plan of paint's restoration are recommended for such unique rock art in the Western Desert of Egypt.

Keywords: Weathering of ancient wall paints, iron oxide content, field and laboratory studies, semi-quantification of damage category

I. Introduction

The archaeological sites are remains that reveal parts of nations' history that we have not lived yet. Weathering processes are among the very deleterious factors that partly or completely demolish such remains. They are acting either physically, chemically and/or biologically solely and/or in combination with different ranks of aggression based on the prevailing environmental conditions at a given area as well as rock's physical and geotechnical properties' limits (Elaine et al., 1992 and Salman et al., 2010). The damage category, especially for a given archaeological site, that can be defined using field and laboratory investigations (Kamh, 2007; Kamh and Azzam, 2008) is not only a result of stone's deterioration, starting from rock's surface grain's liberation up to detachment of mega rock parts via connected fractures or mechanical un-stability of the rock body, but also a factor of wall paints' damage that starts from degradation of original color intensity up to removal of this thin wall paints. It is unusual to find wall paints with its original color intensity, after few years in recent buildings or thousands of years for a given archaeological site, but almost experience fainting color's intensity and/or partial to complete demolishing of these paints.

Previous literatures in this field as well as actual field survey indicated that the ancient Egyptian wall paints, dated back even to the 4th Dynasty i.e. up to 4560 YBP., are highly stable in color's intensity over thousands of years (Shin and Frank, 1993 and Vendrell et al., 1996). Other natural and/or induced processes may result in degradation and/or demolishing of wall paints at a given archaeological site e.g. condensation of air moisture within excavations and semi-closed structures particularly if noticeable difference in air's temperature is recorded from outside to inside this site (Mustoe, 1983; Gauri et al., 1986; Gauri, 1990; Elaine et al., 1992; Waltham, 1993; Salman et al., 2010; Rudrich et al., 2011). The moisture condensation inside a given excavation can be also a result of huge number of tourists or visitors entering such semi-closed site. Air pollutants and/or biological excretions at such painted parts have also been reported as destructive agents to such paints (Salman et al., 2010). Rock's physical and geo-technical properties' limits are among the parameters that define its susceptibility to weathering including paints on it. Recently generated active cracks, particularly the interconnected ones, severely affect on rock's body with its paints through detachment of rock masses with paints on it (GSEGWP, 1977; Robinson and Williams, 1994). Salt weathering is widely recorded as damaging process even for highly durable rocks at a wide range of environments (Flatt, 2002; Angeli et al., 2007; Cardell et al., 2008; Swe and Oguchi, 2009). It acts through one or more mechanism based on salt's type and the prevailing environmental conditions in particular air's temperature and relative humidity (Fitzner and Heinrichs, 2002; Flatt et al., 2007).

Keeping these backgrounds in mind, the present study aims to find out the main reason(s) behind wall paints' detachment (with its holding rock body) and/or obliteration, also to semi-quantify damage category from the archaeological point of view considering Badi-Eshtar and Bannantiu Tombs of XXVI Dynasty (2650 YBP) as case studies at Bahariya Oasis, Western Desert, Egypt.

Geological setting and History of the Study area

Bahariya Oasis is, one of the ten depressions, setting in the heart of the Western Desert of Egypt at a distance of 365km South-west of Giza Governorate. Its capital is Bawiti town, and it has several natural water springs, plants and vegetations. This oasis is oval shaped with maximum length axis 90km running NE-SW direction, and maximum width 40km (Fig. 1). Its rock units are ranging in age from Upper Cretaceous to Oligocene (Said, 1990) and can be arranged from the oldest to the youngest as follows:

Bahariya Formation (Upper Cretaceous "Cenomanian age" 360m thick of alternative thin beds of fine to medium size glauconitic to ferruginous sand and silt, thin iron bands and glauconite can be traced).
 Heiz Formation (Upper Cretaceous "Turonian-Campanian age" unconformably overlying Bahariya Formation with angular unconformity. It is vuggy hard dolomitic beds with thickness up to 30m thick, it is acting as a cap rock for Bahariya Formation at some places of Bahariya Oasis).
 Hefhuf Formation (Upper Cretaceous "Campanian-Maastrichtian age" hard mottled dolomitic thick bed of 43m thick).
 Ain Giffara Formation (Upper Cretaceous "Maastrichtian age" Phosphatic Sandstone beds of 25m thick)
 Radwan Formation (Oligocene Basalt of 25m thick with columnar joints ended by pillow lava on it indicating marine volcanic origin, Unconformable lying on Bahariya Formation).

The historical remains, archaeological sites, at Bahariya Oasis have been recently discovered by chance on falling down one of the animals in a hole of sub-surface archaeological excavation. From that time, continuous and succeeding excavations and exploration of sub-surface structures as well as structures lying underneath sand-piles have been progressed. Bahariya Oasis has many and unique archaeological sites that almost related to 26th Dynasty "2650 YBP" of the Egyptian history. Great Alexander Temple, El-Meftalla Temple, Bannantiu Tombs, the Valley of Golden Monuments are among the very precious detections at Bahariya Oasis.

Bahariya Oasis is a rich field for geological studies regarding its rock units and/or Iron Ore mine "El-Gedida Mine", but it is still virgin for geo-archaeological and restoration studies. The only recorded geo-archaeological study at Bahariya Oasis is that conducted for examining weathering processes acting on Great Alexander and Meftalla Temples as well as Ged Amun Euf Ankh Tombs (Horiya, 2012). It indicated that salt weathering as well as wind blown with sand is almost the main weathering processes at these sites. These sites still require detailed studies to quantify damage category and modes of conservation particularly for wall paints that are considered as the first victim to weathering processes. The wall paints at these sites, represent the main document revealing part of the Egyptian history at Bahariya Oasis, suffer demolishing to pronounced limits that ring a high alarm for defining and quantifying damage categories and examining the best modes of its preservation.

II. Methodology

To achieve the aims of the current study, two sites namely Bannantiu and Badi-Eshtar Tombs (Figs. 1 – 3) have been selected to conduct detailed field and laboratory investigations on them to semi-quantify damage category for the painted walls at the Main Court of these tombs as well as to examine the main reason(s) behind deterioration of these wall paints.

1- Field Investigations

Detailed field description and measuring dimensions of weathering forms and apparent stone's color at painted parts experiencing obliteration have been conducted at these sites preceding the detailed laboratory investigations. This is to group weathering forms and preliminary semi-quantify damage category at these sites from the archaeological point of view using Fitzner and Heinrichs (2002) classifications, for grouping weathering forms and defining its damage category respectively, listed as follows:

Group 1: Loss of stone material (L.S.); includes back weathering represented by cavernous weathering, obliteration of inscriptions and wall paints.

Group 2: Discoloration/ Deposits (D.D.); includes loose salt deposits e.g. salt efflorescence, pollutants as black crust, biological colonization.

Group 3: Detachment (D.T.); includes separation of small or large size part of rock body in the form of granular disintegration "rock meal", scaling, exfoliation.

Group 4: Fissures / Deformation (F.D.); includes all types of fissures i.e. single, map and/or multiple cracks, also describes cracks' aperture width, tilting angel from the vertical and crack's density "number of cracks/square meter" for a given wall side.

After grouping of weathering forms at the study area and its tabulation, the damage category can be defined using Fitzner and Heinrichs (2002) classification:

Damage Category 0: No visible damage can be noted

Damage Category 1: Faint damage can be noted

Damage Category 2: Slight damage can be noted

Damage Category 3: Moderate damage can be noted

Damage Category 4: Severe damage can be noted

Damage Category 5: Very severe damage can be noted

But as this classification is not restricted with any limits or percentages for weathering forms, so, it has been modified in the current study to be more and widely applicable and precisely defines damage category regarding weathering forms listed in the four groups mentioned above. The modified classification of damage category can be presented as follows:

Damage Category 0: No visible damage can be recorded regarding stone's surface and/or its inscriptions and paints.

Damage Category 1: Very slight damage can be recorded i.e. rock body presents weathering forms that are grouped into D.D., D.T. and/or L.S. on its inscriptions and/or paints to less than 5% of the rock body area.

Damage Category 2: Slight damage category can be recorded i.e. rock body presents weathering forms that are grouped into D.D., D.T., L.S. and/or F.D on its inscriptions and/or paints at 5 to 10% of the rock body area.

Damage Category 3: Moderate damage category can be recorded i.e. rock body presents weathering forms that are grouped into D.D., D.T., L.S. and/or F.D. on its inscriptions and/or paints at 10 to 25% of the rock body area.

Damage Category 4: Severe damage category can be recorded i.e. rock body presents weathering forms that are grouped into D.D., D.T., L.S. and/or F.D. on its inscriptions and/or paints at 25 to 50% of the rock body area.

Damage Category 5: Very severe damage category can be recorded i.e. rock body presents weathering forms that are grouped into D.D., D.T., L.S. and/or F.D on its wall mass body and inscriptions only, as paints at D.C. 5 is almost totally demolished, at more than 50% of the rock body area.

On defining damage category for each part of the tombs under investigation regarding each weathering form, the overall damage category of each part considering all weathering forms can be defined using Damage Category including All Weathering forms' Scheme (DCAW) of Fitzner and Heinrichs (2002) that is only based on detailed measuring weathering forms' dimensions. This scheme reflects the degree of urgency and necessity of site's restoration if required.

Air temperature and relative humidity over four field trips to these sites, two times in each of Summer (June and July 2012) and Winter (January and February, 2012) Seasons, have been conducted using thermometer and humidity meter with two sensors for simultaneous measurements inside and outside each site. This is to find out one of the expected reasons of moisture's condensation inside these tombs if measurements proves this, the data will be used in the explanation of wall paints' deterioration at these sites.

2- Laboratory Investigations

Small rock samples had been collected at the parts presenting wall paints' deterioration, then, they have been prepared to cover the required analyses. Those parts used for SEM have been coated with gold and examined at high magnification of SEM (S-2400). Electron Dispersive X-ray (EDX) has been mainly used to check the yellow and brown color content of the collected rock samples as well as to define clay mineral type if noted within rock's texture.

For the geotechnical investigations for the collected rock samples, ultrasonic waves have been used. The rock samples have been prepared for investigation by magneto-structive ultrasonic waves' tool to measure the velocity of these waves

"Cp" in two directions at right angel to each other for the collected samples at these tombs, to find out rock's isotropism. Rock's internal friction "Qc" has also been measured as it reflects rock's porosity and weathering grade (Montoto et al., 1981). Both of Cp and Qc have been measured for the collected rock samples following Kapranos et al (1981) equations listed as follows:

$$[(A_o + A_t) / (A_o - A_t)] = X$$

$$(\pi n / Qc) = \{ \ln [2 / (1 - X)] \} / (1 + X)$$

$$Cp = 2 Lf / n$$

Where A_o and A_t are initial and steady magnitude of the ultrasonic waves; n is the mode number at which we get the best Echo-form for the waves; Qc is material's internal friction; Cp is the velocity of the ultrasonic waves; L is the sample's length "cm"; f is the frequency of the waves.

Rock and pore's properties have been considered in the current study as they had been reported to play an effective role in rock's deterioration and controls rock's susceptibility to weathering (Cardell et al., 2008). It has been conducted for the collected rock samples using MIP-5900 at conditions of low and high mercury pressure (31.04 psia to 33000 psia respectively) to get a measure for all samples' macro- and micro-pores.

The rock's natural moisture content has been measured for the collected rock samples, that had been stored in highly sealed plastic bags to keep its natural moisture content until measurements directly in the laboratory, following the method and equation of Robinson (1974) listed as follows:

Moisture content = $[(W_1 - W_2) / W_1] * 100$, where W_1 is sample's weight at field conditions, W_2 is oven totally dried sample at 105 °C for 24h.

III. Results

The following is a list of field and laboratory investigations conducted for the sites under investigation.

I- Field Investigations

Field investigations are recommended to be conducted as it is less expensive, quick and non-destructive technique for semi-quantitative definition of damage category for a given site (Fitzner and Heinrichs, 2002; Kamh, 2007; and Kamh and Azzam, 2008). The local environmental conditions and detailed description of weathering features are the pre-requests for explanation of weathering mechanism and semi-quantification of damage category at a given site respectively.

The local climatic conditions at the two tombs under investigation represented by temperature and relative humidity inside and outside these tombs had been measured two times in each of Summer and Winter Seasons (Table, 1). Pronounced temperature difference as well as relative humidity from outside to inside these tombs has been recorded particularly in Summer Season. The relative humidity is increased from outside to inside these tombs during Summer (Table, 1).

Table 1: Local climate at the tombs under investigation

Location	Site name	Type	Year and Season	Month	Local Climate inside tombs		Local climate outside tombs	
					Average Temp. C	Average Rh %	Average Temp. C	Average Rh %
Bahariya Oasis	Badi Eshtar Tomb	Rock Art	Winter 2012	Jan.	15	40	12	55
				Feb.	17	39	14	52
			Summer 2012	June	17	66	40	30
				July	18	69	42	29
	Bannantiu Tomb		Winter 2012	Jan.	19	39	18	50
				Feb.	20	40	17	48
			Summer 2012	June	18	67	40	31
				July	19	66	41	30

The sites under investigation suffer weathering including wall paints and its holding bedrock (Fig. 4). Semi-quantification of damage category regarding each weathering form (considering the main court) at each site has been defined using the modified scale of Fitzner and Heinrichs (2002) and weathering forms' dimensions listed in table (2). The overall damage category for the painted walls in the Main Court of each site has been defined considering all weathering forms together using DCAW Scheme (Figs. 5 and 6). It has been indicated that the damage category at Badi Eshtar Tomb ranges from Moderate (at parts with light brown facies "at samples numbers 3 and 4", Fig. 5) to Very severe damage category (at parts with dark brown facies "at samples numbers 1 and 2", Fig. 5). On the other hand, at Bannantiu Tomb, it ranges from Severe (at parts with light color facies "at samples numbers 7 and 8", Fig. 6) to Very severe damage category (at parts with dark brown facies "at samples numbers 5 and 6", Fig. 6). The main reason behind this difference in DC at both tombs will be explained with the detailed laboratory analysis, in the discussion section, conducted for rock samples collected at these tombs.

II- Laboratory Investigations

Detailed laboratory investigations have been conducted on the rock samples collected at light and dark brown color parts representing the bedrock through which these sites had been excavated. This is to examine rock's weathering on micro-scale, clay content and relative difference in elemental composition of these facies that might throw light on the main reason(s) behind deterioration of this bedrock with its wall paints particularly at the dark facies compared with the light color one. The bedrock's geotechnical properties and natural moisture content for the two types of facies have also been measured.

II-1- Micro-petrographic investigation

Two rock samples at each site (one at each of light and dark brown color facies) have been scanned using SEM (S-2400). Great similarity and matching have been noted in texture and mineralogy at both tombs as they had been excavated in the Bahariya Formation and nearly at the same sector of this rock unit. The facies can be identified as fine to very fine sandstone and siltstone with kaolinite and smectite cement either at the light and/or dark brown parts of this bedrock (Figs. 7 and 8). Iron oxide spheres are almost noted in the dark brown samples rather than the light color samples at these sites (Fig. 9). K-feldspar and kaolinite presents deformation and/or loosing cohesion among its lattice and flakes (Figs. 7 and 8).

II-2- Elemental analysis

It has been recommended to be conducted for numerical elemental quantification and identification to specifically differentiate between the light and dark brown facies that hold paints suffering demolishing, the results are listed in table (3). It is clearly noted that SiO₂ represents the main component of these facies as it is siliceous rock in sand and/or silt size. Iron oxide represents a considerable percentage of rock's elemental composition with higher percentages for dark brown facies than light color facies (Table, 3). Other elemental components e.g. Oxides of Al, K are components of clay minerals.

II-3- Geotechnical properties and Natural moisture content

The ultrasonic waves has been widely used as a non-destructive technique to reflect the geotechnical properties of a given material including rocks i.e. semi-quantitatively defines its porosity level that is in an inverse proportional relation with the velocity of these waves "Cp" on one hand, and in a direct proportional relation with rock's internal friction "Qc" on the other hand (Calleja et al., 2000). In the current study, the light as well as dark brown facies have the same mineralogical composition with exception of iron oxide concentration in both (Table, 3), this might affect on rock's geotechnical limits, consequently, this technique has been applied for both facies using the collected rock samples to find out this difference if recorded. The sample's preparation and parameters computation have been conducted following Kapranos et al (1981) method and equations, the data are listed in table (4). A noticeable difference in rock's geotechnical properties limits can be noted from light to dark brown color parts at this bedrock particularly at Bannantiu Tomb; also the bedrock is an-isotropic particularly for the dark brown facies at both tombs and the light brown facies at Bannantiu Tomb

(Table, 4) compared with light color facies at Badi Eshtar Tomb. This an-iso-tropism might be a result of iron oxide concentration (Table, 3) within these facies (Fig. 9) particularly along its lamina

Table 2: Weathering features and damage category at the dark and light brown facies for the tombs under investigation

Site type	Weathering feature, its Group and its Damage Category						
	Group 1 (Loss of Stone material, L.S.)		Group 3 (detachment, D.T.)				Group 4 (Fissures / D.
	Paints Obliteration	D.C. of L.S. (DCLS)	Rock Detachment (D.T.)	D.C. of D.T. (DCDT)	Rock meal (D.T.)	D.C. of D.T. (DCDT)	Cracks type and density
		Main Court		Main Court		Main Court	
Rock Art	12% of wall area	3	8% of wall area at cracked parts with its paints	2	Rock powdering covering an area 9%	2	Single to multiple Connect cracks of average length 0.1cm aperture width covering 10% of wall side
	25% of wall area	4	6% of wall area at cracked parts with its paints	2	Rock powdering covering an area 27%	4	Single to multiple Connect cracks of average length 0.1cm aperture width covering of wall area
Rock Art	16% of wall area	3	4% of wall area at cracked parts with its paints	1	Rock powdering covering an area 9%	2	Single connected cracks of average length 0.75m and aperture width covering 11 wall area
	30% of wall area	4	12% of wall area at cracked parts with its paints	3	Rock powdering covering an area 32%	4	Single to multiple cracks of average length 0.75m and aperture width covering 19 wall area

N.B. L.S. is Group "1" Loss of Stone material; D.T. is Group "3" Detachment of stone material; F.D. is Group "4" Fissures/Deformation

Table 3: X-ray Fluorescence analysis for eight rock samples collected at the tombs under investigation

Location	Site name	Type	Sample No.	Sample color	Elemental Oxide %						
					CaO	SiO2	FeO	K2O	Al2O3	SO2	MnO
Bahariya Oasis	Badi Eshtar Tomb	Rock Art	1	Dark Brown	0.32	76.71	13.02	2.14	1.79	0.69	5.33
			2		0.91	73.02	16.34	1.99	2.56	1.06	4.12
			3	Light Brown	0.06	82.07	1.06	3.86	4.02	1.98	5.95
			4		0.99	85.22	1.11	2.86	3.23	1.58	4.01
	Bannantiu Tomb		5	Dark Brown	0.73	71.75	15.02	2.55	3.04	1.43	5.48
			6		1.03	70.34	16.23	1.95	2.63	0.88	6.94
			7	Light Brown	0.54	83.27	6.12	1.67	3.02	0.77	9.68
			8		0.87	82.97	5.81	1.43	2.89	1.07	8.71

Table 4: Geotechnical properties and Natural moisture content measured for eight rock samples collected at the tombs under investigation

Location	Site name	Type	Sample No.	Sample color	Geotechnical Properties				Rock's Natural Moisture Content %	
					Cp1 “Km/Sec”	Cp2 “km/sec”	Isotropism “Cp1/Cp2”	Qc	Winter	Summer
Bahariya Oasis	Badi Eshtar Tomb	Rock Art	1	Dark	2.26	2.01	1.12	7.20	10.40	14.30
			2	Brown	2.21	2.00	1.11	6.80	11.20	13.80
			3	Light	1.95	1.89	1.03	9.12	7.92	9.12
			4	Brown	1.91	1.88	1.02	9.07	7.88	9.64
	Bannantiu Tomb		5	Dark	2.22	2.03	1.09	6.91	11.60	14.90
			6	Brown	2.24	2.02	1.11	6.71	10.90	14.80
			7	Light	2.02	1.85	1.09	8.62	8.30	9.98
			8	Brown	2.05	1.87	1.10	8.37	8.20	10.57

N.B. Cp1 and Cp2 are velocity of the ultrasonic waves measured parallel to and at right angel to lamination respectively; Qc is rock's internal friction, and Ed is rock's elastic modulus

For detailed investigation and differentiation in rock and pore's properties at the two facies under investigation, MIP has been used, the results are listed in table (5) and the pore size distribution for the two facies at both tombs is graphically presented in figures (10 and 11). Lower values of total porosity, mean pore diameter and total pore area can be noted for dark facies compared with light color facies and vise versa for skeletal density (Table, 5). Pronounced matching in pore properties can be recognized in pore size (radius) distribution as graphically presented from MIP data particularly for dark color facies (Figs. 10 and 11). The Incremental Pore Volume "IPV" data indicates slightly lower values for dark facies compared with light color facies (Table, 6), this might be a result of filling rock pores partially with iron oxide spheres. The micro-porosity has been analyzed to find out the critical pore size or pore size's range at which salt weathering and/or rock's water sorption reaches to maximum limit based on previous literatures (Angeli et al., 2007; Swe and Oguchi, 2009), the percentage of each pore radii range in the examined samples is listed in table (6). This will clarify the reason(s) behind higher damage at dark facies with its wall paints compared with light color facies. On measuring natural moisture content in the two facies during Summer and Winter seasons, it can be noted higher moisture content (%) recorded for samples collected in Summer Season compared with same facies but collected in Winter Season on one hand; and for dark brown facies compared with light color one at the same season on the other hand (Table, 4).

Table 5: Rock pore properties for the samples collected at the sites under investigation using MIP-5900

Location	Site name	Site Type	Sample No.	Sample color	Rock and Pore Properties			
					TPA “m ² /g”	MPD (area) “in micron”	Skeletal density “g/mL”	Total porosity (%)
Bahariya Oasis	Badi Eshtar Tomb	Rock Art	1	Dark	0.032	0.0399	2.450	18.004
			2	Brown	0.031	0.0376	2.420	19.213
			3	Light	2.636	2.1975	2.274	25.196
			4	Brown	2.629	2.1971	2.199	25.321
	Bannantiu Tomb		5	Dark	0.033	0.0399	2.540	18.373
			6	Brown	0.321	0.0395	2.440	19.342
			7	Light	1.342	0.1874	2.355	23.520
			8	Brown	1.289	0.1906	2.328	22.970

N.B. TPA is Total Pore Area; MPD is Mean Pore Diameter;

IV. Discussion

Weathering of a given material is a matter of physical, chemical and/or biological disintegration and/or decomposition of its components. The product is either similar to the original mass but only fragmented probably from boulder to powder size i.e. physical damage, or partly to totally different in composition from the main rock i.e. chemical alteration. The severity of weathering particularly for a given archaeological site is not only a matter of debris volume detached from the main rock mass but also defined by the area and/or mass of the rock mass affected by this weathering particularly those parts holding inscriptions and/or paints that reveal part of ancient history for a given nation (Alison and Heritage, 2007 and Zehnder, 2007). Definition of weathering processes, mechanism(s) and semi-quantification or quantification (if possible) of damage category, all are of value for urgent decisions regarding conservation of a given site. Holding these points into mind, the current study has been conducted on two out of many excavations (rock art) at Bahariya Oasis that still virgin in the field of archaeological excavations and receives less attention for such sort of studies. At the study area, a noticeable difference in temperature from out-door to in-door of these tombs has been recorded particularly in Summer time (Table, 1), this has led to moisture condensation into these tombs particularly in Summer

season where the full situation is reversed regarding relative humidity in Winter season (Table, 1). Based on the modified scale of Fitzner and Heinrichs (2002), the damage category regarding each weathering form at the dark and light color facies for the main court of each tomb has been specified (Table, 2). Then, semi-quantification of overall damage category considering all weathering features has been defined using "DCAW" Scheme of Fitzner and Heinrichs (2002) and plotting D.C. of each group (Table, 2) on this scheme (Figs. 5 and 6). Noticeable difference in overall damage category can be noted from dark brown facies to light brown one in the same tomb e.g. it is moderate and very severe for the light and dark facies at Badi Eshtar Tomb respectively, and severe to very severe for the light and dark facies at Bannantiu Tomb (Figs. 5 and 6) respectively. Binary relationship has been drawn between overall damage category and FeO% for the samples representing light and dark brown facies (Fig. 12). Direct proportional relation has been noted with correlation coefficient $R^2 = 0.5086$, it can be considered as pronounced correlation coefficient but the reason behind its relatively low value is that FeO% in the four samples representing dark facies at the two tombs is nearly the same (Table 3). The net result of this binary relation is that FeO% is an effective factor in rock's susceptibility to weathering. But now, the questions have been raised, how is FeO% content controls rock's susceptibility to weathering?, and is FeO% a deleterious factor on rock's components?.

To answer these two questions, the rock's pore size distribution as well as its natural moisture content measured for eight rock samples representing the facies under investigation (Tables 6 and 4 respectively) in combination with rock's FeO% and pore properties (Tables 3 and 5 respectively) indicate the following two points: (1) as iron oxide percentage increases, the pore diameter, pore area and incremental pore volume as well as rock's iso-tropism are decreased, consequently, rock's total porosity is reduced and its weathering susceptibility is increased if the rock has high percentage of micro-pores with critical pore radii, (2) at critical pore radii value or range that can be defined in this case study to be ranging from 0.1 to 1.0 micron, the rock's sorption for moisture or water is noticeably increased and this is clear in table (4) for the dark brown facies, at both tombs, that has higher percentage of pore radii ranging from 0.1 to 1.0 micron than light brown facies particularly at Badi Eshtar Tomb (Table 6, Fig. 11). At the same time, light color facies at Bannantiu Tomb has relatively higher FeO% than that at Badi Eshtar Tomb (Table, 3), consequently, the pore size distribution is limited to less than 1.0 micron for the former and so, the wall paints at this facies suffers severe DC (Fig. 6). The pore size distribution for light brown facies at Bannantiu Tomb enables more sorption for air moisture compared with that of Badi Eshtar Tomb (Table, 4), consequently, higher DC is recorded for the former than that of the later (Figs. 6 and 5 respectively). Correlating FeO% at the facies under investigation with each of natural moisture content (Table 4), rock's iso-tropism (Table, 4), rock and pore properties as well as pore size distribution (Tables, 5 and 6 respectively) and the overall DC (Figs. 5 and 6), it can be then confirmed with high confidence that FeO% content controls rock's susceptibility to weathering (Fig. 12) by limitation of pore radii to critical pore volume that increases rock's sorption capacity. This high sorption capacity in combination with rock's clay (particularly smectite) content resulted in weakening rock's components cohesion force i.e. it is altered to friable or non coherent material and probably create and/or activate cracks on both micro and mega-scale that may result in detachment of small or big rock masses from the main rock body. It must be kept in mind that the direct proportional relation between FeO% and rock's DC is not absolute where if FeO% is increased above certain limit, then the rock may have high percentage of micro or nano-pores that are not effective in sorption of water molecules and/or salt solutions (Angeli et al, 2007; Benavente et al., 2007).

The probability of salt weathering to be one of the factors responsible for rock's deterioration at the study area is negligible where rock's CaO% as well as SO₂% (for creating sulfate salt) content is very low (Table 3). But in case of reaching salt(s) with salt solution to such bedrock particularly the dark color facies, it is expected to be very deleterious as this pore radii is critical for severe salt crystal growth by crystallization and /or hydration (Flatt, 2002; Cardell et al., 2008; Swe and Oguchi, 2009).

The wider range of pore radii at light brown facies at Badi Eshtar Tomb (≤ 2.5 micron, Table, 6) associated with less FeO% content (i.e. became widely distributed around the critical pore radii "1.0 to 0.1 micron") compared with that range of light brown facies at Bannantiu Tomb with noticeably high FeO% content (i.e. became closely distributed around the critical pore radii, Table 6) resulted in Moderate Overall DC for the former compared with the Severe Overall DC for the later. Conclusively, the FeO% even in the light color facies resulted in noticeable difference in rock's pore radii, consequently, the rock's sorption capacity differed (Table, 4) and so, the overall DC is noticeably varies (Figs. 5 and 6). Although the equality in overall DC for the dark facies at the two tombs (DC=5, Figs. 5 and 6), but this DC slightly differs from each other where it is relatively with higher rank at Bannantiu Tomb compared with Badi Eshtar Tomb, the reason behind that is the damage category Group 3 (DCDT) where the wall area (%) affected by detachment at the former tomb is more than that at the later (Table, 2).

V. Conclusion

The facies under investigation are so similar in mineralogy and elemental composition with exception of iron oxide content that enable its differentiation into two sub-facies. The geotechnical properties' limits and pore size distribution, at the two tombs, are highly matching together particularly for the dark brown facies. The dark facies are expected to be with better geotechnical properties' limits than light color ones, but the pore size distribution that ranges (with higher percentages in the dark facies than light color one) from 0.1 micron to 1.0 micron enables moisture capturing in the pores of the dark facies than light color one. The clay (smectite and kaolinite) content particularly in the dark facies combined with moisture content presents more damage (rock meal and activation of fractures) for it rather than for light color facies. The end result is more demolishing of wall paints at dark facies than light color one. Conclusively, iron

oxide content at Bahariya facies has a pronounced impact on rock's pore size distribution that is ended by higher damage category for dark facies with its wall paints than at light color (less in iron oxide content) one.

Table 6: Pore size distribution and Incremental Pore Volume for the collected rock samples

Location	Site name	Site Type	Sample No.	Sample color	Percentage of Pore Size Distribution and Incremental Pore Volume (mL/g)								
					<0.05 μm	0.05 – 0.1 μm	0.1 – 0.5 μm	0.5 – 1.0 μm	1.0 – 2.5 μm	2.5 – 5.0 μm	> 5.0 μm	IPV “mL/g”	
Bahariya Oasis	Badi Eshtar Tomb	Rock Art	1	Dark Brown	0.000	4.8000	33.920	48.540	6.200	1.360	6.617	0.1160	
			2		0.000	4.6900	33.760	48.930	6.220	1.036	6.494	0.1166	
			3	Light Brown	12.160	8.6100	29.360	23.920	15.620	4.060	6.280	0.1230	
			4		10.880	9.9000	29.450	23.990	16.561	3.920	5.305	0.1226	
	Bannanti u Tomb		5	Dark Brown	0.000	4.800	33.850	49.610	5.215	1.370	6.624	0.1161	
			6		0.000	4.6100	33.267	49.730	6.090	1.340	6.380	0.1187	
			7	Light Brown	18.040	28.720	22.490	13.030	4.521	3.920	9.260	0.1224	
			8		26.030	25.720	18.530	13.020	3.510	3.920	9.280	0.1225	

N.B. IPV is Incremental Pore Volume

VI. Acknowledgement

The authors are deeply grateful to SU, Japan for conducting MIP analysis as well as SEM required for this research. Also, they are appreciating the comments and language reading and corrections by Dr. Heather Allison, MRI, UK.

References

- Alison, S. and A. Heritage, 2007: Evaluating the influence of mixture composition on the Keinetics of salt damage in wall paintings using time Laps Video Imaging with the direct data annotation. *Environmental Geology*, V. 52, P. 303 – 315.
- Angeli, M.; J. P. Bigas; D. Benavente; R. Hebert and C. David, 2007: Salt crystallization in pores: quantification and estimation of damage. *Environmental Geology*, V. 52, P. 205 – 213.
- Benavente, D.; N. Cueto; J. Martinez; M. A. Cura and J. C. Canaveras, 2007: The influence of petrophysical properties on the salt weathering of porous building rocks. *Environmental Geology*, V. 52, P. 215 – 224.
- Calleja, L.; M. Montoto; B. Perez and B. M. Villar, 2000: An Ultrasonic method to analyze the progress of weathering during cyclic salt crystallization tests. *Proceedings of the 9th International Congress on Deterioration and Conservation of Stone*, June 19 – 24, 2000, Amsterdam, Elsevier, 313 – 318.
- Cardell, C.; D. Benavente and J. R. Gordillo, 2008: Weathering of limestone building material by mixed sulfate solutions, characterization of stone micro-structure, reaction products and decay forms. *Material characterization*, V. 59, P. 1371 – 1385.
- Elaine, S.; G. M. McGee; and G. Victor, 1992: Gypsum accumulation on carbonate stone. *Atmospheric Environment*, V. 26B (2), P. 249 – 253.
- Fitzner, b. and K. Heinrichs, 2002: Damage diagnosis on stone monuments- weathering forms, damage categories and damage indices. *Understanding and Managing stone decay*, Prikryl and Viles "eds.", The Karolinum Press, 11 – 56.
- Flatt, R. J., 2002: Salt damage in porous materials: how high supersaturations are generated. *J. Crystal Growth*, V. 242, P. 435 – 454.
- Flatt, R. J.; M. Steiger and G. W. Scheere, 2007: A commented translation of the paper by C. W. Correns and W. Steinborn on crystallization pressure. *Environmental Geology*, V. 52, P. 187 – 203.
- Gauri, K. L.; C. H. George and C. V. Willard, 1986: Cleaning efflorescence from Masonry. *ASTM*, J.R. Clifton “ed”, P. 3 – 13.
- Gauri, K. L., 1990: Decay and preservation of stone in modern environments. *Environmental Geology and Water Science*, V. 15 (1), P. 45 – 54.
- Geological Society Engineering Group Working Party, 1977: The description of rock masses for engineering purposes. *QJEG*, V. 10, P. 355 – 388.

13. Horiya, M. A., 2012: Quantified damage category of some Pharaonic archaeological sites at Bahariya Oasis, Western Desert, Egypt, and Examining their modes of restoration. MSc thesis, Fac. of Sci., Menoufiya Univ., Egypt, Unpublished.
14. Kamh, G. M. E., 2007: Field and laboratory investigations of damage intensity of the Upper Cretaceous monumental sandstone of Dendara Temple, Upper Egypt, a Case study. International Journal for Restoration of Buildings and Monuments, V. 13 (5), P. 331 - 354.
15. Kamh, G. M. E. and R. Azzam, 2008: Field and laboratory investigations to examine the damage category of monumental sandstone in arid regions: Seti I Temple, Upper Egypt, a case study. Int. Journal for Restoration of Buildings and Monuments, V. 14 (3), P. 179 – 196.
16. Kapranos, P. A.; M. H. A. Al-Helaly and V. N. Whittaker, 1981: Ultrasonic velocity measurements in 316 Austenitic Weldments. British Journal of Non-destructive Testing, V. 23 (6), P. 211 – 222.
17. Montoto, M.; L. Callega; B. Perez and R. M. Esbert, 1981: Evaluation in situ of the state of deterioration of monumental Stones by non-destructive ultrasonic techniques. Mat. Res. Soc. Symp. Proc. 1981, V. 185, P. 273 – 284.
18. Mustoe, G. E., 1983: Cavernous weathering in the Capitol reef desert, UTAH. Earth Surface Processes and Landforms, V. 8, P. 517 – 526.
19. Robinson, D. A., 1974: A note on the expression of soil moisture content. J. Area, V. 6; P. 9 – 13.
20. Robinson, D. A. and R. B. G. Williams, 1994: Sandstone weathering and landforms in Britain and Europe. Rock Weathering and Landform Evolution, Robinson and Williams “eds”, P. 371 – 389.
21. Rudrich, J.; T. Bartelsen; R. Dohrmann and S. Siegesmund, 2011: Moisture expansion as a deterioration factor for sandstone used in buildings. Environmental Earth Sciences, V. 63, P. 1573 – 1586.
22. Said, R., 1990: The Geology of Egypt. Rotterda: Balkema, P. 734.
23. Salman, A. B.; F. M. Howari; M. M. El-Sankary; A. M. Wali and M. M. Saleh, 2010: Environmental impact and natural hazards on Kharga Oasis monumental sites, Western Desert of Egypt. Journal of African Earth Sciences, V. 58, P. 341 – 353.
24. Shin, M. and P. Frank, 1993: Environmental monitoring at the Tomb of Nefertari. The Getty Conservation Institute, 4503 Glencoe Avenue, Marina del Rey, CA 90292- 6537 USA), ICOM Committee for conservation, P. 616 – 622.
25. Swe, Y.; and C. T. Oguchi, 2009: Complex relationship between salt type and rock properties in a durability experiment of multiple salt-rock treatments. Earth Surface Processes and Landforms, V. 34, P. 2096 – 2110.
26. Vendrell, M. S.; M. Garcia-valles and S. Alarcon, 1996: Environmental impact on the Roman monuments of Tarragona, Spain. Environmental Geology, v. 27, P. 263 – 269.
27. Waltham, A. C., 1993: Crown hole development in the sandstone caves of Nottingham. QJEG, V. 26, P. 243 – 251.
28. Zehnder, K., 2007: Long-term monitoring of wall paintings affected by soluble salts. Environmental Geology, V. 52, P. 353 – 367.
- 29.



N.B. 1 is Badi Eshtar Tomb, 2 is Bannantiu Tomb

Figure 1: Map of Bahariya Oasis with location of the sites under investigation

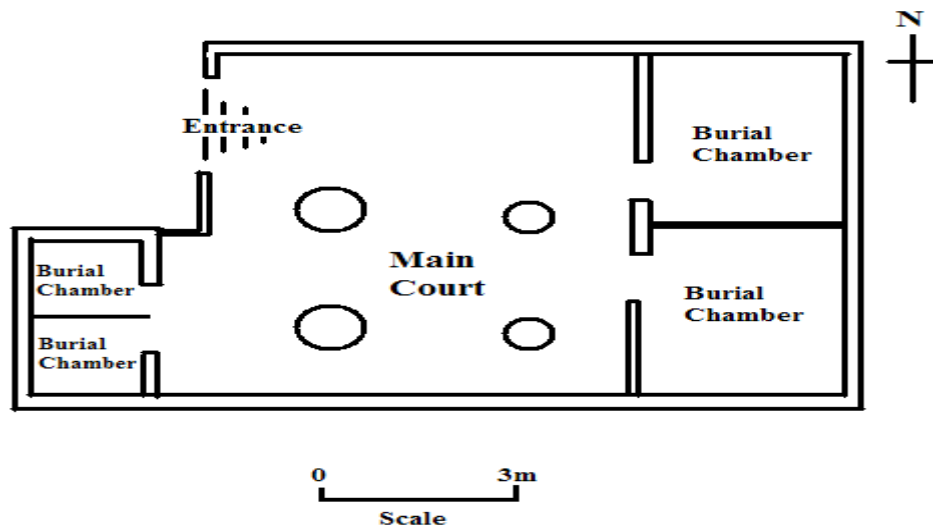


Figure 2: Sketch diagram of Bannantiu Tomb, Bahariya Oasis, Egypt.

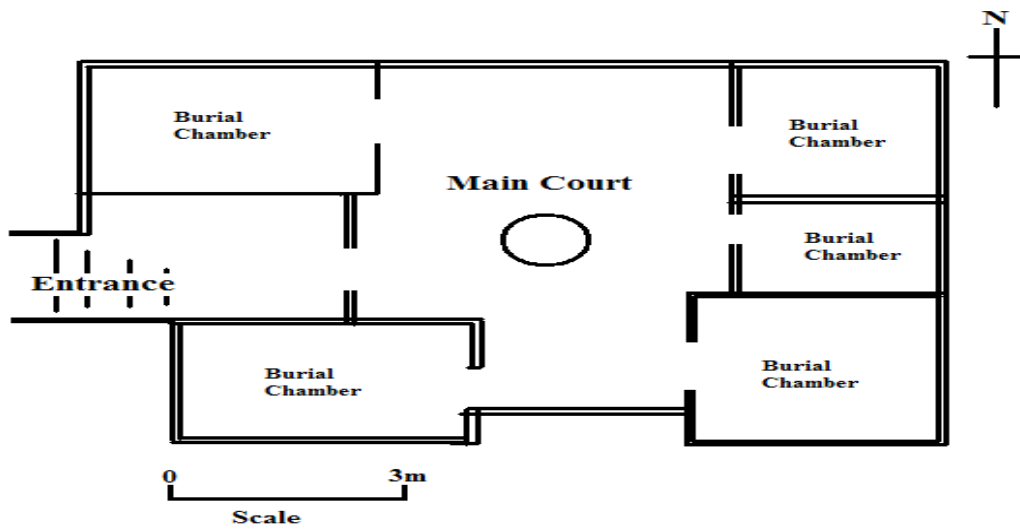


Figure 3: Sketch diagram of Badi Eshtar Tomb, Bahariya Oasis, Egypt

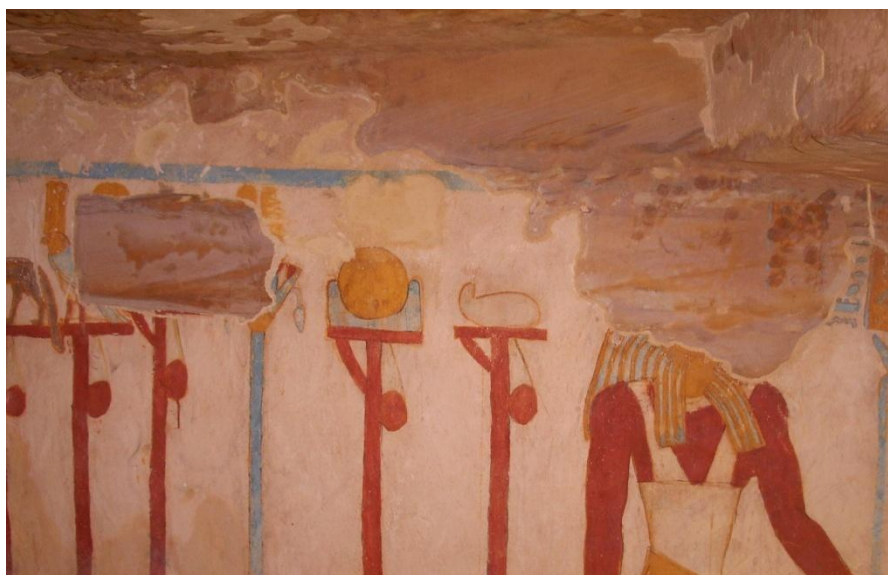


Figure 4: Obliteration of wall paints at dark brown ferruginous facies of the bedrock at Bannantiu Tomb, Bahariya Oasis, Egypt.

		DCDD													
		0			1			2			3				
		4	4	5	4	4	5	4	4	5	4	4	5		
DCLS	0	4	4	5	4	4	5	4	4	5	4	4	5	4	
		3	3	4	3	3	4	3	3	4	3	3	4	3	
		2	2	3	2	2	3	2	2	3	3	3	3	2	
		1	2	3	2	2	3	2	2	3	3	3	3	1	
		0	2	3	2	2	3	2	2	3	3	3	3	0	
	1	4	4	5	4	4	5	4	4	5	4	4	5	4	
		3	3	4	3	3	4	3	3	4	3	3	4	3	
		2	2	3	2	2	3	2	2	3	3	3	3	2	
		1	2	3	2	2	3	2	2	3	3	3	3	1	
		1	2	3	2	2	3	2	2	3	3	3	3	0	
	2	4	4	5	4	4	5	4	4	5	4	4	5	4	
		3	3	4	3	3	4	3	3	4	3	3	4	3	
		2	3	3	3	3	3	2	3	3	3	3	3	2	
		2	2	3	2	2	3	2	2	3	3	3	3	1	
		2	2	3	2	2	3	2	2	3	3	3	3	0	
	3	5	5	5	5	5	5	5	5	5	5	5	5	4	
		4	4	5	4	4	5	4	4	5	4	4	5	3	
		3	3	4	3	3	4	3	3	4	3	3	4	2	
		3	3	4	3	3	4	3	3	4	3	3	4	1	
		3	3	4	3	3	4	3	3	4	3	3	4	0	
	4	5	5	5	5	5	5	5	5	5	5	5	5	4	
		5	5	5	5	5	5	5	5	5	5	5	5	3	
		4	4	5	4	4	5	4	4	5	4	4	5	2	
		4	4	5	4	4	5	4	4	5	4	4	5	1	
		4	4	5	4	4	5	4	4	5	4	4	5	0	
	5	5	5	5	5	5	5	5	5	5	5	5	5	4	
		5	5	5	5	5	5	5	5	5	5	5	5	3	
		5	5	5	5	5	5	5	5	5	5	5	5	2	
		5	5	5	5	5	5	5	5	5	5	5	5	1	
		5	5	5	5	5	5	5	5	5	5	5	5	0	
		0	2	3	0	2	3	0	2	3	0	2	3		
		DCFD													

N.B. DCAW is Damage Category including All Weathering Forms

3	Main Court, Light Brown facies	DCLS	Is Damage category regarding Loss of Stone material
		DCDD	Is Damage Category regarding Discoloration / Deposition
5	Main Court, Dark Brown facies	DCDT	Is Damage Category regarding Detachment
		DCFD	Is Damage Category regarding Fissures/Deformation

Figure 5: DCAW of Fitzner and Heinrichs "2002" for semi-quantification of damage category at the Main Court of Badi Eshtar Tomb, Bahariya Oasis.

		DCDD													
		0			1			2			3				
DCLS	0	4	4	5	4	4	5	4	4	5	4	4	5	4	
		3	3	4	3	3	4	3	3	4	3	3	4	3	
		2	2	3	2	2	3	2	2	3	3	3	3	2	
		1	2	3	2	2	3	2	2	3	3	3	3	1	
		0	2	3	2	2	3	2	2	3	3	3	3	0	
	1	4	4	5	4	4	5	4	4	5	4	4	5	4	
		3	3	4	3	3	4	3	3	4	3	3	4	3	
		2	2	3	2	2	3	2	2	3	3	3	3	2	
		1	2	3	2	2	3	2	2	3	3	3	3	1	
		1	2	3	2	2	3	2	2	3	3	3	3	0	
	2	4	4	5	4	4	5	4	4	5	4	4	5	4	
		3	3	4	3	3	4	3	3	4	3	3	4	3	
		2	3	3	3	3	3	2	3	3	3	3	3	2	
		2	2	3	2	2	3	2	2	3	3	3	3	1	
		2	2	3	2	2	3	2	2	3	3	3	3	0	
	3	5	5	5	5	5	5	5	5	5	5	5	5	4	
		4	4	5	4	4	5	4	4	5	4	4	5	3	
		3	3	4	3	3	4	3	3	4	3	3	4	2	
		3	3	4	3	3	4	3	3	4	3	3	4	1	
		3	3	4	3	3	4	3	3	4	3	3	4	0	
	4	5	5	5	5	5	5	5	5	5	5	5	5	4	
		5	5	5	5	5	5	5	5	5	5	5	5	3	
		4	4	5	4	4	5	4	4	5	4	4	5	2	
		4	4	5	4	4	5	4	4	5	4	4	5	1	
		4	4	5	4	4	5	4	4	5	4	4	5	0	
	5	5	5	5	5	5	5	5	5	5	5	5	5	4	
		5	5	5	5	5	5	5	5	5	5	5	5	3	
		5	5	5	5	5	5	5	5	5	5	5	5	2	
		5	5	5	5	5	5	5	5	5	5	5	5	1	
		5	5	5	5	5	5	5	5	5	5	5	5	0	
		0	2	3	0	2	3	0	2	3	0	2	3		
		DCFD													

N.B. DCAW is Damage Category including All Weathering Forms

4	Main Court, Light Brown facies	DCLS	Is Damage category regarding Loss of Stone material
		DCDD	Is Damage Category regarding Discoloration / Deposition
5	Main Court, Dark Brown facies	DCDT	Is Damage Category regarding Detachment
		DCFD	Is Damage Category regarding Fissures/Deformation

Figure 6: DCAW of Fitzner and Heinrichs "2002" for semi-quantification of damage category at the Main Court of Bannantiu Tomb, Bahariya Oasis.

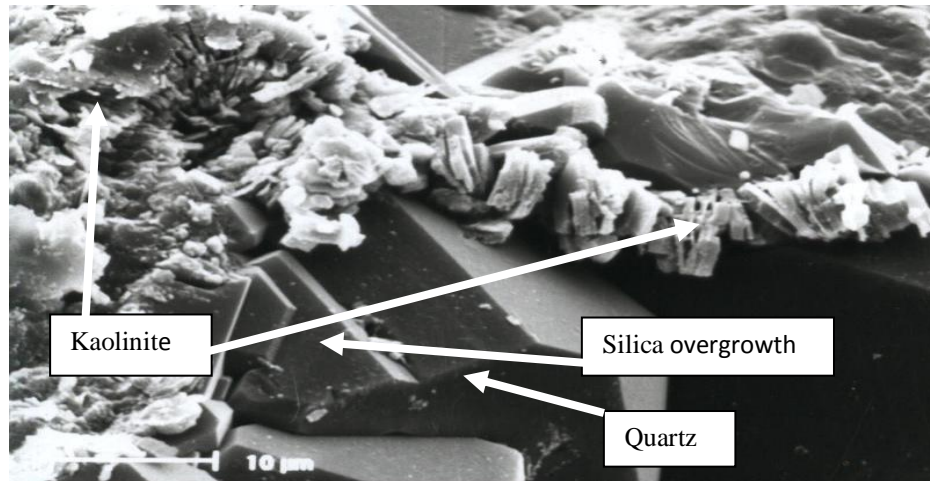


Figure 7: Representative Scanning electron photo-micrograph presenting components of rock sample collected at Badi-Eshtar and Bannantiu Tombs, quartz with silica overgrowth and kaolinite can be noted.

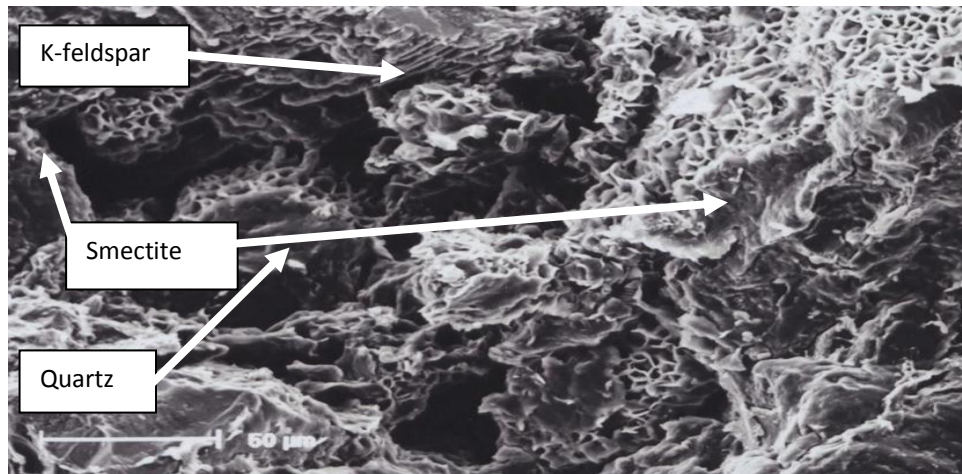


Figure 8: Representative Scanning electron photo-micrograph presenting Quartz, K- feldspar and Smectite for a rock sample collected at the bedrock of Badi-Eshtar and Bannantiu Tombs.

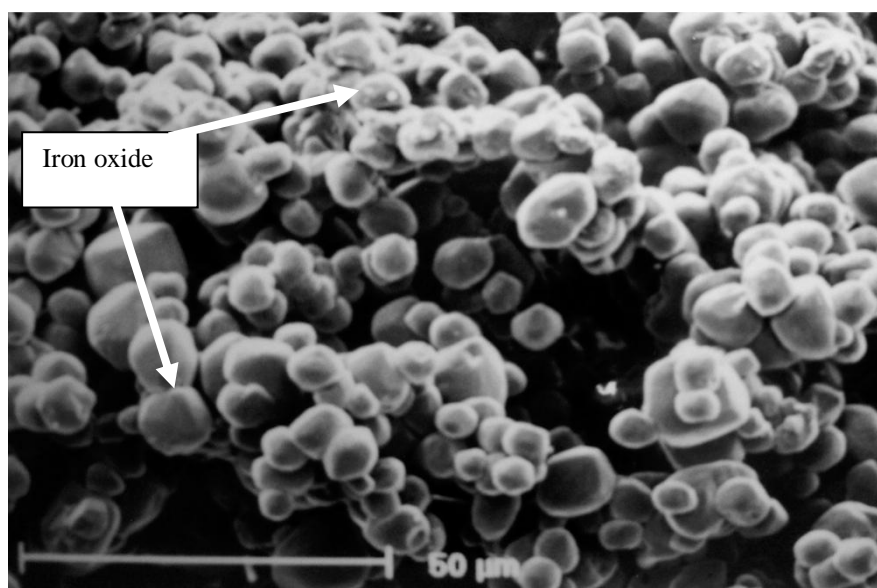


Figure 9: Scanning electron representative photo-micrograph presenting iron oxide balls coating quartz grains of the dark brown sandstone samples at the tombs under investigation.

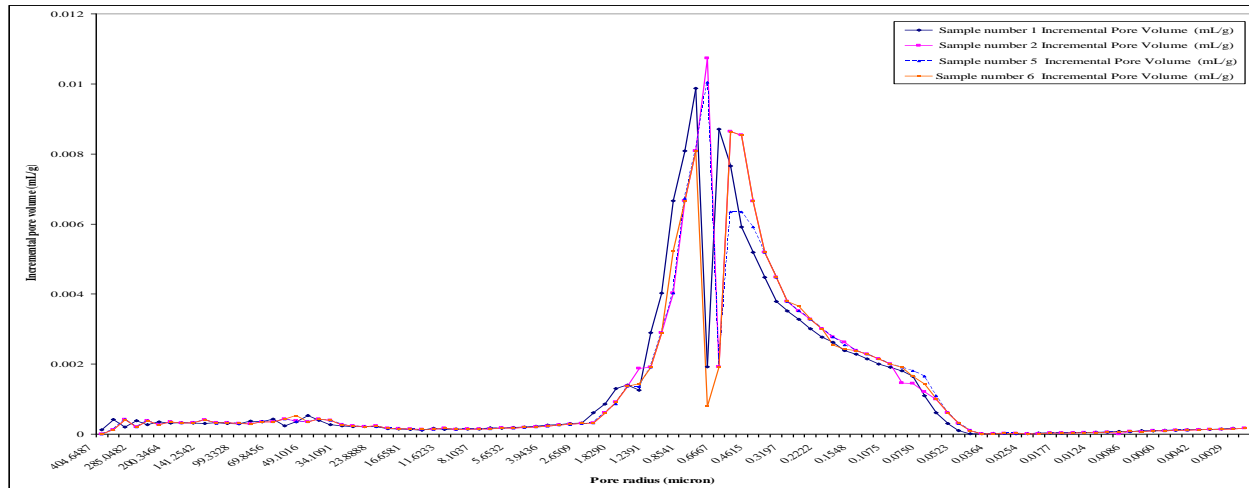


Figure 10: Graphical relationship between pore radius and Incremental pore volume for sandstone samples number 1,2,5 and 6 collected at dark brown facies of Bannantiu and Badi Eshtar Tombs, Bahariya Oasis, Egypt.

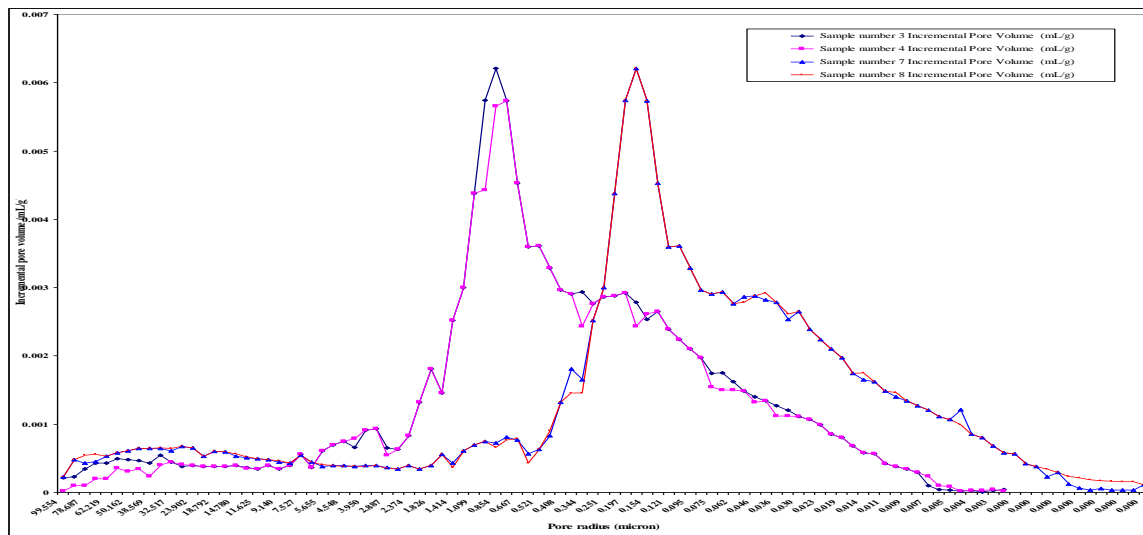


Figure 11: Graphical relationship between pore radius and Incremental pore volume for sandstone samples number 3,4,7 and 8 collected at Light brown facies of Bannantiu and Badi Eshtar Tombs, Bahariya Oasis, Egypt.

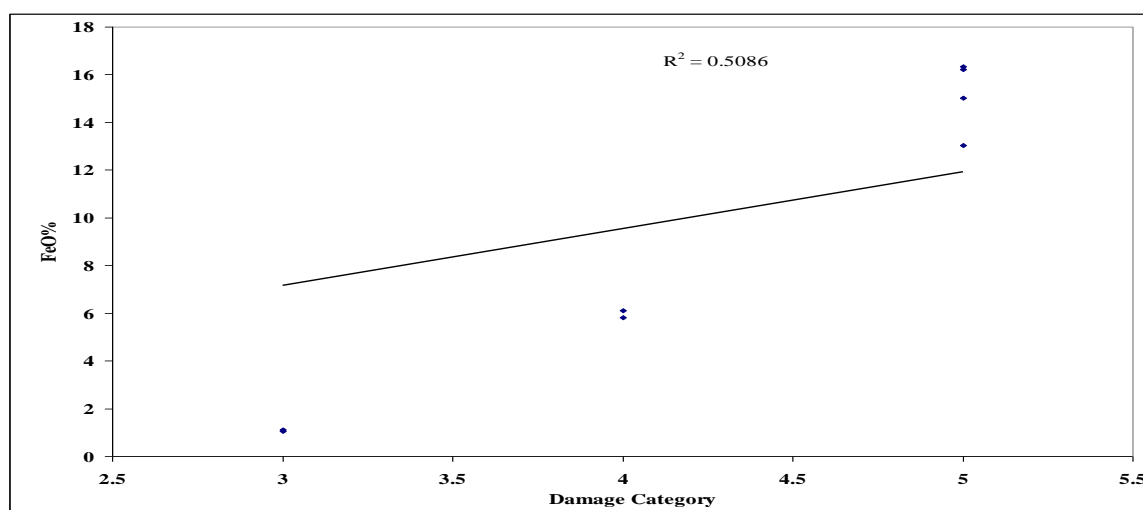


Figure 12: Binary relationship between Overall DC and rock's iron oxide content at the tombs under investigation.

Survey of Routing Scheme in MANET with Clustering Techniques

Neha Gupta¹, Manish Shrivastava², Angad Singh³

I.T. Department, Lakshmi Narain College of Technology, Bhopal, India¹

HOD, I.T. Department, Lakshmi Narain College of Technology, Bhopal, India²

AP, I.T. Department, Lakshmi Narain College of Technology, Bhopal, India³

ABSTRACT: Ad-hoc networking is a model in wireless device interactions, which represent that users wanting to communicate with each other form a temporary network, without any form of centralized administration. Each node participating in the network acts both as host and a router and must therefore be willing to forward packets for other nodes. For this purpose, a routing protocol is needed. This means that the routing protocol should try to minimize control traffic, such as periodic update messages. Cluster formation in Ad-hoc network is an important issue; Clustering in Mobile Ad Hoc Networks (MANETs) has many advantages compared to the traditional networks. But the highly dynamic and unstable nature of MANETs makes it difficult for the cluster based routing protocols to divide a mobile network into clusters and determination of cluster heads for each cluster. In recent years, several routing protocols and Cluster based protocols have been proposed for mobile ad hoc networks and prominent among them are DSR, AODV. This survey paper provides an overview of these protocols by presenting their characteristics, functionality, benefits and limitations and then makes their comparative analysis so to analyze their performance and compare some of existing works on clustering in MANETs. We categorize the works as Location based, Neighbor based, Power Based, Artificial Intelligence Based, Mobility based and Weight Based. We also present the advantages and disadvantages of these techniques and suggest a best clustering approach based on the observation. The objective is to make observations about how the performance of these protocols can be improved.

Keywords: MANET; Routing Protocol; Clustering; AODV; CMDSR.

I. INTRODUCTION

Wireless communication between mobile users is becoming more popular than ever before. This due to recent technological advances in laptop computers and wireless data communication devices, such as wireless modems and wireless LANs. This has led to lower prices and higher data rates, which are the two main reasons why mobile computing continues to enjoy rapid growth. Starting from the development of the packet radio networks (PRNET) in the 1970s and survivable adaptive networks (SURAN) in the 1980s to the global mobile (GloMo) networks in the 1990s and the current mobile ad hoc networks (MANET) [1], the multi-hop ad hoc network has received great amount of research attention.

Mobile Ad hoc Network (MANET), set of wireless mobile node forming a temporary network without the aid of any infrastructure or centralized control. Flexibility and Simplicity of adhoc network attracted everyone and solved many problems of communication where infrastructure establishment/reestablishment is not easy task, such as

Rescue area, Military operations, creates these components, incorporating the applicable criteria that follow.

Modern research area in ad hoc networks has paying attention on MAC and routing strategy. For the reason that of shared wireless broadcast medium, contention, near and far and hidden terminals are common in ad hoc networks and hence MAC demands significant improvement and routing is another issue especially in multi-hop environment.

Routing is also an interesting issue as routes are typically multi-hop. An ad-hoc network has certain characteristics, which imposes new demands on the routing protocol. The most important characteristic is the dynamic topology, which is a consequence of node mobility. Nodes can change position quite frequently, which means that we need a routing protocol that quickly adapts to topology changes. The nodes in an ad-hoc network can consist of laptops and personal digital assistants and are often very limited in resources such as CPU capacity, storage capacity, battery power and bandwidth. Instead the routing protocol should be reactive, thus only calculate routes upon receiving a specific request.

Generally, traditional routing protocols that are used in wired networks can't support routing in fixed wireless networks and mobile networks with fixed access points. Only one-hop routing is required over a link in a wireless network with fixed access points and many fixed wireless network. Routing in mobile ad hoc networks and some fixed wireless networks use multiple-hop routing. Routing protocols for this kind of wireless network should be able to maintain paths to other nodes and in most cases, must handle changes in paths due to mobility. Traditional routing cannot properly support routing in a MANET.

Much wireless technology is based upon the principle of direct point-to-point communication. Popular solutions like Group Standard for Mobile communications (GSM) and Wireless Local Area Network (WLAN) both use an approach where mobile nodes communicate directly with some centralized access point. These types of networks demand centralization for configuration and operation. Contrary to this model is the multi-hop approach. In multi-hop scenarios, nodes can communicate by utilizing other nodes as relays for traffic if the endpoint is out of direct communication range.

A mobile ad-hoc network, MANET [2], uses the multi-hop model. These are networks that can be set up randomly and on-demand. They should be self configuring and all nodes can be mobile resulting in a possibly dynamic network topology.

1.1 Ad-hoc networks

Centralized networks, such as GSM, cannot be used in all situations. Significant examples of such scenarios

include establishing survivable, efficient, dynamic communication for rescue operations, disaster relief efforts and military networks. Such network scenarios cannot rely on centralized and organized connectivity; they can be conceived as applications of MANETs. The set of applications for MANETs is diverse, ranging from small, static networks that are constrained by power sources, to large-scale, mobile, highly dynamic networks.

To enable multi-hop communication in a distributed manner, all nodes should be able to act as routers for each other (see Figure1). Routes are set up and maintained by a routing protocol. MANET routing protocol design is a complex issue considering the possible rapidly changing topology of such networks.

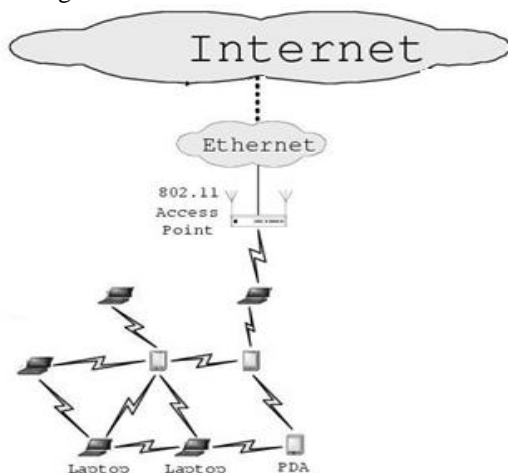
For route maintenance one has two main approaches in MANETs, reactive and proactive. Reactive routing protocols set up traffic routes on-demand, whilst proactive protocols attempt to dynamically maintain a full understanding of the topology.

Ad-hoc networks are not restricted to any special hardware. But today such networks are most likely to consist of nodes utilizing so-called WLAN interfaces. These are wireless interfaces operating according to IEEE specifications 802.11a [3], 802.1b [4] or 802.1g [5]. Throughout this document it is assumed that ad-hoc networks consist of links made up by either WLAN or Ethernet [6] interfaces. IEEE 802.11[7] does not support multi-hop communication by itself. Two modes are defined for communication using WLAN devices:

- Infrastructure mode: The wireless network consists of at least one access point and a set of wireless nodes. This configuration is called a Basic Service Set (BSS). An Extended Service Set (ESS) is a set of two or more BSSs (multiple cells).
- Ad hoc mode: This is a peer-to-peer mode. This configuration is called Independent Basic Service Set (IBSS), and is useful for establishing a network where nodes must be able to communicate directly and without any centralized access point.

The Ad-hoc mode is obviously the mode to use when setting up a MANET, but it lacks one basic requirement: multi-hop. Traffic is only transmitted to neighbors within radio range when using the ad-hoc mode, therefore there is a need for MANET routing protocols to set up and maintain traffic paths.

a) Using Base Station



b) Mobile Ad-hoc network

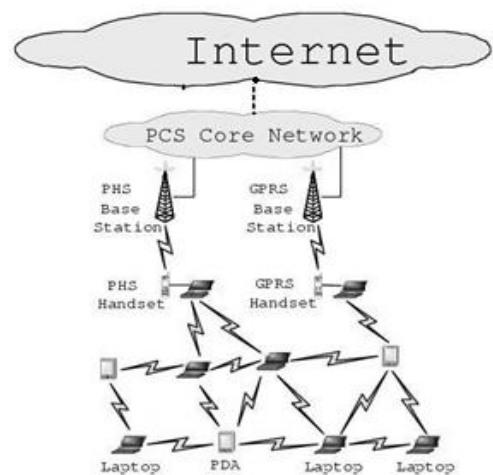


Fig 1: A traditional station scheme compared to an ad-hoc multi-hop network.

II. RELATED WORK

In this section we present some of existing works on survey of clustering in MANETs and Routing protocols. Roberto Carlos Hincapié, et al [8] has presented a survey on clustering techniques for MANET. They introduced some preliminary concepts that form the basis for the development of clustering algorithms. They also discussed the related clustering issues with the network topology, routing schemes, graph partitioning and mobility algorithms. They also described some of the most popular clustering techniques like Lowest-ID heuristic, Highest degree heuristic, DMAC (distributed mobility-adaptive clustering), WCA (weighted clustering algorithm). They also reviewed several clustering algorithms to organize mobile ad hoc networks in a hierarchical manner and explained their advantages and disadvantages.

Ratish Agarwal and Dr. Mahesh Motwani [9] have reviewed several clustering algorithms to organize mobile ad hoc networks in a hierarchical manner and presented their main characteristics. The survey examined the important issues related to cluster-based MANET, such as the cluster structure stability, the control overhead of cluster construction and maintenance, the energy consumption of mobile nodes with different cluster-related status, the traffic load distribution in clusters, and the fairness of serving as cluster heads for a mobile node.

III. EXISTING ROUTING IN MANET

There are three types of flat routing strategies exist in MANET. These are reactive, proactive and hybrid [10].

3.1 Proactive Routing

Proactive MANET protocols are also called as table-driven protocols and will actively determine the layout of the network. Through a regular exchange of network topology packets between the nodes of the network, at every single node an absolute picture of the network is maintained. There is hence minimal delay in determining the route to be taken. This is especially important for time-critical traffic. When the routing information becomes worthless quickly, there are many short-lived routes that are being determined and not used before they turn invalid. Therefore, another

drawback resulting from the increased mobility is the amount of traffic overhead generated when evaluating these unnecessary routes. This is especially altered when the network size increases. The portion of the total control traffic that consists of actual practical data is further decreased. Lastly, if the nodes transmit infrequently, most of the routing information is considered redundant. The nodes, however, continue to expend energy by continually updating these unused entries in their routing tables as mentioned, energy conservation is very important in a MANET system design. Therefore, this excessive expenditure of energy is not desired. Thus, proactive MANET protocols work best in networks that have low node mobility or where the nodes transmit data frequently. Examples of proactive routing protocols are optimized link state routing protocol (OLSR)[11], destination sequenced distance vector routing (DSDV)[12].

3.2 Reactive Protocols

Portable nodes- Notebooks, palmtops or even mobile phones usually compose wireless ad-hoc networks. This portability also brings a significant issue of mobility. This is a key issue in ad-hoc networks. The mobility of the nodes causes the topology of the network to change constantly. Keeping track of this topology is not an easy task, and too many resources may be consumed in signaling. Reactive routing protocols were intended for these types of environments. These are based on the design that there is no point on trying to have an image of the entire network topology, since it will be constantly changing. Instead, whenever a node needs a route to a given target, it initiates a route discovery process on the fly, for discovering out a pathway.

Reactive protocols start to set up routes on-demand. The routing protocol will try to establish such a route, whenever any node wants to initiate communication with another node to which it has no route. This kind of protocols is usually based on flooding the network with Route Request (RREQ) and Route reply (RREP) messages. By the help of Route request message the route is discovered from source to target node; and as the target node gets a RREQ message it send RREP message for the confirmation that the route has been established. This kind of protocol is usually very effective on single-rate networks. It usually minimizes the number of hops of the selected path. However, on multi-rate networks, the number of hops is not as important as the throughput that can be obtained on a given path. Examples of reactive routing protocols are ad-hoc on demand distance vector (AODV)[13], Dynamic source routing(DSR)[14].

3.3 Hybrid Routing

Since proactive and reactive protocols each work best in oppositely different scenarios, hybrid method uses both. It is used to find a balance between both protocols. Proactive operations are restricted to small domain, whereas, reactive protocols are used for locating nodes outside those domains.

Both methods explained before, only demonstrate good performance under certain conditions. But what if a balance point between proactive and reactive routing is found by adjusting the degree to which route information is propagated proactively versus the degree to which it needs to be discovered reactively? If we combine the advantages of both techniques obtaining as a result a particular routing

Parameter	AODV	DSR	DSDV	OLSR	ZRP	CBRP
Control message	3 types- RREQ,RREP,RE RR	3types- RREQ,RREP,RERR	2 type-HELLO & Update	2 type- HELLO and TC	Hello, Update, for inter zone- RREQ,RREP	HELLO ,RREQ,RREP,R ERR
Central Administration	NO	NO	NO	NO	node	Cluster head
Route discover	Each source node broadcast RREQ on demand	Each source node broadcast RREQ on demand	Already have info for all destination	Already have info for all destination	For intra zone have info , but for inter zone broadcast RREQ	For intra cluster have info , but for inter zone broadcast RREQ
Loop free routing	Yes, Due to sequence no.	Yes , due to address in packet header	Yes, due to sequence no.	Yes, due to sequence no.	Yes.	Yes.
Type of routing	Hop by hop	Source routing	Hop by hop	Hop by hop	Hop by hop	Hop by hop, but for inter zone source routing
Link support	Symmetric	Symmetric	Symmetric	Link to MPR- Symmetric, rest can be anything	Symmetric	Supports both Symmetric, Asymmetric
How path is build	By keeping backward pointer and forwards RREQ	Intermediate node insert its address in packer	Next hop is calculated by neighbors routing table	Next hop is calculated by neighbors routing table	Intra zone by routing table, inter zone on demand	Intra cluster by routing table, inter zone on demand
Scalable	Yes but vulnerable to network change	No	No	No	Yes	No
Protocol type	Reactive	Reactive	Proactive	Proactive	Hybrid	Hybrid
Metric	Shortest path	Shortest path	Shortest path	Cost	Shortest path	Shortest path

Advantage	At higher load incur lower delay; Unicast, multicast and broadcast communication possible.	Better in terms of collision; Doesn't flood network with updates; Routes maintained only when communication is done; Single route discovery may result multiple route to same destination	In small network size delay is smallest and throughput is high; Guarantees loop free	Limited broadcasting due to MPR; Being proactive routes to all destination available; Useful in application where less route discovery delay required	It tries to maintain most up to date map of network; Requires less bandwidth; Mobility of cluster head	Use of clustering to minimize on demand route discovery; Link break locally repaired; Mobility of cluster head
Disadvantage	Collision is high; Route discovery latency in high scale network; Lack of efficient maintenance technique	Access delay increases and throughput decrease as increase in network size; Route maintenance mechanism doesn't locally repair broken link; Route cache may stale; Connection set up delay is high; As network grows packet header size grows.	Higher delays for large network; Wastage of bandwidth due to unnecessary updates even if no change; Difficult to determine time delay for advertisement	Due to periodic update bandwidth is wasted; Maintains route most of which never used	Latency for finding new routes; If node not in any zone cannot communicate	Due to source routing, if network size grows packet size increases; Useful in small cluster only

Table 1. The evaluation of DSR, AODV, DSDV, OLSR, ZRP and CBRP in all case.

protocol which is able to adapt himself to the behavior of the network. By a Hybrid routing protocol the following characteristics must be present

- Adaptive: should be applicable to wide range of network characteristics. Node mobility, traffic patterns should be handled easily.
- Flexible: should enable the optimization. Applications should be able to be adapted to the different application-specific metrics at the routing layer. These goals should be set by the network participants
- Efficient and Practical: The protocol should achieve better performance than pure, non-hybrid, strategies without invoking costly low-level primitives. Such as reliable broadcasts and distributed agreements Hybrid protocols try to explode the benefits of both Proactive and Reactive protocols.
- The proactive part of the protocol is reduced to a small neighborhood of a node. The network is divided in small networks in order to decrease the problem of delay.
- The reactive part is used for routing across the network. Routing in large scale networks is implemented to reduce the overhead control problem.

The main difference between the Hybrid Adaptive protocols is the way they implement the PRP and RRP, and the way they define the routing zones. Next, we will briefly describe the most known Hybrid protocol, to finally compare them with each other Example of hybrid protocols are zone routing protocol (ZRP)[15], cluster based routing protocol(CBRP)[16]. Table 1 is description of other important parameters that make a protocol robust and steady in most cases. The evaluation predicts that in spite of slightly more overhead in some cases DSR and AODV in all cases. AODV is still better in Route updating and maintenance process.

IV. CLUSTER BASED ROUTING IN MANETS

4.1 Location Based Clustering

In the location-based routing protocol, the location information of mobile nodes are used to confine routing space into a smaller range. It reduces routing overhead and broadcast storm. [17].

In [17] Tzay-Farn Shih and Hsu Chun Yen have proposed a cluster-based routing protocol, named Core Location-Aided Cluster-based Routing protocol (CLACR). The characteristics of CLACR are stated as the entire network is partitioned into square clusters. In each cluster, the selection of cluster head is done by a cluster head election algorithm. The number of nodes responsible for routing and data transfer is decreased considerably by the usage of the cluster mechanism. It also diminished the routing overhead and increased the route lifetime massively. The path is computed using Dijkstra algorithm in a cluster-by-cluster basis by the CLACR.

4.2 Mobility Based Clustering

In [18] S. Muthuramalingam et al proposed a modified algorithm that uses Weighted Clustering Algorithm (WCA) for cluster formation and Mobility Prediction for cluster maintenance. In a MANET node management is done by Clustering. Cluster formation: At first, a beacon message is send by each node to notify its presence to its neighbors. A beacon message contains the state of the node. A neighbor list is built by each node based on the received beacon messages. The cluster head is elected based on the weight values of the nodes. The node with the lowest weight is chosen as the CH.

Maintenance: It has two distinct types of operations like the battery power threshold property and the node movement to the outside of its cluster boundary. Mobility prediction: The improvement in the weighted clustering algorithm is due to the use of mobility prediction in the cluster maintenance phase.

4.3 Neighbor Based Clustering

In [19] Hui -Yao An et al proposed a Cluster-Based Multipath Dynamic Source Routing in MANET (CMDSR). In this scheme, the hierarchy is used to perform Route Discovery and distributes traffic among diverse multiple paths.

Cluster Architecture: The CMDSR is based on the 3-level hierarchical scheme. The 0-node is the first level of the cluster. 1-cell cluster is the second level of cluster. Here each node of the cell is 1-hop away from the Cluster Head. The 2-server cluster gathers a set of cells of which the Server is the leader. The cluster changes due to the nodal

mobility dynamically. Hence the cluster will be disassembled or reassembled and also the cluster members update at every turn.

4.4 Power Based Clustering

In [20] Pi-Rong Sheu and Chia-Wei Wang proposed an efficient clustering algorithm that can establish a stable clustering architecture by keeping a host with weak battery power from being elected as a cluster head. In their proposed new clustering algorithm, a stable clustering architecture is formed by defining a bottleneck node to be a node with battery power lower than a predefined value Threshold. Bottleneck cluster head refers to the bottleneck node elected as a cluster head. The proposed clustering algorithm is based on the assumption that if the clustering architecture has fewer bottlenecks then the cluster heads have a longer lifetime.

4.5 Artificial Intelligence Based Clustering

In [21] Chongdeuk Lee and Taegwon Jeong proposed a Fuzzy Relevance-based Cluster head selection Algorithm (FRCA). The proposed mechanism selects the cluster head using fuzzy relevance for clustering in wireless mobile ad hoc sensor networks. In the network, the Fuzzy Relevance-based Cluster head selection Algorithm (FRCA)

efficiently clusters and manages sensors using the fuzzy information of node status. The Fuzzy Relevance Degree (FRD) with fuzzy value μ is used to perform and manage clustering in the proposed FRCA. In the proposed algorithm, some nodes acting as coordinators of the clustering are chosen by FRD to perform clustering.

4.6 Weighed Based Clustering

In [22] R. Pandi Selvam and V.Palanisamy presented a flexible weight based clustering algorithm in mobile ad hoc networks. The proposed algorithm is a 2-hop clustering algorithm. The performance of the proposed clustering algorithm showed that it outperformed the existing LID, HD and WCA to make the number of clusters. It also increases the number of nodes, transmission range and maximum displacement.

The weight of each node is calculated by the weight function $w(p)$. The cluster head election is done by comparing the weight of each node with its neighbors in the two hop range. The node with highest weight declares itself as the cluster head. Table 2 shows the comparison of different clustering techniques at a glance.

Table 2. The evaluation of DSR, AODV, DSDV, OLSR, ZRP and CBRP in all cases.

S. No:	Name of protocol	Type	Advantages	Performance metrics	Over head
1.	Core Location-Aided Cluster-Based Routing Protocol for Mobile Ad Hoc Networks[17]	Location based	i) Route life time increases. ii) Collision probability reduced. iii) Broadcast storm problem diminished.	Route construction success ratio, Route set up time, Route life time, Data delivery rate.	yes
2	A Dynamic Clustering Algorithm for MANETs by modifying Weighted Clustering Algorithm with Mobility Prediction[18]	Mobility based	i) Reduce the Power Consumption. ii) Reduces the bandwidth wastage for signals other Than Data. iii) Increase the Stability Of the Cluster.	Minimum life span of nodes, Stability of the Cluster, Throughput, Control overhead, Packet delivery Ratio, Connectivity.	yes
3	A Cluster-Based Multipath Dynamic Source Routing in MANET[19]	Neighbor based	i) improves scalability, ii) Prevents the network flooding. iii) overhead is minimized, iv) Higher and more consistent success delivery ratio. v) Lower error ratio.	average end-to-end delay, Received packets, Success delivery ratio, Error delivery ratio, control overhead.	Yes
4	A Stable Clustering Algorithm Based on Battery Power for Mobile Ad Hoc Networks[20]	Power based	i) better performance, ii) higher stability,	Clustering architecture life time, Minimum battery power, Network lifetime.	No
5	FRCA: A Fuzzy Relevance-Based Cluster Head Selection Algorithm for Wireless Mobile Ad-Hoc Sensor Networks[21]	Artificial intelligence based	i) reduces the overhead ii) Efficient management of node positions and energy. iii) Improvement of routing performance.	Number of clusters, Overhead rate, Cluster head selection rate,	Yes
6	Stable and Flexible Weight based Clustering Algorithm in Mobile Ad hoc Networks[22]	Weighted clustering based	i) stable and flexible against topology changes ii) Increase the number of nodes, transmission range And maximum displacement.	transmission ranges, number of nodes and Maximum displacement.	No

V. CONCLUSION

In this survey paper, an effort has been made to concentrate on the comparative study and performance analysis of various on demand or reactive routing protocols (DSR, AODV and TORA) on the basis of above mentioned performance metrics and gives detailed comparison of various clustering techniques for MANET. The results after analysis have reflected in Table I. The first table is description of parameters selected with respect to low mobility and lower traffic. It has been observed that the performance of all protocols studied was almost stable in sparse medium with low traffic. TORA performs much better in packet delivery owing to selection of better routes using acyclic graph. Table I is evaluation of same parameters with increasing speed and providing more nodes. The results indicate that AODV keeps on improving with denser mediums and at faster speeds. This paper also discussion of weight based approach in the previous section, we can conclude that the weight based clustering approach is the mostly used technique for cluster head selection and the common parameters for weight estimation include node degree, transmission power, mobility, distance and residual battery power. In some cases, stability and connectivity are also taken into account. So we need an artificial intelligence technique like Fuzzy logic or PSO to select the appropriate weight parameters for cluster head thereby minimizing the overhead and maximizing the throughput.

REFERENCES

- [1] Abdulrahman H. Altalhi Golden G. Richard, "Load-Balanced Routing through Virtual Paths: Highly Adaptive and Efficient Routing Scheme for Ad Hoc Wireless Networks", IEEE, 2004.
- [2] S. Corson and J. Macker. MANET RFC 2501, informational edition, January 1999.
- [3] The ieee 802.11a standard. Technical report.
- [4] The ieee 802.11b standard. Technical report.
- [5] The ieee 802.11g standard. Technical report.
- [6] Charles Hornig. A Standard for the Transmission of IP Datagrams over Ethernet Networks RFC894, April 1984.
- [7] ANSI/IEEE 802.11 Std 802.11, 1999 Edition, ieee standards document edition, February 1999.
- [8] Roberto Carlos Hincapié, Blanca Alicia Correa, and Laura Ospina, "Survey on Clustering Techniques for Mobile Ad Hoc Networks," pp.1-8,
- [9] Ratish Agarwal and Dr. Mahesh Motwani, "Survey of clustering algorithms for MANET," International Journal on Computer Science and Engineering Vol.1, issue: 2, pp. 98-104, 2009.
- [10] A Survey of Secure Mobile Ad Hoc Routing Protocols, Loay Abusalah, Ashfaq Khokhar, and Mohsen Guizani IEEE COMMUNICATIONS SURVEYS & TUTORIALS, VOL. 10, NO. 4, FOURTH QUARTER 2008.
- [11] Georgios Kioumourtzis, "Simulation and Evaluation of Routing Protocols for Mobile Ad Hoc Networks", Thesis, Master of Science in Systems Engineering and Master of Science in Computer Science, Naval Postgraduate School, Monterey, California, 2005.
- [12] C. E. Perkins and P. Bhagwat, "Highly dynamic destinationsequenced distance vector routing (DSDV) for mobile computers", Proceedings of ACM SIGCOMM 94, pp. 34-244, 1994.
- [13] A. Kush and S. Taneja, "A Survey of Routing Protocols in Mobile Adhoc Networks", International Journal of Innovation, Management and Technology, Vol. 1, No. 3, pp 279-285, 2010.
- [14] D. B. Johnson, D. A. Maltz, Y.C. Hu, "The Dynamic Source Routing Protocol for Mobile Ad Hoc Networks (DSR)", IETF Internet Draft, 2003.
- [15] Performance Evaluation of ZRP over AODV and DSR in Mobile Adhoc Networks Using Qualnet, European Journal of Scientific Research, SreeRangaRaju, Jitendranath Mungara, 2010
- [16] Comparative Analysis of CBRP, DSR, AODV Routing Protocol in MANET, Mukesh Kumar, Rahul Rishi, International Journal on Computer Science and Engineering 2010.
- [17] T-F. Shih and H-C. Yen, "Core Location-Aided Cluster-Based Routing Protocol for Mobile Ad Hoc Networks," pp223-228, 2006.
- [18] S. Muthuramalingam, R. Raja Ram, Kothai Pethaperumal, and V. Karthiga Devi, "A Dynamic Clustering Algorithm for MANETs by modifying Weighted Clustering Algorithm with Mobility Prediction," International Journal of Computer and Electrical Engineering, Vol. 2, No. 4, pp.709-714, August, 2010.
- [19] H-Y. An, Z. Ling, X-C. Lu, and P. Wei, "A Cluster-Based Multipath Dynamic Source Routing in MANET".
- [20] P-R. Sheu and C-W. Wang, "A Stable Clustering Algorithm Based on Battery Power for Mobile Ad Hoc Networks," Tamkang Journal of Science and Engineering, Vol. 9, No 3, pp. 233-242, 2006.
- [21] Chongdeuk Lee and Taegwon Jeong, "FRCA: A Fuzzy Relevance-Based Cluster Head Selection Algorithm for Wireless Mobile Ad-Hoc Sensor Networks".
- [22] R. Pandi Selvam and V. Palanisamy, "Stable and Flexible Weight based Clustering Algorithm in Mobile Ad hoc Networks," International Journal of Computer Science and Information Technologies, Vol. 2 (2), pp.824-828, 2011.

Design and Simulation of PI Control for Positive Output Triple Lift Luo Converter

N.Dhanasekar¹, Dr.R.Kayalvizhi²

1(Department of Electrical & Electronics, A.V.C.College of Engineering, Mayiladuthurai, India)

2 (Department of Instrumentation, Annamalai University, Chidambaram, India)

ABSTRACT: The positive output triple lift Luo converter is a newly devolved DC-DC converter. The object of this paper is to design and analyze a Proportional – Integral (PI) control for positive output triple lift Luo converter (POTLLC). The positive output triple lift Luo converter performs the voltage conversion from positive source voltage to positive load voltage. The simulation model of the positive output triple lift Luo converter with its control circuit is implemented in Matlab/Simulink. The PI control for positive output triple lift Luo converter is tested for transient region, line changes, load changes, steady state region.

Keywords: DC-DC converter, Matlab, Positive output triple lift Luo converter, Proportional – Integral control, simulink

I. INTRODUCTION

DC-DC conversion technology has been developing rapidly, and DC-DC converters have been widely used in industrial applications such as dc motor drives, computer systems and medical equipments. The output voltage of pulse width modulation (PWM) based DC-DC converters can be changed by changing the duty cycle [1]-[2]. The voltage lift technique is a popular method that is widely applied in electronic circuit design. This technique effectively overcomes the effects of parasitic elements and greatly increases the output voltage. Therefore these converters perform DC-DC voltage increasing conversion with high power density, high efficiency and high output voltage with small ripples [3]. Compared with conventional dc-dc converters, triple-lift Luo converters can implement the output voltages by increasing stage by stage along a geometric progression and obtain higher voltage transfer gains. They are divided into various categories according to their power stage numbers, such as the elementary circuit (single power stage), re-lift circuit (two power stages), triple-lift circuit (three power stages) etc.[4]. Due to the time variations and switching nature of the power converters, their static and dynamic behavior becomes highly non-linear.[5]. A good control for DC-DC converters always ensures stability in arbitrary operating condition. Moreover, good response in terms of rejection of load variations, input voltage variations and even parameter uncertainties is also required for a typical control scheme. The PI control technique offers several advantages compared to PID control methods: stability, even for large line and load variations, reduce the steady error, robustness, good dynamic response and simple implementation [2].

In this paper PI control with zero steady state error and fast response is brought forward. The static and dynamic Performance of PI control for positive output triple lift Luo converter is studied in Matlab/Simulink. For the purpose of optimize the stability of positive output triple lift Luo converter dynamics, while ensuring correct operation in any working condition, a PI control is a more feasible approach. The PI control has been presented as a good alternative to the control of switching power converters [5]-[6]. The main advantage PI control schemes is its insusceptibility to plant/system parameter variations that leads to invariant dynamics and static response in the ideal case [2].

II. CIRCUIT DESCRIPTION AND OPERATION

Triple lift circuit is shown in Fig.1 and it consists of two switches S and S_1 , four inductors L_1 , L_2 , L_3 and L_4 , five capacitors C , C_1 , C_2 , C_3 and C_0 and five freewheeling diodes.

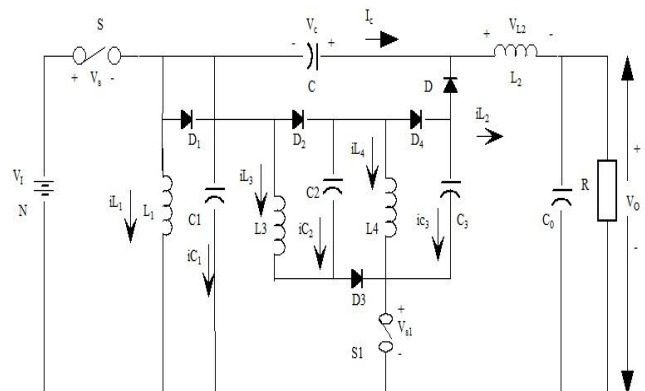


Figure 1 triple lift Luo circuit

Capacitors C_1 , C_2 and C_3 perform characteristics to lift the capacitor voltage V_c by three times the source voltage V_i . L_3 and L_4 perform the function as ladder joints to line the three capacitors C_1 , C_2 and C_3 and lift the capacitor voltage V_c up.

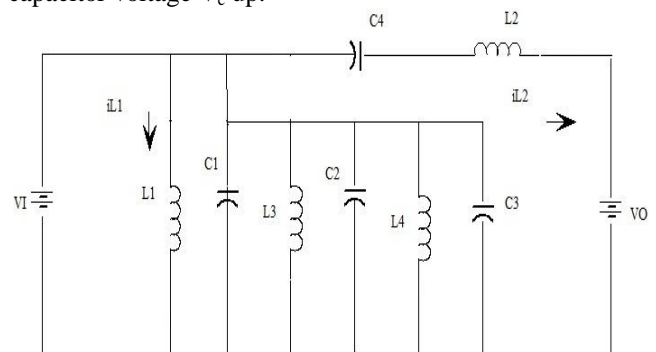


Figure 2 switches S and S_1 are ON

In the description of the converter operation, it is assumed that all the components are ideal and positive output triple lift converter operates in a continuous conduction mode. Fig. 2 and 3 shows the modes of operation of the converter.

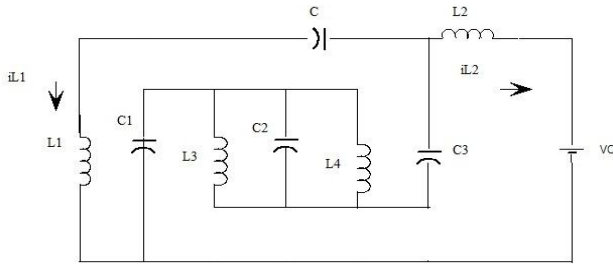


Figure 3 switches S and S₁ are open

The current i_{L2} increases in switches are in ON period kT . And it decreases in switches are in OFF period $(1-kT)$. The output voltage and current are

$$: V_0 = \frac{3V_1}{1-k} \quad (1)$$

$$: I_0 = \frac{(1-k)I_1}{3} \quad (2)$$

The voltage transfer gain in continuous mode is

$$: M_T = \frac{V_0}{V_1} = \frac{3V_1}{1-k} \quad (3)$$

Average current

$$: I_{L1} = \frac{kI_0}{1-k} \quad (4)$$

$$: I_{L2} = I_0 \quad (5)$$

$$: I_{L3} = I_{L4} = I_{L1} + I_{L2} = \frac{I_0}{1-k} \quad (6)$$

Current variations

$$\eta = \frac{k}{M_{T2}} \frac{3R}{2fL} \quad (7)$$

Therefore variation ratio of output voltage v_c is

$$: \varepsilon = \frac{k}{8M_T} \frac{1}{f^2 c_0 L_2} \quad (8)$$

III. DESIGN OF PI CONTROLLER

The PI control is designed to ensure the specifying desired nominal operating point for POTLLC, then regulating POTLLC, so that it stays very closer to the nominal operating point in the case of sudden load disturbances and set point variations. The PI control settings proportional gain (K_p) and integral time (T_i) are designed using Zeigler – Nichols tuning method [6] by applying the step test obtain S – shaped curve of step response of POTLLC. From the S-shaped curve of step response of POTLLC may be characterized by two constants, delay time L and time constant T . The delay time and time constant are determined by drawing a tangent line at the inflection point of the S-shaped curve and determining the intersections of the tangent line with the time axis and line output response $c(t)$. From this value

calculate the proportional gain (K_p) and integral time (T_i) are designed using Zeigler – Nichols tuning method

IV. 4. SIMULATION OF TRIPLE LIFT CONVERTER

The simulations has been performed on the positive output triple lift Luo converter circuit with parameters listed in Table I. The static and dynamic performance of PI control for the positive output triple lift Luo converter is evaluated in Matlab/Simulink

TABLE - I

Parameter name	Symbol	value
Input voltage	V_1	10 volts
Output voltage	V_o	60 volts
Inductors	$L_1, L_2, L_3 \& L_4$	100 μ H
Capacitors	$C, C_1, C_2 \& C_3$	5 μ f
Capacitor	C_0	300 μ f
Switching frequency	f_s	100kHz
Load resistance	R	100 Ω
Duty cycle	k	0.5

The Matlab/Simulink simulation model is shown in Fig.4. The difference between feedback output voltage and reference voltage is given to PI control and output of PI control, change in duty cycle of the power switch (n - channel MOSFET).

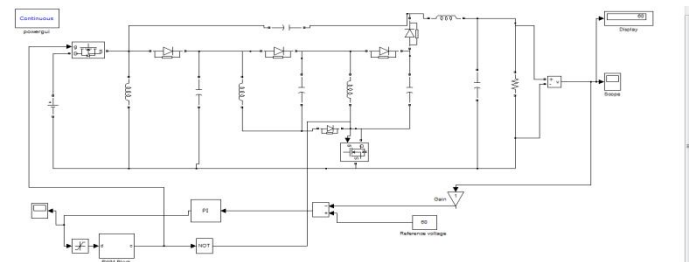


Figure 4 PI control positive output triple lift Luo converter.

The POTLLC performance is done for three regions .they are transient region, line variations and load variations.

4.1 Transient region

Fig 5 shows the output voltage of POTLLC with PI control in the transient region. It can be that the converter output has settled at time of 0.014 sec. with designed PI control.

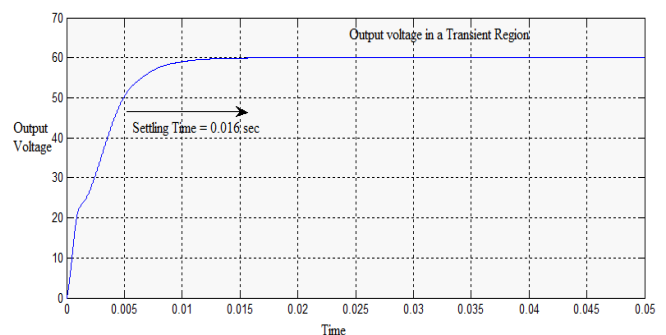


Figure 5 output voltage in transient region

4.2 Line variations

Fig.6 shows the output voltage of converter for input voltage step change from 10 V to 7 V (-30% supply disturbance).the converter output voltage has maximum overshoot of 2.5V and 0.007sec settling time with designed PI control. Fig.7 shows the output voltage variations for the input voltage step change from 10 V to 13 V (+ 30% supply disturbance).the converter output voltage has maximum overshoot of 5 V and 0.012 sec settling time with designed PI control.

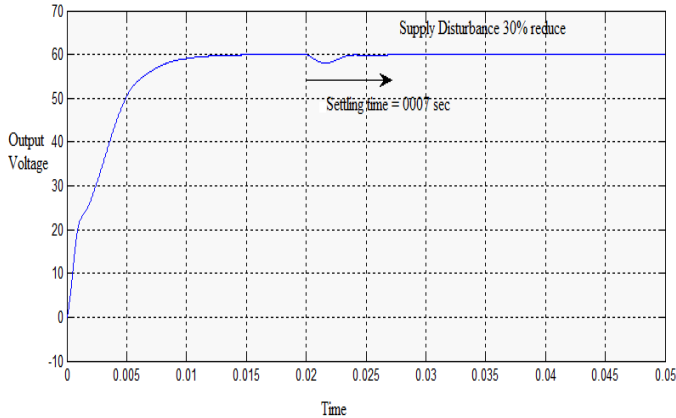


Figure 6 Output voltage - supply change from 10 V to 7 V

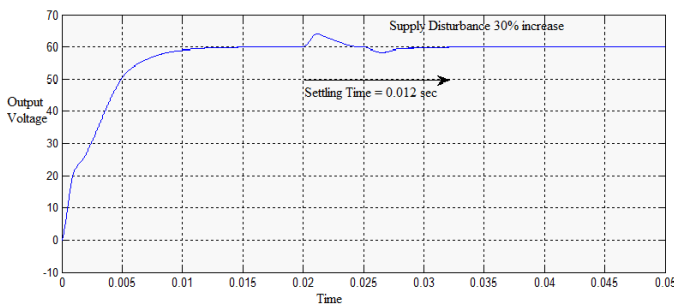


Figure 7 Output voltage - supply change from 10 V to 13V

4.3 Load variations

Fig.8 shows the output voltage with change the load from 100 Ω to 80 Ω (-20% load disturbance).the maximum overshoot is 0.6 V and settled at the 0.005 sec .Fig.9 shows the variation of load from 100 Ω to 120 Ω (+20% disturbance) the maximum overshoot of 0.003 V and settled at 0.00 sec.

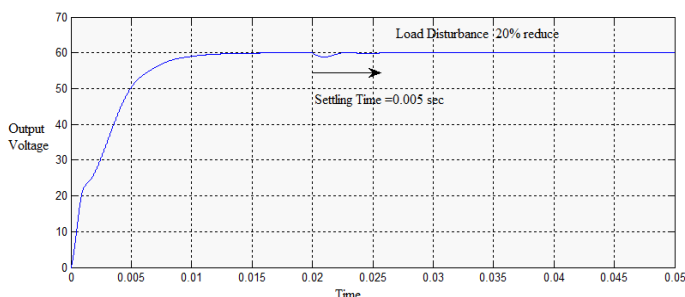


Figure 8 output voltage – load change from 100 Ω to 80 Ω

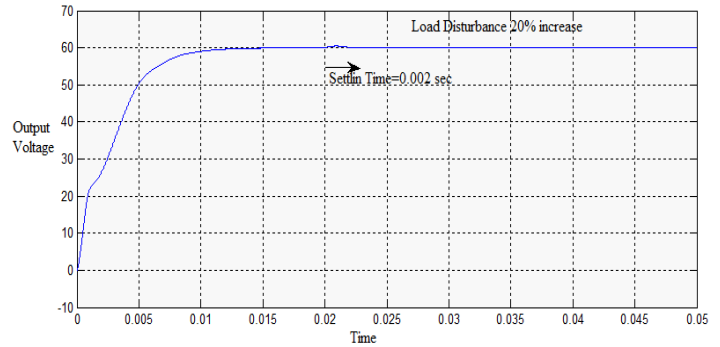


Figure 9 output voltage – load change from 100 Ω to 120 Ω

V. CONCLSION

The positive output triple lift Luo converter (POTLLC) performs the voltage conversion from positive source voltage to positive load voltage. The PI control scheme has proved to be robust and it has been validated with transient region, line and load variations. The positive output triple lift Luo converter with PI control use in applications such as switch mode power supply, medical equipments and high voltage projects etc.

VI. ACKNOWLEDGEMENT

The author wish to thank the A.V.C.College of Engineering Management for their moral support.

REFERENCES

- [1] F.L.Luo and H.Ye, "Positive output super lift converters," IEEE Transaction on power electronics, Vol.18, No. 1, pp. 105-113, January 2003.
- [2] K. Ramesh kumar and S. Jeevanantham." PI Control for positive output elementary super lift luo converter," World Academy of Science, Engineering and Technology. pp. 732-737, March 2010.
- [3] Fang Lin Luo and Hong Ye. Advanced DC/DC Converters. CRC Press, London, U.K.
- [4] R. Kayalvizhi, S.P. Natarajan and AnnRosella. "Design and simulation of PI controller for positive output elementary Luo converter", Journal of Engineering and Technology, AUJET. pp. 90-93.
- [5] T. S. Saravanan , R. Seyezhai and V. Venkatesh "modeling and control of split capacitor type elementary additional series positive output super lift converter", ARPJN Journal of Engineering and Applied Sciences, vol. 7, no. 5, may 2012.
- [6] P. Comines and N. Munro, "PID controllers: recent tuning methods and design to specification", in IEEE Proc. Control Theory Application, vol.149, no.1, pp.46-53, Jan 2002.

A Fuzzy Logic Multi-Criteria Decision Approach for Vendor Selection Manufacturing System

Harish Kumar Sharma¹

National Institute of Technology, Durgapur (WEST BENGAL) - 713209

Abstract: The success of an industry depends on optimization of product cost and for achieving above goal Internal selection should be efficient. In the present study an efficient Multi-Criteria Decision Making (MCDM) approach has been proposed for quality evaluation and performance appraisal in vendor selection. Vendor selection is a Multi-Criteria Decision Making (MCDM) problem influenced by several parameters which are in linguistic. Multiple Performance criteria/attributes. These criteria attributes may be both qualitative as well as quantitative. Qualitative criteria estimates are generally based on previous experience and performance maker's opinion on suitability. Therefore to quantify the linguistic variables fuzzy logic and set theory is used. The fuzzy set theory helps in vagueness of the system. a fuzzy decision approach is developed where are resourcing of vendors to select suitable vendor for materials is made MCDM method has been illustrated in this reporting through a case study.

Keywords: Vendor's selection Fuzzy sets, Decision matrix, Rank, Multiple criteria decision making, weight

I. Introduction

Iron and steel industry is an important basic industry for any industrial economy providing the primary material for construction, automobile machinery and other industries. the importance of maintenance function has increased due to its role in keeping and improving the availability, product quality cost-effectiveness levels. Maintenance costs constitute an important part of the operating budget of manufacturing firms. Maintenance selection is one of the most critical activities for many industries. The selection of an appropriate maintenance may reduce the purchasing cost and also improve competitiveness.

It is impossible for a company to successfully produce, low-cost, high-quality products without satisfactory maintenance. The selection of appropriate maintenance has been one of the most important function for a industries. If the relationship between a supplier and manufacturing industries. Many studies have pointed out that key is to set effective evaluation criteria for the supplier selection

Vendor selection is a common problem for acquiring the necessary materials to support the output of organizations. The problem is to find and evaluate periodically the best or most suitable vendor for the organization based on various vendor. Due to the fact that the evaluation always involves conflicting performance criteria of vendors. The techniques of multiple criteria

decision making (MCDM) are coherently derived to manage the problem (Shyur &Shih, 2006).Evaluating vendors many criteria including quantitative, such as cost, price as well as qualitative, a considerable number of decision models have been developed based on the MCDM theory.

To resolve the problem, this paper suggests evaluating vendor using a multiple levels multiple criteria decision making method under fuzzy logic method maintenance alternative for industries planning of the basis of quantitative and qualitative factors formula are clearly displayed. Classified to benefit and cost criteria has the larger the better, ratings of vendor and importance weights of all the criteria are assessed in linguistic values represented by fuzzy numbers.

- Selection of fuzzy number & their membership functions.
- Fuzzy logic of the scale function
- Averaging the fuzzy numbers as given by the performance makers in terms linguistics variables.
- Determinations of fuzzy normalize weight.
- Overall ranking of alternatives.
- Finally result of multi criteria decision making

In this paper the vendor selection by a MCDM for these logic method identified a criteria based on product, cost ,quality ,service etc. these criteria short out the vendor by using the performance makers P_1, P_2, P_3, P_4, P_5 , and P_N these performance makers gives the data in a logistics variable weight of the criteria then we find the suitable vendor material

II. REVIEW OF PREVIOUS WORK

[1]The vendor selection a focus area of research since the 1966s.literature (Dickson,1966; Weber ,1991)several dimensions are mentioned that are important for the multiple vendor selectiondecision.nmaking,price,quality,delivery,performance,history,capacity,service Production facilities and technical capabilities etc. the problem is how to select vendor that perform optimally on the desired dimensions.[2] Weber et al.(1991) reviewed 74 vendor(supplier) selection articles from 1966 to 1991 and showed that more than 63% of them were in a multi criteria decision making. other researchers also endorsed using a weighted linear method of multiple for the VSP. Gaballa (1974) is the first author who applied mathematical programming to a vendor selection problem in a real case. He used a mixed integer programming .model to minimize the total discounted price of it misallocated to the VSP. Weber

and Current (1993) developed a multi objective MIP for vendor selection and order allocation among the selected vendors .they applied the proposed model in a proposed model in a practical case.[3] Buffa and Jackson (1983) and Sharma et al. (1989), respectively, used linear and non-linear mixed-integer goal programming (GP) for price, service level, delivery and quality goals. Failure base maintenance (FBM) is performed when a failure or breakdown occurs, no action is taken to detect the onset of or to present failure. The maintenance related costs are usually high, but it may be considered cost effective in certain cases.[4] fuzzy multi agent system is proposed for ta-chung chu,Rangnath varma (2011),developed to depict the relationship among parent criteria and their sub-criteria and criteria and the weight of all criteria,[5] amit karami and zhiling Gua We demonstrate that the fuzzy logic approach provides a robust analysis for vendor selection, [6]eleonona botani ,Antonio Rizzi (2007) An adapted multi –criteria approach to suppliers and products selection An application oriented to lead-time reduction. An extensive case study is presented to show the practical application of the methodology

III. METHOD OF SOLUTION

2.1 Fuzzy sets

A fuzzy set A can denoted by $A_i = \{(x, f_A(x)) | x \in U\}$, where U is universe of discourse, x is an element in U, A is a fuzzy set in $f_A(x)$ is the membership function of A x (Kaufmann & gupta, 1991) the larger $f_A(x)$, the stronger the grade of membership for x in A

2.2 Fuzzy numbers

A real fuzzy number A is described as any fuzzy subset of the real line R with membership function f_A which possesses the following properties (Dubois & Prade, 1978

normality with at least one element with degree of

$$\mu_A(x) = \begin{cases} \frac{(x-a)}{(b-a)} & a \leq x \leq b \\ \frac{(c-x)}{(c-a)} & b \leq x \leq c \\ 0 & \text{otherwise} \end{cases} \quad \mu_A(x) = \begin{cases} \frac{(x-a)}{(b-a)} & a \leq x \leq b \\ 1 & b \leq x \leq c \\ \frac{(x-d)}{(c-d)} & c \leq x \leq d \\ 0 & \text{otherwise} \end{cases}$$

- (a) f_A is a continuous mapping from R to [0, 1];
 - (b) $f_A(x) = 0, \forall x \in (-\infty, a]$
 - (c) f_A is strictly increase on [a, b];
 - (d) $f_A(x) = 1, x \in [b, c]$;
 - (e) f_A is strictly decreasing on [c, d];(f) $f_A(x) = 0, \forall x \in [d, \infty)$;
- Where a, b, c and d are real numbers. We may let a = -1, or a=b, or b=c or c=d or d= +1

IV. OPERATIONS ON FUZZY NUMBERS

Let $A=(a_1, b_1, c_1, d_1)$ and $B=(a_2, b_2, c_2, d_2)$ are two trapezoidal fuzzy numbers. Then the operations $+, -, \times, \div$ are expressed (Kaufmann and Gupta 1991) as.

Let

$$A + B = (a_1, b_1, c_1, d_1) + (a_2, b_2, c_2, d_2) \\ = (a_1 + a_2, b_1 + b_2, c_1 + c_2, d_1 + d_2)$$

$$A - B = (a_1, b_1, c_1, d_1) - (a_2, b_2, c_2, d_2) \\ = (a_1 - a_2, c_1 - b_2, c_1 - b_2, d_1 - a_2)$$

$$A \times B = (a_1, b_1, c_1, d_1) \times (a_2, b_2, c_2, d_2) \\ = (a_1 \times a_2, b_1 \times b_2, c_1 \times c_2, d_1 \times d_2)$$

$$\frac{A}{B} = \frac{(a_1, b_1, c_1, d_1)}{(a_2, b_2, c_2, d_2)} \\ = \left(\frac{a_1}{d_2}, \frac{b_1}{c_2}, \frac{c_1}{b_2}, \frac{d_1}{a_2} \right)$$

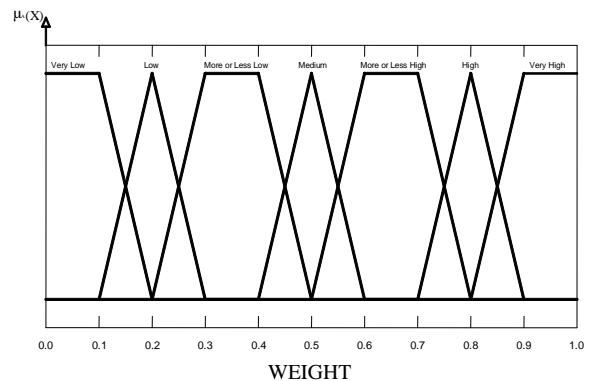
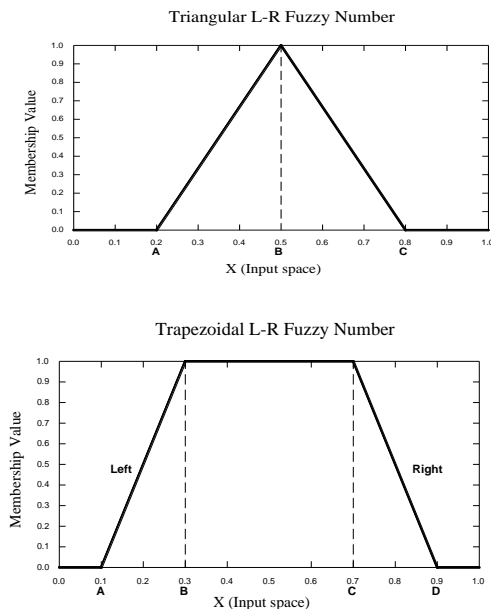


Fig. 2: Graphical representation of fuzzy numbers for linguistic variables.

A fuzzy number is defined as a continuous fuzzy set that contains convexity with one distinct peak and

For the selection of location, seven fuzzy numbers are taken

to describe the level of performance on decision criteria, to avoid difficulties for an performance makers in distinguishing subjectively between more than seven alternatives Salty (1977)

Table 1 shows the fuzzy numbers associated with the corresponding linguistic variables and the same is graphically represented in figure3.

Table 1: Fuzzy numbers and corresponding linguistic variables

Linguistic Variable	Fuzzy Number
VL (Very low)	(0.0, 0.0, 0.1, 0.2)
L (low)	(0.1, 0.2, 0.3, 0.4)
ML/LL (more or less low)	(0.2, 0.3, 0.4, 0.5)
M (Medium)	(0.4, 0.5, 0.5, 0.6)
MH/LH (more or less high)	(0.5, 0.6, 0.7, 0.8)
H(High)	(0.6, 0.7, 0.8, 0.9)
VH (Very high)	(0.8, 0.9, 1.0, 1.0)

Step – 1:

The linguistic variables assigned by the experts for each criteria is translated into fuzzy numbers and the same is represented in the matrix (Fuzzy Decision Matrix).

Step – 2:

Let A_{ar}^j be the fuzzy number assigned to an vendor A_i by the Perfromance makers (P_k) for the decision criterion. C_j , the average of fuzzy numbers is given as

$$A_{ij} = \frac{1}{p} \otimes (a_{i1}^j \oplus a_{i2}^j + \dots + a_{ik}^j); k$$

$$= 1, 2, \dots, p.$$

The average fuzzy score matrix for each criteria is obtained.

Step – 3:

The crisp score (Defuzzified values) for each criteria is obtained. Defuzzification of fuzzy numbers is an operation that produces a non fuzzy crisp value. Defuzzified value is given by the following equation (Kaufman and Gupta, 1991).

Trapezoidal fuzzy number

$$E = \frac{(a + b + c + d)}{4}$$

Triangular fuzzy number

$$E = \frac{(a + 2b + c)}{4}$$

Step – 4:

The normalized weight for each criteria (C_i) is obtained as W_j , Where $J=1, 2, \dots, n$. The normalized weight for each criterion is obtained by dividing the Defuzzified scores of each criterion by the total of all the criteria.

Rating of Suitable Locations:

In similar way as procedure adopted for the calculation of weight criteria, the rating of suitable location is derived as:

- Locations suitable on each of the criteria are to be rated in the linguistic variables by the performance makers, which is converted into fuzzy numbers and the same is represented in the matrix form (Fuzzy Decision Matrix).
- The average fuzzy score matrix for each locations are obtained.
- The crisp score (Defuzzified value) for each location are obtained and same is represented in the matrix form as X_{ij} , where $i=1, 2, \dots, m$ and $J=1, 2, \dots, n$. Where, m is the number of locations, n is the number of criteria.
- Total aggregated score for locations against each criteria is obtained as

$$TS = \{X_{ij}\} \{W_j\}$$

$$TS = \begin{bmatrix} v_{11} & v_{12} & \dots & v_{1j} & \dots & v_{1m} \\ v_{21} & v_{22} & \dots & v_{2j} & \dots & v_{2m} \\ \vdots & \vdots & & \vdots & & \vdots \\ v_{i1} & v_{i2} & \dots & v_{ij} & \dots & v_{im} \\ \vdots & \vdots & & \vdots & & \vdots \\ v_{n1} & v_{n2} & \dots & v_{nj} & \dots & v_{nm} \end{bmatrix} \otimes \begin{bmatrix} w_1 \\ w_2 \\ \vdots \\ w_j \\ \vdots \\ w_n \end{bmatrix} = (v \times w)^t$$

On the basis of the total score obtained for each location against decision criteria, overall scores are obtained, using simple average method, which provide final ranking of locations.

V. CASE STUDY

Steel industries purposed methodology allows the experts to rank the suitable vendor reelection for a magnum steel limited Gwalior (India) companies on the basis of different decision criteria in a more realistic manner. The advantage of fuzzy set theory facilitates the assessment to be made on the basic of linguistic manner, which corresponded to the real lie situations in a much better way for simplicity five perfromance makers E1, E2,, E3, E4, E5 vendor selection projects, were consulted to get the linguistic variables in terms of importance of each of the delusion criteria used to rank the vendor for each criteria's (V_1, V_2, V_3, V_4, V_5).

- material cost(C_1)
- Semi –Raw material cost (C_2)

3. Transportation cost (C₃)
4. Inventory and storage cost (C₄)
5. Production Process cost (C₅)
6. On time delivery (C₆)
7. Percentage waste items (C₇)
8. Flexibility in service (C₈)
9. Financial position (C₉)
10. Inspection (quality control) (C₁₀)

Table.2 show the linguistic variables assigned by the Performance makers to each of the decision criteria are define in the table -1

Table 3: Linguistic variables assigned by the Performance maker's

Criteria	performance maker's				
	E ₁	E ₂	E ₃	E ₄	E ₅
C ₁	H	M	H	H	VH
C ₂	H	H	H	VH	H
C ₃	MH	H	H	VH	VH
C ₄	MH	MH	M	M	M
C ₅	M	M	MH	M	M
C ₆	H	H	VH	H	M
C ₇	MH	VH	M	MH	M
C ₈	M	MH	MH	M	M
C ₉	VH	H	VH	M	H
C ₁₀	MH	MH	M	VH	M

The average fuzzy scores, defuzzified values and normalized weight of criteria are obtained and given in table 3

Table 3: Normalized weight of criteria

criteria	Parameter of average fuzzy scores				Defuzzified Value	Normalized weight
C ₁	0.670	0.767	0.870	0.890	0.800	0.250
C ₂	0.470	0.567	0.670	0.720	0.606	0.190
C ₃	0.670	0.768	0.870	0.920	0.807	0.253
C ₄	0.5	0.6	0.7	0.78	0.66	0.209

	30	33	30	0	9	
C ₅	0.670	0.767	0.870	0.930	0.809	0.253
C ₆	0.560	0.634	0.720	0.800	0.678	0.211
C ₇	0.200	0.300	0.400	0.500	0.350	0.110
C ₈	0.541	0.620	0.720	0.831	0.678	0.211
C ₉	0.422	0.580	0.642	0.720	0.591	0.184
C ₁₀	0.470	0.567	0.670	0.720	0.607	0.190

Rating of alternatives (venders) on criterion (X_i^j)
 Suitability of venders against each criteria are to be rated and linguistic variables are assigned by the experts to the venders table-3 are define in table-1 the linguistic variables are converted into fuzzy numbers

Table 5: Linguistics variables for alternatives

C ₁	V ₁	M	L	M	L	M
	V ₂	H	M	VH	H	M
	V ₃	VH	M	M	VH	VH
	V ₄	VH	VH	H	VH	VH
	V ₅	H	H	M	H	H
C ₂	V ₁	VH	VH	VH	VH	VH
	V ₂	H	H	H	VL	L
	V ₃	H	VH	VH	VH	VH
	V ₄	M	M	VH	H	VH
	V ₅	VH	VH	M	H	H
C ₃	V ₁	L	M	M	M	M
	V ₂	L	M	H	M	H
	V ₃	H	VH	H	H	VH
	V ₄	VH	H	H	H	VH
	V ₅	M	VH	H	VH	H
C ₄	V ₁	VH	VH	M	H	H
		VL	M	M	H	VH
	V ₂					
	V ₃	VH	VH	H	H	M
	V ₄	M	H	H	VH	M
	V ₅	VH	H	M	VH	VH
C ₅	V ₁	M	H	M	L	M
	V ₂	H	L	VL	L	M
	V ₃	M	M	VL	H	H
	V ₄	H	VH	M	M	H

	V ₅	H	M	H	M	VH
C ₆	V ₁	VH	H	VL	H	M
	V ₂	VH	H	M	M	H
	V ₃	L	VL	M	VL	L
	V ₄	L	L	L	H	H
	V ₅	VH	H	H	H	VH
C ₇	V ₁	VL	M	L	VL	L
	V ₂	VL	M	M	M	H
	V ₃	M	M	VL	VL	L
	V ₄	H	H	L	L	VL
	V ₅	H	VH	VH	M	M
C ₈	V ₁	VH	M	L	H	H
	V ₂	VL	VL	L	M	M
	V ₃	H	M	H	H	H
	V ₄	L	M	H	M	H
	V ₅	M	M	H	H	H
C ₉	V ₁	L	M	L	L	L
	V ₂	H	M	H	M	L
	V ₃	L	M	VH	H	M
	V ₄	M	VL	L	L	L
	V ₅	H	H	M	M	VL
C ₁₀	V ₁	H	VL	L	VL	VL
	V ₂	L	H	H	H	M
	V ₃	L	L	VL	VL	VL
	V ₄	M	L	VL	M	VL
	V ₅	M	L	VL	M	H

Table 6: Average fuzzy scores and Defuzzified scores

criteria	Vendo r	Average Fuzzy scores				Defuzz ied score
C ₁	V ₁	0.670	0.767	0.870	0.890	0.799
	V ₂	0.470	0.567	0.670	0.710	0.605
	V ₃	0.670	0.767	0.870	0.880	0.797
	V ₄	0.530	0.633	0.730	0.800	0.674
	V ₅	0.670	0.767	0.870	0.900	0.802
C ₂	V ₁	0.530	0.633	0.730	0.820	0.679
	V ₂	0.200	0.300	0.400	0.500	0.350
	V ₃	0.730	0.833	0.930	0.980	0.869
	V ₄	0.670	0.767	0.870	0.910	0.805
	V ₅	0.600	0.700	0.800	0.900	0.750
C ₃	V ₁	0.530	0.633	0.730	0.850	0.686

	V ₂	0.480	0.530	0.633	0.730	0.593
	V ₃	0.470	0.567	0.670	0.720	0.607
	V ₄	0.330	0.433	0.530	0.450	0.436
	V ₅	0.400	0.500	0.600	0.700	0.550
C ₄	V ₁	0.733	0.830	0.930	0.980	0.868
	V ₂	0.267	0.370	0.470	0.520	0.407
	V ₃	0.400	0.500	0.600	0.700	0.550
	V ₄	0.400	0.500	0.600	0.700	0.550
	V ₅	0.533	0.630	0.730	0.801	0.494
C ₅	V ₁	0.200	0.300	0.400	0.500	0.350
	V ₂	0.730	0.833	0.930	0.980	0.856
	V ₃	0.670	0.767	0.870	0.920	0.807
	V ₄	0.470	0.470	0.567	0.720	0.557
	V ₅	0.530	0.633	0.730	0.820	0.679
C ₆	V ₁	0.470	0.567	0.670	0.720	0.607
	V ₂	0.470	0.567	0.670	0.700	0.602
	V ₃	0.130	0.233	0.330	0.460	0.289
	V ₄	0.530	0.630	0.730	0.820	0.678
	V ₅	0.470	0.570	0.670	0.720	0.608
C ₇	V ₁	0.730	0.830	0.930	0.950	0.860
	V ₂	0.530	0.630	0.730	0.820	0.678
	V ₃	0.400	0.500	0.600	0.700	0.550
	V ₄	0.330	0.430	0.500	0.670	0.483
	V ₅	0.530	0.630	0.730	0.820	0.678
C ₈	V ₁	0.470	0.570	0.670	0.720	0.608
	V ₂	0.730	0.830	0.930	0.980	0.868
	V ₃	0.670	0.767	0.870	0.890	0.800
	V ₄	0.470	0.470	0.567	0.620	0.532
	V ₅	0.530	0.633	0.730	0.820	0.679
C ₉	V ₁	0.470	0.567	0.670	0.720	0.606
	V ₂	0.470	0.567	0.670	0.720	0.607
	V ₃	0.130	0.233	0.330	0.460	0.289
	V ₄	0.530	0.630	0.730	0.820	0.678
	V ₅	0.470	0.570	0.670	0.720	0.608
C ₁₀	V ₁	0.730	0.830	0.930	0.960	0.863
	V ₂	0.530	0.630	0.730	0.830	0.680
	V ₃	0.400	0.500	0.600	0.700	0.550
	V ₄	0.330	0.430	0.500	0.640	0.476
	V ₅	0.530	0.630	0.730	0.820	0.678
	V ₂	0.467	0.567	0.667	0.767	0.617
	V ₃	0.333	0.433	0.530	0.620	0.479

The total scores for each vendor can be calculated matrix as follows

$$TS = \begin{matrix} V_1 & V_2 & V_3 & V_4 & V_5 & W_j \\ \begin{matrix} C_1 \\ C_2 \\ C_3 \\ C_4 \\ C_5 \\ C_6 \\ C_7 \\ C_8 \\ C_9 \\ C_{10} \end{matrix} & \begin{bmatrix} 0.800 & 0.605 & 0.797 & 0.674 & 0.802 \\ 0.679 & 0.350 & 0.869 & 0.805 & 0.750 \\ 0.686 & 0.593 & 0.607 & 0.436 & 0.550 \\ 0.868 & 0.407 & 0.550 & 0.550 & 0.494 \\ 0.350 & 0.856 & 0.807 & 0.557 & 0.679 \\ 0.607 & 0.602 & 0.289 & 0.678 & 0.608 \\ 0.860 & 0.678 & 0.550 & 0.483 & 0.678 \\ 0.608 & 0.808 & 0.800 & 0.532 & 0.629 \\ 0.606 & 0.607 & 0.289 & 0.678 & 0.608 \\ 0.863 & 0.680 & 0.550 & 0.476 & 0.678 \end{bmatrix} & \otimes & \begin{bmatrix} 0.250 \\ 0.190 \\ 0.253 \\ 0.209 \\ 0.254 \\ 0.213 \\ 0.110 \\ 0.212 \\ 0.185 \\ 0.190 \end{bmatrix} \end{matrix}$$

Total scores for vender (V1) on criteria is obtained as-
 $(0.800 \times 0.250) + (0.679 \times 0.190) + (0.686 \times 0.253) + (0.868 \times 0.209) + (0.350 \times 0.254) + (0.607 \times 0.213) + (0.860 \times 0.110) + (0.608 \times 0.212) + (0.606 \times 0.185) + (0.863 \times 0.190) = 1.4035$

Similarly, total scores for vendors (V2), (V3), (V4), (V5) are obtained and provided in table-7. In the selection of suitable vendor for any company, initial investment, qualitative criteria each has equal weight age. Hence the final scores and ranking of vendors are given in table.6

Table 7: Final scores and ranging of vendors.

Vendors	V1	V2	V3	V4	V5
Final Scores	1.4035	1.2859	1.29900	1.2489	1.3353
Rank	1	4	3	5	2

VI. RESULTS CONCLUSION

This paper, presented the fuzzy multi criteria decision approach, the order odd ranking of vendor's for the company's are as **V1 > V5 > V3 > V2 > V4**. The result show V1 is the best location for the company. Has been highlighted to solve multi-criteria decision making problems through a case study of vendor selection. The Study demonstrates the effectiveness of the said MCDM techniques in solving such a vendor selection problem.

VII. ACKNOWLEDGEMENT

Authors would like to thank to Vimal steel corporation ltd., for providing data's to create decision criteria & also thank to Performance maker's for providing linguistic variables to apply fuzzy multi criteria decision approach for selecting the best vendor for a companies.

REFERENCES

- [1] Alexios-patapios kontis and vassilionvyagotis, supplier Selection problem multi-criteria approaches based on DEA, international Scientific Advances in Management & Applied Economics, vol.1.1, no.2, 207-219 (2011)
- [2] Shyur & Shih, 2006. Evaluating vendors many criteria Including quantitative, as well as qualitative, a considerable Number of decision making European Journal of Operation Research, Vol.50, 5-10 (2009)
- [3] Kaufmann, A., & Gupta, M.M, Introduction to Fuzzy Arithmetic theory & application, Van No strand Reinhold, Newyork. vol.1; 5-18 (1991)
- [4] Dickson, Weber, Multi objective linear model for Vendor Selection criteria and methods, European Journal of Operational Research, Vol.50, 2-18 (1991)
- [5] Buffa and Jackson and Sharma, Multi decision making used linear and non-linear programming, Total Quality Environmental Management Vol.3 (4); 521-530 (1994)
- [6] Tu-chung Chu, Rangnath varma, Evaluating suppliers via a multiple criteria decision making method under fuzzy Enviroment, nternational Journal of computers & Industrial Engineering vol, 62; 653-660 (2012)
- [7] Swanson's., 2001. Linking maintenance strategies To performance. International Journal of Production Economics 70, 237-244. (2001)
- [8] Shyur & Shih, 2006. Evaluating vendors many criteria Including quantitative, as well as qualitative, a considerable Number of decision making European Journal of Operational Research, Vol.50, 5-10 (2009)

Existence of Hopf-Bifurcations on the Nonlinear FKN Model

Tarini Kumar Dutta,¹ and Nabajyoti Das,²

1. Professor, Department of Mathematics, Gauhati University, Guwahati -781014 : India
2. Assistant Professor, Department of Mathematics, Jawaharlal Nehru College, Boko-781123: India

Abstract: The principal objectives of this paper are (i) to study the development of a general theory for evaluating supercritical and subcritical Hopf bifurcation in any nonlinear differential equations, and (ii) to determine supercritical and subcritical Hopf bifurcations in a rigorous manner on the the Field-Körös-Noyen or FKN model:

$$\frac{dx}{dt} = \varepsilon^{-1}(qy - xy + x - x^2), \frac{dy}{dt} = \delta^{-1}(-qy - xy + 2fz), \frac{dz}{dt} = x - z.$$

Where $\varepsilon, \delta, q, f$ are adjustable parameters?

Key Words: Supercritical Hopf bifurcation, Subcritical Hopf bifurcation, nonlinear differential equation

2010 AMS Classification: 37 G 15, 37 G 35, 37 C 45

I. Introduction

There has been considerable interest recently in sustained oscillation in chemically reacting systems represented by a set of nonlinear differential equations. These oscillations can be periodic in which case the concentrations of some species undergo regular variations with time or they can be non-periodic in which case the reactor never approaches a globally attracting limit cycle. This later condition has been termed chemical chaos.

Many of these studies have been carried out with the well known Belousov-Zhabotinskii reaction. Periodic chemical reaction such as the Belousov-Zhabotinski reaction provide wonderful example of relaxation oscillation in science [3, 9]. The BZ reaction is one of the first oscillating reactions which is studied systematically [1]. Although there are many reactions involved in the BZ reaction they can be rationally reduced to 5 key reactions, with known values for the rate constants, which capture the basic elements of the mechanism. These five reactions can then be represented by a 3-chemical system in which the overall rate constants can be assigned with reasonable confidence. The model is known as the **Field-Körös-Noyen or FKN model** [6]:

$$\begin{aligned} \frac{dx}{dt} &= \varepsilon^{-1}(qy - xy + x - x^2), \\ \frac{dy}{dt} &= \delta^{-1}(-qy - xy + 2fz), \\ \frac{dz}{dt} &= x - z. \end{aligned}$$

We first highlight some related concepts for completeness of our exploration.

II. Limit cycles

A cyclic or periodic solution of a nonlinear dynamical system corresponds to a closed loop trajectories in the state space. A trajectory point on one of these loops continues to cycle around that loop for all time. These loops are called **cycles**, and if trajectories in the neighborhood to the cycle are attracted toward it, we call the cycle a **limit cycle**. Some limit cycles are shown in the figure 1, where (a) shows an inner limit cycle, (b) an outer limit cycle, (c) a stable limit cycles, (d) an unstable limit cycle, and (e) and (f) periodic orbit that may be called saddle limit cycles [4, 7].

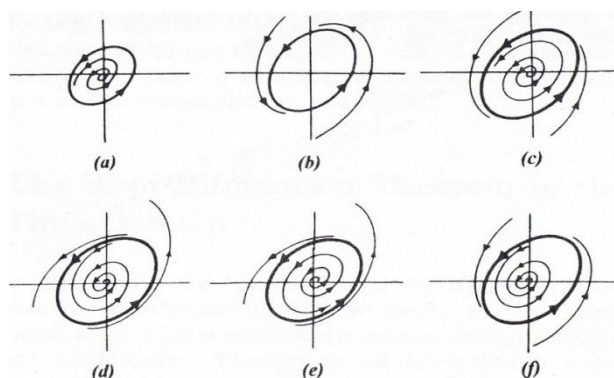


Fig1. Periodic orbits and limit cycles.

III. The Hopf bifurcation theorem in continuous-time

In this discussion we will restrict our discussion on second-order systems of nonlinear ordinary differential equations, although almost all the results and discussions given below can be extended to general n th-order systems. We consider the system:

$$\frac{d\bar{\mathbf{x}}}{dt} = \xi(\bar{\mathbf{x}}; b), \quad \bar{\mathbf{x}} \in \mathfrak{R}^2 \quad (1.1)$$

where b denotes a real parameter on an interval I . We assume that the system is well defined, with certain smoothness on the nonlinear vector field ξ , and has a unique solution for each given initial value $\bar{\mathbf{x}}(t_0) = \bar{\mathbf{x}}$ for each fixed $b \in I$. We also

assume that the system has an equilibrium point $\bar{\mathbf{x}}^*(b)$ and that the associated Jacobian $J = \left. \frac{\partial \xi}{\partial \bar{\mathbf{x}}} \right|_{\bar{\mathbf{x}}=\bar{\mathbf{x}}^*}$ has a single pair of

complex conjugate eigenvalues $\eta(b), \bar{\eta}(b) = \text{Re} \eta \pm i \text{Im} \eta$. Now suppose that this pair of eigenvalues has the largest real part of all the eigenvalues and is such that in a small neighborhood of a bifurcation value b_c , (i) $\text{Re} \eta < 0$ if $b < b_c$, (ii) $\text{Re} \eta = 0, \text{Im} \eta \neq 0$ if $b = b_c$ and (iii) $\text{Re} \eta > 0$ if $b > b_c$. Then, in a small neighborhood of $b_c, b > b_c$, the steady state is unstable by growing oscillations and, at least, a small amplitude limit cycle periodic solution exists about the equilibrium point. The appearance of periodic solutions (all depend on the particular nonlinear function ξ) out of an equilibrium state is called Hopf bifurcation. When the parameter b is continuously varied near the criticality b_c , periodic solutions may emerge for $b < b_c$ (this case is referred to as **supercritical bifurcation**) or for $b > b_c$ (which is referred to as **subcritical bifurcation**) [2, 6, 8].

Armed with these concepts, we now concentrate to our main study and investigation.

IV. The principal investigation

We consider a two-dimensional system $\dot{\bar{\mathbf{x}}} = \xi(\bar{\mathbf{x}}; b), b \in \mathfrak{R}, \bar{\mathbf{x}} = (x, y) \in \mathfrak{R}^2$ where ξ depends smoothly on the real variable parameter b such that for each b near the origin $(0, 0)$ there is an equilibrium point $\bar{\mathbf{x}}^*(b)$ with the Jacobian matrix $D_{\xi_{\bar{\mathbf{x}}}}(\bar{\mathbf{x}}^*(b), b)$ having a complex conjugate pair of eigenvalues $\eta(b), \bar{\eta}(b) = \varphi \pm i\psi$ which cross the imaginary axis as the parameter b passes through $(0, 0)$. Using complex coordinate $z = x + iy$, the system can be expressed in the variable z as

$$\dot{z} = \eta z + A_1 z^2 + B_1 z \bar{z} + C_1 \bar{z}^2 + M_1 z^2 \bar{z} + \dots \quad (1.2)$$

where A_1, B_1, C_1, M_1 are complex constants. By making a suitable change of variables the system can be transformed to a normal form:

$$\dot{w} = w(\eta + a|w|^2) + o(|w|^4), \quad (1.3)$$

where w, a are both complex numbers. We write $a = k + il; k, l \in \mathfrak{R}$. The behavior of the system (1.3) is most conveniently studied using polar coordinate $w = r e^{i\theta}$. From this we obtain, $\dot{w} = e^{i\theta} \dot{r} + i r e^{i\theta} \dot{\theta}$. Hence $\dot{r} = r^{-1} \text{Re}(\bar{w} \dot{w})$ and $\dot{\theta} = r^{-2} \text{Im}(\bar{w} \dot{w})$ and then (1.3) implies

$$\dot{r} = k r^3 + o(r^4), \quad \dot{\theta} = \psi + o(r^2) \quad (1.4)$$

Supercritical and subcritical Hopf bifurcation occur according as $k < 0$ and $k > 0$ respectively. If $k = 0$, considering high order terms we can draw the same conclusion [2].

V. Determination of the indicator of bifurcations: k

Here we are interested in finding the expression for k , whose sign determines the supercritical and subcritical Hopf bifurcation. For this we need the term in $z^2 \bar{z}$. In order to eliminate the quadratic terms, we apply the transformation $w = z + \delta z^2 + \rho z \bar{z} + \bar{\theta} \bar{z}^2$. Then we expand \dot{w} , keeping only terms upto second order (and noting, for example that the difference between z^2 and w^2 is third order, so z^2 can be replaced by w^2 etc.). We have

$$\begin{aligned} \dot{w} &= \dot{z} + 2\delta z \dot{z} + \rho \bar{z} \dot{z} + \rho z \dot{\bar{z}} + 2\theta \bar{z} \dot{\bar{z}} \\ &= \eta z + A_1 z^2 + B_1 z \bar{z} + C_1 \bar{z}^2 + M_1 z^2 \bar{z} + 2\delta z(\eta z + B_1 z \bar{z}) + \\ &\quad \rho \bar{z}(\eta z + A_1 z^2) + \rho z(\eta \bar{z} + \bar{B}_1 z \bar{z}) + 2\theta \bar{z}(\eta \bar{z} + \bar{C}_1 \bar{z}^2) \end{aligned}$$

where cubic terms are neglected other than $z^2 \bar{z}$. We eliminate the quadratic terms by putting

$$\delta = -A_1 / \eta = iA_1 / \psi, \quad \rho = -iB_1 / \psi, \quad \theta = -iC_1 / 3\psi.$$

Then we obtain

$$\dot{w} = \eta w + \left(M_1 + iA_1 B_1 / \psi - i|B_1|^2 / \psi - 2i|C_1|^2 / 3\psi \right) w^2 \bar{w},$$

where again cubic terms are neglected other than $w^2 \bar{w}$, and terms of order higher than 3. We conclude that

$$a = M_1 + iA_1 B_1 / \psi - i|B_1|^2 / \psi - 2i|C_1|^2 / 3\psi.$$

and

$$\begin{aligned} k &= \operatorname{Re}(M_1 + iA_1 B_1 / \psi) \\ &= \operatorname{Re}(M_1) - \psi^{-1} \operatorname{Im}(A_1 B_1). \end{aligned}$$

VI. Extension to three order differential equations

Let us assume that we have a three-dimensional system:

$$\dot{\bar{\mathbf{x}}} = \xi(\bar{\mathbf{x}}), \quad \bar{\mathbf{x}} = (x, y, z)^T, (x, y, z) \in \mathbb{R}^3$$

which has an equilibrium point for which there is one negative eigenvalue and an imaginary pair. The behavior of the system near the equilibrium point can be analyzed by a reduction of the system to a two-dimensional one, as follows. First we choose coordinates so that the equilibrium point is the origin and so that the linearised system is

$$\dot{v} = \rho v, \quad \dot{z} = \lambda z$$

where v is a real variable and z is complex, and $\rho < 0$, $\lambda = i\sigma$.

We can now express the system as

$$\dot{v} = \rho v + \alpha v z + \bar{\alpha} v \bar{z} + \gamma z^2 + \delta z \bar{z} + \bar{\gamma} \bar{z}^2 + \dots$$

$$\dot{z} = \lambda z + p v z + q v \bar{z} + r z^2 + s z \bar{z} + t \bar{z}^2 + d z^2 \bar{z} + \dots$$

If the equation for v were of the form $\dot{v} = \rho v + v f(v, z)$ then the plane $v = 0$ would be invariant, in the sense that solutions starting on this plane stay on it, and we could restrict attention to the behavior on this plane. What we do below is to find a change of variables which converts the system into one which is sufficiently close to this form. We try the change of variables

$$v = w + a z^2 + b z \bar{z} + \bar{a} \bar{z}^2, \text{ where } b \text{ is real.}$$

We obtain

$$\dot{w} = \rho w + \rho a z^2 + \rho b z \bar{z} + \rho \bar{a} \bar{z}^2 + \alpha w z + \bar{\alpha} w \bar{z} + \gamma z^2 + \delta z \bar{z} + \bar{\gamma} \bar{z}^2 - 2a \lambda z^2 - 2\bar{a} \bar{\lambda} \bar{z}^2,$$

neglecting terms of order 3 and higher. Then if we choose

$$a = \gamma \div (2i\sigma - \rho)$$

and

$$b = -\delta \div \rho$$

We have

$$\dot{w} = \rho w + \alpha w z + \bar{\alpha} w \bar{z} + \dots$$

which is of the desired form (as far as of second-order, which turns out to be sufficient). Putting $w = 0$, in the equation for \dot{z} , and retaining only terms of order second and those involving $z^2 \bar{z}$, we obtain

$$\dot{z} = \lambda z + r z^2 + s z \bar{z} + t \bar{z}^2 + \left(\frac{-p\delta}{\rho} + \frac{q\gamma}{2i\sigma - \rho} + d \right) z^2 \bar{z}$$

and using the two-dimensional theory we obtain

$$k = \operatorname{Real} \text{ part of } \left(\frac{-p\delta}{\rho} + \frac{q\gamma}{2i\sigma - \rho} + d + \frac{irs}{\sigma} \right).$$

Supercritical and subcritical Hopf bifurcation occur according as $k < 0$ and $k > 0$ respectively. If $k = 0$, considering high order terms we can draw the same conclusions.

VII. Our main study

For our main study we consider the Field-Körös-Noyen or FKN model:

$$\begin{aligned}\frac{dx}{dt} &= \varepsilon^{-1}(qy - xy + x - x^2), \\ \frac{dy}{dt} &= \delta^{-1}(-qy - xy + 2fz), \\ \frac{dz}{dt} &= x - z.\end{aligned}\tag{1.5}$$

For our purpose, the parameters are fixed as in the FKN model as given below [6]:

$$\varepsilon = 5 \times 10^{-5} = 0.00005, \quad \delta = 2 \times 10^{-4} = 0.0002, \quad q = 8 \times 10^{-4} = 0.0008, \quad f = 0.5$$

With these parameter values the equilibrium points (x^*, y^*, z^*) of the system (1.5) are given by setting the left-hand sides zero and solving the resulting system of equations, to get

$$\begin{aligned}(x^* = 0, y^* = 0, z^* = 0), \\ \text{or } (x^* = -0.0404019999500025, y^* = 1.0202009999750015, z^* = -0.0404019999500025), \\ \text{or } (x^* = 0.0396019999500025, y^* = 0.9801990000249986, z^* = (0.0396019999500025)).\end{aligned}$$

These numerical solutions are found with the help of MATHEMATICA. Out of these equilibrium points

$$(x^* = -0.0404019999500025, y^* = 1.0202009999750015, z^* = -0.0404019999500025)$$

is suitable for our purpose.

Let us take a linear transformation which moves the equilibrium point to the origin. We take $u = x - x^*$, $v = y - y^*$ and $w = z - z^*$.

Then the system (1.5) becomes

$$\begin{aligned}\frac{du}{dt} &= \varepsilon^{-1}(q(v + y^*) - (u + x^*)(v + y^*) + (u + x^*) - (u + x^*)^2) \\ &= 1.38778 \times 10^{-13} - 20000u^2 + u(1212.06 - 20000v) + 824.04v\end{aligned}\tag{1.6}$$

$$\begin{aligned}\frac{dv}{dt} &= \delta^{-1}(-q(v + y^*) - (u + x^*)(v + y^*) + 2f(w + z^*)) \\ &= 3.46945 \times 10^{-14} + u(-5101 - 5000v) + 198.01v + 5000w\end{aligned}\tag{1.7}$$

$$\begin{aligned}\frac{dw}{dt} &= (u + x^*) - (w + z^*) \\ &= 0 + x - z\end{aligned}\tag{1.8}$$

The matrix of linearized system is then of the form

$$M = \begin{bmatrix} 1212.0599985000702 & 824.0399990000501 & 0.0 \\ -5101.004999875007 & 198.0099997500125 & 5000.0 \\ 1.0 & 0.0 & -1.0 \end{bmatrix}$$

The eigenvalues $\rho, \lambda_1, \lambda_2$ of M are

$$\begin{aligned}\rho &= -0.07276521654210118, \\ \lambda_1 &= 704.5713817333121 + 1986.3795683652036i, \\ \lambda_2 &= 704.5713817333121 - 1986.3795683652036i\end{aligned}$$

Let us take

$$D = \begin{bmatrix} \rho & 0 & 0 \\ 0 & \lambda_1 & 0 \\ 0 & 0 & \lambda_2 \end{bmatrix}$$

as the diagonal matrix. Then we obtain

$$M^{-1}D = \begin{bmatrix} -0.0000445755166 & -1.7962166905241 - 5.0640264803776i & -8981.0834526207 + 25320.132401888i \\ -0.0000227379933 & 2.6420105842731 + 7.4485509631315i & 13210.052921365 - 37242.754815658i \\ -0.0000445755166 & -1.7962166905241 - 5.0640264803776i & -9685.6548343540 + 27306.511970253i \end{bmatrix}$$

In order to make the linearized system into a diagonal form, we make the coordinate change by $M^{-1}DU$, where U is the column matrix, $U = [f, g, h]^T$.

$$\text{Now } M^{-1}DU = \begin{bmatrix} (-0.0000445755 + 0.i)f - (1.79622 + 5.06403.i)g - (8981.08 - 25320.1.i)h \\ (-0.000022738 + 0.i)f + (2.64201 + 7.44855.i)g + (12310.1 - 37242.8.i)h \\ (-0.0000445755 + 0.i)f - (1.79622 + 5.06403.i)g - (9685.65 - 27306.5.i)h \end{bmatrix}$$

Putting $u = (-0.0000445755 + 0.i)f - (1.79622 + 5.06403.i)g - (8981.08 - 25320.1.i)h$,
 $v = (-0.000022738 + 0.i)f + (2.64201 + 7.44855.i)g + (12310.1 - 37242.8.i)h$,
 $w = (-0.0000445755 + 0.i)f - (1.79622 + 5.06403.i)g - (9685.65 - 27306.5.i)h$

in equations (1.6) and (1.7), we get

$$\begin{aligned} \frac{du}{dt} &= 1.38778 \times 10^{-13} - 20000(-0.0000445755f - (1.79622 + 5.06403i)g - (8981.08 - 25320.1i)h)^2 \\ &\quad + (-0.0000445755f - (1.79622 + 5.06403i)g - (8981.08 - 25320.1i)h)(1212.06 - \\ &\quad 20000(-0.0000445755f - (1.79622 + 5.06403i)g - (8981.08 - 25320.1i)h)) \\ &\quad + 824.04(-0.000022738f + (2.64201 + 7.44855i)g + (13210.1 - 37242.8i)h) \end{aligned}$$

$$\begin{aligned} \frac{dv}{dt} &= 3.46945 \times 10^{-14} + (-0.0000445755f - (1.79622 + 5.06403i)g - (8981.08 - 25320.1i)h)(-51101 - \\ &\quad 5000(-0.000022738f + (2.64201 + 7.44855i)g + (13210.1 - 37242.8i)h)) + \\ &\quad 198.01(-0.000022738f + (2.64201 + 7.44855i)g + (13210.1 - 37242.8i)h) + \\ &\quad 5000(-0.0000445755f - (1.79622 + 5.06403i)g - (9685.65 - 27306.5i)h). \end{aligned}$$

Finally, under the stated transformation (as described in General theory) the system becomes

$$\begin{aligned} \frac{du}{dt} &= -0.0727652f + (-1.66416 - 4.69172i)fg + (-8320.8 + 23458.6i)fh \\ &\quad + (-211121 + 171325i)g^2 + (2.7189 \times 10^9 + 3.77936 \times 10^{-8}i)gh \\ &\quad + (-5.27803 \times 10^{12} - 4.28312 \times 10^{12}i)h^2 + \dots \end{aligned} \quad (1.9)$$

$$\begin{aligned} \frac{dv}{dt} &= (704.571 + 1986.38i)g + (0.384633 + 1.084339i)fg + (1923.17 - 5421.93i)fh \\ &\quad + (-164870 + 133792i)g^2 + (2.12326 \times 10^9 + 1.93249 \times 10^{-8}i)gh \\ &\quad + (-4.12175 \times 10^{12} - 3.3448 \times 10^{12}i)h^2 + 0.0g^2h + \dots \end{aligned} \quad (1.10)$$

From above, we obtain

$$\begin{aligned} \rho &= \text{Coefficient of } f \text{ in (1.9)} = -0.0727652, \\ p &= \text{Coefficient of } fg \text{ in (1.10)} = 0.384633 + 1.08439i, \\ \delta &= \text{Coefficient of } gh \text{ in (1.9)} = 2.7189 \times 10^9 + 3.77936 \times 10^{-8}i, \\ q &= \text{Coefficient of } fh \text{ in (1.10)} = 1923.17 - 5421.93i, \\ \gamma &= \text{Coefficient of } g^2 \text{ in (1.9)} = -211121 + 171325i, \\ d &= \text{Coefficient of } g^2h \text{ in (1.10)} = 0, \\ r &= \text{Coefficient of } g^2 \text{ in (1.10)} = -164870 + 133792i, \\ s &= \text{Coefficient of } gh \text{ in (1.10)} = 2.12326 \times 10^9 + 1.93249 \times 10^{-8}i, \\ \sigma &= \text{Imaginary part of eigenvalues} = 1986.37957 \end{aligned}$$

Using the above values we can calculate the value of k as

$$k = \text{Real part of } \left(\frac{-p\delta}{\rho} + \frac{q\gamma}{2i\sigma - \rho} + d + \frac{irs}{\sigma} \right).$$

$$\approx -1.28639 \times 10^{11}$$

Hence, we have a supercritical Hopf bifurcation. Similarly, we can study the Hopf bifurcation of a given system for different values of the parameters.

VIII. Conclusion

We think, our method is quite suitable for obtaining Hopf Bifurcation for any order nonlinear differential equations, if Hopf bifurcation exists.

References

- [1] Atkins, P. and Paula, J. D., Atkin's Physical Chemistry, Seventh edition, oxford University Press, 2002
- [2] Das, N. and Dutta, T. K., Determination of supercritical and subcritical Hopf bifurcation on a two-dimensional chaotic model, International Journal of Advanced Scientific Research and Technology, Issue2, Vol. 1, February, 2012
- [3] Field, R. and Burger, M., Oscillations and Travelling Waves in Chemical Systems, Wiley, New York, 1985
- [4] Hilborn, Robert C., Chaos and Nonlinear Dynamics, Oxford University Press, 1994
- [5] Moiola, J. L. and Chen, G., Hopf Bifurcation Analysis: a frequency domain approach, World Scientific, 1996
- [6] Murray, J. D., Mathematical Biology I: An Introduction, Third Edition (2002), Springer
- [7] J. L Moiola and G. Chen, Hopf Bifurcation Analysis: a frequency domain approach, World Scientific, 1996
- [8] Roose, D. and Hlavacek, V., A Direct Method for the computation of Hopf bifurcation points, SIAM J. APPL. MATH., Vol. 45, No. 6, December 1985
- [9] Scott, S. K., Oscillations, Waves, and Chaos in Chemical Kinetics, Oxford Science Publications, Oxford, UK, 1994

Application of Multilevel Voltage-Source-Converter in FACTS Devices for Power System Voltage Control & Reactive Power Compensation

Snehasish Pal¹, Suvarun Dalapati,² and N.C.Ganguly³

¹Associate. Professor, Department of Electrical Engineering, JIS College of Engineering, Block-A, Phase-III, P.O.Kalyani, District Nadia, Pin 741235, West Bengal., INDIA.

²Asst. General Manager (R & D), Electronic Systems Division, Stesalit Limited, Stesalit Towers, E-2/3, Block- EP and GP, Salt Lake, Sector-V, Kolkata- 700091, West Bengal, INDIA.

³Ex-Principal, NIT-Silchar, Assam-788010, INDIA.

Abstract: Voltage control and fast reactive power compensation are two main application area of Static Synchronous Compensator (STATCOM), which is a shunt connected voltage source converter (VSC) based FACTS controller using power semiconductor devices (particularly IGBT, GTO etc.). However, the total Statcom circuitry has complex and coupled system dynamics which require advanced controllers (specially FPGA/DSP based) to achieve well performance. In our paper, we have represented a sixty pulse VSC for producing higher pulse number by combining a twelve pulse converter with a five level VSI in order to obtain the overall performance of the said VSC in a three phase system. As the number of levels increases in the VSI of the Statcom, it will produce a staircase wave with lower value of THD. The simulation results are presented and it is observed that the STATCOM shows excellent response to step change in the reactive current reference & the value of THD is also within the acceptable limit.

Keywords: FACTS, Multilevel converter, Statcom, Voltage stability, Reactive Power Compensation

I. Introduction

The field of voltage control application in power system using FACTS devices has been one of the most active areas in research & development of application of power electronics in power system as a remedy to release the extremely transmission system tension. Several generating station as well as industrial process have increased their power level needs, driven mainly by economy of scale, triggering the development of new power semiconductors, converter topologies and control methods. Amongst the power switching devices, GTO (rating ≈ 4.7 Kv) was the standard for medium voltage transmission system until the advent of high power IGBTs and gate commutated thyristors (GCTs) in the late 1990s [2]. These switching devices are now extensively used in high power application due to their superior switching characteristics, reduced power losses, ease of gate control and snubberless operation.

With the trend of deregulating power industry and installing more distributed generators, the future power system needs to provide sufficient, stable, economic, secure and high quality electric power to various load centres. It is envisaged that FACTS devices or controllers are going to play a critical role in operating the new type of power systems under such a complex operating environment [4]. FACTS technology has been expected to offer the following advantages:-

- a) A major thrust of FACTS technology is the development of power electronic-based systems that provide dynamic Control of the power transfer parameters of transmission voltage, line impedance and phase angle.
- b) It increases the loading capability of lines with the thermal capability.
- c) Provides greater flexibility in sitting new generation.
- d) To reassign power flows at will and on a real time basis.
- e) To bring the transfer capability of transmission line approaching its thermal limit violating the stability criteria.

Amongst the FACTS devices, STATCOM is a new generation of reactive power compensating devices, which is much used in various power system operation and control due to its fast control characteristics as well as continuous compensating capability. The hardware of a STATCOM is similar to the shunt branch of the Unified Power Flow Controller (UPFC) and can be controlled to provide both the real and reactive power compensations. Fig1 shows the schematic diagram of Statcom shunt FACTS controller. As the classical two level VSIs are limited to low or medium power applications due to the device voltage limits, the series connection of switching devices enable the high power two level VSI. With the addition of few components like diodes or capacitors, permitted to enhance the quality of input and output variables, brings out the multilevel VSI (ML-VSI) technology.

This paper presents the design of a sixty pulse vsc based STATCOM, where the five level VSI is utilized as a re-injection circuit. Here sixty-pulse VSC consists of the following components:-

- a) The standard twelve-pulses shunt converter.
- b) A half-bridge diode-clamped inverter providing three-level.
- c) A half-bridge inverter sharing a common split-capacitor power supply providing other two level to the dc pulse.

The proposed STATCOM is used to provide satisfactory performances in performing various reactive power flow control during transient as well as steady state operations of power systems. In order to simulate realistic conditions, three phase power flow is so important. In our proposed model, there are three phase transmission lines unbalanced in high voltage transmission network and also there are one or two phase lines are in some distribution network. The results of various power flow control examples are presented in the matlab/simulink environment to show the successful decision of the sixty-pulse VSC based STATCOM and its effectiveness in voltage and reactive power control in power systems.

II. Aspects of availability Transfer Capability(ATC)

The reasoning behind the development of ATC is based on several principles developed by the 'North American Electric Reliability Council's(NERC)[5].ATC actually is the measurement of the transfer capability remaining in the physical transmission network for further commercial activity, over and above already committed uses.ATC must recognize time variant power flow conditions and the effects of simultaneous transfers/parallel path flow from reliability point of view. Briefly ATC can be defined as [Dobson et al.,2001].

ATC = TTC – CBM – TRM – 'Existing TC'

Where, TTC denotes the 'total transfer capability.'

This capacity is defined by the worst contingency for the defined point-to-point path and the thermal, voltage and stability limits of the path.

CBM denotes the 'capacity benefit margin'.

TRM denotes the 'transmission reliability margin'.

III. Aspects of FACTS devices

Nowadays, centralized control of bulk power system will no longer be possible because of the development of distributed generation systems and thus traditional vertically integrated utility structures will no longer be used much. FACTS devices can provide a solution to a number of potential problems such as uneven power flow through the system, more transmission losses, lower stability margin(both transient and dynamic), sub-synchronous oscillations and greater voltage fluctuations. The majority of the FACTs topologies are designed to minimize the problems by controlling the amount and direction of reactive power (mainly) flows through the coupling transformer reactance (X), which lies between bus and VSC (Ref Fig 2).

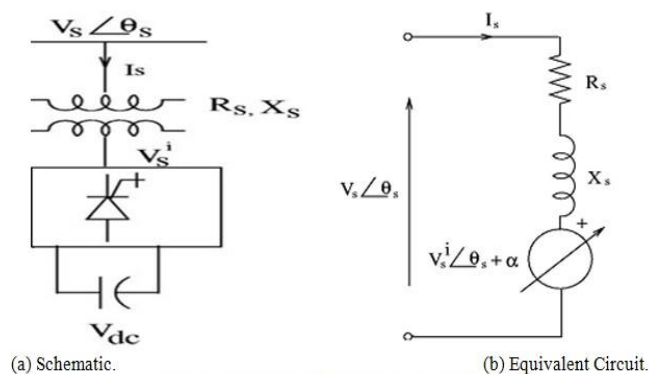


Fig. 1. STATCOM shunt FACTS controller.

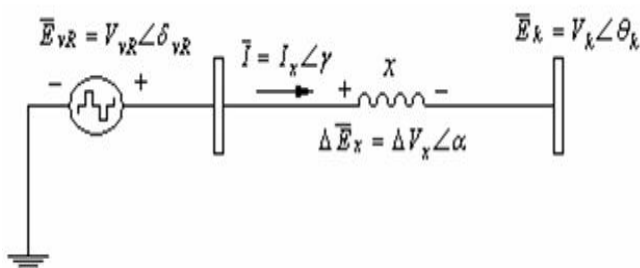


Fig. 2. Equivalent one-phase circuit of the STATCOM.

$E_{vR} \rightarrow$ Represents the STATCOM's terminals voltage.(acts as variable voltage source) and V_{vR} is a function of the STATCOM's capacitor rating.

$E_k \rightarrow$ Voltage at the power system bus,k.

$\Delta E_x \rightarrow$ voltage drop in the coupling reactance, X

The incorporation of battery energy storage systems(BESS) is required into the FACTs devices to overcome the problems of uneven active power flow, transient and dynamic instability, subsynchronous oscillations and lower quality of power by proper active power control. The possibility of controlling the power flow in an electric power system without generation rescheduling or topological changes can improve the performance effectively. with increased loading of power system, combined with de regulation of power industry, motivates the use of power flow control as a very cost effective means by using power- electronics based controllers. There are several methods for finding the optimal locations of FACTS devices in both vertically integrated and unbundled power systems [7].

However, the drawback of FACTs/ESS devices, is the size of the storage systems for FACTs integration, particularly BESS may be too high for practical use in transmission-level applications. Voltage instability occurs in large battery systems, where multiple cells are placed in series. However large oscillations can be mitigated with modest power injection from a storage system, and thus it is possible to consider design for FACTs converters that take advantage of smaller voltage energy systems (SVES).Multilevel inverter can replace standard VSC to decreasing the required BESS voltage. Additionally, it can provide improved voltage quality, decreased switching frequencies, reduced power losses, decreased stress on individual switching devices, and enable more effective use of ESSs.

IV. Modeling of the STACOM with Five Level VSI

FACTS devices have the ability to allow power systems to operate in a more flexible, secure, economic and sophisticated way. When transmission constraints make certain combinations of generation and demand unviable due to the potential of outages, FACTs devices may be used to improve the system performance by controlling the power flows in the grid.

A schematic representation of a traditional six pulse (two levels) STATCOM is shown in Fig 3.

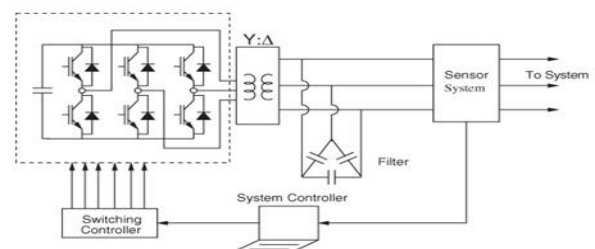


Fig 3:- Schematic of the traditional six pulses STATCOM.

It is composed of a VSC and its associated shunt connected transformer with system bus. The transformer is used as a link between the VSC and the system bus. To explain the basic principle of STATCOM, it is considered that the coupling transformer is lossless and in this way, its equivalent one-phase circuit has already been depicted in fig 2.

In fig 2, if we take $\theta_k = 0$ as the reference, the following equations are obtained when STATCOM supplying power to the bus :-

$$\vec{E}_k = \vec{E}_{VR} - \Delta \vec{E}_x \quad \dots\dots\dots(1)$$

$$P = \frac{V_{VR} V_k}{x} \sin \delta_{VR} \quad \dots\dots\dots(2)$$

$$Q = \frac{V_{VR}^2}{x} - \frac{V_{VR} V_k}{x} \cos \delta_{VR} \quad \dots\dots\dots(3)$$

Under normal operating conditions, to compensate for the power losses that exist in its interior, a small amount of active power must flow into the VSC. Normally there is always a slight phase difference between δ_{VR} and θ_k . A STATCOM without accompanying energy storage is used primarily for reactive power support and voltage related problems can be significantly reduced by STATCOM controlled reactive power injection. The problems of transient & dynamic stability, uneven active power flow, sub-synchronous oscillation and power quality issues can be impacted more effectively by active power control. Incorporating an ESS, such as batteries, superconducting magnetic energy storage (SMES), fuel cells into a STATCOM device can provide dynamic decentralized active power capabilities and give transmission service providers much needed flexibility for reducing transmission level power flow problems, if the dc voltage of the STATCOM is closely regulated.

The present VSC represents six pulse five level inverter topology which greatly reduces the harmonic distortion on the ac side i.e. at the output side of the STATCOM as well as decreases stress on the electronic components due to decreased voltages and lower switching losses. To improve efficiency and control of VSC multilevel converter uses a variety of PWM strategies, amongst which SVPWM control strategy is very much effective. This type of inverters also reduces the size of the individual energy storage units without compromising performance. Since the dc voltage no longer requires direct control, it is possible to design controls to vary the output reactive power (or voltage) and active power independently by varying the magnitude and angle of the fundamental component of the injected current. A five level cascaded converter with unequal voltage levels can be converted into a nine level converter [8]. e.g. if the batteries of the five level converter are rearranged such that dc voltage V_1 and V_2 are unequal, then a nine level stair case output voltage waveform can be synthesized.

Due to the potential for charge imbalance of the capacitors, diode clamped converters (DCMLI) are used less frequently than cascaded inverters in industrial applications. However two most recent advances in charge-balancing circuit or to use space vector modulation [19]. Since a balancing circuit is required for optimal operation, several connections can be used to better

utilize the STATCOM/BESS. e.g., the number of batteries can be reduced by placing them across the inner dc link capacitors. This reduced system is called a STATCOM/2BESS.

V. Optimum Location of FACTS devices

The primary function of a STATCOM is to provide voltage regulation within the power system. To provide best performance, a STATCOM should be placed at those buses which provide high voltage response for incremental changes in reactive power injection. The main objective for FACTS device placement may be one of the following:-

- 1.Reduction in the real power loss of a particular line.
2. Reduction in the total system real power loss.
- 3.Reduction in the total system reactive power loss.
- 4.Maximum relief of congestion in the system.

For the first three objectives, sensitivity approach of the total system reactive power loss w.r.t the control variables of the FACTS devices based methods may be used. If the objective of the placement of FACTS devices is maximum relief of congestion, the devices may be placed in the most congested lines. One means of quantifying the sensitivity in voltage magnitude to changes in reactive power is to use a voltage security indicator such as the singular value decomposition of the system Jacobian :-

$$J = U \Sigma V^T = \sum_{i=1}^n \sigma_i u_i v_i^T \quad \dots\dots\dots(4)$$

Where u_i and v_i are the columns of the $n \times n$ orthonormal matrices U and V , and Σ is a diagonal matrix of positive real singular values σ_i , so that

$$\sigma_1 \geq \sigma_2 \geq \sigma_3 \geq \dots \geq \sigma_n \geq 0 \quad \dots\dots\dots(5)$$

The smallest singular value σ_n is an indicator of the proximity to the static voltage limit, the right singular vector V_n corresponding to σ_n indicates the sensitive voltage magnitudes and angles and the left singular vector u_n corresponding to σ_n indicates the most sensitive direction for changes of active and reactive power injections. At the critical loading point, the relatively large elements of left singular vector u_n will correspond to those system buses, which are highly sensitive to reactive power injections. If we place the STATCOM at these buses, most effective voltage regulation can be obtained.

VI. Mathematical Modeling of the STATCOM in D-Q Reference Frame

When switching functions are approximated by their fundamental frequency components, neglecting harmonics, a STATCOM can be modeled by transforming the three-phase voltages and currents to D-Q variables using Kron's transformation. The STATCOM can be represented functionally, as shown in Fig.1. Magnitude control of the converter output voltage is achieved by modulating the conduction period affected by the dead angle β of a converter while the dc voltage is kept constant. The converter output voltage can be represented in the D-Q reference frame as:

$$\begin{aligned} V_s^i &= \sqrt{V_{sD}^2 + V_{sQ}^2} \\ V_{sD}^i &= k_m V_{dc} \sin(\theta_s + \alpha) \\ V_{sQ}^i &= k_m V_{dc} \cos(\theta_s + \alpha) \end{aligned} \quad (6)$$

The following equations in the D-Q variables can be given for describing STATCOM:

$$\frac{dI_{sD}}{dt} = -\frac{R_s \omega_B}{X_s} I_{sD} - \omega_o I_{sQ} + \frac{\omega_B}{X_s} [V_{sD} - V_{sD}^i] \quad (7)$$

$$\frac{dI_{sQ}}{dt} = \omega_o I_{sD} - \frac{R_s \omega_B}{X_s} I_{sQ} + \frac{\omega_B}{X_s} [V_{sQ} - V_{sQ}^i] \quad (8)$$

$$\frac{dV_{dc}}{dt} = -\frac{\omega_B}{b_c} I_{dc} - \frac{\omega_B}{b_c R_p} V_{dc} \quad (9)$$

Where,

$$I_{dc} = -[k_m \sin(\theta_s + \alpha) I_{sD} + k_m \cos(\theta_s + \alpha) I_{sQ}] \quad (10)$$

I_{sD} and I_{sQ} are the D-Q components of the STATCOM current, θ_s is the phase angle of the bus voltage and α is the angle by which the fundamental component of the converter output voltage leads the STATCOM bus voltage V_s . k_m is the modulation index and for a three-level converter it is a function of the dead angle β and is given by $k_m = k^1 \cos \beta$,

where $k^1 = k^p$. $k = \frac{4\sqrt{6}}{\pi}$ for 24-pulse converter. p is the transformation ratio of STATCOM interfacing transformer. In a three level 24-pulse converter, the dc voltage reference may be adjusted by a slow controller to get the optimum harmonic performance at $\beta_{\text{optimum}} = 3.75^\circ$ in the steady state.

VII. Simulink Model

In our proposed system (Fig.4), the STATCOM is connected to bus through a coupling transformer with resistance and reactance respectively. In the Power circuit diagram of the STATCOM, the converter has multipulse or a multilevel configuration. With Five level converter topology, the magnitude of the ac output voltage of VSI can be changed by varying the dead angle with fundamental switching frequency. This higher level topology of the VSI greatly reduces the THD much more than two-level VSI. Here, the Statcom is connected to a 25 KV,60 Hz.

System, where fixed load and variable loads are existing in different buses.

The STATCOM output is coupled on parallel with the network. A 12,000 μ F capacitor is used as dc voltage source for the inverter. The standard response time is typically chosen to be of the order of a hundred microseconds (i.e. 0.1s). To control the output voltage of VSI, PWM Strategy has been used not only for fast communications to reach a lower THD but also it can be effectively used during unbalanced operation of the system.

The design of a sixty pulse VSC based STATCOM, where the five level VSI is utilized is shown below. Here sixty-pulse VSC consists of the following components :-

- The standard twelve-pulses shunt converter.
- A half-bridge diode-clamp inverter providing three-level.
- A half-bridge inverter sharing a common split-capacitor power supply providing other two level to the dc pulse.

The proposed STATCOM is used to provide satisfactory performances in performing various reactive power flow control during transient as well as steady state operations of power systems.

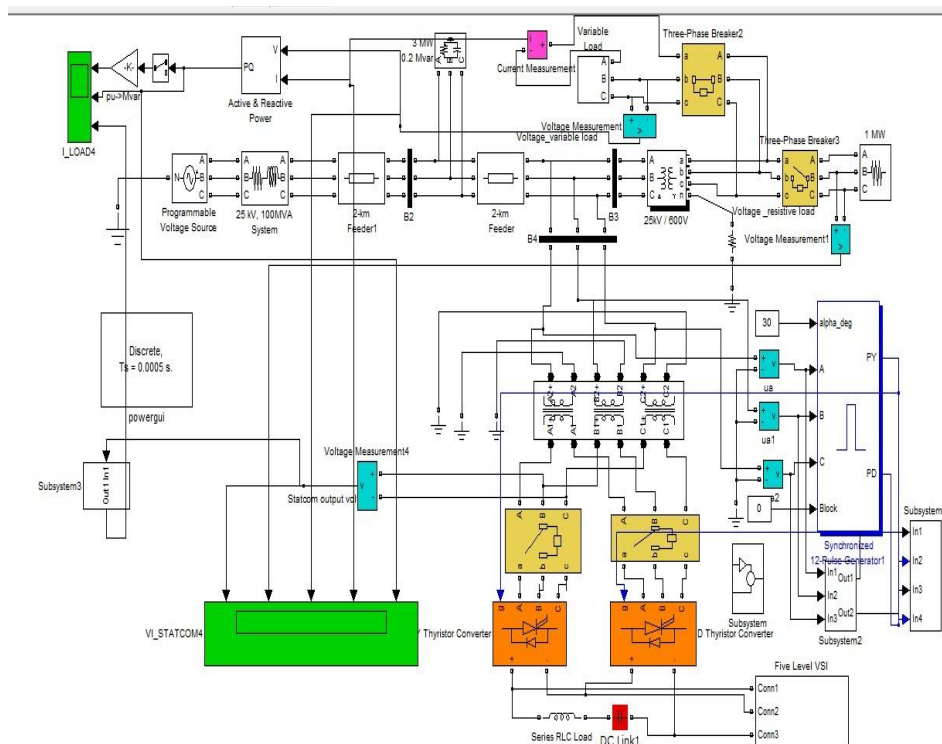


Fig 4: Proposed simulink model of 64 pulse STATCOM

Output Scope :-

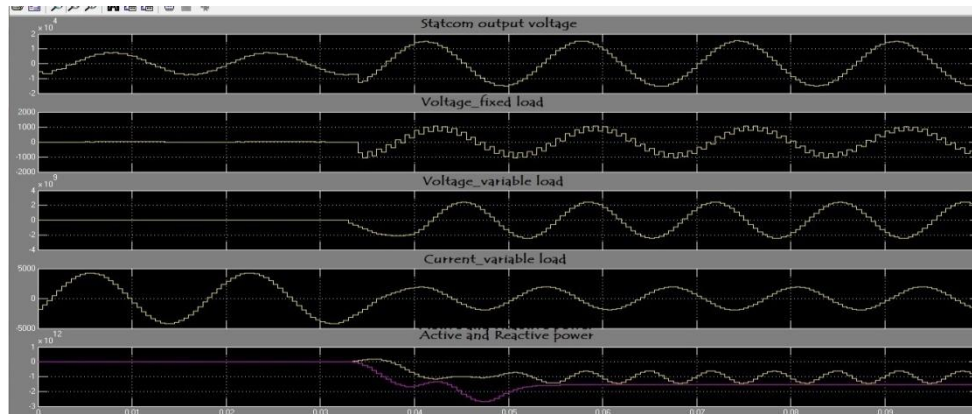


Fig 5 : Output waveforms of the simlink model.

FFT Analysis :-

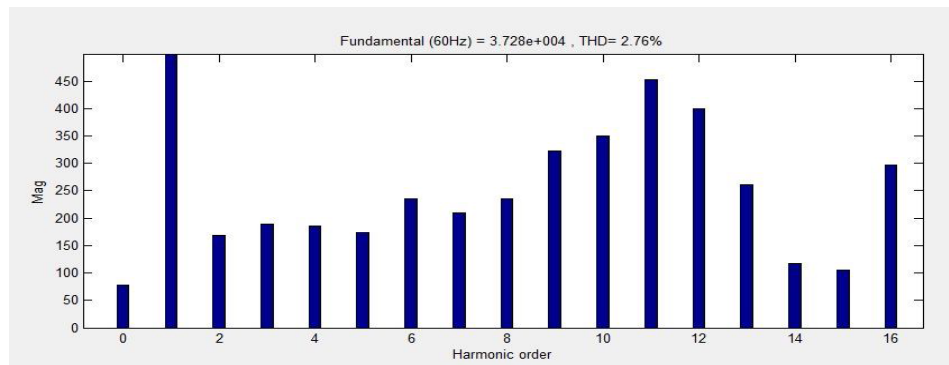


Fig6.Output Voltage waveform of Fixed Load

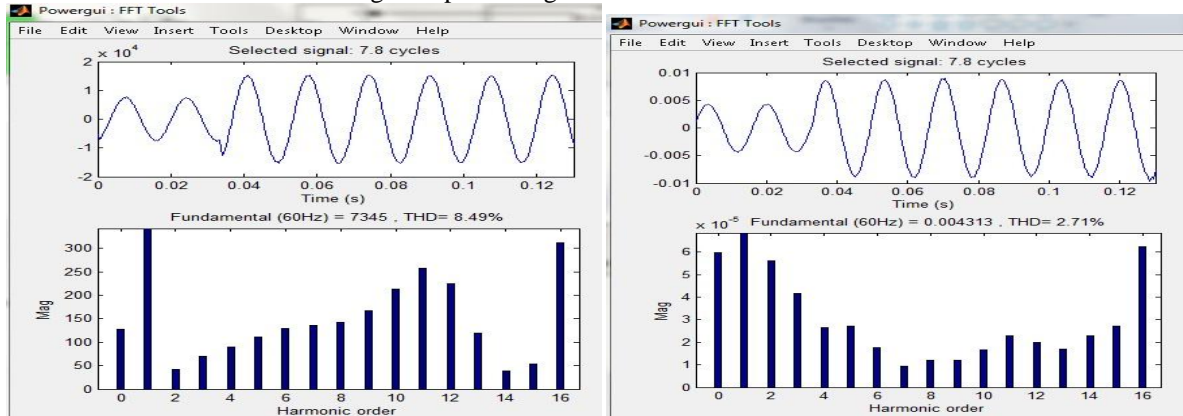


Fig 7 : Output voltage(left) and current(right) waveform of STATCOM

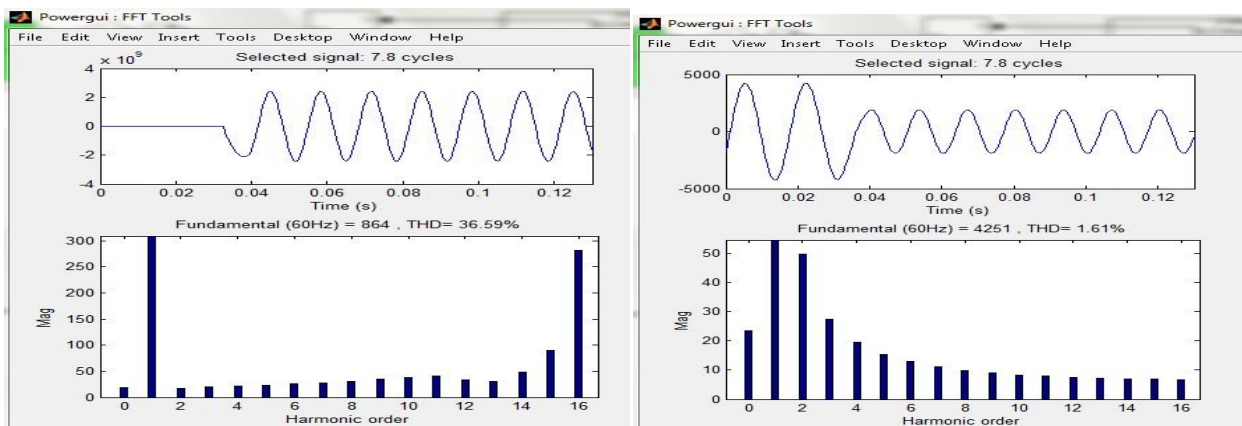


Fig 8: Output voltage (left) and current (right) waveform of variable load

VIII. Conclusion

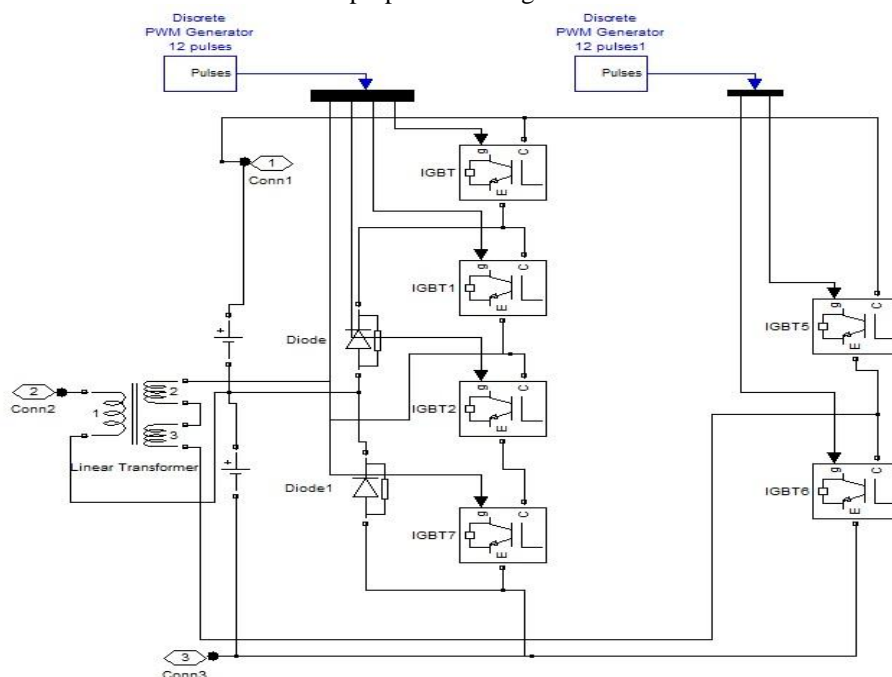
This paper has presented the state-of-art and development of multilevel VSCs for high power rating transmission system application within the STATCOM. Due to improved dynamic performance, extended operating range, increased availability, reduced line harmonics and an adjustable power factor at the point of common coupling, multilevel VSIs are used as VSC within the STATCOM. The main feature of the proposed system and switching strategy is that it can fast modify the switching patterns of the internal power electronics switches of the given STATCOM to achieve the desired voltage across the load terminals. The mathematical modeling of the STATCOM for power system applications is also presented here. The diode-clamped converter(which provides three level part of the five level VSI) provides a large operating range and the ability to use fewer batteries with a balancing circuit. The increase of the converter power of multilevel VSCs will enable replacement of thyristor based CCVs and LCIs in the near future.

References

- [1] K.R.Padiyar . and N.Prabhu. (2006) 'Design and Performance evaluation of sub synchronous damping controller with STATCOM', IEEE Transactions on Power Delivery, July, Vol. 21, No. 3, pp.1398-1405.
- [2] P.K.Steimer.;H.E.Gruning.;J.Werninger.;E. Carroll.;S.Klaka;S.Linder,(1999) ' IGCT –A new emerging technology for high power, low cost inverter', IEEE India Appl. Mag, July / August, Vol. 5, No. 4, pp. 12-18.
- [3] Y.Chang ,C. Wian , M.L.Crow ,S. Pekarek and S.Atcitty. (2006) 'A comparison of diode-clamped and cascaded multilevel converters for a STATCOM with energy storage', IEEE Trans, India Elctron, April, Vol. 53, No. 2., pp. 477-485.
- [4] K.Li,J.Liu, Z.Wang and B.Wei. (2007) 'Strategies and operating point optimization of STATCOM control for voltage unbalance utilization in three-phase three wire systems', IEEE Trans. PD, January, Vol. 22, No. 1 pp. 413-422.
- [5] I.Dobson , S.Greene, R.R.Raman , C.L.Demarco , F.L.Alvarado, M.Glavic,J. Zhang. andR. Zimmerman (2001), ' Electric Power Transfer Capability: Concepts, Applications, Sensitivity and Uncertainty', November, PSERC Publication, pp. 01—34.
- [6] Wu G. Yokoyama, J. He and Y.Yu (1998) 'Allocation and control of FACTS devices for steady state stability enhancement of large-scale power system', Proceedings of IEE International Conference on Power System Technology, August,1998, Vol. 1, INSPEC Accession Number: 6111205, pp. 357-361.
- [7] S.Pal and S.Dalapati, "Digital Simulation of Eighty Four Pulse STATCOM for improvement of Power Quality",Int.J.of Engg,Research & Indu Appls.,Vol.5,No.III,Aug.2012:pp.225-236.
- [8] Y.Liu,Z. Zhao, C.Quian and X. Zhou (2000) 'A novel three phase multilevel voltage source converter', proceedings IPEMC, August, Vol. 3, pp. 1172-1175,.
- [9] M.Botao ,L. Congwei , Z.Wang and L. Fahai (2002) ' New SVPWM Control with balance dc voltages', in proceedings Annual conference IEEE India Electron Society, November, Vol. 2, pp. 903 – 907.
- [10] B.R.Lin (2000) ' Analysis and implementation of a three level PWM rectifier/inverter,' IEEE Transactions on Aerospace and Electronic Systems, July, Vol. 36, No. 3, pp. 948 – 956.

Appendix :-

The five level VSI which has been proposed in the given simulink model is shown below :-



Response Spectrum Modal Analysis of Buildings using Spreadsheets

Ravi Kant Mittal¹, P. Prashanth²

¹Assistant Professor, Department of Civil Engineering

Birla Institute of Technology and Science, Pilani-333031, India,

²Formerly Graduate Students, Department of Civil Engineering

Birla Institute of Technology and Science, Pilani-333031, India

ABSTRACT: Seismic analysis of any structure is now mandatory requirement for design of structures. These analyses are very time consuming and tedious. Problem is to be analyzed as per country code only (e.g. IS 1893-2002 for India) in which building is situated. An attempt has been made to make these analyses simple using spread sheets. Spread sheet has been prepared for analysis of structure by response spectrum analysis using SRSS method and CQC method.

Keywords: Earthquake analysis, Response spectrum analysis, Modal combination, SRSS, CQC.

I. INTRODUCTION

Understanding and mastering the seismic analysis of structures is a challenging yet essential element in the field of civil engineering [1-2]. Use of spreadsheets in Civil engineering is reported by various authors [3-7]. In this paper, an Excel-based analysis tool is presented, which attempts to address some of the challenges associated with the problem. The basic principle of the approach is anchored in the need and desire to empower the designer to explore effects of the various parameters on the response of the structure in an environment designed to generate rigorous solutions. The paper also explores the benefits of coupling programming and spreadsheet calculations.

II. RESPONSE SPECTRUM MODAL ANALYSIS OF BUILDINGS USING IS 1893(PART1)-2002

As per IS 1893 (part1)-2002 [8], dynamic analysis shall be performed to obtain the design seismic force, and its distribution to different levels along the height of the building and to the various lateral load resisting elements, for the following buildings:

- Regular buildings — Those greater than 40 m in height in Zones IV and V, and those greater than 90 m in height in Zones II and III.
- Irregular buildings - All framed buildings higher than 12 m in Zones IV and V, and those greater than 40 m in height in Zones II and III. Dynamic analysis may be performed by The Response Spectrum Method. Procedure is summarized in following steps.
 - Modal mass (M_k) – Modal mass of the structure subjected to horizontal or vertical as the case may be, ground motion is a part of the total seismic mass of the Structure that is effective in mode k of vibration. The modal mass for a given mode has a unique value, irrespective of scaling of the mode shape.

$$M_k = \frac{\left[\sum w_i \phi_{ik} \right]^2}{g \sum w_i \phi_{ik}^2}$$

Where

g = acceleration due to gravity,

ϕ_{ik} = mode shape coefficient at floor i in mode k

W_i = Seismic weight of floor i.

(b) Modal Participation factor (P_k) – Modal participation factor of mode k of vibration is the amount by which mode k contributes to the overall vibration of the structure under horizontal or vertical earthquake ground motions. Since the amplitudes of 95 percent mode shape can be scaled arbitrarily, the value of this factor depends on the scaling used for the mode shape.

$$P_k = \frac{\sum w_i \phi_{ik}}{\sum w_i \phi_{ik}^2}$$

(c) Design lateral force at each floor in each mode – The peak lateral force (Q_{ik}) at floor i in

Mode k is given by

$$Q_{ik} = A_{hk} \phi_{ik} P_k W_i$$

Where,

A_{hk} = Design horizontal spectrum value using natural period of vibration (T_k) of mode k.

$$= (Z/2)(I/R)(S_a/g)$$

Z= zone factor for the maximum considered earthquake (MCE), Z/2 stands for DBE

I= Importance factor depending upon the functional use of the structures

R= Response Reduction factor

S_a/g = Average response acceleration coefficient for rock or soil sites as given by response spectra and based on appropriate natural periods and damping of the structure

(d) Storey shear forces in each mode – The peak shear force (V_{ik}) acting in storey i in mode k is given by

$$V_{ik} = \square \square Q$$

(e) Storey shear force due to all modes considered – The peak storey shear force (V_i) in storey i due to all modes considered is obtained by combining those due to each mode as per SRSS or CQC methods.

SRSS method

If the building does not have closely spaced modes, than the peak response quantity (λ) due to all modes considered shall be obtained as per Square Root of Sum of Square method

$$\lambda = \sqrt{\lambda_1^2 + \lambda_2^2 + \lambda_3^2 + \lambda_4^2 + \dots}$$

Response Quantity λ could be any response quantity of interest such as base shear, force in a member etc.

CQC method

$$\lambda = \sqrt{\sum_{i=1}^r \sum_{j=1}^r \lambda_i \rho_{ij} \lambda_j}$$

Where,

r = Number of modes being considered,

ρ_{ij} = Cross-modal coefficient

i = Response quantity in mode i (including sign)

j = Response quantity in mode j (including sign)

$$\rho_{ij} = \frac{8\zeta^2(1+\beta)\beta^{1.5}}{(1-\beta^2)^2 + 4\zeta^2\beta(1+\beta)^2}$$

β_{ij} = frequency ratio = ω_j/ω_i

ω_i = circular frequency in ith mode

ω_j = circular frequency in jth mode

ζ = modal damping ratio (2% and 5% respectively for steel and RC buildings)

III. BUILDING THE SPREADSHEET

A large set of parameters, some of which are interrelated, is involved in the analysis. In order to facilitate the interaction between the designer and the spreadsheets, which may seem intimidating at first glance, the cell values that require an input by the user are highlighted in light pink and the ones that will be automatically generated are highlighted in dark grey. Calculations are highlighted using orange colour and outputs of those calculations are shown in light grey.

Some of the calculations involve trial and error procedures and loops. In such instances, Visual BASIC macros were assigned to specifically created buttons for the purpose of running these loops and obtaining the required parameter value with minimal effort. The idea is to lessen time spent on performing tedious and repetitive tasks which encroach on the "quality-learning time" and reduce the tedium to a few mouse clicks while maintaining the advantages of spreadsheet interfaces. It is important to add here that the automated processes do not create "black boxes" invisible to the student, but merely perform those tasks that are fully understood and clearly explained.

After entering all the required parameters the response of the structures, expressed in terms of forces can be calculated using the formulae given in the spread sheet. Macros are used for the generation and clearing of rows corresponding to each storey. Logic used for macros is

shown in figure. Macros are displayed in blue in colour. Necessary parameters are given as input in specified cells the values that are shown in dark grey cells are used for calculation of base shear and lateral storey forces. In this method weights, fundamental time period of modes and mode shapes of structure are to be inputted in their specified location. No. of stories is also to be given as input. Macros are used here also for adding and clearing of rows corresponding to floors for the convenience of calculations. Calculations for A_h , S_a/g and frequencies are also shown. Using these inputs and with formulae given in [8], base shear (V_B) has been calculated using excel. The design base shear (V_B) obtained by response spectrum modal analysis shall be compared with a base shear (V'_B) calculated using a fundamental period T_a , Where V_B is less than V'_B , all the response quantities (for example member forces, displacements, storey forces, storey shears and base reactions) shall be multiplied by (V_B/V'_B). Calculations and results of this method are shown in the following figures

Total width of the building(m)	6			
Total breadth of the building(m)	6			
Total height of the building(m)	12			
Number of Storeys	4			
Start		Clear		
City				
Zone	4			
Structure	Important			
Soil type	rocky/hardsoil			
Lateral load resisting system	steel MRF as per SP6(6)			
seismic intensity,Z	0.24			
Importance factor,I	1.5			
Response reduction factor,R	5			
% Damping	5			
Multiplying factor	1			

```

Sub Sheet1Start()
Dim i As Integer
For i = 1 To Range("c6").Value Step 1
Rows("44:44").Select
Selection.Insert Shift:=xlDown, CopyOrigin:=xlFormatFromLeftOrAbove
Range("A44").Select
ActiveCell.FormulaR1C1 = 1
Range("A45").Select
Next i
End Sub

Sub Sheet1Clear()
Macro3 Macro
For i = Range("c6").Value To 1 Step -1
Rows("44:44").Select
Selection.Delete Shift:=xlUp
Range("c6").Select
Next i
End Sub

```

An example of complexity of formula for selecting S_a/g value is shown in below figure

Fundamental natural period of vibration of the structure with brick infill,				
in the direction of	$T_a = 0.09H/\sqrt{I_d}$ $T_a = 0.075H/0.75$			
Width	0.484			
Breadth	0.441			
S_a/g in direction of				
Width	$=IF(S14="rocky/hardsoil",IF(C25<0.1,DATA(D25,IF(AND(0.1<C25,C25<0.4),DATA(E25,DATA(F25)),IF(S14="medium soil",IF(C25<0.1,DATA(D26,IF(AND(0.1<C25,C25<0.55),DATA(E26,DATA(F26)),IF(C25<0.1,DATA(D27,IF(AND(0.1<C25,C25<0.67),DATA(E27,DATA(F27)))))))))$			
Breadth	$=IF(logical_test,(value_if_true),(value_if_false))$			

Total width of the building(m)	6
Total breadth of the building(m)	6
Total height of the building(m)	12
Number of Storeys	4
<input type="button" value="Start"/> <input type="button" value="Clear"/>	
City	
Zone	4
Structure	Important
Soil type	rocky/hardsoil
Lateral load resisting system	steel MRF as per SP6(6)
seismic intensity,Z	0.24
Importance factor,I	1.5
Response reduction factor,R	5
% Damping	5
Multiplying factor	1

CALCULATIONS			
Fundamental natural period of vibration of the strcture with brick infill,			
in the direction of		Ta=0.09h/vd	Ta=0.075h^0.75
	Width	0.484	
	Breadth	0.441	
S _a /g in direction of			
	Width	2.068010798	
	Breadth	2.068010798	
A _h in direction of			
	Width	0.074448389	
	Breadth	0.074448389	

seismic weight= dead weight of the structure+part of imposed load

Q ₁	Q ₂	Q ₃	Q ₄	
21.33272	2.51865	54.35947	7.344951	
43.69239	2.826667	-31.9922	-15.2732	
61.68749	-1.014	-26.0497	42.76274	
71.32689	-4.09144	29.18655	-22.6613	
0	0	0	0	
V ₁	V ₂	V ₃	V ₄	
198.0395	0.239871	25.50414	12.17318	
176.7068	-2.27878	-28.8553	4.828225	
133.0144	-5.10545	3.136873	20.1014	
71.32689	-4.09144	29.18655	-22.6613	
correction factor				4.279801
V ₁	200.0458	V _{1c}	856.1565	
V ₂	179.1268	V _{2c}	766.6272	
V ₃	134.6581	V _{3c}	576.3098	
V ₄	80.43417	V _{4c}	344.2423	

For calculation of base shear using this CQC method, user has to input frequency ratio matrix in the specified matrix. Using the formulae given in IS 1893, cross modal coefficients are calculated and shown in the form of a matrix shown in orange colour. λ matrix is the base shears calculated for each mode. This λ and λ^T matrices are used for calculating the base shears of the structure. Correction factor is again to be calculated and multiplied to the outputs. Inputs, calculations and results for some input values are shown in the following figures.

Input frequency ratio matrix				
	β_1	β_2	β_3	β_4
β_1	1	2.919	0	0
β_2	0.343	1	0	0
β_3	0	0	0	0
β_4	0	0	0	0

Cross modal coefficient				
	ρ_1	ρ_2	ρ_3	ρ_4
ρ_1	1	0.006857	0	0
ρ_2	0.006876	1	0	0
ρ_3	0	0	0	0
ρ_4	0	0	0	0

	V ₁	V ₂	V ₃	V ₄
198.0395	0.239871	25.50414	12.17318	
176.7068	-2.27878	-28.8553	4.828225	
133.0144	-5.10545	3.136873	20.1014	
71.32689	-4.09144	29.18655	-22.6613	

V ₁ ^T	198.0395	176.7068	133.0144	71.32689
V ₂ ^T	0.239871	-2.27878	-5.10545	-4.09144
V ₃ ^T	25.50414	-28.8553	3.136873	29.18655
V ₄ ^T	12.17318	4.828225	20.1014	-22.6613

Base shear (CQC Method)			
V ₁	266.3184	V _{1c}	856.1565
V ₂	2.28973	V _{2c}	7.36099
V ₃	38.37948	V _{3c}	123.3818
V ₄	13.1265	V _{4c}	42.19889
Correction factor			3.214785

IV. CONCLUSION

In this paper, the process of development and use of a spreadsheet-based tool for the analysis of multi storey frame under seismic loading is documented. In summary, making of excel spreadsheet for seismic analysis of a multi storey frame is found to be fruitful since the calculation time and energy consumed for these analyses using this spreadsheet is negligible when compared to manual calculations.

REFERENCES

- [1] Chopra, A.K., *Dynamics of Structures: Theory and Application to Earthquake Engineering* (Pearson Education, 4th edition, 2012).
- [2] Duggal, S. K., *Earthquake Resistant Design of Structures* (Oxford University Press, 2007).
- [3] Davies, S. R., *Spreadsheets in Structural Engineering* (Longman Scientific and Technical, 1995).
- [4] Goodchild, C. H., and Lupton, J, Spreadsheets and the structural engineer, *Struct. Eng.*, 77(3), 1999, 21–22.
- [5] Hegazy, T., and Ayed, A., Simplified spreadsheet solutions: Models for CPM and TCT analyses, *Cost Engrg. J.*, 41(7), 1999, 26–33.
- [6] Kabalan K. Y. and El-Hajj, A., Digital filter design using spreadsheets, *Comp Appl Eng Educ*, 7, 1999, 9-15.
- [7] Low BK, Tang WH., Efficient spreadsheet algorithm for first-order reliability method. *J Eng Mech ASCE*, 133(12), 2007, 1378–87.
- [8] IS 1893(Part1):2002, Criteria for earthquake resistant design of structures, Part 1 General provisions and buildings, *Bureau of Indian Standard*, 2002.

An Algorithm Based Simulation Modeling For Control of Production Systems

Srinivas Viswanath V¹, R Ramanujam², VM Nistane³

^{1,2}Mechanical Engineering, VIT University, India,

³Mechanical Engineering, VNIT Nagpur, India.

ABSTRACT: This paper describes an algorithm based simulation approach for the design of a flexible production system Which allows the implementation of logic during the system design stage. The Algorithm design approach is built around the basic concept of supervisory control based on limited Automation. We provide the optimal inventory control policy and characterize its structural properties for the single-period model. Through an extensive numerical study, we demonstrate that applied programmed methodology is sufficiently accurate and close to optimal. The system resources are modeled to be monitored for real-time control. Real-time control issues including deadlock resolution, resource failures in various modes of operation and recovery from failures while sustaining desirable logical system properties are integrated into the logical design for simulating the supervisory controller.

Keywords: Algorithm, Automated systems, Inventory control, Production systems, simulation.

I. INTRODUCTION

Evaluation of existing performance levels of discrete parts production plant design is quite difficult and has to go with Algorithm based simulation models. Current commercial software for the simulation of production system designs does not incorporate models of the sensory data collection and electronic control systems that will eventually drive the operation of the factory that the simulation is modeling. This leaves the control system design architecture as a separate design task to be performed later.

Consequently, the impact of the control system on system performance is evaluated after the construction of the plant. Integration of control system design into plant simulation models requires modeling the plant in terms of events that will have to be monitored, recorded, and used for control. In principle, the software used to control the simulated factory operations could also be used to drive the operations of the actual factory after it is constructed. The traditional hierarchical decomposition approach to the design and control of production systems includes the strategic level (initial design) at the top, followed by the tactical (system configuration) and operational levels (part dispatching) towards the bottom. The control systems as they are referred to in this paper, reside below the operational decisions layer and deal with real-time control of the production system, which includes deadlock resolution and recovery from resource failures.

1.2. Algorithm based simulation

The primary contribution of Algorithm based approaches is through their ability to facilitate links between the analysis and specification of a real system and the design and implementation of an action model for that real system where the structure and behavior of entities are readily modeled as objects. An object, in the

Algorithm based paradigm, is a collection of data (attributes) together with all the operations (methods) which access or alter that data (Hill, 1996). Some or all of these operations could be used to provide a uniform external interface to other parts of the system. Other objects in the system can interact with this object only through requests for the object to execute its operations. The ability of the Algorithm based paradigm to provide a direct representation for real world objects comes with four unique features associated with it, data abstraction, and dynamic binding.

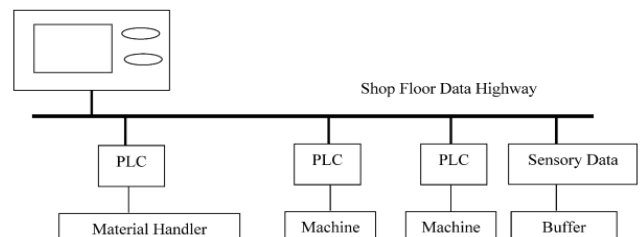


Fig 1.1 System design for Automation

Algorithm based simulations have now been produced in many languages, however it is important to emphasize that the use of Algorithm based methods is not dependent on any particular programming language (Jones & Powell, 1993). This paper presents an Algorithm based design approach for the simulation of flexible production systems. The approach is an extension of Boucher, Yalcin, and Tai (2000) in scope, design and implementation. The methodology in Boucher et al. (2000) integrates real-time supervisory control and physical system simulation using ARENA simulation coupled with control modules developed using C programming language. The proposed approach in this paper extends the scope by integrating resource failures and recovery from failure procedures. The Algorithm based design and implementation approach pursued in this work is also different, and has proven to be more effective with respect to ease of implementation, debugging and extensibility. In this paper, CCC, which is an Algorithm based extension to the C programming language, is used. The important features of the described framework are: (1) integrates control system design into the simulation of the physical process, (2) horizontally and vertically extendible within the production system design and control functions hierarchy (3) the mathematical foundation based on finite automata formalism allows for logical as well as quantitative analysis of the system, (4) facilitates the design and implementation of robust and formal controller models and algorithms that can service a variety of system designs, resolve deadlocks, and accommodate a range of resource failures, and (5) allows an analyst to design and evaluate the impact of different control programs on factory performance, and evaluation of various production system designs in a 'plug'n play' fashion.

II. Physical system

The physical system considered is a fully automated flexible production cell that has a number of single capacity machines and a central material-handling device, such as a robot, that interconnects these machines. There is an input and an output buffer where parts can be loaded and unloaded to and from the cell via the material-handling device. Each machine and the material handler are assumed to have their own internal controller as well as a Programmable Logic Controller (PLC) that it is connected to which coordinates its interactions with the rest of the components in the system. The cell controller monitors the machine PLCs for machine failures, repair completions, event start and finish signals, etc.

III. Algorithm based design framework

In order to simulate the real-time control activities, the system model must consider several factors such as the status of machines and material handlers, processing requirements of the parts in the system, sequencing of the operations required by these parts and contingencies such as equipment breakdowns. The proposed Algorithm based design approach contains constructs to model: (1) production cell, (2) the control structure to accomplish desired system behavior, and (3) communication between the cell and its controller. The modeling of the cell includes the definition of machines, robots, input and output buffers, their interactions and associated contingencies such as resource failures.

IV. Methodology

4.1. Mathematical Model:

As discussed earlier in the previous chapter the production process WIP inventory was increasing and there was increase in the loss of utilization of resources as well. So there is a need of proper scheduling technique which takes care of this problem. The Gantt charts can be one of the techniques to tackle this problem but the problem with the technique is that it is a slow and time consuming process [5]. Each and every time we need to charts and also beyond a certain limit of time span it is difficult to read the charts. As the number of operations or number of batches in the scheduling increases in order to accommodate the larger time span either the Gantt charts have to be huge or the resolution has to be sacrificed. If there is a mathematical tool by which we can solve the above discussed problem then it will be much easier to get the schedule. Inventory has problems. The proposed technique requires the daily attainment of the track grinding that is the last operation of production process. Here the logic of process is reverse type of process i.e., last process requests number of parts for before process. The same amount of parts are prepared and sent, no excess parts are send. So inventory levels are balanced and no excessive stocks are maintained.

MATHEMATICAL MODEL FORMULATION LOGIC:

Day	BGTG	ODG	FG	SB	Heat	GS	total inventory
1	3536	0	3438		30000		37974
2	3555		8000		22000		33555
3	3495	8000			14000		25495
4	3668	0	8000		6000		17668
5	3778	0	0		36000		39778
6	3356	0	0		28000		31356
7	3669	8000	0		20000		31669
		Average Inventory					29702

4.2 Calculation of Buffer Stock / Inventory Levels

The Proposed system supports level production. It helps to maintain stable and efficient operations. The question of how many proposed to use is a basic issue in tuning a proposed system. If your factory makes products using mostly standard, repeated operations, the number of proposed can be determined using the formula The number of proposed you need dependent on the number of pallets or containers and their capacity. Lead times, safety margins or buffer inventory , and transportation time for proposed retrieval are also important factors. Several questions must be answered when deciding the number of proposed to use.

- How many products can be carried on a pallet?
- How many transport lots are needed, given the frequency of transport?
- Will a single product or mixed products be transported?

4.3. Inventory Level:

Inventory level is very important in between the process. That is also called as safety stock level which is calculated as below.

$$\text{Inventory level} = [\text{Daily Production Requirement} * (1 + \alpha)]$$

Daily Production requirement for COMPONENT 1

Outer Ring = 4000 components

According to monthly plan If safety factor $\alpha=1$,

Inventory level for COMPONENT 1

$$\text{Outer Ring} = \text{DR} * (1 + \alpha) = 4000 * (1 + 1) = 8000.$$

4.2. Simulation inputs

The input files to the simulation describe the processing times and the routing of the part types in the cell representing the full set of alternative production sequences for the parts. There are two types of files. The partplantstate[i].txt specifies the machine which can perform the required operation on part typei in a particular state. The partprocessplan[i].txt describes the state transitions for the part typei and the processing time for that part in each state. Together, they contain all the information to generate the corresponding Finite Automata models of the parts. At the beginning of each simulation, the user also specifies the number of machines in the cell model and the number of parts to be processed in the plant during the simulation. The user may also simulate resource failures in the plant by specifying failure-rates and repair rates for the resources. These set of details are complete in themselves in describing the structure and behavior of the plant comprehensively.

The constructor of the cell class is used as an initialization procedure to create the buffer, the machine, the material handler and the part objects that form the cell object, and to create certain information-arrays from the input files. These arrays capture all the information on the cell behavior and are henceforth, used by the supervisor to formulate a control strategy.

4.2. Simulation logic

The simulation logic is implemented in the object-oriented model through the updating of the attributes of the component objects and the interactions among these components are modeled through the message-passing facility in the object-oriented approach. The event handler object monitors the buffers and the machines in the cell and queues and relays appropriate event signals to the supervisor object. The supervisor object then evaluates the request based on the current state of the system and the control strategy and sends back the decision to allow/disallow the request back to the cell object, which executes the move if it is allowed. If the move is not allowed, it is sent to the end of the queue of events requested in the event handler object to be

evaluated again when the system state changes. The flow of information within the simulation is illustrated in flow chart. The simulation starts with the arrival of a part to the input buffer. The event handler sends the load new part signal to the supervisor based on the change in the buffer object's attributes. The supervisor generates a new control pattern, evaluates the move requested using the `evaluate_newpart_request()` and the `evaluate_move_request()` methods. The response is evaluated by the `evaluate_response()` method of the cell, and if it is allowed, the `execute_event()` method of the material handler, `load_machine()` method of the cell and `load_part()` method of the machine are sequentially invoked. The current states of the cell, the machine and the part are updated using their respective `update_state()` methods. Based on the processing time of the required operation, the `mark_event()` method of the event handler object schedules the part to be unloaded when the processing is complete.

V. Implementation Phase

5.1 Action Plan:

In this section action plan has been discussed.

5.1.1 To Decide Proposed Methodology:

After study of the existing process it was found that maximum inventory and lack of utilization of available resources is with production process. In the Process of production WIP inventory was increasing more so to avoid this it was decided to implement Toyota Production System PROPOSED Methodology.

5.2 Monitoring Phase:

Having implemented Proposed Algorithm Methodology the next most important step is to monitor the flow of materials. This step is important so as to know whether an Just In Time, Toyota implementation is successfully running or not.

5.2.1 Steps in Monitoring Phase:

- Daily production fulfillments according to Monthly plan
- Attend daily Production Meeting
- Update Current status of Notice Board
- Attend breakdown and know the root cause
- Calculation of WIP inventory at starting of

Take every problem for discussion with team and after answering it design the solution on paper and gather necessary tools to implement these solution. Getting proposal from top management is major thing it depend on understanding solution designed and how that can solve the problem associated with the existing process.

5.2.2 Simulation logic:

The simulation logic is implemented in the Algorithm based model through the updating of the attributes of the component objects and the interactions among these components are modeled through the message-passing facility in the Algorithm based approach. The event handler object monitors the buffers and the machines in the cell and queues and relays appropriate event signals to the supervisor object. The supervisor object then evaluates the request based on the current state of the system and the control strategy and sends back the decision to allow/disallow the request back to the cell object, which executes the move if it is allowed. If the move is not allowed, it is sent to the end of the queue of events requested in the event handler object to be

evaluated again when the system state changes.

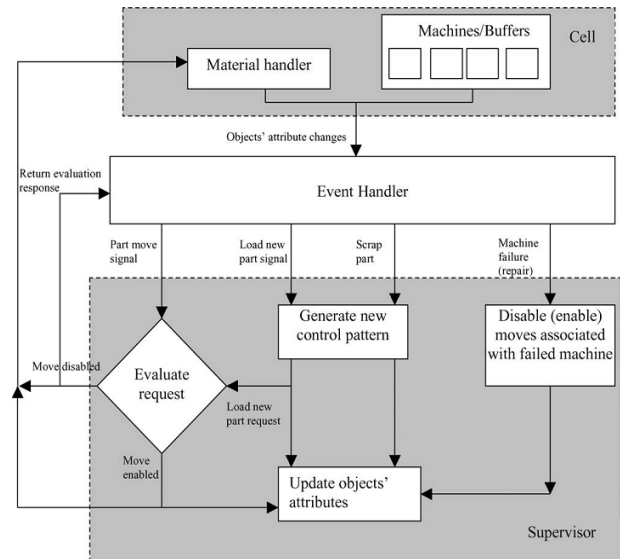


Fig 5.1 Flow of materials and Application Logic

Simulation outputs the output produced by the simulation model is captured in data files and includes event trace information, system performance information, and supervisory controller computation complexity information. The trace information includes a trace of the events ordered by time for understanding the behavior of the system. The system performance information includes measures such as the throughput, resource utilization, etc. Also, included are the state space and response time of the supervisory controller to keep track of computational complexity.

VI. Summary and conclusions;

Integration of control requirements into plant simulation models requires modeling the plant in terms of events that have to be monitored, recorded, and used for control. In this paper we describe an Algorithm based approach to the design of flexible production system simulation that allow the implementation of control logic during the system design phase. The Algorithm based design approach is structured around formal supervisory control theory. While Algorithm based design approaches have several advantages for software development, especially in specifying intra-object relationships, the interactions between objects in a complex system are difficult to capture.

References:

- [1]. Buffer stocks controlled traditional by KANBAN methodology .kumar and Rao.The journal of operations research 51, 195-294
- [2]. Inventory management with periodic ordering and minimum order quantities. The Journal of the Operational Research Society 49, 1085-1094.
- [3]. Ross, S., 1992. Applied Probability Models with Optimization Applications. Dover, New York.
- [4]. Scarf, H., 1960. The optimality of (s,S) policies in the dynamic inventory problem.
- [5]. Narayanan, S., Bodner, D. A., Sreekanth, U., Govindaraj, T., McGinnis, L. F., & Mitchell, C. M. (1998). Research in object-oriented manufacturing simulations: An assessment of the state of the art.IIE Transactions, 30, 795-810.
- [6]. Smith, J. S., Hoberecht, W. C., & Joshi, S. B. (1996). A shop-floor control architecture for computer-integrated manufacturing. IIE Transactions, 28, 783-794.
- [7]. Smith, J. S., & Joshi, S. B. (1993). Message-based part state graphs (MPSG) for shop floor control. Proceedings of the second IIE research conference, Los Angeles, CA.
- [8].

System Modeling Corporation (1999).Arena professional edition reference guide, Swickley, PA.

- [9]. Tang, M. X., & Smothers, T. (1991). Towards object-oriented simulation. IEEE Colloquium on Object-Oriented Simulation and Control, 7/1–7/4.
- [10]. Venkatesh, S., Smith, J. S., Deuermeier, B., & Curry, G. (1998). Deadlock detection and resolution for discrete-event simulation: Multiple-unit seizures. IIE Transactions, 30, 201–216.
- [11]. Yalcin, A. (2004). Re-configurable supervisory control of automated manufacturing cells with resource failures. Robotics and Computer Integrated Manufacturing, 20(2), 111–119.
- [12]. Deuermeier, B., Curry, G., Duchowski, A. T., & Venkatesh, S. (1997). An automatic approach to deadlock detection and resolution in discrete simulation systems. INFORMS Journal on Computing, 9(2), 195–205.
- [13]. Hill, D. R. C. (1996). Object-oriented analysis and simulation. Reading, MA: Addison-Wesley.
- [14]. Jones, J. A., & Powell, K. A. (1993). Building object-oriented simulations with CCC. Proceedings of the winter simulation conference, Los Angeles, 79–88.

Ac to Dc Conversion Using Active PFC

ANITHA.U,¹ SAMPATH KUMAR BOINI,²

(PG Scholar, Department of Electrical And Electronics Engineering, Teegala Krishna Reddy Engineering College/JNTU HYDERABAD, INDIA)

(Associate Professor, Department of Electrical and Electronics Engineering, Teegala Krishna Reddy Engineering College /JNTU HYDERABAD, INDIA)

ABSTRACT: In the modern power distribution system, majority of loads draw reactive power and/or harmonic currents from ac source along with main active power currents. These non-unity powerfactor linear and non-linear loads cause low efficiency of supply system, poor power-factor, destruction of other equipments due to excessive stresses and EMI problems. Active filters have been considered an effective solution to reduce these problems. This paper presents an Active Power Filter (APF) based on simple control technique to provide reactive power and harmonics compensation or non-linear single-phase loads. A voltage source inverter with carrierless hysteresis PWM current control is used to form an APF. A simple P-I (proportional-integral) dc bus voltage controller with reduced energy storage capacitor is employed in the APF. A diode rectifier fed capacitive load and ac voltage regulator fed inductive load as the non-linear loads are taken on ac mains to demonstrate the effectiveness of the proposed APF for reactive power and harmonic compensation. The operation, and simulation results of the proposed scheme are presented.

Keywords: Active, power-factor correction, ac/dc converters, sinusoidal line current.

I. INTRODUCTION

With the development in advanced power semiconductor devices, more and more switch-mode power supplies (SMPS's) and other power switching circuits are used in modern power system. Due to the nonlinear behavior of power switched circuits, distorted currents are normally drawn from the line, resulting in low power factor (usually less than 0.67) [1] and high total harmonic distortion (THD). The equation relating the pf and THD is:

$$PF = \frac{1}{\sqrt{1 + THD^2}} \times \cos\phi.$$

Traditionally, to improve power factor of a given power electronic system, normally a power factor correction (PFC) circuit is designed and placed in front end of the system, which in turn interfaced with the load. This PFC circuit may be an independent unit followed by a dc-dc converter, or an inseparable part of circuit incorporated into the power supply of the load, namely two-stage PFC to perform the input current shaping [2-3] and single-stage PFC power supply, respectively. Because the line voltage is normally not distorted (near sinusoidal), the basic idea of PFC is design circuits with certain means to force the line current to follow the waveform of the line voltage.

Because of the nature of PFC, there exists an unbalance of instantaneous power between the input power,

which is an alternative quantity with two times the line frequency, and its dc output power. Therefore, power factor correction involves processing the input power in certain way that it stores the excessive input energy when the input power is larger than the dc output power, and releases the stored energy when the input power is less than the dc output power. To accomplish the above task, at least one energy storage element must be included in the PFC circuit.

In most PFC circuits [4-7], normally an input inductor is used in series with line bridge rectifier in order to smooth the line current. The input inductor can operate in either continuous conduction mode (CCM) or discontinuous conduction mode (DCM). In DCM, the input inductor is no longer a state variable since its state in a given switching cycle is independent on the value in the previous switching cycle. The input inductor operating in DCM cannot hold the excessive input energy because it must release all its stored energy before the end of each switching cycle.

In addition, if discontinuous conduction mode is applied, the input current is normally a train of triangle pulses with nearly constant duty ratio. In this case, an input filter is necessary for smoothing the pulsating input current. The DCM input circuit can be one of the basic dc-dc converter topologies.

In recent years, many switching circuits like the flyback and the boost using DCM input technique were reported. Several single-stage single-switch (S^4) PFC circuits [8-10] have been reported. These circuits are especially attractive in low power applications with increased efficiency and reduced cost.

II. SOLUTIONS FOR PFC

The solutions for PFC can be divided into two groups, according to the input current shape: sinusoidal or nonsinusoidal.

A. Sinusoidal Line Current

For comparison, we have selected as a reference the afore mentioned cascade association of converters. All of them as shown in Fig 1, except passive filters, involve the use of two converters (PFP plus dc-dc) with their respective control loops.

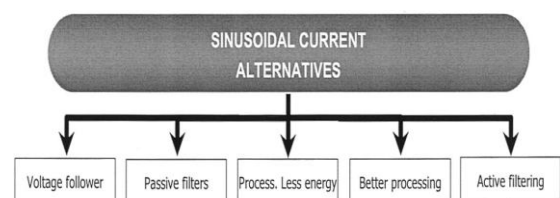


fig.1. Alternatives to the two stage approach.

B. Nonsinusoidal Line Current

Since Regulations allow harmonic currents, designers may take advantage of that, simplifying the circuitry and using new topologies as shown in Fig 2 , mainly in low power applications.

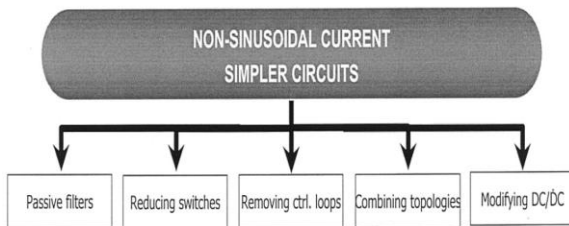


fig.2. Alternatives to the two stage approach for non sinusoidal line current.

III. PROPOSED CONVERTER CIRCUIT AND ITS OPERATION

Different circuits as shown in FIG 3 are proposed for power factor correction in AC to DC conversion process.

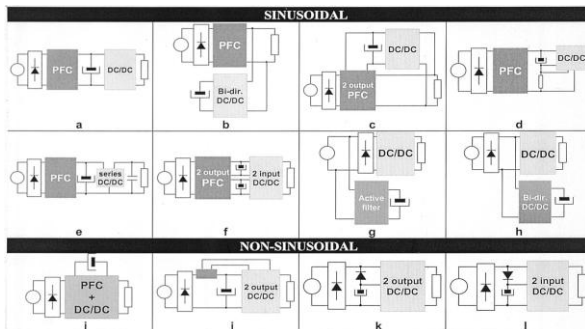


fig.3 Proposed circuits for PFC.

A new technique of active PFC as shown in Fig 4. is proposed.

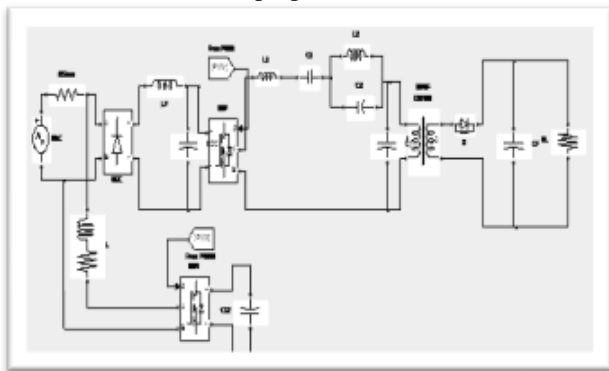


fig.4 Proposed Active PFC circuit.

3.1 PRINCIPLE OF OPERATION

The sinusoidal mains voltage is rectified through the front end bridge diode rectifier. A voltage from the auxiliary winding which is rectified using half bridge diode rectifier is added to the rectified voltage. This forces the input current to follow a sinusoidal shape and flow in discontinuous manner.

The full bridge PI controlled PWM converter topology provides a good choice to control the converter. Four MOSFET switches (Q1 - Q4) and a high frequency power transformer are used to form the full bridge. The

capacitor C_b is used to block any net dc voltage E_{om} appearing across the transformer primary and saturating it. The gate conducting, positive voltage is applied to the primary and when Q2, Q4 are conducting, negative voltage is applied to it. During other periods the primary voltage is zero and energy stored in the output filter capacitor free-wheels through the secondary.

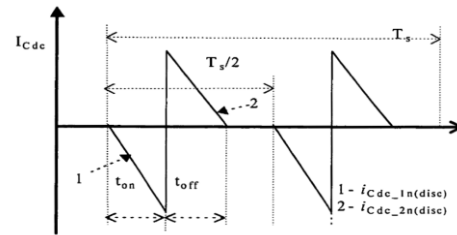


fig.5 Current through filter capacitor on secondary.

3.2 ACTIVE FILTERING

The use of active filters with the parallel configuration is very common in high power installations (from tens of kW). The two quadrant active filter is in charge to obtain a sinusoidal line current even when the load is nonlinear.

The shunt connected single phase active power filter is based on the principle of injection of harmonic currents into the ac system of the same amplitude but opposite in phase to that of the load harmonic currents. The detailed block diagram in Fig. 5 displays the proposed circuit.

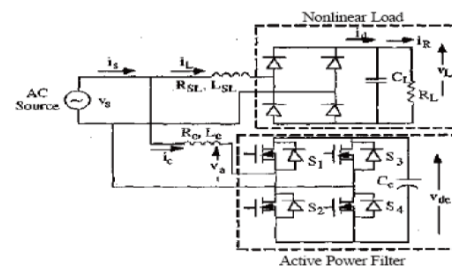


fig.6 Basic Circuit of Single Phase APF

Fig. 5 shows the basic circuit of APF Including inverter having an energy storage capacitor on dc side. Pulse width modulation (PWM) is employed to generate gating Pulses to the switches of APF. The dc based load fed from diode bridge rectifier with a capacitor is a non-linear load on the ac mains. The proposed APF is to eliminate harmonics and to improve the power factor of supply. The major parts constituting APF are described in brief:

3.2.1 INTERFACE FILTER

The filter provides smoothing and isolation for high frequency components. Control of the injected current waveshape is limited by the switching frequency of the inverter and the available driving voltage across the interfacing inductance. The driving voltage across the interfacing inductance determines the maximum di/dt that can be achieved by the filter. This is important because high values of di/dt may be needed to cancel higher order harmonic components. A large value of interfacing inductance is better for isolation but it limits the ability of an active filter to cancel higher order harmonics.

3.2.2 PWM CONTROLLER

A simplified P-I (Proportional-Integral) control of the dc capacitor average voltage is used to generate reference source current in phase with ac source voltage to result in unity power factor of the source current. The pulse width modulation (PWM) is employed to generate gating signal for MOSFETs to control the phase and magnitude of the inverter output.

3.2.3 ACTIVE SHUNT FILTER

The current drawn by the load is non-sinusoidal and have all odd harmonics. The load current is expressed as:

$$i = i_1 + i_h \quad (1)$$

Where, i_1 is the fundamental component of the load current and i_h is the harmonic current. Now active filter current is given by:

$$i_{afh} = i_h \quad (2)$$

Supply current is given by applying KCL at PCC:

$$i_s = i - i_{afh} \quad (3)$$

Combining equations (1), (2) and (3):

$$i_s = i_1 \quad (4)$$

Equation (4) theoretically shows that with SPAPF the supply current harmonics can be compensated completely.

3.3 FLYBACK TRANSFORMER / LINE OUTPUT TRANSFORMER

Unlike mains transformers and audio transformers, a LOPT is designed not just to transfer energy, but also to store it for a significant fraction of the switching period. This is achieved by winding the coils on a ferrite core with an air gap. The air gap increases the reluctance of the magnetic circuit and therefore its ability to store energy. The current does not flow simultaneously in primary and secondary (output) windings. Because of this the flyback transformer is really a loosely coupled inductor rather than classical transformer, in which currents do flow simultaneously in all magnetically coupled windings.

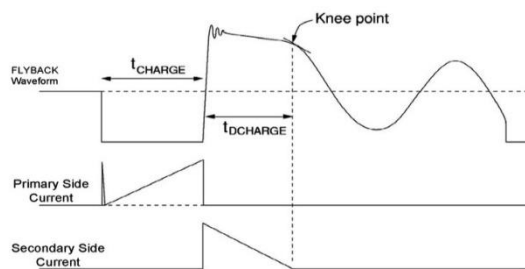


Fig.7 Waveforms of Flyback transformer.

The primary winding of the flyback transformer is driven by a switch from a DC supply. When the switch is

switched on, the primary inductance causes the current to build up in a ramp.

When the switch is turned off, the current in the primary winding collapses leaving the energy stored in magnetic core. The voltage in the output winding rises very quickly (usually less than a microsecond) until it is limited by the load conditions. Once the voltage reaches such level as to allow the secondary current to flow, then the current in the secondary winding begins to flow in a form of a descending ramp.

The cycle then can be repeated. If the secondary current is allowed to discharge completely to zero (no energy stored in the core) then it is said that the transformer works in discontinuous mode.

IV. SIMULATION DIAGRAM

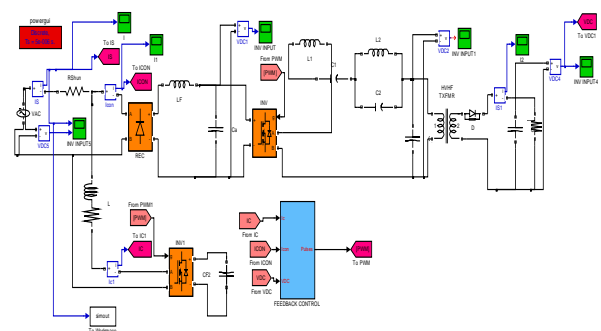


fig.8 MATLAB Simulation diagram of Active PFC

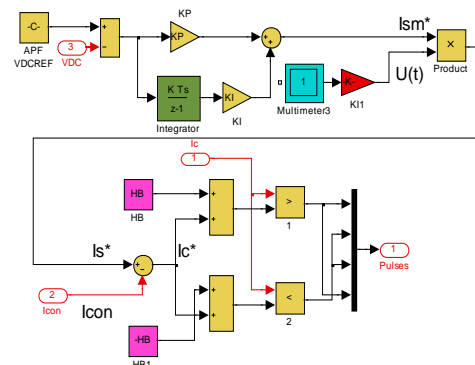


fig.9 MATLAB Simulation diagram of PI control.

V. SIMULATION RESULTS:

5.1 DC-DC LINK OUTPUT VOLTAGE

The resultant voltage across the dc-dc link capacitor placed in the secondary of the flyback transformer:

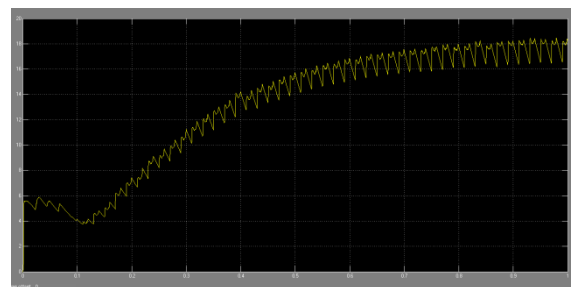


fig.10 Resultant voltage across dc-dc link.

5.2 FLYBACK CONVERTER INPUT

The required high frequency pulsating source required to drive the dc-dc link:

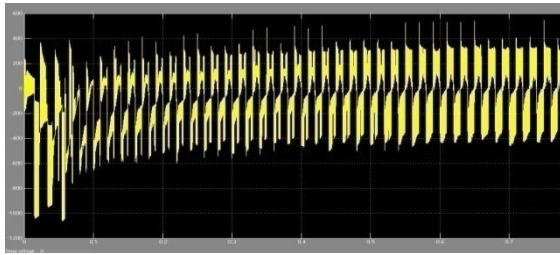


fig.11 High frequency pulsating source.

5.3 INPUT CURRENT HARMONICS

The PFC properties of a active flyback converter can be estimated from the given plots:

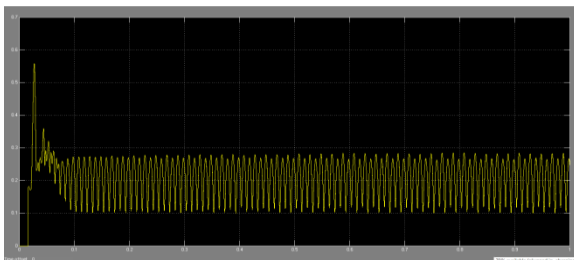


fig.12 Harmonic spectrum of supply current.

5.4 OUTPUT CURRENT HARMONICS

Harmonic content of the current waveform obtained from a rectifier circuit

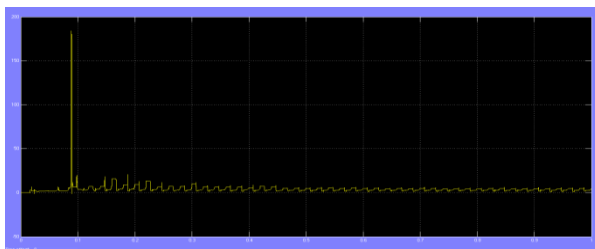


fig.13 Harmonic spectrum of output current.

Harmonic content of the current waveform of a active PFC converter

As can be clearly seen, the higher order harmonics are considerably reduced in the line current by using a active PFC.

VI. CONCLUSION

In this paper, a new ac/dc converter based on a active PFC scheme has been presented. The proposed method produces a current with low harmonic content to meet the standard specifications as well as high efficiency. This circuit is based on adding an active shunt filter using voltage source inverter. The input inductor can operate in DCM to achieve lower THD and high power factor. By properly designing the converter components, a tradeoff between efficiency and harmonic content can be established to obtain compliance with the regulation and efficiency as high as possible.

REFERENCES

- [1] J. Goren, and B. Curchic, "Single Stage Sence Resonant Power Factor correctors," LEEEMEL EC'96 Conz Rec., pp. 242-247, October 1996.
- [2] Barbi and J.L. Freitas Vieira, "A High power factor PWM-ZVS Single Stage Power Supply," HPFC93 Con\$ Proc., pp. 209-219, May 1995.
- [3] Y.Jiang F.C.Lee, "Single -Stage Single-Phase Parallel Power Factor Correction Scheme," IEEE PESC '94 Con\$ Rec., pp. 1 145- 1 15 1, June 1994.
- [4] L. Huber, J. Zhang, M. Jovanovic, and F.C. Lee, "Generalized topologies of single stage input-current-shaping circuits," IEEE Trans.Power Electron., vol. 16, no.4, pp. 508-513, Jul. 2001.
- [5] H. Wei, I. Batarseh, G. Zhu, and K. Peter, "A Single - switch AC-DC converter with PF correction," IEEE Trans Power Electro., vol.15,no. 3, pp. 421-430, May 2000.
- [6] H. L. Do, "Singlestage single-switch power factor correction AC - DC converter," Inst. Electr. Eng. Proc. Electr. Power Appl., vol.152, no. 6, pp.1578-1584, Nov. 2005.
- [7] J. Qian, Q. Zhao, and F.C. Lee, "Single-stage Singleswitch power factor correction ac - dc converters with dc-bus voltage feedback for universal line applications," IEEE Trans Power Electron.vol.13, no. 6, pp. 1079-1088, Nov. 1998.
- [8] Hussain S. Athab, and Dylan Dah - Chuan Lu, "A high-Efficiency AC/DC Converter with Quasi-Active Power Factor Correction", IEEE Transactions on Power Eelectronics, vol. 25, NO. 5, MAY 2010.
- [9] J. Sebastian, A. Femandez, P. Villegas, J. Prieto M.Hemando, and, "New topologies of Active input current shapers to allow AC-to-DC converters with asymmetrically driven transformers to comply with the IEC-1000-3-2," IEEE TransPower Electron., vol. 17, no. 4, pp. 493-501, Jul.2002.
- [10] N. Vazquez, J. Lopez, J. Arau, C. Hernandez, And Elias Rodriguez, "A different approach to implement an active input current shaper," IEEE Trans. Ind. Electron., vol. 52, no. 1, pp.132 -138, Feb. 2005.

AUTHORS BIOGRAPHY



Anitha.U received B.Tech Degree in Electrical & Electronics Engineering from Siddhartha College of Engineering and Technology in 2002. She is presently working towards her M.Tech degree in Power Electronics from Teegala Krishna Reddy engineering college (JNTU), Hyderabad. Her areas of interest are in Voltage Control , Inverters and Transmission.



Sampath Kumar Boini is an Associate Professor in Teegala Krishna Reddy Engineering College, (JNTU) Hyderabad. He received B.Tech degree in Electrical & Electronics Engineering from Jawaharlal Nehru Technological University, Hyderabad in 2005 and M.Tech degree in Power Systems from Jawaharlal Nehru Technological University, Hyderabad in 2007. His areas of interest are Electrical power transmission & distribution, Power system operation and stability.

A Review on Two-Temperature Thermoelasticity

¹²Kiran Bala

¹ Research scholar in Mathematics, Singhania University, Rajasthan, India .

²Department of Mathematics, Government College, Barwala, Panchkula, Haryana, India

ABSTRACT: The present paper deals with the review on the development of the theory of two-temperature thermoelasticity. The basic equations of two-temperature thermoelasticity in context of Lord and Shulman [6] theory and Green and Naghdi[15] theories of generalized thermoelasticity are reviewed. Relevant literature on two-temperature thermoelasticity is also reviewed.

KeyWords: Two-temperature, generalized thermoelasticity, basic equations

1. INTRODUCTION

Thermoelasticity deals with the dynamical system whose interactions with the surrounding include not only mechanical work and external work but the exchange of heat also. Changes in temperatures causes thermal effects on materials. Some of these thermal effects include thermal stress, strain, and deformation. Thermal deformation simply means that as the "thermal" energy (and temperature) of a material increases, so does the vibration of its atoms/molecules and this increased vibration results in what can be considered a stretching of the molecular bonds - which causes the material to expand. Of course, if the thermal energy (and temperature) of a material decreases, the material will shrink or contract. Thus, thermoelasticity is based on temperature changes induced by expansion and compression of the test part. Thus, the theory of thermoelasticity is concerned with predicting the thermomechanical behaviour of elastic solids. It represents a generalization of both the theory of elasticity and theory of heat conduction in solids. The theory of thermoelasticity was founded in 1838 by Duhamel [1], who derived the equations for the strain in an elastic body with temperature gradients. Neumann [2], obtained the same results in 1841.

However, the theory was based on independence of the thermal and mechanical effects. The total strain was determined by superimposing the elastic strain and the thermal expansion caused by the temperature distribution only. The theory thus did not describe the motion associated with the thermal state, nor did it include the interaction between the strain and the temperature distributions. Hence, thermodynamic arguments were needed, and it was Thomson [3], in 1857 who first used the laws of thermodynamics to determine the stresses and strains in an elastic body in response to varying temperatures.

There are three types of thermoelasticity i.e. uncoupled, coupled and generalized thermoelasticity. The theory of classical uncoupled theory of thermoelasticity predicts two phenomena not compatible with physical observations. First, the equation of heat conduction of this theory does not contain any elastic term contrary to the fact that the elastic changes produce heat effects. Second, the heat equation is of parabolic type predicting infinite speeds of propagation for heat waves. The classical uncoupled and coupled thermoelastic theories of Biot[4] and Nowacki[5]

have an inherent paradox arising from the assumption that the thermal waves propagate at infinite velocity and it is a physically unreasonable result.

Generalized thermoelasticity theories have been developed with the objective of removing the paradox of infinite speed of heat propagation inherent in the conventional coupled dynamical theory of thermoelasticity in which the parabolic type heat conduction equation is based on Fourier's law of heat conduction. This newly emerged theory which admits finite speed of heat propagation is now referred to as the hyperbolic thermoelasticity theory, since the heat equation for rigid conductor is hyperbolic-type differential equation. The first generalized theory of thermoelasticity is due to Lord and Shulman [6] who coupled elasticity with a way in which temperature can travel with a finite wave speed. The approach of Lord and Shulman [6] begins with the full nonlinear equations but they are mainly interested in developing a linear theory since they begin with "small strains and small temperature changes". The second generalization to the coupled theory is known as the generalized theory with two relaxation times. Muller[7] introduced the theory of generalized thermoelasticity with two relaxation times. A more explicit version was then introduced by Green and Laws [8], Green and Lindsay [9] and independently by Suhubi[10]. In this theory the temperature rates are considered among the constitutive variables. This theory also predicts finite speeds of propagation for heat and elastic waves similar to the Lord-Shulman theory. It differs from the latter in that Fourier's law of heat conduction is not violated if the body under consideration has a centre of symmetry. Dhaliwal and Sherief[11] extended the Lord and Shulman (L-S) theory for an anisotropic media. Chandrasekharaiah[12] referred to this wave-like thermal disturbance as "second sound". These writers investigate the propagation of a thermal pulse in a thermoelastic shell employing each of the linearized equations for the three thermoelastic theories, Classical, Lord-Shulman and Green-Lindsay. Their numerical results typically demonstrate that Classical theory leads to a smooth pulse while that of Lord-Shulman is less smooth showing discontinuities in derivatives. The theory of Green and Lindsay [9] leads to strong pulse behaviour displaying distinct jumps such as to the behaviour of stainless steel run tanks which holds cryogenic liquids for rocket fuel at NASA's John C. Stennis Space Centre, the strong pulse solution is definitely of interest.

Green and Naghdi[13-15] proposed three new thermoelastic theories based on entropy equality than the usual entropy inequality. The constitutive assumption for the heat flux vector are different in each theory. Thus they obtained three theories which are called thermoelasticity of type I, thermoelasticity of type II and thermoelasticity of type III. Green and Naghdi[15] postulated a new concept in generalized thermoelasticity which is called the

thermoelasticity without energy dissipation. The principal feature of this theory is that in contrast to the classical thermoelasticity, the heat flow does not involve energy dissipation. Also, the same potential function which is defined to derive the stress tensor is used to determine the constitutive equation for the entropy flux vector. In addition, the theory permits the transmission of heat as thermal waves at finite speeds. Dhaliwal and Wang [16] formulated the heat-flux dependent thermoelasticity theory for an elastic material with voids. This theory includes the heat-flux among the constitutive variables and assumes an evolution equation for the heat-flux. Hetnarski and Ignaczak [17] examined five generalizations to the coupled theory and obtained a number of important analytical results. Literature on generalized thermoelasticity is available in the books like "Thermoelastic Solids" by Suhubi [10], "Thermoelastic Deformations" by Iesan and Scalia [18], "Thermoelastic Models of Continua" by Iesan [19], "Thermoelasticity with Finite Wave Speeds" by Ignaczak and Ostoja-Starzewski [20] etc.

II. LITERATURE SURVEY

Chen and Gurtin [21] and Chen et al. [22-23] have formulated a theory of heat conduction in deformable bodies, which depends on two distinct temperatures, the conductive temperature Φ and the thermodynamic temperature T . The two-temperature theory involves a material parameter $a^* > 0$. The limit $a^* \rightarrow 0$ implies that $\Phi \rightarrow T$ and hence classical theory can be recovered from two-temperature theory. The two-temperature model has been widely used to predict the electron and phonon temperature distributions in ultrashort laser processing of metals. For time-independent situations, the difference between these two temperatures is proportional to the heat supply, and in the absence of any heat supply, the two temperatures are identical. For time-dependent problems, however, and for wave propagation problems in particular, the two temperatures are in general different, regardless of the presence of a heat supply. The two temperatures T and Φ and the strain are found to have representations in the form of a travelling wave plus a response, which occurs instantaneously throughout the body. Warren and Chen [24] investigated the wave propagation in the two-temperature theory of thermoelasticity. Following Boley and Tolins, [25], they studied the wave propagation in the two-temperature theory of coupled thermoelasticity.

Youssef [26] developed a new theory of generalized thermoelasticity by taking into account the theory of heat conduction in deformable bodies, which depends on two distinct temperatures, the conductive temperature and the thermodynamic temperature where the difference between these two temperatures is proportional to the heat supply. Youssef and Al-Harby [27] studied the state-space approach of two-temperature generalized thermoelasticity of infinite body with a spherical cavity subjected to different types of thermal loading. Youssef and Al-Lehaibi [28] applied the state space techniques of two-temperature generalized thermoelasticity to one-dimensional problem of half-space subjected to thermal shock and traction free. Youssef [29] studied two-dimensional problem of a two-temperature generalized thermoelastic half-space subjected to ramp type heating. Youssef and Bassiouny [30] used the theory of two-

temperature generalized thermoelasticity, based on the theory of Youssef to solve boundary value problems of one-dimensional finite piezoelectric rod with loading on its boundary with different types of heating. Abbas and Youssef [31] analysed a finite element model of two-temperature generalized magneto-thermoelasticity. Ezzat et al. [32] studied the two-temperature theory in generalized magneto-thermo-viscoelasticity. Mukhopadhyay and Kumar [33] studied thermoelastic interactions on two-temperature generalized thermoelasticity in an infinite medium with a cylindrical cavity. Youssef [34] constructed a model of two-temperature generalized thermoelasticity for an elastic half-space with constant elastic parameters. Ezzat and Awad [35] derived the equations of motion and the constitutive relations for the theory of micropolar generalized two-temperature thermoelasticity. Kaushal et al. [36] solved the boundary-value problem in frequency domain in the context of two generalized theories of thermoelasticity (Lord and Shulman, Green and Lindsay) by employing the Hankel transform. Kumar et al. [37] established a variational principle of convolutional type and a reciprocal principle in the context of linear theory of two-temperature generalized thermoelasticity, for a homogeneous and isotropic body. Kumar and Mukhopadhyay [38] investigated the propagation of harmonic plane waves in elastic media in the context of the linear theory of two-temperature-generalized thermoelasticity. Youssef [39] solved a problem of thermoelastic interactions in an elastic infinite medium with cylindrical cavity thermally shocked at its bounding surface and subjected to moving heat source with constant velocity. Youssef and El-Bary [40] studied two-temperature generalized thermoelasticity with variable thermal conductivity. Awad [41] wrote a note on the spatial decay estimates in non-classical linear thermoelastic semi-cylindrical bounded domains. El-Karamany [42] presented two-temperature theory in linear micropolar thermoviscoelastic anisotropic solid. El-Karamany and Ezzat [43] introduced the two general models of fractional heat conduction law for non-homogeneous anisotropic elastic solid, obtained the constitutive equations for the two-temperature fractional thermoelasticity theory, proved uniqueness and reciprocal theorems and established the convolutional variational principle. El-Karamany and Ezzat [44] gave the constitutive laws for two-temperature Green-Naghdi theories and proved that the two-temperature thermoelasticity theory admits dissipation of energy and the theory of elasticity without energy dissipation is valid only when the two-temperatures coincide. Ezzat and El-Karamany [45] studied the two-temperature theory in generalized magneto-thermoelasticity with two relaxation times. Ezzat and El-Karamany [46] constructed fractional order heat conduction law in magneto-thermoelasticity involving two temperatures. Miglani and Kaushal [47] studied the axisymmetric deformation in generalized thermoelasticity with two temperatures. Mukhopadhyay et al. [48] presented the theory of two-temperature thermoelasticity with two phase-lags. Singh and Bijarnia [49] studied the propagation of plane waves in anisotropic two-temperature generalized thermoelasticity. Youssef [50] presented a theory of two-temperature thermoelasticity without energy dissipation. Banik and Kanoria [51] studied the effects of three-phase-lag on two-temperature generalized thermoelasticity for

infinite medium with spherical cavity. Bijarnia and Singh [52] studied the propagation of plane waves in an anisotropic generalized thermoelastic solid with diffusion. Ezzat et al. [53] introduced both modified Ohm's and Fourier's laws to the equations of the linear theory of magneto-thermo-viscoelasticity involving two-temperature theory, allowing the second sound effects obtained the exact formulas of temperature, displacements, stresses, electric field, magnetic field and current density. Singh and Bala [54] studied the reflection of P and SV waves from the free surface of a two-temperature thermoelastic solid half-space.

III. THE BASIC EQUATIONS OF TWO-TEMPERATURE GENERALIZED THERMOELASTICITY

Following Youssef [26], the basic equations of two-temperature anisotropic thermoelasticity in context of Lord and Shulman [6] theory are

The stress-strain temperature relations :

$$\sigma_{ij} = c_{ijkl} e_{kl} - \gamma_{ij} (T - \Phi_0) \quad (1)$$

The displacement-strain relation :

$$e_{ij} = 1/2(u_{i,j} + u_{j,i}) \quad (2)$$

The equation of motion:

$$\rho \ddot{u}_i = \sigma_{ji,j} + \rho F_i \quad (3)$$

The energy equation :

$$-q_{i,i} = \rho T_0 \dot{S} \quad (4)$$

The modified Fourier's law :

$$-K_{ij} \Phi_{,j} = q_i + \tau_0 \dot{q}_i \quad (5)$$

The equations (1) to (5) gives the basic equations of isotropic two-temperature thermoelasticity in context of Lord and Shulman theory as :

$$K \Phi_{,ii} = \rho c_E (\dot{\theta} + \tau_0 \ddot{\theta}) + \gamma T_0 (\dot{e}_{kk} + \tau_0 \ddot{e}_{kk}) \quad (6)$$

$$\rho \ddot{u}_i = (\lambda + \mu) u_{i,jj} + \mu u_{i,jj} - \gamma \theta_{,i} + \rho F_i \quad (7)$$

$$\sigma_{ij} = 2\mu e_{ij} + (\lambda e_{kk} - \gamma \theta) \delta_{ij} \quad (8)$$

Following Youssef [50], the basic equations for isotropic two-temperature thermoelasticity in context of Green and Naghdi [15] theory are :

The heat equations :

$$T_0 \gamma \delta_{ij} \dot{e}_i + \rho c_E \ddot{T} = K^* \Phi_{,ii} \quad (9)$$

The constitutive equation :

$$\sigma_{ij} = 2\mu e_{ij} + (\lambda e_{kk} - \gamma \theta) \delta_{ij} \quad (10)$$

The equations of motion :

$$\rho \ddot{u}_i = (\lambda + \mu) u_{i,jj} + \mu u_{i,jj} - \gamma T_{,i} + \rho F_i \quad (11)$$

Here, T is the mechanical temperature, $\Phi_0 = T_0$, is the reference temperature, where $\theta = |T - T_0|$ and $\frac{\theta}{T_0} \ll 1$, σ_{ij} is the stress tensor, e_{kl} is the strain tensor, c_{ijkl} is tensor of elastic constants, γ_{ij} is stress-temperature tensor, F_i is the external forces per unit mass, ρ is the mass density, q_i is the heat conduction vector, K_{ij} is the thermal conductivity tensor, c_E is the specific heat at constant strain, u_i are the components of the displacement vector, S is the entropy per unit mass, τ_0 is the thermal relaxation time (which will ensure that the heat conduction equation will predict finite speeds of heat propagation), $\gamma = (3\lambda + 2\mu)\alpha_t$, and α_t is the thermal expansion coefficient, λ and μ are called Lamé's elastic constants, δ_{ij} is the Kronecker delta symbol, Φ is the

conductive temperature and satisfying the relation $\Phi - T = a^* \Phi_{,ii}$, where $a^* > 0$, is the two-temperature parameter and K, K^* are material characteristic constants.

IV. ACKNOWLEDGEMENTS

Author is highly grateful to Dr. Baljeet Singh, Assistant Professor, Post Graduate Government College, Sector 11, Chandigarh for his valuable guidance while preparing this review.

REFERENCES

- [1] J. M. C. Duhamel, Me moires sur le calcul des actions mol éculaires développées par les changements de température dans les corps solides, Mémoires par Divers Savans (Acad. Sci. Paris), 5, 1838, 440-498.
- [2] K. E. Neumann, Die Gesetze der Doppelbrechung des Lichts in comprimierten und ungleichförmig erwärmten unkrystallinischen Körpern, Pogg. Ann., Physics Chem., 54, 1841, 449-476.
- [3] W. Thomson, On the Thermo-Elastic and Thermo-Magnetic Properties of Matter, Quarterly Journal of Mathematics, 1, 1857, 57-77.
- [4] M.A. Biot, Theory of propagation of elastic waves in a fluid-saturated porous solid. I. Low frequency range. II. Higher frequency range, Journal of Acoustical Society of America, 28, 1956, 168-191.
- [5] W. Nowacki, Couple stresses in the theory of thermoelasticity I, Bulletin L'Académie Polonaise des Sciences, Série des Sciences Technology, 14, 1966, 129-138.
- [6] H. Lord and Y. Shulman, A generalized dynamical theory of thermoelasticity, Journal of the Mechanics and Physics of Solids, 15, 1967, 299-309.
- [7] I.M. Muller, The Coldness, a universal function in thermoelastic bodies, Archive for Rational Mechanics and Analysis, 41, 1971, 319-332.
- [8] A. E. Green and N. Laws, On the entropy production inequality. Archive for Rational Mechanics and Analysis, 45, 1972, 47-53.
- [9] A. E. Green and K. A. Lindsay, Thermoelasticity, Journal of Elasticity, 2, 1972, 1-7.
- [10] E. S. Suhubi, A.C. Eringen, Thermoelastic solids in Continuum Physics II, (Ch. 2 ed.). (Academic, Press, New York, 1975).
- [11] R. S. Dhaliwal and H. H. Sherief, Generalized thermoelasticity for anisotropic media, Quarterly of Applied Mathematics, 33, 1980, 1-8.
- [12] D. S. Chandrasekharaiah, Thermoelasticity with second sound : A Review, Applied Mechanics Review, 39 1986, 355-376.
- [13] A. E. Green and P. M. Naghdi, A re-examination of the basic postulates of thermomechanics, Proceedings of Royal Society of London: A, 432, 1991, 171-194.
- [14] A. E. Green and P. M. Naghdi, On undamped heat waves in an elastic solid. J. Thermal Stresses 15, 1992, 253-264.
- [15] A. E. Green and P. M. Naghdi, Thermoelasticity without energy dissipation, Journal of Elasticity, 31, 1993, 189-209.
- [16] R. S. Dhaliwal and J. Wang, A heat-flux dependent theory of thermoelasticity with voids, Acta Mechanica, 110, 1993, 33-39.
- [17] R. B. Hetnarski and J. Ignaczak, Generalized thermoelasticity, Journal of Thermal Stresses, 22, 1999, 451-476.
- [18] D. Iesan and A. Scalia, Thermoelastic deformations, (Kluwer Academic Publisher, 1996).
- [19] D. Iesan, Thermoelastic models of continua (Solid Mechanics and its Applications, Springer, 2004).

- [20] J. Ignaczak and M. Ostoj-Starzewski, *Thermoelasticity with finite wavespeeds*, (Oxford University Press, 2009).
- [21] P.J. Chen and M. E. Gurtin, On a theory of heat conduction involving two temperatures, *Z. Angew. Math. Phys.* 19 (1968) 614-627.
- [22] P.J.Chen., M. E. Gurtin and W. O. Williams, A note on non-simple heatconduction, *Z. Angew. Math. Phys.* 19, 1968, 969-970.
- [23] P.J Chen., M. E. Gurtin and W. O. Williams, On the thermodynamics of non-simple elastic materials with two temperatures, *Z. Angew. Math. Phys.*, 20, 1969, 107-112.
- [24] W. E. Warren, and P. J. Chen, Wave propagation in the two temperature theory of thermoelasticity, *Acta Mech.*, 16, 1973, 21-33.
- [25] B. A. Boley and I. S. Tolins, Transient coupled thermoelastic boundary value problems in the halfspace, *J. Appl. Mech.(ASME)*, 29, 1962, 637-646.
- [26] H.M Youssef,., Theory of two-temperature-generalized thermoelasticity, *IMA Journal of Applied Mathematics*, 71, 2006, 383-390.
- [27] H.M Youssef and A. H. Al-Harby, State-space approach of two-temperature generalized thermoelasticity of infinite body with a spherical cavity subjected to different types of thermal loading, *Archive of Applied Mechanics*, 9, 2007, 675-687.
- [28] H.M. Youssef and E.A. Al-Lehaibi., State-space approach of two-temperature generalized thermoelasticity of one-dimensional problem, *International journal of solids and structures*, 44, 2007, 1550-1562.
- [29] Youssef, H.M., Two-dimensional problem of a two-temperature generalized thermoelastic half-space subjected to ramp-type heating, *Computational Mathematics and Modeling*, 19, 2008, 201-216.
- [30] H.M. Youssef and E. Bassiouny, Two-Temperature Generalized Thermoelasticity for One Dimensional Problems-State Space Approach, *Computational Methods in Science and Technology*, 14, 2008, 55-64.
- [31] I.A. Abbas, and H.M. Youssef, Finite element analysis of two-temperature generalized magneto-thermoelasticity *Archive of Applied Mechanics*, 79, 2009, 917-925.
- [32] M.A. Ezzat, and A.S. El-Karamany, State Space Approach of Two-Temperature Magneto-Viscoelasticity Theory with Thermal Relaxation in a Medium of Perfect Conductivity, *Journal of Thermal Stresses*, 32, 2009, 819-838.
- [33] S. Mukhopadhyay and R. Kumar, Thermoelastic Interactions on Two-Temperature Generalized Thermoelasticity in an Infinite Medium with a Cylindrical Cavity, *Journal of Thermal Stresses*, 32, 2009, 341-360.
- [34] H.M. Youssef, A Two-temperature generalized thermoelastic Medium Subjected to a moving heat source and ramp-type heating : A state-space approach, *Mathematical Sciences Publishers*, 4, 2009, 1637-1649.
- [35] M.A. Ezzat and E.S. Awad, Constitutive relations, uniqueness of solution, and thermal shock application in the linear theory of micropolar generalized thermoelasticity involving two temperatures, *Journal of Thermal Stresses*, 33, 2010, 226-250.
- [36] S. Kaushal, R. Kumar and A. Miglani, Response of frequency domain in generalized thermoelasticity with two temperatures, *Journal of Engineering Physics and Thermophysics*, 83, 2010, 1080-1088.
- [37] R. Kumar, R. Prasad and S. Mukhopadhyay, Variational and reciprocal principles in two-temperature generalized thermoelasticity, *Journal of Thermal Stresses*, 33, 2010, 161-171.
- [38] R. Kumar and S. Mukhopadhyay, Effects of thermal relaxation times on the plane wave propagation under two-temperature thermoelasticity, *International Journal of Engineering Science*, 48, 2010, 128-139.
- [39] H.M. Youssef, Two-temperature generalized thermoelastic in finite medium with cylindrical cavity subjected to moving heat source, *Archive of Applied Mechanics*, 80, 2010, 1213-1224.
- [40] H.M. Youssef and A. A. El-Bary, Two-Temperature Generalized Thermoelasticity with Variable Thermal Conductivity, *Journal of Thermal Stresses*, 33, 2010, 187-201.
- [41] E. S. Awad, A Note on the Spatial Decay Estimates in Non-Classical Linear Thermoelastic Semi-Cylindrical Bounded Domains, *Journal of Thermal Stresses*, 34, 2011, 147-160.
- [42] A. S. El-Karamany, Two-Temperature Theory in Linear Micropolar Thermo-viscoelastic Anisotropic Solid, *Journal of Thermal Stresses*, 34, 2011, 985-1000.
- [43] A. S. El-Karamany and M.A Ezzat, Convolutional variational principle, Reciprocal and Uniqueness theorems in linear fractional two-temperature thermoelasticity, *Journal of Thermal Stresses*, 34, 2011, 264-284.
- [44] A.S. El-Karamany and M.A. Ezzat, On the Two-Temperature Green-Naghdi Thermoelasticity Theories, *Journal of Thermal Stresses*, 34, 2011, 1207-1226.
- [45] M.A. Ezzat, and A.S. El-Karamany, Two-Temperature Theory in Generalized Magneto-Thermoelasticity with Two relaxation times, *Meccanica*, 46, 2011, 785-794.
- [46] M.A. Ezzat and A.S. El-Karamany, Fractional order heat conduction law in magneto-thermoelasticity involving two temperatures, *Zeitschrift für Angewandte Mathematik und Physik (ZAMP)*, 62, 2011, 937-952.
- [47] A. Miglani and S. Kaushal, Axi-Symmetric Deformation in Generalized Thermoelasticity with Two Temperatures, *Arabian Journal for Science and Engineering*, 36, 2011, 1581-1595.
- [48] S. Mukhopadhyay, R. Prasad and R. Kumar, On the Theory of Two-Temperature Thermoelasticity with Two Phase-Lags, *Journal of Thermal Stresses*, 34, 2011, 352-365.
- [49] B. Singh and R. Bijarnia, Propagation of plane waves in anisotropic two temperature generalized thermoelasticity, *Mathematics and Mechanics of Solids*, 17, 2011, 279-288.
- [50] H.M. Youssef, Theory of two-temperature thermoelasticity without energy dissipation, *Journal of Thermal Stresses*, 34, 2011, 138-146.
- [51] S. Banik and M. Kanoria, Effects of three-phase-lag on two-temperature generalized thermoelasticity for infinite medium with spherical cavity, *Applied Mathematics and Mechanics*, 33, 2012, 483-498.
- [52] R. Bijarnia and B. Singh, Propagation of plane waves in an anisotropic generalized thermoelastic solid with diffusion, *Journal of Engineering Physics and Thermophysics*, 85(2), 2012, 442-448.
- [53] M.A. Ezzat, M. Zakaria and A. A. El-Bary, Two-Temperature theory in thermo-electric viscoelastic material subjected to modified Ohm's and Fourier's Laws, *Mechanics of Advanced Materials and Structures*, 19, 2012, 453-464.
- [54] B. Singh and K. Bala, Reflection of P and SV waves from the free surface of a two-temperature thermoelastic solid half-space, *Journal of Mechanics of Materials and Structures*, 7, 2012, 183-193.

Design and Fabrication Of Manually Track Parabolic Solar Disc for In-House Cooking

Yogesh R. Suple¹ N.N. Suraskar²

Asst. Prof. Mechanical Engineering Department, Kavikulguru Institute of Technology & Science, Ramtek (India)

Abstract: Human civilization has been witnessing a gradual shift towards cleaner fuels—from wood to coal, from coal to oil, from oil to natural gas; renewables are the present demand. In this fabrication work a primary reflecting parabolic surface concentrates the solar radiation on it and reflects them on to the secondary reflectors. This secondary reflector then focus the incident radiation at the point of interest, thus generated heat can be used for cooking purpose. In this work the biaxial sun tracking mechanism is developed which can be operated from the cooking place (in-house).

Keywords: In-house cooking, manual bi-axial tracking, parabolic disc, solar energy.

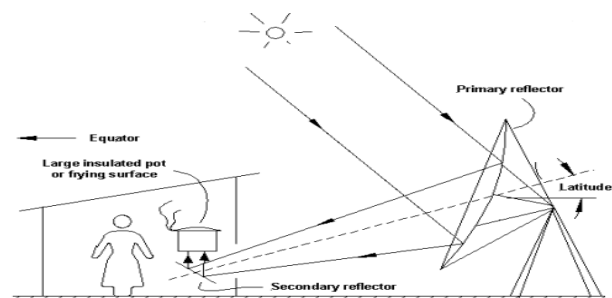
I. INTRODUCTION

Energy crisis in today's world is the most stressed term that present day scientists are working upon. Solar energy should be the answer to the above problem. In the rural parts of the country it is observed that the sources of energy for the daily purposes are less these results in many difficulties like cooking purposes, thus the people have to use unhealthy practices like dunk cakes and charcoal it causes severe health hazards and pollution. The use of solar energy to cook food presents a viable alternative to the use of fuelwood, kerosene, and other fuels traditionally used in developing countries for the purpose of preparing food. Solar cooking can be used as an effective mitigation tool with regards to global climate change, deforestation, and economic debasement of the world's poorest people. In the concentrating type of solar collector, solar energy is collected and concentrated so that higher temperatures can be obtained. The basic idea that leads to the development of the parabolic reflector is to make solar cooking as comfortable as possible. At the same time the device should be build in such a way that it allow, it to be constructed in any rural welding workshop in a country after a certain period of training. As the conventional solar cooker is exposed to the day light therefore the operator needs to stay under direct sunlight for constantly paying attention on the cooker to maintain the temperature even. In parabolic solar cooker this problem of operator to constantly stand under direct sunlight in hot and humid condition is eliminated. The concentrating reflector provides the sunlight directly into the kitchen for preparation of food. The main objectives of this paper are: 1) To promote solar energy technologies to meet cooking energy requirements of a family in rural area. 2) Reduction in the consumption of traditional

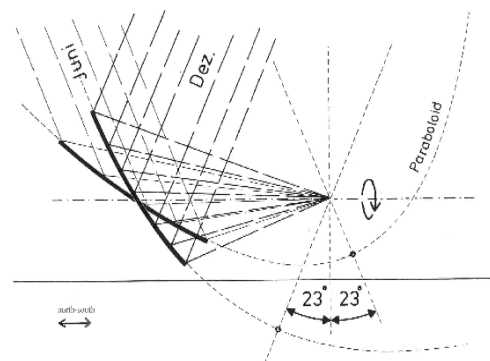
II. Working Principle of Parabolic Solar cooker

To make cooking simple and comfortable the cooking-place should not have to be moved, even better, it should be inside the house and the concentrating reflector

outside in the sun. The best solution is an eccentric, parabolic reflector which rotates around as axis parallel to earth- axis synchronous with the sun. Additionally the reflector is adjusted to the seasons by making it flexible in a simple way.



The system of parabolic cooker comprises a primary reflector, a secondary reflector, and tracking mechanism. The primary reflector produces a converging beam of sunlight aligned with an axis of rotation which is parallel to the axis of the earth, and which passes through the centers of both reflectors. The tracking unit rotates the primary reflector around its axis of rotation, keeping the reflected beam aligned with the axis of rotation as the sun moves. The fixed secondary reflector reflects the beam from the primary reflector onto a cooking pot or frying surface as shown in above figure. In the course of the seasons the incident angle of the solar radiation varies $\pm 23.5^\circ$ in relation to the perpendicular earth-axis. The paraboloid has to perform the same change of inclination in order to stay directed to the sun. Otherwise it's not possible to obtain a sharp focal point. But the centre of the reflector and the position of the focus are not allowed to move as shown in figure.



With the help of a simple mechanical tracking system the solar disc rotates in the direction of the movement of the Sun to give continuous and accurate solar energy concentration. For a fully tracking the sun normal to the primary reflector must be normal to the solar beam.

Therefore, the reflector's azimuth and altitude angles must coincide with the sun's azimuth angle and the complement to the sun's altitude angle. The incidence angle is equal to zero. Therefore,

Inclination angle (β) = $\cos^{-1}[\sin \delta \sin \phi + \cos \delta \cos \phi \cos \omega]$

And surface azimuth angle

$$\gamma = \sin^{-1} \left[\frac{\cos \delta \sin \omega}{\sin \beta} \right]$$

where

ϕ is the latitude of location,

δ is the declination angle and

ω is the hour angle.

III. Fabrication of Experimental Set up

The various elements of the setup (Parabolic Concentrating Solar Cooker) are as follows:

- Primary Reflector
- Cooking unit with secondary reflector
- Manual tracking mechanism

3.1 Primary Reflector

The primary reflector is the basic element of the revolutionary concept developed by Wolfgang Scheffler.

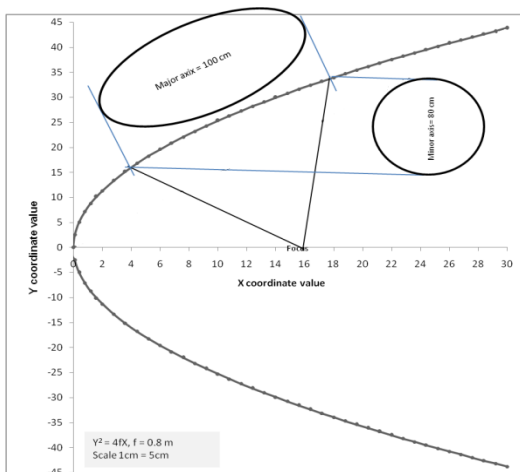
3.1.1 Design Considerations

The various factors taken into consideration for formulating the primary reflector are

- Focal distance from the primary reflector (vertical as well as horizontal)
- Concentration ratio to be achieved.
- Aperture area of the primary reflector.
- Central depth.
- Elliptical area of primary reflector.

The general equation of parabola is $Y^2 = 4f \times X$

Where, X and Y are polar co-ordinates and f is the distance of focus from origin. (f = 80 cm)



$A_p = \pi/4 \times \text{major axis} \times \text{minor axis}$, where A_p is the aperture area.

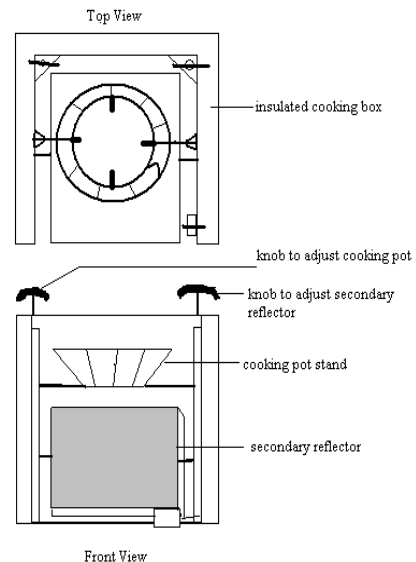
3.1.2 Primary Reflector Specifications

The various specifications of primary reflector with its frame are shown in table 1.

1.	Concentrator type	paraboloidal
2.	Aperture area	0.628 m ²
3.	Aperture diameter	0.8 m
4.	Length of circumference	3 m
5.	Focal length	0.8 m
6.	Receiver diameter	14 cm
7.	Receiver area	0.015 m ²
8.	Optical concentration ratio	40

3.2 Cooking Unit with Secondary Reflector

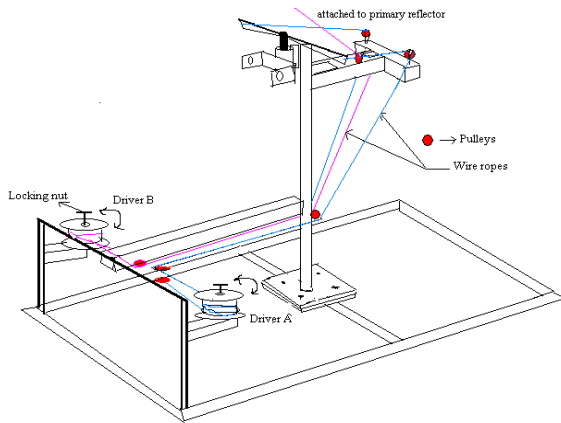
The main purpose of secondary reflector is to trap the incoming heat at the focal point & onto a well defined point under the vessel placed at a certain height. The design of the secondary reflector plays a vital role to the over all objective of heat entrapment. The provision of the adjustment of the cooking pot height as per the requirement and secondary reflector position and inclination with respect to the position of primary reflector is the unique feature of the cooking unit fabricated as shown in figure.



Part	Material	Specifications
Cooking unit with Secondary Reflector	Stainless steel	300 x 250 x 1.5 mm
	MS sheet	1250 x 750 x 1 mm
	MS bar	10 mm, 06 mm
	MS Angle	20 x 20 x 2 mm
	Insulation	Glass wool

3.3 Manual Tracking Mechanism

The main purpose of the tracking mechanism is to trace the path of sun movement through the entire day. This is achieved by manual or automated tracking mechanism. In this paper manual tracking mechanism is developed, which will be operated from the cooking place (kitchen). Manual sun tracking arrangement is designed to track both the axis by using the wire ropes and pulleys. Two Rotating drivers are provided to which the wire ropes are attached as shown in figure.



Out of two one rotating driver is for adjusting or setting primary reflector as per the solar altitude angle and another one is to adjust azimuth angle. The operator has to rotate these two rotating drivers to set the orientation of primary reflector normal to the sun once in 10 to 15 minutes. The material used for the fabrication of manual tracking mechanism is shown in table 2 with its specifications.

Part	Material	Specifications
Drivers (Rotating)	MS sheet MS	203 mm OD, 152 mm ID
Pulley	MS	30 mm ID, 10 mm thick
Wire rope	Steel	2 mm Ø
Thrust bearing	51104	20 ID x 35 OD x 10 mm
Bushes & Pins	MS round bar	20 ID & 20 OD

IV. Working of Parabolic Solar Cooker



The parabolic disc is installed in an open area facing the South. The cooking place and vessels faces the North. A 0.628 m² area parabolic solar concentrator is used for concentrating solar radiation on a focal area where the secondary reflector is placed. The reflector disc can be Easily rotated to adjust the reflector according to sun orientation. The secondary reflector diverts the solar energy on the cooking vessel and the heating begin. With the help of a wire ropes and pulleys manually operated simple mechanical tracking arrangement the solar disc rotates in the direction of the movement of the Sun to give continuous and accurate solar energy concentration. These wire ropes are attached to rotating drivers. By rotating this drivers regulated tracking motion to follow the path of the sun throughout the day.

V. CONCLUSION

In an age where domestic fuel costs are rising each year, the solar cooker is a real boon. Reasonably priced, easy-to-use and completely trouble-free, the solar cooker is an ideal supplement to the conventional cooking appliances. Solar cooking is entirely non-polluting and has no ill effects on health. Unique feature of cooker is the sun tracking arrangement. Though it is manually operated but fully controlled within the kitchen only. That means the operator doesn't need to go in sunny place to set primary reflector normal to sun rays every time.

References

- [1] Sukhatme, S.P. *Solar Energy Principles of Thermal Collection and Storage* Tata McGraw-Hill publishing company Ltd., New Delhi 2005.
- [2] Garg HP, Parkash J. *Solar Energy fundamentals and applications* New Delhi: Tata McGraw-Hill, 2000. pp 166-175.
- [3] Pohekar SD, Ramachandran M. *Multi-criteria evaluation of cooking energy alternatives for promoting parabolic solar cooker in India*. Renew Energy 2004;29:1449–60.
- [4] A.V.Sonune, S.K.Philip *Development of a domestic concentrating cooker* Renewable energy 28 (2003) 1225-1234
- [5] Jose M.Arenas *Design, development and testing of a portable parabolic solar kitchen* Renewable energy 32 (2007) 257-266.
- [6] S. R. Kalbande, A. N. Mathur, S. Kothari I & S. N. Pawar. *Design, Development and Testing of Paraboloidal Solar Cooker* Karnataka J. Agric. Sci., 20(3), (571-574): 2007
- [7] U.S.Mirdha, S.R.Dhariwal. *Design optimization of solar cooker* Renewable energy 33 (2008) 530-544.

Optimization of Lipase Enzyme Activity Produced By *Bacillus Amyloliquefaciens* Isolated From Rock Lobster *Panlirus Homarus*

T. Selvamohan¹, V. Ramadas² and T. A. Sathya³

¹P.G & Research Department of Zoology, R.D.Govt Arts College, Sivagangai – 630 561, Tamil Nadu, India

^{2,3}Department of Microbiology, Sivanthi Aditanar College, Pillayarapuram - 629 501, Nagercoil, Tamilnadu, India

Abstract: The production of extracellular lipase (triacylglycerol hydrolase) is a widely distributed phenomenon among eukaryotic and prokaryotic microorganisms. Microbial lipases have mostly been employed in food and detergent industry for purposes such as the ripening of cheese and an additive to laundry detergent. Lipase producing organisms were isolated from Rock Lobster (*Panlirus homarus*). *Bacillus amyloliquefaciens* was found to be the highly active strain for lipase enzyme production. The most suitable for lipase production is fish bone and the maximum amount of paranitrophenyl palmitate released is found to be 0.84 µg/ml/min at 48hrs of incubation. The optimum temperature and pH for the organism was found to be 47°C and 9, the amount of paranitrophenyl palmitate released was recorded as 0.89 µg/ml/min and 0.74 µg/ml/min for various substrates such as Glycerol, Olive Oil, Coconut Oil and Fishbone. Lipase production was obtained at different substrate concentration and the bacterial species yield maximum production of lipase and it was analysed by spectrophotometric method.

Keywords: Rock lobster (*Panlirus homarus*) – *Bacillus amyloliquefaciens*, Optimization of Lipase enzyme with different substrates..

I. INTRODUCTION

Lipases are enzymes capable of hydrolyzing the ester bonds of water-insoluble substrates at the interface between substrate and water. It is well known that the reaction is reversible and this enzyme can catalyse ester synthesis and transesterification since lipases can catalyse numerous different reactions they have been widely used in industrial applications, such as in food, chemical, pharmaceutical and detergent industries [1]. Many microorganisms are known as good producers of extracellular lipases [2].

Lipases occur widely in bacteria, yeast and fungi [3]. Most of the lipase research focuses on the production of extracellular lipases through a wide variety of microorganisms. Studies on the production of extracellular lipases with *Bacillus* have shown variations among different strains. However, the requirement for lipid carbon source remains essential for enzyme production. Lipase producing organisms are isolated from Lobster (*Panlirus homarus*) and that the wild and cultured lobsters harbours a diverse bacterial flora which includes the dominant genera like *Aeromonas*, *Pseudomonas*, *Bacillus*, *E.coli*, *Salmonella* and *Vibrio* [4]. These organisms are having the ability to produce enzymes. These enzymes are produced during the utilization of certain nutrients such as proteins, lipid and carbohydrate. Lipases have potential applications in detergent, oleo chemical, paper manufacturing, cosmetics,

pharmaceuticals, and agrochemical industries. They are also employed in organic chemical processing, biosurfactant synthesis, nutrition and biomedical sciences [5].

Most of the commercial lipases produced are utilized for flavour development in dairy products and processing of other foods, such as meat, vegetables, fruit, baked foods, milk products and beer. Lipases are extensively used in dairy industry for the hydrolysis of milk fat. The dairy industry uses lipases to modify the fatty acid and chain lengths, to enhance the flavours of various cheeses. Lipases enzyme also accelerates cheese ripening and the lipolysis of butter, fat and cream [6]. The objective of this study was the production of lipase and characterization of the enzyme with regards to its stability in relation to temperature, P^H and the optimization of the temperature and P^H conditions for obtaining higher lipase activity.

II. MATERIAL AND METHODS

2.1 Collection of Sample:

Lobster sample was collected in a sterile bag from the fish market near Kanyakumari, Tamil Nadu, India and brought to the laboratory within 15 minutes.

2.2 Isolation of Intestinal Flora of Lobster:

The intestine of the lobster was dissected out aseptically and homogenized with 0.089% of NaCl solution. The homogenate was serially diluted and spread on sterilized nutrient agar plates and incubated at 37°C for 24 hours. The colonies were counted for TVC (Total viable Count). The dominant colonies were isolated and streaked in nutrient agar slants as master culture.

2.3 The Composition of Production Medium Used For Lipase Production:

The production medium was prepared for lipase production by the *Bacillus amyloliquefaciens* in the following composition.

- | | | |
|-------------------|---|------------|
| • Peptone | - | 3% (w/v) |
| • Yeast Extract | - | 1% (w/v) |
| • Sodium Chloride | - | 0.5% (w/v) |
| • Olive Oil | - | 1% (w/v) |
| • P ^H | - | 7 |

2.4. Assay of Lipase Enzymes

2.4.1. Optimization of Fermentation Media:

The fermentation media prepared was optimized with following factors such as Incubation period, P^H, Temperature and Lipid Substrates.

2.4.1.1. Optimization by Incubation Period:

The organisms were subjected to different incubation periods such as 24, 48 and 72 hours using production media.

2.4.1.2. Optimization by different P^H

The microorganisms isolated from the rock lobster were incubated in the production media containing different P^H varied from 5, 7 & 9.

2.4.1.3. Optimization by different temperature

The microorganism in the production media was incubated at different temperature 27°C, 37°C, and 47°C.

2.4.1.4. Optimization by Lipid Substrate

In order to optimize the enzyme lipase different lipid substrates were used, such as, Glycerol, Olive oil, Coconut oil, Fish Bone and chicken intestine.

2.4.1.5. Enzyme Assay

Microbial Culture was assayed for lipase enzyme activity using Spectrophotometric method and results were recorded.

2.5. Principle

In the present investigation one unit (U) of lipase activity was defined as the amount of enzyme solution liberating 1µmol of p-nitrophenol per minute under standard assay conditions.

2.6. Reagents Required

To carry out the study following reagents were required such as, Reaction Buffer (500µl) (It contains the mixture of 50 mM Tris Hcl (P^H 9.0) and Triton X-100), 2-Propanol (20µl) p-nitrophenylpalmitate (P^{NPP})

The spectrophotometric method, using P-nitrophenyl Palmitate as substrate was applied for rapid and routine measurement of the lipase activity. Enzyme or blank solution (480µl) was added to the reaction buffer (500µl) which has 50mM Tris-HCl (P^H 9.0) with variable concentrations of Triton x-100. The content was incubated at 25°C for 5 minute and ten millimolar P^{NPP} in 2-propanol (20µl) was added to the enzyme buffer solution and shaken well. The mixture was emulsified for 2 minutes at 50°C. The progress of the reaction was followed by monitoring the change in the absorbance at 400nm over a period of 5 minutes at 50°C using Perkin-Ealmer Spectrophotometer. The molar extinction coefficient of P-nitrophenol ($E=16.900M^{-1}Cm^{-1}$) was estimated from the absorbance measured at 400 nm of standard solutions of P^{NPP}.

III. RESULTS

The enzymatic activity was assayed with different substrates like Glycerol, Olive oil, Coconut oil and Fish bone. The production of lipase was observed at varying pH (5, 7 & 9), temperature (27°C, 37°C & 47°C), substrate concentration (0.1, 0.2, 0.3, and 0.4) and at different time intervals (24, 48, and 72 hrs). Lipase producing organisms was isolated from rock lobster and was noted as *k₁*. It was identified as lipase positive organism by comparing with Bergey's Manual of Determinative Bacteriology and this organism was the highly active strain for lipase production.

The effect of lipase production by the *Bacillus amyloliquefaciens* (*k₁*) with various substrates (glycerol, olive oil, coconut oil and fish bone) at different incubation periods (24hrs, 48hrs and 72hrs) were carried out and the results were indicated in Fig.1. The most suitable substrate for lipase production was identified as fish bone, and the maximum amount of paranitrophenyl palmitate released was recorded as 0.84 µg/ml/min at 48 hrs of incubation period. The minimum amount of paranitrophenyl palmitate was released with olive oil was recorded as 0.10 µg/ml/min at 48hrs of incubation time.

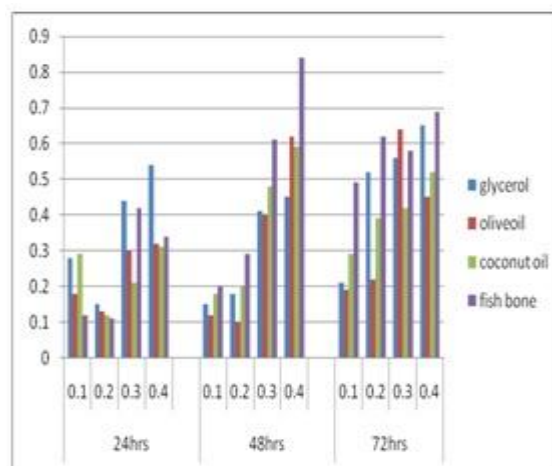


Fig.1 Effect of different substrates on lipase production by *Bacillus amyloliquefaciens* (*K₁*)

The effect of pH on lipase production at various incubation time intervals have been carried out and the results were indicated in Fig. 2. At 48hrs of incubation at pH 9, the *Bacillus amyloliquefaciens* (*k₁*) showed the maximum production lipase and the amount of paranitrophenyl palmitate released was recorded as 0.89 µg/ml/min, whereas the minimum production was noted at pH 5 at 24hrs of incubation period and the amount of paranitrophenyl palmitate released was recorded as 0.31 µg/ml/min.

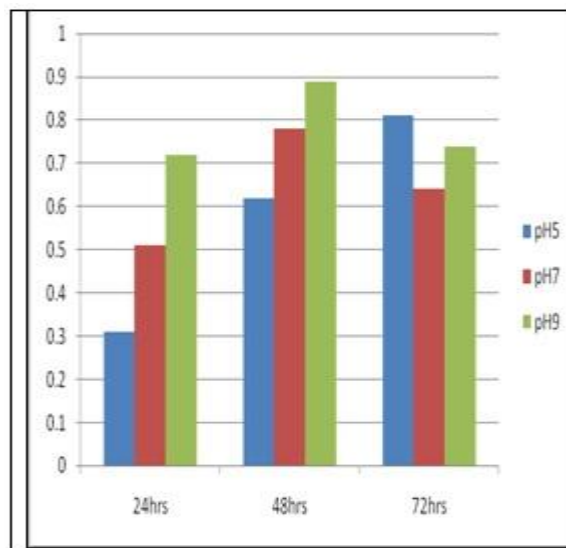


Fig.2 Effect of different pH on lipas production by *Bacillus amyloliquefaciens* (*K₁*)

The effect of different temperatures on lipase production at various time intervals was shown in Fig.3. At 72hrs of incubation at 47°C, the *Bacillus amyloliquefaciens* (k1) showed a maximum production and the amount of paranitrophenyl palmitate released recorded was 0.74 µg/ml/min, whereas the minimum production observed at 37°C at 24hrs and the amount of paranitrophenyl palmitate released was recorded as 0.43 µg/ml/min.

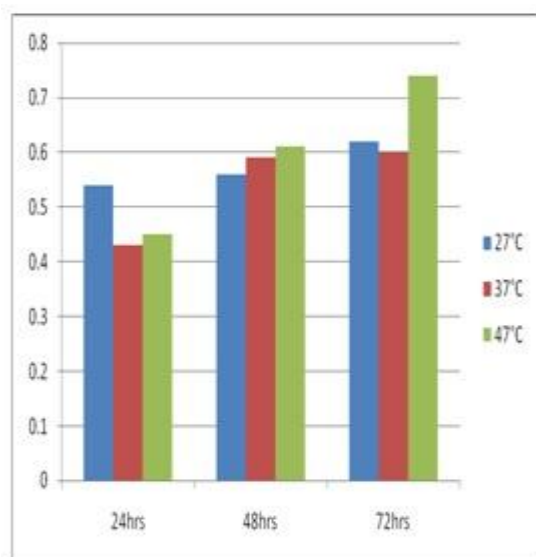


Fig.3 Effect of different temperature on lipase production by *Bacillus amyloliquefaciens* (K1)

IV. DISCUSSION

Lobsters harbors a diverse bacterial flora and most of the microorganisms produce enzymes. Lipase producing microorganism isolated from the lobster was identified as *Bacillus amyloliquefaciens* (k1). The lipase enzyme activity was assayed with varying pH, temperature and substrates at different time intervals. In the present study the effect of lipase enzyme activity with the fish bone as a substrate showed the maximum production (0.84 µg/ml/min) at 48hrs of incubation and the minimum amount of paranitrophenyl palmitate released in olive oil as a substrate was recorded as 0.10 µg/ml/min at 48hrs of incubation. Among the various substrates, gingili oil cake and wheat bran were found to be the best substrates [7]. Whereas in the present investigation, the fish bone used as substrate was found to be the best with a high enzyme production.

At 48hrs of incubation with pH 9, the *Bacillus amyloliquefaciens* (k1) showed the maximum production and the amount of paranitrophenyl palmitate released was recorded as 0.89 µg/ml/min and the minimum production at pH 5 at 24hrs the amount of paranitrophenyl palmitate released was 0.31 µg/ml/min. The lipase enzyme was active in the range of pH 7.5-9.5, and the maximal activity was observed at pH 9.0. It is a characteristics that the most microbial lipases, the optimum pH falls on the alkaline side. In present study the similar trend was observed that pH was optimum and it falls on the alkaline side [8].

At 72hrs of incubation at 47°C the *Bacillus amyloliquefaciens* (k1) showed the maximum production and the amount of paranitrophenyl palmitate released was observed as 0.74 µg/ml/min and the minimum production noted at 37°C at 24hrs, and the amount of paranitrophenyl

palmitate released was recorded as 0.43 µg/ml/min. In contrast, in the present study, the P^{NPP}-hydrolysing activity had a clear temperature which is "optimum" at 37°C even though the enzyme was fully stable up to 80°C for at least 15 min, which is much longer than the duration of the activity assay [9].

The overall properties showed by *Bacillus amyloliquefaciens* (k1) indicated that the cloned lipase is a mesophilic enzyme acting on a broad range of pH that becomes inactivated only by a limited number of lipase inhibitors. In the present study, pH was varied using different substrates concentration [10]. In connection with their biochemical properties, both lipolytic enzymes display different substrate specificities [11]. In the present study the substrate specificities are done using Glycerol, Coconut Oil, Olive Oil, and Fish Bone as substrates.

The cell produces lipases in order to obtain the energy required to form new cells from the available carbon sources and at the same time it does a normal metabolic activity irrespective of growth [12]. Comparing results of lipolytic activities with those of other research studies is difficult owing to the different methodologies used by different groups. However, comparing the results obtained in this work with those reported using the same methodology and reaction substrate.

Glucose, Olive Oil, Peptone and FeCl₃ 6H₂O were found to have more significance on lipase production by *Candida rugosa*. [13]. In the present study glucose, olive oil, coconut oil and fish bone are used as substrates and among that fish bone showed the highest enzymatic production.

References

1. Harwood, J. 1989. The versatility of lipase for Industrial uses. *Trends Biochem. Sci.* 14: 12-126.
2. Ratledge, C., Tan, K.M. 1990. Oils and fats Production degradation and utilization by yeasts. In: Verachter, H., Mot, D. (Eds), *Yeasts, Biotechnology and Biocatalysis*, Marcel Dekker, New York. PP.223-253.
3. Jaeger, K.E., B.W. Dijkstra, M.T. Reetz. 2000. Bacterial Biocatalysts Molecular biology, three – dimensional structures, and biotechnological application. *Annu-Rev-Microbiol.* 53: 315-351.
4. Oxley, A.P.A., W. Shipton, Owen. 2002. Bacterial flora from the gut of wild and cultured banana prawn. *Applied Microbiology.* 93: 214-218.
5. Pandey, A., S. Benjamin, P. Nigam, C.R. Soccol and N. Krieger 1999. Realm of microbial lipases in biotechnology. *Biotechnol Appl.* 29: 119-131.
6. Sharma, R., Y. Chisti and U. Banerjee. 2001. Production, Purification, Characterization and applications of lipase. *Biotechnol. Adv.*, 19: 627-662
7. Kamini, N.R., J.G.S. Mala and R. Puvanakrishnan. 1998. Lipase production from *Aspergillus niger* by solid-state fermentation using gingelly oil cake. *Process Biochemistry.* 33: 505-511.
8. Kambourova, M.N., R. Kirilova, A. Mandiva, A. Derekora 2003. Purification and properties of thermostable lipase from a thermophilic *Bacillus stearothermophilus* MCF. *Journal of Molecular Catalysis B. Enzymatic.* 22: 307-313.

9. Fitter N, R.Hermann, N.A. Dencher, A. Blume, T.Hauss. 2001. Preliminary characterisation of a lipolytic enzymes. *Journal of Molecular catlysis*. 40: 10723
10. Prim, N., Blanco, A. Martinez, J., Pastor, F.I.J and Diaz P. 2000. A gene coding for a cell- bound esterase from *Paenibacillus sp.* *Dpt of Microbiology*. 43: 237-240
11. Eggert T. Van Pouderoyen G, Dijkstra BW, Jaegerk. 2001. Lipolytic enzymes Lip A and Lip B from *Bacillus subtilis* differ in regulation of gene expression, biochemical properties and three dimensional structure. *FEBS Lett*. **502**: 89-92.
12. Shu, and Lin. **2006**. Purification and Partial characterization of a lipase from *Antrodia cinnamomea*. *Process Biochem*. **41**: 734-738.
13. Aravindan Rajendran., Anbumathi Palanisamy and Viruthagiri Thangavelu. **2008**. Evaluation of medium components by placket-Burman statistical design for lipase production by *Candida rugosa I* and kinetic modeling. *Chinese Journal of Biotechnoogy*. **24**(3): 436-444.

Free Expansion and Thermal Stress Analysis of a Corner Welded Joint by Finite Element Method

¹ K.Ashok Kumar ² T.N.Charyulu ³ Dr. CH.Srinivasa Rao ⁴ P. Surendra Babu

¹ M.Tech. Scholar, Nova College of Engineering & Technology, Jangareddygudem, West Godavari, A.P. INDIA.

² Head, Department of Mechanical Engineering, Nova College of Engineering & Technology, Jangareddygudem, West Godavari, A.P.

^{3,4} Department of Mechanical Engineering, KHIT, Guntur, A.P.

ABSTRACT: In Arc welding heat is transferred to the joint by an electrode. During manual metal Arc Welding this heat is transferred by melting the electrode. The stresses generated in welded plate are due to temperature raise and can be simple and thermal stresses. The stresses generated will cause distortion and changing the shape of the welded plates. The study of the distortion and residual stresses is found major importance in the area of shipbuilding boiler works and machine tool structures. The finite element method is one of the numerical techniques used mostly for the stress analysis of welded joints.

The present paper deals with the simulation of arc welding process for the study of stresses due to free expansion and temperature rise. ANSYS 11.0, commercial software is used for modeling and simulation of the present problem. The FE analysis is carried two stages in the first stage thermal stresses analysis has been carried to estimate time dependent temperature. The temperature output of the first stage is given as input in the structural analysis i.e. in the second stage. The structural analysis has been carried of the corner joint with and without fixed boundary conditions along the length of the joint. The output of the combined thermal and structural analysis involves von mises stresses, strains and deformation. The results have been compared with theory and are in good agreement for both free expansion and thermal stress analysis.

Keywords: Arc Welding, Finite Element Method, Free expansion, Thermal stresses & Deformation.

I. Introduction and Background

Arc welding is a fusion type of welding process used for joining of structural elements for a wide range of applications e.g. guide way for trains, ships, bridges, building structures, automobiles, and nuclear reactors etc. In Arc welding, either direct or alternating electric current is continuously supplied to create an electric arc that generates enough heat to melt the metal and form a weld.

The research activity in welding simulation started decades ago. The Theory of moving Sources of Heat and Its Application to Metal Treatments [1]. Thermo mechanical Analysis of the Welding Process Using the Finite Element Method [2]. Over the past few years, Finite Element Simulation of Welding of Large Structure [3] and Prediction of Welding Distortion [4]. The work done by the Friedman et al has been verified by 3-D computational modeling and Analysis of Residual Stress and Deformation Due to Welding [5].

The transient temperature distributions and temperature variations of the welded plates during welding

were predicted and Thermal Analysis of the Arc Welding Process: Part 1. General Solutions [6]. The Effects of Root Opening on Mechanical Properties, Deformation and Residual Stress of Weldments [7]. Effects of welding speed, energy input and heat source distribution on temperature variations in butt joint welding [8]. Simulation on the thermal cycle of a welding process by space-time convection-diffusion finite element analysis [9]. Numerical and experimental investigation into effect of temperature field on sensitization of Alloy 690 butt welds fabricated by gas tungsten arc welding and laser beam welding [10]. Modeling the transient heat transfer for the controlled pulse key-holing process in plasma arc welding [11].

The problem of welding distortion during large steel fabrications leads to dimensional inaccuracies and misalignments of structural members, which can result in corrective tasks or rework when tolerance limits are exceeded. This in turn, increases the cost of production and leads to delays. Therefore, the problems of distortion and residual stresses are always of great concern in welding industry. Even though ample of work has been carried on welding phenomenon still there is a lacuna in the study of the effects of heat input, welding speed, restraint, plate curvature, and gap on arc welding responses. Thus the objective of the present paper is to simulate the complex arc welding process using the finite element code ANSYS and study the Von mises Stresses, Strains, and distortion due to thermo-mechanical response.

II. Finite Element Modeling:

The corner welded joint has been modeled using two number 3-dimensional rectangular plates to obtain an L-shape. The dimensions of both the horizontal and vertical plates are of length of 0.28m, width 0.1m and thickness of 0.006m. The temperature-dependent Material Properties shown in Table –I are given as input. Solid 70 and Solid 185 elements have been used for meshing in the thermal analysis and Structural Analysis is respectively. The number of element divisions in X&Y Directions are 10 and along Z-Direction is 28. The FE mesh of the model in Figure-1.

Table-1: Temperature-Dependent Material Properties

Temperatures (Celsius)	Modulus of Elasticity (MPa)	Poisson Ratio	Thermal Ex. Coef. ($10^{-6}/^{\circ}\text{C}$)	Thermal Conductivity ($\text{W/m}^{\circ}\text{K}$)	Specific Heat ($\text{J/kg}^{\circ}\text{K}$)
0	314	0.2786	10	51.9	450
100	349	0.3095	11	51.1	499.2
300	440	0.331	12	46.1	565.5
450	460	0.338	13	41.05	630.5
550	410	0.3575	14	37.5	705.5
600	330	0.3778	14	35.6	773.3
720	58.8	0.3738	14	30.64	1080.4
800	58.8	0.4238	14	26	931
1450	1.29	0.4738	15	29.45	437.93
1510	1.0	0.499	15	29.7	400
1580	0.01	0.499	15	29.7	735.25
5000	0.01	0.499	15.5	42.2	400

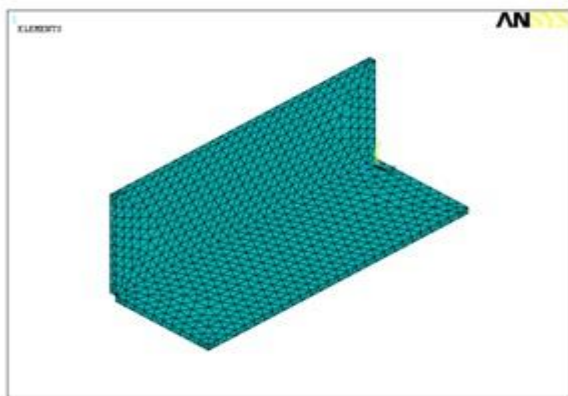


Figure-1: FE Mesh of the model

A heat input of 1200 W is given at the welded joint i.e. between the plates along the centre line. Convection is applied on the exposed surface with a film coefficient of $h=5000 \text{ w/m}^2\text{ }^{\circ}\text{C}$ and the bulk temperature of 25°C . The surface temperature of the specimen is Zero. The simulation has been carried for thermal analysis in a time period of 1200 seconds. The number of sub steps are 20 the time at the end of load step is 1200seconds on the size of the time step is 60. For simple stresses due to free expansion, no fixed boundary condition is applied along the joints and the joint is constrained along the length for thermal stresses. The Newmark algorithm has been used to run the simulation with transient effects. The temperatures obtained from thermal analysis are imported in to structural analysis for getting thermal stresses and strains.

III. Results & Discussion

The results and discussions drawn from the present work include the temperature distribution with respect to time in thermal analysis and estimation of Von mises stresses, Strains by combined Thermo-mechanical analysis. The variation of temperatures in all(X, Y &Z) directions with respect to time is shown in Figure 2. The temperature rises initially at a slower rate and rapid rate later but the rate is uniformly increasing and is due to cold condition of work piece at initial stages.

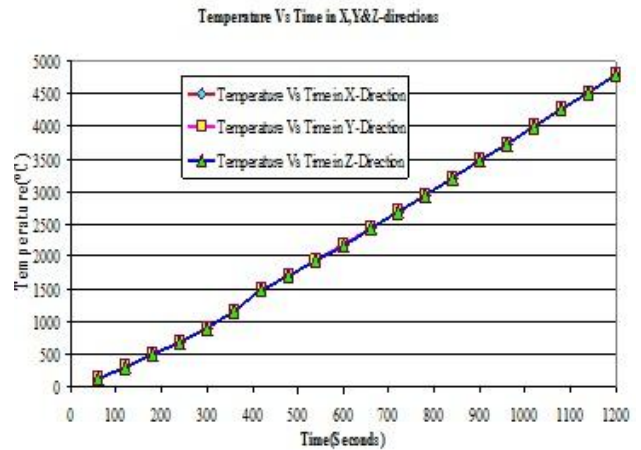


Figure-2: Temperature Vs Time

3.1 Displacements: The displacement of the horizontal plate in X, Y&Z directions with respect to the dimensionless parameter(X/L) for free expansion (simple stress analysis) and temperature stresses are shown in Figure 3 and 4 respectively.

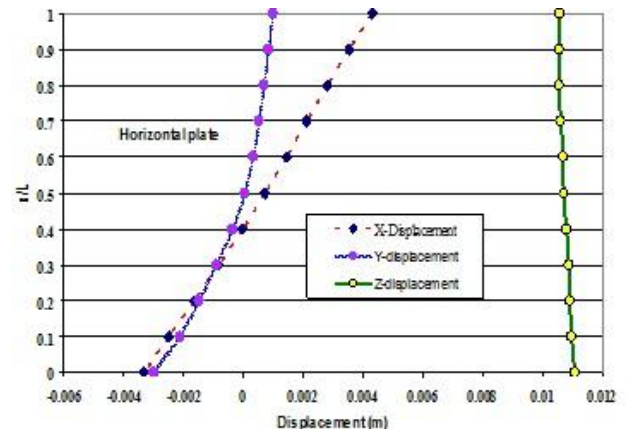


Figure-3: Displacements in Horizontal Plate (Free Expansion)

It is observed that the displacement in z-direction is more for both the simple stress and thermal stress analysis for the horizontal plate (Figure-3 & 4). The deformation is more for free expansion and is less for thermal analysis with structural boundary conditions

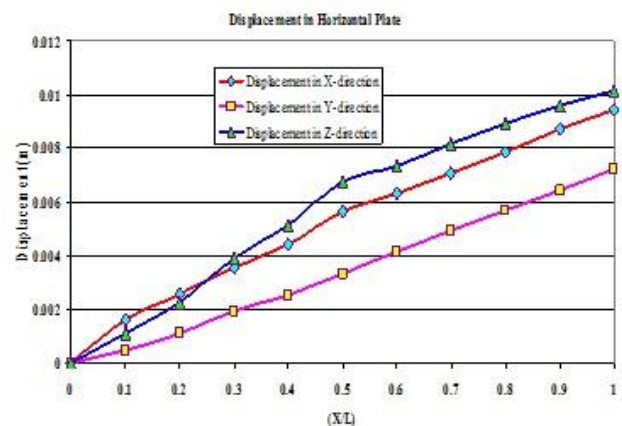


Figure-4: Displacements in Horizontal Plate.

This is due to the fact that the welded plate acts like a fin fixed at one end and free at the other end. For the same dimensionless parameter, the maximum deformation in Z-direction for free expansion is 0.015mm and it is 0.01mm. The displacement is continuously increasing from line of welding to the other end for structural boundary condition and is falling along the length for free expansion. The behaviour is opposite in X and Y-directions. The similar trend is also observed for vertical plate.

3.2 Von mises Stresses: The variation of Von mises Stresses are shown in Figure-5 and Figure-6 for free expansion and thermal respectively. For both the analysis, the maximum stresses are found in X-direction i.e. along the width of the plates.

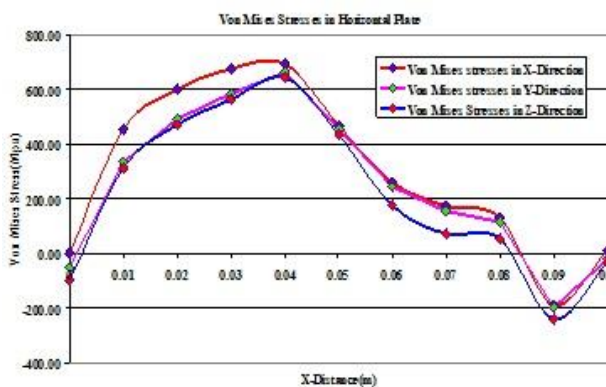


Figure-5: Von mises Stresses in horizontal Plate (Free Expansion)



Figure-6: Von mises Stresses in horizontal Plate

The highest stress value of 692 Mpa is found at a distance of 40mm from the origin in X-direction and a minimum value of compressive stress of 240 Mpa at the extreme end of the horizontal plate. Similarly for thermal analysis, the highest stress value of 1510 Mpa is found at a distance of 10mm from the origin in X-direction and a minimum value of compressive stress 315 Mpa at the extreme end of the horizontal plate.

Because of the thin plate effect, the stresses are uniform in vertical and horizontal plates of the Joint (Figure-7) for free expansion and is different from thermal analysis. The cumulative effect of temperature raise at the welded joint and the heat input at the origin causing more thermal stresses at the origin (Figure-8) due to fixed boundary conditions.

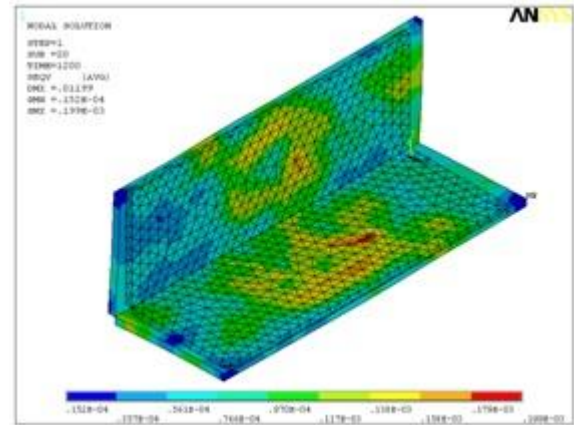


Figure-7: Von mises Stresses (X, Y & Z directions)-Free Expansion

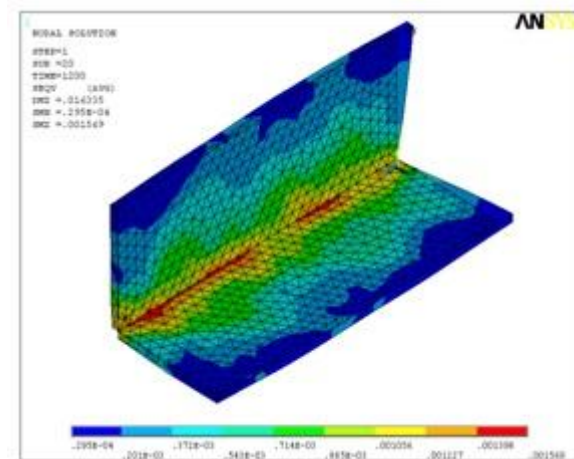


Figure-8: Von mises Stresses (X, Y & Z directions)

3.3 Von mises Strain: The variation of Von Mises strain in X-direction for the horizontal plate for both the analyses are shown in Figure-9 and Figure-10 respectively. It is found that the strain is more in the direction width and is due to the surface exposed to convection.

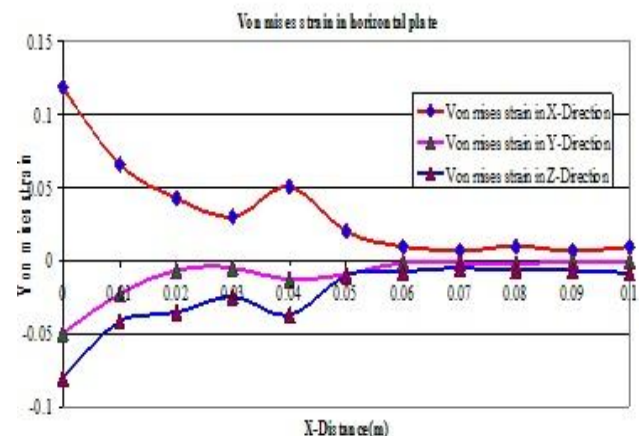


Figure-9: Von mises Strain in Horizontal Plate (Free Expansion)

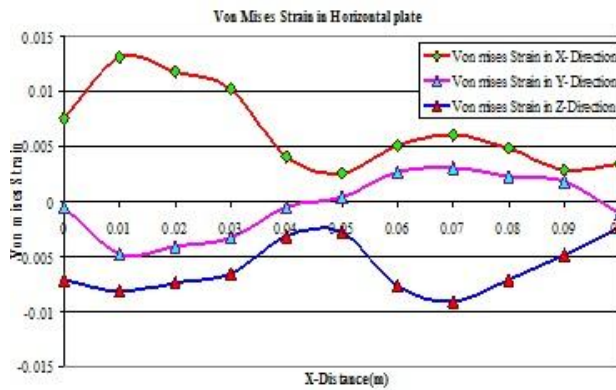


Figure-10: Von mises Strain in Horizontal Plate

Since the heat loss from the surface by convections time dependent and no temperature boundary conditions have applied, the deformation is more X-direction. It is evident that the fin effect is more in X-direction for thermal analysis than free expansion analysis.

IV. Conclusion:

The simulation of arc welding process for the study of stresses due to free expansion and temperature rise has been carried successfully. The temperatures obtained by thermal analysis have been used to obtain stress-strain values and distortion during combined thermo-mechanical analysis. Initially the vonmises stresses and strains have been obtained for free expansion process and compared with the structural boundary conditions. It is observed that the stresses are more for fixed conditions due to fin effect and heat loss through the exposed surface due to convection. The results for thermal analysis have been compared with theoretical values and are found in good agreement.

References:

- [1]. Rosenthal D. "The Theory of moving Sources of Heat and Its Application to Metal Treatments", Transactions of A.S.M.E., Nov. 1946, p 849-866.
- [2]. Friedman E., "Thermomechanical Analysis of the Welding Process Using the Finite Element Method", Transaction of the ASME, 1975, p 206-213.
- [3]. Brown S., and Song H., "Finite Element Simulation of Welding of Large Structure", Journal of Engineering for Industry, vol. 144, 1992, p 441-451.
- [4]. Michaleris P. and Debicari A., "Prediction of Welding Distortion", Welding Journal, April 1997, p 172-180.
- [5]. Okumoto Y., "Analysis of Residual Stress and Deformation Due to Welding", 17th International Conference on Offshore Mechanics and Arctic Engineering, 1998, p 1-7.
- [6]. Komanduri R. and Hou Z., "Thermal Analysis of the Arc Welding Process: Part I. General Solutions", Metallurgical and Materials Transactions B, vol. 31B, Dec. 2000, p 1353-1370.
- [7]. Jang G., Kim H., and Kang S., "The Effects of Root Opening on Mechanical Properties, Deformation and Residual Stress of Weldments", Welding Research Supplement, March 2001, p 80-89.
- [8]. D. Gery , H. Long and P.Maropoulos" Effects of welding speed, energy input and heat source distribution on temperature variations in butt joint welding" August 2005, pp.393-401.
- [9]. Shaodong Wang and John Goldak "Simulation on the thermal cycle of a welding process by space-time convection-diffusion finite element analysis" May 2009, pp. 936-947.
- [10]. Hwa Teng Lee, Chun Te Chen and Jia Lin Wu "Numerical and experimental investigation into effect of temperature field on sensitization of Alloy 690 butt welds fabricated by gas tungsten arcwelding and laser beam welding" September 2010, pp.1636-1645
- [11]. Junhua Sun, Chuan Song Wu and Yanhui Feng "Modeling the transient heat transfer for the controlled pulse key-holing process in plasma arc welding" September 2011, pp.1664-1671.

Customized IVR Implementation Using Voicexml on SIP (Voip) Communication Platform

Kranti Kumar Appari¹

(ECE Department, JNT University, India)

ABSTRACT : An innovative application for communication platform based on SIP (VoIP) protocol is presented in this paper.

The Voice Server is an Open-standards-based voice services framework that interprets the VoiceXML dialog markup language. It is designed to serve as a VoiceXML interpreter implementation for VoIP platform. Although it is perfectly suitable for PC desktop applications, it can be integrated with any telephony platform, messaging suite or communications solution intended to implement the VoiceXML functionality to execute feature rich voice enabled applications like: auto-attendant, email-by-phone, voice dialing, message notification and reminders, contact book look-up, business transaction enablement, customer relationship management and utility applications (driving directions, flight tracking, audio newsmagazines, prescription refilling).

It also allows input via speech recognition (SR) or "touch tone" DTMF and dialog prompting via synthesized speech (TTS) or recorded audio playback. And the experience with the platform shows that, it could be widely utilized in enterprises, groups and organizations with low-cost because of those improvements.

Keywords: Voice Over Internet Protocol (VoIP), Session Initiation Protocol (SIP), VoiceXML, Text-To-Speech (TTS), Dual-tone multi-frequency (DTMF), IPPBX (Internet Protocol Private Branch Exchange)

I. INTRODUCTION

A browser is a client application program that takes one or more input streams on a platform and executes an application that lives on one or more document servers by interpreting markup. In the case of VoiceXML, the application consists of the call flow logic, the prompts for the application, and any associated grammars, the document server executes portions of the application dialog by delivering VoiceXML markup to the browser in response to a document request. The markup interpreter renders the VoiceXML markup within an interpreter context, perhaps changing the context, and then makes calls into the implementation platform. The implementation platform contains all of the resources needed by the markup interpreter to render the dialog. This application deployed in IPPBX.

A private branch exchange (PBX) is a telephone routing system that directs all calls from outside lines and routes them to the appropriate phone. This type of system is most commonly used in an office space. PBXs make connections

among the internal telephones of a private organization usually a business and also connect them to the public switched telephone network (PSTN) via trunk lines.

IP Communication solutions offer migration at an organization's preferred pace. By integrating with most of the major legacy PBXs and voicemail systems, as well as other business applications, most leading IP players empower customers to migrate to full IP based on their business needs, instead of being forced to adopt technologies due to limitations like interoperability of the various business applications. Successful customer migration to IPPBX communications is as much about processes as it is about technologies. Understanding this, leading industry players have developed detailed plans and processes that make migration smoother, faster, and easier for companies of all sizes.

In the IP communications world, telephony is just one of the services in the network. And, this service is available from anywhere in the network, independent of location. For example, a multisite business may deploy the call control (IP PBX) software only at the central site, then enable the remote sites to access the service remotely over the network.

II. SYSTEM ANALYSIS

2.1 Existing Systems

Till date different kinds of browsers are being used to browse the web content like Internet explorer, Mozilla, Netscape etc. which needs a typical computer and network connectivity to the web content. A web browser is a Software Application which enables a user to display and interact with text, images, videos, music and other information typically located on a Web Page at a website on the World Wide Web or a Local Area Network. Text and images on a Web page can contain hyperlinks to other Web pages at the same or different website.

2.2 Proposed System

The existing internet protocol network is connecting VOIP (Voice over Internet Protocol) together enabling users to make a call in a hassle free environment. Just a stable internet connection is required and a user can make a call from anywhere in the world independent of the location. Proprietary systems are easy to outgrow: Adding more phone lines or extensions often requires expensive hardware modules. In some cases an entirely new phone system is required. Not so with an IP PBX: a standard computer can easily handle a large number of phone lines and extensions just add more phones to your network to expand.

2.3 Feasibility Study

a) Operation Feasibility:

It is much easier to operate unlike the traditional web browsers. This project has been proposed in a user-friendly environment where the hardware requirement is very less. No proprietary software is required.

b) Technical Feasibility:

VoiceXML scripting is much easier to design. Any layman can understand VXML code. The hardware complexity is very less. All this project requires is a stable Internet connection, a processor with 1GB of RAM.

c) Cost Feasibility:

This project has one of the major benefits i.e. that most of the software that are being used here all available for Open Sources. The set up cost is very less. Just a stable Internet connection is required and a user can access it from anywhere in the world independent of the location.

2.4 Model Used

When the user places a call to the designated VoiceXML extension the call gets handed over to the pre-recorded hunt group. The particular code for a call flow gets activated when a call is placed. After the session is established successfully Asterisk gateway interface invokes the VoiceXML browser and calls the initial VoiceXML script hosted on the same server. Voice Glue starts interpreting the VoiceXML code for audio output and the user input by way of DTMF signals or voice commands.

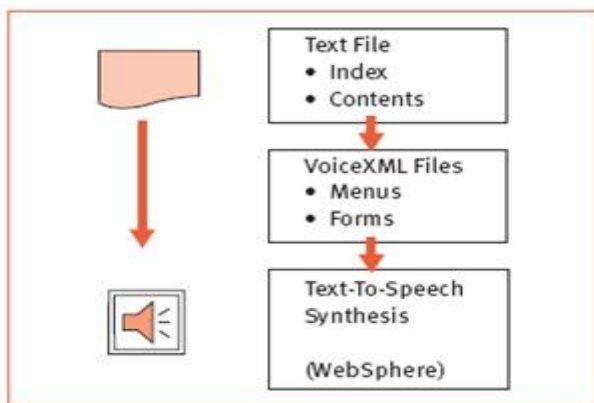


Fig 1: Text-To-Speech (TTS)

User can control the navigation of VoiceXML code with user's commands. Once the user is finished with his operation on VoiceXML the control is handed over to Asterisk (IPPBX). Asterisk comes as a part of preconfigured code terminates the call after the control is handed over from Voice Glue.

VoiceXML is a key used to transfer text to speech or database entries to speech in a very flexible way. Any text with its index of contents can be transferred from the document file into forms and menus of VoiceXML files that can be read out by text-to-speech synthesis tools like Web Sphere.

III. TECHNOLOGY OVERVIEW

3.1 Voice Over Internet Protocol (VoIP)

In just a few years, the old circuit-switched voice-centric communications network will give way to a data-centric, packet-oriented network that seamlessly supports data, voice, and video with a high quality of service. The

switching equipment, protocols, and links are already being put into place. A transition network is currently in place that joins the packet data world with the circuit-switched world. Integrated access solutions are being installed that support integrated data, voice, and other media into the Internet or the PSTN.

Voice over Internet Protocol (VoIP) is a protocol optimized for the transmission of voice through the Internet or other packet switched networks. VoIP is often used abstractly to refer to the actual transmission of voice (rather than the protocol implementing it). VoIP is also known as IP Telephony, Internet telephony, Broadband telephony, Broadband Phone and Voice over Broadband. "VoIP" is pronounced voyp.

Despite a number of technological issues, real-time multimedia transmission (voice and video) over IP networks and the Internet has largely been worked out. Advanced compression techniques have reduced voice data transfer rates from 64 Kbits/sec to as little as 6 Kbits/sec. Voice over IP or VoIP can potentially allow users to call worldwide at no charge (except for the fee paid to service providers for Internet access). A user's IP address basically becomes a phone number. Additionally, computer-based phone systems can be linked to servers that run a variety of interesting telephony applications, including PBX services and voice messaging.

One of the best reasons to support packet telephony can be seen in the service limitations of the traditional telephone system. The switches are mostly proprietary with embedded call control functions and service logic. That makes it difficult to add new services. In addition, the end devices-telephones-are limited in functionality to a 12-key pad! In contrast, new services are easy to add in the IP telephony world because users simply add new telephony applications on their computers and communicate with other users who are running the same telephony applications.

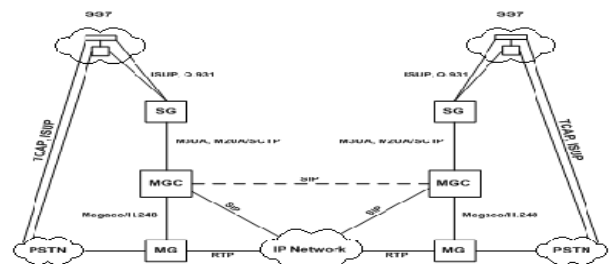


Fig 2: VoIP Architecture

3.2 Session Initiation Protocol (SIP)

There are many applications of the Internet that require the creation and management of a session, where a session is considered an exchange of data between an association of participants. The implementation of these applications is complicated by the practices of participants: users may move between endpoints, they may be addressable by multiple names, and they may communicate in several different media sometimes simultaneously. Numerous protocols have been authored that carry various forms of real-time multimedia session data such as voice, video, or text messages.

The Session Initiation Protocol (SIP) works in concert with these protocols by enabling Internet endpoints

(called user agents) to discover one another and to agree on a characterization of a session they would like to share. For locating prospective session participants, and for other functions, SIP enables the creation of an infrastructure of network hosts (called proxy servers) to which user agents can send registrations, invitations to sessions, and other requests. SIP is an agile, general-purpose tool for creating, modifying, and terminating sessions that works independently of underlying transport protocols and without dependency on the type of session that is being established. SIP is generic protocol for every IP capable access networks.

The Session Initiation Protocol (SIP) is an application-layer control (signaling) protocol for creating, modifying, and terminating sessions with one or more participants. It can be used to create two-party, multiparty, or multicast sessions that include Internet telephone calls, multimedia distribution, and multimedia conferences. SIP is designed to be independent of the underlying transport layer; it can run on TCP, UDP. It was originally designed by Henning Schulzrinne (Columbia University) and Mark Handley (UCL) starting in 1996. It is a 3GPP (Third Generation Partnership Project) signaling protocol. It is one of the major signaling protocols used in Voice over IP (VoIP).

SIP handles the signaling part of a communication session.

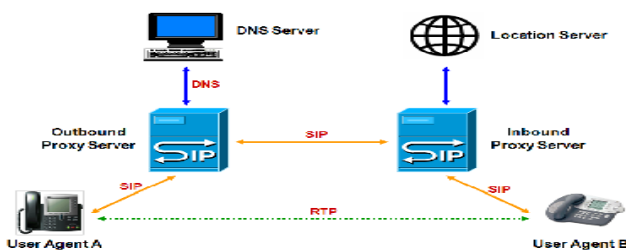


Fig 3: SIP Trapezoid Architecture

SIP handles the signaling part of a communication session. It serves as a carrier for the Session Description Protocol (SDP). SDP handles the media portion of the session. The transmission of voice and video content are done by the Real-time Transport Protocol (RTP). A SIP session thus involves packet streams of RTP. SIP is a part of the protocols involved in a multimedia session. The latest version of the specification is RFC 3261 from the IETF SIP Working Group.

3.3 Internet Protocol Private Branch Exchange (IPPBX)

An IP PBX or VOIP phone system replaces a traditional PBX or phone system and gives employees an extension number, the ability to conference, transfer and dial other colleagues. All calls are sent via data packets over a data network instead of the traditional phone network.

An IP PBX is a complete telephony system that provides telephone calls over IP data networks. Typically an IP PBX system is a piece of software running on a server. Depending on the workload, that server can also be performing other tasks, but usually it is dedicated and also acts as the VoIP system's connection to the internet.

An IP PBX is a telephone switching system inside an enterprise that switches calls between Voice over IP (VoIP) users on local lines and lets all users share a certain number of external telephone lines. The typical IP PBX can

also switch calls between a VoIP user and a traditional telephone user, or between two traditional telephone users much like a conventional PBX does. The IP PBX is also able to connect to traditional PSTN lines via an optional gateway so upgrading day to day business communication to this most advanced voice and data network

Internet protocol private branch exchange (IP PBX) market offers a ray of hope in the otherwise depressed European telecommunications industry. Encouraging developments in this market have seen enterprises beginning to replace their time division multiplexing (TDM) voice networks with IP enabled/converged voice data networks.

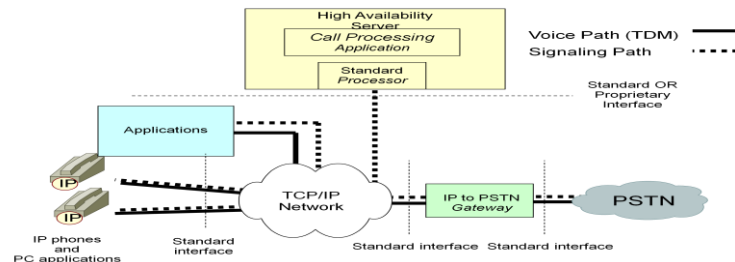


Fig 4: IPPBX Architecture

An IP PBX or IP Telephone System consists of one or more SIP phones, an IP PBX server and optionally a VOIP Gateway to connect to existing PSTN lines. The IP PBX server functions in a similar manner to a proxy server: SIP clients, being either soft phones or hardware-based phones, register with the IP PBX server, and when they wish to make a call they ask the IP PBX to establish the connection. The IP PBX has a directory of all phones/users and their corresponding SIP address and thus is able to connect an internal call or route an external call via either a VOIP gateway or a VOIP service provider.

3.4 VoiceXML

The Extensible Markup Language (XML) is a general-purpose markup language. It is classified as an extensible language because it allows its users to define their own elements. Its primary purpose is to facilitate the sharing of structured data across different information systems, particularly via the Internet, and it is used both to encode documents and to serialize data.

In 1998, W3C hosted a conference on voice browsers. By this time, AT&T and Lucent had different variants of their original PML, while Motorola had developed VoxML, and IBM was developing its own SpeechML. Many other attendees at the conference were also developing similar languages for dialog design; for example, such as HP's TalkML and Pipe Beach's VoiceHTML.

The Voice XML Forum was then formed by AT&T, IBM, Lucent, and Motorola to pool their efforts. The goal of the Voice XML Forum was to define a standard dialog design language that developers could use to build conversational applications.

In 2000, the Voice XML Forum released Voice XML 1.0 to the public. Shortly thereafter, Voice XML 1.0 was submitted to the W3C as the basis for the creation of a new international standard. Voice XML 2.0 is the result of

this work based on input from W3C Member companies, other W3C Working Groups, and the public.

Voice XML is designed for creating audio dialogs that feature synthesized speech, digitized audio, recognition of spoken and DTMF key input, recording of spoken input, telephony, and mixed initiative conversations. Its major goal is to bring the advantages of Web-based development and content delivery to interactive voice response applications. A common architecture is to deploy banks of voice browsers attached to the Public Switched Telephone Network (PSTN) so that users can use a telephone to interact with voice application.

Here is a short example of Voice XML. This is a Hello World example:

```
<?xml version="1.0"?>
<vxml
version="2.0"xmlns="http://www.w3.org/2001/vxml">
  <form>
    <block>Hello World!</block>
  </form>
</vxml>
```

The top-level element is <vxml>, which is mainly a container for dialogs. There are two types of dialogs: forms and menus. Forms present information and gather input; menus offer choices of what to do next. This example has a single form, which contains a block that synthesizes and presents "Hello World!" to the user. Since the form does not specify a successor dialog, the conversation ends.

The architectural model assumed by this document has the following components. A document server (e.g. a Web server) processes requests from a client application, the VoiceXML Interpreter, through the VoiceXML interpreter context. The server produces VoiceXML documents in reply, which are processed by the VoiceXML interpreter. The VoiceXML interpreter context may monitor user inputs in parallel with the VoiceXML interpreter.

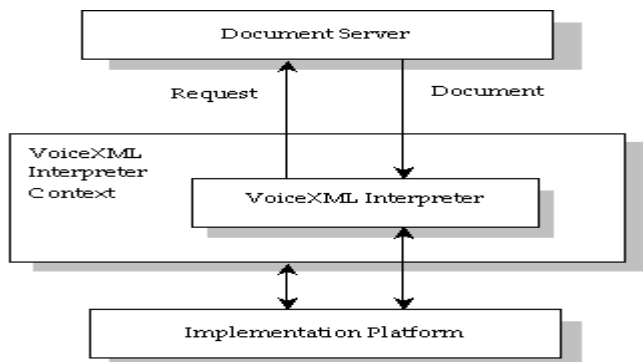


Fig 5: VoiceXML Architecture

For example, one VoiceXML interpreter context may always listen for a special escape phrase that takes the user to a high-level personal assistant, and another may listen for escape phrases that alter user preferences like volume or text-to-speech characteristics.

The implementation platform is controlled by the VoiceXML interpreter context and by the VoiceXML interpreter. For instance, in an interactive voice response application, the VoiceXML interpreter context may be responsible for detecting an incoming call, acquiring the initial VoiceXML document, and answering the call, while

the VoiceXML interpreter conducts the dialog after answer. The implementation platform generates events in response to user actions (e.g. spoken or character input received, disconnect) and system events (e.g. timer expiration).

Some of these events are acted upon by the VoiceXML interpreter itself, as specified by the VoiceXML document, while others are acted upon by the VoiceXML interpreter context.

The language describes the human-machine interaction provided by voice response systems, which includes:

- 1) Output of synthesized speech (text-to-speech)
- 2) Recognition of spoken input
- 3) Recognition of DTMF input
- 4) Recording of spoken input
- 5) Control of dialog flow
- 6) Telephony features such as call transfer and disconnect

The language provides means for collecting character and/or spoken input, assigning the input results to document-defined request variables, and making decisions that affect the interpretation of documents written in the language. A document may be linked to other documents through Universal Resource Identifiers (URIs).

VoiceXML has become a standard and has the following advantages:

- 1) Reduces development costs
- 2) Separation between dialogue system components
- 3) Portability of application
- 4) Re-use of Internet infrastructure
- 5) VoiceXML is becoming a standard
- 6) Reduces dialogue system development time
- 7) Additional functions can be implemented
- 8) Can develop own dialogue system with free VoiceXML browsers

IV. SYSTEM DESIGN

4.1 UML Diagrams:

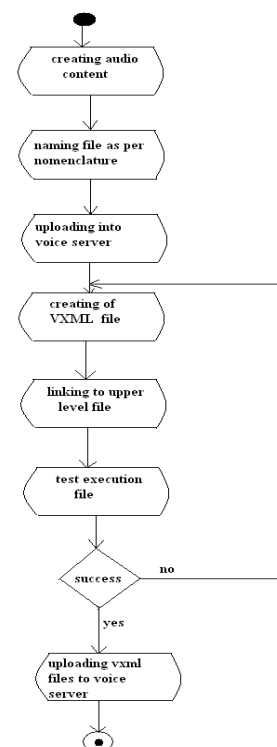


Fig 6: Creating Audio Database

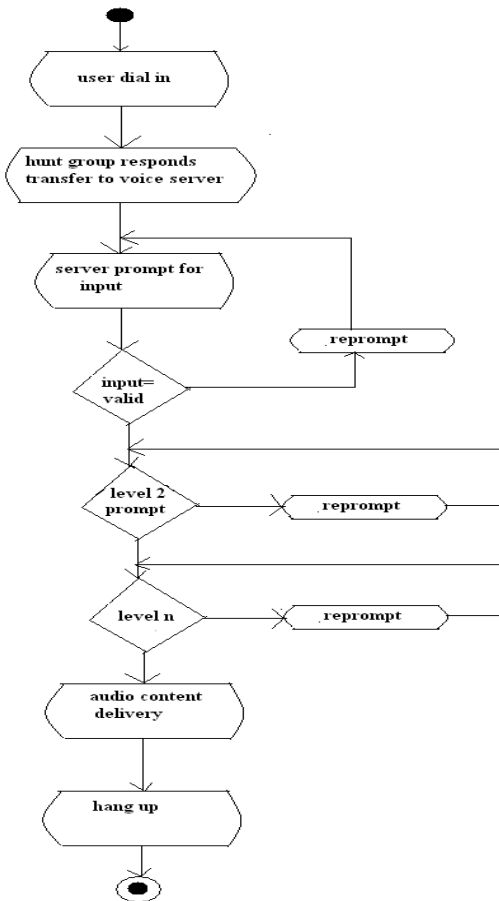


Fig 7: Flow of Execution

V. TESTING AND IMPLEMENTATION

Test 1:

Placing two concurrent call on the vxml system

Test 2:

Checking the code how when wrong option selected

5.1 Test Execution:

Case 1:

Call from two extensions 101,102 simultaneously

Case 2.1:

After the welcome message select ECE by pressing choice 3

CASE 2.2

After selecting ECE we choose first year by pressing 1.

5.2 Result

Case 1:

Two calls successfully able to hear the welcome message on both the calls

Case 2.1:

Able to hear the welcome message of ECE department and prompts to select year

Case 2.2:

The calls suppose to go to the year level menu but call get routed Thank you and it got hang up.

VI. CONCLUSION

In this paper, we proposed the Customized IVR implementation using VoiceXML on VoIP platform. VoiceXML provides flexibility at robust technology which delivers its output in form of audio which will be very much useful to all kinds of people starting from the very busy business man to layman who doesn't even know how to read.

VoiceXML enables all its robust features in lines with existing coding methodology used in today's very popular HTML and XML. It makes the development of VoiceXML very easier and adoptable to presently existing system.

References

- [1] Benbin Chen, Wenchao Zhou, Yiyang Li ,Donghui Guo, Innovative application of SIP protocol for communication platform , Anti-Counterfeiting Security and Identification in Communication (ASID), 2010 International Conference, IEEE,2010
- [2] Larson, J.A, W3C Speech Interface Languages: VoiceXML, Vol 24, IEEE, 2007
- [3] Jianfeng Zhu, Zhuang Li, Yuchun Ma, Yulin Huang, Realization of Extended Functions of SIP-Based IP-PBX, Vol 3, IEEE, 2010
- [4] Prasad, J.K., Kumar, B.A, Analysis of SIP and realization of advanced IP-PBX features , Vol 6, IEEE, 2011
- [5] Gokhale, S.S , Jijun Lu, Signaling performance of SIP based VoIP: a measurement-based approach , Vol 2, IEEE, 2005

Contribution of Axial Deformation in the Analysis of Rigidly Fixed Portal Frames

Okonkwo V. O.¹, Aginam C. H.², and Chidolue C. A.³

¹²³Department of Civil Engineering Nnamdi Azikiwe University, Awka Anambra State-Nigeria

ABSTRACT: In this work the stiffness equations for evaluating the internal stress of rigidly fixed portal frames by the displacement method were generated. But obtaining the equations for the internal stresses required non-scalar or parametric inversion of the structure stiffness matrix. To circumvent this problem, the flexibility method was used taking advantage of the symmetrical nature of the portal frame and the method of virtual work. These were used to obtain the internal stresses on rigidly fixed portal frames for different cases of external loads when axial deformation is considered. A dimensionless constant s was used to capture the effect of axial deformation in the equations. When it is set to zero, the effect of axial deformation is ignored and the equations become the same as what can be obtained in any structural engineering textbook. These equations were used to investigate the contribution of axial deformation to the calculated internal stresses and how they vary with the ratio of the flexural rigidity of the beam and columns and the height to length ratio of the loaded portal frames.

Keywords: Axial deformation, flexural rigidity, flexibility method, Portal frames, stiffness matrix,

I. INTRODUCTION

Structural frames are primarily responsible for strength and rigidity of buildings. For simpler single storey structures like warehouses, garages etc portal frames are usually adequate. It is estimated that about 50% of the hot-rolled constructional steel used in the UK is fabricated into single-storey buildings (Graham and Alan, 2007). This shows the increasing importance of this fundamental structural assemblage. The analysis of portal frames are usually done with predetermined equations obtained from structural engineering textbooks or design manuals. The equations in these texts were derived with an underlying assumption that deformation of structures due to axial forces is negligible giving rise to the need to undertake this study. The twenty first century has seen an astronomical use of computers in the analysis of structures (Samuelsson and Zienkiewi, 2006) but this has not completely eliminated the use of manual calculations from simple structures and for easy cross-checking of computer output (Hibbeler, 2006). Hence the need for the development of equations that capture the contribution of axial deformation in portal frames for different loading conditions.

II. DEVELOPMENT OF THE MODEL

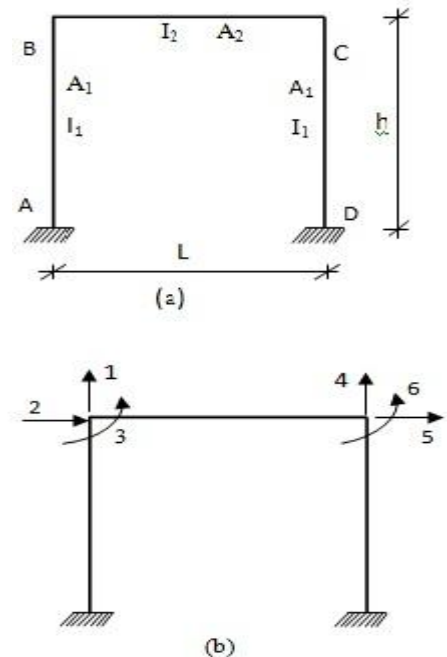


Figure 1: A simple portal frame showing its dimensions and the 6 degrees of freedom

The analysis of portal frames by the stiffness method requires the determination of the structure's degrees of freedom and the development of the structure's stiffness matrix. For the structure shown in Figure 1a, the degrees of freedom are as shown in Figure 1b. I_1 and A_1 are respectively the second moment of inertia and cross-sectional area of the columns while I_2 and A_2 are the second moment of inertia and cross-sectional area of the beam respectively. The stiffness coefficients for the various degrees of freedom considering shear deformation can be obtained from equations developed in Ghali et al (1985) and Okonkwo (2012) and are presented below

The structure's stiffness matrix can be written as:

$$K = \begin{bmatrix} k_{11} & k_{12} & k_{13} & k_{14} & k_{15} & k_{16} \\ k_{21} & k_{22} & k_{23} & k_{24} & k_{25} & k_{26} \\ k_{31} & k_{32} & k_{33} & k_{34} & k_{35} & k_{36} \\ k_{41} & k_{42} & k_{43} & k_{44} & k_{45} & k_{46} \\ k_{51} & k_{52} & k_{53} & k_{54} & k_{55} & k_{56} \\ k_{61} & k_{62} & k_{63} & k_{64} & k_{65} & k_{66} \end{bmatrix} \quad (1)$$

Where k_{ij} is the force in coordinate (degree of freedom) i when there is a unit displacement in coordinate (degree of freedom) j . They are as follows:

$$k_{11} = \frac{EA_1}{h}$$

$$k_{12} = 0$$

$$k_{13} = \frac{6EI_2}{l^2}$$

$$k_{14} = -\frac{12EI_1}{h^3}$$

$$k_{15} = 0$$

$$k_{16} = \frac{6EI_2}{l^2}$$

$$k_{22} = \frac{12EI_1}{h^3} + \frac{EA_2}{l}$$

$$k_{23} = \frac{6EI_1}{h^2}$$

$$k_{24} = 0$$

$$k_{25} = -\frac{EA_2}{l} \quad . \quad . \quad . \quad (2)$$

$$k_{26} = 0$$

$$k_{33} = \frac{4EI_2}{l} + \frac{4EI_1}{h}$$

$$k_{34} = -\frac{6EI_2}{l^2}$$

$$k_{35} = 0$$

$$k_{36} = \frac{2EI_2}{l}$$

$$k_{44} = \frac{12EI_2}{l^3} + \frac{EA_1}{h}$$

$$k_{45} = 0$$

$$k_{46} = -\frac{6EI_2}{l^2}$$

$$k_{55} = \frac{12EI_1}{h^3} + \frac{EA_2}{l}$$

From Maxwell's Reciprocal theorem and Betti's Law $k_{ij} = k_{ji}$ (Leet and Uang, 2002).

When there are external loads on the structure on the structure there is need to calculate the forces in the restrained structure F_o as a result of the external load.

The structure's equilibrium equations are then written as

$$\{F\} = \{F_o\} + [K]\{D\} \quad . \quad . \quad . \quad (3)$$

$$\{F_o\} = \begin{Bmatrix} k_{10} \\ k_{20} \\ k_{30} \\ k_{40} \\ k_{50} \\ k_{60} \end{Bmatrix} \quad . \quad . \quad . \quad . \quad . \quad . \quad (4)$$

Where k_{io} is the force due to external load in coordinate i when the other degrees of freedom are restrained.

$$\{D\} = \begin{Bmatrix} d_1 \\ d_2 \\ d_3 \\ d_4 \\ d_5 \\ d_6 \end{Bmatrix} \quad . \quad . \quad . \quad . \quad . \quad . \quad (5)$$

Where d_i is the displacement in coordinate i .

$$\{F\} = \begin{Bmatrix} F_1 \\ F_2 \\ F_3 \\ F_4 \\ F_5 \\ F_6 \end{Bmatrix} \quad . \quad . \quad . \quad . \quad . \quad . \quad (6)$$

Where F_i is the external load with a direction coinciding with the coordinate i (McGuire et al, 2000).

By making $\{D\}$ the subject of the formula in equation (3)

$$\{D\} = [K]^{-1}\{F - F_o\} \quad . \quad . \quad . \quad . \quad (7)$$

Once $\{D\}$ is obtained the internal stresses in the frame can be easily obtained by writing the structure's compatibility equations given as

$$M = M_r + M_1d_1 + M_2d_2 + M_3d_3 \quad . \quad . \quad . \quad (8)$$

Where M is the internal stress (bending moment) at any point on the frame, M_r is the internal stress at the point under consideration in the restrained structure while M_i is the internal stress at the point when there is a unit displacement in coordinate i .

To solve equation (8) there is need to obtain $\{D\}$. $\{D\}$ can be obtained from the inversion of $[K]$ in equation (7). Finding the inverse of K parametrically (i.e. without substituting the numerical values of E , h , l etc) is a difficult task. This problem is circumvented by using the flexibility method to solve the same problem, taking advantage of the symmetrical nature of the structure and the principle of virtual work.

III. APPLICATION OF THE FLEXIBILITY MODEL

The basic system or primary structure for the structure in Figure 1a is given in Figure 2. The removed redundant force is depicted with X_1 .

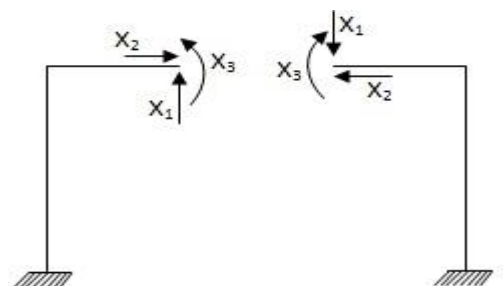


Figure 2: The Basic System showing the removed redundant forces

The flexibility matrix of the structure can be determined using the principle of virtual work.

By applying the unit load theorem the deflection in beams or frames can be determined for the combined action of the internal stresses, bending moment and axial forces with

$$D = \int \frac{\bar{M}M}{EI} ds + \int \frac{\bar{N}N}{EA} ds \quad (9)$$

Where \bar{M} and \bar{N} are the virtual internal stresses while M and N are the real/actual internal stresses.

E is the modulus of elasticity of the structural material

A is the cross-sectional area of the element (McGuire et al, 2000; Nash, 1998)

If d_{ij} is the deformation in the direction of i due to a unit load at j then by evaluating equation (9) the following are obtained:

$$d_{11} = \frac{l_1 GA_1 l^3 + 6l_2 A_1 l^2 h + 12l_1 l_2 h}{12EI_1 l_2 A_1} \quad (10a)$$

$$d_{12} = 0 \quad (10b)$$

$$d_{13} = 0 \quad (10c)$$

$$d_{22} = \frac{2A_2 h^3 + 3l_1 l}{3EI_1 A_2} \quad (10d)$$

$$d_{23} = \frac{-h^2}{EI_1} \quad (10e)$$

$$d_{33} = \frac{ll_1 + 2hl_2}{EI_1 l_2} \quad (10f)$$

From Maxwell's Reciprocal theorem and Betti's Law $d_{ij} = d_{ji}$.

The structure's compatibility equations can be written thus

$$\begin{bmatrix} d_{11} & d_{12} & d_{13} \\ d_{21} & d_{22} & d_{23} \\ d_{31} & d_{32} & d_{33} \end{bmatrix} \begin{Bmatrix} X_1 \\ X_2 \\ X_3 \end{Bmatrix} + \begin{Bmatrix} d_{10} \\ d_{20} \\ d_{30} \end{Bmatrix} = 0 \quad (11a)$$

$$\text{i.e. } fF + d_o = 0 \quad (11b)$$

Where F is the vector of redundant forces X_1, X_2, X_3 and d_o is the vector deformation d_{10}, d_{20}, d_{30} due to external load on the basic system (Jenkins, 1990).

$$F = f^{-1}(-d_o) \quad (12)$$

$$f^{-1} = \frac{Adj[f]}{\det[f]} \quad (13)$$

(Stroud, 1995)

$$f^{-1} = \begin{bmatrix} \frac{1}{d_{11}} & 0 & 0 \\ 0 & \frac{d_{33}}{d_{22}d_{33}-d_{23}^2} & \frac{-d_{32}}{d_{22}d_{33}-d_{23}^2} \\ 0 & \frac{-d_{23}}{d_{22}d_{33}-d_{23}^2} & \frac{d_{22}}{d_{22}d_{33}-d_{23}^2} \end{bmatrix} \quad (14)$$

From equations 10a – 10f

$$\frac{1}{d_{11}} = \frac{12EI_1 l_2 A_1}{l_1 A_1 l^3 + 6l_2 A_1 l^2 h + 24l_1 l_2 h} \quad (15a)$$

$$\frac{d_{33}}{d_{22}d_{33}-d_{23}^2} = \frac{3EI_1 A_2 (ll_1 + 2hl_2)}{2A_2 h^3 ll_1 + 3l_1^2 l^2 + A_2 h^4 l_2 + 6hll_1 l_2} \quad (15b)$$

$$\frac{d_{32}}{d_{22}d_{33}-d_{23}^2} = \frac{-3EI_1 l_2 GA_2 h^2}{2A_2 h^3 ll_1 + 3l_1^2 l^2 + A_2 h^4 l_2 + 6hll_1 l_2} \quad (15c)$$

$$\frac{d_{22}}{d_{22}d_{33}-d_{23}^2} = \frac{EI_1 l_2 (2A_2 h^3 + 3l_1 l)}{2A_2 h^3 ll_1 + 3l_1^2 l^2 + A_2 h^4 l_2 + 6hll_1 l_2} \quad (15d)$$

Equation (12) is evaluated to get the redundant forces and these are substituted into the structures force equilibrium (superposition) equations to obtain the internal stresses at any point.

$$M = M_o + M_1 X_1 + M_2 X_2 + M_3 X_3 \quad (16)$$

Where M is the required stress at a point, M_o is the stress at that point for the reduced structure, M_i is stress at that point when the only the redundant force $X_i = 1$ acts on the reduced structure.

For the loaded portal frame of Figure 3, the deformations of the reduced structure due to external loads are

$$d_{10} = 0 \quad (17a)$$

$$d_{20} = \frac{wh^2 l^2}{8EI_1} \quad (17b)$$

$$d_{30} = \frac{-wl^2 (ll_1 + 6hl_2)}{24EI_1 l_2} \quad (17c)$$

By substituting the values of equations (17a) – (17c) into equations (12)

$$X_1 = 0 \quad (18a)$$

$$X_2 = \frac{-A_2 l_1 wh^2 l^3}{4(2A_2 h^3 ll_1 + 3l_1^2 l^2 + A_2 h^4 l_2 + 6hll_1 l_2)} \quad (18b)$$

$$X_3 = \frac{wl^2 (2A_2 h^3 ll_1 + 3l_1^2 l^2 + 3A_2 h^4 l_2 + 18hll_1 l_2)}{24(2A_2 h^3 ll_1 + 3l_1^2 l^2 + A_2 h^4 l_2 + 6hll_1 l_2)} \quad (18c)$$

Evaluating equation (16) for different points on the structure using the force factors obtained in equations (18a) – (18c)

$$M_A = \frac{2wl^3 l_1 (h^3 A_2 - 3ll_1)}{12(2A_2 h^3 ll_1 + 3l_1^2 l^2 + A_2 h^4 l_2 + 6hll_1 l_2)} \quad (19)$$

$$M_B = \frac{-2wl^3 l_1 (2h^3 A_2 + 3ll_1)}{24(2A_2 h^3 ll_1 + 3l_1^2 l^2 + A_2 h^4 l_2 + 6hll_1 l_2)} \quad (20)$$

$$M_C = \frac{-2wl^3 l_1 (2h^3 A_2 + 3ll_1)}{24(2A_2 h^3 ll_1 + 3l_1^2 l^2 + A_2 h^4 l_2 + 6hll_1 l_2)} \quad (21)$$

$$M_C = \frac{-wl^3 l_1 (8l_2 h^3 + s_2 l^3 l_1)}{12[4h^3 l_2 (2ll_1 + hl_2) + s_2 l^3 l_1 (ll_1 + 2hl_2)]}$$

$$M_D = \frac{2wl^3 I_1 (h^3 A_2 - 3lI_1)}{12(2A_2 h^3 lI_1 + 3l_1^2 l^2 + A_2 h^4 l_2 + 6hlI_1 l_2)} \quad (22)$$

For the loaded portal frame of Figure 4, the deformations of the reduced structure due to external loads are

$$d_{10} = \frac{-wl(l^3 I_1 A_1 + 8hl^2 I_2 A_1 + 64hlI_1 l_2)}{128EI_1 l_2 A_1} \quad (23a)$$

$$d_{20} = \frac{wh^2 l^2}{16EI_1} \quad (23b)$$

$$d_{30} = \frac{-wl^2(lI_1 + 6hl_2)}{48EI_1 l_2} \quad (23c)$$

By substituting the values of equations (23a) – (23c) into equations (12)

$$X_1 = \frac{3wl(l^3 I_1 A_1 + 8hl^2 I_2 A_1 + 64hlI_1 l_2)}{32(lI_1 A_1 l^3 + 6l_2 A_1 l^2 h + 24hlI_1 l_2)} \quad (24a)$$

$$X_2 = \frac{-2wh^2 l^3 A_2 I_1}{16(2A_2 h^3 lI_1 + 3l_1^2 l^2 + A_2 h^4 l_2 + 6hlI_1 l_2)} \quad (24b)$$

$$X_3 = \frac{wh^3 l^2 A_2 (3hl_2 + 2lI_1) + 3wl^3 I_1 (lI_1 + 6hl_2)}{48(2A_2 h^3 lI_1 + 3l_1^2 l^2 + A_2 h^4 l_2 + 6hlI_1 l_2)} \quad (24c)$$

$$\text{Let } \beta = \frac{s_2}{s_1} \quad (25)$$

Evaluating equation (16) for different points on the structure using the force factors obtained in equations (24a) – (24c)

$$M_A = \frac{wl^2[h^3 A_2 (3hl_2 + 8lI_1) + 3lI_1 (lI_1 + 6hl_2)]}{48(2A_2 h^3 lI_1 + 3l_1^2 l^2 + A_2 h^4 l_2 + 6hlI_1 l_2)} - \frac{wl^4 A_1 (5lI_1 + 24hl_2)}{64(lI_1 A_1 l^3 + 6l_2 A_1 l^2 h + 24hlI_1 l_2)} \quad (26)$$

$$M_B = -\frac{wl^4 A_1 (5lI_1 + 24hl_2)}{64(lI_1 A_1 l^3 + 6l_2 A_1 l^2 h + 24hlI_1 l_2)} + \frac{wl^2[h^3 A_2 (3hl_2 + 2lI_1) + 3lI_1 (lI_1 + 6hl_2)]}{48(2A_2 h^3 lI_1 + 3l_1^2 l^2 + A_2 h^4 l_2 + 6hlI_1 l_2)} \quad (27)$$

$$M_C = -\frac{3wl^2(l^3 I_1 A_1 + 8hl^2 I_2 A_1 + 64hlI_1 l_2)}{64(lI_1 A_1 l^3 + 6l_2 A_1 l^2 h + 24hlI_1 l_2)} + \frac{wl^2[h^3 A_2 (3hl_2 + 2lI_1) + 3lI_1 (lI_1 + 6hl_2)]}{48(2A_2 h^3 lI_1 + 3l_1^2 l^2 + A_2 h^4 l_2 + 6hlI_1 l_2)} \quad (28)$$

$$M_D = -\frac{3wl^2(l^3 I_1 A_1 + 8hl^2 I_2 A_1 + 64hlI_1 l_2)}{64(lI_1 A_1 l^3 + 6l_2 A_1 l^2 h + 24hlI_1 l_2)} + \frac{wl^2[h^3 A_2 (3hl_2 + 8lI_1) + 3lI_1 (lI_1 + 6hl_2)]}{48(2A_2 h^3 lI_1 + 3l_1^2 l^2 + A_2 h^4 l_2 + 6hlI_1 l_2)} \quad (29)$$

For the loaded portal frame of Figure 5, the deformations of the reduced structure due to external loads are

$$d_{10} = -\frac{wlh^3}{12EI_1} \quad (30a)$$

$$d_{20} = \frac{wh^4}{8EI_1} \quad (30b)$$

$$d_{30} = \frac{-wh^3}{6EI_1} \quad (30c)$$

By substituting the values of equations (30a) – (30c) into equations (12)

$$X_1 = \frac{wh^3 lI_2 A_1}{lI_1 A_1 l^3 + 6l_2 A_1 l^2 h + 24hlI_1 l_2} \quad (31a)$$

$$X_2 = \frac{-wh^4 A_2 (3lI_1 + 2hl_2)}{8(2A_2 h^3 lI_1 + 3l_1^2 l^2 + A_2 h^4 l_2 + 6hlI_1 l_2)} \quad (31b)$$

$$X_3 = \frac{wh^3 l_2 (-h^3 A_2 + 12lI_1)}{24(2A_2 h^3 lI_1 + 3l_1^2 l^2 + A_2 h^4 l_2 + 6hlI_1 l_2)} \quad (31c)$$

Evaluating equation (16) for different points on the structure using the force factors obtained in equations (31a) – (31c)

$$M_A = -\frac{wh^2(lI_1 A_1 l^3 + 5A_1 l^2 h l_2 + 24hlI_1 l_2)}{2(lI_1 A_1 l^3 + 6l_2 A_1 l^2 h + 24hlI_1 l_2)} + \frac{wh^3(9h^2 lI_1 A_2 + 5A_2 h^3 l_2 + 12lI_1 l_2)}{24(2A_2 h^3 lI_1 + 3l_1^2 l^2 + A_2 h^4 l_2 + 6hlI_1 l_2)} \quad (32)$$

$$M_B = \frac{wh^3 l^2 I_2 A_1}{2(lI_1 A_1 l^3 + 6l_2 A_1 l^2 h + 24hlI_1 l_2)} + \frac{wh^3 l_2 (-h^3 A_2 + 12lI_1)}{24(2A_2 h^3 lI_1 + 3l_1^2 l^2 + A_2 h^4 l_2 + 6hlI_1 l_2)} \quad (33)$$

$$M_C = -\frac{wh^3 l^2 I_2 A_1}{2(lI_1 A_1 l^3 + 6l_2 A_1 l^2 h + 24hlI_1 l_2)} + \frac{wh^3 l_2 (-h^3 A_2 + 12lI_1)}{24(2A_2 h^3 lI_1 + 3l_1^2 l^2 + A_2 h^4 l_2 + 6hlI_1 l_2)} \quad (34)$$

$$M_D = -\frac{wh^3 l^2 I_2 A_1}{2(lI_1 A_1 l^3 + 6l_2 A_1 l^2 h + 24hlI_1 l_2)} + \frac{wh^3(9h^2 lI_1 A_2 + 5A_2 h^3 l_2 + 12lI_1 l_2)}{24(2A_2 h^3 lI_1 + 3l_1^2 l^2 + A_2 h^4 l_2 + 6hlI_1 l_2)} \quad (35)$$

For the loaded portal frame of Figure 6, the deformations of the reduced structure due to external loads are

$$d_{10} = -\frac{Pa^2 l}{2EI_1} \quad (36a)$$

$$d_{20} = 0 \quad (36b)$$

$$d_{30} = 0 \quad (36c)$$

By substituting the values of equations (36a) – (36c) into equations (12)

$$X_1 = \frac{6Pa^2 lI_2 A_1}{A_1 lI_1 l^3 + 6A_1 h l^2 l_2 + 24hlI_1 l_2} \quad (37a)$$

$$X_2 = 0 \quad (37b)$$

$$X_3 = 0 \quad (37c)$$

Evaluating equation (16) for different points on the structure using the force factors obtained in equations (37a) – (37c)

$$M_A = -Pa \left(1 - \frac{3al^2 I_2 A_1}{A_1 I_1 l^3 + 6A_1 h l^2 I_2 + 24h I_1 I_2} \right) \quad (38)$$

$$M_B = \frac{3Pa^2 l^2 I_2 A_1}{A_1 I_1 l^3 + 6A_1 h l^2 I_2 + 24h I_1 I_2} \quad (39)$$

$$M_C = -\frac{3Pa^2 l^2 I_2 A_1}{A_1 I_1 l^3 + 6A_1 h l^2 I_2 + 24h I_1 I_2} \quad (40)$$

$$M_D = Pa \left(1 - \frac{3al^2 I_2 A_1}{A_1 I_1 l^3 + 6A_1 h l^2 I_2 + 24h I_1 I_2} \right) \quad (41)$$

For the loaded portal frame of Figure 7, the deformations of the reduced structure due to external loads are

$$d_{10} = -\frac{Pa^2 l}{4EI_1} \quad (42a)$$

$$d_{20} = \frac{Pa^2(3h-a)}{6EI_1} \quad (42b)$$

$$d_{30} = -\frac{Pa^2}{2EI_1} \quad (42c)$$

By substituting the values of equations (42a) – (42c) into equations (12)

$$X_1 = \frac{3Pa^2 l^2 I_2 A_1}{I_1 A_1 l^3 + 6I_2 A_1 l^2 h + 24h I_1 I_2} \quad (43a)$$

$$X_2 = \frac{-Pa^2 A_2 [I_1 (3h-a) + h I_2 (3h-2a)]}{2(2A_2 h^3 I_1 + 3I_1^2 l^2 + A_2 h^4 I_2 + 6h I_1 I_2)} \quad (43b)$$

$$X_3 = \frac{-Pa^2 I_2 (-h^3 A_2 + ah^2 A_2 + 3I_1 l)}{2(2A_2 h^3 I_1 + 3I_1^2 l^2 + A_2 h^4 I_2 + 6h I_1 I_2)} \quad (43c)$$

Evaluating equation (16) for different points on the structure using the force factors obtained in equations (43a) – (43c)

$$M_A = -Pa + \frac{3Pa^2 l^2 I_2 A_1}{2(I_1 A_1 l^3 + 6I_2 A_1 l^2 h + 24h I_1 I_2)} + \frac{Pa^2 [A_2 I_1 l (3h^2 - ah) + I_2 (2A_2 h^3 - aA_2 h^2 + 3I_1 l)]}{2(2A_2 h^3 I_1 + 3I_1^2 l^2 + A_2 h^4 I_2 + 6h I_1 I_2)} \quad (44)$$

$$M_B = \frac{3Pa^2 l^2 I_2 A_1}{2(I_1 A_1 l^3 + 6I_2 A_1 l^2 h + 24h I_1 I_2)} + \frac{Pa^2 I_2 (-h^3 A_2 + ah^2 A_2 + 3I_1 l)}{2(2A_2 h^3 I_1 + 3I_1^2 l^2 + A_2 h^4 I_2 + 6h I_1 I_2)} \quad (45)$$

$$M_C = -\frac{3Pa^2 l^2 I_2 A_1}{2(I_1 A_1 l^3 + 6I_2 A_1 l^2 h + 24h I_1 I_2)} + \frac{Pa^2 I_2 (-h^3 A_2 + ah^2 A_2 + 3I_1 l)}{2(2A_2 h^3 I_1 + 3I_1^2 l^2 + A_2 h^4 I_2 + 6h I_1 I_2)} \quad (46)$$

$$M_D = -\frac{3Pa^2 l^2 I_2 A_1}{2(I_1 A_1 l^3 + 6I_2 A_1 l^2 h + 24h I_1 I_2)} + \frac{Pa^2 [A_2 I_1 l (3h^2 - ah) + I_2 (2A_2 h^3 - aA_2 h^2 + 3I_1 l)]}{2(2A_2 h^3 I_1 + 3I_1^2 l^2 + A_2 h^4 I_2 + 6h I_1 I_2)} \quad (47)$$

For the loaded portal frame of Figure 8, the deformations of the reduced structure due to external loads are

$$d_{10} = -P \left[\frac{a^2 I_1 A_1 (3l-2a) + 6h I_2 (al A_1 + 2I_1)}{12EI_1 I_2 A_1} \right] \quad (48a)$$

$$d_{20} = \frac{Pa h^2}{2EI_1} \quad (48b)$$

$$d_{30} = -\frac{Pa(al I_1 + 2h I_2)}{2EI_1 I_2} \quad (48c)$$

By substituting the values of equations (48a) – (48c) into equations (12)

$$X_1 = \frac{P(a^2 I_1 A_1 (3l-2a) + 6h I_2 (al A_1 + 2I_1))}{I_1 A_1 l^3 + 6I_2 A_1 l^2 h + 24h I_1 I_2} \quad (49a)$$

$$X_2 = \frac{-3Pa h^2 I_1 A_2 (l-a)}{2(2A_2 h^3 I_1 + 3I_1^2 l^2 + A_2 h^4 I_2 + 6h I_1 I_2)} \quad (49b)$$

$$X_3 = \frac{Pa[h^3 A_2 (2al I_1 + h I_2) + 3I_1 l (al I_1 + 2h I_2)]}{2(2A_2 h^3 I_1 + 3I_1^2 l^2 + A_2 h^4 I_2 + 6h I_1 I_2)} \quad (49c)$$

Evaluating equation (16) for different points on the structure using the force factors obtained in equations (49a) – (49c)

$$M_A = -Pa + \frac{Pl[a^2 I_1 A_1 (3l-2a) + 6h I_2 (al A_1 + 2I_1)]}{2(I_1 A_1 l^3 + 6I_2 A_1 l^2 h + 24h I_1 I_2)} + \frac{Pa[A_2 h^3 (-aI_1 + h I_2 + 3I_1 l) + 3I_1 l (al I_1 + 2h I_2)]}{2(2A_2 h^3 I_1 + 3I_1^2 l^2 + A_2 h^4 I_2 + 6h I_1 I_2)} \quad (50)$$

$$M_B = -Pa + \frac{P(a^2 I_1 A_1 (3l-2a) + 6h I_2 (al A_1 + 2I_1))}{2(I_1 A_1 l^3 + 6I_2 A_1 l^2 h + 24h I_1 I_2)} + \frac{Pa[h^3 A_2 (2al I_1 + h I_2) + 3I_1 l (al I_1 + 2h I_2)]}{2(2A_2 h^3 I_1 + 3I_1^2 l^2 + A_2 h^4 I_2 + 6h I_1 I_2)} \quad (51)$$

$$M_C = -\frac{Pl[a^2 I_1 A_1 (3l-2a) + 6h I_2 (al A_1 + 2I_1)]}{2(I_1 A_1 l^3 + 6I_2 A_1 l^2 h + 24h I_1 I_2)} + \frac{Pa[h^3 A_2 (2al I_1 + h I_2) + 3I_1 l (al I_1 + 2h I_2)]}{2(2A_2 h^3 I_1 + 3I_1^2 l^2 + A_2 h^4 I_2 + 6h I_1 I_2)} \quad (52)$$

$$M_D = -\frac{Pl[a^2 I_1 A_1 (3l-2a) + 6h I_2 (al A_1 + 2I_1)]}{2(I_1 A_1 l^3 + 6I_2 A_1 l^2 h + 24h I_1 I_2)} + \frac{Pa[A_2 h^3 (-aI_1 + h I_2 + 3I_1 l) + 3I_1 l (al I_1 + 2h I_2)]}{2(2A_2 h^3 I_1 + 3I_1^2 l^2 + A_2 h^4 I_2 + 6h I_1 I_2)} \quad (53)$$

IV. DISCUSSION OF RESULTS

The internal stress on the loaded frames is summarized in table 1. The effect of axial deformation is captured by the dimensionless constant s taken as the ratio of the end translational stiffness to the shear stiffness of a member.

$$S_1 = \frac{12EI_1}{h^3} \cdot \frac{h}{EA_1} = \frac{12I_1}{h^2 A_1} \quad (54)$$

$$S_2 = \frac{12EI_2}{l^3} \cdot \frac{l}{EA_2} = \frac{12I_2}{l^2 A_2} \quad (55)$$

When the axial deformation in the columns is ignored $S_1 = 0$ and likewise when axial deformation in the beam is

ignored $s_2 = 0$. If axial deformation is ignored in the whole structure, $s_1 = s_2 = 0$.

The internal stress equations enable an easy investigation into the contribution of axial deformation to the internal stresses of statically loaded frames for different kinds of external loads.

For frame 1 (figure 3), the moment at A, M_A is given by equation (19). The contribution of axial deformation in the column ΔM_A is given by

$$\Delta M_A = M_{A(\text{from equation 19})} - M_{A(\text{from equation 19 when } s_2=0)}$$

$$= \frac{wl^3 I_1}{12} \left[\frac{4h^3 I_2 + s_2 l^3 I_1}{4h^3 I_2 (2l I_1 + h I_1) + s_2 l^3 I_1 (l I_1 + 2h I_2)} - \frac{1}{2l I_1 + h I_2} \right] \quad (56)$$

Equation (56) gives the contribution of axial deformation to M_A as a function of h , l , I_1 , I_2 and s

By considering the case of a portal frame of length $l = 5\text{m}$, $h = 4\text{m}$. Equation 56 was evaluated to show how the contribution of axial deformation varied with I_1/I_2 . The result is shown in Table 2. When plotted on a uniform scale (Figure 9) the relationship between ΔM_B and I_1/I_2 is seen to be linear. This was further justified by a linear regression analysis of the results in Table 2 which was fitted into the model $\Delta M_A = P_1 \frac{I_1}{I_2} + P_2$ to obtain $P_1 = -0.004815$ and $P_2 = 0.0001109$ and the fitness parameters sum square of errors (SSE), coefficient of multiple determination (R^2) and the root mean squared error (RMSE) gave 1.099×10^{-7} , 0.999952 and 0.0001105 respectively. From Table 2 when $I_1/I_2 = 0$, $\Delta M_A \cong 0$ and when $I_1/I_2 = 10$; $\Delta M_A = -0.0479$ which represent only a 5% reduction in the calculated bending moment.

In like manner by evaluating the axial contribution in the beam, ΔM_B for varying I_1/I_2 of the portal frame, Table 3 was produced. This was plotted on a uniform scale in Figure 10. From Figure 10 it would be observed that there is also a linear relationship between ΔM_B and I_1/I_2 . When fitted into the model $\Delta M_B = P_3 \frac{I_1}{I_2} + P_4$ it gave $P_3 = -0.006502$ and $P_4 = -0.0003969$ for the fitness parameters sum square of errors (SSE), coefficient of multiple determination (R^2) and the root mean squared error (RMSE) of 6.51×10^{-7} , 0.9999 and 0.000269 respectively.

By pegging I_1/I_2 to a constant value of 0.296 and the variation of ΔM_A with respect to h/L investigated, Table 4 was generated. A detailed plot of Table 4 was presented in Figure 11. From Table 4 when $h/L = 0$; $\Delta M_A = -3.125$ (about 30% drop in calculated bending moment value) while at $h/L > 0$, ΔM_A dropped in magnitude exponentially to values below 1. In like manner, when the variation of ΔM_B with respect to h/L was investigated, Table 5 was generated. A detailed plot of Table 5 was presented in Figure 12. From Table 5 when $h/L = 0$; $\Delta M_A = -4.1667$ (about 40% drop in calculated bending moment value) while at $h/L > 0$, ΔM_A dropped in magnitude exponentially to values below 1.

V. CONCLUSION

The flexibility method was used to simplify the analysis and a summary of the results are presented in table 1. The equations in table 1 would enable an easy evaluation of the internal stresses in loaded rigidly fixed portal frames considering the effect of axial deformation.

From a detailed analysis of frame 1 (Figure 3), it was observed that the contribution of axial deformation is generally very small and can be neglected for reasonable values of I_1/I_2 . However, its contribution skyrockets at very low values of h/l i.e. as $h/l \Rightarrow 0$. This depicts the case of an encased single span beam and a complete departure from portal frames under study. This analysis can be extended to the other loaded frames (Figures 4 – 8) using the equations in Table 1. These would enable the determination of safe conditions for ignoring axial deformation under different kinds of loading.

REFERENCES

- Ghali A, Neville A. M. (1996) *Structural Analysis: A Unified Classical and Matrix Approach* (3rd Edition) Chapman & Hall London
- Graham R, Alan P.(2007). *Single Storey Buildings: Steel Designer's Manual* Sixth Edition, Blackwell Science Ltd, United Kingdom
- Hibbeler, R. C.(2006). *Structural Analysis*. Sixth Edition, Pearson Prentice Hall, New Jersey
- Leet, K. M., Uang, C.,(2002). *Fundamental of Structural Analysis*. McGraw-Hill ,New York
- McGuire, W., Gallagher R. H., Zienkiewicz, R. D.(2000). *Matrix Structural Analysis*, Second Edition, John Wiley & Sons, Inc. New York
- Nash, W.,(1998). *Schaum's Outline of Theory and Problems of Strength of Materials*. Fourth Edition, McGraw-Hill Companies, New York
- Okonkwo V. O (2012). *Computer-aided Analysis of Multi-storey Steel Frames*. M. Eng. Thesis, Nnamdi Azikiwe University, Awka, Nigeria.
- Reynolds, C. E.,and Steedman J. C. (2001). *Reinforced Concrete Designer's Handbook*, 10th Edition) E&FN Spon, Taylor & Francis Group, London
- Samuelsson A., and Zienkiewicz O. C.(2006), Review: History of the Stiffness Method. *International Journal for Numerical Methods in Engineering*. Vol. 67: 149 – 157
- Stroud K. A.,(1995). *Engineering Mathematics*. Fourth Edition, Macmillan Press Ltd, London.

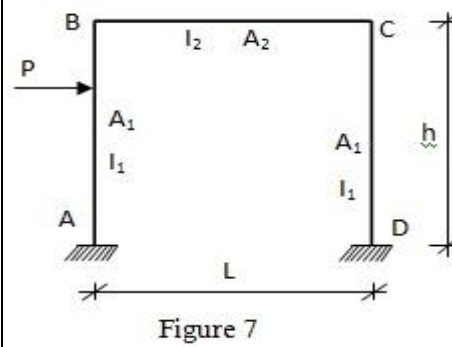
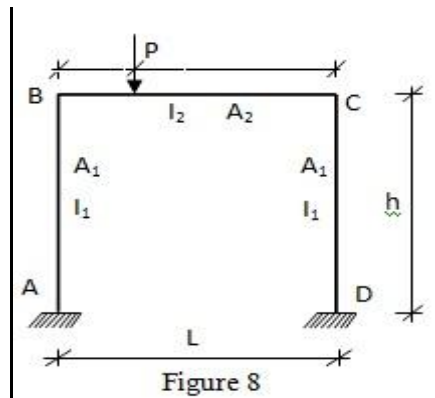
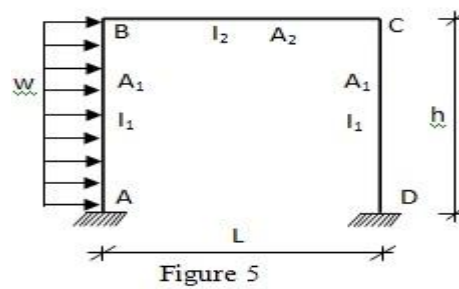
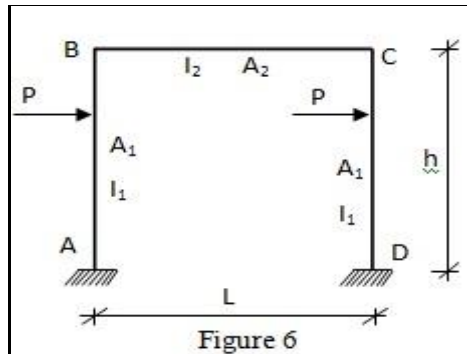
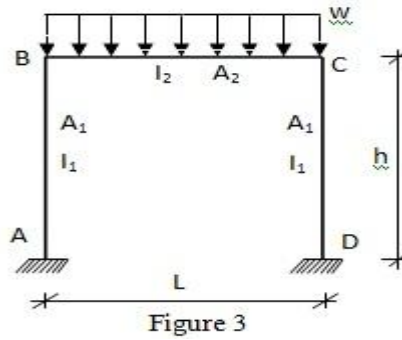
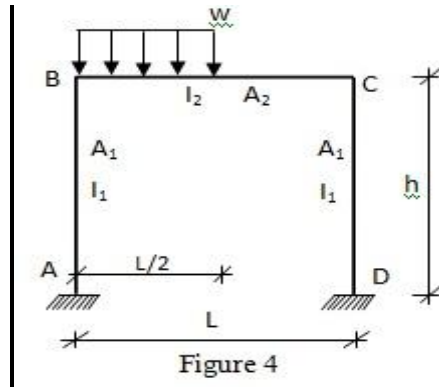
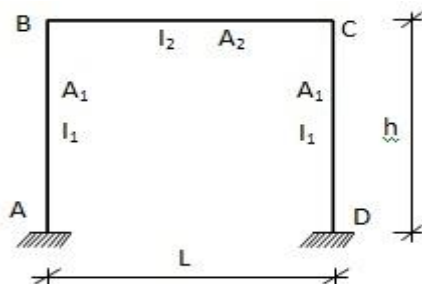


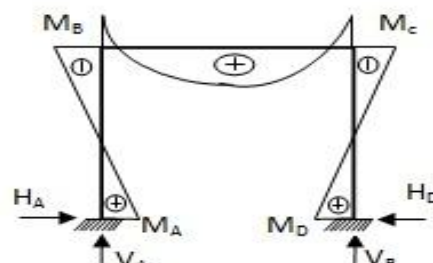
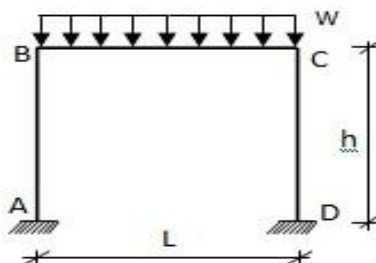
Table 1: Internal stresses for a loaded rigid frame



A_1 = Cross-sectional area of the columns
 I_1 = Second moment of area of the column cross-section
 A_2 = Cross-sectional area of the beam
 I_2 = Second moment of area of the beam cross-section

S/No LOADED FRAME

REMARKS

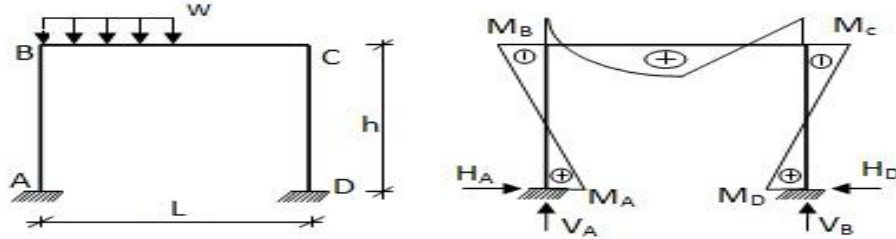


$$M_A = M_D = \frac{wl^3 I_1 (4h^3 I_2 - s_2 l^3 I_1)}{12[4h^3 I_2 (2lI_1 + hI_2) + s_2 l^3 I_1 (lI_1 + 2hI_2)]}$$

$$M_B = M_C = \frac{-wl^3 I_1 (8I_2 h^3 + s_2 l^3 I_1)}{12[4h^3 I_2 (2lI_1 + hI_2) + s_2 l^3 I_1 (lI_1 + 2hI_2)]}$$

$$V_A = V_D = \frac{wl}{2} \quad H_A = H_D = \frac{wh^2 l^3 I_1 I_2}{4h^3 I_2 (2lI_1 + hI_2) + s_2 l^3 I_1 (lI_1 + 2hI_2)}$$

See equations (19) – (22)



$$M_A = \frac{wl^2 [4h^3 I_2 (3hI_2 + 8lI_1) + l^3 I_1 (s_1 lI_1 + 6s_2 hI_2)]}{48[4h^3 I_2 (2lI_1 + hI_2) + s_2 l^3 I_1 (lI_1 + 2hI_2)]} - \frac{wl^4 (5hI_1 + 24hI_2)}{64(l^2 I_1 + 6hl^2 I_2 + 2s_1 h^3 I_2)}$$

$$M_B = -\frac{wl^4 (5hI_1 + 24hI_2)}{64(l^2 I_1 + 6hl^2 I_2 + 2s_1 h^3 I_2)} + \frac{wl^2 [4h^3 I_2 (3hI_2 + 2lI_1) + s_2 l^3 I_1 (lI_1 + 6hI_2)]}{48[4h^3 I_2 (2lI_1 + hI_2) + s_2 l^3 I_1 (lI_1 + 2hI_2)]}$$

$$M_C = -\frac{wl(3I_1 l^3 + 24I_2 l^2 h + 16s_1 h^3 I_2)}{64(I_1 l^3 + 6I_2 l^2 h + 2s_1 h^3 I_2)} + \frac{wl^2 [4h^3 I_2 (3hI_2 + 2lI_1) + s_2 l^3 I_1 (lI_1 + 6hI_2)]}{48[4h^3 I_2 (2lI_1 + hI_2) + s_2 l^3 I_1 (lI_1 + 2hI_2)]}$$

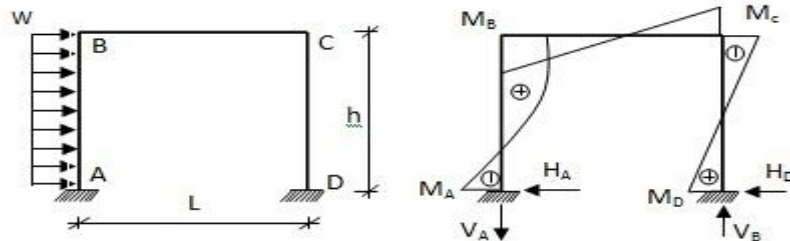
$$M_D = \frac{wl^2 [4h^3 I_2 (3hI_2 + 8lI_1) + l^3 I_1 (s_1 lI_1 + 6s_2 hI_2)]}{48[4h^3 I_2 (2lI_1 + hI_2) + s_2 l^3 I_1 (lI_1 + 2hI_2)]} - \frac{wl(3I_1 l^3 + 24I_2 l^2 h + 16s_1 h^3 I_2)}{64(I_1 l^3 + 6I_2 l^2 h + 2s_1 h^3 I_2)}$$

$$V_D = \frac{wl(3I_1 l^3 + 24hI_2 l^2 + 16s_1 h^3 I_2)}{32(I_1 l^3 + 6hl^2 I_2 + 2s_1 h^3 I_2)} \quad V_A = \frac{wl}{2} - V_D$$

$$H_A = H_D = \frac{wh^2 l^3 I_1 I_2}{2[4h^3 I_2 (2lI_1 + hI_2) + s_2 l^3 I_1 (lI_1 + 2hI_2)]}$$

See equations (26) – (29)

3



$$M_A = -\frac{wh^2 (I_1 l^3 + 5hl^2 I_2 + 2s_2 h^3 I_2)}{2(I_1 l^3 + 6hl^2 I_2 + 2s_1 h^3 I_2)} + \frac{wh^3 I_2 (9h^2 lI_1 + 5h^3 I_2 + s_2 l^3 I_1)}{6[4h^3 I_2 (2lI_1 + hI_2) + s_2 l^3 I_1 (lI_1 + 2hI_2)]}$$

$$M_B = \frac{wh^3 l^2 I_2}{2(I_1 l^3 + 6hl^2 I_2 + 2s_1 h^3 I_2)} + \frac{wh^3 I_2 (-4h^3 I_2 + s_2 l^3 I_1)}{6[4h^3 I_2 (2lI_1 + hI_2) + s_2 l^3 I_1 (lI_1 + 2hI_2)]}$$

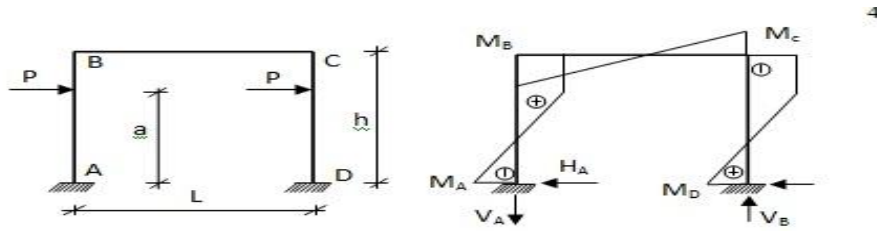
$$M_C = -\frac{wh^3 l^2 I_2}{2(I_1 l^3 + 6hl^2 I_2 + 2s_1 h^3 I_2)} + \frac{wh^3 I_2 (-4h^3 I_2 + s_2 l^3 I_1)}{6[4h^3 I_2 (2lI_1 + hI_2) + s_2 l^3 I_1 (lI_1 + 2hI_2)]}$$

$$M_D = -\frac{wh^3 l^2 I_2}{2(I_1 l^3 + 6hl^2 I_2 + 2s_1 h^3 I_2)} + \frac{wh^3 I_2 (9h^2 lI_1 + 5h^3 I_2 + s_2 l^3 I_1)}{6[4h^3 I_2 (2lI_1 + hI_2) + s_2 l^3 I_1 (lI_1 + 2hI_2)]}$$

$$V_A = V_B = \frac{wh^3 lI_2}{I_1 l^3 + 6I_2 l^2 h + 2s_1 I_2 h^3}$$

$$H_D = \frac{wh^4 I_2 (3l_1 + 2hl_2)}{2[4h^3 I_2 (2l_1 + hl_2) + s_2 l^3 I_1 (l_1 + 2hl_2)]} \quad H_A = wh - H_D$$

See equations (32) – (35)

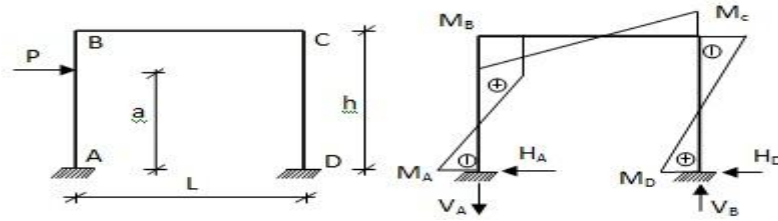


$$M_A = -Pa \left(1 - \frac{3al^2 I_2}{l_1 l^3 + 6hl^2 I_2 + 2s_1 h^3 I_2} \right) \quad M_B = \frac{3Pa^2 l^2 I_2}{l_1 l^3 + 6hl^2 I_2 + 2s_1 h^3 I_2} \quad H_D$$

$$M_C = -\frac{3Pa^2 l^2 I_2 A_1}{A_1 l_1 l^3 + 6A_1 hl^2 I_2 + 24h l_1 l^2} \quad M_D = Pa \left(1 - \frac{3al^2 I_2}{l_1 l^3 + 6hl^2 I_2 + 2s_1 h^3 I_2} \right)$$

$$V_A = V_B = \frac{6Pa^2 l I_2}{l^3 I_1 + 6l^2 hl I_2 + 2s_1 h^3 I_2} \quad H_A = H_B = P$$

See equations (38) – (41)



$$M_A = -Pa + \frac{3Pa^2 l^2 I_2}{2(l_1 l^3 + 6hl^2 I_2 + 2s_1 h^3 I_2)} + \frac{Pa^2 [4l_1 l_2 hl(3h-a) + l_2 (8h^3 I_2 - 4ah^3 I_2 + s_2 l^3 I_1)]}{2[4h^3 I_2 (2l_1 + hl_2) + s_2 l^3 I_1 (l_1 + 2hl_2)]}$$

$$M_B = \frac{3Pa^2 l^2 I_2}{2(l_1 l^3 + 6hl^2 I_2 + 2s_1 h^3 I_2)} + \frac{Pa^2 l_2 (-4h^3 I_2 + 4ah^2 I_2 + s_2 l^3 I_1)}{2[4h^3 I_2 (2l_1 + hl_2) + s_2 l^3 I_1 (l_1 + 2hl_2)]}$$

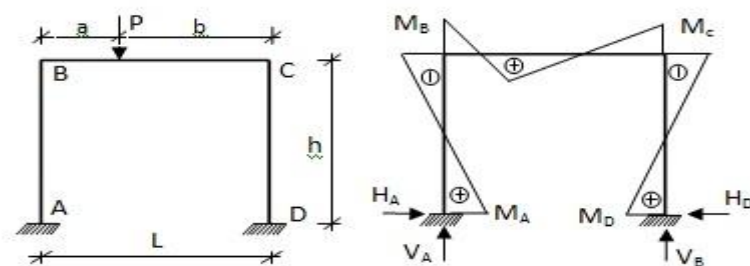
$$M_C = -\frac{3Pa^2 l^2 I_2}{2(l_1 l^3 + 6hl^2 I_2 + 2s_1 h^3 I_2)} + \frac{Pa^2 l_2 (-4h^3 I_2 + 4ah^2 I_2 + s_2 l^3 I_1)}{2[4h^3 I_2 (2l_1 + hl_2) + s_2 l^3 I_1 (l_1 + 2hl_2)]}$$

$$M_D = -\frac{3Pa^2 l^2 I_2}{2(l_1 l^3 + 6hl^2 I_2 + 2s_1 h^3 I_2)} + \frac{Pa^2 [4l_1 l_2 hl(3h-a) + l_2 (8h^3 I_2 - 4ah^3 I_2 + s_2 l^3 I_1)]}{2[4h^3 I_2 (2l_1 + hl_2) + s_2 l^3 I_1 (l_1 + 2hl_2)]}$$

$$V_A = V_B = \frac{3Pa^2 l I_2}{l^3 I_1 + 6l^2 hl I_2 + 2s_1 h^3 I_2}$$

$$H_D = \frac{2Pa^2 l_2 [l_1 (3h-a) + hl_2 (3h-2a)]}{4h^3 I_2 (2l_1 + hl_2) + s_2 l^3 I_1 (l_1 + 2hl_2)} \quad H_A = P - H_D$$

See equations (44) – (47)



$$M_A = -Pa + \frac{Pl[a^2I_1(3l-2a)+hI_2(6al+s_1h^2)]}{2(I_1l^3+6hl^2I_2+2s_1h^3I_2)} + \frac{Pa[4h^3I_2(-aI_1+hI_2+3lI_1)+s_2l^3I_1(aI_1+2hI_2)]}{2[4h^3I_2(2lI_1+hI_2)+s_2l^3I_1(lI_1+2hI_2)]}$$

$$M_B = -Pa + \frac{Pl[a^2I_1(3l-2a)+hI_2(6al+s_1h^2)]}{2(I_1l^3+6hl^2I_2+2s_1h^3I_2)} + \frac{Pa[4h^3I_2(2aI_1+hI_2)+s_2l^3I_1(aI_1+2hI_2)]}{2[4h^3I_2(2lI_1+hI_2)+s_2l^3I_1(lI_1+2hI_2)]}$$

$$M_C = -\frac{Pl[a^2I_1(3l-2a)+hI_2(6al+s_1h^2)]}{2(I_1l^3+6hl^2I_2+2s_1h^3I_2)} + \frac{Pa[4h^3I_2(2aI_1+hI_2)+s_2l^3I_1(aI_1+2hI_2)]}{2[4h^3I_2(2lI_1+hI_2)+s_2l^3I_1(lI_1+2hI_2)]}$$

$$M_D = -\frac{Pl[a^2I_1(3l-2a)+hI_2(6al+s_1h^2)]}{2(I_1l^3+6hl^2I_2+2s_1h^3I_2)} + \frac{Pa[4h^3I_2(-aI_1+hI_2+3lI_1)+s_2l^3I_1(aI_1+2hI_2)]}{2[4h^3I_2(2lI_1+hI_2)+s_2l^3I_1(lI_1+2hI_2)]}$$

$$V_D = \frac{P[a^2I_1(3l-2a)+6ahlI_2+s_1h^3I_2]}{l^3I_1+6hl^2I_2+2s_1h^3I_2} \quad V_A = P - V_D$$

$$H_A = H_B = \frac{6Pa h^2 I_1 I_2 (l-a)}{4h^3 I_2 (2lI_1+hI_2)+s_2 l^3 I_1 (lI_1+2hI_2)}$$

See equations (50) – (53)

Table 2: Axial deformation contribution ΔM_A for different values of I_1/I_2

w=1kN/m L = 5m H = 0.4m h = 4m						
I_1/I_2	0	1	2	3	4	5
ΔM_A	0	-0.0045	-0.0095	-0.0144	-0.0192	-0.0241
I_1/I_2	6	7	8	9	10	
ΔM_A	-0.0289	-0.0337	-0.0384	-0.0432	-0.0479	

Table 3: Axial deformation contribution ΔM_B for different values of I_1/I_2

w=1kN/m L = 5m H = 0.4m h = 4m						
I_1/I_2	0	1	2	3	4	5
ΔM_B	0	-0.0066	-0.0135	-0.0201	-0.0267	-0.0332
I_1/I_2	6	7	8	9	10	
ΔM_B	-0.0396	-0.0460	-0.0524	-0.0587	-0.0651	

Table 4: Axial deformation contribution ΔM_A for different values of h/l

w=1kN/m L = 5m $I_1/I_2 = 0.296$						
h/l	0	0.1	0.2	0.3	0.4	0.5
ΔM_A	-3.1250	-0.5409	-0.0823	-0.0239	-0.0096	-0.0047
h/l	0.6	0.7	0.8	0.9	1.0	
ΔM_A	-0.0026	-0.0015	-0.0010	-0.0006	-0.0004	

Table 5: Axial deformation contribution ΔM_B for different values of h/l

$$w = 1 \text{ kN/m} \quad L = 5 \text{ m} \quad I_1/I_2 = 0.296$$

h/l	0	0.1	0.2	0.3	0.4	0.5
ΔM_A	-4.1667	-0.7668	-0.1208	-0.0359	-0.0146	-0.0072
h/l	0.6	0.7	0.8	0.9	1.0	
ΔM_A	-0.0040	-0.0024	-0.0015	-0.0010	-0.0007	

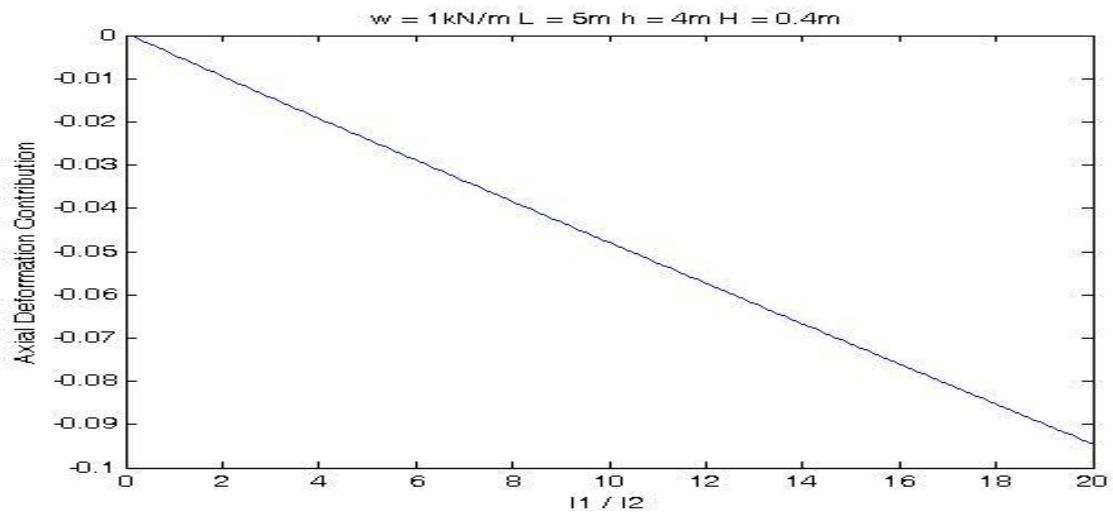


Figure 9: A graph of ΔM_A against I_1/I_2

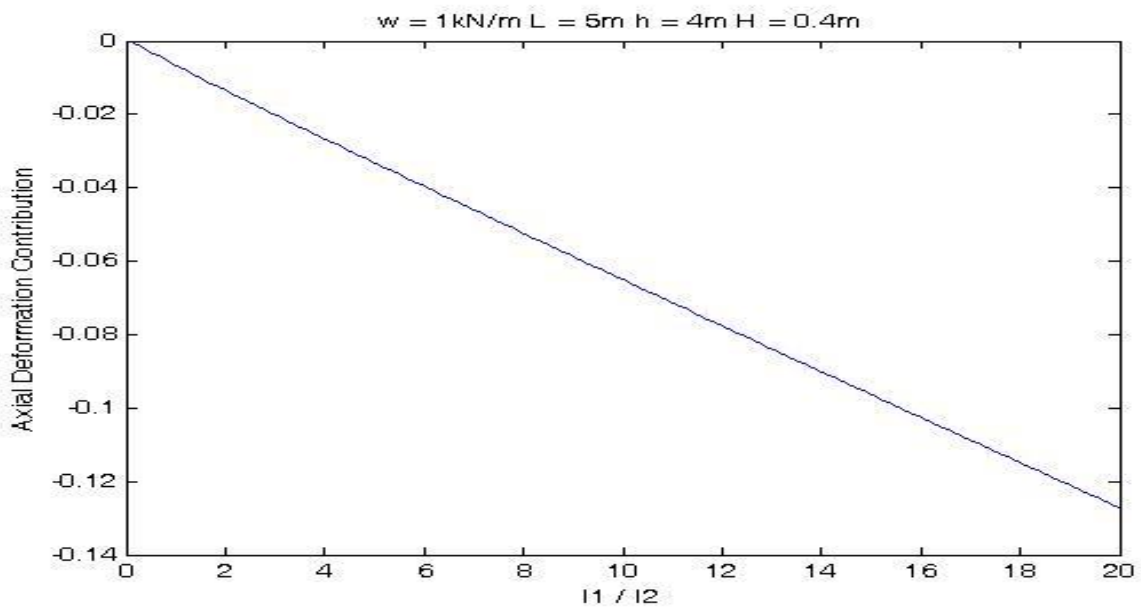


Figure 10: A graph of ΔM_B against I_1/I_2

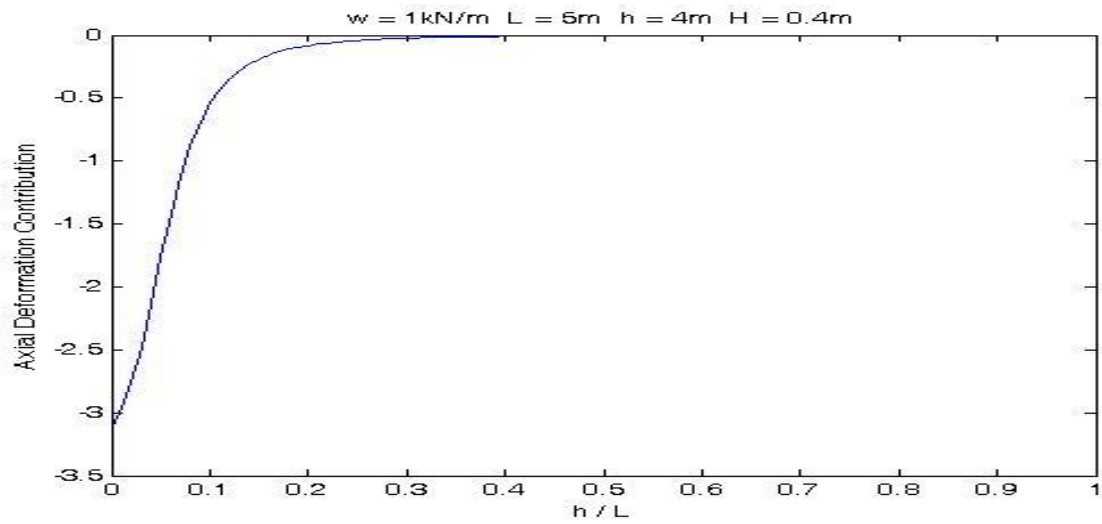


Figure 11: A graph of ΔM_A against h/L

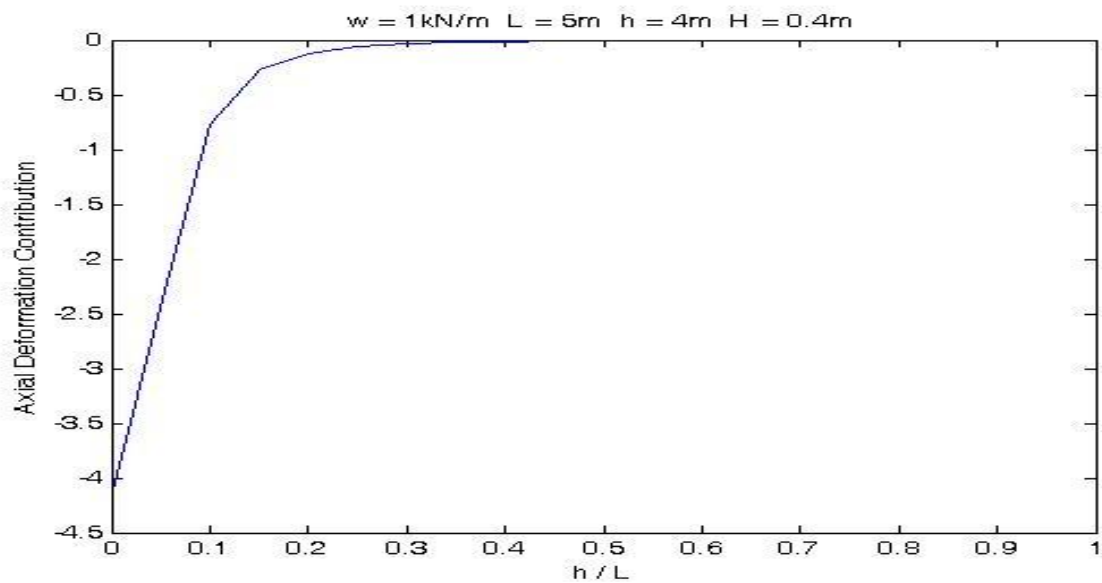


Figure 12: A graph of ΔM_B against h/L

Real Power Loss Reduction in Distribution Systems Using Ant Colony Optimization Adapted By Graph Theory

Shaik Mohammad shakeer¹, P.Suresh babu²

M.Tech student¹, Assistant Professor^{2, 1, 2} Department of EEE A.I.T.S Engineering College Rajampet, kadapah, India

Abstract: This paper presents an efficient method for the reconfiguration of radial distribution systems for minimization of real power loss using adapted ant colony optimization. The conventional ant colony optimization is adapted by graph theory to always create feasible radial topologies during the whole evolutionary process. This avoids tedious mesh check and hence reduces the computational burden. The initial population is created randomly and a heuristic spark is introduced to enhance the pace of the search process. The effectiveness of the proposed method is demonstrated on IEEE 14 & 30-bus real distribution system. The simulation results show that the proposed method is efficient and promising for reconfiguration problem of radial distribution systems.

IndexTerms: Ant colony optimization, distribution network, graph theory, real power loss, and reconfiguration

I. INTRODUCTION

DISTRIBUTION networks are generally structured in mesh but operated in radial configuration for effective co-ordination of their protective schemes and to reduce the fault level. The reconfiguration of a distribution system is a process that alters feeder topological structure by managing the open/close status of sectionalizing and tie-switches in the system under contingencies or under normal operating conditions. Reconfiguration of radial distribution systems is a very effective and efficient means to reduce distribution network losses, improve voltage profile, to manage load congestion and to enhance system reliability. The aim of distribution network reconfiguration is to find a radial operating configuration that optimizes certain objectives while satisfying all the operational constraints without islanding of any node(s). A lot of research work has been carried out to solve distribution network reconfiguration problems.

These research efforts can be broadly classified into traditional approaches and AI based approaches. The traditional approaches include heuristic optimization techniques and classical optimization techniques. Merlin *et al.* [1] were first to report a method for distribution network reconfiguration to minimize feeder loss. They formulated the problem as mixed integer non-linear optimization problem and solved it through a discrete branch and-bound technique. Later on [2]-[7] also suggested different branch exchange heuristic algorithms. The complexity of reconfiguration problem increases with the exponential growth in the size of modern distribution networks and the heuristic techniques fails to provide a quality solution. Therefore, the researchers diverted towards various stochastic-based search techniques. Nara *et al.* [8] introduced genetic algorithm (GA) for reconfiguration of distribution networks for loss minimization. Later, several

GA based methods [9]-[14] have been used for reconfiguration of distribution networks. Mendoza *et al.* [13] proposed a new methodology for minimal loss reconfiguration using GA with the help of fundamental loops. They restricted the search space of GA by modifying the genetic operators. Enacheanu *et al.* [14] presented a method based on GA for the loss minimization in distribution networks, using matroid theory and graph theory. Some other population-based meta-heuristic techniques, e.g., immune algorithm [15], evolutionary algorithm [16], simulated annealing [17], [18], tabu-search [19]-[21], particle swarm optimization [22] and ant colony optimization [23]-[27] etc. also have been attempted to solve the reconfiguration problem of distribution network.

The reconfiguration of distribution system for loss minimization is a complex, combinatorial optimization problem. The application of these population based search techniques to solve the reconfiguration problem of distribution networks faces an additional difficulty of maintaining the radiality constraint throughout the evolutionary process. These methods in the literature provide different ways of maintaining radiality constraint, but, they are incomplete as they may generate infeasible intermediate solutions during the evolutionary process.

These infeasible intermediate solutions have to be rejected and the process is to be repeated until it gets a feasible individual, which may be time consuming. This paper presents a new codification to represent feasible radial topologies of distribution system for the meta-heuristic search techniques. For this purpose some rules are framed with the help of graph theory. As the ant colony optimization (ACO) is one of the latest meta-heuristic techniques based on swarm intelligence and considered to be an efficient method for solving the large-scale.

The formulation of the loss minimization problem is discussed in Section II. The conventional ACO is explained in Section III. The modifications proposed in the conventional ACO are discussed in Section IV, in Section V the proposed codification for AACO is illustrated with the help of an example. In Section VI the application results of the proposed method are presented and finally concluded in Section VII.

II. PROBLEM FORMULATION FOR MINIMAL POWER LOSS

The distribution networks reconfigured frequently to optimize operational efficiency and maintain power quality.

The principal objective of distribution network reconfiguration is to find the radial operating structure having minimum real power loss while satisfying various operating constraints. All the loads are assumed of the nature of constant power. The reconfiguration problem of

distribution networks for loss minimization is formulated as below:

$$\text{Minimize} \quad \sum_{n=1}^E R_n \frac{P_n^2 + Q_n^2}{|V_n|^2} \quad (1)$$

$$\text{Subject to} \quad I_n \leq I_{\max}^n \quad (2)$$

$$V_{\min} \leq V_n \leq V_{\max} \quad (3)$$

$$\Phi(i) = 0 \quad (4)$$

where, V_n , P_n and Q_n are voltage, real power and reactive power at the sending end of the n th branch respectively, R_n is the resistance of the n th branch and E is the total number of branches in the system. Equation (1) corresponds to the objective function to be optimized and represent total real power loss of the distribution system. Equation (2) corresponds to limit branch current and substation current capacities within permissible limits. Equation (3) considers voltage constraints for each node of the system. Equation (4), deals with the radial topology constraint, it ensures radial structure of the i th candidate topology.

III. ANT COLONY OPTIMIZATION

Ant colony optimization (ACO) is a population-based meta-heuristic technique for solving combinatorial optimization problems, initially proposed by Marco Dorigo in 1992 in his PhD thesis [28], inspired by the behavior of ants in finding paths from the nest to food and back to the nest. The original idea has since diversified to solve a wider class of numerical problems, and as a result, several problems have emerged, drawing on various aspects of the behavior of ants. Ant communication is accomplished primarily through chemicals called pheromones. Other ants perceive the presence of pheromone and tend to follow paths where pheromone concentration is higher. An ant will move from node i to node j with probability

$$P_{i,j} = \frac{(\tau_{i,j}^\alpha)(\eta_{i,j}^\beta)}{\sum (\tau_{i,j}^\alpha)(\eta_{i,j}^\beta)} \quad (5)$$

where $\tau_{i,j}$ is the amount of pheromone on edge $i-j$, α is a parameter to control the influence of $\tau_{i,j}$, $\eta_{i,j}$ is the desirability of edge $i-j$ (a priori knowledge, typically $1/d_{i,j}$; $d_{i,j}$ is the distance between node i and j) and β is a parameter to control the influence of $\eta_{i,j}$. While moving from node i to j , the ant updates the pheromone on the edge $i-j$. To escape local minima, pheromone evaporation is used. Evaporation is applied uniformly to all edges with a simple decay coefficient ρ . The pheromone update is given by

$$\tau_{i,j} = (1 - \rho)\tau_{i,j} + \Delta\tau_{i,j} \quad (6)$$

where $\tau_{i,j}$ is the amount of pheromone on a given edge $i-j$, ρ is the rate of pheromone evaporation and $\Delta\tau_{i,j}$ is the amount of pheromone deposited, typically given by

$$\Delta\tau_{i,j}^k = \begin{cases} 1/C_k, & \text{if ant } k \text{ travels on edge } i-j \\ 0, & \text{otherwise} \end{cases} \quad (7)$$

where C_k is the cost of the k th ant's tour (typically length).

IV. PROPOSED ADAPTIVE ANT COLONY OPTIMIZATION

While the conventional ACO is applied to solve the reconfiguration problem of distribution networks, the radiality constraint imposes main hurdle since a large number of infeasible individuals appears during initialization as well as at intermediate stages of the evolutionary process. These infeasible individuals may be transformed into the feasible ones using some engineering knowledge base. The proposed methodology creates feasible individuals all times for ACO by encoding the Individual ant with the help of graph theory [29] and the terms are redefined in the context of distribution network reconfiguration, as described in the next sub-sections.

A. Ant encoding using Graph Theory

The graph of the given distribution network can be obtained by closing all tie-switches. The radial configuration in which the distribution networks must operate should not possess any closed path with all nodes energized. These radial configurations are called *trees* of the distribution network graph (DNG). The *co-tree* is the complement of a *tree*. The elements of *co-tree* are called *links*. When one *link* is added in its corresponding *tree*, one *fundamental loop* is formed. In the distribution network reconfiguration problem, ants may be encoded by a set of definite number of switches to be opened (*links*). The number of *links* or the *fundamental loops* of a DNG is unique [29] and is given by $L = E - N + 1$ (8) where, E is total number of elements (sectionalizing and tie switches) of the network and N is total number of nodes of the network.

The reconfiguration problem of distribution network can be defined as to find that particular *tree*, i.e., *co-tree*, which optimizes all objectives and satisfies all constraints set by the optimization problem. Therefore, while using ACO ants may be encoded to represent a *co-tree*. If the ant population is selected randomly for initialization, as in case of the conventional ACO, a large number of infeasible topologies will generate, moreover some infeasible topologies may appear during the evolutionary process, which increases the computational burden. Therefore, in the proposed AACO, some rules are framed to generate only feasible radial topologies. Before framing these rules, let us define

- (i) Principal Node: The junction of three or more elements of the distribution network graph (DNG).
- (ii) Exterior Node: The node located at the perimeter of the DNG.
- (iii) Interior Node: The node located inside the perimeter of the DNG.
- (iv) Loop Vector: It is the set of elements constituting closed path in a DNG. The total number of loop vectors for a given DNG are L_k , where $k = 1, 2, 3, \dots, L$.
- (v) Common Branch Vector: It is the set of elements which are common between any two *loop vectors* of a DNG. The *common branch vector* C_{ij} , containing the set of elements common between two *loop vectors* L_i and L_j .
- (vi) Prohibited Group Vector: It is the set of the *common Branch vectors* incident to interior node(s) of the DNG.

The *prohibited group vector* $R_{m1} \ m2 \ m3 \ \dots$, isolate principal interior node(s) $m1, m2, m3 \ \dots$ of the DNG.

Now, the following rules are framed to create feasible

individuals during the whole evolutionary process of AACO: Rule 1: The m th member of the individual must belong to *loop vector* L_m . Rule 2: Only one member from a *common branch vector* can be selected to form an individual. Rule 3: All the *common branch vectors* of any *prohibited group vector* cannot participate simultaneously to form an individual. The Rule 1 and Rule 2 prevent islanding of exterior and interior nodes respectively whereas Rule 3 prevents the islanding of principal interior nodes of the DNG. Therefore, while encoding the individual ant for AACO, these three rules ensure the radial topology of the network without islanding of any node(s) and thus it avoids tedious mesh checks. In general, the ant encoding in real numbers may be defined as shown in Fig. 1, where each member Z_m represents the open switch of the distribution network in real number. The ant consists of L such members, where the Z_m belongs to the *loop vector* L_m ; $m = 1, 2, \dots, L$.

$Z_1 \in L_1$	$Z_2 \in L_2$...	$Z_m \in L_m$...	$Z_L \in L_L$
---------------	---------------	-----	---------------	-----	---------------

Fig. 1. Ant encoding for the proposed AACO

In this paper, the conventional ACO is adapted using fundamentals of graph theory to generate feasible individuals. Therefore the proposed ACO is named as Adapted Ant Colony Optimization (AACO). The AACO transforms infeasible individual, whenever generated, into feasible ones under the guidance of the rules framed.

B. Initialization using Heuristic Spark

In the proposed algorithm, one individual of better fitness is created using the heuristics of [2], which may be called as heuristic spark. However, the remaining individuals are created randomly under the guidance of rules framed to maintain the diversity. The heuristic spark ignites the search engine of the proposed AACO as the other individuals are influenced by it. In the due course of time, these individuals will get better descendents and this enhances the pace of the ACO.

C. Edge Selection

In ant codification shown in Fig. 1, the member Z_m indicates that an ant is standing at switch Z_m and to implement Rule 1 its search is restricted to corresponding *loop vector* L_m .

An edge is defined as the imaginary path between one switch to another switch in the loop. In the next iteration, the probability of the movement of the ant from current switch position i to all other switch positions within *loop vector* L_m is evaluated using (5) based on the pheromone concentration and desirability. The desirability in the context of reconfiguration is redefined in the next sub-section. The edge having the maximum probability is selected. This process of selecting switch is used for each loop separately, in the guidance of Rule 2 and Rule 3, such that the resultant ant represents a radial network. Fig.

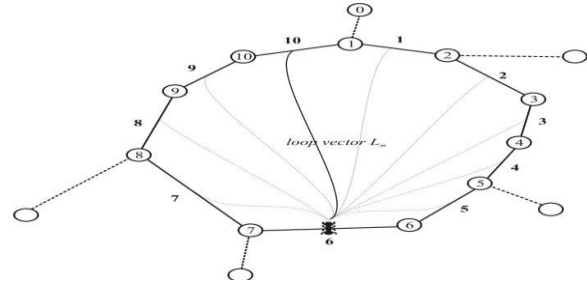


Fig. 2. Edge Selection of the ant within loop vector L_m

The loop shown in Fig. 2 is a part of any meshed network. The encircled numbers represent the nodes and numbers without circle represent switch position in a *loop vector* L_m . It is also shown that an artificial ant is standing at switch position 6. If its probability of the selection of edge from switch position 6 to switch position 10 is maximum, shown by solid line in the figure,

D. Desirability

In ant colony optimization, the term desirability is normally defined as the reciprocal of the distance between two nodes. For the reconfiguration problem it is redefined in terms of the sending end voltage of each line for the best radial network obtained; as sending end voltage will keep on decreasing as its distance from the source increasing. A desirability matrix is created for each *loop vector*. The matrix D_m is the desirability matrix for *loop vector* L_m and the element D_{mij} represents the desirability of selection of switch j from switch i . The value of D_{mij} is defined as

$$D_{mij} = \begin{cases} V_i - V_j, & i \neq j \\ \lambda V_i, & i = j \end{cases} \quad (9)$$

$$\Delta \tau_{i,j}^k = \begin{cases} 1/P_k, & \text{if ant } k \text{ travels on edge } i-j \\ 0, & \text{otherwise} \end{cases} \quad (10)$$

where P_k is real power loss of the radial configuration obtained by the k^{th} ant's travel.

F. Global Update

The ants communicate the best location of food with other ants. To implement this behavior of ants for reconfiguration problem extra pheromone is added for the edge from each switch in the *loop vector* to the switch of the corresponding *loop vector* of global best solution. For the *loop vector* L_m

$$\tau_{i,j} = \tau_{i,j} + \sigma \Delta \tau_{i,j}$$

G. Hunting Group

In ant colony the responsibility of a particular group is to explore new possible food location irrespective of the pheromone deposition.

H. Elitism

At the end of each iteration, all the tours visited by ants are evaluated and the ant with the best fitness is preserved for the next iteration.

I. Termination

The algorithm is terminated if all the ants of the current population reach to the solution with same fitness or the iteration number reaches the predefined maximum iteration

number. The flow chart of the proposed AACO is shown in the Fig. 3.

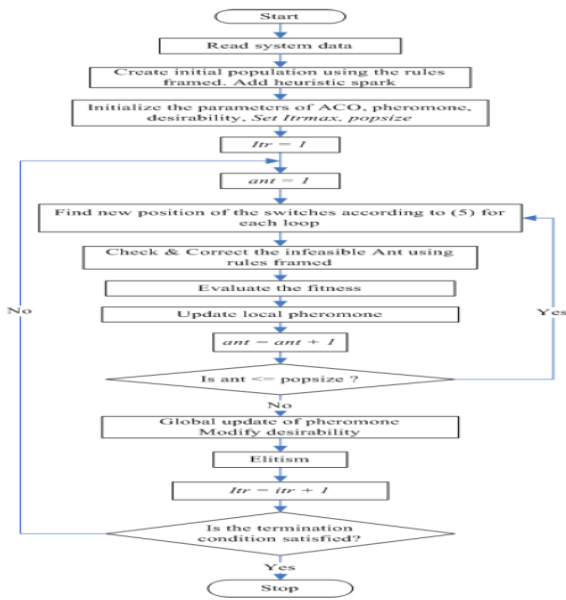


Fig. 3. Flow chart of the proposed AACO

V. ILLUSTRATION OF THE PROPOSED CODIFICATION

To understand the application of graph theory in the proposed codification, let us consider the example of IEEE 14-bus system, shown in the Fig. 4. For this system $E=17$, $N=14$ and $L=16-14+1=3$. Therefore, there are three loop vectors. According to their position in the loop, each switch is assigned a position number as shown. For IEEE 30-bus system $L=35-31+1=5$. Such that there are five loops

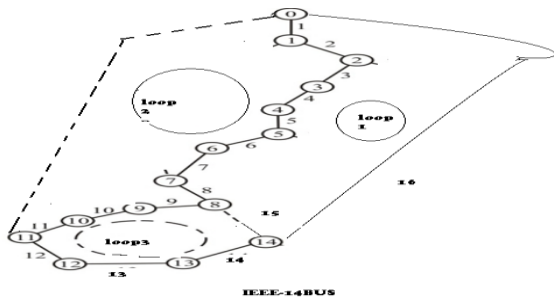
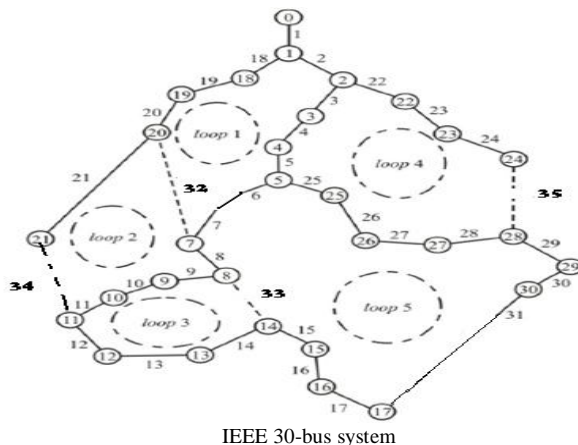


Fig. 4. IEEE 14-bus system



IEEE 30-bus system

In this section, the effectiveness of the proposed algorithm is tested on balanced IEEE 14-bus test distribution system [5], [31]. The initial configuration, system rated line voltage, nominal real and reactive loadings, real power loss and minimum node voltage of these test systems. The proposed AACO is implemented with the ant population size and maximum iterations as shown in Table V. The parameters α , β , ζ , ρ and σ are adjusted for their optimal values by hit and trial and the final values are. The simulation results for these aforementioned test distribution systems and are found to be either identical or better with the results

Test and Results of IEEE 14 & 30 bus

From Bus to bus		PL(LF)	PL(ACO)	PL(AACO)
1.0000	2.0000	12.9630	5.7350	4.8280
1.0000	5.0000	11.6430	7.1320	6.7740
2.0000	3.0000	9.5990	6.8760	6.6640
2.0000	4.0000	5.0870	3.7500	2.7500
2.0000	5.0000	2.8210	2.1810	1.1810
3.0000	4.0000	0.9630	0.1910	0.1910
4.0000	5.0000	1.4940	1.4470	1.4170
4.0000	7.0000	1.6310	1.6830	1.6520
4.0000	9.0000	1.2870	1.2760	1.2510
5.0000	6.0000	5.1520	6.2470	5.2470
6.0000	11.0000	0.2690	0.2650	0.2650
6.0000	12.0000	0.1680	0.1670	0.1670
6.0000	13.0000	0.4940	0.4860	0.4860
7.0000	8.0000	1.1110	1.1460	1.1460
7.0000	9.0000	1.0500	1.0730	1.0500
9.0000	10.0000	0.0200	0.0280	0.0200
9.0000	14.0000	0.2040	0.2120	0.2020
10.0000	11.0000	0.1390	0.1330	0.1320
12.0000	13.0000	0.0100	0.0100	0.0100
13.0000	14.0000	0.2280	0.2220	0.2220

IEEE30 bus

From-Bus	To-Bus	RPL(without)	RPL(ACO)	RPL(AACO)
1.0000	2.0000	16.3620	6.4790	4.4329
1.0000	3.0000	11.5060	7.0560	5.5006
2.0000	4.0000	3.3718	3.1450	3.2245
2.0000	5.0000	62.0440	58.8760	57.0890
2.0000	6.0000	5.7961	5.7000	5.7890
3.0000	4.0000	0.4810	0.4110	0.6741
4.0000	6.0000	2.1020	1.9870	2.2117
4.0000	12.0000	9.2030	8.9530	9.7453
5.0000	7.0000	0.5630	0.5110	0.5015
6.0000	7.0000	2.2520	2.1560	2.4501
6.0000	8.0000	0.0790	0.0710	0.0820
6.0000	9.0000	0.8090	0.8070	0.8879
6.0000	10.0000	3.8120	3.8040	3.9844
6.0000	28.0000	0.1240	0.1260	0.1264
8.0000	28.0000	0.0006	0.0002	0.0006
9.0000	10.0000	0.6350	0.6330	0.6443
9.0000	11.0000	0.3060	0.3280	0.4328
10.0000	17.0000	0.0220	0.0320	0.0202
10.0000	20.0000	0.1850	0.1850	0.1825
10.0000	21.0000	0.0480	0.0490	0.0494
10.0000	22.0000	0.0860	0.0880	0.0887
12.0000	13.0000	0.0680	0.1100	0.1182
12.0000	14.0000	0.3030	0.3190	0.3129

12.0000	15.0000	0.8260	0.8300	0.8608
12.0000	16.0000	0.1072	0.1080	0.1183
14.0000	15.0000	0.0250	0.0280	0.0281
15.0000	18.0000	0.2360	0.2460	0.2496
15.0000	23.0000	0.0850	0.0925	0.0955
16.0000	17.0000	0.2110	0.2436	0.2446
18.0000	19.0000	0.0060	0.0031	0.0071
19.0000	20.0000	0.0110	0.0080	0.0110
21.0000	22.0000	0.0007	0.0006	0.0001
22.0000	24.0000	0.0385	0.0340	0.0403
23.0000	24.0000	0.0074	0.0090	0.0097
24.0000	25.0000	0.0224	0.0238	0.0276
25.0000	26.0000	0.0923	0.0950	0.0945
25.0000	27.0000	0.0245	0.0232	0.0220
27.0000	28.0000	0.6362	0.6309	0.6390
27.0000	29.0000	0.1485	0.1510	0.1510
27.0000	30.0000	1.0863	1.0670	1.0770
29.0000	30.0000	0.5860	0.5770	0.5670

NOTE: PL=power Loss, RPL=Real power loss, ACO=Ant colony optimization, AACO=Adaptive ant colony optimization

VI. CONCLUSIONS

The reconfiguration of distribution network is assuming significant importance in the context of modern distribution systems. In this paper, a new codification for the population based meta-heuristic techniques to solve reconfiguration problem of distribution networks is presented. In the proposed method, the topological concepts of *loop vectors*, *common branch vectors* and *prohibited group vectors* have been introduced with the help of graph theory and some rules are framed to avoid generation of infeasible individuals during each stage of the proposed AACO. Several parameter of the conventional ACO are redefined in the context of the reconfiguration of the distribution networks. Moreover, the proposed method incorporates the advantages of heuristics to increase the pace of the search techniques without losing diversity. The objective function for loss minimization is optimized using AACO. The proposed method has been extended on three different IEEE-33,70 and 135 BUS distribution networks. The simulation results show that the method provides a promising tool for reconfiguration problem of distribution network and can be extended to incorporate multi-objective problem without any significant computational burden

REFERENCES

- [1] A. Merlin and H. Back, "Search for a minimum-loss operating spanning tree configuration in an urban power distribution", Proc. 5th Power System Computation Conf., Cambridge, U.K., pp. 1-18, 1975.
- [2] S. Civanlar, J. J. Grainger, H. Yin and S. S. H. Lee, "Distribution feeder reconfiguration for loss reduction", IEEE Trans. Power Delivery, vol. 3, pp. 1217-1223, 1988.
- [3] D. Shirmohammadi and W. H. Hong, "Reconfiguration of electric distribution networks for resistive line loss reduction", IEEE Trans. Power Delivery, vol. 4 (1), pp. 1492-1498, 1989.
- [4] S. K. Goswami and S. K. Basu, "A New algorithm for the reconfiguration of distribution feeders for loss minimization", IEEE Trans. Power Delivery, vol. 7 (3), pp. 1482-1491, 1992.
- [5] M. E. Baran and F. F. Wu, "Network reconfiguration in distribution systems for loss reduction and load balancing", IEEE Trans. Power Delivery, vol. 4 (2), pp. 1401-1407, 1989.
- [6] J. A. Martín and A. J. Gil, "A new heuristic approach for distribution systems loss reduction", Electric Power Systems Research, vol. 78, (11), pp. 1953-1958, Nov. 2008.
- [7] V. N. Gohokar, M. K. Khedkar and G. M. Dhole, "Formulation of distribution reconfiguration problem using network topology: a generalized approach", Electric Power Systems Research, vol. 69 (2-3), pp. 304-310, May 2004.
- [8] K. Nara, A. Shiose, M. Kiagawa and T. Ishihara, "Implementation of genetic algorithm for distribution system loss minimum reconfiguration", IEEE Trans. Power Systems, vol. 7 (3), pp. 1044-1051, 1992.
- [9] M. Lin, F. S. Cheng, and M. T. Tsay, "Distribution feeder reconfiguration with refined genetic algorithm", IEE Proc. Generation Transmission and Distribution, 147, pp. 349-354, 2000.
- [10] J. Z. Zhu, "Optimal reconfiguration of electric distribution network using refined genetic algorithm", Electrical Power System Research, vol. 62, pp. 37-42, 2002.
- [11] Y. Y. Hong and S. Y. Ho, Determination of network configuration considering multiobjective in distribution systems using genetic algorithms, IEEE Trans. on Power System, vol. 20 (2), pp. 1062-1069, May 2005.
- [12] K. Prasad, R. Ranjan, N. C. Sahoo and A. Chaturvedi, "Optimal configuration of radial distribution system using fuzzy mutated genetic algorithm", IEEE Trans. on Power Delivery, vol. 20 (2), pp. 1211-1213, 2005.
- [13] J. Mendoza, R. Lopez, D. Morales, E. Lopez, P. Dessante and R. Moraga, "Minimal loss reconfiguration using genetic algorithms with restricted population and addressed operators: real application", IEEE Trans. on Power Systems, vol. 21 (2), pp. 948-954, May 2006.
- [14] B. Enacheanu, B. Raison, R. Caire, O. Devaux, W. Bienia and N. HadjSaid, "Radial Network Reconfiguration Using Genetic Algorithm Based on the Matroid Theory", IEEE Trans. on Power Systems, vol. 23 (1), pp. 186-195, Feb. 2008,
- [15] C. H. Lin, C. S. Chen, C. J. Wu and M. S. Kang, "Application of immune algorithm to optimal switching operation for distribution loss minimization and load balance", IEE Proc. Generation Transmission and Distribution, vol. 150 (2), pp. 183-189, 2003.
- [16] A. C. B. Delbem, A. C. Pd L. F. Carvalho and N. G. Bretas, "Main chain representation of evolutionary algorithms applied to distributionsystem reconfiguration", IEEE Trans. on Power System, vol. 20 (1), pp. 425- 436, Feb. 2005.

A Novel Bidirectional DC-DC Converter with Battery Protection

Srinivas Reddy Gurrula¹, K.Vara Lakshmi²

¹(PG Scholar Department of EEE, Teegala Krishna Reddy Engineering college, JNTU- Hyd, AP, INDIA)

² (Assistant professor Department of EEE, Teegala Krishna Reddy engineering college, JNTU-Hyd, AP, INDIA)

ABSTRACT: This paper presents the implementation of a bidirectional dc-dc converter to protect a battery from overcharging and undercharging. The proposed converter circuit provides low voltage stresses across the switches, higher step-up and step-down voltage gains and efficiency is also high when compared to conventional boost/buck converter. The proposed control circuit controls the charging and discharging of the battery. The operating principle and steady state analysis for the step-up and step-down modes are discussed only in continuous conduction mode. Finally, 13/39-V prototype circuit is implemented to verify the performance of proposed converter.

Keywords: Battery, Bidirectional dc-dc converter, coupled inductor.

I. INTRODUCTION

BIDIRECTIONAL dc-dc converters are used to transfer the power between two dc sources in either direction. These converters are widely used in applications, such as hybrid electric vehicle energy systems, uninterrupted power supplies, fuel-cell hybrid power systems, photovoltaic hybrid power systems, and battery chargers. Many bidirectional dc-dc converters have been researched. The bidirectional dc-dc flyback converters are more attractive due to simple structure and easy control [2], [10]. However, these converters suffer from high voltage stresses on the power devices due to the leakage inductor energy of the transformer. In order to recycle the leakage inductor energy and to minimize the voltage stress on the power devices, some literatures present the energy regeneration techniques to clamp the voltage stress on the power devices and to recycle the leakage inductor energy [11], [12]. Some literatures research the isolated bidirectional dc-dc converters, which include the half bridge [5], [6] and full-bridge types [9]. These converters can provide high step-up and step-down voltage gain by adjusting the turns ratio of the transformer.

For non-isolated applications, the non-isolated bidirectional dc-dc converters, which include the conventional boost/buck [1], [4], [8], multilevel [3], three-level [7], sepic/zeta [16], switched capacitor [17], and coupled inductor types [18], are presented. The multilevel type is a magnetic-less converter, but 12 switches are used in this converter. If higher step-up and step-down voltage gains are required, more switches are needed.

The total system is useful to avoid the damage to the life of the Batteries. Because of overcharging and undercharging batteries will produce hot spots inside the battery such that the batteries not survive for long time. The following sections will describe the operating principles and steady-state analysis for the step-up and step-down modes in continuous conduction mode only. In

order to analyze the steady-state characteristics of the proposed converter, some conditions are assumed: The ON-state resistance $R_{DS(ON)}$ of the switches and the equivalent series resistances of the coupled inductor and capacitors are ignored; the capacitor is sufficiently large; and the voltages across the capacitor can be treated as constant.

II. CIRCUIT CONFIGURATION AND STEADY STATE ANALYSIS

A. STEP-UP MODE

Fig. 1 shows the conventional bidirectional dc-dc boost/buck converter. The proposed converter in step-up mode is shown in Fig. 2. The pulse-width modulation (PWM) technique is used to control the switches S_1 and S_2 simultaneously. The switch S_3 is the synchronous rectifier.

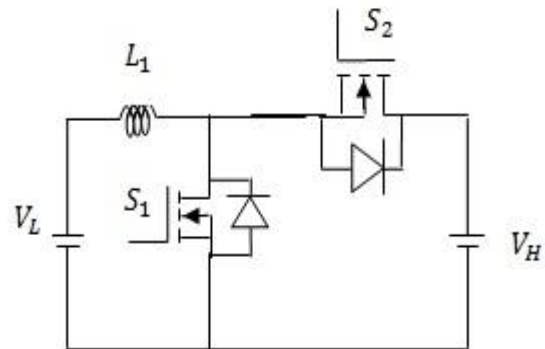


Fig1. Conventional bidirectional DC-DC boost/buck converter

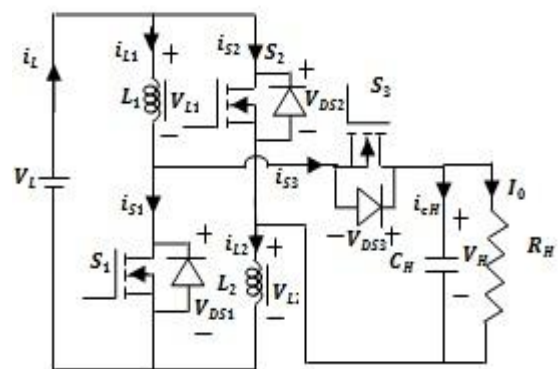


Fig.2. Proposed converter in step-up mode

Since the primary and secondary winding turns of the coupled inductor is same, the inductance of the coupled inductor in the primary and secondary sides are expressed as

$$L_1 = L_2 = L \quad (1)$$

Thus, the mutual inductance M of the coupled inductor is given by

$$M = k\sqrt{L_1 L_2} = kL \quad (2)$$

where k is the coupling coefficient of the coupled inductor. The voltages across the primary and secondary windings of the coupled inductor are as follows:

$$v_{L1} = L_1 \frac{di_{L1}}{dt} + M \frac{di_{L2}}{dt} = L \frac{di_{L1}}{dt} + kL \frac{di_{L2}}{dt} \quad (3)$$

$$v_{L2} = M \frac{di_{L1}}{dt} + L_2 \frac{di_{L2}}{dt} = kL \frac{di_{L1}}{dt} + L \frac{di_{L2}}{dt} \quad (4)$$

Fig. 3 shows some typical waveforms in continuous conduction mode (CCM). The operating principles and steady-state analysis of CCM is described as follows.

1) *Mode 1*: During this time interval $[t_0, t_1]$, S_1 and S_2 are turned on and S_3 is turned off. The energy of the low-voltage side V_L is transferred to the coupled inductor. Meanwhile, the primary and secondary windings of the coupled inductor are in parallel. The energy stored in the capacitor C_H is discharged to the load. Thus, the voltages across L_1 and L_2 are obtained as

$$v_{L1} = v_{L2} = V_L \quad (5)$$

Substituting (3) and (4) into (5), yielding

$$\frac{di_{L1}(t)}{dt} = \frac{di_{L2}(t)}{dt} = \frac{V_L}{(1+k)L}, \quad t_0 \leq t \leq t_1 \quad (6)$$

2) *Mode 2*: During this time interval $[t_1, t_2]$, S_1 and S_2 are turned off and S_3 is turned on. The low-voltage side V_L and the coupled inductor are in series to transfer their energies to the capacitor C_H and the load. Meanwhile, the primary and secondary windings of the coupled inductor are in series. Thus, the following equations are found to be

$$i_{L1} = i_{L2} \quad (7)$$

$$v_{L1} + v_{L2} = V_L - V_H \quad (8)$$

Substituting (3), (4), and (7) into (8), yielding

$$\frac{di_{L1}(t)}{dt} = \frac{di_{L2}(t)}{dt} = \frac{V_L - V_H}{2(1+k)L}, \quad t_1 \leq t \leq t_2 \quad (9)$$

By using the state-space averaging method, the following equation is derived from (6) and (9):

$$\frac{DV_L}{(1+k)L} + \frac{(1-D)(V_L - V_H)}{2(1+k)L} = 0 \quad (10)$$

Simplifying (10), the voltage gain is given as

$$G_{CCM(step-up)} = \frac{V_H}{V_L} = \frac{1+D}{1-D} \quad (11)$$

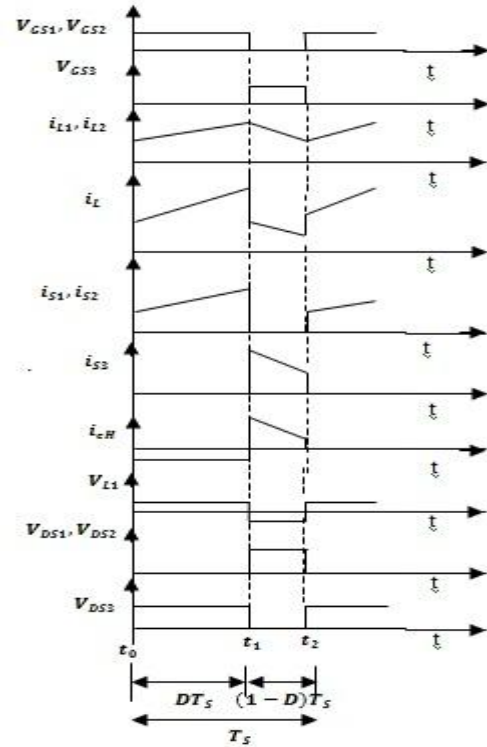


Fig.3. waveforms of proposed converter in step-up mode in CCM mode of operation

B. STEP-DOWN MODE

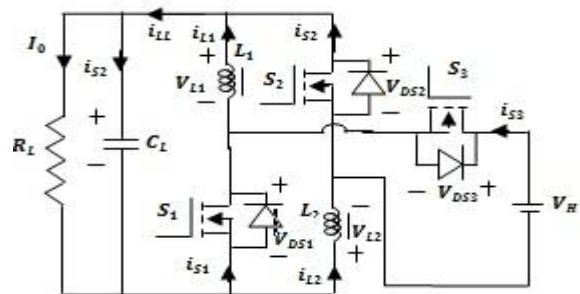


Fig.4. Proposed converter in step-down mode

Fig. 4 shows the proposed converter in step-down mode. The PWM technique is used to control the switch S_3 . The switches S_1 and S_2 are the synchronous rectifiers. Fig. 5 shows some typical waveforms in CCM. The operating principle and steady-state analysis of CCM is described as follows.

1) *Mode 1*: During this time interval $[t_0, t_1]$, S_3 is turned on and S_1/S_2 are turned off. The energy of the high-voltage side V_H is transferred to the coupled inductor, the capacitor C_L , and the load. Meanwhile, the primary and secondary windings of the coupled inductor are in series. Thus, the following equations are given as:

$$i_{L1} = i_{L2} \quad (12)$$

$$v_{L1} + v_{L2} = V_H - V_L \quad (13)$$

Substituting (3), (4), and (12) into (13), yielding

$$\frac{di_{L1}(t)}{dt} = \frac{di_{L2}(t)}{dt} = \frac{V_H - V_L}{2(1+k)L}, \quad t_0 \leq t \leq t_1 \quad (14)$$

2) *Mode 2*: During this time interval $[t_1, t_2]$, S_3 is turned off and S_1/S_2 are turned on. The energy stored in the coupled inductor is released to the capacitor C_L and the load. Meanwhile, the primary and secondary windings of the coupled inductor are in parallel. Thus, the voltages across L_1 and L_2 are derived as

$$v_{L1} = v_{L2} = -V_L \quad (15)$$

Substituting (3) and (4) into (15), yielding

$$\frac{di_{L1}(t)}{dt} = \frac{di_{L2}(t)}{dt} = -\frac{V_L}{(1+k)L}, \quad t_1 \leq t \leq t_2 \quad (16)$$

By using the state space averaging method, the following equation is obtained from (14) and (16):

$$\frac{D(V_H - V_L)}{2(1+k)L} - \frac{(1-D)V_L}{(1+k)L} = 0 \quad (17)$$

Simplifying (17), the voltage gain is found to be

$$G_{CCM(step-down)} = \frac{V_L}{V_H} = \frac{D}{2-D} \quad (18)$$

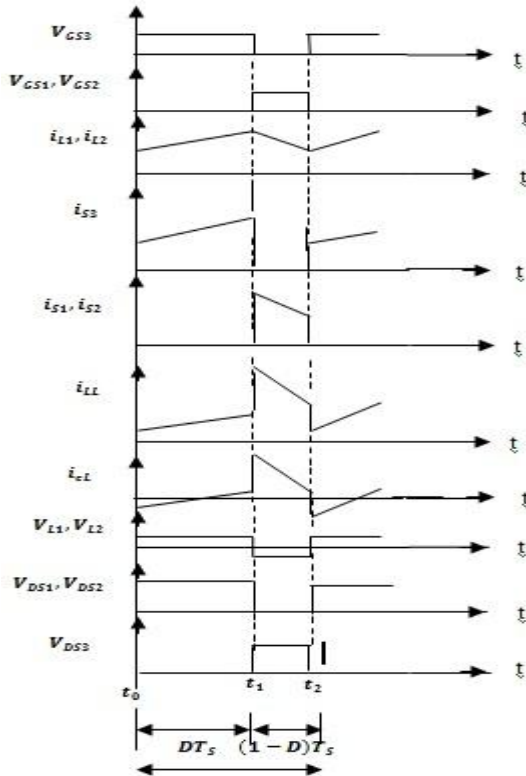


Fig.5. waveforms of proposed converter in step-down mode in CCM mode of operation

III. ANALYSIS OF BATTERY PROTECTION

The basic model of a battery is shown in the fig.6.

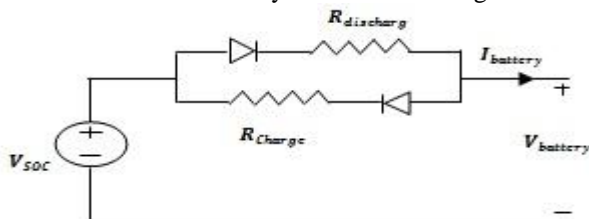


Fig.6. basic model of a battery

With the current flow in the battery there is some resistive drop in electrodes and resistance offered to the movement of ions, are modeled as electrical resistances here.

Battery capacity is defined as the current that discharges in 1hour. So the battery capacity should be in Ampere-hours. In practice the relationship between battery capacity and discharge current is not linear.

Peukert's Law relates battery capacity to discharge rate:

$$C = I^k t \quad (19)$$

where C is the battery capacity, I is the discharge current, t is the discharge time, k is the Peukert coefficient, typically 1.1 to 1.3.

The output voltage of the bidirectional dc-dc converter is connected to the three Lead-Acid batteries which are connected in series.

Table-1: charge limits of a 12V battery

	Fully charged	Discharged completely
State of charge	100%	0%
Voltage	12.7V	11.6V

Let a single battery fully charged voltage is V_1 and completely discharged voltage will be V_2 . Here three batteries of V_1 each are connected in series so that the fully charge voltage ($3 \times V_1$) V is the overcharged voltage. Similarly ($3 \times V_2$) V is the undercharged voltage.

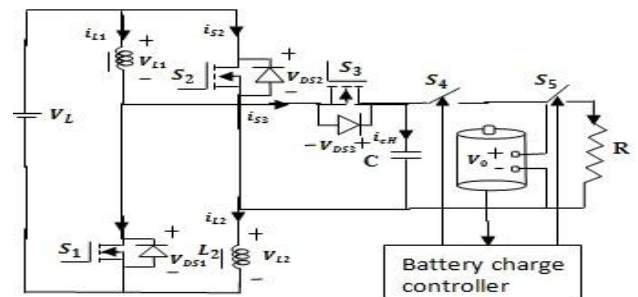


Fig.7. Battery charge controller in step-up mode

Initially S_4 and S_5 both switches are in closed condition. Whenever the voltage across batteries is greater than or equal to ($3 \times V_1$) V, switch S_4 will open. Under this condition load will fed from the batteries. Means under overcharged condition supply to batteries and load from the bidirectional dc-dc converter is disconnected. While discharging if the voltage across the batteries is less than or equal to ($3 \times V_2$) V switch S_5 will open.

The total system is useful to avoid the damage to the life of batteries. Because of overcharging and undercharging batteries will not survive for long time.

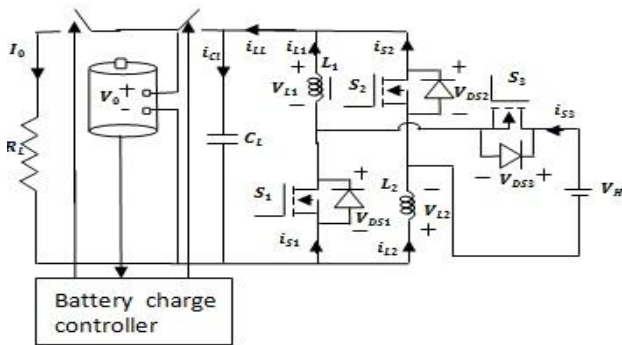


Fig.8.Battery charge controller in step-down mode

The output voltage of the bidirectional dc-dc converter is connected to a single Lead-Acid battery. The output voltage across the battery is limited by the battery charge controller so that controlling the charging and discharging of the battery. The operation principle is same as in step-up mode.

IV. EXPERIMENTAL RESULTS

Simulation of novel bidirectional dc-dc converter with battery protection was performed by using MATLAB SIMULINK to confirm the above analysis. The electric specifications and circuit components are selected as $V_L = 13$ V, $V_H = 39$ V, $f_s = 50$ kHz, $P_0 = 200$ W, $C_L = C_H = 330$ μ F, $L_1 = L_2 = 15.5$ μ H ($r_{L1} = r_{L2} = 11$ m Ω). Also, MOSFET IRF3710 ($V_{DS} = 100$ V, $R_{DS(ON)} = 23$ m Ω , and $I_D = 57$ A) is selected for S_1, S_2 and S_3 .

Some experimental results in step-up mode are shown in Figs. 9-15. Fig.9 shows the waveform of the output voltage across the battery. It shows that the voltage across the battery is limited in the range of overcharging and undercharging levels. Fig.10 shows the waveform of the input current. Figs.11 and 12 and 13 show the switch currents across the switches. Fig. 14 shows the waveform of the coupled-inductor i_{L1} and fig.15 shows the coupled-inductor current i_{L2} . The source current is double of the level of the coupled-inductor current during S_1/S_2 ON-period and equals the coupled-inductor current during S_1/S_2 OFF-period. It can be observed that i_{L1} is equal to i_{L2} . The source current equals to the coupled-inductor current during S_3 ON-period and is double of the level of the coupled-inductor current during S_3 OFF-period. Fig.16 shows the output voltage across the battery.

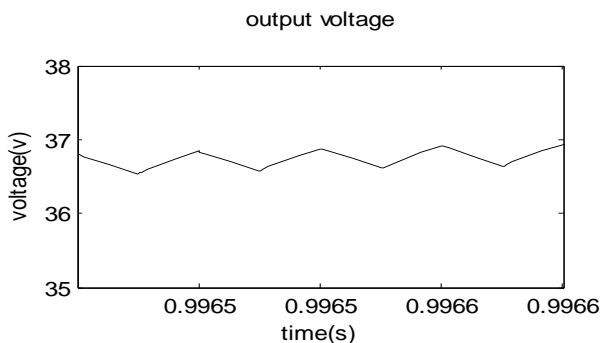


Fig.9. simulation result for the output voltage

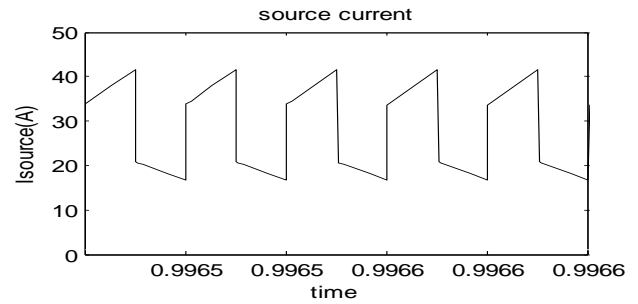


Fig.10. simulation waveform for the source current

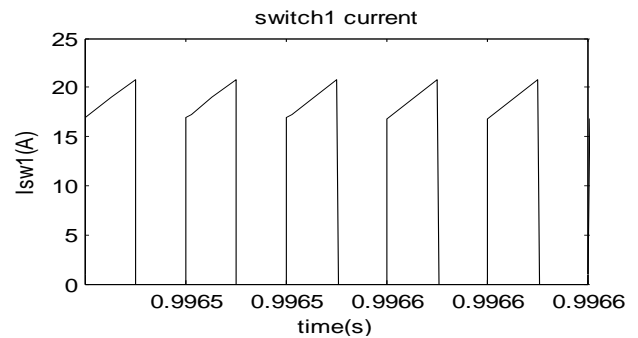


Fig.11. simulation result for the switch1 current

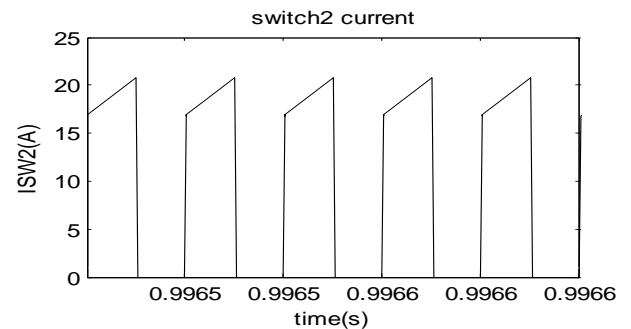


Fig.12. simulation result for the switch2 current

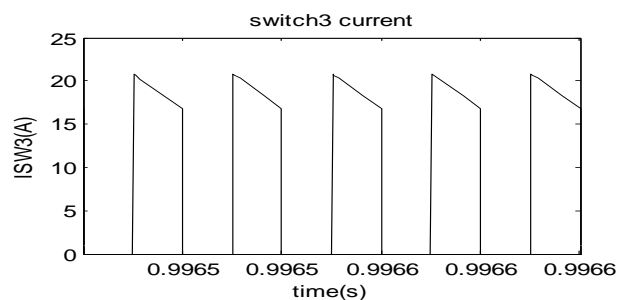


Fig.13. simulation result for the switch3 current

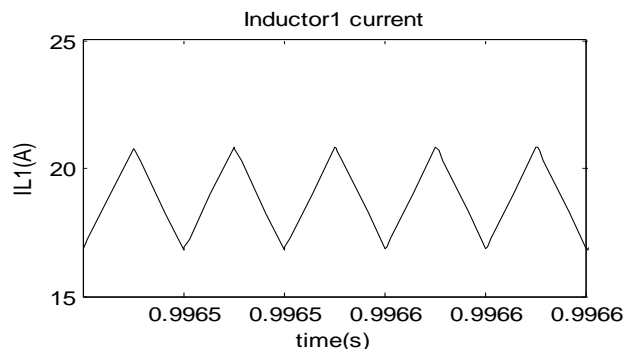


Fig.14. simulation result for the coupled inductor1 current

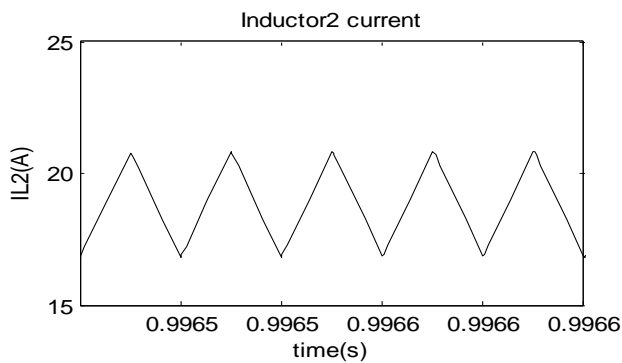


Fig.15. simulation result for the coupled inductor2 current

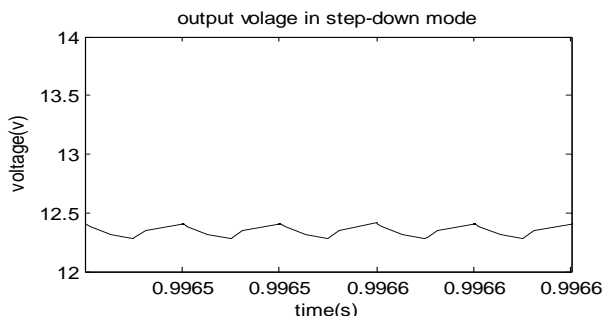


Fig.16. simulation result for the coupled inductor2 current

V. CONCLUSION

In this paper, a novel bidirectional dc–dc converter with battery protection is proposed. The circuit configuration of the proposed converter is very simple. The operation principle, including the operation modes and steady-state analysis is explained in detail. The proposed converter has higher step-up and step-down voltage gains and lower average value of the switch current than the conventional bidirectional boost/buck converter. From the experimental results, it is seen that the experimental waveforms agree with the operating principle and steady-state analysis.

REFERENCES

- [1] M. B. Camara, H. Gualous, F. Gustin, A. Berthon, and B. Dakyo, "DC/DC converter design for supercapacitor and battery power management in hybrid vehicle applications—Polynomial control strategy," *IEEE Trans. Ind. Electron.*, vol. 57, no. 2, pp. 587–597, Feb. 2010.
- [2] T. Bhattacharya, V. S. Giri, K. Mathew, and L. Umanand, "Multiphase bidirectional flyback converter topology for hybrid electric vehicles," *IEEE Trans. Ind. Electron.*, vol. 56, no. 1, pp. 78–84, Jan. 2009.
- [3] F. Z. Peng, F. Zhang, and Z. Qian, "A magnetic-less dc–dc converter for dual-voltage automotive systems," *IEEE Trans. Ind. Appl.*, vol. 39, no. 2, pp. 511–518, Mar./Apr. 2003.
- [4] A. Nasiri, Z. Nie, S. B. Bekiarov, and A. Emadi, "An on-line UPS system with power factor correction and electric isolation using BIFRED converter," *IEEE Trans. Ind. Electron.*, vol. 55, no. 2, pp. 722–730, Feb. 2008.
- [5] G. Ma, W. Qu, G. Yu, Y. Liu, N. Liang, and W. Li, "A zero-voltage-switching bidirectional dc–dc converter with state analysis and soft-switching-oriented design consideration," *IEEE Trans. Ind. Electron.*, vol. 56, no. 6, pp. 2174–2184, Jun. 2009.
- [6] F. Z. Peng, H. Li, G. J. Su, and J. S. Lawler, "A new ZVS bidirectional dc–dc converter for fuel cell and battery application," *IEEE Trans. Power Electron.*, vol. 19, no. 1, pp. 54–65, Jan. 2004.
- [7] K. Jin, M. Yang, X. Ruan, and M. Xu, "Three-level bidirectional converter for fuel-cell/battery hybrid power system," *IEEE Trans. Ind. Electron.*, vol. 57, no. 6, pp. 1976–1986, Jun. 2010.
- [8] Z. Liao and X. Ruan, "A novel power management control strategy for stand-alone photovoltaic power system," in *Proc. IEEE IPEMC*, 2009, pp. 445–449.
- [9] S. Inoue and H. Akagi, "A bidirectional dc–dc converter for an energy storage system with galvanic isolation," *IEEE Trans. Power Electron.*, vol. 22, no. 6, pp. 2299–2306, Nov. 2007.
- [10] K. Venkatesan, "Current mode controlled bidirectional flyback converter," in *Proc. IEEE Power Electron. Spec. Conf.*, 1989, pp. 835–842.
- [11] G. Chen, Y. S. Lee, S. Y. R. Hui, D. Xu, and Y. Wang, "Actively clamped bidirectional flyback converter," *IEEE Trans. Ind. Electron.*, vol. 47, no. 4, pp. 770–779, Aug. 2000.
- [12] F. Zhang and Y. Yan, "Novel forward-flyback hybrid bidirectional dc–dc converter," *IEEE Trans. Ind. Electron.*, vol. 56, no. 5, pp. 1.
- [13] H. Li, F. Z. Peng, and J. S. Lawler, "A natural ZVS medium-power bidirectional dc–dc converter with minimum number of devices," *IEEE Trans. Ind. Appl.*, vol. 39, no. 2, pp. 525–535, Mar. 2003.
- [14] B. R. Lin, C. L. Huang, and Y. E. Lee, "Asymmetrical pulse-width modulation bidirectional dc–dc converter," *IET Power Electron.*, vol. 1, no. 3, pp. 336–347, Sep. 2008.
- [15] Y. Xie, J. Sun, and J. S. Freudenberg, "Power flow characterization of a bidirectional galvanically isolated high-power dc/dc converter over a wide operating range," *IEEE Trans. Power Electron.*, vol. 25, no. 1, pp. 54–66, Jan. 2010.
- [16] I. D. Kim, S. H. Paeng, J. W. Ahn, E. C. Nho, and J. S. Ko, "New bidirectional ZVS PWM sepic/zeta dc–dc converter," in *Proc. IEEE ISIE*, 2007, pp. 555–560.
- [17] Y. S. Lee and Y. Y. Chiu, "Zero-current-switching switched-capacitor bidirectional dc–dc converter," *Proc. Inst. Elect. Eng.—Elect. Power Appl.*, vol. 152, no. 6, pp. 1525–1530, Nov. 2005.
- [18] R. J. Wai and R. Y. Duan, "High-efficiency bidirectional converter for power sources with great voltage diversity," *IEEE Trans. Power Electron.*, vol. 22, no. 5, pp. 1986–1996, Sep. 2007.
- [19] L. S. Yang, T. J. Liang, and J. F. Chen, "Transformerless dc–dc converters with high step-up voltage gain," *IEEE Trans. Ind. Electron.*, vol. 56, no. 8, pp. 3144–3152, Aug. 2009.

Nonlinear Control of UPFC in Power System for Damping Inter Area Oscillations

¹M.Praveen Kumar, ²P B Chennaiah

¹EEE,M.Tech student, AITS, Rajampet, Kadapa , A.P, India,

²EEE, Associate Professor, AITS, Rajampet, Kadapa, A.P, India,

Abstract: This paper introduces a new nonlinear control of flexible ac transmission systems (FACTS) controllers for the purpose of damping interarea oscillations in power systems. FACTS controllers consist of series, shunt, or a combination of series-shunt devices which are interfaced with the bulk power system through injection buses. Controlling the angle of these buses can effectively damp low frequency interarea oscillations in the system. The proposed control method is based on finding an equivalent reduced affine nonlinear system for the network from which the dominant machines are extracted based on dynamic coherency. It is shown that if properly selected, measurements obtained from this subsystem of machines are sufficient inputs to the FACTS controllers to stabilize the power system. The effectiveness of the proposed method on damping interarea oscillations is validated on the 68 bus, 16 generator system of the New England/New York network.

IndexTerms: Coherent groups, dominant machines, flexible ac transmission systems (FACTS), interarea oscillation, nonlinear control, phasor measurement unit (PMU), wide-area control.

I. INTRODUCTION

AS high voltage power electronics become less expensive and have a wider-range of operation, flexible ac transmission systems (FACTS) controllers will become more prevalent in the transmission system to control active power flow across congested corridors and ensure voltage security. In addition, FACTS controllers can provide promising solutions to many of the stability problems that occur within the bulk power system. FACTS controllers can be categorized into three major groups: shunt devices such as the Static Synchronous Compensator (STATCOM), series devices such as the static synchronous series compensator (SSSC) and series shunt devices such as the unified power flow controller (UPFC). In addition to steady-state solutions such as power flow and voltage control, an added benefit of FACTS controllers deployed in the transmission system is that they can also effectively Control active power oscillations that can damage generators, increase line losses, and increase wear and tear on network components.

Therefore developing suitable control strategies is a requirement before FACTS can be confidently utilized in the power system. Several authors have investigated utilizing FACTS, especially UPFCs to damp interarea oscillations using a variety of control approaches [1]–[10]. Interarea oscillations can occur in a system because of contingencies such as sudden load changes or faults. In [1]–[5], oscillation damping is based on a linear control approach to the UPFC and power system, whereas other authors consider nonlinear control systems theory and Lyapunov Energy Functions [6]–[10]. Typically, nonlinear approaches are more effective for large perturbations or when the power system state strays significantly from the initial operating point.

The approach proposed in this paper provides a general nonlinear method for using multiple FACTS controllers in a power network for the purpose of damping interarea oscillations. In this paper, it is shown that any FACTS device capable of changing its interface bus angle(s) with the network can be used to mitigate power system oscillations. Using this method, it will be shown that both shunt and series FACTS controllers can be used for this purpose. The control method is based on finding a reduced nonlinear affine state space system for the network which can be controlled by feedback of selected measurements of rotor frequencies. While frequency measurements (such as from FNET [11]) have made wide area control of the power networks feasible, it is still not reasonable to expect that the full set of frequency measurements is available for controller use. Therefore, an approach is proposed to use a reduced set of measurements from a subset of machines in the system.

II. UPFC MODEL

The UPFC is the most versatile FACTS device. It consists of a combination of a shunt and series branches connected through the DC capacitor as shown in Fig. 1. Models for the STATCOM and SSSC can be easily extracted from the UPFC model by considering the shunt and series converters individually. The series connected inverter injects a voltage with controllable magnitude and phase angle in series with the transmission line, therefore providing active and reactive power to the transmission line. The shunt-connected inverter

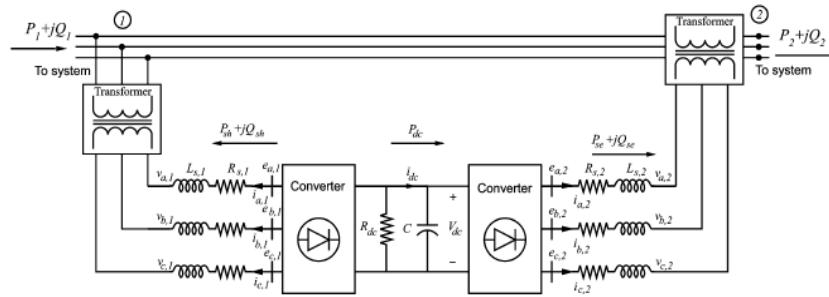


Fig. 1. Unified power flow controller diagram.

Provides the active power drawn by the series branch plus the losses and can independently provide reactive compensation to the system. The UPFC model is given by [12] as shown in (1)–(5) at the bottom of the next page, where the parameters are as shown in Fig. 1. The currents i_{d1} and i_{q1} are the dq components of the shunt current. The currents i_{d2} and i_{q2} are the dq components of the series current. The voltages $V_1 \angle \theta_1$ and $V_2 \angle \theta_2$ are the sending end and receiving end voltage magnitudes and angles, respectively. The UPFC is controlled by varying the phase angles (α_1, α_2) and (k_1, k_2) magnitudes of the converter shunt and series output voltages (e_1, e_2), respectively.

The power balance equations at bus 1 are given by

$$0 = V_1 \left((i_{d1} - i_{d2}) \cos \theta_1 + (i_{q1} - i_{q2}) \sin \theta_1 \right) - V_1 \sum_{j=1}^n V_j Y_{1j} \cos(\theta_1 - \theta_j - \phi_{1j}) \quad (1)$$

$$0 = V_1 \left((i_{d1} - i_{d2}) \sin \theta_1 - (i_{q1} - i_{q2}) \cos \theta_1 \right) - V_1 \sum_{j=1}^n V_j Y_{1j} \sin(\theta_1 - \theta_j - \phi_{1j}) \quad (2)$$

and at bus 2

$$0 = V_2 \left(i_{d2} \cos \theta_2 + i_{q2} \sin \theta_2 \right) - V_2 \sum_{j=1}^n V_j Y_{2j} \cos(\theta_2 - \theta_j - \phi_{2j}) \quad (3)$$

$$0 = V_2 \left(i_{d2} \sin \theta_2 + i_{q2} \cos \theta_2 \right) - V_2 \sum_{j=1}^n V_j Y_{2j} \sin(\theta_2 - \theta_j - \phi_{2j}) \quad (4)$$

III. SYSTEM MODEL

For control development purposes, several initial assumptions are made. The first assumption is that the system loads are modeled as constant impedance loads and can therefore be absorbed into the bus admittance matrix. Second, the generators are modeled as the classical “transient reactance behind constant voltage” model. Note that these assumptions are for control development *only*—the proposed control is validated with the full nonlinear 10-th order power system model given in the Appendix [13]. In addition, the proposed control is developed for the UPFC; control development for the STATCOM and SSSC follows a similar procedure and is therefore not explicitly detailed.

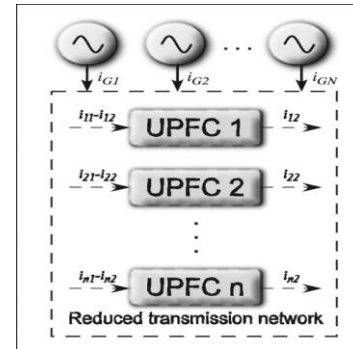


Fig. 2. Equivalent power system from the controller viewpoint.

Using the load impedance model, the only points of current injection into the network are the generator internal buses and the UPFC sending and receiving end buses. Using Kron reduction, the transmission network can be reduced to an admittance matrix of size $(N + n \times N + n)$ where N is the number of generator buses and n is the number FACTS current injections in the system. Fig. 2 illustrates the reduced system showing the points of current injection. Each UPFC has two current injections i_1 and i_2 , at the sending and receiving ends, respectively; a STATCOM and SSSC have only one current. The generator current injections are given by i_G .

The classical model for the reduced network including the UPFCs.

Mechanical power, inertia constant and angular speed, respectively, of machine; and is synchronous speed. The summation represents the active power injected at each current injection point, including FACTS buses.

IV. CONTROLLER DESIGN

The controller design consists of three stages.

A. Stage I

The objective of the first design stage is to find the desired changes in mechanical powers required to stabilize the system. To obtain the amount of mechanical power required, it is initially assumed that the mechanical powers PM_j are inputs into the system model. Note that this is *only* for controller development; in the final control, it is not required that the generator mechanical powers actually vary.

Under this assumption, the system models are

$$\dot{x} = F(x) + GU \quad (5)$$

where as shown in (13)–(15) at the bottom of the page and $x = [\delta_1 \omega_1 \delta_2 \omega_2 \dots \delta_N \omega_N]$.

Since it is only required that the system frequencies return to steady-state rapidly, a subset of (12) is

$$\dot{x} = f(x_1) + gu \quad \dots\dots\dots(6)$$

where $x_1 = [\delta_1 \delta_2 \dots \delta_N]$ and $x_2 = [\omega_1 \omega_2 \dots \omega_N]$

$$f(x_1) = \begin{bmatrix} -\frac{1}{M_1} E_1 \sum_{k=1}^{N+n} E_k Y_{1k} \cos(\delta_1 - \delta_k - \phi_{1k}) \\ \vdots \\ -\frac{1}{M_N} E_N \sum_{k=1}^{N+n} E_k Y_{Nk} \cos(\delta_N - \delta_k - \phi_{Nk}) \end{bmatrix} \quad \dots\dots\dots(7)$$

$$g = \begin{bmatrix} \frac{1}{M_1} & \dots & 0 \\ \vdots & \ddots & \vdots \\ 0 & \dots & \frac{1}{M_1} \end{bmatrix} \quad \dots\dots\dots(8)$$

$$u = [Pm_1 Pm_2 \dots Pm_n]$$

Letting x_{1s} , x_{2s} , and u_s denote the steady-state values of x_1 , x_2 and u , respectively, then the error in generator rotor frequencies becomes

$$e = x_2 - x_{2s} \quad \dots\dots\dots(9)$$

and

$$\dot{e} = f(x) - f(x_{1s}) - gu_s + g u_d \quad \dots\dots\dots(10)$$

Equation (21) can be stabilized with input u_d so that

$$u_d = g^{-1} [-f(x_1) + f(x_{1s}) - gu_s + Ke] \quad \dots\dots\dots(11)$$

where K is a positive definite matrix and

$$\dot{e} = -Ke \quad \dots\dots\dots(12)$$

B. Stage II

In Stage I, the required changes in the generator's mechanical powers were found that stabilize the system. In Stage II, these changes are translated into control signals to the FACTS controllers. As noted previously, the generator mechanical powers do not actually change as a consequence of the proposed control. Therefore, using the desired active power changes, a new control signal is introduced

$$\Delta u = u_{desired} - u_{actual} \quad \dots\dots\dots(13)$$

Where $u_{desired}$ and u_{actual} are the desired and actual values for the generator mechanical powers. This mismatch is translated into the desired changes in the FACTS' bus voltage angles, as shown in (25) at the bottom of the page, where

$$L = [L_1, \dots, L_N]^T$$

$$\bar{\Delta} = [\Delta\delta_1, \dots, \Delta\delta_n]^T$$

The nonlinear system is solved numerically for $\bar{\Delta}$. Note that if $N \neq n$, then the system of equations is not square and an exact solution is not possible. In this case, the equations are solved to find the best fit to $\bar{\Delta}$ which minimizes the error. These values are then used to calculate the desired current injections i_{d1}^* , i_{q1}^* , i_{d2}^* , i_{q2}^* from the power balance (1)–(4).

C. Stage III

In Stage III, the desired current injections are translated into actual control values for the FACTS controllers. As before, this approach is developed for the UPFC only, noting that similar approaches can be developed for the SSSC and STATCOM. To find the actual control inputs, a predictive control based on [14] is used. The basic methodology of predictive control is to design an asymptotically stable controller such that in an

affine nonlinear system, the output $y(t)$ tracks a prescribed reference value $\omega(t)$ in terms of a given performance:

$$\dot{x} = f(x(t)) + g(x(t))u(t) \quad \dots\dots\dots(14)$$

$$y_i(t) = h_i(x(t)) \quad i=1, \dots, m \quad \dots\dots\dots(15)$$

Where m is the number of outputs equal to the number of inputs in $u(t)$. The receding horizon performance index is given by

$$J = \frac{1}{2} \int_0^T (\hat{y}(t+\tau) - \hat{\omega}(t+\tau))^2 d\tau \times (\hat{y}(t+\tau) - \hat{\omega}(t+\tau)) d\tau \quad \dots\dots\dots(16)$$

where T is the predictive period. The actual control input $u(t)$ is given by the initial value of the optimal control input $\hat{u}(t+\tau)$ for $0 \leq \tau \leq T$ and $u(t+\tau)$ when $\tau=0$.

The optimal predictive control law is given by

$$u(t) = -(L_g l_f^{p-1} h(x))^{-1} (K M_p + L_f^p h(x) - \omega^{(\rho)}(t)) \quad \dots\dots\dots(17)$$

where ρ is the relative degree for the system outputs (assuming that all outputs have the same relative degree) and L is the Lie derivative defined by

$$L_\mu v = \frac{\partial v}{\partial x} \mu \quad \dots\dots\dots(18)$$

The matrix K is given by

$$M_\rho = \begin{bmatrix} h(x) - w(t) \\ L_f^1 h(x) - w^{[1]}(t) \\ \vdots \\ L_f^{\rho-1} h(x) - w^{[\rho-1]}(t) \end{bmatrix} \quad \dots\dots\dots(19)$$

The matrix K is the first rows of the matrix $\psi_{rr}^{-1} \psi_{pr}^T$ where

$$\psi_{rr} = \begin{bmatrix} \psi_{(\rho+1, \rho+1)} & \dots & \psi_{(\rho+1, \rho+r+1)} \\ \psi_{(\rho, \rho+1)} & \dots & \psi_{(\rho, \rho+r+1)} \end{bmatrix} \quad \dots\dots\dots(20)$$

$$\psi_{pr} = \begin{bmatrix} \psi_{(1, \rho+1)} & \dots & \psi_{(1, \rho+r+1)} \\ \psi_{(\rho, \rho+1)} & \dots & \psi_{(\rho, \rho+r+1)} \end{bmatrix} \quad \dots\dots\dots(21)$$

Where

$$\psi_{ij} = \frac{r^{i+j-1}}{(i-1)!(j-1)!(i+j-1)!}, \quad i, j=1, \dots, \rho+r+1 \quad \dots\dots\dots(22)$$

And

$$\bar{T} = \text{diag}\{T, \dots, T\} \in R^{m \times m}$$

Returning to (1)–(5), the relative degree for all of the outputs is $\rho = 1$ and assuming the control order to be $r = 0$, then the control law for the UPFC becomes

$$u_1 = \frac{-3L_1}{\omega_s V_{dc} T} (i_{d1} - i_{d1}^*) + \frac{R_1}{V_{dc}} i_{d1} - \frac{L_1}{V_{dc}} i_{q1} + \frac{V_1 \cos \theta_1}{V_{dc}} + \frac{L_1}{\omega_s V_{dc}} \frac{d}{dt} i_{d1}^* \quad \dots\dots\dots(23)$$

$$u_2 = \frac{-3L_1}{\omega_s v_{dc} T} (i_{q1} - i_{q1}^*) + \frac{R_1}{V_{dc}} i_{q1} - \frac{L_1}{V_{dc}} \frac{di_{q1}}{dt} + \frac{V_1 \sin \theta_1}{V_{dc}} + \frac{L_1}{\omega_s v_{dc}} \frac{d}{dt} i_{q1}^* \dots\dots\dots(24)$$

$$u_3 = \frac{-3L_1}{\omega_s v_{dc} T} (i_{d2} - i_{d2}^*) + \frac{R_1}{V_{dc}} i_{d2} - \frac{L_1}{V_{dc}} \frac{di_{d2}}{dt} + \frac{V_2 \cos \theta_2}{V_{dc}} - \frac{V_1 \cos \theta_1}{V_{dc}} \frac{L_2}{\omega_s v_{dc}} \frac{d}{dt} i_{d2}^* \dots\dots\dots(25)$$

$$u_4 = \frac{-3L_2}{\omega_s v_{dc} T} (i_{q2} - i_{q2}^*) + \frac{R_2}{V_{dc}} i_{q2} - \frac{L_2}{V_{dc}} \frac{di_{q2}}{dt} + \frac{V_2 \sin \theta_2}{V_{dc}} - \frac{V_1 \sin \theta_1}{V_{dc}} + \frac{L_1}{\omega_s v_{dc}} \frac{d}{dt} i_{q1}^* \dots\dots\dots(26)$$

These inputs are then translated into the control inputs for the UPFC

$$k_1 = \sqrt{u_1^2 + u_2^2} \dots\dots\dots(27)$$

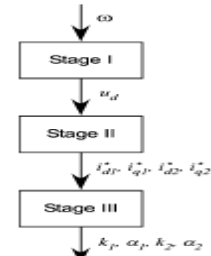


Fig. 3. Three stage control process.

$$\alpha_1 = \tan^{-1} \frac{u_2}{u_1} \dots\dots\dots(28)$$

$$k_2 = \sqrt{u_3^2 + u_4^2} \dots\dots\dots(29)$$

$$\alpha_2 = \tan^{-1} \frac{u_4}{u_3} \dots\dots\dots(30)$$

The three stage control process and outcomes of each stage are summarized in Fig.3

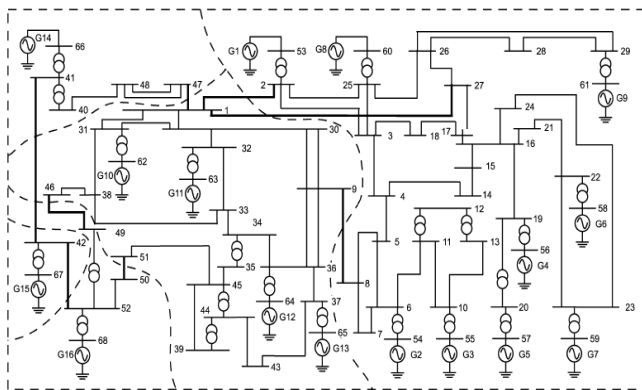


Fig. 4. The 68 bus, 16 generator test system

V. SELECTIVE FEEDBACK MEASUREMENTS BASED ON DOMINANT MACHINES

The control method proposed in the previous section requires generator rotor frequencies to be implemented. Although with recent advances in wide area frequency measurement (FNET) it may be possible to provide synchronized global measurements, it is still not feasible to assume that all generator rotor frequencies are simultaneously available. However, it is reasonable to assume that a *subset* of the measurements are available for feedback and the remainder of the states can be estimated based on the available measurements. The most probable machines to obtain measurements from are those machines which dominate coherent groups.

There are numerous methods for calculating coherent groups in the literature [15]–[18]. In [18], the coherency identification method is based on modal analysis and Gaussian elimination with full pivoting on the selected eigenvectors of the system to find the reference generators and their group members.

The selected eigenvectors are chosen based on the lowest oscillatory modes of the system. Once the dominant machines are found, a reduced order system is computed which captures the “slow” dynamics of the original system. In this process, the remaining unmeasured states of the system can be estimated based on the states which are measured via singular perturbation [13]. Let the dominant

machines be ordered from 1 to Q and the rest of the machines be numbered from Q+1 to N, then the changes in the non-dominant machines can be approximated using a zero-th order model by

$$\begin{bmatrix} X_{Q+1,Q+1} & \dots & X_{Q+1,N} \\ \vdots & \ddots & \vdots \\ X_{N,Q+1} & \dots & X_{N,N} \end{bmatrix} \begin{bmatrix} \Delta \delta_{Q+1} \\ \vdots \\ \Delta \delta_N \end{bmatrix} = \begin{bmatrix} \sum_{k=1}^Q X_{Q+1,k} \Delta \delta_k - \sum_{k=N+1}^{N+n} X_{Q+1,k} \Delta \delta_k \\ \vdots \\ \sum_{k=1}^Q X_{N,k} \Delta \delta_k - \sum_{k=N+1}^{N+n} X_{N,k} \Delta \delta_k \end{bmatrix} \dots\dots(31)$$

Where

$$x_{ij} = \frac{\mu_{ij}}{\mu_{ii}} \dots\dots\dots(32)$$

And

$$\mu_{ij} = -E_i E_j Y_{ij} \sin(\delta_i - \delta_j - \varphi_{ij}) \quad i \neq j \dots\dots(33)$$

$$\mu_{ii} = -\sum_{k \neq i}^{N+n} E_i E_j Y_{ij} \sin(\delta_i - \delta_j - \varphi_{ij}) \quad i = j \dots\dots\dots(34)$$

Note that when only the dominant machines are selected for the control action, only the rows corresponding to the dominant machines will be used thereby reducing the order of the system. This is advantageous since the pseudo-inverse required to solve the set of equations is more nearly square providing better convergence.

VI. EXAMPLE AND RESULTS

Although the control has been developed using the classical generator model, the control approach will be validated using the full 10th order model which includes an exciter/AVR, turbine, and governor dynamics. The model is given in the Appendix. The proposed control is validated on the 68 bus, 16 generator New England/New York test system shown in Fig. 4. The coherent groupings corresponding to the five slowest modes are indicated by the dashed lines in Fig. 4. The network data and coherent groupings are the same as in [19]. The transmission tie lines are shown with bold lines. The reference generators for the five areas are G5, G13, G14, G15, and G16.

TABLE I FACTS PARAMETERS

	R_1	L_1	R_2	L_2	R_p	C
UPFC	0.01	0.15	0.001	0.015	25	1400
STATCOMs	0.01	0.10	n/a	n/a	25	1200

Choosing the appropriate number of FACTS controllers in the network is based on the number of coherent areas. As a rule of thumb, it is best to match the number of current injections with the number of modes. For example, five current injections can be used to control the interarea oscillations between five areas. In the 68 bus example, four current injections are used: one UPFC (two injections) and two STATCOMS (one injection each). In this paper, the UPFC is placed on line 1–2 with the shunt converter on bus 2 and the STATCOMS have been placed on buses 47 and 49. The placements of the FACTS controllers were heuristically chosen to be at buses at the edge of the areas as might occur in practice. Several researchers have addressed the problem of optimal placement of FACTS controllers. In [20], the authors utilize modal sensitivity to determine placement of TCSCs. Eigenvalue shift is used as a placement strategy for SVCs in [21]. [22] focuses on the determination of the best bus placement for SVCs to damp interarea oscillations. Another recent work addresses the use of modal controllability indices specifically for FACTS placement for oscillation damping [23].

The parameters of the FACTS controllers are given in Table I. The per unit approach is the same as in [24] on a 100 MW, 100 kV base.

In the simulations, a solid three-phase fault is applied to bus 30 at 0.2 seconds and cleared at 0.3 seconds. The dynamic responses to this fault are shown for the following cases:

- Case 1) proposed control, all measurements available;
- Case 2) proposed control, only dominant machine measurements available;
- Case 3) linear control (taken from [25]).

Note that in Case 2), the estimation approach proposed in Section V is used to obtain approximations to the non-measured states.

Fig.5 shows a subset of the generator speeds with no FACTS controllers in the system compared to Case 1). Not all responses are shown for the sake of brevity. The selected generators are taken from four of the five coherent areas (generator 15 is by itself in an area and is not shown). Note that the generators go unstable as a result of the fault, but the proposed control is able to stabilize the system and rapidly mitigate the oscillations.

Fig. 6 shows the active power injections of the UPFC. The series injection is shown in the top figure and the shunt injection is shown in the bottom figure. In this figure, Case 2 (bold) is compared to Case 3 (thin). These series active power injection for the proposed control is very modest; therefore the rating of the series transformer and converter do not need to be overly large. The shunt active power is related to the series active power

$$-P_{shunt} = P_{series} - \frac{V_{dc}^2}{R_{dc}} \dots \dots \dots (35)$$

Therefore P_{shunt} will be opposite in polarity to P_{series} and will differ in magnitude by the losses in the converter. Furthermore, during transients the dc link capacitor will charge or discharge active power. Also note

that by definition, the shunt active power absorbed is positive, thus during steady-state the STATCOM will absorb active power and the figures indicate a positive value. The shunt converter injects active power into the system during the fault. Similar behavior is displayed by the STATCOMs as shown in Fig. 8. Fig. 9 shows the dc link capacitor voltages. The UPFC and one of the STATCOMs experience a drop of approximately 5% whereas the second STATCOM experiences a slight increase in voltage. This is reasonable, since to damp oscillations, it may be necessary to inject active power in some areas and absorb active power in other areas.

VII. CONCLUSIONS

A three stage nonlinear control scheme has been proposed for damping interarea oscillations using multiple FACTS controllers. Any FACTS device that can control its interface bu angle(s) with the power network can utilize this control approach. The method uses the generators' frequencies as the feedback data for the control. Using measurements from the dominant generators and estimating the rest of the states based on equivalent reduced systems is shown to considerably reduce the number of needed global measurements for control. Based on the simulation results, the proposed method shows promising results for wide-area control of power systems. There are several issues which need to be considered however.

There is a considerable computational burden for the controller which requires fast processors for real-time performance. However, good coherent groupings will lower the computation time by improving the estimation process. Future work will also consider the effect of time delays and communication noise in the measured states on the control effectiveness. Sensitivity of the proposed method to system uncertainties and topology changes will also be studied.

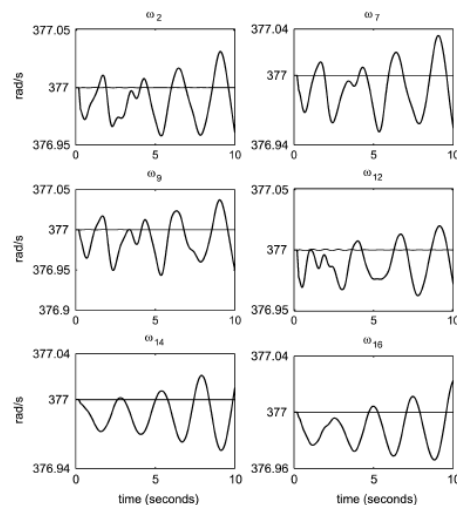


Fig. 5. Generator speeds for no FACTS controllers (bold) and Case 1 (thin).

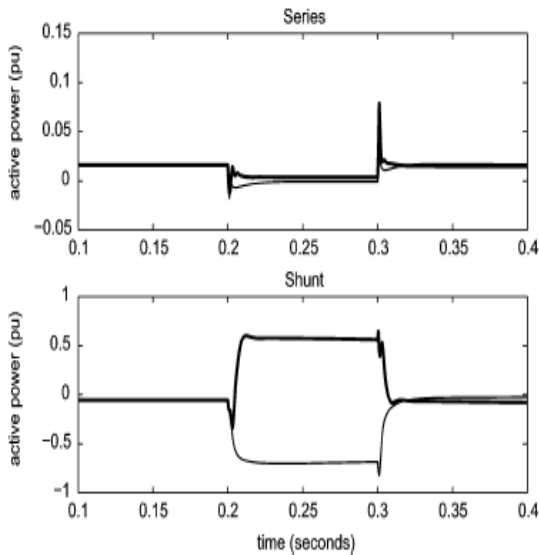


Fig. 6. UPFC injected active power: Series (top) and shunt (bottom); Case 2 (bold) and Case 3 (dashed).

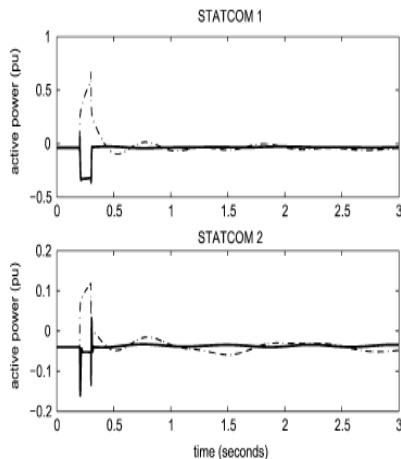


Fig. 7. STATCOM active power injection: Case 2 (bold), Case 3 (dashed).

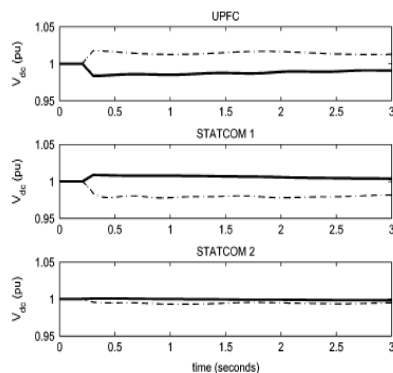


Fig. 8. FACTS Vdc: Case 2 (bold) and Case 3 (dashed).

REFERENCES

[1] H. Wang, "A unified model for the analysis of FACTS devices in damping power system oscillations—Part III: Unified power flow controller," *IEEE Trans. Power Del.*, vol. 15, no. 3, pp. 978–983, Jul. 2000.

[2] B. C. Pal, "Robust damping of interarea oscillations with unified power flowcontroller," *Proc. Inst. Elect. Eng., Gen. Transm. Distrib.*, vol. 149, no. 6, pp. 733–738, Nov. 2002.

[3] B. Chaudhuri, B. C. Pal, A. Zolotas, I. Jaimoukha, and T. Green, "Mixed-sensitivity approach to H_{∞} control of power system oscillations employing multiple FACTS devices," *IEEE Trans. Power Syst.*, vol. 18, no. 3, pp. 1149–1156, Aug. 2004.

[4] M. M. Farsangi, Y. H. Song, and K. Y. Lee, "Choice of FACTS device control inputs for damping interarea oscillations," *IEEE Trans. Power Syst.*, vol. 19, no. 2, pp. 1135–1143, May 2004.

[5] N. Tambey and M. L. Kothari, "Damping of power system oscillations with unified power flow controller (UPFC)," *Proc. Inst. Elect. Eng., Gen. Transm. Distrib.*, vol. 150, pp. 129–140, Mar. 2003.

[6] M. Ghandhari, G. Andersson, and I. A. Hiskens, "Control Lyapunov functions for controllable series devices," *IEEE Trans. Power Syst.*, vol. 16, no. 4, pp. 689–694, Nov. 2001.

[7] S. Robak, M. Januszewski, and D. D. Rasolomampionona, "Power system stability enhancement using PSS and Lyapunov-based controllers: A comparative study," in *Proc. IEEE Power Tech Conf., Bologna, Italy, 2003*, vol. 3, p. 6.

[8] C.-C. Chu and H.-C. Tsai, "Application of Lyapunov-based adaptive neural network UPFC damping controllers for transient stability enhancement," presented at the *IEEE Power Energy Soc. General Meet., Pittsburgh, PA, Jul. 20–24, 2008*.

[9] A. Bidadfar, M. Abedi, M. Karari, and C.-C. Chu, "Power swings damping improvement by control of UPFC and SMES based on direct Lyapunov method application," presented at the *IEEE Power and Energy Soc. General Meet., Pittsburgh, PA, Jul. 20–24, 2008*.

[10] M. Januszewski, J. Machowski, and J. W. Bialek, "Application of the direct Lyapunov method to improve damping of power swings by control of UPFC," *Proc. Inst. Elect. Eng., Gen., Transm. Distrib.*, vol. 151, pp. 252–260, Mar. 2004.

[11] Z. Zhong, C. Xu, B. J. Billian, L. Zhang, S. J. Tsai, R. W. Conners, V. A. Centeno, A. G. Phadke, and Y. Liu, "Power system frequency monitoring network (FNET) implementation," *IEEE Trans. Power Syst.*, vol. 20, no. 4, pp. 1914–1921, Nov. 2005.

[12] L. Dong, M. L. Crow, Z. Yang, and S. Atcitty, "A reconfigurable FACTS system for university laboratories," *IEEE Trans. Power Syst.*, vol. 19, no. 1, pp. 120–128, Feb. 2004.

[13] P. Sauer and M. A. Pai, *Power System Dynamics and Stability*. Upper Saddle River, NJ: Prentice-Hall, 1998.

[14] W.-H. Chen, D. J. Balance, and P. J. Gawthrop, "Optimal control of nonlinear systems: A predictive control approach," *Automatica*, vol. 39, pp. 633–641, 2003.

[15] J. H. Chow, R. Galarza, P. Accari, and W. W. Price, "Inertial and slow coherency aggregation algorithms for power system dynamic model reduction," *IEEE*

Trans. Power Syst., vol. 10, no. 2, pp. 680–685, May 1995.

- [16] S. Gees, “A modal-coherency technique for deriving dynamic equivalents,” IEEE Trans Power Syst., vol. 3, no. 1, pp. 44–51, Feb. 1998.
- [17] M. L. Ourari, L.-A. Dessaint, and V.-Q. Do, “Dynamic equivalent modeling of large power systems using structure preservation technique,” IEEE Trans. Power Syst., vol. 21, no. 3, pp. 1284–1295, Aug. 2006.
- [18] J. H. Chow, Ed., Time-Scale Modeling of Dynamic Networks With Applications to Power Systems. Berlin, Germany: Springer-Verlag, 1982.
- [19] G. Rogers, Power System Oscillations. Norwell, MA: Kluwer, 2000.
- [20] E. V. Larsen, J. J. Sanchez-Gasca, and J. H. Chow, “Concepts for design of FACTS controllers to damp power swings,” IEEE Trans. Power Syst., vol. 10, no. 2, pp. 948–956, May 1995.
- [21] P. Pourbeik and M. J. Gibbard, “Simultaneous coordination of power system stabilizers and FACTS device stabilizers in a multimachine power system for enhancing dynamic performance,” IEEE Trans. Power Syst., vol. 13, no. 2, pp. 473–479, May 1998.
- [22] N. Martins and L. T. G. Lima, “Determination of suitable locations for power system stabilizers and static VAR compensators for damping electromechanical oscillations in large scale power systems,” IEEE Trans. Power Syst., vol. 5, no. 4, pp. 1455–1469, Nov. 1990.
- [23] B. K. Kumar, S. Singh, and S. Srivastava, “Placement of FACTS controllers using modal controllability indices to damp out power system oscillations,” Proc. Inst. Eng. Technol., Gen., Transm., Distrib., vol. 1, no. 2, pp. 252–260, Mar. 2007.
- [24] C. Schauder and H. Mehta, “Vector analysis and control of advanced static VAR compensators,” Proc. Inst. Elect. Eng., C, vol. 140, no. 4, 1993.
- [25] M. Zarghami and M. L. Crow, “Discussion of effective control of interarea oscillations by UPFCs,” presented at the 39th North American Power Symp., Las Cruces, NM, Oct. 2007.



M Praveen Kumar received B.Tech Degree in Electrical & Electronics Engg. from JNT University, Hyderabad, India. Presently he is with Annamacharya Institute of Technology & Sciences, Rajampet, A.P, India, in Dept. of EEE and pursuing his M.Tech. His research interests includes power systems, FACTS,



P.B Chennaiah received B.Tech Degree in Electrical & Electronics Engg. from JNT University, Anantapur, India. M.Tech degree in electrical engineering from JNT University, Hyderabad. Presently he is with Annamacharya Institute of Technology & Sciences, Rajampet, A.P, India, in Dept. of EEE as an Associate professor. His research includes optimization techniques in power systems, FACTS,

Voltage Clamped Dc-Dc Converter with Reduced Reverse Recovery Current And Stability Analysis

Dharamalla. ChadraSekhar,¹ D. Jagan,²

^{1,2} Assistant Professor /GATE Engineering College / JNTU, Hyderabad/ AP /INDIA.

Abstract: this paper in vest gates a high-efficiency clamped-voltage dc-dc converter with reduced reverse-recovery current And switch-voltage stress. In the circuit topology, it is designed by way of the combination of in duct or and transformer to increase the corresponding voltage gain. Moreover, one additional inductor provides the reverse-current path of the transformer to enhance the utility rate of magnetic core. In addition, the voltage-clamped technology issued to reduce the switch-voltage stress so that it can select the Scotty diode in the output terminal for all aviating the reverse recovery current and decreasing the witching and conduction losses. Fur the more; the closed-loop control methodology is utilization the proposed scheme to overcome the voltage-drift problem of power source under the variation of loads. Thus, the proposed converter topology has a favor able voltage-clamped effect and superior conversion efficiency. Some experimental results via an example of a proton exchange membrane fuel cell (PEMFC) power source with a 250-W nominal rating are given to demonstrate the effectiveness of the proposed power-conversion strategy.

Index Terms: Converter, fuel cell, proton-exchange membrane (PEM), reverse recovery, voltage clamped.

I. INTRODUCTION

INRECENT years, dc-dc converter switch steep voltage ratio are usually require din many industrial applications, e.g., the front-end stage for clean energy sources, the dc backup energy system for an uninterruptible power supply (UPS), high-intensity discharge (HID) lamps for automobile head lamps, And the telecommunication industry[1]–[3].The conventional boost converters cannot provide such a high dc-voltage ratio due to the losses associated with the inductor, filter capacitor, main switch, and output diode. Even for an extreme duty cycle, It will result in serious reverse-recovery problems and increase The rating of the output diode. As a result, the conversion efficiency is degraded, and the electromagnetic interference (EMI) problem is severe under this situation [4].In order to increase the conversion efficiency and voltage gain, many modified boost converter topologies have been investigated in the past decade[5]–[10].

Although voltage-clamped techniques are manipulated in the converter design to overcome the severe reverse-recovery problem of the output diode in high-level voltage applications, there still exist over large switch-voltage stresses, and the voltage gain is limited by the turn-ON time of the auxiliary switch [5], [6].da Silva et al. [7] presented a boost soft-single-switch converter, which has only one single active switch. It is able to operate with soft switching in a pulse width modulation (PWM) way without high voltage and current stresses. Unfortunately, the voltage gain is limited below four in order to achieve the function of

soft switching. In [8] and [9], coupled inductors were employed to provide ea high step-up ratio and to reduce the switch-voltage stress substantially, and the reverse-recovery problem of the output diode was also alleviated efficiently.

In this case, the leakage energy of the coupled inductor is another problem as the main switch was turned OFF. It will result in a high voltage ripple a cross the main switch due to the resonant phenomenon induced by the leakage current. In order to protect the switch devices, either a high-voltage-rated device with higher RDS (ON) or a snubber circuit is usually adopted to deplete the leakage energy. Consequently, the power-conversion efficiency will be degraded. Zhao and Lee [10] introduced a family of high-efficiency high-step-up dc-dc converters by only adding one addition diode and a small capacitor. It can recycle the leakage energy an

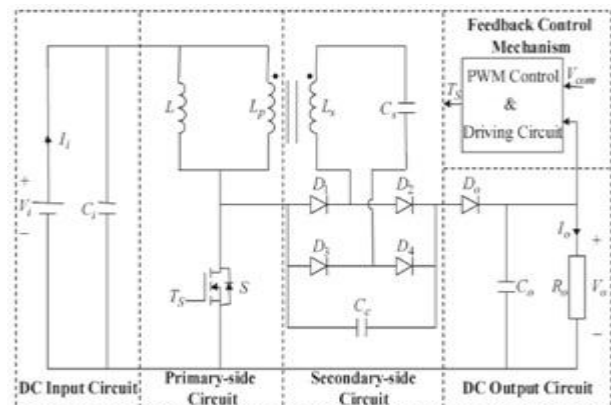


Fig. 1. System configuration of a high-efficiency voltage-clamped dc-dc converter.

Alleviate the reverse-recovery problem. However, a snubber circuit is still required in the output diode terminal with extra energy losses.

Nowadays, fuel cells are in the news because they appear to be one of the most efficient and effective solutions to the environmental pollution problem [11]–[17]. A fuel cell is an energy conversion device that produces electricity by electrochemically combining fuel (hydrogen) and oxidant (oxygen from the air) gases through electrodes, across an ion conduction electrolyte. This process produces much higher conversion efficiency than any conventional thermal-mechanical system, because it operates without combustion and extracts more electricity from the same amount of fuel. This system has the merits of high efficiency, energy security, reliability, pollution free, and quiet operations. Fuel cells have been known to science for more than 160 years and have recently become the subject of intense research and development. Up to the present, many demonstration projects have shown fuel-cell systems to be feasible for portable power, transportation, utility power and on-site power generation in a variety of building applications.

For portable power, a fuel cell with a fuel container can offer a higher-energy density and more convenience than conventional battery systems. Moreover, portable power packs using fuel cells can be lighter and smaller in volume for an equivalent amount of energy. In transportation applications, fuel cells offer higher efficiency and better part-load performance than conventional engines. In stationary power applications, low emissions permit fuel cells to be located in high-power requirement areas, where they can supplement the existing utility grid. Using fuel cells and hydrogen technology, electrical power can be delivered cleanly, efficiently and sustainably where and when required. The greatest research interests throughout the world have focused on proton-exchange membrane

(PEM) and solid oxide cell stacks. Specially, PEM fuel cell (PEMFC) has promising characteristics as follows: 1) the by-product waste is water; 2) low-temperature operation; and 3) they use a solid polymer as the electrolyte that reduces concerns related to construction, transportation, and safety issues [16]. Thus, it seems to be a good alternative source for distributed generation systems.

The aim of this study is to design a high-efficiency voltage clamped dc-dc converter with reduced reverse-recovery current and switch-voltage stress to provide a stable constant dc voltage. To achieve this goal, the manipulation of inductor and transformer is adopted to increase the voltage gain and to enhance the utility rate of the magnetic core. Moreover, the voltage-clamped technology is used for reducing the switch voltage stress and solving the reverse-recovery problem. In addition, the closed-loop control methodology is utilized in the proposed converter to overcome the voltage-drift problem of power source under the variation of loads. The prototype is developed for a PEMFC application requiring an output power of 310 W, an output voltage of 200 V, and an input voltage varying from 27 to 37.5 V. The remainder of this study is organized as follows. Section II presents the converter design and analyses in detail. Experimental results for a PEMFC power source with a 250-W nominal rating are provided to validate the effectiveness of the proposed power conversion system in Section III. Conclusions are drawn in Section IV.

II. CONVERTER DESIGN AND ANALYSES:

A newly designed converter topology is depicted in Fig. 1, where it contains five parts including a dc-input circuit, a primary-side circuit, a secondary-side circuit, a dc-output circuit, and a feedback-control mechanism. The major symbol representations are summarized as follows. V_i and I_i denote the dc-input voltage and current, and C_i is the input filter capacitor in the dc-input circuit. L_p represents the primary inductor of the transformer; L is the additional inductor in the primary-side circuit; and S is the main switch. L_s denote the secondary inductor of the transformer; C_s and C_c are the balanced capacitor and clamped capacitor in the secondary-side circuit; and D_1 , D_2 , D_3 , and D_4 are the rectifier diodes. V_o and I_o describe the output voltage and current; R_o is the output load; D_o , and C_o are the output diode and filter capacitor in the output circuit. V_{com} and T_S are the output-voltage command and switch-driving signal in the feedback-control mechanism, respectively.

The equivalent circuit and state definition of the newly designed converter is depicted in Fig. 2, where the

transformer is modeled as an ideal transformer with a secondary leakage inductor (L_k). The turn's ratio of this ideal transformer is defined as

$$n = \frac{N_2}{N_1} \quad (1)$$

Where N_1 and N_2 are the primary and secondary winding turns. The additional inductor (L) is located in parallel with the primary side of the transformer. Moreover, the rectifier diodes (D_1 , D_2 , D_3 , and D_4) are connected between the primary and secondary sides of the transformer. The voltages across the additional inductor, the main switch, the ideal transformer primary and secondary winding, the secondary leakage inductor, the balanced capacitor, and the output diode are v_L , v_{DS} , v_{Lp} , v_{Ls} , v_{Lk} , v_{Cs} , and v_{Do} , respectively. The clamped capacitor C_c is assumed to be large enough to be viewed as a constant voltage source, V_{Cc} . The conductive voltage drops of the main switch

(S) And all diodes (D_1 , D_2 , D_3 , D_4 , and D_o) are neglected to simplify the circuit analyses. The characteristic waveforms of the proposed high-efficiency converter are depicted in Fig. 3. In addition, Fig. 4 illustrates the operational modes in one switching cycle, and the detailed operation stages are described as follows.

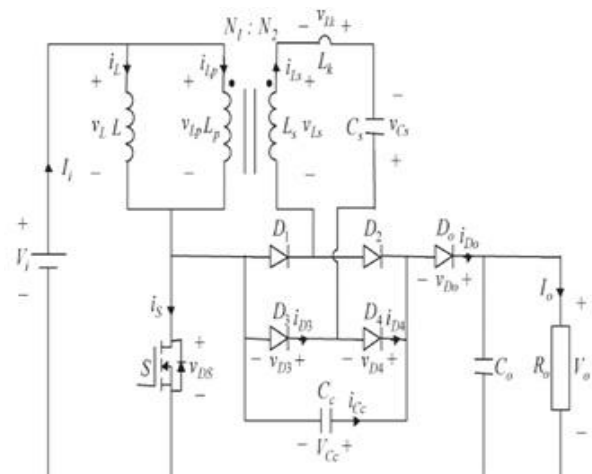


Fig. 2. Equivalent circuit.

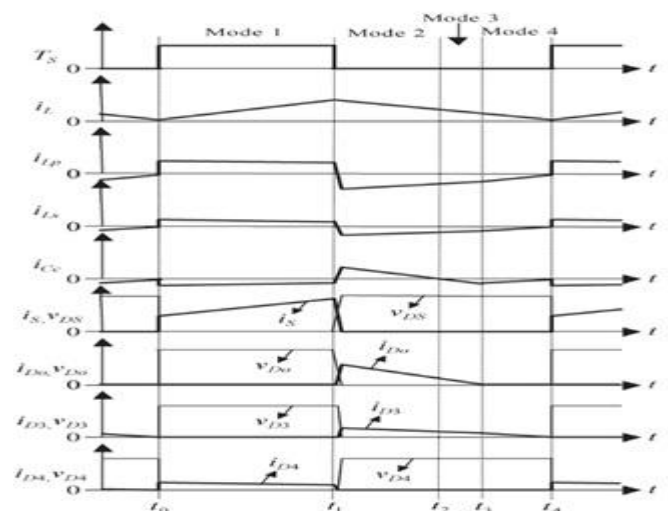


Fig. 3. Characteristic waveforms.

A. Mode 1 ($t_0 - t_1$) [Fig. 4(a)]

At time $t = t_0$, the main switch (S) is turned ON. At the same time, the diodes (D_1 and D_4) become conducted, and other diodes (D_2 , D_3 , and D_o) are reverse biased. The additional inductor (L) and clamped capacitor (C_c) are linearly charged by the input-voltage source (V_i) through the transformer. Applying Kirchhoff's law [4], the voltages of v_L , v_{Lp} , v_{Ls} , and v_{Lk} during this period can be expressed as

$$v_L = v_{Lp} = V_i \quad (2)$$

$$v_{Ls} = nV_i \quad (3)$$

$$v_{Lk} = V_{Cc} - nV_i - v_{Cs} \quad (4)$$

According to (2)–(4), the rate of change of the additional inductor current (i_L), the primary-side current (i_{Lp}), and the secondary-side current (i_{Ls}) of the transformer can be represented as

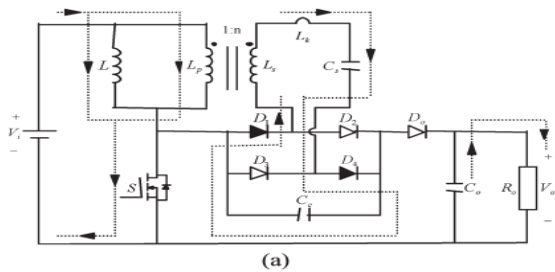
$$\frac{di_L}{dt} = \frac{V_i}{L} \quad (5)$$

$$\frac{di_{Lp}}{dt} = \frac{V_{Cc} - nV_i - v_{Cs}}{L_k} + \frac{V_i}{L_p} \quad (6)$$

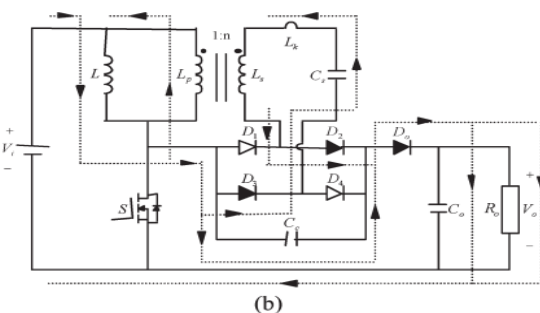
$$\frac{di_{Ls}}{dt} = \frac{V_{Cc} - nV_i - v_{Cs}}{L_k} \quad (7)$$

B. Mode 2 ($t_1 - t_2$) [Fig. 4(b)]

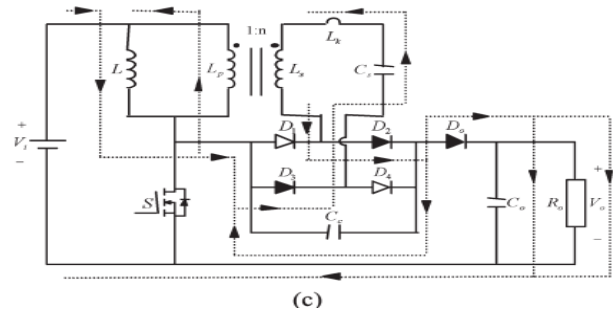
At time $t = t_1$, the main switch (S) is turned OFF. At this time, the diodes (D_2 , D_3 , and D_o) become forward biased to start conducting, and other diodes (D_1 and D_4) are reverse biased. The stored energy of the additional inductor (L) and clamped capacitor (C_c) in Mode 1 is released to output loads. Moreover, the transformer can be operated at four quadrants to enhance the utility rate of the magnetic core and to keep the clamped voltage (V_{Cc}), since the additional inductor (L) supplies energy to the output terminal by way of the transformer. Applying Kirchhoff's law [4], the voltage and current relations of each element during this mode can be described by



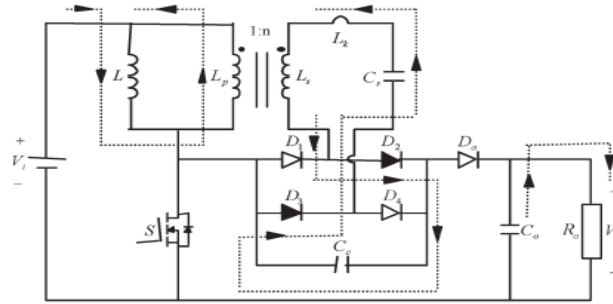
(a)



(b)



(c)



(d)

Fig.4.Operational modes: (a) mode 1 [$t_0 - t_1$]; (b) mode 2 [$t_1 - t_2$]; (c) mode 3 [$t_2 - t_3$]; (d) mode 4 [$t_3 - t_4$].

$$v_L = v_{Lp} = V_i + V_{Cc} - V_o \quad (8)$$

$$v_{Ls} = n(V_i + V_{Cc} - V_o) \quad (9)$$

$$v_{Lk} = -V_{Cc} - v_{Cs} - n(V_i + V_{Cc} - V_o) \quad (10)$$

$$v_{DS} = V_i - V_L = V_o - V_{Cc} < V_o \quad (11)$$

$$i_{D_o} = i_L + i_{Lp} = i_{Cc} - i_{Ls} \quad (12)$$

Where i_{Do} is the current of the output diode D_o ; i_{Cc} is the current of the clamped capacitor C_c . According to (11), the cutoff voltage of the main switch (S) is clamped at $V_o - V_{Cc}$. Moreover, the main switch (S) with low-voltage-rated capacity can be selected since the switch-voltage stress (v_{DS}) is smaller than the output voltage (V_o). The selection of a low-voltage-rated device with lower $R_{DS} (ON)$ is useful for improving the conversion efficiency. Referring to (8)–(10), the rate of change of i_L , i_{Lp} and i_{Ls} is given by

$$\frac{di_L}{dt} = \frac{V_i + V_{Cc} - V_o}{L} \quad (13)$$

$$\frac{di_{Lp}}{dt} = \frac{-V_{Cc} - v_{Cs} - n(V_i + V_{Cc} - V_o)}{L_k} + \frac{V_i + V_{Cc} - V_o}{L_p} \quad (14)$$

$$\frac{di_{Ls}}{dt} = \frac{-V_{Cc} - v_{Cs} - n(V_i + V_{Cc} - V_o)}{L_k} \quad (15)$$

C. Mode 3 ($t_2 - t_3$) [Fig. 4(c)]

$$\frac{di_{Cc}}{dt} = \frac{V_i + V_{Cc} - V_o}{L} + \frac{V_i + V_{Cc} - V_o}{L_p} + 2 \left[\frac{-V_{Cc} - v_{Cs} - n(V_i + V_{Cc} - V_o)}{L_k} \right] \quad (16)$$

$$\frac{di_{D_o}}{dt} = \frac{V_i + V_{C_c} - V_o}{L} + \frac{V_i + V_{C_c} - V_o}{L_p} + \frac{-V_{C_c} - v_{C_s} - n(V_i + V_{C_c} - V_o)}{L_k} \quad (17)$$

$$\frac{di_{L_p}}{dt} = -\frac{di_L}{dt} = -\frac{V_i + V_{C_c} - V_o}{L} \quad (18)$$

$$\frac{di_{L_s}}{dt} = -\frac{V_i + V_{C_c} - V_o}{L} - \frac{V_i + V_{C_c} - V_o}{L_n} \quad (19)$$

$$v_{C_s} = \frac{nV_i(2d-1)}{2(1-d)} \quad (20)$$

$$V_{C_c} = \frac{nV_i}{2(1-d)} \quad (21)$$

$$V_o = \frac{2+n}{2(1-d)} V_i \quad (22)$$

At time $t = t_2$, the residual energy of the clamped capacitor (C_c) is discharged entirely, i.e., $i_{C_c}(t_2) = 0$. Immediately, the clamped capacitor (C_c) is charged by the energy of the additional inductor (L) through the transformer, and the rate of change of the clamped-capacitor current (i_{C_c}) can be denoted as Moreover, the stored energy of the additional inductor (L) is released continuously to the output terminal by way of the transformer. The rate of charge of i_{D_o} is given by

$$v_{DS} = \frac{V_i}{(1-d)} \quad (23)$$

$$v_{DS} = \frac{2V_o}{(2+n)} \quad (24)$$

D. Mode 4 ($t_3 - t_4$) [Fig. 4(d)]

At time $t = t_3$, the clamped-capacitor current (i_{C_c}) equals to the secondary-side current (i_{L_s}) of the transformer, and the output diode current (i_{D_o}) decays to 0, i.e., $i_{D_o}(t_3) = 0$. During this period, the voltage of the output diode (v_{D_o}) Maintains the zero status until the main switch (S) is turned ON. Moreover, the magnitude of the additional inductor current (i_L) is equal to the one of the primary-side current (i_{L_p}). According to (13) and (14), the rate of change of i_{L_p} and i_{L_s} can be represented as Since the secondary leakage inductor (L_k) and the change rate of i_{L_s} in the transformer are very small, the voltage of the secondary leakage inductor (v_{L_k}) can be neglected. According to the concept of the zero average voltage across the inductor over one period [4], the voltages of v_{C_s} , V_{C_c} , and V_o for steady state operation can be described via (2), (4), (8), and (10) as.

Since the voltage difference may be caused by the secondary inductor of the transformer, as $d = 0.5$, the major function of the balanced capacitor (C_c) is used for keeping the cutoff voltages of the rectifier diodes (D_1 , D_2 , D_3 , and D_4) balanced. Moreover, it also can avoid the overlarge current that passed through the rectifier diodes. According to (22), the voltage gain can be tuned by regulating the turn's ratio (n) in the transformer to overcome the boost- ratio limitation of the conventional converter. In addition, the

switch-voltage stress (v_{DS}) can be calculated(11),and (22) as

Where d is the duty cycle of the main switch (S). Continuously, the main switch (S) is turned ON at time $t = t_4$ to begin the next switching cycle.

By analyzing (24), the switch-voltage stress (v_{DS}) is not related to the dc-input voltage (V_i) and duty cycle (d) if the values of the output voltage (V_o) and the turns ratio (n) are fixed. Thus, it can ensure that the sustainable voltage of the main switch (S) is constant. As long as the dc-input voltage is not higher than the rated voltage of the main switch, the high-efficiency voltage clamped dc-dc converter can be applied well to the low-voltage power sources even with large voltage variations, e.g., fuel cell, solar cell, etc.

Fuel-cell generation systems have been receiving more attention in the last years due to the advantages of high-conversion efficiency, low aggression to the environment, no moving parts, and superior reliability and durability. Owing to the electrochemical reaction, fuel cell has the power quality of low voltage and high current. However, the fuel-cell stack with high output voltage is difficult to fabricate and it may be failure when any single cell is inactive. Besides, the output voltage is varied easily with respect to the load variations. In order to satisfy the requirement of high-voltage demand, a stable boost converter with high voltage gain and superior conversion efficiency is necessary to utilize the fuel-cell energy more efficiently. The validity of the proposed converter is verified by the following experimental results via an example of a PEMFC power source.

III. EXPERIMENTAL RESULTS

In order to verify the effectiveness of the designed converter topology, the clean energy of a PEMFC system is utilized for the low-voltage power source in the proposed high-efficiency voltage-clamped dc-dc converter, and its application circuit is depicted in Fig. 5. The PEMFC system used in this study is the PowerPEM™-PS250 manufactured by the H power Company. It is a dc power source with 250-W dc nominal power rating.

The system operates on an ambient air and clean pressurized hydrogen fuel. The fuel-cell system consists of a (40) cell stack of the PEM type, mechanical auxiliaries, and electronic control module. In experimentation, the high-efficiency voltage-clamped dc-dc converter is designed to operate from the fuel-cell variability dc input, $V_i = 27-37.5$ V, to deliver a constant dc output, $V_o = 200$ V, with the maximal capability of output power, $P_{o,max} = 330$ W. If the maximal value of main switch voltage (v_{DS}) is arranged for clamping at 50 V, the turns ratio can be determined as $n = (2V_o/v_{DS(max)}) - 2 = 6$ according to (24). As can be seen from Figs. 3 and 4, the voltage stress of the output diode (v_{D_o}) is the same as the switch-voltage stress. In addition, the voltage stresses of rectifier diodes (v_{D1} , v_{D2} , v_{D3} , and v_{D4}) can be calculated via (21) and (23) as $n v_{DS}/2 = 150$ V. For conservative consideration, the main switch (FQI90N08, 80 V), the output diode (Schottky diode SR20100, 100 V), and the rectifier diodes (Schottky diode SR20200, 200 V) are adopted in the experimental converter.

In order to solve the problem of the fuel-cell output voltage varied with the variations of loads, the proposed converter with dc-voltage feedback control is utilized to ensure the system stability, and a PWM control IC TL494 is adopted to

achieve this goal of feedback control. The prototype with the following

Specifications are designed in this section to illustrate the design procedure given in Section II:

Switching frequency $f_s = 100$ kHz;

Turns ratio $n = 6$;

Additional inductor $L = 5.9$ μ H;

Primary inductor of transformer $L_p = 213.6$ μ H

Secondary inductor of transformer $L_s = 7689.6$ μ H;

Secondary leakage inductor $L_k = 0.6$ μ H;

Balanced capacitor $C_s = 4 \times 6.8$ μ F;

Clamped capacitor $C_c = 6 \times 4.7$ μ F;

Input filter capacitor $C_i = 3300$ μ F;

Output filter capacitor $C_o = 3 \times 4.7$ μ F;

Main switch S : FQI90N08 (80 V,

RDS (ON) = 16 m Ω);

Output diode D_o : Schottky diode

SR20100 (100 V, 20 A);

Rectifier diodes D_1, D_2, D_3, D_4 :

Scotty diode SR20200 (200 V, 20 A).

Fig. 5 depicts the experimental voltage and current curves of the main switch (S) at 310-W output power. As can be seen from this figure, the shaken switch voltage at the beginning is caused by the line inductor when the switch is turned OFF. Fortunately, the steady state of this switch-voltage stress is about 50 V due to the utilization of voltage-clamped technique, and it is much smaller than the output voltage, $V_o = 200$ V. It has the merit of selecting a low-voltage-rated device in order to reduce the conduction loss of the switch.

The experimental current waveforms of the additional inductor (L), in parallel with the transformer, primary inductor of transformer (L_p), and secondary inductor of transformer (L_s) at 310-W output power, are depicted in Fig. 5(c). By observing the currents of i_{Lp} and i_{Ls} , it is obvious that the transformer is manipulated during the four-quadrant operation so that the utility rate of the magnetic core is improved to exhibit the transformer characteristics completely. The experimental voltage and current responses of the diodes (D_o, D_3 , and D_4) at 310-W output power are depicted in Fig. 5. From these results, the reverse-recovery currents in these diodes are small to give the credit to the utilization of Schottky diodes with extremely low switching and conduction losses. Thus, it can alleviate the reverse-recovery problem for further raising the conversion efficiency. As can be seen from Fig. 5(a) and (b),

The balanced capacitor (C_s) can be used for balancing the current and cutoff voltage of the diodes (D_3 and D_4) when the condition of $d = 0.5$ holds. For verifying the voltage-clamped property, the experimental voltage responses of the output voltage (V_o), clamped capacitor (C_c), output diode (D_o), and main switch (S) at 310-W output power are depicted. As can be seen from this figure, the output voltage, $V_o = 200$ V, is strode mainly across the clamped capacitor in the secondary-side circuit (i.e., $V_{Cc} = 150$ V). Thus, the switch-voltage stress and the cutoff voltage of the output diode are clamped at about 50 V. In order to examine the robust performance of the proposed converter scheme, the experimental results of the converter output voltage (V_o), output current (I_o), and the PEMFC output current (I_i) under the step load variation between no load (0 W) and full load (310 W) are depicted Fig. 10.

According to Fig. 10, the converter output voltage, $V_o = 200$ V, is insensitive to the variation of loads due to the closed-loop control, and the output current ripple is also slightly extreme as a result of the high switching frequency. Fig. 11 summarizes the conversion efficiency of the proposed converter and the PEMFC output voltage under different output powers. From the experimental results, the measure of efficiency of the proposed converter operating at 310-W output power is 95.6%, and the maximal efficiency is 96.5% at 190-W output power. The above experimental results agree well with those obtained from the design procedure given in Section II. However, slight differences in these results are attributed to the factor of system uncertainties in practical applications.

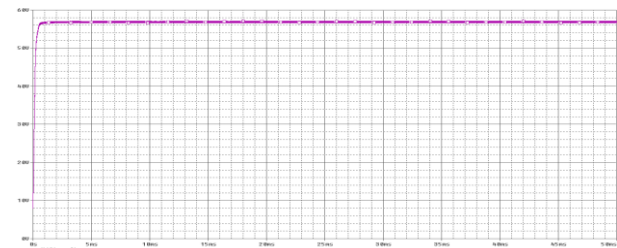


Fig 5 (a)output voltage

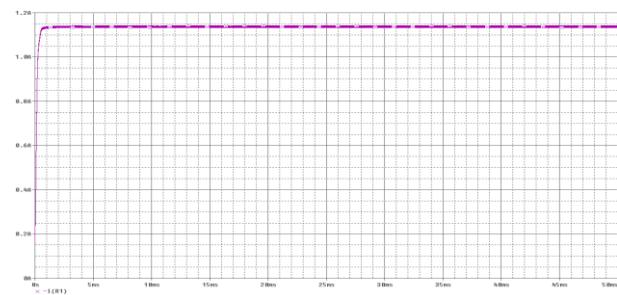


Fig 5 (b)output current:

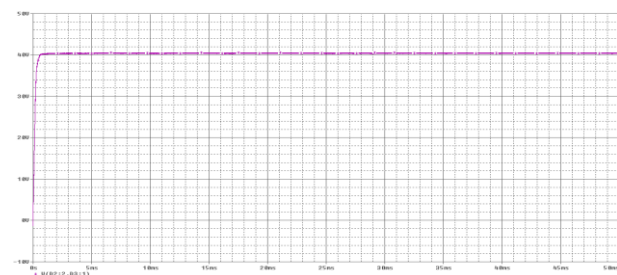


Fig 5 (c) clamped capacitor voltage

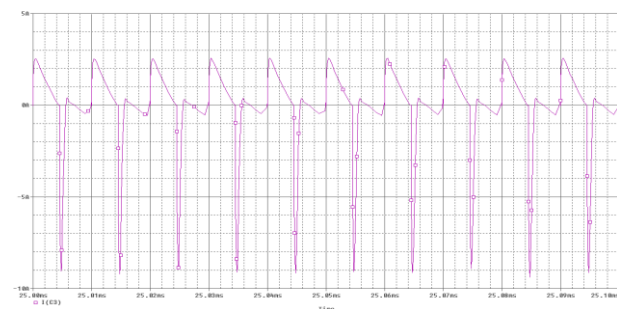


Fig 5 (d) clamped capacitor current

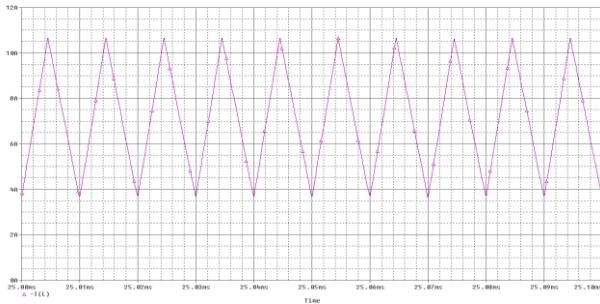


Fig 5 (e) Inductor current:

IV. CONCLUSION

This paper has successfully developed a high-efficiency voltage-clamped dc-dc converter with reduced reverse recovery current and switch-voltage stress, and this converter has been applied well to a PEMFC system with a power quality of low voltage and high current. According to the experimental results, the maximal efficiency was measured to be over 96%, which is comparatively higher than the conventional converter with the same voltage gain. The newly designed converter circuit has the following improvements compared to the previous work.

- 1) It can select the main switch with lower sustainable voltage for alleviating the switch conduction loss due to the utilization of voltage-clamped technique.
- 2) All diodes in this circuit topology are Schottky diodes with the reduction of switching and conduction losses.
- 3) The additional inductor is used for providing the reverse current path of the transformer to raise the utility rate of the magnetic core.
- 4) Additional snubber circuits for absorbing the voltage spikes in the diodes are not required to further cut down the manufacture cost.
- 5) There is no circulating current to overcome the problem of degenerate efficiency under slight loads.
- 6) The voltage-drift problem of power source under the variation of loads can be solved by the closed-loop control methodology.

This new converter topology provides designers with an alternative choice to convert renewable energy efficiently, and it also can be extended easily to other power-conversion systems for satisfying high-voltage demands.

V. ACKNOWLEDGMENT

The authors would like to express their gratitude to the Referees and the Associate Editor for their useful comments and suggestions.

REFERENCES

- [1] I. Barbi and R. Gules, "Isolated dc-dc converters with high-output voltage for TWTAs telecommunication satellite applications," *IEEE Trans. Power Electron.*, vol. 18, no. 4, pp. 975–984, Jul. 2003.
- [2] O. Abutbul, A. Gherlitz, Y. Berkovich, and A. Ioinovici, "Step-up switching-mode converter with high voltage gain using a switched-capacitor circuit," *IEEE Trans. Circuits Syst. I, Fundam. Theory Appl.*, vol. 50, no. 8, pp. 1098–1102, Aug. 2003.
- [3] K. C. Tseng and T. J. Liang, "Novel high-efficiency step-up converter," *Proc. Inst. Elect. Eng.—Electr. Power Appl.*, vol. 151, no. 2, pp. 182–190, Mar. 2004.

- [4] N. Mohan, T. M. Undeland, and W. P. Robbins, *Power Electronics: Converters, Applications, and Design*. New York: Wiley, 1995.
- [5] M. M. Jovanovic and Y. Jang, "A new soft-switched boost converter with isolated active snubber," *IEEE Trans. Ind. Appl.*, vol. 35, no. 2, pp. 496–502, Mar./Apr. 1999.
- [6] C. M. C. Duarte and I. Barbi, "An improved family of ZVS-PWM active-clamping DC-to-DC converters," *IEEE Trans. Power Electron.*, vol. 17, no. 1, pp. 1–7, Jan. 2002.
- [7] E. S. da Silva, L. dos Reis Barbosa, J. B. Vieira, L. C. de Freitas, and V. J. Farias, "An improved boost PWM soft-single-switched converter with low voltage and current stresses," *IEEE Trans. Ind. Electron.*, vol. 48, no. 6, pp. 1174–1179, Dec. 2001.
- [8] K. Hirachi, M. Yamanaka, K. Kajiyama, and S. Isokane, "Circuit configuration of bidirectional DC/DC converter specific for small scale load leveling system," in *Proc. IEE Power Conversion Conf.*, Osaka, Japan, 2002, pp. 603–609.
- [9] C. W. Roh, S. H. Han, and M. J. Youn, "Dual coupled inductor fed isolated boost converter for low input voltage applications," *Electron. Lett.*, vol. 35, no. 21, pp. 1791–1792, Oct. 1999.
- [10] Q. Zhao and F. C. Lee, "High-efficiency, high step-up dc-dc converters," *IEEE Trans. Power Electron.*, vol. 18, no. 1, pp. 65–73, Jan. 2003.
- [11] K. Ro and S. Rahman, "Two-loop controller for maximizing performance of a grid-connected photovoltaic-fuel cell hybrid power plant," *IEEE Trans. Energy Convers.*, vol. 13, no. 3, pp. 276–281, Sep. 1998.
- [12] M. D. Lukas, K. Y. Lee, and H. Ghezal-Ayagh, "Development of a stack simulation model for control study on direct reforming molten carbonate fuel cell power plant," *IEEE Trans. Energy Convers.*, vol. 14, no. 4, pp. 1651–1657, Dec. 1999.
- [13] —, "An explicit dynamic model for direct reforming carbonate fuel cell stack," *IEEE Trans. Energy Convers.*, vol. 16, no. 3, pp. 289–295, Sep. 2001.
- [14] A. Boudghene Stambouli and E. Traversa, "Fuel cells, an alternative to standard sources of energy," *Renew. Sustain. Energy Rev.*, vol. 6, no. 3, pp. 297–306, Sep. 2002.
- [15] M. W. Ellis, M. R. Von Spakovsky, and D. J. Nelson, "Fuel cell systems: Efficient, flexible energy conversion for the 21st century," *Proc. IEEE*, vol. 89, no. 12, pp. 1808–1818, Dec. 2001.
- [16] J. M. Correa, F. A. Farret, J. R. Gomes, and M. G. Simoes, "Simulation of fuel-cell stacks using a computer-controlled power rectifier with the purposes of actual high-power injection applications," *IEEE Trans. Ind. Appl.*, vol. 39, no. 4, pp. 1136–1142, Jul./Aug. 2003.
- [17] K. Green and J. C. Wilson, "Future power sources for mobile communications," *IEE Electron. Commun. Eng. J.*, vol. 13, no. 1, pp. 43–47, Feb. 2001.



Dharamalla.ChandraSekhar-

was born in Andhra Pradesh, INDIA in 1982. He received the B.Tech degree from JNTU Hyderabad in 2004 and M.Tech degree in Power Electronics from JNTU Hyderabad in 2010.

Since July 2004-Sept 2008 he has been Assistant Professor in the Department of Electrical and Electronics in Hi-Tech Engineering College. From October-2008 he was been working as a Head of Department of Electrical and Electronics Engineering in GATE Engineering College, JNTUH, AP. His areas of interest are Electrical Machines, Power Electronics and Drives, Control Systems and Electrical Circuits.



D Jagan -

was born in Andhra Pradesh, INDIA in 1988. He received the B.Tech degree from JNTU Hyderabad in 2010, the M.Tech degree in Power Electronics from JNTU Ananthapur In 2012.

Since July 2010-Oct 2012 he has been Assistant Professor in the Department of Electrical and Electronics in GATE Engineering College, JNTUH, and AP. His areas of interest are Electrical Machines, Power Electronics and Drives, Control Systems and Electrical Circuits.

Geotechnical Investigation of Soils: A Case Study of Gombe Town (Sheet 152NW), North Eastern Nigeria

Stephen J. Mallo,¹ Ikani N. Akuboh²

Department of Geology and Mining University of Jos, Nigeria

Abstract: This work focuses mainly on the Geotechnical properties of mapped areas in Gombe town which forms part of the Upper Benue trough. Representative soil samples were collected from these areas and were investigated for their Geotechnical properties with a view to classifying for their suitability or otherwise for infrastructural development. Hitherto, this has not been done in the Gombe town area. The recent growth which is associated with urbanization in Gombe Township calls for appropriate geotechnical investigation of soils of the area. Twelve representative samples were collected from different locations of the mapped areas around Kanol, Hamatatu, Wurro Daji, Kalshing Forest, Titi Baba, Chongo, Danba, Wurro Ladde, Pantame, Tempure, Tonde, and Kulalum. Samples from each site were collected at 1m depth and analyzed using the following tests: Moisture content test, Particle size distribution test, Atterberg limit test, Specific gravity test, Compaction test. All these tests were carried out using the BS 1377, (1990) Parts 1 - 9 specification. Based on the test results obtained from the study areas, comparison were made with some standard specifications and it was revealed that samples from Pantame, Hamatatu, Tonde, Chongo and Kulalum areas are clayey soils which are unsuitable for most engineering construction because they have poor bearing capacities. While soils from Kalshingi forest, Titi baba, Wuro ladde, Danba, Tempure, Kanol and Wuro Daji are clayey sands. This group would make better sub-grade materials for civil engineering construction.

Key words: Geotechnical investigation; Rock Formation; Upper Benue Trough; Sandstones

I. Introduction

The mapped area lies within the Gongola arm of the Upper Benue trough of Northeastern Nigeria. It forms an integral part of Gombe (Sheet 152 NW) and lies within the 11°06' and 11°15'E and latitude 10°25'30'' and 10°16'30'' N. It encompasses Gombe Township and its surrounding villages (Fig.1)

The Gombe region located in Northeastern Nigeria falls within one of the geographical domains of the Benue trough (Upper Benue Trough). The Nigerian Benue Trough is an approximately 1000km long and 50- 150km wide intercontinental basin, elongated in a direction and overlies the Precambrian shield of West African Mobile Belt (Benkhelil 1989; Guiraud 1990). It was described by Carter et al. (1963) and Wright (1976) as a fault bounded depression filled by 6000m thick marine coastal and fluvial sediments which were compressionally folded in a non-orogenic shield environment.

The sedimentary sequence, which is underlain by Basement complex rocks, spans over a considerable area around, Bima Sandstone at the base, Yolde Formation, Pindiga Formation, and finally the Gombe Sandstones at the top. The Bima sandstone is Albian in age, while the overlying Cretaceous rock represents a marine sequence and represents a time range from Lower Turonian to Maastrichtian. The Bima sandstone is succeeded by transitional beds, which pass upwards into a marine sequence of Turonian to Senonian age. Continental conditions were re-established in the Maastrichtian and resulted in the deposition of the Gombe Sandstone. The Pan-African orogeny (600 million years) which is the last known tectonic episode to have affected the Basement complex, have lead to deformation of the sandstone formations, forming faults and joints, and also the orogeny has cause an upliftment of the Basement complex there by forming Inliers (Gombe and Liji hills) of considerable height around the Gombe area.

The Upper Benue Trough has generated as much controversy compared to other sedimentary rocks. This is because most of the sequences such as the Basement rocks and sedimentary rocks are well exposed and can be studied in details. The earliest detailed work on the geology of the Upper Benue Trough was carried out by Carter et al, (1963). Other works include; Allix (1983), Guiraud (1990).

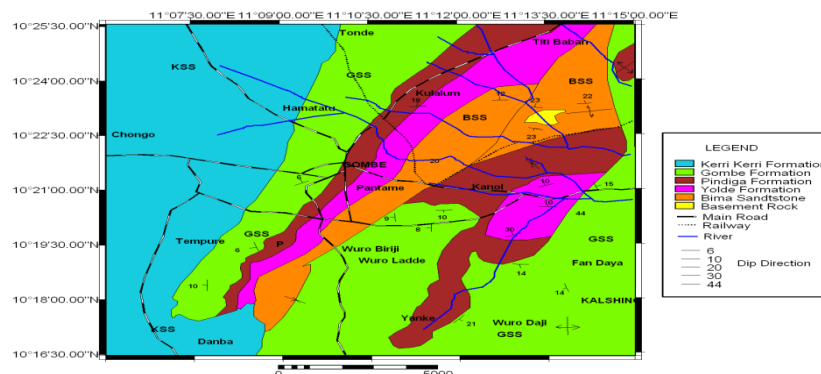


Fig.1: Geological map of the study area.

II. Methodology

The methodology of research involved desktop survey followed by reconnaissance survey and collection of representative samples. Field equipment used for the study and sampling include a map of the study area, Sampling bags, Sampling tube for undisturbed samples, Global Position System (GPS), Ilwis software, Camera, Measuring tape, Twain Masking tape, Markers, Field note book, Pen, Pencil, Geological hammer, Shovels, Diggers and compass clinometers. A detailed geological field mapping which entailed ground traversing, description of the rock types, identification of sedimentary and tectonic deformation structures (such as joints and faults), delineation of formational boundaries and dip and strike measurements were recorded on a base map. Representative samples were taken from Kanol (Central part of the study area), Hamatatu (Northeastern part), Wuro Daji (Southeastern part), Kalshing Forest (South east), Titi Baba (North east) Chongo (North east), Danba (Southwest), Wurro Ladde (South east), Pantame (Central), Tempure (South west), Tonde (North east) and Kulalum (North east), (Fig.2).

The soil samples were subjected to laboratory testing for natural water content, grain size analysis, Atterberg's Limit Test (Liquid limit and Plastic limit test), Standard compaction Test and Specific Gravity test.

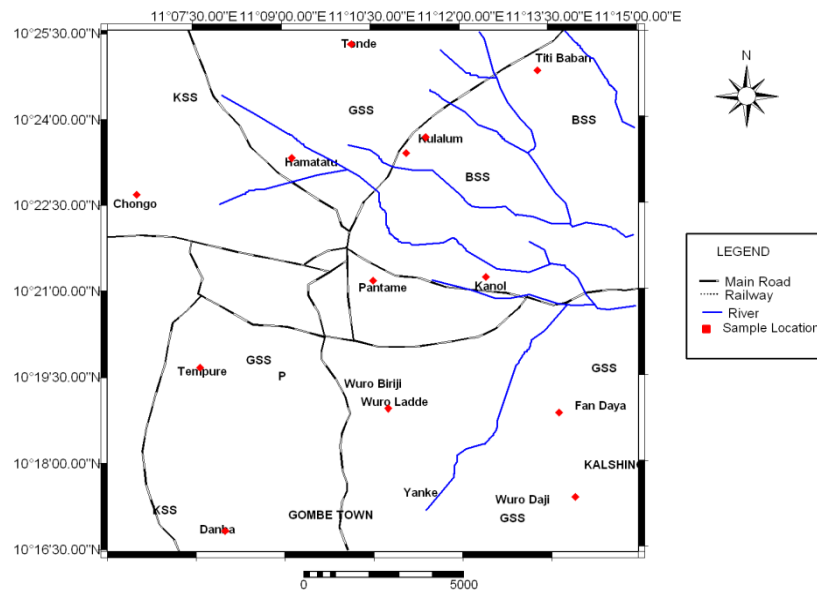


Fig.2: Sample location map of the study area.

Geology

The mapped area is characterized by two major rock types: The basement complex rocks represented by the rocks of the Migmatite Gneiss Complex of Nigeria and the Cretaceous sedimentary sequence which encompasses; The Bima Sandstone Formation; The Yolde Formation; The Pindiga Formation and the Gombe Sandstone

The crystalline basement rocks in the mapped area are represented by the rock types of the migmatite Gneiss Complex of Nigeria. They outcrop in the North-eastern part of the study area forming the Gombe inlier. Exposures of these rocks were also encountered along stream channels in the Northeastern part of the area. The basement rocks constitute about 2% of the mapped area. The rock type is predominantly gneisses of medium to coarse grained texture and mesocratic in color. The alternations of light and dark colored band of minerals are very obvious.

The Bima sandstone formation represents the basal formation of the Cretaceous rocks of the Upper Benue trough in the study area. The rocks of the formation are better exposed along stream channels and gullies, though hilly outcrops of highly cemented Bima sandstone were encountered close to the Gombe hill in the northeastern part of the study area. The Bima sandstone Formation consists about 20% of the mapped area. They consist predominantly of medium to coarse grained sandstones interbedded with thin layer of grey to purple clays. The sandstones are generally friable and range in color from cream white to brown. Bima sandstones were observed in Pantame, Kanol, and Danba areas.

The Yolde Formation occupies about 15% of the mapped area. The formation was encountered in the southwestern and northeastern parts of the study area and is mainly exposed along river channels. The lithological units of this formation include fine-coarse-grained sandstones with very thick units of grey shale. The sandstones vary in color from light grey to reddish. Sections of the Yolde Formation are well exposed in the Pantame, Titi Baba.

This formation constitutes 25% of the mapped area. It consists of dark grey shales which become silty towards the top and occasionally contain horizons of milky-grey impure Marls coated with fibrous limestone that show syntaxial calcite minerals growth pattern. Exposures of the Pindiga Formation were encountered in Kulalum area. They are best exposed in river valleys and gullies.

The Gombe Sandstone Formation is the most widespread sedimentary rock in the study area as it constitutes about 35% of the area. It is found exposed as hills and along river channels and valleys. The Gombe Sandstone Formation consists of fine-grained buff to red coloured sandstones which are often parallel laminated, cross-laminated or cross-

bedded. Clay interbeds are present at some horizons. Outcrops of the Gombe Sandstone dominate the southeastern parts of the mapped area and some part of Northeast and tend to show high degree of weathering. The sandstones are also characterized by ferruginized capping. The Keri-Keri formation was identified at Chongo and Tempure having fine to medium grained sandstone, Trough cross bedding and amalgamated bedding. Traces, Erosional surfaces (Fig.3), oolitic and pacilithic materials that are highly ferruginized, Clay clasts and paraconglomerate were all identified.

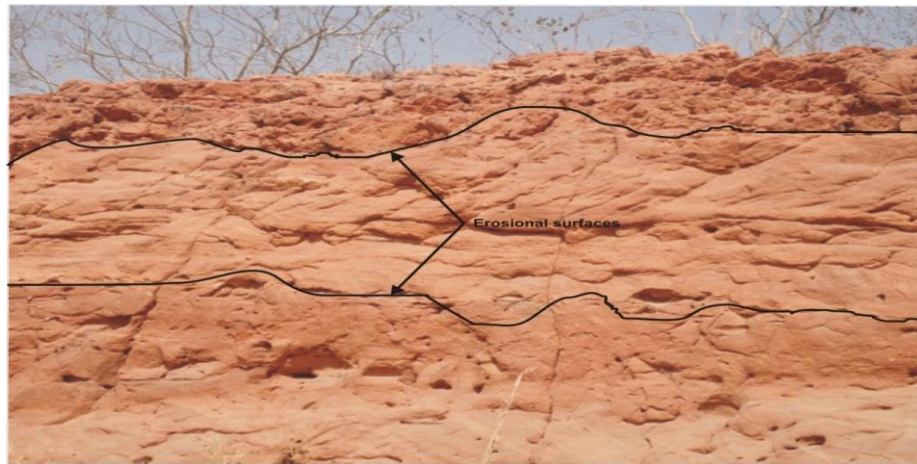


Fig.3: Amalgamated sandstone bed in Keri Keri Formation

III. Materials and Methods

Testing refers to the determination of the soil characteristics or properties using laboratory experiment. Representative samples were taken for laboratory analysis under strict adherence to the rules and procedures for soil tests as prescribed in the BS 1377 manual. Preparation of samples for each test depends on the procedure required for such test to be carried out. Some samples were first sun dried before making use of them in the laboratory while some were used in their natural state. Laboratory equipment such as electric oven, sieve shaker, casagrande liquid limit apparatus, density bottle with distilled and gassing machine were deployed for the analysis. The results of experiments are shown in Table 1.

Table 1: Geotechnical laboratory Test Results

S/N	Sample Location	Sample Point	Field Description	Natural Moisture content %	OMC %	MDD g/cm ³	Specific Gravity g/cm ³	Liquid Limits g/cm ³	Plastic Limits g/cm ³	Plasticity index	Percentage Passing sieve no. 200
				M			GS	LL	PL	PI	
1	Kanol	Sample L2	Brownish sandstone	3.92	8.7	2.49	2.56	23.2	16.0	7.2	20.10
2	Kulalum	Sample H	Brownish - Greyish fissile shale	33.66	15.0	1.945	2.55	64.2	33.3	30.9	83.32
3	Pantame	Sample P	(Greyish- Reddish Clayey Sand	6.73	11.0	2.58	2.62	30.3	17.2	13.1	42.64
4	Kalshing forest	Sample K	Brownish - Reddish Sandstone	7.68	5.9	2.449	2.59	24.1	5.4	18.7	14.26
5	Hamatatu	Sample Z4	Brownish - Reddish sandstone	2.10	10.8	2.359	2.57	30.1	13.4	16.7	42.99
6	Titi Baba	Sample G3	Medium - coarse grained sand	2.03	8.7	2.50	2.58	26.9	17.3	9.6	16.70....
7	Wuro Ladde	Sample G1	Fine grained sandstone	10.95	8.1	2.14	2.51	25.7	16.2	9.5	27.63
8	Chongo	Sample C5	Very fine sand	6.41	9.4	2.775	2.63	22.2	14.9	7.3	35.83
9	Damba	Location M	Fine sand	8.44	8.3	2.831	2.54	31.8	18.9	12.9	28.99
10	Tonde	Sample Z2	Brownish - Reddish sandstone	7.95	10.5	2.37	2.62	31.7	20.7	11.0	82.52
11	Wuro Daji	Sample B	Brownish - reddish sandstone	5.80	9.3	2.80	2.59	20.9	15.6	5.3	19.80
12	Tempure	Sample C4	Reddish - medium sandstone	6.52	6.3	2.7	2.60	22.5	13.4	9.1	17.75

IV. Discussion

Grain size distribution: A soil consists of an assemblage of discrete particles of different of various shapes and sizes. For the other entire engineering test to be effective, determination of the particle sizes is important due to its strong relationship with the engineering behavior. Some relevant and useful information can be obtained from a grain size distribution curve. Such information includes the percentage larger or finer than a given size and their uniformity or the range in grain size distribution.

The American Association of State Highway and Transportation Officials (AASHTO) classification is a widely used method for classifying soils for earth work structures, particularly sub-grades, bases, sub-bases, embankments. The system separates soils into granular and silt clays groups. It classifies soils into seven (7) groups based on particles size distribution, liquid limit and plasticity.

Furthermore, the unified soil classification system divide soil into two main groups: coarse –grained and fine-grained defined by a set of two letters, a prefix and a suffix. The coarse grained designation is assigned to soils for which over 50%, by weight of the material is retained by the no. 200 sieve (0.75mm). Within the coarse grained, the prefix G is assigned to the soils if more than 50%, pass through the no. 4 sieve (4.7mm); G and S is follow by suffix that describes the gradation; W- well graded; P- poorly graded; M- containing silt; C- containing clay.

According to AASHTO classification, soil samples from Pantame (P), Hamatutu (Z4), Chongo(C5), Kulalum(H) and Tonde(Z2) contain more than 35% of the soil passing through sieve No. 200 hence the soils are in the Silty Clay Group and all the aforementioned samples fall under group A-6 with the exception of kulalum which falls under A-7. On this basis they can therefore be classified as poor materials. Samples from Kanol (K), Kalshingi forest (L2), Titi baba(G3), Wuro ladde (G1), Danba(M), Wuro Daji(B) and Tempure(C4) have less than 35% passing through No 200 sieve and thus falls under A-2 group of the granular materials which are regarded as the silt or clayey gravel and sand group of soils. They are excellent to good subgrade materials.

From the classification, soil sample whose Liquid limit values do not exceed 40 (which is the maximum value for A – 2 soils) and Plasticity Index not more than 11 (which is the maximum value for A- 2 soil are said to be high in quality. Samples from Kashing Forest (L2), Titi Baba (G3), Wuro Ladde (G1), Wuro Daji (B), and Tempure (C4) falls within the range of liquid limit for A – 2 materials, hence these soils can be regarded as good materials.

However, plastic index for Danba(M) and Kanol(K) are greater than 11(below the maximum value of A-2 soils) and samples from Kulalum have higher liquid limit values of 64.2, which exceeds 41 been the minimum liquid limit and having . The non-satisfaction of the liquid limit and plastic index requirement indicates that the soil is actually poor in quality when compared to A – 2 soils. The high liquid limit values could be due to increasing porosity leading to increased moisture content as in the case with gravel and sand group of soils. The soil will require improvement before it can be used as an A- 2 materials. Based on the Unified Soils Classification System (USCS), Kanol, Pantame, Kalshingi forest, Hamatatu, Titi Baba, Wurro Ladde, Chongo, Danba, Wurro Daji and Tempure belong to coarse grained group, while Tonde and Kulalum are under the fine grained group.

Atterberg limit: The atterberg limits are an empirically developed but widely used procedure for establishing and describing the consistency of cohesive soil thereby providing useful information regarding soil strength, behaviour, stability and type and state of consolidation besides its use to identify the soil classification. Consistency is frequently used to describe the degree of firmness (e.g soft, medium, firm, or hard) and the consistency of cohesive soil is strongly affected by the water content of the soil. A gradual increase of the water content, for example, may transform dry clay from perhaps a solid state to a semi-solid state, to a plastic state and after further moisture increase, increase into a liquid state. The water content at the corresponding junction points on these states are known as the shrinkage limit, plastic limit and the liquid limit respectively.

The result of the liquid limit(LL) and plastic limit (PL) and plasticity index (PI) for the soil investigated shows that the liquid limit ranges between 20.9 and 64.2, while the plasticity index ranges between 5.3 and 30.9.

According to the guideline of Federal Ministry of Works (1997), the liquid limit should not exceed 35% to be suitable for use as sub-grade and sub-base or base course materials, hence Kalshing Forest, Pantame, Kanol, Hamatatu, Wurro Ladde, Titi Baba, Chongo, Danba, Tonde, Wurro Daji and Tempure can be regarded as fairly good for sub-base or base course materials except for soil sample from Kulalum whose liquid limit is higher (64.2%).

Based on the British Soil Classification Systems, samples from Kalshing Forest, Pantame, Kanol, Hamatatu, Wurro Ladde, Titi Baba, Chongo, Danba, Tonde, Wurro Daji and Tempure have low plasticity and low liquid limit while sample from Kulalum have high plasticity and low liquid limit.

Generally, soils with high liquid limit (LL) are clays with poor engineering properties too weak in strength. Soils with intermediate plasticity index and liquid limit would make better engineering properties while those with low plasticity and liquid limit as displayed by most of the samples in the study area would have fair to good engineering properties,

According to the specification for Roads and Bridges, Ministry of Works, Bauchi (1990), Samples from Kashing Forest, Pantame, Kanol, Hamatatu, Titi Baba, Wuro Ladde, Chongo, Danba, Tonde, Wuro Daji and Tempure have fulfilled the requirement to be used as fill materials with liquid limit(LL) ranging from 0 – 45% and plasticity index of 0 – 20%. Samples from Kulalum showed high liquid limit and high plastic limit and hence would not make good fill materials.

All the samples collected were plotted on a Casagrande Unified Soil Classification Plasticity Chart (Fig.4) and from the plots samples from Pantame, Hamatatu, and Tonde are classified as Clay soils with low plasticity index. Sample 4 appears outside the U – line which could be attributed to laboratory error.

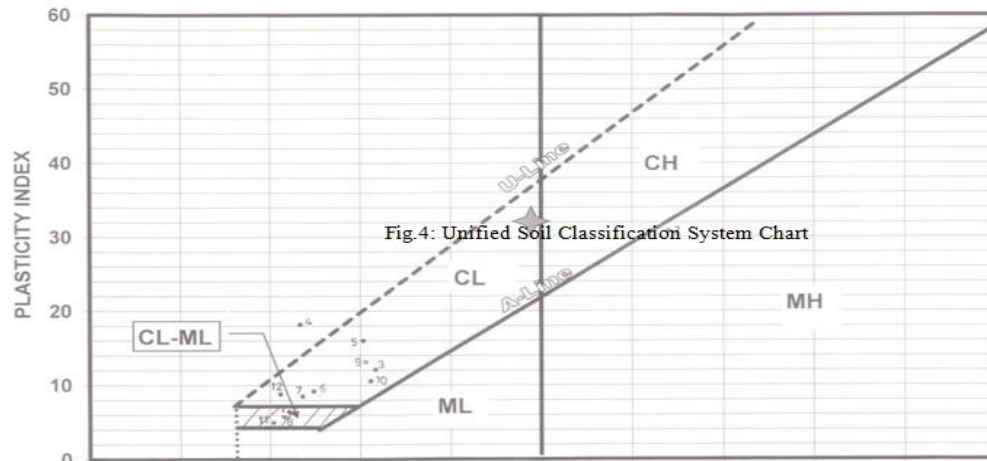


Fig.4: Unified Soil Classification System Chart

(Table 2) provides the classification of soils using the Attenburg limits. From the results, indicates samples from Danba, Wurro, Ladde, Titi Baba, Tempure, and Kalshing are Clayey sands having low plasticity index. However, those samples from Kanol, Chongo and Wurro Daji contain silty clays of low plasticity index, while Kulalum sample is Clay soil with high plasticity. The Plasticity index of soils is a function of their swelling potentials.

Table 2: Classification of fine soils using the Atterberg limits

SAMPLE	USCS	GROUP SYMBOL	LIQUID LIMIT	PLASTICITY INDEX
PANTAME	Clay	CL	30.3	13.1
HAMATATU	Clay	CL	30.1	16.7
TITI BABA	Clayey sand	CL(s)	26.9	9.6
WURRO LADDE	Clayey sand	CL(s)	25.7	9.5
DANBA	Clayey sand	CL(s)	31.8	12.9
TONDE	Clay	CL	31.7	11.0
TEMPURE	Clayey sand	CL(s)	22.5	9.1
KALSHING FOREST	Clayey sand	CL(s)	24.1	18.7
KANOL	Clayey silt	CL – ML	23.2	7.2
CHONGO	Clayey silt	CL – ML	22.2	7.3
WURRO DAJI	Clayey silt	CL – ML	20.9	5.3
KULALUM	Clay	CH	64.2	30.9

Shrinkage limit: Soil samples from Kanol, Pantame, Klashing Forest, Hamatatu, Titi Baba, Wurro Ladde, Chongo, Danba, Tonde, Wurro Daji, and Tempure have low degree of expansion and shrinkage limit <15 (Table 6) and this implies that they are likely to develop cracks when used as fills or embankments. It is important to note that among the above samples some showed plasticity values higher than 12 which is the highest limit for class 1 and can thus be classified as low-medium degree of expansion and shrinkage limit. The sample from Hamatatu falls under class 4 with shrinkage limits >60 and a very high degree of expansion. Such soils are unsuitable for most engineering purposes.

Compaction: When soils are used as construction materials in any type of field or embankment, they nearly always require compaction to prevent settlement and to reduce permeability. With all soils, an increase in the compactive effort, results in an increase in the maximum density and a decrease in optimum water content, (Smith, 1975).

When the values of dry densities and moisture content are plotted, the resulting curve has a peak value of dry density and corresponding moisture content (OMC). The reason for this is that at low moisture values, the soil is stiff and difficult to compact resulting in a low density with a high void ratio. As the moisture is increased the water lubricates the soil, increasing the workability and producing high dry density and low void ratios.

The specification for road and bridges, (1975) states the significance of the moisture – density test as an aid in the field compaction of soils so as to develop the best engineering properties of the material, since it is assumed that the strength or shearing resistance of the soil increases with higher densities.

The moisture density relationship, i.e. the compactive curves (not shown in this paper) showed a maximum dry density ranging from 1945 g/m^3 for the lowest curve at and 2831 kg/m^3 for the highest curve at an optimum content of 5.9 and 15.0% respectively. Since the curve indicates the maximum bulk density to which the soil may be compacted by a given force and the water content of the soil that is optimum for maximum compaction, when the soil is either drier or wetter than these values, the compaction will be more difficult, Brady and Well (1999).

Based on the range of values anticipated for the standard moisture density test stated above, the soils in the study area falls in the clays and silt clay range which also agree with the results indicated by the Atterberg limit classification and grain size distribution.

The results show that, to compact a soil in the field, the sample with the least optimum moisture content will require small amount of water to bring each to its highest density. It could also mean that the samples with high range of moisture absorption capacity may have an advantage in an exceptionally moist area and may easily become saturated and so lose its strength relatively fast, (Alabo, et al., 1984).

According to the criterion by the researchers for determining the suitability of soil for construction of embankment, samples from Kanol, Kalshing forest, and Tempure are proven to be excellent while samples from Chongo and Wurro Daji are good to excellent materials that are suitable for construction. Some of the soils in the study areas exhibit fair to good engineering properties. The areas include; Pantame, Hamatatu, Titi Baba, Wurro Ladde, Danba, Tonde while sample taken from Kulalum have poor engineering properties and therefore will have poor bearing qualities.

Specific gravity: This is the ratio of weight in air of a given volume of soil solids to the weight of an equal volume of distilled water, at a given temperature. The specific gravity of engineering soils usually varies between 2.6 to 2.8. If it is less than 2.6, it may indicate possible presence of organic matter (IS). It can be deduced from that samples from Pantame, Tempure, Chongo, and Tonde have their specific gravity values to be between 2.60 to 2.63, which makes them good materials for engineering construction. The least value is from Wurro Ladde whose value is 2.51. Based on the above it can be deduced that most of the samples are fair for use as sub-grade materials.

Natural Moisture Content: From (Table 3), it is observed that the average moisture content are low for samples gotten from Titi Baba, Hamatatu, Kanol, Wurro Daji, Chongo, Tempure, Pantame, Kulshing Forest, Tonde, Danba, Wurro Ladde ranging from 2.03 to 10.95%, hence they may constitute good construction materials, such as subgrades for roads and foundations. Wikipedia, (2009) suggests that soils with low percentage (%) moisture content, (less than 16%), have a good property for construction. The Kulalum reading on the other hand, is very high, the moisture content value is 33.66% . According to Wikipedia (2009), soils that have more than 16% natural moisture content is assumed to be a saturated soil and will not be good as a construction material.

Table 3: Moisture content values from study area

Sample location	Natural Moisture Content
Kanol	3.92
Kulalum	33.66
Pantame	6.73
Kulshing forest	7.68
Hamatatu	2.10
Titi Baba	2.03
Wurro Ladde	10.95
Chongo	6.41
Danba	8.44
Tonde	7.95
Wurro Daji	5.80
Tempure	6.52

V. Conclusion

The geotechnical properties obtained shows that soil samples from Pantame, Hamatatu, Tonde, Chongo and Kulalum areas are clayey soils which are unsuitable for most engineering construction because they have poor bearing capacities. They would make fair to poor sub grades because of their grain sizes and relatively high plasticity index but can be useful as dam embankment materials.

Samples collected from Kalshingi forest, Titi baba, Wuro ladde, Danba, Tempure, Kanol and Wuro Daji are clayey sands. This group has better engineering properties as they would make good subgrade materials for road construction and they are also good as fill materials.

Generally all the soils in the study area are clayey in nature and hence great care must be taken when they are put to use in engineering construction. This is because clays can be expansive in nature especially when they come in contact with water.

References

1. Allix, C. (1983): The Benue trough Structure and Evolution. 172 – 201.
2. Benkhelil J. (1986) Structure et Evolution geodynamique du bassin intracontinental de la Benoue (Nigeria). Unpublished These Doctoral d' Etat, Univeristy of Nice, 266p.
3. Benkhelil J. (1989): Origin and Evaluation of the Cretaceous Benue Trough (Nigeria). Journal of African Earth Sciences, 8, (1/3), 251- 282.
4. Benkhelil J., Dainelli P., Ponsaro J.I, Popoff, M. and Sauggl (1983): The Benue Trough wrench fault related basins on the border of the Equatorial atlantic.
5. Brady, C.N and Well, R.R (1999): The nature and properties of soils. 5thed. New Jersey Prentice Hall.
6. British Standard 1377 Part 1 (1990): General Requirement and Sample Preparation. British Standard Institute, London.
7. British Standard 1377 Part 2 (1990): Classification Test. British Standard Institute, London.

8. British Standard 1377 Part 4 (1990): 3 Determination of dry density/moisture content relationship, British Standard Institute.
9. British Standard 1377 Part 4 (1990): 3, 2 Preparation of soil sample for compaction Test, British Standard Institute, London.
10. British Standard 1377 Part 4 (1990): 4.0 Determination of Dry densities and Maximum densities of samples. British Standard Institute, London.
11. British Standard 1377 Part 4 (1990): 7.5 Calculation and plotting. British Standard Institute, London.
12. Carter, I.D, Barber, W. Tait, E.A (1963): The Geology of parts of Adamawa, Bauchi, Gombe and Borno provinces in Northeastern Nigeria. Bulletin Geological Survey of Nigeria. No 30.
13. Federal Ministry of Works and Housing (1997): General specification for roads and bridges. Federal Highway Department.
14. Giraud, M (1990): Tectono – Sedimentary Framework of Early Cretaceous Continental Lima Formation of Upper Benue Trough. N.E Nigeria. Journal of Africa Earth Science. 21, (1/2), 341 – 353.
15. Guiraud, M. (1990): Tectono-sedimentary framework of Early Cretaceous Continental Lima formation of Upper Benue Trough. N.E Nigeria. Journal of African Earth Science. 21, (1/2), 341 — 353.
16. Wright J.B (1976): Origin of the Benue Trough. In Geology of Nigeria. C.A Kogbe (ed) Elizabethan Pub.Co.

Automation of Raw Material Transfer Process from Quarry to Silos in Cement Plant

D.R. Pongallu¹, P.H. Zope², S. R. Suralkar³

¹Lecturer E&TC Department, G.H. Raisoni polytechnic Jalgaon, India

²Assitant Professor, E&TC Department, SSBTCOET Jalgaon, India

³HOD and Associate Professor, E&TC Department, SSBTCOET Jalgaon, India

ABSTRACT: Cement is an essential component of infrastructure development. The market demand of cement is increasing continuously but still now most of those plants aren't up to the mark technologically, an integrated solution of material handling in cement plant is presented in this paper to meet the increasing production needs. This innovative thinking will help to reduce energy consumption and improve operational efficiency as most of the energy is consumed to transfer the bulk materials between intermediate stages. The automation process is done using programmable logic controller (PLC)[1]. The focus of this paper is to implement ladder logic for automation process in cement plant and the hardware used for it.

Keywords: Automation, PLC, ladder logic, level detector, silos.

I. INTRODUCTION

India is the second largest producer of cement in the world but still it is not enough for our increasing needs. The overall concept of manufacturing process is taken from ACC CEMENT LTD and various cement manufacturing groups of India. This paper only reviews the flow of materials through the various stages to a particular place.

The whole operation is timing controlled, the devices are turned on sequentially one after another by on delay timer and also turned off sequentially one after another by off delay timer. There are various types of sensors and level detectors are used in each and every critical point to control the entire operation and to reduce the unwanted running of machineries. [3] cement plant has various process in manufacturing we will discuss the process automation of raw material transfer from quarry to silos. The word automation is used frequently in modern discourse to describe all manner of things that involve machines and electronics performing tasks previously performed by humans. Nonetheless, automation still has a finite and quantifiable meaning when referring to its implementation in a modern cement manufacturing facility.

This paper will focus on offering an overview of industrial automation that gives the reader a framework for about the equipment, systems, programming used for automation and methodologies involved in implementing a modern automation system. [2]. Automation is defined as "automatically controlled operation of an apparatus, process, or system by mechanical or electronic devices that take the place of human organs of observation, effort, and decision. [4]

II. HARDWARE

1. Instruments, Actuators, and Sensors

The sensors connected to the process can be as simple as a limit switch or can be as complicated as an on-

line X-ray analyzer. Examples of traditional discrete (switch) sensors include the classic limit switch, temperature switch, pressure switch, flow switch, level switches of numerous designs, photoeyes, and input devices such as push buttons and pilot lights. Switches are digital devices that provide a simple contact which indicate their state: on or off. Instruments such as thermocouples or pressure transmitters are analog devices capable of providing a continuous range of measurement readings from 0 to 100% of range and reporting their data with a changing voltage or current output. As for outputs, motor starters and solenoids are generally digital devices, opening or closing depending on whether they are fed with power from a system output or not. Other actuators, such as valve positioners and adjustable speed drives, are variable and will accept a 4–20-mA control signal to command them to go to 0–100% of their range.

Most instruments today can be enhanced in with intelligent versions. These intelligent instruments have on-board microprocessors that allow for functionality beyond the basic measurement of the primary variable. They can monitor and report additional process variables, support multiple configurations, totalize flow, and monitor and report on their own health. Often, they have significant on-board diagnostics. Motor starters can now monitor various aspects of the health of the motor. They can report current, phase voltage, motor power, motor power factor, and running hours and can tell you exactly why a trip occurred (i.e., overload, ground fault, or short circuit?). They can even tell you when the coil in the contactor is about to fail. Likewise, variable frequency drives can report the same information and even more.

On the plus side, these intelligent instruments can tell you far more about your process than simply the temperature or pressure at a single point. The information given by an intelligent motor starter can help in managing energy costs and predicting motor failures before it happens. Furthermore, if you suspect a fault with one of these instruments, the on-board diagnostic information can often lead you directly to the cause if the device has not already notified you of the problem on its own. To setup and configure intelligent instruments correctly we need to have proper knowledge about the instruments. For all of these types of instruments, the additional information can only be accessed remotely or in real time if you add a serial communication line to the instrument in addition to or in lieu of the primary voltage, current, or contact output. Otherwise, data are trapped in the device and only available at the local display. [2]

2. Intelligent Devices and Integrated Subsystems

In addition to the sensors and actuators that one would typically relate with an automated system, vendors are continually striving to provide tighter integration and communication between the controller and some of the newer, more specialized, and more complex systems that one may find in an automation system. To narrow the communications gap between these complex subsystems and the rest of the control system, vendors have started to offer interface cards that reside in the same card rack with the PLC or HDCS controller. Putting these two elements in the same rack allows them to communicate over the backplane of the chassis, thus enabling the passing of large amounts of control and process data at high rates of speed. The PLC can then use this information from the subsystem in its control program and can execute various commands in the subsystem program without going through a hardwired interface.

Numerous intelligent subsystems are available in the market with controller cards that will reside in the same card rack as the PLC. These include scales and load cell controllers, radio frequency identification tag readers, motion controllers, and numerous forms of communication interfaces, from basic RS-232 to proprietary network protocols. Another interesting development is the availability of actuators with small amounts of I/O that are equipped with the ability to communicate over I/O networks. An example of this is the availability of intelligent valve controllers that will reside on the I/O network. No individual wiring of the individual solenoids or switches back to I/O modules is required. By simply connecting the serial I/O network cable to the valve controller and doing some configuration, limit switches and position status can be read and each solenoid becomes individually addressable and can be actuated directly from the program. This cuts down on the field wiring required to install and operate the valves. [2]

3. I/O Systems

Your I/O system is the equipment that takes input signals from the sensors and turns them into digital bits for your process controller to read. It also takes the bits from your process controller and turns them into voltage signals to drive your motor starters and valves. Traditional I/O systems involve a card rack that is populated with individual input and output cards. Each card usually handles 8, 16, or 32 points and is tailored to the specific voltage and current characteristics of the signals it will accept: 24 Vdc, 120 Vac, mV (for thermocouples), or 4–20 mA for other analog instruments. Many vendors offer diagnostic versions of their cards. These diagnostic cards not only tell you if the input signal from the device is present but also tell you if the signal wire is broken or short circuited. Generally, I/O racks are placed in an electrical room or marshalling panel that is centrally located to the majority of the sensors on the process. Since a single rack can handle several hundred I/O points, often there is several hundred feet of signal wire from the rack to each device. With this concentration of input capability, one or two rack locations can then cover the entire facility, with hundreds of individual wiring runs going from the rack to each device.

An option to concentrating all of the I/O into several centrally located racks is the concept of distributed I/O. In this arrangement, several small I/O modules of 8–16

points each are located in the field, nearer to the devices they monitor. This concept reduces the amount of field wiring from the device to the I/O module and puts the module close to the monitored process or equipment. Often, skid mounted equipment can be supplied with all I/O factory wired to one of these modules mounted on board the skid.

Regardless of whether it is rack, distributed, or point I/O, all of these solutions need to communicate back to the PLC over a serial network. In the past, vendors provided separate proprietary networks that talked only to their I/O and to devices from selected partners. These original networks ran at baud rates in the 50–200 K range.

Modern I/O networks now run in the 2–4 MBd range. Other developments include the growing use of the Ethernet as an I/O device network. Another consideration with proprietary I/O networks is the ability to place intelligent devices directly on these networks. Often, equipment such as variable frequency drives or scale controllers contain a large amount of data that is of value to the control system and operator. Placing these devices on the PLC's I/O network allows these data to be easily communicated to the PLC for use in controlling the process or for passing data through for display on the system HMI.

To manage the amount of data available in intelligent instruments, vendors have introduced a number of networks that are designed to connect directly to the instruments themselves. These networks are generically referred to as field buses and are intended to run from the controller to the instrument, then on to the next instrument in daisy chain fashion. In this configuration, they replace both the I/O modules and the individual runs from the I/O module to the devices. Currently, there are several competing standards for these device networks. Some, such as Device Net and ASI, are designed primarily for digital data and are intended for simple devices such as limit switches or photoeyes. Others, such as Profibus and Foundation Fieldbus, are intended for analog instruments with greater amounts of data to transmit. All of them have special cabling installation and connection requirements, require engineering configuration and setup of both the instruments and the networks themselves, and work only with instruments specifically manufactured and certified for that network.

As you can see, there are numerous options when it comes to I/O solutions. Each has its advantages and disadvantages. The traditional rack I/O usually provides the lowest per point cost and allows you to centralize all of your I/O equipment in one clean, secure, and environmentally controlled room. On the other hand, unless your process is concentrated in a small area, it requires long wiring runs to connect to the devices in the field. Distributed I/O modules allow you to reduce the length of the wiring runs to your devices. However, they are slightly more expensive, often place the module in the field in a hostile or even hazardous environment, and require that the I/O communication network be run out in the field to their location. Finally, field bus networks offer savings in the costs of installation wiring, allow the instruments to provide large amounts of data to the controller and operator interface, and ease the configuration of the instruments by allowing the maintenance technician to access all instruments from one PC connected to the bus. On the

minus side, the instruments can be more expensive, the instruments and network require engineering to configure and setup, and the networks can be difficult to trouble shoot if problems arise. [2]

III. RAW MATERIAL TRANSFER FROM QUARRY TO DIFFERENT SILOS

Cement industries typically produce Portland cement. Most of the raw materials used are extracted from the earth through mining and quarrying. Those are lime (calcareous), silica (siliceous), alumina (argillaceous), and iron (ferriferous). As limestone is the prime constituent of cement, the major cement plants are located near the good quality lime stone quarry. At first lime stones and quarry clays are fed to primary crusher house for raw crushing. Then the materials are transferred to secondary crusher house. After that the crushed materials are fed to the stock pile. Inside the stock pile there is a stacker/reclaimer which segregates the raw material quality wise in to different stacks. The stacking and reclaiming systems operate independently. There are also four additives- iron ore, bauxite, laterite and flourspar into the stack pile to get required composition of cement. The additives are brought to the stack pile by conveyor C4. Then according to the requirement limestone, iron ore, bauxite, laterite and flourspar are transferred to different silos by their respective conveyors. Inside each silo there are three level detectors which detect the level of materials inside it. [1] The process is shown in fig.1

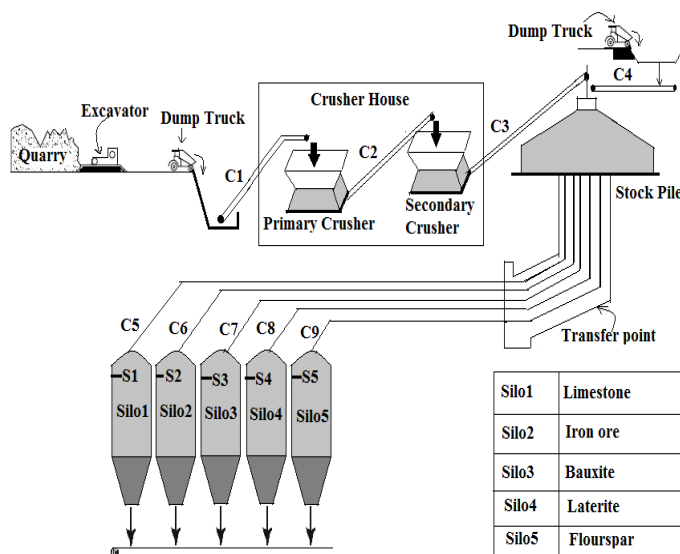


Fig 1. Raw Material Transfer from Quarry to Different Silos

IV. Process Automation

To make this process fully automatic a PLC unit is used. PLC takes real time decision depending upon the various field level input signals from various sensors placed in different critical points and sends the decision to the output devices.

1) Input

Pushbutton [PB(1-9)], Upper level detector [S(1-5)], conveyor[C4].

2) Output

Conveyor [C (1-3, 5-9)], Primary crusher(PC), Secondary crusher(SC), Stacker/reclaimer system(S/R)

3) Process Description

At first an operator starts the entire process by pressing a push button PB1. As soon as the operator presses PB1, conveyor C1 starts rolling and the bulk materials i.e. lime stones are taken from quarry by conveyor C1 to primary crusher (PC). The primary crusher will start by an on delay timer TT1. After some time delay, required for primary crushing C2 starts running and the raw crushed materials are transferred to secondary crusher (SC). This time on delay is defined by timer TT2. The secondary crusher (SC) is started together with C2. Conveyor C3 will start after a time on delay (TT3) of starting the secondary crusher to transfer the material from crusher house to stock pile. There are two pushbutton switches PB3 and PB4 inside the stock pile. Now if PB3 is closed manually, the stacker /reclaimer system (S/R) starts directly or after a time on delay(TT4) of starting either conveyor C3 or C4.

Pushbutton PB4 is provided to stop the stacker/reclaimer system manually. For safe operation each and every process should be turned off sequentially. So to achieve these five off-delay timers are used i.e. TT5, TT6, TT7, TT8, TT9. When conveyor C1 are on, the timer TT5 is true. The Done bit of TT5 is latched with PC. When the primary crusher (PC) is on, the timer TT6 is true. The Done bit of TT6 is latched with C2. TT7 is latched with the secondary crusher (SC) which remains true till C2 remains on. Timer TT8 remains true till SC is running. The done bit of TT8 is latched with the C3. TT9 remains true till conveyor C3 is on. There are also an off delay timer TT10 which remains true till C4 is on. Now due to any fault or any other reason if emergency plant shutdown is required, the operator presses PB2. As soon the operator presses PB2 at first conveyor C1 will stop.

Then according to the PLC programming the primary crusher(PC), conveyor(C2), secondary crusher(SC), conveyor(C3) and S/R will go off sequentially. The same things will happen in case of conveyor C4. Push button switches PB5, PB6, PB7, PB8, PB9 are the operating switches of limestone conveyor (C5), iron ore conveyor (C6), bauxite conveyor (C7), laterite conveyor(C8), flourspar conveyor(C9) respectively.

Through these conveyors the materials are transferred to their respective silos. S1, S2, S3, S4, S5 are the upper level detectors of different silos. If upper level detector is high, the corresponding conveyor i.e. C5, C6, C7, C8, C9 will be off. [1]

V. PLC Ladder Logic Program

The PLC is programmed using ladder logic which is used to control the whole process of automation i.e. raw material transfer from quarry to silos.

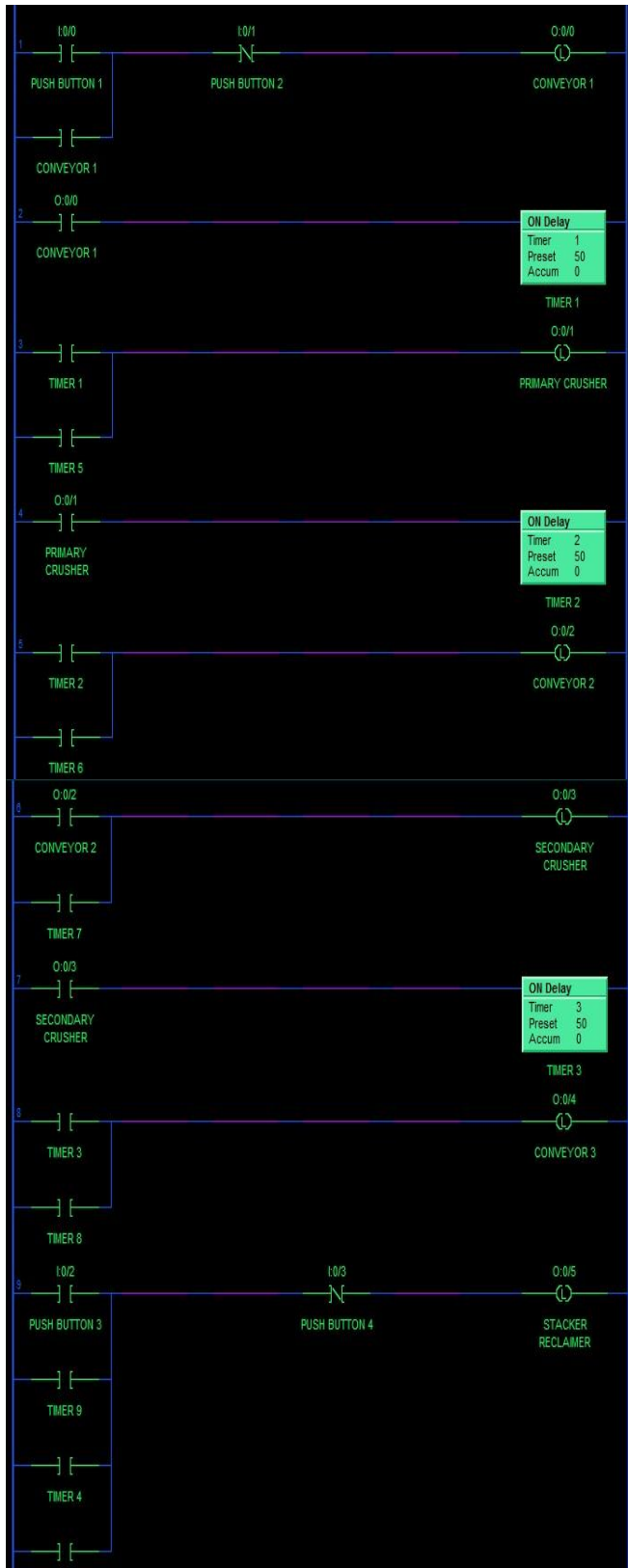


Fig -2(a) Ladder logic for raw material transfer from quarry to silos

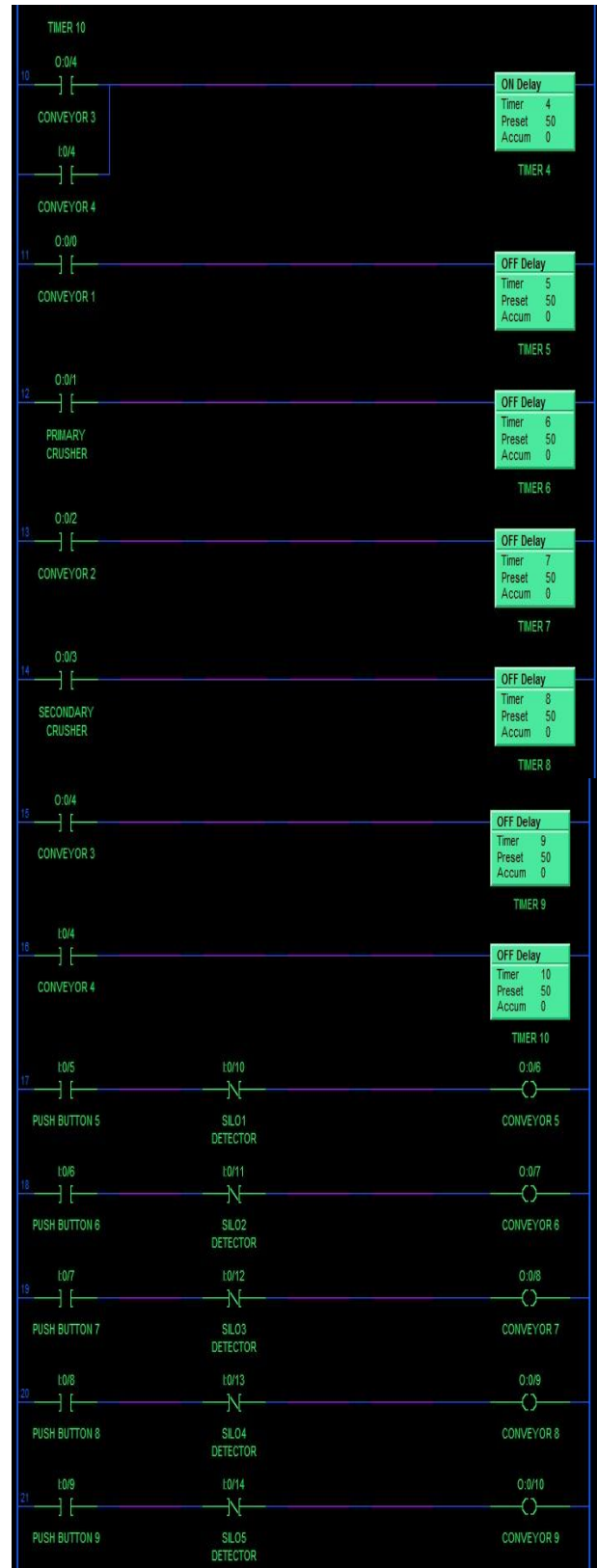


Fig -2(b) Ladder logic for raw material transfer from quarry to silos

VI. CONCLUSION

Though India is the second largest producer of cement in the world, still those industries need to further concentrate on modernization and upgradation of technology, optimization of operations and increased application of automation and information technology which reduces the

energy consumption, production cost and increases the production speed [5]. So this paper is appropriate to fulfil those requirements of the cement industries. This innovative automation process is highly flexible and easily adaptable to new and existing situations. Automation provides some form of monitoring capabilities and provisions for programmable troubleshooting which reduces the downtime. The automation process also has flexibilities in programming and control techniques. As the PLC does intelligently the overall operation and as it has centralized control futures. So it also helps to reduce the manpower and at the same time it reduces the workers' strain. [6]

References

- 1) "PROCESS AUTOMATION OF CEMENT PLANT", Akash Samanta, Ankush Chowdhury, Arindam Dutta, International Journal of Information Technology, Control and Automation (IJITCA) Vol.2, No.2, April 2012 pages(63-68)
- 2) "Power of Automation" GREGORY DIFRANK, An overview, technology, and implementation, 1077-2618/08/\$25.00©2008 IEEE
- 3) "Automation of coal handling plant", Arindam Dutta, Ankush Chowdhury, Sabhyasachi karforma, Subhabrata Saha, Saikat Kundu, Dr. Subhasis Neogi, in Pro.of conf. on control communication and power Engineering 2010,ACEEE, paper- 67-146-149,p (147-149).
- 4) Automation. Webster's Third New International Dictionary, Unabridged, [Online]. Available: <http://unabridged.merriam-webster.com>
- 5) , "Material mix control in cement plant automation" A.K. Swain, 0272- 1708/95/\$04.00@1 995IEEE, August 1995.pages(23-27).
- 6) "Record Growth and Modernisation in Indian Cement Industry", A quarterly information carrier of ncb services to the industry, VOL IX NO 4 DECEMBER 2007, seminar special, ISSN 0972-3412.
- 7) Madhuchanda Mitra and Samarjit Sen Gupta, Programmable Logic Controllers and Industrial Automation an Introduction, ISBN-81-87972-17-3, 2009, pages (1-51).
- 8) www.vitalsystems.com/superlogic version 6.2.1
- 9) Programmable controllers, theory & implementation, second edition by L.A.Bryan, E.A.Bryan

Estimation of Cost Analysis for 4 Kw Grids Connected Solar Photovoltaic Plant

Rohit Pandey¹, Dr. M.K.Gaur², Dr. C.S.Malvi³

Department of Mechanical Engineering, Madhav Institute of Technology and Science Gwalior (M.P.) 474005, INDIA

ABSTRACT: The depletion of fossil fuel resources on a worldwide basis has necessitated an urgent search for alternative energy sources to meet up the present day demands. Solar energy being a clean, inexhaustible and environment-friendly potential resource among all renewable energy options. But in the present scenario, there is a need of continuous supply of energy, which cannot be full filled by alone wind energy system or solar photovoltaic system due to seasonal and periodic variations. Therefore, in order to satisfy the load demand the combination of solar and conventional conversion units are now being implemented as a Grid connected energy systems. The objective of this work is to estimate the cost analysis for 4 KW grid connected solar photovoltaic plant and developed a system based on the potential estimations made for a chosen area of 50m². The specifications of equipment are provided based on the availability of the component in India. Annual energy generation by proposed Grid connected SPV power plant is calculated.

KEYWORDS: Solar energy, Grid connected SPV system.

I. INTRODUCTION

Photovoltaic's offer consumers the ability to generate electricity in a clean, quiet and reliable way. Photovoltaic systems are comprised of photovoltaic cells, devices that converted light energy directly into electricity. It is anticipated that photovoltaic systems will experience an enormous increase in the decades to come. However, a successful integration of solar energy technologies into the existing energy structure depends also on a detailed knowledge of the solar resource. But to note it is essential to state the amount of literature on solar energy, the solar energy system and PV grid connected system is enormous. Grid interconnection of photovoltaic (PV) power generation system has the advantage of more effective utilization of generated power. However, the technical requirements from both the utility power system grid side and the PV system side need to be satisfied to ensure the safety of the PV installer and the reliability of the utility grid. For this survey we have gone through different books, journals and papers to get its keen knowledge.

II. LITERATURE REVIEW

Souvik Ganguli et.al (2009) [1] presented a Estimation of Grid Quality Solar Photovoltaic Power Generation Potential and its Cost Analysis in Some Districts of West Bengal. The objective of their work was to estimate the potential of grid quality solar photovoltaic power in some districts of West Bengal (Birbhum, Burdwan, Hooghly, Howrah and Kolkata), study the solar radiation level and potential of the above mentioned districts and finally develop a system corresponding to the potential.

Equipment specifications were provided based on the system developed and finally cost analysis was also carried out.

A.S. Elhodeiby et.al (2011) [2] presented a performance analysis of 3.6 kW Rooftop grid connected solar photovoltaic system in Egypt. The system was monitored for one year and all the electricity generated was fed into the 220 V, 50 Hz low voltage grid to the consumer. D.Picault et.al (2009) [3] presented an over view of current architectures used in grid connected systems, five key points for comparison based on topology upgradeability, performance under shaded conditions, degraded mode operation, investment costs and ancillary service participation. The proposed method can be adapted to the user's particular needs and expectations of the photovoltaic plant. These evaluation guidelines may assist grid-tied PV system users to choose the most convenient topology for their application by weighting the evaluation criteria Phil Bolduc et.al [4] presented a paper about performance of a grid –connected PV system with energy storage. One kilowatt amorphous photovoltaic system has been operated in a grid-connected mode with energy storage. The purpose of the system development and performance experiment is to investigate the additional value a gridconnected system garners with dispatchable battery energy storage. These values are then weighed against the added cost of the system and inefficiencies incurred in the charging and discharging of the battery.

R. Ramkumar et.al (1993) [5] presented a paper of photovoltaic systems including a discussion of major U.S. and international activities. After a brief review of system types and output characteristics, various system configurations were discussed and a classification based on photovoltaic (PV) system rating was provided. Modeling, design, and economic Considerations were briefly discussed. The worldwide status of PV system technology was discussed with a view to making an assessment of the future. The assessment presented includes some specific areas for further research and development.

Eduardo Román et.al (2006) [6] presented a performance of a grid connected PV system with energy storage. three kilo watt amorphous photovoltaic system has been operated in a grid-connected mode with energy storage. The purpose of the system development and performance experiment is to investigate the additional value a grid connected system garners with dispatch able battery energy storage. These values are then weighed against the added cost of the system and inefficiencies incurred in the charging and discharging of the battery.

Evert Nieuwlaar (1997) [7] presented an over view of current power generation used in grid connected systems, the points for comparison based on, performance under shaded conditions, degraded mode operation, investment costs and ancillary service participation. The

proposed method can be adapted to the user's particular needs and expectations of the photovoltaic plant. These evaluation guidelines may assist grid-tied PV system users to choose the most convenient topology for their application by weighting the evaluation criteria.

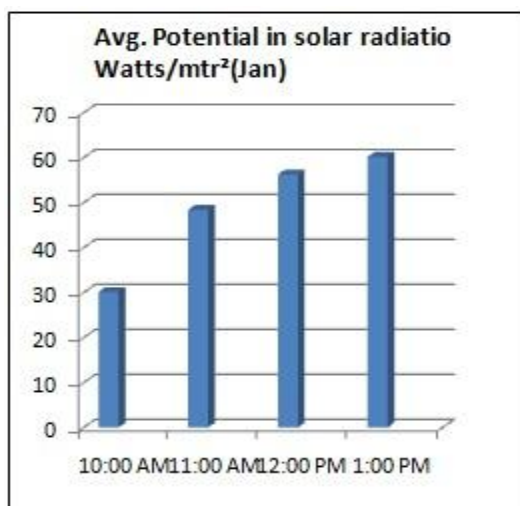
Kosuke Kurokawa et.al (2002) [8] presented paper about the cost analysis of very large scale PV system on the world desert. a 100 MW very large scale photovoltaic power generation (VLS-PV) system was estimated assuming that it is installed on the world deserts, which are Sahara, Negev, Sonora, Great Sandy and Gobi desert. PV array was dimensioned in detail in terms of array layout, support, foundation, wiring and so on.

III. METHODOLOGY

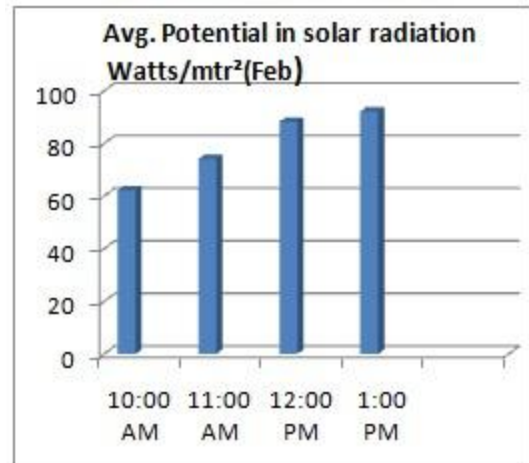
To find out the cost analysis for 4 KW grid connected solar PV plant in India, the solar radiation over different months measured. Then the diurnal variations, average monthly output are find out and related graphs are plot for showing the variation. We started our project work from January month. So we measured value of solar radiation from January to April month after that we calculated the diurnal variations, average monthly output for four months (Jan 2012 to April 2012). Thus from these data we can estimate the rating of solar PV power plant for Indore. For estimation of solar potential we need reading of solar radiation for our site. For the better understanding of the methodology, the measured radiation data sheet of Indore district for the month of April 2012 has been given as a sample. The diurnal variation for four months are plotted. From that the monthly output are calculated. Input solar radiation means how much amount of solar radiation is coming from sun and Output solar radiation means how much amount of solar radiation we can utilize to generate electricity which is depends upon the efficiency of the PV module. For calculating the output the efficiency of the PV module is taken as 13.2%. Chosen area for the estimated plant capacity is considered as 50 m².

3.1 Graphs for Diurnal Variations (Jan 2012 to April 2012)

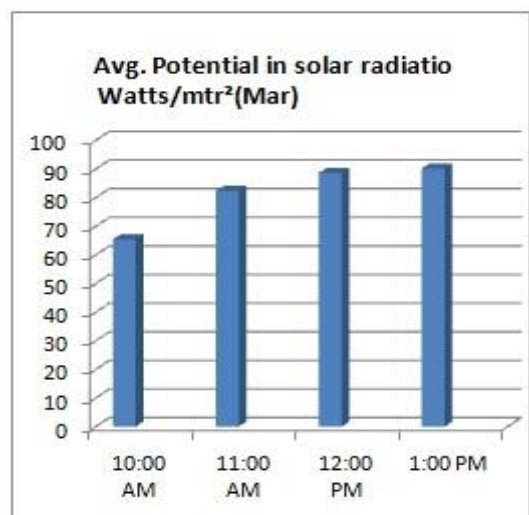
Graph is plotted between average solar radiation available in Watts/mtr² and different time interval of day for different months.



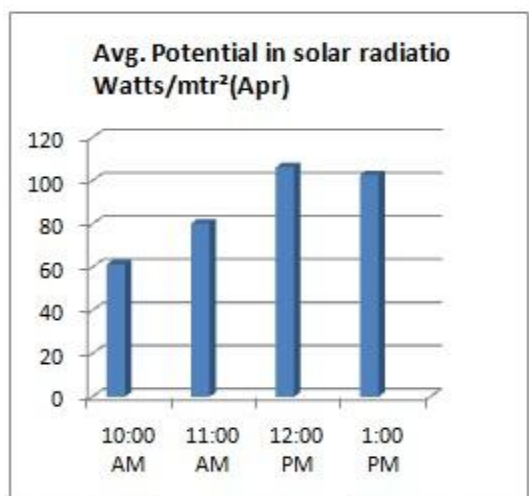
Graph 1



Graph 2



Graph 3



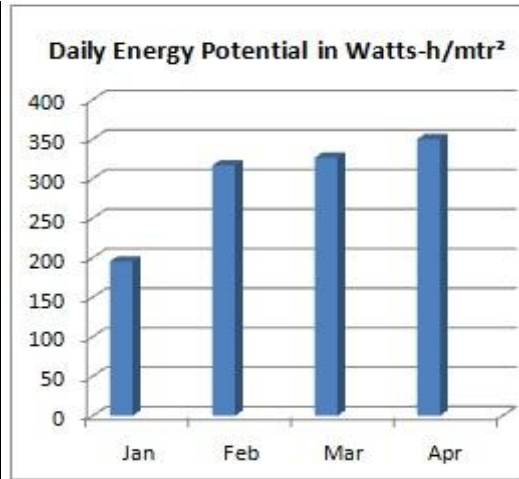
Graph 4

IV. TOTAL POTENTIAL

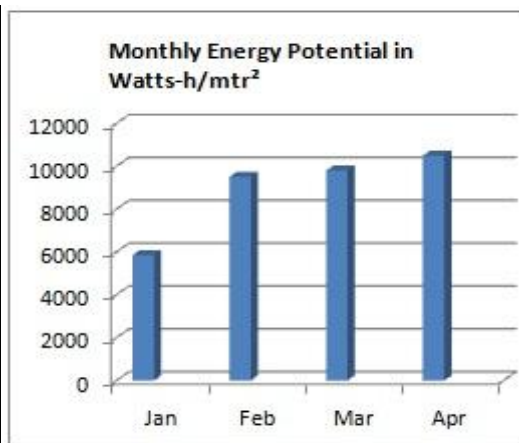
Here the average yearly energy output is calculated by multiplying average monthly energy output with total number of month 12. The daily energy output also calculated for various months shown in 2nd coulomb. Monthly energy output is calculated by multiplying the

number of days of month with the daily energy output shown in 3rd coulomb for various months. Kilowatt-Hour (kWh) means 1,000 thousand watts acting over a period of 1 hour. The kWh is a unit of energy. 1 kWh=3600kJ.

4.1 Graph for Daily & Monthly Energy Potentials (Watt/mtr²-hr)



Graph 5,6



V. COST ANALYSIS FOR 4 KW GRID CONNECTED SOLAR PV

VI. PLANT

A. Cost of Solar panels: - we use the BP 5128 most powerful module manufactured by BP Solar [34], cost of solar panel is Rs.140 per watt. So cost of 150 watt panel is (150 × 140) Rs.21000.

We use 40 numbers of panels so Cost estimate for total panels used (40 × 21000) Rs.840000.

B. Cost of 3-φ Inverter: - Only one piece of 10.5 - 12 KVA or 10 KW of an inverter Power Conditioning Unit is used, multiply the size of the inverter by Rs. 25 per rated watt.

Cost estimate for Inverter (25 × 10000) Rs. 250000.

C. Cost of 3-φ step up Transformer: - Only one piece of 12 KVA or 10 KW of a step up. Transformer is used, multiply the size of the Transformer by Rs. 20 per rated watt.

Cost estimate for Inverter (20 × 10000) Rs. 200000.

Subtotal: Rs.1290000.

D. Multiply the subtotal above by 0.2 (20%) to cover balance of system costs (wire, fuses, switches, etc.).

Cost Estimate for Balance of System: (1290000 × 0.2) Rs. 258000.

Total Estimated PV System Cost is Rs.1548000.

VI. CONCLUSION

The design described is based on the potential measured. System sizing and specifications are provided based on the design made. Finally, cost analysis is carried out for the proposed design. Total Estimated PV System Cost is Rs1548000. The methodology adopted seems satisfactory for determining the possible plant capacity for an arbitrarily chosen area.

VII. ACKNOWLEDGEMENT

The authors would like to thank MPUVN Limited for providing data's to estimate the Grid connected solar photovoltaic system & also thank to experts for providing valuable guidance.

REFERENCES

1. Souvik Ganguli and Sunanda Sinha, "A Study and Estimation of Grid Quality Solar Photovoltaic Power Generation Potential in some districts of West Bengal Patiala, Page(s): 522-528, 29-30th Oct., 2009.
2. A.S. Elhodeiby, H.M.B. Metwally and M.A. Farahat, "Performance analysis of 3.6KW Rooftop grid connected photovoltaic system Egypt. International Conference on Energy Systems and Technologies (ICEST 2011) 11-14 March 2011, Cairo, Egypt.
3. D. Picault, B. Raison, and S. Bacha, "Guidelines for evaluating grid connected PV system topologies". IEEE International Conference on Industrial Technology. Page(s): pp. 1-5, 2009.
4. Phil Bolduc, David Lehmicke & Joseph Smith, "Performance of a grid connected PV system with energy storage". IEEE Photovoltaic. Page(s): 1159 – 1162, 1993.
5. R. Ramkumar & J. E. Bigger, "Photovoltaic Systems". Proceedings of IEEE. Volume: 81, Page(s): 365 – 377, 1993.
6. Eduardo Román, Ricardo Alonso & Pedro Ibañez, "Intelligent PV Module for Grid- Connected PV Systems", IEEE Transactions on Industrial electronics, Vol.53.No.4, Page(s): 1066 – 1073, August 2006.
7. Evert Nieuwlaar & Erik Alsema, Environmental aspects of PV power systems", Report on the IEA PVPS Task1 Workshop, 25-27 June 1997, Utrecht TheNetherlands. Report no. 97072, December 1997.
8. Kosuke Kurokawa, Kazuhiko Kato, Masakazu Ito, Keiichi Komoto, Tetsuo Kichim, & Hiroyuki Sugihara "The cost analysis of very large scale PV system on the world desert". Photovoltaic Specialists IEEE Conference, Page(s): 1672 – 1675, 2002.

Airy Function Based Papr Reduction Method for Ofdm Systems

K.HEMANAGENDRA SANKAR¹, Prof K.ASHOK BABU²

^{1, 2}Department of ECESri Indu college of Engg and Tech, Hyderabad, A. P, India

Abstract: Orthogonal Frequency division multiplexing (OFDM) is widely used technique in modern day wireless communication systems which provides robustness to channel fading and immunity to impulse interference. Despite of its advantages, one of the major drawbacks of OFDM system is very high peak-to-average power ratio (PAPR). Among the various PAPR reduction techniques, companding appears attractive for its simplicity and effectiveness. In this paper novel companding technique based on mathematical airy function is proposed which offers improved bit error rate, minimizes out-of-band interference and reduce PAPR effectively. Simulation results illustrates the performance of the system under Additive White Gaussian Noise (AWGN) and further evaluation is done for comparing the proposed companding technique with previous techniques.

Keywords: OFDM, OBI, PAPR, Companding

I. INTRODUCTION

Orthogonal Frequency Division Multiplexing (OFDM) has significant ability to support high data rates for wide area coverage, robustness to multipath fading, immunity to impulse interference [1,2]. However one of the major drawbacks of OFDM signal is its large envelope fluctuation, likely resulting in large peak-to average power ratio (PAPR), which distorts the signal if the transmitter contains the non-linear components such as power amplifiers and these may causes deficiencies such as intermodulation, spectral spreading and change in signal constellation. Minimizing PAPR allows higher Average power to be transmitted for a fixed peak power and improving the overall signal to noise ratio at the receiver.

Some of the methods proposed in literature to reduce the PAPR of OFDM signals include several techniques such as amplitude clipping, tone reservation (TR), active constellation extension (ACE) and coding [1,2][13], selective mapping [3], partial transmitting [4]. In [5], optimal companding coefficient is determined to enlarge small OFDM signals along with PAPR reduction. In [6], non-linear companding scheme is described by a single valued function which allows to be transformed before amplification. In exponential companding OFDM signals are transformed into uniformly distributed.

The idea behind these methods is that by clipping the peaks [8] of OFDM signal which is the simplest technique but it causes additional clipping noise and out-of-band interference (OBI) which degrades the system performance. But in μ -law companding, the PAPR is reduced at the expense of increasing the average power. In order to overcome the problem of increase of average power and to have efficient PAPR reduction, a non-linear companding technique namely exponential companding has been developed. In this paper, a simple but effective novel new companding technique which uses the special airy

function to reduce the peak-to-average power ratio of OFDM signal is proposed.

II. PEAK TO AVERAGE POWER RATIO (PAPR)

An OFDM signal can be expressed as

$$s(t) = \frac{1}{\sqrt{N}} \sum_{k=0}^{N-1} S_k e^{j2\pi kt/NT}, \quad t \in [0, NT] \quad (1)$$

Where S_k is the complex based band modulated symbol and N is the number of subcarriers

Let S^m be the m -th OFDM symbol, then its PAPR is defined as

$$\text{PAPR}_m = \frac{\|s^{(m)}\|_{\infty}^2}{E[\|s^{(m)}\|^2]/N} \quad (2)$$

The peak power occurs when modulated symbols are added with the same phase. The effectiveness of a PAPR reduction technique is measured by the complementary cumulative distribution function (CCDF), which is the probability that PAPR exceeds some threshold [11, 12], i.e.

$$\text{CCDF} = \text{Probability}(\text{PAPR} > \text{PAPR}_0) \quad (3)$$

III. PROPOSED METHOD

In OFDM system, the ideal case is to reduce the PAPR to make the amplitude of the complex baseband signal constant. Quantification of the OBI caused by companding requires the knowledge of the power spectral density (PSD) of the companded signal. Unfortunately analytical expression of the PSD is in general mathematically intractable, because of the nonlinear companding transform involved. Here we take an alternative approach to estimate the OBI. Let $f(x)$ be a nonlinear companding function, and $x(t) = \sin(\omega t)$ be the input to the compander. The companded signal $y(t)$ is:

$$y(t) = f[x(t)] = f[\sin(\omega t)] \quad (4)$$

We now propose a new companding technique using a smooth function, namely the airy special function. The companding function is as follows:

$$f(x) = \beta \cdot \text{sign}(x) \cdot [\text{airy}(0) - \text{airy}(\alpha \cdot x)] \quad (5)$$

Where $\text{airy}(\cdot)$ is the airy function of the first kind

$$\text{Ai}(x) = \frac{1}{\pi} \int_0^{\infty} \cos\left(\frac{1}{3}t^3 + xt\right) dt, \quad (6)$$

Where α is the parameter that controls the degree of companding β is the factor adjusting the average output power of the compander to the same level as the average input power:

$$\beta = \sqrt{\frac{E[|x|^2]}{E[\text{airy}(0) - \text{airy}(\alpha|x|)^2]}} \quad (7)$$

The de-companding function is the inverse of $f(x)$:

$$f^{-1}(x) = \frac{1}{\alpha} \cdot \text{sign}(x) \cdot \text{airy}^{-1} \left[\text{airy}(0) - \frac{|x|}{\beta} \right] \quad (8)$$

IV. EXPERIMENTAL RESULTS

The spectrums of the uncompressed and compressed OFDM signals by the proposed scheme are illustrated in Fig.1. From the simulation results; it is observed that the proposed algorithm produces OBI almost 3dB lower than the exponential algorithm, 10dB lower than the μ -law. Fig.2 depicts the CCDF of the three companding schemes. The new algorithm is roughly 1.5dB inferior to the exponential, but surpasses the μ -law by 6dB. The BER vs. SNR is plotted in Fig.3 proposed algorithm has improved bit error rate compared with exponential and μ -law algorithms. The amount of improvement increases as SNR becomes more.

One more observation from this simulation is that unlike the exponential companding whose performance is found almost unchanged under different degrees of companding, the new algorithm is flexible in adjusting its specifications simply by changing the value of α in the companding function.

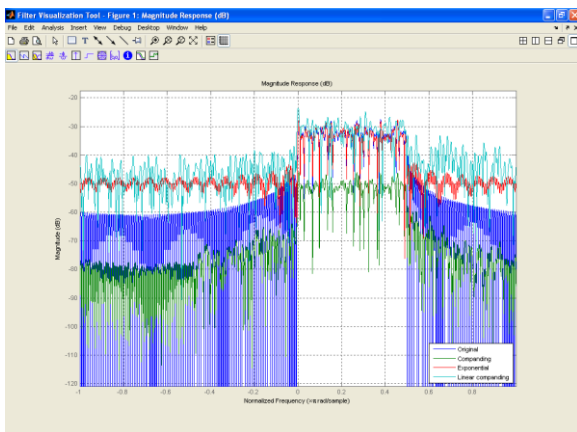


Figure 1: Power spectral density of original and companded signals (companded i/p power = 3dBm, $\alpha = 30$)

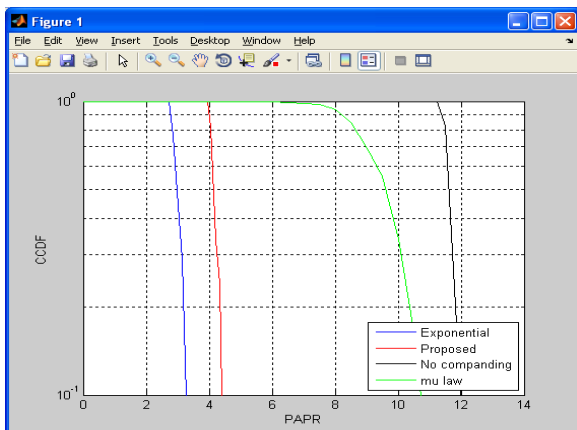


Figure 2: Complimentary Cumulative Distribution function of original and companded signals companded i/p power = 3dBm, $\alpha = 30$)

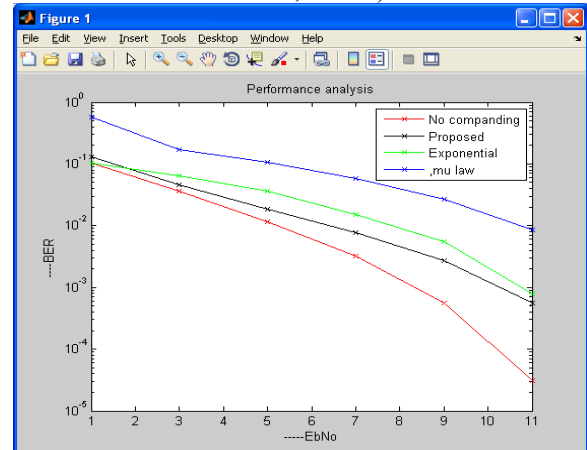


Figure3: BERVs SNR for original and companded signals in AWGN channel and Linear LDPC coding (companded i/p power = 3dBm, $\alpha = 30$)

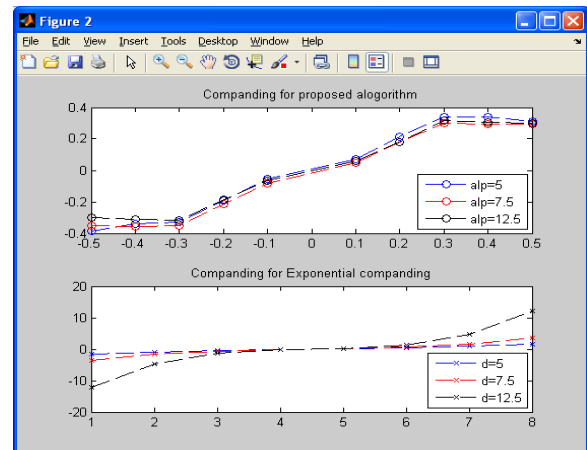


Figure 4: Comparative analysis between the proposed and the exponential companding transform

V. CONCLUSION

An attractive and simpler companding algorithm is proposed to effectively reduce PAPR problem in Orthogonal Frequency Division Multiplexing (OFDM) with mathematical airy function. By careful selection of the control parameter α explained in the paper, the PAPR reduction can be achieved in a better way and the BER performance can be improved. Simulation results show, that the proposed algorithm offers improved performance in terms of BER and OBI while reducing PAPR effectively compared with exponential and μ -law companding schemes.

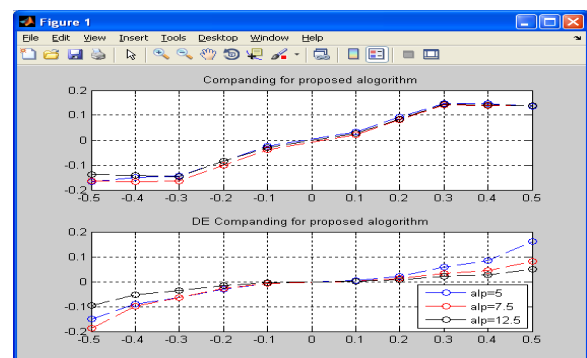


Figure 5: Proposed companding method analysis for companding and de-companding

REFERENCES

- [1] R.van Nee and R.Prasad, "OFDM for Wireless Multimedia Communications. Boston, MA: Artech House, 2000.
- [2] S.H.Han and J. H. Lee, "An Overview of peak-to-averagepower ratio reduction techniques for multicarrier transmission," *IEEE Wireless Commun.*, vol. 12, pp. 56-65, Apr. 2005.
- [3] R.W.Bauml, R.F.H.Fischer, and J.B. Huber, "Reducing thepeak-to-average power ratio of multi carrier modulation byselective mapping," *IEE Electron. Lett.*, vol.32, pp. 2056-2057, Oct. 1996.
- [4] S.H Muller and J.B.Huber, "OFDM with reduced peak-toaverage power ratio by optimum combination of partial transmit sequences," *IEE Electron. Letters*, vol .33,pp. 368-369, Feb.1997.
- [5] X. Wang, T. T. Tjhung, and C. S. Ng, "Reduction of peak-toaveragepower ratio of OFDM system using a companding technique," *IEEE Trans. Broadcast.*, vol. 45, no. 3, pp. 303-307, Sept. 1999.
- [6] T. Jiang and G. Zhu, "Nonlinear companding transform forreducingpeakto- average power ratio of OFDM signals,"*IEEE Trans. Broadcast.*, vol. 50, no. 3, pp. 342-346, Sept.2004.
- [7] T. Jiang, Y. Yang, and Y. Song, "Exponential compandingtechnique for PAPR reduction in OFDM systems, *IEEETrans.Broadcast*" vol. 51, no. 2, pp. 244-248, June 2005.
- [8] J.Akhtman, B.Z. Bobrovsky , and L.Hanzo, "Peak-to-averagepower ratio reduction for OFDM modems," in *Proc. 57thIEEE Semi-Annual Vehicular Technology Conf. (VTC '03)*,vol. 2, Apr. 2003. pp 1188-1192.
- [9] B.S. Krongold and D.L.Jones , "PAR Reduction in OFDMvia active constellation extension ," *IEEE Trans . Broadcast*,vol. 49, pp. 258-268, Sep. 2003.
- [10] Zhan T.andParhi K.K, "Joint regular LDPC Code andDecoder/Encoder Decoder," *IEEE Transactions on signalprocessing*, vol.52, no.4, pp. 1065-1079,2004.
- [11] R.Van Nee and A. de Wild, "Reducing the peak-to-averagepower ratio of OFDM,"*Proc .IEEE vehicular technologyConf.(VTC'98)*, pp. 2072-2076,May 1998.
- [12] H. Ochiai and H. Imai, "On the distribution of the peak-toaverage power in OFDM signals," *IEEE transactions onCommunications*, vol.49, pp.282-289, Feb.2001.
- [13] T. Jiang and Y. Imai, "An Overview: Peak-To-Average PowerRatio Reduction Techniques for OFDM Signals," *IEEETransactions on Broadcasting*, Vol. 54, No. 2, 2008, pp. 257-268doi:10.1109/TBC.2008.915770
- [14] J. Kim and Y. Shin, "An Effective Clipping CompandingScheme for PAPR Reduction of OFDM Signal," *IEEEInternational Conference on Communications 2008, Beijing,2008*, pp. 668-672.
- [15] M.SushanthBabu and Prof.K.KishanRao, "OFDMPerformance with Optimum Training Symbols in WiMaX802.16e", *IEEE International Conference on InformationTechnology on Real*



Mr.K.HEMANAGENDRASANKAR

GRADUATE IN SWARNA BHARATHI INSTITUTE OF SCIENCE AND TECHNOLOGY IN **ELECTRONICS AND COMMUNICATIONS**.NOW PURSING MASTERS IN DIGITAL ELECTRONICS AND COMMUNICATION SYSTEMS(DECS) FROM SRI INDU COLLEGE OF ENGG AND TECH.



I EXPRESS MY GRATITUDE TO **Dr.K.ASHOK BABU** Professor & HEAD OF THE DEPARTMENT (ECE) OF AND HIS CONSTANT COOPERATION ,SUPPORT AND PROVIDING NECESSARY FACILITIES THROUGH OUT THE M.Tech PROGRAM .HE HAS 16 YEAR FO EXPERINCE ,AT BOTH B.Tech AND M.Tech LEVEL AND WORKING AS A PROFESSOR IN SRI INDU COLLEGE OF ENGG AND TECHNOLOGY.

Different Image Fusion Techniques –A Critical Review

Deepak Kumar Sahu¹, M.P.Parsai²

^{1, 2}(Department of Electronics & Communication Engineering, Jabalpur Engineering College, Jabalpur MP, India)

ABSTRACT : Image Fusion is a process of combining the relevant information from a set of images into a single image, where the resultant fused image will be more informative and complete than any of the input images. Image fusion techniques can improve the quality and increase the application of these data. This paper presents a literature review on some of the image fusion techniques for image fusion like, primitive fusion (Averaging Method, Select Maximum, and Select Minimum), Discrete Wavelet transform based fusion, Principal component analysis (PCA) based fusion etc. Comparison of all the techniques concludes the better approach for its future research.

Keywords: Discrete Wavelet Transform (DWT), Mean Square Error (MSE), Normalized correlation (NC), Peak signal to noise ratio (PSNR), Principal Component Analysis (PCA),

I. INTRODUCTION

Image fusion means the combining of two images into a single image that has the maximum information content without producing details that are non-existent in the given images[1][2]. With rapid advancements in technology, it is now possible to obtain information from multi source images to produce a high quality fused image with spatial and spectral information [2] [3]. Image Fusion is a mechanism to improve the quality of information from a set of images. Important applications of the fusion of images include medical imaging, microscopic imaging, remote sensing, computer vision, and robotics .Use of the Simple primitive technique will not recover good fused image in terms of performance parameter like peak signal to noise ratio (PSNR), Normalized correlation (NC), and Men square error (MSE). Recently, Discrete Wavelet Transform (DWT) and Principal Component Analysis(PCA),Morphological processing and Combination of DWT with PCA and Morphological techniques have been popular fusion of image[4][5][6]. These methods are shown to perform much better than simple averaging, maximum, minimum.

This report is organized as follows: Section II presents brief description of image Fusion techniques, Section III gives Performance Measures parameter of Fusion techniques , Section IV presents performance comparison of those techniques and finally, conclusion is presented in Section V.

II. IMAGE FUSION TECHNIQUES

The process of image fusion the good information from each of the given images is fused together to form a resultant image whose quality is superior to any of the input images .Image fusion method can be broadly classified into two groups –1.Spatial domain fusion method 2.Transform domain fusion

In spatial domain techniques, we directly deal with the image pixels. The pixel values are manipulated to achieve desired result. In frequency domain methods the

image is first transferred in to frequency domain. It means that the Fourier Transform of the image is computed first. All the Fusion operations are performed on the Fourier transform of the image and then the Inverse Fourier transform is performed to get the resultant image. Image Fusion applied in every field where images are ought to be analyzed. For example, medical image analysis, microscopic imaging, analysis of images from satellite, remote sensing Application, computer vision, robotics etc [7][8]. The fusion methods such as averaging, Brovey method, principal component analysis (PCA) and IHS based methods fall under spatial domain approaches. Another important spatial domain fusion method is the high pass filtering based technique. The disadvantage of spatial domain approaches is that they produce spatial distortion in the fused image. Spectral distortion becomes a negative factor while we go for further processing such as classification problem [8].

Spatial distortion can be very well handled by frequency domain approaches on image fusion. The multi resolution analysis has become a very useful tool for analyzing remote sensing images. The discrete wavelet transform has become a very useful tool for fusion. Some other fusion methods are also there such as Laplacian-pyramid based, Curvelet transform based etc. These methods show a better performance in spatial and spectral quality of the fused image compared to other spatial methods of fusion [8].

There are various methods that have been developed to perform image fusion. Some well-known image fusion methods are listed below [3]:-

- (1) Intensity-hue-saturation (IHS) transform based fusion
- (2) Principal component analysis (PCA) based fusion
- (3) Multi scale transform based fusion:-
 - (a) High-pass filtering method
 - (b) Pyramid method:-(i) Gaussian pyramid (ii) Laplacian Pyramid (iii) Gradient pyramid (iv) Morphological pyramid (v) Ratio of low pass pyramid
 - (c) Wavelet transforms:- (i) Discrete wavelet transforms (DWT) (ii) Stationary wavelet transforms (iii) Multi-wavelet transforms
 - (d) Curvelet transforms

2.1 IMAGE FUSION ALGORITHMS

Due to the limited focus depth of the optical lens it is often not possible to get an image that contains all relevant objects in focus. To obtain an image with every object in focus a multi-focus image fusion process is required to fuse the images giving a better view for human or machine perception. Pixel-based, region-based and wavelet based fusion algorithms were implemented [9].

2.1.1. SIMPLE AVERAGE

It is a well documented fact that regions of images that are in focus tend to be of higher pixel intensity. Thus

this algorithm is a simple way of obtaining an output image with all regions in focus. The value of the pixel $P(i, j)$ of each image is taken and added. This sum is then divided by 2 to obtain the average. The average value is assigned to the corresponding pixel of the output image which is given in equation (1). This is repeated for all pixel values.

$$K(i, j) = \{X(i, j) + Y(i, j)\} / 2 \quad (1)$$

Where $X(i, j)$ and $Y(i, j)$ are two input images.

2.1.2. SELECT MAXIMUM

The greater the pixel values the more in focus the image. Thus this algorithm chooses the in-focus regions from each input image by choosing the greatest value for each pixel, resulting in highly focused output. The value of the pixel $P(i, j)$ of each image is taken and compared to each other. The greatest pixel value is assigned to the corresponding pixel [7] [9].

2.2. DISCRETE WAVELET TRANSFORM (DWT)

Wavelets are finite duration oscillatory functions with zero average value [1]. They have finite energy. They are suited for analysis of transient signal. The irregularity and good localization properties make them better basis for analysis of signals with discontinuities. Wavelets can be described by using two functions viz. the scaling function $f(t)$, also known as 'father wavelet' and the wavelet function or 'mother wavelet'. Mother wavelet (t) undergoes translation and scaling operations to give self similar wavelet families as given by Equation.

$$\psi_{a,b}(t) = \frac{1}{\sqrt{a}} \psi\left(\frac{t-b}{a}\right), (a, b \in \mathbb{R}), a > 0 \quad (2)$$

The wavelet transform decomposes the image into low-high, high-low, high-high spatial frequency bands at different scales and the low-low band at the coarsest scale which is shown in fig: 2. The L-L band contains the average image information whereas the other bands contain directional information due to spatial orientation. Higher absolute values of wavelet coefficients in the high bands correspond to salient features such as edges or lines [1][7][10]. The basic steps performed in image fusion given in fig. 1.

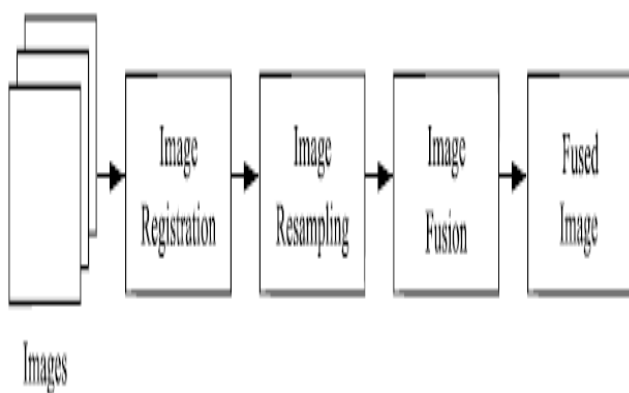


Fig1: Preprocessing of image fusion

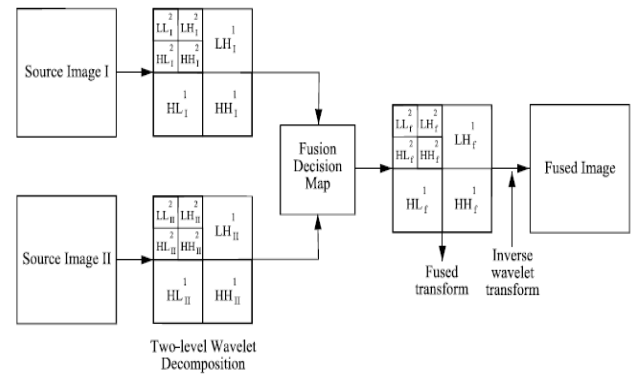


Fig. 2: Wavelet Based image fusion

The wavelets-based approach is appropriate for performing fusion tasks for the following reasons:-

- (1) It is a multi scale (multi resolution) approach well suited to manage the different image resolutions. Useful in a number of image processing applications including the image fusion [3][7].
- (2) The discrete wavelets transform (DWT) allows the image decomposition in different kinds of coefficients preserving the image information. Such coefficients coming from different images can be appropriately combined to obtain new coefficients so that the information in the original images is collected appropriately.
- (3) Once the coefficients are merged the final fused image is achieved through the inverse discrete wavelets transform (IDWT), where the information in the merged coefficients is also preserved.

2.3. PRINCIPAL COMPONENT ANALYSIS (PCA)

PCA is a mathematical tool which transforms a number of correlated variables into a number of uncorrelated variables. The PCA is used extensively in image compression and image classification. The PCA involves a mathematical procedure that transforms a number of correlated variables into a number of uncorrelated variables called principal components. It computes a compact and optimal description of the data set. The first principal component accounts for as much of the variance in the data as possible and each succeeding component accounts for as much of the remaining variance as possible. First principal component is taken to be along the direction with the maximum variance. The second principal component is constrained to lie in the subspace perpendicular of the first. Within this Subspace, this component points the direction of maximum variance. The third principal component is taken in the maximum variance direction in the subspace perpendicular to the first two and so on. The PCA is also called as Karhunen-Loève transform or the Hotelling transform. The PCA does not have a fixed set of basis vectors like FFT, DCT and wavelet etc. and its basis vectors depend on the data set [11].

III. PERFORMANCE MEASURES

The general requirements of an image fusing process are that it should preserve all valid and useful pattern information from the source images, while at the same time it should not introduce artifacts that could interfere with subsequent analyses. The performance

measures used in this paper provide some quantitative comparison among different fusion schemes, mainly aiming at measuring the definition of an image.

3.1 PEAK SIGNAL TO NOISE RATIO (PSNR)

PSNR is the ratio between the maximum possible power of a signal and the power of corrupting noise that affects the fidelity of its representation [2][9]. The PSNR measure is given by:-

$$PSNR(dB) = 20 \log \frac{255\sqrt{3MN}}{\sqrt{\sum_{i=1}^M \sum_{j=1}^N (B'(i,j) - B(i,j))^2}} \quad (3)$$

Where, B - the perfect image, B' - the fused image to be assessed, i - pixel row index, j - Pixel column index, M , N - No. of row and column

3.2 ENTROPY (EN)

Entropy is an index to evaluate the information quantity contained in an image. If the value of entropy becomes higher after fusing, it indicates that the information increases and the fusion performances are improved. Entropy is defined as:-

$$E = - \sum_{i=0}^{L-1} p_i \log_2 p_i \quad (4)$$

Where L is the total of grey levels, $p = \{p_0, p_1, \dots, p_{L-1}\}$ is the probability distribution of each level [9].

3.3 MEAN SQUARED ERROR (MSE)

The mathematical equation of MSE is given by the equation (5)

$$MSE = \frac{1}{mn} \sum_{i=1}^m \sum_{j=1}^n (A_{ij} - B_{ij})^2 \quad (5)$$

Where, A - the perfect image, B - the fused image to be assessed, i - pixel row index, j - pixel column index, m , n - No. of row and column

3.4 NORMALIZED CROSS CORRELATION (NCC)

Normalized cross correlation are used to find out similarities between fused image and registered image is given by the following equation (6)

$$NCC = \frac{\sum_{i=1}^m \sum_{j=1}^n (A_{ij} * B_{ij})}{\sum_{i=1}^m \sum_{j=1}^n (A_{ij})^2} \quad (6)$$

IV. COMPARISON BETWEEN VARIOUS FUSION TECHNIQUES

In the reference [9] ,[12] we found that the value of the PSNR and Entropy in average method is less than as compared to value of other frequency domain method like SWT and laplacian method which means fused image are not exactly to registered image. That is why transform domain method are more suitable as compared to spatial domain method. But in some case Spatial domain play a very important role in image fusion that contain high spatial information in fused image. Same thing is also noticed in [2] and [4]. Table is given below.

Table1: Statics result of different fusion methods for lena image [9].

Fusion method	PSNR	IOI	EN
Average	25.4810	0.9848	7.2228
Select maximum	26.8663	0.9939	7.2071
L a p l a c i a n pyramid	57.1387	0.9854	7.2297
Morphological pyramid	54.1061	0.9788	7.2053
SWT	59.1387	0.9851	7.2322
P r o p o s e d method	67.0832	0.9977	7.2494

In [3][4][8][11] the proposed advanced DWT fusion method is compared with existing transform domain methods. Table2 show the advanced DWT method gives higher IQI and entropy.

Table2: Image quality evaluation results of the fused images tested on the two simulated image pair lena I1 and lena I2 [4]

Imagery	Ref.	Input A	Input B	Eval.	Laplacian	Gradient	Contrast	Ratio	Morpho.	DWT	aDWT
Lena-I1	7.31	7.29	7.29	Entropy	7.46	7.2	7.44	7.38	7.38	7.42	7.45
	147.77	89.53	116.55	SF	145.59	121.98	145.9	92.68	126.03	142.19	151.71
				IQI	0.96	0.93	0.96	0.92	0.93	0.96	0.96
				RMSE	3.03	22.27	1.53	5.91	8.79	2.06	2.75
Lena-I2	7.31	7.36	7.33	Entropy	7.56	7.34	7.47	7.35	7.42	7.53	7.52
	147.77	92.34	119.76	SF	152.18	125.92	116.14	81.28	121.62	150.93	159.17
				IQI	0.95	0.94	0.94	0.9	0.92	0.94	0.95
				RMSE	11.31	15.17	14.85	13.41	8.51	12.47	6.74

In [2] a new fusion method based on combination of pixel and energy rule is proposed. Comparison with pixel and energy method show the proposed method gives better result.

Table3: Comparison between pixel region and hybrid fusion rule based on MSE and PSNR [2].

Source images	Fusion Rule	MSE	PSNR in decibels
CT/MRI Scan	Pixel	207.56	24.96
	Energy	206.22	25.03
	Hybrid	190.95	25.32
Clocks	Pixel	106.27	27.87
	Energy	85.92	28.79
	Hybrid	67.97	29.81
Cameraman	Pixel	180.57	25.56
	Energy	120.28	27.33
	Hybrid	114.29	27.55
Girl	Pixel	411.15	21.99
	Energy	428.84	21.81
	Hybrid	275.73	23.73
Lenna	Pixel	233.62	24.45
	Energy	188.52	25.38
	Hybrid	109.05	27.75

4.1 COMPARISON OF DIFFERENT IMAGE FUSION TECHNIQUES:-

S.N	Fusion Technique/Algorithm	Domain	Measuring Parameters	Advantages	Disadvantages
1.	Simple Average[12][9]	Spatial	PSNR-25.48 EN-7.22	This is the simplest method of image fusion.	The main disadvantage of Pixel level method is that this method does not give guarantee to have a clear objects from the set of images.
2.	Simple Maximum[8][12]	Spatial	PSNR-26.86 EN-7.20	Resulting in highly focused image output obtained from the input image as compared to average method.	Pixel level method are affected by blurring effect which directly affect on the contrast of the image
3.	PCA[11]	Spatial	NC-0.998 PSNR-76.44	PCA is a tools which transforms number of correlated variable into number of uncorrelated variables, this property can be used in image fusion.	But spatial domain fusion my produce spectral degradation.
4.	DWT[3][4][8]	Transform	RMSE-2.06 EN-7.42	The DWT fusion method may outperform the slandered fusion method in terms of minimizing the spectral distortion. It also provide better signal to noise ratio than pixel based approach.	In this method final fused image have a less spatial resolution.
5.	Combine DWT, PCA[7][9]	Transform	PSNR-67.08 EN-7.24	Multi level fusion where the image undergoes fusion twice using efficient fusion technique provide improved result .output image contained both high spatial resolution with high quality spectral content.	This method is complex in fusion algorithm. Required good fusion technique for better result.
6.	Combination of Pixel & Energy Fusion rule [2]	Transform	PSNR=27.75	Preserves boundary information and structural details without Introducing any other inconsistencies to the image.	Complexity of method increases.

V. CONCLUSION:-

Although selection of fusion algorithm is problem dependent but this review results that spatial domain provide high spatial resolution. But spatial domain have image blurring problem. The Wavelet transforms is the very good technique for the image fusion provide a high quality spectral content. But a good fused image have both quality so the combination of DWT & spatial domain fusion method (like PCA) fusion algorithm improves the performance as compared to use of individual DWT and PCA algorithm. Finally this review concludes that a image fusion algorithm based on combination of DWT and PCA with morphological processing will improve the image fusion quality and may be the future trend of research regarding image fusion.

REFERENCES

- [1]. Deepali A.Godse, Dattatraya S. Bormane (2011) "Wavelet based image fusion using pixel based maximum selection rule" International Journal of Engineering Science and Technology (IJEST), Vol. 3 No. 7 July 2011, ISSN : 0975-5462
- [2]. Susmitha Vekkot, and Pancham Shukla "A Novel Architecture for Wavelet based Image Fusion". World Academy of Science, Engineering and Technology 57 2009
- [3]. Shih-Gu Huang, "Wavelet for Image Fusion"
- [4]. Yufeng Zheng, Edward A. Essock and Bruce C. Hansen, "An Advanced Image Fusion Algorithm Based on Wavelet Transform – Incorporation with PCA and Morphological Processing"
- [5]. Shrivsubramani Krishnamoorthy, K P Soman, "Implementation and Comparative Study of Image Fusion Algorithms". International Journal of Computer Applications (0975 – 8887) Volume 9– No.2, November 2010
- [6]. Jonathon Shlens, "A Tutorial on Principal Component Analysis". Center for Neural Science, New York University New York City, NY 10003-6603 and Systems Neurobiology Laboratory, Salk Insitute for Biological Studies La Jolla, CA 92037
- [7]. Gonzalo Pajares , Jesus Manuel de la Cruz "A wavelet-based image fusion tutorial" 2004 Pattern Recognition Society.
- [8]. Chetan K. Solanki Narendra M. Patel, "Pixel based and Wavelet based Image fusion Methods with their Comparative Study". National Conference on Recent Trends in Engineering & Technology. 13-14 May 2011
- [9]. M .Chandana,S. Amutha, and Naveen Kumar, " A Hybrid Multi-focus Medical Image Fusion Based on Wavelet Transform". International Journal of Research and Reviews in Computer Science (IJRRCS) Vol. 2, No. 4, August 2011, ISSN: 2079-2557
- [10]. Stavri Nikolov Paul Hill David Bull Nishan Canagarajah "WAVELETS FOR IMAGE FUSION"
- [11]. V.P.S. Naidu and J.R. Raol, "Pixel-level Image Fusion using Wavelets and Principal Component Analysis". Defence Science Journal, Vol. 58, No. 3, May 2008, pp. 338-352 Ó 2008, DESIDOC
- [12]. Anjali Malviya, S. G. Bhirud ." Image Fusion of Digital Images" International Journal of Recent Trends in Engineering, Vol 2, No. 3, November 2009

Some Dynamical Behaviours of a Two Dimensional Nonlinear Map

Tarini Kumar Dutta¹, Debasish Bhattacharjee², Basistha Ram Bhuyan³

¹Department of Mathematics; Gauhati University; Guwahati 781014; INDIA

²Department of Mathematics; B. Borooah College; Guwahati 781007; INDIA

³Department of Mathematics; LCB College; Guwahati 781011; INDIA

Abstract: We consider the Nicholson Bailey model

$$f(x,y) = (Lx e^{-ay}, x(1 - e^{-ay}))$$

Where L and a are adjustable parameters, and analyse dynamical behaviours of the model. It is observed that the steady state occurs when there is no predator and prey for a certain range of the control parameters and that there exists a certain region of the control parameters in which the natural equilibrium state never occurs. In that case a modified version of the model is considered by taking care of the unboundedness of the prey system. It is further found that the model follows the stability of period-doubling fashion obeying Feigenbaum universal constant δ and at last attains infinite period doubling route leading to chaos in the system. The bifurcation points are calculated numerically and after that the accumulation point i.e. onset of chaos is calculated based on the experimental values of bifurcation points.

Key Words: Period-Doubling Bifurcation/ Periodic orbits / Feigenbaum Universal Constant Accumulation point

2010 AMS Classification: 37G15, 37G35, 37C45

I. Introduction:

The Nicholson Bailey model [14] was developed in 1930's to describe population dynamics of host-parasite (predator-prey) system. It has been assumed that parasites search hosts at random and that both parasites and hosts are assumed to be distributed in a non-contiguous ("clumped") fashion in the environment. However the modified version of the Nicholson-Bailey model has been discussed many times by many authors [1, 2, 6, 9, 10, and 11].

In this present discussion in section 1.2 we verify the stability and dynamic behaviour of the model analytically and then in section 1.3 the modified form of the model has been taken which restricts the unboundedness of the model to some extent. The detailed dynamical behaviour of a particular form of its class has been studied and it has been observed that the map follows period doubling bifurcation route to chaos proving that the natural equilibrium changes its nature from periodic order to chaos. In section 1.4 numerical evaluations has been carried out to prove the geometrical behaviour. Lastly, in section 1.5 the calculation of the accumulation point from where chaos starts has been evaluated numerically, [3, 5, 6, 8, 12, and 13].

1.1 Nicholson-Bailey model:

The model as discussed by Nicholson and Bailey is as follows:

$$x_{n+1} = Lx_n e^{-ay_n}$$

$$y_{n+1} = x_n (1 - e^{-ay_n}),$$

where x_{n+1} represents the number of hosts (or prey) at stage n and y_{n+1} represents number of parasites (or predator) at n th stage. The difference equation can also be written in the function form as follows:

$$f(x,y) = (Lx e^{-ay}, x(1 - e^{-ay}))$$

1.2.1 Steady state of the above system:

The fixed point is given as follows:

$$Lx e^{-ay} = x \tag{1.2.1.1}$$

$$x(1 - e^{-ay}) = y \tag{1.2.1.2}$$

Clearly (0,0) is one of the fixed points. Let $x \neq 0$ then

$$e^{-ay} = \frac{1}{L} \quad \text{i.e. } -ay = \log\left(\frac{1}{L}\right) \quad \text{i.e. } y = -\frac{1}{a} \log\left(\frac{1}{L}\right) \quad \text{from (1.2.1.1)}$$

From (1.2.1.2) we have

$$x \left(1 - \frac{1}{L}\right) = -\frac{1}{a} \log\left(\frac{1}{L}\right)$$

$$\text{i.e. } x = -\frac{\frac{1}{a} \log\left(\frac{1}{L}\right)}{1 - \frac{1}{L}}$$

Thus the fixed points are $\left(-\frac{\frac{1}{a} \log\left(\frac{1}{L}\right)}{1 - \frac{1}{L}}, -\frac{1}{a} \log\left(\frac{1}{L}\right)\right)$ and (0,0). However at $L=1$, (1.2.1.1) gives $y=0$ and it automatically satisfy (1.2.1.2) for any value of x. Hence any (x,0) is a fixed point for $L=1$.

1.3.2 Stability of the equilibrium points:

Now the Jacobian matrix is given by

$$\begin{pmatrix} Le^{-ay} & -aLxe^{-ay} \\ 1 - e^{-ay} & axe^{-ay} \end{pmatrix} \quad \text{The eigenvalues of which are:}$$

$$\frac{1}{2}e^{-ay}(L+ax - 4ae^{ay}Lx + (L+ax)^2) \text{ and}$$

$$\frac{1}{2}e^{-ay}(L+ax - \sqrt{-4ae^{ay}Lx + (L+ax)^2})$$

For fixed point (0,0), the eigenvalues are 0, L. This shows that (0,0) is a stable solution till L=1. However for other fixed points say (x,y), we have

$e^{-ay} = \frac{1}{L}$, hence the eigenvalues become

$$\frac{1}{2L}(L+ax - \sqrt{-4aL^2x + (L+ax)^2}) \text{ and } \frac{1}{2L}(L+ax + \sqrt{-4aL^2x + (L+ax)^2})$$

In particular for L=1, the eigenvalues are ax, 1. Thus if ax<1 one of the eigenvalues become less than 1. That is why at L=1 the trajectory converges to (x,0) such that ax<1.

Now for the period-doubling bifurcation point,

$$\frac{1}{2L}(L+ax + \sqrt{-4aL^2x + (L+ax)^2}) = -1$$

$$\text{i.e. } L+ax + \sqrt{-4aL^2x + (L+ax)^2} = -2L$$

$$\text{i.e. } 3L+ax = \sqrt{-4aL^2x + (L+ax)^2}$$

$$\text{i.e. } (3L+ax)^2 = -4aL^2x + (L+ax)^2$$

$$\text{i.e. } 8L^2 + 4aLx + 4aL^2x = 0$$

$$\text{i.e. } 2L + ax + aLx = 0$$

$$\text{i.e. } L = -\frac{ax}{2+ax} \quad (1.2.2.1)$$

$$\text{Putting } x = -\frac{\frac{1}{a} \log(\frac{1}{L})}{1-\frac{1}{L}} \text{ in (1.2.2.1) we have } ax = \frac{\log(t)}{t-1}$$

From eq (1.2.2.1) we have,

$$L = -\frac{\log(t)}{(t-1)(2+\frac{\log(t)}{t-1})}$$

$$\text{i.e. } \frac{1}{t} = \frac{-\log(t)}{2(t-1)+\log(t)} \text{ i.e. } -t \log(t) - \log(t) = 2(t-1)$$

$$\text{i.e. } -\log t(t+1) = 2(t-1)$$

if t>1 then l.h.s. is negative and r.h.s. is positive.

If t<1 then l.h.s. is positive but r.h.s. is negative. Hence there is no solution i.e. period doubling bifurcation does not occur.

$$\frac{1}{2L}(L+ax + \sqrt{-4aL^2x + (L+ax)^2}) = 1$$

$$\text{i.e. } L+ax + \sqrt{-4aL^2x + (L+ax)^2} = 2L$$

$$\text{i.e. } -L+ax = \sqrt{-4aL^2x + (L+ax)^2}$$

$$\text{i.e. } (-L+ax)^2 = -4aL^2x + (L+ax)^2$$

$$\text{i.e. } -4aLx + 4aL^2x = 0$$

$$\text{i.e. } -ax + aLx = 0$$

$$\text{i.e. } L=1 \quad (1.2.2.2)$$

Again we consider the stability of the other fixed point $(-\frac{\frac{1}{a} \log(\frac{1}{L})}{1-\frac{1}{L}}, -\frac{1}{a} \log(\frac{1}{L}))$

Now we consider the expression $-4aL^2x + (L+ax)^2$ for the fixed point $(-\frac{\frac{1}{a} \log(\frac{1}{L})}{1-\frac{1}{L}}, -\frac{1}{a} \log(\frac{1}{L}))$. The simplified expression is

$$\frac{-2(-1+L)^2(-1+2L)+2L \log[L](-1+L^2-L \log[L])}{(-1+L)^3 L} = g(L)$$

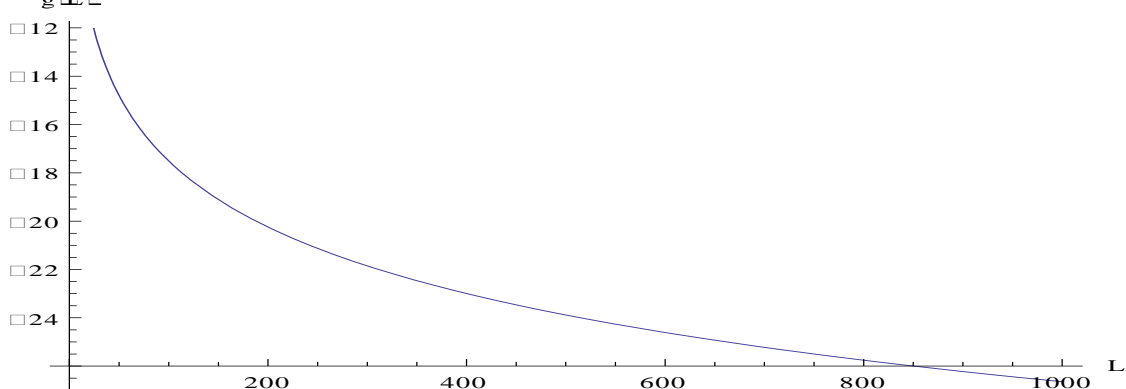


Fig 1.2.2.a : Abcissa represents the control parameter L and ordinate represents g(L)

Clearly, g(L) is negative for L>1

Hence magnitude of the eigenvalues become

$$\left| \frac{1}{2L} \left(L + ax - \sqrt{-4aL^2x + (L + ax)^2} \right) \right| = \frac{1}{2L} \sqrt{(L + ax)^2 - (L + ax)^2 + 4aL^2x}$$

$$= \sqrt{ax} = \sqrt{\frac{L \log L}{L-1}} = h(L) \text{ (say).}$$

For $L > 1$ and for large value of L , the above expression shows the graph as

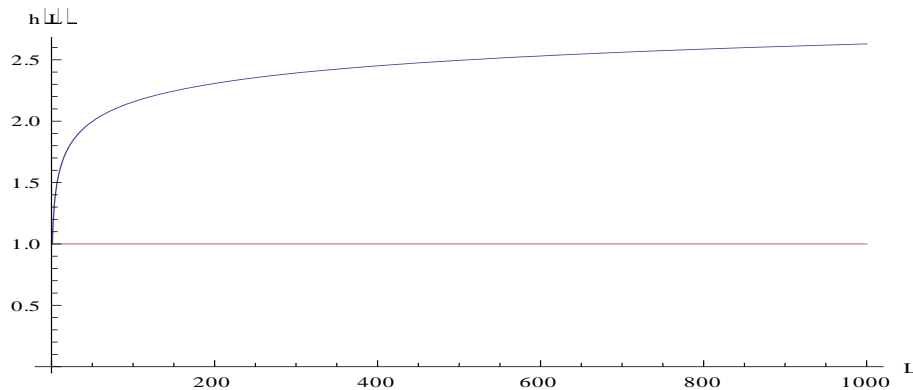


Fig 1.2.2.b: Abcissa represents the control parameter L and ordinate represents $h(L)$

Hence the fixed point is unstable, and this shows that the model has been made to fulfill the fact that equilibrium stage never occurs for predator system in nature.

We now take a modified version of the Nicolson Bailey model, i.e. we take

$$x_{n+1} = Lx_n e^{-ay_n - x_n^2}$$

$$y_{n+1} = x_n (1 - e^{-ay_n})$$

The additional term $e^{-x_n^2}$ with x_{n+1} helps to restrict the unlimited growing of host(or prey).

1.3 Dynamical behaviour of the map keeping “a” constant:

We now fix the parameters say “a” and keep varying L to analyse the detailed dynamical behaviours of the map. Let us take $a=0.1$. On inspection it can be seen that $(0,0)$ is a fixed point of the model satisfying the equation

$$f(x,y) = (x,y) = (Lxe^{-ay - x^2}, x(1 - e^{-ay}))$$

$$\text{i.e. } \begin{aligned} x &= Lxe^{-ay - x^2} \\ y &= x(1 - e^{-ay}) \end{aligned} \quad (1.3.1)$$

Using “Mathematica” software we generate the bifurcation diagram for the observation of the whole dynamical behaviour of the map as L is varied.

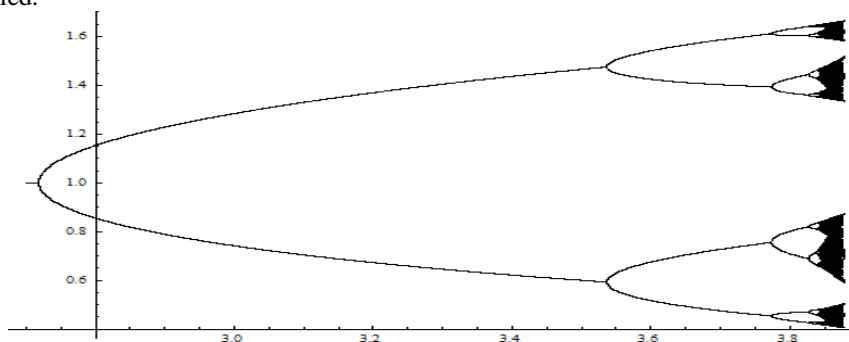


Fig 1.3.a: The figure is generated using 20000 points of which the last 300 points are taken at every parameter value of L , and plotted the x coordinate of the point (x,y) vs. L .

The eigen values of the linearised form are as follows:

$$\frac{1}{2} e^{-x^2 - 2ay} (e^{ay} L + a e^{x^2 + ay} x - 2e^{ay} Lx^2 \pm \sqrt{(-e^{ay} L - a e^{x^2 + ay} x + 2e^{ay} Lx^2)^2 - 4e^{x^2 + 2ay} (a e^{ay} Lx - 2aLx^3)})$$

can be re-written as

$$\frac{1}{2L} (e^{ay} L + aLx - 2e^{ay} Lx^2 \pm \sqrt{(-e^{ay} L - aLx + 2e^{ay} Lx^2)^2 - 4e^{ay} L(a e^{ay} Lx - 2aLx^3)})$$

The diagram shows that the model follows period doubling route to chaos on increasing the control parameter L . For $(0,0)$ the eigenvalues are $0, L$, which says that $(0,0)$ loses stability at $L=1$. Let (x_0, y_0) be a fixed point of the map f where neither of x_0, y_0 are equal to zero. The fixed point is stable till both the eigen values at x_0, y_0 are less than 1 in modulus. However the first bifurcation point can be obtained from the equations (1.2.1) and $\min\{\lambda_1, \lambda_2\} = -1$. If we now begin to increase the value of L exceeding the bifurcation point, the fixed point (x_0, y_0) loses its stability and there arises around it two points, say, $(x_{21}(L), y_{21}(L))$ and $(x_{22}(L), y_{22}(L))$ forming a stable periodic trajectory of period 2. On increasing the value of L one of the eigen values starts decreasing from positive values to negative and when we reach a certain

value of L , we find that one of the eigenvalues of the Jacobian of f^2 becomes -1 , indicating the loss of stability of the periodic trajectory of period two. Thus, the second bifurcation takes place at this value L_2 of L . We can repeat the same process, and find that the periodic trajectory of period 2^n becomes unstable and a periodic trajectory of period 2^{n+1} appears in its neighbourhood for all $n=1,2,3,\dots$, [5,6,8,10].

1.4 Numerical Method for Obtaining Bifurcation Points:

We have used Newton-Raphson method to obtain the periodic points which has been proved to be worthy for sufficient accuracy and time saving.

The Newton Recurrence formula is

$\bar{x}_{n+1} = \bar{x}_n - Df(\bar{x}_n)^{-1}f(\bar{x}_n)$, where $n = 0,1,2,\dots$ and $Df(\bar{x})$ is the Jacobian of the map f at the vector $\bar{x} = (x_1, x_2)$ (say). We see that this map f is equal to $f^k - I$ in our case, where k is the appropriate period. The Newton formula actually gives the zero(s) of a map, and to apply this numerical tool in our map one needs a number of recurrence formulae which are given below.

Let the initial point be (x_0, y_0) and let $M(x,y) = Lxe^{-ay-x^2}$, $N(x,y) = x(1 - e^{-ay})$,

Let $A_0 = \frac{\partial M}{\partial x}|_{(x_0,y_0)}$, $B_0 = \frac{\partial M}{\partial y}|_{(x_0,y_0)}$, $C_0 = \frac{\partial N}{\partial x}|_{(x_0,y_0)}$, $D_0 = \frac{\partial N}{\partial y}|_{(x_0,y_0)}$

and $A_k = \begin{pmatrix} \frac{\partial M}{\partial x}|_{(x_k,y_k)} & \frac{\partial M}{\partial y}|_{(x_k,y_k)} \\ \frac{\partial N}{\partial x}|_{(x_k,y_k)} & \frac{\partial N}{\partial y}|_{(x_k,y_k)} \end{pmatrix} \begin{pmatrix} A_{k-1} & B_{k-1} \\ C_{k-1} & D_{k-1} \end{pmatrix} \quad \forall k \geq 1$

Since the fixed point of the map f is a zero of the map

$F(x,y) = f(x,y) - (x,y)$, the Jacobian of $F^{(k)}$ is given by

$$J_k - I = \begin{pmatrix} A_k - 1 & B_k \\ C_k & D_k - 1 \end{pmatrix}. \text{ Its inverse is } (J_k - I)^{-1} = \frac{1}{\Delta} \begin{pmatrix} D_k - 1 & -B_k \\ -C_k & A_k - 1 \end{pmatrix}$$

where $\Delta = (A_k - 1)(D_k - 1) - B_k C_k$, the Jacobian determinant. Therefore, Newton's method gives the following recurrence formula in order to yield a periodic point of F^k

$$x_{n+1} = x_n - \frac{(D_k - 1)(\bar{x}_n - x_n) - B_k(\bar{y}_n - y_n)}{\Delta}$$

$$y_{n+1} = y_n - \frac{(-C_k)(\bar{x}_n - x_n) + (A_k - 1)(\bar{y}_n - y_n)}{\Delta}$$

where $F^k(\bar{x}_n) = (x_n, y_n)$

1.4.1 Numerical Methods for Finding Bifurcation Values:

As described above for some particular value of $L=L_1$ say, the fixed point of f^k is calculated and hence the eigenvalues of J_k can be calculated at the fixed point. Let $(x_1, y_1), (x_2, y_2), \dots, (x_k, y_k)$ be the periodic points of f at L_1 . Let λ_1, λ_2 be the two eigenvalues of J_k at L_1 , let $I(k, L_1) = \min\{\lambda_1, \lambda_2\}$, where $n=2^k$ is the period number. Then we search two values of "L" say L_{11} and L_{22} such that $(I(k, L_{11}) + 1)(I(k, L_{22}) + 1) < 0$. Then the existence of n^{th} bifurcation point is confirmed in between L_{11} and L_{22} . Then we may apply some of the numerical techniques viz. Bisection method or Regula Falsi method on L_{11} and L_{22} for sufficient number of iterations to get L such that $I(k, L) = -1$.

Our numerical results are as follows:

Table 1.4.1.a: Bifurcation points calculated with the above numerical procedure are given as follows:

Period	Bifurcation point
n=1	2.71828182845904523536028747135266249775724709369995957496696
n=2	3.53684067130120359837043484826459115405423168841443588327400
n=4	3.77415543777691650197392802578931393394103470516281183784919
n=8	3.82788212068493762703545087588566660131789524411227589313294
n=16	3.83954703996904224281164775272528029534621679916918934834796
n=32	3.84205211923591357428498949577187590314662912792561150844422
n=64	3.84258895757543669502842561849603953670354363149648649855300
n=128	3.84270394654591339735557484998431661721920300008353132976556
n=256	3.84272857434341121053856237571767662232417602736345292594595
n=512	3.84273384889445086737896598441474166356789762228260539689561
n=1024	3.842734978543189743621418854360407234045741604974429302522640
n=2048	3.84273522047942178512266708047918352493564928024817333443963

The Feigenbaum universal constant is calculated using the experimentally calculated bifurcation point using the following formula $\delta_n = \frac{A_n - A_{n-1}}{A_{n+1} - A_n}$, where A_n represents n^{th} bifurcation point. The values of δ_n are as follows.

$\delta_1=3.44925372743685$
 $\delta_2=4.41707460112493$
 $\delta_3=4.60583409104533$
 $\delta_5=4.65650705682990$
 $\delta_6=4.66635685725543$
 $\delta_7=4.66860723509033$
 $\delta_8=4.66907243682318$
 $\delta_9=4.66917417475885$
 $\delta_{10}=4.66919570494443$
 $\delta_{11}=4.66920034814159$

It may be observed that the map obeys Feigenbaum universal behaviour as the sequence $\{\delta_n\}$ converges to δ as n becomes very large.

1.5 Accumulation Point:

The accumulation point can be calculated by the formula $A_\infty=(A_2-A_1)/(\delta-1)$, where δ is Feigenbaum constant. But it has been observed that $\{\delta_n\}$ converges to δ as $n \rightarrow \infty$. Therefore a sequence of accumulation point $\{A_{\infty,n}\}$ is made using the formula $A_{\infty,n}=(A_{n+1}-A_n)/(\delta-1)$ [8]. From the above experimental values of bifurcation points and using $\delta=4.669201609102990671853204$ the sequence of values is constructed as follows:

$A_{\infty,1} = 3.75992975989513108127$
 $A_{\infty,2} = 3.83883293216342125972$
 $A_{\infty,3} = 3.84252472924989889705$
 $A_{\infty,4} = 3.84272618369752118495$
 $A_{\infty,5} = 3.84273485066736624607$
 $A_{\infty,6} = 3.84273526688103365882$
 $A_{\infty,7} = 3.84273528550809836535$
 $A_{\infty,8} = 3.84273528637510680165$
 $A_{\infty,9} = 3.84273528641454422260$
 $A_{\infty,10} = 3.84273528641636195462$
 $A_{\infty,11} = 3.84273528641644509866$

It may be observed that the sequence converges to the point 3.842735286416 After which chaotic region starts.

References:

1. Beddington, J.R., Free, C.A., Lawton, J.H., "Dynamic Complexity in Predator-Prey models framed in difference equations", Nature, 225(1975),58-60.
2. Comins, H.N., Hassel, M.P., May, R., "The spatial dynamics of host-parasitoid systems", Journal of Animal Ecology, vol-61(1992), pp-735-748.
3. Falconer, K.J., "Fractal Geometry: Mathematical Foundations and Applications", John Wiley publication, 1998
4. Feigenbaum, M.J., "Qualitative Universality for a class of non-linear transformations", J. Statist. Phys, 19:1(1978), 25-52.
5. Feigenbaum, M.J., "Universality Behavior in non-linear systems", Los Alamos Science, 1.(1980), 4-27.
6. Hassel, M.P., Comins, H.N., May, R., "Spatial structure of chaos in insect population dynamics", Nature, Vol-353(1991), pp-255-258.
7. Henon, M., "A two dimensional mapping with a strange attractor", Comm. Math. Phys. Lett. A 300(2002), 182-188
8. Hilborn, R.C., "Chaos and Non-linear dynamics", Oxford Univ. Press. 1994.
9. Hone, A.N.W., Irle, M.V., Thurura, G.W., "On the Neimark-Sacker bifurcation in a discrete predator-prey system", 2009.
10. Kuznetsov, Y., "Elements of Applied Bifurcation Theory", Springer(1998).
11. May, R.M., "Simple Mathematical Models With Very Complicated Dynamics", Nature, Vol.261(1976), 459.
12. Murray, J.D., "Mathematical Biology 1: An Introduction, Third Edition", Springer. 1997
13. Murray, J.D., "Mathematical Biology II: Spatial Models and Biomedical Applications", Springer, 2001
14. Nicholson, A.J., Bailey V.A., "The Balance of Animal Populations-Part-1", Proceedings of the Zoological Society of London, Vol-105, issue-3(1935), pp-551-598

Evaluation Of Vehicular Noise Pollution In The City Of Hebron, Palestine

Zuhdi Salhab¹, Husein Amro²

^{1,2}(Renewable Energy and Environment Research Unit-REERU, Palestine Polytechnic University, Hebron, Palestine)

ABSTRACT: Noise generally is known as unwanted and unwelcome sound. It is considered as the most pervasive pollutant besides the emission pollutants. Noise pollution generated from vehicles with its influence on life quality and the environment may be considered as a hot topic in scientific research and one of the main concerns of the world, especially in urban areas. Because in Palestinian Territories (PT), there are neither legal legislations nor sufficient studies on noise pollution, this paper was carried out to evaluate vehicular noise level in Hebron city (the largest city of about two hundred thousand population), located at the south of (PT). Noise measurements were taken at two chosen areas with high population density, heavy traffic, commercial and residential buildings. The value of equivalent level noise (L_{Aeq}) was measured during three intervals ranged from 7-8 am (peak traffic hours), 14-15 pm (peak traffic hours), and 17-18 pm (non-peak traffic hours) in June 2012. Noise pollution was measured and analyzed and it was noticed that the maximum average of noise level was measured 83.05 dB(A) from 14 to 15 pm, while the minimum average was measured 74.4 dB(A) from 17 to 18 pm. The results showed and emphasized that in regard to high (L_{Aeq}) compared with international legislations, implementing strategy and greater priority must be devoted to control the noise levels.

Keywords: Hebron, L_{Aeq} , noise level, noise pollution, traffic.

I. INTRODUCTION

The word "noise" is derived from the Latin word "nausea" meaning seasickness. Noise can be defined as the level of sound that exceeds the acceptable level and creates an annoyance. Noise is any sound independent of loudness which can produce an undesired physiological or psychological effect on an individual group. Noise is a major source of friction between individuals [1]. The major sources of noise are industrial noise, community noise and traffic noise. Out of three parameters, the source that affects the most is traffic or vehicular noise. In this traffic noise, almost two- third of the total noise pollution in an urban area is contributing by vehicle noise.

Vehicle noise includes the following sources:

- Engines.
- Exhaust systems.
- Tires interacting with the road.
- Horns.
- Aerodynamic friction and by the interaction between vehicles.
- Sounds of cooling fans, gearboxes and brakes.

The increase in magnitude and severity of traffic noise depends on the following factors [2]:

- Population growth and urbanization associated with the growing number of automobiles.
- Vehicle type, its mode of operation and flow.
- Dimension, position and surface materials of the roads.
- City prior planning.

- City center crossroad signal system.
- Commercial and industrial activities in the residential areas, in addition to high traffic density.
- Disobeying traffic rules.

All the above mentioned factors combined together lead to increased vehicular noise levels.

Noise pollution does not get noticed and it is not like a kind of chemical reaction. It is only like a wave which widespread in the air and does not have any stable and normally observable effect like water or soil pollution. Noise pollution is regarded as a significant criterion in determining the quality of life in cities and affects the social welfare [3].

1.1 Noise Pollution; its Magnitude, Sources, and Effect

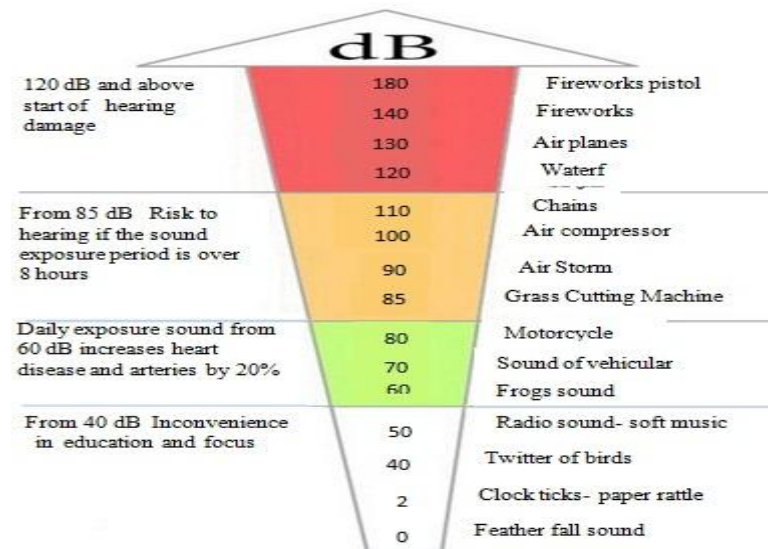


Fig.1. Noise pollution sources and influence due to its levels in (dB)

In general, previous figure schematically illustrates the magnitude of noise pollution, sources, and its influence on human beings [4].

1.2 Typical Traffic Noise Levels

The typical traffic noise levels can be summarized as follows [5]:

- Areas with heavy traffic or close to loud speakers: 80-105 dB(A).
- Areas with over flying aircrafts: 90-100 dB(A).
- At railway stations, busy markets, and traffic junctions: 70-90 dB(A).
- Industries markets and residential areas close to traffic: 60-80 dB(A).
- Residential areas that are away from heavy traffic roads or other noisy sources: 40-60 dB(A).

Regarding the above mentioned, the study and investigation of noise are necessary before presenting the noise control policies in order to investigate the distribution

of existing noise levels compared to noise standard levels and then finding out the main sources of noise. Hence came the importance of this study.

II. STUDY AREA PROFILE

2.1 Why Hebron city

In the Palestinian Territories, geographical point of view Hebron city is about of 35 km north of Jerusalem. It is one of the most dynamic cities. It was chosen to achieve the goals of this study for the following reasons:

- It is considered as the largest and the most populated city.
 - The increasing number of people is accompanied by an increase in the industrial and commercial utilities which requires an increase in the number of vehicles.
 - Hebron is considered as the biggest and the most important industrial and commercial center.
 - The growth rate due to immigration from the countryside and the purpose of shopping increases the proportion of noise pollution.
 - A big ratio of older vehicle model causes pollution and noise. Since then, ignoring the control procedure results in neglecting the necessity of maintenance operation needed for these vehicles.
 - The city of Hebron features from other cities in Palestinian Territories that is still adhering to the customs and traditions, especially those are related to happy occasions and weddings: that are vehicles used for this purpose are going in ceremonial convoys in the streets and these festivals consist of numerous number of vehicles (cars and buses).
- The result then is making a very annoying sound with the use of horns and musical instruments. In addition, they cause traffic jam through over the streets which increases the noise.
- Due to limited availability of land resources, finances and occupation, many important roads are in the commercial and residential areas. Hens there will be some adverse and environmental effects including physiological and psychological effects to those living close to these corridors.

Figure 2 shows a general view photographed for one of these occasions in Hebron streets.



Fig.2 View of occasion (wedding party in streets of Hebron city)

Due to explosion of population in Hebron city (about 250.000 people-Palestinian Central Bureau of Statistics 2011), rapid industrialization and highest growth rate in vehicles number made the traffic problems and noise pollution very complicated. Table 1 shows the

number of registered vehicles in Hebron city (the number of unregistered vehicles is neglected).

Table I. Composition of registered vehicles in Hebron city

Type of vehicles	Number of vehicles
Private cars	31124
Trucks	8673
Taxi	2155
Vehicles without custom duties	1243
Buses	459
Others	166

*(Statistics of Palestinian Ministry Of Transport-2012).

2.2 Site Selection

To measure the traffic noise pollution, the first task was site selection. So, due to surveys of different areas and nature of noise problem in Hebron city, a two cross roads (squares) where the continuous uninterrupted flow of vehicles occurs were selected. The first crossroad was Sebta square (figure 3) which matches the north of the city to the south and the severs with the city center.

The second cross road was Ras Al- Joura square which extends towards the north of the city and the south through the city center (figure 4).

2.3 Noise Measurement Instrument

For traffic noise problems it is useful to measure the equivalent sound level L_{Aeq} . Such information was obtained using the sound level meter model *Noise Pro Series DLX 1* with upper limit 114 dB (and with accessories such as microphone Random Incidence Corrector) available at REERU at Palestine Polytechnic University (figure 5).



Fig.3 Sebta square view of the noise measurement site



Fig.4 Ras Al- Joura square view of the noise measurement site



Fig. 5 Sound level meter

III. MEASUREMENT PROCEDURE

The measurement procedure was as follows:

- Measurements were performed in two days in June 2012 with a sunny day.
- Before taking the measurements, the sound level meter was suitably calibrated according to level meter producer instructions.
- The sound level meter was placed on the pavement of the street at a height of about 1.2 m and at a distance of about 7.5 m from the existing road level as shown in figure 6.

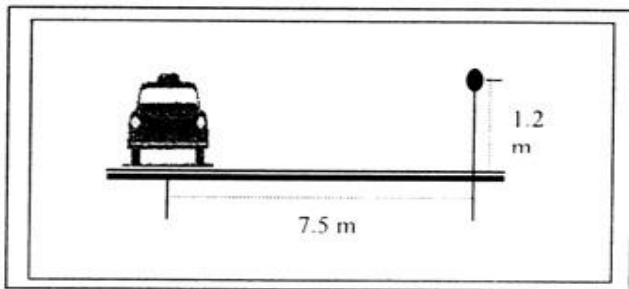


Fig.6 Location of the sound level meter

- The sound level meter was provided with a windscreen to minimize the influence of wind during measurements.
- The 15 time duration is considered during every hour measurement.
- A vehicle count was recorded based on various classification of vehicles.
- Noise level for different categories of vehicles was measured during three intervals ranged from 7-8 am (peak traffic hours), 14-15 pm (peak traffic hours), and 17-18 pm (non-peak traffic hours).

After all noise measurements in two sites (areas), statistical evaluation was done. Results are illustrated in tables 2-5 and figures 6-7.

Table II. Septa Square 15 minute measurement period

Day time	Measurement periods (minute)	Vehicle Types			LAeq (dB)
		Car	Van	Lorry	
8:00	15	55	25	10	78.4
	30	103	36	21	79.7

14:00-15:00 pm	45	40	25	18	75.8
	60	47	63	13	75
	15	119	36	12	85.8
	30	108	32	19	82.6
	45	64	21	10	78.8
17:00-18:00 pm	60	140	32	20	85
	15	119	42	19	85.5
	30	125	23	11	81.8
	45	101	42	10	79
	60	92	36	8	71.1

Table III. The average measurement Septa Square

Day time	Car and Van	Lorry	Average LAeq (dB)
7:00- 8:00 am	394	62	77.225
14:00-15:00 pm	552	61	83.05
17:00-18:00 pm	580	48	79.35

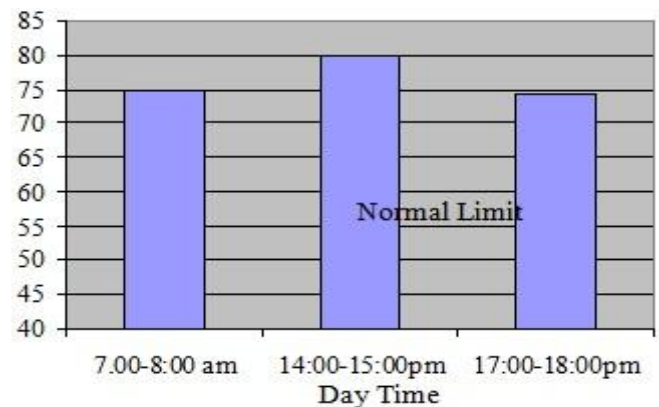


Fig. 6 The average measurement Septa Square

Table IV. Ras Al-Joura Square 15 minute measurement period

Day time	Measurement periods (minute)	Vehicle Types			LAeq (dB)
		Car	Van	Lorry	
7:00-8:00 am	15	112	100	6	74
	30	122	81	11	74.7
	45	40	38	18	75.8
	60	46	55	12	75
14:00-15:00 pm	15	180	91	21	81.5
	30	188	105	20	82.4
	45	132	78	20	78.8
	60	123	82	26	77.2
17:00-18:00 pm	15	157	83	30	71.5
	30	142	70	23	75
	45	157	83	22	80
	60	182	86	14	71.1

Table V. The average measurement Ras Al-Joura Square

Day time	Car and Van	Lorry	Average LAeq (dB)
7:00- 8:00 am	594	47	74.875
14:00-15:00 pm	979	87	79.975
17:00-18:00 pm	960	89	74.4

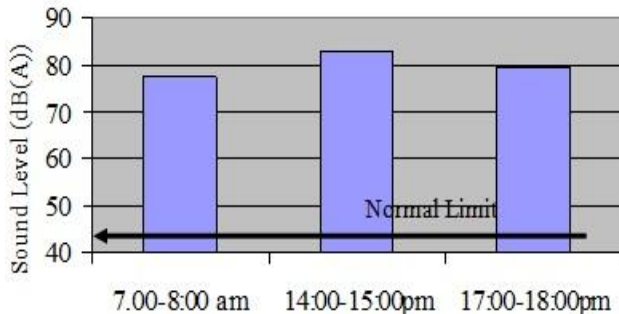


Fig. 7 The average measurement Ras Al-Joura Square

IV. RESULTS AND DISCUSSION

There have been many studies on noise levels in recent years in various countries. In one of these studies (Zeid et al., 2000), the noise level in Arraba city in the Occupied Palestinian Territories since 1948, was found to be 67 dB(A), from 20 measuring points. In Curitiba in Brazil, at 93% of the measurement points, the noise level was over the limit value 65 dB(A) and it was over high noise of being 75dB(A) at 40.3% of these points (Zannin et al., 2002). In Beijing (Li et al., 2002) Capital Cities, Assiut (Ali, 2004), Messina (Piccolo et.al., 2005) noise levels exceed the allowed values

Evaluation of traffic noise has several uses, including estimating current noise exposure along roadways, assessing the effect of roadway changes and determining (predicting) the performance of noise abatement options. The basic and main elements of traffic noise evaluation are the traffic source levels and the propagation of sound between traffic and receiver.

Evaluation of noise measurement was based on a limit value of 55 dB(A) in noise control regulation in Egypt (international standards used are limited to 65 dB(A)) and it was found from the measurements that allowed limit values were exceeded of all measurement points (higher than 65 dB(A)). The highest noise value (85.8 dB(A)) was recorded in Sebta Square at peak traffic hours between 14:00-15:00 pm, while the minimum noise value was (71.1 dB(A)) between 17:00-18:00 pm at the same location. The maximum average LAeq was (83.05 dB(A)) and the average minimum value was (77.225 dB(A)).

Noise also exceeded the (65 dB(A)) allowed limit value on Ras Al-Joura square as it is shown in tables 4-5 and figure 7 (almost (80 dB(A)).

V. CONCLUSION

Regarding the data achieved during noise measurement and the high equivalent noise level in all research conducted in the investigation areas, implementing strategies to control the noise in the Palestinian Territories is very necessary and urgent. The results proved that noise pollution must be devoted more attention and reached serious levels and it has become one of the major environmental problems. Therefore, protections related to planning, technical, biological, legislative and educational issues should be taken in order to avoid negative effects of noise pollution on the environment and human beings. In addition, the awareness of the population about the risk of noise pollution is the most effective noise control.

REFERENCES

- [1] Jobair Ben Alam, Mdi., Rauf. A.F.M.A. and Ahmed M.F, Traffic Induced Noise Pollution in Dhaka, *Journal of Civil Engineering*, The Institute of Engineers, CF29, vol 1, 2001, pp 55-63.
- [2] BhavenTandel, Dr. Joel Macwan, Patrik, Ruperal N., Urban Corridors Noise Pollution: A Case Study of Surat City, India, *International Conference on Environment and Industrial Innovation*, 2011, vol 12, pp 144-148.
- [3] G. Cammarat, S. Cavalieri, Noise Prediction in Urban Traffic by a Neural Approach, *International Workshop on Artificial Neural Networks*, 1993, Sitgaes, Barcellona, Spain.
- [4] Wael A. O. Noise *Pollution Levels in Al-Shurouk City*, Environmental Affairs Ministry, Egypt, 2008, p 23.
- [5] T. Subramani, M. Kavitha, K.P. Sivaraj, Modelling of Traffic Noise Pollution, *International Journal of Engineering Research and Applications (IJERA)*, 2(3), 2012, p 3176.

Analysis and Experimental Of 3-Dimensional AOA with Directional Antenna on Narrowband MIMO Capacity

Charinsak Saetiaw¹, Saksit Summart², Chanchai Thongsopa³

^{1,2,3}(School of Telecommunication Engineering, Suranaree University of Technology, Thailand)

ABSTRACT: Recently, many works have considered a physical property of antenna in MIMO channel models, such as radiation pattern effective for MIMO system. However, effect of antenna for MIMO with different algorithms is required and also with different environments of signal behavior at each end of the link. Thus, a traditional antenna such as Omni-directional antenna generally is used to design MIMO systems. In this paper, we analyze the performance of directional antenna in different environment of signal spread for multiple-input-multiple-output (MIMO). We incorporate 3-dimensional (3D) of signal spread matching with directional antenna into a narrow-band MIMO channel model separately. This channel model allows us to investigate effect of distribution of signal coming to antenna combined with antenna radiation pattern to MIMO capacity in various propagation environments. We perform MIMO capacity simulations of a system with various antennas radiation pattern property. Uniform and peaky distribution models of angle of arrival (AOA) in azimuth and elevation planes are used in the simulations. We have shown that directional antennas reduce the narrow-band MIMO capacity when the AOA is uniformly distributed. If the AOA is peaky distributed, such as Laplacian distribution or Gaussian distribution, the narrow-band MIMO capacity is improved when the directional antennas with proper alignment to the mean AOA. However, radiation pattern will show some limitation of the antenna properties, such as gain and beam-width will affect to the capacity. This will trade off with limit an antenna for difference environment of propagation for MIMO by gain and beam-width. The proposed model is validated by narrow-band MIMO capacity measurements. Omni-directional monopole and Yagi-Uda with different gain and beam-width is used in the experiments. The experiments are performed in an anechoic chamber for reference and compared with indoor and outdoor scenario. The result verifies that the capacity with directional antenna is greater than isotropic capacity in proper scenarios.

Keywords: channel capacity, 3D-radiation pattern, multiple-input multiple-output (MIMO) system

I. INTRODUCTION

It has been shown that systems with multiple antennas at both transmitter and receiver, called MIMO systems, linearly increase the capacity of a wireless link with the number of antennas [1]. The MIMO systems exploit the channel uncertainty to create multiple independent paths between the transmitter and receiver. The uncertainty of the channel is significantly influenced by fading phenomena of the wireless channel. Fading correlation is considered to be a major factor that reduces the MIMO capacity [2]. The MIMO capacity also depends

On array element radiation patterns [3-6]. Unlike the fading Correlation, the radiation Patterns do not depend on a propagation environment.

Analysis performance of antenna design in a propagation channel for MIMO and antenna diversity systems has become many of publications. The resulting understanding has led to the practice of designing antenna arrays whose element radiation patterns are nearly orthogonal, as such a criterion leads to good performance in multi-antenna systems under specific assumptions such as the propagation environment. In practically, design of the antenna is likely to be used in different environments, such as indoor, outdoor, office and so on. The question is which type of antenna will improve in those environments. However, many works have recently reported best antenna characteristics for MIMO systems operating in a specific propagation environment [7], [8]. Furthermore, to compare antennas performance is not an easy task, since it is difficult to replicate the same channel conditions for different measurements. The solution for antenna properties must be optimal for the specific propagation channel that they considered. While these reported techniques are usually discovered, they need to consider the transmitted and received antenna characteristics together but the designs are interdependent.

This paper presents MIMO capacity results for directional antenna arrays in relevant environments using in- and outdoor environment and proposes a simplify model for analyze the antenna radiation characteristics based on stochastic characteristics of the propagation at receiver. We generalize the channel model so that it can take 3-dimension or 3D antenna property including antenna pattern effect on the system capacity into consideration.

There are two major contributions in this paper.

- i) Investigate the effect of directional antenna with combined AOA distribution on the MIMO capacity in difference environment by simulations.
- ii) Verify the simulation results by measurement in the real propagation scenarios compare with a result from simulations.

This paper is organized as follow. The next section, the proposed channel model of special correlation with directional antenna and propagation spread is discussed for multiple antenna systems. Simulations of the MIMO capacity in various propagation environments are presented in section three. Section four will report the results from our MIMO channel measurements and finally, the simulations comparing results will be reported.

II. ANALYSIS MIMO MODEL

2.1. Narrow-bands MIMO model

In this section, a brief review of "one-ring" channel model is given. Then, the proposed model of the MIMO system with the effect from pattern of directional

antenna is discussed. The end of this section presents a technique for MIMO capacity calculation with effect of both antenna pattern property and a spread of AOAs.

Let \mathbf{x} be a vector of the transmitted signals with n_T transmit antennas and \mathbf{y} be a vector of the received signals with n_R receive antennas. Then the MIMO system model [1],[2],[9] is given by

$$\mathbf{y} = \mathbf{H}\mathbf{x} + \mathbf{n} \quad (1)$$

Where \mathbf{n} is an $(n_R \times 1)$ additive noise vector introduced at the receiver and \mathbf{H} is an $(n_R \times n_T)$ channel matrix.

The following assumptions are made in order to compute channel capacity for this model.

- \mathbf{H} Is a matrix of i.i.d. zero mean Gaussian random variables h_{ij} with variance σ_h^2 .
- \mathbf{n} is a vector of i.i.d. zero mean Gaussian random variables n_i with variance σ_n^2 .
- The transmitter has knowledge of channel statistics and the receiver knows \mathbf{H} .
- The total transmit power P_{total} is allocated uniformly to each transmit antenna as $P = P_{total}/n_T$.

However, we consider a model for a narrowband with a specific band of frequency spectrum. Let x and y be a transmitted and received signal respectively. The system model for a narrowband wireless system with single antenna at the both ends can be written as

$$y = hx + n \quad (2)$$

Where h and n are the channel impulse response and additive noise respectively.

However, to describe a channel in spherical coordinate that will be used for antenna radiation pattern or antenna gain and incident wave for either antenna will show in Fig. 1. An incoming signal will come over $[0, 360]$ or $[0, 2\pi]$ for azimuth plane (ϕ) and $[0, 180]$ or $[0, \pi]$ for elevation plane (θ) respectively. We can be calculated antenna gain from the far-field radiation pattern in 3D using [10] we have,

$$G(\theta, \phi) = \frac{4\pi U(\theta, \phi)}{P} \quad (3)$$

Where $G(\theta, \phi)$ and P are antenna gain as a function of angle and total power respectively. $U(\theta, \phi)$ Is radiation intensity of antenna given by?

$$U(\theta, \phi) = \frac{1}{2\eta} \left[|E_\theta(\theta, \phi)|^2 + |E_\phi(\theta, \phi)|^2 \right] \quad (4)$$

Where E_θ and E_ϕ is electric field component of antenna. Substituting (4) into (3) gives

$$G(\theta, \phi) = k \left(|E_\theta(\theta, \phi)|^2 + |E_\phi(\theta, \phi)|^2 \right) \quad (5)$$

Where $k = 4\pi / 2\eta P$.

The antenna radiation pattern is deterministic phenomena whereas the channel impulse responses are stochastic process. The incoming electromagnetic waves are stochastic process due to the randomness of the channel. Since the antenna is used for converting statistical electromagnetic waves to an electrical signal, the output electrical signal will be a stochastic process. However, the

output stochastic process will not be the same with the input process because the antenna radiation pattern influences the input process as a transfer function. In other words, the randomness of the channel is altered by the antenna radiation pattern. The radiation pattern directly influences the capacity. In an ideal channel case, the antenna pattern is needed to be Omni-direction. However, in a certain propagation environment, the Omni-directional antenna may not be an optimal choice for maximizing the capacity.

A model for the channel including the effect of the radiation pattern is needed. We propose a MIMO channel model with antenna radiation pattern in 3-dimension. In this paper, the channel impulse responses, the angle of arrival and the antenna pattern can be modeled separately in the proposed model.

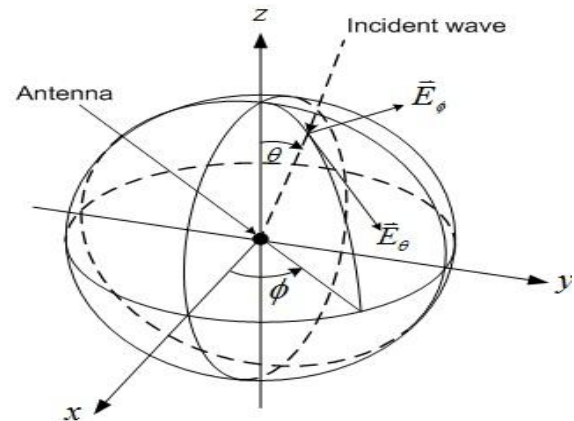


Fig.1 Spherical coordinate system.

For Omni-directional antenna, the direction of incoming signal derived as closed-form expressions. The distributions of AOA have a closed-form as a Uniform, Gaussian and Laplacian distribution have been introduced [11-13]. For these three distributions will use the AOA as indexing variables. So, the modified channel impulse response with the effect of the directional antenna and spread of AOA for a narrowband wireless system can be written as

$$h_a = G(\theta, \phi)h \quad (6)$$

Where h is in frequency domain for narrowband system model.

The main advantage of the proposed model is that the channel impulse response and antenna pattern for different environments of AOA can be treated as one single function or separately depend on environment selected. The channel impulse response can be obtained from either a wireless channel measurement [7] or an analytic model [6],[14-16]. Whereas either a full wave electromagnetic simulation or antenna radiation pattern measurement can be used to obtain radiation or antenna gain pattern. By using (6) for the modified channel impulse responses with antenna pattern and a spread of AOA, each row of the channel matrix is given by

$$h_i^a = [G_i(\theta_1, \phi_1)h_{i1} \quad \dots \quad G_i(\theta_{n_r}, \phi_{n_r})h_{in_r}] \quad (7)$$

Where $G_i(\theta_i, \phi_i)$ is the radiation pattern of i -th receive antenna. Hence, the channel matrix with the effect of receive antenna radiation patterns and a spread of AOA can be written as

$$\mathbf{H}_a = [h_1^a \ h_2^a \ \dots \ h_{n_r}^a]^T \quad (8)$$

The MIMO system model in (1) with the effect received antenna radiation pattern and AOA can be written as

$$\mathbf{y} = \mathbf{H}_a \mathbf{x} + \mathbf{n} \quad (9)$$

The narrowband MIMO capacity is a function of the channel matrix will given by

$$C = \log \det \left(\mathbf{I}_{n_r} + \frac{P}{\sigma_n^2} \mathbf{H}_a \mathbf{H}_a^T \right) \quad (10)$$

Where P the signal is power and σ_n^2 is the noise power. To calculate the capacity with effect of directional antenna and a spread of AOA, random matrices are generated by using (7) each realization of the channel matrix is obtained by using (9) and (10) where the AOA for each receive antenna is generated based on environments scenarios selected.

2.2. Distributions Function of AOA

For 3D Model, the propagation distribution for both azimuth and elevation planes are independent and identically distributed (i.i.d.) random variables. However, the distribution of the propagation directions are defined for azimuth and elevation plane. So, in literature measurement results suggest three candidates for AOA distribution in azimuth plane, Uniform, Gaussian and double exponential or Laplacian distributions [17]. The uniform distribution, which assumes that all the incoming waves are come from all direction in the azimuth plane, with an independent random phase for each azimuth direction with equal probability. The other distribution function can be written as follows.

1) Gaussian function:

$$\psi(x) = A_1 \exp \left[-\frac{(x - \mu)^2}{2b^2} \right] \quad (11)$$

2) Double exponential function:

$$\psi(x) = \begin{cases} A_2 \exp \left[-\frac{\mu - x}{b^-} \right], & x < \mu \\ A_2 \exp \left[-\frac{x - \mu}{b^+} \right], & x \geq \mu \end{cases} \quad (12)$$

If the spread parameters b^- and b^+ are equal, the double exponential function become Laplacian function as show in Fig. 2. Where coefficients $A_1 = 1/\sqrt{2\pi b^2}$ and $A_2 = 1/2b$.

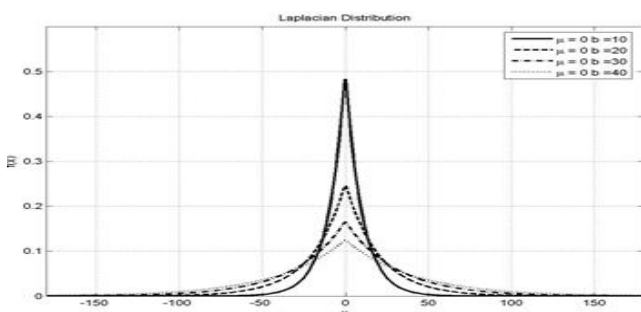


Fig. 2 Laplacian distribution.

III. SIMULATIONS

The MIMO capacity in (10) is evaluated using Monte Carlo simulations. Then, 10,000 instances of channel and collect the statistics of MIMO channel capacity were generated. In the simulations, 4 transmits and 4 receive antennas are used at the both ends. The signal to noise ratio (P/n) is calculated from a result of measurement that will discuss for detail later. The AOAs are generated using Uniform, Gaussian and Laplacian distribution in both azimuth and elevation plane depend on scenarios that will be describe as,

Scenario I – a measurement has been setting up in a laboratory room that has a desk and partition. The measurement space is 15.00m. x 7.00m. x 3.00m., as shown in Fig. 3. So, the distribution in azimuth plane is used and elevation will be uniformed on both planes.

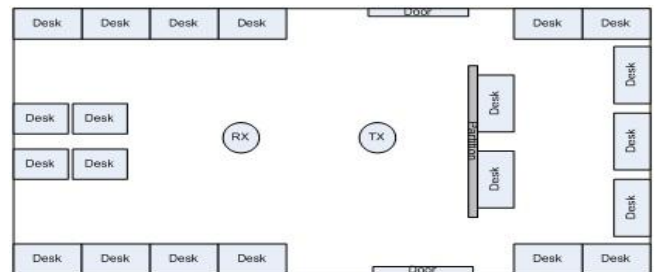


Fig. 3 Diagram of TX and RX location for indoor scenarios.

Scenario II – a measurement has setting up in a parking yard with a wide area opened. So, the distribution in azimuth plane using a peaky distribution with spread parameter is normal distribution. So, we will use both Gaussian and a double-sided exponential function with equal spread parameters or Laplacian on both planes in this scenario.

For AOA in 3D model, we will combine the AOA of the incoming multipath at the receiver both spherical angles θ and ϕ . The joint pdf $p(\theta, \phi)$ is written in terms of the conditional pdf of θ for a given ϕ ; $p_\theta(\theta|\phi)$, and the marginal pdf $f_\phi(\phi)$ Thus,

$$p(\theta, \phi) = p_\phi(\phi) f_\theta(\theta|\phi) \quad (13)$$

So, the result of distribution of AOA in both azimuth and elevation plane can be written as,

1) Gaussian function:

$$\psi(\theta, \phi) = B_1 \exp \left[-\left(\frac{(\theta - \mu_\theta)^2}{2b_\theta^2} + \frac{(\phi - \mu_\phi)^2}{2b_\phi^2} \right) \right] \quad (14)$$

2) Double exponential function:

$$\psi(\theta, \phi) = \begin{cases} B_2 \exp \left[-\left(\frac{\mu_\theta - \theta}{b_\theta^-} + \frac{\mu_\phi - \phi}{b_\phi^-} \right) \right], & \theta < \mu_\theta, \phi < \mu_\phi \\ B_2 \exp \left[-\left(\frac{\theta - \mu_\theta}{b_\theta^+} + \frac{\phi - \mu_\phi}{b_\phi^+} \right) \right], & \theta \geq \mu_\theta, \phi \geq \mu_\phi \end{cases} \quad (15)$$

When coefficients $B_1 = A_1^2$ and $B_2 = A_2^2$. The center of distribution and direction of antenna must point into the direction of the main lobe of antenna. So, the distribution will shift an angle that the distribution mainly distributed that match to main lobe of an antenna we used. For simulation, a monopole antenna is used as a reference scenario and other three type of Yagi-Uda are used to investigate the effect of antenna radiation pattern with difference AOA distribution to the channel capacity.

The 3D radiation patterns of antennas are obtained from CST microwave studio 2009. The radiation pattern in the simulations, 5-element, 9-element, 13-element Yagi-Uda antennas are show in Fig. 4 and Fig. 5 for azimuth and elevation plane respectively.

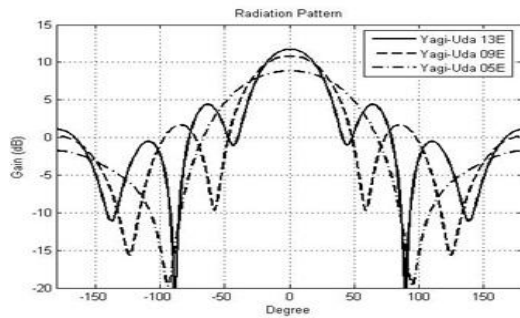


Fig. 4 The radiation pattern for Yagi-Uda on azimuth plane.

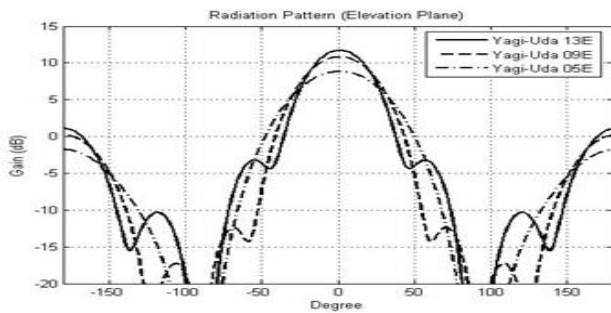


Fig. 5 The radiation pattern for Yagi-Uda on elevation plane.

The actual antenna pattern properties such as gain and HPBW from measurement compare to a result from CST is similarly on both azimuth and elevation planes as show in table 1 and table 2. Where the gains are with respect to Omni-directional antenna in dBi and HPBW are in degrees. Antennas at receiver are equipped with uniform linear arrays (ULA) of the same type antennas. Furthermore, it is assumed that antenna spacing at both sides is the same at transmitter and receiver, each has four antennas.

The MIMO capacities were compared in terms of the Complementary Cumulative Distribution Functions (CCDF). The performance of each antenna type is varied by different scenarios referring to the different AOA distribution and the outage capacity observation. The channel capacity at a given outage probability q , denoted by C_q . The 10% outage channel capacities will be written as $C_{0.1}$.

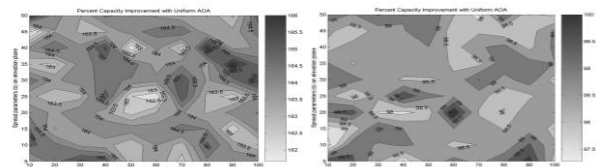
Table 1. Antenna property from CST for simulation.

Antenna Type	Azimuth-HPBW (Degree)	Elevation-HPBW (Degree)	Gain (dBi)
Isotropic	-	-	1.00
Yagi-05E	86.4	59.0	8.84
Yagi-09E	58.8	48.0	10.83
Yagi-13E	44.9	40.0	11.70

Table 2. Actual antenna property used in measurement.

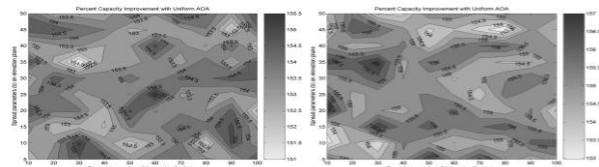
Antenna Type	Azimuth-HPBW (Degree)	Elevation-HPBW (Degree)	Gain (dBi)
Monopole	95.0	85.0	4.32
Yagi-05E	84.0	60.0	8.58
Yagi-09E	56.0	50.0	9.71
Yagi-13E	45.0	40.0	10.55

In order to access the capacity performance of directional antennas, the downlink of a point-to-point narrowband MIMO system is considered, operating at the frequency of 2.45 GHz. It is assumed the 3D scattering environment can be represented by a scenarios selected as describe before.



a) Isotropic Antenna

b) Yagi-Uda 5E Antenna



c) Yagi-Uda 9E Antenna

d) Yagi-Uda 13E Antenna

Fig. 6 Percent capacity outage with different spread parameter on 3D for scenarios I with Uniform AOA.

3.1 Scenario I

In this scenario, a distribution of AOA is uniformed on both planes. We generate channel with a distribution of AOA for 10000 instants. The AOAs are concentrated around the mean. The spread parameter is a parameter to control the randomness of the AOA. So, the result of the 10% outage channel capacities counted from CCDF will be compare to ideal case of isotropic antenna

with different spread parameter of AOA distribution on azimuth and elevation plane will be investigated.

varied with a spread parameter in both planes. When the spread increases, it decreases the capacity on both ways.

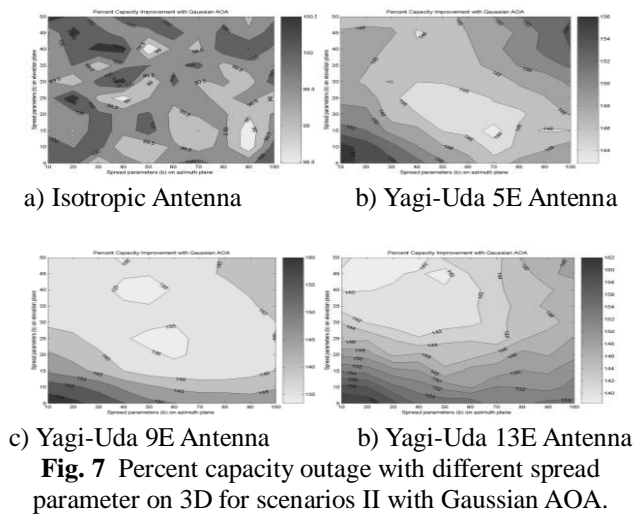


Fig. 7 Percent capacity outage with different spread parameter on 3D for scenarios II with Gaussian AOA.

The spread parameter between 10 to 100 degree on azimuth and 5 to 50 degree on elevation plane has been investigated. The 10% outage channel capacities for four types of antenna show in Fig. 6. The capacity is about 166%, 157% and 155% for 5E 9E and 13E Yagi-Uda antenna. All capacity is greater than the ideal case due to the gain of each antenna but not affect a spread of AOA changed.

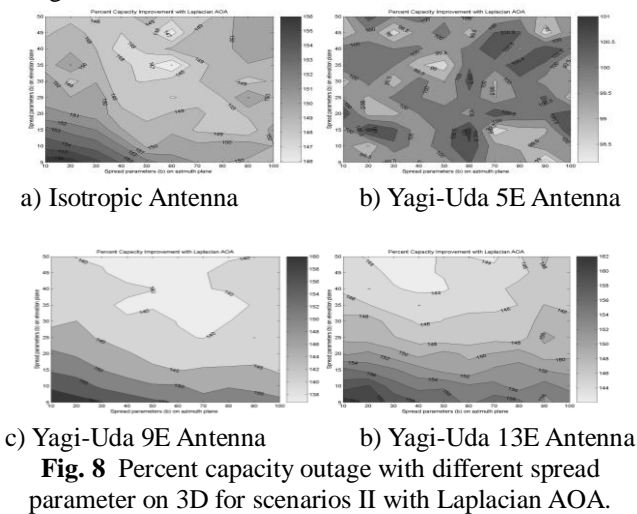


Fig. 8 Percent capacity outage with different spread parameter on 3D for scenarios II with Laplacian AOA.

3.2 Scenario II

In this scenario, the antenna is located so that the direction of maximum directivity is aligned with the mean of AOA of the Yagi-Uda antenna is used. The 10% outage channel capacities in (8) for all antenna types are shown in Fig. 7 and 8 for Gaussian and Laplacian AOA environment respectively.

It can be seen that the directional antennas maximize the system capacity show in Fig. 7 for Gaussian AOA. of the Yagi-Uda 5E, Yagi-Uda 9E and Yagi-Uda 13E is about 156%, 162% and 160% more than the ideal case. For Laplacian AOA in Fig.8, The result of Yagi-Uda 5E, Yagi-Uda 9E and Yagi-Uda 13E is about 156%, 162% and 160% more than the ideal case.

In this scenario, the capacity improvement is

IV. EXPERIMENTAL MEASUREMENTS

In this section, the capacity of a directional antenna, 5-elements 9-element and 13-elements Yagi-Uda, is measured. A Monopole antenna is used in the experiment for comparison with those three Yagi-Uda antennas. The 4-monopole array is used in the experiment as a transmit antenna. At the receiver, 4-Yagi-Uda array is used. The system is 4x4 MIMO.

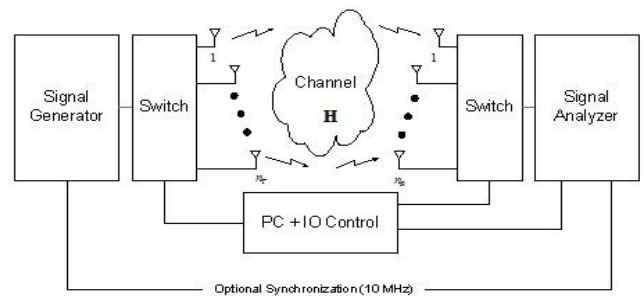


Fig. 9 Diagram of narrowband MIMO channel measurement system.

The block diagram of the capacity measurement system is shown in Fig. 9. The capacity measurements are performed by using the signal scheme in [18]. This signal is loaded into the E4433 signal generator. The received signals are store in the signal analyzer MXA9020A.

Table 3. Mutual Coupling level (S21).

Distance(Lambda)	Monopole	Yagi-05E	Yagi-09E	Yagi-13E
d=0.5	-34.73	-22.49	-23.27	-21.10
d=1.0	-36.41	-31.42	-30.91	-25.23
d=1.5	-46.20	-35.42	-34.05	-32.02
d=2.0	-43.49	-42.39	-41.52	-39.25
d=2.5	-50.21	-41.04	-41.86	-54.28
d=3.0	-44.42	-48.78	-52.52	-41.12
d=3.5	-52.33	-42.03	-67.43	-47.67
d=4.0	-53.16	-48.21	-62.91	-52.91

The antenna separations in the array are determined by mutual coupling measurements measuring in an anechoic chamber for monopole and all type of Yagi-Uda. The mutual coupling with various antenna separations is shown in table 3. Normally, the mutual coupling will effect to capacity when antenna space less than $\lambda/2$. So, the mutual coupling is less than -40 dB when the antenna separation is greater than 2λ . Finally, we choose the antenna separation of 2λ in the experiments to neglect the mutual coupling [19-20].

4.1 MIMO Capacity Calculation.

A comparison of the MIMO capacity achieved by each type of antenna array must be made using measurements from various scenarios. Directive antennas may increase SNR and also reduce the multipath signals that can be received by the antennas at the same time. To separate these two effects we firstly quantify whether there is a MIMO capacity reduction with directive antennas at constant SNR. To make a fair comparison shown in simulation, a monopole antenna closed to an isotropic antenna in all measurement scenarios is used to compare result with a simulation. Average channel capacity of monopole is measured as reference for normalized as follows.

A reference SNR measurement is made at each scenario using monopole ULAs with antenna spacing of 2λ . Mutual coupling is assumed to have negligible effect on receiver SNR for such large spacing. The reference measurement is made using the same grid positions and frequencies used for all site measurements. A reference noise variance is computed as before while the reference channel variance is computed as [21]

$$\sigma^2 = \frac{1}{n_T n_R} \sum_{i=1}^{n_T} \sum_{j=1}^{n_R} |h_{ij}|^2 \quad (17)$$

The normalized ensemble average channel capacity is then computed as

$$\overline{C_N} = \frac{\overline{C_H}}{C(\sigma_{h,r}^2, \sigma_n^2)} \quad (18)$$

Where $C(\sigma_{h,r}^2, \sigma_n^2)$ is the i.i.d. Gaussian channel capacity corresponding to the reference SNR measurement and computed by Monte Carlo simulation of the system defined in Section 3. The computed reference channel capacity is assumed to be able to achieve in the best case scenario of no mutual coupling and no channel correlation. This capacity normalization is a departure from the traditional method in which the measured channel matrices are normalized and SNR is scaled freely.

4.2 Field Measurement Procedure

Table 4. Measurement parameter for all scenarios

Parameter	Value
Transmitter antenna gain	4.32dB
Receiver antenna gain (Yagi-Uda 13E)	10.55dB
Receiver antenna gain (Yagi-Uda 09E)	9.71dB
Receiver antenna gain (Yagi-Uda 05E)	8.58dB
Receiver antenna gain (Monopole)	4.32dB
Distance from TX. ant. To RX. ant.	3.0 m.
Total transmission cable loss	-11.48dB

A measurement campaign is performed by using the QPSK signal generator that broadcasts a 50 MHz IF excitation signal at 2.45 GHz from each transmit antenna. The transmitted signal from each antenna is captured at each receive antenna by using a manual-switch. For far-field measurement, this transmitter and receiver will have 3 meter distance. A MXA9020A signal analyzer was used to measure a propagation gain that is used in this paper. A complete calibration of each radio's gain, phase noise and frequency offset was performed prior to field measurements.

It has been shown that the statistical property of AOA in outdoor propagation environment has peaky characteristic [22]. The measurement parameters are shown in table 4.

4.3 Measurement Results

This section presents the results from an indoor and outdoor measurement campaign using a measurement instrument test-set with the Yagi-Uda and monopole antennas. Measured channel capacity results from difference measurement scenarios are presented to show the effect of antenna radiation pattern and AOA distribution in environment. Before using the measurement result, it must normalize capacity as show in section 4.1. An average SNR at receive antenna from all measurement scenario as scenario I, scenario II and anechoic chamber are shown in table 5.

A reference SNR measure in chamber that will extremely have direct line of sight signal. That result show a difference scattering effect to SNR for both scenarios.

Table 5. Average receive power from measurements.

Antenna Type	Scenario I	Scenario II	Chamber
Monopole	-46.18	-46.33	-46.26
Yagi-05E	-43.56	-40.18	-39.49
Yagi-09E	-42.05	-38.87	-38.32
Yagi-13E	-40.76	-37.32	-37.20

Table 6. Improvement of 10% outage capacity from measurements.

Antenna Type	Scenario I	Scenarios II	Chamber
Monopole	100%	100%	100%
Yagi-05E	116%	143%	131%
Yagi-09E	134%	156%	141%
Yagi-13E	136%	164%	147%

However, a comprehensive set of results is presented for both scenarios. A fair comparison of MIMO performance is made between the Yagi-Uda and the reference monopole from simulation result as shown in table 6. A directional antenna in scenarios not be improved MIMO capacity but in scenarios II, directional antenna will improve MIMO

capacity. Finally, directional antenna that has gain and direction match to AOA spread will improve MIMO capacity in condition as the direction of antenna is correctly.

V. CONCLUSIONS

This research proposes proposed the channel model for MIMO capacity calculation. The proposed model can be used to calculate the MIMO capacity with the presence of 3D antenna radiation pattern.

The proposed model allows us to model the 3D antenna pattern. The elements spacing are 2λ for decrease effect of mutual coupling. However, not only radiation pattern of the element influences the narrowband MIMO capacity but also the statistical property of AOA. We have shown that directional antennas are not attractive for MIMO systems in a scenario where the randomness of AOA is high. In a scenario with AOA concentrating on a single value, the antenna position is crucial to the capacity. If the antenna is point into the mean AOA, then the capacity is increased. The results from measurement show that the AOA and antenna radiation pattern influence narrowband MIMO capacity from simulation be confirmed.

On the other hand, in rich scattering environments, the power gain of directional antennas is no more helpful, since the signal power is dispersed over a large extent of directions. The limited beam-width of directional antennas will decrease in the effective angular spread which severely increases the correlation. Therefore Omni-directional antennas outperform in these situations. These results suggest the following general guidelines for selection of antenna type. Our results show that choosing the suitable antenna, operating SNR and antenna spacing are other factors that should also be considered together with the spread of AOA.

VI. ACKNOWLEDGEMENTS

This work was supported by Suranaree University of Technology (SUT) and advised by Ms. Natthanant Summat on the paper report writing.

REFERENCES

- [1] G.J. Foschini and M.J. Gan, On limits of wireless communications in fading environment when using multiple antennas, *Wireless Personal Communications*, 6(3), 1998, 311-335.
- [2] D.S. Shiu, G.J. Foschini, M.J. Gans and J.M. Kahn, Fading correlation and its effect on the capacity of multi-element antenna systems, *Proc. IEEE 1998 International Conference on Universal Personal Communications*, 1998, 429-433.
- [3] K. Yu and B. Ottersten, Models for MIMO propagation channels: A review, *Wirel. Commun. Mob. Comput.*, 2(7), 2002, 653-666.
- [4] B. Wang, and A.G. Burr, Effect of element radiation patterns on the capacity of MIMO system, *Proc. IEEE Int. Symp. on Microwave, Antenna, Propagation and EMC Tech. for Wireless Comms*, 2005, 1448 - 1451.
- [5] C. Saetiauw, A. Intrapanich, C. Thongsopa, Effect of Spatial Correlation with Directional Antenna on MIMO Capacity, *Proc. of ISAP2007*, 2007, 1334-1338.
- [6] H.S. Rad and S. Gazor, The impact of non-isotropic scattering and directional antennas on MIMO multicarrier mobile communication channels, *IEEE Transactions on Communications*, 56(4), 2008, 642-652.
- [7] D. Chizhik, J. Ling, P.W. Wolniansky, R.A. Valenzuela, N. Costa, and K. Huber, Multiple-input-multiple-output measurements and modeling in Manhattan, *IEEE J. Sel. Areas Commun.*, 21, 2003, 321-331.
- [8] K.I. Pedersen, P.E. Mogensen, and B.H. Fleury, Power azimuth spectrum in outdoor environments, *Electron. Lett.*, 33(18), 1997, 1583-1584.
- [9] I.E. Telatar, Capacity of multi-antenna Gaussian channels AT&T Bell Labs, Tech. Rep., 1995.
- [10] C.A. Balanis, *Antenna Theory: Analysis and Design*, 3rd Edition, John Wiley & Sons Inc, 2005.
- [11] K.I. Pedersen, P.E. Mogensen, and B.H. Fleury, A stochastic model of the temporal and azimuthally dispersion seen at the base station in outdoor propagation environments, *IEEE Trans. Veh. Technol.*, 49(2), 2000, 437-447.
- [12] Q.H. Spencer, B.D. Jeffs, M.A. Jensen, and A.L. Swindlehurst, Modeling the Statistical Time and Angle of Arrival Characteristics of an Indoor Multipath Channel, *IEEE Journal on Selected Areas in Communications*, 18, 2000, 347-360.
- [13] F. Adachi, M. Feeny, A. Williamson, and J. Parsons, Cross-Correlation between the Envelopes of 900 MHz Signals Received at a Mobile Radio Base Station Site, *IEEE Proceedings Pt. F*, 133, 1986, 506-512.
- [14] W.C.Y. Lee, Effects on correlation between two mobile radio base-station antennas, *IEEE Trans. Commun.*, 21, 1973, 1214-1224.
- [15] J. Salz and J. Winters, Effect of Fading Correlation on Adaptive Arrays in Digital Mobile Radio, *IEEE Transactions on Vehicular Technology*, 43, 1994, 1049-1057.
- [16] C. Saetiauw, A. Intrapanich, C. Thongsopa, Relations Between 3-Dimensions Antenna Pattern and Narrowband MIMO Capacity, *Proc. Microwave Conference, APMC2007*, 2007, 1 - 4.
- [17] K. Kalliola, K. Sulonen, H. Laitinen, O. Kivekäs, J. Krogerus, and P. Vainikainen, Angular power distribution and mean effective gain of mobile antenna in different propagation environments, *IEEE Transactions on Vehicular Technology*, 51(5), 2002, 823-838.
- [18] D.W. Browne, W. Zhu, and M.P. Fitz, A signaling scheme and estimation algorithm for characterizing frequency selective MIMO channels, *Proc. IEEE Veh. Technol. Conf.*, 2005.
- [19] T. Svantesson and A. Ranheim, Mutual coupling effects on the capacity of multielement antenna systems, *Proc. IEEE ICASSP*, 2001, 2485-2488.
- [20] I. Gupta and A. Ksienski, Effect of mutual coupling on the performance of adaptive arrays, *IEEE Trans. Antennas Propag.*, 31, 1983, 785-791.
- [21] D.W. Browne, M. Manteghi, M.P. Fitz, Y. Rahmat-Samii, Experiments With Compact Antenna Arrays for MIMO Radio Communications, *Antennas and Propagation, IEEE Transactions on*, 54(11), 2006, 3239-3250.
- [22] M. Alsehaili, S. Noghianian, D.A. Buchanan and A.R. Sebak, Angle-of-Arrival Statistics of a Three-Dimensional Geometrical Scattering Channel Model for Indoor and Outdoor Propagation Environments, *IEEE Antennas and Wireless Propagation Letters*, 9, 2010, 946-949.

On The Zeros of Polynomials

M. H. Gulzar

Department of Mathematics University of Kashmir, Srinagar, 190006, India

Abstract: In this paper we extend Enestrom -akeya theorem to a large class of polynomials with complex coefficients by putting less restrictions on the coefficients . Our results generalise and extend many known results in this direction.

(AMS) Mathematics Subject Classification (2010) : 30C10, 30C15

Key-Words and Phrases: Polynomials, Zeros, Bounds

I. Introduction and Statement of Results

Let $P(z)$ be a polynomial of degree n . A classical result due to Enestrom andakeya [9] concerning the bounds for the moduli of the zeros of polynomials having positive coefficients is often stated as in the following theorem(see [9]) :

Theorem A (Enestrom-akeya) : Let $P(z) = \sum_{j=0}^n a_j z^j$ be a polynomial of degree n whose coefficients satisfy

$$0 \leq a_1 \leq a_2 \leq \dots \leq a_n.$$

Then $P(z)$ has all its zeros in the closed unit disk $|z| \leq 1$.

In the literature there exist several generalisations of this result (see [1],[3],[4],[8],[9]). Recently Aziz and Zargar [2] relaxed the hypothesis in several ways and proved

Theorem B: Let $P(z) = \sum_{j=0}^n a_j z^j$ be a polynomial of degree n such that for some $k \geq 1$,

$$ka_n \geq a_{n-1} \geq \dots \geq a_1 \geq a_0.$$

Then all the zeros of $P(z)$ lie in

$$|z + k - 1| \leq \frac{ka_n + |a_0| - a_0}{|a_n|}.$$

For polynomials ,whose coefficients are not necessarily real, Govil and Rehman [6] proved the following generalisation of Theorem A:

Theorem C: If $P(z) = \sum_{j=0}^n a_j z^j$ is a polynomial of degree n with $\operatorname{Re}(a_j) = \alpha_j$ and $\operatorname{Im}(a_j) = \beta_j$, $j=0,1,2,\dots,n$, such that

$$\alpha_n \geq \alpha_{n-1} \geq \dots \geq \alpha_1 \geq \alpha_0 \geq 0,$$

where $\alpha_n > 0$, then $P(z)$ has all its zeros in

$$|z| \leq 1 + \left(\frac{2}{\alpha_n}\right) \left(\sum_{j=0}^n |\beta_j|\right).$$

More recently, Govil and Mc-tume [5] proved the following generalisations of Theorems B and C:

Theorem D: Let $P(z) = \sum_{j=0}^n a_j z^j$ be a polynomial of degree n with $\operatorname{Re}(a_j) = \alpha_j$ and $\operatorname{Im}(a_j) = \beta_j$, $j=0,1,2,\dots,n$.

If for some $k \geq 1$,

$$k\alpha_n \geq \alpha_{n-1} \geq \dots \geq \alpha_1 \geq \alpha_0,$$

then $P(z)$ has all its zeros in

$$|z + k - 1| \leq \frac{k\alpha_n - \alpha_0 + |\alpha_0| + 2\sum_{j=0}^n |\beta_j|}{|\alpha_n|}.$$

Theorem E: Let $P(z) = \sum_{j=0}^n a_j z^j$ be a polynomial of degree n with $\operatorname{Re}(a_j) = \alpha_j$ and $\operatorname{Im}(a_j) = \beta_j, j=0,1,2,\dots,n$.

If for some $k \geq 1$,

$$k\beta_n \geq \beta_{n-1} \geq \dots \geq \beta_1 \geq \beta_0,$$

then $P(z)$ has all its zeros in

$$|z + k - 1| \leq \frac{k\beta_n - \beta_0 + |\beta_0| + 2\sum_{j=0}^n |\alpha_j|}{|\beta_n|}.$$

M.H.Gulzar [7] proved the following generalisations of Theorems D and E.

Theorem F: Let $P(z) = \sum_{j=0}^n a_j z^j$ be a polynomial of degree n with $\operatorname{Re}(a_j) = \alpha_j$ and $\operatorname{Im}(a_j) = \beta_j, j=0,1,2,\dots,n$.

If for some real number $\rho \geq 0$,

$$\rho + \alpha_n \geq \alpha_{n-1} \geq \dots \geq \alpha_1 \geq \alpha_0,$$

then $P(z)$ has all its zeros in the disk

$$\left| z + \frac{\rho}{\alpha_n} \right| \leq \frac{\rho + \alpha_n + |\alpha_0| - \alpha_0 + 2\sum_{j=0}^n |\beta_j|}{|\alpha_n|}.$$

Theorem G: Let $P(z) = \sum_{j=0}^n a_j z^j$ be a polynomial of degree n with $\operatorname{Re}(a_j) = \alpha_j$ and $\operatorname{Im}(a_j) = \beta_j, j=0,1,2,\dots,n$.

If for some real number $\rho \geq 0$,

$$\rho + \beta_n \geq \beta_{n-1} \geq \dots \geq \beta_1 \geq \beta_0,$$

then $P(z)$ has all its zeros in the disk

$$\left| z + \frac{\rho}{\beta_n} \right| \leq \frac{\rho + \beta_n + |\beta_0| - \beta_0 + 2\sum_{j=0}^n |\alpha_j|}{|\beta_n|}.$$

The aim of this paper is to give generalizations of Theorem F and G under less restrictive conditions on the coefficients. More precisely we prove the following :

Theorem 1: Let $P(z) = \sum_{j=0}^n a_j z^j$ be a polynomial of degree n with $\operatorname{Re}(a_j) = \alpha_j$ and $\operatorname{Im}(a_j) = \beta_j, j=0,1,2,\dots,n$. If

for some real numbers $\rho \geq 0, 0 < \sigma \leq 1$,

$$\rho + \alpha_n \geq \alpha_{n-1} \geq \dots \geq \alpha_1 \geq \sigma\alpha_0,$$

then $P(z)$ has all its zeros in the disk

$$\left| z + \frac{\rho}{\alpha_n} \right| \leq \frac{\rho + \alpha_n - \sigma(|\alpha_0| + \alpha_0) + 2|\alpha_0| + 2\sum_{j=0}^n |\beta_j|}{|\alpha_n|}.$$

Remark 1: Taking $\sigma = 1$ in Theorem 1, we get Theorem F. Taking $\rho = (k-1)\alpha_n, \sigma = 1$, Theorem 1 reduces to Theorem D and taking $\rho = 0, \alpha_0 > 0$ and $\sigma = 1$, we get Theorem C.

Applying Theorem 1 to $P(tz)$, we obtain the following result:

Corollary 1 : Let $P(z) = \sum_{j=0}^n a_j z^j$ be a polynomial of degree n with $\operatorname{Re}(a_j) = \alpha_j$ and $\operatorname{Im}(a_j) = \beta_j, j=0,1,2,\dots,n$.

If for some real numbers $\rho \geq 0, 0 < \sigma \leq 1$ and $t > 0$,

$$\rho + t^n \alpha_n \geq t^{n-1} \alpha_{n-1} \geq \dots \geq t \alpha_1 \geq \sigma \alpha_0,$$

then $P(z)$ has all its zeros in the disk

$$\left| z + \frac{\rho}{t^{n-1}\alpha_n} \right| \leq \frac{\rho + t^n \alpha_n - \sigma(|\alpha_0| + \alpha_0) + 2|\alpha_0| + 2 \sum_{j=0}^n |\beta_j| t^j}{t^{n-1} |\alpha_n|}.$$

In Theorem 1, if we take $\alpha_0 \geq 0$, we get the following result:

Corollary 2 : Let $P(z) = \sum_{j=0}^n a_j z^j$ be a polynomial of degree n with $\operatorname{Re}(a_j) = \alpha_j$ and $\operatorname{Im}(a_j) = \beta_j, j=0,1,2,\dots,n$.

If for some real numbers $\rho \geq 0$,

$$0 < \sigma \leq 1,$$

$$\rho + \alpha_n \geq \alpha_{n-1} \geq \dots \geq \alpha_1 \geq \sigma \alpha_0 \geq 0,$$

then $P(z)$ has all its zeros in the disk

$$\left| z + \frac{\rho}{\alpha_n} \right| \leq 1 + \frac{\rho + 2(1-\sigma)\alpha_0 + 2 \sum_{j=0}^n |\beta_j|}{|\alpha_n|}.$$

If we take $\rho = \alpha_{n-1} - \alpha_n \geq 0$ in Theorem 1, we get the following result:

Corollary 3 : Let $P(z) = \sum_{j=0}^n a_j z^j$ be a polynomial of degree n with $\operatorname{Re}(a_j) = \alpha_j$ and $\operatorname{Im}(a_j) = \beta_j, j=0,1,2,\dots,n$,

such that

$$\alpha_n \geq \alpha_{n-1} \geq \dots \geq \alpha_1 \geq \sigma \alpha_0 > 0.$$

Then $P(z)$ has all its zeros in

$$\left| z + \frac{\alpha_{n-1}}{\alpha_n} - 1 \right| \leq \frac{\alpha_{n-1} + 2(1-\sigma)\alpha_0 + 2 \sum_{j=0}^n |\beta_j|}{|\alpha_n|}.$$

Taking $\sigma = 1$ in Cor.3, we get the following result:

Corollary 4 : Let $P(z) = \sum_{j=0}^n a_j z^j$ be a polynomial of degree n with $\operatorname{Re}(a_j) = \alpha_j$ and $\operatorname{Im}(a_j) = \beta_j, j=0,1,2,\dots,n$,

such that

$$\alpha_n \geq \alpha_{n-1} \geq \dots \geq \alpha_1 \geq \alpha_0 > 0.$$

Then $P(z)$ has all its zeros in

$$\left| z + \frac{\alpha_{n-1}}{\alpha_n} - 1 \right| \leq \frac{\alpha_{n-1} + 2 \sum_{j=0}^n |\beta_j|}{|\alpha_n|}.$$

If we apply Theorem 1 to the polynomial $-iP(z)$, we easily get the following result:

Theorem 2: Let $P(z) = \sum_{j=0}^n a_j z^j$ be a polynomial of degree n with $\operatorname{Re}(a_j) = \alpha_j$ and $\operatorname{Im}(a_j) = \beta_j, j=0,1,2,\dots,n$,

If for some real numbers $\rho \geq 0, 0 < \sigma \leq 1$,

$$\rho + \beta_n \geq \beta_{n-1} \geq \dots \geq \beta_1 \geq \sigma \beta_0,$$

then $P(z)$ has all its zeros in the disk

$$\left| z + \frac{\rho}{\beta_n} \right| \leq \frac{\rho + \beta_n - \sigma(|\beta_0| + \beta_0) + 2|\beta_0| + 2 \sum_{j=0}^n |\alpha_j|}{|\beta_n|}.$$

On applying Theorem 2 to the polynomial $P(tz)$, one gets the following result:

Corollary 5 : Let $P(z) = \sum_{j=0}^n a_j z^j$ be a polynomial of degree n with $\operatorname{Re}(a_j) = \alpha_j$ and $\operatorname{Im}(a_j) = \beta_j$,

$j=0,1,2,\dots,n$. If for some real numbers $\rho \geq 0, 0 < \sigma \leq 1$ and $t > 0$,

$$\rho + t^n \beta_n \geq t^{n-1} \beta_{n-1} \geq \dots \geq t \beta_1 \geq \beta_0,$$

then $P(z)$ has all its zeros in the disk

$$\left| z + \frac{\rho}{t^{n-1} \beta_n} \right| \leq \frac{\rho + t^n \beta_n - \sigma(|\beta_0| + \beta_0) + 2|\beta_0| + 2 \sum_{j=0}^n |\alpha_j| t^j}{t^{n-1} |\beta_n|}.$$

II. Proofs of the Theorems

Proof of Theorem 1.

Consider the polynomial

$$\begin{aligned} F(z) &= (1-z)P(z) \\ &= (1-z)(a_n z^n + a_{n-1} z^{n-1} + \dots + a_1 z + a_0) \\ &= -a_n z^{n+1} + (a_n - a_{n-1})z^n + \dots + (a_1 - a_0)z + a_0 \\ &= -a_n z^{n+1} + (\alpha_n - \alpha_{n-1})z^n + \dots + (\alpha_1 - \alpha_0)z + \alpha_0 - i\beta_n z^{n+1} + i(\beta_n - \beta_{n-1})z^n \\ &\quad + \dots + i(\beta_1 - \beta_0)z + i\beta_0 \\ &= -\alpha_n z^{n+1} - \rho z^n + (\rho + \alpha_n - \alpha_{n-1})z^n + (\alpha_{n-1} - \alpha_{n-2})z^{n-1} + \dots + (\alpha_1 - \alpha_0)z \\ &\quad + (\alpha_0 - \alpha_0)z + \alpha_0 + i\{-\beta_n z^{n+1} + (\beta_n - \beta_{n-1})z^n + \dots + (\beta_1 - \beta_0)z + \beta_0\}. \end{aligned}$$

Then

$$\begin{aligned} |F(z)| &= \left| -\alpha_n z^{n+1} - \rho z^n + (\rho + \alpha_n - \alpha_{n-1})z^n + (\alpha_{n-1} - \alpha_{n-2})z^{n-1} + \dots + (\alpha_1 - \alpha_0)z \right. \\ &\quad \left. + (\alpha_0 - \alpha_0)z + \alpha_0 + i\{-\beta_n z^{n+1} + (\beta_n - \beta_{n-1})z^n + \dots + (\beta_1 - \beta_0)z + \beta_0\} \right| \\ &\geq |z|^n \left\{ \begin{aligned} &|\alpha_n z + \rho| - |\rho + \alpha_n - \alpha_{n-1}| - |\alpha_0| \frac{1}{|z|^n} - |\alpha_1 - \alpha_0| \frac{1}{|z|^{n-1}} \\ &-(1-\sigma)|\alpha_0| - \sum_{j=2}^{n-1} |\alpha_j - \alpha_{j-1}| \frac{1}{|z|^{n-j}} \end{aligned} \right\} \\ &\quad - |-\beta_n z^{n+1} + \dots + (\beta_1 - \beta_0)z + \beta_0|. \end{aligned}$$

Thus, for $|z| > 1$,

$$\begin{aligned} |F(z)| &> |z|^n \left\{ \begin{aligned} &|\alpha_n z + \rho| - (\rho + \alpha_n - \alpha_{n-1}) - |\alpha_0| - (\alpha_{n-1} - \alpha_{n-2}) - \dots - (\alpha_2 - \alpha_1) \\ &-(\alpha_1 - \alpha_0) - (1-\sigma)|\alpha_0| \end{aligned} \right\} \\ &\quad - (|\beta_n| + |\beta_0|) - \sum_{j=1}^n (|\beta_j| + |\beta_{j-1}|) \\ &= |z|^n \left[|\alpha_n z + \rho| - \left\{ \rho + \alpha_n - \sigma(|\alpha_0| + \alpha_0) + 2|\alpha_0| + 2 \sum_{j=0}^n |\beta_j| \right\} \right] \\ &> 0 \end{aligned}$$

if

$$|\alpha_n z + \rho| > \rho + \alpha_n - \sigma(|\alpha_0| + \alpha_0) + 2|\alpha_0| + 2 \sum_{j=1}^n |\beta_j|.$$

Hence all the zeros of $F(z)$ whose modulus is greater than 1 lie in the disk

$$\left| z + \frac{\rho}{\alpha_n} \right| \leq \frac{\rho + \alpha_n - \sigma(|\alpha_0| + \alpha_0) + 2|\alpha_0| + 2 \sum_{j=0}^n |\beta_j|}{|\alpha_n|}.$$

But those zeros of $F(z)$ whose modulus is less than or equal to 1 already satisfy the above inequality. Hence it follows that all the zeros of $F(z)$ lie in the disk

$$\left| z + \frac{\rho}{\alpha_n} \right| \leq \frac{\rho + \alpha_n - \sigma(|\alpha_0| + \alpha_0) + 2|\alpha_0| + 2\sum_{j=0}^n |\beta_j|}{|\alpha_n|}.$$

Since all the zeros of $P(z)$ are also the zeros of $F(z)$, it follows that all the zeros of $P(z)$ lie in the disk

$$\left| z + \frac{\rho}{\alpha_n} \right| \leq \frac{\rho + \alpha_n - \sigma(|\alpha_0| + \alpha_0) + 2|\alpha_0| + 2\sum_{j=0}^n |\beta_j|}{|\alpha_n|}.$$

This completes the proof of Theorem 1.

REFERENCES

- [1] N. Anderson , E. B. Saff , R. S.Verga , An extension of the Enestrom-Kakeya Theorem and its sharpness, SIAM. Math. Anal. , 12(1981), 10-22.
- [2] A.Aziz and B.A.Zargar, Some extensions of the Enestrom-Kakeya Theorem , Glasnik Matematiki, 31(1996) , 239-244.
- [3] K.K.Dewan, N.K.Govil, On the Enestrom-Kakeya Theorem, J.Approx. Theory, 42(1984) , 239-244.
- [4] R.B.Gardner, N.K. Govil, Some Generalisations of the Enestrom-Kakeya Theorem , Acta Math. Hungar Vol.74(1997), 125-134.
- [5] N.K.Govil and G.N.Mc-tume, Some extensions of the Enestrom-Kakeya Theorem , Int.J.Appl.Math. Vol.11,No.3,2002, 246-253.
- [6] N.K.Govil and Q.I.Rehman, On the Enestrom-Kakeya Theorem, Tohoku Math. J.,20(1968) , 126-136.
- [7] M.H.Gulzar, On the Location of Zeros of a Polynomial, Anal. Theory. Appl., vol 28, No.3(2012)
- [8] A. Joyal, G. Labelle, Q.I. Rahman, On the location of zeros of polynomials, Canadian Math. Bull.,10(1967) , 55-63.
- [9] M. Marden , Geometry of Polynomials, IInd Ed.Math. Surveys, No. 3, Amer. Math. Soc. Providence,R. I,1996.
- [10] G.V. Milovanoic , D.S. Mitrinovic and Th. M. Rassias, Topics in Polynomials, Extremal Problems, Inequalities, Zeros, World Scientific Publishing Co. Singapore,New York, London, Hong-Kong, 1994.

A Novel Three-Phase Three-Leg AC/AC Converter Using Nine IGBTs

Mr. V. Sambasiva Rao¹, Mr. M. Lokya², Chalasani Hari Krishna³

Abstract: This paper proposes a novel three-phase nine-switch ac/ac converter topology. This converter features sinusoidal in- puts and outputs, unity input power factor, and more impor- tantly, low manufacturing cost due to its reduced number of active switches. The operating principle of the converter is elaborated; its modulation schemes are discussed. Simulated semiconductor loss analysis and comparison with the back-to-back two-level voltage source converter are presented. Finally, experimental results from a 5-kVA prototype system are provided to verify the validity of the proposed topology.

Index Terms: AC/AC converter, pulsewidth modulation (PWM), reduced switch count topology.

I. INTRODUCTION

THREE-PHASE ac/dc/ac and ac/ac converters with variable frequency (VF) and variable voltage operation have found Wide applications in the industry. The most popular configura- tion uses voltage source inverter (VSI) with a diode rectifier as the front end for adjustable speed drives (ASDs), uninterruptible power supplies (UPS), and other industrial applications [1]. This configuration features low cost and reliable operation due to the use of a diode rectifier, but it generates highly distorted input line currents and does not have regenerative or dynamic braking capability. These problems can be mitigated by using a back-to-back two-level voltage source converter (B2B 2L-VSC), shown in Fig. 1, where a pulsewidth modulation (PWM) voltage source rectifier is used to replace the diode rectifier [2].

The B2B 2L-VSC requires a relatively high number (12) of active switches such as insulated gate bipolar transistors (IG- BTs). It also needs a dc-link capacitor that is responsible for a limited lifespan and increased cost. To reduce the device count and minimize/eliminate the dc-capacitor filter, various converter topologies have been proposed in the literature. The first ap- proach reported in [3]–[5] puts two dc capacitors in cascade

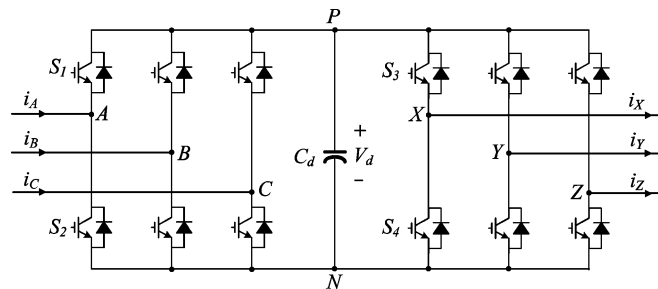


Fig. 1. B2B 2L-VSC.

And takes their midpoint as one of the input–output terminals, whereby an entire phase leg for the rectifier and/or inverter can be saved. It is also possible to reduce the total number of switches, as the second approach suggests [6], [7], by sharing one of the three phase legs between the rectifier and inverter with proper control. In addition, combined use of dc midpoint con- nection and phase leg sharing has been proposed in [8], where only four legs are needed to perform three- phase ac to ac con- version with bidirectional power flow and power factor control. Although all the earlier references achieve the goal of reducing the number of switches and thus reducing the cost, they unexcep- tionally have limits or involve complex control due to their un- balanced topological structure. For unidirectional applications, diodes can be used in place of active switches in the rectifier part, such as the VIENNA rectifier [9], three-phase three-switch buck-type rectifier [10], and three- phase three-switch two-level rectifier [11]. These converters may also be regarded as topolo- gies with a saved number of switches, despite their employment of a large number of diodes.

Unlike VSCs that inevitably require the dc-link stage, the matrix converter [12] presents a radical change in topology and directly converts a fixed ac input voltage to an adjustable ac output voltage. It features sinusoidal input–output, controllable power factor, and is capable of bidirectional energy transfer from the supply to the load or vice versa. Since there is no dc- link circuit, the dc capacitor in the VSC is not necessary here, leading to cost reduction as well as improved reliability and longevity. However, the conventional matrix converter (CMC) normally requires 18 active switches and its switching scheme is complex. The high semiconductor cost and complex control have made this topology less attractive. Similar to the situation of VSCs, efforts to reduce the number of active switches for a matrix converter have been made in recent publications [13], [14], where a couple of topological variants such as the sparse matrix converter (SMC) were proposed. The SMC provides

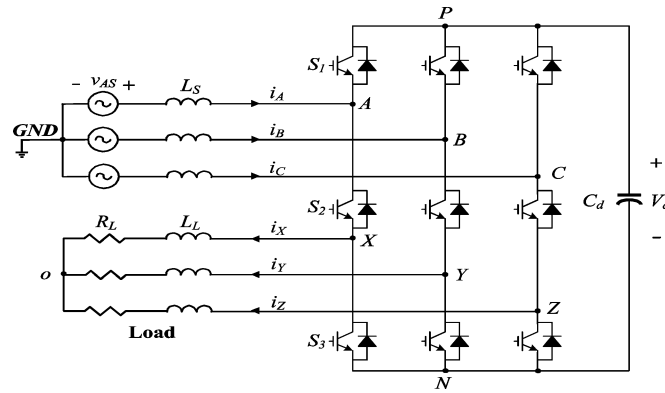


Fig. 2. Proposed nine-switch ac/ac converter with a quasi-dc link.

Equivalent functionality to the CMC. It employs 15 switches with the semiconductor cost still higher than that of the B2B 2 L-VSC. In this paper, a novel one-stage three-phase ac/ac converter topology is proposed. Different from all other existing topologies, this converter has only three legs with only nine active switches for bidirectional ac/ac power conversion.

II. NINE-SWITCH CONVERTER TOPOLOGY

Fig. 2 shows the proposed three-phase nine-switch converter topology. This converter has only three legs with three switches installed on each of them. The novelty herein is that the middle switch in each individual leg is shared by both the rectifier and the inverter, thereby reducing the switch count by 33% and 50% in comparison to the B2B 2L-VSC and CMC, respectively. The input power is delivered to the output partially through the middle three switches and partially through a quasi-dc-link circuit. For the convenience of discussion, we can consider that the rectifier of the nine-switch converter is composed of the top three and middle three switches, whereas the inverter consists of the middle three and bottom three switches.

The converter has two modes of operation: 1) constant frequency (CF) mode, where the output frequency of the inverter is constant and also the same as that of the utility supply, while the inverter output voltage is adjustable; and

TABLE I
SWITCHING STATES AND CONVERTER LEG VOLTAGES

(a) Back-to-back converter						
Switching State	S_1	S_2	S_3	S_4	v_{AN}	v_{XN}
1	On	Off	On	Off	V_d	V_d
2	Off	On	Off	On	0	0
3	On	Off	Off	On	V_d	0
4	Off	On	On	Off	0	V_d

(b) Proposed nine-switch converter					
Switching State	S_1	S_2	S_3	v_{AN}	v_{XN}
1	On	On	Off	V_d	V_d
2	Off	On	On	0	0
3	On	Off	On	V_d	0

2) VF mode, where by switches S_1 and S_2 in the rectifier, whereas the inverter leg voltage v_{XN} can be controlled by S_3 and S_4 in the inverter. This means that the rectifier and inverter leg voltages can be controlled independently. The B2B 2L-VSC has four switching states per phase, as defined in Table I.

For the nine-switch topology, the control of the input and output voltages has to be accomplished through the three switches on each leg. Because the middle switches are shared by the rectifier and inverter, the proposed converter has only three switching states per phase, as listed in Table I. It can be observed that switching state 4 for the B2B 2L-VSC does not exist in the nine-switch converter, which implies that the inverter leg voltage v_{XN} cannot be higher than the rectifier leg voltage v_{AN} at any instant. This is, in fact, the main constraint for the switching scheme design of the nine-switch converter.

Carrier-based continuous PWM schemes for modulating the 2L-VSC, such as sinusoidal PWM (SPWM), space vector PWM (SVPWM), and third-harmonic injection PWM (THIPWM), are well established in the literature [15]. The principles of

these methods can all be applied to the nine-switch converter but a little modification would be necessary, because when designing the switching pattern for the nine-switch converter, the switching constraint discussed earlier must be satisfied.

III. MODULATION SCHEMES

A. Switching Constraint

The reduction of the number of switches in the proposed converter topology imposes certain switching constraints for the switching pattern design. In the B2B 2L-VSC shown in Fig. 1, the rectifier leg voltage v_{AN} , which is the voltage at node A with respect to the negative dc bus N, can be controlled compared with a common triangular carrier v_c . The generated rectifier and inverter leg voltages v_{AN} and v_{XN} are also shown in the figure. This arrangement guarantees that switch state 4 in the B2B 2L-VSC is eliminated here for the nine-switch converter.

B. Modulation Scheme for CF-Mode Operation

Taking SPWM as an example, Fig. 4 illustrates the modified scheme for CF-mode operation, where m_r and m_i are the rectifier and inverter modulation indexes

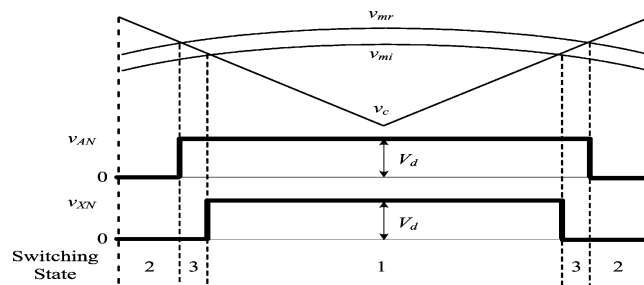


Fig. 3. PWM waveform generation, where switching state 4 of the B2B 2L-VSC is eliminated.

Fig. 3 illustrates the generalized carrier-based modulation scheme in a single switching period for the nine-switch converter. The rectifier modulating wave v_{mr} and the inverter modulating wave v_{mi} are arranged such that v_{mr} is not lower than applications in UPS, whereas the VF mode can be applied to v_{mi} at any instant of time. These two modulating waveforms are variable-speed drives.

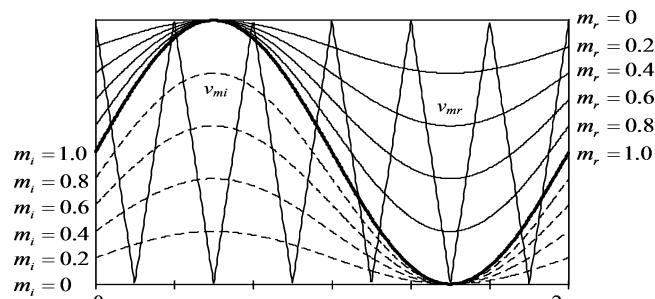


Fig. 4. SPWM scheme for CF-mode operation.

The peak-to-peak magnitude of the sinusoid divided by the peak-to-peak magnitude of the carrier), respectively. The difference between this scheme and the traditional SPWM for 2L-VSC is that here the modulating waves of the rectifier (solid line) and the inverter (dashed line) are placed in a single dc plane and compared to a common triangular carrier wave. The gate signals are generated at the waveforms' intersections with the carrier. To prevent the modulating waves from intersecting each other, the rectifier's modulating waves are lifted to the top of the dc plane whereas the inverter's are pushed to the bottom by adding proper dc offsets. In this way, the switching constraint of the nine-switch converter can be satisfied. In practice, the rectifier side modulation can be synchronized to the grid via a phase-locked loop (PLL). The freedoms of choosing its modulation index m_r and firing angle α between the modulating wave and the grid can be employed to control the dc voltage and the input power factor. The inverter-side modulation index m_i can be freely selected to adjust the output magnitude. If the

inverter's modulating wave is set in phase with the rectifier's, as in the case shown in Fig. 4, both the rectifier and inverter's modulation indexes can simultaneously reach a maximum of unity.

C. Modulation Scheme for VF-Mode Operation

Fig. 5 shows the SPWM modulation scheme for the VF mode of operation. In this case, the inverter's modulation index and

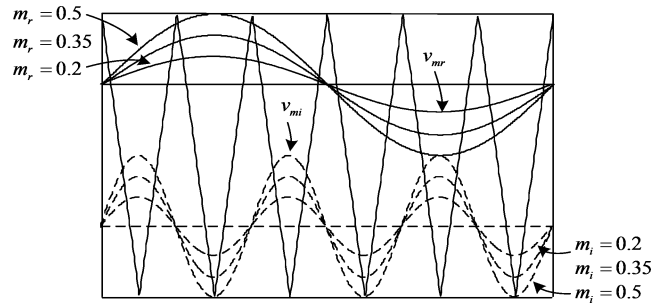


Fig. 5. SPWM scheme for VF-mode operation.

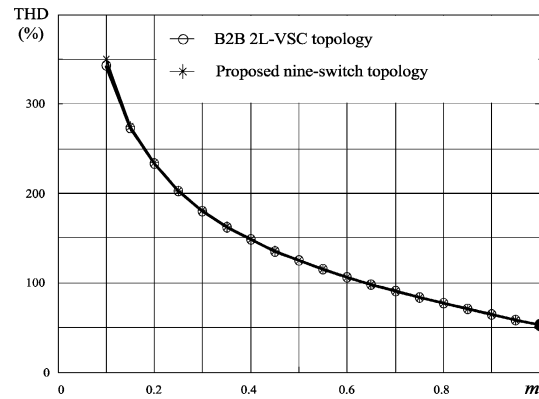
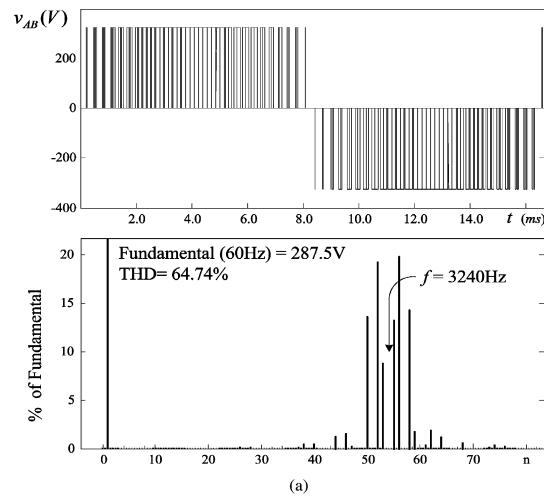


Fig. 6. Rectifier input voltage waveform, spectrum, and THD (CF-mode operation). (a) Rectifier input voltage waveform and spectrum. (b) THD comparison

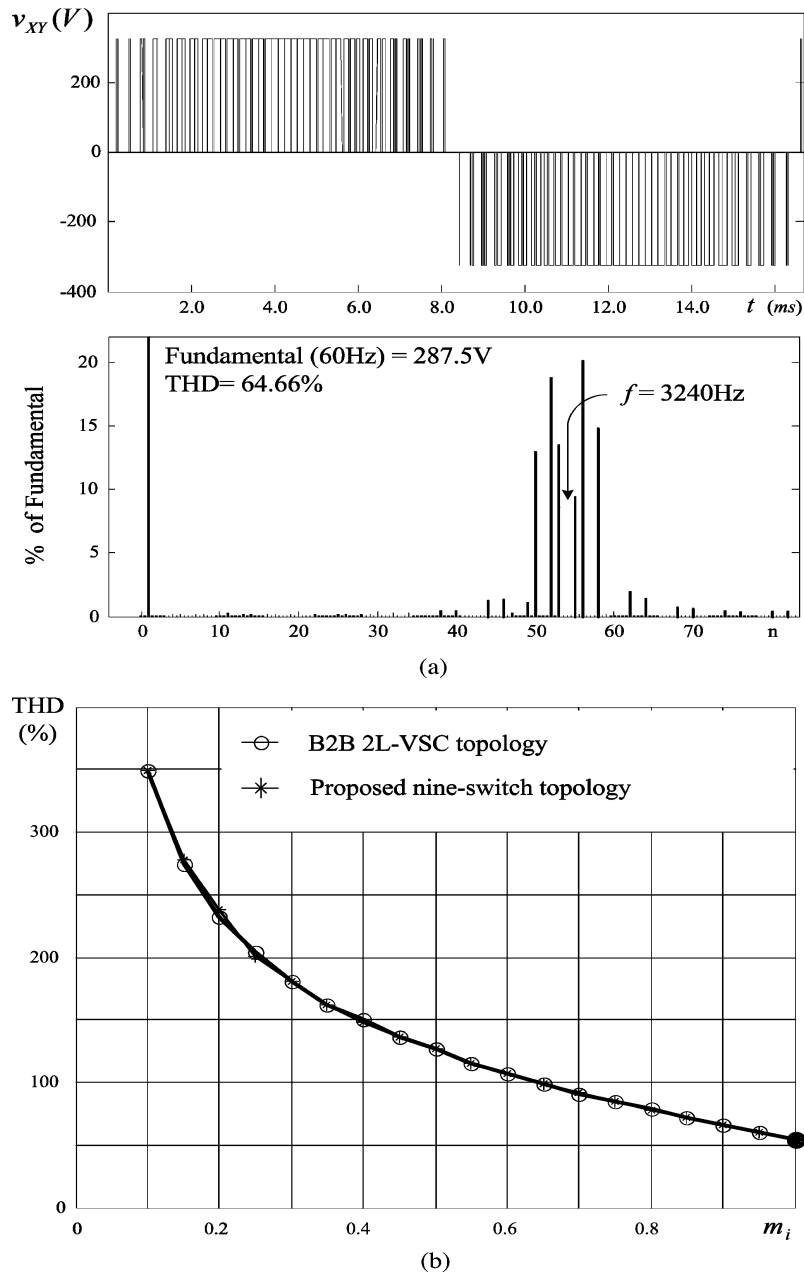


Fig. 7. Inverter output voltage waveform, spectrum, and THD (CF-mode operation). (a) Inverter output voltage waveform and spectrum. (b) THD comparison.

phase angle can both be adjusted independently from the rectifier's. In order to satisfy the switching constraint discussed earlier, the sum of the two modulation indexes m_r and m_i of the rectifier and inverter must not exceed 1. For matching the input and output ratings, we limit both of their maximums to 0.5. It can be observed from the figure that both the rectifier and inverter's modulating waves can only be adjusted within half of the carrier's magnitude (which represents the dc voltage); therefore, the dc voltage v_d of the converter is twice as high as the rated dc voltage of a B2B 2L-VSC with the same ac ratings. This is different from the situation of the CF mode with identical input and output phases, in which the dc voltage of the converter can be tightly controlled and maintained at around its rated value.

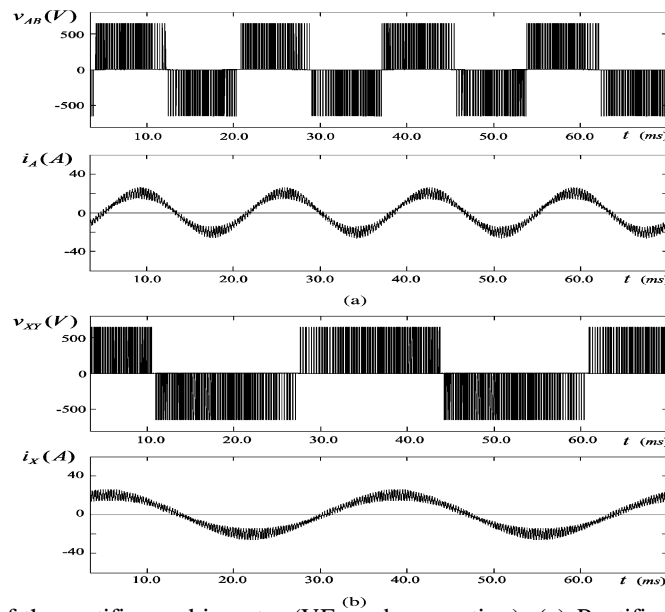


Fig. 8. Simulated waveforms of the rectifier and inverter (VF-mode operation). (a) Rectifier input waveforms at 60 Hz. (b) Inverter output waveforms at 30 Hz.

It should be pointed out that although the added dc offsets guarantee that the instant value of v_{m_r} is always higher than that of v_{m_i} , they are of zero sequence in the three phases and have no effect on the input/output ac magnitudes. In fact, if the inverter's modulation index is selected to be higher than the rectifier's, e.g., $m_i = 0.5$ and $m_r = 0.2$, the fundamental component of the inverter output voltage v_{XY} will be higher than that of the rectifier input voltage v_{AB} .

IV. SIMULATION ANALYSIS

The performance of the proposed nine-switch converter topology is simulated with the Matlab/Simulink software. In the simulation, the utility supply is rated at 208 V and 60 Hz with a source inductance of $L_s = 2.5$ mH. The converter is rated at 5 kVA and is driving a three-phase RL load of $R_L = 8\Omega$ and $L_L = 2.5$ mH. The dc capacitor C_d is 2350 μ F. SVPWM method is used to modulate the converter for its superior performance over SPWM and higher dc voltage utilization. The rectifier is controlled by a vector control scheme with unity power factor operation. The inverter output voltage is not detected, and therefore, is not tightly controlled. The switching frequency of both

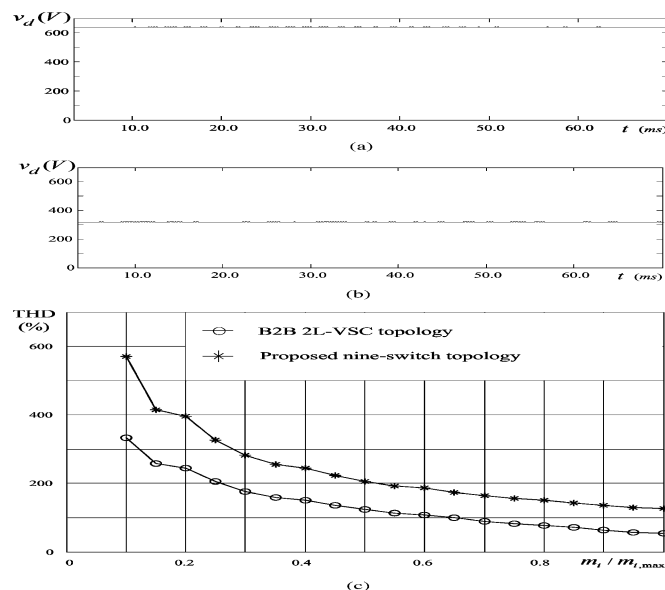


Fig. 9. Comparison of dc voltage and inverter output THD with full utility supply (VF-mode operation). (a) DC voltage of nine-switch converter. (b) DC voltage of B2B 2L-VSC. (c) THD comparison of inverter output.

rectifier and inverter is 3240 Hz. Both CF and VF modes of operation are investigated.

A. CF-Mode Operation

Fig. 6(a) shows the simulated waveform of the rectifier input voltage v_{AB} and its harmonic spectrum with the converter operating in the CF mode. The modulation indexes for the rectifier m_r and inverter m_i are both set at 0.9 and the dc voltage is maintained at 320 V. The frequency of the dominant switching harmonics is centered around 3240 Hz, which is the carrier frequency and also the switching frequency of the converter. The low-order harmonics are negligibly small.

Fig. 6(b) illustrates the total harmonic distortion (THD) curve of the rectifier input voltage v_{AB} versus the rectifier modulation index m_r of the nine-switch converter. The THD curve of the input voltage of the B2B 2L-VSC operating at the same switch-

TABLE II
RATED SYSTEM PARAMETERS

	Nine-Switch (CF)	Nine-Switch (VF)	B2B 2L-VSC
Rated dc voltage V_{dR}	320V	640V	320V
Rated IGBT voltage $V_{CE,R}$ / current $I_{C,R}$	600V/50A	1200V/50A	600V/50A
Rated switching power $V_{CE,R}I_{C,R}n$	270kVA	540kVA	360kVA

TABLE III
INTERPOLATED PARAMETERS FOR LOSS CALCULATION

	600V/50A IGBT BSM50GB60DLC	1200V/50A IGBT BSM50GB120DLC
V_{T0}	1.12	1.55
r_{CE}	0.0218	0.024
V_{D0}	0.8	1.0
r_D	0.0072	0.013
A_{onT}	0	0
B_{onT}	0.0103	0.139
A_{offT}	0.15	1.4
B_{offT}	0.017	0.096
A_{offD}	0.65	1.32
B_{offD}	0.0175	0.047

ing frequency is also plotted. It can be noted that the harmonic performance of the nine-switch converter is the same as that of its counterpart.

Fig. 7(a) shows the simulated waveform and spectrum of the inverter output voltage v_{XY} with a fundamental frequency of 60 Hz. It is interesting to note that the inverter output voltage waveform, its fundamental component, and THD are very close to those of the rectifier given in Fig. 6.

Similar to Fig. 6(b), Fig. 7(b) gives the THD comparison of the inverter output voltage v_{XY} between the nine-switch converter and the B2B 2L-VSC, with respect to the inverter modulation index m_i . It can be seen that the inverter out-put THD characteristics are identical to that of the rectifier input.

B. VF-Mode Operation

Fig. 8 shows the simulated rectifier input and inverter output waveforms when the converter operates in the VF mode. The rectifier operates at 60 Hz while the inverter operates at 30 Hz. The modulation indexes for the rectifier and inverter are both 0.45. The figure illustrates that the rectifier and the inverter can operate independently with different fundamental frequencies. Fig. 9(a) and (b) presents the VF-mode dc voltage comparison between the nine-switch converter and the B2B 2L-VSC. Due to the boost nature of the rectifier, the dc voltage v_d of the nine-switch converter in VF mode becomes twice that in the CF mode, which is also the rated value of a B2B 2L-VSC with identical ac ratings. A THD comparison of the inverter output voltage v_{XY} versus the normalized inverter modulation index $m_i / m_{i,max}$ is shown in Fig. 9(c), where the maximum

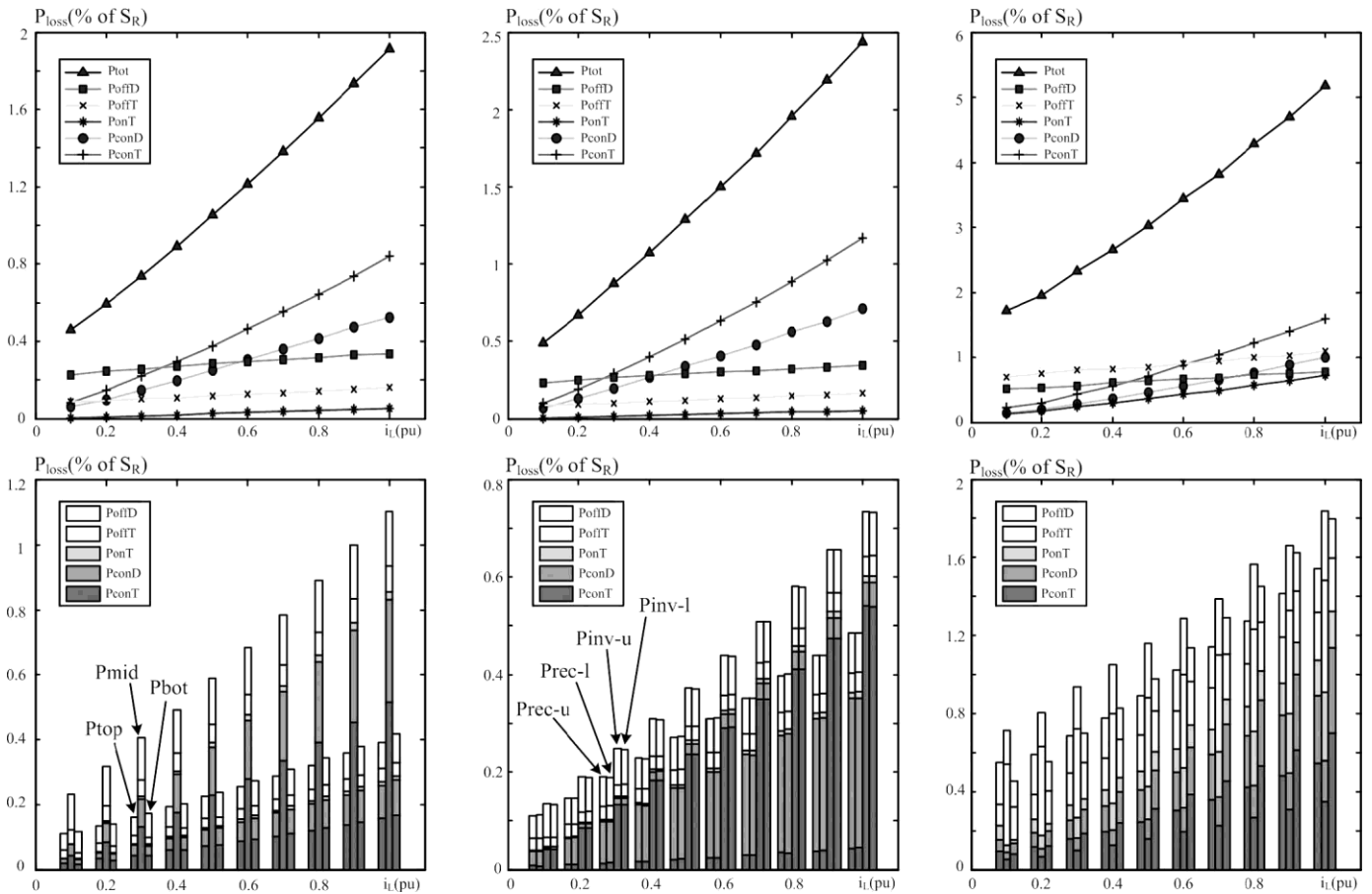


Fig. 10. Semiconductor loss versus load current i_L . (a) Nine-switch converter (CF mode). (b) B2B 2L-VSC. (c) Nine-switch converter (VF mode).

modulation index m_i , \max for the nine-device converter and the B2B 2L-VSC are 0.5 and 1, respectively. It can be noted that with the same ac-side voltage magnitudes, the THD of the nine-switch converter output is much higher than that of a competitive B2B 2L-VSC because of the lower modulation index that the nine-switch converter is working at.

V. SIMULATED SEMICONDUCTOR LOSS ANALYSIS

To further study the operating mechanism of the proposed nine-switch converter, it would be necessary to investigate the converter's power loss profile. In this section, a comparative study is presented for the nine-switch converter and the B2B 2L-VSC. The system parameters and rated switching power of the converters are listed in Table II. For all the converters, the base value of the system power S_R and the source/load side line single switch is used instead. The loss model for the IGBTs incorporated in the simulation is expressed in (1)–(5), where semiconductor losses are abbreviated as P_{conT} (conduction loss of IGBT), P_{conD} (conduction loss of diode), P_{onT} (turn-on loss of IGBT), P_{offT} (turn-off loss of IGBT), and P_{offD} (reverse recovery loss of diode) [17]. All the losses are averaged over the output fundamental cycle T_1 . Constants such as V_{T0} , r_{CE} , A_{onT} , and B_{onT} are derived by linear interpolation from a commercial manufacturer's datasheet and are specified in Table III. The accuracy of this model is acceptable provided that the switching and dead time, as well as the switching frequency ripple, is neglected; also, the junction temperature of the switches is assumed constant when the converter's switching frequency is much higher than its input-output frequency voltage are 5 kVA and 208 V. Due to the nine-switch converter's distinctive topological structure, input-output currents flowing through the switches a convenient way to obtain detailed loss information on every

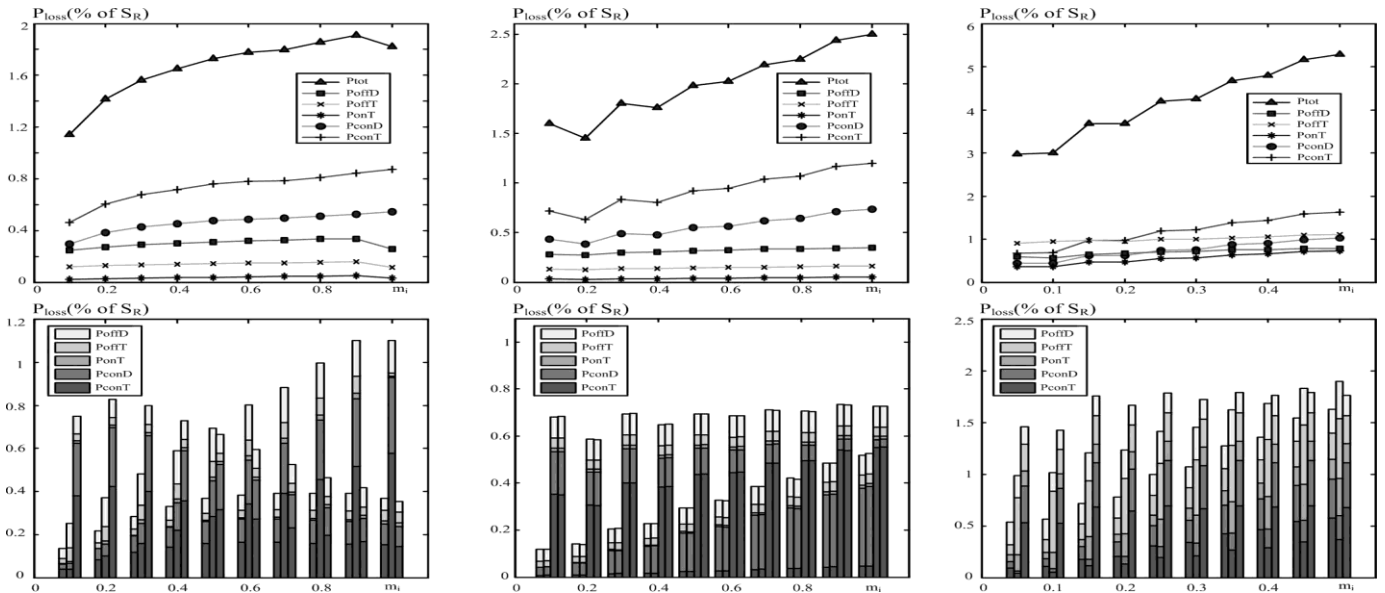


Fig. 11. Semiconductor loss versus output modulation index m_i . (a) Nine-switch converter (CF mode). (b) B2B 2L-VSC. (c) Nine-switch converter (VF mode).

$$P_{\text{off } T} = \frac{(A_{\text{off } T} + B_{\text{off } T} i_c)}{T_1} \quad (4)$$

$$P_{\text{off } D} = \frac{(A_{\text{off } D} + B_{\text{off } D} i_F)}{T_1} \quad (5)$$

loss profile no matter which mode it is in. Therefore, the loss diagram of the two modes for B2B 2L-VSC is shown in the same figure. Note that the CF-mode nine-switch converter and the B2B 2L-VSC are simulated with the 600-V IGBT parameters,

In order to perform a comparative evaluation, a B2B 2L-VSC with identical power rating is also simulated with the derived loss model. Using the same parameters, modulation and control scheme, and being simulated in the same working conditions, the simulation results can help reveal some of the commonalities and differences between the two converters.

The simulated loss diagrams for the nine-switch converter and the B2B 2L-VSC are shown in Figs. 10 and 11. In addition to the aforementioned individual losses, P_{tot} indicates the total semiconductor loss of the studied converter. For the nine-switch Converter, P_{top} , P_{mid} , and P_{bot} denote losses in the top, middle, and bottom three switches, respectively. For the 2L-VSC, losses on the upper and lower switches in the rectifier and inverter are denoted as $P_{\text{rec-u}}$, $P_{\text{rec-l}}$, $P_{\text{inv-u}}$, and $P_{\text{inv-l}}$. Both converters are simulated in CF and VF mode with system specifications identical to those given in Section IV. However, it was verified from simulation that if parameters other than the output fundamental frequency are not changed, the B2B 2L-VSC keeps the same Whereas the VF-mode nine-switch converter requires the use of the 1200-V IGBT. Switching losses $P_{\text{on } T}$, $P_{\text{off } T}$, and $P_{\text{off } D}$ are proportionally scaled with respect to the converters' operating dc voltages in the simulation.

Fig. 10 shows the losses in both converters as a function of the normalized load current in per unit value (p.u.). The converters are operated with unity input power factor, a switching frequency of 3240 Hz, and the inverter modulation index of 0.9. From the figure, it can be seen that the total semiconductor loss of both CF- and VF-mode nine-switch converters follows a similar trend to the B2B 2L-VSC with respect to the load current change, although the CF-mode loss is always lower than that of the B2B 2L-VSC due to its partial single-stage power transfer nature. Unlike the B2B 2L-VSC that possesses a symmetrical structure, the loss distribution on the top, middle, and bottom switches are not even in the CF-mode nine-switch converter. In general, the middle three switches dissipate more than twice the loss of those from the top three and bottom three switches, which is evident in Fig. 10(a). The VF-mode nine-switch converter losses, shown in Fig. 10(c), have a more balanced distribution on the switches but are significantly higher than those of

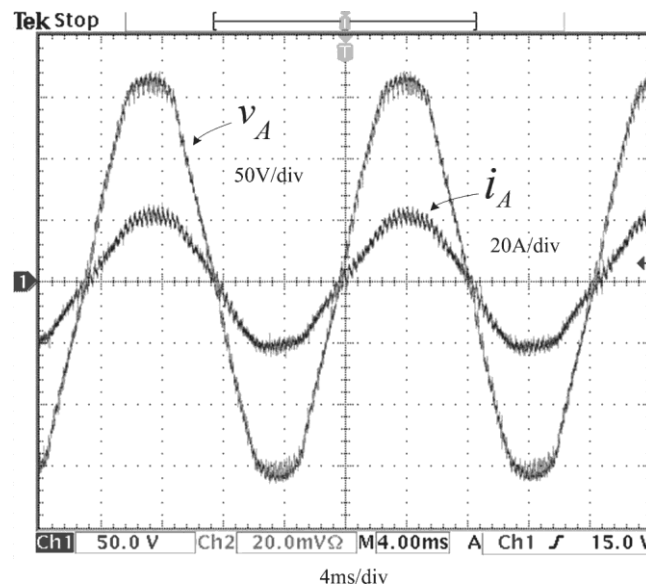


Fig. 12. Unity input power operation of the rectifier.

The B2B 2L-VSC and CF mode nine switch. This is due to its doubled dc voltage and the necessity to use IGBT devices with higher ratings.

In Fig. 11, the changing parameter becomes the converter's output modulation index m_i . A drop of total semiconductor loss can be observed at the end of the curve in Fig. 11(a); this is due to joined pulses at maximum modulation index that leads to reduced times of switchings.

Loss dependency on switching frequency and input and output power factors provide similar information, and therefore, are not illustrated here for the sake of brevity.

VI. EXPERIMENTAL VERIFICATION

A 5-kVA prototype system was built and tested. The values of the supply voltage, source inductance L_S , dc capacitor C_d , and RL load parameters are the same as those given in the simulation.

A. Unity Power Factor Operation

The input power factor of the converter can be leading, lagging, or unity. Fig. 12 shows the measured supply phase voltage v_A and line current i_A of the converter with unity power factor operation. During the test, the dc voltage was maintained at 320 V by the rectifier, and the converter modulation index was $m_r = m_i = 0.9$. It should be noted that the control of the rectifier and inverter is decoupled, and therefore, the inverter operation will not affect the operation of the rectifier.

B. CF-Mode Operation

Fig. 13 shows measured voltage and current waveforms when the inverter operates with the same frequency as that for the rectifier. The modulation index of the rectifier and inverter was 0.9, while the dc voltage of the converter was 320 V. The harmonic

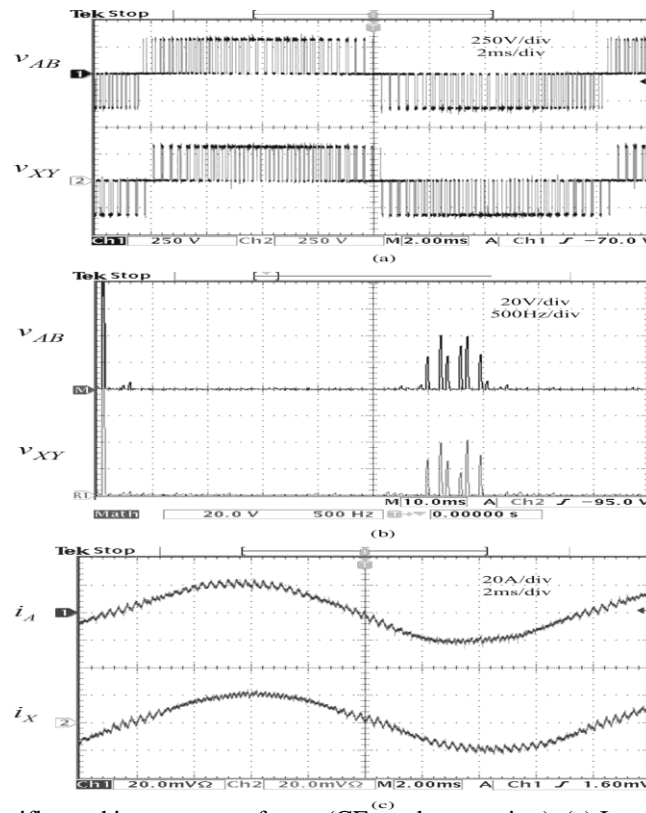


Fig. 13. Measured rectifier and inverter waveforms (CF-mode operation). (a) Input and output voltages. (b) Voltage spectrum. (c) Input and output currents.

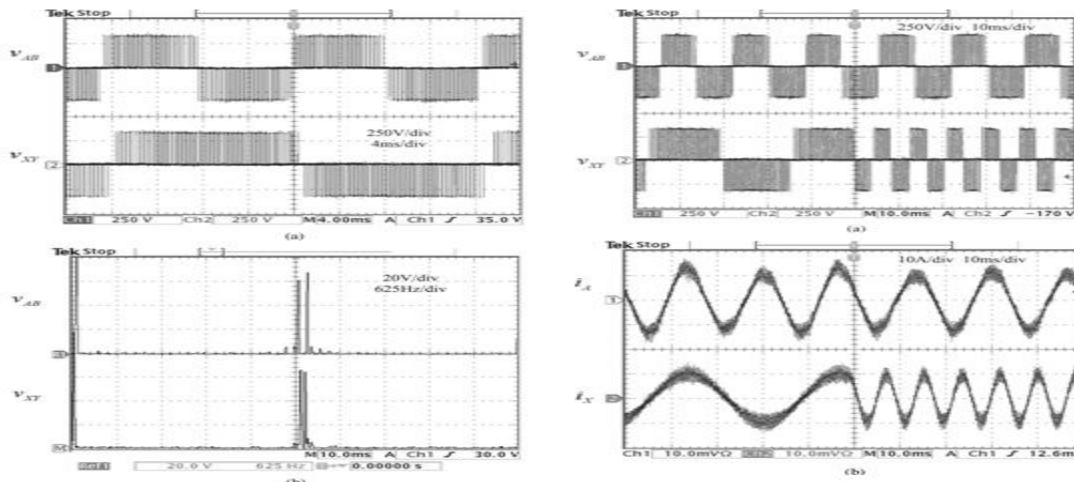


Fig. 14. Measured waveforms and spectrum (VF mode operation). (a) Input and output voltages. (b) Spectrum. spectrum of v_{AB} and v_{XY} matches very well with the simulation results in Figs. 6 and 7.

C. VF-Mode Operation

Fig. 14 illustrates the converter input and output voltage waveforms and their harmonic spectrum at the input frequency of 60 Hz and the output frequency of 30 Hz. The modulation index for the rectifier and the inverter is 0.45. The supply voltage in this case is reduced to half of the rated voltage of 208 V such that the dc voltage can remain at 320 V. The spectrum shows that the frequency of the dominant harmonics is centered around 3240 Hz, while all the low-order harmonics are eliminated.

Fig. 15 shows the dynamic response of the converter input and output waveforms when the converter output frequency has a step increase from 30 to 120 Hz. It demonstrates that the control for the converter input and output variables is independent and decoupled, similarly to that of the B2B 2L-VSC.

VII. CONCLUSION

A novel nine-switch PWM ac/ac converter topology was proposed in this paper. The topology uses only nine IGBT devices for ac to ac conversion through a quasi dc-link circuit. Compared with the conventional back-to-back PWM VSC using 12 switches and the matrix converter that uses 18, the number of switches in the proposed converter is reduced by 33% and 50%, respectively. The proposed converter features sinusoidal inputs and outputs, unity input power factor, and low manufacturing cost. The operating principle of the converter was elaborated, and modulation schemes for constant and VF operations were developed. Simulation results including a semiconductor loss analysis and comparison were provided, which reveal that the proposed converter, while working in CF mode, has an overall higher efficiency than the B2B 2L-VSC at the expense of uneven loss distribution. However, the VF-mode version requires IGBT devices with higher ratings and dissipates significantly higher losses, and thus, is not as attractive as its counterpart. Experimental verification is carried out on a 5-kVA prototype system.

REFERENCES

- [1] B. Wu, *High-power Converters and AC Drives*. Piscataway, NJ: IEEE/Wiley, 2006.
- [2] B. Singh, B. N. Singh, A. Chandra, K. Al-Haddad, A. Pandey, and D.P. Kothari, "A review of three-phase improved power quality AC-DC converters," *IEEE Trans. Ind. Electron.*, vol. 51, no. 3, pp. 641-660, Jun. 2004.
- [3] F. Blaabjerg, S. Freysson, H. H. Hansen, and S. Hansen, "A new optimized space-vector modulation strategy for a component-minimized voltage source inverter," *IEEE Trans. Power Electron.*, vol. 12, no. 4, pp. 704-714, Jul. 1997.
- [4] R. L. A. Ribeiro, C. B. Jacobina, E. R. C. da Silva, and A. M. N. Lima, "AC/AC converter with four switch three phase structures," in *Proc. IEEE PESC*, 1996, vol. 1, pp. 134-139.
- [5] K. Gi-Taek and T. A. Lipo, "VSI-PWM rectifier/inverter system with a reduced switch count," *IEEE Trans. Ind. Appl.*, vol. 32, no. 6, pp. 1331-1337, Nov./Dec. 1996.
- [6] A. Bouscayrol, B. Francois, P. Delarue, and J. Niiranen, "Control implementation of a five-leg AC-AC converter to supply a three-phase induction machine," *IEEE Trans. Power Electron.*, vol. 20, no. 1, pp. 107-115, Jan. 2005.
- [7] C. B. Jacobina, I. S. de Freitas, E. R. C. da Silva, A. M. N. Lima, and R. L. A. Ribeiro, "Reduced switch count DC-link AC-AC five-leg converter," *IEEE Trans. Power Electron.*, vol. 21, no. 5, pp. 1301-1310, Sep. 2006.
- [8] C. B. Jacobina, I. S. de Freitas, and A. M. N. Lima, "DC-link three-phase-to-three-phase four-leg converters," *IEEE Trans. Ind. Electron.*, vol. 54, no. 4, pp. 1953-1961, Aug. 2007.
- [9] J. Minibock and J. W. Kolar, "Novel concept for mains voltage proportional input current shaping of a VIENNA rectifier eliminating controller multipliers," *IEEE Trans. Ind. Electron.*, vol. 52, no. 1, pp. 162-170, Feb. 2005.
- [10] T. Nussbaumer, M. Baumann, and J. W. Kolar, "Comprehensive design of a three-phase three-switch buck-type PWM rectifier," *IEEE Trans. Power Electron.*, vol. 22, no. 2, pp. 551-562, Mar. 2007.
- [11] F. A. B. Batista and I. Barbi, "Space vector modulation applied to three-phase three-switch two-level unidirectional PWM rectifier," *IEEE Trans. Power Electron.*, vol. 22, no. 6, pp. 2245-2252, Nov. 2007.
- [12] P. W. Wheeler, J. Rodriguez, J. C. Clare, L. Empringham, and A. Weinstein, "Matrix converters: A technology review," *IEEE Trans. Ind. Electron.*, vol. 49, no. 2, pp. 276-288, Apr. 2002.
- [13] L. Wei, T. A. Lipo, and H. Chan, "Matrix converter topologies with reduced number of switches," in *Proc. IEEE PESC*, 2002, vol. 1, pp. 57-63.
- [14] J. W. Kolar, F. Schafmeister, S. D. Round, and H. Ertl, "Novel three-phase AC-AC sparse matrix converters," *IEEE Trans. Power Electron.*, vol. 22, no. 5, pp. 1649-1661, Sep. 2007.
- [15] A. M. Hava, R. J. Kerkman, and T. A. Lipo, "Simple analytical and graphical methods for carrier-based PWM-VSI drives," *IEEE Trans. Power Electron.*, vol. 14, no. 1, pp. 49-61, Jan. 1999.
- [16] F. Blaabjerg, U. Jaeger, and S. Munk-Nielsen, "Power losses in PWM-VSI inverter using NPT or PT IGBT devices," *IEEE Trans. Power Electron.*, vol. 10, no. 3, pp. 358-367, May 1995.
- [17] Infineon Technologies, Application Note ANIP9931E—Calculation of Major IGBT Operating Parameters. Germany: Infineon Technologies, 1999.



Mr. V. SAMBASIVA RAO was born in 1984. I received B.Tech degree from Jawaharlal Nehru Technological University, Hyderabad in the year 2006. He is presently working as Assistant Lecture in the Department of Electrical and Electronics Engineering at S.E.S.N.M POLYTECHNIC, Andhra Pradesh, India.



Mr. M. LOKYA was born in 1984. He graduated from KAKATIYA UNIVERSITY, in the year 2005. He Received M.Tech degree from Jawaharlal Nehru Technological University, Hyderabad in the year 2011. He is presently working as Assistant Professor in the Department of Electrical and Electronics Engineering at Mother Teresa Institute of Science and Technology, Andhra Pradesh, India.



Chalasani Hari Krishna was born in 1982. He graduated from Jawaharlal Nehru Technological University, Hyderabad in the year 2003. He received M.E degree from Satyabama University, Chennai in the year 2005. He presently Associate Professor in the Department of Electrical and Electronics Engineering at Mother Teresa Institute of Science and Technology, India. His research area includes DTC and Drives. He presented 11 research papers in various national and international conferences and journals. His research areas include PWM techniques, DC to AC converters and control of electrical drives

Stability of the Equilibrium Position of the Centre of Mass of an extensible Cable Connected Satellites System In Case Of Circular Orbit

Dinesh Tiwari¹, Dr. Brijendra Kumar Singh²,

¹(Research Scholar Department of Mathematics, J.P. University, Chapra, India

²(Department of Mathematics, J.P. University, Chapra, India)

Abstract: In a linear motion of a system of two cable connected satellites, one stable equilibrium point exists when perturbative forces like solar radiation pressure, shadow of the earth, oblateness of the earth, air resistance and earth's magnetic force act simultaneously. Many research workers obtained the stable point in case of any one of above mentioned perturbative forces. We have obtained one stable point of equilibrium in case of perturbative forces like the shadow of the earth due to solar pressure and air resistance acting together on the motion of two cable-connected satellites. Liapunov's theorem has been exploited to test the stability of the equilibrium point.

I. Introduction

The present paper is concerned with the stability of the equilibrium point of the centre of mass of the system of two satellites connected by a light, flexible and extensible cable under the influence of the shadow of the earth due to solar pressure and air resistance in case of circular orbit. Beletsky; V.V. is the pioneer worker in this field. This paper is an attempt towards generalization of work done by him.

II. Equations of motion

The equations of motion of one of the two satellites moving along keplerian elliptic orbit in Nechvill's coordinates may be obtained by using Lagrange's equations of motion of first kind in the form:

$$\left. \begin{aligned} x'' - 2y' - 3\rho x + f\rho\rho' + A\psi_1\rho^3 \cos \epsilon \cos(v - \alpha) &= -\bar{\lambda}_\alpha \left[1 - \frac{\ell_0}{r} \right] x \\ y'' + 2x' + f\rho^2 - A\rho^3\psi_1 \cos \epsilon \sin(v - \alpha) &= -\bar{\lambda}_\alpha \left[1 - \frac{\ell_0}{r} \right] y \\ z'' + z - A\psi_1 \sin \epsilon &= -\bar{\lambda}_\alpha \left[1 - \frac{\ell_0}{r} \right] z \end{aligned} \right\} \quad \text{----- (1)}$$

Where

$$\rho = \frac{1}{1 + e \cos v}; r = \sqrt{x^2 + y^2 + z^2}$$

V= True anomaly of the centre of mass of the system.

$$A = \frac{p^3}{\mu} \left[\frac{B_1}{m_1} - \frac{B_2}{m_2} \right] = \text{Solar pressure parameter.}$$

$$f = \frac{a_1 p^3}{\sqrt{\mu p}} = \text{Air resistance parameter}$$

ψ_1 = Earth's shadow function parameter

$$\bar{\lambda}_\alpha = \frac{p^3}{\mu} \lambda_\alpha; \ell_0 \text{ is the natural length of the cable connecting two satellites.}$$

Here dashes denotes differentiations with respect to true anomaly v

The condition of constraint is given by

$$x^2 + y^2 + z^2 \leq \frac{\ell_0^2}{\rho^2} \quad \text{----- (2)}$$

For circular orbit of the centre of mass of the system, we must have e=0 and so

$$\rho = \frac{1}{1 + e \cos v} = 1 \text{ and } \rho' = 0$$

Putting $\rho=1$ and $\rho'=0$ in (1), we get the equations of motion for two dimensional case

$$\left. \begin{aligned} x''-2y'-3x+A\psi_1 \cos \in \cos(v-\alpha) &= -\bar{\lambda}_\alpha \left[1 - \frac{\ell_0}{r} \right] x \\ \text{and } y''+2x'+f-A\psi_1 \cos \in \sin(v-\alpha) &= -\bar{\lambda}_\alpha \left[1 - \frac{\ell_0}{r} \right] y \end{aligned} \right\} \text{----- (3)}$$

Where $r = \sqrt{x^2 + y^2}$

The condition of constant given by (2) takes the form:

$$x^2 + y^2 \leq \ell_0^2 \text{----- (4)}$$

We also assume that in case of circular orbit, the true anomaly v for the elliptic orbit will be replaced by τ whose value is as follows:

$$\tau = \omega_0 t \text{----- (5)}$$

Where ω_0 is the angular velocity of the centre of mass of the system in case of circular orbit and t is the time.

Hence (3) can be written as

$$\left. \begin{aligned} x''-2y'-3x+A\psi_1 \cos \in \cos(\tau-\alpha) &= -\bar{\lambda}_\alpha \left[1 - \frac{\ell_0}{r} \right] x \\ y''+2x'+f-A\psi_1 \cos \in \sin(\tau-\alpha) &= -\bar{\lambda}_\alpha \left[1 - \frac{\ell_0}{r} \right] y \end{aligned} \right\} \text{----- (6)}$$

When in (4), the inequality sign holds, then the free motion of the system will take place otherwise the motion will be constrained.

Therefore, we have three types of motion

- (i) Free motion (in case of loose string)
- (ii) Constrained motion (in case of tight string)
- (iii) Evolutional motion (combination of free and constrained motion)

To find the Jacobian integral of the problem, we averaged the periodic terms in (6) as follows:

$$\left. \begin{aligned} \frac{1}{2\pi} \left[\int_{\psi_1=0}^{\theta} A \cos \in \cos(\tau-\alpha) d\tau + \int_{\psi_1=1}^{2\pi-\theta} A \cos \in \cos(\tau-\alpha) d\tau \right] &= \frac{-A \cos \in \cos \alpha \sin \theta}{\pi} \\ \text{and} \\ \frac{1}{2\pi} \left[\int_{\psi_1=0}^{\theta} A \cos \in \sin(\tau-\alpha) d\tau + \int_{\psi_1=1}^{2\pi-\theta} A \cos \in \sin(\tau-\alpha) d\tau \right] &= \frac{A \cos \in \sin \alpha \sin \theta}{\pi} \end{aligned} \right\} \text{---- (7)}$$

Where θ is taken to be constant

Thus, the equations of motion (6) of the system are being described by using averaged values given by (7) in the form:

$$\left. \begin{aligned} x''-2y'-3x - \frac{A \cos \in \cos \alpha \sin \theta}{\pi} &= -\bar{\lambda}_\alpha \left[1 - \frac{\ell_0}{r} \right] x \\ y''+2x'+f - \frac{A \cos \in \sin \alpha \sin \theta}{\pi} &= -\bar{\lambda}_\alpha \left[1 - \frac{\ell_0}{r} \right] y \end{aligned} \right\} \text{----- (8)}$$

We find that the equations of motion given by (8) do not contain time t explicitly. Hence, there must exist Jacobi's integral for the problem.

Multiplying the first equation of (8) by $2x'$ and the second equation of (8) by $2y'$ and adding them together and then integrating, we get Jacobi's integral in the form.

$$\begin{aligned} x'^2 + y'^2 - 3x^2 - \frac{1}{\pi} 2Ax \cos \in \cos \alpha \sin \theta - \frac{1}{\pi} 2Ay \cos \in \sin \alpha \sin \theta \\ + 2fy + \bar{\lambda}_\alpha \left[(x^2 + y^2) - 2\ell_0 \sqrt{x^2 + y^2} \right] = h \text{----- (9)} \end{aligned}$$

Where h is the constant of integration

Equation given by (9) can be written as

$$\begin{aligned} x'^2 + y'^2 = 3x^2 + \frac{2}{\pi} Ax \cos \in \cos \alpha \sin \theta + \frac{2}{\pi} Ay \cos \in \sin \alpha \sin \theta \\ - 2fy - \bar{\lambda}_\alpha \left[(x^2 + y^2) - 2\ell_0 \sqrt{x^2 + y^2} \right] + h \text{----- (10)} \end{aligned}$$

The curve of zero velocity can be obtained in the form.

$$3x^2 + \frac{2}{\pi} Ax \cos \epsilon \cos \alpha \sin \theta + \frac{2}{\pi} Ay \cos \epsilon \sin \alpha \sin \theta - 2fy - \bar{\lambda}_\alpha \left[(x^2 + y^2) - 2\ell_0 \sqrt{x^2 + y^2} \right] + h = 0 \quad \text{----- (11)}$$

Hence we conclude that the satellite of mass m_1 will move inside the boundaries of different curves of zero velocity represented by (11) of (10) for different values of Jacobian constant h .

III. Equilibrium point of the problem

We have obtained the system of equations given by (8) for the motion of the system in rotating frame of reference. It has been assumed that the system is moving with effective constraints and the connecting level of the two satellites of masses m_1 and m_2 respectively will always remain tight.

The equilibrium positions of the system are given by the constant values of the coordinates in the rotating frame of reference.

Now, let $x = x_0$ and $y = y_0$ give the equilibrium position where x_0 and y_0 are constants

Hence, $x' = 0 = x''$ and $y' = 0 = y''$

Thus, equations given by (8) take the form:

$$\left. \begin{aligned} -3x_0 - \frac{A}{\pi} \cos \epsilon \cos \alpha \sin \theta &= -\bar{\lambda}_\alpha \left[1 - \frac{\ell_0}{r_0} \right] x_0 \\ f - \frac{A}{\pi} \cos \epsilon \sin \alpha \sin \theta &= -\bar{\lambda}_\alpha \left[1 - \frac{\ell_0}{r_0} \right] y_0 \\ \text{where } r_0 &= \sqrt{x_0^2 + y_0^2} \end{aligned} \right\} \quad \text{----- (12)}$$

From (12) it follows that it is very difficult to get the solution in its present form. Hence we are compelled to make the following assumptions ; $\alpha = 90^\circ$. Hence the sun rays are assumed to be in the direction perpendicular to the line of the perigee of the circular orbit of the centre of mass of the systems.

Hence on putting $\alpha = 90^\circ$ in (12), we get

$$\left. \begin{aligned} -3x_0 &= -\bar{\lambda}_\alpha \left[1 - \frac{\ell_0}{r_0} \right] x_0 \\ f - \frac{A \cos \epsilon \sin \theta}{\pi} &= -\bar{\lambda}_\alpha \left[1 - \frac{\ell_0}{r_0} \right] y_0 \end{aligned} \right\} \quad \text{----- (13)}$$

From 13, we get the equilibrium point as

$$\left[0, \frac{\frac{A \cos \epsilon \sin \theta}{\pi} + \bar{\lambda}_\alpha \ell_0 - f}{\bar{\lambda}_\alpha} \right] \quad \text{----- (14)}$$

It can be easily seen that the equilibrium position given by (14) gives a meaningful value of Hook's modulus of elasticity if $\left(\frac{A \cos \epsilon \sin \theta}{\pi} - f \right)$ is positive.

IV. Stability of the system

We shall study the stability of equilibrium point given by (14) of the system in the sense of Liapunov. For this,

$$\text{Let } a = x = 0 \text{ and } b = y = \frac{\frac{A \cos \epsilon \sin \theta}{\pi} + \bar{\lambda}_\alpha \ell_0 - f}{\bar{\lambda}_\alpha}$$

Let δ_1 and δ_2 be the small variations in x_0 and y_0 respectively. For the given position of equilibrium (o, b) given by (14). Hence, we get

$$\left. \begin{aligned} x &= 0 + \delta_1 \text{ and } y = b + \delta_2 \\ \therefore x' &= \delta_1' \text{ and } y' = \delta_2' \\ x'' &= \delta_1'' \text{ and } y'' = \delta_2'' \end{aligned} \right\} \quad \text{----- (15)}$$

Hence on putting $\alpha = 90^\circ$ in equations (8) and using (15), we get

$$\left. \begin{aligned} \delta_1'' - 2\delta_2' - 3\delta_1 &= -\bar{\lambda}_\alpha \left[1 - \frac{\ell_0}{r} \right] \delta_1 \\ \text{and } \delta_2'' - 2\delta_1' + f - \frac{A \cos \theta \sin \theta}{\pi} &= -\bar{\lambda}_\alpha \left[1 - \frac{\ell_0}{r} \right] (b + \delta_2) \end{aligned} \right\} \text{----- (16)}$$

Where $r = \sqrt{\delta_1^2 + (b + \delta_2)^2}$

Multiplying the first equation and the 2nd equation of (16) by $2\delta_1'$ and $2(b + \delta_2)'$ respectively and adding these together and then integrating, we get Jacobi's integral in the form:

$$\delta_1^{1^2} + \delta_2^{1^2} - 3\delta_1^2 + 2f(b + \delta_2) - \frac{2A \cos \theta \sin \theta (b + \delta_2)}{\pi} + \bar{\lambda}_\alpha [\delta_1^2 + (b + \delta_2)^2] - 2\bar{\lambda}_\alpha \ell_0 [\delta_1^2 + (b + \delta_2)^2]^{1/2} = h \text{----- (17)}$$

Where h is the constant of integration.

To test the stability in the sense of Liapunov, we take Jacobi's integral given by (17) as Liapunov's function $v(\delta_1', \delta_2', \delta_1, \delta_2)$ and is obtained expanding the terms of (17) as

$$\begin{aligned} v(\delta_1', \delta_2', \delta_1, \delta_2) &= \delta_1^{1^2} + \delta_2^{1^2} + \delta_1^2 \left[\bar{\lambda}_\alpha - 3 - \frac{\bar{\lambda}_\alpha \ell_0}{b} \right] \\ &\quad + \delta_2^2 [\bar{\lambda}_\alpha] \\ &\quad + \delta_2 \left[2f - \frac{2A \cos \theta \sin \theta}{\pi} + 2b\bar{\lambda}_\alpha - 2\bar{\lambda}_\alpha \ell_0 \right] \\ &\quad + 2fb - 2b\bar{\lambda}_\alpha \ell_0 - \frac{2bA \cos \theta \sin \theta}{\pi} \\ &\quad + O(3) \\ &= h \end{aligned} \text{----- (18)}$$

Where $O(3)$ stands for third and higher order terms in δ_1 and δ_2 . By Liapunov's theorem on stability, it follows that the only criterion for given equilibrium position $(0, b)$ to be stable is that V defined by (18) must be positive definite and for this the following three conditions must be satisfied:

$$\left. \begin{aligned} \text{(i)} \quad &2f - \frac{2A \cos \theta \sin \theta}{\pi} + 2b\bar{\lambda}_\alpha - 2\bar{\lambda}_\alpha \ell_0 = 0 \\ \text{(ii)} \quad &\bar{\lambda}_\alpha - 3 - \frac{\bar{\lambda}_\alpha \ell_0}{b} > 0 \\ \text{(iii)} \quad &\bar{\lambda}_\alpha > 0 \end{aligned} \right\} \text{----- (19)}$$

$$\text{(i) Can be seen to be satisfied if we put } b = \frac{\frac{A \cos \theta \sin \theta}{\pi} + \bar{\lambda}_\alpha \ell_0 - f}{\bar{\lambda}_\alpha}$$

(ii) and (iii) can be seen to be since

$$\begin{aligned} b &= \frac{\frac{A \cos \theta \sin \theta}{\pi} + \bar{\lambda}_\alpha \ell_0 - f}{\bar{\lambda}_\alpha} > 0 \text{ and } \bar{\lambda}_\alpha > 0 \\ \Rightarrow \frac{A \cos \theta \sin \theta - f}{\bar{\lambda}_\alpha} > 0 &\Rightarrow A \cos \theta \sin \theta - f > 0 \end{aligned}$$

Thus, all the above three conditions given in (19) are satisfied. Hence, we conclude that the equilibrium point $(0, b)$ given by (14) of the system is stable in the sense of Liapunov.

References

- [1] Beletsky; V.V. : Kosmicheskie Isslodovna, Russia p.p. 827-840; 1969
- [2] Sharma; B.: The motion of a system of two cables connected satellites in the atmosphere Ph.D. thesis, submitted to B.U.; Muz; 1974
- [3] Thakur; H.K.: The motion of a system of two satellites connected by extensible cable, Ph.D. thesis, submitted to B.U.: Muz; 1975.

Control Scheme of Multi Level Cascaded H-Bridge STATCOM

Gollapalle Pullaiah¹, S.Sarada,²

¹M Tech student, Department of EEE Annamacharya institute of technology and sciences Rajampet, India

²Assistant professor Department of EEE Annamacharya institute of technology and sciences Rajampet, India

Abstract: This paper presents a control scheme of cascaded H-bridge STATCOM in three-phase power systems. Cascaded H-bridge STATCOM has merits in point of switching losses, output harmonics, and the number of circuit components. But every H-bridge cell has isolated dc capacitors. So the balancing problem of capacitor voltages exists. Since STATCOM is often requested to operate under asymmetrical condition by power system faults, capacitor voltage balancing between phase clusters is particularly important. Solving this problem, a technique using zero-sequence voltage and negative-sequence current is proposed. By this scheme, the STATCOM is allowed to operate under asymmetrical conditions by power system faults. The validity is examined by digital simulation under one line and two-lines fault circuit condition.

IndexTerms: Capacitor voltage balancing, cascaded H-bridge, multilevel converter, negative-sequence current, STATCOM, zero sequence voltage.

I. INTRODUCTION

CASCADED H-bridge multilevel converter consists of series connected H-bridge cells. It has merits of switching losses of semiconductor device and harmonics in output voltage. And it is considered to be suitable for STATCOM in power system application, because it requires less number of circuit components compared with diode-clamped multilevel converter or flying capacitor multilevel converter and STATCOM does not have to handle real power [1]–[3]. But every H-bridge cell has isolated dc capacitor and balancing problem of capacitor voltages exists in this configuration [3]–[8]. STATCOM is often requested to operate under asymmetrical condition by power system faults, such as one line grounding or two-lines short circuit [9]. These kinds of faults cause unbalance of power system voltage [10] and unbalance current flows into each phase cluster. So capacitor voltage balancing between phase clusters is particularly important. Recently, several methods of voltage balancing between phase clusters are proposed [4], [5]. One method is based on zero-sequence voltage injection [4]. However it needs wide margin of dc capacitor voltage compared with rated power system voltage when the unbalance of power system voltage is large. The other method handles the capacitor voltage unbalance by independently controlling active power of individual phase cluster, but unbalance of power system voltage is not considered [5]. By these reasons, the circuit condition in which these methods are effective is considered to be limited in practical use. We also had proposed a capacitor voltage balancing method using negative-sequence current [11]. It does not need wide margin of dc capacitor voltage and can handle large unbalance of power system voltage. However the output current of the STATCOM using the method is uniquely determined by the unbalance of power system voltage and function of the STATCOM is limited.

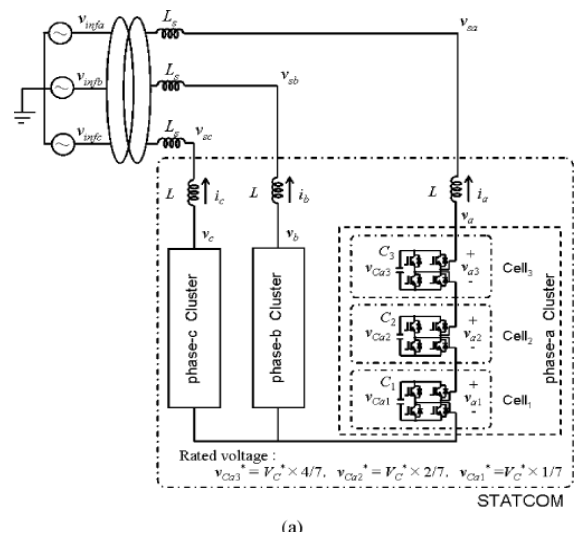
So we introduce a different control method using zero-sequence voltage in this paper. By this method, the STATCOM can control output current almost freely. But it needs wide margin of dc voltage under large power system voltage unbalance, similar to the method proposed in [5]. To avoid this, we exclusively use the two methods depending on the extent of voltage unbalance. The validity is examined by digital simulation under one line and two-lines fault circuit condition.

II. MAIN CIRCUIT AND CONTROL SCHEME

A. Main Circuit and Basic Operation

Fig. 1(a) shows the main circuit of cascaded H-bridge STATCOM in this paper [11]. It is composed of three-phase clusters. Each phase cluster consists of three H-bridge cells. The dc capacitor voltages are set to $V_c, 2V_c, 4V_c$, in a phase cluster. Fig. 1(b) shows an example of output waveform. Voltage level from -7 to +7 can be generated by combining the capacitor voltages. The level is decided according to the calculation flow shown in Fig.

1(c). Then the cluster outputs the nearest voltage level to reference. Conventional cascaded H-bridge multilevel converter may require high number of H-bridge cells for low current distortion. But the proposed circuit configuration can output 15-level voltage in spite of only three cells. So, lower conduction losses of semiconductor devices are expected. For dc voltage balancing in each phase cluster, the control Method proposed here uses the fact that several switching patterns are available when a phase cluster outputs particular voltage levels. An example is shown in Fig. 2. When a phase cluster outputs voltage “ V_c ”, “ $2V_c - V_c$ ”, “ $4V_c - 2V_c - V_c$ ” and charged or discharged capacitors are different. These patterns are selected



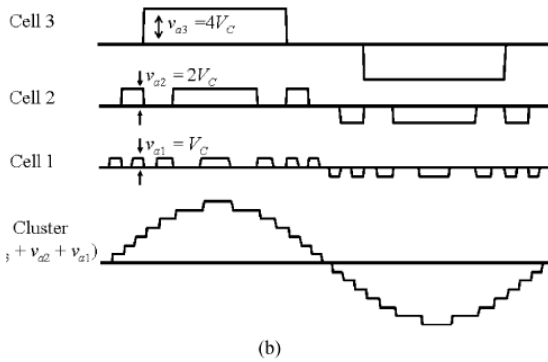


Figure1 Circuit configuration and operation, (a) Main circuit, (b) Example of output waveform, (c) Decision method of output level.

According to the relation between V_{c1} , V_{c2} , and V_{c3} . When $4V_{c1} \geq 2V_{c2}$ and V_{c3} , output pattern “ V_c ” is selected. When $2V_{c2} > 4V_{c1}$ and V_{c3} out pattern

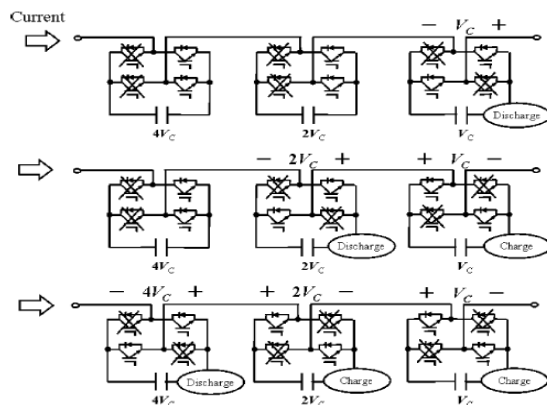
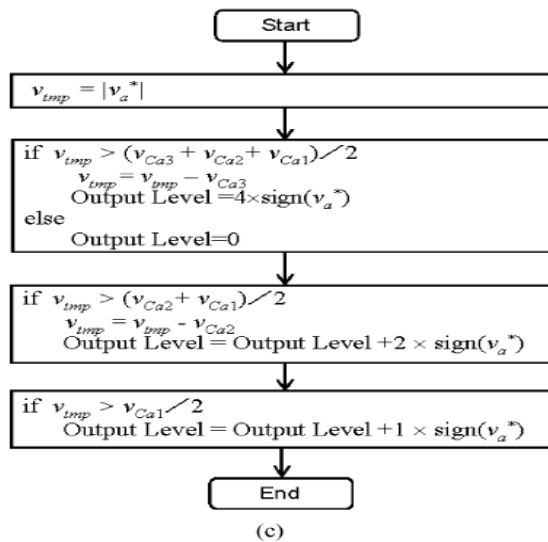


Figure2 An example of voltage balancing between the H-bridge cells

Output pattern “ $2V_c - V_c$ ” is selected when $V_{c3} > 2V_{c2}$ and $4V_{c1}$, out pattern “ $4V_c - 2V_c - V_c$ ” is selected. To use same switching pattern in $1/4$ cycle, the capacitor voltages are measured [rad] of ac side phase angle. Table I shows the all operational patterns and decision method. It is used when the polarities of STATCOM output voltage and current are same. “1” indicates that the cell outputs voltage to positive direction and its capacitor is discharged. “-1”

indicates that the cell output voltage to negative direction and its capacitor is charged. It is similar when the polarity of the output current is opposite. By this method, capacitor voltage ratio between H-bridge cells in a phase cluster is controlled.

TABLE I
DECISION TABLE OF OPERATIONAL PATTERN FOR VOLTAGE BALANCING

Output Level	Cell ₃	Cell ₂	Cell ₁	Condition
1			1	$4v_{c1} \geq 2v_{c2}$ and $4v_{c1} \geq v_{c3}$
		1	-1	$2v_{c2} \geq v_{c3}$ and $2v_{c2} > 4v_{c1}$
	1	-1	-1	$v_{c3} > 4v_{c1}$ and $v_{c3} > 2v_{c2}$
2		1		$2v_{c2} \leq v_{c3}$
	1	-1		$2v_{c2} < v_{c3}$
3		1	1	$2v_{c2} \leq v_{c3}$ and $4v_{c1} \geq v_{c3}$
	1		-1	$v_{c3} > 4v_{c1}$ and $2v_{c2} > 4v_{c1}$
	1	-1	1	$v_{c3} > 2v_{c2}$ and $4v_{c1} \geq 2v_{c2}$
4	1			
5	1		1	$4v_{c1} \geq 2v_{c2}$
	1	1	-1	$4v_{c1} < 2v_{c2}$
6	1	1		
7	1	1	1	

Table I shows the all operational patterns and decision method. It is used when the polarities of STATCOM output voltage and current are same. “1” indicates that the cell outputs voltage to positive direction and its capacitor is discharged. “-1” indicates that the cell output voltage to negative direction and its capacitor is charged. It is similar when the polarity of the output current is opposite. By this method, capacitor voltage ratio between H-bridge cells in a phase cluster is controlled.

B. Capacitor Voltage Balancing Between Phase Clusters:

STATCOM is often requested to operate under symmetrical condition by power system faults, such as one line grounding or two-lines short circuit. These kinds of faults cause unbalance of power system voltage and unbalance current flows into each phase cluster. Then capacitor voltage unbalance between phase clusters occurs.

So we had proposed a capacitor voltage balancing method using negative-sequence current [11]. The negative-sequence current i_{na} , i_{nb} , i_{nc} , for capacitor voltage balancing is expressed as

$$\begin{pmatrix} i_{na} \\ i_{nb} \\ i_{nc} \end{pmatrix} = \sqrt{\frac{2}{3}} K_{nvca} \begin{pmatrix} \cos(\omega t) \\ \cos\left(\omega t + \frac{2\pi}{3}\right) \\ \cos\left(\omega t - \frac{2\pi}{3}\right) \end{pmatrix} + \sqrt{\frac{2}{3}} K_{nvca} \begin{pmatrix} \cos\left(\omega t + \frac{2\pi}{3}\right) \\ \cos\left(\omega t - \frac{2\pi}{3}\right) \\ \cos(\omega t) \end{pmatrix} + \sqrt{\frac{2}{3}} K_{nvca} \begin{pmatrix} \cos\left(\omega t - \frac{2\pi}{3}\right) \\ \cos(\omega t) \\ \cos\left(\omega t + \frac{2\pi}{3}\right) \end{pmatrix} \quad (1)$$

Where Kn is a gain and v_{ca}, v_{cb}, v_{cc} are the sum of capacitor voltages in a phase cluster, as shown

$$\begin{aligned} V_{Ca} &= \sum_{k=1,2,3} V_{Cak} \\ V_{Cb} &= \sum_{k=1,2,3} V_{Cbk} \\ V_{Cc} &= \sum_{k=1,2,3} V_{Cck} \end{aligned} \quad (2)$$

Here, it is assumed that the STATCOM shown in Fig. 1 operates under the asymmetrical circuit condition, as shown

$$\begin{pmatrix} V_a \\ V_b \\ V_c \end{pmatrix} = \sqrt{\frac{2}{3}} V_p \begin{pmatrix} \cos(\omega t) \\ \cos(\omega t - \frac{2\pi}{3}) \\ \cos(\omega t + \frac{2\pi}{3}) \end{pmatrix} + \sqrt{\frac{2}{3}} V_n \begin{pmatrix} \cos(\omega t + \varphi) \\ \cos(\omega t + \frac{2\pi}{3} + \varphi) \\ \cos(\omega t - \frac{2\pi}{3} + \varphi) \end{pmatrix} \quad (4)$$

And its output current is controlled as shown in (4). Where, the first term is the active current to compensate converter losses. The second term is the reactive current output to power system. The third term is the negative-sequence current for voltage balancing, as shown in (1)

$$\begin{pmatrix} i_a \\ i_b \\ i_c \end{pmatrix} = \sqrt{\frac{2}{3}} i_{pd}^* \begin{pmatrix} \cos(\omega t) \\ \cos(\omega t - \frac{2\pi}{3}) \\ \cos(\omega t + \frac{2\pi}{3}) \end{pmatrix} + \sqrt{\frac{2}{3}} i_{pq}^* \begin{pmatrix} -\sin(\omega t) \\ -\sin(\omega t - \frac{2\pi}{3}) \\ -\sin(\omega t + \frac{2\pi}{3}) \end{pmatrix} + \begin{pmatrix} i_{na} \\ i_{nb} \\ i_{nc} \end{pmatrix} \quad (5)$$

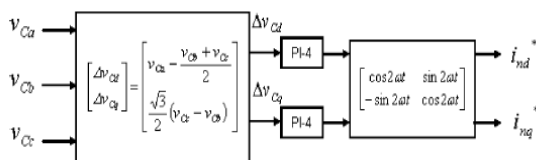


Fig. 3. Calculation method of negative-sequence current for voltage balancing between phase clusters.

Then, the average real powers of each phase clusters are calculated as

$$\begin{pmatrix} P_a \\ P_b \\ P_c \end{pmatrix} = \begin{pmatrix} \frac{w}{2\pi} \int_0^{\frac{2\pi}{w}} v_a \cdot i_a dt \\ \frac{w}{2\pi} \int_0^{\frac{2\pi}{w}} v_b \cdot i_b dt \\ \frac{w}{2\pi} \int_0^{\frac{2\pi}{w}} v_c \cdot i_c dt \end{pmatrix}$$

$$= \frac{V_p K_n}{2} \begin{pmatrix} V_{Ca} - V_c \\ V_{Cb} - V_c \\ V_{Cc} - V_c \end{pmatrix} + \begin{pmatrix} P \\ P \\ P \end{pmatrix} + \begin{pmatrix} P_{na} \\ P_{nb} \\ P_{nc} \end{pmatrix} \quad (6)$$

Where

$$V_c = \frac{V_{Ca} + V_{Cb} + V_{Cc}}{3} \quad (7)$$

$$P = \frac{V_{pdpd}^*}{3} + \frac{V_n K_n}{3} \left[v_{ca} \cos \varphi + v_{cb} \cos \left(\varphi - \frac{2\pi}{3} \right) + v_{cc} \cos \left(\varphi - \frac{2\pi}{3} \right) \right] \quad (8)$$

$$P_{na} = \frac{V_{nipd}^*}{3} \cos(\varphi) + \frac{V_{nipq}^*}{3} \sin(\varphi)$$

$$P_{nb} = \frac{V_{nipd}^*}{3} \cos \left(\varphi - \frac{2\pi}{3} \right) + \frac{V_{nipq}^*}{3} \sin \left(\varphi - \frac{2\pi}{3} \right) \quad (9)$$

$$P_{nc} = \frac{V_{nipd}^*}{3} \cos \left(\varphi + \frac{2\pi}{3} \right) + \frac{V_{nipq}^*}{3} \sin \left(\varphi + \frac{2\pi}{3} \right)$$

In (5), the first term is proportional to the error between the individual capacitor voltage V_{ca}, V_{cb}, V_{cc} , and the average capacitor voltage V_c expressed as (6) and (2). The second term is the same for each phase cluster. The third term is almost independent of V_{ca}, V_{cb}, V_{cc} , as expressed in (8). So the error of the individual capacitor voltage is decreased by use of the negative-sequence currents shown in (1)

Besides i_{na}, i_{nb}, i_{nc} can be expressed on dq-axes, as shown

$$\begin{pmatrix} i_{nd}^* \\ i_{nq}^* \end{pmatrix} = \begin{pmatrix} \cos 2\omega t & \sin 2\omega t \\ -\sin 2\omega t & \cos 2\omega t \end{pmatrix} K_n \begin{pmatrix} V_{Ca} - \frac{V_{Cb} + V_{Cc}}{2} \\ \frac{\sqrt{3}}{2} (V_{Cc} - V_{Cb}) \end{pmatrix} \quad (10)$$

So PI controller is actually used to calculate i_{na}, i_{nb}, i_{nc} in the control block of proposed STATCOM, instead of gain K_n , to make the error between the individual capacitor voltage and the average capacitor voltage zero, as shown in Fig. 3. However the output current of the STATCOM using the negative-sequence current method is uniquely determined by unbalance of power system voltage and function of the STATCOM is limited. For example, the STATCOM becomes impossible to compensate negative-sequence current by unbalanced loads. So we introduce a different control method using zero-sequence voltage in this paper. The zero-sequence voltage for capacitor voltage balancing is expressed as

$$V_O = \frac{\Delta P_a(i_b, i_c) i_a + \Delta P_b(i_c, i_a) i_b + \Delta P_c(i_a, i_b) i_c}{i_a i_b - (i_a, i_b)^2}$$

$$\Delta P_a = V_a' \cdot i_a - \frac{1}{3} \sum_{k=a,b,c} V_k' \cdot i_k$$

+Kop

$$\left(\frac{1}{3} \sum_{k=a,b,c} \sum_{j=1,2,3} \frac{1}{2} C_j V_{caj} - \sum_{j=1,2,3} \frac{1}{2} C_j V_{cbj} \right)$$

$$\Delta P_b = V_b' \cdot i_b - \frac{1}{3} \sum_{k=a,b,c} V_k' \cdot i_k$$

+Kop

$$\left(\frac{1}{3} \sum_{k=a,b,c} \sum_{j=1,2,3} \frac{1}{2} C_j V_{ckj} - \sum_{j=1,2,3} \frac{1}{2} C_j V_{cbj} \right)$$

$$\Delta P_c = V_c' \cdot i_c - \frac{1}{3} \sum_{k=a,b,c} V_k' \cdot i_k$$

$$\left(\frac{1}{3} \sum_{k=a,b,c} \sum_{j=1,2,3} \frac{1}{2} C_j V_{ckj} - \sum_{j=1,2,3} \frac{1}{2} C_j V_{ccj} \right)$$

(11)

where bold text means phasor, v_a', v_b', v_c' , are positive and negative-sequence components of STATCOM output voltage, i_a, i_b, i_c are STATCOM output current, Kop is a gain, operator “.” means scalar product of complex vector. To handle

Instantaneous value at time t , it is substituted by the calculation as follows:

$$x, y = \frac{w}{2\pi} \int_{t-\frac{2\pi}{w}}^t x(t) \times y(t) d\tau \quad (12)$$

where x and y are arbitrary phasor in (10) and $x(t)$ and $y(t)$ are their instantaneous value. w is angular frequency of power system. By using v_o shown in (10), STATCOM output power from each phase is calculated as follows. See equation (12) at the bottom of the page. From (12), it is understood that the STATCOM outputs same power from each phase when the capacitor voltage of each phase is balanced. Even if capacitor voltage unbalance occurs, it is corrected by the second term of (12). It can be easily confirmed that the time constant to correct the capacitor voltage unbalance is $1/kop$.

However, this method requires a wide dc voltage margin. For example, it is assumed that two-line short circuit occurs in power system and positive positive and negative sequence of STATCOM output voltage becomes

$$\left. \begin{aligned} V_a' &= 1 + j0 \\ V_b' &= -0.5 + j0 \\ V_c' &= -0.5 + j0 \end{aligned} \right\} \quad (13)$$

At this time v_o shown in (10) is calculated as follows

$$V_o = 0.5 + j0 \quad (14)$$

Then statcom output voltages becomes as follows:

$$\left. \begin{aligned} V_a &= V_a' + V_o = 1.5 + j0 \\ V_b &= V_b' + V_o = 0 + j0 \\ V_c &= V_c' + V_o = 0 + j0 \end{aligned} \right\} \quad (15)$$

As mentioned before, the STATCOM using must output 1.5 times voltage compared with only using positive and negative sequence voltage at the circuit condition shown in (13). To avoid this, we exclusively use the two voltage balancing methods depending on the extent of voltage unbalance. The zero-sequence voltage method is used normally. The negative-sequence current method is used under large unbalance of power system voltage. The decision method shown in Fig. 4 is used to select these two methods. Input V_c^* is capacitor voltage necessary for outputting reference voltage of the STATCOM. The calculation method of V_c^* is described in next section. Input v_{nd}, v_{nq} is the negative-sequence component of power system voltage on reverse rotated frame, described in the next section.

$$P_a = (V_a' + V_o) \cdot i_a = V_a' \cdot i_a - \Delta P_a$$

$$= \frac{1}{3} \sum_{k=a,b,c} V_k' \cdot i_k + Kop \left[\sum_{j=1}^3 \frac{1}{2} C_j V_{caj} - \frac{1}{3} \sum_{k=a,b,c} \sum_{j=1}^3 \frac{1}{2} C_j V_{ckj} \right]$$

$$P_b = (V_b' + V_o) \cdot i_b = V_b' \cdot i_b - \Delta P_b$$

$$= \frac{1}{3} \sum_{k=a,b,c} V_k' \cdot i_k + Kop \left[\sum_{j=1}^3 \frac{1}{2} C_j V_{cbj} - \frac{1}{3} \sum_{k=a,b,c} \sum_{j=1}^3 \frac{1}{2} C_j V_{ckj} \right] \quad (12)$$

$$P_c = (V_c' + V_o) \cdot i_c = V_c' \cdot i_c - \Delta P_c$$

$$= \frac{1}{3} \sum_{k=a,b,c} V_k' \cdot i_k + Kop \left[\sum_{j=1}^3 \frac{1}{2} C_j V_{ccj} - \frac{1}{3} \sum_{k=a,b,c} \sum_{j=1}^3 \frac{1}{2} C_j V_{ckj} \right]$$

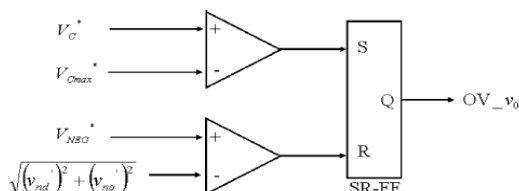
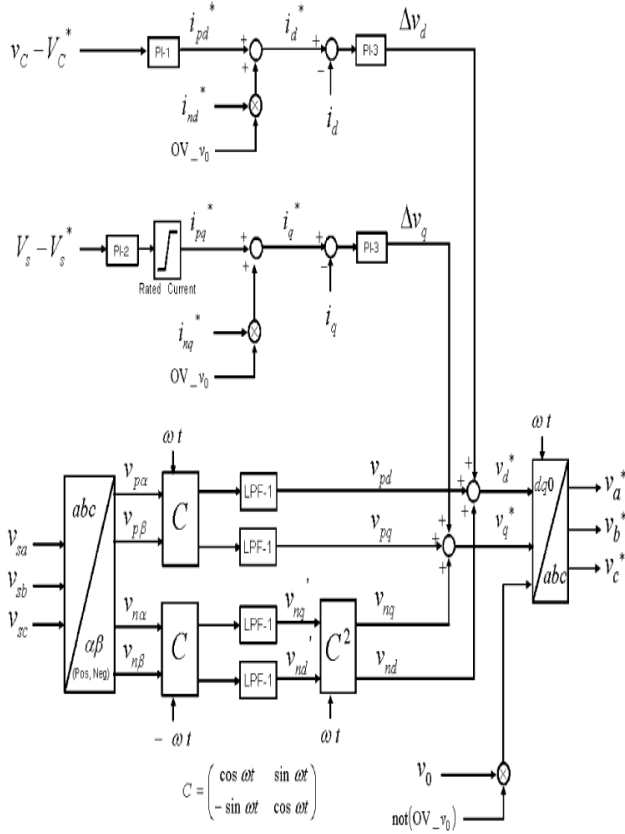


Fig. 4. Decision method of voltage balancing between phase clusters.



If power system voltage is balanced, $v'nd, v'nq$ is enough lower than limit value V^*NEG shown in Fig. 4. Then over voltage flag "OV-vo" shown in Fig. 4 is set to 0 and the zero-sequence voltage method is selected. Once asymmetrical power system fault occurs, vo shown in (10) may become rather high and may become higher than limit value V^*cmax shown in Fig. 4. At this time, the flag "OV-vo" is set to 1 and the negative-sequence current method is selected. After clearing the fault, $v'nd, v'nq$, returns to a value low enough and the zero-sequence voltage method restarts.

V^*cmax is set depending on withstand voltage of the STATCOM components such as dc capacitor. is set to a value low enough to use the zero-sequence voltage method

C. Control Scheme for STATCOM

Fig. 5 shows the control block of the STATCOM shown in

Fig. 1. The STATCOM is designed to control the positive sequence voltage V_s at the grid connection point to reference V^*s by q-axis current i^*pq .

The average capacitor voltage v_c is controlled to reference V^*c by d-axis current i^*pd . Where, v_c is from (6) and (2). The dc voltage is varied according to the STATCOM output voltage shown in Fig. 6. The reason why this method is adopted is to use as many voltage levels of the cascade H-bridge multilevel converter as possible, regardless of the peak of STATCOM output voltage. In addition, the control element "7/6.5" shown in Fig. 6 acts to set the peak of reference v^*a, v^*b, v^*c in the middle of output level 6 and 7.

The zero-sequence voltage shown in (10) or the negative sequence current i^*nd, i^*nq shown in Fig. 3 are

used for capacitor voltage balancing between phase clusters. If over voltage flag OV-vo shown in Fig. 4 is set to 0, then vo is transformed to

$$\max_{k=a,b,c} \left(\sqrt{2} \times \sqrt{\frac{1}{T} \int_{t-T}^t v_k^*(\tau)^2 d\tau} \right) \rightarrow \text{LPF-2} \rightarrow \times \frac{7}{6.5} \rightarrow V_c^*$$

Fig. 6. Calculation method of capacitor voltage reference.

The detection method of the grid voltage, shown in under part of Fig. 5, is designed to control the STATCOM output current accurately under asymmetrical circuit conditions by power system faults. The grid voltage is once decomposed to positive sequence and negative sequence by the method shown in Fig. 7. The control element "lag90" delays the input, for 1/4 cycle at fundamental frequency of ac voltage and outputs. For example, v_a, v_b these are expressed as

$$\begin{pmatrix} v_a \\ v_b \end{pmatrix} = V_p \begin{pmatrix} \cos \omega t \\ \sin \omega t \end{pmatrix} + V_n \begin{pmatrix} \cos(\omega t + \phi_n) \\ -\sin(\omega t + \phi_n) \end{pmatrix} \quad (16)$$

Then $v'a, v'\beta$ are calculated as

$$\begin{pmatrix} v'a \\ v'\beta \end{pmatrix} = V_p \begin{pmatrix} \sin \omega t \\ -\cos \omega t \end{pmatrix} + V_n \begin{pmatrix} \sin(\omega t + \phi) \\ \cos(\omega t + \phi) \end{pmatrix} \quad (17)$$

From (16) and (17), positive sequence v_p^α, v_p^β and negative sequence v_n^α, v_n^β are calculated as follows:

$$\begin{aligned} \begin{pmatrix} v_p^\alpha \\ v_p^\beta \end{pmatrix} &= \frac{1}{2} \begin{pmatrix} v_a - v_b' \\ v_b + v_a' \end{pmatrix} = V_p \begin{pmatrix} \cos \omega t \\ \sin \omega t \end{pmatrix} \\ \begin{pmatrix} v_n^\alpha \\ v_n^\beta \end{pmatrix} &= \frac{1}{2} \begin{pmatrix} v_a + v_b' \\ v_b - v_a' \end{pmatrix} = V_n \begin{pmatrix} \cos(\omega t + \phi_n) \\ -\sin(\omega t + \phi_n) \end{pmatrix} \end{aligned} \quad (18)$$

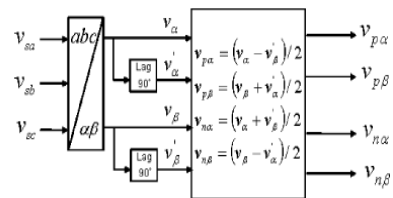


Fig. 7. Decomposition from grid voltage to positive and negative sequence.

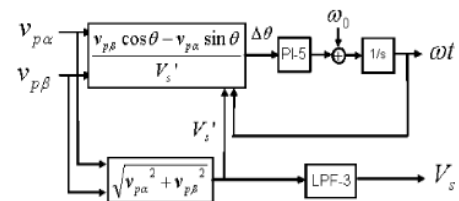


Fig. 8. Phase angle and voltage detection method.

TABLE II
CIRCUIT PARAMETERS

Rated AC Voltage	V_s^*	3 ϕ AC 6600V
Rated Reactive Power	Q	1MVA
Line angular frequency	ω_0	$2\pi \times 60$ rad/s
Line Inductance	L_s	4.64mH (4%)
AC link Inductance	L	11.6mH (10%)
DC Capacitance	C_3	1mF
	C_2	2mF
	C_1	4mF
Rated Capacitor Voltage	V_{C3}^*	3900V
	V_{C2}^*	1950V
	V_{C1}^*	975V

The feature of this method is that the appropriate values are obtained in about 1/4 cycle even if sudden change of occurs by power system faults. After transformation and low pass filtering, the positive sequence other hand are once rotated to reverse direction of transformation. Here, the negative-sequence voltage is also obtained as dc components. After low pass filtering, the output values are rotated two times to forward direction of transformation.

And the negative-sequence voltage are obtained accurately. The time constant of low pass filter does not have to be long, ie. the delay time of low pass filter is not long, because the filter is requested to eliminate only harmonic component of ac side voltage. As a result, the STATCOM can respond to power system faults quickly, and the error of capacitor voltage between phase clusters is expected to be small even in the transient state by the faults. In addition, these are used for PLL, shown in Fig. 8, to synchronize the phase angle to positive sequence of the grid voltage. And the positive sequence voltage at grid point is also obtained by this control block diagram.

III. SIMULATION RESULT

Digital simulation using EMTP (Electro Magnetic Transient Analysis Program) has been carried out to verify the effectiveness of the proposed scheme for the circuit shown in Fig. 1. The TABLE III CONTROL PARAMETERS

TABLE III
CONTROL PARAMETERS

PI-1 : Proportional gain	K_{Cp}	0.1
Integral gain	K_{Ci}	1.0
PI-2 : Proportional gain	K_{Vp}	0.5
Integral gain	K_{Vi}	50
PI-3 : Proportional gain	K_{Ip}	25
Integral gain	K_{Ii}	100
PI-4 : Proportional gain	K_{mp}	0.1
Integral gain	K_{mi}	1.0
LPF-1 : Time constant	T_1	0.001
LPF-2 : Time constant	T_2	0.2
LPF-3 : Time constant	T_3	0.01
Proportional gain	K_{op}	30
Limit for Zero Seq. Voltage	V_{Cmax}^*	7000
Limit for neg. seq. Current	V_{NBG}^*	1320

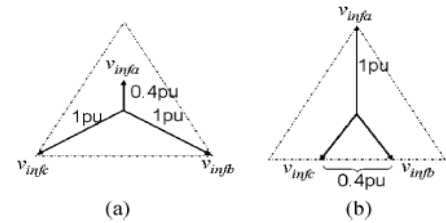
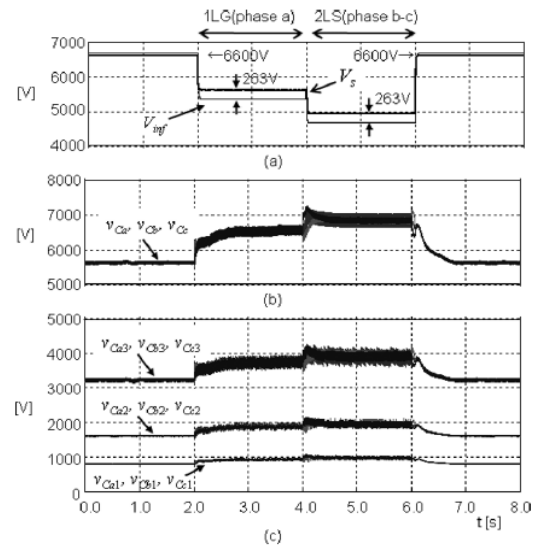
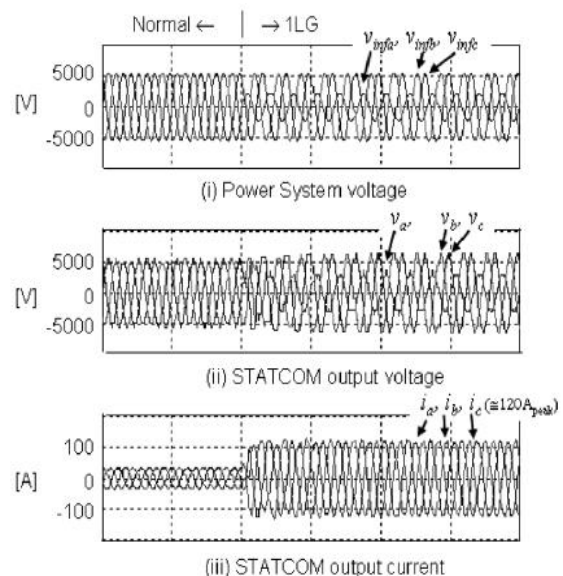


Fig. 9. Source voltage under faults. (a) 1LG. (b) 2LS.



Circuit parameters are given in Table II. Rated reactive power is 1 MVA. The sum of rated capacitor voltage is $825V+1650V+3300V=5575V$ slightly higher than the peak voltage of ac system which is $.5389V$. The capacitance 1 mF, 2 mF, 4 mF are chosen so that the capacitor voltage ripple are less than about 5% of their rated voltage at outputting rated reactive power. The ac reactance 11.6 mH is equivalent to 10% at rated reactive power. The control parameters are given in Table III.



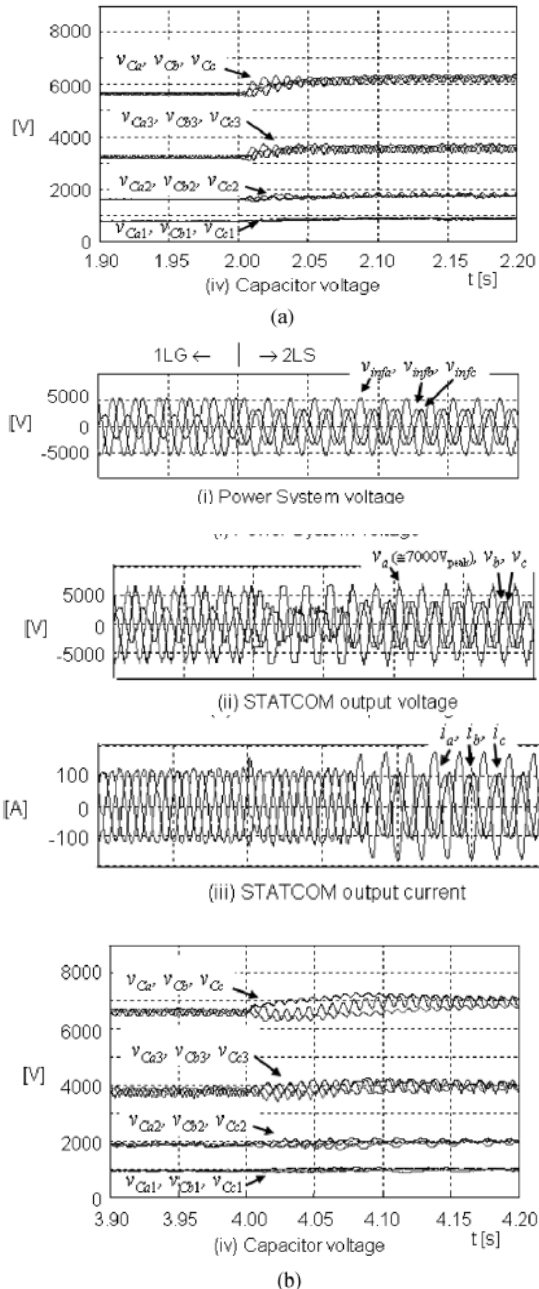


Fig. 11. Simulation result (Proposal: zero seq. voltage + negative seq. current control). (a) Normal \rightarrow 1LG. (b) 1LG \rightarrow 2LS.

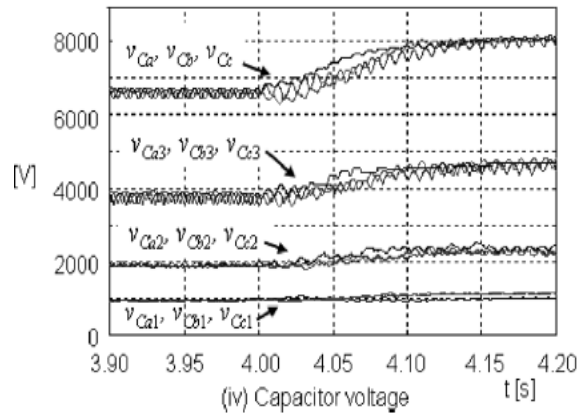
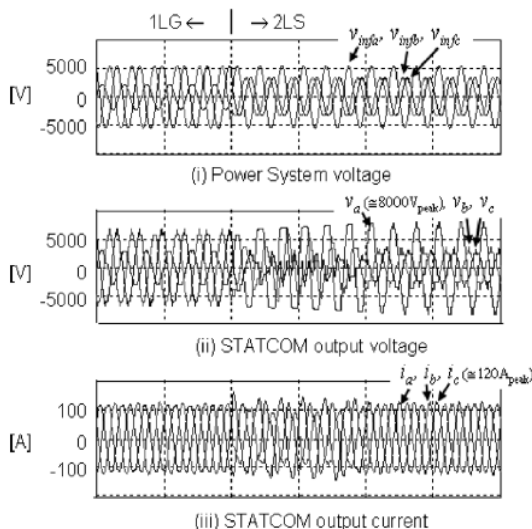


Fig. 12. Simulation result (only zero-sequence voltage control).

The simulation result of power system voltage and capacitor voltages are shown in Fig. 10. The STATCOM compensates power system voltage. As a result, grid connection voltage is 263 V higher than source voltage during 1LG and 2LS. Before 1LG the capacitor voltages of phase clusters are balanced and the voltage ratio of H-bridge cells is controlled to 1:2:4. At the starting point of 1LG and 2LS, the capacitor voltages of phase clusters are once unbalanced. But they are rebalanced soon. Fig. 11 shows the power system voltage, STATCOM output voltage, STATCOM output current and capacitor voltages. Under normal condition or 1LG the zero-sequence voltage method is used and balanced current are output, as shown in Fig. 11(a). The peak value of the currents is about 120 A. On the other hand, the negative-sequence current method is used and the STATCOM output unbalanced current under 2LS, as shown in Fig. 11(b). By this, the capacitor voltages are balanced. During this time, the peak value of STATCOM output voltage is about 7000 V. If the zero-sequence voltage method was used under 2LS, the STATCOM outputs balanced current, as shown in Fig. 12. But the peak value of the STATCOM output voltage is about 8000 V. Thus, the STATCOM had to output high voltage and a wide margin of dc capacitor voltage was needed. As described before, the combination of two capacitor voltage method realizes reasonable circuit design and flexible function of the STATCOM.

IV. CONCLUSION AND FUTURE SCOPE

This paper presented a configuration and control scheme of cascaded H-bridge STATCOM in three-phase power system. We proposed a control method using zero-sequence voltage and negative-sequence current. The two methods are used exclusively depending on the extent of voltage unbalance. By this method, STATCOM can operate flexibly under normal power system condition and does not need wide margin of dc capacitor voltage under large asymmetrical condition. The validity is examined by digital simulation under one line and two-lines fault circuit condition. The simulation results showed the effectiveness of proposed STATCOM. In addition, proposed control scheme can be used for other type of applications, such as PV(photovoltaic) inverter systems. It expands applicable scope of cascaded H-bridge multilevel converter.

REFERENCES

- [1] F. Z. Peng, J. S. Lai, J. W. McKeever, and V. Coevering, "A multilevel voltage-source inverter with separate dc sources for static var generation," *IEEE Trans Ind. Appl.*, vol. 32, no. 5, pp. 1130–1138, Sep./Oct. 1996.
- [2] J. Arrillaga, Y. H. Liu, and N. R. Watson, *Flexible Power Transmission*. Hoboken, NJ: Wiley, 2007, pp. 158–160.
- [3] O. Alizadeh and S. Farhangi, "Voltage balancing technique with low switching frequency for cascade multilevel active front-end," presented at the 7th Int. Conf. Power Electronics, Daegu, Korea, Oct. 2007.
- [4] R. E. Betz and T. J. Summers, "Using a cascaded H-bridge STATCOM for rebalancing unbalanced voltages," presented at the 7th Int. Conf. Power Electronics, Daegu, Korea, Oct. 2007.
- [5] H. Akagi, S. Inoue, and T. Yoshii, "Control and performance of a transformerless cascade PWM STATCOM with star configuration," *IEEE Trans Ind. Appl.*, vol. 43, no. 4, pp. 1041–1049, Jul./Aug. 2007.
- [6] Q. Song, W. Liu, Z. Yuan, W. Wei, and Y. Chen, "DC voltage balancing technique using multi-pulse optimal PWM for cascade H-bridge inverters based STATCOM," in *Proc. IEEE 35th Power Electronics Specialists Conf.*, Aachen, Germany, Jun. 2004, vol. 6, pp. 4768–4772.
- [7] C. Cecati, A. Dell'Aquila, M. Liserre, and V. G. Monopoli, "A passivity-based multilevel active rectifier with adaptive compensation for traction applications," *IEEE Trans. Ind. Appl.*, vol. 39, no. 5, pp. 1404–1413, Sep./Oct. 2003.
- [8] C. Cecati, A. Dell'Aquila, M. Liserre, and V. G. Monopoli, "Design of H-bridge multilevel active rectifier for traction systems," *IEEE Trans. Ind. Appl.*, vol. 39, no. 5, pp. 1541–1550, Sep./Oct. 2003.
- [9] T. Fujii, S. Funahashi, N. Morishita, M. Azuma, H. Teramoto, N. Iio, H. Yonezawa, D. Takayama, and Y. Shinki, "A STATCOM for the Kanzaki substation," presented at the Int. Power Electronics Conf., Niigata, Japan, Apr. 2005.
- [10] M. H. J. Bollen, "Voltage recovery after unbalanced and balanced voltage dips in three-phase system," *IEEE Trans. Power Del.*, vol. 18, no. 4, pp. 1376–1381, Oct. 2003.
- [11] N. Hatano and T. Ise, "A configuration and control method of cascade H-bridge STATCOM," presented at the IEEE Power Energy Soc. General Meeting, Pittsburgh, PA, Jul. 2008.

Gecko Stick

Pramod Murali Mohan¹, Sagar Ayare², Sandesh Pai³

¹(Mechanical Engineering, Visvesvaraya Technological University, India

^{2, 3}(Electronics & Telecommunication Engineering, Mumbai University, India

ABSTRACT : Irony of nature's incredible fact's led us to delineate about a remarkable natural capability of Gecko, a type of lizard. This paper dwells around the anatomy of Gecko's foot whose capability of sticking and clinging to any surface whether vertical or upside down and walking over. This has led the scientists around the world to captivate its supernatural qualities and implement it in today's world. The paper also outlines about its application in today's world carving out niche technology on various frontiers.

Keywords: Setae, Spatulae, van-der Waals force, geckel, lithography.

I. INTRODUCTION

Being able to climb like spider man is every child's fantasy. But today's technology is only one step behind from achieving this due to GECKOSTICK. The term geckostick is derived from the gecko which actually is a species of lizards.

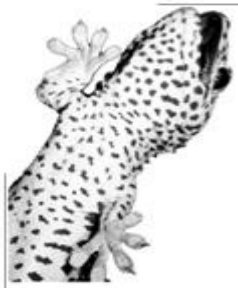


Fig. 1 Gecko

Geckos are a superhero's envy when it comes to their ability to climb rapidly up just about any vertical surface. Unlike other climbing animals and insects, the small lizards have no need for suction cups, velcro-like hooks, electrostatic attraction or sticky secretions.

Despite a century of anatomical studies, nobody could ever figure out just how the lizard does it. Now, researchers at the University of California at Berkeley, Stanford University and Lewis & Clark College in Portland, Ore., are taking interest on these species and their remarkable ability to climb any kind of surfaces.

II. GECKO FOOT STRUCTURE

Researchers have discovered that a gecko uses an elaborated array of toe hairs that form intermolecular bonds with the surface as it walks. Gecko uses these intermolecular bonds to climb a vertical wall, stick upside down or even cling to polished glass

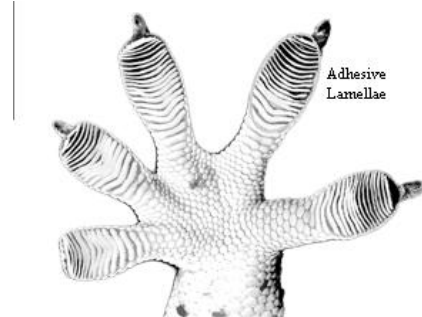


Fig. 2 Gecko's Foot

Each five-toed foot of the GECKO has about 500,000 microscopic foot-hairs called ``**SETAE**``. Each seta is no more than about 5 microns in diameter –i.e. about one-tenth the diameter of a human hair. These setae are lined up in rows on the gecko's toes.

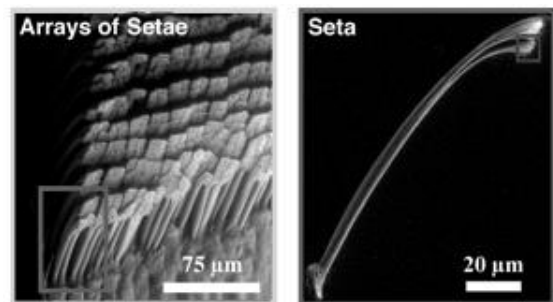


Fig. 3 Setae

Further each of this single seta divided to form an array of split ends which are bunch of 400 to 1,000 tiny structures. These submicroscopic, funnel-shaped pads, or spatula as it is called, measure about 200 nanometers.

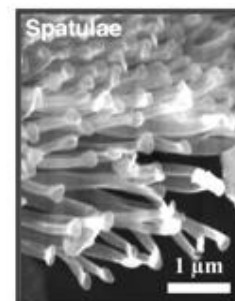


Fig. 4 Spatulae

These spatulae, numbering perhaps a billion per gecko, are around 10 millionths of an inch across, and when spread out, begin to interact with a surface at a molecular level.

III. GECKO'S ADHESION

The gecko moves with a peculiar motion of curling and uncurling its toes, up to 15 times a second.

A climbing gecko moves in such a way that when it presses a foot down, the toe hairs splay out and the spatulae spread out. This allows the spatulae to get extraordinarily close to the target surface so that subtle intermolecular attractions initiate. Essentially, the lizards may be grabbing onto walls with the same atomic-scale "glue", known as van der Waals forces, that make enzymes biochemically "sticky."

The gecko tries to find the proper angle and pressure by moving its toes. The adhesive force of one spatula may not amount to much, but collectively they generate an impressive force. As the gecko begins curling its feet again, an angle of around 30 starts to break the molecular force and the bond is released, leaving no residue.

IV. 'VAN-DER WAALS' FORCES

In physical chemistry, the **Van der Waals** force is the attractive or repulsive forces between molecules (or between parts of the same molecule) other than those due to covalent bonds or to the electrostatic interaction of ions with one another or with neutral molecules.

The ability of geckos to climb on sheer surfaces is due to van der Waals force. These "van der Waals" forces arise when unbalanced electrical charges around molecules attract one another. The cumulative attractive force of billions of setae allows geckos to scurry up walls and even hang upside down on polished glass. The reptile's grip is only released when it peels its foot off the surface.

V. ARTIFICIAL SATAE

Inspired by the remarkable hairs that allow geckos to hang single-toed from steep walls and scamper along ceilings, a team of researchers led by engineers at the University of California, Berkeley, has created an array of synthetic micro-fibers that uses very high friction to support loads on smooth surfaces i.e. 'geckel'.

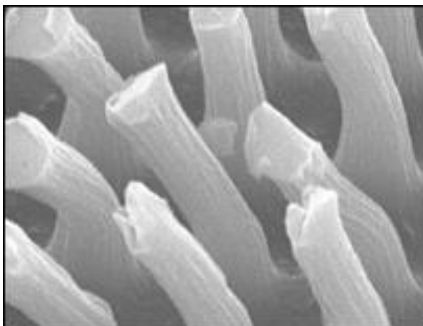


Fig. 5 Geckel is composed of millions of mushroom-shaped hairs

Each synthetic fiber in geckel is made from a material called kapton having dimensions same as gecko hairs. The hair-covered tape is made using a mould created by a lithographic process.

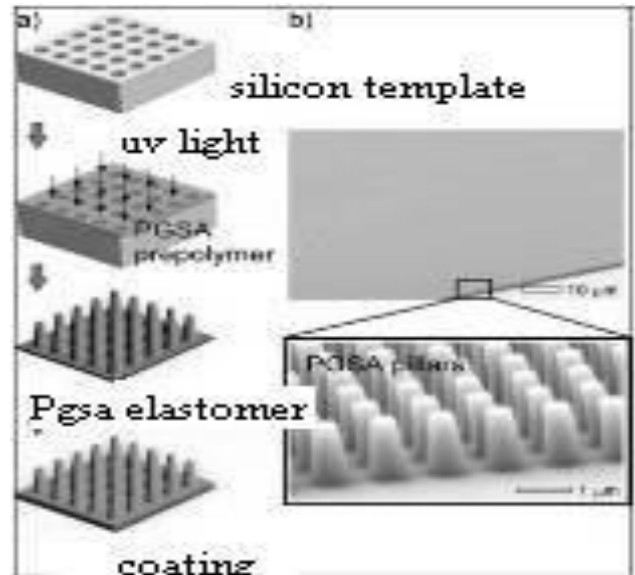


Fig. 6 Process of lithography

A piece of tape one centimeter square holds around 100 million of these artificial setae and could support a weight of one kilogram. Its staying power comes from coating fibrous silicone, similar in structure to a gecko's foot, with a polymer that mimics the "glue" used by mussels.

Unlike other adhesives inspired by the nimble reptiles, "geckel" can attach to both wet and dry surfaces and even in vacuums.

Tests showed that the material could be stuck and unstuck more than 1,000 times, even when used under water. The researchers said that other materials had only demonstrated "a few contact cycles". Removing the polymer coating drastically reduced its efficiency.

VI. APPLICATIONS

The adhesion of the gecko finds its applications in various fields especially in medical and technology field. Scientists just can't resist trying to copy the remarkable way these animals stick to walls using feet covered in millions of microscopic hairs. Moreover the fact that gecko adhesion works in a vacuum means the system could be used for space works.

A. Mecho-Gecko:

One small step for a gecko is proving to be one giant leap for robot designers. iRobot has built gecko-inspired robots called 'Mecho-gecko'.

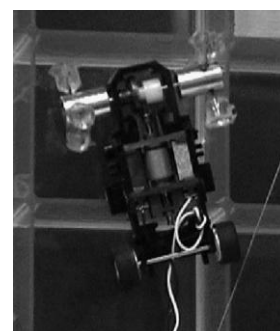


Fig. 7 Mecho-Gecko

The Mecho-Gecko's three legs are tipped with a pressure-sensitive adhesive to mimic the unroll-and-peel-off manner in which geckos climb.

B. Stickybot:

Stickybot, developed by Mark Cutkosky and his team at Stanford University in California, has feet with synthetic setae made of an elastomer. These tiny polymer pads ensure a large area of contact between the feet and the wall, maximizing the van-der Waals stickiness.



Fig. 8 Stickybot

The Pentagon is interested in developing gecko-inspired robots. A Stickybot-type robot would also make an adept planetary rover or rescue bot.

C. Robot crawlers:

Robot crawlers, used in aviation to check for flaws or defects, currently use suction to attach themselves to the wings or fuselage, but they also have hoses and other peripherals attached. 'Synthetic Gecko' would eliminate the need for this.

D. Disaster Rovers:

After the big earthquake hits, emergency responders must have the superhero-like skills of the gecko for keeping them safe from collapsing buildings as they try to find survivors.

Robots inspired by the gecko's multi-purpose tail and incredible sticky feet could be the first ones to explore the unstable, potentially dangerous rubble in search of life, saving time and the lives of rescuers.

E. Biodegradable tape:

- Biodegradable tape could replace surgical sutures and staples.
- It could also be used to deliver drugs to organs, including the heart.
- The tape could be laid down in one motion, potentially shortening patients' time in surgery.
- It could also help doctors during laparoscopic surgeries, which are performed through a small incision.
- The tape might also be used to reinforce sutures and staples used when a segment of the gastrointestinal tract is removed during gastric bypass surgery.

- The tape could release drugs that promote healing as it seals the incision.
- After heart attacks, patients often have regions of damaged tissue that don't get enough oxygen. This can lead to heart failure. Injecting a stem-cell-attracting factor encourages tissue regeneration, but sticking needles into the heart is dangerous. A patch of medical tape might deliver these factors at lower risk.

F. Parking:

A patch of the material one-meter-squared would hold the weight of a family-sized car.

G. Athletics:

From this type of material we can also make super-grip shoes for athletes.

H. Automobiles:

Tyres could be made that can hold the road better in all weathers.

I. Geckobot

Inspired by the unparalleled characteristic of gecko i.e. Stickiness of its spatula, over a decade research and development is being carried out to build Geckobot- A climbing Robot. This is built using simple features using Peeling mechanism, stable climbing of bots using active tail for centre of gravity balance during its ascent and descent.[1,2]

For these geckobot to stick to the surface different attachment methods have been employed over a period,

1. Suction adhesion
2. Magnetic adhesion
3. Grasping technique

Of the late, recently evolved mechanism is Passive attachment mechanism. The typical Tokay gecko weighs 300g and 35cm in length has a footpad of fibrillar dry adhesive. The geckobot's footpad is built with synthetic dry adhesive to achieve this passive attachment mechanism.[3]

A typical rough surface has an average roughness value of 10, in which case the contact area of the mating surface is very small. For better adhesion the mating surface area has to be divided into minute contact areas. Surface Energy method can be employed to gauge the adhesion force in-order to calculate the effect of division of contacts.

Based on the Johnson-Kendall-Roberts (JKR) theory the spatula of a gecko is considered as a hemisphere of radius R . The adhesion force of a single contact is F_{ad} given by:[4]

$$F_{ad} = \frac{3}{2} \pi W_{ad} R, [4]$$

Where W_{ad} is the work of adhesion (energy per unit area).

Based on the principal of contact splitting, for a constant area and 'n' number of spatula, the radius of one spatula

$$R' = R / \sqrt{n}.$$

The total adhesion force for the multiple contacts

$$F_{ad}' = F_{ad} * n = \frac{3}{2} * \pi * W_{ad} * R' * n = \frac{3}{2} * \pi * W_{ad} * \frac{R}{\sqrt{n}} * n = F_{ad} * \sqrt{n}.$$

In order to realize the relation a bit more in depth let us consider three case studies which helps us visualizing the variation of adhesion force, energy required per unit area and the radius of spatula.

For this let us consider three cases as mentioned below:

Case 1:

Let us consider the number of contacts i.e. spatula varies in steps for 200 from 200 to 1000. The radius of spatula varies from 0.1μm to 0.5 μm in steps of 0.05 μm. Let the energy required per unit area be unity. The figure 1 depicts the adhesion force vs radius of spatula plotted against the number of contacts.

Case 2:

The radius of spatula varies from 0.1μm to 0.5 μm in steps of 0.05 μm. Let the energy required per unit area be unity. The adhesion force required varies from 5μN-50μN in steps of 5μN. The figure 2 shows the variation of energy required per unit area vs the adhesion force plotted against the different radius of spatula.

Case 3:

Let us consider the number of contacts i.e. spatula varies in steps for 200 from 200 to 1000. The adhesion force required varies from 5μN-50μN in steps of 5μN. The figure 3 shows the variation of total adhesion force vs number of spatula plotted against single contact adhesion force required.

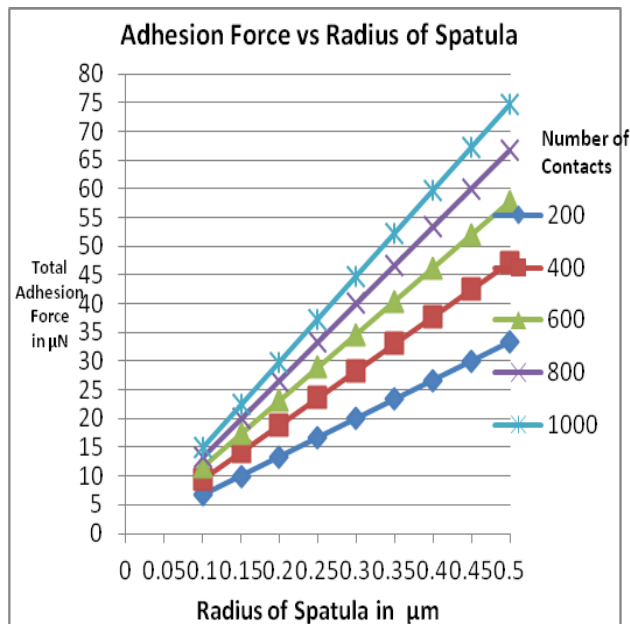


Fig. 7 Adhesive Force vs Radius of Spatula

From the above figure it is clearly evident that the adhesion force linearly varies with the radius of spatula.

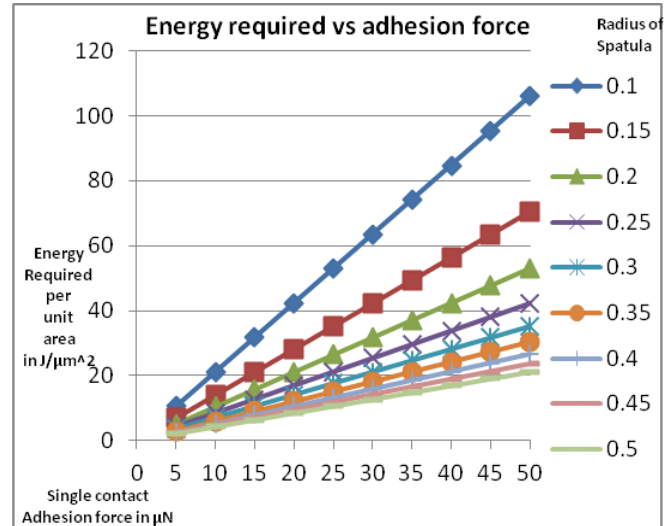


Fig. 8 Energy required vs adhesive force

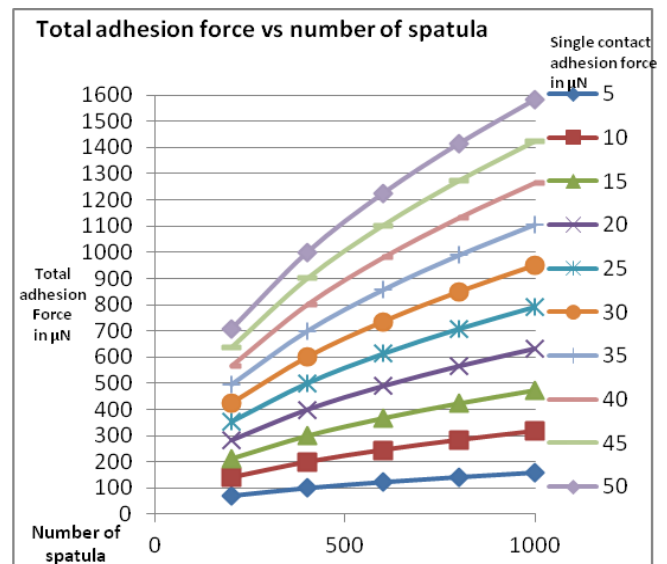


Fig. 9 Total adhesive force vs number of spatula

VII. Discussion

- The adhesion force varies linearly with radius of spatula and energy required per unit area.
- The total adhesion force varies exponentially with multiple contact points.
- These case studies give us a glimpse of adhesion force exerted by the gecko footpad for their movement. This study can be carried out further for the synthetic dry adhesive of different material by applying JKR theory, Derjaguin-Muller-Toporov Hypothesis, Maugis and Barquins Models.
- The charisma of this geckobot is its ability of independency, safe sticking and walking mechanism for enriched job skill.
- To built a geckobot an extensive analysis has to be carried out before building a virtual prototype of Gecko and testing it. This involves structural, thermal, dynamic, kinematics analysis. Later the life cycle testing and evaluation has to be carried out on the prototype to check the feasibility and performance.
- These Geckobot are built as scaled climbing robots employed for many applications such as wall cleaning, Boiler drum cleaning in thermal power

plant, rescue of people, exploration of hazardous places, analysis of navy dock.

- This is just one of the application that's been cited by studying the natural aspects of a gecko-foot.

VIII. CONCLUSION

The advent of geckos has proved to be a boon in both the technological and medical fields, hence opening a new horizon. This shows that Nature is awe-inspiring. There is so much engineering knowledge to be gained from studying biological systems. One as Gecko led us to ruminate about its application in various fields. Recent advents have taken place in Nanotechnology based on this gecko-foot sticky concept.

References

- [1] Gecko, a climbing robot for walls cleaning, F. Cepolina, R.C. Michelini, R.P. Razzoli, M. Zoppi, PMAR Lab – Dept. of Mechanics and Machine Design, University of Genova, Via all'Opera Pia 15/A. 16145 Genoca, Italy submitted at 1st Int.Workshop on Advances in service Robotics ASER03, March 13-15, Bardolino, Italia,2003.
- [2] Design and Analysis of Gecko-like Robot by MENG Cai, WANG Tianmiao, GUAN Shengguo, ZHANG Long, WANG Jing, and LI Xiaohu at CHINESE JOURNAL OF MECHANICAL ENGINEERING Vol. 24, No. *, 2011.
- [3] Geckobot: A Gecko Inspired Climbing Robot Using Elastomer Adhesives by Ozgur Unver, Ali Uneri, Alper Aydemir and Metin Sitti, Department of Mechanical Engineering, Carnegie Mellon Univesity, Pittsburgh.
- [4] Surface forces and their contribution to adhesion and adherence in glass fibre-reinforced polymer composited – A thesis submitte to the faculty of Mechanical Engineering of the University of Technology Dresden (Germany) by Victoria Dutschk for the PhD degree Mai, 2000.
- [5] Autumn, Kellar;. (2002). "Evidence for van der Waals adhesion in gecko setae".
- [6] Lee, Haeshin; Lee, Bruce P.; Messersmith, Phillip B. (2007). "A reversible wet/dry adhesive inspired by mussels and geckos"
- [7] A.J. Kinloch, Adhesion and Adhesives: Science and Technology, Chapman and Hall, 1987

GA Based Multi-Objective Time-Cost Optimization in a Project with Resources Consideration

Sultana Parveen,¹ Surajit Kumar Saha,²

¹ Associate Professor, Department of Industrial and Production Engineering, Bangladesh University of Engineering and Technology, Dhaka, Bangladesh.

² Post-Graduate Student, Department of Industrial and Production Engineering, Bangladesh University of Engineering and Technology, Dhaka, Bangladesh.

ABSTRACT: Project planner's main goal is to complete project with minimal time as well as minimal cost. Much effort (e.g. resources which demand cost) is required to complete the project in shorter time. There is a trade-off relationship between activity duration and its resources. This study employed a GA based multi-objective approach for time-cost trade-off using resources-time tradeoff as input. Combining with modified adaptive weight approach (MAWA), this proposed optimization model can find out best optimal solution and Pareto front which provides flexibility to planners and decision makers in making efficient time-cost decisions. This proposed model was developed in MATLAB and applied to test problems. However, it is illustrated that this model could be useful to solve bigger networks in practice.

Key words: Critical path method (CPM); Time-cost trade-off problem (TCTP); Resources-time trade-off; Multi-objective optimization; Genetic algorithm (GA).

I. Introduction

A project is a group of activities. According to precedence relationship of the activities project planner has to plan the execution order to complete the project. So, all activities are arranged in a network using arrows and nodes, maintaining their logical sequence. Among the paths a critical path is the longest continuous path which defines the total project time. Hence, critical path method (CPM) is widely recognized project planning and scheduling tool which deals with deterministic time duration of activities to schedule the project.

In a project, there are three major elements, such as project duration, project cost and resources. These are depended to each other. The activity duration is a function of resources (i.e. crew size, equipments and materials) availability. On the other hand, resources demand direct costs. Therefore, the relationship between project time and direct cost of each activity is a monotonously decreasing curve. It means if activity duration is compressed then there is leading to an increase in resources and so that direct costs. But, project indirect costs increase with the project duration. Hence, relationship between project time and cost is trade-off (Geem, 2010). So, in a project it needs multi-objective approach to minimize both projects time and cost by varying options of the critical activities.

Traditionally, time-cost trade-off problem (TCTP) is a deterministic scheduling problems, it is assumed that all data are available. Several mathematical models such as linear programming (Kelly, 1961; Hendrickson and Au, 1989; Pagnoni, 1990), integer programming, or dynamic programming (Butcher, 1967; Robinson, 1975; Elmaghraby, 1993; De, Dunne and Wells, 1995) and LP/IP hybrid (Liu, Burns and Feng, 1995; Burns, Liu and Feng, 1996) models are used to solve TCTPs. Meyer and Shaffer (1963) and Patterson and Huber (1974) use mixed integer programming. However, for large number of activity in network and complex problem, integer programming needs a lot of computation effort (Feng, Liu and Burns, 1997). Since, these are suitable for small project.

Some heuristic models, such as Fondahl's (1961) method, effective cost slope model of Siemens (1971), structural stiffness model (Moselhi, 1993) and structural model (Prager, 1963) could only optimize one objective at a time but the solution is not guaranteed to be the global optimal (Xiong and Kuang, 2008). Li and Love (1997) and Hegazy (1999) introduced GA to solve deterministic TCT problems, but yet remained as a single-objective optimization tool.

Some researchers have tried to introduce evolutionary algorithms to find global optima such as genetic algorithm (GA) (Feng, Liu and Burns, 1997; Gen and Cheng, 2000; Zheng, Ng and Kumaraswamy, 2004) the particle swarm optimization algorithm (Yang, 2007), ant colony optimization (ACO) (Xiong and Kuang, 2008; Ng and Zhang 2008) and harmony search (HS) (Geem, 2010). The model of Feng, Liu and Burns (1997) might be inefficient to obtain optima for the large TCT problem. Gen and Cheng (2000) and Zheng, Ng and Kumaraswamy (2004) have drawback that they may be entrapped into local optima for TCT problems.

In this study another evolutionary algorithm, genetic algorithm is induced to solve TCT problem incorporating modified adaptive weight approach (MAWA) (Zheng, Ng and Kumaraswamy, 2004). Moreover, this study has used discrete relationship between activity time and resources except relationship between activity time and cost to find optima in TCT problem. Penalty for delay above the desired project completion time is also added for TCT in this study. When compared with models of Gen and Cheng (2000) and Zheng, Ng and Kumaraswamy (2004), the new model saved fittest solution of each generation in fittest table and evaluated performances of them again to obtain best optimal solution. Finally, this proposed algorithm solved two example test cases and found out best optimal solutions and Pareto set solutions.

II. Problem Formulation

In TCT problems, there are twin objectives-minimize both project time and cost. The durations of each activity and their corresponding resources (i.e. crew sizes, equipments and materials) are included to measure direct costs in present project cost function.

$$C = \sum_{i=1}^l \sum_{j=1}^r C_{dij} + C_{id} \quad 1$$

Where, C is the total project cost, C_{dij} the direct cost of resources type j at activity i, C_{id} the indirect cost of project, r total number of resource types and l the total number of activity.

For any type of resource at any activity, the direct cost depends on whether the number required exceeds that available limit (Supply limit). When demanded resource is available, the normal cost rate of that resource is applied. However, if the activity requires more than available limit of resource the extra premium cost rate is added for each extra unit of resource. Thus,

$$C_{dij} = R_{ij}^r \times M_{ij} \times t_i + P_{ij} \times t_i \times (R_{ij}^r - R_{ij}^n) \quad 2$$

Where, R_{ij}^r is number of resource type j required by activity i on time t, R_{ij}^n the number of resource type j of activity i on time t available at normal condition, M_{ij} the cost rate of resource type j of activity i, P_{ij} the premium rate of resource type j of activity i above normal condition and t_i the time of activity i.

The premium is added when number of resources j of activity i exceeds of availability, so that the P_{ij} is given by

$$P_{ij} = \begin{cases} V_{ij} - M_{ij}, & R_{ij}^r > R_{ij}^n \\ 0, & R_{ij}^r \leq R_{ij}^n \end{cases} \quad 3$$

Where, V_{ij} is the cost rates of resources type j at activity i above normal availability limit.

The indirect cost of project C_{id} depends on total project time and desired project time, thus

$$C_{id} = T \times C_L + D \times (T - T_a) \quad 4$$

$$D = \begin{cases} C_p, & T > T_a \\ 0, & T \leq T_a \end{cases} \quad 5$$

Where, C_L the indirect cost rate, C_p the delay fine rate for unit time delay and desired project time T_a . If the project duration is more than the desired project duration, then delay fine will be added.

The total project time T is given by

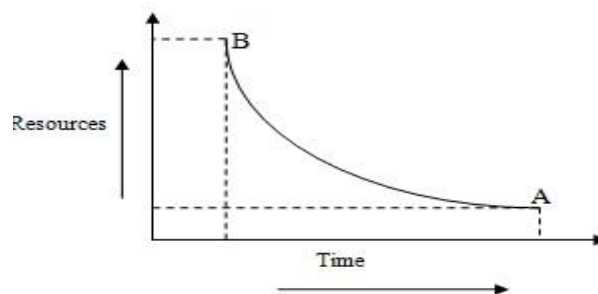
$$T = \max \{EST_i + t_i \mid i = 1, 2, \dots, l\} \quad 6$$

Where, EST_i the earliest starting time of activity i.

The objective functions for TCTP are Eq. (1) and (6), to minimize project cost, C and time. Eq. (6) is also used to find the critical path and total duration of the project.

For TCTP, resources-time trade-off curve acts as input in this study shown in Figure 1 which was originally developed by (Chua, Chan and Govinda, 1997). The curve was developed from a consideration of varying of resources such as crew sizes, equipments and materials, their productivity and cost rates. It is shown in Figure 1 that, resources of activity decreases with as activity duration increases. That means much resources (correlated direct cost) are required to complete the activity in shorter time. Hence, the purpose of this study is to minimize resources so that project cost of shorted schedule for TCT.

Figure 1 level of resources-time trade-off input.



III. Modified Adaptive Weight Approach

This study applies the modified adaptive weight approach (MAWA) proposed by Zheng, Ng and Kumaraswamy (2004) to deal with the multi-objective TCTPs. This utilizes some useful information from the current population to generate an adaptive weight for each objective, and thereby exerts a search pressure towards the ideal point. Under the MAWA (Zheng, Ng and Kumaraswamy, 2004), the adaptive weights are formulated through the following four conditions:

1. For $Z_c^{\max} \neq Z_c^{\min}$ and $Z_t^{\max} \neq Z_t^{\min}$,

$$v_c = \frac{Z_c^{\min}}{Z_c^{\max} - Z_c^{\min}} \quad 7$$

$$v_t = \frac{Z_t^{\min}}{Z_t^{\max} - Z_t^{\min}} \quad 8$$

$$v = v_c + v_t \quad 9$$

$$w_c = v_c / v \quad 10$$

$$w_t = v_t / v \quad 11$$

$$w_c + w_t = 1 \quad 12$$

2. For $Z_c^{\max} = Z_c^{\min}$ and $Z_t^{\max} = Z_t^{\min}$,

$$w_c = w_t = 0.5 \quad 13$$

3. For $Z_t^{\max} = Z_t^{\min}$ and $Z_c^{\max} \neq Z_c^{\min}$

$$w_c = 0.1, w_t = 0.9 \quad 14$$

4. For $Z_t^{\max} \neq Z_t^{\min}$ and $Z_c^{\max} = Z_c^{\min}$

$$w_c = 0.9, w_t = 0.1 \quad 15$$

Zheng, Ng and Kumaraswamy (2004) propose a fitness formula in accordance with the proposed adaptive weight:

$$f(x) = w_t \frac{Z_t^{\max} - Z_t + \gamma}{Z_t^{\max} - Z_t^{\min} + \gamma} + w_c \frac{Z_c^{\max} - Z_c + \gamma}{Z_c^{\max} - Z_c^{\min} + \gamma} \quad 16$$

Here, γ = random number (between 0 and 1).

Where, Z_c^{\max}, Z_t^{\max} = maximal value for the objective of total cost and time, respectively, in the current population; Z_c^{\min}, Z_t^{\min} = minimal value for the objective of total cost and time, respectively, in the current population; w_c, w_t = adaptive weights, respectively, on cost and time derived from the last generation, v_c, v_t = value for the criterion of cost and time respectively; v = value for the project; w_c = adaptive weight for the criterion of cost; and w_t = adaptive weight for the criterion of time, Z_c represents the total cost of the x th solution in the current population; Z_t represents the time of the x th solution in the current population.

IV. Genetic Algorithm

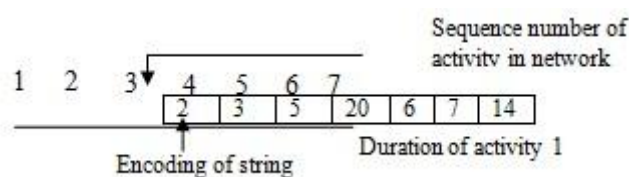
Genetic algorithms (GAs) are global search and optimization techniques modeled from natural genetics, and they explore the search space by incorporating a set of candidate solutions in parallel (Holland, 1975). GA for TCTP is used for selecting an optimal option to perform each activity of a project. This study applied simple GA for TCTP.

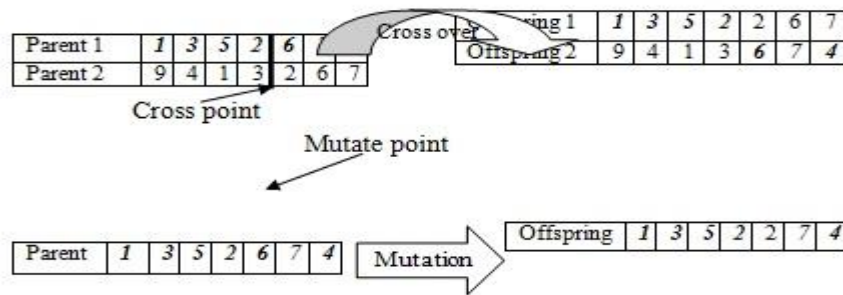
GAs procedure begins by generating an initial collection of random solutions that are encoded in the form of strings (or chromosome). A string is collection of genes which represent decision variables of problem. The number of string in population is referred to as population size. Strings are evaluated on their performances with respect to the fitness function in the population and fitter strings are selected by selection operator. Best strings exchange information and mutate to produce offspring chromosomes that are evaluated and can replace less fit member in the population to create new population for next generation. Thus, the best solutions are evolved through successive generation.

In TCTP perspective, each gene in the chromosome represents duration of an activity in the network. Crossover and mutation operations are performed to exploit and explore potential solution. In this study, single point crossover and uniform mutation are used. To evaluate the performance of strings Eq. (16) is used as a fitness equation (or objective function) in GA search.

GA is a robust and random search algorithm for TCTP. The GAs differ from conventional searching tools in that they operate on a set of solutions rather than a single solution, and hence multiple frontiers are searched simultaneously within a single run. This advantage makes GAs the most suitable searching engine for complicated multi-criteria optimization problems (Zheng and Ng, 2005).

Figure 2 Mechanism of GA.

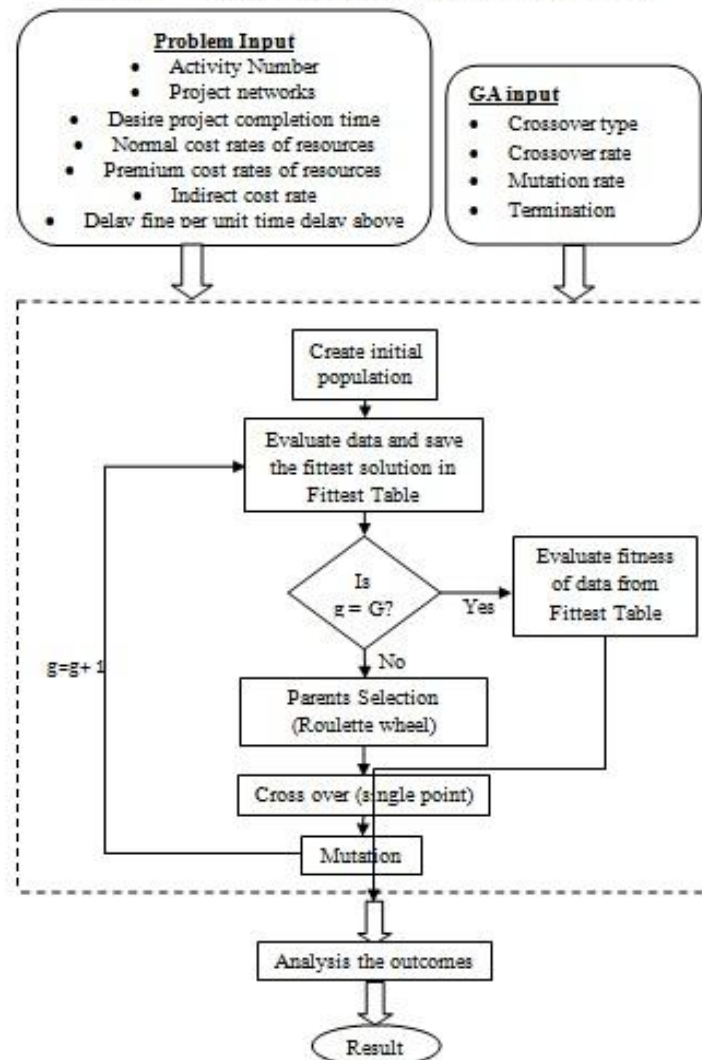




V. GA Based TCTP Solver

The operation of GA based model for TCTP is shown in Fig. 3. The proposed multi-objective time-cost optimization problem has been solved with genetic algorithm technique which is coded in MATLAB 7.7.0.471 (R2008b) and run on personal computer having Intel (R) Pentium (R) Dual CPU 2.80 GHz and 512 MB of RAM. One folder is created where inputs are given into text files. For each activity, one text file is used for time schedules and their corresponding resources and another text file is used for resource cost rates at available and above available limit and resources available limit. All GA parameters are inputted through dialogs.

Figure 3 Operation of the GA based model for TCTP



VI. Problem solving and results

6.1 Example 1

A project of seven activities is taken as an example which was derived by Zheng, Ng and Kumaraswamy (2004). Table 1 shows available activity options and corresponding durations and costs. This study was developed including the resources-time trade-off as input, so that the cost of each option was taken as resources to fit the case into the proposed

model. Indirect cost rate was \$1500/day. The robustness of the new proposed model in the deterministic situation was compared with two other previous models: (1) MAWA model (Zheng, Ng and Kumaraswamy, 2004) and (2) Gen and Cheng (2000) model.

Table 1 Options for seven activity example 1.

Activity Number	Precedent Activity	Option	Duration (days)	Direct cost (\$)
1		1	14	23,000
		2	20	18,000
		3	24	12,000
2	1	1	15	3,000
		2	18	2,400
		3	20	1,800
		4	23	1,500
		5	25	1,000
3	1	1	15	4,500
		2	22	4,000
		3	33	3,200
4	1	1	12	45,000
		2	16	35,000
		3	20	30,000
5	2,3	1	22	20,000
		2	24	17,500
		3	28	15,000
		4	30	10,000
6	4	1	14	40,000
		2	18	32,000
		3	24	18,000
7	5,6	1	9	30,000
		2	15	24,000
		3	18	22,000

Table 2 Results of example 1 of the three models

Models	Optimal solutions							
	Time (day)	Cost (\$)	Durations of activity (Day)					
Gen and Cheng (2000)	79	256,400	24	18	15	16	22	14 15
MAWA (Zheng, Ng and Kumaraswamy, 2004)	66	236,500	14	15	15	20	28	18 9
The new model	60	233500	14	15	15	12	22	24 9
	62	233000	14	15	15	20	24	18 9
	63	225500	14	15	15	16	24	24 9
	67	224000	14	15	15	20	28	24 9
	68	220500	14	15	15	20	30	24 9

The new model was able to find Pareto optimal front. Since, Gen and Cheng (2000) and Zheng, Ng and Kumaraswamy (2004) did not propose any Pareto front. Moreover, the finally obtained solutions by these two models as shown in table 2 respectively were not global optimal solutions. The new proposed model showed Pareto optimal solutions and best optimal solution (project time = 60 days and cost = \$233500) in Table 2.

6.2 Example 2

A hypothetical case of 8 activities was developed to fit into the proposed model. Here, activities had several options of time and resources. A detail of example 2 is shown in table 3. Delay fine (\$2500/day) was also added if project completion time is more than 50 days. Indirect cost rate of project was taken \$1000/day. The parameters of the GA model were selected to solve the example 2, such as the generation number = 1000, population size = 200, crossover rate = 0.2 and mutation rate = 0.5.

The proposed model found the Pareto front as shown in Table 4 and Figure 5. The result of project example 2 is shown in Figure 4. The best optimal solution was the solution of time= 47 days, cost= \$ 2.552×10⁵ and activity duration 7-6-7-15-5-9-10-3. The critical path of the best optimal solution is 1→3→4→5→7→8.

Table 3 Activity data of the project example 2.

Activity	Precedent activity	Time (days)	Resources (units/day)	Resources cost rates at available and above available limit (\$/unit/day) and available limit (units/day) respectively for each resources
1		6	10	7 19 400,500,7; 200,350,5;
		7	7	5 15 75,120,15
2	1	4	9	16 200,350,7; 125, 200,12
		6	7	10
		8	5	7
		9	4	6
3	1	7	13	9 200,350,9; 50,150,7
		9	9	6
		10	7	5
4	2,3	12	5	16 9 5 400,500,3; 200,350,10;
		15	3	10 6 2 70,200,12;
		18	2	8 4 2 120,160,3
5	4	5	15	300,500,12
6	3	5	20	12 200,350,15; 30,70,9
		7	15	8
		9	8	6
		12	6	5
7	2,5,6	9	17	200,350,14
		10	14	
8	7	3	4	200,350,2
		5	2	

Table 4 Pareto front for example 2.

Optimal solutions									
Time (days)	Cost (\$) (10 ⁵)	Durations of activities							
45	2.709	6	6	7	15	5	9	9	3
46	2.607	7	6	7	15	5	9	9	3
47	2.552	7	6	7	15	5	9	10	3
48	2.527	7	9	9	15	5	9	9	3
49	2.47	7	9	9	15	5	12	10	3
50	2.458	7	9	10	15	5	12	10	3

Figure 4 Results of example 2.

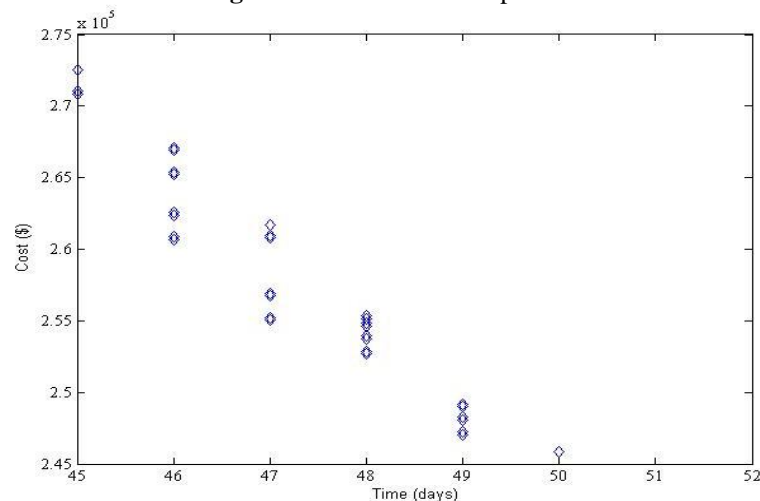
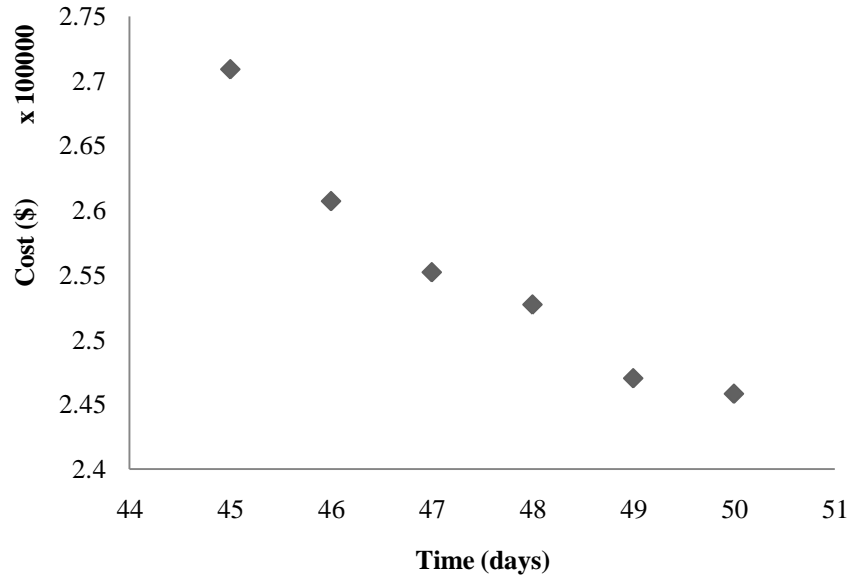


Figure 5 Pareto front of example 2.



VII. Conclusions

The GA based multi-objective time-cost trade-off problem solver was originally developed to minimize both project time and cost by assigning one optimal option of time and resources to each activity in the project network. Here, activity resources and time were directly used to calculate project cost. Incorporating MAWA, the TCTP solver integrated the project time and cost in single objective. Moreover, it was illustrated that this algorithm can define the Pareto front of the problem. So that, the decision maker gets options to solve project according to his desire. This GA based TCTP solver took much iterations but it was a robust and random searching algorithm so that it resisted the trials to entrap in local optima. Thereby, the development of the GA based multi-objective approach provides an efficient model to solving project time-cost optimization with resources consideration.

The performance of the presented model can be further analyzed in terms of number of iteration by comparing it with other best known algorithms for multi-objective TCT project scheduling. The algorithm can also be extended by considering limited resources time-cost trade-off with other different types of fuzzy numbers.

References

- [1] Burns, S.A., Liu, L. and Feng, C.W. (1996) 'The LP/IP hybrid method for construction time-cost trade-off analysis', *Constr. Manag. Econ.*, Vol. 14, No. 3, pp. 265-276.
- [2] Butcher, W.S. (1967) 'Dynamic programming for project cost-time curve', *Journal of Construction Division, ASCE*, Vol. 93 (C01), pp. 59-73.
- [3] Chua, D.K.H., Chan, W.T. and Govinda, K. (1997) 'A time-cost trade-off model with resource consideration using genetic algorithm', *Civil. Eng. Syst.*, Vol. 14, pp. 291-311, 1997.
- [4] De, P., Dunne, E. J. and Wells, C. E. (1995) 'The discrete time-cost trade-off problem revisited', *Eur. J. Operational Res.*, Vol. 81, pp. 225-238.
- [5] Elmaghraby, S. E. (1993) 'Resource allocation via dynamic programming in activity networks', *Eur. J. Operational Res.*, Vol. 64, pp. 199-215.
- [6] Feng, C.W., Liu, L. and Burns, S.A. (1997) 'Using genetic algorithms to solve construction time-cost trade-off problems', *Journal of Computing in Civil Engineering, ASCE*, Vol. 11, No. 3, pp. 184-189.
- [7] Fondahl, J. W. (1961) *A non-computer approach to the critical path method for the construction industry*, Technical Report No. 9, The Construction Institute, Department of Civil Engineering, Stamford University.
- [8] Geem, Z. W. (2010) 'Multiobjective optimization of time-cost trade-off using harmony search', *Journal of Construction Engineering and Management, ASCE*, Vol. 136, No. 6, pp. 711- 716.
- [9] Gen, M. and Cheng, R. (2000) *Genetic Algorithms & Engineering Optimization*, Wiley-Interscience, New York.
- [10] Hegazy, T. (1999) 'Optimization of construction time-cost trade-off analysis using genetic algorithms', *Canadian Journal of Civil Engineering*, Vol. 26, No. 6, pp. 685-697.
- [11] Hendrickson, C. and Au, T. (1989) *Project Management for Construction*, Prentice-Hall, Inc., Englewood Cliffs, N.J.
- [12] Holland, J.H. (1975) *Adaptation in Natural and Artificial Systems*, University of Michigan Press, Ann Arbor.
- [13] Kelly, James, E. Jr. (1961) 'Critical path planning and scheduling: mathematical basis', *Oper. Res.*, Vol. 9 no. 3, pp. 167-179.
- [14] Li, H. and Love, P. (1997) 'Using improved genetic algorithms to facilitate time-cost optimization', *Journal of Construction Engineering and Management, ASCE*, Vol. 123, No. 3, pp. 233-237.
- [15] Liu, L., Burns, S.A. and Feng, C. (1995) 'Construction time-cost trade-off analysis using LP/IP', *Journal of Construction Engineering and Management, ASCE*, Vol. 121 (4), pp. 446-454.
- [16] Mayer, W. L. and Shaffer, L.R. (1963) 'Extension of the critical path method through the application of integer programming', *Civ. Engrg. Constr. Res. Ser. 2*, Univ. of Illinois, Urbana, III.
- [17] Moselhi, O. (1993) 'Schedule compression using the direct stiffness method', *Canadian Journal of Civil Engineering*, Vol. 20, No. 1, pp. 65-72.

- [18] Ng, S. T. and Zhang, Y. (2008) 'Optimizing construction time and cost using ant colony optimization approach', *Journal of Construction Engineering and Management, ASCE*, Vol. 134, No. 9, pp. 721-728.
- [19] Pagnoni, A. (1990) *Project Engineering: Computer Oriented Planning and Operational Decision Making*, Springer, Berlin.
- [20] Panagiotakopoulos, D. (1977) 'Cost-time model for large CPM project networks', *Journal of Construction Engineering and Management, ASCE*, Vol. 103 (C02), pp. 201-211.
- [21] Patterson, J. H. and Huber, D. (1974) 'A horizon-varying, zero-one approach to project scheduling', *Mgmt. Sci.*, Vol. 20, No. 6, pp. 990-998.
- [22] Prager, W. (1963) 'A structured method of computing project cost polygons', *Manage. Sci.*, Vol. 9, No. 3, pp. 394-404.
- [23] Robinson, D. R. (1975) 'A dynamic programming solution to cost-time tradeoff for CPM', *Mgmt. Sci.*, Vol. 22, No. 2, pp. 158-166.
- [24] Siemens N. (1971) 'A simple CPM time-cost trade-off algorithm', *Management Science*, Vol. 17, No. 6, pp. B-354-OB-363.
- [25] Xiong, Y. and Kuang, Y. (2008) 'Applying an ant colony optimization algorithm-based multiobjective approach for time-cost trade-off', *Journal of Construction Engineering and Management, ASCE*, Vol. 134, No. 2, pp. 153- 156.
- [26] Yang, I.T. (2007) 'Using elitist particle swarm optimization to facilitate bicriterion time-cost trade-off analysis', *J. Constr. Eng. Manage.*, Vol. 133, No. 7, pp. 498-505.
- [27] Zheng, D. X.M., Ng, S.T. and Kumaraswamy, M.M. (2004) 'Applying a genetic algorithm-based multiobjective approach for time-cost optimization', *Journal of Construction Engineering and Management*, Vol. 130, No. 2, pp. 168-176.
- [28] Zheng, D. X. M. and Ng, S. T. (2005) 'Stochastic time-cost optimization model incorporating fuzzy sets theory and nonreplaceable front', *Journal of Construction Engineering and Management, ASCE*, Vol. 131, No. 2, pp. 176- 186.

Structural Analysis of Partitioned Vertical Column

Nitin V. Titave¹, Dr. Satishchandra V. Joshi², Vinay Patil³

¹ (Master of Engineering (Mech. Design Engg.) Student of DYPCOE, Akurdi, University of Pune, India

² (Principal, DYPCOE, Akurdi, University of Pune, India

³ (Department of CAE, Vaftsy CAE, Pune, India

Abstract: Research work in the area of Vertical storage column, used in Ammonium Nitrate pyrolysis Process plant, where in required to design a tall vertical pressure vessel having three partitions, each partition is subjected to different pressures and materials. Evaluation of partitions in partitioned pressure vessel has to be done to know performance of vessel under different pressure condition and ensure structural stability of the system

This paper focuses on Finite Element Analysis of partitioned vertical storage column subjected with given pressure loading condition.

Keywords: Finite Element Analysis [FEA], structural analysis, partitioned vertical column

I. INTRODUCTION

A pressure vessel is a closed container designed to hold gases or liquids at a pressure substantially different from the ambient pressure. The pressure differential is dangerous and many fatal accidents have occurred in the history of their development and operation. Consequently, their design, manufacture, and operation are regulated by engineering authorities backed up by laws. For these reasons, the definition of a pressure vessel varies from country to country, but involves parameters such as maximum safe operating pressure and temperature. [1]

1.1 Process Information:

Pyrolysis is a process, in which Nitrous Oxide is obtained by thermo chemical decomposition of Ammonium Nitrate at elevated temperatures in the absence of oxygen. Ammonium Nitrate pyrolysis synthesis is an exothermic reaction occurring at 200 deg C. Nitrous Oxide generated has lot of Impurities like Ammonium Nitrate fumes, Nitrogen, Other oxides of Nitrogen & Steam. These impurities are removed by washing or Scrubbing, which is a 3 stage process. In first stage, steam gets condensed by water scrubbing, In second stage, residual traces of ammonium nitrate are removed by caustic scrubbing. Finally in third stage, Ammonia gas generated by caustic scrubbing is removed by Acid Scrubbing.

1.2 Objectives of study:

Objectives of study are as follows:

- A detailed understanding of function and configuration of pressure vessel.
- Modeling of partitioned pressure vessel shell
- Finite Element Analysis of model using Ansys.
- Strength enhancement in concern areas of base line design using Ansys.

- Integration of three stages of scrubbing in a single vessel by using partitions

1.3 Types of Non-Linearities:

Nonlinear structural behavior arises from a number of causes, which can be grouped into three principal categories. Contact Nonlinearities are Situations in which contact occurs are common to many different nonlinear applications. Contact forms a distinctive and important subset to the category of changing-status nonlinearities^[2]

Geometric Nonlinearities occurs, if a structure experiences large deformations, its changing geometric configuration can cause the structure to respond nonlinearly.^[2] Material Nonlinearities, when Nonlinear stress-strain relationships are a common cause of nonlinear structural behavior. Many factors can influence a material's stress-strain properties environmental conditions, and the amount of time that a load is applied.^[3]

II. DESIGN SPECIFICATIONS

2.1 Design Specifications:

Three partitions are equispaced and held in place by use of inner shell. Ratio of Inner radius of outer shell and inner radius of Inner shell to be maintained as per 4.5m/2m (Inner shell radius varies between 0.5 m to 2m).

2.2 Material Properties:

The material used for pressure vessel is structural steel (SA 516 Gr 70) and standard properties are:

E= Modulus of elasticity = $2.01 \times 10^{11} \text{ (N/ m}^2\text{)}$

ν = Poisson's ratio = 0.23

Ultimate Tensile strength: 340 MPa

Yield strength: 240 MPa at 27°C temperature

Factor of safety: 1.5

Working Pressure-0.14 Mpa

Analysis performed for two of three compartments are fully occupied to design pressure conditions.

Table 1 shows basic information of overall dimensions of partitioned pressure vessel and the data for analysis

Component thicknesses shown in Table 1 are derived from calculations using ASME 2007 section-VIII, Div-2.^{[4], [5]}

Table1

Dimensions of partitioned vertical column

III. FINITE ELEMENT ANALYSIS

Ansys 12 is used to carry out Analysis. The steps involved in Finite Element Analysis of partitioned Vertical Column are Modeling, Meshing, Applying boundary conditions & solving problem with static structural analysis and this is discussed in detailed manner in this section.

3.1 Modeling:

Fig 1 shows the 3-D model of Partitioned vertical Column. It is created in CAD software Pro-E, and then exported in IGES format for further analysis in ANSYS workbench.

Sl. No.	Parameters	Units	Value
1	Diameter of Vessel External cylinder (d1)	mm	9000
2	Diameter of Vessel Internal cylinder (d2)	mm	4000
3	Vessel Vertical Height	mm	21000
4	Vessel Skirt Height	mm	3000
5	Vessel Top (Flat)	mm	132
6	Vessel Base (Flat)	mm	132
7	Vessel Shell Thickness	mm	102
8	Vessel Skirt Support Thickness	mm	102
9	Partition Thickness	mm	102
10	Design Temperature	deg. C	27°C
11	Angle between each partition	deg.	120°
12	Vessel External cylinder thickness	mm	102
13	Vessel Internal cylinder thickness	mm	102

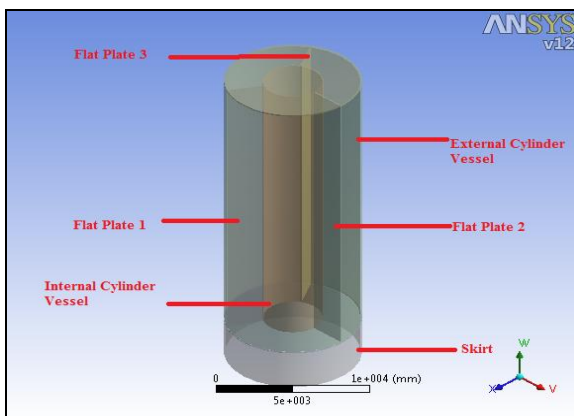


Fig 1: 3-D model of Partitioned vertical column

3.2 Meshing:

Fig.4 shows meshing of model. Assembly model is meshed with 20 node tetrahedron SOLID 186. It is a higher order 3-D 20-node solid element that exhibits quadratic displacement behavior. The element is defined by 20 nodes having three degrees of freedom per node: translations in the nodal x, y, and z directions. The element supports plasticity, hyper elasticity, creep, stress stiffening, large deflection, and large strain capabilities. It also has mixed formulation capability for simulating deformations of nearly incompressible elasto-plastic materials, and fully incompressible hyper elastic materials. [6]

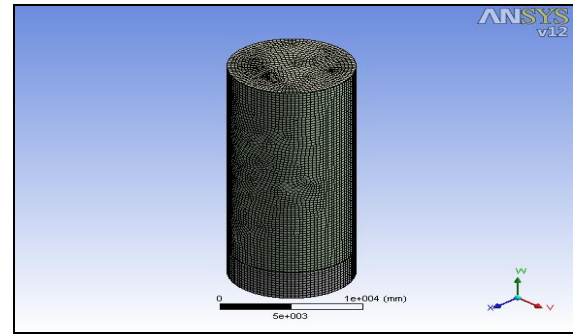


Fig.2: Meshing of Partitioned Vertical Column

3.3 Boundary conditions:

Fig. 3 shows boundary conditions applied to partitioned vertical column, Skirt support is fixed to ground. Internal pressure is acting on vessel wall, partition walls, Flat Top and bottom head and also force due to gravity

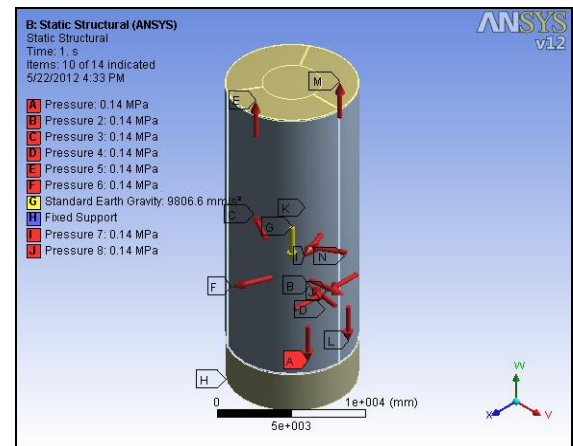


Fig. 3 Boundary Conditions & Constraints

3.4 Analysis Procedure:

Using Ansys workbench, For pressure loading condition of two compartments are fully loaded with designed pressure and one compartment empty, Analysis carried out on single component at a time. Inner cylinder with thickness 102 mm taken for first iteration, with keeping thicknesses of other components constant as per Table 1. Analysis iterations carried out for different element sizes. Plot of No of elements & corresponding maximum von-mises stresses made. In first readings, Von-mises stresses found to be very less as compared to designed allowable stress (Yield strength* Factor of Safety). Then iterations are taken by reducing thickness of inner cylinder until we get safe thickness for inner cylinder. Now keeping Inner cylinder thickness constant, same Analysis procedure carried out for Outer Cylinders, Partitions, Flat top & bottom.

No of Elements	Von-Mises Stress [Mpa]
200267	120.78
264184	106.11
284380	105.27

Fig.4 shows plot of maximum von mises stresses in inner cylinder, Fig. 5 shows maximum von mises stress plot of whole vessel, location of max von mises stress is on partition plate, Fig.6 shows total deformation plot.

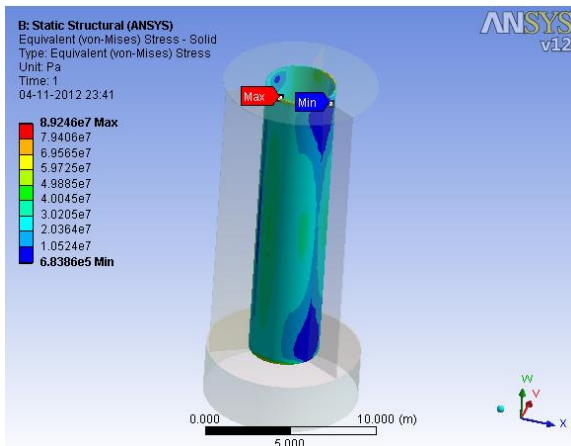


Fig.4: Maximum von mises Stress plot-Inner cylinder

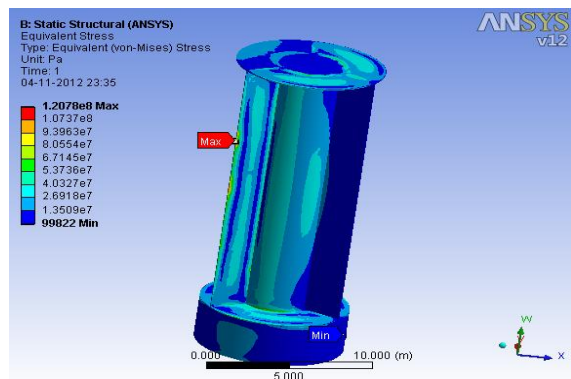


Fig.5: Maximum von mises Stress plot-Partition Plate

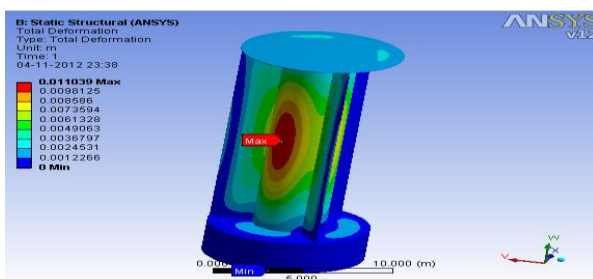


Fig.6: Total Deformation plot (outer shell not shown)

Table 2: Stress Vs. No of Elements

Sr.No.	Dimensions of Components	Von-Mises Stress (MPa)
1	70 mm Vessel Inner Shell thickness	120.78
2	50 mm vessel external shell thickness	91.30
3	80 mm flat partitioned plates	74.00
4	80 mm Top and Bottom covers	66.71

No of Elements Vs Max von mises stresses are shown in Table 2 & Fig. 7 shows plot of number of elements and Von-mises stresses. From graph, it is clear that maximum von-mises stress is approx. upto 120 MPa.

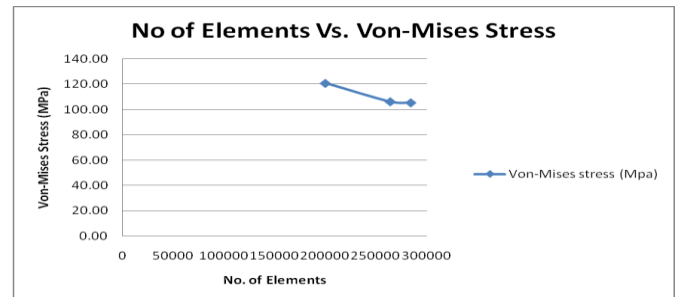


Fig.7: Graph of No of elements Vs Von-Mises stress

IV. RESULTS & DISCUSSIONS:

Results are shown in Table 3:

Table 3: Results of Analysis

V. CONCLUSION

The basic objective was to perform design and analysis of proposed Model of partitioned vertical column. Analytical design of regular pressure vessel is done with reference to ASME 2007 Section VIII, Division-2.

But resultant thicknesses of components seem to be overdesigned. Also calculations of stresses and strains near to end cap not easy to calculate. Finite element analysis is powerful and yet to be simpler approach, which gives accurate results in the field of pressure vessel design. Proposed work is to analyze partition plates critically due to differential pressures, resulting in interference between the vessel and partition and need to analyze in FEA to understand effects on stresses on the Vessel.

VI. ACKNOWLEDGMENT

The Author gratefully thanks to Dr. D.R. Panchagade, PG co-ordinator, Dept. of Mechanical Engg., DYPCOE, Pune for continuous motivation. Authors also gratefully acknowledge the contributions of Vinay Patil of Vafts CAE for his guidance for FEA simulation using Ansys Inc. software.

REFERENCES

- [1] Stephen Tiernan, Martin Fahy, "Dynamic FEA modelling of ISO tank containers", *Journal of Materials Processing Technology* 124 (2002) 126-132
- [2] Proprietary information of POWER GAS INC, PGI USA
- [3] Z. Sanal, Nonlinear analysis of pressure vessels: some examples, *International Journal of pressure vessels and piping* 77 (2000) 705-709
- [4] Deniss R. Moss, *Pressure Vessel Design manual* 2004 (third edition)
- [5] ASME Boiler and Pressure Vessel Code, Section VIII, Divisions 2, 2007, American Society of Mechanical Engineers
- [6] Ansys12.0, *Ansys Manual*, ANSYS Inc

On The Zeros of Certain Class of Polynomials

B.A. Zargar

Post-Graduate Department of Mathematics, U.K, Srinagar.

Abstract: Let $P(z)$ be a polynomial of degree n with real or complex coefficients. The aim of this paper is to obtain a ring shaped region containing all the zeros of $P(z)$. Our results not only generalize some known results but also a variety of interesting results can be deduced from them.

I. Introduction and Statement of Results

The following beautiful result which is well-known in the theory of distribution of zeros of polynomials is due to Enestrom andakeya [9].

Theorem A. If $P(z) = \sum_{j=0}^n a_j z^j$ is a polynomial of degree n such that

(1) $a_n \geq a_{n-1} \geq \dots \geq a_1 \geq a_0 \geq 0$,
 then all the zeros of $P(z)$ lie in $|z| \leq 1$.

In the literature ([2], [5]–[6], [8]–[11]) there exists some extensions and generalizations of this famous result. Aziz and Mohammad [1] provided the following generalization of Theorem A.

Theorem B. Let $P(z) = \sum_{j=0}^n a_j z^j$ is a polynomial of degree n with real positive coefficients. If $t_1 \geq t_2 \geq 0$ can be found such that

(2) $a_j t_1 t_2 + a_{j-1} (t_1 - t_2) a_{j-2} \geq 0, j=1, 2, \dots, n+1, (a_{-1} = a_{n+1} = 0)$,
 then all the zeros of $P(z)$ lie in $|z| \leq t_1$.

For $t_1 = 1, t_2 = 0$, this reduces to Enestrom-akeya Theorem (Theorem A).

Recently Aziz and Shah [3] have proved the following more general result which includes Theorem A as a special case.

Mathematics, subject, classification (2002). 30C10,30C15,

Keywords and Phrases, Enestrom-akeya Theorem, Zeros, bounds.

Theorem C. Let $P(z) = \sum_{j=0}^n a_j z^j$ be a polynomial of degree n . If for some $t > 0$.

(3) $\max_{|z|=R} [ta_0 z^n + (ta_1 - a_0) z^{n-1} + \dots + (ta_n - a_{n-1})] \leq M_3$

Where R is any positive real number, then all the zeros of $P(z)$ lie in

(4) $|z| \leq \max \left\{ \frac{M_3}{|a_n|}, \frac{1}{R} \right\}$

The aim of this paper is to apply Schwarz Lemma to prove a more general result which includes Theorems A, B and C as special cases and yields a number of other interesting results for various choices of parameters a, r, t_1 and t_2 . In fact we start by proving the following result.

Theorem 1. Let $P(z) = \sum_{j=0}^n a_j z^j$ be a polynomial of degree n , If for some real numbers t_1, t_2 with $t_1 \neq 0, t_1 >$

$t_2 \geq 0$

(5) $\max_{|z|=R} |(a_n(t_1 - t_2) + \alpha - a_{n-1}) + \sum_{j=0}^n (a_j t_1 t_2 + a_{j-1}(t_1 - t_2) - a_{j-2}) z^{n-j+1}| \leq M_1$

(6) $\min_{|z|=R} |a_0(t_1 - t_2) + a_1 t_1 t_2 + \beta| + \sum_{j=2}^{n+2} (a_j t_1 t_2 + a_{j-1}(t_1 - t_2) -$

$(a_{j-2}) z^j| \leq M_2$

Where R is a positive real number, then all the zeros of $P(z)$ lie in the ring shaped region.

(7) $\min_{|z|=R} \left(\frac{t_1 t_2 |a_0|}{|\beta| + M_2}, R \right) \leq |z| \leq \max_{|z|=R} \left(\frac{M_1 + |\alpha|}{|a_n|}, \frac{1}{R} \right)$

Taking $t_2=0$, we get the following generalization and refinement of Theorem C.

Corollary 1. Let $P(z) = \sum_{j=0}^n a_j z^j$ be a polynomial of degree n . If for some $t > 0$.

$\max_{|z|=R} |(a_n t + \alpha - a_{n-1}) + \sum_{j=0}^n (a_{j-1} t - a_{j-2}) z^{n-j+2}| \leq M_1$

$\min_{|z|=R} |(a_0 t + \beta) + \sum_{j=0}^{n+2} (a_{j-1} t - a_{j-2}) z^j| \leq M_2$

Where R is a real positive number then all the zeros of $P(z)$ lie in

$$|z| \leq \text{Max}_{|z|=R} \left(\frac{M_1 + |\alpha|}{|a_n|}, \frac{1}{R} \right)$$

In case we take $t=1=R$ in corollary 1, we get the following interesting result.

Corollary 2. Let $P(z) = \sum_{j=0}^n a_j z^j$ be a polynomial of degree n ,

$$\text{Max}_{|z|=R} \{ |a_n + \alpha - a_{n-1}| + |(a_{n-1} - a_{n-2})z + \dots + (a_1 - a_0)z^{n-1} + a_0 z^n| \} \leq M,$$

then all the zeros of $P(z)$ lie in the circle $|z| \leq \text{Max} \left(\frac{M + |\alpha|}{|a_n|}, 1 \right)$

If for some $\alpha > 0$, $\alpha + a_n \geq a_{n-1} \geq \dots \geq a_1 \geq a_0 \geq 0$, then ,

$$\begin{aligned} M &\leq |a_n + \alpha + a_{n-1}| + |a_{n-1} - a_{n-2}| + \dots + |a_1 - a_0| + |a_0| \\ &= (a_n + \alpha - a_{n-1}) + (a_{n-1} - a_{n-2}) + \dots + |a_1 - a_0| + a_0 \\ &= a_n + \alpha \end{aligned}$$

Using this observation in Corollary 2, we get the following generalization of Enestrom-Kakeya Theorem.

Corollary 3. If, $P(z) = a_n z^n + a_{n-1} z^{n-1} + \dots + a_1 z + a_0$, is a polynomial of degree n , such that for some $\alpha \geq 0$,

$$\alpha + a_n \geq a_{n-1} \geq \dots \geq a_0 \geq 0,$$

then all the zeros of $P(z)$ lie in the circle

$$|z| \leq 1 + \frac{2\alpha}{a_n},$$

For $\alpha = 0$, this reduces to Theorem A. If we take $\alpha = a_{n-1} - a_n \geq 0$, then we get Corollary 2, of ([4] Aziz and Zarger).

Next we present the following interesting result which includes Theorem A as a special case.

Theorem 2. Let $P(z) = \sum_{j=0}^n a_j z^j$ be a polynomial of degree n , If for some real numbers with $t_1 \neq 0, t_1 > t_2 \geq 0$

$$(8) \quad \text{Max}_{|z|=R} \left| \sum_{j=0}^n (a_j t_1 t_2 + a_{j-1} (t_1 - t_2) - a_{j-2}) z^{n-j} \right| \leq M_3$$

then all the zeros of $P(z)$ lie in the region

$$(9) \quad |z| \leq r_1,$$

Where ,

$$(10) \quad r_1 = \frac{2M_3}{\{|a_n(t_1 - t_2) - a_{n-1}|^2 + 4|a_n M_3\}^{1/2} - |a_n(t_1 - t_2) - a_{n-1}|}$$

Taking $t_2 = 0$, we get the following result

Corollary 4. Let $P(z) = \sum_{j=0}^n a_j z^j$ be a polynomial of degree n , If for some $t > 0$,

$$\text{Max}_{|z|=R} \left| \sum_{j=0}^n (a_{j-1} t - a_{j-2}) z^{n-j} \right| \leq M_3,$$

then all the zeros of $P(z)$ lie in the region

$$|z| \leq r_1,$$

Where ,

$$r = \frac{2M_3}{\{|a_n t - a_{n-1}|^2 + 4|a_n M_3\}^{1/2} - |a_n t - a_{n-1}|}$$

Remark. Suppose polynomial $P(z) = \sum_{j=0}^n a_j z^j$, satisfies the conditions of

Theorem A, then it can be easily verified that from Corollary 4.

$$M_3 = a_{n-1},$$

then all the zeros of $P(z)$ lie in

$$|z| \leq \frac{2a_{n-1}}{\sqrt{(a_n - a_{n-1})^2 + 4a_n a_{n-1}} - (a_n - a_{n-1})}$$

$$= \frac{2a_{n-1}}{2a_{n-1}} = 1,$$

which is the conclusion of Enestrom-Kekaya Theorem.

Finally, we prove the following generalization of Theorem 1 of ([2], Aziz and Shah).

Theorem 3. Let $P(z) = \sum_{j=0}^n a_j z^j$ be a polynomial of degree n , If α, β are complex numbers and with $t_1 \neq 0, t_2$ are real numbers with $t_1 \geq t_2 \geq 0$ and

$$(11) \quad \text{Max}_{|z|=R} |(a_n(t_1 - t_2) + \alpha - a_{n-1})z + \sum_{j=0}^n a_j t_1 t_2 + a_{j-1}(t_1 - t_2) - a_{j-2} z^{n-j-2}| \leq M_4$$

and,

$$(12) \quad \text{Max}_{|z|=R} |(a_n(t_1 - t_2) + \beta - a_{n-1})z + \sum_{j=2}^{n+2} a_j t_1 t_2 + a_{j-1}(t_1 - t_2) - a_{j-2} z^j| \leq M_5$$

Where $a_{-2} = a_{-1} = 0 = a_{n+1} = a_{n+2}$ and R is any positive real number, then all the zeros of $P(z)$ lie in the ring shaped region.

$$(13) \quad \text{Min}(r_2, R) \leq |z| \leq \max\left(r_1, \frac{1}{R}\right)$$

Where

$$(14) \quad r_1 = \frac{2[|\alpha|R^2|a_n(t_1 - t_2) - a_{n-1} + \alpha| + M_4^2]}{\{(|\alpha|R^2 M_4 + R^2(M_4 - |a_n|)|a_n(t_1 - t_2) + \alpha - a_{n-1}|^2 + 4(|\alpha|R^2|a_n(t_1 - t_2) + \alpha - a_{n-1}| + M_4^2)(|a_n|R^2 M_4)\}^{1/2} - (|\alpha|R^2 M_4 + R^2(M_4 - |a_n|)|a_n(t_1 - t_2) + \alpha - a_{n-1}|)}$$

and

$$(15) \quad \frac{1}{r_2} = \frac{2[R^2|\beta||a_1 t_1 t_2 + a_0(t_1 - t_2) + \beta| - M_5^2]}{R^2\{|a_1 t_1 t_2 + a_0(t_1 - t_2) + \beta|(|a_0|t_1 t_2 - M_5) - |\beta|M_5\} + \{R^4(|a_1 t_1 t_2 + a_0(t_1 - t_2) + \beta|(|a_0|t_1 t_2 - M_5))^2 + 4(|a_0|(|M_5 t_1 t_2) + (R^2|\beta||a_1 t_1 t_2 + a_0(t_1 - t_2) + \beta| + M_5^2)\}^{1/2}}$$

Taking $\alpha = 0, \beta = 0$, in Theorem 3, we get the following.

Corollary 5. Let $P(z) = \sum_{j=0}^n a_j z^j$ be a polynomial of degree n , If $t_1 \neq 0$ and t_2 are real numbers with $t_1 \geq t_2 \geq 0$,

$$\text{Max}_{|z|=R} |\sum_{j=1}^{n+1} (a_j t_1 t_2 + a_{j-1}(t_1 - t_2) - a_{j-2})z^{n-j+2}| \leq M_4,$$

$$\text{Max}_{|z|=R} |\sum_{j=1}^{n+2} (a_j t_1 t_2 + a_{j-1}(t_1 - t_2) - a_{j-2})z^j| \leq M_5,$$

Where R is any positive real number. then all the zeros of $P(z)$ lie in the ring shaped region

$$\text{min}(r_2, R) \leq |z| \leq \max\left(r_1, \frac{1}{R}\right)$$

Where

$$r_1 = \frac{2M_4^2}{\{R^4|(t_1 - t_2)a_n - a_{n-1}|^2 + 4|a_n|R^2 M_4^3\}^{1/2} - |(t_1 - t_2)a_n - a_{n-1}|(M_4 - |a_n|)R^2}$$

$$r_2 =$$

$$\frac{1}{2M_5^2} \left[\{R^4 |a_1 t_1 t_2 + a_0 (t_1 - t_2)|^2 (M_5 - |a_0| t_1 t_2)^2 + 4M_5^3 R^2 |a_0| t_1 t_2\}^{\frac{1}{2}} - R^2 (M_5 - |a_0| t_1 t_2) |a_1 t_1 t_2 + a_0 (t_1 - t_2)| \right]$$

The result was also proved by Shah and Liman [12].

II. LEMMAS

For the proof of these Theorems, we need the following Lemmas. The first Lemma is due to Govil, Rahman and Schmesser [7].

LEMMA. 1. If $f(z)$ is analytic in $|z| \leq 1$, $f(o) = a$ where $|a| < 1$, $f'(o) = b$, $|f(z)| \leq 1$, on $|z| = 1$, then for $|z| \leq 1$.

$$|f(z)| \leq \frac{(1-|a|)|z|^2 + |b||z| + |a|(1-|a|)}{|a|(1-|a|)|z|^2 + |b||z| + (1-|a|)}$$

The example

$$f(z) = \frac{a + \frac{b}{1+a} z - z^2}{1 - \frac{b}{1+a} z - az^2}$$

Shows that the estimate is sharp.

form Lemma 1, one can easily deduce the following:

LEMMA. 2. If $f(z)$ is analytic in $|z| \leq R$, $f(0) = 0$, $f'(0) = b$ and $|f(z)| \leq M$, for $|z| = R$, then

$$|f(z)| \leq \frac{M|z|}{R^2} \frac{M|z| + R^2|b|}{M + |b||z|} \text{ for } |z| \leq R$$

III. PROOFS OF THE THEOREMS.

Proof of Theorem . 1 Consider
(16)

$$\begin{aligned} F(z) &= (t_2 + z)(t_1 - z)P(z) \\ &= -a_n z^{n+2} + (a_n(t_1 - t_2) - a_{n-1})z^{n+1} \\ &\quad + (a_n t_1 t_2 + a_{n-1}(t_1 - t_2) - a_{n-2})z^n \\ &\quad + \dots + (a_n t_1 t_2 + a_0(t_1 - t_2))z + a_0 t_1 t_2 \end{aligned}$$

Let

$$\begin{aligned} &G(z) + z^{n+2} F\left(\frac{1}{z}\right) \\ &= -a_n + (a_n(t_1 - t_2) - a_{n-1})z + (a_n t_1 t_2 + a_{n-1}(t_1 - t_2) - a_{n-2})z^2 + \dots \\ &\quad \dots + (a_1 t_1 t_2 + a_0(t_1 - t_2))z^{n+1} + a_0 t_1 t_2 z^{n+2} \\ &= -a_n - \alpha z + (a_n(t_1 - t_2) + \alpha - a_{n-1})z \\ &\quad + (a_n t_1 t_2 + a_{n-1}(t_1 - t_2) - a_{n-2})z^2 + \dots \\ &\quad \dots + (a_1 t_1 t_2 + a_0(t_1 - t_2))z^{n+1} + a_0 t_1 t_2 z^{n+2} \\ &= -(a_n + \alpha z) + H(z) \end{aligned}$$

Where,

$$H(z) = z \{ (a_n(t_1 - t_2) + \alpha - a_{n-1}) + \sum_{j=0}^n (a_j t_1 t_2 + a_{j-1}(t_1 - t_2) - a_{j-2})z^{n-j} \}$$

Clearly $H(0)=0$ and $\max_{|z|=R} |H(z)| \leq RM_1$,

We first assume that $|a_n| \leq R(M_1 + |\alpha|)$

Now for $|z| \leq R$, by using Schwarz Lemma, we have

$$\begin{aligned} (17) \quad |G(z)| &= |-(a_n + \alpha z) + H(z)| \\ &\geq |a_n| - |\alpha||z| - |H(z)| \\ &\geq |a_n| - |\alpha||z| - |M_1||z| \\ &= |a_n| - (M_1 + |\alpha|)|z| \\ &> 0, \text{ if} \\ |z| &< \frac{|a_n|}{M_1 + |\alpha|} \quad (\leq R) \end{aligned}$$

This shows that all the zeros of $G(z)$ lie in $|z| \geq \frac{|a_n|}{M_1 + |\alpha|}$

Replacing z by $\frac{1}{z}$ and noting that $F(z) = z^{n+2}G\left(\frac{1}{z}\right)$, it follows that all the zeros of $F(z)$ lie in

$$|z| \leq \frac{M_1 + |\alpha|}{|a_n|} \text{ if } |a_n| \leq R(M_1 + |\alpha|)$$

Since all the zeros of $P(z)$ are also the zeros of $F(z)$, we conclude that all the zeros of $P(z)$ lie in

$$(18) \quad |z| \leq \frac{|a_n|}{M_1 + |\alpha|}$$

Now assume $|a_n| > R(M_1 + |\alpha|)$, then for $|z| \leq R$, we have from (17).

$$\begin{aligned} |G(z)| &\geq |a_n| - |\alpha||z| - |H(z)| \\ &\geq |a_n| - |\alpha|R - M_1R \\ &= |a_n| - (|\alpha| + M_1)R > 0, \end{aligned}$$

Thus $G(z) \neq 0$ for $|z| < R$, from which it follows as before that all the zeros of $F(z)$ and hence all the zeros of $P(z)$ lie in $|z| \leq \frac{1}{R}$. Combining this with (18), we infer that all the zeros of $P(z)$ lie in

$$19. \quad |z| \leq \max \left\{ \frac{|a_n|}{M_1 + |\alpha|}, \frac{1}{R} \right\}$$

Now to prove the second part of the Theorem, from (16) we can write $F(z)$ as

$$\begin{aligned} F(z) &= (t_2 + z)(t_1 - z)P(z) \\ &= \\ &= a_0 t_1 t_2 + (a_1 t_1 t_2 + a_0(t_1 - t_2))z + \cdots + (a_n(t_1 - t_2) - a_{n-1})z^{n+1} - a_n z^{n+2} \\ &= a_0 t_1 t_2 - \beta z + (a_1 t_1 t_2 + a_0(t_1 - t_2) + \beta)z + \cdots + (a_n(t_1 - t_2) - a_{n-1})z^{n+1} - a_n z^{n+2} \\ &= a_0 t_1 t_2 - \beta z + T(z) \end{aligned}$$

Where

$$T(z) = z \{ (a_1 t_1 t_2 + a_0(t_1 - t_2) + \beta) + \sum_{j=2}^{n+2} a_j t_1 t_2 + a_{j-1}(t_1 - t_2) a_{j-2} \} z^{j-1}$$

Clearly $T(0)=0$, and $\max_{|z|=R} |T(z)| \leq RM_2$

We first assume that $|a_0 t_1 t_2| \leq |\beta| + M_2$

Now for $|z| \leq R$, by using Schwarz lemma, we have

$$\begin{aligned} |F(z)| &\geq |a_0 t_1 t_2| - |\beta||z| - |T(z)| \\ &\geq |a_0 t_1 t_2| - |\beta||z| - M_2|z| \\ &> 0, \text{ if,} \end{aligned}$$

$$|z| < \frac{a_0 t_1 t_2}{|\beta| + M_2} \quad (\leq R)$$

This shows that $F(z) \neq 0$, for $|z| < \frac{|a_0 t_1 t_2|}{|\beta| + M_2}$, hence all the zeros of $F(z)$ lie in

$$|z| \geq \frac{|a_0 t_1 t_2|}{|\beta| + M_2}$$

But all the zeros of $P(z)$ are also the zeros of $F(z)$, we conclude that all the zeros of $P(z)$ lie in

$$20. \quad |z| \geq \frac{|a_0 t_1 t_2|}{|\beta| + M_2}$$

Now we assume $|a_0 t_1 t_2| > |\beta| + M_2$, then for $|z| \leq R$, we have

$$\begin{aligned} |F(z)| &\geq |a_0 t_1 t_2| - |\beta||z| - |T(z)| \\ &\geq |a_0 t_1 t_2| - |\beta|R - M_2 R \\ &> |t_1 t_2 a_0| - (|\beta| + M_2)R \\ &> 0, \end{aligned}$$

This shows that all the zeros of $F(z)$ and hence that of $P(z)$ lie in

$$|z| \geq R$$

Combining this with (20), it follows that all the zeros of $P(z)$ lie in

$$21 \quad |z| \geq \min\left(\frac{|a_0 t_1 t_2|}{|\beta| + M_2}, R\right)$$

Combining (19) and (20), the desired result follows.

Proof of Theorem 2:- Consider

$$\begin{aligned} 22. \quad F(z) &= (t_2 + z)(t_1 - z)P(z) \\ &= (t_2 + z)(t_1 - z)(a_n z^n + a_{n-1} z^{n-1} + \cdots + a_1 z + a_0) \\ &= -a_n z^{n+2} + (a_n(t_1 - t_2) - a_{n-1})z^{n+1} + \cdots + a_0 t_1 t_2 \end{aligned}$$

Let

$$\begin{aligned} 23. \quad G(z) &= z^{n+2} F\left(\frac{1}{z}\right) \\ &= -a_n + (a_n(t_1 - t_2) - a_{n-1})z + \\ &\quad (a_n t_1 t_2 - a_{n-1}(t_1 - t_2)a_{n-2})z^2 + H(z) \end{aligned}$$

Where

$$H(z) = z^2 \{(a_n t_1 t_2 - a_{n-1}(t_1 - t_2) - a_{n-2}) + \cdots + a_0 t_1 t_2 z^n\}$$

Clearly $H(0) = 0 = H'(0)$, since $|H(z)| \leq M_3 R^2$ for $|z| = R$

We first assume,

$$24 \quad |a_n| \leq MR^2 + R|a_n(t_1 - t_2) - a_{n-1}|$$

Then by using Lemma 2. To $H(z)$, it follows that

$$H|z| \leq \frac{M_3|z|}{R^2} \frac{M_3|z|}{M_3} \max_{|z|=R} |H(z)|$$

Hence from (23) we have

$$|G(z)| \geq |a_n| - |a_n(t_1 - t_2) - a_{n-1}||z| - \frac{|z|^{2M_3}}{R^2} R^2$$

$$> 0, \text{ if}$$

$$M_3|z|^2 + |a_n(t_1 - t_2) - a_{n-1}||z| - |a_n| < 0$$

That is if,

$$25. \quad |z| < \frac{\{|a_n(t_1 - t_2) - a_{n-1}|^2 + 4|a_n|M\}^{1/2} - |a_n(t_1 - t_2) - a_{n-1}|}{2M_3}$$

$$= \frac{1}{r} \leq R$$

If

$$|a_n(t_1 - t_2) - a_{n-1}|^2 + 4|a_n|M_3 \leq (2M_3R + |a_n(t_1 - t_2) - a_{n-1}|)^2$$

Which implies

$$|a_n| \leq M_3R^2 + R|a_n(t_1 - t_2) - a_{n-1}|$$

Which is true by (24). Hence all the zeros of $G(z)$ lie in $|Z| \geq r$. since

$$F(z) = z^{n+2}G(z),$$

It follows that all the zeros of $F(z)$ and hence that of $P(z)$ lie in $|z| \leq r$. We now assume.

$$26. \quad |a_n| \leq M_3R^2 + R|a_n(t_1 - t_2) - a_{n-1}|,$$

then for $|z| \leq R$, from (23) it follows that

$$|G(z)| \geq |a_n| - |a_n(t_1 - t_2) - a_{n-1}||z| - |H(z)|$$

$$\geq |a_n| - R|a_n(t_1 - t_2) - a_{n-1}| - R^2M_3$$

$$> 0, \text{ by (26).}$$

This shows that all the zeros of $G(z)$ lie in $|Z| > R$, and hence all the zeros of $F(z) = z^{n+2}G(\frac{1}{z})$ lie in $|z| \leq \frac{1}{R}$, but all the zeros of $P(z)$ are also the zeros of $F(z)$, therefore it follows that all the zeros of $P(z)$ lie in

$$|Z| \leq \frac{1}{R}$$

27. From (25) and (27), we conclude that all the zeros of $P(z)$ lie in

$$|Z| \leq \max(r, \frac{1}{R})$$

Which completes the proof of Theorem 2.

28. PROOF OF THEOREM 3. Consider the polynomial

$$\begin{aligned}
 F(z) &= (t_2 + z)(t_1 - z)P(z) \\
 &= (t_1 t_2 + (t_1 - t_2)z - z^2)(a_n z^n + a_{n-1} z^{n-1} + \dots + a_1 z + a_0) \\
 &= -a_n z^{n+2} + (a_n(t_1 - t_2) - a_{n-1})z^{n+1} + \dots + (a_n t_1 t_2 \\
 &\quad + (a_{n-1}(t_1 - t_2) - a_{n-2})z^{n+1} + \dots + \\
 &\quad (a_2 t_1 t_2 + a_1(t_1 - t_2) - a_0)z^2 + (a_1 t_1 t_2 + a_0(t_1 - t_2))z + a_0 t_1 t_2)
 \end{aligned}$$

We have,

$$\begin{aligned}
 G(z) &= z^{n+2} F\left(\frac{1}{z}\right) \\
 &= r a_n + (a_n(t_1 - t_2) - a_{n-1})z + (a_n t_1 t_2 + a_{n-1}(t_1 - t_2) - a_{n-2})z^2 \\
 &\quad + \dots + (a_1 t_1 t_2 + a_0(t_1 - t_2))z^{n+1} + a_0 t_1 t_2 z^{n+2} \\
 &= -a_n - \alpha z + (a_n(t_1 - t_2) + \alpha - a_{n-1})z + \\
 &\quad (a_n t_1 t_2 + a_{n-1}(t_1 - t_2) - a_{n-2})z^2 + \dots + \\
 &\quad (a_1 t_1 t_2 + a_0(t_1 - t_2))z^{n+1} + a_0 t_1 t_2 z^{n+2} \\
 &= -a_n - \alpha z + H(z)
 \end{aligned}$$

29.

Where

$$H(z) = \{(a_n(t_1 - t_2) + \alpha - a_{n-1})z + \dots + a_0 t_1 t_2 z^{n+2}\}$$

We first assume that

30. $|a_n| \geq |\alpha|R + M_4$

Then for $|z| < R$, we have

31. $|G(z)| \geq |a_n| - |\alpha||z| - |H(z)|$

Since

$$|H(z)| \leq M_4 \text{ for } |z| \leq R$$

Therefore for $|z| < R$, from (31) with the help of (30), we have

$$|G(z)| > |a_n| - |\alpha|R - M_4$$

therefore, all the zeros of $G(z)$ lie in $|z| \geq R$, in this case. Since $F(z) = z^{n+2} G\left(\frac{1}{z}\right)$ therefore all the zeros of $G(z)$ lie in $|z| \leq \frac{1}{R}$. As all the zeros of $P(z)$ are the zeros of $F(z)$, it follows that all the zeros of $P(z)$ lie in

32. $|z| \leq \frac{1}{R}$

Now we assume $|a_n| < |\alpha|R + M_4$, clearly $H(0) = 0$ and $\alpha - a_{n-1}$, Since by (11), $|H(z)| \leq M_4$, for $|z| = R$, therefore it follows by Lemma 2. that

$$|H(z)| \leq \frac{M_4 |z|}{R^2} \left(\frac{M_4 |z| + R^2 |a_n(t_1 - t_2) - a_{n-1} + \alpha|}{M_4 + |a_n(t_1 - t_2) - a_{n-1} + \alpha||z|} \right)$$

for $|z| \leq R$

Using this in (31), we get,

$$|G(z)| \geq |a_n| - |\alpha||z| - \frac{M_4 |z|}{R^2} \left(\frac{M_4 |z| + R^2 |a_n(t_1 - t_2) - a_{n-1} + \alpha|}{M_4 + |a_n(t_1 - t_2) - a_{n-1} + \alpha||z|} \right)$$

> 0, if

$$\begin{aligned}
 &|a_n|R^2(M_4 + |a_n(t_1 - t_2) - a_{n-1} + \alpha||z|) - |z|\{|\alpha|R^2 \\
 &(M_4 + |a_n(t_1 - t_2) - a_{n-1} + \alpha||z|) + M_4(M_4|z| + R^2 \\
 &|a_n(t_1 - t_2) - a_{n-1} + \alpha|)\} > 0,
 \end{aligned}$$

this implies,

$$\begin{aligned}
 &(|\alpha|R^2 |a_n(t_1 - t_2) - a_{n-1} + \alpha| + M_4^2)|z|^2 + \{|\alpha|R^2 M_4 + \\
 &R^2 M_4 |a_n(t_1 - t_2) - a_{n-1} + \alpha| \dots R^2 M_4 |a_n(t_1 - t_2) - a_{n-1} + \alpha|\} \\
 &|z| - |a_n|R^2 M_4 < 0,
 \end{aligned}$$

This gives,

$$\begin{aligned}
 &|G(z)| > 0, \text{ if} \\
 &|z| < [(|\alpha|R^2 M_4 + R^2(M_4 - |a_n|)|a_n(t_1 - t_2) - a_{n-1} + \alpha|)^2 + \dots \\
 &4(|\alpha|R^2 |a_n(t_1 - t_2) - a_{n-1} + \alpha| + M_4^2)(|a_n|R^2 M_4)]
 \end{aligned}$$

$$\begin{aligned}
 &= \frac{(|\alpha|R^2 M_4 + R^2(M_4 - |a_n|)|a_n(t_1 - t_2) - a_{n-1} + \alpha|)}{2(|\alpha|R^2 |a_n(t_1 - t_2) - a_{n-1} + \alpha| + M_4^2)} \\
 &= \frac{1}{r_1},
 \end{aligned}$$

So, $|z| < R$, if

$$(|\alpha|R^2 M_4 + (M_4 - |a_n|R^2)|a_n(t_1 - t_2) - a_{n-1} + \alpha|)^2 +$$

$$4\{|a|R^2|a_n(t_1-t_2) - a_{n-1} + \alpha| + M_4^2\}\{|a_n|R^2M_4\} \\ < \{2|a||a_n(t_1-t_2) - a_{n-1} + \alpha|R + |a|R^2M_4 + 2RM_4^2 \\ + (M_4 - |a_n|R^2)|a_n(t_1-t_2) - a_{n-1} + \alpha|^2\}$$

That is if,

$$|a_n|R^2M_4 \leq R^2(|a|R^2|a_n(t_1-t_2) - a_{n-1} + \alpha| + M_4^2) + \\ (|a|R^2M_4) + (M_4 - |a_n|R^2)|a_n(t_1-t_2) - a_{n-1} + \alpha|R$$

Which gives

$$|a_n|M_4 \leq M_4\{|a|R + M_4 - |a_n| + R||a|R^2||a_n(t_1-t_2) - a_{n-1} + \alpha| + M_4^2| \\ \{|a|R^2 + M_4 - a_n|\}$$

Which is true because $a_n < |a|R + M_4$,

Consequently, all the zeros of $G(z)$ lie in $|z| \geq \frac{1}{r_1}$, as $F(z) = z^{n+1}G(\frac{1}{z})$, we conclude that all the zeros of $F(z)$ lie $|z| \leq r_1$, since every zero of $P(z)$ is also a zero of $F(z)$, it follows that all the zeros of $P(z)$ lie in

$$33. \quad |z| \leq r_1$$

Combining this with (32) it follows that all the zeros of $P(z)$ lie in

$$34. \quad |z| \leq \max\left(r_1, \frac{1}{R}\right)$$

Again from (28) it follows that

$$F(z) = |a_0t_1t_2 - \beta z + (a_1t_1t_2(t_1-t_2) + \beta)z + \dots + (a_n(t_1-t_2) \\ - a_{n-1})z^{n+2} - a_nz^{n+2}|$$

$$35. \quad \geq |a_0t_1t_2| - |\beta||z| - |T(z)|$$

Where,

$$T(z) = a_nz^{n+2} + (a_n(t_1-t_2) - a_{n-1})z^{n+1} + \dots + \\ (a_0t_1t_2 + a_0(t_1-t_2) + \beta)z$$

Clearly $T(0)=0$, and $T(0) = (a_1t_1t_2 + a_0(t_1-t_2) + \beta)$

Since by (12), $|T(z)| \leq M_5$ for $|z| = R$

using Lemma 2. To $T(z)$, we have

$$F(z) \geq \left| a_0t_1t_2 - |\beta||z| - \frac{M_5|z|}{R^2} (M_5|z| + R^2|a_1t_1t_2| + a_0(t_1-t_2) + \beta)|z| \right| \\ = -(R^2|\beta||a_1t_1t_2| + a_0(t_1-t_2) + \beta| + M_5^2)|z|^2 + \\ \{|a_1t_1t_2| + a_0(t_1-t_2) + \beta|(R^2|a_0t_1t_2| - R^2M_5) - |\beta|R^2M_5\}|z| + M_5R^2|a_1t_1t_2| \\ R^2(M_5 + |a_1t_1t_2 + a_0(t_1-t_2) + \beta||z|)$$

>0, if,

$$(R^2|\beta||a_1t_1t_2| + a_0(t_1-t_2) + \beta| + M_5^2)|z|^2 - \{|a_1t_1t_2| + a_0(t_1-t_2) + \beta|$$

$$(R^2|a_0t_1t_2| - R^2M_5) - |\beta|R^2M_5\}|z| - R^2M_5|a_0t_1t_2| < 0,$$

Thus, $|F(z)| > 0$, if

$$|z| < -R^2\{|a_1t_1t_2 + a_0(t_1-t_2) + \beta|(|a_0t_1t_2 - M_5)||\beta|M_5\}$$

$$-\{R^4(|a_1 t_1 t_2| + a_0(t_1 - t_2)) + \beta |(|a_0| t_1 t_2 - M_5)| |\beta| M_5)^2 \\ + 4(R^2 |\beta| |a_1 t_1 t_2 + a_0(t_1 - t_2)| + \beta | + M_5^2)(R^2 M_5 |a_0| t_1 t_2)\}^{1/2} \\ \frac{r_z}{2(R^2 |\beta| |a_1 t_1 t_2| + a_0(t_1 - t_2) + \beta | + M_5^2)}$$

Thus it follows by the same reasoning as in Theorem 1, that all the zeros of $F(z)$ and hence that of $P(z)$ lie in

36. $|z| \geq \min(r_2, R)$

Combining (34) and (36), the desired result follows.

REFERENCES

- [1] A. Aziz and Q.G Mohammad, On the zeros of certain class of polynomials and related analytic functions, J. Math. Anal Appl. 75(1980), 495-502
- [2] A.Aziz and W.M Shah, On the location of zeros of polynomials and related analytic functions, Non-linear studies, 6(1999),97-104
- [3] A.Aziz and W.M Shah, On the zeros of polynomials and related analytic functions, Glasnik, Matematicke, 33 (1998), 173-184;
- [4] A.Aziz and B.A. Zarger, Some extensions of Enestrem-Kakeya Theorem, Glasnik, Matematicke, 31 (1996), 239-244
- [5] K.K.Dewan and M. Biakham,, On the Enestrom –Kakeya Theorem, J.Math.Anal.Appl.180 (1993), 29-36
- [6] N.K, Govil and Q.I. Rahman, On the Enestrem-Kakeya Theorem, Tohoku Math.J. 20 (1968), 126-136.
- [7] N.K, Govil , Q.I. Rahman and G. Schmeisser, on the derivative of polynomials, Illinois Math. Jour. 23 (1979), 319-329
- [8] P.V. Krishnalah, On Kakeya Theorem , J.London. Math. Soc. 20 (1955), 314-319
- [9] M. Marden, Geometry of polynomials, Mathematical surveys No.3. Amer. Math. Soc. Providence , R.I. 1966
- [10] G.V. Milovanovic, D.S. Mitrinovic, Th.M. Rassias Topics in polynomials, Extremal problems Inequalities, Zeros(Singapore, World Scientific)1994.
- [11] Q.I. Rahman and G.Schmeissier, Analytic Theory of polynomials, (2002), Clarantone, Press Oxford.
- [12] W.M. Shah and A. Liman, On the zeros of a class of polynomials, Mathematical inequalities and Applications, 10(2007), 793-799

Application Of Intelligent Decision Support Systems (Idss) To Calculate The Number Of Sectors For Security Operations In The East Sea Indonesia

Hozairi¹, Ketut Buda Artana², Masroeri³, M.Isa Irawan⁴

¹(Department Of Ocean Engineering, Faculty of Marine Technology, ITS, Indonesia)

²(Department of Mathematics, Faculty Mathematics and Science, ITS, Indonesia)

ABSTRACT: This study discusses the implementation of Fuzzy Analytical Hierarchy Process (FAHP) as part of the Intelligent Decision Support Systems (IDSS) for determining the number of marine security operations sector of eastern Indonesia. There are two types of variables used in this study is a quantitative and qualitative. Quantitative variables were used in conjunction with the ship (C5) is the speed, size, wave height and coverage area. Qualitative variables used are weapons (C1), sector (C2), logistics (C3) and infrastructure (C4). There are 7 decision alternatives used in this study, to determine the optimal number of operational sectors are A1 = 4 sectors, sectors A2 = 5, A3 = 6 sectors, sector A4 = 7, A5 = 8 sectors, A6 and A7 = 9 sectors = 10 sectors. The calculation of the variable weights of 5 criteria using FAHP obtained as follows: C1 = 0.26; C2 = 0.24; C3 = 0.21; C4 = C5 = 0.17 and 0.12. The weight will be multiplied by the weight of sub-criteria of each alternative weighting criteria to produce a decision. Some Navy leaders also give the value of the criteria and sub-criteria for each of the proposed number of sectors with a range of values 50-100. The end result of this research is A1 = 45.843, A2 = 46.134, A3 = 46.008, A4 = 46.201, A5 = 46.232 A6 = 46.015 and A7 = 46.083. Based on calculations FAHP is recommended for the development of the number of sectors in ARMATIM from 7 to 8 sectors that can be monitored and secured by the fleets of the Republic of Indonesia.

Keywords: FAHP, IDSS, Sector, Armatim

I. INTRODUCTION

Republic of Indonesia is an archipelago consisting of 17,504 islands and has a beach along the 81,290 kilometers (Dishidros TNI-AL, 2003). As an island nation with 80% of the sea area and 20% of the land, the threat to the sovereignty and territory of Indonesia is in the sea. The threats are higher because the position of Indonesia is the geography of world trade traffic. The high number of crimes and violations that occurred in Indonesia such as the sea, illegal fishing, illegal logging, illegal mining, illegal migrants, human trafficking and smuggling, this suggests that the weakness of Indonesia's marine security. This is due to the limited number of owned fleet so the extent of the area to be secured, lack of budget, lack of achievement Indonesian warship coverage area and have not optimized the amount of the security zone (sector operations) Indonesian sea.

Based on the above conditions need to do some study and development of decision models capable of working in a dynamic and uncertain environment quickly and accurately. Decision support systems (DSS) is an application of technology that can help leaders determine

the Navy's decision to utilize existing data and models to solve unstructured and semi-structured.

This research aims to design and create an application Intelligent Decision Support System (IDSS) to be able to provide alternative solutions that are easy to adapt to a dynamic environment, the method chosen to build the IDSS is Fuzzy Analytical Hierarchy Process (F-AHP), IDSS is built not to replace the role and function of the human but to help provide an alternative decision. F-AHP is a decision support method is quite popular and has been reliable in addressing the issue in accordance with the criteria of selection of objects is measured qualitatively and quantitatively. F-AHP is one of the ranking methods. F-AHP is a combination of AHP with fuzzy concept approach (Raharjo et al, 2002). F-AHP cover the weaknesses contained in the AHP, the problem of the subjective nature of the criteria that have more. Uncertainty is represented by the sequence numbers of the scale. To determine the degree of membership in F-AHP, use the rules function in the form of triangular fuzzy numbers or Triangular Fuzzy Number (TFN) which is based on the set of linguistics. Thus, the numbers in the level of intensity of interest in AHP is transformed into a set of scales TFN.

II. LITERATURE REVIEW

2.1. IDSS

Intelligent decision support system (IDSS) is the development of decision support systems using the knowledge (the rules of the nature and elements of the problem) such as fuzzy systems, neural networks and genetic algorithm (Sadly 2007). This goal is to help users to access, view, understand, and manipulate data more quickly and easily to help in making decisions. So with intelligent decision support systems can be used to make optimal decisions to approach learning and reasoning ability and the ability of a system grounded in choosing a solution, as was done by an expert in making decisions that will get consistent and effective solution. The process consists of sub-systems organizational system input, sub-systems and sub-structuring problems simulation system state and determining the best solution. The output of Intelligent Decision Support Systems is in the form of reporting solutions, forecasting the impact of its decisions on input and suggestions and explanations effects. Input has a feedback output to obtain an optimal solution in making decisions on effective and efficient.

2.2. AHP

Analytical Hierarchy Process (AHP) is a flexible model that allows individuals or groups to form ideas and limit problems with their own assumptions and generate solutions for them (Thomas L. Saaty, Decision Making for

Leaders; The Analytical Hierarchy Process for Decision in Complex World, 1988). AHP was developed in the early 1970's by Saaty and has been used to assist decision makers from different countries and companies. According to Saaty (1993, p23) AHP is a flexible model that provides an opportunity for individuals or groups to develop ideas and define problems in a way to make their own assumptions and obtain her desired solution. AHP include considerations and values logical.

The working principle of AHP is to simplify the complex problem of unstructured, strategic and dynamic into its parts, as well as arranging the variables in a hierarchy (levels). Then the variable interest rate subjectively assigned a numerical value on the relative importance compared to other variables. From various considerations are then carried out the synthesis to define variables that have the highest priority and role is to influence the outcome of the system. The difference between AHP models with other models of decision-making lies in the type of input use AHP model of human perception is considered 'expert or experts' as the primary input. Criteria experts here are people who understand the real problem, feeling the effects of a problem or have an interest in this. Qualitative measurement of things is very important given the increasingly complex problems of the world and a higher degree of uncertainty. If there are deviations which are too far from the value of a perfect consistency an assessment needs to be repaired or re-structured hierarchy of need.

Analytic hierarchy process (AHP) is a multiple criteria decision-making approach that has been used in most applications related with different areas including evaluation, allocation, selection, benefit-cost analysis, allocation, planning and development, priority and ranking, and decision-making (Korpela, KylaKaheiko, Lehmusvaara & Tuominen, 2002; Crary, Nozick & Whitaker, 2002; Badri, 2001; Beynon, 2002). However, traditional AHP seems inadequate to capture customer values with linguistic expressions and determine the relative importance weight of customer's needs accurately (Kahraman, Cebeci, and Ulukan, 2003). And AHP method is often criticized due to its use of unbalanced scale of judgments and its inability to adequately handle inherent uncertainty and imprecision in the pair-wise comparison process (Deng, 1999). Hence, fuzzy analytic hierarchy process (FAHP) was developed to solve these shortcomings and decision-makers usually are more confident to give interval judgments than fixed value judgments.

2.3. F-AHP

F-AHP is a decision-making tool typically aimed to accommodate conflict of opinion and subjectivity of assessment of several different people. Unlike simple decisions (which consists of only one criterion), the real world must have a lot of criteria and alternatives involved in the decision making. This makes the decision process more complicated because of the conflict of opinion about opinions like inequality priority level of each criterion. Therefore, AHP is capable of breaking a complex problem into elements smaller hierarchy in the form of a simpler assessed can be used for decision making by the number of criteria of more than one or often called multi-criteria decision making.

But on further development of AHP was assessed as having few weaknesses is the inability to capture the vagueness (*vagueness*), uncertainty, imprecision and subjectivity in the assessment made by some people. M Buckley (Hsieh, 2004) developed the concept of Fuzzy AHP (FAHP) is the development of the AHP by integrating fuzzy AHP with synthetic evaluation (FSE). In FAHP use ratio to replace the fuzzy AHP and the exact ratio is also used mathematical operations and fuzzy logic to replace the usual mathematical operations on AHP. Users rate at FAHP fuzzy AHP inability to accommodate the inaccuracy factor (imprecision) and subjectivity in the process of pair wise comparison or paired comparisons for each criterion and alternative. Therefore, the ratio is used which consists of three fuzzy values are the highest values (values above), the average (median) and the lowest value (lower value). The ratio of three fuzzy membership values is usually called triangular fuzzy number (TFN).

There are several variations of FAHP types have been developed:

1. Var Laarhoven and Pedrycz (1983) apply fuzzy triangular number on pair wise comparison ratio. This is what started the emergence of fuzzy AHP method.
2. Kristianto (2002) proposed a model based on Fuzzy FAHP quantification theory in which the aspirations of the evaluators who shaped crisp converted to a fuzzy membership function to look for. This model was considered crisp and aspirations evaluator quantization method involves complex computational operations.
3. Rahardjo (2002) proposed a model with a model FAHP weighted non-additive which is a combination of the weight and the weight of prior information. The weight is the weight of the prior development of AHP and fuzzy weights of weighted fuzzy information entropy. The model uses a weighted fuzzy evaluator and it involves a complicated computing operations.
4. Singgih (2005) have put forward a model that is an extension of the FAHP from Rahardjo (2002) which can use more than one evaluator.

III. FUZZY - AHP

3.1. DEGREES OF MEMBERSHIP AND SCALE OF FUZZY TRIANGLE

Fuzzy AHP method provides a systematic procedure for selecting and justifying the alternatives by using the concept of fuzzy logic and hierarchical structure inherited from traditional AHP method. Moreover, fuzzy AHP method is a popular approach for multiple criteria decision-making and has been widely used in the literature.

Chang (1996) applied triangular fuzzy number to construct the fuzzy pair-wise comparison matrix in AHP and used the extent analysis method for obtaining the synthetic values of the pair-wise comparisons. Sheu (2004) combined fuzzy AHP with fuzzy multi-attribute decision-making approach for identifying global logistics strategies. Kahraman, Cebeci, and Ruan (2004) applied the fuzzy AHP to the comparison of catering firms via customer satisfaction. Chang's extent analysis method (Chang, 1996) provides an easier way to construct fuzzy reciprocal comparison matrix and derive the weight vectors for individual levels of the hierarchical requirements without weight overlapping than the other fuzzy AHP and traditional AHP approaches. In this study, Chang's extent

analysis method (Chang, 1996) is applied to evaluate the relative importance weights of customer relational benefit attributes for searching appropriate relationship marketing strategies.

F-AHP is a combination of methods to approach the concept of Fuzzy AHP (Raharjo, 2002). FAHP cover the weaknesses contained in the AHP, the problem of the subjective nature of the criteria that have more. Uncertainty is represented by the sequence numbers of the scale. Determine the degree of membership of F-AHP developed by Chang using triangular membership function (Triangular Fuzzy Number / TFN). Triangular membership function is a combination of the two lines (linear). Graph triangle membership functions described in terms of triangular curve, such as Figure 1.

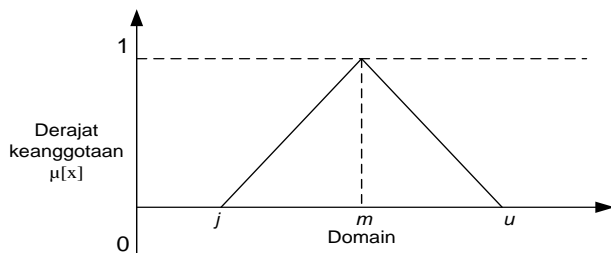


Figure 1. Triangular Membership Function (Chang, 1996)

(Chang, 1996) mendefinisikan nilai intensitas AHP ke dalam skala fuzzy segitiga yaitu membagi tiap himpunan fuzzy dengan dua (2), kecuali untuk intensitas kepentingan satu (1). Skala fuzzy segitiga yang digunakan Chang dapat dilihat pada tabel 1.

Tabel 1. Skala Nilai Fuzzy Segitiga

3.1. STEP-BY-STEP FUZZY-AHP

Different methods have been proposed in the literatures that one of most known of them is Fuzzy Extent Analysis proposed by Chang (1996). The steps of extent analysis can be summarized as follows:

- computing the normalized value of row sums (i.e. fuzzy synthetic extent) by fuzzy arithmetic operations;
- Creating a hierarchical structure and the issues to be resolved between the pairwise comparison matrix to determine the scale criteria TFN
- Determining the value of fuzzy sitesis (S_i) priority using the following formula:

$$S_i = \sum_{j=1}^m M_i^j \times \frac{1}{\sum_{i=1}^n \sum_{j=1}^m M_i^j} \dots\dots\dots (1)$$

Where

$$\sum_{j=1}^m M_i^j = \sum_{j=1}^m il, \sum_{j=1}^m mj, \sum_{j=1}^m uj \dots\dots\dots (2)$$

While

$$\frac{1}{\sum_{j=1}^n \sum_{j=1}^m M_i^j} = \frac{1}{\sum_{i=1}^n ui, \sum_{i=1}^n mi, \sum_{i=1}^n li} \dots\dots\dots (3)$$

- Determining the value of the vector (v) and the ordinate value Defuzifikasi (d').
 If the results obtained in each matrix fuzzy, $M_2 \geq M_1$ ($M_2 = (l_2, m_2, u_2)$) and $M_1 = (l_1, m_1, u_1)$ the value of the vector can be formulated as follows:
 $V(M_2 \geq M_1) = \sup [\mu M_1(x), \min (\mu M_2(y))]$

Or equal to the following equation:

$$V(M_2 \geq M_1) = \begin{cases} 1, & \text{if } m_2 \geq m_1 \\ 0, & \text{if } l_1 \geq \mu_2 \\ \frac{l_1 - \mu_2}{(m_1 - m_2) - (m_1 - l_1)}, & \text{more} \end{cases}$$

If the results of fuzzy values, is greater than k, M_i ($i=1,2,...,k$) the value of the vector can be defined as follows:

$$\begin{aligned} V(M \geq M_1, M_2, \dots, M_k) &= V(M \geq M_1) \text{ and} \\ V(M \geq M_2, M_2) \text{ and} \\ V(M \geq M_k) &= \min V(M \geq M_i) \dots\dots\dots (5) \end{aligned}$$

Assume that:

$$d'(A_i) = \min V(S_i \geq S_k) \dots\dots\dots (6)$$

to $k = 1, 2, \dots, n$; $k \neq i$, then obtained weight value vector.

$$W' = (d'(A_1), d'(A_2), \dots, d'(A_n))^T \dots\dots\dots (7)$$

where $A_i = 1, 2, \dots, n$ is n elements of the decision.

- Normalized weights fuzzy vector (w)

After normalization of the equation (7), then the value of the normalized weight vector is as the following formula:

$$W = (d(A_1), d(A_2), \dots, d(A_n))^T \dots\dots\dots (8)$$

Where W is a non-fuzzy numbers

IV. DISCUSSION

4.1. Criteria and Sub Criteria

After doing the test interviews with the management of the Navy in particular KOARMATIM then obtained criteria and sub-criteria used in determining the number of sectors of maritime security operations in eastern Indonesia, as follows:

Table 1. Criteria and Sub Criteria

N o	Criteri a	Name Of Criteria	Sub Criterie
1	C1	Weapons	<ul style="list-style-type: none"> Coverage Ammunition Maintenance Operational
2	C2	Sector	<ul style="list-style-type: none"> Vulnerability Coordination Potentiality SDAB
3	C3	Logistic	<ul style="list-style-type: none"> Refueling Repair Berth Fresh Water Groceries
4	C4	Infrastructur e	<ul style="list-style-type: none"> Land Manufacture Treatment
5	C5	Ship	<ul style="list-style-type: none"> Coverage Area Speed Type Endurance

Once the criteria and sub-criteria is obtained, further troubleshooting using the F-AHP method.

4.2. FUZZY- AHP

4.2.1. Hierarchy

Hierarchical structure of the problem of determining the optimal number of operational sectors to secure the sea east of the Republic and can be seen figure 2.

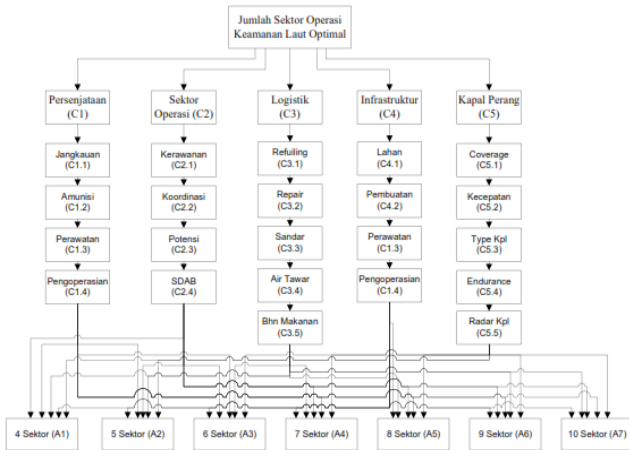


Figure 2. Hierarchical Structure Determination of Total Marine Security Operations Sector Eastern Indonesia

4.2.2. Step By Step F-AHP

The calculation of the value of fuzzy synthesis leads to the approximate total value of each of the criteria, sub-criteria and alternatives in want.

Input value to generate pair-wise assessments use the Chang. However, for ease of calculation then multiplied by 2. For example, the input (0.5, 1; 1.5) will be (1, 2, 3) and so on. Examples of data entry can be seen in Table 2 below:

Table 2. Pair-wise comparison matrix of criteria F-AHP

EVALUASI KRITERIA																
Kriteria Evaluasi	1	2	3	4	5	6	7	8	9	10	11	12	13	14	15	16
SENJATA	1	1	1	1	2	3	1	2	3	1	2	3	1	2	3	1
SEKTOR	0.333	0.5	1	1	1	1	1	2	3	1	2	3	1	2	3	1
LOGISTIK	0.333	0.5	1	0.333	0.5	1	1	1	1	1	2	3	1	2	3	1
INFRASTRUKTUR	0.333	0.5	1	0.333	0.5	1	0.333	0.5	1	1	1	1	1	1	2	3
KAPAL	0.333	0.5	1	0.333	0.5	1	0.333	0.5	1	0.333	0.5	1	1	1	1	1

The next step, the system forms FSE matrix resulting from arithmetic operations rows and columns in table 2, and the resulting matrix in table 3 below:

Table 3. Calculation of fuzzy synthetic extents (FSE)

Fuzzy Synthetic Extent	5	9	13	15.99	27	40	0.025	0.037	0.063	0.125	0.333	0.819
SENJATA	5	9	13	15.99	27	40	0.025	0.037	0.063	0.125	0.333	0.819
SEKTOR	4.333	7.5	11	15.99	27	40	0.025	0.037	0.063	0.108	0.278	0.693
LOGISTIK	3.666	6	9	15.99	27	40	0.025	0.037	0.063	0.092	0.222	0.567
INFRASTRUKTUR	2.999	4.5	7	15.99	27	40	0.025	0.037	0.063	0.075	0.167	0.441
KAPAL	2.332	3	5	15.99	27	40	0.025	0.037	0.063	0.058	0.111	0.315

The next step, the system forms FSE matrix resulting from arithmetic operations rows and columns in table 2, and the resulting matrix in table 3 below. Of the

matrix is to be generated FSE variables such as eigen-vectors, the degree of probability and the normalized matrix. The last step will be generated where the emphasis criteria. These steps are repeated as many times as there sub-criteria.

Before continuing this process it will be calculated IR (Index Ratio) resulting from the division of numbers CI (Consistency Index) and CR (Consistency Ratio) when it is in accordance with the formula Sa'aty then the system will store the data. And so on so that the calculation process is complete until the last sub-criteria. Figure 3 below shows the results of the final weighting generated by the system.

Figure 3. Final calculation

The solution provided by the system can be seen in the display form of the figure 4 below:

Figure 4. Solution from Fuzzy AHP

4.2.3. Data Flow Diagram

Data flow diagram of the system is illustrated below:

a. DFD Level 0

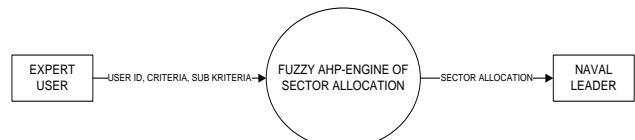


Figure 5. DFD Level 0

Users of this system divided by 2 is Admin and Expert. System provides the AHP calculation to completion ranging from matrix calculations FAHP until normalization process if the user entered the category admin. System generates the final weights of all sub-criteria as well as providing the final calculation in which the ship's captain is authorized to enter a value.

b. DFD Level 1 = User Login

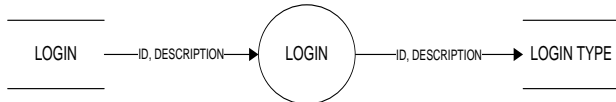


Figure 6. DFD Level 1 for user login

Users of this system divided by 2 is Admin and Expert. System provides the AHP calculation to completion ranging from matrix calculations FAHP until normalization process if the user entered the category admin. System generates the final weights of all sub-criteria as well as providing the final calculation in which the ship's captain is authorized to enter a value.

DFD Level 1 = F- AHP

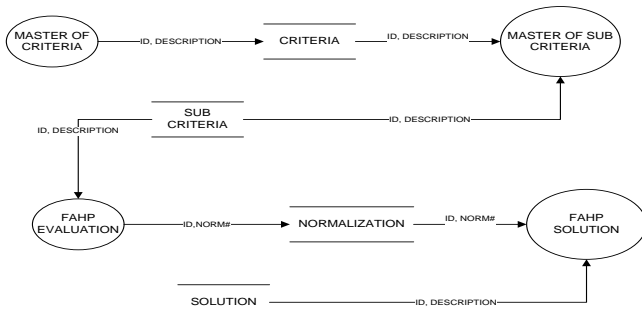


Figure 7. DFD Level 1 for Fuzzy AHP

The system will provide to users who log in with the admin user types allowed for input, edit, add and delete the data on the criteria and sub-criteria are shown in Figure 5.

c. DFD Level 2 = F-AHP

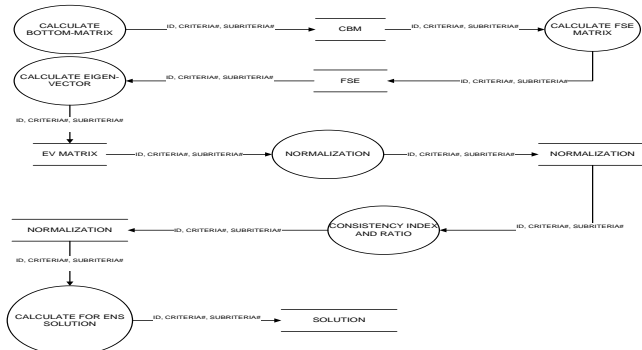


Figure 8. DFD Level 2 for Fuzzy AHP

The system will provide to users who log in with the user as a kind of expert is allowed to perform the calculations step by step in fuzzy AHP are shown in Figure 5 above

DFD above shows the the process of the system FAHP made in this study. The resulting solution is very dependent on the perception of expert user of the criteria and sub-criteria that have been provided.

V. CONCLUSION

Based on the calculation of the fuzzy AHP designed this study are obtained as follows:

1. Infrastructure is the highest criterion value of 0.67. This means that the system is suggested to Armatim to make infrastructure improvements each sector. Including ship infrastructure.
2. Coverage Area is the highest sub-criteria with a value of 0.33. This means that the system is

suggested to Armatim to expand the reach of the patrol boat. This resulted in the renewal of the vessel which supplies both weapons, radar and its cargo could be accounted for reliability. Since the addition of the sector is tantamount to increasing the ability of ships and personnel.

3. Finally, the system prompts the Armatim to increase the number of sectors to be 7 with a value of 45,335. For the current state of the system does not propose an increase but the improvement of the infrastructure sector and ship technology.

REFERENCES

- [1] Ade Supriyanto Sinaga and Ketut Buda Artana, (2012). *Application Of Multiple Attribute Decision Making (MADM) Spread The Planning Naval Base In Eastern Indonesia*. Essay, Department Of Ocean Engineering, Fakulty Of Marine Technology, ITS.
- [2] Chang, D.Y., (1996). *Application of the extent analysis method on fuzzy AHP*. *European Journal of operational Research* 95, 649-655
- [3] Jasril, Elin Haerani and Lis Afrianty, (2011). *Decision Support Systems Employee Selection Method Using FAHP*, *Seminar on Information Technology Applications 2011*, ISSN: 1907-5022. F36 – F43.
- [4] Kahraman, Cengiz, Ufuk Cebeci, and Da Ruan., (2004). *Multi Attribute Comparison of Catering Service Companies Using Fuzzy AHP: The Case of Turkey*, *International Journal Of Production Economics* 87, 171-184.
- [5] Lee, H. S., (2009). *Using Fuzzy AHP to Develop Intellectual Capital Evaluation Model For Assessing their Performance Contribution in a University*, *Expert System with Application*. xxx,xxx-xxx
- [6] Mikhailov.L and Tsvetiniy.P., (2004). *Evaluation of services using a Fuzzy Analytic Hierarchy Process*. *Applied Soft Computing* 5, 22-23
- [7] Satty, T. L., 1980. *The Analytical Hierarchy Process: Planning, PrioritySetting, Resource Allocation*. New York: McGraw-Hill
- [8] Saaty. T.L. 1991. *Pengambilan Keputusan Bagi Para Pemimpin*. PT. Pustaka Binaman Pressindo Jakarta
- [9] Saaty, T.L. 1993. *The Analytical Hierarchy Process*, McGrraw-Hill, New York. 1993.
- [10] Saaty, T. L. 2001. The seven pillars of the analytic hierarchy process. *Multiple Criteria Decision Making in the New Millennium*. M. Koksalan and S. Zionts. 507: 15-37.
- [11] Sadly, M. (2007). *Utilization of Technology Assessment Knowledge-based Expert System in the Management of Natural Resources*,

Acryl Resin Distribution In Lime Tree Wood Determined By ^{241}Am Analyser Of Density Profiles

Ladislav Reinprecht,¹ Ján Iždinský,²

^{1,2}(Department of Mechanical Wood Technology, Technical University of Zvolen, Masarykova 24, Slovakia)

ABSTRACT: The aim of this study was to determine retention and distribution of the polybutylmethacrylate resin Solakryl BT-55 in conserved lime tree wood (*Tilia cordata* Mill.) using conventional method and gamma ray method working with radioisotope ^{241}Am . Conservation of sound lime tree samples 60 x 60 x 60 mm with known densities and density profiles in all three anatomical directions was performed with a 27.5 % toluene acrylic solution (Solakryl BT-55 diluted with toluene in a ratio of 1:1) in autoclave at 20 °C and 0.8 MPa for 5, 30 or 180 minutes.

Total retentions of the acryl resin increased nonlinearly with prolongation of the impregnation process when densities in the oven dry state of conserved samples increased about 20.5 % (5 min), 25.5 % (30 min) or 30 % (180 min). The gamma ray distribution analyses of the acryl resin showed that lime tree wood had the best impregnability in the longitudinal direction. Differential retentions of the solid acrylic resin into samples varied from 0.15 to 0.20 g/cm³ at distance of 5 mm from the axial surfaces, from 0.05 to 0.13 g/cm³ at distance of 20 mm from the axial surfaces, and only from 0.02 to 0.11 g/cm³ in the centre of samples (at distance of 30 mm). Penetrations of the acryl resin in the radial and tangential directions were negligible, unlike the longitudinal direction.

Keywords: acryl resin, distribution, lime tree, radioisotope ^{241}Am , retention

I. INTRODUCTION

Generally, for improving the esthetical, physical and mechanical properties of wood and wooden artefacts are used conservation agents. Efficiency of various conservation processes with natural and synthetic agents depends on more factors related to (1) wood structure, e.g. species, permeability, moisture, geometry, range and degree of damaging by bacteria, fungi, insect, etc., (2) macro- and micro-distribution of the conservation agents in wood which depends on their properties and also on technological parameters of the conservation process, e.g. pressure and time, (3) physical and chemical properties of conservation agents, e.g. viscosity, surface tension, polarity, molecular weight, possibility for reactions with –OH groups of cellulose, etc. [1,2].

Distribution of acryl and other conservation agents in wood can be determined by destructive methods, e.g. on small drilled samples, cross-sections and micro-slides by a scanning electron microscope – SEM [3], and also by various non-destructive methods, e.g. by acoustic, thermographic, nuclear magnetic resonance or radiographic [4, 5, 6].

At analysis the penetration, retention and distribution of conservation agents in wooden objects, similar to estimation of moisture, adhesive, mechanical

behavior, growth rings, knots, or defects caused by fungi and insect, The following stationary or mobile radiographic methods are usually applied [4, 7, 8, 9, 10, 11, 12, 13, 14, 15]:

- Conventional X-ray radiography – one line scanning,
- Gamma rays densitometry – one line scanning,
- X-ray computer tomography scanning (2D and 3D, e.g. SRXTM),
- γ -ray computer tomography scanning (2D and 3D),
- scanning neutron radiography.

The aim of this work was to evaluate the acryl resin “Solakryl BT-55” retention and distribution in lime tree wood in the longitudinal, radial and tangential directions after its pressure impregnation, using one line scanning gamma rays densitometry – the analyzer of density profiles. The density profiles of lime tree samples were monitored before and after conservation and from these profiles the acryl resin amount in defined distances from the external surfaces of conserved samples were computed. Used analyzer of density profiles is based on the measurement of the absorption coefficient attenuate of the gamma-radiation from the isotope ^{241}Am passing through tested material. More other researches preferred this isotope at testing the density and quality of wood and wooden composites [16, 17, 18, etc.].

II. MATERIAL AND METHODS

2.1 Lime tree wood

Samples, 60 mm x 60 mm x 60 mm (longitudinal x radial x tangential), were prepared from one lime tree (*Tilia cordata* Mill.) sound board 1400 x 400 x 100 mm which was previously kiln dried and conditioned on approximately 12 % moisture content. Natural samples without knots or other inhomogeneities were then selected for the experiment. In the oven dry state were determined their total densities “ ρ_N (g/cm³)” and density profiles in three anatomical directions “ $\rho_{N\text{-profile}}$ (g/cm³)”.

2.2 Acryl resin

For the lime tree samples conservation was used commercial product Solakryl BT-55, which contains 55 % of the polybutylmethacrylate (PBMA) and it is manufactured in the Lučební závody, Draslovka a.s. Kolín, Czech Republic. In the experiment was used a 27.5 % solution of the acryl resin. It means the Solakryl BT-55 was diluted with toluene in a weight ratio 1:1 (w/w). This resin is convenient for restoration works, e.g. for consolidation of wooden artefacts. Its basic chemical-physical properties by the technical sheet PND 47-701-93 are as follows: $M_w = 40.103$ g/mol; $\rho = 900$ kg/m³; $T_g = 45$ °C.

2.3 Conservation process

Conservation of the lime tree samples with Solakryl BT-55 was performed in the Dreyer-Holand-

Merten KG device by the pressure-vacuum Lowry technique at a temperature of 20 °C, using pressure of 0.8 MPa, lasting for 5, 30, or 180 minutes. Conserved samples were conditioned 4 weeks at a relative humidity of 50 % and a temperature of 20 °C, then dried in a kiln at 103 ± 2 °C into the oven dry state, and finally re-analyzed their total densities " ρ_C (g/cm³)" and density profiles in three anatomical directions " $\rho_{C-profile}$ (g/cm³)". Volumes of samples remained the same during and after conservation, so the acryl resin was only in lumina and was not able to penetrate into cell walls of wood. It was confirmed by microscopic analyses, as well.

2.4 Total retention of acryl resin

Total retentions " R_S (g/cm³)", i.e. total solid mass retentions of the acryl resin Solakryl BT-55, were calculated as difference between densities of the lime tree samples in their conserved " ρ_C (g/cm³)" and natural " ρ_N (g/cm³)" state by equation 1:

$$R_S = \rho_C - \rho_N \quad (1)$$

2.5 Assessment of acryl resin distribution in wood by the analyzer of density profiles

Density profiles of the natural and conserved lime tree samples were determined again in their oven dry state. Apparatus constructed in laboratories of the Faculty of Wood Sciences and Technology, Technical University in Zvolen was used for these analyses (Fig. 1). Source of the gamma radiation was a low-energy radiant AMG 50. It works with the radioisotope ²⁴¹Am having the energy of 59.5 keV, and its output power is 2.0 GBe.

During measurements, the tested samples were imbedded in initial position on the moving electrical car, then the cover of the emitter was removed and the beam of gamma-rays distributed from the radiant AMG 50 was transmitted through the samples gradually in their all three anatomical directions – longitudinal, radial and tangential. The shift of the samples was always after each 0.2 mm. The analyzer scanned the density profiles of respective samples in one plane (Fig. 1). The intensity of the gamma-radiation after crossing the slots is evaluated by the NaJ (TI) detector which is attached to the single-channel spectrum analyzer IH 10 made by the firm STADOS Prague, Czech Republic. This analyzer is furnished with IMS2 interface that makes it possible to control measure with personal computer [19]. Measurements of the density profiles were carried out in the same position of samples, i.e. in the natural " $\rho_{N-profile}$ (g/cm³)" and then in the conserved " $\rho_{C-profile}$ (g/cm³)" state, what was secured by small cuts on their edges (Fig. 1).

The differential retentions of the acryl resin Solakryl-BT55 into lime tree samples – test pieces " $R_{S-profile}$ (g/cm³)" were calculated separately for their three anatomical directions (as difference between density profile of the conserved and natural sample) in the same plane for defined distances from their outer surface by equation 2:

$$R_{S-profile} = \rho_{C-profile} - \rho_{N-profile} \quad (2)$$

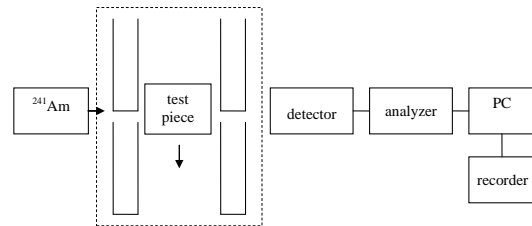


Fig. 1: Working flow diagram of the analyzer of density profiles - densities evaluated by equation 3

$$I = I_0 \cdot e^{-C \cdot \rho \cdot d} \quad (3)$$

where: " I_0 " is the intensity of the incident gamma beam, " I " is the intensity of the gamma beam transmitted through test piece (lime tree sample), " C " is the gamma-beam attenuation coefficient of the test piece, " ρ " is the density of the test piece and " d " is the thickness of the test piece in the direction of gamma beam.

III. RESULTS AND DISCUSSION

Total retentions of the acryl resin Solakryl BT-55 (R_S) into lime tree samples are listed in the Table 1.

Tab. 1: Total retentions of the solid part of acryl resin "Solakryl BT-55" (R_S) into lime tree samples

Time of 0.8 MPA in autoclave	5 min	30 min	180 min
Density of natural samples - ρ_N (g.cm ⁻³)	0.470 (0.017)	0.468 (0.012)	0.467 (0.013)
Density of conserved samples - ρ_C (g.cm ⁻³)	0.566 (0.024)	0.587 (0.022)	0.607 (0.021)
Total retention of acryl - R_S (g.cm ⁻³)	0.096 (0.030)	0.119 (0.023)	0.140 (0.019)

Notes:

- Mean values are always from 6 replicates (5 min → No: A11-A16; 30 min → No: B21-26; 180 min → No: C31-C36)
- Values in the parentheses are the standard deviations

Differential retentions related to a solid part of the acryl resin Solakryl BT-55 ($R_{S-profile}$) into lime tree samples are presented in the Figures 2 and 3. For illustration are shown results only from one replicate selected from six replicates tested at a given impregnation time, i.e. replicates with numbers A-12, B-22 and C-31.

From the total retentions of the acryl resin into lime tree samples established after 5, 30 or 180 minutes of the pressure impregnation process (Table 1), and also from the differential retentions of the acryl resin rated in three anatomical directions of wood (Figs. 2 and 3), it is evident that the penetration kinetic of the conservation agent in wood structure had a non-linear character. Relatively the largest retentions of the acryl resin into lime tree wood were achieved during the first 5 minutes of impregnation while then retentions grew only moderately (Figs. 2 and 3). This result complies with knowledge of [20] and more other researches [e.g. 21] impregnated beech, maple, ash, pine and spruce samples of different dimensions from 15 to 150 minutes) under which the dependence between retention and impregnation time can be expressed by exponential, logarithmic or other non-linear equations.

The distribution analyses confirmed that the best impregnability of lime tree wood with the acryl resin was achieved in its longitudinal direction. This result complies also with a generic penetration model of adhesives for hardwoods proposed by [22] in which the vessel network is dominated. In our experiment, i.e. after pressure impregnation lasting from 5 to 180 minutes, the differential retention of the acryl macromolecules in the longitudinal direction at distance of 5 mm from the axial surfaces of samples varied usually from 0.15 to 0.20 g/cm³, at distance of 20 mm from 0.05 to 0.13 g/cm³, or in their centre – at distance of 30 mm only from 0.02 to 0.11 g/cm³ (Fig. 3).

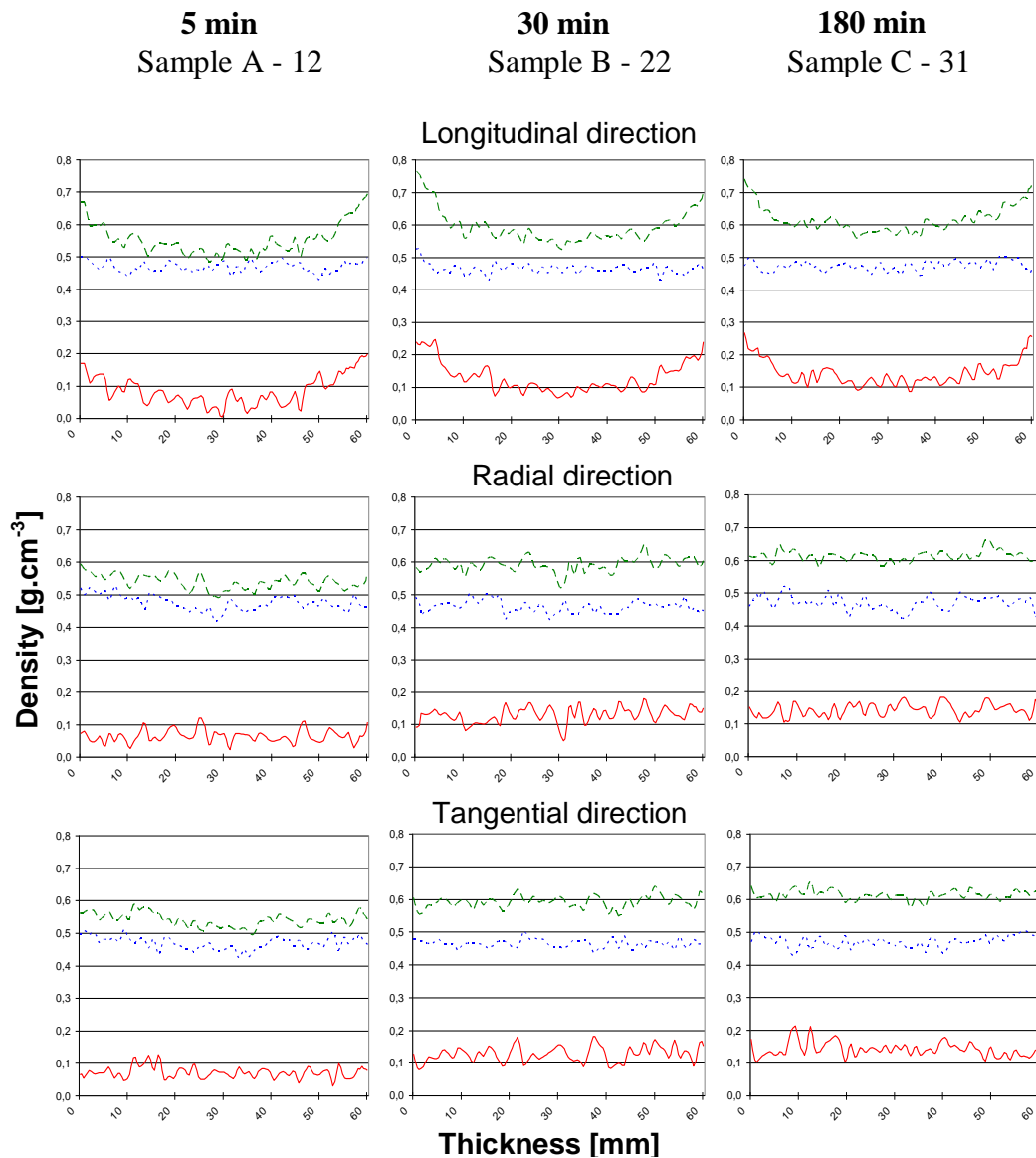


Fig. 2: Density profiles of the natural ($\rho_{N\text{-profile}}$ ) and conserved ($\rho_{C\text{-profile}}$ - - -) lime tree samples 60x60x60mm, and differential retentions of the acryl resin Solakryl BT 55 ($R_{S\text{-profile}}$ —)

Differential retentions of the acryl resin in the radial and tangential directions were negligible. It was indirectly found by almost the same differential retentions which were assessed in the radial and tangential directions of samples from various distances of their outer surfaces (Fig. 3). So, toluene solutions of the acryl resin penetrated into lime tree samples preferentially (or only) in the longitudinal direction (Fig. 3).

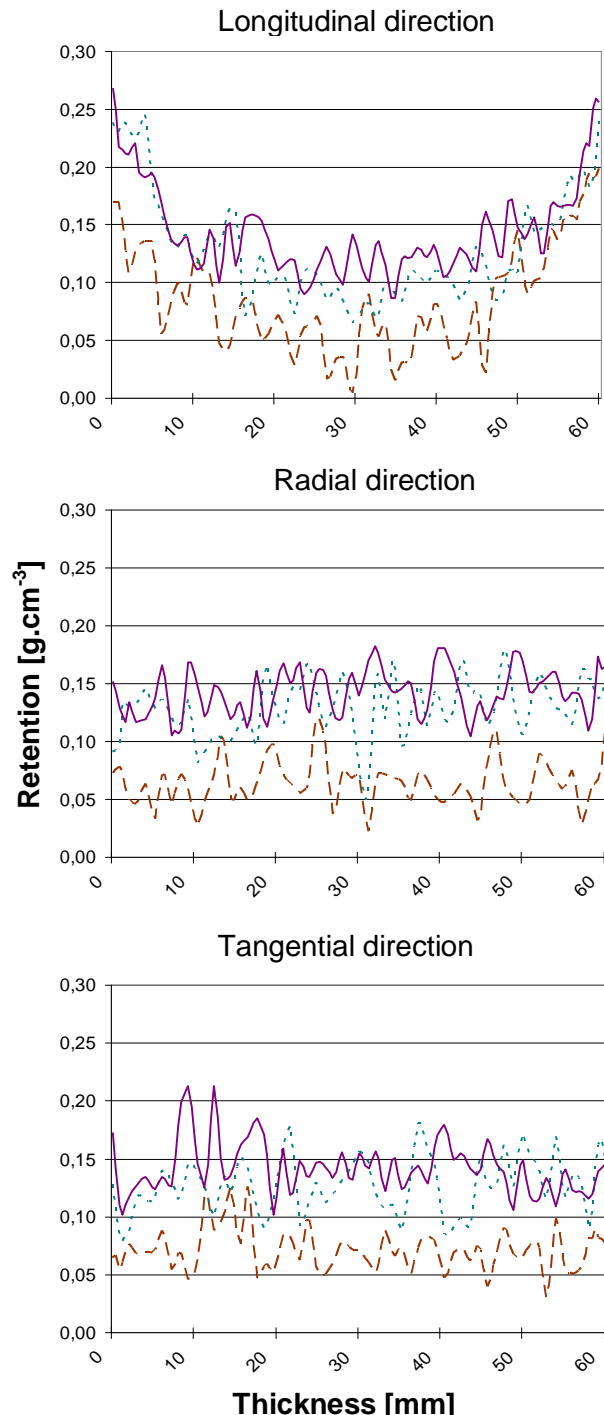


Fig. 3: Differential retentions of the acryl resin Solakryl BT-55 ($R_{S-profile}$) into lime tree samples 60x60x60 mm (see Fig. 2) after 5 minutes ---, 30 minutes or 180 — minutes of the pressure impregnation processes

IV. CONCLUSIONS

The achieved results give the opportunity to do the following conclusions:

- The gamma ray densitometry working with the isotope ^{241}Am is a suitable method for distribution analyses of solid conservation substances, e.g. the acryl resin Solakryl BT-55, in wood.
- Clearly the highest penetration of the acryl resin into lime tree wood occurred from its axial surfaces in the longitudinal direction.
- The most significant penetration and retention of the acryl resin into lime tree wood was measured at beginning of the pressure impregnation processes, and this is in compliance with exponential behavior of transport processes in wood.

V. ACKNOWLEDGEMENTS

The author would like to thank the Grant Agency of the Slovak Republic (Project VEGA No. 1/0574/12/) for financial support of this work.

REFERENCES

- [1] L. Reinprecht, Rekonštrukcia objektov z dreva "Reconstruction of wooden structures" (TU Zvolen – Slovakia, 1998).
- [2] C. A. S. Hill, Wood modification – chemical, thermal and other processes (John Wiley & Sons Ltd, Chichester – UK, 2006).
- [3] L. Reinprecht, and I. Makovíny, Hardening of aminoplasts in modified wood with catalytic and thermic dielectric heating, Modyfikacja drewna, 1987, 288-298.
- [4] A. Unger, A. P. Schniewind, and W. Unger, Conservation of wood artifacts (Springer-Verlag Berlin Heidelberg, 2001).
- [5] E. Lehmann, S. Hartmann, and P. Wyer, Neutron radiography as visualization and quantification method for conservation measures of wood firmness enhancement, Nuclear Instruments and Methods in Physics Research – Section A, 2005, 542: 87-94.
- [6] I. Kučerová, B. Schillinger, E. Calzada, and E. Lehmann, Monitoring transport of acrylate consolidants through wood by neutron radiography, Wood Science for Conservation of Cultural Heritage, 2009, 80-85.
- [7] V. Bucur, S. Garros, A. Navarrete, M.T. de Troya, and R. Guyonnet, Kinetics of wood degradation by fungi with X-ray microdensitometric technique, 10th International Symposium on Nondestructive Testing of Wood, Lausanne – Switzerland, 1996, 209-215.
- [8] I. Kučerová, and J. Lisý, Sledování pruniku impregnační látky do dřeva metodou počítačové tomografie "Study of the penetration ability of consolidating agent into wood by using the X-ray computer tomography" Rekonštrukcia a konzervácia historického dreva '99, TU Zvolen – Slovakia, 1999, 167-170.
- [9] L. Reinprecht, H. Novotná, and V. Štefka, Density profiles of spruce wood changed by brown-rot and white-rot fungi, Wood Research, 52(4), 2007, 17-28.

- [10] D. Mannes, L. Josic, E. Lehmann, and P. Niemz, Neutron attenuation coefficients for non-invasive quantification of wood properties, *Holzforschung*, 63, 2009, 472-478.
- [11] D. Mannes, F. Marone, E. Lehmann, M. Stampononi, and P. Niemz, Application areas of synchrotron radiation tomographic microscopy for wood research, *Wood Sci. Technol*, 44, 2010, 67-84.
- [12] J.Y. Buffiere, E. Maire, J. Adrien, J.P. Masse, and E. Boller, In situ experiments with X ray tool for experimental mechanics, *Experimental mechanics*, 50, 2010, 289-305.
- [13] F. Forsberg, M. Sjodahl, R. Mooser, E. Hack, and P. Wyss, Full three-dimensional measurements on wood exposed to three-point bending: Analysis by use of digital volume correlation applied to synchrotron radiation micro-computed tomography image data, *Strain*, 46, 2010, 47-60.
- [14] E.H. Lehmann, D. Mannes, P. Scherrer, K. Hunger, M. Wörle, S. Braovac, H. Kutzke, and M. Christensen, Wood investigations by means of radiation transmission techniques in the analysis of cultural heritage objects of different size scale, Joint final conference of COST Actions IE0601 and MP0601 - Wood science and conservation: on-going work and challenges for the future, Paris - France, 2011, 53-54.
- [15] P. Hass, F.K. Wittel, M. Mendoza, H.J. Herrmann, and P. Niemz, Adhesive penetration in beech wood: experiments, *Wood Sci. Technol.*, 46, 2012, 243-256.
- [16] F. Divós, S. Szegedi, and P. Raics, Local densitometry of wood by gamma batch-scattering, *Holz als Roh- und Werkstoff*, 54 (4), 1996, 279-281.
- [17] M. Tiitta, H. Olkkonen, T. Lappalainen, and T. Kanko, Density measurement of particleboard, veneer and wood specimens by narrow beam gamma absorption technique, *Nondestructive Testing of Wood*, Lausanne - Switzerland, 1996, 187-200.
- [18] W. Dzbeński, P. Mańkowski, and S. Krzosek, Theoretical and practical usefulness of radiation methods for wood density testing, *Folia Forestalia Polonica – Series B*, 39, 2008, 31-43.
- [19] V. Bahýl, Analyzátor hustotného profilu aglomerovaných materiálov “Analyzer of density profiles of composite materials”, *Drevo*, 47(2), 1992, 48-49.
- [20] J.F. Siau, *Transport processes in wood* (Springer Verlag, New York, 1984).
- [21] L. Reinprecht, and D. Horský, Impregnability of tree species as a function of their shape, Latest achievements in research of structure and physics, IUFRO Conference, TU Zvolen – Slovakia, 1990, 163-177.
- [22] M. Mendoza, P. Hass, F.K. Wittel, P. Niemz, and H.J. Hermann, Adhesive penetration of hardwood: a generic penetration model, *Wood Sci. Technol.*, 46, 2012, 529-549.

A Total Productive Maintenance (TPM) Approach To Improve Overall Equipment Efficiency

Hemant Singh Rajput¹, Pratesh Jayaswal²

¹(Mechanical, M.I.T.S. /R.G.P.V., India)

²(Department of Mechanical Engineering, R.G.P.V. University, India)

ABSTRACT: Good maintenance is fundamental to productive manufacturing system. Total Productive Maintenance (TPM) is an alternative approach to equipment maintenance that seeks to achieve zero breakdowns and zero defects. TPM is an approach to keep the current plant and equipment at its higher productive level through cooperation of all areas of organization. In this paper the selected machines were carefully studied in an industry. Data for past have been analyzed and results achieved are quite encouraging in terms of motivated employees, improvement in overall equipment effectiveness (OEE) and reduction in no. of accidents on shop floor. The analysis has revealed that there are 98% good components, 2% rework losses, where the nine most common causes were identified for the machine stoppages. The OEE was 67% and the six big losses represent 35% loss of the product time. Based on the findings, it was recommended to implement a TPM to improve the OEE of the plant.

Keywords: Manufacturing performance, overall equipment effectiveness implementation, planning, training, TPM, etc.

I. INTRODUCTION

In this competitive world total elimination of waste is necessary for the survival of the organization. The wastes generated due to the failure shutdown of facilities that have been built, with huge investment and also waste such as defective products should be absolutely eliminated. In a manufacturing scenario, the desirable productivity, cost, inventory, quality and delivery all depend on the efficient functioning of the company's facilities. The philosophies like, total quality management (TQM), just in time (JIT), flexible manufacturing systems (FMS), etc. have led to a comprehensive maintenance technique known as total productive maintenance (TPM) [1]. Hartman defines TPM as "Total Productive Maintenance permanently improves the overall effectiveness of equipment with the active involvement of operators" [2]. The aim of TPM to reduce

The six major equipment losses, to zero, have been recognized as necessary for corporate survival. TPM is a unique Japanese system of plant management, developed from preventive maintenance concept. This approach emphasizes the role of teamwork, small group activities, and the participation of all employees to accomplish equipment improvement objectives [3]. It challenges a sense of joint responsibility between operators and maintenance workers, not only to keep the machines running smoothly, but also to extend and optimize their overall performance [4]. It is also defined as, bringing both functions (production and maintenance)

Together by a combination of good working practices, team working,

And continuous improvement [5]. TPM is intended to bring both functions (production and maintenance) together by a combination of good working practices, team working and continuous improvement [6].

II. PILLARES OF TPM

The Japan Institute of Plant Maintenance propose the introduction of TPM program is based on the implementation of a series 8 pillars of TPM in a systematic way to optimize plant and equipment efficiency by crating perfect relationship between man and equipment. The diagram below represents a common structure of TPM. Figure 1

- Autonomous Maintenance / Jishu Hozen.
- Focused Improvement / Kobestu Kaizen.
- Planned Maintenance.
- Quality Maintenance.
- Training.
- Office TPM.
- Safety, Health and Environment.
- Initial Flow Control.

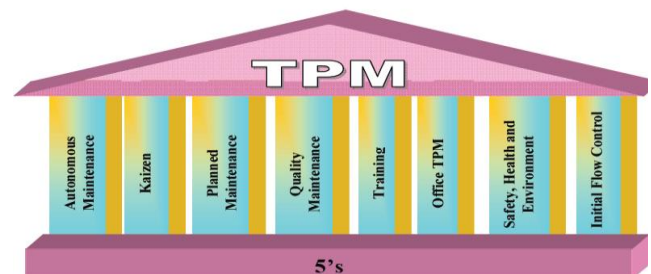


Fig. 1 Pillars of TPM

III. AUTONOMOUS MAINTENANCE/JISHU HOZAN

Japanese name of autonomous maintenance is JISHU HOZEN. This activity is geared towards developing operators to be able to take care of small maintenance tasks, thus freeing up the skilled maintenance people to spend time on more value added activity and technical repairs. The operators are responsible for upkeep of their equipment to prevent it from deteriorating. Autonomous maintenance includes any activity performed by the production department that has a maintenance function and is intended to keep the plant operating efficiently and stable in order to meet production plans [1]. Autonomous maintenance is closely linked with focused improvement in that both support equipment restoration and sustaining basic equipment conditions [14]. Following policies are adopted for developing JISHU HOZEN:

- Uninterrupted operation of equipment's.
- Flexible operators to operate and maintain other equipment's.
- Eliminating the defects at source through active employee participation.
- Stepwise implementation of JH activities.

IV. FOCUSSED IMPROVEMENT/ KAIZEN

Focused improvement includes all activities that maximize the overall effectiveness of equipment, processes and plants through elimination of losses [15]. It includes identification, quantification and elimination of losses that affect productivity, quality, performance, etc. OEE is a key metric of focused improvement. Focused improvement is characterized by a drive for zero losses meaning continuous improvement effort to eliminate any effectiveness losses. Kaizen is a Japanese word for improvement. According to Kaizen, it is a fact that every employee of the company is capable of improving his work and the method of working. Kaizen forms an essential part of TPM.

V. OEE AND SIX MAJOR LOSSES

The literature reveals that no standard exists for calculation of OEE. The OEE calculation is quite general and can be applied to any manufacturing organization [7]. OEE is a measurement used to determine how efficiently a machine is running. Though the definition implies that OEE is the measure of a particular machine, but it can also be used to measure efficiency of product lines, sections of a plant or even the entire plant. Philip Godfrey [8] notes that the effective operation of individual pieces of production equipment, assembly lines or whole factory is dependent on the three factors of OEE [9]. OEE is the most effective measure for driving plant improvement. It continuously focuses the plant on the concept of zero-waste [10]. Unless careful monitoring occurs, the reduced capacity goes unnoticed or is accepted as normal. OEE can be considered to combine the operation, maintenance and management of manufacturing equipment and resources [2]. The losses are divided into six major categories, which affect the overall performance of the equipment namely [10]:

1. Equipment failures/breakdown losses are the time losses and quantity losses caused by defective products.
2. Set-up and adjustment losses are defined as time losses resulting from downtime and defective products that occur when production of one item ends and the equipment is adjusted to meet the requirements of another item.
3. Idling and minor stop losses occur when the production is interrupted by a temporary malfunction or when a machine is idling.
4. Reduced speed losses refer to the difference between equipment design speed and actual operating speed.
5. Reduced yield losses occur during the early stages of production from machine start up to stabilization.
6. Quality defects and reworks are losses in quality caused by malfunctioning of production equipment.

The first two losses are known as down time loss and are used to calculate availability of a machine. The third and fourth are speed losses that determine the performance efficiency and the final two losses are considered to be losses due to defects in the products. OEE is measured in terms of these six losses, which are function of availability, performance rate and quality rate of the machine, production line or factory [11]. And claims, increasing productivity, reducing costs, shrinks inventory, decreasing accidents and promoting employee involvement [12]. Suzuki cites Productivity, Quality, Costs, Delivery, Safety and Morale (PQCDSM), improvement for early TPM implantation.

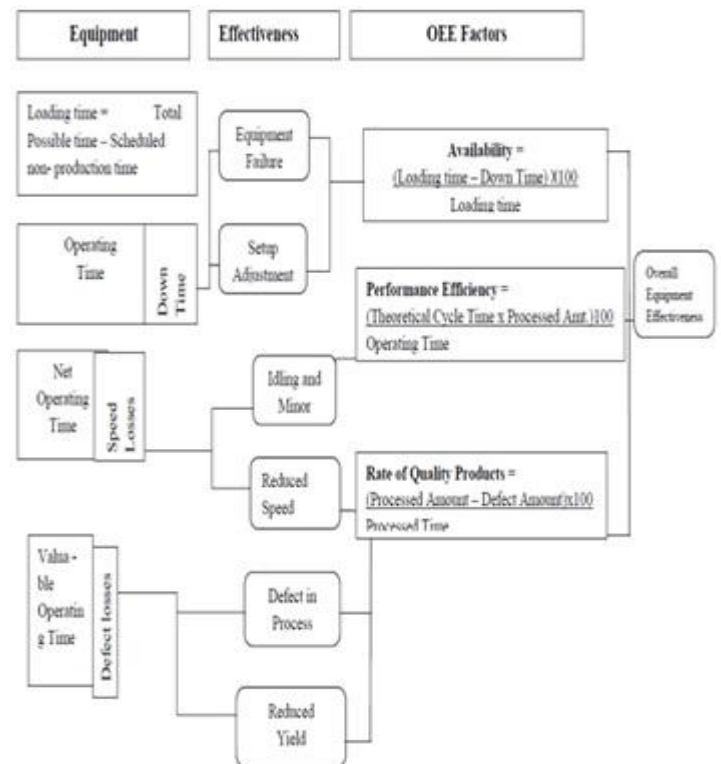


Fig.2 Impact of OEE on Competitiveness [13]

The overall performance of equipment's can be enhanced by identifying and eliminating the root causes. OEE is used as a tool to measure the effectiveness of equipment's to know the current condition. It helps to identify the areas of improvement required in terms of availability, performance efficiency and quality rate of products classifying them into six major losses, as identified by Nakajima in the OEE model [10]. These six major losses are overcome by the Focused Equipment Improvement (FEI) and Autonomous Maintenance (AM) activities of TPM, (Refer fig. 2). These activities will be more effective if carried, in small groups or teams, which are more active, dynamic, self-motivated and also increasing one's-self-confidence of participants.

VI. PROBLEM STATEMENT

Model Machine selected for the implementation of TPM is Shot Peening Machine for the following reasons.

- Poor performance among the other shot -peening machines
- Oldest machine
- Dusty and dark atmosphere
- Poor house-keeping
- Poor safety

VII. OBJECTIVES

The objectives of this case study were,

- Improve equipment reliability and maintainability.
- To cultivate the equipment-related expertise among operators.
- Maximize OEE, through total employee involvement.
- Create an enthusiastic work environment.

VIII. PROPOSED IMPLEMENTATION PLAN FOR TPM

The following plan were used for the implementation of TPM activities,

- Initial cleaning
- Listing and classification of abnormalities
- Why-Why Analysis
- Kaizen
- Jishu Hozan
- Safety

IX. DATA ANALYSIS

First of all out of the whole plant process equipment's bottleneck equipment is identified and was decided to consider this for TPM implementation study. Major losses during the production on this equipment were pointed out using a time study. The study was carried out in all three shifts for two continuous hours in each shift. Two persons standing on either side of the line with the stop watches noted down whenever there was a stop or any other situation occurring, which led to idle or stoppage time on equipment. Three days continuously the study was conducted and finally average of all these readings were calculated in order to decide the final values of various losses on respective equipment. According to study, small interruptions were the biggest contributors to the time losses. So looking into the type of losses it seems that there is lot of scope for improvement in the profitability after implementation of TPM.

Calculation of OEE:

Working days in a month = 30×24 hrs.

Planned down time in a month = 10 hrs.

Setup adjustment losses per day (Which includes material not available, Job setting, rework) = 1.75hrs

Setup adjustment losses per month = 52.5 hrs.

Breakdown time in hrs. Per day = 1 hrs.

Breakdown time per month = 30 hrs.

Total down time per month = (Planned down time + setup adjustment losses + breakdown time)/month = $10 + 52.5 + 30 = 92.5$ hrs. /month

Operating time per month = Running Time - Total down time = 720 hrs. - 92.5 hrs. = 627.5 hrs.

Availability = (loading Time – Down Time)/Loading time = $(720-92.5)/720 = 87.15\%$

Performance efficiency (PE) is calculated as
 $PE = ((TCT \times PA) / OT) \times 100$

Where,

TCT - theoretical cycle time,

PA - processed amount, and

OT - operating time.

Targeted capacity of shot peening machine is 22 MT/hr.

Theoretical cycle time is 2.72min./MT and

Processed Amount (PA) 11000 MT/ month (approx.)

Performance efficiency (PE) = $2.72 \times 11000 / 627.5 \times 100 = 79.4\%$

PE = Speed efficiency \times Rate efficiency

Where,

Speed efficiency = ICT / ACT

ICT - Ideal cycle time and

ACT - Actual cycle time

Rate efficiency = $(PA \times AT) / OT$,

Where,

AT is Actual time. These losses occur due to machine running at slower speed than the designed speed because of vibration and improper maintenance, also due to idle and minor stoppage etc.

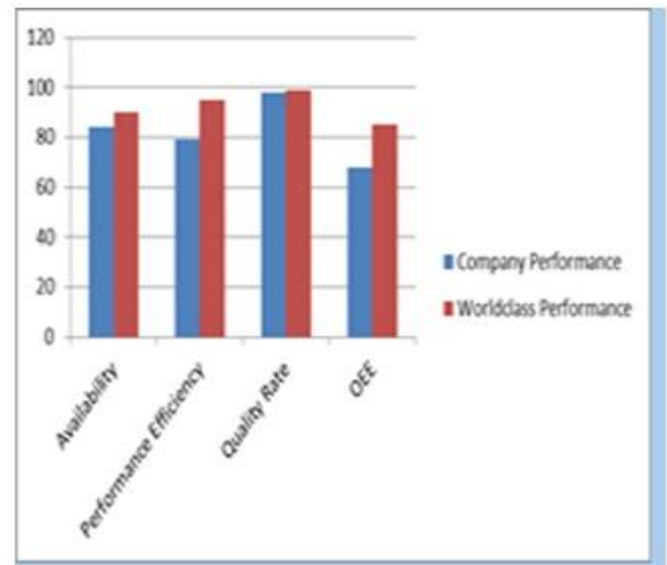
Rate of Quality products = $((PA - DA) / PA) \times 100$

= $(11000 - 220) / 11000 \times 100 = 98\%$.

Defected Amount = 2% of PA = 440 MT (app)

OEE on Shot Peening Machine = Availability \times Performance Efficiency \times Rate of Quality

= $0.8715 \times 0.794 \times 0.98 = 66.4\%$



X. CONCLUSION

The process of recording information must remain simple, but effective for future data analysis .if provisions were made to highlight such problems and possible causes, then it may lead to the correction of common problems such as breakdowns and rework. Ultimately if possible, the aim is to eliminate such causes. Information provided by the trend analysis can provide a basis for forming- long-term plans. The maintenance department can plan spending requirements by using historical information to state the return on investments by contributing to the annual business plan of the company. Therefore if the world-class performance of 85%OEE was

achieved then 20% increase in OEE would have represented enhance the annual earning. To achieve this target efficient maintenance is necessary, in order to establish autonomous maintenance teams, better Communication and team-work must be promoted. It is essential that the company develops an efficient data recording systems, so that up-to date and accurate information will be available to the management. Information provided by the trend analysis can provide a basis for forming long-term plans.

REFERENCES

- [1] Hartman. E, "Successfully Installing TPM in a Non-Japanese Plant", (Pittsburgh, PA, TPM Press, Inc., 1992).
- [2] Bamber, C. J, Sharp, J. M, Hides. M. T, Factors affecting Successful Implementation of Total Productive Maintenance: A UK Manufacturing Case study Perspective, *Journal of Quality in Maintenance Engineering*, Vol.5, 3, 1999, 162-181.
- [3] Bulent Dal, Phil Tugwell, and Richard Greatbanks, "Overall equipment effectiveness as a measure of operational improvement A practical analysis", *International Journal of Operations & Production Management*, 20(12), 2000, 1488-1502.
- [4] Debadyuti Das. "Total Productive maintenance (TPM): A comprehensive tool for achieving excellence in operations system – A case study", *Industrial Engineering Journal* 30 (10), 15, 2001.
- [5] Cooke, F. L., Implementing TPM in plant maintenance: some organizational barriers, *International Journal of Quality and Reliability Management*, 17(9), 2000, 1003-1016.
- [6] Thomas R. Pomorski, *Total Productive Maintenance (TPM) Concepts and Literature Review*, (Brooks Automation, Inc.2004).
- [7] Philip Godfrey, "Overall Equipment Effectiveness" *Manufacturing Engineering*, 81(3), 2002, 109-112.
- [8] K. E, Schroder, Total Productive Maintenance: A contextual View, *Journal of Operations Management*, 17, 1999, 123-144.
- [9] Nakajima, S. *Introduction to TPM: Total Productive Maintenance*, (Productivity Press, Cambridge, MA, 1989).
- [10] Lungberg. O, Measurement of overall equipment effectiveness as a basis for TPM activities, *International Journal of Operation. & Production Management*, 18(5), 1998, 495-507.
- [11] Venkatesh J, *An Introduction to total productive Maintenance*, 2005.
- [12] Suzuki, T., *TPM in Process Industries*, (Portland OR, Productivity Press, 1994)
- [13] Anil Badiger, S., Gandhinathan, R., A Literature Overview on Overall Equipment Effectiveness (OEE), *Journal on Manufacturing Engineering*, 5(3), 2006, 49-56.
- [14] Kunio Shirose, *TPM for Operators*, (Norman Bodek, Productivity, 1992).
- [15] Leflar. J, *Practical TPM*, (Portland OR, Productivity Press, 2001).
- [16] Anil Badiger, S., Gandhinathan, R., Impact of Focused Improvement and Autonomous Maintenance on OEE: A study, *The ICFAI Journal of Operations Management*, 5(2) 2006, 23-34.
- [17] Brave. S.B, Birajdar. H.S, Bhongade. A.S, and Hemant Chaudhari, Application of Total Productive Maintenance (TPM) to vertical boring machine, *Industrial Engineering Journal*, 33(7), 2004 22-27.
- [18] Tajiri. M, Gotoh. F, *TPM Implementation -A Japanese Approach*, (Mc Graw Hill, New York, 1992).

X-Ray Diffraction Analysis of the Microscopies of Some Corrosion-Protective Bitumen Coatings

T. N. Guma,¹ P.B., Madakson,² D.S. Yawas,³ S.Y. Aku,⁴

¹Department of Mechanical Engineering Nigerian Defence Academy Kaduna, Nigeria.

^{2, 3, 4} Department of Mechanical Engineering Ahmadu Bello University Zaria, Nigeria.

Abstract: The most important versatile and widely used method for corrosion protection of steelworks is by paint or organic coatings. Information about microscopy of a protective coating is essential to understand the basic determinants of its attributes and improvement requirements. Bitumen has been an important material for the protection of steelworks in the world's petroleum or other chemical and water industries. Bitumen is however attended with some undesirable characteristics and it can vary widely in quality from one source to another. A previous study has shown that Nigeria has abundant bitumen resources for sustained exploitation as common and economical coat-inhibitors of steel corrosion in her economy. In this paper, the micro-structural make-ups of coatings produced with bitumens harvested from the country's critical bitumen resources by a bath dipping process at a temperature of 230°C and cooled to room temperature are investigated through the analysis. The results show that about 3.75 to 4.847% of each coating is constituted by five to seven of 14 listed different mineral phases; and there is variation in quantity and types of these phases even in coatings produced at the same temperature with bitumen from the same source.

Keywords: Corrosion of steelworks, protective coatings, Nigerian bitumens, bath-dipping process, microscopy, XRD analysis.

I. INTRODUCTION

The levels of material structure which are of greatest interest in material science and engineering are the microstructure, the substructure and the crystal structure. The mechanical, physical, chemical, electrical and magnetic properties of a material such as strength, wear resistance, hardness, corrosion resistance, high and low temperature behaviours; defects such as porosities, segregations, discontinuities, etc are strongly dependent on its micro-structure (Raghavan, 1990; INTERNET, 2012b). Microscopy is the technical field of using microscopes to view samples that cannot be seen with the unaided eye, to understand and provide basic information on their microstructures. There are three well-known branches of microscopy: optical, electron, and scanning probe microscopy. Characteristics distances observable by optical microscopy are around 100nm, by electron microscopy 0.15 – 2.5nm, and by X-ray diffraction 0.01nm; and scanning probe microscopy has minimum scan-spot size and other limitations resolution to about 1nm. The majority of our knowledge about atomic positions and intermolecular distances is gained from X-ray diffraction measurement. X-ray Diffraction (XRD) is a high-tech, non-destructive technique for analyzing a wide range of materials including fluids, metals, minerals, polymers, catalysts, plastics, pharmaceuticals, thin-film coatings, ceramics, solar cells and semi conductors. The technique finds innumerable practical applications in various industries, including microelectronics, power generation, aerospace, and many more. The XRD analysis can easily detect the existence of defects in a particular crystal, its resistance level to stress, its texture, its size and degree of crystallinity and virtually any other variable relating to the sample's basic structure (Hull and John, 1989; Bodor, 1991; INTERNET, 2012b).

Corrosion of carbon steel is a prime corrosion problem in all quarters and the commonest, most versatile and widely used method to counteract it by paint or organic coatings. It is estimated that about 90% of all steel are corrosion-protected by paints or organic coatings. The quality of a protective coating however, depends greatly on the quality of the coating material and method. Bitumen is an organic material that has been in use for corrosion protection of transmission pipelines and other aspects of plants in the world's petroleum or other chemical and water industries; and coatings based on it show excellent resistance to industrial pollution (Guma et al, 2010; 2011a-b; 2012a-b). However, bitumen is in most cases not used in its original form, but modified or supported because of certain undesirable characteristics of the material which include (Jackson and Ravindra, 1996):

- i. Its ability to exist in solid, semisolid, or very high and low viscous liquid state; and change its hardness or consistency with temperature.
- ii. Its not being mechanically tough enough to withstand much wear or stress.
- iii. Its ability to crack under cold weather.
- iv. Its poor resistance to organic solvents.
- v. The dependence of its engineering properties on temperature, duration of loading, and the applied stress.

Nigeria's economy is petroleum-dependent and a lot of wastages occur in it through the corrosion process. The country has abundant bitumen resources for sustained exploitation as common, economical, and effective coat-inhibitors of steel corrosion in her economy. Test-evaluation of corrosion resistance of five different coatings of 0.81 to 1.46mm thicknesses with each of three harvested bitumens from the country's critical bitumen resources with assigned identification names OndoS-A, OndoS-B, and KPB was carried out to substantiate that fact. OndoS-A and OndoS-B were natural bitumens collected from rich and clear deposits in a waterlogged surface area, and underground through a standard extraction hole respectively at Agbabu village in Ondo State of the country while KPB was a synthetic bitumen produced with the blend of

Nigerian crude and Iran's Basara crude as feedstock at the country's most important synthetic bitumen outfit-Kaduna Refining and Petrochemical Company. The coatings were applied on low carbon steel specimens by a bath-dipping process at temperatures in the range of 170 to 230°C and cooled to room temperature. The resistance of each coating to corrosion deterioration of each of the basic mechanical properties of low carbon steel was evaluated. It was found that the bitumens differed physioco-chemically in characteristics properties and, their coatings generally exhibited appreciable inhibition performances; and KPB coatings the highest performance while those of Ondo S-A the least. Moreover, as coating thickness decreased with increase in the coating temperature, the corrosion protection performance decreased (Illston et al, 1979; Pain.Dec.Con., 1995; Alwan, 2010; Guma et al (2010, 2-2011a-b, 2012a); INTERNET, 2012b). The prime objectives of this paper is therefore,

- i. To understand the distinct microscopical make-ups of the bath-dip produced coatings with KPB and Ondo S-A which exhibited the highest and lowest corrosion inhibition performances respectively by proper XRD analysis.
- ii. To present the information for consideration in any methodical modification strategy of bitumens of such characteristic structures and the coating method to improve the coatings for better service performance, and relevant researches on bitumen and other coating technologies.

II. METHODOLOGY

Principles of X-ray diffraction analyses

The concept of X-ray diffraction analysis originates from the established fact that when parallel X-ray 1, 2, 3, 4, 6 of the same wavelength produced by some source are linearly incident on different crystal planes of atoms of a sample separated by a distance 'd' from one another as shown in figure 1 below, there is constructive

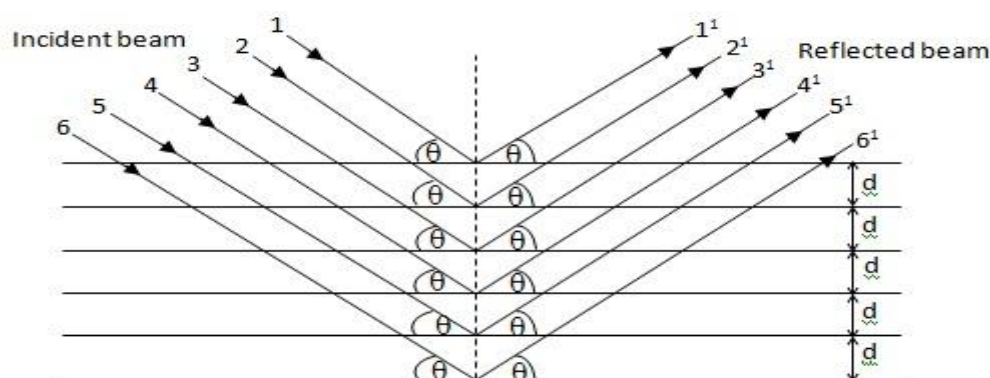


Fig. 1: X-ray diffraction pattern

interference of respectively diffracted (reflected) X-ray $1'$, $2'$, $3'$, $4'$, $6'$,... at an angle θ with each plane on which the ray is incident. In other words the rays are in phase and there is resultant energy leaving the sample. The condition for which there is constructive but not destructive interference has been determined and expressed in Bragg's Law (Raghavan, 1990; Bodor, 1991) as,

$$2d\sin\theta = n\lambda \dots\dots\dots 1$$

Where; $n = 1, 2, 3, 4, \dots$, and λ is the wavelength of the X-ray. The greater the value of λ the larger is the value of θ , while the greater the value of d , the smaller is θ for a given λ . If λ is known and measured, then the value of n/d follows, and if the order can be found, the value of the spacing (d) of the reflecting planes is determined. By putting together the information on various sets of reflecting planes obtained in this way with the X-ray spectrometer, the first crystal structure were made. This follows that properly diffracted rays by atoms of crystals of any materials sample in accordance to Bragg's law can be used to analyze such sample based on the information obtained from the rays. A material that contains various structural discontinuities or inhomogenities will have them manifested in its degree of crystallinity at their locations and will be revealed in its microscopy by the energy intensities of the diffracted rays. This is because crystal atoms of the same size and nature will always produce diffracted X-rays of the same nature and intensities, while those of different sizes and natures will produce different diffraction information. XRD analysis is performed with an automated diffractometer and the sample data can be analyzed by the search/match and accept method using a computerized software with library of diffraction information on different inorganic, organic, and crystalline phases (Raghavan, 1990; Bodor, 1991; INTERNET, 2012c).

The mechanical assembly of the diffractometer that makes up the sample holder, detector arm and associated gearing is referred to as the goniometer. There are two types of goniometer, the THETA (θ) and 2-THETA (2θ) goniometers, but the 2-THETA, goniometer has better accuracy over the THETA when θ is small and is most widely used. For example, Figure 2 below shows the 2-THETA Bragg Brentano goniometer and its parts arrangement, with the sample in position. The X-ray tube and the detector of the goniometer can both be made to move simultaneously over the angular range 2-THETA.

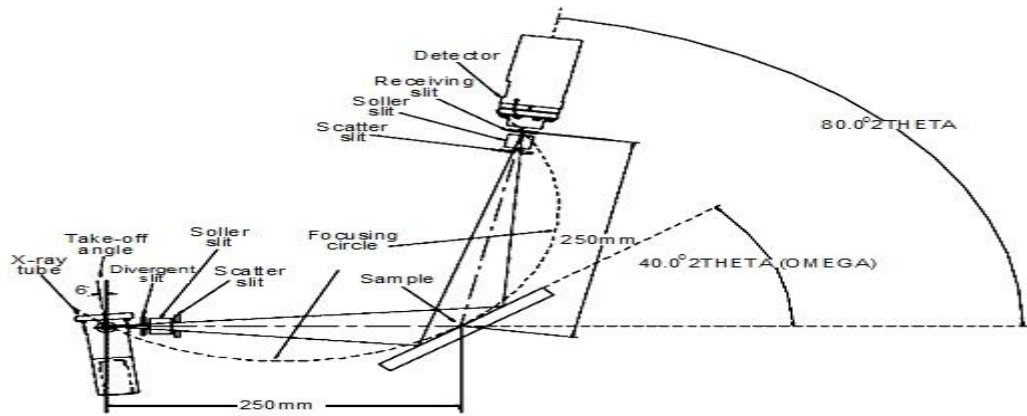


Fig. 2: The Bragg Brentano 2-THETA goniometer (INTERNET, 2012a).

Materials and Facilities

The main materials and facilities used were as follows:

- The remaining bitumen samples of Ondo S-A, and KPB which were used by Guma et al (2010, 2011a-b, 2012)
- The Japanese-made Shimadzu-1200 model diffractometer with complete accessories
- A Bunsen burner
- A mercury-in-glass thermometer with a measuring range of up to 360°C
- A with-handle steel cup
- A thin-lip crucible tong

Specimen preparation and XRD Analysis

A portion of the KPB was detached in a reasonable quantity with a steel spoon and the end with the bitumen placed inside the cup. The thermometer was inserted into the bitumen. The cup was heated with the Bunsen burner by gas-firing and control to the thermometer-monitored temperature of 230°C. This caused most of the bitumen on the spoon to drain off into the cup and the spoon was removed. The specimen loading glass slide of the diffractometer's goniometer was held with the tong and about 75% of it dipped in the bitumen bath at that temperature for 30 seconds and withdrawn and allowed to cool to room temperature for 30 minutes to produce coating (No. 1) of KPB on it in accordance to Illston et al, 1979; Pain.Dec.Con., 1995; Guma et al (2010, 2011a-b, 2012).

The other part of the specimen slide that was not dipped in the heated bitumen was used to hold it in the goniometer's slide attachment slit. The XRD was taken at room temperature using the diffractometer with counter monochromatic Cu-K α radiation (from a Cu tube) of wavelength-0.15406nm. The voltage and current settings were 40KV and 30mA, respectively. The coating was examined in a continuous mode over the maximum angle range of the goniometer from $2\theta = 0$ to 120° . The scanning speed, sampling pitch and preset time were $2\theta = 7^\circ/\text{min}$, 0.02 and 0.17sec respectively.

With these, the diffractogram, reference peak intensities, reference high and low intensity peaks and, the performed search/match and accept information on the coating; were produced with the diffractometer's computer. To investigate any microstructural variation in coatings with bitumen from the same source, the procedure was repeated with another portion of KPB after properly cleaning the cup with kerosene, water and detergent to produce another coating (No. 2) with another portion of KPB. The coating was then scanned with a range of 2θ from 3 to 60° which also covered the major characteristic reflection for all conditions in the coating; and scan speed of 5 deg/min, sampling pitch of 0.02 deg, and preset time of 0.24sec respectively. The described test procedure for coating (No.1) with KPB was similarly repeated with Ondo S-A after similarly cleaning the cup off of the KPB portion.

III. RESULTS AND DISCUSSION

The diffractograms for KPB coating Nos. 1 & 2, and Ondo S-A and an example is shown for the coating No.1 in Figure 3. The scan peak counts intensities for KPB coating (No. 1 & 2) and Ondo S-A were also obtained and an example is shown for the case of KPB coating No. 1 in Table 1, together with the corresponding 2θ scan, observed d-spacing in Angstrom, intensity in counts, intensity match ratio (I/II), and Full Width at Half Maximum at lower angle side (FWHM). The obtained reference peaks of high and low intensities for KPB coating (No. 1 & 2), and Ondo S-A with the diffractometer's computer software were also obtained and an example is shown in Figure 4 for coating No.1. The overall print out result for coating Nos 1&2, and Ondo SA are shown respectively in Tables 2, 3, and 4; showing the scale factor (S), line match ratio (L), density (Dx), percentage composition by weight (Wt %) and intensity (I) for the observed microstructure.

Microstructural analysis of the coating shows that the as-prepared Ondo S-A coating is constituted of five different mineral phases which are principally; Lead Oxide, Magnesium Silicate Hydroxide, Chromium Nitride, Magnesium Silicate Hydroxide, and Calcium Silicate Hydroxide Hydrate totaling to the tune of 3.75% of the scanned area. Results for KPB coating No. 1 show the presence of Sucrose, Sucrose Octaacetate, Nickel Iodide Triethylamine N-oxide, Codeine Phosphate Dihydrate and Barium Neodymium Titanium Oxide mineral phases totaling to the tune of 4.374% within the scanned area. The identified principal mineral phases in KPB coating No. 2 are Hcl, Zirconium Oxide, Codeine Phosphate Dihydrate,

Nickel Iodide Triethylamine N-oxide, Sucrose Octaacetate and Sodium Aluminium silicates totaling to a 4.847 within the scanned area.

The difference between the as-produced KPB coatings (Nos. 1 & 2) is in the presence or absence of the Sucrose, Iron Chromium Oxide, Sodium Aluminum Silicate, Hcl, Barium Neodymium Oxide in one or the other. This means that, there are some microstructural variations in the as-produced coatings even with bitumen from the same source.

IV. CONCLUSION

Bitumens are usually coat-applied within the temperature range of 150 – 250°C and in the oxidized form for corrosion protection of steelworks (Illston et al, 1979; Pain.Dec.Con., 1995). A previous study has shown that coatings of 0.81 to 1.73mm thicknesses produced by the bath-dipping process with bitumens harvested from critical sources in Nigeria can provide appreciable or complete inhibition of corrosion deterioration of the basic mechanical properties of low carbon steel. XRD is a versatile, non-destructive method that will reveal detailed information about the chemical composition, crystallography and microstructure of all types of natural and manufactured materials; that cannot be revealed by the optical and most other methods of microscopy analysis. XRD analyses of microscopies corrosion-protective coatings of bitumens harvested from different critical sources in Nigeria which were produced at 230°C and subsequently cooled to room temperature has been conducted. The results indicate that 3.75 to 4.847% of each of the coatings consists of five to seven of 14 listed distinct mineral phases and coatings of bitumens from even the same source will have variation in these phases.

V. RECOMMENDATION

The information presented in this paper is recommended to be considering in any methodical modification or improvement strategy in utilizing the abundant Nigerian bitumen resources for corrosion protection of steelwork in her petroleum-dependent economy or elsewhere, and for relevant research purposes.

REFERENCES

- [1] Bodor, G. (1991) Structural Investigation of Polymers, Ellis Horwood Limited Chichester, England pp. 230 – 357.
- [2] Von Fraunhofer, J.A. (1975). Paul Elek Scientific Book Limited, London, England pp 116 – 119.
- [3] Hull, B. and John, V. (1989) Non-destructive Testing, English Language Book Society, Macmillan Houndmills pp 1 – 6.
- [4] INTERNET. Basic of X-ray Diffraction. <http://epswww.unm.edu/xrd/xrdbasics.pdf> (10/10/2012a)
- [5] INTERNET. http://www.bruker-axs.com/x_ray_diffraction.html (10/10/2012b)
- [6] INTERNET. Nigerian Bitumen. <http://farriconsulting.blogspot.com/2011/02/bitumenexploitation-and-exploration-in.htm> (10/10/2012c)
- [7] Guma, T.N; Madakson, P.B; Yawas. D.S; and Aku S.Y; Effects of Some Bitumen Coating Treatments on the Hardness Corrosion of Low Carbon Steel, International Research Journal in Engineering Science and Technology, Vol. 7, No. 1 Edna Ben Publishers, Owerri, Nigeria, 2010.
- [8] Guma, T.N; Madakson, P.B; Yawas. D.S; and Aku S.Y; Assessment of Capability Levels of Bitumen From Nigerian Sources to Coat-inhibit Tensile Strength Corrosion of Low Carbon Steel, International Research Journal Engineering Science Vol. 3, No. 1 Pan-African Book Company, Accra Ghana, 2011.
- [9] Guma, T.N; Madakson, P.B; Yawas. D.S; and Aku S.Y; Assessment of Capability Levels of Bitumen From Nigerian Sources to Coat-inhibit Impact Strength Corrosion of Low Carbon Steel, International Journal of Mechanical Engineering Vol. 3, No. 1 Blackwell Publications, Lagos, Nigeria 2011b.
- [10] Guma, T.N; Madakson, P.B; Yawas. D.S; and Aku S.Y; Effects of Some Bitumen Coating Treatment on the Corrosion Fatigue Strength on Low Carbon Steel, Accepted for Publication International Journal of Science and Advanced Technology, Dhaka, Bangladesh (2012a).
- [11] Guma, T.N; Madakson, P.B; Yawas. D.S; and Aku S.Y; Assessment of Physicochemical Properties of Some Bitumen from Nigeria Resources. Nigerian Journal of Basic and Applied Sciences, Published by Usmanu Danfodiyo University Sokoto, Nigeria Vol. 20, No. 1 & 2, (2012b).
- [12] Illston, J.M., Dinivoodie, J.M. and Smith, A.A (1979). Concrete, Timber and Metals: The Nature and Behaviour of Structural Materials. Van Nostrand Reinhold Company Ltd, London, England pp. 569 – 615.
- [13] Pain.Dec.Con. (1995). Painting and Decoration Craftman's Manual and Textbook 8th Edition. Published by Painting and Decorating Contractors of America Fairfax Va, pp. 7 – 15.
- [14] Jackson, N. Ravindra, K.D. (1996). Civil Engineering Materials. Macmillan Press Ltd, London, England pp. 53 – 64.

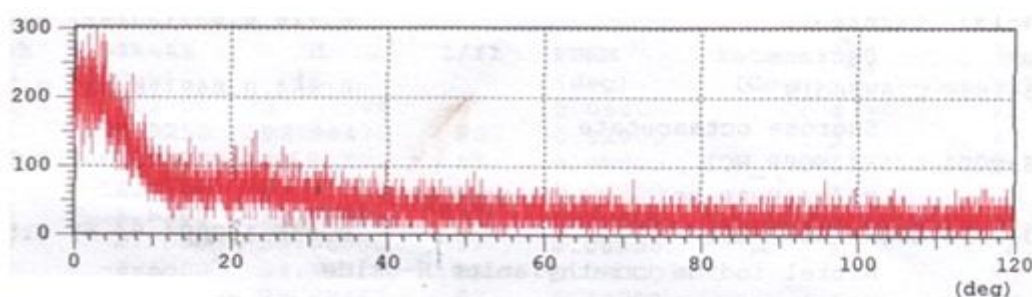


Fig. 3: Diffractogram Obtained with KPB Coating No. 1

Strongest 3 peaks

no.	peak no.	2Theta (deg)	d (Å)	I/I1	FWHM (deg)	Intensity (Counts)	Integrated Int. (Counts)
1	10	4.0000	22.07195	100	0.40000	6	110
2	7	2.5600	34.48329	83	0.08000	5	33
3	2	0.8250	106.99472	83	0.11000	5	41

#Peak Data List

Peak no.	2Theta (deg)	d (Å)	I/I1	FWHM (deg)	Intensity (Counts)	Integrated Int. (Counts)
1	0.2500	353.07979	67	0.06000	4	22
2	0.8250	106.99472	83	0.11000	5	41
3	1.1600	76.09602	67	0.08000	4	21
4	1.4700	60.04918	33	0.06000	2	6
5	1.8100	48.76992	33	0.14000	2	32
6	2.2600	39.06000	17	0.00000	1	0
7	2.5600	34.48329	83	0.08000	5	33
8	2.9550	29.87467	67	0.17000	4	37
9	3.4800	25.36881	17	0.00000	1	0
10	4.0000	22.07195	100	0.40000	6	110
11	4.7200	18.70653	17	0.00000	1	0
12	5.1600	17.11235	50	0.04000	3	21
13	5.6550	15.61551	33	0.03000	2	3
14	5.9400	14.86691	50	0.04000	3	13
15	6.3200	13.97384	83	0.04000	5	31
16	6.9700	12.67207	50	0.06000	3	25
17	7.5350	11.72309	33	0.09000	2	13
18	8.2300	10.73461	33	0.14000	2	15
19	9.0200	9.79613	17	0.00000	1	0
20	11.0600	7.99341	50	0.04000	3	18
21	11.5500	7.65537	33	0.06000	2	19
22	12.0600	7.33276	33	0.08000	2	16
23	12.3600	7.15544	33	0.16000	2	25
24	12.7000	6.96463	17	0.00000	1	0
25	13.4150	6.59499	67	0.19000	4	54
26	13.7200	6.44905	17	0.00000	1	0
27	14.0200	6.31173	50	0.04000	3	17
28	14.3200	6.18017	17	0.00000	1	0
29	14.7450	6.00298	50	0.05000	3	21
30	15.4500	5.73061	50	0.06000	3	24
31	15.9800	5.54172	33	0.28000	2	44

32	16.38.50	5.40564	50	0.05000	3	14
33	16.6400	5.32337	17	0.00000	1	0
34	17.6000	5.03511	50	0.04000	3	18
35	18.3000	4.84405	50	0.04000	3	20
36	18.7600	4.72630	50	0.04000	3	19
37	19.0800	4.64775	17	0.00000	1	0
38	19.4000	4.57180	33	0.08000	2	9
39	20.5700	4.31433	50	0.06000	3	16
40	20.0400	4.25904	50	0.08000	3	24
41	21.2400	4.17972	17	0.00000	1	0
42	21.7400	4.08471	50	0.04000	3	19
43	21.9000	4.04428	50	0.04000	3	18
44	22.2200	3.99755	33	0.12000	2	27
45	22.6900	3.91579	83	0.10000	5	68
46	23.3400	3.80819	33	0.16000	2	37
47	23.5200	3.77905	50	0.04000	3	11
48	23.8900	3.72175	33	0.14000	2	25
49	24.2200	3.67178	17	0.00000	1	0
50	24.5400	3.62462	50	0.04000	3	17
51	25.0400	3.55337	17	0.00000	1	0
52	25.5700	3.48090	50	0.06000	3	29
53	26.1300	3.40756	50	0.06000	3	28
54	26.6600	3.34101	50	0.08000	3	24
55	27.2700	3.26764	33	0.22000	2	26
56	27.7500	3.21220	33	0.10000	2	21
57	28.1900	3.16306	33	0.06000	2	17
58	28.7600	3.10165	50	0.04000	3	19
59	29.3000	2.04570	17	0.00000	1	0
60	27.7400	3.00164	50	0.04000	3	21
61	30.3200	2.94552	17	0.00000	1	0
62	30.9000	2.89155	67	0.20000	4	72
63	31.2800	2.85728	50	0.04000	3	17
64	31.6700	2.82298	50	0.10000	3	42
65	31.9800	2.79632	33	0.04000	2	17
66	32.2500	2.77352	67	0.14000	4	57
67	32.6600	2.73973	17	0.00000	1	0
68	33.0500	2.70819	50	0.06000	3	36
69	33.9200	2.64069	33	0.08000	2	24
70	34.3000	2.61230	67	0.12000	4	48
71	34.8700	2.57089	33	0.22000	2	44
72	35.5100	2.52601	33	0.06000	2	16

73	35.9000	2.49946	17	0.00000	1	0
74	36.0800	2.48740	33	0.04000	2	19
75	36.2400	2.47678	50	0.04000	3	23
76	37.1600	2.41755	1	0.00000	0	0
77	38.0600	2.36243	50	0.08000	3	32
78	38.5900	2.33119	33	0.06000	2	14
79	38.9000	2.31332	17	0.00000	1	0
80	42.1900	2.14023	33	0.06000	2	9
81	43.5600	2.07604	17	0.00000	1	0
82	44.2300	2.04613	33	0.06000	2	11
83	44.7800	2.02227	17	0.00000	1	0
84	46.1200	1.96658	50	0.08000	3	20
85	46.7400	1.94193	17	0.00000	1	0
86	52.0400	1.75593	33	0.04000	2	8
87	52.4800	1.74224	50	0.04000	3	19
88	53.2400	1.71915	17	0.00000	1	0
89	54.5400	1.68120	33	0.16000	2	27
90	55.0000	1.66822	33	0.04000	2	9
91	55.8800	1.64402	17	0.00000	1	0
92	61.1200	1.51503	33	0.08000	2	21
93	62.6600	1.48144	17	0.00000	1	0
94	66.5100	1.40472	33	0.14000	2	22
95	66.7700	1.39988	33	0.10000	2	13
96	67.3600	1.33904	17	0.00000	1	0
97	68.4000	1.37044	33	0.08000	2	10
98	70.5200	1.33434	17	0.00000	1	0
99	72.1400	1.30831	33	0.04000	2	9
100	72.8200	1.29776	17	0.00000	1	0
101	77.2500	1.23402	33	0.14000	2	19
102	77.5400	1.23013	17	0.00000	1	0
103	84.2000	1.14897	50	0.04000	3	24
104	84.1500	1.14291	33	0.18000	2	53
105	86.3000	1.12632	1	0.00000	0	0
106	87.7800	1.11110	33	0.04000	2	11
107	88.6400	1.10252	17	0.00000	1	0
108	90.0500	1.08889	33	0.10000	2	21
109	90.8800	1.08110	17	0.00000	1	0
110	91.5400	1.07502	33	0.08000	2	13
111	91.8000	1.07265	17	0.00000	1	0
112	100.0800	1.00493	33	0.04000	2	10
113	100.4000	1.00262	17	0.00000	1	0

114	101.8700	0.99210	33	0.26000	2	42
115	102.5600	0.98730	17	0.00000	1	0
116	104.4700	0.97441	33	0.26000	2	47
117	104.8600	0.97185	50	0.12000	3	32
118	105.4100	0.96829	33	0.18000	2	23
119	105.8200	0.96566	17	0.00000	1	0
120	112.2600	0.92773	33	0.08000	2	13
121	112.5600	0.92611	17	0.00000	1	0
122	114.4000	0.91641	33	0.04000	2	14
123	114.9800	0.91344	17	0.00000	1	0
124	115.6000	0.91031	33	0.08000	2	15
125	115.9200	0.90872	17	0.00000	1	0
126	117.5100	0.90098	33	0.18000	2	30
127	117.9200	0.89904	1	0.00000	0	0
128	118.2600	0.89744	33	0.04000	2	13
129	118.7600	0.89511	1	0.00000	0	0
130	119.2700	0.89277	33	0.14000	2	31

Table 1: Reference Peak Intensities for KPB Coating No. 1

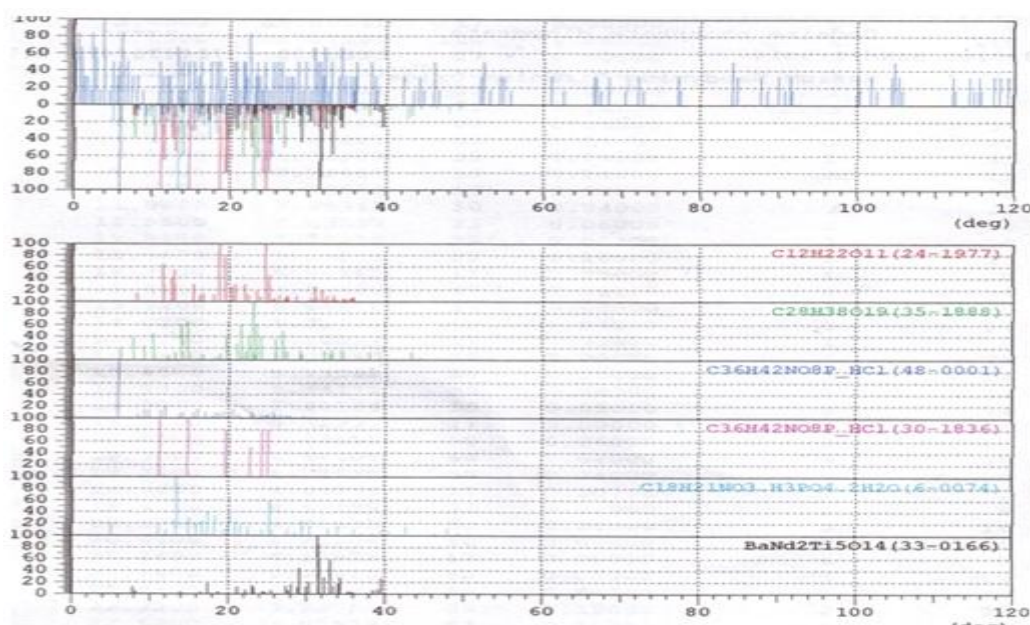


Fig. 4: Reference Peaks of High and Low Intensities for KPB Coating No. 1

<Entry Card>

No.	Card	Chemical Formula	S	L	d	I
		Chemical Name (Mineral Name)	Dx	WT% S.G.		
1	24-1977	C12H22O11	0718	0.833 (35/42)	0.799 -----	0.666
		Sucrose		-----	-----	
2	35-1888	C28H38O19	0.834	0.848 (28/33)	0.745-----	0.632
		Sucrose octaacetate		-----	-----	
3	48-0001	C36H42NO8P_HCL	0.838	0.838 (25/30)	0.712-----	0.593

		C36H42NO8P_HCL (C36H42NO8P_HCL) -----			
4	30-1836 C36H42NO8P_HCL	0.476	1.000 (6/6)	0.593-----0.593	
	Nickel iodide triethylamine N-oxide	-----		-----	
5	6-0074 C18H21NO3 .H3PO4. 2H2O	0.924	0.775 (31/40)	0.733-----0.568	
	Codeine phosphate dehydrate	-----		-----	
6	33-0166 BaNd2Ti5O14	0.833	0.714 (30/42)	0.792-----0.566	
	Barium Neodymium Titanium Oxide	-----		-----	

Table 2: Search/Match and Accept Result for KPB Coating No. 1

<Entry Card>

No.	Card	Chemical Formula	S	L	d	I
		Chemical Name (Mineral Name)	Dx	WT%	S.G.	
1	48-0001 C36H42NO8P_HCl		0.874	0.767 (23/30)	0.741-----0.568	
		C36H42NO8P_HCl (C36H42NO8P_HCl)	-----		-----	
2	22-1025 Zr3O		0.383	0.750 (12/16)	0.702-----0.526	
		Zirconium Oxide	-----		-----	
3	6-0074 C18H21NO3. H3PO4. 2H2O		0.706	0.775 (31/40)	0.672-----0.521	
		Codeine phosphate dehydrate	-----		-----	
4	30-1836 C18H21NO3. H3PO4. 2H2O	0.300	0.833 (5/6)	0.622-----0.519		
		Nickel iodide triethylamine N-oxide	-----		-----	
5	24-0511 C18H21NO3. H3PO4. 2H2O	0.460	0.700 (7/12)	0.739-----0.517		
		Iron Chromium Oxide	-----		-----	
6	35-1888 C28H38O19		0.652	0.758 (25/33)	0.683-----0.517	
		Sucrose octaacetate	-----		-----	
7	10-0393 Na (Si3A1) 08		0.678	0.738 (31/42)	0.688-----0.508	
		Sodium Aluminum Silicate (Albite, disorder	-----		-----	

Table 3: The Search/Match and Accept Result for KPB Coating No. 2

<Entry Card>

No.	Card	Chemical Formula	S	L	d	I
		Chemical Name (Mineral Name)	Dx	WT%	S.G.	
1	8-0019 Pb3O4		0.715	0.795 (31/39)	0.812 ----- 0.646	
		Lead Oxide (Minium, syn)	-----		-----	
2	13-0558 Mg3Si4O10 (OH)2		0.614	0.900 (27/30)	0.708----- 0.637	
		Magnesium silicate hydroxide (Talc-2/ITM/	-----		-----	
3	11-0065 CrN		0.444	0.875 (7/10)	0.720-----0.630	
		Chromium Nitride (Carlsbergite, syn)	-----		-----	
4	29-1493 Mg3Si4O10 (OH)2		0.463	0.800 (12/15)	0.759 -----0.607	
		Magnesium Silicate Hydroxide (Talc-2/ITM	-----		-----	
5	29-0382 Ca14Si24O58 (OH)8.2H2O		0.729	0.786 (33/42)	0.752-----0.591	
		Calcium Silicate Hydroxide Hydrate (Trusc	-----		-----	

Table 4: Search/Match and Accept Result for Ondo S-A Coating

Online Business Frauds: A Case Study of an Online Fraud Survey Company

PROF (DR) YASHPAL SINGH BIST¹, DR CHARU AGARWAL,²
UTTARA BANSAL,³

¹Professor faculty of mngt studies, Daas College of Mngt & Tech Dehradun (UK),
^{2, 3}(Associate Professors, Deptt of computer science, Daas College of Mngt & Tech Dehradun (UK).

ABSTRACT: “Fraud and falsification are highly destructive to market capitalism and, more broadly, to the underpinnings of our society. Our market-system depends critically on trust. Trust in the word of our colleagues and trust in the word of those with whom we do businesss”

----Alan Greenspan

The relationship between a customer and a business organization can stand only on the pillars of trust, faith, fair dealing and mutual expectation. Remove any pillar and the business will collapse but in the great Internet fraud factory these pillars are non-existent. Just a Google search for “internet fraud” pops out 26 lacks results in less than 28 sec indicating the huge menace the global networked world is facing, it’s a vicious cycle of greed, ignorance and fast money, which prods the victims to believe in these surreal scams, they invest their hard-earned money and time. The fraudsters spin their web of lies and deceit, dangling the lure of easy money and false commitments they wait to devour their victim of their self esteem and trust, brutally savaging their faith in the internet, worst still in majority of cases the victims have no redressal’ mechanism in their country as where to complain since these fraudsters leave no physical and legal footprints .The onus no doubt lies with the unsuspecting victims but its also up to the various countries to make their legal IT Laws stringent and strong so that these fraudsters are treated as global frauds and be strictly dealt with. Government organizations and NGO’s should educate the netizens on the “human trust” traps laid for them on the information superhighway. This paper deals with the various dubious mechanisms of fraudulent solicitations made by internet fraudsters, what can be done and why do we fall for it. We specially investigate the online survey frauds.

Keyword: Business Ethics, Internet fraud, Investment frauds, Business frauds, Online survey fraud, Nigerian letter fraud, Fraud management system

THE BROAD CATEGORIES OF INTERNET BASED SCAMS ARE

I. Investment related internet scams

- (a) Online auction and retail schemes
- (b) Online Survey frauds

II. Business Fraud:

- (a) Purchase frauds
- (b) Online automotive fraud
- (c) Counterfeit cashier's check scam
- (d) PayPal Fraud
- (e) Call tag scam
- (f) Money transfer fraud
- (g) Target youth frauds

III. Target elder fraud

(1)Investment related internet scams:

- (a)Online auction and retail schemes
- (b)Online survey frauds

(a)In an online auction scheme, a fraudster starts an auction on a site such as eBay or TradeMe with very low prices and no reserve price, especially for typically high priced items like watches, computers, or high value collectibles. The fraudster accepts payment from the auction winner, but either never delivers the promised goods, or delivers an item that is less valuable than the one offered—for example, a counterfeit, refurbished, or used item.

Online retail schemes, involve complete online stores that appear to be legitimate. As with the auction scheme, when a victim places an order through such a site, their funds are taken but no goods are sent, or inferior goods are sent. However the eBay Site has introduced certain financial control mechanisms and thus until the user is not satisfied with the product the seller will not get the money and in case even after 15 days the buyer fails to inform ebay, ebay believe that the product payment.

Fraud Management in the online retail environment:

A staggering 28% of all online retail orders are affected by fraud². This has direct impact on the ecommerce profitability, operating efficiency and scalability. G.S Paintal of Infosys in his white paper "Fraud Management in the online retail environment" Recommends the following security steps:

- 1) Online payments authorizations of credit cards (This ensures that the card is not stolen or lost and has enough credit in it)
- 2) Address Verification services (AVS) (It Checks billing address of customer with the billing address in the card)
- 3) Use of card verification code (CVV.CVV2)(its 3 or 4 digit number printed at the backside of credit card and ensures that the card was physically present at the time of purchasing)
- 4) Negative files (it consists of a file having data of stolen cards, fake addresses, hacked emails etc)
- 5) Risk predication models/Electronic data warehousing system (Here special soft wares are used which analyzes data from millions of online sales and each prospective order is run through this algorithm and checked for any suspicious attributes)
- 6) Manual reviews (It's the same as above but is done manually, its time consuming)
- 7) Verified by Visa/Master card secure code (these have advanced security mechanisms which take onus of the transactions)

According to Paintal we must have a well modular architecture which clearly defines:

- (1) Ecommerce store front 2) Payment gateways 3)order management system 4)fraud management system and electronic data ware housing analytics

(b) Online Survey frauds:

The question is are there any online survey companies which are genuine, Yes, but its almost impossible to find, a Google search of "online surveys" prompts out 77,3000 results. But in case you are interested be cautious, according to audri and Jim of *Internet ScamBusters*TM, ignore all spam solicitations. They are all scams. Secondly, use a search engine to see if you can find info on the company, including complaints³. ASIAN countries like India, Bangladesh, Nepal etc have recently witnessed a surge in ONLINE SURVEY FRAUDS notably **Speakasia** has swindled huge amounts of money. Home Minister R R Patil of Maharastra said the Speakasia fraud could be as big as Rs 2,000 crore and the money sent out of the country. The minister cautioned people against investing money in companies which make unbelievable promises and said economic offences to the tune of Rs 699.70 crore were reported in the state in 2010 alone.

Patil said cases had been reported against the Singapore-based company in other parts of the world and added that about 20 lakh people could have been duped in all. "We acted as soon as we received a complaint in the matter"⁴

Speak Asia was registered in Singapore, and it costs nothing.

Company Background:

The company name is: SpeakAsia Online Pte Ltd.

formerly known as : Haren Technology Pte. Ltd.

Earlier known as: PAN Automotives Pte. Ltd

(Compliance rating for this company is Non Compliant currently)

Prior to this name they were operating under:

HAREN VENTURES PTE. LTD.

Formerly HAREN AUTO PARTS PTE. LTD.

Formerly HAREN MULTICONSULT TRADE SERVICES PTE. LTD.

Search found <8> matches
Displaying Page <1> of <1>

S/No.	Registration No. <small>Click below hyperlink to buy entity information.</small>	Entity Name	Partial Address	Status ^②	Compliance Rating for Annual Filing ^③ <small>Click on icon for details of compliance records</small>
1	53023024X	HAREN AUTO & HEAVY EQUIPMENTS	EMERALD HILL ROAD	Cancelled	-
2	52885731B	f.k.a HAREN AUTOMOTIVES & COMPONENTS	CHIN SWEE ROAD	Terminated	-
3	200613527C	HAREN MULTICONSULT TRADE SERVICES	BUKIT BATOK CRESCENT	Live	✓
4	53034470W	HAREN VENTURES PTE. LTD.	JALAN SULTAN	Live	-
5	200705083Z	f.k.a HAREN AUTO PARTS PTE. LTD.	LORONG 23 GEYLANG	Struck off	-
6	52998195E	f.k.a HAREN MULTICONSULT TRADE SERVICES PTE. LTD.	RACE COURSE ROAD	Cancelled	-
7	35495100M	HARENE'S	YISHUN STREET	Terminated	-
8	200618809D	HARENRA STORE	71 UBI CRESCENT	Live	✗
		HAREN TECHNOLOGY PTE. LTD. n.k.a SPEAKASIA ONLINE PTE. LTD. f.k.a PAN AUTOMOTIVES PTE. LTD.			

Notes:
1. n.k.a means "now known as"
2. f.k.a means "formerly known as"
3. Compliance rating is available for "Live" companies only.
4. Compliance rating for the company is based on real-time information.

Source: www.psi.gov.sg

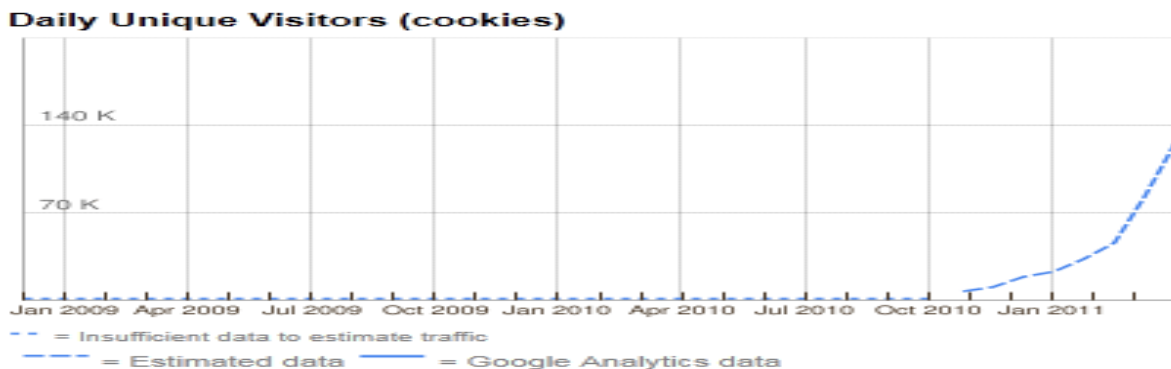
- a) There is a defunct website too <http://www.hmtservices.com> where we can see is that there is no relation between the survey they used to do for products ,also in the link spare parts there is no mention of any product obviously it was all a fake website.

- b) When doing little more research on the address of the company the same address is used for different companies. A simple Google can throw a few names which I am listing below. Some of the companies having the same address are: Valves.Com Pte Ltd, SBS Consulting Pte. Ltd.
- c) The company has a franchisee model so at the face of it you are not paying anything directly to the company "Speak Asia" and it goes in the name of the franchise (bank account) and who further pass that money to someone in Mumbai and all get to keep a certain % out of it.
 If it's such a big company they should provide an option to pay online through credit card directly to them instead of making so many layers of people accepting payments on company's behalf and would have helped them with instant signups.
- d) If you watch YouTube for their Torch Bearers 2011 meet they were talking about opening a TV Channel by August 2011. Very nice and ambitious plan but doesn't it require a lot of regulatory processes and time and huge "money". But the ground reality is that they don't have a single registered office in India. There are claims that it will be open in May 2011 in Mumbai.
- e) We found that they were using SurveyMonkey as their survey tool and only recently purchased Novi Survey. However established proven businesses with multi million dollars in revenue build there own software tools in-house.
- f) They claimed they were getting good business in Singapore / Malaysia / Indonesia but after searching the Alexa site we find that the traffic is mainly in India and Bangladesh only.

Screenshot from Alexa:

Speakasiaonline.com's Regional Traffic Ranks	
Country	Rank
 Bangladesh	43
 India	91

The below screen shot shows the amount of traffic per day in speakasia website



The traffic in India

View data for: India		
Traffic statistics		All traffic statistics are estimates ?
	Country	Worldwide
Unique visitors (estimated cookies) ?	990K	990K
Unique visitors (users) ?	910K	920K
Reach	1.6%	0.0%
Page views	98M	110M
Total visits	3.9M	4.2M
Avg visits per visitor	4.2	4.6
Avg time on site	21:40	21:40

g) Speak asia advertised heavily on IPL matches, daily newspapers, the celebrities were not even paid in full⁵

h) Again when you do some research on the domain: SpeakAsiaOnline.com

this was registered on **21 January 2010** and they started working in India from February 2010. So the point is that the whole scheme is not that OLD as the company proclaims that it is working since 2006. Earlier the company was doing agreements with Franchisee through the name "Haren Auto Parts Pte. Ltd.", which again changed to Haren Ventures Pte. Ltd.

Registrant:
 Speakasia Online Pte. Ltd.

71 Bukit Batok Crescent #10-08 Prestige
 Singapore, 658071
 Singapore

Registered through: GoDaddy.com, Inc. (<http://www.godaddy.com>)
 Domain Name: SPEAKASIAONLINE.COM
 Created on: 21-Jan-10
 Expires on: 21-Jan-13
 Last Updated on: 06-Nov-10

Administrative Contact:
 asia.speak support@speakasiaonline.com
 Speakasia Online Pte. Ltd.
 71 Bukit Batok Crescent #10-08 Prestige
 Singapore, 658071
 Singapore
 +65.91234567

The address mentioned on their WHOIS doesnt match with their registered company address.
 WHOIS Record says:

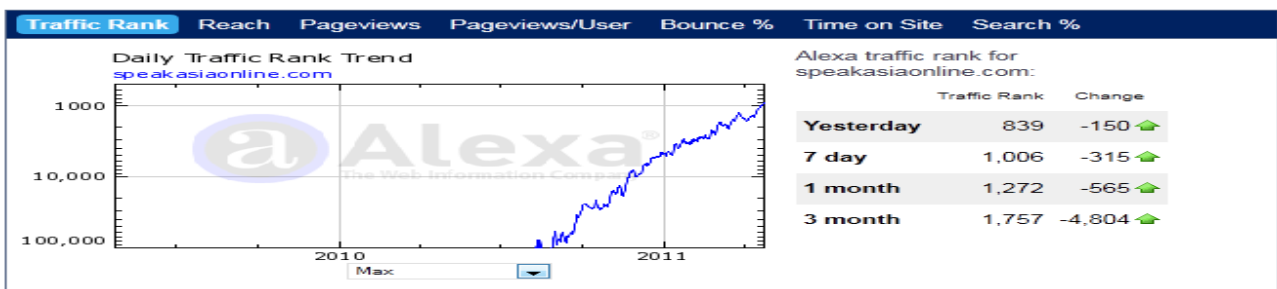
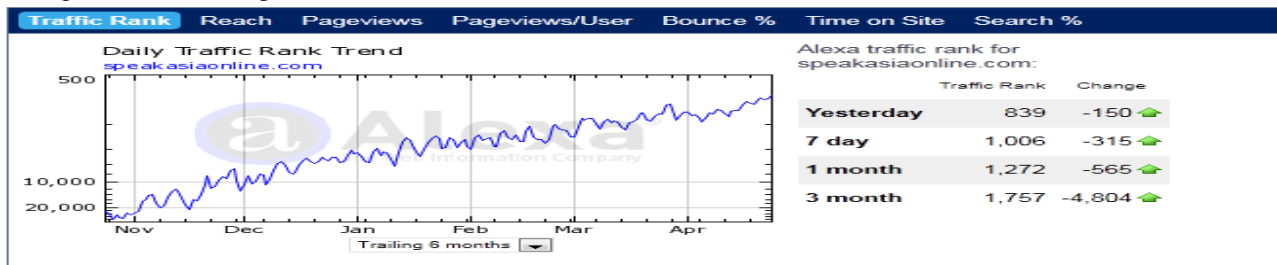
Speakasia Online Pte. Ltd

.71 Bukit Batok Crescent #10-08 Prestige
 Singapore, 658071
 Singapore
 Company website mentions:

Speak Asia Online Pte. Ltd.

Address: 10 Ubi Crescent, #07-68, Ubi Techpark,
 Singapore 408564

h) The site indeed got a lot of traffic and that certainly makes them one of the fastest growing website, their current Alexa ranking is at 839 (as on april 2011)



i) Speakasia was like a Ponzi scheme

. For the first three month it is actually paid from its pocket and after that since users had obviously multiplied they started getting more money as planned by them.

j) legal problems: Speakasia knew that since the company was registered in Singapore thus in order to recover 11000 Rs one would have to go to Singapore to file case which as we can comprehend will be not feasible , secondly the company was selling E-Zine and the victim had paid 11000 towards that and not towards the Survey. Your payment of Rs.1000 / 2 surveys is toward the Surveys you fill. So on that ground too the company is safe

k) Yes one do receive a online receipt for the money that one pays from Speak Asia and here is the screenshot. Earlier it was given from "Online Surveys Today" which I doubt that any such company even exists though the address was same as SpeakAsia Online Pte. Ltd. and later it is changed to Haren Ventures Pte. Ltd.but they had later changed the address to a new address ,see screen shots below

Online Surveys Today :: <http://www.speakasiaonline.com/receipt.aspx?UName=>

Online Surveys Today
10 Ubi Crescent, #07-68, Ubi Techpark,
Singapore 408564
Receipt No:
Date :

Receipt

Received with thanks from
an amount of \$220 towards purchase of 52 subscription for
E-Zine. Subscription code No

This is a Computer generated receipt, hence it does not require an Authorised Signature .

Speak Asia :: Receipt http://speakasiaonline.com/panelist/accounts_receipt_view.aspx?id=

SPEAK ASIA

Haren Ventures Pte Ltd. (HVP)
3, Temasek Boulevard # 01-K10, Suntec City Mall,
Singapore 038983
Receipt No:
Date : 10 April, 2011

Receipt

Received with thanks from
an amount of \$ 200.00 towards purchase of Premium Subpanel
Subscription Code :
52 issues of e zine - Surveys Today.

This is Computer generated receipt, no need for Authorised Signature .

References (<http://blog.investraction.com/2011/04/speak-asia-scam-or-for-real.html>,
<http://www.suchetadatal.com/?id=90890ade-4fcf-f284-4da58466269d&base=sections&f>,
<http://www.moneylife.in/article/speakasia-still-cant-show-valid-legal-documents/15551.html>
http://www.aboutindiatoday.gen.in/2011_02_01_archive.html
<http://timesofindia.indiatimes.com/city/nagpur/Another-co-goes-to-town-with-easy-money-scheme/articleshow/7523895.cms>
Things to know before making money from online surveys firms article appeared on The economic times on 09/05/2011
What could have been done: The Indian government should have woken up to the fact that the advertisements were released in all leading print and broadcast media and every govt department ,be it vigilance ,or
(2)Business Fraud:

(a)Purchase frauds

Purchase fraud occurs when a criminal approaches a merchant and proposes a business transaction, and then uses fraudulent means to pay for it, such as a stolen or fake credit card. As a result, merchants do not get paid for the sale. Merchants who accept credit cards may receive a chargeback for the transaction and lose money as a result.

(b)Online automotive fraud

A fraudster posts a nonexistent vehicle for sale to a website, typically a luxury or sports car, advertised for well below its market value. The details of the vehicle, including photos and description, are typically lifted from sites such as eBay Motors or Autoscout24. An interested buyer, hopeful for a bargain, emails the fraudster, who responds saying the car is still available but is located overseas. The scam artist then instructs the victim to send a deposit via wire transfer to initiate the "shipping" process. The unwitting victim wires the funds, and subsequently discovers they have been scammed.

(c) Counterfeit cashier's check scam

Landlords placing advertisements on Craigslistrent.com receive an e-mail response from a prospective renter from a foreign country, typically a student fresh out of secondary education (high school in the U.S.). The first inquiry seems legitimate. The second usually comes with request for more information and an attachment from a fake company set up by the scam artist indicating that the "student" has won a part-time scholarship from the company. (The fraudster will often set up a fake website for the company, in order to make the attachment seem legitimate.) The scam comes with the third e-mail: a request for the victim's name and address so that the "company" can send a cashier's check to cover the rent and the "student's" travel costs.

The victim is instructed to cash the check and wire the difference back to the student so that they can travel to the destination country. In the United States, banks consider cashier's checks to be "guaranteed funds" and will typically cash them instantly. However, unlike a certified check, the bank that cashes a cashier's check can still take back the money from the depositor if the check is counterfeit or "bounces". Because of the lag between the cashing and clearing of the check, the victim does not realize that they have been had until their account is debited for the amount they wired to the fraudster, plus any fees for the bounced check.

(d)PayPal Fraud

In a **collection in person PayPal scheme**, the scammer targets eBay auctions that allow the purchaser to personally collect the item from the seller, rather than having the item shipped, and where the seller accepts PayPal as a means of payment.

The fraudster uses a fake address with a post office box when making their bids, as PayPal will allow such an unconfirmed address. Such transactions are not covered by PayPal's seller protection policy. The fraudster buys the item, pays for it via PayPal, and then collects the item from the victim. The fraudster then challenges the sale, claiming a refund from PayPal and stating that they did not receive the item. PayPal's policy is that it will reverse a purchase transaction unless the seller can provide a shipment tracking number as proof of delivery; PayPal will not accept video evidence, a signed document, or any form of proof other than a tracking number as valid proof of delivery. This form of fraud can be avoided by only accepting cash from buyers who wish to collect goods in person.

(e)Call tag scam

In a call tag scam, criminals use stolen credit card information to purchase goods online for shipment to the legitimate cardholder. When the item is shipped, the criminal receives tracking information via email. They then call the cardholder and falsely identify themselves as the merchant that shipped the goods, saying that the product was mistakenly shipped and asking permission to pick it up when it is delivered. The criminal then arranges the pickup, using a "call tag" with a different shipping company. The victim usually doesn't notice that a second shipping company is picking up the product, and the shipping company has no knowledge it is participating in a fraud scheme. The cardholder may later notice the charge on his statement and protest the charge, generating a chargeback to the unsuspecting merchant.

(f)Money transfer fraud: consists of an offer of employment transferring money to a foreign company, supposedly because it costs too much to do it through other methods. The prospective victim receives an email like

Dear Sir/Madam I'm the C.E.O of XXXXX Textiles. We'd like to offer you additional earnings \$2000 – \$8000 per month. It's easy and will not take a lot of time. No costs, No Investments, Work Part Time or Full Time. Up to \$2000 Part Time and \$8000 Full Time. Work from Home with a Business Opportunity that no job could ever offer. Use your own computer to make money and make a CAREER as your own boss. I would like to know if you are interested. Work will consist of receiving of the payments from our clients in USA and Canada. All you would be doing is receiving these payments that would come to you via the mail system in your country, have them cashed and remit the rest to me. I would be willing to pay you 10% of whatever payment you process. These payments would come in different forms. We are always facing serious difficulties when it comes to selling our products to Americans; they are always offering to pay with Different Modes, which are difficult for me to cash here in the UK. Because of a hold of almost three weeks that would be placed on them before they clears the banks here in the UK. Unfortunately we can't open the bank accounts in all the countries we work with and because of that we seek for a representative/bookkeeper in USA and Canada. Respond only if you will like to work from home part-time/full time and get paid weekly without leaving or it affecting your present job. (PAY IS GOOD)If interested please reply with the information below to

Email: XXXXXX@XXXXXX.com EMPLOYMENT APPLICATION FORM:

FULL NAME.....

ADDRESS (P.O Box Not Accepted).....

CITY.....STATE.....ZIPCODE....

PHONE..... CELL PHONE.....

AGE.....SEX.....

PRESENT OCCUPATION.....

RECENT BANK..... XXXXXX XXXXXXXX ARTS AND CRAFTS

99-98 XXXXXX STREET XXXXXXXXXX

LONDON,WG2B 6TD

+44-999-999-9999 Best Regards,

Mr. XXXXX XXXXX

The fraudsters then send fake checks or postal money orders, in the hopes that the victims will cash the fake money instruments and send money to the scammers before the fraud is discovered.

Because the fraudsters are often able to get the victim's personal information, including their Social Security number or bank account number, these scams often become phishing scams as well, leading to identity fraud.

Why can't a pyramid scheme work?

The fact that a pyramid scheme cannot work for all, or even most participants can be proven mathematically and shown by this example:

This table shows how many new paying members must be recruited at each level for programs (schemes) that require each new member to recruit 4, 5, 6, 7, or 8 new members.

Level	Each person must recruit Members that must be recruited by each level (total) to be profitable for that level if each member must recruit the following new members:				
	4	5	6	7	8
1	4	5	6	7	64
2	16	25	36	49	512
3	64	125	216	343	4096
4	256	625	1,296	2401	32,768
5	1,024	3125	7,776	16,807	262,144
6	4,096	15,625	46,656	117,649	2,097,152
7	16,384	78,125	279,936	823,543	16,777,216
8	65,536	390,625	1,679,616	5,764,801	134,217,728
9	262,144	1,953,125	10,077,696	40,353,607	1,073,741,824
10	1,048,576	9,765,625	60,466,176	282,475,249	8,589,934,592
11	4,194,304	48,828,125	362,797,056	1,977,326,743	68,719,476,736
12	16,777,216	244,140,625	2,176,782,336	13,841,287,201	
13	67,108,864	1,220,703,125	13,060,694,016		

You will notice that the reddish colored cells signify levels that are unachievable because there aren't that many people on earth (approximately 6 billion people)! The orange colored cells signify levels that are practically unachievable: there are no existing companies on earth with this many employees or members. The yellow colored cells indicate levels that are mathematically possible, but would mean that the company would be huge by most standards (7,000 to 1 million employees) and this is VERY unlikely. The uncolored cells are levels that are possible and maybe even practically achievable - by really good con men! This does NOT mean that we are recommending them.

IV. Target youth frauds:

- (a) **Internet ticket fraud**
- (b) **Nigerian letter 419 fraud.**

(a) Internet ticket fraud

A variation of Internet marketing fraud offers tickets to sought-after events such as concerts, shows, and sports events. The tickets are fake, or are never delivered. The proliferation of online ticket agencies, and the existence of experienced and dishonest ticket resellers, has fueled this kind of fraud. Many such scams are run by British ticket touters, though they may base their operations in other countries. A prime example was the global Beijing Olympic Games ticket fraud run by US-registered **Xclusive Leisure and Hospitality**, sold through a professionally-designed website, www.beijingticketing.com, with the name "Beijing 2008 Ticketing". On 4 August it was reported that more than AU\$50 million worth of fake tickets had been sold through the website. On 6 August it was reported that the person behind the scam, which was wholly based outside China, was a British ticket tout, Terance Shepherd.

(b) **Nigerian letter 419 fraud:** Nigerian letter frauds combine the threat of impersonation fraud with a variation of an advance fee scheme in which a letter mailed from Nigeria offers the recipient the "opportunity" to share in a percentage of millions of dollars that the author—a self-proclaimed government official—is trying to transfer illegally out of Nigeria. The recipient is encouraged to send information to the author, such as blank letterhead stationery, bank name and account numbers, and other identifying information using a fax number provided in the letter. Some of these letters have also been received via e-mail through the Internet. The scheme relies on convincing a willing victim, who has demonstrated a "propensity for larceny" by responding to the invitation, to send money to the author of the letter in Nigeria in several installments of increasing amounts for a variety of reasons.

Payment of taxes, bribes to government officials, and legal fees are often described in great detail with the promise that all expenses will be reimbursed as soon as the funds are spirited out of Nigeria. In actuality, the millions of dollars do not exist, and the victim eventually ends up with nothing but loss. Once the victim stops sending money, the perpetrators have been known to use the personal information and checks that they received to impersonate the victim, draining bank accounts and credit card balances. While such an invitation impresses most law-abiding citizens as a laughable hoax, millions of dollars in losses are caused by these schemes annually. Some victims have been lured to Nigeria, where they have been imprisoned against their will along with losing large sums of money. The Nigerian government is not sympathetic to victims of these schemes, since the victim actually conspires to remove funds from Nigeria in a manner that is contrary to Nigerian law. The schemes themselves violate section 419 of the Nigerian criminal code, hence the label "419 frauds."

V. Miscellaneous interent frauds :

(a) Phishing

(b) Pharming

(a) Phishing

Phishing is the act of masquerading as a trustworthy person or business to fraudulently acquire sensitive information, such as passwords and credit card details, that a victim might think reasonable to share with such an entity. Phishing usually involves seemingly official electronic notifications or messages, such as e-mails or instant messages. It is a form of social engineering.

Fraudsters have widely used e-mail spam messages posing as large banks like Citibank, Bank of America, or PayPal in phishing attacks. These fraudsters copy the code and graphics from legitimate websites and use them on their own sites to create legitimate-looking scam web pages. These pages are so well done that most people cannot tell that they have navigated to a scam site. Phishers will also add what appears to be a link to a legitimate site in an e-mail, but use specially-crafted HTML source code that actually links to the scammer's fake site. Such links can be often revealed by using the "view source" feature in the e-mail application to look at the destination of the link, or by putting the mouse pointer over the link and looking at the URL then displayed in the status bar of the web browser. **Examples of phishing attacks**⁷

Subject: Windows Account Alert™

From: Windows Microsoft™ Center (war.veteran@hotmail.com)

Sent: Fri 4/30/10 7:58 AM

To: accountprotectteam2010 @ hotmail.com **Microsoft Live Account Alert!!!** Dear Account Owner This Email is from Microsoft Customer Care and we are sending it to every Hotmail Email User Accounts Owner for safety. we are having congestion's due to the anonymous registration of Hotmail accounts so we are shutting down some Hotmail accounts and your account was among those to be deleted. Please verify your account and let us know if you still want to use this account. If you are still interested please confirm your account by filling the space below. Your User name, password, date of birth and your country information would be needed to verify your account.

- Username:
- Password:
- Date of Birth:
- Country or Territory:

Confirm you're E-mail by filling out your Login Information below after clicking the reply button, or your account will be suspended within 48 hours for security reasons. Sincerely,
The Windows Live Hotmail Team

(b) Pharming

Pharming occurs when a hacker redirects website traffic from a legitimate website to the hacker's fraudulent website by exploiting vulnerabilities in the Domain Name System (DNS). By corrupting a computer's knowledge of how a site's domain name maps to its IP address, the attacker causes the victim's computer to communicate with the wrong server—a technique known as domain hijacking.

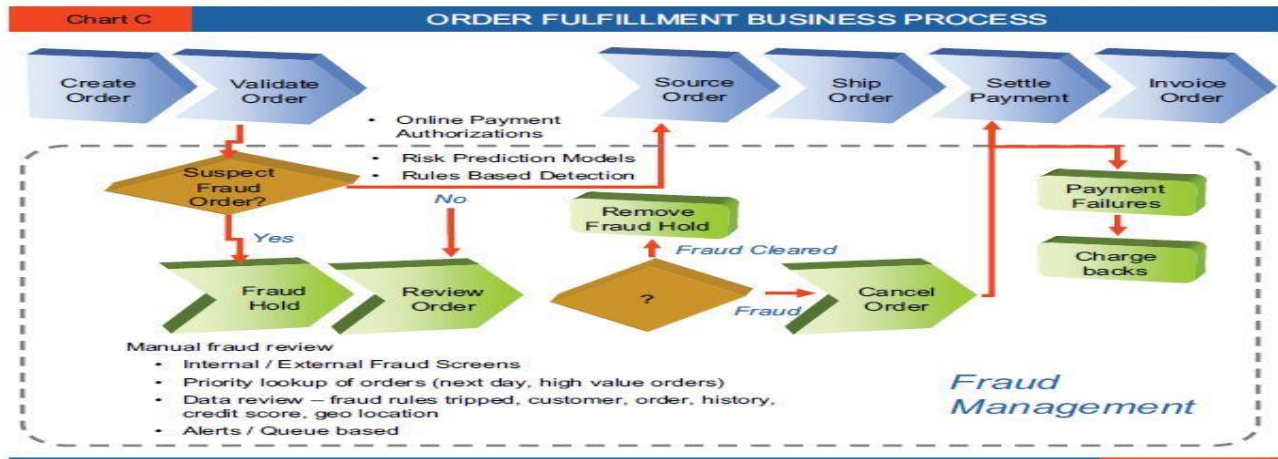
By constructing a fake web site that looks like a legitimate site that might ask for the user's personal information, such as a copy of a bank's website, the fraudster can "phish", or steal by means of false pretenses, a victim's passwords, PIN or bank account number. The combination of domain hijacking with a phishing website constitutes farming.

Although many such sites use the Secure Sockets Layer (SSL) protocol to identify themselves cryptographically and prevent such fraud, SSL offers no protection if users ignore their web browsers' warnings about invalid SSL server certificates. Such warnings occur when a user connects to a server whose SSL certificate does not match the address of the server.

VI. DEFENDING THE FAITH IN VIRTUAL WORLD:

Web has become the prominent part of our life so we need a complete protection which can retain our faith. As we have been facing a problem of cyber laws in India which has no relevant result. Cyber act 2005 does not protect the users from fraud because there is no solution of virtual world crime in real world so we need some virtual guards who can catch them in their world. Infosys is working on this concept very passionately since they have introduced the system on line fraud

management system. Almost 28% of all online orders are affected by fraud. The efficiency of the fraud management process thus has a direct impact on ecommerce profitability, operating efficiency and scalability.



VII. CONCLUSION:

Easy money always been a razzmatazz, everyone wants to be around it. People those who get buzzed around it in initial stage get benefited and finally the easy money maker get benefited. The ponzi schemes are luring the people since it came in existence and people are being cheated too. It's totally illogical to make money from ponzi schemes for investors. Only three levels are possible⁶ after that only company can make out money from so called Ponzi schemes. One thing is having a high level of paradox in this issue and that is, internet literate people are the victim of these fraud so only awareness is not a sufficient solution. A real but virtual guardian is required to shield investor from the great internet fraud factories. Ethics are conventional but cyber ethics has to be implemented with all its new definitions and code of conducts. Notions are changed but the rate of change measured high in virtual world. Now we are in a situation where we are supposed to start an ethical debate on cyber ethics from scratch.

REFERENCES:

- [1] Remarks by Alan Greenspan former federal reserve chairman on CNBC, July 16, 2002, quoted by Patricia Aburdene in Megatrends 2010: The Rise of Conscious Capitalism .
- [2] Infosys white paper on "Fraud Management in the online retail environment" by G.S Paintal ,www.infosys.com
- [3] <http://www.scambusters.org/onlinesurveys.html> ,Internet ScamBusters™ The #1 Publication on Internet Fraud By Audri and Jim Lanford Issue #150)
- [4] <http://www.indianexpress.com/newsspeak-asia-fraud-rs-2-000-crore825777>
- [5] http://www.suchetadalal.com/?id=a60a3ffc-a8bd-0368-492e822e450e&base=sub_sections_content&f&t=Home+Trade%27s+%27starry%27+gameplan
- [6] described in pyramid table mentioned above.
- [7] http://en.wikipedia.org/w/index.php?title=Internet_fraud&action=edit§ion=26

Stress-Strain Behaviours Of Two Stage Lime-Cement Treated Expansive Soils

Charles Lucian

Ardhi University (ARU), Box 35176, Dar es Salaam, Tanzania

Abstract: The aim of this research work is to examine the stress-strain behaviours of Two Stage Lime-Cement Stabilized Expansive Soil. The stress-strain of stabilized soils under different loading conditions is essential to properly understand how the material will behave when exposed to applied load. An investigation has been performed on soils stabilized in two stage lime-cement process in different combinations of binders with the purpose of demonstrating the impact of different loading conditions. The binders used were lime, cement, and a combination of lime and cement with a mellowing period between them. Strains at failure were recorded on all tested samples. The results show that while the untreated sample exhibited a ductile behavior, the lime treated samples exhibited brittle behavior but the two stage lime-cement treatment changed the brittle behaviour of lime treated soils to more ductile ones. This abrupt change from brittle to ductility is strongly linked to the influence that the two stage lime-cement treatment has on the deformation behaviour of treated soils.

Keywords: Two-stage stabilization, unconfined compressive tests, and stress-strain behaviour.

I. Introduction

Treated expansive soils behave differently with different loads resulting in varying degrees of initial strength gains and final strength development to support foundations for building purposes. The strength gain and stability in treated soils are due to complex chemical reactions which take place between the soil, water and admixtures. The immediate initial strength gains in expansive soils are a result of cation exchange and flocculation of clay particles in the presence of lime. The final strength development depends on admixtures content, soil water content, soil type, curing duration, temperature and stress state. The final strength generally refers to the soil's ability to support the loads imposed by buildings or structure preferably without failure.

Information about the material's behaviour under load is well captured by monitoring the relationship between stress and strain for a material. When a material is loaded with the applied load, it produces a stress, which then causes a material to deform. The degree of soil deformation is governed not only by the interplay between the magnitude of stress levels (loading) applied to the soil and the rigidity of the soil in controlling these external stresses but also by internal stresses. The internal resistance of the material to counteract the applied load is called internally induced stress, and the arising deformation is known as strain. The internal stresses arise from physico-chemical mechanisms and microstructural behavior of soils. The applied stress is contained as long as the strength of the soil arising from its physico-chemical mechanisms and microstructural behavior remains above the stresses required to maintain equilibrium. It is unfortunate that expansive soils that shrink and swell because of changes in moisture content always have their stress equilibrium constantly disturbed. Expansive soil which has been treated with appropriate binders, will have higher internal effective stress and has little tendency to deform.

Typical expansive soils often display linear relationship between stress and strain over a short range of load, followed by non-linearity small-strain stiffness over the rest range of loading. When the soil is treated with cement, lime or a combination of the two, the failure stress increases and the ultimate strain required to reach the maximum principal stress difference decreases. It is postulated that the addition of lime alone, decreases the rate of strength gain and the addition of cement significantly increases the initial rate of strength in treated soils (Indraratna et al., 1995 and Madhyannapu et al., 2009). Therefore, the addition of either lime or cement results in brittle behaviour associated with low strain and high strength than those of non-treated soils. For both treated and untreated soils, the maximum peak shear strength is taken as the peak stress of the soil stress-strain curve or the shear strength at critical state when the stress-strain relationship levels off. If the stress-strain curve does reach the peak before the end of shear strength test, the shear strength at a strain of 15% to 20% is considered to be the shear resistance (Salgado et al., 2000).

The stress strain behaviour of lime treated expansive soils has been extensively investigated (Tuncer and Basma, 1991, Nalbantoglu, 2006, Khatlab et al., 2007, Sharma et al., 2008, and Yin and Tong, 2011). Likewise, the stress strain behaviour of cement treated expansive soils has received the attention of numerous researchers (Anagnostopoulos, 2006, Al-Zoubi, 2008 and Kamruzzaman, 2009). Cautiously, the stress-strain behaviours of lime and cement treated soils has been examined by a number of researchers (Kennedy and Tahmovessi, 1987, Jacobson, 2002 and Puppala et al., 2005). Nevertheless, each of the treatment studied behaves in a different way depending on the binder systems used. Although many researchers have studied the stress-strain behaviours of soils with cementing agent like lime and cement and a combination of the two, not many of these researchers have explored the stress-strain behaviours of two stage lime-cement stabilization mixtures with mellowing period between them. This paper therefore presents experimental results in stress-strain plot obtained from tests conducted on remolded expansive soil specimens stabilized with lime, cement, and lime-cement with the mellowing period between them.

II. Materials and Experimental Methodology

Description of the Area

The site from where the samples were taken is found in Kibaha Township in Tanzania. Kibaha Township is located in eastern Tanzania, about 40 km west of Dar es Salaam (the commercial capital city of Tanzania), along the Dar Es Salaam-Morogoro highway. It's positioned at an altitude of about 155 m above sea level and located approximately by geographic latitude and longitude of 06°46'S and 38°55'E respectively. It is within the coastal belt where expansive clay soils are predominant (Lucian, 2009 & 2011).

III. Soil Samples

The soil samples used in this study were taken in their natural expansive conditions from a depth of 1.3 m to 1.5 m below the ground level in a 3.5 m deep test pit. The samples were carefully wrapped in cling-films and aluminium foil and transported to the soil laboratory at the College of Engineering and Technology (CoET) at the University of Dar es Salaam in Tanzania. In the laboratory, the basic soil properties were determined and they are shown in Table 1. The soil is classified as a very stiff active clayey SAND of high plasticity (SCH) with expansive behaviour. Furthermore, the other soil samples were stabilized using lime, cement as a whole and in combinations of the two (with the mellowing period between them) at different proportions for Unconfined Compressive Strength (UCS).

Table 1: Basic Properties of Native Expansive Soil

PROPERTY	VALUE	PROPERTY	VALUE
Liquid limit (%)	60.2	Sand (%)	55
Plastic limit (%)	23.5	Silt (%)	11
Plasticity index (%)	36.7	Clay (%)	29
Swell potential, (S) (%)	19.2	Bulk density (ρ), kg/m ³	2120
Swell pressure (P_s), kPa	560	Dry density (ρ_d), kg/m ³	1910
Gravel (%)	5	Density of solids(ρ_s), kg/m ³	2650

IV. Binders Used

Two stabilizer materials, Lime and Cement, were used in this study. The cement used in this research was an Ordinary Portland Cement, Twiga brand from Tanzania Portland Cement at Wazo Hill, Tegeta, Dar es Salaam which was purchased from a local supplier. The hydrated lime used in this study was also obtained locally in Tanzania. To obtaining a higher level of fineness of the binder, the hydrated lime was sieved through No. 40 sieve before mixing.

V. Specimens Preparation

Soil samples were dried, ground and sieved through No. 40 sieve and oven dried at 50°C for 24 hours. Based on the Initial Consumption of Lime which was established to be 5.3%, lime was added at the rate of 4%, 6%, 8% and 10% by weight of dry soil. Also, some of lime-modified soil samples were allowed to mellow for 4 hours in a sealed container before treating with different ranges of cement contents of 2%, 4% and 6%. All treated soils were compacted using a modified Proctor effort (BSI, 1990), extruded from the compaction mold, and sealed in a plastic bag, cured at room temperature for a period of 7, 14 or 28 days, trimmed to appropriate 110 mm high and 52.4 mm diameter sizes and their stress-strain behaviours measured by running Unconfined Compressive Strength (UCS) test.

VI. Laboratory Testing Procedures

To assess the stress-strain behaviour of treated specimens, unconfined compression strength (UCS) tests were conducted in accordance with TMHI-1986, Method A14 (NITTRI, 1986). In the unconfined compression test, the prior compacted, cured soil samples and trimmed specimens were placed in the loading machine between the lower and upper plates. Before starting the loading, the upper compression plate was just brought barely into contact with the specimen and the deformation was set to zero at the start of the test. The tests were performed at a strain rate of approximately 2% per minute. The load and deformation values were recorded and load-deformation curve drawn. The loading was continued until the load values decreased or remained constant with increasing strain, indicating specimen's failure. Prior to testing, specimens were carefully weighed and measured and soonest after specimen testing the mode of failure was recorded (Figure 1). The Unconfined Compressive Strength of a stabilized material was recorded as the load in kN/m² (kPa) required to crush a cylindrical specimen, at a rate of 140 kN/m² per second (140 kPa/s).



Figure 1: UCS Test - specimens crushed to total failure

VII. Experimental results and Discussion

In the light of this research, the stress-strain behaviour of soil specimens treated with different admixtures, proportions and curing times has been investigated based on unconfined compression tests. The stress-strain behaviours of treated expansive soil specimens cured for 7, 14 and 28 days are represented in Figures 2, 3 and 4 respectively. For comparison purposes, Figure 2 shows stress-strain behaviours of natural soil specimen compacted using the same procedure as the one used for treated samples. Strain at the onset of failure corresponding to the maximum stress was recorded on each tested sample. At its natural state, the maximum compressive strength of untreated expansive soils reached 106 kPa at a strain of about 1.8%, with no true failure points observed. Indeed, the untreated specimens exhibited a ductile behavior with a continuous deformation until a steady state was reached. Upon treatment with considerable amount of lime (8% and 10%), the Unconfined Compressive Strength (UCS) increased considerably but the shear failure mode of specimens was close to brittle failure and the specimens strain is less than that of the natural soil. For lime treated specimens the shear strength increased significantly over small strain increments until the peak value was reached followed by a sudden drop in shear strength. It implies that the addition of considerable amount of lime to the expansive soils increased stiffness, peak strength, and brittleness. Unfortunately, the addition of reasonable amount of cement (2%, 4% and 6%) to expansive soils did not produce significant increase in strength. The addition of cement greater than the mention percent cannot justify the cost of further addition of pricey cement.

In contrast, the stress-strain curves of mellowed lime-cement treated soils exhibited gradual pronounced peaks, depending on the lime-cement proportions and curing time (Figures 2, 3 & 4). All strain-stress behaviours shown in the Figures reveal that the two-stage stabilized samples approached residual strength more gradually and maintained certain post-yield failure strength for all tested curing periods. This may be explained by the fact that addition of cement to a lime-modified sample increases the rate and extent of gradual strength development, whereas cement treatment of unmodified soil generates lower strength due to poor workability of the plastic soil that results into a non-uniform material and formation of chunks.

Furthermore, the unconfined compression strength increased with the curing period (Figures 2, 3 and 4). The figures indicate that almost all treated specimens, irrespective of the kind of admixtures, gained most of their strength within the first fourteen days of curing and no significant increase in 28 days of curing. Interestingly, lime treated specimens developed highest initial values within 7 days of curing indicating that the initial rapid hydration process took place within the first few days. At 14 and 28 days of curing, the strength values for lime treated specimens showed an increase in fracture strain and a reduction in strength due to degradation during curing. Furthermore, Figure 2 shows that during the first seven days of curing there is a linear reduction in the strain at failure that becomes stable when increasing the period of curing to 14 and 28 days as shown in Figure 3 and Figure 4 respectively. In 28 days curing period (Figure 3), USC increased from 106 kPa of untreated soil to 462 kPa and 2.65 MPa for 4% and 10% lime contents respectively. Two-stage stabilized soil with 4% lime and 2% cement increased the UCS to 1.05 MPa, 1.32 MPa and 1.55 MPa in 7, 14 and 28 days curing periods, respectively (Figures 2, 3 & 4), whereas 4% lime-and-6% cement resulted in the UCS of 2.25 MPa, 2.43 MPa and 2.51 MPa in the same curing periods. Higher percentages of lime and cement produced higher UCS values, up to 3.0 MPa in 28 curing days. For reasonably graded material, the minimum Unconfined compression Strength (UCS) of 800 kPa suggested by NAASRA (1986) can be used to base the selection of the two stage operation.

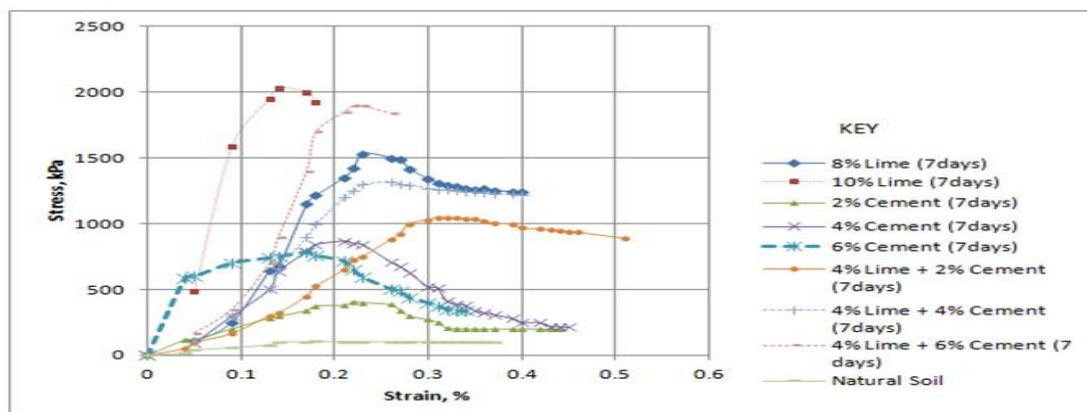


Figure 2: Stress- strain relationship of stabilized expansive soil specimens treated with different proportions of admixtures and cured for 7 days

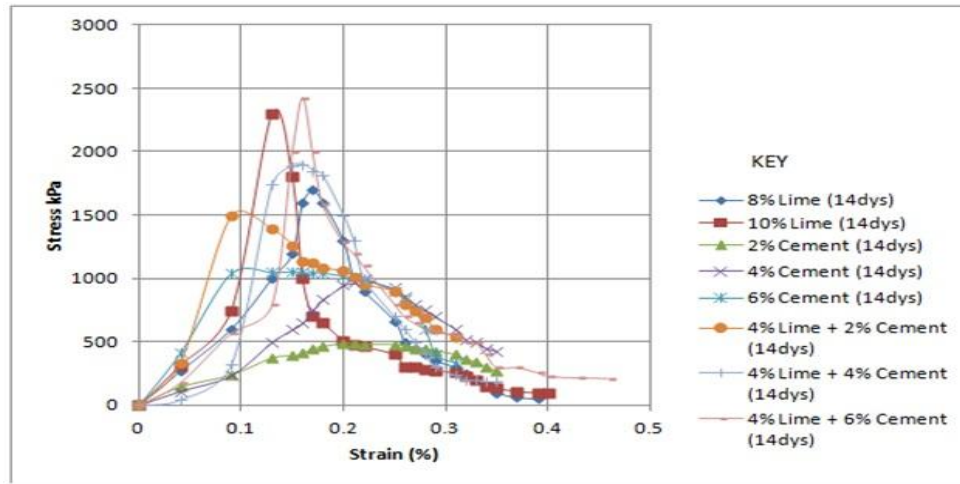


Figure 3: Stress- strain relationship of stabilized expansive soil specimens treated with different proportions of admixtures and cured for 14 days

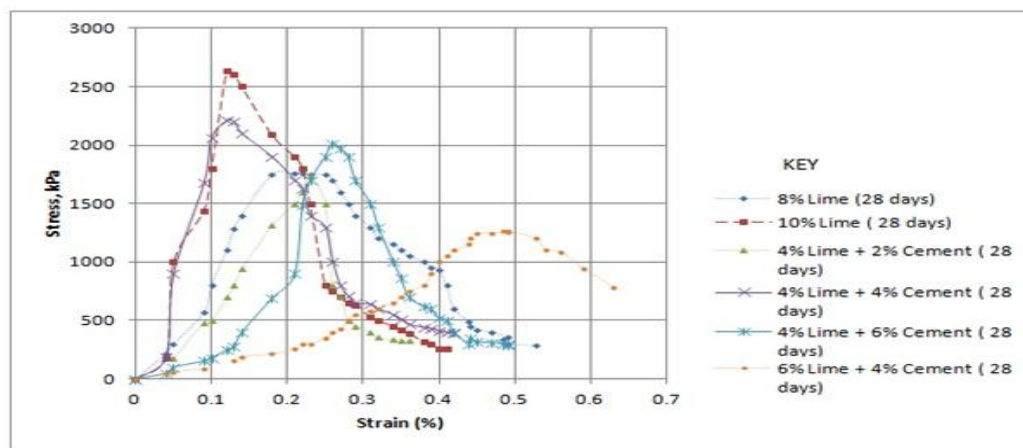


Figure 4: Stress- strain relationship of stabilized expansive soil specimens treated with different proportions of admixtures and cured for 28 days

VIII. Conclusions

This study has discussed the results of the stress-strain behaviours of lime, cement and Two Stage Lime-Cement Stabilized Expansive Soils in unconfined compressive strength (UCS) tests. In general test results indicated the strength, deformation characteristics and stress strain behaviours of treated soils depend on mix proportion and curing duration. In comparison with those of treated specimens, the untreated sample exhibited a ductile behavior associated with lower strength and higher failure strain.

The test results of treated specimens indicated that the unconfined compressive strengths increase with the increase in the quantity of stabilizer. For example, the increase in lime portion induced greater initial strength development at a lower strain to peak strength. The stress-strain curves obtained from unconfined compression strength tests showed sharp peak with an abrupt drop in peak implying that the lime treated specimens exhibited brittle behavior. The lower strain to peak strength and higher strength for lime specimens indicates that the immediate cation exchange and flocculation of expansive clay particles in the presence of lime induce apparent and more friable modified specimens.

Also, treating expansive soils with cement alone did not work well. All cement treated specimens tested were characterized by large deformation or strain but inadequate strength. Furthermore, the unconfined strength for cement treated specimens did not increase in direct proportion with cement content. Lastly, the length of curing had little effect on stress-strain behaviour of cement treated specimens.

The two stage lime-cement treatment indeed struck the right balance between lime modification and cement treatment. The two stage stabilization changed the brittle behaviour of lime treated soils where the specimens were more ductile thus required larger strain to reach ultimate failure. The strain curves of mellowed lime-cement treated soils exhibited gradual pronounced peaks, depending on the lime-cement proportions and curing time. Prolonged curing time showed more improvement in two stage lime-cement treatment than lime or cement treatment alone. It implies that cement stabilization needs pre-treatment with lime to reduce the plasticity of the soil and improve its workability before cement is added to improve the strength of clayey soils. Therefore, two-stage stabilization is strongly recommended whenever expansive soils similar to that in Kibaha region along the coast - Chalinze belt is to be improved for construction purposes. Importantly, the 4% lime and 2% cement two stage operation conform conveniently with NAASRA (1986) standard specification.

IX. Acknowledgement

The author is grateful to the Swedish International Development Cooperation Agency (SIDA) for the funding that made this research possible. The tireless efforts of the laboratory staff of College of Engineering and Technology (CoET) for carrying out the laboratory tests whose results have been used in this research deserve very special recognition.

References

- [1] Al-Zoubi, M. S. (2008). Undrained Shear Strength and Swelling Characteristics of Cement Treated Soil. *Jordan Journal of Civil Engineering*, Vol. 2, No. 1, pp. 53-62.
- [2] Anagnostopoulos, C. A. (2006). Physical and Engineering Properties of Cement Stabilized Soft Soil Treated with Acrylic Resin Additive, Chapter 28 in the *Expansive Soils, Recent Advance in Characterization and Treatment*. Edited by Al-Rawas, A. A. and Goosen, M. F. A., Taylor & Francis group, London, UK.
- [3] BSI, 1990. *Methods of test for soils for civil engineering purposes (BS 1377: Part 4: 1990)*. British Standards Institution, London.
- [4] Indraratna, A. S., Balasubramanian, A. K. and Khan, M. J. (1995). Effect of fly ash with lime and cement on the behavior of soft clay. *Quarterly Journal of Engineering Geology and Hydrogeology*, Vol. 28, No. 2, pp. 131-142
- [5] Jacobson, J (2002). *Factors Affecting Strength Gain in Lime-Cement Columns and development of a laboratory Testing Procedure*. MSc Thesis, Virginia Polytechnic Institute and State University, Blacksburg, Virginia
- [6] Kamruzzaman, A., Chew, S., and Lee, F. (2009). "Structuration and Destructuration Behavior of Cement-Treated Singapore Marine Clay." *Journal Geotechnical and Geoenvironmental. Engineering*, Vol. 135, No. 4, pp. 573-589
- [7] Kennedy, T. W. and Tahmouessi, M. (1987). Lime and Cement Stabilization. *Lime Notes, Updates an Lime Application in Construction*, Issue 2, National Lime Association, Virginia
- [8] Khattab, S. A., Al-Mukhtar, M. and Fleureau, J.-M. (2007). Long-Term Stability Characteristics of a Lime-Treated Plastic Soil. *Journal of Materials in Civil Engineering*, Vol. 19, No. 4, pp. 358-366
- [9] Lucian, C. (2009), "Spatial Variability of Expansive Soil Properties at Different Scale within Kibaha, Tanzania", *The Global Journal of Agricultural Sciences*, vol. 8, No.1, pp. 95-100
- [10] Lucian, C. (2011), "Geotechnology to Determine the Depth of Active Zone in Expansive Soils in Kibaha, Tanzania", *Global Journal of Pure and Applied Science*, Vol. 17, No. 2, pp. 189 -195.
- [11] Madhyannapu, R. S., Puppala, A. J., Bhadriraju, V. and Nazarian, S. (2009). Deep Soil Mixing (DSM) Treatment of Expansive Soils. *ASCE Geotechnical Special Publication, USA & China Joint Conference on Ground Improvement*, Orlando, Florida, pp. 130-139.
- [12] NAASRA. (1987). *Pavement Design: A Guide to the Structural Design of Road Pavements*. National Association of Australian State Road Authorities (NAASRA), Sydney.
- [13] Nalbantoglu, Z. (2006). Lime Stabilization of Expansive Soils, Chapter 23 in the *Expansive Soils, Recent Advance in Characterization and Treatment*. Edited by Al-Rawas, A. A. and Goosen, M. F. A., Taylor & Francis group, London, UK.
- [14] Puppala, A. J, Bhadriraju, V. and Madhyannapu, R. S. (2005). Small Strain Shear Moduli of Lime-Cement Treated Expansive Soils, *ASCE Geotechnical Special Publication*, No. 156, pp. 58-70
- [15] Sharma, R., Phanikumar, B., and Rao, B. (2008). "Engineering Behavior of Remolded Expansive Clay Blended with Lime, Calcium Chloride, and Rice-Husk Ash." *Journal of Materials in Civil Engineering*, Vol. 20, No. 8, pp. 509-515.
- [16] Salgado, R., Bandini, P. and Karim, A. (2000). Shear Strength and Stiffness of Silty Sand. *Journal of Geotechnical and Geoenvironmental Engineering*, ASCE, Vol. 126 No. 5 pp 451-462
- [17] TMH1 - Technical Methods for Highways (1986). *Standard Methods of Testing Road Construction Materials*, National Institute for Transportation and Road Research (CSIR), Pretoria
- [18] Tuncer, E. R. and Basma, A. A. (1991). Strength and Stress-Strain Characteristics of a Lime Treated Cohesive Soil, *Transportation Research Record*, Vol. 1295, pp. 70-79
- [19] Yin, J. and Tong, F. (2011). Constitutive modeling of time-dependent stress-strain behaviour of saturated soils exhibiting both creep and swelling. *Canadian Geotechnical Journal*, Vol. 48, No. 12, pp. 1870-1885

Sliding Mode Control of DSTATCOM Using Seven Level Multilevel Inverter

VUYYURU SWAPNA,¹ ASWANI KUMAR EEDARA,²

¹M-Tech Scholar, Power Electronics, Department of Electrical And Electronics Engineering, SASI institute of Technology and Engineering Tadepalligudem (A.P), India,

²Head of the Department & Asst. Professor Department of Electrical and Electronics Engineering, SASI institute of Technology and Engineering Tadepalligudem (A.P), India,

Abstract: In distribution system (DS), the majority of power consumption has been drawn in reactive loads. These loads are drawn in low power factor and therefore give rise to reactive power burden in the distribution system. So that DSTATCOM controller is used to compensate reactive power, correction of power factor and elimination of current harmonics. This paper presents the 7-Level Cascaded H-bridge Inverter as DSTATCOM for compensation of Balanced and Unbalanced Linear and Non-Linear Loads by using Level Shifted and Phase Shifted PWM techniques. The advantage of CHB Inverter is reducing the number of switches and thus switching losses. The simulation verification of the derived results are provided through a three-phase distribution static compensator (DSTATCOM) model. The application in the three-phase system has been shown through simulation studies

Index Terms: Cascaded H-bridge multilevel inverter (CHBMLI), distribution static compensator (DSTATCOM), Multiband hysteresis modulation, switching characterization.

I. INTRODUCTION

The multilevel power conversion has been receiving increasing attention in the past few years for high power application [4]. Numerous topologies have been introduced and studied extensively for utility and drive applications in the recent literature. These converters are suitable in high voltage and high power applications due to their ability to synthesize waveforms with better harmonic spectrum and attain higher voltage with a limited maximum device rating [1], [4]. There are various current control methods for two-level converters [5]. Hysteresis control of power converters, based on instantaneous current errors, is widely used for the compensation of the distribution system as it has good dynamic characteristics and robustness against parameter variations and load non-linearities [6].

A DSTATCOM is a voltage source converter (VSC) based device. When operated in a current control mode, it can improve the quality of power by mitigating poor load power factor, eliminating harmonic content of load.

In this paper, a generalized multiband hysteresis modulation has been proposed for the sliding-mode control of CHBMLI controlled systems. A frequency-domain method is proposed for the switching characterization of the multilevel inverter using Tsypkin's method and the describing function of nonlinear relay [23]. A hierarchical switching scheme is used for the equal-power-rated modular cells of the cascaded multilevel inverter. Sequential swapping of the hierarchy is done for applications involving balancing of the capacitor voltages. The simulation and

experimental verification of the derived results have been obtained through a single-phase DSTATCOM model. The application has been shown through simulation results for a three-phase distribution-system compensation using DSTATCOM.

II. SLIDING-MODE CONTROL OF DSTATCOM

In this section, a sliding-mode control for distribution system load voltage control using DSTATCOM is presented briefly [13]. A DSTATCOM-compensated distribution system is shown in Fig. 1.

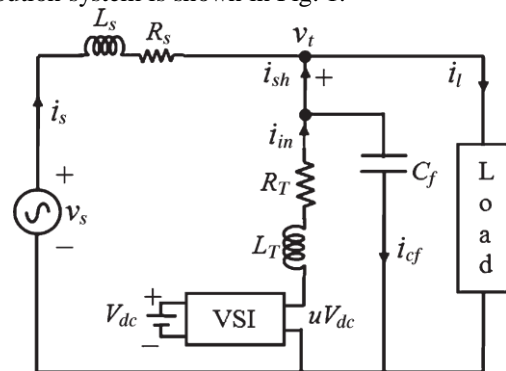


Fig.1. Load voltage control using DSTATCOM.

The distribution system consists of a load that is supplied from voltage source v_s through a feeder (R_s , L_s), as shown in Fig. 1. DSTATCOM consists of a VSI that is connected to the load through an interfacing inductance L_T . Resistance R_T represents the equivalent resistance in the shunt path. Voltage V_{dc} represents the net dc-link voltage of the VSI. Filter capacitor C_f is connected in the shunt. The currents flowing through the different branches are source current i_s , load current i_l , current through the filter capacitor i_{cf} , inverter output current i_{in} , and current injected in the shunt branch i_{sh} . The net controllable voltage at the output of the VSI is uV_{dc} , where u is defined as the control input and represents the switching logic of the inverter. It assumes discrete values between -1 and $+1$, depending upon the number of levels of the VSI, e.g., -1 , $-1/2$, 0 , $+1/2$, and $+1$, for a five-level inverter.

In order to design a control law independent of the load and source parameters, the following state vector is defined: $z^T = [\dot{v}_t \ v_t]$. State variable v_t is the terminal voltage or point-of-Common-coupling (PCC) voltage and \dot{v}_t is its derivative. Considering the terminal voltage as output, the state-space representation of the system shown in Fig. 1 can be written as

$$\dot{z} = Fz + g_1 u + g_2 d$$

$$vt=hoz \quad (1)$$

Where

$$F = \begin{bmatrix} -R_T & -1 \\ L_T & C_f L_T \\ 1 & 0 \end{bmatrix} g_1 = \begin{bmatrix} V_{dc} \\ C_f L_T \\ 0 \end{bmatrix} g_2 = \begin{bmatrix} 1 \\ 0 \end{bmatrix}$$

$$h_o = \begin{bmatrix} 0 & 1 \end{bmatrix}$$

Variable d is considered to be a periodic source that depends upon the shunt current as

$$d = -\frac{1}{C_f} \left(\frac{di_{sh}}{dt} \right) - \left(\frac{R_T}{C_f L_T} \right) i_{sh} \quad (2)$$

State vector $z(t)$ is required to track reference vector $z_r(t)$. This reference state vector comprises the reference for the terminal voltage and its derivative defined as $z_r = [\dot{v}_{tref} \ v_{tref}]^T$. It is desired to derive a model following the sliding-mode control for the sinusoidal reference with frequency ω_0 , as given by

$$v_{tref}(t) = V_{tref} \sin(\omega_0 t - \delta P) \quad (3)$$

where V_{tref} is the amplitude of the reference terminal voltage and δ is its phase angle with respect to the reference phase of source voltage v_s .

The design of sliding-mode control requires two conditions to be satisfied [11], [24], i.e., reaching and sliding phases. Let us choose a switching surface, which will be called here onward as switching function s_e that is defined by the following control law:

$$s_e = K z_e = k_1 (\dot{v}_{tref} - \dot{v}_t) + k_2 (v_{tref} - v_t) \quad (4)$$

where z_e is the error state vector defined as

$$z_e = (z_r - z) = [\dot{v}_{tref} - \dot{v}_t \quad v_{tref} - v_t]^T \quad (5)$$

In (4), K is the feedback gain matrix with two nonzero positive gains, namely, k_1 and k_2 . The existence condition of sliding-mode control is expressed as

$$\dot{s}_e > 0, \text{ when } s_e < 0$$

$$\dot{s}_e < 0, \text{ when } s_e > 0 \quad (6)$$

If u in (1) is chosen by the following variable-structure control law:

$$u = +1, \text{ for } s_e > 0$$

$$u = -1, \text{ for } s_e < 0 \quad (7)$$

Such that it complies with the existence condition (6), the system will then operate in sliding mode, and z_e will tend toward the origin. It is shown in [11] that, under sliding mode, the error state dynamics is governed by the state-space equation

$$\dot{z}_e = F^* z_e \quad (8)$$

Where

$$F^* = \begin{bmatrix} -K_2 & 0 \\ K_1 & 0 \\ 1 & 0 \end{bmatrix}$$

For a positive value of (k_2/k_1) , the sliding surface is stable. The states under sliding mode follow the references independent of the system and load parameters [13].

Under ideal sliding-mode control (7), the switches used in the VSI need to be fully rated and operate at very high switching frequency. A multiband hysteresis modulation using a cascaded multilevel inverter will be discussed hereinafter so as to bring the device ratings into the limits of practical insulated-gate bipolar-transistor (IGBT) switches with the desired maximum switching frequency.

III. MULTIBAND HYSTERESIS MODULATION

The graphical representations of the cascaded multilevel inverter with the proposed generalized multiband hysteresis

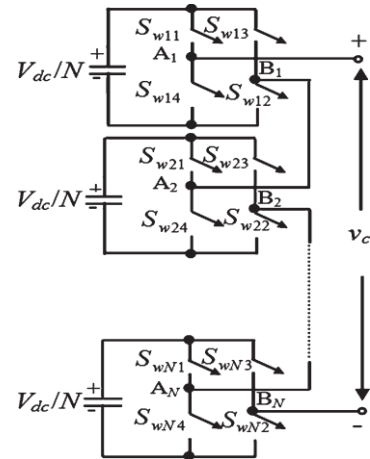


Fig.2. Cascaded n -level inverter using N number of H-bridges.

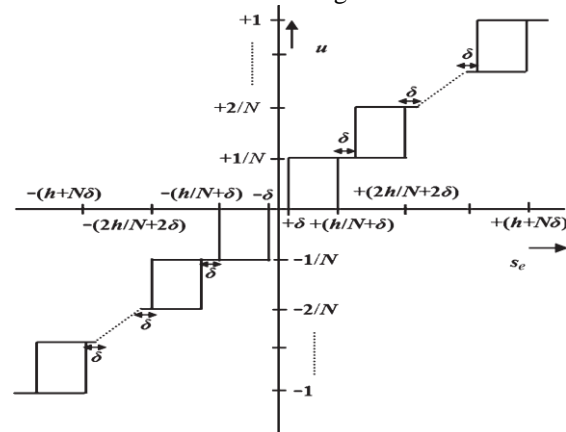


Fig. 3. Multiband hysteresis modulation.

Modulations are shown in Figs. 2 and 3, respectively, [20]. Fig. 2 shows a general n -level ($n = 3, 5, 7, \dots$) cascaded multilevel inverter topology. The basic building block of the cascaded inverter is an H-bridge. The switches $S_{w11}, S_{w12}, \dots, S_{wN4}$ shown in Fig. 2 represent an IGBT with an anti parallel diode. The number of such H-bridges required for an n -level inverter is $N = (n - 1)/2$. For higher voltage/power-rating applications, the switching frequency and device ratings are limited. Therefore, it is desirable to distribute the voltage and power stress among the number of devices. For an n -level inverter, the voltage stress on the semiconductor switches and the dc-link capacitor is $1/N$ times the net dc-link voltage V_{dc} required. The voltage output of the n -level inverter is denoted by $v_c = u V_{dc}$. Fig. 3 shows the proposed multiband hysteresis modulation. The frequency spectrum of the output voltage can be appropriately shifted to the high-frequency region

and that the magnitude of the switching harmonics in the output voltage will also be reduced significantly.

The number of hysteresis loops in each odd quadrant, as shown in Fig. 3, is N , which is the same as the number of H-bridges in the cascaded multilevel inverter. Parameter h is the net hysteresis band, and δ is a small dead zone introduced to avoid any overlapping between adjoining loops [20].

A. Seven-Level Modulation

For a Seven-level modulation, three H-bridges are required. The corresponding multiband hysteresis modulation is shown graphically in Fig 2. The detailed control algorithm for a seven-level inverter based on the multiband hysteresis modulation is described in the Following:

Condition 1: if $se(t) > 0$, then

Condition 1.1:

if $se(t) > +\delta$, then
 $u(t) = +1/2$, for $+(h/2 + \delta) < se(t) < +(h/2 + 2\delta)$
 $u(t) = +0$ for $se(t) < \delta$

Condition 1.2 :

if $se(t) > +(h/2 + 2\delta)$, then

$u(t) = +1$, for $se(t) > +(h/2 + 2\delta)$
 $u(t) = +1/2$, for $se(t) < +(h/2 + 2\delta)$ (9a)

Condition 2 : if $se(t) < 0$, then

Condition 2.1 :

if $se(t) < -\delta$, then
 $u(t) = -1/2$, for $-(h/2 + \delta) > se(t) > -(h/2 + 2\delta)$
 $u(t) = +0$, for $se(t) > -\delta$

Condition 2.2 :

If $se(t) < -(h/2 + 2\delta)$, then
 $u(t) = -1$, for $se(t) < -(h/2 + 2\delta)$
 $u(t) = -1/2$, for $se(t) > -(h/2 + 2\delta)$ (9b)

With this scheme, the modulator has seven levels of output, i.e., $u = -1, -1/2, -3/2, 0, +3/2, +1/2$, and $+1$. The time-domain representation of seven-level hysteresis modulation, showing switching function $se(t)$ and seven-level switching logic $u(t)$, following the algorithm (9a) and (9b).

B. Hierarchical Switching Scheme

There are many switching combinations for obtaining the same level of inverter output voltage [25]. In this section, a switching scheme is proposed to follow the algorithm given in (9) for obtaining the seven-level output, which can easily be extended to the further higher level inverter. The scheme leads to a unique switching pattern corresponding to each level in the output. In this scheme, the switching stress of all the switches of the same H-bridge is equal. For the seven-level modulation discussed in the previous section, the following two hierarchies are chosen, 1) level-3 H-bridge, 2) level-5 H-bridge and 3) level-7 H-bridge

For Condition 1 in (9a), the left-leg switches of both H-bridges shown are kept at low switching frequency, i.e., switches Sw11, Sw14, Sw21, and Sw24 change their states at the fundamental frequency as follows:

Condition 1: $se > 0$, Switches Sw1 and Sw21 are ON. (10a)

Under steady-state condition, switching function se varies at the fundamental frequency. Therefore, the left-leg switches operate at this frequency for the positive half-cycle.

The right-leg switches of the H-bridges, i.e., Sw13, Sw12, Sw23, and Sw22, operate at high switching frequency for the positive half-cycle of switching function se , following the multiband hysteresis modulation. Each hierarchical bridge will operate for that corresponding level of the output only. The position of switches in the other H-bridge will remain fixed in this period. Consider the various cases of Condition 1 in (9) as follows.

Condition 1.1: (Level-3 operation); $se > +\delta$, switch Sw23 Remains ON, and

Case 1: Sw12 is ON, for $u = +1/2$,
 such that $v_c = +V_{dc}/2$

Case 2: Sw13 is ON, for $u = 0$,
 such that $v_c = 0$.

Condition 1.2: (Level-5 operation); $se > +(h/2 + 2\delta)$, Switch Sw12 remains ON, and

Case 1: Sw22 is ON for $u = +1$,
 such that $v_c = +V_{dc}$

Case 2: Sw23 is ON for $u = +1/2$,
 such that $v_c = +V_{dc}/2$

Now, for Condition 2 in (9b), i.e., $se < 0$, the right-leg switches of all the H-bridges are kept at low switching frequency, i.e., switches Sw13, Sw12, Sw23, and Sw22 change their states at the fundamental frequency for the negative half-cycle of se as follows:

Condition 2: $se < 0$, switches Sw13 and Sw23 are ON. (10b)

The left-leg switches, in this case, i.e., Sw11, Sw14, Sw21, and Sw24, operate at high switching frequency for the negative half-cycle of switching function se .

Condition 2.1: (Level-3 operation); $se < -\delta$, switch Sw21 Remains ON, and

Case 1: Sw14 is ON, for $u = -1/2$,
 Such that $V_c = -V_{dc}/2$

Case 2: Sw11 is ON, for $u = 0$,
 Such that $V_c = 0$.

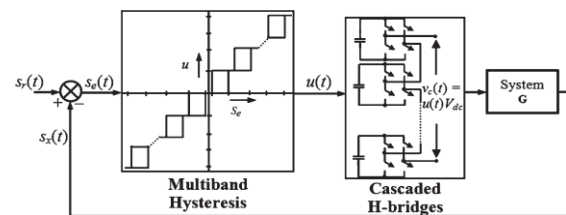


Fig. 4 Block diagram for a generalized n -level inverter-controlled system using multiband hysteresis modulation

Condition 2.2: (Level-5 operation); $se < -(h/2 + 2\delta)$,
 SwitchSw14 remains ON, and
 Case 1:Sw24 is ON, for $u=-1$,
 Such that $VC=-Vdc$
 Case 2:Sw21 is ON, for $u=-1/2$,
 such that $vc=-Vdc/2$.

The hierarchical switching scheme can easily be extended to any higher level inverter modulation. For an n -level inverter, there are N hierarchical H-bridges. Each is assigned as level-3, level-5 . . . or level- n H-bridge. It will be shown in the following section that a sequential change in the hierarchy of each H-bridge leads to the equal average switching of all the H-bridges.

C. Switching Characterization

In this section, an expression relating the desired maximum switching frequency fc of the switching elements in the H-bridges of the cascaded multilevel inverter, and the hysteresis band h of the multiband hysteresis modulation, as shown in Fig. 3, has been obtained.

The block diagram represents the steady state condition of the system [13], [15]. Under steady state, it is assumed that the low-frequency reference vector s is tracked by the controlled vector x against low-frequency perturbations such as source voltage and nonlinear load under closed loop. The difference of the two vectors generates switching function se , as given by (4). Using (1), the following systems are defined:

$$\begin{aligned} Gu(s) &= VdcG(s) \\ &= K(sI - F) - 1g1 \\ &= \frac{(V_{dc} / C_f L_T)(k_1 s + k_2)}{s^2 + (R_T / L_T)s + (1 / C_f L_T)} \quad (11) \end{aligned}$$

It has been shown in [13] that the hysteresis band h required for a given maximum switching frequency $fc (= \omega_c / 2\pi)$, using the switching transition concept of Tsytkin's method, for a two level hysteresis modulation shown in Fig. 7, can be obtained using the following:

$$h = -4\pi \text{Im} (H(\omega_c)) \quad (12)$$

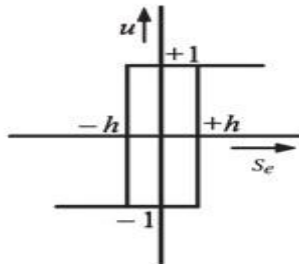


Fig. 5 Two-level hysteresis modulation.

Where

$$\text{Im}\{H(\omega_c)\} = \sum_{n=1(2)}^{\infty} \frac{1}{n} \text{Im}\{G_u(jn\omega_c)\}$$

Also, it is well known from the describing-function theory that the describing function of the nonlinear hysteresis shown in Fig. 5 with hysteresis band h is given by [23]

$$N_x(X) = \frac{4}{\pi X^2} \left[(X^2 - h^2)^{1/2} - jh \right] \quad (13)$$

Its inverse can be obtained as

$$-\frac{1}{N_x(X)} = -\frac{\pi}{4} \left[(X^2 - h^2)^{1/2} + jh \right] \quad (14)$$

Where X is the amplitude of the limit cycle and represents the minimum amplitude of switching ripples in switching function se [13], over one cycle of the fundamental frequency, based upon the first harmonic linearization. Equating (14) and system transfer function $Gu(j\omega)$ gives relation (12), based upon the first harmonic approximation at frequency ω_c .

Proposition 1: The effective maximum switching frequency f_{ce} , as seen in the output of an n -level inverter, following the multiband hysteresis modulation shown in Fig. 3, is the same as that for the two-level inverter, i.e., fc with the same net hysteresis band length h . The magnitude of switching ripples in the output is reduced by $1/2N$ times as compared to that present in the case of the two-level inverter.

Proof: It is assumed that the variable-structure control for multiband hysteresis modulation satisfies the existence condition (6) for the switching surface se shifted correspondingly for different levels in Fig. 3. Consider now the n -level inverter operating in a k th level at a particular instant under steady state. Then, the $(k-1)/2 = p$ th H-bridge having a k th hierarchy must be operating at that particular instant following the p th band in Fig. 3. For example, if a five-level inverter is used and if this inverter is at level-3 operation at a particular instant under steady state, then the first H-bridge must be operating following the first hysteresis band in the first quadrant and this H-bridge has a level-3 hierarchy. Consider again the p th hysteresis band in Fig. 3. The hysteresis band length starts from $[(p-1)h/N + p\delta]$ and ends at $[ph/N + p\delta]$. The output levels corresponding to these points are $(p-1)/N$ and p/N , respectively. Therefore, the net band length is h/N , and the difference in the net operating level is $1/N$. Now, let us place this hysteresis band symmetrically around the origin, as.

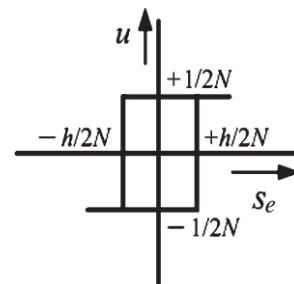


Fig. 6. Switching characterization of an n -level inverter using the PTH hysteresis band.

Shown in Fig. 6. This is based on the assumption made earlier that switching surface se may be shifted correspondingly for different levels for the purpose of analysis. The describing function of the hysteresis band shown in Fig. 6 can be obtained as

$$N_{X'}(X') = \frac{1}{\pi(NX')^2} \left[\{(2NX')^2 - h^2\}^{\frac{1}{2}} - jh \right] \quad (15)$$

where X' is a limit-cycle amplitude in switching function se for an n -level-inverter-controlled system. The negative inverse of (15) yields

$$-\frac{1}{N_{X'}(X')} = \frac{\pi}{4} \left[\{(2NX')^2 - h^2\}^{\frac{1}{2}} + jh \right] \quad (16)$$

By comparing (16) with (14), it can be seen that the imaginary parts of the two equations are the same. Therefore, this leads to the same condition (12) of the switching of the two level inverter. Hence, the effective maximum switching frequency f_{ce} of an n -level inverter and the maximum switching frequency f_c of a two-level inverter, for the same net hysteresis band h , are the same. Although, on instantaneous basis, the number of switches participating in this switching operation is two out of $4N$ switches in a multilevel inverter, therefore the average switching frequency of each switch will be less than $f_{ce}/2N$. The switching loss will also be distributed in the case of the multilevel inverter. A comparison of the real parts of (14) and (16) yields the following:

$$X' = \frac{X}{2N} \quad (17)$$

This implies that the amplitude of the limit cycle or ripples in switching function se is reduced by $1/2N$ times as compared to that for the two-level inverter. Also, since switching input u toggles between $-1, \dots, -2/N, -1/N, 0, +1/N, 2/N, \dots, +1$, the net pulse height of the switching pulses are $1/N$ compared to $(1 - (-1)) = 2$ in the case of the two-level inverter. Hence, the magnitude of switching ripples in the output of the multilevel-inverter-controlled system is reduced to $(1/2N)$ times as compared to the two-level-inverter-controlled system for the same effective switching frequency.

IV. MATLAB/SIMULINK MODEL and SIMULATION RESULTS

Case 1: Five level inverter as DSTATCOM

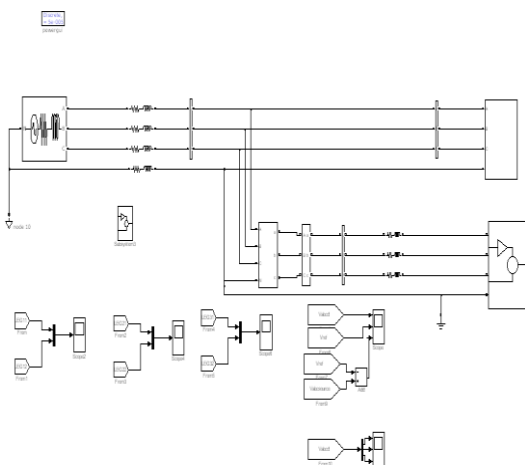


Fig. 7 Simulation circuit of DSTATCOM with 5-level VSI.

Fig.7 shows the simulation circuit of the DSTATCOM with 5-level inverter topology.

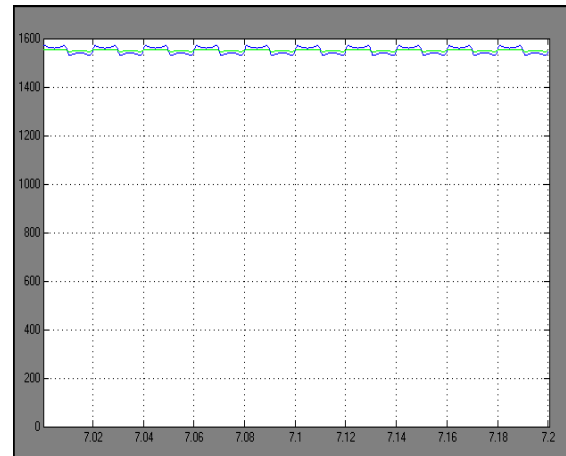


Fig.8 DC-link voltages Vdc1 and Vdc2.

Fig.8 shows the DC-link voltages Vdc1 and Vdc2, which varies with the operation of the DSTATCOM.

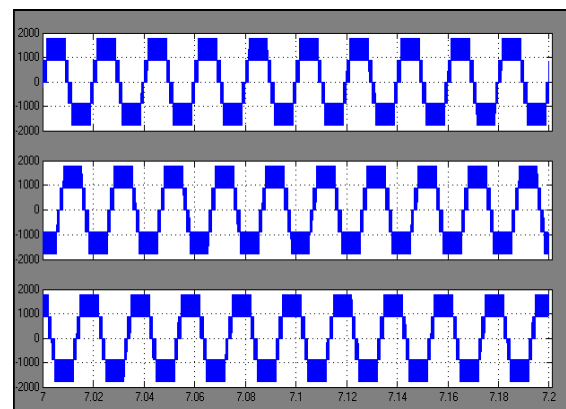


Fig.9 Five-level inverter output voltages of three phases.

Fig.9 shows the five level inverter output voltages of the three phases.

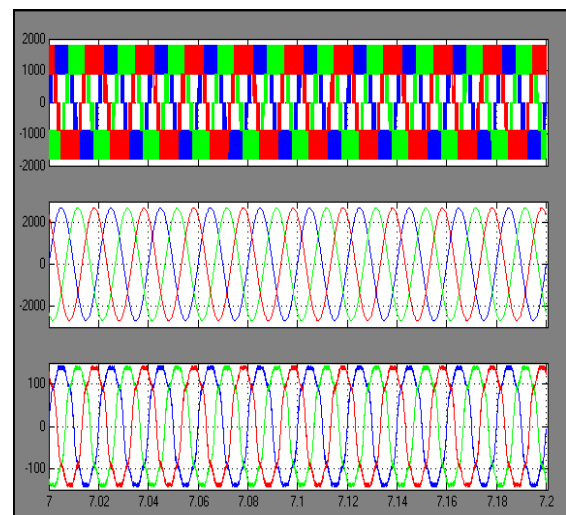


Fig.10 Three phase inverter voltage, Source voltage and source current

Fig.10 shows the three phase inverter output voltage, source voltage and current which are not having harmonics.

Case 2: Seven level inverter as DSTATCOM

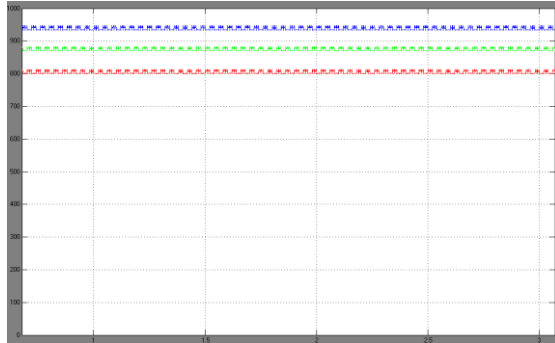


Fig. 11 DC-link voltages Vdc1 and Vdc2.

Fig. 11 shows the DC-link voltage of Vdc1 and Vdc2 of leg 1 of seven levels VSI.

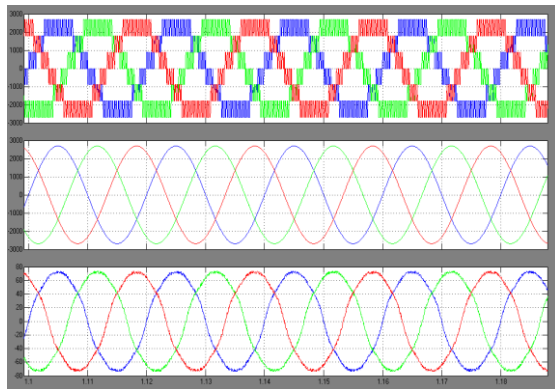


Fig.12 Inverter output voltage, Source voltage and source current.

Fig.12 shows the output voltage waveform the inverter, source voltage and source current of the system with seven level DSTATCOM.

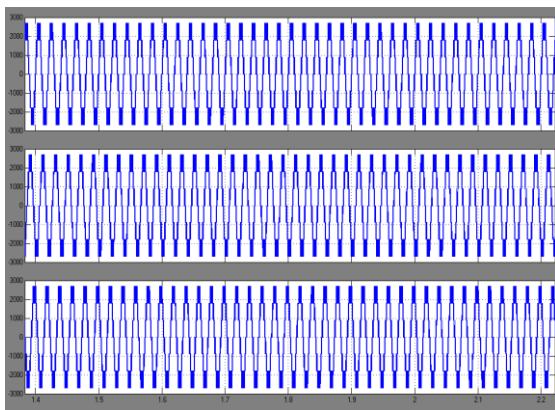


Fig.13 Seven level inverter output voltages of the inverter.

Fig.13 shows the seven level inverter output voltages of the inverter which is connected to the system.

VI. CONCLUSION

In this paper, a proposal has been made for a DSTATCOM based on a five-level and seven levels Cascaded multilevel inverter. The basic concepts and structure of the DSTATCOM are discussed. The multiband hysteresis modulation proposed in this paper has shifted the switching components toward higher frequencies and has hence reduced the switching ripple content in the output controlled voltage. The simulation results verify the control scheme proposed. The sequential swapping of hierarchy for each cell yields the self-balancing capability in case the dc-link voltage is supported by the capacitors. The simulation

results confirm that the proposed DSTATCOM offers satisfactory performance.

REFERENCES

- [1] J. S. Lai and F. Z. Peng, "Multilevel converters—A new breed of power converters," IEEE Trans. Ind. Appl., vol. 32, no. 3, pp. 509–517, May/Jun. 1996.
- [2] J. Rodriguez, J. S. Lai, and F. Z. Peng, "Multilevel inverters: A survey of topologies, controls and applications," IEEE Trans. Ind. Electron., vol. 49, no. 4, pp. 724–738, Aug. 2002.
- [3] J. Rodriguez, S. Bernet, B. Wu, J. O. Pontt, and S. Kouro, "Multilevel voltage-source-converter topologies for industrial medium-voltage drives," IEEE Trans. Ind. Electron., vol. 54, no. 6, pp. 2930–2945, Dec. 2007.
- [4] P. Lezana, J. Rodriguez, and D. A. Oyarzun, "Cascaded multilevel inverter with regeneration capability and reduced number of switches," IEEE Trans. Ind. Electron., vol. 55, no. 3, pp. 1059–1066, Mar. 2008.
- [5] Z. Du, L. M. Tolbert, J. N. Chiasson, and B. Ozpineci, "Reduced switching-frequency active harmonic elimination for multilevel converters," IEEE Trans. Ind. Electron., vol. 55, no. 4, pp. 1761–1770, Apr. 2008.
- [6] J. I. Leon, R. Portillo, S. Vazquez, J. J. Padilla, L. G. Franquelo, and J. M. Carrasco, "Simple unified approach to develop a time-domain modulation strategy for single-phase multilevel converters," IEEE Trans. Ind. Electron., vol. 55, no. 9, pp. 3239–3248, Sep. 2008.
- [7] J. I. Leon, S. Vazquez, A. J. Watson, L. G. Franquelo, P. W. Wheeler, and J. M. Carrasco, "Feed-forward space vector modulation for single-phase multilevel cascaded converters with any dc voltage ratio," IEEE Trans. Ind. Electron., vol. 56, no. 2, pp. 315–325, Feb. 2009.
- [8] M. A. Pérez, P. Cortés, and J. Rodríguez, "Predictive control algorithm technique for multilevel asymmetric cascaded H-bridge inverters," IEEE Trans. Ind. Electron., vol. 55, no. 12, pp. 4354–4361, Dec. 2008.
- [9] M. S. Carmeli, F. Castelli-Dezza, and G. Superti-Furga, "Generalized decoupling method for current-controlled multiswitching systems," IEEE Trans. Ind. Electron., vol. 56, no. 2, pp. 348–349, Feb. 2009.
- [10] C. C. Hua, C. W. Wu, and C. W. Chuang, "A digital predictive current control with improved sampled inductor current for cascaded inverters," IEEE Trans. Ind. Electron., vol. 56, no. 5, pp. 1718–1726, May 2009.
- [11] M. Carpita and M. Marchesoni, "Experimental study of a power conditioning system using sliding mode control," IEEE Trans. Power Electron., vol. 11, no. 5, pp. 731–742, Sep. 1996.
- [12] L. Malesani, L. Rossetto, G. Spiazzi, and A. Zuccato, "An AC power supply with sliding-mode control," IEEE Ind. Appl. Mag., vol. 2, no. 2, pp. 32–38, Sep./Oct. 1996.

AUTHORS PROFILE



VUYYYURU SWAPNA received her B.Tech degree in St. Ann's College of Engineering and technology and she is pursuing her M.Tech degree from Sasi Institute of Technology and Engineering with the specialization of Power Electronics. Her area of interests are Power Electronics.



ASWANI KUMAR EEDARA received the B.Tech. Degree in Electrical and Electronics Engineering from the JNTU college of Engineering Hyderabad, India in 2005 and the M.E. degree in Power Systems from the University College of Engineering Osmania University Hyderabad in 2008. He worked as Project Trainee at General Electric-consumer and Industrial Hyderabad for one year. He has been on the faculty of SASI Institute of Technology and Engineering at Tadepalligudem as an Assistant Professor in Department of Electrical and Electronics Engineering since 2008. He has been working as Head of the Department of E.E.E. since MAY 2012. He is member of IAENG. He is presently doing his research in the area of Power Electronics applications in Power systems at JNTU Kakinada. His areas of interest are FACTS Controllers, Evolutionary algorithms, Modeling and simulation of Power Electronics and Power Systems.

An Application of 2d Rigid Link Theory in Flexible Link Manipulator: Kinematics

Mahesh A. Makwana¹, Arvind N. Nakiya²

¹(Department of Mechanical Engineering, Sardar Vallabhbhai National Institute of Technology, Surat, India

²(Department of Electrical Engineering, Nirma University, Ahmedabad, India

ABSTRACT: This paper presents kinematic and dynamic modeling techniques for flexible robots. The main emphasis is to discretize whole flexible link in very small parts each considering as a rigid link. This approach is based on a "discretization method". In kinematics position or deflection is solved by deflection of cantilever beam theory while orientation is solved by forward kinematics. Dynamics is solved by applying Lagrange-Euler formulation.

Keywords: Discretization, Dynamics, Flexible link manipulator (FLM), Kinematics, Rigid link manipulator

I. INTRODUCTION

1.1 Kinematics of rigid link

Kinematics is the branch of physics which involves the description of motion, without considering the forces which produce the motion (dynamics or kinetics, on the other hand, involves an examination of both a description of motion and the forces which produce it). A subset of kinematics is that of rigid body kinematics concerns the motions of one or more rigid bodies. A rigid body experiences zero deformation. In other words, all points lying on a rigid body experience no motion relative to each other [1].

There are seven methods to solve kinematics as:

1. Forward Kinematics
2. Inverse Kinematics
3. Algebraic method
4. Geometric method
5. Symbolic elimination method
6. Continuation method
7. Iterative method

1.2 Kinematics of flexible link

In rigid robot manipulator kinematics can be described by employing Denavit-Hartenberg representation. The main idea is to use 4x4 transformation matrices which can be determined uniquely as a function of only 4 parameters. However this procedure cannot be used directly to describe the kinematics of a FLM due to link deformation. In order to overcome this drawback, the procedure has been modified by including some transformation matrices which take link elasticity into account. A description of Denavit-Hartenberg representation of rigid body is assumed to be known.

In general, the homogeneous transformation of frame i with respect to the base frame can be characterized through the following composition of consecutive transformation:

$${}^0T_i = A_1 E_1 A_2 E_2 \dots A_{i-1} E_{i-1} = T_{i-1} A_i \quad (1)$$

$$\text{or} \quad T_i = A_i \quad (2)$$

Where A_i is the standard homogeneous transformation matrix for joint i due to rigid motion and E_i is the homogeneous transformation matrix due to link i length and deflection. Notice that, even though the superscript is not explicitly indicated, each transformation matrix is referred to the frame determined by the preceding transformation.

The transformation matrix A_i can be computed just like in the case of the rigid body. On the other hand, the transformation matrix E_i deserves special attention. Assuming small link deformation, E_i can be expressed by:

$$E_i = \begin{bmatrix} 1 & \cos\left(\frac{\pi}{2} + \theta_{zi}\right) & \cos\left(\frac{\pi}{2} - \theta_{yi}\right) & l_i + \delta_{xi} \\ \cos\left(\frac{\pi}{2} - \theta_{zi}\right) & 1 & \cos\left(\frac{\pi}{2} + \theta_{xi}\right) & \delta_{yi} \\ \cos\left(\frac{\pi}{2} + \theta_{yi}\right) & \cos\left(\frac{\pi}{2} - \theta_{xi}\right) & 1 & \delta_{zi} \\ 0 & 0 & 0 & 1 \end{bmatrix} \quad (3)$$

Where θ_{xi} , θ_{yi} , θ_{zi} are the angles of rotation, and δ_{xi} , δ_{yi} , δ_{zi} represent link i deformation along x , y , z , respectively, being l_i the length of link without deformation. By taking into account the fact $\cos(\pi/2 + \alpha) = -\sin(\alpha)$ and assuming small angles, so that $\sin(\alpha) = \alpha$ is valid, the matrix E_i can be approximated as

$$E_i = \begin{bmatrix} 1 & -\theta_{zi} & \theta_{yi} & l_i + \delta_{xi} \\ \theta_{zi} & 1 & -\theta_{xi} & \delta_{yi} \\ -\theta_{yi} & -\theta_{xi} & 1 & \delta_{zi} \\ 0 & 0 & 0 & 1 \end{bmatrix} \quad (4)$$

1.3 Dynamics of rigid-link

Manipulator dynamics is concerned with the equations of motion, the way in which the manipulator moves in response to torques applied by the actuators, or external forces. The history and mathematics of the dynamics of serial-link manipulators is well covered by Paul and Hollerbach[2].

There are methods by which we can solve the dynamics of the rigid manipulator as:

1. Newton-Euler formulation
2. Lagrange-Euler formulation
3. Generalized d'Alembert equation of motion

There are two problems related to manipulator dynamics that are important to solve:

- Inverse dynamics in which the manipulator's equations of motion are solved for given motion to determine the generalized forces and
- Direct dynamics in which the equations of motion are integrated to determine the generalized coordinate response to applied generalized forces.

To derive the dynamic equations of motion of manipulators

types of methods can be followed for rigid link.

1.3.1 Lagrange-Euler Formulation

The general motion equation of a manipulator can conveniently be expressed through the direct application of the Lagrange-Euler formulation to non-conservative system. Many investigators utilize the Denavit-Hartenberg matrix representation to describe the spatial displacement between the neighboring link coordinate frame to obtain link kinematics information and they employ the L-E equation to derive dynamic equation of manipulator.

The derivation of the dynamic equation of an n degree of freedom manipulator is based on the understanding of:

- The 4X4 homogeneous coordinate transformation matrix, ${}^{i-1}A_i$, which describes the spatial relationship between the ith and (i-1)th link coordinate frame. It relates the point fixed in link i expressed in homogeneous coordinates with respect to i^{th} coordinate system to the (i-1)th coordinates system.

- The Lagrange-Euler equation

$$\frac{d}{dt} \left[\frac{\partial L}{\partial \dot{q}_i} \right] - \frac{\partial L}{\partial q_i} = \tau_i, i=1,2,\dots,n \quad (5)$$

Where

L= Lagrangian function= kinetic energy K – potential energy P

K= total kinetic energy of the robot arm

P= total potential energy of robot arm

q_i =generalized coordinates of the robot arm

\dot{q}_i =first time derivative of the generalized coordinates, q_i

τ_i = generalized force or (torque) applied to the system at joint i to drive link i

From the above lagrangian equation one is required to properly choose a set of generalized coordinates to describe the system. Generalized coordinates are used as a convenient set of a coordinates which completely describe the location of a system with respect to reference coordinate frame.

1.4 Dynamics of flexible link

There are methods by which we can solve the dynamics of the flexible manipulator as:

1. Newton-Euler formulation
2. Langrange-Euler formulation
3. Generalized d'Alembert equation of motion
4. Recursive Gibbs-Appell formulation
5. Finite dimensional approximation
6. Hamilton's principle and FE approach
7. Assume mode method and Langrange approach

1.4.1 Dynamics using Lagrange-Euler approach

In order to obtain a set of differential equations of motion to adequately describe the dynamics of a flexible link manipulator, the Lagrange-Euler approach can be used. A system with n generalized coordinates q_i must satisfy n differential equations of the form

$$\frac{d}{dt} \left[\frac{\partial L}{\partial \dot{q}_i} \right] - \frac{\partial L}{\partial q_i} + \frac{\partial D}{\partial \dot{q}_i} = \tau_i \quad i=1, 2, \dots, n \quad (6)$$

Where L is the so called Lagrangian which is given by $L=K-P$; K represents the kinetic energy of the system and P the

potential energy. Also, D is the Rayleigh's dissipation function which allows dissipative effects to be included, and τ_i is the generalized force acting on q_i .

II. MATHEMATICAL ANALYSIS

2.1 Problem statement

A flexible robotic arm having length of 0.500 m, width of 0.08 m, thickness of 0.001 m having point load at B as shown in figure of 0.200 kg. Modulus of elasticity of link material is 20 GPa consider as an example.

Kinematics and Dynamics of the flexible link using rigid link theories (deflection of cantilever beam, Forward kinematics and Lagrange-Euler approach) with discretization approach are to be solved.

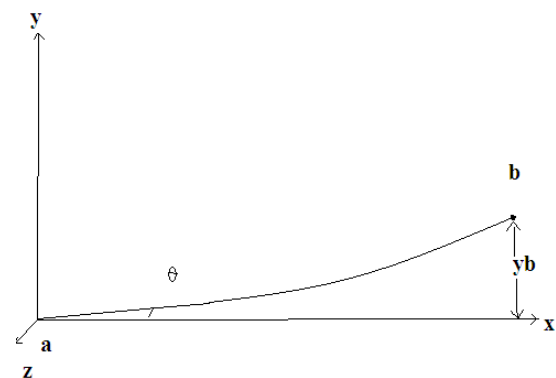


Fig.1 Deflection of flexible link

SOLUTION

$$L=500 \text{ mm} \quad E=2 \times 10^5 \text{ N/mm}^2$$

$$w=80 \text{ mm}$$

$$t=1 \text{ mm} \quad W=20 \text{ KN/m}$$

Let,

- Moment of inertia of link is I, given as

$$I = \frac{wt^3}{12} \quad (7)$$

$$I = \frac{80 \times 1^3}{12} \quad (8)$$

$$I=6.66 \text{ mm}^4$$

$$\text{Flexure rigidity } F=EI=13.32 \times 10^6 \text{ N-mm}^2$$

Deflection of link is given as

$$y_b = \frac{WL^3}{3EI} \quad (9)$$

$$y_b = \frac{20 \times (500)^3}{3 \times 13.32 \times 10^6}$$

$$y_b=62.56 \text{ mm}$$

Now to use cantilever beam deflection theory for flexible link, discretize whole link in 50 parts each having length of 10 mm and find deflection of point B.

So deflection for single link,

$$y_1 = \frac{Wl_1^3}{3EI}$$

$$y_1 = \frac{20 \times (10)^3}{3 \times 13.32 \times 10^6}$$

$y_1 = 0.0005 \text{ mm}$

Deflection of all the links (1 to 50) calculated as above and angle of each from horizontal axis.

TABLE Deflection and angle of each link

Link no. (n)	Deflection from fixed point A (y_n)	Deflection (Y_n)= $y_n - y_{n-1}$	θ from each point $\theta_n = \tan^{-1} Y_n$
1	0.0005	0.0005	0.0028
2	0.0040	0.0035	0.0200
3	1.0130	0.0090	0.0515
4	0.0320	0.0190	0.1088
5	0.0625	0.0305	0.1747
6	0.1081	0.0456	0.2612
7	0.1716	0.0635	0.3638
8	0.262	0.0846	0.4847
9	0.3648	0.1086	0.6222
10	0.5005	0.1357	0.7774
11	0.6661	0.1656	0.9487
12	0.8648	0.1987	1.1383
13	1.0995	0.2347	1.3444
14	1.3733	0.2738	1.5683
15	1.6891	0.3158	1.8087
16	2.0500	0.3609	2.0669
17	2.4589	0.40879	2.3415
18	2.9181	0.4600	2.6337
19	3.4329	0.5140	2.9424
20	4.0040	0.5711	3.2686
21	4.6351	0.6311	3.6111
22	5.3293	0.6942	3.9711
23	6.0895	0.7602	3.9711
24	6.9189	0.8294	4.7412
25	7.8203	0.9014	5.1507
26	8.7967	0.9764	5.5596
27	9.8513	1.0546	6.0201
28	10.9869	1.1356	6.4787
29	12.2067	1.2198	6.9545
30	13.5135	1.3068	7.4452
31	14.9104	1.3969	7.9521
32	16.4004	1.4900	8.4747
33	17.9864	1.5860	9.0120
34	19.6716	1.6852	9.5656
35	21.4589	1.7873	10.1334
36	23.3513	1.8924	10.7159
37	25.3518	2.0005	11.3126
38	27.4634	2.1116	11.9234
39	29.6891	2.2257	12.5477
40	32.0320	2.3429	13.1859
41	34.4949	2.4629	13.8360
42	37.0810	2.5861	14.4995
43	39.7932	2.7122	15.1747
44	42.6346	2.8414	15.8619
45	45.6081	2.9735	16.5598
46	48.7167	3.1086	17.2683
47	51.9634	3.2467	17.9870
48	55.3513	3.3879	18.7158
49	58.8833	3.5320	19.4532
50	62.5625	3.6795	20.2010

For whole link,

$$y_{total} = y_b = \sum_{n=1}^{50} y_n - y_{n-1}$$

$$y_{total} = y_b = 62.5628 \text{ mm}$$

(10)

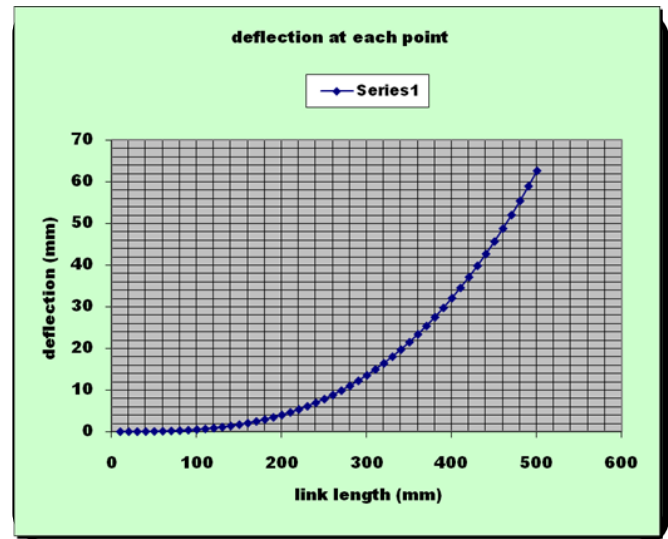


Fig.2 Deflection at each point

The deflection of link is 62.5628 mm which has been manually founded. The same result has been founded using ANSYS is 62.563 mm with two digit precision.

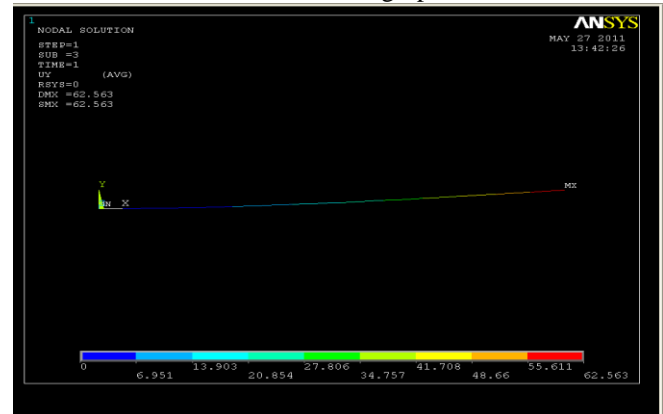


Fig.3 Nodal solution Y-component displacement

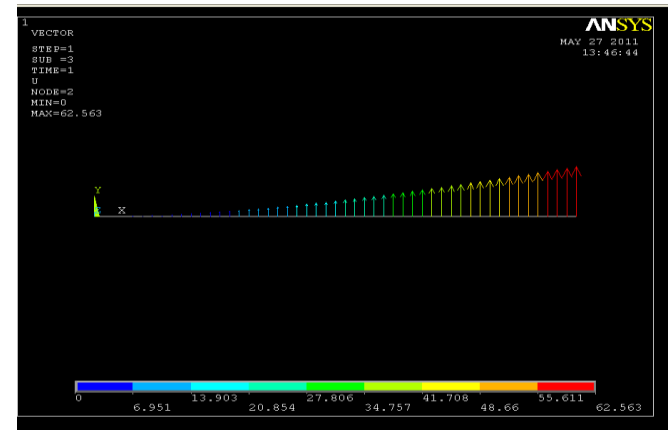


Fig.4 Predefine vector plot on ANSYS

Same as to find rotation of link discretize whole link in 50

equal parts and find each link rotation matrix and use forward transformation for n rigid link will give rotation matrix of flexible link.

Rotation of θ angle with respect to Z- axis[1].

$$R_{z,\theta} = \begin{bmatrix} \cos\theta & -\sin\theta & 0 \\ \sin\theta & \cos\theta & 0 \\ 0 & 0 & 1 \end{bmatrix} \quad (11)$$

For link-1-50, rotation matrices are

So ${}^0R_{50} = {}^0R_1 {}^1R_2 {}^2R_3 \dots {}^{49}R_{50}$

$${}^0R_{10} = \begin{bmatrix} 0.337 & -0.899 & 0 \\ 0.899 & 0.337 & 0 \\ 0 & 0 & 1 \end{bmatrix}$$

III. CONCLUSION

From above given approach of discretizing the flexible link in number of rigid links one can solve the kinematics and dynamics of the flexible link. Usually this approach is very much applicable in hyper-redundant or serpentine type of robot.

Future scope: Solve the dynamics by discretizing approach. By applying Lagrange-Euler theory of motion equation of rigid link for number of links and considering that the flexible link is made of from number of small rigid links one can solve dynamics for flexible link.

REFERENCES

- [1] Fu K.S., Robotics: Control & Sensing, Vision & Intelligence, (Tata McGraw-Hill, pp.12-144-2008).
- [2] Book, De luca and Siciliano, Flexible Link Manipulator: Modeling, Nonlinear Control And Observer, 2003.
- [3] Hollerbach J.M., A recursive Lagrangian formulation of manipulator Dynamics and a comparative study of Dynamics Formulation Complexity, IEEE Transactions on System, Man, and cybernetics, Vol. SMC-10, No.11, November 1980.
- [4] Wen Chen, Dynamic modeling of multi-link flexible robotic manipulators, Institute of Mechanics, Technical University of Munich, Garching, Germany, 6 August 1999.
- [5] W.J. Book, Modeling, design, and control of flexible manipulator arms: A tutorial review, Proc. of the IEEE Conference on Decision and Control, San Francisco, CA, (1990) 500–506.

An Overview of PLC Based Control Panel System for External Plunge Grinding Machine and CNC Machine

Arvind N. Nakiya¹, Mahesh A. Makwana²

¹(Department of Electrical Engineering, Nirma University, Ahmedabad, India

²(Department of Mechanical Engineering, Sardar Vallabhbhai National Institute of Technology, Surat, India

ABSTRACT: Automation is the process of handling various parameters of process like temperature, flow, level etc. without presence of responsible person. In industrial field, Automation and control have greatly improve in industrial manufacturing in the world. Technological advancement in automation and control over the past decades have contributed greatly to improve the productivity of virtually all manufacturing industries throughout the world. In the development of automation controllers the trend has been to move towards soft controllers so as to provide better control, more flexibility and more reliability with intelligent diagnostics of machine faults. So industries have gradually moved from conventional relay logic control to programmable logic control and then to computerized numeric control. In this paper all the required control and motor performance data will be taken to a personal computer via PLC for further analysis. Various results are obtained and discussed.

Keywords: Computerized Numeric Control (CNC), External plunge Grinding machine (EPG), Personal Computer (PC), Programmable Logic Controller (PLC), Pulse per revolution (ppr)

I. INTRODUCTION

Almost any production line, machine function or process can be automated using a PLC. The speed and accuracy of the operation can be greatly enhanced using this type of control system. But the biggest benefit in using a PLC is the ability to change and replicate the operation or process while collecting and communicating vital information. Since there were problems related to large electrical panels with a number of electrical components and extensive wiring, people felt the need for software logic controllers? So they gave birth to Programmable Logic Controller (P.L.C) wherein the control logic is developed in ladder diagram, a software logic control, with a number of inputs taken from the environment and generating the outputs, depending on the logic programmed, to the environment. This helped to control any machine sequence with small electrical panels, less number of electrical components and less wiring with more flexibility to change machine sequence. These fulfilled some of their needs but the desire to obtain software controlled automation with accuracy necessitated the development of Computer Numeric Control (C.N.C). In order to have better control for positioning, controlled speed and quick reversal of direction of slide movement, servo motors having less inertia, along with servo drives are interfaced with the C.N.C. The user based part program decoded by the C.N.C. provides the desired profile with the control being transferred to P.L.C. and drives as and when required. Special measuring devices

as locators, gauges being interfaced with the C.N.C. through independent controllers provide more accuracy. [1]

Advantages of PLC are as below;

- Reliability in operation
- Flexibility in control techniques
- Flexibility in programming
- Large quantity of contacts
- Online/offline modifications
- Cost effective for controlling complex systems
- Small physical size, shorter project time
- In-house simulation and testing of project
- Speed in operation
- Ability to communicate with computer systems
- Security [2]

II. PROGRAMABLE LOGIC CONTROLLER

2.1 A programmable logic controller is a specialized computer. Since it is a computer, it has all the basic component parts contained in any other computer, a central processing unit, memory, input interfacing, and output interfacing.

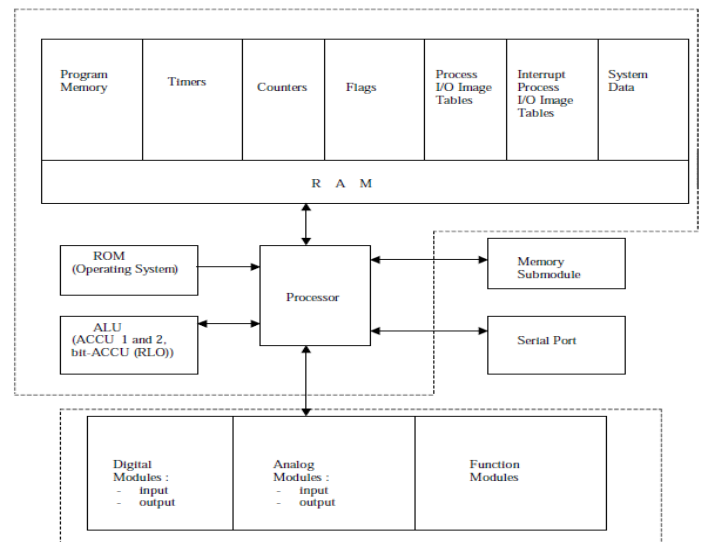


Fig.1 functional units of a typical PLC

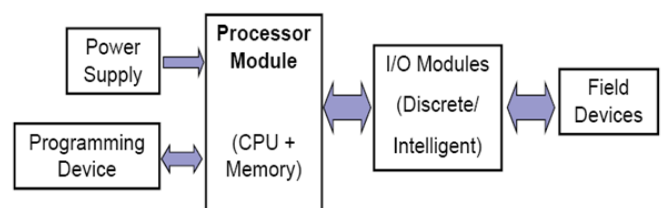


Fig.2 Block Diagram of PLC

The block diagram of Programmable Logic Controller is shown in Fig.2 The processor is a solid state

device designed to replace relays, timers, counter etc. The necessary voltage and current requirement for the internal working of the PLC is generated by the power supply. The field element is interfaced to the input or output section. Typical input or output section, typical input element are push buttons, limit switches, proximity switches, relay contacts, selector switches, thumb wheels etc. Typical output elements are solenoid valves relay coils, indicator lights LED display etc.



Fig.3 PLC based control panel for EPG

Fig.3 shows PLC based control panel system for external plunge grinding machine. In this control panel system Mitsubishi Q series PLC is used. PLC controls all inputs and outputs. Wheel is fed directly into the work piece in external plunge grinding. In this paper external plunge grinding is used for bearing application.

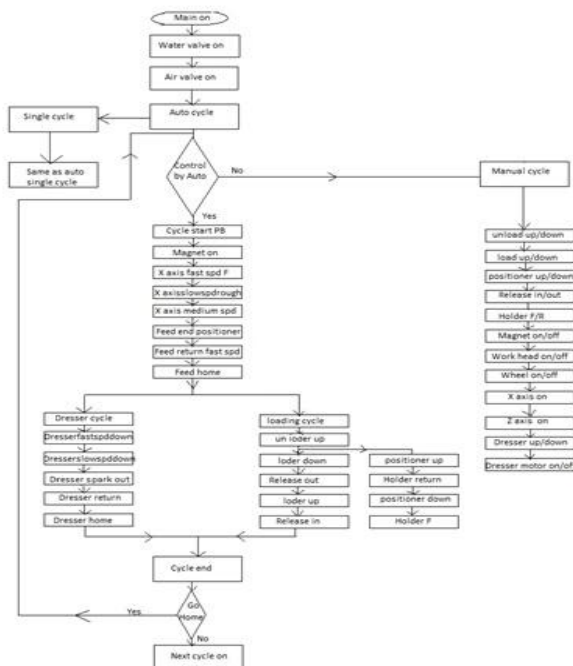


Fig.4 Flow chart of EPG machine

Operation of machine is done by three cycles. Single cycle, multi cycle and manual cycle. Machine operation is done in manual and auto both modes. In auto cycle one cycle is over the next cycle is automatic on.

2.2 Computer Numeric Control (CNC): The major components associated with a CNC system are power supply, PLC, servo drives, Touch monitor and keyboard and some special controllers might be interfaced for specific accuracy requirements such as precise positioning of job, accurate sizing of any machining operations. The power unit supplies constant 24V D.C. to the system. PLC interfaced with the CNC is programmed for the machine sequence. The part program of the CNC determines the operational sequence of the machine. To clarify the machine sequence and operational sequence CNC-PLC interface has been dealt later in this paper. Servo drives are used in conjunction with servo motors for better variable speed control with less response time as the inertia of the rotor is less. The diagram (1) has shown below shows the CNC block diagram with the necessary interfaces for a single axis machine [3].

There are two types of servo drives:

- (1) Constant torque-speed drives used for axis motors
- (2) Constant power drives used for spindle motors

The external inputs and outputs from the machine are connected to the PLC through the I/O interface of PLC. The system program of the CNC executes the part program, reads the machine data, perform the calculations.

CNC reads in the signal from the axis encoder from the measuring card which is placed in one of the slots of the controller. Thus having the machine data as pitch of the ball-screw, number of encoder pulses generated and resolution of the encoder mounted on the slide the distance moved by the slide can be calculated as [4].

Distance = $(p/r) * e_p$ (here backlash compensation is not taken into account)

Where p = pitch of ball-screw (mm)

r = resolution of encoder in (ppr)

e_p = number of encoder pulses generated

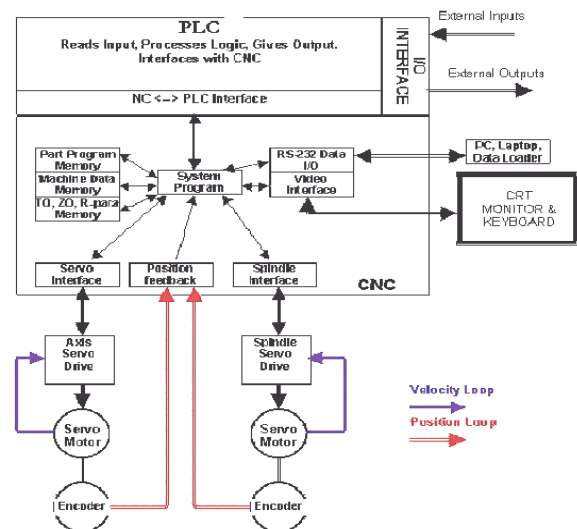


Fig. 5 CNC block diagram

This provides the positional feedback to the system. The velocity feedback is directly fed to the drive from the encoder or tachogenerator of the servo motor. The diagram (5) below shows the interface of the CNC with the servo drives. CNC sends a drive enable signal to a drive and the drive tends to retain its position unless some command for movement is send from the CNC. To give feed command CNC along with the drive enable signal sends a reference

voltage to the drive in the range of +/-10V proportional to the desired speed. The +/- sign denotes the direction of movement [5].

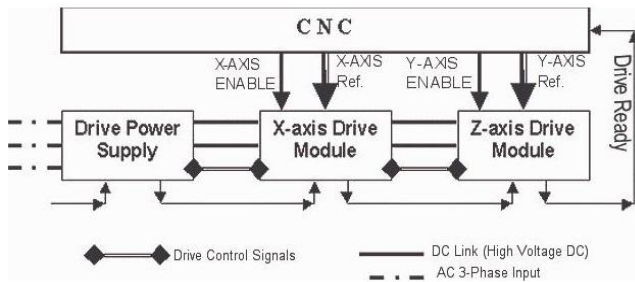


Fig 6 Drive-CNC interface diagram

The reference voltage is calculated as:

$$\text{Reference voltage} = (10/n) * S$$

Where n = maximum speed i.e. rated speed of motor (r.p.m)

S = desired speed (r.p.m)

The drive calculates the commanded speed from the reference voltage and calculates the actual motor speed from the motor encoder feedback to the drive. Thus the error is known and by changing the frequency and phase voltage drive tries to minimize the error to maintain the desired speed. If the drives and motors are in healthy condition then a drive ready signal is sent to the PLC. If this signal is missing then fault appears and axes movements or spindle operations are not possible.

III. EXPERIMENTAL RESULT

Many PLC processors have an RS-232 port that is normally used for programming the PLC. The RS-232 standard is based on a low/false voltage between +3 to +15V, and a high/true voltage between -3 to -15V (+/-12V is commonly used). Fig.7 shows the experimental result of output of hydraulic machine derived by GT-Developer software.

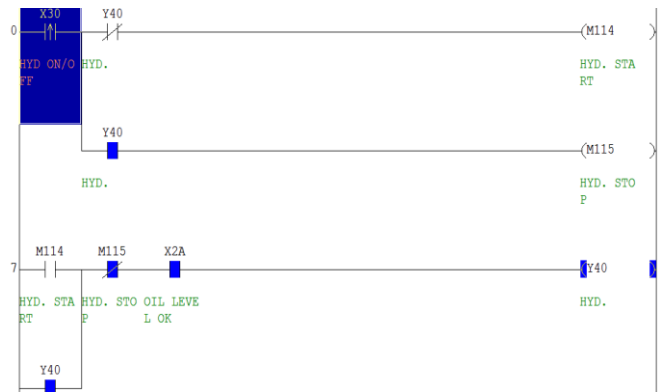


Fig. 7 Experimental result

IV. CONCLUSION

The paper gives a broad overview of PLC and CNC controllers in machine automation and grinding application. Certain other factors are also involved but it could not be presented in this paper. However the topics dealt with will give a brief idea for the basic functioning of PLC and CNC controllers. By automation we can improve the productivity in the industry. We continuously monitor the state of input devices and make the decision based upon a custom program to control the state devices connected as output.

REFERENCES

- [1] Pradeep Chatterjee, An over view of PLC and CNC in machine automation.
- [2] Bolton, w., Programmable Logic Controllers: An Introduction, Butterworth-Heinemann, 1997.
- [3] Douglas V. Hall, Microprocessors and Interfacing (Programming and Hardware), Tata McGraw-Hill, 1992.
- [4] Pradeep Kumar srivastava, Programmable logic controllers.
- [5] K.V Ram, a Course of CNC Maintenance.

Effect of Modified AA5356 Filler on Corrosion Behavior of AA6061 Alloy GTA Welds

¹N. Ramanaiah ²B. Balakrishna, ³K. Prasad Rao

¹ Professor Dept. of Metallurgical and materials Engineering, IITM, Chennai.

² Associate Professor, Dept. of Mechanical Engineering, JNTU (K), Kakinada

³Associate Professor, Dept. of Mechanical Engineering, AUCE, Visakhapatnam,

Abstract: The corrosion behavior of the fusion zone of gas tungsten arc (GTA) welds of AA6061 alloy was studied. Role of gas tungsten arc welding techniques such as continuous current (CC) and pulsed current (PC) and reference filler (AA5356) were studied. Role of different grain refiners such as scandium, zirconium and Tibor in the reference filler was studied. Dynamic polarization testing was used to determine the pitting corrosion resistance of the fusion zone. Optical studies was carried out to find the mechanism of corrosion. The fusion zone of welds made with the 0.5%Sc with AA5356 filler with PC technique shown better corrosion resistance.

I. Introduction

Gas tungsten arc welding (GTAW) process is widely used for joining aluminium alloys for various applications in the aerospace, defence and automotive industries. Fusion welding leads to physical, chemical and metallurgical changes in aluminium alloys¹. One of the reasons for the chemical changes in the fusion zone of welds is due to the different chemical compositions of the filler materials used. The resistance to corrosion of aluminum alloy welds is affected by the alloy being welded, the filler alloy and the technique used. When localised corrosion does occur in aluminium welds, it may take the form of preferential attack of the weld bead, pitting, intergranular attack or exfoliation may occur in a heat affected zone (HAZ) a short distance from the weld bead. Welds in Al-Mg-Si alloys (AA6061) generally have a good resistance to atmospheric corrosion, but in specifically corrosive environments such as seawater localised corrosion may occur. Selection of proper filler wire is important to avoid cracking during welding and to optimize corrosion resistance. When the solution potential of the filler is the same as that of the base metal, optimum corrosion resistance is obtained. In some cases, an intermetallic phase formed by the base metal and filler wire determines the final corrosion resistance of the weld.

In general, the welding procedure that has the lowest influence on the microstructure has the least chance of reducing the corrosion resistance of aluminum weldments. Though literature on the corrosion behavior of aluminium alloys is available, the same cannot be said of their welded counterparts in view of the chemical and microstructural changes caused by welding.

Gas tungsten arc welding (GTAW) is widely applied method to join aluminum alloys and detailed studies on the effect of alternate current pulsing technique on the Corrosion behavior of heat treatable aluminum alloys are not fully available in the literature. The present investigation Corrosion behavior of AA6061 gas tungsten arc welds is studied. It was intended to study the effects of different current modes, viz., such continuous current (CC) and pulsed current (PC) and application of AA5356 filler containing different grain refiners such as scandium, zirconium and Tibor.

II. Experimental details

The investigations were carried out on AA6061 (6 mm thick) alloy in T6 temper. Base metal-T6 was solution treated (at 530°C for 1 h) and artificially aged (at 160°C for 18 h). The composition of the base alloy and AA5356 filler wire is given in Table 1. The alternate current (AC) GTAW process was used. Autogenous, bead-on-plate, full penetration welds were produced. The weld bead was made perpendicular to the sheet rolling direction. Prior to welding, the base material coupons, reference fillers and grain refiners were wire brushed and thoroughly cleaned with acetone. Weighed filler material and grain refiner master alloy strips (Al-Sc, Al-Zr and Al-Tibor) of uniform cross section were press fitted into a rectangular groove machined in the base plate and tack welded. Details of the welding parameters are presented in Tables 2 and 3. The chemical compositions of fusion zone deposited with AA5356 fillers is shown in Table 4. The scandium content of the fusion zones was varied by varying the size of the groove in the base metal and size of the filler strip. The chemical compositions of fusion zone deposited with AA5356 fillers containing grain refiners is shown in Table 4. Two types of current modes were used: CC and PC. Optimum welding parameters based on previous work² were used. Specific details of CC GTAW and PC GTAW are given in Table 2 and 3.

Table 1
Chemical Composition of the base metal and filler

Material	Mg	Si	Fe	Mn	Cu	Al
AA6061 –base metal	0.96	0.73	0.24	0.33	0.23	Balance
AA5356-filler	5.00	0.27	0.40	0.10	0.10	Balance

Table 2
Welding parameters used for CC welding

Welding parameter	Selection
Current	66 A
Speed	3.5 mm/s
Voltage	12–15 V
Electrode	Thoriated W, 2 mm dia
Shielding gas	Argon

Table 3
Welding parameters used for PC welding

Welding parameter	Selection
Peak current (I_p)	88 A
Background current (I_b)	44 A
Speed	3.5 mm/s
Voltage	12–15 V
Pulse frequency	6 Hz
Pulse on-time	50% of cycle time
Electrode	Thoriated W, 2 mm dia
Shielding gas	Argon

Actual composition of fusion zones is given in Table 4. The samples of welds from the fusion zone region were polished on Emery papers and disc cloth to remove the very fine scratches. Polished surfaces were etched with Keller's reagent. The microstructures were recorded with an image analyzer attached to the metallurgical microscope. A software based PAR Basic electrochemical system was used for conducting corrosion testing of the fusion zone. Potentiodynamic polarisation testing was used to determine the pitting corrosion resistance.

Saturated calomel electrode (SCE) and carbon electrode were used as reference and auxiliary electrodes respectively. All the experiments were conducted in 3.5% NaCl solutions with the pH adjusted to 10. The potential scan was carried out at 0.166 mV s⁻¹ with an initial potential of 20.25 V (OC, open circuit) SCE to the final potential of pitting. The exposure area for these experiments was 1cm². The potential at which the current increases drastically is treated as critical pitting potential (Epit). Specimens exhibiting more positive potential were considered as those with better pitting corrosion resistance.

Table 4
Chemical Composition (Wt %) of the fusion zone with AA5356 and grain refiners to fusion zone through AA5356

Material	Mg	Si	Fe	Mn	Cu	Sc	Ti	Zr	Al
AA5356-filler		2.83	0.26	0.20	0.13	0.15	-	-	-
AA5356+0.25%Sc		2.75	0.27	0.20	0.10	0.12	0.24	-	-
AA5356+0.50%Sc		2.70	0.26	0.20	0.19	0.11	0.48	-	-
AA5356+Zr			2.80	0.26	0.21	0.12	-	-	0.14
AA5356+Tibor	2.77		0.25	0.20	0.12	-	0.15	-	Bal

III. Results and discussion

3.1. Microstructures

Micrograph of the base metal is shown in the Fig. 1a. It shows number of Mg₂Si particles present in artificially aged (T6) alloy. The microstructure was columnar (Fig. 1b) without grain refiners and significant grain refinement was noticed when grain refiners were added to the fusion zone (Fig. 1c).

3.2. Effect of grain refiners

Pitting potentials of fusion zone deposited with AA5356 filler with grain refiners are shown in Table 5. For comparative purposes, pitting potentials of base metal and fusion zone obtained without grain refiners also shown in Table 5.

It can be seen from the results that filler metal composition and welding technique have strong influence on the pitting potentials of fusion zone of AA6061 alloy. The pitting potentials of fusion zone of this alloy is found to be in the range of -690 - -580mV depending on the filler composition and process technique.

Fusion zone with AA5356 without grain refiners showed the least pitting potential. As for technique, CC welds showed greater pitting corrosion susceptibility than PC welds. The pitting corrosion susceptibility was found to decrease with additions of grain refiners to fusion zone through AA5356 filler metal. Among the grain refiners studied filler metal with 0.5%Sc was observed to provide the highest pitting corrosion resistance followed by Tibor.

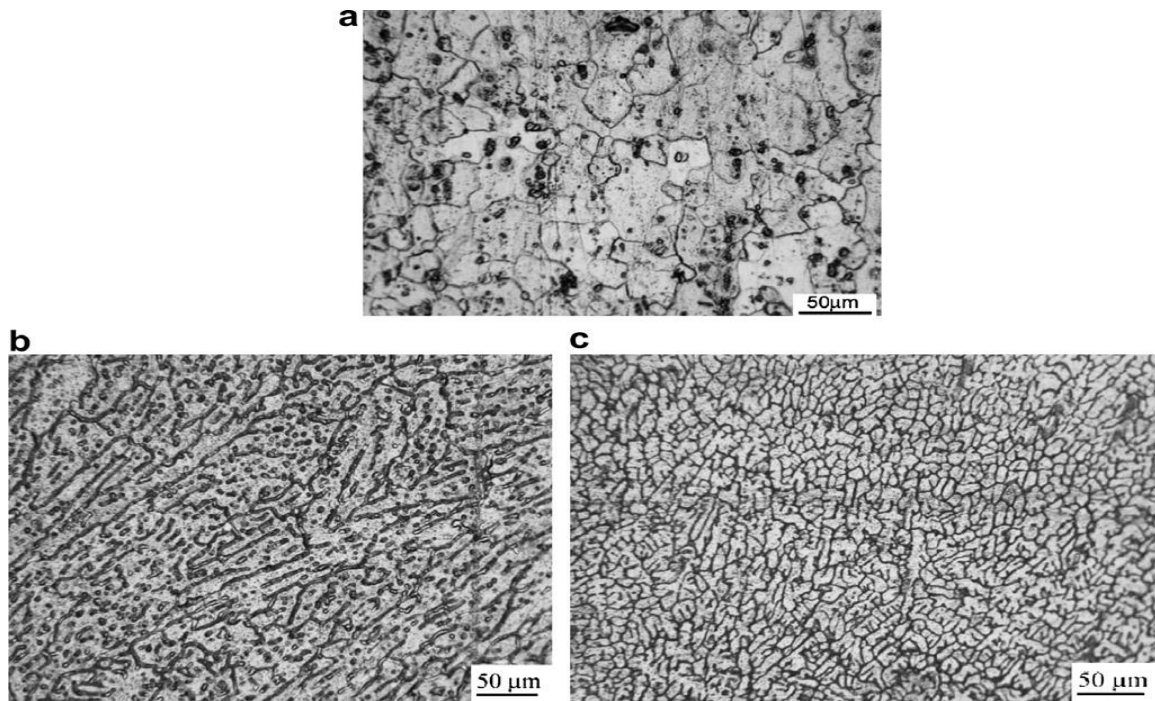


Fig. 1. Micrographs of (a) Base Metal-T6 and (b) Fusion Zone AA5356 CC
(C) Fusion Zone AA5356 + 05%Sc, PC

Table 5

Pitting potentials of fusion zone with AA5356 filler and grain refiners to fusion zone through AA5356

Filler	Epit mV (SCE)	
	CC	PC
AA5356-filler	-690	-651
AA5356+0.25%Sc	-655	-644
AA5356+0.50%Sc	-618	-580
AA5356+Zr	-655	-645
AA5356+Tibor	-644	-633

These results can be discussed in the light of their micro structural aspects. Welds made with AA5356 filler (without grain refiners, with CC) showed larger size of pits and pit density (Fig. 2a and b) Than PC indicating poor pitting corrosion resistance. Significant reduction in the size of pits and number of pits was observed with 0.5%Sc addition to AA5356filler. It showed reduction in pitting density and number of pits among the filler metals studied (Fig. 3c). Pit size was also reduced with Tibor, Zr addition (Fig. 3 d-e). Pit density was less with Tibor when compared to Zr addition. Out of all the grain refiners studied 0.5% Sc, PC resulted lowest pit density. These results indicate that fusion zone composition has got a significant effect on pitting corrosion resistance of AA6061. Ganiev ET al³, compared corrosion potential of pure aluminum to that of Sc addition to pure aluminum. Vyazovikina⁴ proposed that corrosion potential improvement in in Al-Zn alloys are due to the presence of Al₃Sc particles and Sinyavskii et al⁵ reported that the presence of Al₃Sc improved the corrosion potential of Al-Zn~Mg-Cu alloys. It seems that the genera trend is that addition of Sc to Aluminum alloy makes it slightly more noble.

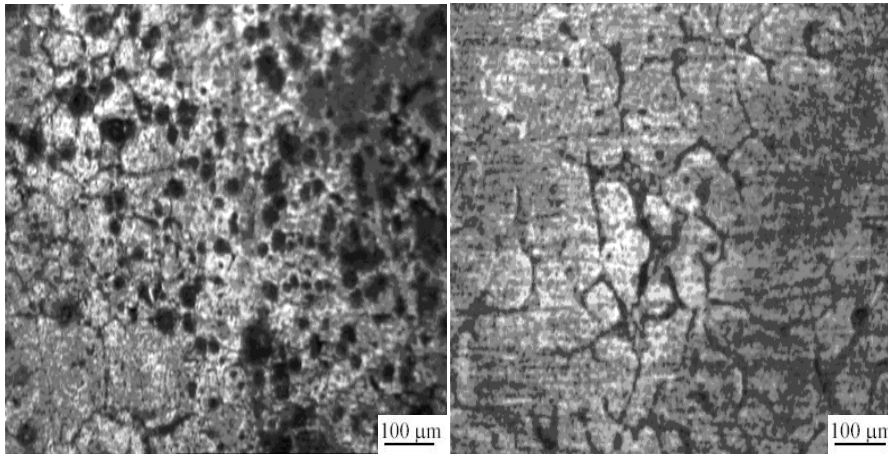


Fig. 2 Optical micrographs of fusion zone after corrosion test
(a) AA5356 CC (b) AA5356PC

3.3 Effect of welding technique

High thermal gradients, characteristic of conventional continuous current (CCW), the segregation of elements and liquid film formation at the grain boundaries of gas tungsten arc welding (CCTIG) limits the use of base metal properties such as strength and corrosion resistance.⁶

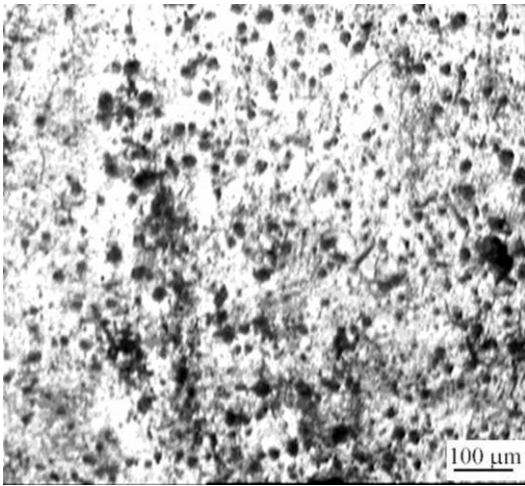
In case of PC GTA welding, cycling of the welding current from a high level to a low level at a selected regular frequency. The high level or the peak current is generally selected to give adequate penetration and bead contour, while the low level or the background current is set at a level sufficient to maintain a stable arc. This permits arc energy to be used efficiently to fuse a spot of controlled dimensions in a short time producing the weld as a series of overlapping nuggets and limits the wastage of heat by conduction into the adjacent parent material in normal constant current welding. Metallurgical advantages of PC welding frequently reported in the literature include refinement of fusion zone grain size and substructure, reduced width of HAZ, control of segregation, etc. All these factors help in improving weld mechanical properties. The enhanced fluid motion in the weld pool homogenizes the weld metal composition and helps in reducing the segregation and porosity. Therefore the improved pitting and general corrosion resistance of the fusion zone of the PC GTA AA6061 welds compared to that of CC GTA welds, was attributed to the reduced segregation and refining of the eutectics of the fusion zone.

IV. Conclusions

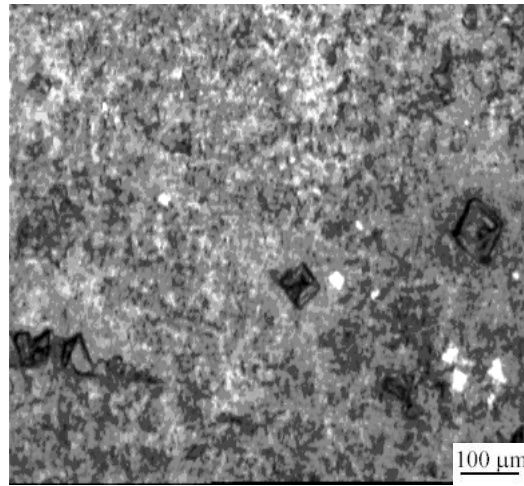
1. Pitting corrosion resistance of AA6061 alloy was relatively less when pulsed current GTA welding was adopted compared to continuous current.
2. Pitting corrosion resistance of AA6061 alloy was relatively less when filler materials contained grain refiners such as scandium, Zr or TiB₂. The highest Pitting corrosion resistance was found with 0.5%Sc containing AA5356 filler material.
3. Highest Pitting corrosion resistance in AA6061 alloy welds was noticed when AA5356 filler containing 0.5%Sc was used with pulsed arc GTA welding.

References

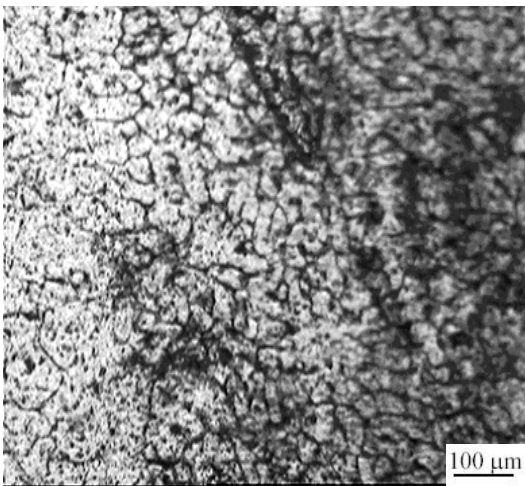
1. Davis, J. R.: 'Corrosion of aluminium alloys', 2nd ed., 2000, Metals Park, OH, ASM International.
2. Prasad Rao, K., Ramanaiah, N., Viswanathan, N., 2008, Mat. Des. 29, 179-186.
3. Ganiev, I. N., 1995, *Prot. Met.*, 31, 543-546.
4. Vyazovikina, N. V., 1999, *Prot. Met.*, 35, 448-453.
5. Sinayaskii, V. S., V.D. Valkov and E. Titkova, 1998, *Prot. Met.*, 34, 549-555.
6. S. Kou: 'Welding metallurgy', 2nd edn.; 2003, NY, Wiley.



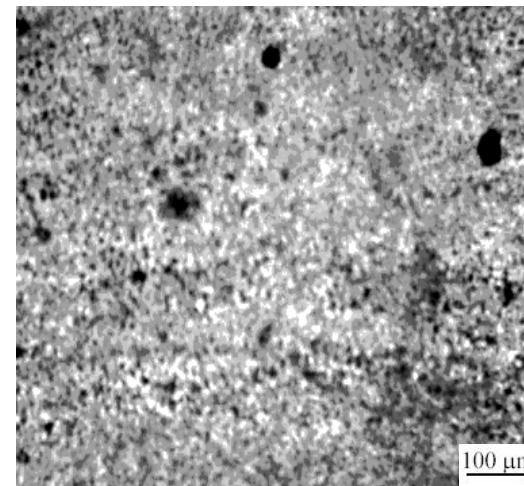
(a)



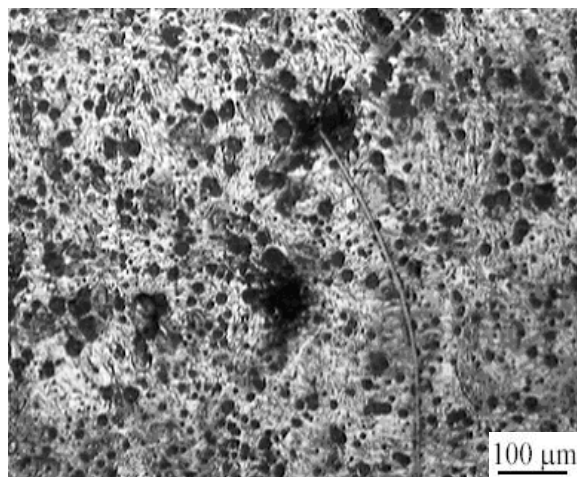
(b)



(c)



(d)



Optimal Motion Planning For a Robot Arm by Using Artificial Bee Colony (ABC) Algorithm

P.V. Savsani,¹ R. L. Jhala,²

¹(Research Scholar PAHER University, Udaipur, Rajasthan, India)

²(Professor, Marwadi Education Foundation, Dept. of Mech. Engg., Gujarat, India)

Abstract: This work is concentrated to optimize the trajectory for planer two-link robot. The whole travel of the trajectory is divided into two parts, which consists of fourth order polynomial trajectory for the one part and fifth order trajectory for the second part. There are many optimization algorithms, which can be implemented to solve such problems. Evolutionary algorithms are also tried by many researchers to solve such trajectory optimization problems. Evolutionary algorithms are capable of giving global optimum solution and traditional optimization techniques converge to local optima and so they are not suitable for the trajectory problems. In this work artificial bee colony (ABC) algorithm is implemented to solve trajectory optimization problem. The objective function for the proposed ABC is to minimize traveling time and space, while not exceeding a maximum pre-defined torque. The objective function consist of four parameter, excessive driving torque, total joint traveling distance, total joint Cartesian length and total consumed time for robot motion.

Keywords: Artificial bee colony algorithm, 2R robotic arm, Trajectory.

I. INTRODUCTION

Many researches on optimal trajectory planning have been reported in free workspace as well as in obstacle existence work space. The evolutionary algorithm is extensively used as practical optimization computation methods, because of the advantage that this algorithm can avoid local optimum value. This work focused on the trajectory optimization of 2R robotic arm in free work space as well as circular obstacle existence robot work space using ABC. Forth order and fifth order polynomials are used to describe the segments that connect initial, intermediate and final point at joint space.

In last year's, evolutionary algorithms have been applied in large number of fields. An optimal galloping trajectory proposed by Giju Chae and Jong Hyeon Park[2] which cost low energy and guarantees the stability of the quadruped robot. They optimized trajectory based on energy and stability using GA, which provides a robust and global solution to a multi-body, highly nonlinear dynamic system. For generating smooth trajectory planning for specified path, Zoller and Zentan [3] focused on the problem of the trajectory planning and dealt with constant kinetic energy motion planning. This method produced trajectory characteristics smoother and better than which did obtained from time optimal method. Zhe Tang et al. [6] proposed a third-order spline interpolation based trajectory-planning method to plan a smooth biped swing leg trajectory by reducing the instant velocity change.

Chwa et al. [7] proposed Missile Guidance Algorithm to generate on-line trajectory planning of robot

arms of the interception of a fast maneuvering object. The authors employed the guidance law throughout the tracking phase, and dynamic constraints such as torque and velocity constraints and satisfied the matching condition of the position and velocity at the time of the interception altogether.

Garg and M. Kumar [8] use GA techniques for robot arm to identify the optimal trajectory based on minimum joint torque requirements. The authors use polynomial of 4th degree in time for trajectory representation to joint space variables. Pires and Machado [10] propose a path planning method based on a GA while adopting the direct kinematics and the inverse dynamics. The optimal trajectory is the one that minimize the path length, the ripple in the time evolution and the energy requirements, without any collision with the obstacle in the workspace. S. G. Yue et al. [4] focused on the problem of point-to-point trajectory planning of flexible redundant robot manipulator (FRM) in joint space. The proposed trajectory to minimize vibration of FRMs is based on GA.

Pires et al [5] use genetic algorithm to optimize a planar robot manipulator trajectory. The main purpose of this paper is to present the optimum robot trajectory in free workspace and obstacle existence workspace by using ABC. In the first part of the work mathematical model is formed. In the second part optimization of the developed robot trajectory is done by using ABC.

II. ARTIFICIAL BEE COLONY (ABC) TECHNIQUE

Artificial Bee Colony (ABC) Algorithm is an optimization algorithm based on the intelligent foraging behaviour of honey bee swarm. The colony of artificial bees consists of three groups of bees: employed bees, onlookers and scouts [9,11,12]. An employed bee searches the destination where food is available. They collect the food and returns back to its origin where they perform waggle dance depending on the amount of food available at the destination. The onlooker bee watches the dance and follows employed bee depending on the probability of the available food means more onlooker bee will follow the employed bee associated with the destination having more amount of food. The employed bee whose food source becomes abandoned convert into a scout bee and it searches for the new food source. For solving optimization problems the population is divided into two parts consisting of employed bees and onlooker bees. An employed bee searches the solution in the search space and the value of objective function associated with the solution is the amount of food associated with that solution. Employed bee updates its position using Equation (1) and it updates new position if it is better than the previous position, i.e it follows greedy selection.

$$v_{ij} = x_{ij} + R_{ij}(x_{ij} - x_{kj}) \quad (1)$$

Where v_{ij} is the new position of employee bee, x_{ij} is the current position of employee bee, k is a random number between $(1, N(\text{population size})/2) \neq i$ and $j = 1, 2, \dots, \text{Number of design variables}$. R_{ij} is a random number between $(-1, 1)$. An onlooker bee chooses a food source depending on the probability value associated with that food source, p_i , calculated using Equation (2).

$$p_i = \frac{F_i}{\sum_{n=1}^{N/2} F_n} \quad (2)$$

Where F_i is the fitness value of the solution i and $N/2$ is the number of food sources which is equal to the number of employed bees.

The Employed bee whose position of the food source cannot be improved for some predetermined number of cycles than that food source is called abandoned food source. That employed bee becomes scout and searches for the new solution randomly using Equation (3).

$$x_i^j = x_{\min}^j + \text{rand}(0,1)(x_{\max}^j - x_{\min}^j) \quad (3)$$

The value of predetermined number of cycles is an important control parameter of the ABC algorithm, which is called "limit" for abandonment. The value of limit is generally taken as Number of employed bees. Step by step procedure for the implementation of ABC is given as follows.

Step 1

Initialize ABC parameters which are necessary for the algorithm to proceed. These parameters include population size which indicates the number of employed bees and onlooker bees, number of generations necessary for the termination criteria, value of limit, number of design variables and respective range for the design variables.

Step 2

Generate random population equal to the population size specified. Each population member contains the value of all the design variables. This value of design variable is randomly generated in between the design variable range specified. First half of the population will consist of employed bees. Each population member associated with employed bees indicates each food source.

Step 3

Obtain the value of objective function for employed bees. The value of objective function so obtained indicates the amount of nectar (food) associated with that destination (food source).

Step 4

Update the position of employed bees using Equation (1). If the value of objective function of the new solution is better than the existing solution, replace the existing solution with the new one.

Step 5

Calculate probability associated with the different solutions using Equation (2). Onlooker bee follows a solution depending on the probability of that solution. So more the probability of the solution more will be the onlooker bee following that solution.

Step 6

Update the position of onlooker bees using Equation (1). If the value of objective function of the new solution is better than the existing solution, replace the existing solution with the new one.

Step 7

Identify abandoned solution and replace it with the newly generated solution using Equation (3).

Step 8

Continue all the steps from step 3 until the specified number of generations are reached.

III. MATHEMATICAL MODELLING

For the present work two degree of freedom planar robotic arm is considered as shown in figure 1, where the endeffector is required to move from starting point to goal point in free work space as well as without colliding with the obstacle in work space. For the motion planning, point-to-point trajectory is taken which is connected by several segments with continuous acceleration at the intermediate via point. ABC is used as optimization tool.

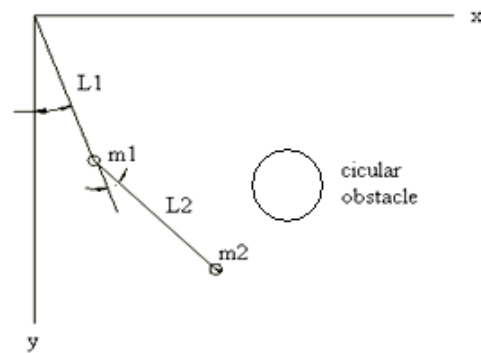


Figure 1 Two degree of freedom planar robotic arm

For the motion planning, point-to-point trajectory is taken which is connected by several segments with continuous acceleration at the intermediate via point as shown in figure 2. For a robot, the number of degrees of freedom of a manipulator is n and the number of end-effectors degree of freedom is m . If one wishes to be able to specify the position, velocity, and acceleration at the beginning and the end of a path segment, a fourth order and a fifth order polynomial are used. Let us assume that there is mp intermediate via points between the initial and final points[1].

$$\theta_{i,i+1}(t) = a_{i0} + a_{i1}t_i + a_{i2}t_i^2 + a_{i3}t_i^3 + a_{i4}t_i^4, \quad (4)$$

$$(i = 0, \dots, mp - 1)$$

Where (a_{i0}, \dots, a_{i4}) are constants, and the constraint are given as:

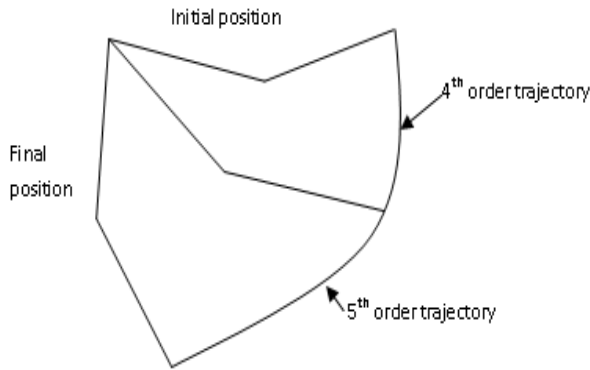


Figure 2 Intermediate point on planed trajectory

$$\theta_i = a_{i0} \quad (5)$$

$$\theta_{i+1} = a_{i0} + a_{i1}T_i + a_{i2}T_i^2 + a_{i3}T_i^3 + a_{i4}T_i^4 \quad (6)$$

$$\dot{\theta} = a_{i1} \quad (7)$$

$$\dot{\theta}_{i+1} = a_{i1} + 2a_{i2}T_i + 3a_{i3}T_i^2 + 4a_{i4}T_i^3 \quad (8)$$

$$\ddot{\theta} = 2a_{i2} \quad (9)$$

Where T_i is the execution time from point i to point $i+1$. The five unknowns can be solved as [1]. The intermediate point $(i+1)$'s acceleration can be obtained as:

$$\ddot{\theta}_{i+1} = 2a_{i2} + 6a_{i3}T_i + 12a_{i4}T_i^2 \quad (10)$$

The segment between the number mp of intermediate points and the final point can be described by fifth order polynomial as:

$$\theta_{i+1}(t) = b_{i0} + b_{i1}t_i + b_{i2}t_i^2 + b_{i3}t_i^3 + b_{i4}t_i^4 + b_{i5}t_i^5, \quad (i = mp) \quad (11)$$

Where the constraints are given as:

$$\theta_i = b_{i0} \quad (12)$$

$$\theta_{i+1} = b_{i0} + b_{i1}T_i + b_{i2}T_i^2 + b_{i3}T_i^3 + b_{i4}T_i^4 + b_{i5}T_i^5 \quad (13)$$

$$\dot{\theta}_i = b_{i1} \quad (14)$$

$$\dot{\theta}_{i+1} = b_{i1} + 2b_{i2}T_i + 3b_{i3}T_i^2 + 4b_{i4}T_i^3 + 5b_{i5}T_i^4 \quad (15)$$

$$\ddot{\theta}_i = 2b_{i2} \quad (16)$$

$$\ddot{\theta}_{i+1} = 2b_{i2} + 6b_{i3}T_i + 12b_{i4}T_i^2 + 20b_{i5}T_i^3 \quad (17)$$

In addition, these constraints specify a linear set of six equations with six unknowns whose solution is explained in [1]. As formulated above, the total parameters to be determined are the joint angles of each intermediate via point ($n \times m_p$ parameters), the joint angular velocities of each intermediate point ($n \times m_p$ parameters), the execution time for each segment ($m_p + 1$ parameters), and the posture

of the final configuration ($n-m$). Therefore, for 2-link robot case, it used $m_p = 1$, $n = 2$ and one degree of freedom of redundancy for the final point, there are six parameters to be determined.

IV. FITNESS FUNCTION

Present robot trajectory use the four parameters to meet the criteria of the robotic manipulator in free work space. All parameters are translated into penalty functions to be minimized. Each parameter is computed individually and is integrated in the fitness function evaluation. The fitness function f_f adopted for evaluating the aspirant trajectories is defined as:

$$f_f = \beta_1 f_{ot} + \beta_2 f_q + \beta_3 f_c + \beta_4 t_T \quad (18)$$

The optimization goal consists in finding a set of design parameters that minimize f_f according to the priorities given by the weighting factors β_i ($i = 1, \dots, 4$), where each different set of weighting factors must results in a different solution. For this work the weight factors are,

$$[\beta_1, \beta_2, \beta_3, \beta_4] = [1, 2, 2, 1].$$

The f_{ot} index represents the amount of excessive driving, in relation to the maximum torque τ_i max, that is demanded for the i^{th} joint motor for the trajectory. The index f_q represents the total joint traveling distance of the manipulator, The index f_c represents total Cartesian trajectory length and The index t_T represents the total consumed time for robot motion. All four index are calculated as given in [1]. For obstacle existence workspace, obstacle avoidance objective function f_{ob} has been combined with free space fitness function to form over all fitness function f , as shown below:

$$f = f_f / f_{ob} \quad (20)$$

By f_{ob} , the robot manipulator has the ability to avoid the obstacle collision during its movement from point to point in side the workspace and it is calculated as [1]. For the present work six parameter are optimized :

$$[q_1, q_2, q_3, \dot{q}_1, \dot{q}_2, \dot{q}_3, t_1, t_2]$$

Where q_i and \dot{q}_i are intermediate joint angle and velocity for i^{th} joint respectively, t_1 is execution time from initial to intermediate via point, and t_2 is execution time from intermediate to final point. Limits of all the variables are as follows:

$$-\pi \leq q_i \leq +\pi \quad (21)$$

$$-\pi/4 \leq \dot{q}_i \leq +\pi/4 \quad (22)$$

$$0.1 \leq t_i \leq 8 \quad (23)$$

$$-\pi \leq q_s \leq +\pi \quad (24)$$

Implementation of ABC

For the case study, robotic arm movement is considered as motion of human hand, which start at ($x=0$ m, $y= -0.76$ m,) and get final position ($x= 0.76$ m, $y= 0$). Various parameters for the illustration are taken as: Length of link 1 =0.3048 m ,Length of link 2=0.3048 m , Mass of link 1 and 2= 175 gms. For ABC maximum generation =2000 and population= 10. The main target here is to minimizing traveling time and space, while not exceeding the predefined torque(joint-1=45 N.m, joint-2=20N.m) ,in free workspace and without collision with any obstacle. Finally results of ABC are discussed.

V. RESULTS AND DISCUSSION

Trajectory of 2R robot is optimized using ABC. Table-1 shows total traveling time, total joint traveling distance and total cartesian trajectory length for both free work space and obstacle avoidance work space.

Table 1 Comparison of optimum results obtained in free workspace and obstacle existence workspace

Result value	Free workspace	Obstacle existence workspace
Total traveling time(sec)	2.0106	2.1078
Total joint traveling distance(rad)	1.5776	6.6167
Total Cartesian trajectory length(m)	3.1403	3.2623
Fitness value	11.2367	16.4495

As noted from the table 1 the values of all the parameters are more in obstacle existence workspace. The amount of increment allows the robot to manipulate in the work space without colliding with obstacle. For the optimum result function evaluation is taken as 20000 for both free and obstacle existence workspace.

Figure 3 shows the variation of joint angle with respect to time in free robot workspace. Dotted line represents the variation of joint angle in free workspace while full line shows the angle variation in obstacle existence workspace. Joint 1 angle varies from 0 to ~ -1.6 rad in 2 sec when the arm moves in free workspace, while it takes more than 2 sec in obstacle existence workspace to cover the same range of angle. Joint 2 angle is almost zero when the robot arm moves in free workspace and variation of 0 to ~1.5 rad in is obtained when it moves in obstacle existence workspace.

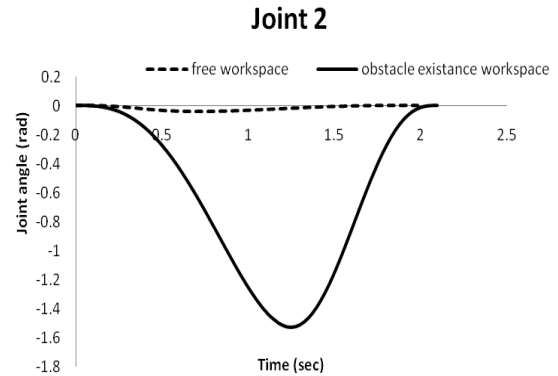
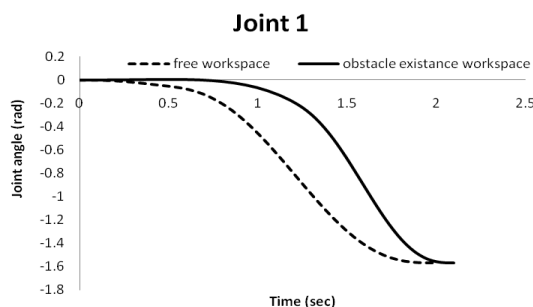


Figure 3 joint angle variation with respect to time

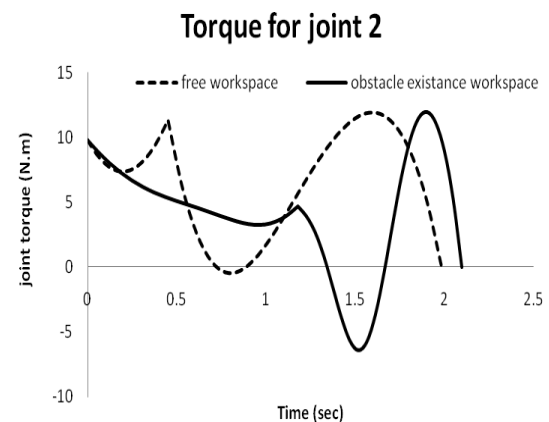
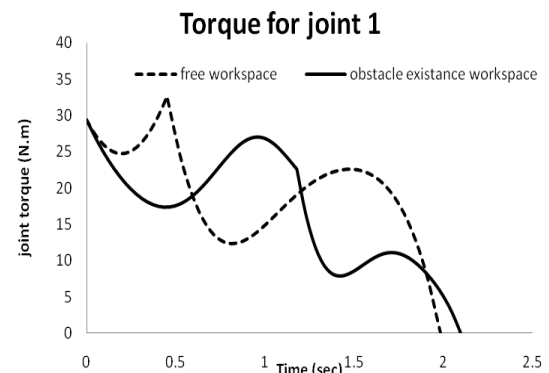


Figure 4 torque variation with respect to time

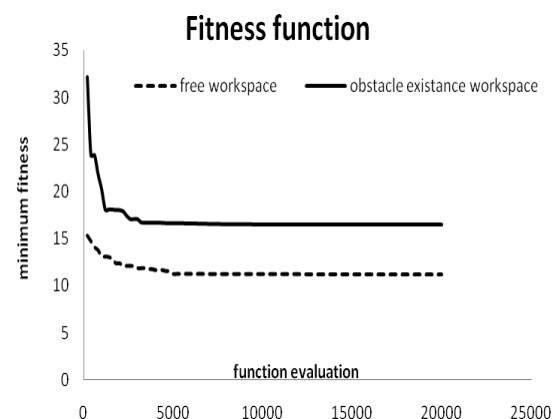


Figure 5 fitness function with function evaluation

Figure 4 depicts that for both the workspace (free and obstacle existence) torque for joint 1 and joint 2 are within the predefined limit. Torque of joint 1 varies from 0 to ~33 Nm and joint 2 varies from 0 to ~ 12 Nm when robot arm manipulate in free workspace over 2 sec. Manipulation of robot arm in obstacle existence workspace gives the torque variation for joint 1 (0 to ~30 Nm) and joint 2 (~ -6 Nm to ~13Nm) over 2.1 sec.

Fitness value variation with free and obstacle existence workspace is shown in figure 5. Fitness value in obstacle existence workspace is more than the fitness value in free workspace.

VI. CONCLUSIONS

Trajectory planning method based on ABC with specific objective functions is presented. Case study of human motion is taken for the 2R planner robotic arm and trajectory is optimized in free and obstacle existence workspace. Comparison shows that fitness value for the free workspace is lesser than value in obstacle existence workspace. The joint torque of the robot did not exceed its maximum pre-defined torque. Since ABC uses the direct kinematics, the singularities do not constitute a problem.

REFERENCES

- [1] Kazem, I. B., Mahdi, A. I., Oudha, A. T. (2008). Motion Planning for a Robot Arm by Using Genetic Algorithm. *Jordan Journal of Mech. and Ind. Engg.* 2, pp. 131-136.
- [2] Chae, G., Park, J., H. (2007). Galloping Trajectory Optimization and Control for Quadruped Robot Using Genetic Algorithm. In: *IEEE International Conference on Robotics and Biomimetics*, pp. 1166-1171.
- [3] Zoller, Z., Zentan, P. (1999). Constant Kinetic Energy Robot Trajectory Planning. *peridica polytechnicaser. Mech. Eng.*, 43(2), pp. 213 – 228.
- [4] Yue, S., G., Henrich, D., Xu, X., L., Toss, S.K. (2002). Point-to-Point Trajectory Planning of Flexible Redundant Robot Manipulators Using Genetic Algorithms. *J. Robotica*, 20, pp. 269—280.
- [5] Solteiro, P., Tenreiro, M., Moura O., 2003, "Fractional Order Dynamic in a Genetic Algorithm". In: *11th International Conference On Advanced Robotics*, pp. 264-269. Colombia, Portugal.
- [6] Tang, Z., Zhou, C., Sun Z. (2003). Trajectory Planning For Smooth Transition of A Biped Robot. In: *IEEE International Conference on Robotic & Automation*, pp. 2455—2460.
- [7] Chwa, D., Kang, J., Im, K., Choi, J. (2003). Robot Arm Trajectory Planning Using Missile Guidance Algorithm. In: *SICE Annual Conference*, pp. 2056-2061.
- [8] Grag, P., Kumar, M. (2002). Optimization Techniques Applied To Multiple Manipulators for Path Planning and Torque Minimization. *Engineering Applications of Artificial Intelligence*, 15(3), pp. 241-252.
- [9] Savsani, V., Rao, R., Vakharia, D. P. (2010). Multi objective optimization of mechanical elements using artificial bee colony optimization technique. *ASME Early Career Technical Journal*
- [10] Solteiro, P., Machado, J. (2000). A GA Perspective Of The Energy Requirement For Manipulators Maneuvering In A Workspace With Obstacles. *Cec 2000-Congress On Evolutionary Computation*, pp. 1110- -1116, Santiago, California, USA.
- [11] Craig, J. (1989). *Introduction to Robotics: Mechanics and Control*. Wesley
- [12] Karaboga, D. (2005). An Idea Based On Honey Bee Swarm For Numerical Optimization. Technical Report-TR06, Erciyes University, Engineering Faculty, Computer Engineering Department.
- [13] Basturk, B. Karaboga, D. (2006). An Artificial Bee Colony (ABC) Algorithm for Numeric function Optimization. *IEEE Swarm Intelligence Symposium*, May 12-14, Indianapolis, Indiana, USA.

Numerical Investigation for Exhaust Gas Emissions for a Dual Fuel Engine Configuration Using Diesel and Hydrogen

PREMAKUMARA. G¹, AKHIL THOMAS², JAYAKRISHNAN. K³, ANIRUDH VUYYALA⁴,
L.M. DAS⁵

¹(CENTRE FOR ENERGY STUDIES, INDIAN INSTITUTE OF TECHNOLOGY, DELHI, INDIA)

²(DEPARTMENT OF MECHANICAL ENGINEERING, INDIAN INSTITUTE OF TECHNOLOGY, BHUBANESWAR, INDIA)

ABSTRACT: A SIMULATION FOR NUMERICAL ANALYSIS OF INTERNAL COMBUSTION ENGINES, BOTH SPARK-IGNITED AND COMPRESSION-IGNITED SYSTEMS, RUNNING ON DUAL FUEL OF HYDROGEN AND ANY HYDROCARBON FUEL DEVELOPED IS PRESENTED IN THIS REPORT. THE PROGRAM CODED USING MATLAB IS USED TO SIMULATE VARIOUS ENGINE CONDITIONS AND DISCERN ITS EFFECT ON THE EMISSIONS. THE ENGINE EMISSIONS, INCLUDING SPECIES LIKE NO_x, CO, AND CO₂, IN ACCORDANCE WITH THE EXTENT OF HYDROGEN FRACTION, THE EQUIVALENCE FUEL-AIR RATIO, COMBUSTION EQUILIBRIUM TEMPERATURE AND PRESSURE ARE SIMULATED. THE PAPER FOCUSES ON SIMULATION OF EXHAUST EMISSIONS WHILE USING H-DIESEL BLEND. SIMULATION ATTEMPTS TO FIND AN OPTIMUM EXTENT OF DUAL-FUELLING, EQUIVALENCE RATIO, COMBUSTION TEMPERATURE FOR HYDROGEN-DIESEL BLEND WITH REGARD TO QUALITY OF EMISSIONS.

Key Words: Dual Fuel, Diesel Hydrogen, Numerical Investigation, Matlab

I. Introduction

Our history tells us one thing that men always tends to go wrong, as if he always beholds to the Murphy's Law which says, 'if anything can go wrong, then it will'. Such an error made by man was his incorrect assessment on availability of petroleum fuels. Till the early 1970s, petroleum was considered as the eternal fuel source when it was realized that the petroleum-based fuels were diminishing fast and at the same time, the rate of consumption of these fuels was increasing at a much faster rate and this presents the trillion dollar quest today, for the best alternative fuel [1]. Looking at this problem, we have a broader aim than just an

alternative to the present fuels, but a better one in terms of its emissions. Considering the effect of global warming which has already made big impact giving us serious warning of its effects has led to the need for an alternative fuels which produce minimum emissions. But there also lies another big problem in terms of economic viability. So, taking all these factors, we look for an environment friendly, economically viable alternative fuel for the existing internal combustion engines.

Over the years, liquefied petroleum gas (LPG), alcohols (both ethanol and methanol), compressed natural gas (CNG), Bio-fuels, hydrogen and a horde of other alternatives were investigated as alternative fuels for both the spark ignition (SI) and compression ignition (CI) engines [1]. Among this, considering Hydrogen's work experience as fuel of the stars and its exceptional properties like high flame speed, high diffusivity, wide flammability limits, and high calorific value etc., researchers do have a glimpse of hope

for it as the answer to the present quest. Hydrogen supplementation was done with fuels like diesel, petrol in order to exploit its properties. Results from Hydrogen supplementation to diesel show improvements in BTFC, Brake power, and emissions [2].

It is a necessity that we have to judge all the factors and its effects on the performance of the engine, when being run by alternative fuels. Conducting experiments is a way of achieving the above said, but it always has its own limitations since many of the possible conditions may not be realized practically. So, a better way of doing this is by theoretical analysis.

There was a time when analytical methods were time consuming and extremely challenging. But today, the scenario is different. With advances in technology, there are enormous and effective ways of theoretically analyzing situations. This paper includes numerical analysis of the exhaust gas emissions from an engine run on dual fuel involving Hydrogen-Diesel blends. The paper involves an indigenously developed simulation program with graphical user interface which is capable of calculating the mole fraction of different components in exhaust emission.

II. The Program

The developed program is capable of simulating the effects of various factors, such as extent of dual-fuelling, the equivalence fuel-air ratio, combustion equilibrium temperature and pressure, on the emission properties as well as calculating the emission properties for a specific set of input values. The species which could be analyzed in the exhaust are CO, NO, CO₂, H₂O, O₂, H₂, O, H, OH and N₂.

For simulating the effects of input parameters on exhaust emissions, we considered three main input parameters, Temperature, equivalence ratio, and extent of dual fuelling, on the exhaust species CO, NO, and CO₂. Out of the different methods possible of simulating the effect, we found three-dimensional surface plots as the apt one in our analysis. In two-dimensional plots, when simulating the effect of two factors on output, there is a limitation that there can be only one variable factor and the effect of other has to be analyzed for various constant values. Surface plots give a wider scope of simulation, since in addition to what is possible in two-dimensional plots, we can simulate the effect of two factors, both being variables at a time on the exhaust properties. And this approach makes it more comparable with real engine simulations.

TABLE.1: Notations used

p	Number of carbon atoms in primary fuel
q	Number of hydrogen atoms in primary fuel
r	Number of oxygen atoms in primary fuel
s	Number of nitrogen atoms in primary fuel
t	Temperature (K)
x	Fraction of Hydrogen in blend
Pres	Pressure (atm)
equ	Equivalence ratio
sto	Stoichiometric fuel-air ratio
K	Equilibrium constant
ni	Concentration of 'i'th product

2.1 Program Interface

A user friendly interface is given to the program as seen in Fig.1 that enables the user to control the hydrocarbon fuel data (the number of Carbon, Hydrogen, Nitrogen, and Oxygen atoms), fraction of Hydrogen in the fuel blend, combustion conditions including equilibrium combustion temperature and pressure, and the equivalence fuel-air ratio. According to the user's choice, the output will be the mole fractions of the compounds CO₂, H₂O, N₂, O₂, CO, H₂, H, O, OH, and NO corresponding to the input set of values or the simulated change in mole fraction of the species with the change in input parameters.

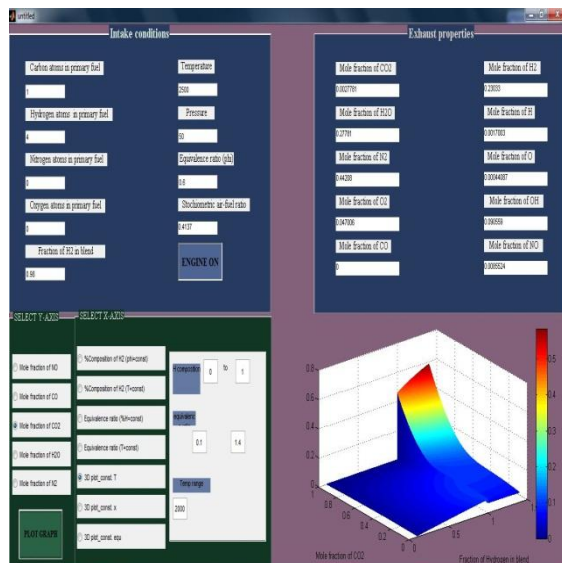


Fig.1 Interface of the program

2.2 Simulations

Mole fractions of NO, CO, H₂O, N₂ and CO₂ can be simulated against varying the factors such as Extent of blending (fraction of hydrogen in blend) for five different values of combustion temperature with equivalence fuel-air ratio kept as a constant in a 2- dimensional plot. Extent of blending for five different values of equivalence fuel-air ratio with combustion temperature kept as a constant.

Equivalence fuel-air ratio for five different values of combustion temperature with extent of blending kept as a constant.

Equivalence fuel-air ratio for five different values of extent of blending with combustion temperature kept as a constant.

Equivalence fuel-air ratio and extent of blending for a constant value of temperature in a three dimensional surface plot.

Equivalence fuel-air ratio and Temperature for a constant value of composition of hydrogen in a three dimensional surface plot.

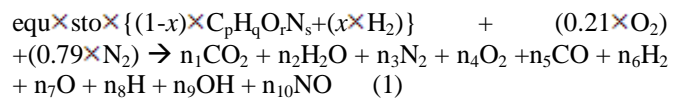
Temperature and composition of hydrogen for a constant value of equivalence fuel-air ratio in a three dimensional surface plot.

2.3 Formation of equations

The program uses a modified version of equilibrium constant method applied by Olikara and Borman to find the solution for the properties of equilibrium gas phase products of combustion of Hydrocarbon fuels. [3] The coding is done for any general dual fuel blend involving hydrogen. The reactant mixture is a blend of a primary fuel of formula CpHqOrNs and H₂ and air.

Lagrange multiplier approach [3] is done with the help of NASA simulation program [5] to restrict the number of species to be considered in the equilibrium constant method. The data showed that if fuel-air ratio is less than 3, the only species of importance because of dissociation are O, H, OH, and NO. In accordance with the results, we considered only 10 products of combustion.

The combustion reaction is hence written as:



Here, stoichiometric fuel-air ratio:

$$\text{sto} = 0.21 \times \left(\frac{1-x}{p+0.25q-0.5r} + 2x \right) \quad (2)$$

Balancing of atoms leads to:

$$\text{C: } \text{equ} \times \text{sto} \times (1-x) \times p = n_1 + n_5 \quad (3)$$

$$\text{H: } \text{equ} \times \text{sto} \times (1-x) \times q + 2x = 2n_2 + 2n_6 + n_8 + n_9 \quad (4)$$

$$\text{O: } \text{equ} \times \text{sto} \times (1-x) \times r + 0.42 = 2n_1 + n_2 + 2n_4 + n_5 + n_7 + n_9 + n_{10} \quad (5)$$

$$\text{N: } \text{equ} \times \text{sto} \times (1-x) \times s + 1.58 = 2n_3 + n_{10} \quad (6)$$

Applying the following approximations, we developed the equations:

$$\text{For } \text{equ} < 1: n_5 = 0 \quad (7)$$

$$\text{For } \text{equ} > 1: n_4 = 0 \quad (8)$$

The equations of products for equivalence fuel-air ratio < 1 are:

$$n_1 = (1-x) \times p \times \text{equ} \times \text{sto} \quad (9)$$

$$n_2 = 1 \times q \times \text{equ} \times \text{sto} / 2 \quad (10)$$

$$n_3 = 1 \times 0.79 + (1-x) \times s \times \text{equ} \times \text{sto} / 2 \quad (11)$$

$$n_4 = (1-x) \times 0.21 \times (1-\text{equ}) \quad (12)$$

$$n_5 = 0 \quad (13)$$

$$n_6 = 0.42x \quad (14)$$

And for equivalence fuel-air ratio > 1;

In this case, considering the equilibrium constant for the water gas reaction [3] and taking values from JANAF tables [7] we get the following equations:

$$K = e^{0.273 - (1.761 \div \frac{t}{1000}) - (1.611 \div (\frac{t}{1000})^2) + (0.283 \div (\frac{t}{1000})^3)} \quad (15)$$

$$a = 1 \times (1-K) \quad (16)$$

$$b = (1-x) \times (0.42 - \text{equ} \times \text{sto} \times (2-r) + k \times (0.42 \times (\text{equ}-1)) + p \times \text{equ} \times \text{sto}) + x \times (0.42 - 2 \times \text{equ} \times \text{sto} + K \times 0.42 \times (\text{equ}-1)) \quad (17)$$

$$c = - (1-x) \times (0.42 \times \text{equ} \times \text{sto} \times p \times (\text{equ}-1) \times k) \quad (18)$$

$$n_5 = \frac{-b \pm \sqrt{b^2 - 4ac}}{2a} \quad (19)$$

$$n_1 = (1-x) \times (p \times \text{equ} \times \text{sto} - n_5) + x \times n_5 \quad (20)$$

$$n_2 = (1-x) \times (0.42 + \text{equ} \times \text{sto} \times (2p-r) + n_5) - x \times (0.42 + n_5) \quad (21)$$

$$n_3 = (1-x) \times (0.79 + s \times \text{equ} \times \text{sto} / 2) + 0.79x \quad (22)$$

$$n_4 = 0 \quad (23)$$

$$n_6 = (1-x) \times (0.42 \times (\text{equ}-1) - n_5) + 0.42x \quad (24)$$

Mole fractions of these products are found out using the equation:

$$y_i = n_i / \sum n_i \quad (25)$$

The six gas-phase reactions are introduced which include the dissociation of hydrogen, oxygen, water, carbon dioxide, and equilibrium OH and NO formation [3]. The equilibrium constants of these reactions [3] had been curve fitted to JANAF table by Olikara and Borman for $600 < t < 4000$ K. Their expressions are of the form:

$$\log_{10} K_i = A_i \times \ln \frac{t}{1000} + \frac{B_i}{t} + C_i + D_i \times t + E_i \times t^2 \quad (26)$$

The values of A, B, C, D, E are obtained from JANAF table. [7]

The mole fraction of rest species are found out using these equilibrium constant values in accordance with the following equations:

$$y_7 = \frac{K_1}{p_{res}^{0.5}} \times y_6^{0.5} \quad (27)$$

$$y_8 = \frac{K_2}{p_{res}^{0.5}} \times y_4^{0.5} \quad (28)$$

$$y_9 = K_3 \times y_6^{0.5} \times y_4^{0.5} \quad (29)$$

$$y_{10} = K_4 \times y_4^{0.5} \times y_3^{0.5} \quad (30)$$

III. Results

Simulations are done for Diesel – H₂ fuel blend emissions under various conditions as discussed before. The results are presented below:

3.1 CO Emissions

It can be observed from Fig.2 that CO emissions increase with increase in temperature. This result is due to the increase in dissociation of CO₂ at higher temperatures which boosts the formation of CO. It can be noted that the emissions of CO are the highest for T=2500K and equ=1.5 in the plot.

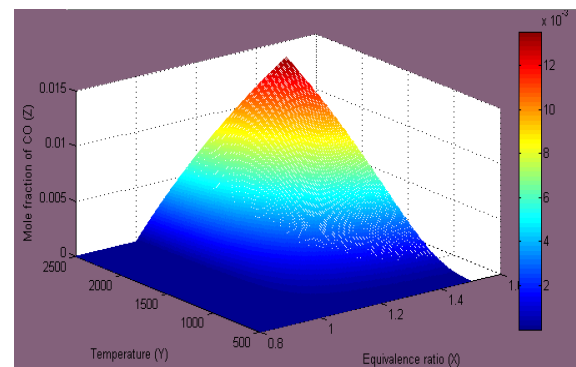


Fig.2: effect of temperature and equivalence ratio on co emissions at x=0.3

Fig.2 also shows that for lean mixtures (equ<1), the CO emissions are negligible which is due to complete combustion of fuel. On the other hand for rich mixtures (equ>1), it can be observed that mole fraction of CO increases with increasing equivalence ratio. This can be attributed to the occurrence of incomplete combustion.

3.2 CO₂ Emissions

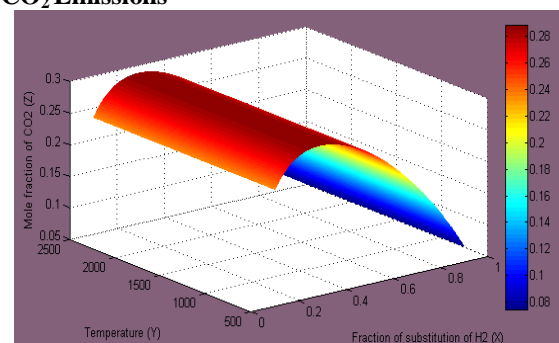


Fig.3: variation of mole fraction of co₂ with change in temperature and hydrogen fraction at equ=0.6

In Fig.3, it can be seen that with the increase in hydrogen fraction, CO₂ emissions first increase and then decrease for equ=0.6. It is observable that maximum CO₂ emissions occur for hydrogen fraction around 0.3. This trend was found to be the same for all other values of equ less than one. For the hydrogen fraction of 0.1, the value of CO₂ mole fraction is 0.24, it is 0.28 for hydrogen fraction 0.3 and for 0.9 the value of mole fraction is 0.1.

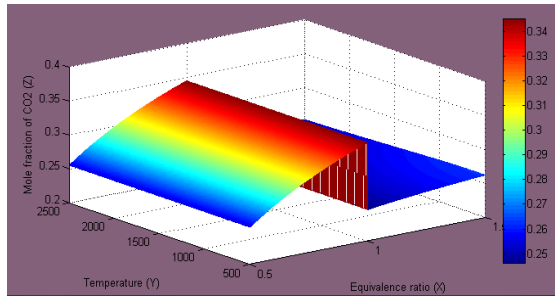


Fig.4: Effect of Temperature and equivalence ratio on CO_2 emissions for $x=0.3$

In Fig.4, it can be observed that for lean mixtures, the mole fraction of CO_2 is almost independent on temperature. However, for rich mixtures it is seen that the mole fraction slightly decreases with increase in temperature. This can be explained as temperature increases, dissociation of CO_2 increases which, on the other hand leads to the increase in mole fraction of CO , a product due to incomplete combustion of rich mixtures.

It is also noticeable that mole fraction of CO_2 shows an increasing trend with increase in equivalence ratio, which is a result of the increase in carbon content (due to increased fuel content). From the plot, a sudden fall in mole fraction at $\text{equ}=1$ is visible, which can be accredited to the incomplete combustion of fuel after $\text{equ}=1$.

3.3 NO_x Emissions

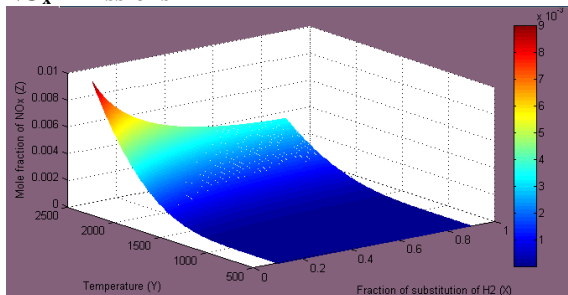


Fig.5: Effect of Temperature and Hydrogen fraction on mole fraction of NO_x for $\text{equ}=0.6$

The Fig.5 shows that for all hydrogen fractions, mole fraction of NO increases with increase in temperature. This is due to the very high dissociation energy of N_2 atoms which demands higher temperatures for its dissociation, which is in turn essential for NO formation. It can also be observed that for a fixed temperature, NO emissions show a slightly decreasing trend with increase in hydrogen fraction.

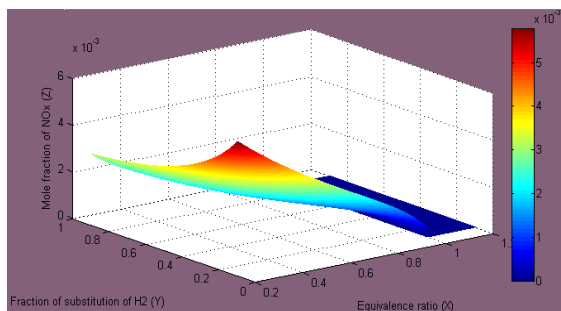


Fig.6: Effect of Equivalence ratio and Hydrogen fraction on mole fraction of NO_x for $T=2000\text{K}$

In Fig.6, the effect of Hydrogen fraction on NO emission is consistent with the earlier result. It can also be observed that as equivalence ratio increases for a given temperature, NO_x emissions decrease and it becomes negligible after $\text{equ}=1$. This can be explained by the decrease in availability of Oxygen after combustion with fuel as equivalence ratio increases.

IV. Conclusions

The effects of equivalence ratio, Temperature and Hydrogen fraction on emission of different species in an H-Diesel blend can be concluded as follows:

The emission of CO is negligible for lean mixtures and increases with equivalence ratio for rich mixtures. Also for rich mixtures, the CO emissions increase with increase in combustion equilibrium temperature.

For lean mixtures, CO_2 emissions increase with increase in equivalence ratio. But with the increase in Hydrogen fraction, the emissions will increase initially, reaches a maximum at around 0.3, and then it will decrease. It is also independent on temperature for lean mixtures, but decrease with increase in temperature for rich mixtures.

The emission of NO is negligible for rich mixtures and decreases with equivalence ratio for lean mixtures. NO emissions also decrease slightly with increase in hydrogen fraction. Also, the emissions increase with increase in temperature.

References

- [1] L.M.Das. 'Hydrogen engine: research and development (R&D) programmes in Indian Institute of Technology (IIT), Delhi'. International Journal of Hydrogen Energy 27 (2002) 953 – 965
- [2] T Narayan Patro. 'Utilisation of hydrogen fuel in small utility CI Engine and its Effect on engine Performance, Emissions and Combustion characteristics', Indian Institute of Technology Delhi, 1990.
- [3] Ferguson CR. Internal combustion engines – applied thermo sciences. John Wiley and Sons; 1986.
- [4] Mathur HB, Khajuria PR. 'Performance and emission Characteristics of a hydrogen-fuelled spark ignition engine.' Int J Hydrogen Energy, 1984:729–36.
- [5] Svehla, R.A and Mcbride, B.J.: "Fortran IV computer program for calculation of thermodynamic and transport properties of complex chemical system", NASA technical notes TND-7056, 1973
- [6] Deshpande NV et.al, Exhaust gas simulation. IE (I) Journal-MC; 2004.
- [7] Yun Xiao. 'Thermodynamic simulation for Engine combustion simulations' UM-MEAM-90-07

Design and Analysis of Canister Testing Chamber

Raj Kiran Ilony¹ & A.Purushotham²

¹M.Tech. (CAD/CAM)

²Professor of Mechanical Engineering SreeNidhi Institute of Science of Technology (An Autonomous Institution under JNTU),
Ghatkser, Hyderabad -501301 A.P.India

ABSTRACT: Canister is used for carrying, storing and launching of missile. During storage and launching, the canister is subjected to internal pressure of 45 kgf/cm² and external pressure of 9 kgf/cm². The canister is generally placed inside the testing chamber. Canister testing chamber is one of the most critical components in Defence Organization. The Primary objective of this paper is to design a canister testing chamber and predicting the failure performance of canister testing chamber using ANSYS a finite element analysis package.

The structure of the canister testing chamber is determined on the basis of empirical of gun design and experimental data of Ballistic Research Laboratories (BRL). First a three- Dimensional model of a canister chamber is made in Uni Graphics and then stress analysis is carried out using ANSYS. Contact analysis on canister testing chamber is also carried out using ANSYS to estimate the gap between contact surfaces of bolt region of canister testing chamber.

Key words: Canister, Testing Chamber, contact analysis, Von Misses stress.

I. INTRODUCTION

The shell of the test setup is made from IS: 2062 plates welded to get 11 meters length and diameter of the shell is 1.5 meters. One end of the test setup will have dished end welded integrally to the cylinder. The other end shall be a hinged door with proper sealing. One of the sides dished end is provided with screw rod to press the dummy dish end for leak proof joint which shall withstand the internal pressure during testing. The screw is actuated by a hand wheel provided through nut. The nut is fixed in a welded housing on the dished end. Between both the mating faces rubber/gasket will be provided to avoid any leak of water during pressure testing.

II. COMPONENTS USED IN CANISTER TESTING CHAMBER

The following are the components which are used in canister.

1. Chamber shells
2. Canister dished ends
3. Support legs
4. Bolts
5. Pressure gauges

III. Modelling of Canister Testing Chamber

The NX software integrates knowledge-based principles, industrial design, geometric modelling, advanced analysis, graphic simulation, and concurrent engineering. The software has powerful hybrid modeling capabilities by integrating constraint-based feature modelling and explicit geometric modelling. In addition to modelling standard geometry parts, it allows the user to design complex free-form shapes such as airfoils and manifolds. It also merges solid and surface modeling techniques into one powerful tool set. The steps involved while developing the 3D model of a canister testing chamber:

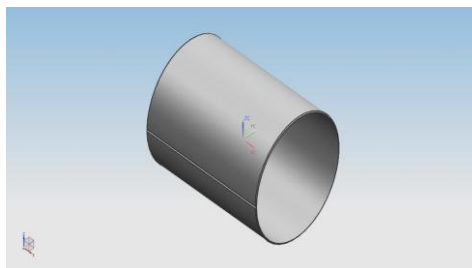


Fig 3.1 3D model of the chamber shell



Fig 3.2 model of the shell head plate 1

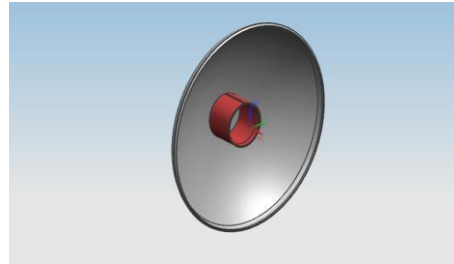


Fig 3.3 model of the shell head plate 2

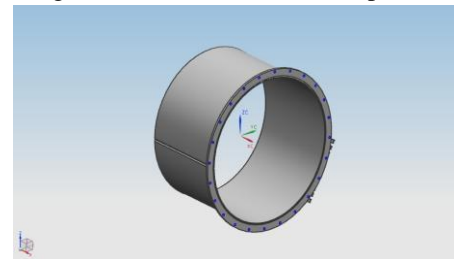


Fig 3.4 model of the spacer

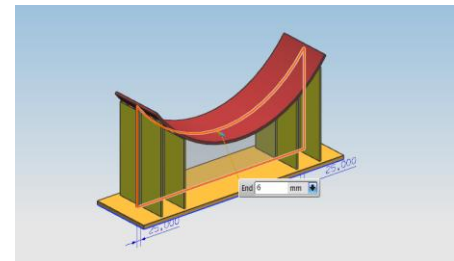


Fig 3.5 model of the bottom supports

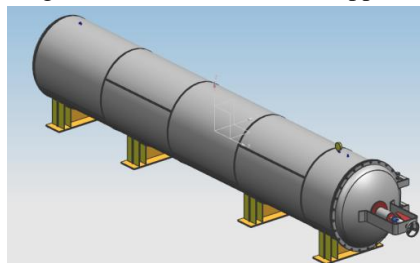


Fig 3.6 model of a canister testing chamber assembly

IV. ANALYSIS OF TESTING CHAMBER

Pressure Analysis

The canister testing chamber is meshed using shell 63 element type. It is a quad 4 node element. Thickness is given as the real constant.

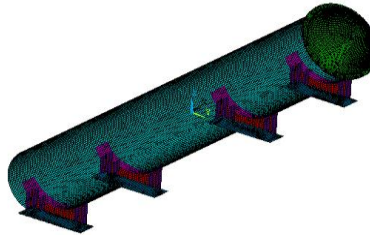


Fig 4.1 Meshing of the canister testing chamber

Boundary Conditions

1. Base plates are constrained in all degrees of freedom
2. Head closure is bolted to chamber using Constraint equations – Simulating bolts
3. Internal pressure of 9 Kgf/cm² is applied
4. Gravity – 9810 mm/sec² is applied to simulate self weight

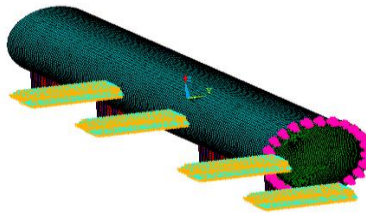


Fig 4.2 Applying gravity for self weight

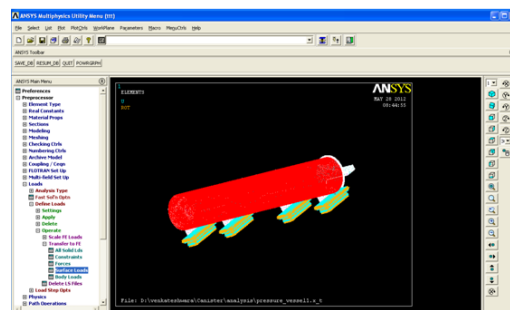
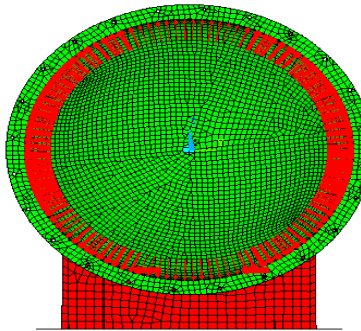


Fig 4.4 Loads condition on canister testing chamber

The canister testing chamber is applied by loading conditions (pressure) upto 9 kgf/cm

V. Contact Gap Analysis

Contact gap analysis is a carried out at the bolting locations of the chamber to check for the leakage of the pressure to the atmosphere. Contact problems are highly nonlinear and require significant computer resources to solve. It is important to understand the physics of the problem and take the time to set up the model to run as efficiently as possible. Contact problems present two significant difficulties. First, we do not know the regions of contact until we've run the problem. Depending on the

loads, material, boundary conditions, and other factors, surfaces can come into and go out of contact with each other in a largely unpredictable and abrupt manner. Second, most contact problems need to account for friction. There are several friction laws and models to choose from, and all are nonlinear. Frictional response can be chaotic, making solution convergence difficult.

Fig 4.3 Application of Internal pressure of 9 Kgf/cm²

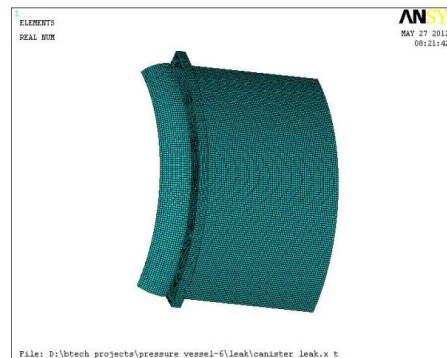


Fig 5.1 Mesh model of the Chamber used for Contact Gap Analysis

Calculation for M12 BOLT:

Bolt preload is computed as follows: $P_i = T / (K D)$

where P_i = bolt preload (called F_i in Shigley).

T = bolt installation torque. = 10858 N-mm

K = torque coefficient = 0.2

D = bolt nominal shank diameter (i.e., bolt nominal size) = 12mm

Torque coefficient K is a function of thread geometry, thread coefficient of friction m_c , and collar coefficient of friction m_c .

$\delta = P L / (E A)$

P = bolt preload = 4524.1 N

L = bolt length = 50mm

E = bolt modulus of elasticity = $2e5$ N/mm²

A = bolt cross-sectional area = $(\pi/4) \cdot d^2$

D = bolt nominal shank diameter = 12mm

δ = measured bolt elongation in units of length = 0.01mm

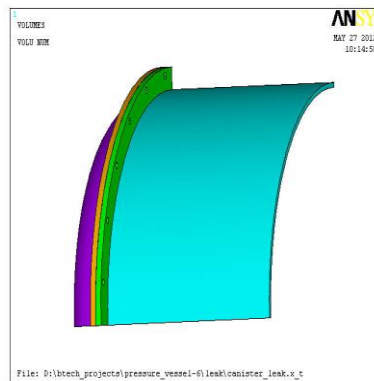


Fig 5.2 Contact created between the mating surfaces

near bolted region

Similarly The Delata Values For M22 And M36 Bolts are.

Intial strain value for M22 bolt is:0.001

Intial strain value for M36 bolt is:0.0003

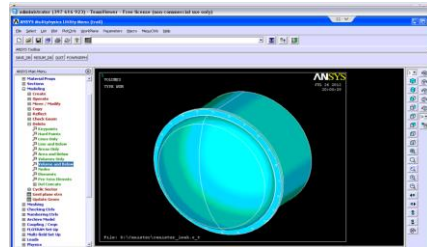


Fig 5.3 Model for the Contact Gap Analysis

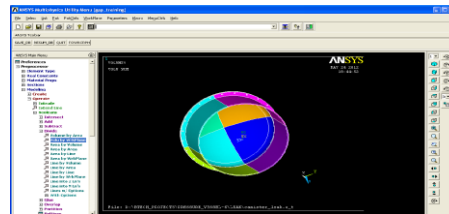


Fig 5.4 Dividing the model into Quarter parts

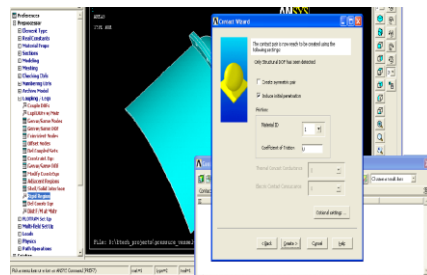


Fig 5.5 Creating surface to surface contact to Shell and Dished end

VI. RESULTS AND DISCUSSIONS

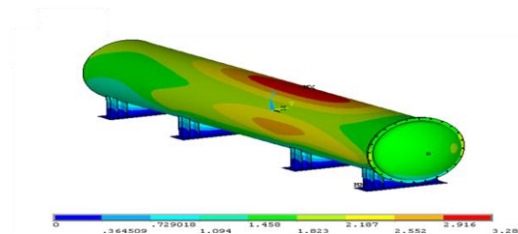


Fig 6.1 Total deflection of testing chamber

Total deflection of the canister testing chamber. Maximum total deflection of 3.2 mm is seen on the canister testing chamber.

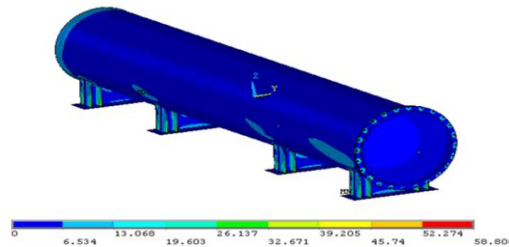


Fig 6.2 von mises stress of testing chamber

Von Mises Stress on the canister testing chamber. Maximum Stress of 58N/mm² is seen on the canister testing chamber.

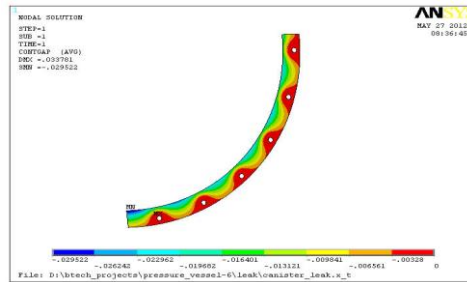


Fig 6.3 Contact Gap for M12 bolt

From the above Fig it can be observed that the VonMises stress is very high at bolt region and also there is an opening of 0.00328mm at the bolt locations. So It is recommended to check for the higher bolt diameter.so,the gap analysis is performed again for M22 bolt diameter.

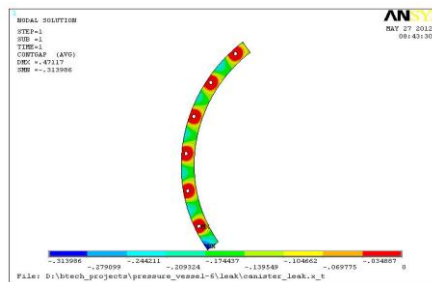


Fig 6.4 Contact Gap for M22 bolt

From the above Fig it can be observed that the VonMises stress is within the limit at bolt region but there is an opening of 0.0034mm at the bolt locations.So It is recommended to check for the higher bolt diameter.so,the gap analysis is performed again for M36 bolt diameter.

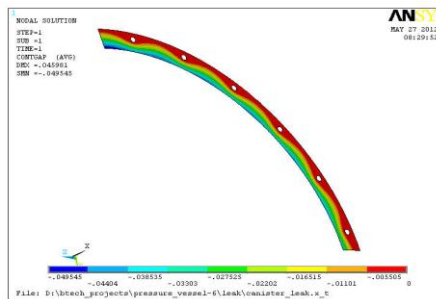


Fig 6.5 Contact gap for M36 bolt

From the above Fig. it can be observed that the VonMises stress is 6 N/mm², within the limit at bolt region and there is no opening at the bolt locations. The contact status is also observed as sticking at the bolting regions. So M36 bolts are the suitable bolt diameter to prevent the leakage of pressure to the atmosphere.

VII. CONCLUSION

In this paper a canister chamber is designed and tested for stresses and leakages using ANSYS simulation studies. The following conclusions can be made from Simulation studies that are carried out in this thesis.

- The maximum vonMises Stress observed on the canister testing chamber is 58 Mpa.
- The maximum deflection observed on the canister testing chamber is 3.2mm.
- The Designed horizontal canister testing chamber is safe of the internal pressure of 9kgf/cm² as the yield strength of material used for canister testing chamber is 260N/mm²
- Nonlinear Contact Gap analysis performed on the canister testing chamber shows free from leakage of pressure.
- Contact gap analysis suggests to use M36 Bolts which gives a gap opening of 0mm and hence M36 bolts recommended for canister testing chamber to avoid the pressure leakage to the atmosphere.

REFERENCES

- [1] Serena, Joseph M (1996). An On-Site Demilitarization Container for Unexploded Ordnance, Proc InstnMech Engrs Part C, No.717-729.
- [2] Charles P. Haber (1976). Dynamic and Structural Analysis of Reusable Shipping & Storage Container for Encapsulated Harpoon Missile, Defense Technical Information Center, Europe.
- [3] Cardinal, J. W., Dobosz, S. A., Pomerening, D. J (1987). Nondestructive Analysis of MK 607 Harpoon Missile container, Southwest research institute, 53-56.
- [4] Local Stresses in Spherical and Cylindrical Shells Due to External Loading, K.K. Wichman, A.G. Hopper, and J.L. Marshen, WRC Bulletin No. 107, December 1968, Revised March 1979.
- [5] Lin, J.I., "A Nonlinear, Explicit, Three-Dimensional Finite Element Code for Solid and Structural Mechanics - User Manual," Lawrence Livermore NationalLaboratory, UCRL-MA-107254, November 1997.

Some New Families on H-Cordial Graphs

Freedra .S¹, Robinson S. Chellathurai²

1, 2(Department of Mathematics, Scott Christian College, Nagercoil – 629 001, INDIA)

Abstract: In this paper some new families on H-cordial graphs are investigated. We prove that the graphs obtained by duplication of vertices as well as edges in cycle C_n , $n \geq 3$ admits H_2 -Cordial labeling. In addition to this we derive that the joint sum of two copies of cycle C_n of even order, a triangle and quadruple in C_r and C_{r+1} respectively for each $r \geq 3$ and complete graph K_n , $n \equiv 1 \pmod{4}$ are H_2 -Cordial labeling. The shadow graph of path P_n for even n and split graph of C_n for even n are H-cordial labeling.

Keywords: H-cordial labeling, H_2 -cordial labeling, joint sum, shadow graphs.

I. INTRODUCTION

We begin with simple, finite, connected and undirected graph $G = (V(G), E(G))$ with p vertices and q edges. For all other standard terminology and notations we follow (Harary, F.1972). We will provide brief summary of definitions and other information which serve as prerequisites for the present investigations.

1.1. Definition: Duplication of a vertex V_k of a graph G produces a new graph G_1 by adding a new vertex V'_k in such a way that $f(v_k) = f(v'_k)$.

1.2. Definition : For a graph G the split graph is obtained by adding to each vertex v , a new vertex v' such that v' is adjacent to every vertex that is adjacent to v in G . The resultant graph is denoted by $\text{spl}(G)$.

1.3. Definition: Consider a cycle C_n . Let $e_k = V_k V_{k+1}$ be an edge in it, and let $e^1 = V_k V'_k$, $e'' = V_{k+1} V'_{k+1}$ be the new edges incident with V_k and V_{k+1} . The duplication of an edge e_k by an new edge, $e'_k = V'_k V'_{k+1}$ produces a new graph G in such a way that $f(V'_k) = f(V'_{k+1})$.

1.4. Definition: Consider two copies of C_n , connect a vertex of the first copy to a vertex of second copy with a new edge, the new graph obtained is called the joint sum of C_n .

1.5. Definition: The shadow graph $D_2(G)$ of a connected graph G is obtained by taking two copies of G say G' and G'' . Join each vertex V' in G' to the neighbours of the corresponding vertex V'' in G'' .

1.6. Definition: If the vertices are assigned values subject to certain conditions then it is known as graph labeling.

The concept of an H-cordial graph is introduced by I-Cahit in 1996 (Bulletin of the ICA).

In [2] proved that if f is an assignment of integer numbers to the edges and vertices of a given graph G such that for each vertex v

$$f(v) = \sum_{e \in I(v)} f(e) \text{ then } \sum_{V \in V(G)} f(v) = 2 \sum_{e \in E(G)} f(e).$$

1.7. Definition: Let $G = (V(G), E(G))$ be a graph. A mapping $f: E(G) \rightarrow \{1, -1\}$ is called H-cordial, if there exists a positive constant k , such that for each vertex v , $|f(v)| = k$, and the following two conditions are satisfied. $|e_f(1) - e_f(-1)| \leq 1$ and $|v_f(k) - v_f(-k)| \leq 1$, where $v(i)$ and $e(j)$ are respectively the number of vertices labeled with i and the number of edges labeled with j .

A graph G is called to be H-cordial, if it admits an H-cordial labeling.

1.8. Definition: An assignment f of integer labels to the edges of a graph G is called to be a H_k – cordial labeling, if for each edge e and each vertex v of G we have $1 \leq |f(e)| \leq k$ and $1 \leq |f(v)| \leq k$ and for each with $1 \leq i \leq k$ we have $|e_f(i) - e_f(-i)| \leq 1$ and $|v_f(i) - v_f(-i)| \leq 1$. A graph G is called to be H_k – cordial if it admits a H_k – cordial labeling.

Ghebleh and Khoeilar proved that K_n is H-cordial if and only if $n \equiv 0$ or $3 \pmod{4}$ and $n \neq 3$. W_n is H-cordial if and only if n is odd.

K_n is H_2 – cordial if $n \equiv 0$ or $3 \pmod{4}$ and K_n is not H_2 -cordial if $n \equiv 1 \pmod{4}$.

C_n is not H-cordial and H_2 – cordial labeling. In [2] showed that triangle and quadruple C_r and C_{r+1} respectively for each $r \geq 3$ are not H_2 – cordial labeling. In this paper we duplicated the vertices and edges of those graphs and obtained a H_2 -cordial labeling.

II. Main Results

2.1. Theorem: The graph obtained by duplication of two vertices in a graph of C_n , $n \geq 3$ admits a H_2 – cordial labeling.

Proof: Let v_1, v_2, \dots, v_n be the vertices of the cycle C_n . Let G be the graph obtained by duplicating two vertices that lies between the edges of the labels +1 and -1.

Without loss of generality let the vertices be v_1 and v_2 , the newly added vertices by v'_1, v'_2 and the edges be 'e' and e_0 .

$E(G) = \{E(C_n), e \text{ and } e_0\}$ where $e = v_1 v'_1$ and $e_0 = v_2 v'_2$.

To define $f : E(G) \rightarrow \{1, -1\}$ two cases are to be considered.

Case (i) n is even.

$$\begin{aligned} f(e_i) &= 1, 1 \leq i \leq n/2 \\ &= -1, n/2+1 \leq i \leq n \\ f(e) &= -1, \quad f(e_0) = 1. \end{aligned}$$

Case(ii) n is odd

$$\begin{aligned} f(e_i) &= 1, 1 \leq i \leq n-1/2 \\ &= -1, \frac{n-1}{2} + 1 \leq i \leq n \end{aligned}$$

In view of the above defined labeling pattern f satisfies the condition for H_2 - cordial labeling as shown in Figure 1. The vertex and the edge conditions are given in Table 1 and Table 2.

2.2 Illustration: Figure 1 shows H_2 -cordial labeling of the graph obtained by duplication of vertices in C_{12}

2.3 Theorem: The graph obtained by duplication of edges in $C_n, n \geq 3$ admits a H_2 -cordial labeling.

Proof: Let v_1, v_2, \dots, v_n be the vertices of the cycle C_n .

Let G be the graph obtained by duplicating edges of C_n that lies between the labels of the vertices 0 and $|2|$.

Without loss of generality, let the edge be $e_1 = v_1 v_2$ and the new edges incident with v_1 and v_2 are $e'_0 = v_1 v'_1, e''_0 = v_2 v'_2$. The duplication of an edge e_1 by another new edge $e'_1 = v'_1 v'_2$. Similarly define the other edge that lies between the vertices of the labels 0 and $|2|$.

Define $f : E(G) \rightarrow \{1, -1\}$; two cases are to be considered.

Case (i) when n is even

$$\begin{aligned} f(e_i) &= 1, \quad 1 \leq i \leq n/2 \\ &= -1, \quad n/2+1 \leq i \leq n \\ f(e_1) &= -1, f(e'_1) = 1, f(e'_0) = 1, f(e''_0) = 1 \end{aligned}$$

Similarly $f(e_2) = 1, f(e'_2) = -1, f(e') = -1, f(e'') = -1$

Case (ii) when n is odd

$$\begin{aligned} f(e_i) &= 1, \quad 1 \leq i \leq n-1/2 \\ &= -1, \quad n/2+1 \leq i \leq n \\ f(e_1) &= 1, f(e'_1) = -1, f(e'_0) = -1, f(e''_0) = -1 \end{aligned}$$

Similarly $f(e_6) = -1, f(e'_6) = 1, f(e') = 1, f(e'') = 1$

In view of the above defined labeling pattern f satisfies the condition for H_2 -cordial labeling as shown in Figure 2. The edge and the vertex conditions are given in Table 3 and Table 4.

2.4 Illustration: H_2 -cordial labeling of the graph obtained by duplication of the edge in C_{11} is shown in figure 2.

2.5 Theorem: Joint sum of two copies of $C_n, n \geq 3$ of even order produce an H_2 -cordial labeling graph.

Proof: Let the vertices of the first copy of C_n by v_1, v_2, \dots, v_n and second copy by $v'_1, v'_2, \dots, v'_n, e_i$ and e'_i where $i \leq n$ be the corresponding edges.

Join the copies of C_n with new edges and let G be the resultant graph. Without loss of generality we assume that the new edges be $e = v_1 v'_1$ and $e' = v_2 v'_2$.

Define $f : E(G) \rightarrow \{1, -1\}$.

When n is even

$$\begin{aligned} f(e_i) &= 1, & 1 \leq i \leq n/2 \\ &= -1, & n/2 + 1 \leq i \leq n; \end{aligned} \quad f(e) = -1, f(e') = 1$$

In view of the above defined labeling pattern f satisfies the condition for H_2 -cordial labeling as shown in Figure 3. The edge and the vertex conditions are given in Table 5.

2.6 Illustration: H_2 -cordial labeling of joint sum of two copies of C_{10} is shown in Figure 3.

2.7 Theorem: The split graph of C_n , $n \geq 3$ of even order is H-cordial.

Proof: Let v_1, v_2, \dots, v_n be the vertices of cycle C_n and v_1', v_2', \dots, v_n' be the newly added vertices when n is even.

Let G be the split graph of cycle C_n with $V(G) = \{v_i, v_i', 1 \leq i \leq n\}$ and

$$E(G) = \{v_i, v_{i+1}, 1 \leq i \leq n-1, v_n v_1, v_i' v_{i+1},$$

$$1 \leq i \leq n-1, v_n' v_1, v_i' v_{i+1}', 1 \leq i \leq n-1, v_n' v_1'\}$$

To define $f : E(G) \rightarrow \{1, -1\}$

$$\begin{aligned} f(e_i) = f(v_i, v_{i+1}) &= 1, 1 \leq i \leq n/2 \\ &= -1, n/2 + 1 \leq i \leq n \\ f(v_n v_1) &= -1 \end{aligned}$$

For $1 \leq i \leq n/2$

$$\begin{aligned} f(v_i, v_{i+1}') &= 1 \text{ if } i \equiv 0, 1 \pmod{4} \\ &= -1 \text{ if } i \equiv 2, 3 \pmod{4} \end{aligned}$$

For $n/2 + 1 \leq i \leq n$

$$\begin{aligned} f(v_i, v_{i+1}') &= -1 \text{ if } i \equiv 1, 2 \pmod{4} \\ &= 1 \text{ if } i \equiv 0, 3 \pmod{4} \end{aligned}$$

$$f(v_n, v_1') = 1$$

For $1 \leq i \leq n/2$

$$\begin{aligned} f(v_i' v_{i+1}) &= 1, \text{ if } i \equiv 1, 2 \pmod{4} \\ &= -1, \text{ if } i \equiv 0, 3 \pmod{4} \end{aligned}$$

For $n/2 + 1 \leq i \leq n$

$$\begin{aligned} f(v_i' v_{i+1}) &= 1 \text{ if } i \equiv 0, 1 \pmod{4} \\ &= -1 \text{ if } i \equiv 2, 3 \pmod{4} \end{aligned}$$

$$f(v_n', v_1) = 1$$

In view of the above defined labeling pattern f satisfies the condition for H-cordial labeling as shown in Figure 4. The edge and the vertex conditions are given in Table 6.

2.8 Illustration: H-cordial labeling of split graph of cycle C_8 is shown in figure 4.

2.9 Theorem: $D_2(P_n)$ is H-cordial labeling for even n .

Proof : Let P_n', P_n'' be two copies of path P_n . We denote the vertices of first copy of P_n by v_1', v_2', \dots, v_n' and the second copy by $v_1'', v_2'', \dots, v_n''$. Let G be $D_2(P_n)$ with $|V(G)| = 2n$ and $|E(G)| = 4n-4$.

Define $f: E(G) \rightarrow \{1, -1\}$

$n \equiv 0, 2 \pmod{4}$

$$\begin{aligned} f(v_i', v_{i+1}') &= 1, & 1 \leq i \leq n/2 \\ &= -1, & n/2 + 1 \leq i \leq n-1 \end{aligned}$$

$$\begin{aligned} f(v_i'', v_{i+1}'') &= 1, & 1 \leq i \leq n-2 \\ &= -1, & n-2 \leq i \leq n \end{aligned}$$

For $1 \leq i \leq n-1$

$$\begin{aligned} f(v_i' v_{i+1}'') &= 1, & i \equiv 0, 1 \pmod{4} \\ &= -1, & i \equiv 2, 3 \pmod{4} \end{aligned}$$

$$f(v_{n-1}' v_n'') = -1$$

For $i \leq i \leq n-1$

$$\begin{aligned} f(v_i'', v_{i+1}'') &= 1, & i \neq j, \quad j = 2, 3, \dots, n-1 \\ &= -1, & i = j \end{aligned}$$

In view of the above defined labeling pattern f satisfied the condition for H-cordial labeling for even n , as shown in Figure 5. The edge and the vertex conditions are given in Table 7.

2.10 Illustration: H-cordial labeling of $D_2(P_6)$ is shown in figure 5.

The duplication of Triangle and quadruple, C_r and C_{r+1} , $r \geq 3$ admits a H_2 -cordial labeling.

Proof: Consider a triangle C_3 and quadruple C_4 . Let the vertices be v_1, v_2, \dots, v_7 and the corresponding edges are e_1, e_2, \dots, e_{13} .

Take an edge $e_1 = v_1 v_2$ be the duplicating edge that lies between the labels of the vertices 0 and $|2|$.

Define $f: E(G) \rightarrow \{1, -1\}$

$$E(G) = \{E(C_3 \& C_4) e', e''\} \text{ where } e' = v_1 v_1'$$

$$e'' = v_2 v_2', e_1' = v_1' v_2'$$

The newly added edges be e_1', e' and e'' .

$$f(v_i, v_{i+1}) = 1, \quad 1 \leq i \leq n-2$$

$$f(v_1, v_n) = -1 \quad f(v_2, v_{n-1}) = -1$$

$$f(v_3, v_{n-1}) = -1 \quad f(v_6, v_n) = -1$$

$$f(e') = f(v_1 v_1') = -1$$

$$f(e'') = f(v_2 v_2') = -1$$

$$f(e_1^1) = f(v_1^1 v_2^1) = -1$$

In view of the above defined labeling pattern f satisfies the condition for H_2 -cordial labeling as shown in Figure 6. The edge and the vertex conditions are given in Table 8.

2.11 Illustration: H_2 -cordial labeling of the graph obtained by duplication of the edge in C_3 & C_4 is shown in figure 6.

2.11 Theorem: The graph obtained by duplication of an edge of the complete graph K_n , $n \equiv 1 \pmod{4}$ admits a H_2 -cordial labeling.

Proof: Let v_1, v_2, \dots, v_n be the vertices of the complete graph K_n . Let G be the graph obtained by duplicating an edge that lies between the vertices of the labels 0 and $|2|$.

Without loss of generality let this edge be e_1 and the newly added edge be e_1' .

$E(G) = \{E(K_n), e_1', e' \text{ and } e''\}$ where

$e_1' = v_1' v_2', e' = v_1 v_1', e'' = v_2 v_2'$

By the definition of duplication of an edge we have $f(v_k') = f(v_{k+1}')$.

Define $f : E(G) \rightarrow \{1, -1\}$

For $1 \leq i \leq n-1$

$$f(v_i, v_{i+1}) = 1, \quad i \equiv 1, 3 \pmod{4}$$

$$= -1, \quad i \equiv 0, 2 \pmod{4}$$

$$f(e_1') = -1$$

$$f(e') = -1$$

$$f(e'') = -1$$

$$f(v_1, v_{n-2}) = -1$$

$$f(v_1, v_{n-1}) = 1, \quad f(v_2, v_n) = 1$$

$$f(v_2, v_{n-1}) = 1$$

$$f(v_3, v_n) = 1$$

:

:

:

In view of the above defined labeling pattern f satisfies the condition for H_2 -cordial labeling as shown in Figure 7. The edge and the vertex conditions are given in Table 9.

2.13 Illustration: H_2 -cordial labeling of the graph obtained by duplicating of an edge K_5 is shown figure 7.

TABLE 1

n	Vertex Condition	Edge Condition
even	$v_f(1) = v_f(-1) = n-(n-2)$ $v_f(2) = v_f(-2) = n-2/2$	$e_f(1)=e_f(-1)=\frac{n+2}{2}$ $e_f(2)=e_f(-2)=0$

TABLE 2

n	Vertex Condition	Edge Condition
odd	$v_f(1) = v_f(-1) = n-(n-2)$ $v_f(-2) = v_f(2)+1 = n-1/2$	$e_f(-1)=e_f(1)+1=\frac{n+3}{2}$ $e_f(2)=e_f(-2)=0$

TABLE 3

n	Vertex Condition	Edge Condition
Odd	$v_f(1) = v_f(-1) = n-(n-2)$ $v_f(-2) = v_f(2)+1 = n+1/2$	$e_f(-1)=e_f(1)+1 = n+7/2$ $e_f(-2)=e_f(2)=0$

TABLE 4

n	Vertex Condition	Edge Condition
Even	$v_f(1) = v_f(-1) = n - (n-2)$ $v_f(-2) = v_f(-2)+1 = n/2$	$e_f(1)=e_f(-1) = n+6/2$ $e_f(2)=e_f(-2)=0$

TABLE 5

n	Vertex Condition	Edge Condition
Even	$v_f(1) = v_f(-1) = n-(n-2)$ $v_f(2) = v_f(-2) = n+6/2$	$e_f(1)=e_f(-1) = n+12/2$ $e_f(2)=e_f(-2)=0$

TABLE 6

n	Vertex Condition	Edge Condition
even	$v_f(2) = v_f(-2) = n$	$e_f(1)=e_f(-1) = \frac{3n}{2}$

TABLE 7

n	Vertex Condition	Edge Condition
Even	$v_f(-2) = v_f(2) + 1 = \frac{n+6}{2}$	$e_f(1)=e_f(-1) = 2n-2$

TABLE 8

n	Vertex Condition	Edge Condition
Odd	$v_f(1) = v_f(-1) = n-1/2$ $v_f(-2) = v_f(2)+1 = 1$	$e_f(-1) = e_f(1)+1 = \frac{n+9}{2}$ $e_f(2) = e_f(-2) = 0$

TABLE 9

n	Vertex Condition	Edge Condition
$n \equiv 1 \pmod{4}$	$v_f(1) = v_f(-1) = n-(n-1)$ $v_f(2) = v_f(-2)+1 = n+1/2$	$e_f(1) = e_f(-1)+1 = n+9/2$ $e_f(2) = e_f(-2) = 0$

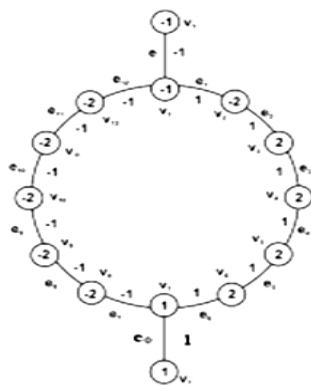


Figure 1 H_2 -cordial labeling of the graph obtained by duplication of the vertices in C_{12}

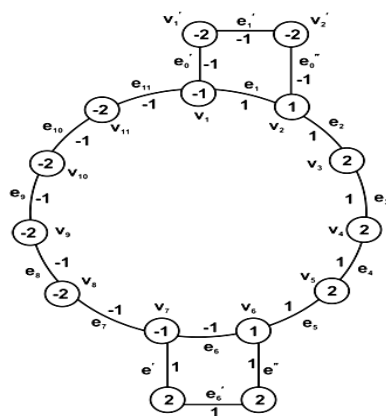


Figure 2: H_2 -cordial labeling of the graph by duplication of the edge in C_{11} .

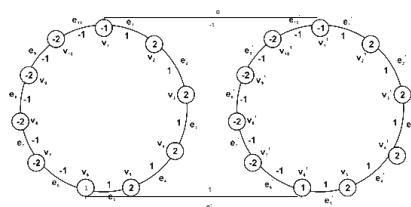


Figure 3 : H_2 -cordial labeling of joint sum of two copies of C_{10} .

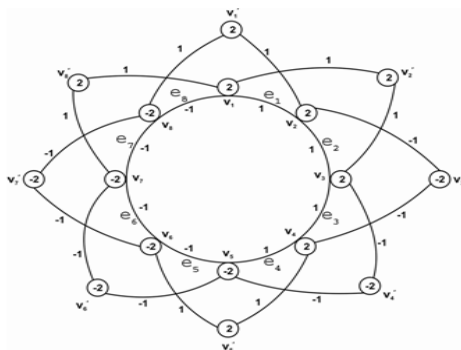


Figure 4 : H -cordial labeling of split graph of cycle C_8

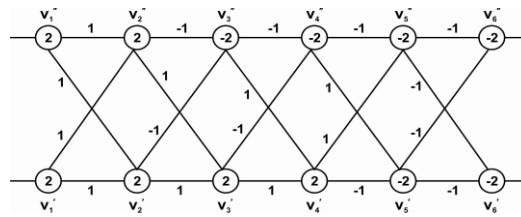


Figure 5: H-cordial labeling of $D_2 (P_6)$

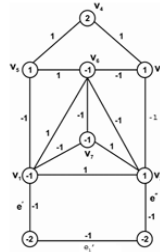


Figure 6: H_2 -cordial labeling of the graph obtained by duplication of the edge in C_3 & C_4

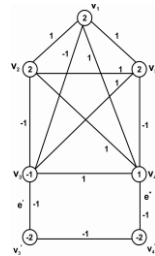
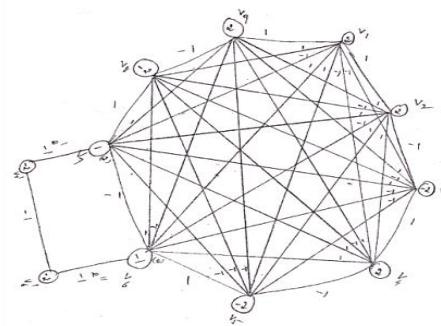


Figure 7 : H_2 -cordial labeling of the graph obtained by duplication of an edge K_5 .

Example : 1

Show that K_9 is a H_2 - cordial labeling by using theorem 2.2



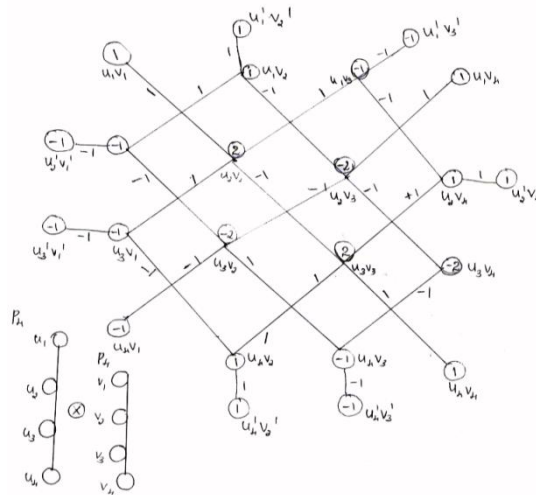
$$V_f(2) = 4, V_f(-2) = 5 \quad V_f(1) = 1 \quad V_f(-1) = 1 ; \quad e_f(1) = 19 \quad e_f(-1) = 20 \quad e_f(2) = 0 \quad e_f(-2) = 0$$

$$\text{For each } i, 1 \leq i \leq 2; |V_f(1) - V_f(-1)| + |V_f(2) - V_f(-2)| = |1-1| + |4-5| \leq 1$$

$$\text{For each } i, 1 \leq i \leq 2; |e_f(1) - e_f(-1)| + |e_f(2) - e_f(-2)| = |19-20| + |0-0| \leq 1$$

$\therefore K_9$ is H_2 Cordial labeling.

Example 2: Show that $P_4 \otimes P_4$ is a H_2 Cordial labeling by using theorem 2.1



$$V_f(2) = 2, V_f(-2) = 3 \quad V_f(1) = 9 \quad V_f(-1) = 9; \quad e_f(1) = 13 \quad e_f(-1) = 13 \quad e_f(2) = 0 \quad e_f(-2) = 0$$

$$\text{For each } i \quad 1 \leq i \leq 2; \quad |V_f(1) - V_f(-1)| + |V_f(2) - V_f(-2)| = |9-9| + |2-3| \leq 1$$

$$\text{For each } i \quad 1 \leq i \leq 2; \quad |e_f(1) - e_f(-1)| + |e_f(2) - e_f(-2)| = |13-13| + |0-0| \leq 1$$

$\therefore P_4 \otimes P_4$ is a H_2 Cordial labeling.

III. Concluding Remarks

Here we investigate seven new families of H-cordial graphs generated by different graph operations. To investigate similar results for other graph families and in the context of different graph labeling problems is an open area of research.

IV. ACKNOWLEDGMENT

The authors are highly thankful to the anonymous referees for constructive suggestions and comments.

REFERENCES

- [1] Cahit, H-cordial graphs, Bull.Inst.Combin.Appl; 18(1996) 87-101.
- [2] M.Ghebleh and R.Khoeilar, A note on "H-cordial graphs", Bull.Inst.Combin.Appl; 31(2001) 60-68.
- [3] Gallian J.A. (2010). A dynamic survey of graph labeling. The Electronics journal of combinatorics 17 # DS6.
- [4] S.K.Vaidya and Lekha Bijukumar, "Some New Families of E-cordial graphs".
- [5] Harary, F. (1972) Graph Theory, Addison Wesley, Reading Massachusetts.

A Robust Data Hiding in Random Macro Blocks of Compressed Video

Susmitha Rayapudi,¹ NagaRaju Ravada,² N.V.G.Prasad,³

Student M. Tech, VLSI & ES, Department of ECE, Sasi Institute of Technology & Engineering, India

M.Tech, Asst. Professor, Department of ECE Sasi Institute of Technology & Engineering, India

M.Tech, Associate. Professor, H.O.D Department of ECE Sasi Institute of Technology & Engineering, India

Abstract: Data hiding in compressed video. We target, finding the macro blocks randomly by Pseudo Random Generation Algorithm. Then encoded the video and reconstructed the frames both forward predictive (P)-frame and bidirectional (B)-frame in compressed video, which are very secured and Compared to data hiding in motion vectors of compressed video. A every frame is searched for achieve to robustness. The secret message bit stream is embedded in the random macro block in each frame of compressed video. The method is implemented and tested for hiding data in order of multiple GOP's and the results are evaluated. The proposed method is performing well.

Keywords: Data hiding, Pseudo Random Generation, Motion Picture Expert Group (MPEG), Group of pictures (GOP), steganography.

I. INTRODUCTION

DATA hiding [1] in digital images seen widely this paper target the internal operation of video compression, specifically the random macro block estimation stage. This is processed internally during the video encoding/reconstruction which can't to be detected by image steganalysis methods and most work applied on data hiding in the macro blocks randomly .In [2] and [3], the data bits of the message are hidden in macro blocks these are called the random block.

The data is encoded as a region where the estimation is only allowed, that specified region. Using the variable macroblock sizes (16x16, 16x8, 8x16, 8x8), the authors in [5] used for the message bit stream to select one of the four sizes for the estimation process. The authors in [6] and [7] embed the data in compressed video. The block matching is constrained to search within the selected sector. The methods in [2]–[7] focused on finding a direct reversible way to identify the at the decoder.

II. PROPOSED METHOD

In this section, we overview lossy video compression to define evaluation metrics. At the encoder, the I-frame is used as a reference frame for encoding a group of (P) frame or (B)-frames. The video is sequenced into groups of pictures (GOPs) whose frames can be encoded in the GOP sequence: [I,B,B,P,B,B,P,B]. Predicted (p)-frames are coded based on nearest I frame and P frame this technique is called forward prediction. B pictures are consider the forward and backward of I and B frames, this technique is called bidirectional predicted (B) frame. Generally, the video compression is assumed to be translational with horizontal component d^x and vertical component d^y and denoted in vector form by $d(x)$ for the spatial variables $x=(x,y)$ in the underlying image.

The search window is constrained by assigning limited n-bits for d ; in other words, both d^x and d^y which corresponds to pixels if the random macro blocks are computed with half-pixel accuracy. A search in the window can be done to find the optimal random estimation satisfying the search criterion which needs many computations, or suboptimal random block can be obtained using expeditious methods .This is based on the video encoding device processing power, the required compression ratio, and the reconstruction quality. Since d does not represent in the video then the frames are able to reconstruct with minimum distortion at the decoder in case of a P-frame. Similar operation is done for the B-frame but with the average of both the forward prediction from a previous reference frame and backward prediction from a next reference frame. E is of the size of an image and is thus lossy compressed using JPEG compression reducing its data size. For every random block estimation method, the pair (d, \tilde{E}) will be different and the data size of the compressed error E will be different. The macro blocks d are lossless coded and thus become an attractive place to hide a message that can be blindly extracted by a special decoder.

The decoder receives the pair (d, \tilde{E}) applies random generation to form P and B or and decompresses \tilde{E} to obtain a reconstructed E_r then the decoder in unable to reconstruct P identically but it alternatively reconstructs.

III. Data hiding

Data hiding in random estimation places at the encoder replaces the regular pair (d, \tilde{E}) due to tampering the motion vectors, to become (d^h, \tilde{E}^h) where the superscript h denotes hiding. We define data hiding in random macroblocks of compressed video in the context of super-channel [9]; the secret message m is hidden in the host video signal $\chi = (d, E)$ to produce the composite signal $s = (d^h, E^h)$. The composite signal is subject to video lossy Compression to become $y = (d^h, E^h)$. The message m should survive the video lossy compression and can be identically extracted from video. This robustness constrain should have low distortion effect on the reconstructed video as well as low effect on the data size (bit rate). Given that m can be identically extracted, in this paper, we use data-hiding algorithms in compressed video which are. The payload should be robust to the video compression.

These observations stimulated our proposal to rely directly on the random macro blocks, such that we choose our macroblocks E . If we tamper with these Blocks, then we will not hav effect on the video reconstruction quality. Since then our selection criteria in this paper can be thought of as in this direction, we choose the random estimation based on the pair (d, E) and not d alone. However, this incurs the difficulty that E is lossy compressed and what we have at the decoder after decompression is actually E_r .

IV. Random Generation

Our data-hiding algorithm is applied at the encoder side, uses the regular pair (d, \tilde{E}) produced, tampers to become d^h and thus replaces them by the pair (d^h, \tilde{E}^h) for each P and B-frame in the GOP. We propose pseudo random generation algorithm for secret message is hidden by random generator it can random generator, generates the random number of macro blocks with in the period, here we can implement the random logic for random blocks, are as good as truly random bits. The algorithm tests the robustness of the hidden message to the quantization effect of the JPEG compression. For the prediction frames E^h it performs the compression by the encoder followed by the decompression performed by the decoder, If the reconstructed prediction frames maintains the same criterion then can be identified by the data extractor for the given value of any macro block, then reconstructed d will be identified by the data extractor and the message will be extracted correctly. Hence, we use an this algorithm by iteratively decrementing for the frame until either the criterion is satisfied for all macro blocks or the stopping value is reached for which we embed no data in this frame, we hide the twenty four values in specified macro blocks of 24 bits i.e RGB have 24 bits in each pixel for that GOP. In the GOP, I-frame using any robust image data-hiding technique or sending them on a separate channel based on the application.

The decoder receives and it can decode without loss and decompresses to obtain a lossy reconstructed Version. During normal operation for viewing the video, the decoder is able to reconstruct or by suitable compensation from reference frame(s). Acting as a new kind of random macroblock estimation, will have two effects on the new compressed video: change in data size and reconstruction quality which are thoroughly. The data extractor operates to extract the hidden message as a special decoder and our proposal is straightforward. After data extraction from the consecutive GOPs the hidden message is reconstructed back by concatenation of the extracted bit stream.

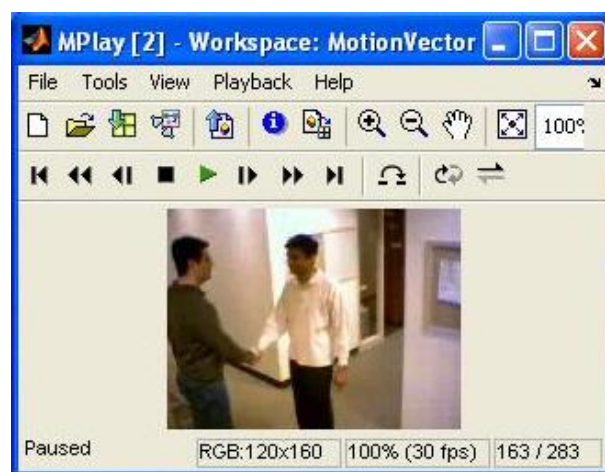
V. RESULTS

We implemented the hiding and extraction Algorithms are integrated them to the MPEG-2 encoder and decoder operation. We used . search Random macroblock estimation algorithms with pixel accuracy. Each test video sequence is organized into consecutive GOP organized as [I,B,B,P,B,B,P,B,B]. The compression to the I-frame and the prediction of the P- and B- frames are implemented. Our algorithm may hide a maximum of bytes per P-frame and B-frame. We evaluated our algorithm which is independent on a threshold T of the random estimation. We have chosen the pixel for [3] total number of embedded bytes (payload) to that of our algorithm for the whole test sequence. The payload for both methods and the associated threshold T of motion vector and Random Macroblock in values of pixels, For each sequence we calculated the overall frames the reconstructed video in effect to the hiding; results. Finally, the data size increase due to hiding the data is measured for each frame and the total data size increase which is accounted for our hiding criteria.

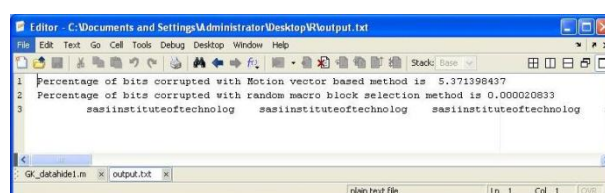
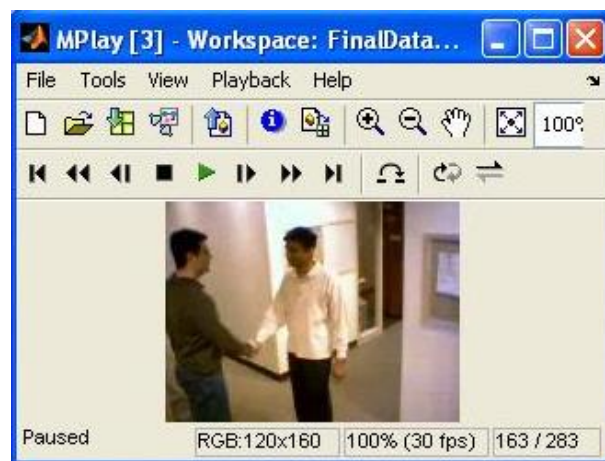
According to the GOP organization among I-, P-, and B, the random blocks of the B-frames can hold a bigger share of the payload than those of the P-frames. However, tampering the motion vectors of B-frames will have more distortive effect. Video than that by P-frames, as the B-frames are bi-directionally optimized to minimize the prediction error. We counted the percentage of hidden bytes in both the P- and B-frames. The usage of the macro blocks of the B-frames is an additional reason that accounts for the enhanced results of our method in both aspects of the data size and the quality of the reconstructed video.

Simulation Results:

Motion vector video:



Random Block video:



We can observe the errors and hidden data in the above simulation output text file.

Data hiding in motion vectors of compressed video error is 5.371398437 when threshold value is 1, Random

macro block method of compressed video error is 0.0000208330.

VI. CONCLUSION

We proposed a new data-hiding method in the random macroblock estimation of MPEG-2 compressed video. Unlike most data-hiding methods in the motion vectors, we chose a different approach that selects those random blocks whose random macro blocks error is low for hiding a bit. The embedding and extraction algorithms are implemented and integrated to the MPEG-2 encoder/decoder and the results are evaluated. This method is found to have very much secured compared with motion vector estimation because easy to guess the where the motion takes place. Hence by using this random macro block method we get very low error when compared to motion vector of compressed video method. So we propose the random estimation macro blocks for hiding and the quality of the video. Future work will be directed towards increasing the size of the embedded.

REFERENCES

- [1] Hussein A. Aly, IEEE Member, Data Hiding in Motion Vectors of Compressed Video Based on Their Associated Prediction Error , IEEE Transactions on information forensics and security, vol. 6, NO. 1, March 2011
- [2] F. A. P. Petitcolas, R. J. Anderson, and M. G. Kuhn, "Information Hiding—A survey," Proc. IEEE, vol. 87, no. 7, pp. 1062–1078, Jul.1999.
- [3] J. Zhang, J. Li, and L. Zhang, "Video watermark technique in motion vector," in Proc. XIV Symp. Computer Graphics and Image Processing, Oct. 2001, pp. 179–182.
- [4] C. Xu, X. Ping, and T. Zhang, "Steganography in compressed video stream," in Proc. Int. Conf. Innovative Computing, Information and Control (ICICIC'06), 2006, vol. II, pp. 803–806.
- [5] P. Wang, Z. Zheng, and J. Ying, "A novel video watermark technique in motion vectors," in Int. Conf. Audio, Language and Image Processing (ICALIP), Jul. 2008, pp. 1555–1559.
- [6] S. K. Kapotas, E. E. Varsaki, and A. N. Skodras, "Data hiding in H.264 encoded video sequences," in IEEE 9th Workshop on Multimedia Signal Processing (MMSP07), Oct. 2007, pp. 373–376.
- [7] D.-Y. Fang and L.-W. Chang, "Data hiding for digital video with phase of motion vector," in Proc. Int. Symp. Circuits and Systems (ISCAS), 2006, pp. 1422–1425.
- [8] X. He and Z. Luo, "A novel steganographic algorithm based on the motion vector phase," in Proc. Int. Conf. Comp. Sc. and Software Eng., 2008, pp. 822–825.
- [9] Generic Coding of Moving Pictures and Associated Audio Information: Video, 2 Editions, SO/IEC13818-2, 2000.
- [10] B. Chen and G. W. Wornell, "Quantization index modulation for digital watermarking and information embedding of multimedia," J. VLSI Signal Process, vol. 27, pp. 7–33, 2001.

[3] J. Zhang, J. Li, and L. Zhang, "Video watermark technique in motion vector," in Proc. XIV Symp.

Wear Behavior of AISI D3 Die Steel Using Cryogenic Treated Copper and Brass Electrode in Electric Discharge Machining

Harpreet Singh,¹ Amandeep Singh²

¹Department of mechanical Engg YCOE Talwandi Sabbo

²Department of mechanical Engg FCET Ferozepur

ABSTRACT: Electric discharge machining is used for machining of hard materials. Tool material is of great importance because it affects material removal rate as well as surface finish of work piece. In this article we study the wear behavior AISI D3 Die steel in EDM and compare the tool wear rate of cryogenic treated copper and brass electrode with simple copper and brass electrode on machining of AISI D3 die steel using current setting as 4A and 8A. The electrolyte is used kerosene oil.

Keyword: Current, EDM, surface finish, Wear

I. Introduction

Technological advances have led to an increasing use of high strength, high hardness materials in manufacturing industries. In the machining of these materials, traditional manufacturing processes are being replaced by more advance techniques like electro discharge machining, electric chemical machining and laser machining. (Lee et al., 2003). In non-traditional processing electrical discharge machining (EDM) has tremendous potential on account of the versatility of its application and it is except to be successfully and commercial utilized in modern industries (Habib, 2009). Electrical discharge machining is highly developed technology which account about 7% of all machine tools sales in the world. (Leao et al., 2004). In EDM process the material removal is achieved by preferential erosion of work piece electrode as controlled discrete discharge are passed between the tool and the work piece in a dielectric medium (Wong et al., 1995). Electric discharge machining one of the most popular non-traditional material removals process and has become basic machining method for the manufacturing industries of aerospace, automotive, nuclear and medical (Kiyak et al., 2007). In the EDM process there is no direct contact between electrode and the component during machining and therefore no deformation occurs even for thin components (Lee et al., 2003). In the EDM process to obtain the maximum material removal with minimum tool wear, the work material and tool must be set at positive and negative electrode (Che Haron et al., 2008). The EDM process is thermal energy based process in which the use of thermal energy to generate heat that melts and vaporized the work piece by the ionization within the dielectric medium. The source of energy used is amplified light, ionized material and high voltage. Examples are laser beam machining, ion beam machining, and plasma arc machining and electric discharge machining (Kiyak et al., 2007). This paper describe the wear behavior of AISI D3 Die steel in EDM and compare tool wear behavior of cryogenic treated copper and brass electrode with simple copper and brass electrode which Assist in choosing optimum electrode

II. Experimental detail

2.1 Work piece material

AISI D3 die steel was used as work piece material. Sample of size 25mm×18mm×6mm were prepared by using wire EDM. The prepare sample were heat treated to improve their hardness. After heat treatment the hardness of work piece material was 58HRc. Table 2.1 shows the chemical composition of work piece material.

Table 2.1 - The chemical composition of AISI D3 die steel

C%	Si%	Mn%	Cr%	Cu%
1.88	0.5	0.38	11.5	0.16

2.2 Tool Preparation

The electrodes having the size of 16 mm diameter and 55 mm length were prepared out of the rods of Copper and Brass for performing the experiments. After preparing the required size the face of all the electrodes was polished so as to get good surface finish using different emery papers ranges from 220 to 2000 grit size following general metallographic procedure. After that half the number of the electrodes of Cu and Br were cryogenically treated to improve properties. Following Table 2.2 and 2.3 show the chemical composition of copper and brass electrode

Table 2.2 - The chemical composition of the copper electrode

Cu%	Zn%	Al%	Bi%	Pb%
99.8	0.057	0.15	0.0011	0.0008

Table 2.3 - The chemical composition of the brass electrode

Cu%	Zn%	Pb%	Sn%	Fe%	Ni%
58.8	37.2	2.7	0.5	0.9	0.16

2.3 Dielectric used

The commonly available kerosene oil is used as dielectric fluid for all the experiments. The properties of the kerosene oil are shown in the Table no. 2.4.

Table 2.4 - Properties of kerosene oil

Surface Tension N/M	Density Kg / M ³	Dynamic Viscosity
0.028	820	2400

2.4. Machining process

Machining was performed on the electronics CNC EDM machine Each experiment was performed for fix time period of 20 min using the input process parameters as current using four different types of electrodes i.e. Cu, cryogenic treated Cu, Br and cryogenic treated Br. The weight of the work pieces and electrodes was done before machining and after machining on the weighing machine with least count of 1 mg

III. Result and discussion

3.1 Influence of the current and electrode material on MRR

The MRR is a measure, defining removal material volume per minute. The mass loss of the material when using different electrodes with different setting of the current i.e. 4A and 8A is shown in the Fig. 3.1. MRR is higher for the high value of the current for all the four different electrodes used. When the pulse current increases from 4A to 8A then the discharge strikes the sample with more intensity.

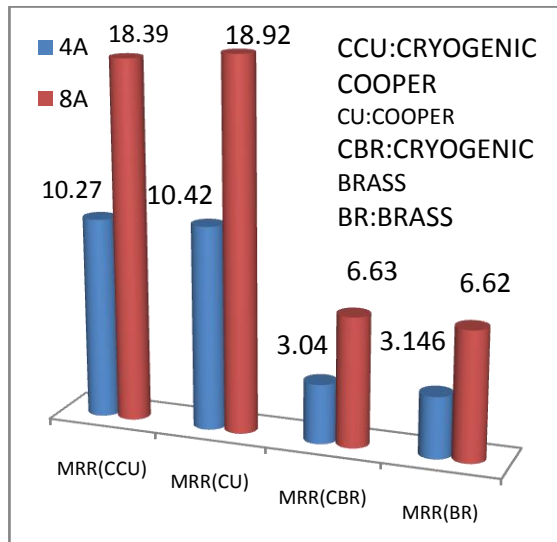


Fig. 3.1- Influence of the electrode material and current on the MRR (% of mass loss)

This result in erosion and cause more MRR (Lee et al., 2003). When the current increase from 4A to 8A then the spark energy increases, this leads to higher crater volume. This higher creator volume causes more MRR (Saha et al., 2009). This trend of MRR is in agreement with the work done by authors Kiyak and Lee (2007). As shown in Fig. 3.1 the maximum material removal is given by the copper electrode among the four different electrodes used, as copper electrode has higher thermal conductivity as compared to the brass electrode (Uhlmann et al., 2008). Further the MRR of cryogenic treated copper electrode and brass electrode is less than the non cryogenic treated electrodes. This may be due to the fact that with the cryogenic treatment of electrodes, the thermal conductivity of the electrodes increases. Due to increase in thermal conductivity of the electrode, heat applied during machining gets dissipated at a faster rate, which results in decrease in heat input at the inter-electrode gap. This further resulted in decrease in MRR. During the EDM process heat is applied for every discharge pulse and rate at which the material is removed depend upon how fast the applied heat is absorbed or dissipated (Abdulkarrem et al., 2009).

3.2 Influence of the Electrode Material and Current on the TWR

The Fig. 3.2 shows that with the increase in current there is increase in TWR for all the four electrodes used in machining. The higher value of current means higher heat energy subjected to electrode and high energy causes more

volume of molten ejected material from the electrode, which results in high TWR (Saha et al., 2009). When the current increase from 4A to 8A then more ionization of the dielectric fluid occur which means that more number of the ions and electrons are striking on the tool surface, due to which more TWR occur (Singh et al., 2010).

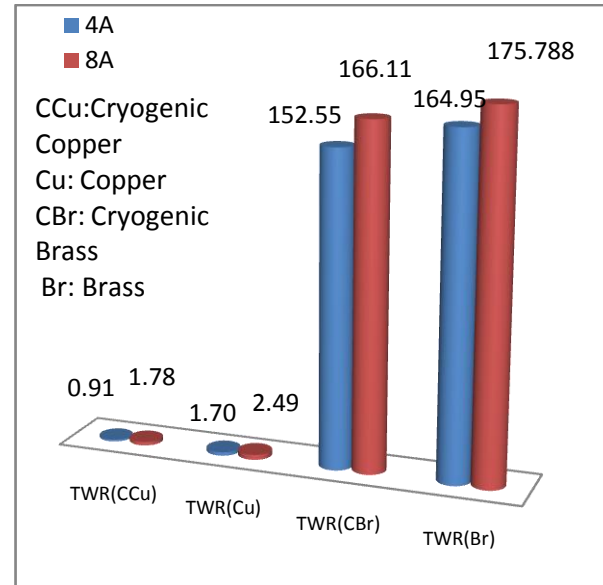


Fig. 3.2- Influence of the electrode material and current on the TWR (% of Tool wear)

Among the cryogenic treated and non cryogenic treated electrodes, the TWR of cryogenic treated electrode is less than the non cryogenic treated electrode. The cryogenic treatment improve the thermal conductivity of electrode material and due to good thermal conductivity there is a reduction is the heat entrapment at the electrode & work piece interface, due to less heat at the interface, there is less volume of metal which gets melted and evaporated, which results in reduction in the tool wear rate.

IV. Summary

- Tool wear of cryogenic treated copper electrode is approximately 50% less than copper electrode at 4 ampere current and 30% less at 8 ampere.
- Tool wear off cryogenic treated brass electrode is 8% least s than brass electrode at 4 ampere and 5% less at 8 ampere.
- Material removal rate of copper electrode is greater 1.4% of cryogenic treated copper electrode at 4 ampere and 2.8% at 8 ampere
- Material removal rate of brass electrode is greater 3.2% of cryogenic treated brass electrode at 4 ampere and same at 8 ampere.

V. Conclusion

Copper electrode is best electrode for high material removal rate. But cryogenic treated copper electrode has very low tool wear as compared to cooper electrode

References

- [1] Abdulkareem, S., Khan, Ahsan A., Konneh, M., Reducing electrode wear ratio using cryogenic cooling during electrical discharge machining. *Int. J. Adv. Manuf. Technol.* 45, (2009). 1146-1151
- [2] Saha, S. K., Choudhury, S.K., Experimental investigation and empirical modelling of the dry electric discharge machining process. *Int. J. Mach. Tools. Manuf.* 49, 2009. 297-308.
- [3] Kiyak, M., Cakir, O., 2007. Examination of machining parameters on surface roughness in EDM of tool steel. *J. Mater. Process.*
- [4] Singh, R., Singh B., Singh, H., Experimental Investigation for Tool Life Enhancement using Cryogenic Treatment. *J. Eng. Sci. Tech.* 4, 2010. 1-4.
- [5] Uhlmann, E., Roehner, M., Investigation on reduction of tool electrode wears in micro-EDM using novel electrode materials. *CIRP J. Manuf. Sci and Technol.* 1, 2008. 92-96.
- [6] Wong, Y.S., Lim, L.C., Lee, L.C., Effects of Flushing of Electro-Discharge Machined Surfaces. *J. Mater Process Technol.* 48, 1995. 299-305.
- [7] Lee, H.T., Tai, T.Y., Relationship between EDM parameters and surface crack formation. *J. Mater. Process. Technol.* 142, 2003 676-683.
- [8] Leao, F. N., Pashby, I. R., 2004. A review on the use of environmentally-friendly dielectric fluids in electrical discharge machining. *J. Mater. Process. Technol.* 149, 2003341-346.
- [9] Haron, C.H Che., Ghani, J.A., Burhanuddin, Y., Seong, Y.K., S wee, C.Y., Copper and graphite electrodes performance in electrical-discharge machining of XW42 tool steel. *J. Mater. Process. Techno.* 201, 2008. 570-573.
- [10] Habib, S. S., Study of the parameters in electrical discharge machining through response surface methodology approach. *App. Math. Model.* 33, 2009. 4397-4407.

A Laboratory Study of Cyclic Plate Load Test on Lime and Rice Husk Ash Treated Marine Clay Subgrade Flexible Pavements

Dr. D. Koteswara Rao,¹ Venkatesh Ganja,² P.R.T Pranav³

¹(Civil Engineering Department, Jawaharlal Nehru Technological University Kakinada, India)

²(Department of Civil Engineering, JNT University, Kakinada, India)

³(Department of Civil Engineering, National Institute of Technology, Warangal, India)

ABSTRACT: Marine clay is an impermeable soil, meaning it holds water, as opposed to permeable soil that allows water to rapidly drain, like a gravel or sand. It is also an expansive soil, such as the marine clay which predominates in almost all countries of the world, which when shrinking or expanding, can damage foundations and structures. The shrink and swell movements are due to changes in soil moisture. Providing uniform soil moisture next to and under your foundation is the only best thing to reduce or minimize the damaging effects of expansive soil. These soils are highly saturated, soft, sensitive and normally consolidated. These usually have low density and low shear strength. The present study involves a study on the strength characteristics of Rice Husk Ash and Lime treated marine clay based on the cyclic plate load test criteria.

Keywords: Marine clay, RHA, Lime, OMC, MDD, FSC, Cyclic Plate Load Test.

I. INTRODUCTION

Many innovative foundation techniques have been devised as a solution to the problem of marine soils. The selection of any one of the techniques is to be done after detailed comparison of all techniques for the well suited technique for the particular system. The various additives used for stabilizing expansive soils are lime, calcium chloride, Rice Husk Ash, fly ash, gypsum, Saw dust and others.

Zhang (2002) undertook an experimental program to study the individual and admixed effects of lime and fly ash on the geotechnical characteristics of soil. They observed reduction in free swell and increase in CBR value. Later on it was observed that lime-fly ash admixtures reduced the water absorption capacity and compressibility of soils.

Phani Kumar and Radhey Sharma (2004) reported that fly ash can be used as an additive in improving the engineering characteristics of soils. They observed the decrease in plasticity and hydraulic conductivity and increase in penetration resistance of blends with increase in fly ash content.

Various remedial measures like soil replacement, pre-wetting, moisture control, chemical stabilization have been practiced with varying degrees of success. Unfortunately the limitations of these techniques questioned their adaptability in all conditions. So work is being done all over, to evolve more effective and practical treatment methods, to alleviate the problems caused to any structures laid on marine clay strata.

Investigation on chemical stabilization (Petry and Armstrong, 1989; Prasada Raju, 2001) revealed that electrolytes like potassium chloride, calcium chloride and ferric chloride may be effectively used in place of conventionally used lime, because of their ready dissolvability in water and supply of adequate cations for ready cation exchange.

II. OBJECTIVES OF THE STUDY

The objectives of the present experimental study are

- To determine the properties of the Marine clay and Rice Husk Ash.
- To evaluate the performance of Marine clay when stabilized with Rice Husk Ash as an admixture and lime as an additive.
- To study the cyclic plate load characteristics of marine clay when stabilized with optimum mix of Rice Husk Ash and lime

III. MATERIAL USED

Marine Clay

The soil used in this study is Marine Clay soil, obtained from Kakinada Sea Ports Limited, Collected at a depth of 1.5m from ground level. Kakinada port is situated on the east coast of India at a latitude of 16° 56' North and longitude of 82° 15' East.

Rice Husk Ash

Locally available Rice Husk Ash was used in the present work.

Lime

Commercial grade lime mainly consisting of 58.67% CaO and 7.4% Silica was used in the study.

Geotextile

PP woven geotextile-GWF-40-220, manufactured by GARWARE –WALL ROPES LTD, Pune, India, was used in this investigation. The tensile strength of woven Geotextile is 60.00kN/m for warp and 45.00kN/m for weft.

Aggregates

Road aggregate of size between 40-20 mm, conforming WBM-III standards was used for the preparation of the base course in the investigation of the modal flexible pavements.

Gravel

For the present investigation, the gravel was collected from Surampalem, East Godavari District, and Andhra Pradesh State, India. The gravel was classified as well graded gravel and was used in this investigation as a gravel cushion on untreated, treated & reinforced marine clay foundation soil bed and also as a sub-base course in all model flexible pavements.

IV. LABORATORY TEST RESULTS

Table1: Variation of OMC and MDD with % variation in RHA

MIX PROPORTION	WATER CONTENT (%)	DRY DENSITY (G/CC)
100% SOIL	36.00	1.270
85%SOIL+15%RHA	27.20	1.430
80%SOIL+20%RHA	27.60	1.480
75%SOIL+25%RHA	29.93	1.486
70%SOIL+30%RHA	27.3	1.430

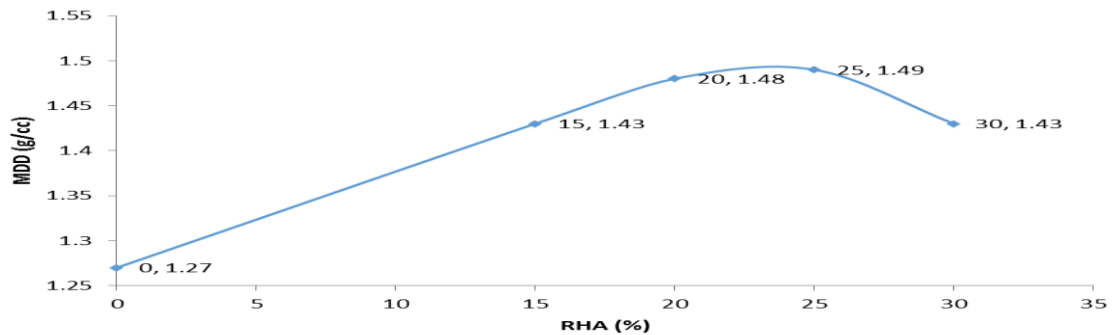


Fig1: Curve showing variation of MDD with % variation of RHA

Table2: variation of soaked CBR values with Rice Husk Ash(%)

MIX PROPORTION	WATER CONTENT (%)	SOAKED CBR
100% SOIL	36.00	1.754
85% SOIL+15% RHA	37.26	2.240
80% SOIL+20% RHA	36.88	2.460
75% SOIL+25% RHA	25.71	8.290
70% SOIL+30% RHA	39.55	2.460

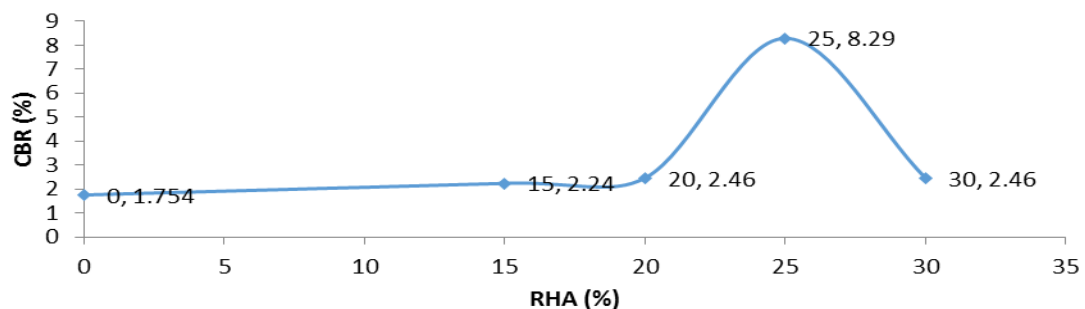


Fig2: CBR Curve with % variation of RHA

Table3: Variation of MDD values with Lime (%)

MIX PROPORTION	WATER CONTENT (%)	MDD (%)
100% SOIL+25% RHA+4% LIME	38.30	1.113
100% SOIL+25% RHA+5% LIME	39.48	1.198
100% SOIL+25% RHA+6% LIME	37.48	1.311
100% SOIL+25% RHA+7% LIME	22.68	1.401
100% SOIL+25% RHA+8% LIME	21.03	1.421
100%SOIL+25%RHA+9%LIME	20.65	1.432
100% SOIL+25% RHA+10% LIME	19.96	1.412

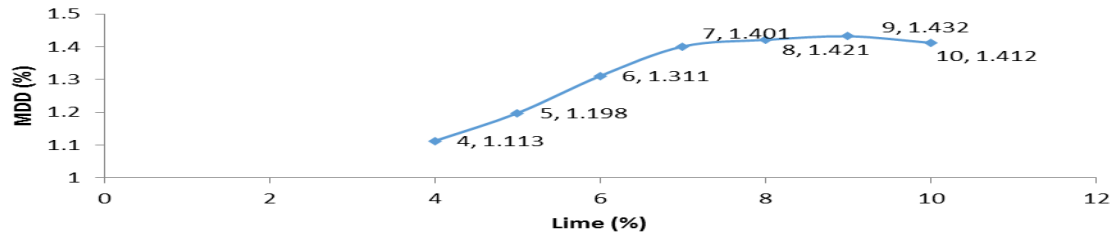


Fig3: Curve showing MDD values with % variation of Lime

Table4: Variation of CBR values of MC+RHA+ Lime

(75%MC+25%RHA+)	WATER CONTENT (%)	SOAKED CBR
4%LIME	38.3	3.126
5%LIME	39.48	3.136
6%LIME	37.48	4.256
7%LIME	22.68	5.384
8%LIME	21.03	6.136
9%LIME	20.65	9.632
10%LIME	19.96	6.272

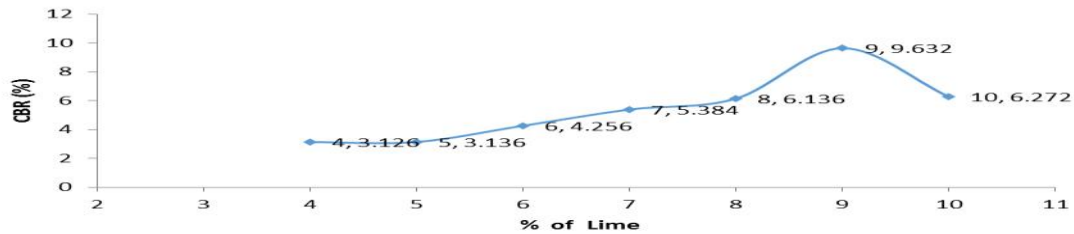


Fig4: Curve showing CBR values with % variation of lime

V. PLATE LOAD TEST RESULTS

LABORATORY CYCLIC PLATE LOAD TESTS ON UNTREATED AND TREATED MARINE CLAY SUBGRADE FLEXIBLE PAVEMENTS USING MODEL TANKS

Cyclic Plate Load Test

Plate Load Test is a field test for determining the ultimate load carrying capacity of soil and the maximum settlement under an applied load. The plate load test basically consists of loading a steel plate placed at the foundation level and recording the settlements corresponding to each load increment. The load applied is gradually increased till the plate starts to sink at a rapid rate. The total value of load on the plate in such a stage divided by the area of the steel plate gives the value of the ultimate bearing capacity of soil. The ultimate bearing capacity is divided by suitable factor of safety (which ranges from 2 to 3) to arrive at the value of safe load capacity of soil.

Cyclic plate load tests were carried out on untreated and treated marine clay flexible pavements in separate model tanks and the woven Geo-textile was used as reinforcement & separator between the treated marine clay subgrade & gravel sub-base and also between the sub base & the base course of model flexible pavement under pressures, viz 500kPa, 560kPa, 630kPa, 700kPa and 1000kPa. The tests were conducted until the failure of the marine clay model flexible pavements at OMC and FSC and the results were given in the Fig5 to Fig8 and Table5.

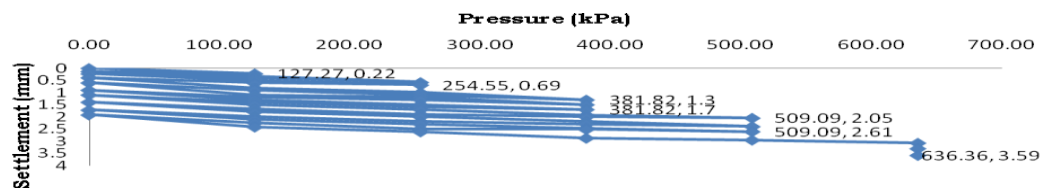


Fig.5 Laboratory Cyclic Plate Load Test results of Untreated Marine Clay Model Flexible Pavement at OMC

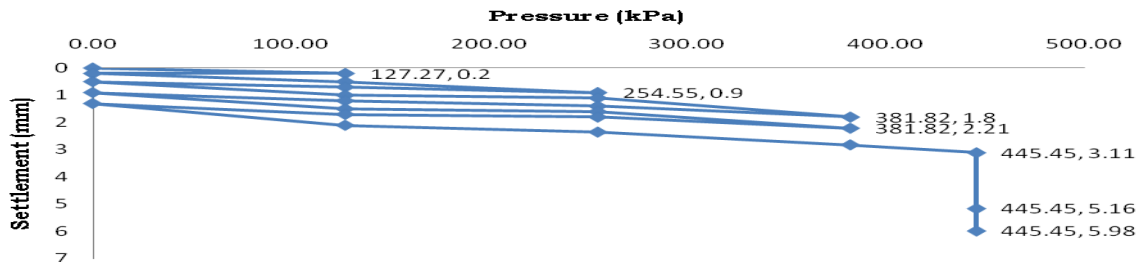


Fig.6 Laboratory Cyclic Plate Load Test results of Untreated Marine Clay Model Flexible Pavement at FSC

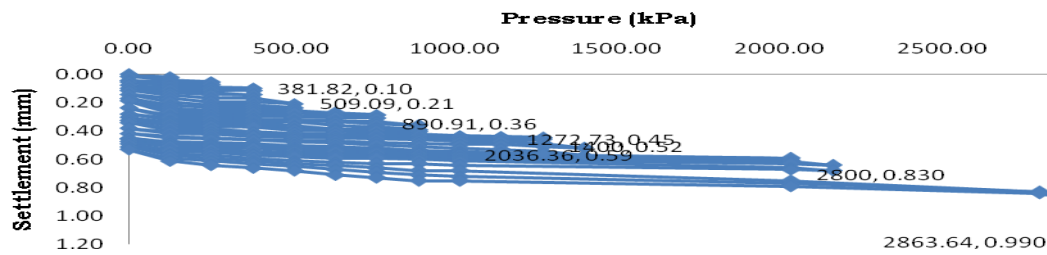


Fig7: Laboratory Cyclic Plate Load Test results of '25% RHA + 9% Lime+ Double Geo textile reinforced Maarine Clay Subgrade Model Flexible Pavement at OMC

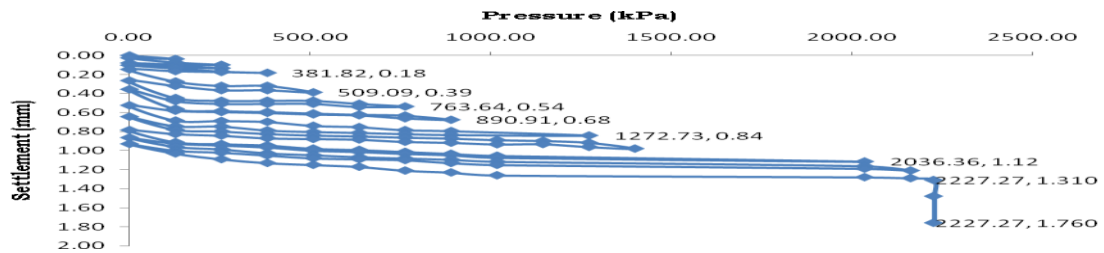


Fig8: Laboratory Cyclic Plate Load Test results of '25% RHA + 9% Lime+ Double Geo textile reinforced Marine Clay Subgrade Model Flexible Pavement at FSC

Table5: Laboratory Cyclic Plate Load test Results of Treated and Untreated Marine Clay Flexible Pavements at OMC & FSC

S. NO	TYPE OF SUBGRADE	SUB-BASE	BASE COURSE	ULTIMATE CYCLIC LOAD (KN/M ²)		SETTLEMENTS (MM)	
				OMC	FSC	OMC	FSC
1	MARINE CLAY	----	-----	63	31	2.75	4.71
2	MARINE CLAY + 15% RHA	-----	-----	190	127	1.9	2.20
UNTREATED AND TREATED MARINE CLAY MODEL FLEXIBLE PAVEMENTS							
3	UNTREATED MARINE CLAY FLEXIBLE PAVEMENT	GRAVEL	WBM-II	509	381	2.52	2.21
4	4%LIME+15% RHA + MARINE CLAY	GRAVEL	WBM-II	1300	900	1.6	2.05
5	4% LIME+ 15% RHA + MARINE CLAY AND GEO-TEXTILE PROVIDED AS REINFORCEMENT & SEPARATOR	GRAVEL	WBM-II	1800	1400	1.80	1.96
6	4% LIME+ 15% RHA + MARINE CLAY AND GEO-TEXTILE PROVIDED AS REINFORCEMENT & SEPARATOR	GRAVEL	WBM-II	2800	2200	0.83	1.21

VI. CONCLUSION

It was noticed from the laboratory investigations of the cyclic plate load test results that, the ultimate load carrying capacity of the treated marine clay model flexible pavement has been increased from 509kPa to 2800kPa at OMC and 381kPa to 2200kPa at FSC when compared with untreated marine clay model flexible pavement.

VII. ACKNOWLEDGEMENTS



Dr. D. Koteswara Rao, Professor of Civil Engineering, University College of Engineering, JNTUK KAKINADA, East Godavari District, Andhra Pradesh, India.



G. Venkatesh, Graduate Student (Civil Engg.)-2012, University College of Engineering, JNTUK KAKINADA, East Godavari District, Andhra Pradesh, India



P.R.T. Pranav, Postgraduate student (2012-14) (Geotechnical Engineering), National Institute of Technology, Warangal, Andhra Pradesh, India

REFERENCES

Journal Papers:

- [1] Al Quadi LL, Laboratory Evaluation of Geo synthetics Reinforced Pavement Sections, TRR-1739, TRB, 1994, pp. 25-31.
- [2] Al-Omari, R.R and Oraibi, W.K (2000), Cyclic behavior of reinforced expansive clay, Jr. of the Japanese Geotechnical Society of Soils and Foundations, Vol. 40, No. 2; 2000, pp.1-8.
- [3] Al-Rawas, N.M (2000), Effect of curing and temperature on Rice Husk Ash stabilization, Proc. Of Second Australian Conf. on Engineering Materials, Sydney, 1981, pp.611-662
- [4] Ambily, A.P and Gandhi, S.R (2004), Experimental and Theoretical Evaluation of Stone Column in Soft Clay, ICGGE, pp 201-206.
- [5] Anandarajah. A and Chu. J (1997), Laboratory Determination of shear strength parameters for marine clay, Journal of the Institution of Engineers, Singapore, Vol.14, No.3, pp 39-46
- [6] AnandJ.Puppala, Ekarin Wattanasanticharoen and LaureanoR.Hoyos (2003), Ranking of Four Chemical and Mechanical Stabilization Methods to Treat Low-Volume Road Subgrades in Texas, Jr.-Transportation Research Record, Vol. 1819B, 2003, pp. 63-71.
- [7] Arvind Kumar, Baljit Singh Walia and Asheet Bajaj (2007), Influence of Flyash, Polyester Fibers on Compaction and Strength Properties of Expansive Soil, J.Mat in Civil Engineering, ASCE, Vol. 19, Issue. 3, 2007, pp. 242-248
- [8] D. Koteswara Rao (2004), The performance studies on Geo-grid as reinforcement in the flexible pavement construction, IGC-2004
- [9] Chandrasekhar, B.P., PrasadaRaju, G.V.R (1999), Calcium Chloride on Properties of Expansive Soil for Pavement Subgrades, Proc. Of IGC-99, Calcutta, 1999, pp 279-282.
- [10] Rama Rao. R and Satyanarayana P.V.V (2003) "use of RHA, Lime and Gypsum in strengthening sub-grade and sub base in low cost roads" National conference on modern cement concrete and bituminous roads, Vizag PP 374-379.

Books:

- [11] Gopal Ranjan, A.J.R. Rao, a text book on "Fundamentals of soil mechanics."
- [12] Ghassan Abood Habeeb and Hilmi Bin Mahmud (2011), Study on properties of rice husk ash and its use as cement replacement material.
- [13] Desai, I.D. and Oza, B.N (1977), Influence of Anhydrous Calcium Chloride on the Shear Strength of Expansive Soil, Proc. of the 1st

A Study of Periodic Points and Their Stability on a One-Dimensional Chaotic System

Dr. Nabajyoti Das

Assistant Professor, Department of Mathematics Jawaharlal Nehru College, Boko District: Kampur, State: Assam, Country: India

Abstract: This paper highlights three objectives of the quadratic iterator

$$x_{n+1} = F(x_n) = ax_n^2 - bx_n, \quad n = 0, 1, 2, \dots$$

Where $x_n \in [0, 4]$, a and b are tunable parameters. Firstly, by adopting suitable numerical methods and computer programs we evaluate the period-doubling: $1 \rightarrow 2 \rightarrow 4 \rightarrow 8 \rightarrow \dots$ bifurcations, a route from order into chaos. Secondly, we analyze the stability of periodic points. Thirdly, we draw the bifurcation diagram in order to support our period doubling orbits and chaotic region, and some illuminating results are obtained as the measure of chaos.

Key Words: Period-doubling bifurcation/ Periodic orbits / Chaos / Bifurcation diagram/ Stability of periodic points.

2010 Classification: 37 G 15, 37 G 35, 37 C 45

I. Introduction

Period-doubling: $period\ 1 \rightarrow period\ 2 \rightarrow period\ 4 \rightarrow \dots \rightarrow period\ 2^k \rightarrow \dots \rightarrow chaos$

Bifurcations, as a universal route to chaos, is one of the most exciting discoveries of the last few years in the field of nonlinear dynamical systems. This remarkable discovery was made by the theoretical physicist Mitchell J. Feigenbaum in the mid-1970s. The initial universality discovered by Feigenbaum in one-dimensional iterations with the logistic map, $x_{n+1} = \lambda x_n(1 - x_n)$ and the trigonometric sine function, $x_{n+1} = A \sin(\pi x_n)$ has successfully led to discover that large classes of nonlinear systems exhibit transitions to chaos which are universal and quantitatively measurable.

If S be a suitable function space and H , the hyper surface of co-dimension 1 that consists of the maps in S having derivative -1 at the fixed point, then the Feigenbaum universality is closely related to the doubling operator, T acting in S defined by

$$(Tf)(x) = -\alpha f(f(\alpha^{-1}x)), \quad f \in S$$

Where $\alpha = 2.5029078750957\dots$, a universal scaling factor. The principal properties of T that lead to universality are

- (i) T has a fixed point 'g' ;
 - (ii) The linearized transformation $DT(g)$ has only one eigenvalue δ greater than 1 in modulus; here $\delta = 4.6692016091029\dots$
 - (iii) The unstable manifold corresponding to δ intersects the surface H transversally. In
- One dimensional case, these properties have been proved by Lanford [8]. Furthermore, one of his fascinating discoveries is that if a family f presents period doubling bifurcations then there is an infinite sequence $\{b_n\}$ of bifurcation values such that

$$\lim_{n \rightarrow \infty} \frac{b_n - b_{n-1}}{b_{n+1} - b_n} = \delta,$$

Where δ a universal number is already mentioned above. Moreover, his observation suggests that there might be a universal size-scaling in the period doubling sequence designated as the Feigenbaum α value

$$\alpha = \lim_{n \rightarrow \infty} \frac{d_n}{d_{n+1}} = 2.5029\dots$$

Where d_n is the size of the bifurcation pattern of period 2^n just before it gives birth to period 2^{n+1} ? The birth and flowering of the Feigenbaum universality with numerous nonlinear models has motivated our research enterprise [1, 6, 7, 9, and 10].

We now highlight some useful concepts which are absolutely useful for our purpose.

1.1 Discrete dynamical systems

Any C^k ($k \geq 1$) map $E: U \rightarrow \mathbb{R}^n$ on the open set $U \subset \mathbb{R}^n$ defines an n -dimensional **discrete-time** (autonomous) smooth dynamical system by the state equation

$$\bar{x}_{t+1} = E(\bar{x}_t), \quad t = 1, 2, 3, \dots \quad (1.1)$$

Where $\bar{x}_t \in \mathfrak{R}^n$ is the state of the system at time t and E maps \bar{x}_t to the next state \bar{x}_{t+1} . Starting with an initial data \bar{x}_0 , repeated applications (iterates) of E generate a discrete set of points (the orbits) $\{E^t(\bar{x}_0) : t = 0, 1, 2, 3, \dots\}$, where $E^t(\bar{x}) = \underbrace{E \circ E \circ \dots \circ E}_{t \text{ times}}(\bar{x})$ [9].

1.2 Definition: A point $\bar{x}^* \in \mathfrak{R}^n$ is called a **fixed point** of E if $E^m(\bar{x}^*) = \bar{x}^*$, for all $m \in \mathbf{C}$.

1.3 Definition: A point $\bar{x}^* \in \mathfrak{R}^n$ is called a **periodic point** of E if $E^q(\bar{x}^*) = \bar{x}^*$, for some integer $q \geq 1$.

1.4 Definition: The closed set $A \in \mathfrak{R}^n$ is called the attractor of the system $\bar{x}_{t+1} = E(\bar{x}_t)$, if (i) there exists an open set $A_0 \supset A$ such that all trajectories \bar{x}_t of system beginning in A_0 are definite for all $t \geq 0$ and tend to A for $t \rightarrow \infty$, that is, $\text{dist}(\bar{x}_t, A) \rightarrow 0$ for $t \rightarrow \infty$, if $\bar{x}_0 \in A_0$, where $\text{dist}(\bar{x}, A) = \inf_{\bar{y} \in A} \|\bar{x} - \bar{y}\|$ is the distance from the point \bar{x} to the set A , and (ii) no eigensubset of A has this property.

1.5 Definition: A system is called chaotic if it has at least one chaotic attractor.

1.6 Diffeomorphism: Let A and B are open subsets of \mathfrak{R}^n . A map $E : A \rightarrow B$ is said to be a **diffeomorphism** if it is a bijection and both E and E^{-1} are differentiable mapping. E is called a C^k -differentiable if both E and E^{-1} is C^k -maps.

1.7: Stability Theorem: A sufficient condition for a periodic point \bar{x} of period q for a diffeomorphism $E : \mathfrak{R}^n \rightarrow \mathfrak{R}^n$ to be stable is that the eigenvalues of the derivative $DE^q(\bar{x})$ are less than one in absolute value.

Armed with all these ideas and concepts, we now proceed to concentrate to our main aim and objectives

II. Feigenbaum Universality

We consider a one-dimensional map of the interval $x_{n+1} = F(x_n, b) \equiv F(x_n, b)$, where b is a control parameter. We are interested in the maps with quadratic maxima where, as the key system parameter b increases, a stable fixed point gives birth to a stable 2-cycle, which then gives birth to a stable 4-cycle, and so on until at $b = b_\infty$ all cycles of order 2^n are unstable and the invariant set of the map consists of 2^∞ points. Our model belongs to this category.

The condition for a fixed point is that $x^* = F(x^*, b)$ corresponding to a one-cycle. In order to decide the stability of the fixed point, we set $\delta x = x - x^*$ and study the approximate linear map $\delta x_{n+1} = F'(x^*, b)\delta x_n$

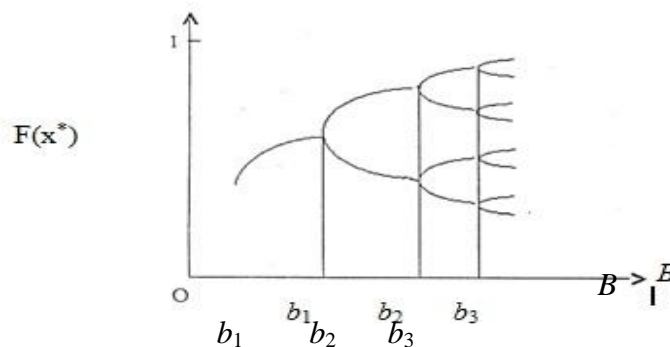


Fig2.1 Feigenbaum tree from order to chaos

Whose solution is? $\delta x_n = F'(x^*, b)^{n-1} \delta x_0$

A fixed point is stable if $|F'(x^*, b)| < 1$ an unstable if $|F'(x^*, b)| > 1$ and the value b_1 where $F'(x^*, b_1) = -1$ signals a bifurcation. After the value $b = b_1$ is passed, the point $x^*(b)$ becomes unstable and there appear around it two points $x_{11}^*(b)$ and $x_{12}^*(b)$ forming a stable periodic trajectory of period-2. The differences

$$\left| x_{11}^*(b) - x^*(b_1) \right| \text{ And } \left| x_{12}^*(b) - x^*(b_1) \right|$$

Are of order $(b - b_1)^{1/2}$ as $(b - b_1) \rightarrow 0$, while $|x^*(b) - x^*(b_1)| = o(b - b_1)$. thus, under period-doubling bifurcations the previously stable fixed point becomes unstable, and a stable periodic trajectory of period-2 appears near it.

As the parameter is further increased, the original fixed point continues to exist as an unstable fixed point, and all the remaining points are attracted towards the stable periodic trajectory of period-2. This happens upto some value $b = b_2$ at which the periodic trajectory of period-2 loses stability in such a way that

$$\left. \frac{dF^2(x, b_1)}{dx} \right|_{x=x_{11}^*} = \left. \frac{dF^2(x, b_2)}{dx} \right|_{x=x_{12}^*} = -1$$

We can then repeat the same arguments and find that the periodic trajectory of period-2 becomes unstable and a periodic trajectory of period-4 appears near it. As b is continuously increased, an infinite sequence $\{b_n\}$ of parameter values emerges such that at $b = b_n$ there is a loss of stability of the periodic trajectory of period 2^{n-1} and a periodic

Trajectory of period 2^n arises. By now, we can imagine what happens when

$$b = b_\infty = \lim_{n \rightarrow \infty} b_n;$$

The map $F(x, b_\infty)$ has an invariant set, say A Cantor's type surrounded by infinitely many unstable periodic trajectories of periods 2^n . Moreover, all the points except those belonging to these unstable trajectories and their inverse images are attracted to A under the action of $F(x, b_\infty)$. Feigenbaum universality in its simplest form means that the sequence $\{b_n\}$ behaves in a universal manner, that is, $b_\infty - b_n \approx C\delta^{-n}$, where the constant C depends on the family F , while δ is the Feigenbaum universal constant. Moreover, the structure of the attractor A , in particular, its Hausdorff dimension, and the behaviour of the iterates F^n in a neighborhood of $b = b_\infty$ do not depend on A [2--5].

III. Feigenbaum δ (delta) to make predictions

One possible and very useful interpretation of the universality of the Feigenbaum constant δ would be by using it for quantitative prediction. At a more practical level, the existence of δ allows us to make quantitative predictions about the behavior of a nonlinear system, even if we cannot solve the equations describing the system. More importantly, this is true even if we do not know what the fundamental equations for the system are, as is often the case. For example, if we observe that a particular system undergoes a period-doubling bifurcation from period-1 to period-2 at a parameter value b_1 , and from period-2 to period-4 at a value b_2 , then we can use δ to predict that the system will make a transition from period-4 to period-8 at b_3 given by

$$b_3 \approx \frac{b_2 - b_1}{\delta} + b_2 \quad (1.1)$$

Observing the first two period-doublings produces no guarantee that a third will occur, but if it does occur, equation (1.1) gives us a reasonable prediction of the parameter value near

Which we should look to see the transitions. Similarly $b_4 \approx \frac{b_3 - b_2}{\delta} + b_3$, and so on [10].

IV. Numerical method for obtaining periodic points

To find a periodic point of our model we apply the Newton-Recurrence formula:

$$x_{n+1} = x_n - \frac{1}{\left[\frac{d}{dx} g(x_n) \right]} g(x_n), \quad \text{where } n = 1, 2, 3, \dots$$

[We later see that this map g equals $F_n I$, where I is the identity function]

The Newton formula actually gives the zero(s) of a map, and to apply this numerical tool, one needs a number of recurrence formulae which are given below:
 Let the initial value of x be x_0 . Then

$$F(x_0) = ax_0^2 - bx_0 = x_1(\text{say}),$$

$$F^2(x_0) = F(F(x_0)) = F(x_1) = ax_1^2 - bx_1 = x_2(\text{say}),$$

Proceeding in this manner, the following recurrence formula can be established:

$$x_n = ax_{n-1}^2 - bx_{n-1}, \quad n = 1, 2, 3, \dots$$

V. Numerical Method for Finding Bifurcation Values

The derivative of F^n can be obtained as follows:

$$\left. \frac{dF}{dx} \right|_{x=x_0} = 2ax_0 - b$$

Again, by the chain rule of differentiation we get

$$\left. \frac{d(F^2)}{dx} \right|_{x=x_0} = \left. \frac{dF}{dx} \right|_{F(x_0)} \left. \frac{dF}{dx} \right|_{x=x_0} = (2ax_1 - b)(2ax_0 - b), \quad \text{where } x_1 = F(x_0)$$

Proceeding in this way we can obtain

$$\left. \frac{d(F^n)}{dx} \right|_{x=x_0} = (2ax_{n-1} - b) \dots (2ax_0 - b)$$

We recall that the value of b will be the bifurcation value for the map F^n when its derivative $\frac{d(F^n)}{dx}$ at a periodic point equals -1 . Also the Feigenbaum theory says that

$$b_{n+2} \approx b_{n+1} + \frac{b_{n+1} - b_n}{\delta}, \quad \text{where } n = 1, 2, 3, \dots \quad (1.2)$$

and δ is the Feigenbaum universal constant. We notice that if we put

$$I = \frac{dF^n}{dx} + 1,$$

Then I turn out to be a function of the parameter b . The bifurcation value of the parameter b of the period n occurs when $I(b)$ equals zero. This means, in order to find a bifurcation value of period n , one needs the zero of the function $I(b)$, which is given by the Secant method, applied to the function $I(b)$ which is given by

$$b_{n+1} = b_n - \frac{I(b_n)(b_n - b_{n-1})}{I(b_n) - I(b_{n-1})} \quad (1.3)$$

This method depends very sensitively on the initial condition.

VI. Our model and associated universal results

Our concerned model is

$$F(x) = ax^2 - bx \quad (1.4)$$

Where $x \in [0, 4]$, a and b are tunable parameters. To find points of period-one, it is necessary to solve the equation given by $F(x) = x$ which gives the points that satisfy the condition $x_{n+1} = x_n$ for all n . The solutions are $x_1^* = 0$ and $x_2^* = (1+b)/a$. If we fix $a = -1$, the function F is maximum at $x = -b/2$ and its maximum value equals $b^2/4$. Taking this as 4, we have $b = \pm 4$. We again fix $b \in [-4, -1]$ for our purpose. In this case, the fixed points of F are the intersection of the graphs of $y = F(x)$ and $y = x$.

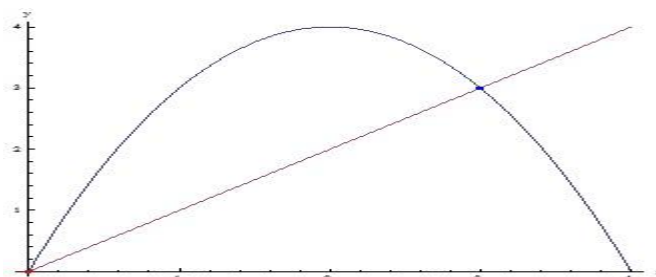


Figure 1.1 Graphs of $y = F(x)$ and $y = x$ for $b = -4$

The periodic points x_1^* (Red) and x_2^* (Blue) are shown in the figure (1.1). The stability of the critical points may be determined using the following theorem:

Using stability theorem, we have $\left| \frac{d}{dx} F(x_1^*) \right| = |-b| > 1$. Thus the fixed point $x_1^* = 0$ is always unstable for all $b \in [-4, -1[$ and $\left| \frac{d}{dx} F(x_2^*) \right| = |b+2|$, the point $x_2^* = -1-b$ stable for $-3 < b < -1$. For example, if we take the parameter value $b = -2.9$, then the orbit generated by the initial point $x_0 = 1.5$ attracted to the fixed point $x_2^* = 1.9$ in the figure 1.2.

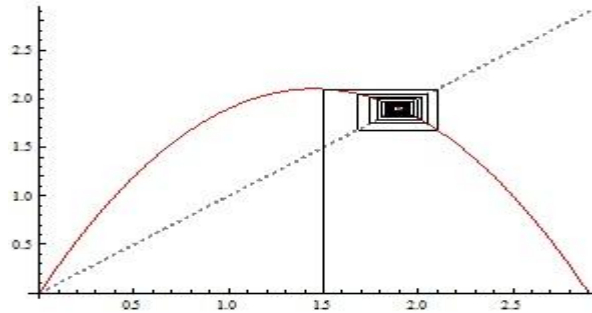


Figure 1.2 Staircase for the initial point $x_0 = 1.5$ and parameter $b = -2.9$

Having studied the dynamics of the quadratic iterator F in detail for parameter values between -1 and -3, we continue to decrease b beyond -3. For such small parameter values the fixed point x_2^* is not stable anymore, it is unstable. Hence, the **first bifurcation value** is $b_1 = -3$. To find points of period 2, we consider the iterated map $F^2(x)$. Here,

$$F^2(x) = -b(-bx - x^2) - (-bx + x^2)^2$$

The periodic points of $F^2(x)$ are given by the equation

$$F^2(x) = x \quad (1.5)$$

Which gives $x = x_1^*, x_2^*, x_{11}^*, x_{12}^*$, where

$$x_1^* = 0, x_2^* = -1-b, x_{11}^* = 1/2(1-b-\sqrt{-3+2b+b^2}), x_{12}^* = 1/2(1-b+\sqrt{-3+2b+b^2})$$

These four points are the intersection of the graphs of $y = F^2(x)$ and $y = x$, in the figure 1.3. The periodic points x_1^*, x_2^*, x_{11}^* and x_{12}^* are marked as A1, A2, B1 and B2.

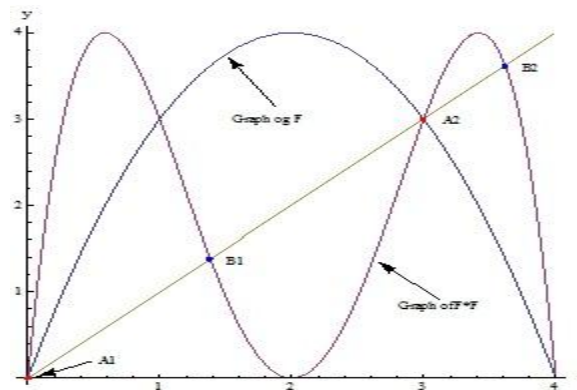


Figure 1.3 Graphs of $y = F^2(x)$ and $y = x$ for $b = -4$

Stability of the first two fixed points is already discussed. Let us discuss the stability of the new points: x_{11}^* and x_{12}^* . We

note that these new solutions are defined only for $b \leq -3$. Moreover, at $b = -3$, $x_{11}^* = x_{12}^* = \frac{1}{2}(1-b)$, i.e., these two

solutions bifurcate from the fixed point x_2^* . The points x_{11}^* and x_{12}^* form a two-cycle, one being the image of the other.

Thus, at parameter $b = -3$, our map orbits undergo period-doubling bifurcations. Just above $b = -3$ the orbits converge to a single value of x . Just below $b = -3$, the orbits tend to this alternation between two values of x .

Let us see how the derivatives of the map function $F(x)$ and of the second iterate function $F^2(x)$ change at the bifurcation value. The equation:

$$\left. \frac{dF(x)}{dx} \right|_{x=x_2^*} = b + 2 \quad (1.6)$$

tells us that function $\frac{dF(x)}{dx}$ passes through the value -1 as b decreases through -3. Next we can evaluate the derivative of the second iterate function by using the chain-rule of differentiation:

$$\frac{dF^2(x)}{dx} = \frac{d}{dx}[F(F(x))] = \left. \frac{dF}{dx} \right|_{F(x)} \left. \frac{dF}{dx} \right|_x$$

If we now evaluate the derivative at one of the above two new fixed points, say x_{11}^* , then we find

$$\left. \frac{dF^2(x)}{dx} \right|_{x_{11}^*} = \left. \frac{dF}{dx} \right|_{x_{12}^*} \left. \frac{dF}{dx} \right|_{x_{11}^*} = \left. \frac{dF^2(x)}{dx} \right|_{x_{12}^*} \quad (1.7)$$

In arriving at the last result, we made use of $x_{12}^* = F(x_{11}^*)$ for the two fixed points. Equation (1.7) states a rather surprising and important result—

The derivative of $F^2(x)$ are the same at both the fixed points that are actually part of the two-cycle. This result implies that both of these fixed points are either attracting or both are repelling, and that they have the same ‘degree’ of stability or instability. Again, since the derivative of $F(x)$ equals -1 for the parameter $b = -3$, equation (1.7) tells us that the derivative of $F^2(x)$ equals +1 for $b = -3$. As b decreases further, the derivative of $F^2(x)$ increases and the fixed points become stable. Besides, the unstable fixed point of $F(x)$ located at x_2^* is also an unstable fixed point of $F^2(x)$.

The 2-cycle fixed points of $F^2(x)$ continue to be stable fixed points until parameter value $b_2 = -3.449489742783...$ we have values of x_{11}^* and x_{12}^* as 1.5176380902051063.... and 2.931851652577893.... respectively at $b_2 = -3.449489742783...$ Also for this value of b

$$\left. \frac{dF^2(x)}{dx} \right|_{x=1.5176380902051063..} = -1, \quad \left. \frac{dF^2(x)}{dx} \right|_{x=2.931851652577893...} = -1$$

The above results guarantee that if a system is stable or unstable at a periodic point, then the system is so at any other periodic point. So our study will be completed if we study the dynamics at any of the periodic points. We can find that for values of b smaller than b_2 , the derivative is more negative than -1. Hence for b values smaller than b_2 , the 2-cycle points are repelling fixed points. We find that for values just smaller than b_2 , the orbits settle into a 4-cycle, that is, the orbit cycles among 4 values which we can label as

$$x_{21}^*, x_{22}^*, x_{23}^*, x_{24}^*.$$

These points are nothing but the intersection of the graphs of $y = F^4(x)$ and $y = x$. To determine these periodic points analytically, we need to solve an eight degree equation, namely $F^4(x) = x$ which is manually cumbersome and time consuming. Therefore, for finding periodic points, bifurcation values of F^4 as well as for higher iterated map functions, we have to write a computer program. We write here a C-program for our purpose.

Using the relation (1.2), an approximate value b_3' of b is obtained. Since the Second method needs two initial values, we use b_3 and a slightly large value, say $b_3 + 10^{-4}$ as the two initial values to apply this method and ultimately obtain b_3 . In the like manner, the same procedure is employed to obtain the successive bifurcation values b_4, b_5 , etc. to our requirement. Through our numerical mechanism, we obtain some periodic points and bifurcation values. In the Table 1.1 Period doubling cascades are shown:

VII. Period doubling cascade

Table 1.1

Period	One of the Periodic points	Bifurcation Points.
1	$x_1 = 2.000000000000...$	$b_1 = -3.000000000000...$
2	$x_2 = 1.517638090205...$	$b_2 = -3.449489742783...$
4	$x_3 = 2.905392825125...$	$b_3 = -3.544090359552...$
8	$x_4 = 3.138826940664...$	$b_4 = -3.564407266095...$
16	$x_5 = 1.241736888630...$	$b_5 = -3.568759419544...$
32	$x_6 = 3.178136193507...$	$b_6 = -3.569691609801...$
64	$x_7 = 3.178152098553...$	$b_7 = -3.569891259378...$
128	$x_8 = 3.178158223315...$	$b_8 = -3.569934018374...$
256	$x_9 = 3.178160120824...$	$b_9 = -3.569943176048...$
512	$x_{10} = 1.696110052289...$	$b_{10} = -3.569945137342...$
1024	$x_{11} = 1.696240778303...$	$b_{11} = -3.569945557391...$
...

Based on these values, the ratios of successive separations of bifurcation points are given by,

$$\frac{b_2 - b_1}{b_3 - b_2} \approx \frac{b_3 - b_2}{b_4 - b_3} \approx \frac{b_4 - b_3}{b_5 - b_4} \approx \frac{b_5 - b_4}{b_6 - b_5} \approx \frac{b_6 - b_5}{b_7 - b_6} \approx \dots \approx \frac{b_k - b_{k-1}}{b_{k+1} - b_k}$$

And have a particular scaling associated with them. We see that

$$\begin{aligned} \delta_1 &= \frac{b_2 - b_1}{b_3 - b_2} = 4.751446218163496..., & \delta_2 &= \frac{b_3 - b_2}{b_4 - b_3} = 4.65625101778075..., \\ \delta_3 &= \frac{b_4 - b_3}{b_5 - b_4} = 4.66824223480187..., & \delta_4 &= \frac{b_5 - b_4}{b_6 - b_5} = 4.668773947278035..., \\ \delta_5 &= \frac{b_6 - b_5}{b_7 - b_6} = 4.66913201146184..., & \delta_6 &= \frac{b_7 - b_6}{b_8 - b_7} = 4.66918299485741..., \\ \delta_7 &= \frac{b_8 - b_7}{b_9 - b_8} = 4.66919831388462..., & \delta_8 &= \frac{b_9 - b_8}{b_{10} - b_9} = 4.66920002791641..., \\ \delta_9 &= \frac{b_{10} - b_9}{b_{11} - b_{10}} = 4.66920287863952..., & & \text{And so on.} \end{aligned}$$

The ratios tend to a constant as k tends to infinity: more formally

$$\lim_{k \rightarrow \infty} \left[\frac{b_k - b_{k-1}}{b_{k+1} - b_k} \right] = \delta = 4.669201...$$

The nature of δ is universal i.e. it is the same for a wide range of different iterators

VIII. Bifurcation diagram

The different behaviors of a system for different values of the parameter can be qualitatively analyzed by using a bifurcation diagram, which is created by plotting the asymptotic orbits of the maps (y axis) generated for different values of the parameter (x axis). A bifurcation diagram is essentially a diagram of attractors, because almost all initial points are attracted to the points shown in the figure of our model, provided a sufficient

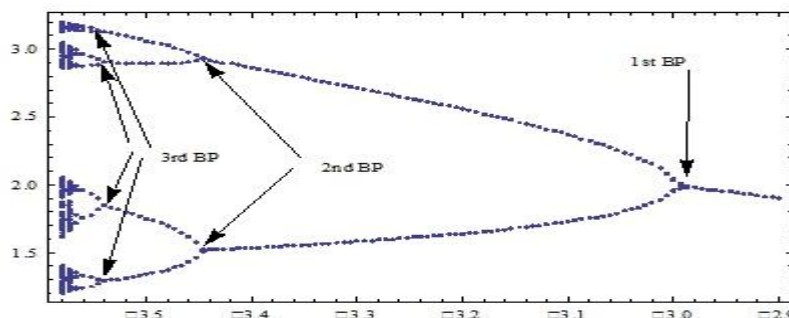


Figure 1.4 Bifurcation diagram for b in the range $-3.6 \leq b \leq -2.9$

Numbers of transients have been thrown away [9, 10]. Fixed points and periodic points are trivial attractor, while the darkened vertical segments are chaotic attractors. Just beyond $b = -3.96995$ (approx) the system becomes chaotic. However, the system is not chaotic for all parameter values b smaller than -3.56995 (approx). If we zoom into the details of the bifurcation diagram by changing to smaller and smaller scales both in x and in b , we see that within the chaotic region, there are many *periodic windows*, that is, lucid intervals where only periodic orbits exist instead of chaotic output.

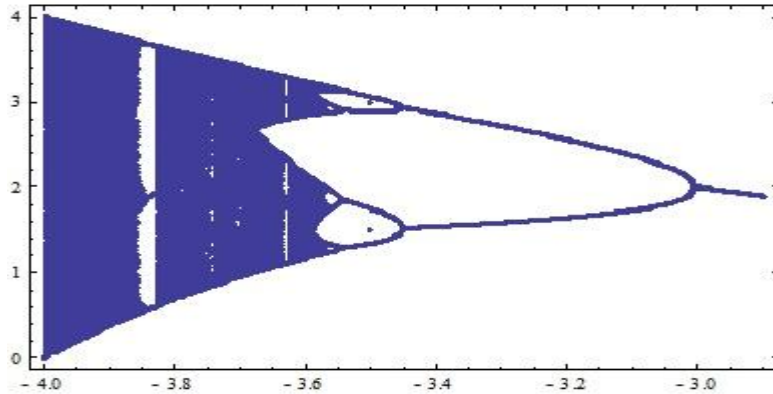


Figure 1.5 Bifurcation diagram for b in the range $-4.0 \leq b \leq -2.9$

IX. Conclusion

The study of chaos in population models is quite interesting. Although there are so many methods for finding bifurcation values, we have developed own numerical mechanism for establishing Feigenbaum tree of bifurcation values leading to chaotic region the study of which is intrinsically marvelous. Our method seems to be applicable to all the chaotic models.

X. Acknowledgement:

I am grateful to **Dr. Tarini Kumar Dutta**, Senior Professor of the Department of Mathematics, Gauhati University, Assam: India, for a valuable suggestion for the improvement of this research paper.

References

- [1] Deveney R.L. "An introduction to chaotic dynamical systems", Addison-Wiseley Publishing Company, Inc
- [2] Davie A. M. and Dutta T. K., "Period-doubling in Two-Parameter Families," Physica D, 64,345-354, (1993).
- [3] Das, N. and Dutta, N., "Time series analysis and Lyapunov exponents for a fifth degree chaotic map", Far East Journal of Dynamical Systems Vol. 14, No. 2, pp 125-140, 2010
- [4] Das, N., Sharmah, R. and Dutta, N., "Period doubling bifurcation and associated universal properties in the Verhulst population model", International J. of Math. Sci. & Engg. Appls. , Vol. 4 No. I (March 2010), pp. 1-14
- [5] Dutta T. K. and Das, N., "Period Doubling Route to Chaos in a Two-Dimensional Discrete Map", Global Journal of Dynamical Systems and Applications, Vol.1, No. 1, pp. 61-72, 2001
- [6] Feigenbaum .J M, "Quantitative Universality for Nonlinear Transformations" Journal of Statistical Physics, Vol. 19, No. 1, 1978.
- [7] G. Chen and X. Dong, From Chaos to Order: Methodologies, Perspectives and Applications, World Scientific, 1998
- [8] Lanford III O. E., "A Computer-Assisted Proof of the Feigenbaum Conjectures", Bull.Am.Math.Soc. 6, 427-34 (1982)
- [9] Peitgen H. O., Jurgens H... and Saupe D., "Chaos and Fractal", New Frontiers of Science, Springer Verlag, 1992,
- [10] Hilborn R. C "Chaos and Nonlinear Dynamics", second edition, Oxford University Press, 1994
- [11] Sandri M., Numerical calculation of Lyapunov Exponents, University of Verona, Italy.

Examination of Surface Roughness Using Different Machining Parameter in EDM

Harpreet Singh,¹ Amandeep Singh²

¹(Department of mechanical engg YOCE Talwandi sabbo)

²(Department of mechanical engg FCET Ferozepur)

ABSTRACT: Electrical discharge machining (EDM) is one of the important non-traditional machining processes and it is widely accepted as a standard machining process in the manufacture of forming tools to produce molds and dies. Since its introduction to manufacturing industry in late 1940s, EDM became a well-known machining method. The method is based on removing material from a work piece by means of a series of repeated electrical discharges, produced by electric pulse generators at short intervals, between an electrode (tool) and a part being machined in dielectric fluid medium. This paper describes the effect of different materials on surface roughness produced. Paper helps in choosing right type of electrode material for specific purpose.

Keyword: Current, EDM, surface roughness.

I. INTRODUCTION

Electric discharge machining (EDM) is one of the most popular non-traditional material removal processes and has become a basic machining method for the manufacturing industries of aerospace, automotive, nuclear, medical and die-mold production. The theory of the process was established by two Soviet scientists B.R. and N.I. Lazarenko in the middle of 1940s. They invented the relaxation circuit and a simple servo controller tool that helped to maintain the gap width between the tool and the profitable and produced first EDM machine in 1950s.

Major development of EDM was observed when computer numerical control systems were applied for the machine tool industry. Thus, the EDM process became automatic and unattended machining method [1]. The process uses thermal energy to generate heat that melts and vaporizes the work piece by ionization within the dielectric medium. The electrical discharges generate impulsive pressure by dielectric explosion to remove the melted material. Thus, the amount of removed material can be effectively controlled to produce complex and precise machine components. However, the melted material is flushed away incompletely and the remaining material resolidifies to form discharge craters. As a result, machined surface has micro cracks and pores caused by high temperature gradient which reduces surface finish quality there have been many published studies considering surface finish of machined materials by EDM. It was noticed that various machining parameters influenced surface roughness and setting possible combination of these parameters was difficult to produce optimum surface quality. The influences of some machining parameters such as pulsed current [2-9], pulse time [2-6,8,9], pulse pause time [2,5,9], voltage [4,6], dielectric liquid pressure [4,6,8,10] and electrode material [11] have been examined. The

present study examines the effects of current, and electrode material on surface roughness in the AISI D3 tool steel.

II. EXPERIMENTAL PROCEDURES

The experimental study was carried out on CNC EDM machine as shown in Fig. 3.1 available at central tool room, Ludhiana. The machine is manufactured by electrical machine tool limited, Pune. This machine is completely computerized. This machine performs its function automatically after the required parameters are entered in the program. The control panels of CNC EDM having following components like graphical desktop, keyboard, voltmeter and ammeter. In this machine a mild steel tank is used in which the dielectric fluid flow. The tank was sufficiently filled with the dielectric fluid (Kerosene oil).

The work piece was held in the fixture assembly and the electrode was held in the clamping device. Fig 1 is showing electric discharge machine available at central tool room Ludhiana.



Fig1. CNC EDM Machine (CTR Ludhiana)

Each experiment was performed for fix time period of 20 min using the input process parameters as shown in Table 3.5 using four different types of electrodes i.e. Cu, cryogenic treated Cu, Br and cryogenic treated Br.

A cylindrical pure copper with a diameter of 22mm was used as an electrode. Table 1 is showing the Input process parameters of EDM

Table 1. Input process parameters of EDM

Supply voltage	110V
Working time	20minutes
Total size	16mm
Tool material	Copper, Brass, Cryogenic copper, cryogenic Brass
Work material	H13 Di-Steel
Current	4A,8A

III. EXPERIMENTAL RESULTS AND DISCUSSION

First part of the experimental study carried out for machined workpiece surface finish quality.

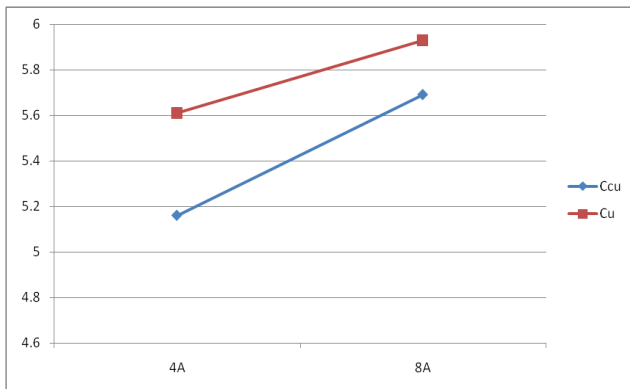


Fig1. Surface roughness of cryogenic treated copper electrode and copper electrode

The SR produced by using four different types of electrodes is shown in the Fig. 4.2. It is observed that the brass electrode gives the better surface finish as compare to the copper electrode. Among the brass electrode and cryogenic treated brass electrode, the cryogenic treated brass electrode has given better surface finish. This may be due to fact that cryogenic treatment of the brass resulted in improving the thermal conductivity [12]. Due to which heat generated at the tool work piece interface gets dissipated at a faster rate. This results in lowering the value of heat at the tool electrode interface, which further resulted in producing small creators on the work piece surface, as a rest of which better surface is produced. Among the copper and cryogenic treated copper electrode the cryogenic treated electrode has given better surface finish. The reason for this is same as that for the brass electrode

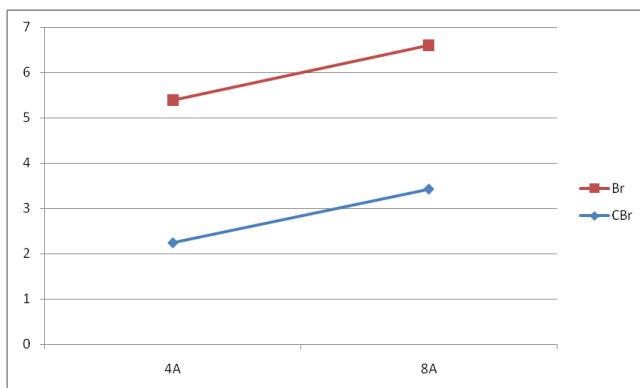


Fig2. Surface roughness of cryogenic treated Brass electrode and Brass electrode

Surface roughness results were noticed for electrode surface roughness. It was observed that the surface roughness of electrode was better when applying smaller pulsed current and pulse time. When pulsed current and pulse time increased, electrode surface presented a higher surface roughness. Pulsed current had an effect on surface roughness of electrode at low pulse time, but the influence of pulse time was more significant than pulsed

current at higher pulse times. The effect of pulse pause time was insignificant.

IV. CONCLUSION

- Surface roughness increased with increasing pulsed current and pulse time
- Increasing wear on electrode surface is unavoidable during EDM process. Therefore, work piece surface roughness will be increasing due to wear rate on electrode.
- Wear on electrode surface is unavoidable during EDM process. Surface roughness of machined work piece would increase when surface quality of electrode decreases due to pulsed current density.

V. ACKNOWLEDGEMENTS

Authors would like to thank central tool room, ludhiana. for kind encouragement and technical support. They are also thankful to Mech.Engg department YOCE Talwandi saboo and FCET ferozshah for his sincere help throughout this research.

REFERENCES

- [1] K.H. Ho, S.T. Newman, State of the art electrical discharge machining (EDM), Int. J. Mach. Tools Manuf. 43 (2003) 1287–1300.
- [2] P.V. Ramarao, M.A. Faruqi, Characteristics of the surfaces obtained in electro-discharge machining, Prec. Eng. 4 (1982) 111–113.
- [3] C.C. Wang, B.H. Yan, H.M. Chow, Y. Suzuki, Cutting austempered ductile iron using an EDM sinker, J. Mater. Process. Technol. 88 (1999) 83–89.
- [4] S.H. Lee, X.P. Li, Study of the effect of machining parameters on the machining characteristics in electrical discharge machining of tungsten carbide, J. Mater. Process. Technol. 115 (2001) 344–358.
- [5] H.S. Halkacı, A. Erden, Experimental investigation of surface roughness in electric discharge machining (EDM), in: Proceedings of the 6th Biennial Conference (ESDA 2002), Istanbul, Turkey, 2002, pp. 1–6.
- [6] S.H. Lee, X. Li, Study of the surface integrity of the machined workpiece in the EDM of tungsten carbide, J. Mater. Process. Technol. 139 (2003) 315–321.
- [7] Y.H. Guu, H. Hocheng, C.Y. Chou, C.S. Deng, Effect of electrical discharge machining on surface characteristics and machining damage of AISI D2 tool steel, Mater. Sci. Eng. A 358 (2003) 37–43.
- [8] C. C. og'un, B. Kocabas., A. O' zgedik, Experimental and theoretical investigation of workpiece surface roughness profile in EDM, J. Fac. Eng. Arch. 19 (2004) 97–106 (in Turkish).
- [9] Y. Keskin, H.S. Halkacı, M. Kızıl, An experimental study for determination of the effects of machining parameters on surface roughness in electrical discharge machining (EDM), Int. J. Adv. Manuf. Tech. 28 (2006) 1118–1121.
- [10] A. O' zgedik, C. C. og'un, An experimental investigation of tool wear in electric discharge machining, Int. J. Adv. Manuf. Tech. 27 (2006) 488–500.
- [11] S. Singh, S. Maheshwari, P.C. Pandey, Some investigations into the electric discharge machining of hardened tool steel using different electrode materials, J. Mater. Process. Technol. 149 (2004) 272–277.
- [12] Zhisheng, W., Ping, S., Jinrui, L., Shengsun, H., 2003. Effect of deep cryogenic treatment on electrode life and microstructure for spot welding hot dip galvanized steel. Mater. Des. 24, 687–692.

Computer-Aided Optimal Design and Finite Element Analysis of a Plain Milling Cutter

K. Lalitha Babu¹, M. Kumara Swamy²

¹PG student, Department of Mechanical Engineering, University College of engineering

²Department of Mechanical Engineering, University College of engineering, JNTUK- Kakinada, A.P, INDIA

Abstract: Plain Milling is one of the progressive enhancements of miniaturized technologies which have wide range of application in industries and other related areas. Plain milling cutters are widely used in roughing and finishing of parts. The milling cutter geometry and distribution of inserts on the cutter body vary significantly in industry depending on the application. This paper presents a generalized mathematical model of plain milling cutter for the purpose of predicting cutting forces, dimensional surface finish, stress, and strain. A sample of plain milling cutter modeling and analysis examples are obtained by using the design and analysis is carried out using the software's like CATIA V5 and ANSYS.

Milling like any metal cutting operation is used with an objective of optimizing surface roughness at micro level and economic performance at macro level. In addition to surface finish, modern manufacturers do not want any compromise on the achievement of high quality, dimensional accuracy, high production rate, minimum wear on the cutting tools, cost saving and increase of the performance of the product with minimum environmental hazards. In this Paper the design aspects of plain milling cutter is analyzed. The objective considered is the design and modeling of plain milling cutter and to analyse various stress components acting on it. Various designing strategies are considered to design the effective plain milling cutter like outer diameter, inner diameter, radius, teeth angle etc.

Keywords: ANSYS, CATIA, Cutter, High Speed Steel, Plain Milling, Speed

I. Introduction

Modeling and simulation of machining processes is a critical step in the realization of high quality machined parts. To precisely simulate the machining operations, accurate models of cutting tools used in the machining processes are required. In metal cutting industry, a plain mill cutter plays an important role for obtaining the desired shape and size of a component. [1]. A variety of helical end mill cutters are used in the industry. Helical cylindrical, helical slab, taper helical and special purpose plain mills are widely used in aerospace, automotive and die machining industries. The analysis of the geometry of the tool surfaces and cutting flutes along with the cutting forces acting on the plain mill plays an important part in the design of the plain mill and the quality of the manufacturing process. Traditionally, the geometry of cutting tools has been defined using the principles of projective geometry. Constantly growing competition between all manufacturers on the global market leads, among the others, to important requirements concerning improving both machining accuracy and economic efficiency of manufacturing [2] this competition is very intense in the case of various products in aviation industry.

II. Milling cutters

Classification of milling cutters according to their design, HSS cutters like end mills, slitting cutters, slab cutters, angular cutters, form cutters and many cutters are made from high-speed steel (HSS)[8]. Brazed cutters are Very limited numbers of cutters (mainly face mills) are made with brazed carbide inserts. This design is largely replaced by mechanically attached cutters. Mechanically attached cutters are the vast majority of cutters in this category [3]. Carbide inserts are either clamped or pin locked to the body of the milling cutter. Basically, milling operations are divided into to peripheral milling, Face milling and Plain milling. The End milling process is widely used in industry because of versatility and effectiveness.

[4] The plain Mill has edges in the side surface and the bottom surface. During the operation in plain milling, vibration is considered to be one of the most important while machining. Three different types of mechanical vibrations such as free vibrations, forced vibrations and self-excited vibrations that arise due to the lack of dynamic stiffness, stability of the machine parts, vibrations generated under unsuitable cutting conditions creates serious problem as it causes excessive tool wear, noise, tool breakage, and deterioration of the surface quality. The milling cutter is a multiple point cutting tool. The cutting edge may be straight or in the form of various contours that are to be reproduced upon the work piece. The relative motion between the work piece and the cutter may be either axial or normal to the tool axis. In some cases a combination of the two motions is used. [5] For example, form-generating milling cutters involve a combination of linear travel and rotary motion. The figure below shows the various angles and geometry of a milling cutter.

2.1 Types of milling operations:

Owing to the variety of shapes possible and its high production rates, milling is one of the most versatile and widely used machining operations. The geometric form created by milling fall into three major groups:

- Plane surfaces: the surface is linear in all three dimensions. The simplest and most convenient type of surface;
- Two-dimensional surfaces: the shape of the surface changes in the direction of two of the axes and is linear along the third axis. Examples include cams;

- Three-dimensional surfaces: the shape of the surface changes in all three directions. Examples include die cavities, gas turbine blades, propellers, casting patterns, etc. [6]

All of these classifications can have either a vertical or horizontal spindle configuration.

2.2 Plain milling cutter Nomenclature:

The nomenclature of a plain milling cutter is shown in the figure (1).

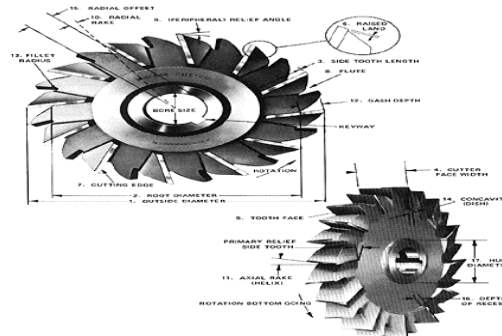


Figure 1: Nomenclature of plain milling cutter

III. Finite Element Analysis of Plain milling cutter

In order to perform a finite element analysis, it is necessary to determine the forces acting on the cutter. From the given conditions the force acting on the cutter (W) may be calculated as:

$$W = \frac{60,000H}{\pi Dn} \quad \text{- Equation (1)}$$

where H is the power, in kW, n is the speed, in rpm, and D is the diameter of the cutter. The stress calculation at the tip of the tooth of the cutter is estimated based on the concept of gear tooth stresses. The stress at each speed is determined by [7]:

$$\sigma = \frac{6Wl}{Ft^2} \quad \text{- Equation (2)}$$

The maximum allowable stress at the tip of the cutter is determined as:

$$\sigma_{\text{allowable}} = \frac{S_t K_L}{K_T K_R} \quad \text{-Equation (3)}$$

S_t (AGMA bending strength) = 44,000 psi

K_R (reliability factor) = 1

Whereas: K_L (life factor) = 1

IV. Dimensions of a Plain Milling Cutter:

The various dimensions chosen for the cutter are shown in figure (2)

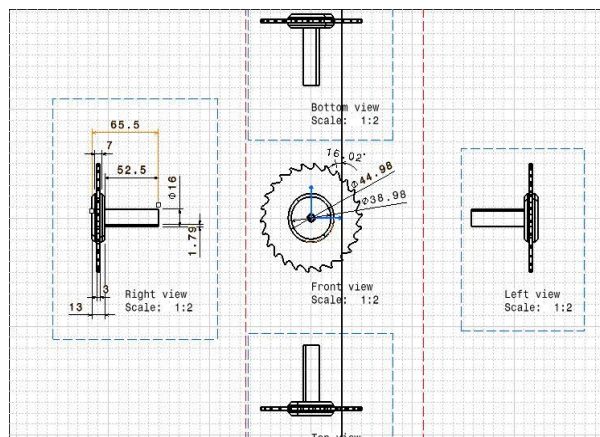


Figure 2: Dimensions of Plain milling cutter

V. Material Properties:

High Speed steel is the material chosen for the milling cutter and the properties are tabulated in Table 1:

Tensile strength (Mpa)	900/1000
Young Modulus E (Mpa)	200000/210000
Compressive Strength(Mpa)	3000/3200
Ductility(compression) %	8/10
Thermal Expansion $^{\circ}\text{C}$	11.5/11.8
Thermal Conductivity(W/m k)	17/18
Specific Heat (J/Kg K)	500/540

Table 1: Properties of High speed Steel milling cutter

From the above data plain milling cutter is designed using CATIA and then model will be analysis by using ANSYS software.

VI. Modeling of Plain Milling Cutter using CATIA:

CATIA V5 is used to model the plain milling cutter and various views are presented in Fig. (3)

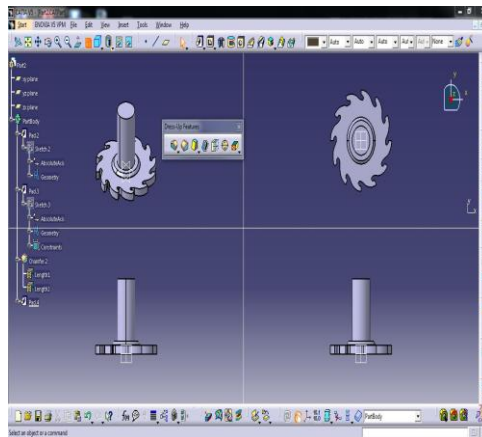


Fig. (3) 3D view of the plain milling cutter.

VII. Analysis of Single Tooth using ANSYS:

The Cutting Forces (loads) on the cutter for five different speeds are calculated (Refer Table.2) and the same are applied on the tip of the cutter modal. The variation in stresses and strains on cutter from ANSYS are Shown in Fig.4.The results are tabulated in Table 2.

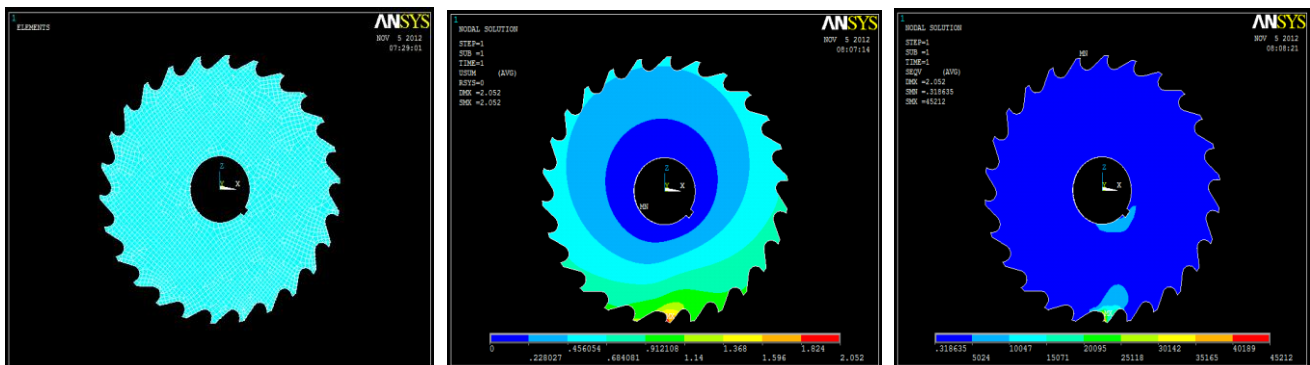


Fig.4(a) Meshed modal of 3D profil Fig.4 (b) Deformation of the cutter at 50 rpm Fig.4(c) Stress at speed 50 rpm

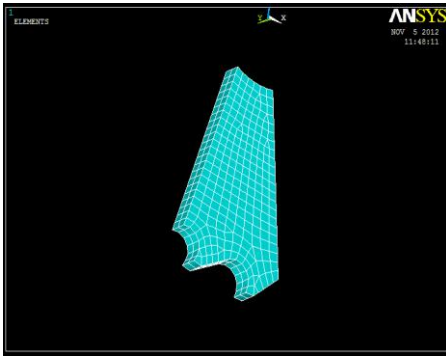


Fig.4 (d) Meshed model of single tooth profile

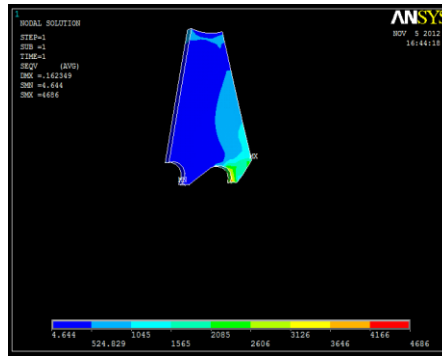


Fig.4 (e) Stress plot at 50 rpm

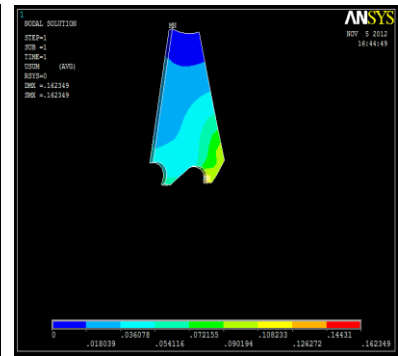


Fig.4 (f) Deformation at 50 rpm

S.no	DI A	SPEED	LOAD	STRESS (Model)	STRESS (Theoretical)
1	100	50	2101.911	4521	4056
2	100	100	1050.955	2261	2207.6
3	100	500	210.1911	2243	2220.8
4	100	1000	105.0955	226.049	223.5
5	100	2000	52.54777	112.485	108.19

Table 2: Results obtained from the analysis

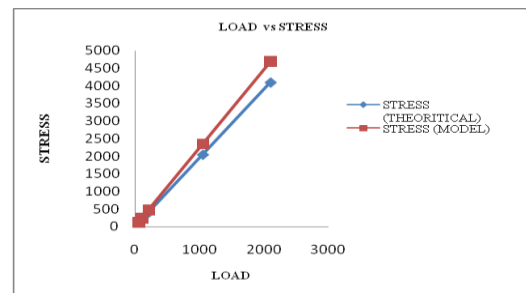


Figure 5: Plot Load Vs Stress

Represents the graph between different loads with model, and theoretical stress

VIII. Conclusion

The main objective of this study has been to perform a detailed computer-aided design and analysis of a plain milling cutter by integrating solid modeling and finite element analysis. Any cutter, single point or multiple point, can be designed based on the approach presented here. It could even be ventured that this approach can be used to design any complex mechanical component or system. Specifically for the cutter design, it produced the cutting variables that yield the minimum cost of manufacturing. The different design activities, such as design solid modeling, and finite element analysis, have been integrated. As is evident, approach presented in this paper is flexible and easy to use. Finally the design and analysis is carried out using the software's CATIA V5 and ANSYS. The values obtained are compared with the model and theoretical stress values of the plain milling cutter

IX. Acknowledgment

I would like to thank my Guide, Associate Professor Mr.M.KUMARA SWAMY for his time and support. In addition, I would like to thank my friends for sharing their experience in CATIA, ANSYS. Finally, I would like to thank my family for their support and putting up with me for these past few months moral and financial support during my studies.

References

- [1] N and K. Jha and Kathryn Hornik, "Integrated computer-aided optimal design and FEA of a plain milling cutter", Mechanical Engineering Department, Manhattan College, Riverdale, NY, USA
- [2] E. Abele, Y. Atlantis, and C. Brasher, "Machine tool spindle units", CIRP Annals – Manuf. Technol., vol. 59, pp. 781-802, 2010.
- [3] C. Li, Y. Ding, and B. Lu, "Development and Key Technology in High Speed Cutting", J. Qingdao Technol. Univ., vol. 30, pp. 7-16, Feb. 2009.
- [4] Kronenberg, M. Machining Science and Application. Pergamon Press, 1966
- [5] ASTM. Fundamentals of Tool Design, 1985
- [6] Draghici, G. and Paltinea, C. Calculation by convex mathematical programming of the optimal cutting condition when cylindrical milling. Int. J. Mach tool Des. Res. xxxx, 14, 143-160
- [7] Shigley, J.E. and Mischke, C.R. Mechanical Engineering Design, Fifth Edition. McGraw Hill book Company, 1989.
- [8] A text book of Machine design R.S Khurmi, and J.K Gupta. 2008 edition S.Chand publications.

A Novel CPU Scheduling Algorithm–Preemptive & Non-Preemptive

Sukumar Babu Bandarupalli¹, Neelima Priyanka Nutulapati²,
Prof. Dr. P.Suresh Varma³

¹(Computer Science & Engg, Vijaya Institute of Technology for Women, India)

²(MCA & CSE Dept, SRK Institute of Technology, India)

³(Computer Science & Dean, Adikavi Nannaya University, India)

ABSTRACT: The main objective of this paper is to introduce a new CPU algorithm called A Novel CPU Scheduling Algorithm which acts as both preemptive and non-preemptive based on the arrival time. The proposed algorithm helps to improve the CPU efficiency in real time uni-processor-multi programming operating system. CPU Scheduling is the basis of multi-programmed operating system. The scheduler is responsible for multiplexing processes on the CPU. There are many scheduling algorithms available for a multi-programmed operating system like FCFS, SJF, Priority, Round Robin etc. In this paper, the results of the existing algorithms (FCFS, SJF, Priority and Round Robin) are compared with the proposed algorithm.

Keyword: Operating System, uni-processor, uni programming, multi-programming, Resource utilization, Scheduling, FCFS, SJF, Priority, Round Robin, ERR etc.

I. INTRODUCTION

Operating system performs variety of tasks in which scheduling is one of the basic task. Scheduling is heart of any computer system since it contains decision of giving resources between possible processes. Sharing of computer resources between multiple processes is also called scheduling [1]. Process is a smallest work unit of a program which requires a set of resources for its execution that are allocated to it by the CPU. These processes are many in number and keep coming in a particular fashion, different scheduling techniques are employed that enable faster and efficient process execution thereby reducing the waiting time faced by each process and increasing CPU utilization. A process has five basic states namely NEW, Ready, Running, Waiting and Terminate [1] [2].

Throughout its lifetime a process migrates between various scheduling queues by different schedulers until it gets terminated. These queues mainly contain the ready queue which contains set of processes ready for CPU response. The second queue is the device or the I/O queue which contains all the processes that are waiting for I/O response [1]. The operating system must select processes for scheduling from these queues in a specific manner. This selection process using a particular scheduling technique is carried out by schedulers. Schedulers in general try to maximize the average performance of a system according to the given criterion [3]. Scheduling algorithms are broadly classified into preemptive and non-preemptive scheduling disciplines.

The algorithm proposed in this article is both preemptive and non-preemptive in nature and attempts to give fair CPU execution time by focusing on average waiting time and turnaround time of a process.

This article comprises of the following sections: Section 2 presents scheduling parameters, which will decide against which parameters the new CPU algorithm will be tested. Section 3 introduces existing scheduling algorithms. Section 4 explains the proposed Algorithm – A Novel CPU Scheduling algorithm. Section 5 contains pseudo code of the proposed algorithm. Section 6 explains the two basic elements that make up the simulation and provide an interactive user interface. Section 7 presents a graphical comparison of the new algorithm with existing algorithms. Section 8 will provide conclusion of the work.

II. SCHEDULING PARAMETERS

THERE ARE DIFFERENT SCHEDULING ALGORITHMS WITH DIFFERENT CHARACTERISTICS WHICH DECIDE SELECTION OF PROCESS USING DIFFERENT CRITERIA FOR EXECUTION BY CPU. THE CRITERIA FOR A GOOD SCHEDULING ALGORITHM DEPEND, AMONG OTHERS, ON THE FOLLOWING MEASURES [1].

- A. **CPU Utilization:** It is the average fraction of time, during which the processor is busy [2, 4].
- B. **Throughput:** It refers to the amount of work completed in a unit of time. The number of processes the system can execute in a period of time. The higher the number, the more work is done by the system [4].
- C. **Waiting Time:** The average period of time a process spends waiting. Waiting time may be expressed as turnaround time less the actual execution time [4].
- D. **Turnaround time:** The interval from the time of submission of a process to the time of completion is the turnaround time [4].
- E. **Response time:** Response time is the time from submission of a request until the first response is produced [4].
- F. **Priority:** give preferential treatment to processes with higher priorities [4].
- G. **Fairness:** Avoid the process from starvation. All the processes must be given equal opportunity to execute [4].

III. OVERVIEW OF EXISTING CPU SCHEDULING ALGORITHMS.

A. *FIRST COME FIRST SERVED (FCFS) Scheduling.*

It is the simplest CPU Scheduling algorithm. The criteria of this algorithm is 'the process that requests first, holds the CPU first' or which process enter the ready queue first is served first [3]. The workload is processed in the order of arrival time, with no preemption [2]. Once a process has been submitted to the CPU, it runs into completion without being interrupted. Such a technique is fair in the case of smaller processes but is quite unfair for long an unimportant job [5]. Since FCFS does not involve context switching therefore it has minimal overhead. It has low throughput since long processes can keep processor occupied for a long time making small processes suffer. As a result waiting time, turnaround time and response time can be low [6].

B. *Shortest Job First (SJF) Scheduling.*

The criteria of this algorithm are which process having the smallest CPU burst, CPU is assigned to that process next. If two process having the same CPU burst time FCFS is used to break up the tie [3]. SJF can be worked as preemptive and non-preemptive in nature based on the arrival time and burst time of the processes. SJF reduces average waiting time of the processes as compared to FCFS. SJF favors shorter processes over longer ones which is an overhead as compared to FCFS. It selects the job with the smallest burst time ensuring CPU availability for other processes as soon as the current process reaches its completion. This prevents smaller processes from suffering behind larger processes in the ready queue for a longer time [5] [7].

C. *Priority Based Scheduling.*

In this algorithm, priority is associated with each process and on the basis of that priority CPU is allocated to the processes. Higher priority processes are executed first and lower priority processes are executed at the end. If multiple processes having the same priorities are ready to execute, control of CPU is assigned to these processes on the basis of FCFS [1]. Priority Scheduling can be preemptive and non-preemptive in nature.

D. *Round Robin (RR) Scheduling.*

It is a preemptive scheduling algorithm. It is designed especially for time sharing systems. In this algorithm, a small unit of time called time quantum or time slice is assigned to each process [2]. When the time quantum expired, the CPU is switched to another process. Performance of Round Robin totally depends on the size of the time quantum.

IV. PROPOSED WORK: NOVEL CPU SCHEDULING ALGORITHM

The proposed algorithm A Novel CPU Scheduling algorithm is both preemptive and non-preemptive in nature. In this algorithm a new factor called condition factor (F) is calculated by the addition of burst time and arrival time ie., $F = \text{Burst Time} + \text{Arrival Time}$.

This factor f is assigned to each process and on the basis of this factor process are arranged in ascending order in the ready queue. Process having shortest condition factor (F) are executed first and process with next shortest factor (F) value is executed next. By considering the arrival time the new algorithms acts as preemptive or non-preemptive.

Proposed CPU scheduling algorithm reduces waiting time, turnaround time and response time and also increases CPU utilization and throughput.

The working procedure of A Novel Preemptive Scheduling of Preemptive and Non Preemptive algorithm is as given below:

- ✓ Take the list of processes, their burst time and arrival time.
- ✓ Find the condition factor F by adding arrival time and burst time of processes.
- ✓ First arrange the processes, burst time, condition factor based on arrival time ascending order.
- ✓ Iterate step a, b until burst time becomes zero.
 - a. If arrival time of first and second process are equal the arrange them based on their condition factor f.
 - b. Decrement the burst time and increment arrival time by 1
- ✓ When burst time becomes find the waiting time and turnaround time of that process.
- ✓ Average waiting time is calculated by dividing total waiting time with total number of processes.
- ✓ Average turnaround time is calculated by dividing total turnaround time by total number of processes.

V. PSEUDO CODE

Initialization variables

Burst time[n] \leftarrow 0
Arrival time[n] \leftarrow 0
Numprocess[n] \leftarrow 0
Factor[i] \leftarrow 0
Turn[n] \leftarrow 0
Wait[n] \leftarrow 0
Temp \leftarrow 0
Current time \leftarrow 0
Wait time=0

Turn time=0
 Avgwaitime=0.0
 Avgturntime=0.0
 Read burst time[n] and arrival time[n]
 Compute factor[i] <- bursstime[i] + arrival time[i]

a. Pseudo code for Non Preemptive

Arrange the elements in ascending order based on condition factor

```

For i ← 0 to n-1
  For j ← I to n
    If factor[i] > factor[j]
      Temp ← burst time[i]
      Burst time[i] ← burst time[j]
      Burst time[j] ← temp
      Temp ← arrival time[i]
      Arrival time[i] ← arrival time[j]
      Arrival time[j] ← temp
      Temp ← factor[i]
      Factor[i] ← factor[j]
      Factor[j] ← temp
  End for
For i ← 0 to n
  Begin
    Wait[i]=wait[i]+burst time[i]
    Turn[i]=wait[i]+btime[i]
    Wait time = wartime + wait[i]
    turn time = turn time + turn[i]
  End
Avgwaittime = wait time/n
Avgturntime = turn time/n
    
```

b. Pseudo code for Preemptive

Arrange the elements in ascending order based on arrival time

```

For i ← 0 to n-1
  For j ← I to n
    If factor[i] > factor[j]
      Temp ← burst time[i]
      Burst time[i] ← burst time[j]
      Burst time[j] ← temp
      Temp ← arrival time[i]
      Arrival time[i] ← arrival time[j]
      Arrival time[j] ← temp
      Temp ← factor[i]
      Factor[i] ← factor[j]
      Factor[j] ← temp
  End for
For i ← 0 to n-1
  For j ← I to n
    If atime[i] == atime[j] then sort elements in ascending order based on factor[i] and factor[j]
    If burs time! =0 && atime==current time
      Begin
        Atime[i] =atime[i]+1
        Btime[i] =btime[i]-1
        Current time++
        If btime[i]==0
          turn time=current time
        End
      End
    For i ← 0 to n
      Begin
        Wait [i]=turn[i]-btime[i]-atime[i]
        turn [i]=turn[i]+atime[i]
        Wait time = wartime + wait[i]
        Turn time = turn time + turn[i]
      End
    End
  End
End
    
```

End

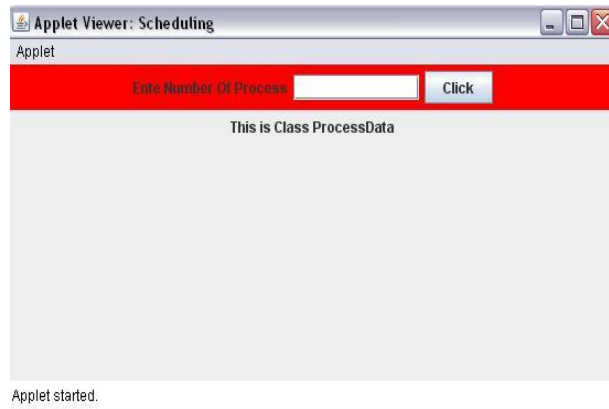
Avgwaittime = wait time/n

Avgturntime = turn time/n

VI. SIMULATION DESIGN

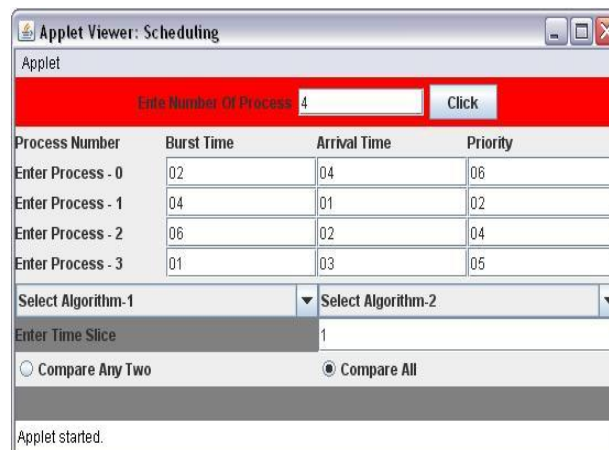
The simulation provides an interactive GUI interface to the user through which a user can input data related to different processes then applying different algorithms based on the algorithm choices given in the simulator. The simulator employs JAVA swings.

The front end user interfaces are designed using java awt's and swings. The parent screen i.e., screen1 allows the user to enter number of processes to be in execution.



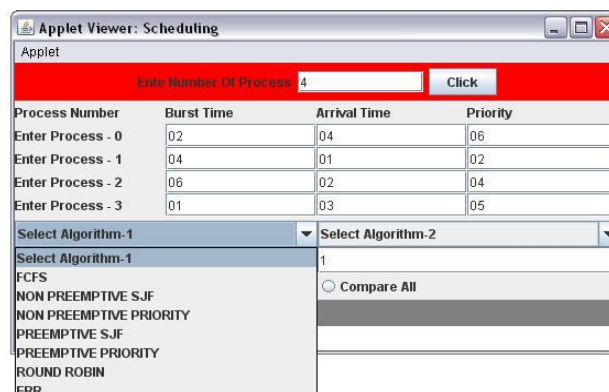
Screen1 : Enter Number of Process

Screen 2 allows the user to enter the details of the processes burst time, arrival time and priority.



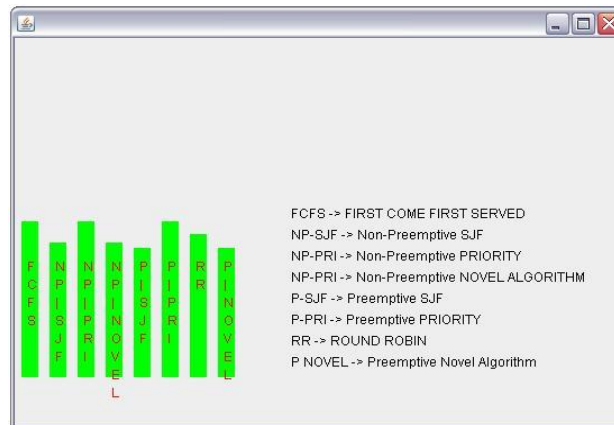
Screen 2: Enter Burst , Anival and Priority of processes

Screen 3 shows that a user can compare any two algorithms of his choice or he can compare all the scheduling algorithms.



Screen 3: Selection of Algorithm1 and Algorithm2

Screen 4 shows the Graphical Comparison of all the algorithms



Screen 4 : GUI Comparision of All Algorithms

Screen 5 shows the non-graphical comparison of all the algorithms

C:\WINDOWS\system32\cmd.exe - appletviewer scheduling.java

```
D:\sukumar\new sukumar\Novel Combinatory Algorithm>javac scheduling.java
D:\sukumar\new sukumar\Novel Combinatory Algorithm>appletviewer scheduling.java
```

Compare All Algorithms

Algorithm Name	Avg Waiting	Avg Turn Around
FCFS	4.7	8.0
NON PREEMPTIVE SJF	2.7	6.0
NON PREEMPTIVE PRIORITY	4.7	8.0
NON PREEMPTIVE NOVEL	2.7	6.0
PREEMPTIVE SJF	2.2	5.5
PREEMPTIVE PRIORITY	4.7	8.0
ROUND ROBIN	3.5	6.7
PREEMPTIVE NOVEL	2.2	5.5

Screen 5 : CUI Comparision of All Algorithms

VII. COMPARISON OF PROPOSED ALGORITHM WITH OTHER CPU SCHEDULING ALGORITHMS.

To compare the performance of the proposed scheduling algorithm it was implemented and compared with the existing scheduling algorithm. GUI and CUI figures, shows the comparison between the proposed algorithm with existing algorithms.

Example 2: Screen 6 takes different processes burst time and arrival time and priority values

Applet Viewer: Scheduling

Applet

Enter Number Of Process 5 Click

Process Number	Burst Time	Arrival Time	Priority
Enter Process - 0	010	0	03
Enter Process - 1	01	01	01
Enter Process - 2	02	02	03
Enter Process - 3	01	03	04
Enter Process - 4	05	04	02

Select Algorithm-1 Select Algorithm-1

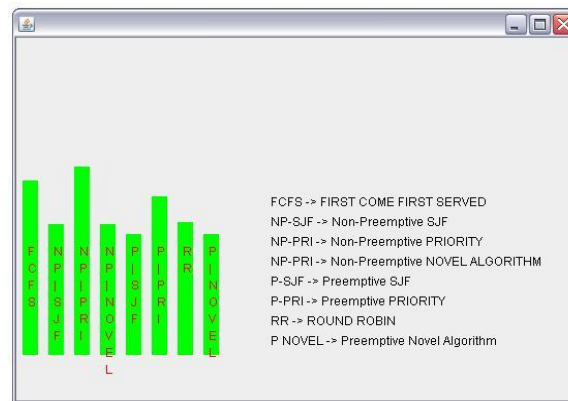
Enter Time Slice 1

☐ Compare Any Two ☒ Compare All

Applet started.

Screen 6: Example 2 for different set of Processes

Screen 7 shows the graphical representation of example 2



Screen 7: Example 2 GUI Comparison

Screen 8 shows the non-graphical representation of example 2

```
C:\WINDOWS\system32\CMD.exe - appletviewer Scheduling.java
```

```
D:\sukumar\new sukumar\Novel Combinatory Algorithm>javac Scheduling.java
```

```
D:\sukumar\new sukumar\Novel Combinatory Algorithm>appletviewer Scheduling.java
```

Compare All Algorithms

Algorithm Name	Avg Waiting	Avg Turn Around
FCFS	7.6	11.4
NON PREEMPTIVE SJF	3.2	7.0
NON PREEMPTIVE PRIORITY	9.0	12.8
NON PREEMPTIVE NOVEL	3.2	7.0
PREEMPTIVE SJF	2.2	6.0
PREEMPTIVE PRIORITY	6.0	9.8
ROUND ROBIN	3.4	7.2
PREEMPTIVE NOVEL	2.2	6.0

Screen 8: Example 2 CUI Comparison

Example 3: Screen 9 takes different processes burst time and arrival time and priority values

Applet Viewer: Scheduling

Enter Number Of Process: 6 Click

Process Number	Burst Time	Arrival Time	Priority
Enter Process - 0	04	01	04
Enter Process - 1	06	02	01
Enter Process - 2	010	03	08
Enter Process - 3	05	04	02
Enter Process - 4	020	05	03
Enter Process - 5	01	06	06

Select Algorithm-1: Select Algorithm-1

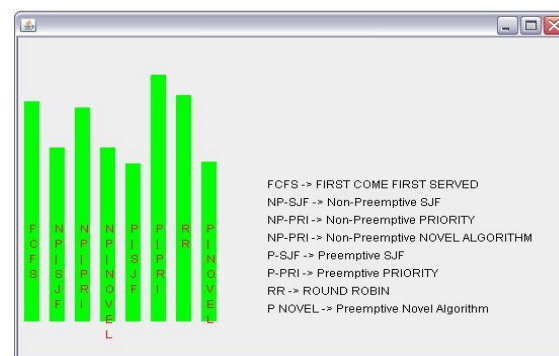
Enter Time Slice: 1

☐ Compare Any Two ☒ Compare All

Applet started.

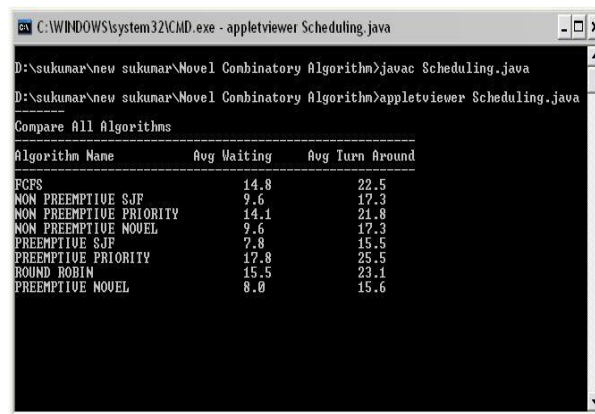
Screen 9: Example 2 for different set of processes

Screen 10 shows the graphical representation of example3



Screen 10: Example 3 GUI Comparison

Screen 11 shows the non-graphical representation of example3



Algorithm Name	Avg Waiting	Avg Turn Around
FCFS	14.8	22.5
NON PREEMPTIVE SJF	9.6	17.3
NON PREEMPTIVE PRIORITY	14.1	21.8
NON PREEMPTIVE NOVEL	9.6	17.3
PREEMPTIVE SJF	7.8	15.5
PREEMPTIVE PRIORITY	17.8	25.5
ROUND ROBIN	15.5	23.1
PREEMPTIVE NOVEL	8.0	15.6

Screen 11: Example 3 CUI Comparison

VIII. CONCLUSION

The paper presents a new CPU scheduling algorithm called A Novel Pre-emptive and Non Pre-emptive CPU Scheduling Algorithm. Paper also contains simulation interface and its working, which interactively takes input from the user and compares the process set against different algorithm pairs. The result of the simulation for different process sets using different scheduling algorithms has been presented graphically in this piece of work. The last half of the paper provides analytical result with each set of graph. From the above graphs and results from example 1, 2 and 3, it is clear that proposed algorithm is more efficient than FCFS, Pre-emptive Priority and Non Pre-emptive Priority, Round Robin. And also observed that proposed algorithm gives almost equal performance like a SJF Pre-emptive and Non Pre-emptive algorithm

REFERENCES

- [1] Abraham Silberschatz, Peter Baer Galvin, Greg Gagne, "Operating System Concepts", Sixth Edition.
- [2] Milan Milenkovic, "Operating Systems Concepts and Design", McGRAM-HILL, Computer Science Series, second edition.
- [3] P. Balakrishna Prasad, "Operating Systems" Second Edition.
- [4] A. Dhore "Opeating Systems", Technical Publications.
- [5] M. Dietel, "Operating Systems", Pearson Education, Second Edition.
- [6] <http://en.wikipedia.org/wiki/Scheduling>
- [7] M Gary Nutt, "Operating systems – A Modern Perspective, Second Edition, Pearson Education, 2000.

Implementation of Incremental Conductance MPPT with Direct Control Method Using Cuk Converter

Divya Teja Reddy Challa¹, I. Raghavendar²

¹(PG student Department of EEE, Teegala Krishna Reddy Engineering college, JNTU- Hyd, AP, INDIA)

²(Associate Professor Head of the Department of EEE, Tee gala Krishna Reddy engineering college, JNTU-Hyd, AP, INDIA)

ABSTRACT: This paper presents simulation of incremental conductance (IncCond) maximum power point tracking (MPPT) used in solar array power systems with direct control method. The main difference of the proposed system to existing MPPT systems includes elimination of the proportional-integral control loop and investigation of the effect of simplifying the control circuit. The resultant system is capable of tracking MPPs accurately and rapidly without steady-state oscillation, and also, its dynamic performance is satisfactory. The IncCond algorithm is used to track MPPs because it performs precise control under rapidly changing atmospheric conditions. MATLAB and SIMULINK were employed for simulation studies. Simulation results indicate the feasibility and improved functionality of the system.

IndexTerms: incremental conductance (IncCond), maximum power point tracking (MPPT), photovoltaic (PV) system.

I. INTRODUCTION

RECENTLY, energy generated from clean, efficient, and environmentally friendly sources has become one of the major challenges for engineers and scientists [1]. Among all renewable energy sources, solar power systems attract more attention because they provide excellent opportunity to generate electricity while greenhouse emissions are reduced [1]–[3]. It is also gratifying to lose reliance on conventional electricity generated by burning coal and natural gas. Regarding the endless aspect of solar energy, it is worth saying that solar energy is a unique prospective solution for energy crisis. However, despite all the aforementioned advantages of solar power systems, they do not present desirable efficiency [4], [5].

The efficiency of solar cells depends on many factors such as temperature, insolation, spectral characteristics of sunlight, dirt, shadow, and so on. Changes in insolation on panels due to fast climatic changes such as cloudy weather and increase in ambient temperature can reduce the photovoltaic (PV) array output power. In other words, each PV cell produces energy pertaining to its operational and environmental conditions [6], [7]. In addressing the poor efficiency of PV systems, some methods are proposed, among which is a new concept called “maximum power point tracking” (MPPT). All MPPT methods follow the same Goal which is maximizing the PV array output power by tracking the maximum power on every operating condition.

A. MPPT Methods

There is a large number of algorithms that are able to track MPPs. Some of them are simple, such as those based on voltage and current feedback, and some are more complicated, such as perturbation and observation (P&O) or

the incremental conductance (IncCond) method. They also vary in complexity, sensor requirement, speed of convergence, cost, range of operation, popularity, ability to detect multiple local maxima, and their applications [8]–[10]. Having a curious look at the recommended methods, hill climbing and P&O [11]–[16] are the algorithms that were in the center of consideration because of their simplicity and ease of implementation. Hill climbing [14], [17] is perturbation in the duty ratio of the power converter, and the P&O method [15], [18] is perturbation in the operating voltage of the PV array. However, the P&O algorithm cannot compare the array terminal voltage with the actual MPP voltage, since the change in power is only considered to be a result of the array terminal voltage perturbation. As a result, they are not accurate enough because they perform steady-state oscillations, which consequently waste the energy [8]. By minimizing the perturbation step size, oscillation can be reduced, but a smaller perturbation size slows down the speed of tracking MPPs. Thus, there are some disadvantages with these methods, where they fail under rapidly changing atmospheric conditions [19]. On the other hand, some MPPTs are more rapid and accurate and, thus, more impressive, which need special design and familiarity with specific subjects such as fuzzy logic [20] or neural network [21] methods. MPPT fuzzy logic controllers have good performance under varying atmospheric conditions and exhibit better performance than the P&O control method [8]; however, the main disadvantage of this method is that its effectiveness is highly dependent on the technical knowledge of the engineer in computing the error and coming up with the rule-based table. It is greatly dependent on how a designer arranges the system that requires skill and experience. A similar disadvantage of the neural network method comes with its reliance on the characteristics of the PV array that change with time, implying that the neural network has to be periodically trained to guarantee accurate MPPs.

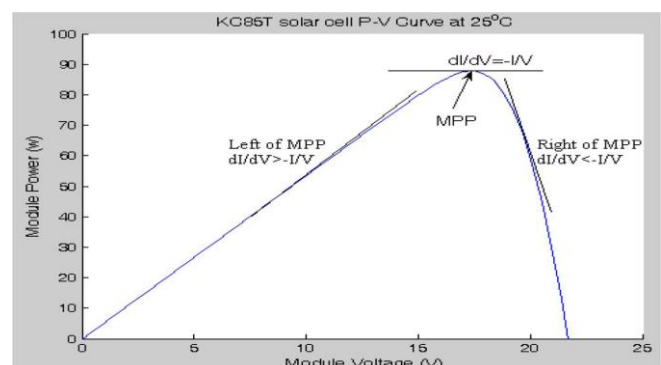


Fig. 1 Basic idea of the IncCond method on a P - V curve of a solar module

The IncCond method is the one which overrides over the aforementioned drawbacks. In this method, the array terminal voltage is always adjusted according to the MPP voltage. It is based on the incremental and instantaneous conductance of the PV module [6], [19], [22], [23].

Fig. 1 shows that the slope of the PV array power curve is zero at the MPP, increasing on the left of the MPP and decreasing on the right-hand side of the MPP. The basic equations of this method are as follows [24]:

$$\frac{dI}{dV} = -\frac{I}{V} \quad \text{at MPP} \quad (1)$$

$$\frac{dI}{dV} > -\frac{I}{V} \quad \text{left of MPP} \quad (2)$$

$$\frac{dI}{dV} < -\frac{I}{V} \quad \text{right of MPP} \quad (3)$$

Where I and V are the PV array output current and voltage, respectively. The left-hand side of the equations represents the IncCond of the PV module, and the right-hand side represents the instantaneous conductance. From (1)–(3), it is obvious that when the ratio of change in the output conductance is equal to the negative output conductance, the solar array will operate at the MPP. In other words, by comparing the conductance at each sampling time, the MPPT will track the maximum power of the PV module. The accuracy of this method is proven in [8], where it mentions that the IncCond method can track the true MPPs independent of PV array characteristics.

Also, Roman *et al.* [25] described it as the best MPPT method, where it has made a comprehensive comparison between P&O and the IncCond method with boost converter and shows that the efficiency of experimental results is up to 95%. In [10], efficiency was observed to be as much as 98.2%, but it is doubtful of the IncCond method reliability issues due to the noise of components. Some modifications and reformations were proposed on this method so far, but since this method inherently has a good efficiency, the aforementioned amendments increase the complexity and cost of the system and there was no remarkable change in system efficiency.

TABLE I
COMPARISON OF COMMON MPPT METHODS

MPPT technique	Speed	Complexity	Reliability	Implementation
Fractional I_{sc}	Medium	Medium	Low	Digital/Analog
Fractional V_{oc}	Medium	Low	Low	Digital/Analog
IncCond	Varies	Medium	Medium	Digital
Hill climbing	Varies	Low	Medium	Digital/Analog
Fuzzy logic	Fast	High	Medium	Digital
Neural network	Fast	High	Medium	Digital

In [6], the variable-step-size IncCond method has been compared with the fixed-step-size one. The variable step size with constant-voltage-tracking startup system has a performance of 99.2%, while the fixed step size has good efficiency as much as 98.9% due to the chosen small step

size. Hence, it was revealed that with proper step size selection, the efficiency of the IncCond method is satisfactory. Table I shows a detailed comparison of the major characteristics for the aforementioned MPPT methods, with a focus on speed of convergence, complexity of implementation, reliability to detect real MPPs with varying weather conditions, and preferred method for implementation.

B. Direct Control Method

Conventional MPPT systems have two independent control loops to control the MPPT. The first control loop contains the MPPT algorithm, and the second one is usually a proportional (P) or P–integral (PI) controller. The IncCond method makes use of instantaneous and IncCond to generate an error signal, which is zero at the MPP; however, it is not zero at most of the operating points. The main purpose of the second control loop is to make the error from MPPs near to zero [8]. Simplicity of operation, ease of design, inexpensive maintenance, and low cost made PI controllers very popular in most linear systems. However, the MPPT system of standalone PV is a nonlinear control problem due to the nonlinearity nature of PV and unpredictable environmental conditions, and hence, PI controllers do not generally work well [26]. In this paper, the IncCond method with direct control is selected. The PI control loop is eliminated, and the duty cycle is adjusted directly in the algorithm. The control loop is simplified, and the computational time for tuning controller gains is eliminated. To compensate the lack of PI controller in the proposed system, a small marginal error of 0.002 was allowed. The objective of this paper is to eliminate the second control loop and to show that sophisticated MPPT methods do not necessarily obtain the best results, but employing them in a simple manner for complicated electronic subjects is considered necessary. Embedded MATLAB function generates pulse width modulation (PWM) waveform to control the duty cycle of the converter switch according to the IncCond algorithm.

II. PV MODULE AND MPPT

The basic structural unit of a solar module is the PV cells. A solar cell converts energy in the photons of sunlight into electricity by means of the photoelectric phenomenon found in certain types of semiconductor materials such as silicon and selenium. A single solar cell can only produce a small amount of power. To increase the output power of a system, solar cells are generally connected in series or parallel to form PV modules. PV module characteristics are comprehensively discussed in [3], [6], [11], [28], and [29], which indicate an exponential and nonlinear relation between the output current and voltage of a PV module. The main equation for the output current of a module is [6]

$$I_o = n_p I_{ph} - n_p I_{rs} \left[\exp \left(k_o \frac{v}{n_s} \right) - 1 \right] \quad (4)$$

where I_o is the PV array output current, v is the PV output voltage, I_{ph} is the cell photocurrent that is proportional to solar irradiation, I_{rs} is the cell reverse saturation current that mainly depends on temperature, k_o is a constant, n_s represents the number of PV cells connected in series, and n_p represents the number of such strings connected in parallel. In (4), the cell photocurrent is calculated from

$$I_{ph} = [I_{scr} + k_i(T - T_r)] \frac{S}{100} \quad (5)$$

Where I_{scr} cell short-circuit current at reference temperature and radiation; k_i short-circuit current temperature coefficient; T_r cell reference temperature; S solar irradiation in mill watts per square centimeter. Moreover, the cell reverse saturation current is computed from

$$I_{rs} = I_{rr} \left[\frac{T}{T_r} \right]^3 \exp \left(\frac{qE_G}{kA} \left[\frac{1}{T_r} - \frac{1}{T} \right] \right) \quad (6)$$

Where T_r cell reference temperature; I_{rr} reverse saturation at T_r ; E_G band-gap energy of the semiconductor used in the cell.

Figs. 2(a) and (b) show the effect of varying weather conditions on MPP location at $I-V$ and $P-V$ curves. Fig. 3 shows the current-versus-voltage curve of a PV module. It gives an idea about the significant points on each $I-V$ curve: open-circuit voltage, short-circuit current, and the operating point where the module performs the maximum power (MPP). This point is related to a voltage and a current that are V_{mpp} and I_{mpp} , respectively, and is highly dependent on solar irradiation and ambient temperature [7].

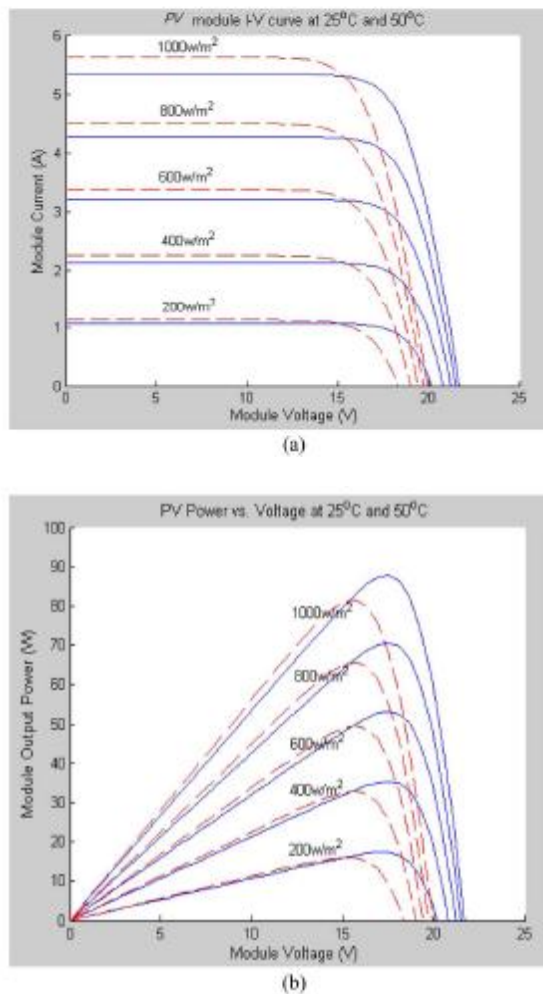


Fig. 2 Maximum power with varying weather conditions $[-25^\circ\text{C}, -50^\circ\text{C}]$.

(a) $I-V$ curves. (b) $P-V$ curves.

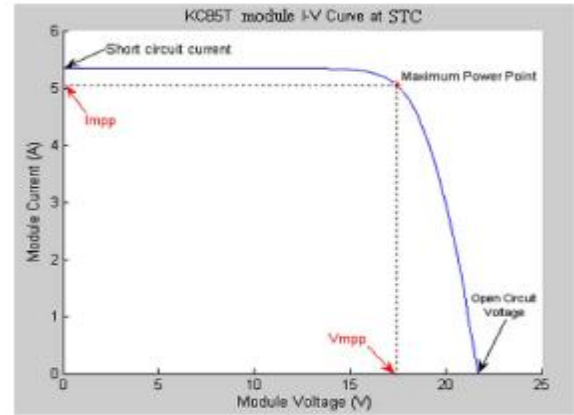


Fig. 3 Current-versus-voltage curve of a PV module.

In Fig. 2, it is clear that the MPP is located at the knee of the $I-V$ curve, where the resistance is equal to the negative of differential resistance [25], [30]

$$\frac{V}{I} = -\frac{V}{I} \quad (7)$$

This is following the general rule used in the P&O method, in which the slope of the PV curve at the MPP is equal to zero.

$$\frac{dP}{dV} = 0 \quad (8)$$

Equation (8) can be rewritten as follows:

$$\frac{dP}{dV} = I \frac{dV}{dV} + V \frac{dI}{dV} \quad (9)$$

$$\frac{dP}{dV} = I + V \frac{dI}{dV} \quad (10)$$

And hence

$$I + V \frac{dI}{dV} = 0 \quad (11)$$

This is the basic idea of the IncCond algorithm. One noteworthy point to mention is that (7) or (8) rarely occur in practical implementation, and a small error is usually permitted [24]. The size of this permissible error (e) determines the sensitivity of the system. This error is selected with respect to the swap between steady-state oscillations and risk of fluctuating at a similar operating point. It is suggested to choose a small and positive digit [24], [31]. Thus, (10) can be rewritten as

$$I + V \frac{dI}{dV} = e \quad (12)$$

In this paper, the value of “ e ” was chosen as 0.002 on the basis of the trial-and-error procedure. The flowchart of the IncCond algorithm within the direct control method is shown in Fig. 4. According to the MPPT algorithm, the duty cycle (D) is calculated. This is the desired duty cycle that the PV module must operate on the next step. Setting a new duty cycle in the system is repeated according to the sampling time.

III. SELECTING PROPER CONVERTER

When proposing an MPP tracker, the major job is to choose and design a highly efficient converter, which is supposed to operate as the main part of the MPPT. The efficiency of switch-mode dc-dc converters is widely discussed in [1]. Most switching-mode power supplies are well designed to function with high efficiency. Among all the topologies available, both Cuk and buck-boost converters provide the opportunity to have either higher or lower output voltage compared with the input voltage. Although the buck-boost configuration is cheaper than the Cuk one, some disadvantages, such as discontinuous input current, high peak currents in power components, and poor transient response, make it less efficient. On the other hand, the Cuk converter has low switching losses and the highest efficiency among non isolated dc-dc converters.

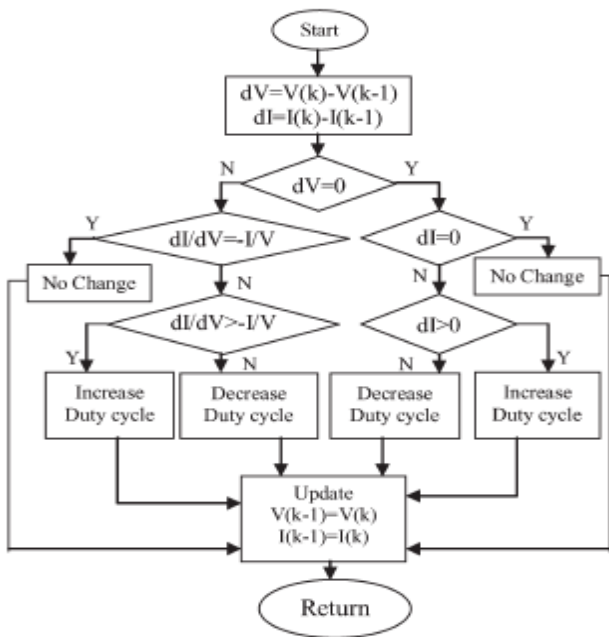


Fig. 4 Flowchart of the IncCond method with direct control

It can also provide a better output-current characteristic due to the inductor at the output stage. Thus, the Cuk configuration is a proper converter to be employed in designing the MPPT. Figs. 5 and 6 show a Cuk converter and its operating modes, which is used as the power stage interface between the PV module and the load. The Cuk converter has two modes of operation. The first mode of operation is when the switch is closed (ON), and it is conducting as a short circuit. In this mode, the capacitor releases energy to the output. The equations for the switch conduction mode are as follows:

$$v_{L1} = V_g \quad (13)$$

$$v_{L2} = -v_1 - v_2 \quad (14)$$

$$i_{c1} = i_2 \quad (15)$$

$$i_{c2} = i_2 - \frac{v_2}{R} \quad (16)$$

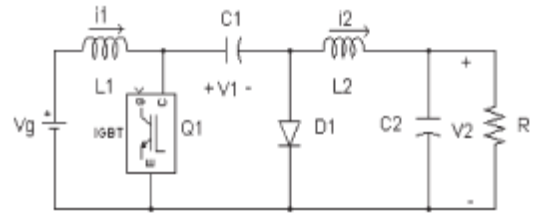


Fig. 5 Electrical circuit of the Cuk converter used as the PV power-stage interface

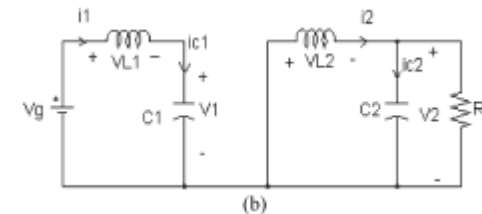
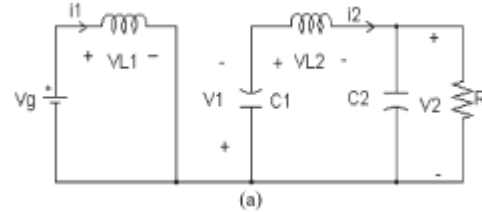


Fig. 6 Cuk converters with (a) switch ON and (b) switch OFF

On the second operating mode when the switch is open (OFF), the diode is forward-biased and conducting energy to the output. Capacitor C1 is charging from the input. The equations for this mode of operation are as follows:

$$v_{L1} = V_g - v_1 \quad (17)$$

$$v_{L2} = -v_2 \quad (18)$$

$$i_{c1} = i_1 \quad (19)$$

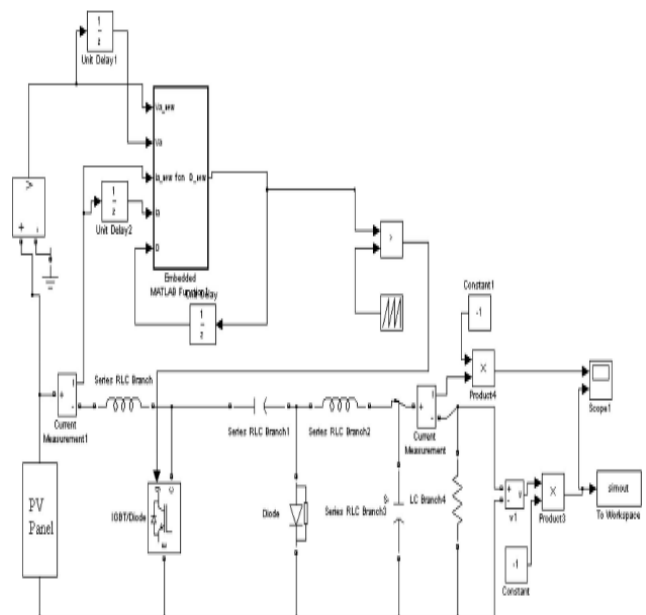


Fig.7 Simulation diagram of the proposed system

$$i_{c2} = i_2 - \frac{v_2}{R} \quad (20)$$

The principles of Cuk converter operating conditions state that the average values of the periodic inductor voltage and capacitor current waveforms are zero when the converter operates in steady state. The relations between output and input currents and voltages are given in the following:

$$\frac{V_o}{V_{in}} = -\left(\frac{D}{1-D}\right) \quad (21)$$

$$\frac{I_{in}}{I_o} = -\left(\frac{D}{1-D}\right) \quad (22)$$

Some analysis of Cuk converter specifications are provided in [32], and a comparative study on different schemes of switching converters is presented in the literature [33].

The components for the Cuk converter used in simulation were selected as follows:

- 1) Input inductor L1 = 5 mH;
- 2) Capacitor C1 (PV side) = 47 μ F;
- 3) Filter inductor L2 = 5 mH;
- 4) Switch: insulated-gate bipolar transistor [(IGBT)];
- 5) Freewheeling diode;
- 6) Capacitor C2 (filter side) = 1 μ F;
- 7) Resistive load = 10 Ω ;
- 8) Switching frequency = 10 kHz;

IV. SIMULATION RESULTS

Fig.7 shows the simulation diagram of the proposed system. The PV module is modeled using electrical characteristics to provide the output current and voltage of the PV module. The provided current and voltage are fed to the converter and the controller simultaneously. The PI control loop is eliminated, and the duty cycle is adjusted directly in the algorithm. To compensate the lack of PI controller in the proposed system, a small marginal error of 0.002 is allowed. The illumination level is taken at 1000 W/m². Fig. 8 shows the change in duty cycle adjusted by the MPPT to extract the maximum power from the module. Figs.9, 10 and 11 shows the wave forms of the output voltage, current and power.

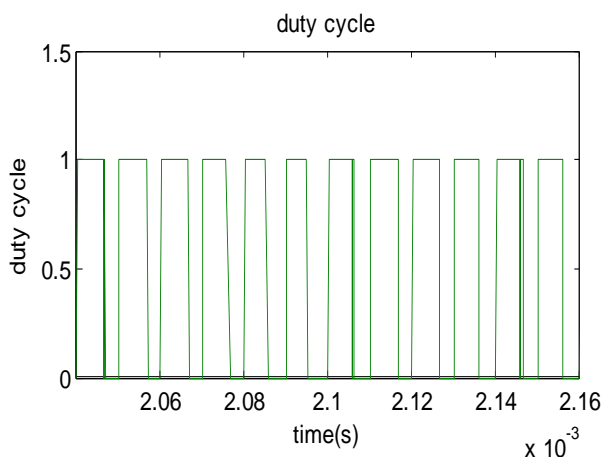


Fig. 8 Change in (a) duty cycle

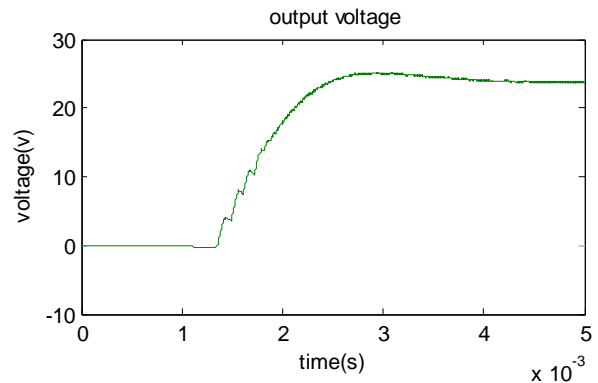


Fig. 9 output voltage of the converter

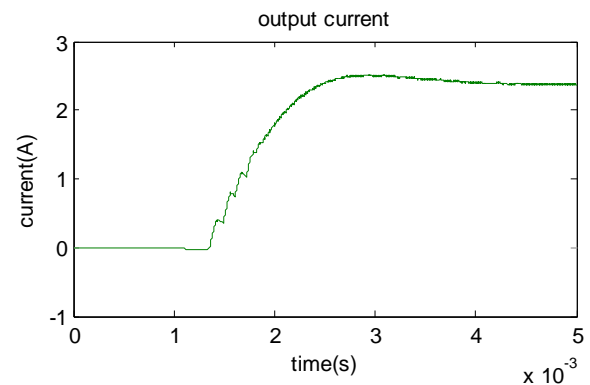


Fig. 10 output current of the converter

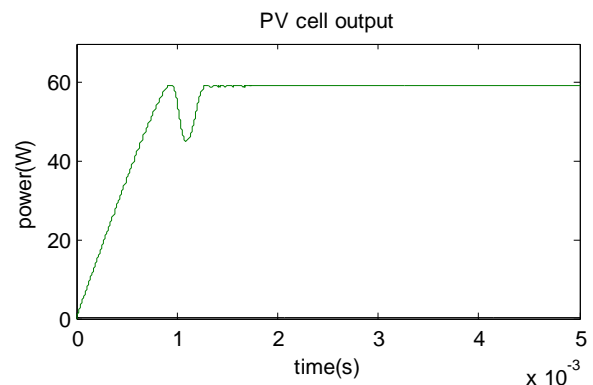


Fig. 11 PV cell output power

V. CONCLUSION

In this paper, a fixed-step-size IncCond MPPT with direct control method was employed, and the necessity of another control loop was eliminated. The proposed system was simulated and the functionality of the suggested control concept was proven. From the results acquired during the simulations it was confirmed that, with a well-designed system including a proper converter and selecting an efficient and proven algorithm, the implementation of MPPT is simple. The results also indicate that the proposed control system is capable of tracking the PV array maximum power and thus improves the efficiency of the PV system and reduces low power loss and system cost.

REFERENCES

- [1] R.-J. Wai, W.-H. Wang and C.-Y. Lin, "High-performance stand-alone Photovoltaic generation system," *IEEE Trans. Ind. Electron.*, vol. 55, no. 1, pp. 240–250, Jan. 2008.
- [2] W. Xiao, W. G. Dunford, P. R. Palmer, and A. Capel, "Regulation of photovoltaic voltage," *IEEE Trans. Ind. Electron.*, vol. 54, no. 3, pp. 1365–1374, Jun. 2007.
- [3] N. Mutoh and T. Inoue, "A control method to charge series-connected ultra electric double-layer capacitors suitable for photovoltaic generation systems combining MPPT control method," *IEEE Trans. Ind. Electron.*, vol. 54, no. 1, pp. 374–383, Feb. 2007.
- [4] R. Faranda, S. Leva, and V. Maugeri, *MPPT Techniques for PV Systems: Energetic and Cost Comparison*. Milano, Italy: Elect. Eng. Dept. Politecnico di Milano, 2008, pp. 1–6.
- [5] Z. Yan, L. Fei, Y. Jinjun, and D. Shanxu, "Study on realizing MPPT by improved incremental conductance method with variable step-size," in *Proc. IEEE ICIEA*, Jun. 2008, pp. 547–550.
- [6] F. Liu, S. Duan, F. Liu, B. Liu, and Y. Kang, "A variable step size INC MPPT method for PV systems," *IEEE Trans. Ind. Electron.*, vol. 55, no. 7, pp. 2622–2628, Jul. 2008.
- [7] F. M. González-Longatt, "Model of photovoltaic module in Matlab," in *2do congreso iberoamericano de estudiantes de ingenieria: a eléctrica, electrónica y computación*, ii cibelec, 2005, pp. 1–5.
- [8] T. ESRAM and P. L. Chapman, "Comparison of photovoltaic array maximum power point tracking techniques," *IEEE Trans. Energy Convers.*, vol. 22, no. 2, pp. 439–449, Jun. 2007.
- [9] V. Salas, E. Olias, A. Barrado, and A. Lazaro, "Review of the maximum power point tracking algorithms for stand-alone photovoltaic systems," *Sol. Energy Mater. Sol. Cells*, vol. 90, no. 11, pp. 1555–1578, Jul. 2006.
- [10] G. Petrone, G. Spagnuolo, R. Teodorescu, M. Veerachary, and M. Vitelli, "Reliability issues in photovoltaic power processing systems," *IEEE Trans. Ind. Electron.*, vol. 55, no. 7, pp. 2569–2580, Jul. 2008.
- [11] C. Hua, J. Lin, and C. Shen, "Implementation of a DSP-controlled photovoltaic system with peak power tracking," *IEEE Trans. Ind. Electron.*, vol. 45, no. 1, pp. 99–107, Feb. 1998.
- [12] T. Noguchi, S. Togashi, and R. Nakamoto, "Short-current pulse-based maximum-power-point tracking method for multiple photovoltaic-and converter module system," *IEEE Trans. Ind. Electron.*, vol. 49, no. 1, pp. 217–223, Feb. 2002.
- [13] N. Mutoh, M. Ohno, and T. Inoue, "A method for MPPT control while Searching for parameters corresponding to weather conditions for PV generation systems," *IEEE Trans. Ind. Electron.*, vol. 53, no. 4, pp. 1055–1065, Jun. 2006.
- [14] N. Femia, G. Petrone, G. Spagnuolo, and M. Vitelli, "Optimization of perturb and observe maximum power point tracking method," *IEEE Trans. Power Electron.*, vol. 20, no. 4, pp. 963–973, Jul. 2005.
- [15] N. Femia, D. Granozio, G. Petrone, G. Spagnuolo, and M. Vitelli, "Predictive & adaptive MPPT perturb and observe method," *IEEE Trans. Aerosp. Electron. Syst.*, vol. 43, no. 3, pp. 934–950, Jul. 2007.
- [16] E. Koutroulis, K. Kalaitzakis, and N. C. Voulgaris, "Development of a Microcontroller-based, photovoltaic maximum power point tracking control System," *IEEE Trans. Power Electron.*, vol. 16, no. 1, pp. 46–54, Jan. 2001.
- [17] S. Jain and V. Agarwal, "A new algorithm for rapid tracking of approximate maximum power point in photovoltaic systems," *IEEE Power Electron. Lett.*, vol. 2, no. 1, pp. 16–19, Mar. 2004.
- [18] A. Pandey, N. Dasgupta, and A. K. Mukerjee, "Design issues in implementing MPPT for improved tracking and dynamic performance," in *Proc. 32nd IECON*, Nov. 2006, pp. 4387–4391.
- [19] K. H. Hussein, I. Muta, T. Hoshino, and M. Osakada, "Maximum photovoltaic power tracking: An algorithm for rapidly changing atmospheric conditions," *Proc. Inst. Elect. Eng.—Gener. Transmits. Distrib.*, vol. 142, no. 1, pp. 59–64, Jan. 1995.
- [20] T.-F. Wu, C.-H. Chang and Y.-H. Chen, "A fuzzy-logic-controlled singlestage converter for PV-powered lighting system applications," *IEEE Trans. Ind. Electron.*, vol. 47, no. 2, pp. 287–296, Apr. 2000.
- [21] M. Veerachary, T. Senjyu, and K. Uezato, "Neural-network-based maximum-power-point tracking of coupled-inductor interleaved-boostconverter-supplied PV system using fuzzy controller," *IEEE Trans. Ind. Electron.*, vol. 50, no. 4, pp. 749–758, Aug. 2003.
- [22] B. Liu, S. Duan, F. Liu, and P. Xu, "Analysis and improvement of maximum power point tracking algorithm based on incremental conductance method for photovoltaic array," in *Proc. IEEE PEDS*, 2007, pp. 637–641.
- [23] Y.-C. Kuo, T.-J. Liang and J.-F. Chen, "Novel maximum-power-pointtracking controller for photovoltaic energy conversion system," *IEEE Trans. Ind. Electron.*, vol. 48, no. 3, pp. 594–601, Jun. 2001.
- [24] D. Sera, T. Kerekes, R. Teodorescu, and F. Blaabjerg, *Improved MPPT Algorithms for Rapidly Changing Environmental Conditions*. Aalborg, Denmark: Aalborg Univ./Inst. Energy Technol., 2006.
- [25] E. Roman, R. Alonso, P. Ibanez, S. Elorduzapatarietxe, and D. Goitia, "Intelligent PV module for grid-connected PV systems," *IEEE Trans. Ind. Electron.*, vol. 53, no. 4, pp. 1066–1073, Jun. 2006.
- [26] F. Salem, M. S. Adel Moteleb, and H. T. Dorrah, "An enhanced fuzzy-PI controller applied to the MPPT problem," *J. Sci. Eng.*, vol. 8, no. 2, pp. 147–153, 2005.
- [27] M. Fortunato, A. Giustiniani, G. Petrone, G. Spagnuolo, and M. Vitelli, "Maximum power point tracking in a one-cycle-controlled single-stage photovoltaic inverter," *IEEE Trans. Ind. Electron.*, vol. 55, no. 7, pp. 2684–2693, Jul. 2008.
- [28] I.-S. Kim, M.-B. Kim and M.-J. Youn, "New maximum power point tracker using sliding-mode observer for estimation of solar array current in the grid-connected photovoltaic system," *IEEE Trans. Ind. Electron.*, vol. 53, no. 4, pp. 1027–1035, Jun. 2006.
- [29] W. Xiao, M. G. J. Lind, W. G. Dunford, and A. Capel, "Real-time identification of optimal operating points in photovoltaic power systems," *IEEE Trans. Ind. Electron.*, vol. 53, no. 4, pp. 1017–1026, Jun. 2006.
- [30] J.-H. Park, J.-Y. Ahn, B.-H. Cho and G.-J. Yu, "Dual-module-based maximum power point tracking control of photovoltaic systems," *IEEE Trans. Ind. Electron.*, vol. 53, no. 4, pp. 1036–1047, Jun. 2006.
- [31] W. Wu, N. Pongratananukul, W. Qiu, K. Rustom, T. Kasparis, and I. Batarseh, "DSP-based multiple peak power tracking for expandable power system," in *Proc. 18th Annu. IEEE Appl. Power Electron. Conf. Expo.*, Feb. 2003, vol. 1, pp. 525–530.
- [32] D. Maksimovic and S. Cuk, "A unified analysis of PWM converters in discontinuous modes," *IEEE Trans. Power Electron.*, vol. 6, no. 3, pp. 476–490, Jul. 1991.
- [33] K. K. Tse, B. M. T. Ho, H. S.-H. Chung, and S. Y. R. Hui, "A comparative study of maximum-power-point trackers for photovoltaic panels using switching-frequency modulation scheme," *IEEE Trans. Ind. Electron.*, vol. 51, no. 2, pp. 410–418, Apr. 2004.

A Heuristic Algorithm to Reduce Information Overhead Based On Hierarchical Category Structure

Kishore Kumar Reddy¹, M M M K Varma²

¹(M.Tech, Department of CSE, Sri Sivani College of Engineering, Andhra Pradesh, India

² (Assistant Professor, Department of CSE, Sri Sivani College of Engineering, Andhra Pradesh, India

Abstract : Database systems are being increasingly used for interactive and exploratory data retrieval. In such retrieval queries often cause in too many answers, this phenomenon is referred as “information overload”. In this paper, we proposed a solution which can automatically categorize the results of SQL queries to address this problem. The proposed solution dynamically generate a labeled hierarchical category structure where users can determine whether a category is relevant or not by checking its label and can explore the relevant categories and ignore other categories to reduce information overload. In the proposed solution, an analytical model is designed to estimate information overload faced by a user for a given exploration. Based on the model, we formulate the categorization problem as a cost optimization problem and develop heuristic algorithms to calculate the min-cost categorization.

Keywords: Data Mining, Information Overload, Categorization, Ranking, Discretization

I. Introduction

Database systems are being increasingly used for interactive and exploratory data retrieval [1, 2, 8, 14]. In such retrieval, queries often result in too many answers. Not all the retrieved items are relevant to the user, only a few result set is relevant to the user. Unfortunately, user needs to check all the retrieved items to find relevant information need to the user query. This phenomenon is commonly referred to as “information overload”. Consider a scenario, real-estate database that maintains information like the location, price, number of bedrooms etc. of each house available for sale. Suppose that a potential buyer is looking for homes in the Seattle/Bellevue Area of Washington, USA in the \$200,000 to \$300,000 price range. The above query, henceforth referred to as the “Homes” query, returns 6,045 homes when executed on the MSN House&Home home listing database. Information overload makes it difficult for the user to differentiate the interesting and uninteresting items, which leads to a huge wastage of user’s time and effort. Information overload can happen when the user is not certain about the query. In such a situation, user can pose a broad query in the beginning to avoid exclusion of potentially interesting results. For example, a user shopping for a home is often not sure of the exact neighbourhood she wants or the exact price range or the exact square footage at the beginning of the query. Such broad queries may also occur when the user is naïve and refrains from using advanced search features [8]. Finally, information overload is inherent when users are interested in browsing through a set of items instead of searching among them.

In the context internet text search, there has been two canonical ways to avoid information overload. First, they group the search results into separate categories. Each

category is assigned a descriptive label examining which the user can determine whether the category is relevant or not. Then user can visit the relevant categories and ignore the remaining ones. Second, they present the answers to the queries in a ranked order. Thus, categorization and ranking present two complementary techniques to manage information overload. After browsing the categorization hierarchy and/or examining the ranked results, users often reformulate the query into a more focused narrower query.

Therefore, categorization and ranking are indirectly useful even for subsequent reformulation of the queries.

In contrast to the internet text search, categorization and ranking of query results have received much less attention in the database field. Recently ranking of query results has gained some attention. But all the existing methods have not critically examined the use of categorization of query results in a relational database. Hence in this paper, categorization of database query results presents some unique challenges that are not addressed in various search engines/web directories. In all the existing search engines, the category structures are created a priori and the items are tagged in advance as well. At search time, the search results are integrated with the pre-defined category structure by simply placing each search result under the category it was assigned during the tagging process. Since such categorization is independent of the query, the distribution of items in the categories is susceptible to skew: some groups can have a very large number of items and some very few.

For example, a search on ‘databases’ on Amazon.com yields around 34,000 matches out of which 32,580 are under the “books” category. These 32,580 items are not categorized any further (can be sorted based on price or publication date or customer rating) and the user is forced to go through the long list to find the relevant items. This defeats the purpose of categorization as it retains the problem of information overload. In this paper, we propose techniques to automatically categorize the results of SQL queries on a relational database in order to reduce information overload. Unlike the “a priori” categorization techniques described above, we generate a labelled hierarchical category structure automatically based on the contents of the tuples in the answer set. Since our category structure is generated at query time and hence tailored to the result set of the query at hand, it does not suffer from the problems of a priori categorization discussed above.

This paper discusses how such categorization structures can be generated on the fly to best reduce the information overload. We begin by identifying the space of categorizations and develop an understanding of the exploration models that the user may follow in navigating the hierarchies. Such understanding helps us compare and contrast the relative goodness of the alternatives for

categorization. This leads to an analytical cost model that captures the goodness of a categorization. Such a cost model is driven by the aggregate knowledge of user behaviours that can be gleaned from the workload experienced on the system. Finally, we show that we can efficiently search the space of categorizations to find a good categorization using the analytical cost models. Our solution is general and presents a domain-independent approach to addressing the information overload problem. We perform extensive experiments to evaluate our cost models as well as our categorization algorithm.

The rest of the paper is organized as section 2: discuss about the related work, section 3: discuss about basics of categorization section 4: presents the Proposed Solution, section 5: discuss about cost model, section 6: categorization algorithm, section 7: discuss about Experimental setup, section 8: concludes the paper.

II. Related Work

OLAP and Data Visualization: Our work on categorization is related to OLAP as both involve presenting a hierarchical, aggregated view of data to the user and allow to drilldown/roll-up the categories [13]. However, in OLAP, the user needs to manually specify the grouping attributes and grouping functions [13] in our work, those are determined automatically. Information visualization deals with visual ways to present information [6]. It can be thought as a step after categorization to the further reduce information overload: given the category structure proposed in this paper, we can use visualization techniques visually display the tree [6].

Data Mining: The space in which the clusters are discovered is usually provided there whereas, in categorization, we need to find that space. Second, existing clustering algorithms deal with either exclusively categorical [11] or exclusively numeric spaces [17] in categorization, the space usually involves both categorical and numeric attributes. Third, the optimization criteria are different while it is minimizing inter-cluster distance in clustering to decrease information overload. Our work differs from classification where the categories are already given their along with a training database of labelled tuples and we need predict the label of future, unlabeled tuples [12].

Discretization/Histograms: The discretization assumes that there is a class assigned to each numeric value and uses the entropy minimization heuristic [10]. On the other hand, the histogram bucket selection is based on minimization of errors in result size estimation [5, 15].

Ranking: Ranked retrieval has traditionally been used in Information Retrieval in the context of keyword searches over text/unstructured data [3] but has been proposed in the context of relational databases recently [2,4,14]. Ranking is a powerful technique for reducing information overload and can be used effectively in complement with categorization. Although categorization has been studied extensively in the text domain [9, 16] to the best of our knowledge, this is the first proposal for automatic categorization in the context of relational databases.

III. Basics of Categorization

Space of Categorizations

Let R be a set of tuples. R can either be a base relation or a materialized view or it can be the result of a query Q . We assume that R does not contain any aggregated or derived attributes, i.e., Q does not contain any GROUP BYs or attribute derivations (Q is a SPJ query). A hierarchical categorization of R is a recursive partitioning of the tuples in R based on the data attributes and their values. We define a valid hierarchical categorization T of R inductively as follows.

Base Case: Given the root or “ALL” node (level 0) which contains all the tuples in R , we partition the tuples in R into an ordered list of mutually disjoint categories (level 1 nodes) using a single attribute.

Inductive Step: Given a node C at level $(l-1)$, we partition the set of tuples $tset(C)$ contained in C into an ordered list of mutually disjoint subcategories (level l nodes) using a single attribute which is same for all nodes at level $(l-1)$. We partition a node C only if C contains more than a certain number of tuples. The attribute used is referred to as the categorizing attribute of the level l nodes and the subcategorizing attribute of the level $(l-1)$ nodes. Furthermore, once an attribute is used as a categorizing attribute at any level, it is not repeated at a later level, i.e., there is a 1:1 association between each level of T and the corresponding categorizing attribute. We impose the above constraints to ensure that the categorization is simple, intuitive and easily understandable to the user.

Associated with each node C is a category label and a tuple-set as defined below:

Category Label: The predicate label(C) describing node C . For example, the first child of root (rendered at the top) has label ‘Neighbourhood $\in \{\text{Redmond, Bellevue}\}$ ’ while the first child of the above category has label ‘Price: 200K–225K’.

Tuple-Set: The set of tuples $tset(C)$ (called the tuple-set of C) contained in C either appearing directly under C (if C is a leaf node) or under its subcategories (if C is a non-leaf node). Formally, $tset(C)$ is the set of tuples, among the ones contained in the parent of C , which satisfy the predicate label(C). In other words, $tset(C)$ is the subset of tuples in R that satisfies the conjunction of category labels of all nodes on the path from the root to C .

The label of a category unambiguously describes to the user which tuples, among those in the tuple set of the parent of C , appear under C . Hence, user can determine whether C contains any item that is relevant or not by looking just at the label and hence decide whether to explore or ignore C .

IV. Proposed Model

We present two models capturing two cases in data exploration. One scenario is that the user explores the result set R using the category tree T until finds relevant tuple $t \in R$. For example, the user may want to find every home relevant to her in the “Homes” query. In order to ensure that user finds every relevant tuple and needs to examine every

tuple and every category label except the ones that appear under categories she deliberately decides to ignore. Another scenario is that the user is interested in just one (or two or a few) tuple(s) in R so she explores R using T till she finds that one (or few) tuple(s). For example, a user may be satisfied if she finds just one or two homes that are relevant to her. For the purpose of modeling, we assume that, in this case, the user is interested in just one tuple, i.e., the user explores the result set until finds the first relevant tuple. We consider these two cases because they both occur commonly and they differ in their analytical models.

Exploration Model for 'All' case

Figure 1 describes the exploration model for all case the user starts the exploration by exploring the root node. Given user has decided to explore the node C, if C is a non-leaf node, user non-deterministically chooses one of the two options

Option 'SHOWTUPLES': Browse through the tuples in tset(C). Note that the user needs to examine all tuples in tset(C) to make sure that she finds every tuple relevant to her.

Option 'SHOWCAT': Examine the labels of all the n subcategories of C, exploring the ones relevant to her and ignoring the rest. More specifically, she examines the label of each subcategory C_i starting from the first subcategory and non-deterministically chooses to either explore it or ignore it. If user chooses to ignore C_i , simply proceeds and examines the next label (of C_{i+1}). If user chooses to explore C_i , it does so recursively based on the same exploration model, i.e., by choosing either 'SHOWTUPLES' or 'SHOWCAT' if it is an internal node or by choosing 'SHOWTUPLES' if it is a leafnode. After she finishes the exploration of C_i , user goes ahead and examines the label of the next subcategory of C (of C_{i+1}). Note that we assume that the user examines the subcategories in the order it appears under C it can be from top to bottom or from left to right depending on how the tree is rendered by the user interface.

If C is a leaf node, 'SHOWTUPLES' is the only option (option 'SHOWCAT' is not possible since a leaf node has no subcategories).

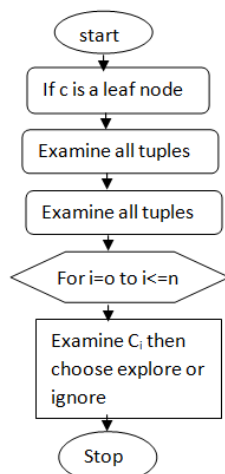


Figure 1: Flow chart model of exploration of node C in 'All' case

Exploration Model for 'One' Scenario

The user starts the exploration by exploring the root node. Given that the user has decided to explore a node C, user non-deterministically choose one of the two options

Option 'SHOWTUPLES': Check the tuples in tset(C) starting from the first tuple in tset(C) till user finds the first relevant tuple. In this paper, we do not assume any particular ordering/ranking when the tuples in tset(C) are presented to the user.

Option 'SHOWCAT': Examine the labels of the subcategories of C starting from the first subcategory till the first one she finds interesting. As in the 'ALL' case, user checks the label of each subcategory C_i starting from the first one and non-deterministically chooses to either explore it or ignore it. If user chooses to ignore C_i , simply proceeds and checks the next label. If user chooses to explore C_i , it does so recursively based on the same exploration model. We assume that when she drills down into C_i , user finds at least one relevant tuple in tset(C_i); so, unlike in the 'ALL' case, the user does not need to examine the labels of the remaining subcategories of C.

V. Cost Estimation

Since we want to generate the tree imposes the least possible information overload on the user, we need to estimate the information overload that a user will face during an exploration using a given category T.

Cost Model for 'ALL' case

Let us first consider the 'ALL' case. Given a user exploration X using category tree T, we define information overload cost, or simply cost (denoted by Cost All(X, T)), as the total number of items examined by the user during X. This definition is based on the assumption that the time spent in finding the relevant tuples is proportional to the number of items the user needs to examine more the number of items user needs to examine, more the time wasted in finding the relevant tuples, higher the information overload.

Cost Model for 'ONE' Scenario

The information overload cost CostOne (T) that a user will face, on average during an exploration using a given category tree T is the number of items that a user will need to examine till user finds the first relevant tuple. Let us consider the cost CostOne(C) of exploring the subtree rooted at C given that the user has chosen to explore C, CostOne (T) is simply CostOne (root). If the user goes for option 'SHOWTUPLES' for C and frac (C) denotes the fraction of tuples in tset(C) that she needs to examine, on average, before she finds the first relevant tuple, the cost, on average, is frac(C)*|tset(C)|. If user goes for option 'SHOWCAT', the total cost is ($K*i + \text{CostOne}(C_i)$) if C_i is the first subcategory of C explored by the user (since the user examines only i labels and explores only C_i).

$$\text{CostOne}(C) = P_w(C) * \text{frac}(C) * |\text{tset}(C)| + (1 - P_w(C)) * \sum_{i=1}^n \left(\prod_{j=1}^{i-1} (1 - P(C_j)) * P(C_i) * (K * i + \text{CostOne}(C_i)) \right)$$

VI. Categorization Algorithm

Since we know how to compute the information overload cost $Cost_{All}(T)$ of a given tree T , we can enumerate all the permissible category trees on R , compute their costs and pick the tree T_{opt} with the minimum cost. This enumerative algorithm will produce the cost-optimal tree but could be prohibitively expensive as the number of permissible categorizations may be extremely large.

Hence we present our preliminary ideas to reduce the search space of enumeration. First we present our techniques in the context of 1-level categorization i.e., a root node pointing to a set of mutually disjoint categories which are not subcategorized any further.

Reducing the Choices of Categorizing Attribute

Since the presence of a selection condition on an attribute in a workload query reflects the user's interest in that attribute, attributes that occur infrequently in the workload can be discarded right away while searching for the min-cost tree. Let A be the categorizing attribute chosen for the 1-level categorization. If the occurrence count $N_{Attr}(A)$ of A in the workload is low, the SHOWTUPLES probability $Pw(\text{root})$ of the root node will be high. Since the SHOWTUPLES cost of a tree is typically much higher than its SHOWCAT cost and the choice of partitioning affects only the SHOWCAT cost, a high SHOWTUPLES probability implies that the cost of the resulting tree would have a large first component ($Pw(\text{root}) * |tset(\text{root})|$) which would contribute to a higher total cost. Therefore, it is reasonable to consider eliminating such low occurring attributes without considering any of their partitioning.

Specifically, we eliminate the uninteresting attributes using the following simple heuristic: if an attribute A occurs in less than a fraction x of the queries in the workload, i.e., $N_{Attr}(A)/N < x$, we eliminate A . The threshold x will need to be specified by the system designer/domain expert. For example, for the home searching application, if we use $x=0.4$, only 6 attributes, namely neighborhood, price, bedroomcount, bathcount, property-type and square footage, are retained from among 53 attributes in the MSN House2Home dataset.

VII. Experimental Evaluation

To evaluate the performance of the proposed model, we present the results of an extensive empirical study we have conducted to evaluate the accuracy of our cost models in modeling information overload and evaluate our cost-based categorization algorithm and compare it with categorization techniques that do not consider such cost models. Our experiments consist of a real-life user study as well as a novel, large-scale, simulated, cross-validated user-study. For both studies, our dataset comprises of a single table called ListProperty which contains information about real homes that are available for sale in the whole of United States. The ListProperty contains 1.7 million rows (each row is a home) and, in addition to other attributes, has the following non-null attributes: location (neighborhood, city, state, zip code), price, bedroomcount, bathcount, year-built, property-type (whether it is a single family home or condo etc.) and square-footage.

Accurate Cost Model: There is a strong positive correlation between the estimated average exploration cost and actual exploration cost for various users. This indicates that our workload-based cost models can accurately model information overload in real life.

Better Categorization Algorithm: Our cost-based categorization algorithm produces significantly better category trees compared to techniques that do not consider such analytical models.

Table 1: Pearson's Correlation between estimated cost and actual cost

Subset	Correlation
1	0.39
2	0.98
3	0.32
4	0.48
5	0.16
6	0.16
7	0.19
8	0.76
All	0.90

To further confirm the strength of the positive correlation between the estimated and actual costs, we compute the Pearson Correlation Coefficient for each subset separately as well as together in Table 1. The overall correlation (0.9) indicates almost perfect linear relationship while the subset correlations show either weak (between 0.2 and 0.6) or strong (between 0.6 and 1.0) positive correlation. This shows that our cost models accurately model information overload faced by users in real-life.

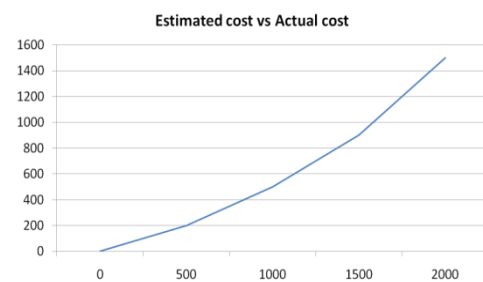


Figure 2: Correlation between actual cost and estimated cost

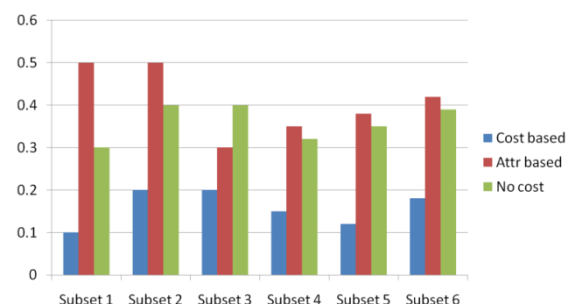


Figure 3: Cost of various techniques

Figure 2 plots the estimated cost against the actual cost for the 800 explorations. The plot along with the trend line (best linear fit with intercept 0 is $y = 1.1002x$) shows that the actual cost incurred by users has strong positive correlation with the estimated average cost.

Figure 3 compares the proposed technique with the Attr-cost and No cost techniques based on the fractional cost averaged over the queries in a subset.

VIII. Conclusion

Database systems are being increasingly used for interactive and exploratory data retrieval. In such retrieval queries often cause in too many answers, this phenomenon is referred as “information overload”. In this paper, we proposed a solution which can automatically categorize the results of SQL queries to address this problem. The proposed solution dynamically generate a labeled hierarchical category structure where users can determine whether a category is relevant or not by checking its label and can explore the relevant categories and ignore other categories to reduce information overload. In the proposed solution, an analytical model is designed to estimate information overload faced by a user for a given exploration. Based on the model, we formulate the categorization problem as a cost optimization problem and develop heuristic algorithms to calculate the min-cost categorization. Our proposed cost-based categorization algorithm produces significant better category trees compared to techniques that do not consider such cost-models.

References

- [1] S. Agrawal, S. Chaudhuri and G. Das. DBExplorer: A System for Keyword Search over Relational Databases. In Proceedings of ICDE Conference, 2002.
- [2] S. Agrawal, S. Chaudhuri, G. Das and A. Gionis. Automated Ranking of Database Query Results. In Proceedings of First Biennial Conference on Innovative Data Systems Research (CIDR), 2003.
- [3] R. Baeza_yates and B. Ribiero-Neto, Modern Information Retrieval, ACM Press, 1999.
- [4] N. Bruno, L. Gravano and S. Chaudhuri, Top-k Selection Queries over Relational Databases: Mapping Strategies and Performance Evaluation. In ACM TODS, VO, 27, No. 2, June 2002.
- [5] N. Bruno, S. Chaudhuri and L. Gravano. STHoles: A Multidimensional Workload-Aware Histogram. Proc. of SIGMOD, 2001.
- [6] S. Card, J. MacKinlay and B. Shneiderman. Readings in Information Visualization: Using Vision to Think, Morgan Kaufmann; 1st edition (1999).
- [7] J. Chu-Carroll, J. Prager, Y. Ravin and C. Cesar, A Hybrid Approach to Natural Language Web Search, In Proc. of Conference on Empirical Methods in Natural Language Processing, July 20
- [8] S. Dar, G. Entin, S. Geva and E. Palmon, DTL's DataSpot: Database Exploration Using Plain Language, In Proceedings of VLDB Conference, 1998.
- [9] S. Dumais, J. Platt, D. Heckerman and M. Sahami, Inductive learning algorithms and representations for text categorization, In Proc. Of CIKM Conference, 1998.
- [10] U. Fayyad and K. Irani. Multi-Interval Discretization of Continuous-Valued Attributes for Classification Learning. Proc. of IJCAI, 1993.
- [11] V. Ganti, J. Gehrke and R. Ramakrishnan. CACTUS - Clustering Categorical Data Using Summaries. KDD, 1999.
- [12] J. Gehrke, V. Ganti, R. Ramakrishnan, W. Loh. BOATOptimistic Decision Tree Construction. Proc. of SIGMOD, 1999.
- [13] J. Gray, S. Chaudhuri, A. Bosworth, A. Layman, D. Reichart, M. Venkatrao, F. Pellow and H. Pirahesh. Data Cube: A Relational Aggregation Operator Generalizing Group-By, Cross-Tab, and Sub-Totals. Journal of Data Mining and Knowledge Discovery", Vol 1, No. 1, 1997.
- [14] V. Hristidis and Y. Papakonstantinou, DISCOVER: Keyword Search in Relational Databases, In Proc. of VLDB Conference, 2002
- [15] V. Poosala, Y. Ioannidis, P. Haas, E. Shekita. Improved Histograms for Selectivity Estimation of Range Predicates. Proc. of SIGMOD, 1996.
- [16] F. Sebastiani, Machine learning in automated text categorization, ACM Computing Surveys, Vol. 34, No. 1, 2002.
- [17] T. Zhang, R. Ramakrishnan and M. Livny. BIRCH: an efficient data clustering method for very large databases. Proc. of ACM SIGMOD Conference, 1996.

Security Attacks on Routing Protocols in Ad Hoc Wireless Networks

Simanta Sarma¹, Binita Devi²

¹(HOD & Asstt. Professor, Department of Computer Science, S.B.M.S College, Sualkuchi, Assam, India)

²(Senior Faculty, Surojit Academy, Assam)

ABSTRACT: In this Research paper we describe mobile ad hoc networking and Security Attacks on Routing Protocols in Ad Hoc Wireless Networks. Moreover we discuss Characteristics of differentiate ad hoc wireless networks and Problems about the routing protocols. We discuss Solutions for Routing Protocols in Ad Hoc Wireless Networks. This paper we discuss Security and protection of Aware Ad Hoc Routing. We discuss for another process of modification of Ad Hoc Wireless Networks and the security criteria of the mobile ad hoc network and present the main attack types that exist in it. Finally we survey the current security solutions for the mobile ad hoc network.

KEY WORDS: Mobile Ad Hoc Wireless Network, Security, routing protocols, SAR, Secure Routing, ARAN, CONFIDANT, SEAD.

I. Introduction

Mobile Ad-hoc Networks are a collection of two or more devices equipped with wireless communications and networking Capability. These devices can communication with other nodes that immediately within their radio range. The nodes can be regarded as wireless mobile hosts with limited power and constrained bandwidth. For the later, the nodes should deploy an intermediate node to be the router to route the packet from the source toward the destination. Ad hoc networks are self-configurable and autonomous systems consisting of routers and hosts, which are able to support modality and organize themselves arbitrarily. This means that the topology of the ad hoc network changes dynamically and unpredictably. Moreover, the ad hoc network can be either constructed or destructed quickly and autonomously without any administrative server or infrastructure.

1.1. Characteristics of differentiate ad hoc wireless networks:

An ad hoc network has many characteristics that contrast sharply with fixed networks or last-hop wireless networks. First, there is no infrastructure support. All routers are mobile and can communicate with each other only when they are in transmission range. Second, ad hoc wireless nodes are resource constrained, with limited processing and memory capacity, and are usually powered with batteries. Finally, the communication medium in an ad hoc wireless network, i.e., radio waves, infrared, etc., can be easily eavesdropped. Hostile environments like battlefields or commando rescue operations are some of the important target application areas for ad-hoc wireless networks. We get the different types of characteristics of ad hoc networks. i.e.

1.1.1. Dynamic Network Topology:

This is triggered by node mobility, nodes leaving or joining the network, node inoperability due to the lack of power resources, etc. Nonetheless, the network connectivity should be maintained in order to allow applications and services to operate undisrupted.

1.1.2. Fluctuating Link Capacity:

The effects of high bit error rate are more profound in wireless communication. More than one end-to-end path can use a given link in ad hoc wireless networks, and if the link were to break, could disrupt several sessions during period of high bit transmission rate.

1.1.3. Distributed Operations

The protocols and algorithms designed for an ad hoc wireless network should be distributed in order to accommodate a dynamic topology and an infrastructure less architecture.

Wireless devices are battery powered, therefore there is a limited time they can operate without changing or replenish their energy resources. Designing energy efficient mechanisms are thus an important feature in designing algorithms and protocols.

II. Attacks on ad hoc wireless networks

In this paper we are concerned with security of routing protocols in ad hoc wireless networks. Routing is an important operation, providing the communication protocol for data delivery between wireless devices. Providing a secure system can be achieved by preventing attacks or by detecting them and providing a mechanism to recover for those attacks. Attacks on ad hoc wireless networks can be classified as active and passive attacks, depending on whether the normal operation of the network is disrupted or not.

1.2. Passive Attack

In passive attacks, an intruder the data exchanged without altering it. The attacker does not actively initiate malicious actions to cheat other hosts. The goal of the attacker is to obtain information that is being transmitted, thus violating the message confidentiality. Since the activity of the network is not disrupted, these attackers are difficult to detect.

1.3. Active Attack:

In active attacks, an attacker actively participates in disrupting the normal operation of the network services. A malicious host can create an active attack by modifying packets or by introducing false information in the ad hoc network. It confuses routing procedures and degrades network performance. Active attacks can be divided into internal and external attacks.

1.3.1. External Attack

External Attacks are carried by nodes that are not legitimate part of the network. In external attacks, it is possible to disrupt the communication of an organization from the parking lot in front of the company office.

1.3.2. Internal Attack

Internal Attacks are from compromised nodes that were once legitimate part of the network. In ad hoc wireless network as authorized nodes, they are much more severe and difficult to detect when compared to external attacks.

III. Problems about the routing protocols

In this paper, we examine there are different types of problems about the routing protocols. i.e.

- First of all, consider the rapid passing pattern. We define the rapid passing pattern to be one node passing through the whole network very quickly. Such a rapid passing node will generate the following affects to the whole network. First, the topology of the network changed rapidly, which will lead to the lost of packets. Second, we have to modify every node's routing table that within the communication distance of the rapid-passing node, that will greatly improve the consumption of the bandwidth and the overhead of the networks. Third, obviously there will be tremendous delay of the data sending to the rapid-moving node.
- Transmission between two hosts over a wireless network does not necessarily work equally well in both directions. Thus, some routes determined by some routing protocols may not work in some environments.
- Many routing protocols may create redundant routes, which will greatly increase the routing updates as well as increase the whole networks overhead.

3.1. Energy Consumption of Wireless Ad-hoc Networks

Energy consumption is also one of the most important performance metrics for wireless ad hoc networks, it directly relates to the operational lifetime of the networks. Energy consumption is also one of the most important performance metrics because it directly relates to the operational lifetime of the network. Most research efforts are focused on performance comparisons and trade-off studies between various low energy routing and self-organization protocols, while keeping other system parameters fixed. As a result, very little has been revealed about the relationship between the aggregate energy consumption and non-protocol parameters such as node density and network coverage area.

IV. Security in Wireless Ad-hoc Networks

Security is an important thing for all kinds of networks including the Wireless Ad Hoc Networks. It is obviously to see that the security issues for Wireless Ad Hoc Networks are difficult than the ones for fixed networks. This is due to system constraints in mobile devices as well as frequent topology changes in the Wireless networks. The system constraints include low-power, small memory and bandwidth, and low battery power. Everybody knows that the core requirement for military applications dealing with trust and security! That is to say, security is the most important issue for ad hoc networks, especially for those security sensitive applications. The main Ad-hoc Networks applications of MANET are in military and emergency, all these applications are security-sensitive. MENAT can not satisfy the security requirement of the applications of the architecture of MANET. There are several factors of security that we should consider. In this process maintain and develop of all military information secured in wireless ad-hoc networks.

4.1. Availability

First, Availability ensures the survivability of network services despite denial of service attacks. This security criterion is challenged mainly during the denial-of-service attacks, in which all the nodes in the network can be the attack target and thus some selfish nodes make some of the network services unavailable area.

4.2. Confidentiality

Confidentiality ensures that certain information is never disclosed to unauthorized entities. In other words, in order to maintain the confidentiality of some confidential information, we need to keep them secret from all entities that do not have the privilege to access them.

4.3. Integrity

Integrity guarantees that a message being transferred is never corrupted. A message can be removed, replayed or revised by an adversary with malicious goal, which is regarded as malicious altering; on the contrary, if the message is lost or its content is changed due to some benign failures, which may be transmission errors in communication or hardware errors such as hard disk failure, then it is categorized as accidental altering.

4.4. Authentication

Authentication enables a node to ensure the identity of the peer node. If there is not such an authentication mechanism, the adversary could impersonate a benign node and thus get access to confidential resources, or even propagate some fake messages to disturb the normal network operations.

4.5. Non repudiation

Non repudiation ensures that the sender and the receiver of a message cannot disavow that they have ever sent or received such a message. This is useful especially when we need to discriminate if a node with some abnormal behavior is compromised or not: if a node recognizes that the message it has received is erroneous, it can then use the incorrect message as an evidence to notify other nodes that the node sending out the improper message should have been compromised.

4.6. Authenticity

Authenticity is essentially assurance that participants in communication are genuine and not impersonators [4]. It is necessary for the communication participants to prove their identities as what they have claimed using some techniques so as to ensure the authenticity. If there is not such an authentication mechanism, the adversary could impersonate a benign node and thus get access to confidential resources, or even propagate some fake messages to disturb the normal network operations.

4.7. Anonymity

Anonymity means that all the information that can be used to identify the owner or the current user of the node should default be kept private and not be distributed by the node itself or the system software. This criterion is closely related to privacy preserving, in which we should try to protect the privacy of the nodes from arbitrary disclosure to any other entities.

4.8. Ordering

Out-of-order updates can also affect the correctness of the routing protocols. These messages may not reflect the true state of the network and may propagate false information. Ad hoc routing protocols have sequence numbers that are unique within the routing domain to keep updates in order.

4.9. Timeliness

Routing updates need to be delivered in a timely fashion. Update messages that arrive late may not reflect the true state of the links or routers on the network. They can cause incorrect forwarding or even propagate false information and weaken the credibility of the update information. If a node that relays information between two large connected components is advertised as "down" by malicious neighbors, large parts of the network become unreachable. Most ad hoc routing protocols have timestamps and timeout mechanisms to guarantee the freshness of the routes they provide.

V. Security Aware Ad Hoc Routing (SAR)

We present a description of our protocol and its behavior and enumerate the metrics we deploy to measure the quality of ad hoc routing security of an ad hoc route discovered by our protocol. Finally & originally, ad hoc routing protocols were based on medications or augmentations to traditional routing protocols for wired networks [8]. These protocols send updates and react to topology changes, using monitoring and other infrastructure support to maintain routing tables. We study & developed the Current research focuses on pure on-demand [12, 17] routing protocols, and more recently, on augmentations that exploit additional information available on the ad-hoc nodes [26, 20, 21] to improve the quality of routes and reduce performance overheads. Most of the protocols that have been proposed so far focus on discovering the shortest path between two nodes as fast as possible. Some protocols trade performance and simplified management to obtain bounded sub-optimal paths to speed up the route discovery process [28, 16].

5.1. Protocol

Protocol is a set of rules created for the process of communication with another computer or with an operating system. In the original protocol, when a node wants to communicate with another node, it broadcasts a Route Request or RREQ packet to its neighbors. The RREQ is propagated to neighbors of neighbors and so on, using controlled flooding. The RREQ packets set up a reverse path to the source of the RREQ on intermediate routers that forward this packet. Moreover, SAR, we embed our security metric into the RREQ packet itself, and change the forwarding behavior of the protocol with respect to RREQs. Intermediate nodes receive an RREQ packet with a particular security metric or trust level. SAR ensures that this node can only process the packet or forward it if the node itself can provide the required security or has the required authorization or trust level. Protocol maintain in rule regulation of Wireless Network.

5.2. Matrices of Protocol

We enumerate different techniques to measure or specify the quality of security of a route discovered by our generalized SAR protocol. The first technique is the explicit representation of trust levels using a simple hierarchy that reflects organizational privileges. SAR provides applications the ability to incorporate explicit trust levels into the route discovery process. Most organizations have an internal hierarchy of privileges. SRP defends against attacks that disrupt the route discovery process and guarantees to identify the correct topological information. The basic idea of SRP is to set up a security association (SA) between a source and a destination node without the need of cryptographic validation of the communication data by the intermediate nodes. For example, in our battlefield scenario, the military ranks of the users of the ad hoc nodes form an explicit partial-ordering of privilege levels. A simple way of incorporating trust levels into ad hoc networks is to mirror the organizational hierarchy, and associate a number with each privilege level. These numbers represent the security/importance/capability of the mobile nodes and also of the paths. Simple comparison operators can sort these levels to reflect their position in the actual hierarchy. We develop our notion of the "*level of protection*" associated with security of information in transit in routing protocol packets. Specifically, in SAR, the aim is to protect any information or behavior that can update or cause a change to the routing on cooperating nodes involved in an ad hoc routing protocol.

5.3. ARAN

A Secure Routing Protocol for Ad Hoc Networks (ARAN) [12] is an on demand protocol designed to provide secure communications in managed open environments. Nodes in a managed-open environment exchange initialization parameters before the start of communication. Each node in ARAN receives a certificate after securely authenticating its identity to a trusted certificate server R. Nodes use these certificates to authenticate themselves to other nodes during the exchange of routing messages. The certificate contains the node's IP address, its public key, as well as the time of issuing and expiration. These fields are concatenated and signed by the server R. A node P receives a certificate as: $R \rightarrow P : cert_P = [IP_P, L_P, r, f] L_R^-$. All the fields are concatenated and signed with source node I's private key. A combination of the nonce number (Q_I) and timestamp (r) is used to obtain data freshness and timeliness property. Source node I broadcasts a Route Discovery Packet (RDP) for a destination D as $I \rightarrow \text{brdcst} : [RDP, IP_D, cert_I, Q_I, r] L_I^-$. If G is the first node on the reverse path, REP packet is sent as $D \rightarrow G : [REP, IP_I, cert_D, Q_I, t] L_D^-$. But nodes use an ERR message to report links in active routes broken due to node movement.

5.4. Cooperation of Nodes Fairness in Dynamic Ad-hoc NeT-works (CONFIDANT)

Cooperation of Nodes Fairness in Dynamic Ad-hoc NeTworks (CONFIDANT) [2] protocol is designed as an extension to reactive source-routing protocol such as DSR. Each node in this protocol monitors their neighbors and updates the reputation accordingly. If they detect any misbehaving or malicious node, they can inform other friend nodes by sending an ALARM message. When a node receives such an ALARM either directly from another node or by listening to the ad hoc network, it calculates how trustworthy the ALARM is based on the source of the ALARM and the total number of ALARM messages about the misbehaving node.

5.5. Rushing attacks

Rushing attacks [9] are mostly directed against on demand routing protocols such as DSR. To counter such attacks, a generic secure route discovery component called Rushing Attack Prevention (RAP) is used. RAP combines the following mechanisms: Secure Neighbor Detection, Secure Route Delegation, and Randomized Route Request Forwarding.

5.6. Attacks using Impersonation

In impersonation attacks, an intruder assumes the identity and privileges of another node in order to consume its resources or to disturb normal network operation. An attacker node achieves impersonation by misrepresenting its identity. This can be done by changing its own IP or MAC address to that of some other legitimate node. Some strong authentication procedures can be used to stop attacks by impersonation.

5.6.1. Man-in-the-Middle Attack

In this attack, a malicious node reads and possibly modifies the messages between two parties. The attacker can impersonate the receiver with respect to the sender, and the sender with respect to the receiver, without having either of them realize that they have been attacked.

5.6.2. Sybil Attack

In the Sybil attack [16], an attacker pretends to have multiple identities. A malicious node can behave as if it were a larger number of nodes either by impersonating other nodes or simply by claiming false identities. Sybil attacks are classified into three categories: direct/indirect communication, fabricated/stolen identity, and simultaneity. In the direct communication, Sybil nodes communicate directly with legitimate nodes, whereas in the indirect communication messages sent to Sybil nodes are routed through malicious nodes.

VI. Attack on Ad-hoc network and Secured Attacks using Modification

This attack disrupts the routing function by having the attacker illegally modifying the content of the messages. Examples of such attacks include redirection by changing the route sequence number and redirection with modified hop count that can trigger the black hole attack. Some other modification based attacks are presented next.

6.1. Misrouting Attack

In the misrouting attack, a non-legitimate node sends data packet to the wrong destination. This type of attack is carried out by modifying the final destination address of the data packet or by forwarding a data packet to the wrong next hop in the route to the destination.

6.2. Detour Attack

In this type of attack, the attacker adds a number of virtual nodes in to a route during the route discovery phase. As a consequence, the traffic is diverted to other routes that appear to be shorter and might contain malicious nodes which could create other attacks.

6.3. Blackmail Attack

Blackmail attack causes false identification of a good node as malicious node. In ad hoc wireless networks, nodes usually keep information of perceived malicious nodes in a blacklist. An attacker may blackmail a good node and tell other nodes in the network to add that node to their blacklists as well, thus avoiding the victim node in future routes.

6.4. Resource Consumption Attack

In Fabrication attack part of resource consumption attack is a malicious node deliberately tries to consume the resources (e.g. battery power, bandwidth, etc.) of other nodes in the network. The attack can be in the form of unnecessary route requests, route discovery, control messages, or by sending stale information. For example, in routing table overflow attack, a malicious node advertises routes to non-existent nodes, thus causing routing table overflow. By using packet replication attack, an adversary consumes bandwidth and battery power of other nodes.

6.5. Routing Table Poisoning

In Fabrication attack part of routing table poisoning is a malicious node sends false routing updates, resulting in sub-optimal routing, network congestion, or network partition.

6.6. Rushing Attack

In Fabrication attack part of rushing attack is malicious node in rushing attack attempts to tamper Route Request packets, modifying the node list, and hurrying its packet to the next node.

6.7. Black Hole

In Fabrication attack part of black hole is a malicious node advertise itself as having the shortest path to all nodes in the network (e.g. the attacker claims that it is a level one node). The attacker can cause DoS by dropping all the received packets.

6.8. Masquerading

During the neighbor acquisition process, a outside intruder could masquerade an nonexistent or existing IS by attaching itself to communication link and illegally joining in the routing protocol domain by compromising authentication system. The threat of masquerading is almost the same as that of a compromised IS.

6.9. Replay

An attacker that performs a replay attack injects into the network routing traffic that has been captured previously. This attack usually targets the freshness of routes, but can also be used to undermine poorly designed security solutions.

6.10. Wormhole Attack

In the wormhole attack, two compromised nodes can communicate with each other by a private network connection. The attacker can create a vertex cut of nodes in the network by recording a packet at one location in network, tunneling the packet to another location, and replaying it there. The wormhole can drop packets or it can selectively forward packets to avoid detection. It is particularly dangerous against different network routing protocols in which the nodes consider themselves neighbor after hearing a packet transmission directly from some node.

6.11. Tunneling Attack

In a tunneling attack, two or more nodes collaborate and exchange en-capsulated messages along existing data routes. For example, if a Route Request packet is encapsulated and sent between two attackers, the packet will not contain the path traveled between the two attackers. This would falsely make the receiver conclude that the path containing the attackers is the shortest path available.

VII. Security at the physical and data link layers and Solutions for Routing Protocols in Ad Hoc Wireless Networks

In this paper, we survey the security solutions in the mobile ad hoc networks. First we analyze the main security criteria for the mobile ad hoc networks, which should be regarded as a guideline for us to find the solutions to the security

issues in the mobile ad hoc networks. We then point out various attack types that mainly threaten the mobile ad hoc networks. The Wireless Ad hoc Networks are a flawed architecture for the following solution technical reasons:

- The most important thing for the networks is security. It is even important for Wireless Ad hoc Networks because its applications are in military. The MANET cannot appropriately solve the problem of the security.
- Routing is also a big problem. All the routing protocols for Wireless Ad hoc Networks are need patches. In security at physical and data link layers are two types of faults that may occur in a routing algorithm: (i) faults whose effect is stochastically indistinguishable from ordinary link failures caused by the mobility of the system, radio interference, power failure etc, and (ii) faults whose effect can be distinguished from ordinary failures. Malicious faults tend to be of the second type, although the first type should not be excluded.

In this process of Message encryption and digital signatures are two important mechanisms for data integrity and user authentication. There are two types of data encryption mechanisms, symmetric and asymmetric (or public key) mechanisms. Symmetric cryptosystems use the same key (the secret key) for encryption and decryption of a message, and asymmetric cryptosystems use one key (the public key) to encrypt a message and another key (the private key) to decrypt it. Public and private keys are related in such a way that only the public key can be used to encrypt messages and only the corresponding private key can be used for decryption purpose. Even if attacker comprises a public key, it is virtually impossible to deduce the private key. Any change to the message will produce a different hash result even when the same hash function is used. A MAC, which is a cryptographic checksum, is computed by the message initiator as a function of the secret key and the message being transmitted and it is appended to the message. The recipient re-computes the MAC in the similar fashion upon receiving the message.

7.1 Secure Efficient Ad hoc Distance Vector (SEAD)

Secure Efficient Ad hoc Distance Vector (SEAD) [7] is a proactive routing protocol, based on the design of DSDV [19]. Besides the fields common with DSDV, such as destination, metric, next hop and sequence number, SEAD routing tables maintain a hash value for each entry. We collect all the nodes are creating, maintaining all the part of control ad-hoc secure process routing protocols update packets. This paper is concerned with protecting routing updates, both periodic and triggered, by preventing an attacker to forge better metrics or sequence numbers in such update packets.

SEAD provides a robust protocol against attackers trying to create incorrect routing state in other node by modifying the sequence number or the routing metric. SEAD does not provide a way to prevent an attacker from tampering next hop or destination field in a routing update. Also, it cannot prevent an attacker to use the same metric and sequence number learned from some recent update message, for sending a new routing update to a different destination.

7.2 ARIADNE

ARIADNE, an efficient on-demand secure routing protocol, provides security against arbitrary active attackers and relies only on efficient symmetric cryptography. It prevents attackers from tampering uncompromised routes consisting of uncompromised nodes. ARIADNE ensures point-to-point authentication of a routing message by combining a shared key between the two parties and MAC. DSR, it consists of two basic operations, route discovery and route maintenance. ARIADNE makes use of efficient combination of one way hash function and shared keys. Pre-hop hashing mechanism, a one-way hash function that verifies that no hop is omitted, is also used in Ariadne. In the case of any dead link, a Route Error message is sent back to the initiator. Errors are generated just as regular data packets and intermediate nodes remove routes that use dead links in the selected path.

7.3. TIARA

Techniques for Intrusion-Resistant Ad Hoc Routing Algorithms (TIARA) mechanisms protect ad hoc networks against denial-of-service (DoS) attacks launched by malicious intruders. TIARA addresses two types of attacks on data traffic which are flow disruption and resource depletion.

7.4. Secure Routing Protocol (SRP)

Secure Routing Protocol (SRP) [17], is another protocol extension that can be applied to many of the on demand routing protocols used today. SRP defends against attacks that disrupt the route discovery process and guarantees to identify the correct topological information. The basic idea of SRP is to set up a security association (SA) between a source and a destination node without the need of cryptographic validation of the communication data by the intermediate nodes. SRP assumes that this SA can be achieved through a shared key KST between the source S and target T. The source S initiates the route discovery by sending a route request packet to the destination T. The SRP uses an additional header called SRP header to the underlying routing protocol (e.g. AODV) packet. Otherwise it calculates the keyed hash of the request fields and if the output matches SRP MAC then authenticity of the sender and integrity of the request are verified. In case of a match, it compares reply IP source-route with the exact reverse of the route carried in reply packet. If the two routes match then S calculates the MAC by using the replied route, the SRP header fields, and the secure key between source and destination. SRP suffers from the lack of validation mechanism for route maintenance messages as it does not stop a malicious node from harming routes to which that node already belongs to. SRP is immune to IP spoofing because it secures the binding of the MAC and IP address of the nodes but it is prone to wormhole attacks and invisible node attacks.

7.5. Defense Mechanisms against Wormhole Attacks

In order to prevent the wormhole attacks, the packet leashes mechanism [33] proposes to add additional information (referred as leashes) to the packets in order to restrict packet's maximum allowed transmission distance. Geographical leash and temporal leash can be used to detect and stop wormhole attacks. Geographical leash insures that the recipient of the packet is within a certain distance from the sender while temporal leash is used to enforce an upper bound on the packet's life time, thus restricting packet's maximum travel distance. Temporal leash uses packet's expiration time to detect a wormhole. The expiration time is computed based on the allowed maximum transmission distance and the speed of light. A node will not accept any packet if this expiration time has passed.

7.6. BISS

Building Secure Routing out of an Incomplete Set of Security Associations (BISS) [48], the sender and the receiver can establish a secure route, even if, prior to the route discovery, only the receiver has security associations established with all the nodes on the chosen route. Thus, the receiver will authenticate route nodes directly through security associations. The sender, however, will authenticate directly the nodes on the route with which it has security associations, and indirectly (by exchange of certificates) the node with which it does not have security associations. The operation of BISS ROUTE REQUEST relies on mechanisms similar to direct route authentication protocols. When an initiator sends a ROUTE REQUEST, it signs the request with its private key and includes its public key PQR in the request along with a certificate sl signed by the central authority binding its id with PQR .

VIII. Related Work

We develop our notion of the "level of protection" associated with security of information in transit in routing protocol packets. Specifically, in SAR, the aim is to protect any information or behavior that can update or cause a change to the routing tables on cooperating nodes involved in an ad hoc routing protocol. Attacks on the trust hierarchy can be broadly classified as Outsider Attacks and Insider Attacks, based on the trust value associated with the identity or the source of the attack. SAR modifies the behavior of route discovery, tying in protocol behavior with the trust level of a user. What is also needed is a binding between the identities of the user with the associated trust level. Routes discovered by SAR come with "quality of protection" guarantees. The techniques enabled by SAR can be easily incorporated into generic ad hoc routing protocols as illustrated by our implementation example - SAODV. In this chapter we discuss security services and challenges in an ad hoc wireless network environment. We research examine and classify major routing attacks and present a comprehensive survey on the state-of-the-art mechanisms and solutions designed to defeat such attacks. All routing protocol develops and executed from secured in this related process.

IX. Conclusions

We briefly introduce in this paper, the basic characteristics of the mobile ad hoc network. Because of the emergence of the concept pervasive computing, there is an increasing need for the network users to get connection with the world anytime at anywhere, which inspires the emergence of the mobile ad hoc network. SAR enables the discovery of secure routes in a mobile ad hoc environment. Its integrated security metrics allow applications to explicitly capture and enforce explicit cooperative trust relationships. In addition, SAR also provides customizable security to the flow of routing protocol messages themselves. In this paper, we examine security services and challenges in an ad hoc wireless network environment. We examine and classify major routing attacks and present a comprehensive survey on the state-of-the-art mechanisms and solutions designed to defeat such attacks. Finally we prove the current security solutions for the mobile ad hoc networks. In the end, we examine several security techniques that can help protect the mobile ad hoc networks from external and internal security threats. Even if parallel model checking approaches were used, our conclusion is that it is at this point not feasible to provide a proof for topologies of any significant size by modeling the protocol directly secured in ad-hoc wireless network.

X. Acknowledgements

The authors would like to thank everyone, whoever remained a great source of help and inspirations in this humble presentation. The authors would like to thank Gauhati University, Assam (Teaching Staff of Department of Computer Science); S.B.M.S College, Sualkuchi, Assam; CMJ University for providing necessary facilities to carry out this work.

References

- [1] J. Broch and D. B. Johnson. The Dynamic Source Routing Protocol for Mobile Ad Hoc Networks. IETF Internet Draft, October 1999.
- [2] W. Du, J. Deng, Y. S. Han, and P. K. Varshney, A Pairwise Key Predistribution Scheme for Wireless Sensor Networks, ACM CCS 2003, Oct. 2003, pp. 42-51.
- [3] R. Kravets, S. Yi, and P. Naldurg, A Security-Aware Routing Protocol for Wireless Ad Hoc Networks, In ACM Symp. On Mobile Ad Hoc Networking and Computing, 2001.
- [4] Data Integrity, from Wikipedia, the free encyclopedia, http://en.wikipedia.org/wiki/Data_integrity.
- [5] P. Papadimitratos and Z. J. Hass, Secure Routing for Mobile Ad Hoc Networks, in Proceedings of SCS Communication Networks and Distributed Systems Modeling and Simulation Conference (CNDSS), San Antonio, TX, January 2002.
- [6] Y. -C. Hu, D. B. Johnson, and A. Perrig, Rushing Attacks and Defense in Wireless Ad Hoc Network Routing Protocols, WiSe 2003, 2003.

- [7] S.Chessa, P.Santi, "Comparison Based System-Level Fault Diagnosis in Ad-Hoc Networks", Proc. IEEE 20th Symp. on Reliable Distributed Systems (SRDS), New Orleans, pp. 257-266, October 2001.
- [8] B. Leiner, R. Ruth, and A. R. Sastry, "Goals and challenges of the DARPA GloMo program," IEEE Personal Communications, vol. 3, no. 6, pp. 34-43, December 1996.
- [9] A Distributed Light-Weight Authentication Model for Ad-hoc Networks.
- [10] T. H. Clausen, G. Hansen, L. Christensen, and G. Behrmann, The Optimized Link State Routing Protocol, Evaluation Through Experiments and Simulation, Proc. of IEEE Symp. On Wireless Personal Mobile Communications 2001, Sep. 2001.
- [11] L. Zhou and Z. J. Haas. Securing Ad Hoc Networks. IEEE Network Magazine, November 1999.
- [12] F. Wang, Brian Vetter, and Shyhtsun Felix Wu. Secure routing protocols: Theory and practice. Technical Report, North Carolina State University.
- [13] B. Smith, S. Murthy, and J.J. Garcia-Luna-Aceves. Securing the Border Gateway Routing Protocols. In Global internet '96, London, UK, November 1996.
- [14] C. E. Perkins and E. M. Royer. Ad-hoc On-Demand Distance Vector Routing. In The Second IEEE Workshop on Mobile Computing Systems and Applications, New Orleans, LA, USA, February 1999.
- [15] Jim Parker, Discussion Record for the 1st MANET Reading Group Meeting
- [16] http://logos.cs.umbc.edu/wiki/eb/index.php/February_10%2C_2006 (Authorization required).
- [17] Jiejun Kong, Xiaoyan Hong, Yunjung Yi, JoonSang Park, Jun Liu and Mario Gerlay, A Secure Ad-hoc Routing Approach Using Localized Self-healing Communities, in Proceedings of the 6th ACM International Symposium on Mobile Ad Hoc Networking and Computing, pages 254-265, Urbana-Champaign, Illinois, 2005.
- [18] Y. Zhang and W. Lee, Intrusion Detection in Wireless Ad-hoc Networks, in Proceedings of the 6th International Conference on Mobile Computing and Networking (MobiCom 2000), pages 275-283, Boston, Massachusetts, August 2000.
- [19] K. Sanzgiri, B. Dahill, B. N. Levine, C. Shields, and E. M. Belding-Royer, A Secure Routing Protocol for Ad Hoc Networks, in Proceedings of ICNP'02, 2002.
- [20] Bissias, G.D., Liberatore, M., Jensen, D., Levine, B.N., "Privacy vulnerabilities in encrypted HTTP streams" In Proc. Privacy Enhancing Technologies Workshop (PET 2005).
- [21] J. Nam, S. Cho, S. Kim, and D. Won, "Simple and Efficient Group Key Agreement Based on Factoring" Proc. Int'l Conf. Computational Science and Its Applications (ICCSA '04), pp. 645-654, 2004.
- [22] Panagiotis Papadimitratos, Zygmunt J. Haas, "Secure message transmission in mobile ad hoc networks, Ad Hoc Networks" IEEE 2003, 193-209.
- [23] Thomas S. Messerges, ohnas Cukier, Tom A.M. Kevenaar, Larry Puhl, Rene truijk, Ed Callaway, "A Security Design for a General Purpose, Self-Organizing, Multihop Ad Hoc Wireless Network" 1st ACM Workshop Security of Ad Hoc and Sensor Networks Fairfax, Virginia 2003.
- [24] Yih-chun hu, adrian perrig, "A Survey of Secure Wireless ad hoc routing" IEEE security & privacy May-June 2004.
- [25] Ljubica Blazevic, Levente Buttyan, Srdan Capkun, Silvia Giordano, Jean-Pierre, Hubaux and Jean-Yves Le Boudec, "Self-Organization in Mobile Ad-Hoc Networks: the Approach of Terminodes".
- [26] J. A. Freebersyser and B. Leiner, "A DoD perspective on mobile ad hoc networks," in Ad Hoc Networking, C. E. Perkin, Ed. Addison-Wesley, 2001, pp. 29-51.
- [27] B. Leiner, R. Ruth, and A. R. Sastry, "Goals and challenges of the DARPA GloMo program," IEEE Personal Communications, vol. 3, no. 6, pp. 34-43, December 1996.
- [28] Perkins, C., Belding-Royer, E., Das, S.: Request for Comments: Ad hoc on-demand distance vector (AODV) routing. <http://www.ietf.org/rfc/rfc3561.txt> (2003).
- [29] Johnson, D.B., Maltz, D.A., Hu, Y.C.: Internet draft: The dynamic source routing protocol for mobile ad hoc networks (DSR). <http://www.ietf.org/internet-drafts/draft-ietf-manet-dsr-09.txt> (2003).
- [30] S. Buchegger and J. L. Boudec, Performance Analysis of the CONFIDANT Protocol Cooperation Of Nodes Fairness In Dynamic Ad-hoc NeTworks, In Proc. of IEEE/ACM Symposium on Mobile Ad Hoc Networking and Computing (MobiHOC), Jun. 2002.

Isolation and Molecular Characterization of Anti-Cancerous Compound Producing Marine Bacteria by Using 16S rRNA Sequencing and GC-MS Techniques

Sai Lakshman Mithun.V¹, C.S.V.Ramachandra Rao²

Department of Biotechnology, DVR & Dr.HS MIC College of Technology, Kanchikacherla, Andhra Pradesh, India.

Abstract: Extracts from microorganisms have served as a valuable source of diverse molecules in many drug discoveries. Identification of microbial strains having promising biological activities and purifying the bio-molecules which are responsible for the biological activities, have led to the discovery of many bioactive molecules. Extracts of bacteria in vitro tested on various cancer cell lines. The lyophilized bacterial extract powder was dissolved in various chemical solvents like Methanol, Chloroform and Ethyl acetate. From them cytotoxic assays was performed the extracts were screened on HCT 15 and MES-SA cancer cell lines to study the cytotoxic potential. Where the Ethyl acetate showed the inhibition 87.34% when compared to other solvents. The Ethyl acetate extract of isolate showed promising results by MTT assay and Trypan blue staining. Identification of the microorganism, the selected isolates was characterized by using the 16s rRNA sequencing based on microbial characterization, the compound produced by bacteria was analyzed by GC-MS technique. The organism was identified as *Micrococcus luteus* and biochemical tests of the extracts were also carried out.

Key words: Anticancer, Bacterial extracts, MTT assay, HCT 15 cell line, MES-SA cell line.

I. INTRODUCTION

Cancer is a disease in which a cell, or a group of cells represents uncontrolled growth invasion (intrusion on and distortion of adjacent tissues), and metastasis (spread from one part to another part in the body through lymph or blood). These three malignant properties differentiate cancer from benign tumors, which are self-limited and do not invade or metastasize while the malignant tumors are not self limited and metastasize. Most of cancers occur form a tumor; the oncology is deals with the study, diagnosis, treatment, and prevention of cancer and it's a branch of medicine. Cancer is a human tragedy that affects people at all ages with the risk in most types increasing with age. Cancers are primarily an environmental disease with 90-95% of cases due to modification in lifestyle and environmental factors and 5-10% due to genetics Cancer is caused.

By both external factors (tobacco, chemicals, radiation and infectious organisms) and internal factors (inherited mutations, hormones, immune conditions and mutation that occurs from metabolism). Common environmental factors leading to cancer death include: tobacco 25-30%, diet and obesity 30-35%, infections 15-20%, radiation, stress, lack of physical activity and environmental pollutants. [B Dhorajiya et al., 2011].

Early discovery of carcinogens by John Hill, an English physician, 1761. In it he made the first causal link between substances in the environment and cancer when he described a relationship between tobacco snuff and nasal cancer. This brought about the awareness of carcinogens (chemical agents that have been demonstrated to cause cancer). That associated particular occupations with an increased risk of developing specific forms of cancer the forerunner to the field of public health and cancer.[C. A. Almeida and S. A. Barry, 2010].

Natural products have played an important role in treating and preventing human diseases. Natural products with medicinal value have come from various sources viz., terrestrial plants, terrestrial microorganisms, marine organisms, and terrestrial vertebrates and invertebrates the microbial extracts have served as a valuable source of diverse molecules in many drug discovery efforts and led to the isolation of several important drugs. [Newman *et al.*, 2002]. The chemical composition of bioactive compounds of microbial origin is often highly complex. Organic compounds from aqua to terrestrial microorganisms have extensive use in the treatment of many diseases and serve as compounds of interest both in their natural form and as templates for synthetic modification. These compounds provided important contributions to the discovery of antibacterial agents like penicillins, cephalosporins, tetracyclines, and polypeptides, immunosuppressive agents like cyclosporine, ant diabetic agent like acarbose, cholesterol-lowering agents like lovastatin and mevastatin and anti cancer agents like peplomycin, pentostatin, and epirubicin [Butler, 2005; Sneader, 2005]

II. MATERIALS AND METHODS

Screening and isolation of bacterial strains:

Collection of soil sample:

Marine soil samples were collected from Bay of Bengal coast of Machilipatnam, Krishna district, AP, India. About 15 grams of soil sediments were collected in a sterile polythene bags and stored at 4°C until further use. The soil samples were stored under sterile conditions for preventing the bacterial cross contamination. Then the sample was serially diluted to till 10⁻⁶ dilution by adding 1 gram of soil to 10ml of distilled water.

Screening for bacterial single isolates:

From the serially diluted samples, 100µl of sample was poured on Nutrient Agar plates (Himedia). From the 10^{-5} and 10^{-6} dilutions the single isolated bacterial colonies were obtained on agar plates by the procedure according to [Shirai *et al.* (1989).], The bacterial pure cultures were isolated.

Sub culturing of bacterial isolates:

The inoculum was prepared by transferring a single colony of the isolates into 5 ml of the corresponding medium. This inoculum was transferred to 95 ml of the corresponding broth and bacterial isolates were incubated at 37° c for 2 -3 days .this broth was used for the extraction of bioactive metabolites.

Preparation of bacterial extracts:

The culture broth was centrifuged at 3000 rpm for 15 min to obtain a clear supernatant. Components were extracted successively dissolved with chemical solvents such as chloroform (C), Methanol (M) and Ethyl acetate (E) and followed by vacuum evaporation of these extracts to obtain the dry extracts by vacuum rotary evaporator. [Angel TreasaThomas *etal.*, 2011]

Sample preparation for biological studies:

The bacterial crude extracts were dissolved in 1 ml DMSO and transferred to sterile vials of 2 ml capacity; these samples were stored at room temperature for further use, protected from light.

Maintenance of cancer cell lines:

Human colorectal adenocarcinoma Cancer cells (HCT 15) and Human uterine cancer cells (MES-SA) were maintained in Dulbecco's modified essential medium (DMEM) supplemented with 4.5 g/l glucose and 2mm l-glutamine and 5% fetal bovine serum (FBS) (growth medium) at 37⁰c in 5% CO₂ incubator.

Trypan blue dye exclusion technique:

A cell suspension was made with a fixed volume of cells (e.g. 1ml). Although an aseptic technique is not essential in all stages of this procedure, 50uL of cell suspension was taken and mixed it with an equal volume of trypan blue. Solution was well mixed using a pipette. It transfers to a hemocytometer and then counted live cell as clear form and dead cell as blue cells. After staining with trypan blue solution counting should commence <5minutes as after that time the cells will begin to take up the dye. The hemocytometer was placed on the stage of an inverted microscope.

Focus was adjusted and power until a single counting square fills the field. The number of cells per ml, and the total number of cells were counted using the following formula:

Calculate percent viability by using formula:

% viability = (live cell count/total cell count) ×100

Anticancer assay:

Micro culture tetrazolium (MTT) assay:

The monolayer cell culture was trypsinized and the cell count was adjusted to 1ml using medium. To each well of 96 well microtitre plates, 0.1ml of diluted cell suspension was added. After 72 hour, the sample solution in wells was flicked off and 50µl of MTT dye was added to each well. The plates were gently shaken and incubated for 4 hours at 37° c in 5% CO₂ incubator. The supernatant was removed, 50 µl of Propanol was added, and the plates were gently shaken to solubilize the formed formazan. The absorbance was measured using a micro plate reader at a wavelength of 490 nm. The percentage growth inhibition was calculated using the Formula below:

The percentage growth inhibition was calculated using following formula:

%cell inhibition= $100 - \{(At - Ab) / (Ac - Ab)\} \times 100$

Where,

At= Absorbance value of test compound

Ab= Absorbance value of blank

Ac=Absorbance value of control [T. Mosmann, *J. Immunol. Methods*]

Identification of microorganism:

Biomass culture for anticancer activity assays was carried out in 500 mL conical flasks at 37°C temperature. Total DNA was extracted and PCR amplification was performed according to the method described by [Fawley and Fawley (2004)] using following primers:

Forward primer- 5¹ GGCGAACGGGTGAGTAA 3¹

Reverse primer- 5¹ ACTGCTGCCTCCCGTAG 3¹

The Genomic DNA was isolated from the overnight grown bacterial culture was amplified with universal bacterial primers. A 25µl of reaction mixture contains 15µl of master mix (10 x assay buffer, dntp's, Taq polymerease and MgCl₂), 1µl of forward primer, 1µl of reverse primer, 2µl of template DNA and 6µl of distilled water. PCR was carried out by the thermal cycler under the following conditions- An intialization step at 94°C for 4min followed by 30 cycles of 94°C for 1min, 52°C for 1min, 72°C for 1.15min followed by final extension at 72°C for 1min and holding temperature at 10°C for

1min. The amplified DNA fragments were observed by agarose gel electrophoresis in 2% agarose gel and sequenced. The unknown bacterium was identified using GenBank database. The amplified PCR products were directly sequenced in an ABM Prism 3100-Avant Sequencer. The obtained sequences were analyzed using BLAST tool to get the relative identification of each bacterial species. PCR samples were purified, after that the bacterial extracts were subjected to thin layer chromatography for detecting the activity of extract and their components

Screening of Bacterial metabolite with GC-MS:

The active bacterial extract which was showing the maximum inhibition on cancer cell lines growth was analyzed by Gas Chromatography and Mass Spectrophotometer, using this technique the main compound having the anticancerous activity can be detected

III. RESULTS AND DISCUSSION

Cancer cells were tested with Chloroform, Methanol and Ethyl acetate bacterial extracts cell viability was evaluated by MTT assay. A gradual decrease in the viability of HCT 15 and MES-SA cancer cells were observed in for all the bacterial extracts used in the study. The bacteria was identified as *Micrococcus luteus* by 16s r RNA sequencing.

MTT cell growth inhibition assay was taken as in vitro measure of anticancer activity of bacterial extracts by using different cancer cell lines. Ethyl acetate extracts of bacteria are effective in inhibiting cancer cell growth of the two cancer cell lines. Therefore present invitro studies on ethyl acetate bacterial extracts demonstrate the remarkable anticancer potentials due to the presence of active principles may responsible for this anti cancer activity. Hence *Micrococcus luteus* Ethyl acetate extracts can be used as a potent natural source of anticancer agent. The GC-MS analyses the bacterial extract and compound identified as pyrrolo (1, 2- α) pyrazine, 1,4 dione hexahydro 3-(2-methylpropyl)

Isolation of pure cultures:

The bacterial pure cultures were isolated by serial dilution and streak plating on nutrient agar medium and selected bacterial colonies were sub cultured in to nutrient broth, and then the bacterial cultures were lyophilized and dissolved in chemical solvents. These bacterial extracts were dissolved in DMSO for long period further use.



FIGURE 1: Isolation of pure culture

Trypan blue staining Report:

The trypan blue staining was performed and the cancer cell line viability cell proliferation as shown below

Table 1: Trypan blue staining % of Viability of cancer cells

Cell line	% viability	Live cell count	Total cell count	pH
MES-SA	81.1%	1.72×10^5	2.12×10^5	7.5
HCT 15	72%	1.728×10^5	2.40×10^5	6.9

GC-MS Report:

Gas chromatography and mass spectrophotometer analyses the bacterial extract and the metabolite produced by bacteria is identified as Pyrrolo [1, 2- α] pyrazine-1, 4-dione, hexahydro-3-(2-methylpropyl)

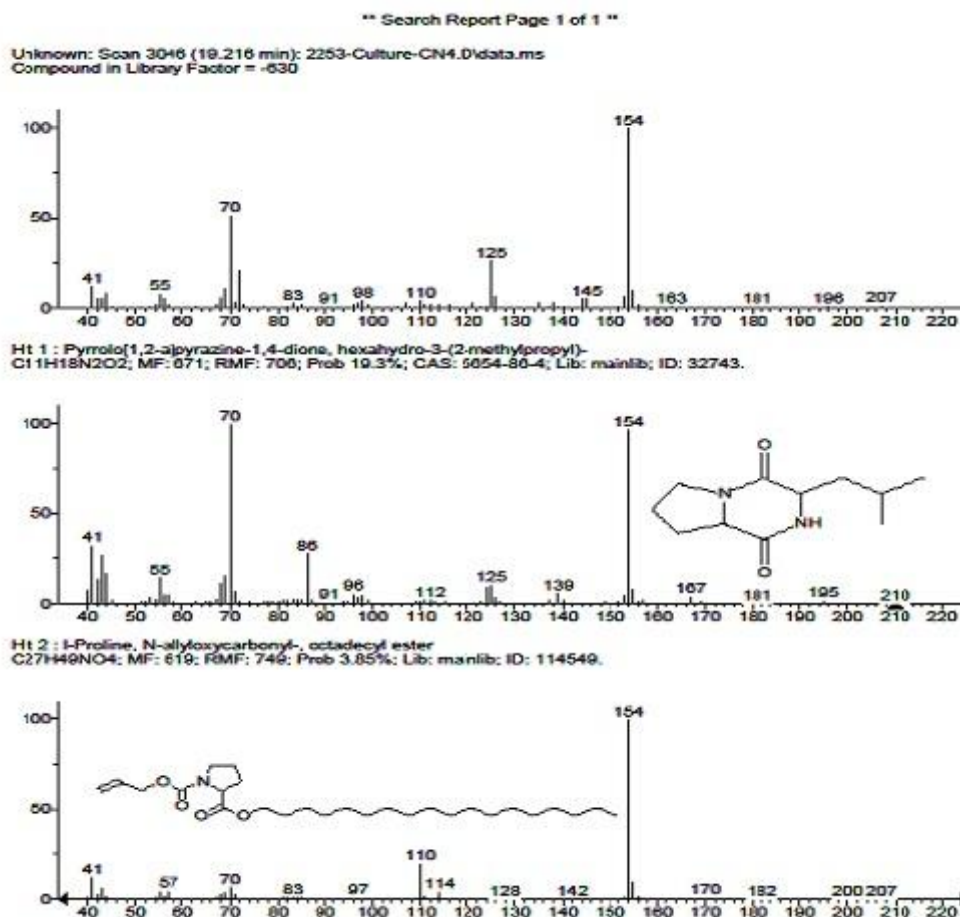


FIGURE 1: GC-MS analysis report with bacterial extract

16s rRNA sequencing report:

The selected bacterial extract sample was analyzed by using 16s rRNA sequencing, the isolate was identified as *Micrococcus luteus*

>mt_16srRNA

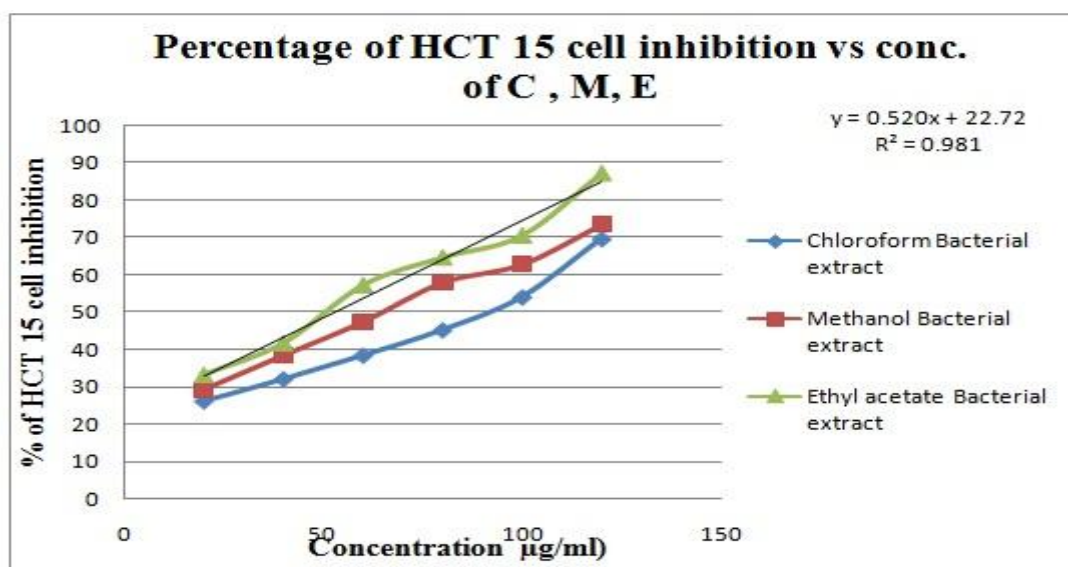
CGCATGGTGGGTGTTGGAAAGATTTATCGGTTTTGGATGGACTCGCGGCCTATCAGCTTGTTGGTGAGGT
 AATGGCTACCAAGGCGACGACGGGTAGCCGGCCTGAGAGGGTGACCGGCCACACTGGGACTGAGACACG
 GCCAGACTCCTACGGGAGGCAGCAGTGGGGAATATTGCACAATGGGCGCAAGCCTGATGCAGCGACGCC
 GCGTGAGGGATGACGGCCTTCGGGTTGTAAACCTCTTTCAGTAGGGAAGAAGCGAAAGTGACGGTACCTG
 CAGAAGAAGCACCGGCTAACTACGTGCCAGCAGCCGCGGTAATACGTAGGGTGCGAGCGTTATCCGGAAT
 TATTGGGCGTAAAGAGCTCGTAGGCGGTTTGTCTGCGTCTGTCTGTAAGTCCGGGGCTTAACCCCGGATC
 TGCGGTGGGTACGGGCAGACTAGAGTGCAGTAGGGGAGACTGGAATTCCTGGTGTAGCGGTGGAATGCGC
 AGATATCAGGAGGAACACCGATGGCGAAGGCAGGTCTCTGGGCTGTAAGTGGCCTGACGCTGAGGAGCGAAAGCA
 TGGGAGCGAAGCAGATTAGATACCTAGTCCAGTCCCGTAACGTTGGCAGTACTAGGTGTGGGGACCA
 TTCCACGGTTTCCGCGCCGACGCTAACGCATTAAGTGCCCCGCTGGGAGTACGGCCGCAAGGCTAAAA
 CTCAAAGGAATTGACGGGGGCGCACAAGCGCGGAGCATGCGGATTAATTCGATGCAACGCGAAGAAC
 CTTACCAAGGCTTGACATGTTCTCGATCGCCGTAGAGATACGGTTTCCCTTTGGGGCGGGTTCACAGGT
 GGTGCATGGTTGTCTGTCAGCTCGTGTCTGTGAGATGTTGGGTTAAGTCCCGCAACGAGCGCAACCCTCGTT
 CCATGTTGCCAGCACGTCGTGGTGGGACTCATGGGAGACTGCCGGGGTCAACTCGGAGGAAGGTGAGGA
 CGACGTCAAATCATCATGCCCTTATGTCTTGGGCTTACGCATGCTACAATGGCCGGTACAATGGGTTG
 CGATACTGTGAGGTGGAGCTAATCCCAAAAAGCCGGTCTCAGTTCGGATTGGGGTCTGCAACTCGACCCC

MTT assay Report:

From the Table 2 and graph 1: we can say that as the concentration of Chloroform, Methanol and Ethyl acetate bacterial extracts increased from 20 to 120 µl/ml, the % HCT 15 cancer cell growth inhibition was increased from 26.19 % to 69.76 % in chloroform bacterial extract, 29.45% to 73.56 % in Methanol bacterial extract and 33.24 % to 87.34% in Ethyl acetate bacterial extract, that means they induces a cell arrest to inhibit the growth of the HCT 15cancer cells. The Ethyl acetate bacterial extract showing the promising results

Table 2: Percentage of HCT 15 cell inhibition at various concentrations

Concentration µg/ml	Percentage of HCT 15 cell inhibition		
	Chloroform Bacterial extract	Methanol Bacterial extract	Ethyl acetate Bacterial extract
20	26.19	29.45	33.24
40	32.12	38.62	41.77
60	38.47	47.56	57.33
80	45.28	58.08	64.73
100	54.11	62.9	70.65
120	69.76	73.56	87.34



Graph 1: Effect of Chloroform, Methanol and Ethyl acetate bacterial extracts on HCT 15 cancer cell growth inhibition

IV. CONCLUSION

Bacterial extracts of the metabolites were *in vitro* tested for their cytotoxic potential on various cancer cell lines. The extracts were screened on HCT 15 and MES-SA cell lines. The Ethyl acetate extract of bacterial isolate showed promising results by MTT assay and Trypan blue staining. The isolate was identified as *Micrococcus luteus* sps by using 16s rRNA typing, GC-MS analyses the bacterial extract and the metabolite is identified as Pyrrolo [1, 2-a] pyrazine-1,4-dione, hexahydro-3-(2-methylpropyl) showing promising results were obtained with anti cancerous activity

V. ACKNOWLEDGEMENTS

SAI LAKSHMAN MITHUN.V would like to thank Department of Biotechnology, DVR& Dr.HS MIC College of Technology, Kanchikacherla, and Andhra Pradesh for their cooperation to complete this work For Masters degree

REFERENCES

- [1] Angel TreasaThomas , Josyula Venkata Rao, Volety Mallikarjuna Subramanian , Hariharapura Raghu Chandrasekhar, Naseer Maliyakkal, Tukaram Kedar Kisan, Alex Joseph, Nayanabhirama Udupa, In vitro anticancer activity of microbial isolates from diverse habitats, Brazilian Journal of Pharmaceutical Sciences, vol. 47, n. 2, apr./jun., 2011
- [2] B Dhorajiya, M Malani, B Dholakiya, Extraction and Preservation Protocol of Anti-Cancer Agents from Marine World, Chemical Sciences Journal, CSJ-38, accepted version, Oct 22, 2011
- [3] Angel.T.T, Venkata rao.J, Jesilm.A, Subrahmanyam.V.M, Venkatesh.K.B, Udupa.N. Antimicrobial profile of extremophiles from aqua to terrestrial habitats. Pharmacology online, v.1, p.111-126, 2009.
- [4] T. Mossman, J. Immunol. Methods; 1983, 65, 55.

- [5] Sanjay patel. Nirav gheewala, Ashok suthar, Anand shah, In-vitro cytotoxicity activity of solanum nigrum extract against Hela cell line and vero cell line, International Journal of Pharmacy and Pharmaceutical Sciences, Vol. 1, Suppl 1, Nov.-Dec. 2009
- [6] CLARDY. J. Discovery of new compounds in nature. Proc. Amer. Phil. Soc., v.151, p.201-210, 2007.
- [7] BUTLER, M.S. Natural products to drugs: natural products derived compounds in clinical trials. Nat. Prod. Rep., v.25, p.475-516, 2008.
- [8] HARLEY, J.P.; PRESCOTT, L.M. Laboratory exercises in microbiology. 5. ed. Columbus: The MC Graw Hill Companies, 2002. P.13-16, 125-207.
- [9] ATTA–UR-RAHMAN.; IQBAL, C.E.; WILLIAM, J.T. Bioassay techniques for drug development. Amsterdam: Harwood Academic Publishers, 2001. P.1-5
- [10] Phillips HJ and Terryberry JE. Counting actively metabolizing tissue cultured cells. Cell Research 1957; 13: 341-347.
- [11] Masters RW. Animal cell culture, Trypan Blue Assay sop. 3rd ed. 2000, p. 1 – 3
- [12] Skehan P, Storeng R, Scudiero D, Monks A, McMahon J, Vistica D et al. Evaluation of Colorimetric Protein and Biomass Stains for Assaying Drug Effects upon Human Tumor Cell Lines. Proceedings of the American Association for Cancer Research 1989; 30: 612.
- [13] Skehan P, Storeng R, Scudiero D, Monks A, McMahon J, Vistica D et al. New Colorimetric Cytotoxicity Assay for Anticancer-Drug Screening. Journal National Cancer Institute 1990; 82(13), 1107-1112.
- [14] Masters RW. Animal cell culture, Cytotoxicity and viability assays. 3rd ed. 2000, p. 202-203.
- [15] JEFFREY, M.E.; LINDA, S.A.; ANDREW, O.M. A rapid and simple MTT based spectrophotometric assay for determining drug sensitivity in monolayer culture. Tissue Cult. Meth, v.11, p.15-17.
- [16] McCloud TG, 2010. High Throughput Extraction of Plant, Marine and Fungal Specimens for preservation of Biologically Active Molecules. Marine Drugs, 15: 4526-4563
- [17] MARIANNA, J.; JAMES, P.K.; RONALD, R.R. Macquarimicins, microbial metabolites from Micromonospora I. Discovery, taxonomy, fermentation and biological properties. J. Antiriot., v.48, p.462-466, 1995
- [18] Newman DJ, Cragg GM, 2007. Natural products as sources of new drugs over the last 25 years. Natural Products, 70: 461–477.
- [19] Rajeev Kumar Jha, and Xu Zi-rong, 2004 Biomedical Compounds from Marine organisms, Marine drugs 2,123-124
- [20] Alejandro M.S. MAYER and Kirk R. GUSTAFSON, Marine pharmacology in 2000: Anti tumor and cytotoxic compounds, International journal of Cancer: 105, 291–299 (2003)

Optimal Design of an I.C. Engine Cylinder Fin Arrays Using a Binary Coded Genetic Algorithms

G.Raju¹, Dr. Bhramara Panitapu², S. C. V. Ramana Murty Naidu³

^{1,3}(Mechanical Engineering Department, Kallam Haranadhareddy Institute of Technology, Guntur, A.P, INDIA.

²(Mechanical Engineering Department, JNTUH College of Engineering, Hyderabad, A.P, INDIA.

ABSTRACT: Optimization is a technique through which better results are obtained under certain circumstances. In the present study maximization of heat transfer through fin arrays of an internal combustion engine cylinder have been investigated, under one dimensional, steady state condition with conduction and free convection modes. Traditional methods have been used, in the past, to solve such problems. In this present study, a non-traditional optimization technique, namely, binary coded Genetic Algorithm is used to obtain maximum heat transfer and their and their corresponding optimum dimensions of rectangular and triangular profile fin arrays.

This study also includes the effect of spacing between fins on various parameters like total surface area, heat transfer coefficient and total heat transfer. The aspect ratios of a single fin and their corresponding array of these two profiles were also determined. Finally the heat transfer through both arrays was compared on their weight basis. Results show the advantage of triangular profile fin array.

Keywords: Aspect Ratio, Genetic Algorithms, Heat Transfer, Heat Transfer per unit Mass, Objective function, Optimization, Rectangular Fin Array, Triangular Fin Array.

1. INTRODUCTION

Fins are extended surfaces often used to enhance the rate of heat transfer from the cylinder surface. Fins are generally used on the surface which has very low heat transfer coefficient. Straight fins are one of the most common choices for enhancing better heat transfer from the flat surfaces. The rate of heat flow per unit basis surface increase in direct proportion to the added heat conducting surface. The arrangement of fins and their geometry in an array are the most important criteria, to dissipate heat from the cylinder surface.

Optimization is a method of obtained the best results under the given circumstances. It plays an important role in the design of energy transfer components. While designing fins and their arrays, optimization helps to reduce the material cost and weight. The present study, aimed at maximizing heat transfer with a given mass, by applying optimization technique called Genetic Algorithm. For engine cylinder, the combustible gas temperature is taken as 698 K and the environment is at 298 K.

2. NOMENCLATURE

b	=	Thickness of the fin [mm]
C	=	Violation coefficient
F	=	Fitness Value
Gr	=	Grashoff's number
h	=	Heat Transfer Coefficient [W/m ² -K]

H	=	Width of the Fin [mm]
K _a	=	Thermal conductivity of air [W/m-K]
K _f	=	Thermal conductivity of fin [W/m-K]
M _f	=	Mass of fin [Kg]
Nu	=	Nusselt Number
N _p	=	Population Size
Pr	=	Prandtl number
Q _{a1}	=	Total Heat Transfer through Rectangular fin array [W]
Q _{fa1}	=	Heat Transfer trough fins in Rectangular fin array [W]
Q _{sa1}	=	Heat Transfer through spacing in rectangular array [W]
Q _{a2}	=	Total Heat Transfer through Triangular fin array [W]
Q _{fa2}	=	Heat Transfer trough fins in Triangular fin array [W]
Q _{sa2}	=	Heat transfer through spacing in Triangular array [W]
Q _m	=	Heat Transfer per unit mass of Rectangular fin array [W/Kg]
(Q _{a1}) _m	=	Maximum heat transfer through Rectangular fin array [W]
R	=	Penalty Parameter
s	=	Spacing between the fins [mm]
T _a	=	Ambient Temperature [K]
T ₀	=	Base Temperature [K]
W	=	Width of the base plate [mm]

2.1. Greek Symbols:

ρ	=	Density of the fin material [Kg/m ³]
θ ₀	=	Temperature difference at the base [K]
λ	=	Length of the fin [mm]
φ(x)	=	Modified objective function.

3. MATHEMATICAL FORMULATION

In actual practice, the bore is a cylindrical one, with cross-section as circular and the surface temperature varies along the stroke. But in the present investigation, the surface of the cylinder is assumed as a flat, with constant, uniform temperature and the fins are straight. This study is carried out under one-dimensional steady state conduction and convection heat transfer. This problem may be stated mathematically, based on the following assumptions:

1. The principal heat transfer is along the x-direction
2. Thermal conductivity of the fin material is to be constant and steady state conditions will prevail.
3. Temperature gradient at the tip of the fin is assumed as zero.

3.1. Straight Fin Array of Rectangular Profile:

The heat flow equation for a rectangular fin array as show in Fig.1 is obtained by assuming the each fin having the same base temperature T_0 .

The total heat transfer from the base plate by conduction and free convection through an array is

$$Q_{a1} = Q_{fins} + Q_{spacing} = Q_{fa1} + Q_{sa1}$$

$$Q_{a1} = \left(\frac{W}{s+b}\right) H \theta_0 \left[\sqrt{2hk_f b} \tanh \left[\frac{2h\lambda}{k_f b} \right] + hs \right] \text{---- (1)}$$

The constraints are expressed in normalized form as follows

$$\left(\frac{W}{s+b}\right) [\rho \lambda b H - m_f] \leq 0 \text{----- (2)}$$

$$8b - \lambda \leq 0 \text{----- (3)}$$

$$\lambda - 10b \leq 0 \text{----- (4)}$$

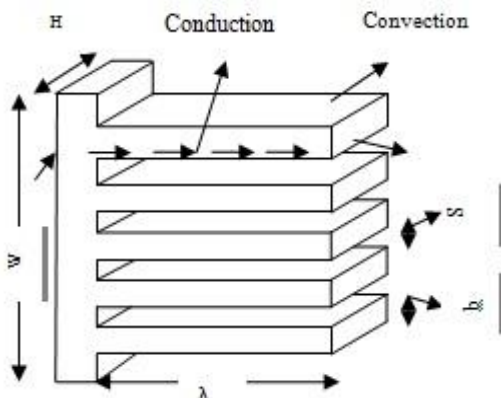


Fig.1 Geometry of Rectangular Fin Array

3.2. Straight Fin Array of Triangular Profile:

The heat flow equation for a triangular fin array as show in Fig.2 is obtained by assuming the each fin having the same base temperature T_0 .

The total heat transfer from the base plate by conduction and free convection through an array is

$$Q_{a1} = \left(\frac{W}{s+b}\right) H \theta_0 \left[\sqrt{2hk_f b} \frac{I_1 \left(2 \sqrt{\frac{2h\lambda}{k_f b}} \right)}{I_0 \left(2 \sqrt{\frac{2h\lambda}{k_f b}} \right)} + hs \right] \text{---- (5)}$$

The constraints are expressed in normalized form as follows

$$\left(\frac{W}{s+b}\right) \left[\frac{1}{2} \rho \lambda b H - m_f \right] \leq 0 \text{----- (6)}$$

$$8b - \lambda \leq 0 \text{----- (7)}$$

$$\lambda - 10b \leq 0 \text{----- (8)}$$

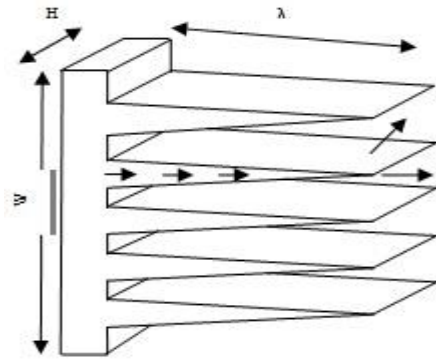


Fig.2 Geometry of Triangular Fin Array

3.3. Effect of fin spacing on heat transfer coefficient (h):

At a given temperature difference and the width of the fin, the heat transfer coefficient is varies with spacing, length and its thickness. The heat transfer coefficient can be calculated by using Nusselt number.

$$h = \left[\frac{(Nu)k_a}{\left(\frac{H}{2}\right)} \right] \text{----- (9)}$$

Nusselt number (Nu) is taken as,

$$\text{If } 10^6 < \left[Gr \cdot Pr \cdot \frac{s \cdot W}{(s+b)\lambda} \right] < 2.5 \times 10^7$$

$$Nu = 5.22 \times 10^{-3} \left[Gr \cdot Pr \cdot \frac{s \cdot W}{(s+b)\lambda} \right]^{0.57} \left[\frac{2\lambda}{H} \right]^{0.656} \left[\frac{2s}{H} \right]^{0.412}$$

$$\text{If } \left[Gr \cdot Pr \cdot \frac{s \cdot W}{(s+b)\lambda} \right] \geq 2.5 \times 10^7$$

$$Nu = 2.787 \times 10^{-3} \left[Gr \cdot Pr \cdot \frac{s \cdot W}{(s+b)\lambda} \right]^{0.745} \left[\frac{2\lambda}{H} \right]^{0.656} \left[\frac{2s}{H} \right]^{0.412}$$

4. OPTIMIZATION TECHNIQUE

Introduction: Classical search and optimization techniques demonstrate a number of difficulties when faced with complex problems. Over the few years, a number of search and optimization techniques, different in principle from classical methods, are getting increasingly more attention. These methods mimic a particular natural phenomenon to solve an optimization problem. Genetic Algorithm and simulated annealing are a few of these techniques. The major reason for GA's popularity in various search and optimization problems is its global perspective, widespread applicability and inherent parallelism.

Genetic Algorithms are computerized search and optimization algorithms based on the mechanics of natural genetics and selection. Genetic algorithms originally proposed by John Holland at the University of Michigan. The aim of his research has been to rigorously explain the adaptive process of natural system and to design artificial systems that retain the important mechanisms of validity of the techniques for function optimization. Genetic algorithms are computationally simple, but powerful in their search for improvement. Gold berg [2] describe the nature of genetic algorithm of choice by combining a Darwinian survival of the fittest procedure with a structured, but randomized, information exchange to form a canonical search procedure that is capable of addressing a

broad spectrum of problems. Genetic algorithms are the search procedures based on natural genetics. Genetic algorithms differ from traditional optimization techniques in many ways. A few are listed as per [2].

- Genetic algorithm doesn't require a problem specific knowledge to carry out a search.
- Genetic algorithms work on coded design variables, which are finite length strings.
- Genetic algorithm uses a population of points at a time in contrast to the single point approach by the traditional optimization methods.
- Genetic algorithm use randomized operator, in place of the deterministic ones. The random operators improve the search process in an adaptive manner.

The four properties, separation of domain knowledge from search, working on coded design variables, population processing and randomized operators, give the genetic algorithms their relative merit.

The various genetic operators that have been identified are reproduction, crossover, mutation, dominance, inversion, intra-chromosomal duplication, deletion, translocation, segregation, speciation, migration and sharing. The present study concentrates on a simple genetic algorithm with reproduction, crossover and mutation operations only to optimize the fin and fin arrays of rectangular and triangular profiles.

The Reproduction operator emphasizes the survival of the fittest in the genetic algorithm. There are many ways of achieving effective reproduction. One simple scheme selects individual strings in the population on the proportionate basis for reproduction according to their fitness. Fitness is defined figure of merit, which is either maximized or minimized. In the effective reproduction, individuals with higher fitness values have higher probability of being selected for mating and subsequent genetic action.

Crossover is a recombination operator, which proceeds in three steps. First, the reproduction operator makes a match of two individual strings for mating. Then a cross-site is selected at random along the string length and position values are swapped between the two strings, following pair be $A = (11111)$ and $B = (00000)$. If the random selection of a cross-site is two, then the new strings following the crossover would be $A' = (00111)$ and $B' = (11000)$. This is a single site crossover. Strings A' and B' are the off spring of A and B and are then placed in the new population of the next generation.

Mutation is the random flipping of the bits or gene that is changing a 0 to 1 and vice versa. Mutation is employed to give new information and reintroduce divergence into a convergent population. This is a tool to avoid local maxima, which is a common problem in stochastic algorithms. It also prevents problem from becoming saturated with chromosome that all look alike. The working of this simple Genetic algorithm for discrete structural optimization is explained in detail in the following section.

4.1. Working Principle of Genetic Algorithm:

This Algorithm is a population based search and optimization technique and it is an iterative procedure. Instead of working with a single solution, a GA is works

with a number of solutions, which are collectively known as population. The working cycle of a GA, is expressed in the form of a flow chart in Fig.4.

The operation of a GA begins with a population of initial solution chosen at random. Thereafter, the fitness value of objective function of each solution is computed. The population is then operated by three operators, namely reproduction, crossover and mutation to create a second population. This new population is further evaluated and tested for termination. First iteration of these operations is known as generation in GA.

4.1.1. Example: Straight Fin Array of Rectangular Profile

The working of genetic algorithm for design optimization of rectangular fin array is described below. The mathematical programming formulation of this problem can be written as follows: Maximize Q_{a1} subjected to $G_i(x) \leq 0, i = 1, 2, \dots, m$. Since the objective is to maximize the heat transfer through fin array of rectangular profile.

Genetic algorithms are ideally suited for unconstrained optimization problems. As the present problem is a constrained optimization one, it is necessary to transform it into an unconstrained problem to solve it using genetic algorithm. This transformation method achieves by using penalty function, which is explained in earlier section.

A violation co-efficient 'C' is computed in the following manner.

If $G_i(x) > 0$, then $c_i = G_i(x)$ or

If $G_i(x) \leq 0$, then $c_i = 0$

$$\therefore C = \sum_{i=1}^m C_i \text{-----} (10)$$

'M' is the number of constraints.

Now the modified objective function is written, incorporating the constraint violation as:

$$\varphi(x) = Q_{a1}(1 + RC) \text{-----} (11)$$

4.1.2. Individual string of length 30:

'R' is the penalty parameter, which is selected, depending on the influence of a violated individual in the next generation. Design variables are thickness, length and spacing between the fins and the values are taken in the range of 0 to 5, 0 to 148 and 0 to 9 mm respectively. There are three design variables can take one of the values between minimum and maximum values in the given range. A binary string of length 10 is capable of representing different values between the ranges given. As there are three groups, the total length of the string becomes 30 with the substring of length 10 each shown in Fig.3. A substring (0000000000) will represent the first value that is 0 mm, and (1111111111) will represent the upper limit values 5, 148 and 9 mm for b , λ and s respectively. Any intermediate values can be represented with appropriate bit coding.

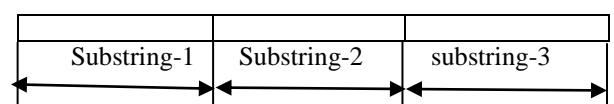


Fig.3 string length

In the present study, the twenty-first generation, shown in Table-3 & 5, all the population satisfies under the given constraint conditions. That is for all population in 21st generation the violation coefficient is zero and also the average fitness value is almost equal to the best fitness value in the population. In the present work number of generation is the criterion for termination.

Population size: 10
 Number of generations: 21
 Crossover Probability: 0.8
 Mutation probability: 0.05

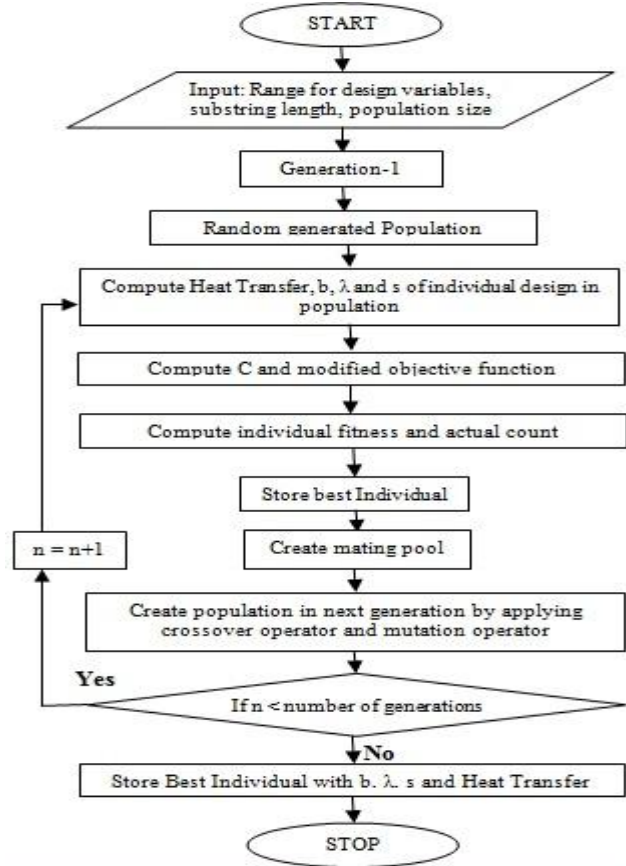


Fig.4 Flow Chart

5. RESULTS AND DISCUSSION

5.1. RESULTS:

Table-1: Comparison of Aspect (λ/b) Ratio

Fin Profile	Single fin	Fin array
Rectangular	8.896	9.94
Triangular	8.227	9.31

Table-2: Comparison of results (Base area 100x100mm²)

Optimized parameter	Rectangular Fin Array	Triangular Fin Array
Maximum Heat Transfer	158.9546W	84.43306W
Length of the Fin	46.72mm	45.37mm
Fin Thickness	4.70mm	4.87mm
Fin Spacing	7.54mm	11.71mm
Aspect Ratio (λ/b)	9.94	9.31
Heat Transfer per unit mass	327.07 W/Kg	468.08 W/Kg

Table-3: Population of Rectangular fin array from 20th Generation

Pop. No.	Population from generation-20		
	Group-1	Group-2	Group-3
(1)	(2)	(3)	(4)
1	1111000010	0101000011	1101011010
2	1111000010	0101000011	1101010000
3	1111000110	0101000011	1101010010
4	1111000010	0101000011	1101000010
5	1111000010	0101000011	1101010010
6	1111000000	0101000011	1101001110
7	1111000010	0101000011	1101011010
8	1111000010	0101000011	1101011010
9	1111000010	0101000011	1101010010
10	1111000010	0101000011	1101011010

Table-4: Results of Rectangular fin array at 21st Generation

b mm	λ mm	s mm	Q_{a1} Watts	C	F
(1)	(2)	(3)	(4)	(5)	(6)
4.70	46.72	7.54	158.9546	0.00	0.99272
4.70	46.72	7.46	158.7835	0.00	0.99272
4.72	46.72	7.47	158.4214	0.00	0.99270
4.70	46.72	7.33	158.5297	0.00	0.99271
4.70	46.72	7.47	158.8184	0.00	0.99272
4.69	46.72	7.44	158.9488	0.00	0.99272
4.70	46.72	7.54	158.9546	0.00	0.99272
4.70	46.72	7.54	158.9546	0.00	0.99272
4.70	46.72	7.47	158.8184	0.00	0.99272
4.70	46.72	7.54	158.9546	0.00	0.99272

Table-5: Population of Triangular fin array from 20th Generation

Pop No.	Population from generation-20		
	Group-1	Group-2	Group-3
(1)	(2)	(3)	(4)
1	1111100110	0101011101	0100001000
2	1111100110	0101011101	0100000010
3	1111100110	0101011101	0100000000
4	1111100110	0101011101	0100010000
5	1111100110	0101011101	0100000000
6	1111100110	0101011101	0100011100
7	1111100110	0101000110	1101011000
8	1111100110	0101011101	1101011000
9	1111100110	0101011101	0100000000
10	1111100110	0101011101	0100000000

Table-6: Results of Triangular fin array at 21st Generation

b mm	λ mm	s mm	Q _{a2} Watts	C	F
(1)	(2)	(3)	(4)	(5)	(6)
4.87	45.37	3.61	64.88708	0.00	0.98232
4.87	45.37	3.53	64.29686	0.00	0.98221
4.85	45.37	3.50	64.09313	0.00	0.98216
4.87	45.37	3.72	65.64494	0.00	0.98257
4.87	45.37	3.50	64.09546	0.00	0.98216
4.86	45.37	3.88	66.71828	0.00	0.98285
4.87	42.38	11.71	79.63562	0.00	0.98559
4.87	45.37	11.71	84.43306	0.00	0.98640
4.87	45.37	3.50	64.09546	0.00	0.98216
4.87	45.37	3.50	64.09546	0.00	0.98216

5.2. DISCUSSION:

In this Paper, the nature of thermal and physical parameters was studied for rectangular and triangular profile fin arrays. The optimum heat transfer for a given mass of fins was obtained by using genetic algorithms method. From the results

- For a given length of the fin the heat transfer through rectangular fin array is increases with spacing at first, attains a maximum value and then decreases. As the spacing increases, the heat transfer increases due to increasing the exposed base area in between the fins, beyond the optimum spacing, the heat transfer decreases with spacing due to decreasing the number of fins. Also for a given spacing the heat transfer increases with the length of the fin due to increase in surface area of the fins.
- For a given spacing the total surface area available for heat transfer through rectangular profile fin array is more than the triangular profile fin array.
- For a given length, width and spacing between the fins, the heat transfer per unit mass for rectangular fin array is less than the triangular fin array.
- For a given length of the fins the heat transfer per unit mass increases with spacing due to reduction in number of fins thereby mass of the fins and also heat transfer coefficient increases with spacing.
- Spacing between the fins for triangular fin array is more than the rectangular fin array for maximum heat transfer therefore the heat transfer coefficient for triangular fin array is higher.

6. CONCLUSIONS

In the present work, an attempt is made to optimize rectangular and triangular profile fins and their fin arrays using genetic algorithm method also compared their performance on weight and heat transfer basis. In this regard, the following conclusions are made;

1. Heat transfer through triangular fin array per unit mass is more than that of heat transfer through rectangular fin array. Therefore the triangular fins are preferred than the rectangular fins for automobiles, central processing units, aero-planes, space vehicles etc... where weight is the main criteria.
2. At wider spacing, shorter fins are more preferred than longer fins.

3. The aspect ratio for an optimized fin array is more than that of a single fin for both rectangular and triangular profiles.
4. The GA is able to find optimal solution.
5. The GA does not require gradient information of the objective function.
6. The present work limited to one dimensional steady state heat transfer

REFERENCES

- [1] Eckert, E. R. G., and Drake, R. M., "Analysis of Heat and Mass Transfer" McGraw Hill, New York, 1972.
- [2] Goldberg, D. E., "Genetic Algorithms in Search Optimization and Machine learning," Addison-Wesley publishing company, USA, 1989.
- [3] Das, A. K. and D. K. Pratihari, "Optimal Design of Machine Elements using Genetic Algorithms," IE (I) Journal-MC-Vol.83, October 2002.
- [4] Dhar, P. L. and Arora, C. P., "Optimum design of finned surfaces" Journal of the Franklin Institute, 1976, 301, pp. 379-392.
- [5] Rong-Hua Yeh, "Analysis of Thermally Optimized Fin Array in Boiling Liquids," Int. J. Heat Mass Transfer, Vol.40, No.5, pp. 1035-1044, 1997.

Synthesis and Characterization of Ferrate (VI) Alkali Metal by Wet Method

A.El Maghraoui¹, A.Zerouale², M.Ijjaali³, Sajieddine Mohamed⁴

¹ Laboratoire de chimie de la matière condensée (LCMC), Faculté des sciences et techniques, université sidi Mohammed ben abdellah. B.P. 2202 FES (Morocco).

² Laboratoire de Physique et Mécanique des Matériaux, Faculté des Sciences et Techniques Beni Mellal, Université Sultan Moulay Slimane (morocco).

Abstract: The synthèses of ferrate (VI) appearstobe very délicate, this Is due to the instabilité That gives them their High oxidizing power. Although the existence of alkaline ferrate has been cited testified for a centurya [1], [2], they have not been a considérable number of studies, because of the instabilité and difficultés encountered during their préparation.

The wetoxydation passes through the oxydation of a ferric solution to form the solution of ferrate (VI) in strongly alkaline medium. As the solution of ferrate Can decompose quickly, protocols of washing and drying precipitation are required to obtain a stable and solid (Ockerman and Schreyer, 1951) [3]; (Schreyer et al, 1953) [4]. The wet method, considered the most practical is still very expensive (Lee et al, 2004) [5]. The phases obtained were caractérisé by IR X- ray, Spectrometry, Mössbauer spectroscopy, and analysis thermogravimetric.

Keywords: Ferrates; bactericidal; oxidant; flocculant, coagulant.

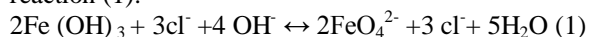
I. Introduction

Our purpose is to prepare compounds based on iron (VI) stable and the track their degradation over time. The preparation phase of Na_2FeO_4 was performed by wet method. Their oxidizing power makes it possible to use them as oxidizing and disinfection agent in water Treatment. It first reacts in the form of iron (VI) by causing oxidation duringwhich it's is reduced to Fe (III). However, the iron (III) is used to treat waste water to precipitate the phosphate.

The induced oxidation is not accompanied by unwanted byproducts.

II. Synthesis

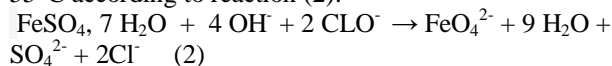
Publications and patents on methods of K_2FeO_4 synthesis [6], [7], [8] recommend the use of a ferric salt, which led us to use ferric sulfate derived from an initial Oxidation of ferrous sulphate by household bleach. H.HROSTOWSKI and A. SCOTT [9] proposed in1950 a method of preparation of ferrates , with a purity rate of 97% by oxidation of ferric chloride by sodium hypochlorite in a concentrated solution of sodium hydroxide at a temperature between 50 ° C and 55 ° C. This synthesis is carried out by applying the following reaction (1):



However, for environments in which were operating H.HROSTOWSKI and Al, in this case in highly concentrated NaOH, Na_2FeO_4 is assumed to be very soluble while NaCl has precipitated in the solution [10]. A separation by filtration is then mode possible.

Procedure

Mixing the hydrated iron sulphate $\text{FeSO}_4 \cdot 7\text{H}_2\text{O}$ and Clo bleach concentrated in a basic medium. The mixture is stirred for one hour at a temperature between 50°C and 55°C according to reaction (2):



Na_2FeO_4 recovery is done by vacuum filtration. This phase is dried in an oven at 120 °C for 12 hours then placed in a desiccators. During these tests; we find that the yield of the oxidation of ferric sulphate varies with temperature in Figure 1.

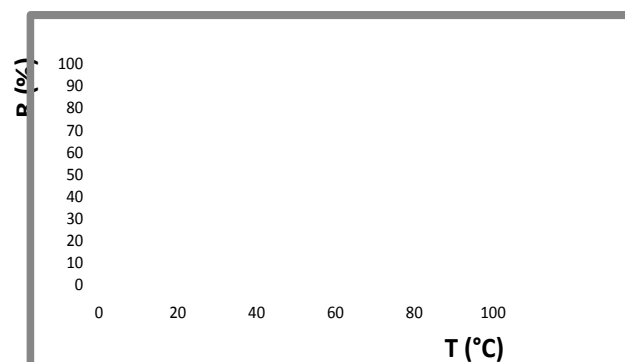


Figure. 1. Performance of the oxidation of ferric sulfate as a function of the température in concentrated NaOH.

III. Characterizations

1. Infrared spectrometry

The appearance of an infrared spectrum is related to the symmetry of the molecule or study group for FeO_4^{2-} with tetrahedral structure, we expected to find out: First, the fundamental bands characteristic of a symmetry T_d : either bands ν_3 and ν_4 from the two degenerate modes of vibration: the symmetric stretching and angular deformation within the tetrahedron resulting in inactive modes in infrared absorption, bands ν_1 and ν_2 must be absent from the spectra [11]. On the other hand, a similarity between the infrared spectra of isomorphous series [12].

The presence of a band ν_1 and a triplet for ν_3 (elongation of the tetrahedron) have led w. Griffith [13] to

consider a lower symmetry in $2d$, very close to $2s$ for the FeO_4^{2-} anion.

IR spectroscopy is a quantitative method for the determination of Iron (VI) in the ferrate compounds. The shape of the spectra is related to the symmetry of the molecule or FeO_4^{2-} group (tetrahedral structure). The

Na_2FeO_4 IR spectrum Figure .2 showed in the field of high frequency an identical appearance to that obtained (mode 825 and 780 cm^{-1}) P. Tarte and g.nizete [14].

By comparing the outgoing lines 825 cm^{-1} , 750 cm^{-1} in the IR spectrum Figure. 2. Na_2FeO_4 phase with that of P. Tarte and G. Nizete [14], we notice that there is a great similarity of these spectra with an isomer shift of Na_2FeO_4 rays that, could be caused by of the preparation and crystallization.

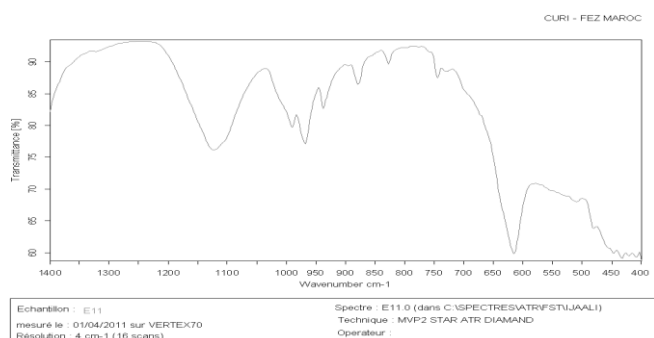
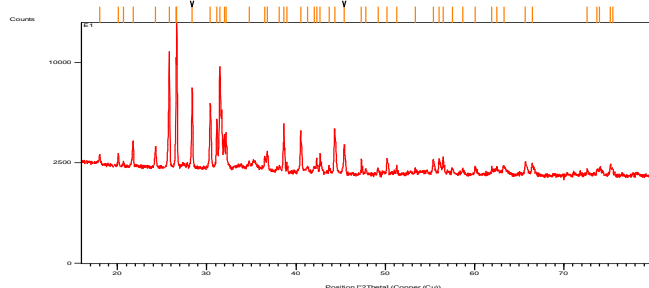


Figure. 2. Spectrometer infra-red Na_2FeO_4 .

2. X-Ray diffraction

Measures by a radiation ray diffractometer $CuK\alpha$ of a compound of Na_2FeO_4 ferrate powder Figure .3 make it possible to verify the crystal structure of ferrate [15], [16], and demonstrate the existence of an isomorphism with K_2FeO_4 and $BaFeO_4$ as proved by Stuart Licht, Vera. Naschitz and collaborators [17]. The X-ray diffraction is one of the means used to verify the presence of ferrate. The spectrum obtained on Na_2FeO_4 bears a strong similarity with that of isomorphous compounds. There is a splitting of the lines corresponding to planes (102), (202), (013), (200), (020), (112) [18], [19], [20], [21]. The results obtained by infrared support those of XRD.



Figure; 3. Diffractometer XR of Na_2FeO_4

3. ATG spectrum

Two decomposition stages were obtained in the TGA curve up to 500°C Figure 4. A first above 100°C corresponding to the

evolution of water weakly adsorbed by the sample and a second step between 210 and 310°C corresponding to the release of O_2 Scholder et al [27] and [28].

The two stages of decomposition was accompanied

By one endothermic heat effects as measured by DTA.

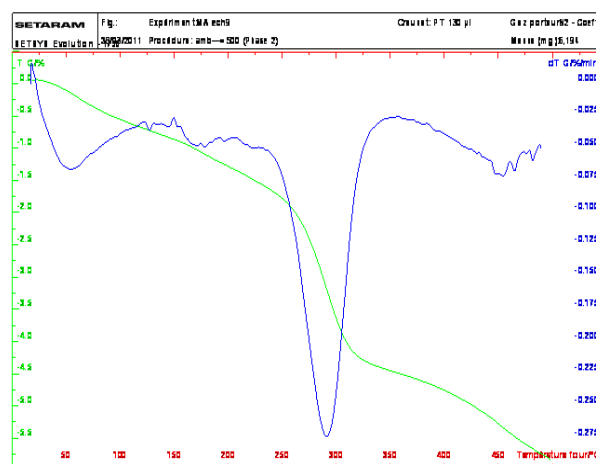


Figure. 4. ATG spectrum of Na_2FeO_4 .

IV. Tracking ferrate degradation as a Function of time

Analysis by Mössbauer spectroscopy

The Mössbauer effect is obvious benefit to the absorption of a photon γ by a nucleus of ^{57}Fe (present at a rate of about 2.6 percent in the natural iron): we gradually make the energy of the emitted photon vary by the speed of the source (^{57}Co). When the latter reaches a value equal to the difference between the energy level of the core in its ground state ($l = 1/2$) and its level in the excited state ($l = 3/2$) the photon is absorbed. This phenomenon translates into a peak on the spectrum Mössbauer spectroscopy also helped to Highlight the existence of magnetic order at low temperature [22], [23], [24], [25], [26].

Na_2FeO_4 characterization by Mössbauer spectroscopy after ten months of storage at room temperature reveals a degradation of Iron (VI) with time according to the spectrum in Figure. 5. It is in the form of a enlarged magnetic component calculated by the superposition of two sextuplets and a paramagnetic component adjusted by a paramagnetic doublet. The hyperfine parameters deduced from the calculation are given in chart below.

Table: hyperfine parameters deduced from the calculation of the spectrum after ten months of storage.

H_{hyp} = champ hyperfin, A = poids de la composante en % du spectre total.

	Composante élargie						Composante paramagnétique		
	Sextuplet 1			Sextuplet 2			Doublet		
	H_{hyp} (kOe)	ISO (mm/s)	A (%)	H_{hyp} (kOe)	ISO (mm/s)	A (%)	ΔE_Q (kOe)	ISO (mm/s)	A (%)
2	490	0,22	7,5	449	0,34	1,6	0,512	0,35	90,7

This degradation is manifested spectrum of the isomer shift to 0.22 mm/s for sextuplet 1 and 0.34 mm/s for sextuplet 2 (see table). While the iron sextuplet (VI) comes close to -1. [22], [23], [24], [25], [26]. This isomer shift is due to the degradation of Fe (VI) to iron (III) because of moisture.

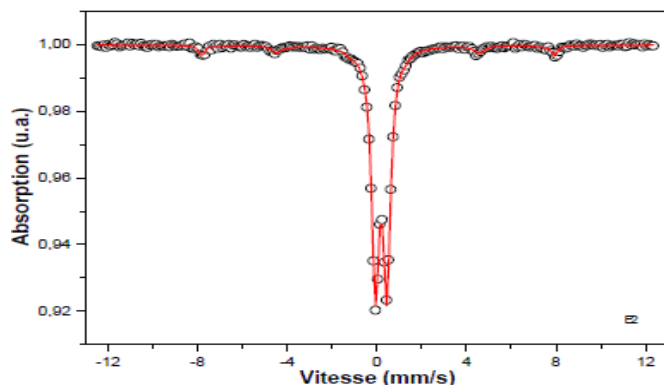


Figure. 5. Mössbauer spectrometer Na_2FeO_4 after ten months of storage.

V. Conclusion

We developed a ferrate (VI) alkaline, ie Na_2FeO_4 , by Wet method at a temperature between 50 °C and 55 °C.

The synthesized ferrate present diffractogram similar to those given in the literature.

Infrared spectroscopy shows that we are dealing with a compound containing the FeO_4^{2-} group.

Mössbauer spectroscopy of iron allowed us to visualize the oxidation of iron and therefore control the rate of iron (VI), and the monitoring of its degradation in iron (III) over time.

The XRD spectrum of Na_2FeO_4 is isomorphic to that of K_2FeO_4 literature given by the literature. The TGA spectra show a peak at 100 °C corresponding to the departure of water and a peak at 295 °C corresponding to the decomposition of Na_2FeO_4 .

REFERENCES

Journal Papers:

- [1] B. Von Helfferich, K. Lang, Zeit. Anorg. Chem. 263, P.169 1950.
- [2] R. J. Audette, J. W. Quail, Inorg. Chim, 11, 8, P. 1904, 1972.
- [3] G. W. Thompson, L.T. Ockerman, J. M. Schreyer, 1951
- [4] , Preparation and purification of potassium ferrate VI,
- [5] J. Am. chem. Soc., 73, PP. 1379 - 1381, 1951.
- [6] J. M. Schreyer, G. W. Thompson, L. T. Ockerman, 1953, Potassium ferrate (VI), Inorg. Synthesis, 4, PP. 164 – 169, 1953.
- [7] Y. H. Lee, M. Cho, J.Y. Kim, Jayson., 2004, Chemistry of ferrate (Fe(VI)) in aqueous solution and its application as a green chemical, J. Ind. Eng. Chem., 10, PP. 161-171, 2004.
- [8] R. Scholder, H. Bunsen, F. Kindervater, W. Zeiss, Z. Anorg. Allg. Chem, 282, p. 268, 1955.
- [9] J. M. Schreyer, G. w. Thompson, L. T. Ockerman, inorganic synthèse, IV, p.164, 1953.
- [10] G.W. Thompson, L.T. Ockerman, J.M. Schreyer, J. Am. Chem. Soc, 73, p.1379, 1951.
- [11] H. Hrostowski, A. Scott, J. Chem. Phys., 18, p.105, 1960.
- [12] A. Hooker, Chem. And Met. Eng., 23, p. 961, 1920.
- [13] N. Becarud, C. Duval, C.R. Acad. Sci, 257, p.1930, 1963.
- [14] F. Gonzales- Vilchez, W. Griffith, J. Chem. Soc. Dalton.p. 1416, 1972.
- [15] W. Griffith, J. Chem. Soc, A, p. 1467, 1966.
- [16] P. Tarte, G. Nizet, Spectrochimica acta, 20, p.503, 1964.
- [17] B. Von Helfferich, K. lang, Zeit. Anorg. Chem. 263, P. 169, 1950.
- [18] H. Von Krebs, Z. Anorg. Chem, 263, p. 175, 1950.
- [19] S. Licht, V. Naschitz, L. Halperin, N. Halperin, L. Lin, J. Chen, S. Ghosh and B. Liu, J. Power Sources, 101, pp. 167–176, 2001.
- [20] Y.L. Wang, S.H. Ye, Y.Y. Wang, J.S. Cao, and, F. Wu Electrochemical Acta, Volume 54, Pages 4131-4135, Issue 16, 30 June 2009.
- [21] He. Weichun, Wang. Jianming, Shao. Haibo, Zhang. Jian Qing. And Cao. Chu-nan, Electrochemistry Communications, Volume 7, Issue 6, June 2005, Pages 607-611.
- [22] R.J. Audette, J.W. Quail, Inorg. Chim, 11, 8, P.1904, 1972.
- [23] Xu. Zhihua, Wang. Jianming, Shao. Haibo, Tang. Zheng, zhang. Jianqing, Electrochemistry communications 9, p. 371-377, 2007.
- [24] A. Ito, K. Ono, j. phys. Soc. Japan, 26, p. 1548, 1969.
- [25] T. Shinjo, T. Ichida, T. Takada, J. Phys. Soc. Japan, 26, p.1547, 1969.
- [26] T. Shinjo, T. Ichida, T. Takada, J. Phys. Soc. Japan, 29, 1, p. 111, 1970.
- [27] G. Hoy, M. Corson, j. Of magnetism and magnetic materials 15, 18, p.627, 1980.
- [28] F. Menil, J. Phys. Chem. Solids, 46, 7, p.763, 1985.
- [29] R. Scholder, H. Bunsen, F. Kindervater and W. Zeiss, Z. Anorg. Allgem. Chem. 282, pp.268-279, 1955.
- [30] R. Scholder, Angew. Chem. I, pp. 220 - 224, 1962.

The Need for Integration of Disaster Management into Engineering Curriculum

Shimi Lawrence,¹ Dr.E.S.M.Suresh²

^{1,2} (Department of Civil Engineering, NITTTR, Chennai, India)

ABSTRACT: *Disasters are happening in this world as a natural phenomenon or as anthropogenic activities. Organizations and agencies involved in Disaster Management find it necessary to recruit professionals having specific skills and knowledge, who can contribute to a more holistic understanding of the development, vulnerability and mitigation of disasters. These professionals should be involved in conceptual work, evaluation studies and in the prediction of disasters scientifically. Engineering Education is supposed to educate the budding Engineers, to solve the real and complex problems faced by the world, to have a successful career at their place of work and also in their life. A modified curriculum has to be formulated including Disaster Management as a core paper for engineering students rather than an Elective paper as in some Indian Universities. All Engineering fields are prone to some sort of hazard. Depending on the nature of this hazard, Disaster management component may be included in each and every subject so that the student will be able to understand the practical aspect of the subject better.*

Keywords: Curriculum, Disaster Management, Engineering Education, Interdisciplinary learning.

I. INTRODUCTION

A disaster, according to WMO, can be defined as a catastrophic consequence of natural phenomena or a combination of phenomena resulting in injury, loss of life or input in a relatively large scale and some disruption to human activities. Disaster response cannot be handled by Legislation alone. The entire community needs to be aware and be a part of the process. Adequate Research and planning is needed to focus on ways to mitigate the impact of disasters.

Engineers are required for safe and effective response of the disaster. For this, they shall be trained on the various disasters that can happen in their respective field of Engineering. Government and Technical Institutions should aim at focusing Disaster Awareness and Management at all levels of Educational Institutions and produce quality professionals. For this, the curriculum should include Security Preparedness, Security Education, Hazard Awareness and Disaster Management.

India, being a country of diverse hypsographic and climatologic conditions has to face 70% of the cultivable land prone to drought, 60% of the land area prone to earthquake, 12% to floods, 8% to cyclones, 85% of the land area is vulnerable to a number of natural hazards and 22 states are categorized as multi hazards states [1].

II. DISASTER MANAGEMENT IN ENGINEERING EDUCATION

Engineering Education is supposed to educate the Engineers, to solve the real world problems. An Engineer has to have adequate theoretical knowledge and be able to adopt it for use in his/her practical work. In Engineering Education, Disaster Management is provided as a core paper, an elective or not at all in the curriculum. Engineers actually have to control, manage, improve and develop technological processes using their theoretical knowledge and skills according to the knowledge they acquire during their four or five year Engineering Degree Program.

2.1. Disaster Management Education.

Disasters vary from place to place. Cyclones, Tsunamis in coastal areas, Droughts in and around deserts, landslides in mountainous areas, avalanches at high altitudes etc... People living in coastal areas suffer a disaster, which is entirely different from that of the people living near mountainous areas. Education, in the context of Disaster Management, is the process of enlightening the mankind about the nature, extent and methods to deal with the disasters, which facilitates them in facing Disaster rather than got caught without understanding how to react. Public awareness and education were identified as regional gaps that should be addressed at the national and local levels, for an effective Disaster Management System. [2].

Students are expected to develop skills and behaviors during the course of their study at an Engineering College. The properly designed curriculum serves as a link between different courses in the curriculum as well as provides connections to real – world applications, which can serve as a motivator for students to master and retain the course content. In actual practice, Engineers are engaged in problem – solving and design using their technical knowledge attained during their period of study as students.

They should be able to communicate properly, at the right time. They shall be trained to work as in teams without hesitation, and shall be informed and explained about the need and importance of teamwork in Disaster Management aspect. There shall be proper communication between technical and nontechnical persons. Therefore, teamwork shall be a process of information exchange between two or more groups or individuals, regarding disaster risks and mitigation measures to be taken, according to the severity of the situation.

Engineering Education educates Engineers as designers who can adjust and act according to the situation. Curriculum Development shall be based on the model of Engineering Practice that includes Conceiving, designing, implementing, and operating on the curriculum. [3], which is a model based on technical problem – solving and design.

2.2. Who is a Disaster Management Engineer?

An Engineer has to have adequate theoretical knowledge and be able to adopt it for use in his/her practical work as and when required. Engineers have to control, manage, improve and develop technological processes and aggregates using their theoretical knowledge and skills. Practical work experience in the form of Field visits, Industrial visits, should become a key component in Engineering Curricula.

2.3 Emergency Preparedness

Emergency Preparedness synonymously used for civil protection. It refers to the process of managing, coordinating, operating, in the various stages of the disaster cycle: hazard and risk mitigation, disaster preparedness, emergency response, recovery and reconstruction. [4], shows that Training and Education have long been acknowledged to be a vital part of emergency preparedness as they are the vital elements in the drive to turn emergency management into a full – fledged profession. Personal Training is one of the most important elements for capacity building and developing a disaster preparedness plan. Training is the process of changing a given behavior pattern to a desired behavior pattern.

III. INTERDISCIPLINARY MODE OF LEARNING IN HIGHER EDUCATION

Interdisciplinary Learning is a methodology that includes learners from different disciplines that work closely together contributing their knowledge, skills and experience to support, enhance the contributions and attributes of each discipline.

The Interdisciplinary Learning initiatives are proliferating throughout higher education at an unprecedented rate. They can be found in general education replacing and augmenting distribution requirements; in emerging disciplines, such as cultural and gender studies, environmental studies, neuroscience, in new pedagogies such as collaborative learning and web – based instruction and in new curriculum designs such as learning communities, capstone courses and service learning.

In interdisciplinary service learning, students from different fields, disciplines or professions, share service and learning objectives. Service Learning is a teaching and learning approach in which the students are engaged in activities that address human and community needs together with structured opportunities, intentionally designed to promote student learning and development.

3.1 Problem Based Learning

Civil Engineering is a key profession to the incorporation of sustainability into our society [5]. As the environment is constantly degraded by the human actions, there is a need to equip Civil Engineering Students with a wider horizon on concepts, in terms of the Sustainability into the society. Problem Based Learning (PBL) gives the students to experience Real Life Problem Solving, Project Management, Interpersonal Skills of Written and Verbal Communication, Working Productively in a Team, Work Integrated Education and Leadership Skills. Team work, by its nature, promotes the multidisciplinary aspect of solution techniques. PBL emphasizes students' pre – existing

knowledge and start with “what the students know” to the “unknown”. Problem or Project Based Learning (PBL) helps students to develop deeper understanding of the subject area by focusing on a realistic problem. It helps the Engineering students (learner) adopt a change in mindset from teacher-dependence to self reliance. It develops life – long learning skills.

Problem-based learning begins with the presentation of an authentic problem stated as it might be encountered by the practitioners. It supports the application of problem-solving skills required in “practice.” Students assume responsibility for their own learning and faculty act as facilitators. It develops Research Skills. Students need to learn how to get information when it is needed and will be current, as this is an essential skill for professional performance. The role of the instructor is to facilitate the application and development of effective problem-solving processes. Instructors must avoid making students dependent on them for what they should learn and know professionally.

Therefore, the students shall be given an opportunity to learn problem based than theoretical. They shall be given option to study the present scenario available in the country, in the context of disasters and then apply their engineering skills to solve the situation. In the context of this research, the identified problem is to manage disasters effectively so that the country will not face much impact on the environmental policies, financial policies and the people.

In the problem, the factors to be considered are the landscape of the country, the Coastal areas, the educational and economic background of the people, Environmental Impact Assessment of the disasters and the feasible engineering solutions in the case of the outcome of a disaster, with respect to the area affected. By this way, the casualties are minimized, waste and destruction of structures minimized. The most important among all the factors is the Disaster Management Education among the Engineers and the Community.

The Students /Engineers shall be able to apply knowledge of Basic Mathematics, Science & Engineering, Techniques, Skills and Modern Engineering Tools for Engineering Practice, Design a System, Components, or Processes to meet the desired needs within realistic constraints such as Economic, Environmental, Social, Political, Ethical, Health & Safety, Manufacturability and Sustainability. They should be able to function in multidisciplinary teams and work professionally. But the key factor is proper efficient communication. The solutions to these Engineering problems shall be obtained from the global, economic, environmental and societal context. Their Project work should be to tie different concepts together and see how they are used to solve realistic concepts.

IV. CURRICULUM INTEGRATION

Curriculum is a living, organic instrument to help teachers and institutions to find optimal ways to educate the youth. Curriculum reform is seen as a core of the ongoing efforts of Education Development and Quality Improvement. It provides students a richer academic experience by broadening the context and applicability of information and skills that are learned. It should challenge

students to solve real world problems. Educational researchers found out that an integrated curriculum can result in greater intellectual curiosity, enhanced problem-solving skills, and higher achievement in their career.

Curriculum Integration model can be referred to as the Problem Based Model. Integrated approach to curriculum, enable teachers and students to go beyond the strict disciplinary boundaries and respond to issues that may be more immediately relevant and motivating young people. Curriculum Integration aims at the interdependence and independence of the students. They will be able to perceive the curriculum as relevant to their learning needs and teaching learning process is enhanced more effectively than through a separate subject approach. (Figure 1.)

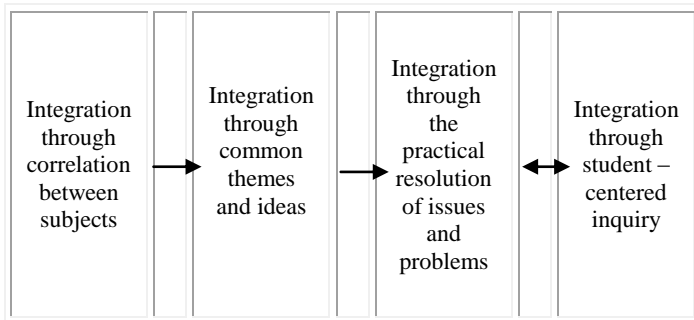


Figure 1. Relationship between the integrative curriculum and teaching learning continuum.

Curriculum integration can improve the effectiveness of education. [6]

Therefore, the contents that the students should compulsorily be aware of in the Management of Disaster perspective are identified, and shall be divided proportionately among various core papers to facilitate the students. There comes the need of Integrating Disaster Management components into the Engineering Curriculum.

V. CONCLUSION

As India is a country of various anthropogenic disasters and natural disasters, it becomes necessary for the future generation of Engineers to be familiar with preventive measures and the Disaster Management practices. As this is a period of globalization, the promising Engineers should be competent enough, who are very much informed and acquainted with the practices of safe, secure and sustainable humanity. For this, their curriculum should be sufficiently rich. In the Disaster Management context, when the Engineers are in their students' years itself, they shall be given information, advertently or inadvertently into their minds, which will be useful for their personal life and also in their duty towards humanity.

REFERENCES

- [1] "Landslide Studies in India", Y.P.SHARDA, LHI, E&E Division, Geological Survey of India, Delhi. www.iypeinsa.org/updates-09/art-20.pdf dt. 20.07.2011
- [2] Goel. S. L. Encyclopedia of Disaster Management. Vol 1 & 2. Policy and Administration (Deep & Deep Publications, 2006).
- [3] Trevelyan.J, "Engineering Education requires a better model of Engineering Practice", Proceedings of the Research in Engineering Education Symposium, 2009.
- [4] Alexander D., Bramati L., and Simonetta M., "Emergency Preparedness Training and Education in Lombardy Region, Italy: Survey of Supply and Demand", Natural Hazards Review, ASCE/ AUGUST 2009, VOL 10. NO.3, pp77 – 83.
- [5] Chau. K .W Incorporation of sustainability concepts into a Civil Engineering Curriculum. Journal of Professional Issues in Engineering Education and Practice, ASCE/ July 2007, pp 188-191.
- [6] Erikson T., Shumway.S, "Integrating the Study of Technology into the Curriculum: A Consulting Teacher Model", Journal of Technology Education, Vol 18, No.1, fall 2006, pp 27-38.

An Optimized BCD Adder Using Reversible Logic Gates

K.Rajesh¹, D A Tatajee²

^{1, 2} Department of ECE, A I E T, Visakhapatnam, India,

ABSTRACT: Reversible logic implementation plays an important role in VLSI design. Nowadays, It has voluminous applications in quantum computing, optical computing, quantum dot cellular automata and digital signal processing, low power CMOS design, nanotechnology. Adders are key components in many computational units, so design efficient binary coded decimal (BCD) adder using reversible gates is needed. It is not possible to calculate quantum cost without implementation of reversible logic. This paper proposes a new design for BCD adder that optimized in terms of quantum cost, memory usage and number of reversible gates. The important reversible gates used for reversible logic synthesis are NOT gate, CNOT gate, Toffoli gate, peres gate, TR gate and MTSG gate.

Key words: Reversible logic, quantum cost, Toffoli gate, Peres gate, MTSG gate, nanotechnology.

I. Introduction

Power dissipation is one of the most important factors in VLSI circuit design. Irreversible logic circuits dissipate $KT \cdot \log_2$ joules heat energy [1]. Where K is Boltzmann's constant and T is the absolute temperature at which the computation is performed. The amount of energy dissipated in a system bears a direct relationship to the number of bits erased during the computation. Some bits erased means some information is lost. Bennet showed that the $KT \cdot \log_2$ joules energy dissipation would not occur if a computation is carried out in a reversible manner. Reversible computation can be performed through circuits that do not lose information [2].

As the Moore's law continues to hold, the processing power doubles every 18 months [1]. The current irreversible technologies will dissipate a lot of heat and can reduce the life of the circuit. The reversible logic operations do not erase the information and dissipate very less heat. Thus, Reversible logic is likely to be in demand in high speed power aware circuits. The main challenges of designing reversible circuits are to reduce number of gates, memory usage, delay and quantum cost. This paper presents a new design of reversible BCD adder. The hardware complexity of this design is very less when compared to the existing once.

II. Basic Definitions of Reversible Logic

In this section, the basic definitions and ideas to the reversible logic and few reversible gates which are used and relevant with this research work.

2.1. Reversible logic

It is an n-input, n-output logic function in which there is a one-to-one correspondence between the inputs and outputs [3]. Because of this one to one mapping the input vector can be uniquely determined from the output vector.

2.2. Quantum cost

Quantum cost refers to the cost of circuit in terms of the cost of primitive gate. It is calculated knowing the number of primitive reversible logic gates required to realize the circuit [4].

2.3. Delay

The delay of a logic circuit is the maximum number of gates in a path from any input line to any output line. This definition is based on the following assumptions [2]

- (i) Each gate performs computation in one unit time.
- (ii) All inputs to the circuit are available before the Computation begins.

2.4. Hardware complexity

Hardware complexity refers to the total number of logic operations in a circuit. Means the total number of AND, OR and EXOR operation in a circuit.

2.5. Ancilla inputs

This refers to the number of inputs that are to be maintaining constant at either 0 or 1 in order to synthesize the given logical function [5].

2.6. Garbage outputs

Garbage outputs are the unutilized outputs in reversible circuits which maintain reversibility but do not perform any useful operations [6].

III. Reversible Logic Gates

3.1. CNOT GATE

CNOT gate is also known as controlled-not gate. It is a 2*2 reversible gate. The CNOT gate can be described as:

$$IV = (A, B) \quad (1)$$

$$Ov = (P=A, Q=A \oplus B) \quad (2)$$

IV and Ov are input and output vectors respectively. Quantum cost of Cnot gate is 1[14]. Figure 1 shows a 2*2 CNOT gate and its symbol.

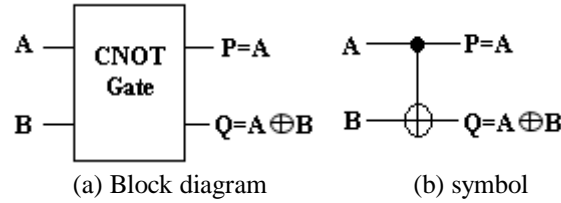


Figure 1: CNOT Gate

3.2. TOFFOLI GATE

Toffoli gate is a 3*3 reversible gate [14]. The input vector is I (A, B, C) and output vector is O (P, Q, R). The Toffoli gate can be described as:

$$Iv = (A, B, C) \quad (3)$$

$$Ov = (P=A, Q=B, R = AB \oplus C) \quad (4)$$

Quantum cost of Toffoli gate is 5. Figure 2 shows a 3*3 Toffoli gate and symbol.

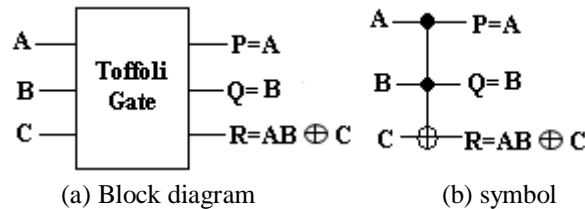


Figure 2: Toffoli Gate

3.3. PERES GATE

Peres gate is a 3*3 reversible gate. It is also known as New Toffoli gate. It is constructed from CNOT gate and Toffoli gate [2]. The Peres gate can be described as:

$$Iv = (A, B, C) \quad (5)$$

$$Ov = (P=A, Q=A \oplus B, R=AB \oplus C) \quad (6)$$

I_v and O_v are input and output vectors orderly. Quantum cost of Peres gate is 4. The Peres gate and its symbol is shown in Figure 3.

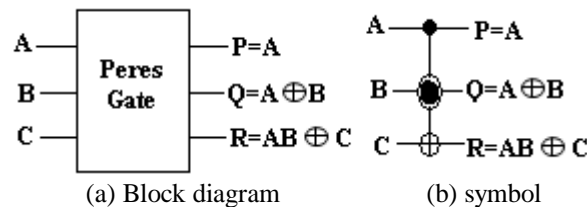


Figure 3: Peres Gate

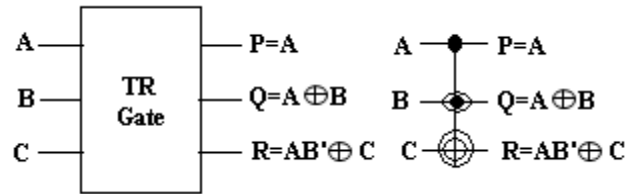
3.4. TR GATE

TR gate full name is Thapliyal-Ranganathan gate. It is a 3*3 reversible gate [8]. The TR gate can be described as:

$$IV = (A, B, C) \quad (7)$$

$$Ov = (P=A, Q=A \oplus B, R=AB' \oplus C) \quad (8)$$

I_v and O_v are input and output vectors orderly. Quantum cost of TR gate is 4. The TR gate and its symbol are shown in figure 4.



(a) Block diagram

(b) symbol

Figure 4: TR Gate

3.5. MTSG GATE

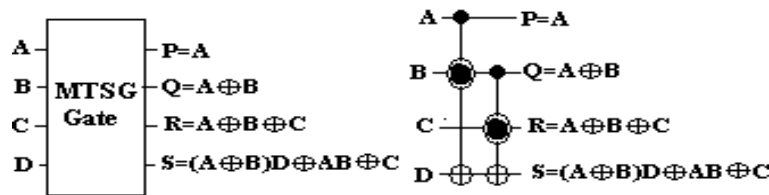
MTSG gate is a 4*4 reversible gate. The MTSG gate can be described as:

$$I_v = (A, B, C, D) \quad (9)$$

$$O_v = (P = A, Q = A \oplus B, R = A \oplus B \oplus C) \quad (10)$$

$$S = (A \oplus B)D \oplus AB \oplus C \quad (11)$$

I_v and O_v are input and output vectors orderly. Quantum cost of MTSG gate is 6[9]. MTSG will be very useful to design reversible circuits as the quantum cost of the MTSG is very low as compared to the TSG gate[9]. it is constricted from cascading of two Pares gates. By providing '0' in the D input, easily realize the full-adder from the MTSG gate. A reversible full adder can be realized at least one gate. For designing n-bit binary ripple carry adder n MTSG gates are required. The MTSG gate and its symbol is shown in figure 5.



(a) Block diagram

(b) symbol

Figure 5: MTSG Gate

IV. Block Diagram of BCD Adder

A BCD adder is a circuit that adds two BCD numbers and produces a sum also in BCD form. Figure 6 shows the block diagram of BCD adder. A BCD adder must include three major parts. Those are

- (i) Binary adder
- (ii) Over 9 detection unit
- (iii) Correction unit

Binary adder performs addition operation on two BCD numbers and one-bit carry input. Over 9 detection unit recognizes if the result of first part is more 9 or not. If the result is more than 9 it produces 1 otherwise 0. Correction unit, if the output of detector is 1 then the sum is added by 6, else added by 0.

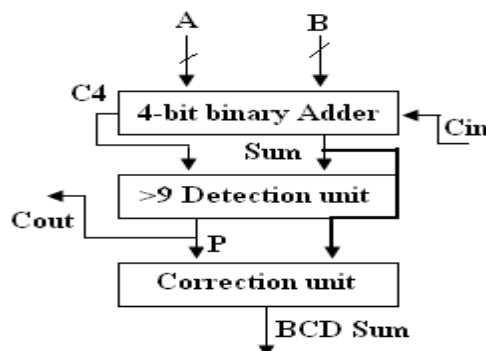


Figure 6: Block diagram of BCD adder

A conventional BCD adder is shown in figure 7. The first part 4-bit binary adder is cascade of four full adders. The second part detection unit is constructed by using two AND gates and one OR gate. The third part correction unit adds 0 to the binary number if the binary result is less than 10 and adds 6 to the binary result if it is more than 9. Binary full adder is a

basic circuit for designing binary arithmetic units such as n-bit binary adder, sub tractor and multiplier. In same manor a BCD adder/subtract or is a basic circuit for designing BCD arithmetic units such as BCD n-bit adder/sub tractor.

V. Efficient Design of Reversible BCD Adder

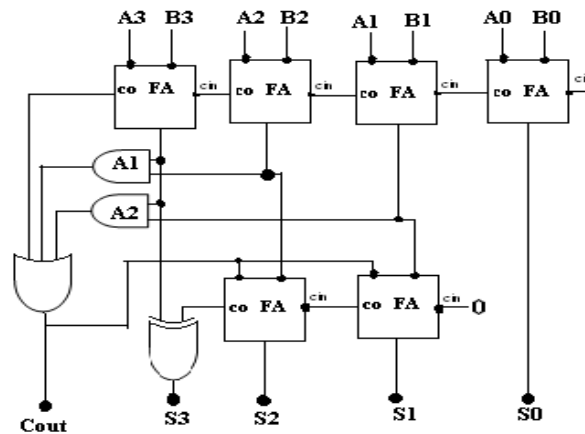


Figure 7: An irreversible BCD adder

This is the equivalent design of the approach shown in figure 7. Proposed reversible BCD adder optimized for the number of reversible gates, memory usage and quantum cost. The proposed design of BCD adder is shown in figure 8. In first part 4 MTSG gates are connected in series. It can Work as 4-bit binary adder produce sum and carry [2]. Second part is equivalent design of over 9 detection unit and correction unit [8].

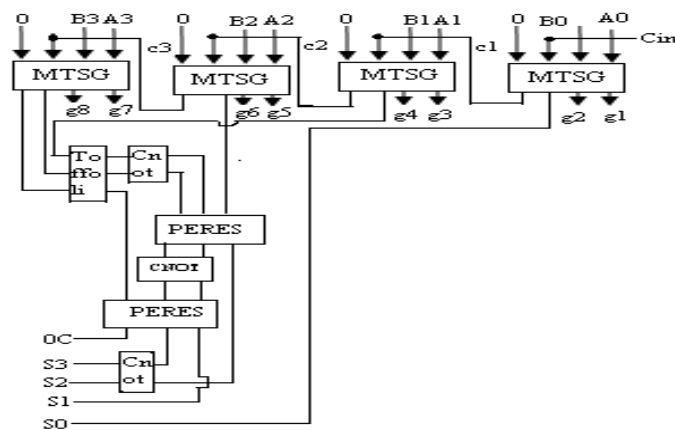


Figure 8: Proposed design of reversible BCD adder

5.1. Quantum cost calculation

For n-bit proposed methodology needs n MTSG gates working in series thus in this stage has the quantum cost is $6n$. In next stage $(n-3)$ toffoli gates are working in series thus in this stage quantum cost is $5(n-3)$. In next stage $(n-3)$ CNOT gates are working in series thus in this stage quantum cost is $(n-3)$. In next stage $(n-3)$ Peres gates are working in series thus in this stage quantum cost is $4(n-3)$. In next stage $(n-3)$ CNOT gates are working in series thus in this stage quantum cost is $(n-3)$. In next stage $(n-3)$ Peres gates are working in series thus in this stage quantum cost is $4(n-3)$. In next stage $(n-3)$ CNOT gates are working in series thus in this stage quantum cost is $(n-3)$.

Thus the total quantum cost of n bit reversible BCD adder is $6n+5(n-3)+n-3+4(n-3)+n-3+4(n-3)+n-3=22n-48$. In this paper we are discuss about 4-bit reversible BCD adder so quantum cost of proposed reversible BCD adder is 40. Number of reversible gates used in this design is 10.

VI. Results and Discussions

The proposed reversible BCD adder design has quantum cost 4 and delay is 11.228ns. To construct proposed BCD adder 10 reversible gates and 10 BELS and 6 slices are required. A comparison with the existing designs of the Reversible BCD adder is illustrated in Table 1. The design in [8] is the best existing design literature considering the Number of reversible gates, Quantum cost, Delay and BELS. It Needs 36 reversible gates and has the quantum cost 70 and it require 9 slices. The delay of design in [8] is 11.153ns. it can be observed from the comparison table that the proposed design is better than the design in [8] in terms of number of reversible gates, area, delay, quantum cost. Thus the proposed design is efficient compared to existing designs. Simulation Results of proposed Reversible BCD Adder is shown in figure 9. Apply a0 a1 a2 a3 is 0 0 1 1 respectively and similarly b0 b1 b2 b3 is 1 1 0 0 respectively and give the input carry is 0. It produces the result, carry out is 1 and s0 s1 s2 s3 is 0 1 0 1 respectively which is equivalent to the 15 in decimal form.

TABLE 1
A Comparison of Reversible BCD Adders

BCD Adder	No. of slices	No. Of gates	Quantm cost	Delay (ns)	BELS
Existing [14]	9	36	70	12.15	22
Proposed Design	6	10	40	11.22	10

VII. Conclusion

In this paper, reversible logic was implemented for BCD adder. By comparing the existing design with proposed design is less costly in terms of number of gates and quantum cost and delay and area and BELS. The proposed design is highly optimized. The efficient design of the BCD adder depends on the Design methodology used for designing the reversible ripple carry adder and the reversible binary to BCD converter. Thus for future research, efficient design schemes for reversible ripple carry adder and the reversible binary to BCD converter is an interesting area to investigate.

References

- [1] Himanshu Thapliyal, M.B.Srinivas, and M.Zwolinski, "A Beginning in the Reversible Logic Synthesis of Sequential Circuits", MAPLD
- [2] M. Thomsen and R.Gluck, "Optimized reversible binary-coded decimal adders," J. Syst. Archit., vol. 54, no. 7, pp. 697–706, 2008.
- [3] M. Mohammadi, M. Haghparast, M. Eshghi, and K. Navi, "Minimization optimization of reversible bcd-full adder/subtract or using genetic algorithm and don't care concept," International J. Quantum Information,
- [4] A. K. Biswas, M. M. Hasan, A. R. Chowdhury, and H. M. Hasan Babu, "Efficient approaches for designing reversible binary coded decimal adders," Microelectron. J., vol. 39, no. 12, pp. 1693–1703, 2008.
- [5] H.Thapliyal and N. Ranganathan, "Design of efficient reversible binary subtractors based on a new reversible gate," in Proc. the IEEE Computer Society Annual Symposium on VLSI, Tampa, Florida, May 2009, pp.229–234.
- [6] Y. Takahashi and N. Kunihiro, "A linear-size quantum circuit for addition with no ancillary qubits," Quantum Information and Computation, vol. 5, no. 6, p. 440448, 2005.
- [7] Sreehari Veeramachaneni, M.Kirthi Krishna, Lingamneni Avinash, Sreekanth Reddy P, M.B.Srinivas "Novel, High-speed 16-Digit BCD Adders Conforming to IEEE 754r Format" IEEE Computer society Annual Symposium on VLSI 2007
- [8] Majid Mohammadi, Mohammad Eshghi, Majid Haghpaarast and Abbas "Design and of Reversible BCD Adder/Subtractor Circuit for Quantum and Nanotechnology Based systems" World applied Sciences Journal 4(6):787-792, 2008
- [9] M.A.Nielsen and I. L. Chuang, Quantum Computation and Quantum Information. New York: Cambridge Univ. Press, 2000.
- [10] T. Toffoli, "Reversible computing," MIT Lab for Computer Science, Tech. Rep. Tech memo MIT/LCS/TM-151, 1980.
- [11] A. Peres, "Reversible logic and quantum computers," Phys. Rev. A, Gen.Phys., vol. 32, no. 6, pp. 3266–3276, Dec. 1985.
- [12] H. Thapliyal and N. Ranganathan, "Design of reversible sequential circuits optimizing quantum cost, delay and garbage outputs," ACM Journal of Emerging Technologies in Computing Systems, vol. 6, no.4, Article 14, pp. 14:1–14:35, Dec. 2010.
- [13] S.A. Cuccaro, T. G. Draper, S. A. Kutin, and D. P. Moulton, "A new quantum ripple-carry addition circuit," <http://arXiv.org/quantph/0410184>, Oct 2004.
- [14] Y. Takahashi, S. Tani, and N. Kunihiro, "Quantum addition circuits' and unbounded fan-out," <http://arxiv.org/abs/0910.2530>, Oct 2009.
- [15] Himanshu Thapliyal, Nagarajan Ranganathan, "A New Reversible Design of BCD Adder" 978-3-9810801-7-9/DATE11/@2011 EDAA.

Preform Shape Optimization of Connecting Rod Using Finite Element Method and Taguchi Method

Md. Israr Equbal¹, Rajkumar Ohdar², Md. Nadeem Bhat³, Suhail Ahmad lone⁴

^{1,2}Department of Forge technology, NIFFT, Ranchi 834003, India

³Department of Foundry and Forge technology, NIFFT, Ranchi 834003, India,

⁴Department of Material science and Engineering, NIFFT, Ranchi, 834003, India

ABSTRACT : Preform design in forging processes is an important aspect for improving the forging quality and decreasing the production cost. The objective of this paper is to obtain an optimal preform shape in the consideration of the influence of the metal flow deformation in closed die forging process. Finite element method based DEFORMTM 3D software in conjunction with Taguchi method has been used to simulate the closed die forging process and then performing a series of optimization iterations in order to obtain the optimal shape of the billet based on forging load minimization. The goal of the simulation and optimization process is to minimize the forging load and produce defect-free forgings. The optimal shape of the billet that gives minimum forging load with complete die filling was obtained after several optimization iterations. The approach used in this study could be extended to the optimization of more complicated forging products.

Keywords: Preform, Hot forging, Optimization, Finite element analysis, Taguchi method.

I. INTRODUCTION

In the forging process of complicated parts, the selection of appropriate preform shapes is crucial. The preform design in metal forging plays a key role in improving product quality, such as ensuring defect-free property and proper metal flow. In addition, it may produce more uniform strain distribution through the final forging product. Thus, the metallurgical and mechanical properties reduce the material waste and less die wear may be achieved [1]. In designing this process, preform shape, final shape and material behaviour should be contemplated in a way to fill the die cavity completely. Furthermore, the designer should regard the process not causing any defect or undesirable properties. Main purpose of the preform design process is achieving the following:

- Assuring the metal flow without any defect and appropriately filling of the die.
- Minimizing the material wastes in the flash.
- Minimizing the die wear.
- Obtaining the desirable grain flow and suitable mechanical properties.

Traditionally, forging process design and forging process plan has employed trial & error methods which are a time consuming process and expensive. However, in the recent years a significant increase of computer and numerical simulations are reported based on finite element (FE) analysis of forging process. Moreover, traditional techniques have been substituted into numerically based analysis. Therefore, more robust and efficient computer based approaches have been introduced recently. As a result, a large number of investigations have been reported by different scientists in the preform design field.

Zhao G. et al. [2] apply a method, which employs an alternative boundary node release criterion in the FEM simulation of a backward deformation of forging processes. The method makes use of the shape complexity factor, which provides an effective measure of forging difficulty. Bramley [3] initiated a reversed method by Upper Bound Elemental Technique (UBET) and has attained the preform shape by reversing the velocity field direction to a minimum amount for whole of the energy distribution rate which optimized by contact conditions. Biglari et al. [4] succeed to design optimum axisymmetric forging preforms by combining the backward tracing and fuzzy logic concepts. A new approach is introduced by Yiguo, L., et al. [5] for pre-form design called Simulation Block Technique (SBT) in which, the two half-parts of the forging die is imaginarily separated from their closed position, they move backward from each other in opposite direction of the forward (normal) forging process, so that the initial billet or a pre-form can be obtained, the model incorporates the use of UBET. Kang, B., S., et al. [6] presented pre-form shapes design in forging of rib-web shaped plane-strain parts were designed using rigid-plastic finite element method in order to obtain flash-less part. The preform was obtained by changing the aspect ratio- the height to width ratios of the rib geometry used in the analysis. An optimization approach for the design of intermediate forging die shapes using backward deformation simulation and design optimization was developed by Han, C., S., et al. [7]. This approach could determine the pre-form die shapes from the final part shape by imposing constraints on the plastic deformation of the material. In this paper computer simulation of the connecting rod using DEFORM (Design Environment for Forming) is adopted for the purpose of optimizing the preform shape. Deform is a Finite Element Method (FEM) based process simulation system designed to analyze various forming and heat treatment processes used by metal forming and related industries. By simulating manufacturing processes on a computer, this advanced tool allows designer and engineers to

- Reduce the need for costly shop floor trials and redesign of tooling and process.
- Improve tool and die design to reduce production and material costs.
- Shorten lead-time in bringing a new product to market.

II. METHODOLOGY

The main objective of closed die forging are complete die filling without defects viz. cracks, fold-over, wrinkles with minimum forging load. The goal of the simulation is to find out the shape of the billet that leads to a minimum forging load and complete die filling without any defects. Taguchi's experimental method is utilized to design the process parameter combinations to identify the relative influence of each parameter considered in the study. Study of the influence of design related variables on output performance characteristics are time consuming and costly during the real-time forging process.

Whereas finite element method (FEM) based simulation software permits simulation of the system in solving linear and non-linear problems in a cost effective and timely manner. In this paper the effect of design parameters viz. flash thickness, flash width, corner radii and fillet radii on perform has been studied in order to obtain minimum forging load with complete die filling along with minimum material loss by using FEM based DEFORM™ 3D V6.1 to simulate and validate the optimum result. For simulation purpose 3-D modeling software CATIA V5 is used to model part and dies. Final part and its die are as shown in Fig. 1 and Fig. 2. Dies and billets are drawn in such a manner that they are Z-axis aligned. As DEFORM™ accepts only '.STL' files, upper die, lower die and billets are saved with 'STL' extension.

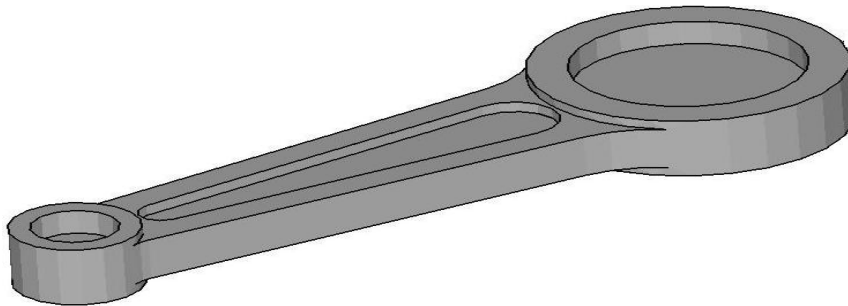


Figure 1: 3D CAD model of connecting rod

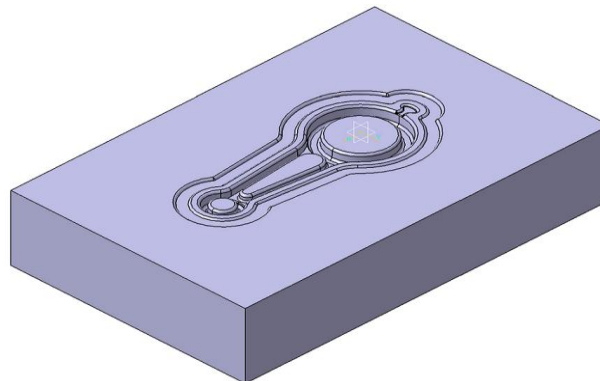


Figure 2: Die of Connecting rod

The material of connecting rod is AISI 1045 alloy steel, whereas AISI-H-13 die steel is used as die material and their properties are given in Table I.

Table I: Material Properties

Property	Component	Die	Units
Density	7870	7800	Kg/m ³
Poisson's Ratio	0.29	0.3	---
Elastic modulus	200	210	GPa
Tensile strength	585	1990	MPa
Yield strength	505	1650	MPa
Hardness	84	45	HRC
Thermal conductivity	51.9	24.6	W/m-K

III. DESIGN CONSIDERATIONS

3.1 Determination of Stock Size

The factors in estimating the stock size include the size and shape of the forging, method of heating and method of forging.

The terms used in weight calculation are

Net weight – it is the weight of forging as per the given dimension of the component.

Net weight = volume of forging × density of material

Volume of forging = 45700 mm³

Density of material = $7.86 \times 10^{-6} \text{ kg/mm}^3$

Net weight = 0.36 kg

Flash loss – it is the loss of extra material comes out when the top and bottom die block has filled. It is determined by flash thickness and flash width.

$$\begin{aligned}\text{Flash loss} &= 15 \text{ to } 20 \% \text{ of the net weight} \\ &= 0.20 \times 0.36 \\ &= 0.072\end{aligned}$$

Gross weight- the amount of material required to fabricate a forging.

$$\begin{aligned}\text{Gross weight} &= \text{net weight} + \text{losses} \\ &= 0.36 + 0.072 \text{ kg} \\ &= 0.43 \text{ kg}\end{aligned}$$

3.2 Design of Flash

The purpose of the flash is to control the metal flow within the die cavity. The flash normally cools faster than the main body of the forging and hence results resistance in metal flow outwards. The consequence of this flow restriction, metal is forced to take an alternative route, the path of least resistance, which normally results in filling dipper die cavities. The flash thickness and width is directly related to the amount of waste material, acts as a pressure release valve for the almost incompressible work metal and restrict the outward flow of the metal so that remote corners and deeper cavities can be filled up. The finisher impression generally includes as provision for flash. The flash depression can be in either die or in both dies.

Thus design of flash dimensions plays a vital role in metal filling. While designing for flash, care must be taken in selecting flash thickness, as thickness being small will necessitate greater energy or extra blows to bring forging to size, on the other hand thickness being more may cause inadequate die filling. Thus a balanced condition is needed with just enough volume of metal to ensure that the flash thickness provided would force the work-metal to fill the impression properly without causing excess wear and pressure. Flash thickness is calculated by using the various formulas as given in Table II.

Table II: Design of Flash

Author	Flash thickness	Result
Bruchanov & Rebelskii [8]	$t = 0.015\sqrt{A}$	1 mm
Thomas [9]	$t = 0.016D$	1.25mm
Vieregge [10]	$t = 0.017D + \frac{1}{\sqrt{D+5}}$	1.5 mm
Neuberger & Mockel [11]	$t = 0.89\sqrt{W} - 0.017W + 1.13$	1.67mm
Teterin & Tarnovski [12]	$t = 2\sqrt[3]{W} - 0.001W - 0.009$	1.4 mm

Here,

A= plan projected area including flash land = 3950 mm²

D= equivalent diameter = 72 mm

W= forging weight = 0.36 kg

3.3 Fillet and Corner radii

Filletts and corners are curved surface connecting ribs, bosses and webs, and are defined by their transverse section. A corner is a convex arc, which joins two intersecting sides at an external angle of more than 180°, whereas fillet is a concave arc, which joins two intersecting sides at an external angle of less than 180°. Design of fillet and corner affect grain flow, forging pressure requirement, die wear, grain flow, amount of metal to be removed during machining, amount of cut grain at junction and cost of dies and forgings. Proper selection of fillet and corner radii is vital in designing dies for forgings. Sharp corners must be avoided in forging design as they weaken both the dies and finished forgings. A sharp internal corner or very small fillet in forging introduces a danger of cracking in heat treatments while the corresponding sharp external corner on the die prevents a satisfactory flow of metal in impression and may result in a defective forging.

3.4 Press selection

The main requirement selecting the press to produce a given forging is an estimate of the forging load. This will depend on the material, forging temperature, forging complexity and flash and land dimension.

For non circular forging

$$P^1 = P \times \left[1 + 0.1 \times \sqrt{\frac{2}{b}} \right] \quad (1)$$

$$P = 8 \times (1 - 0.001 \times D_{\text{reduced}}) \times \left(1.1 + \frac{20}{D_{\text{reduced}}} \right)^2 \times S_1 \times \sigma \quad (2)$$

Where, D_{reduced} = Reduced diameter of Non- Circular forging including flash land = $1.13(S_1)^{1/2} = 72 \text{ mm}$

S_1 = Plan projected area of Non-Circular forging including flash land = 6130 mm²

σ = Tensile strength at forging temperature=6.5 kg/mm²

b= Average width of forging including flash land = S_1/L_{\max} =39.3 mm

L_{\max} = maximum length of forging at parting plane including flash land= 156mm

$P=8 \times (1-.001 \times 72) \times 1.898 \times 6130 \times 6.5 = 561526$ kg

$P^1 = P \times [1 + 0.1 \times 0.225] = 574$ ton

For simulation work press capacity is taken 574 ton

IV. TAGUCHI EXPERIMENTAL DESIGN

Taguchi design of experiment is a powerful analysis tool for modeling and analyzing the influence of control factors on performance characteristics. The most important stage in this method lies in the selection of control factors. An exhaustive literature review reveals that the optimized preform shape largely influenced by flash thickness (F_T), flash width (F_W), corner radius (R_C), fillet radius (R_F). These parameters each at three levels are considered for the present study. The operating conditions under which test are carried are shown in Table III.

Table III: Factors and their levels

Factors	Symbol	Level			Unit
		1	2	3	
Flash thickness	F_T	1	1.5	2	mm
Flash width	F_W	6	8	10	mm
Corner radius	R_C	1.5	2	3	mm
Fillet radius	R_F	2	3	5	mm

The total degree of freedom (DOF) for four factors each at three levels is 8. Therefore L_9 orthogonal array [13] is selected for experimental design and is shown in Table IV.

Table IV: Taguchi Design for Preform (All dim. are in mm)

Flash thickness	Flash width	Corner radii	Fillet radii
1	6	1.5	2
1	8	2	3
1	10	3	5
1.5	6	2	5
1.5	8	3	2
1.5	10	1.5	3
2	6	3	3
2	8	1.5	5
2	10	2	2

V. PREFORM DESIGN

Preform design is one of the most important aspects in metal forming process design. Pre-form impression allows adequate metal distribution in the final impression. Thus, defect-free, complete die fill and small metal losses into flash can be achieved by a properly designed perform. If the component has varied cross-section as in case of spanner, connecting rod, break, pedal lever etc. it is necessary to reduce or increase cross sectional area of the bar at desired points with a view to improve die life. This will necessitate the preforming operation before finishing. For better quality forging productions, care must be taken that in the finishing impression to minimize deformation to achieve final shape. Traditionally, the preform design is based on empirical or approximate analysis, requiring time consuming and expensive trial-and-error. Hence it is necessary to optimize the perform design in order to minimize the above drawbacks.

The following procedure is used to design preform impression from forging drawing.

- The plan and the elevation of forging are laid out to full scale.
- An estimated outline of the flash of the forging preside is than laid out.
- The forging is then divided into various element based on geometric shape.
- Vertical lines are drawn through largest and smallest cross sectional area of each element found as above.
- The area of the above cross section is calculated and to each such area, cross sectional area of flash is added (flash width× flash thickness).
- From the base line of above measurement are plotted and connected with smooth line, then the cross sectional area of perform at each line is determined.
- The diameter “D” of the perform is evaluated at each element using the equation 3.

$$D = (4 \times A / \pi)^{(1/2)} \quad (3)$$

Where D – equivalent diameter

A - Total area (flash area + job section area)

Thereafter, the dimension D is symmetrically plotted about the reference line. These points are finally connected with a smooth curve as shown in Fig.3. A perform impression having this as an approximate contour can provide smooth

flow of metal from blank into perform and finally finisher impression. For the present work 9 such performs and their dies were designed for different values of flash thickness, flash width corner and fillet radii [14].

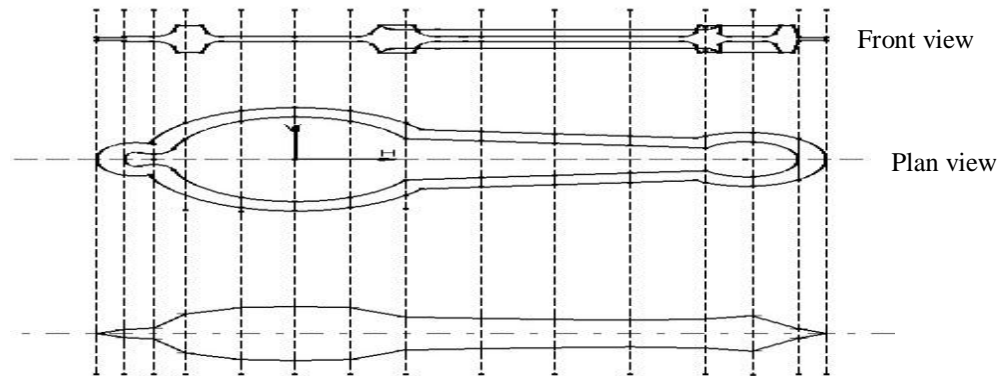


Figure 3: Preform shape of Connecting rod

VI. COMPUTER SIMULATION AND ANALYSIS OF THE FORGING PROCESS

Main objective of this study is to investigate the effect of design parameters on preform shape. The computer simulation of hot forging process has been done to obtain the optimum perform shape. The DEFORM™-3D V6.1 software package was employed in the present research for the simulation and analysis of results. So far most FE based software that simulate billet forming processes that consider only plane-strain or axis symmetric deformations. Since many industrial parts such as connecting rods have very complex geometries, the metal flow is three dimensional and cannot be properly modelled with a two dimensional approximation. Therefore, a three dimensional simulation of the manufacturing process must be performed to get adequate results. The commercial package DEFORM™-3D V6.1 offers the possibility of simulating three dimensional material flows of complex geometries.

Main objective of this paper is to investigate the effect of process and design parameter to die performance and quality of the forged part. In this study, computer simulation of hot forging process has been done to obtain the optimum design and process parameters. The DEFORM™-3D V6.1 software package was employed in the present research for the simulation and analysis. DEFORM essentially consists of three parts, described below.

6.1 Pre-processor

The pre-processor includes (i) an input module for iterative data input verification, (ii) an automatic mesh generation program which creates a mesh by considering various process related parameters such as temperature, strain, strain-rate as well as die and work piece geometry; and (iii) an interpolation module that can interpolate various simulation results of an old mesh onto a newly generated mesh. The combined and the automated use of the modules for automatic mesh generation and interpolation, called automatic remeshing, allow a continuous simulation of a forming process without any intervention by the user, even if several remeshings are required. This automatic remeshing capability drastically reduces the total processing time of finite element analysis. All the input data generated in the pre-processor can be saved (i) in a text form which enables the user to access the input data through any text editor; and /or (ii) in a binary form which is used by the simulation engine explained below.

6.2 The simulation engine

The actual FEM-based analysis is carried out in this portion of DEFORM. This simulation engine is based on a rigid – plastic FE formulation and can handle a multiple number of billets (either dense material or porous material, or combination of these materials) and dies (either rigid or linear elastic) with non-isothermal simulation capability. The simulation results are stored in binary form and accessed by the user through the post – processor.

6.3 Post processor

The post processor is used to display the results of the simulation in graphical or alphanumeric form. Thus, available graphic representations include (i) FE mesh; (ii) contour plots of distributions of strain, stress, temperature etc, (iii) velocity vectors, and (iv) load – stroke curves. Two other useful capabilities in the post –processor are (i) ‘point tracking’, which provides deformation histories of selected points in the workpiece throughout the deformation; and (ii) ‘flownet’, which allows the user to observe the deformation of circles or rectangles ‘inscribed’ on the undeformed workpiece for any desired step through the simulation [15].

There are some assumed models in this paper, including that the plastic material model and the rigid die model are assumed. The velocity of the moving ram is kept constant. The strain rate at the first of deformation is equal to 2 S^{-1} . All the simulations started with 45000 elements. Table V shows the assumed models.

Table V: Operation parameters assigned to complete the simulation

Problem Type	Closed die hot forging
Forging Equipment	Mechanical press
No. of elements	45000
Mesh type	Tetrahedral
Simulation mode	Isothermal
Primary die	Top die
Const. Envir. Temp.	20 ⁰ c
Billet Temp.	1050 ⁰ c
Die Temp.	300 ⁰ c
Friction Coeff.	0.3 with lubrication
Die velocity	1.5 mm/s

VII. RESULTS

Simulations are run as per Taguchi experiment plan based on the experimental layout depicted in Table 4, and respective value of forging load for each simulation run are converted into their respective S/N ratios as per equation 1 and are given in Table VI.

Table VI: L9 orthogonal array with their response

Exp. No.	Parameters				Response		
	F _T	F _W	R _C	R _F	Forging load(N) (10 ⁶)	S/N Ratio	Complete filling
1	1	6	1.5	2	7.86	-17.9085	No
2	1	8	2	3	7.29	-17.2546	No
3	1	10	3	5	9.73	-19.7623	No
4	1.5	6	2	5	3.82	-11.6413	Yes
5	1.5	8	3	2	7.53	-17.5359	No
6	1.5	10	1.5	3	6.25	-15.9176	Yes
7	2	6	3	3	3.17	-10.0212	Yes
8	2	8	1.5	5	3.47	-10.8066	Yes
9	2	10	2	2	4.01	-12.0629	No

After conducting the experiments according to Taguchi's experimental design we observed that in experiment no. 1, 2, 3 and 5 the problem of underfilling occurred and the forging load was also very high. This is due to small flash thickness and improper value of corner and fillet radii. While during experiment no. 9 problem of underfilling occur because it has been observed that material is going out in the form of flash without filling die cavity completely.

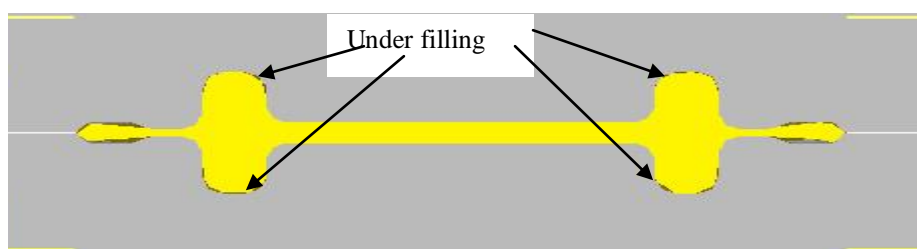


Figure 4. Critical areas of underfilling during Simulation

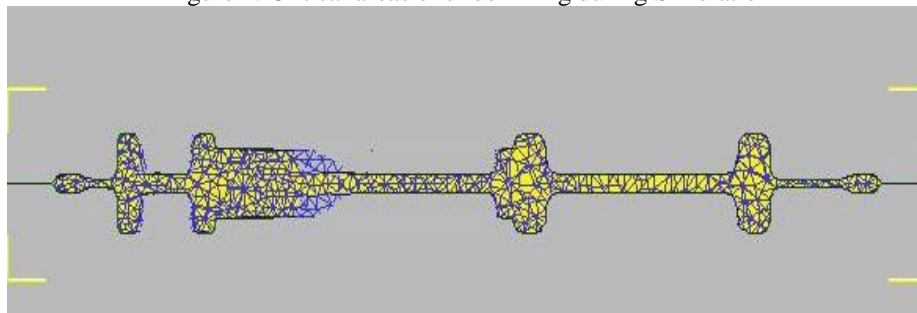


Figure 5. Complete die filling achieved during simulation

VIII. DISCUSSION

Data analysis is made using MINITAB R14 software at 95% of confidence. Main effect plot (Fig. 6) is used to determine the optimum factor levels for minimum forging load, which F_T3 , F_W1 , R_C1 and R_F2 are corresponding to the largest values of S/N ratio for all control parameters. Relative influence of each factor is determined by analysis of variance method (ANOVA) presented in Table VII.

Table VII: ANOVA Table for forging load

Parameters	Degree of freedom	Sum of square	Variance	% Contribution	F- value
Flash thickness	2	81.234	40.617	77.1526	6.72
Flash width	2	11.966	5.983	11.3648	0.99
Corner radii	-	6.797*	-	-	-
Fillet radii	-	5.293*	-	-	-
Error	4	12.09	6.045		
Total	8	105.29			

*pooled

ANOVA depicts that the process parameter namely Flash thickness and Flash width are the most significant parameters affecting the Forging load. Fillet radius and corner radius shows the least contribution. It is necessary to mention that confidence level of 95% is used for analysis purpose, so p-value less than 0.05 will establish the significance of factor.

Adequacy of analysis is carried out using Anderson–Darling (AD) test and results are illustrated in Fig. 7, which shows that data follows normal distribution and develop procedure is suitable enough to explore the design space.

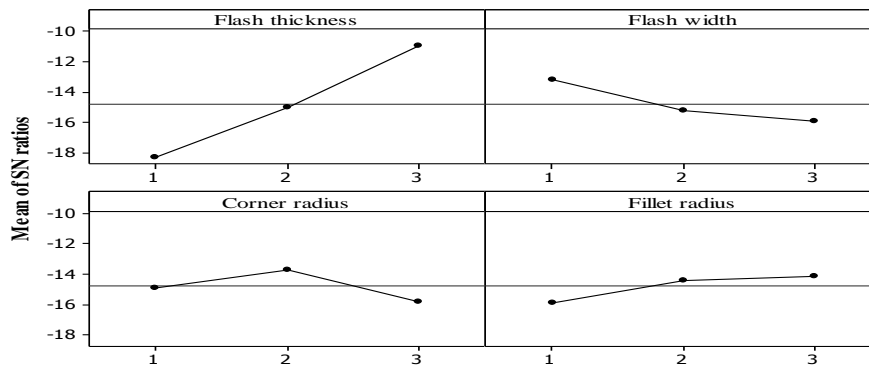


Figure 6: S/N ratio response graph for forging load

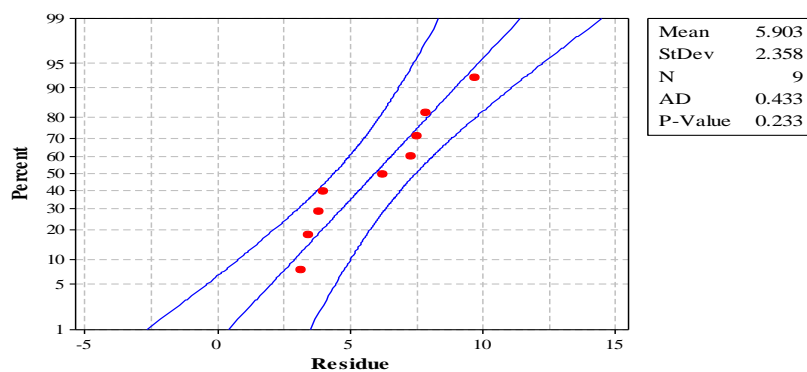


Figure 7: Normal probability plot of residue at 95% of confidence

IX. CONFIRMATION EXPERIMENT

For confirmation purpose process is simulated at optimum factor level setting keeping all the simulation parameter fixed as given in Table 5. Fig. 8 shows the optimal forging load value of 2.13×10^6 N. At this load the complete die filling is achieved with maximum yield (Fig. 9). On comparing the simulation results with Taguchi predictive model which is 2.17×10^6 small error of 1.84 % indicate the Taguchi experimental plan has proceeded in a smooth manner.

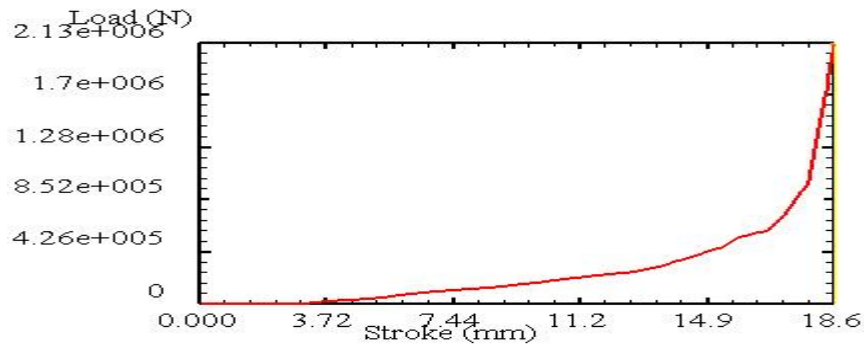


Figure 8: Load vs. stroke curve showing minimum forging load

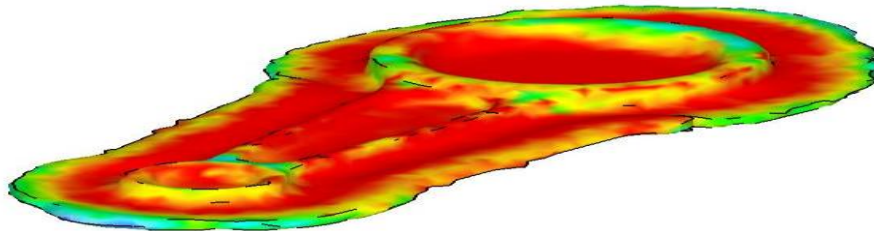


Figure 9: Complete die filling with maximum forging yield and without any defect

X. CONCLUSION

FEM-based computer simulation has been used to optimize the design parameters viz. flash thickness, flash width, corner radius and fillet radius on perform shape of connecting rod. Using Taguchi method, design parameters were optimized individually for forging load. In order to study the significance of the parameters in effecting the quality characteristics of interest i.e. forging load ANOVA has been performed. The conformation experiment was conducted by taking the optimized value (output of Taguchi's experiment) and was simulated once again. The results shows that at optimum factor level setting complete die filling is achieved with minimum forging load. It is found that optimization can be achieved quickly and efficiently through the use of simulation software. Modeling provides more information about the process i.e. load requirement and metal flow at different stages of the process. These techniques are also cheaper than performing tryouts with actual dies and equipments.

References

- [1] M. Sedighi, M. Hadi, and S. Kolahdouz, Optimization of Preform in Close Die Forging by Combination Of Neural Network and Genetic Algorithm, World Applied Sciences Journal, 7 (11), 2009, 1464-1473.
- [2] G. Zhao, E. Wright, R. V. Grandhi, Computer aided preform design in forging using the inverse die contact tracking method, International Journal of Machine Tools & Manufacturing, 36 (7), 1996, 755-769.
- [3] A. N. Bramley, Upper bound elemental technique (ubet) and ubet in 3d and tetrahedral upper bound analysis (teuba) fast method for forging simulation and preform design, Journal of Materials Processing Technology, 116, 2001, 80-83.
- [4] F. R. Biglari, N. P. O. Dowd and R. T. Fenner, Optimum design of forging dies using fuzzy logic in conjunction with the backward deformation method, Int. J. Mach. Tool Manuf. 38, 1998.
- [5] L. Yiguo and S. Sheng, Reverse Simulation using the Simulation Block Technique and its Application in the Precision Forging Process, Journal of Material Processing Technology, 63, 1997.
- [6] B. S. Kang, J. H. Lee, B. M. Kim and J. C. Choi, Process Design in Flashless Forging of Rib-Web Shaped Plane Strain Components by the Finite Element Method, Journal of Material Processing Technology, 47 1995.
- [7] C. S. Han, R.V. Grandhi and R. Srinivasan, Optimum Design of Forging Die Shape using Nonlinear Finite Element Analysis, AIAAJournal, 31, 1993.
- [8] A.N. Bruchanov and A.V. Rebelski, Closed die forging and warm forging (Verlag Technik 1995).
- [9] A. Thomas, Forging handbook, die design (Drop forging research association limited, Sheffield 1981).
- [10] Vieregge, K., Contribution to flash design in closed die forging, doctoral dissertation, Technical university of Hanover 1969.
- [11] F. Neuberger and S. Pannasch, Material Consumption in Die Forging of Steel (Fertigungstechnik und Betrieb 1962).
- [12] G.P. Teterin and I.J. Tarnovskij, Calculation of Plastic Dimensions in Forging Axisymmetric Parts in hammers (Kuznechno- Stampovochnoe proizvodstv 1968).
- [13] R.K. Roy, A primer on the taguchi method (Van Nostrand Reinhold, New York 1990).
- [14] G.D. Satish, N.K. Singh and R.K. Ohdar, Preform optimization of pad section of front axle beam using DEFORM, Journal of materials processing technology, 203, 2007, 102-106.
- [15] S.I. Oh, W.T. Wu, J.P. Tang and Vedharayagam, A Capabilities and applications of FEM code DEFORM, The Perspective of the developer, Journal of Material Processing Technology, 27, 1991, 25-42.

Idol Immersion Activities Cause Heavy Metal Contamination in River Budhabalanga, Balasore, Odisha, India

Kausik Kumar Das¹, Tanuja Panigrahi,² Dr. R.B.Panda³

¹Research Scholar P.G. Dept. Of Environmental Science, F.M. University, Balasore.

²Associate Professor in P.G. Dept. Of Environmental Science, F.M. University, Balasore.

ABSTRACT: Balasore town in the state Odisha, India is situated in the bank of river Budhabalanga. The impact of idol immersion on water quality of Budhabalanga River is discussed, for this purpose Balighat point was selected as sampling station because huge number of idol like Ganesh idol, Durga idol, Viswakarma idol etc. are immersed on this Ghat of Budhabalanga River. Water samples were collected at morning hours during pre immersion, during immersion and post immersion in the periods of idol immersions. The immersion of idol of Lord Ganesh, Lord Viswakarma and Goddess Durga during month of August to October is a major source of contamination and sedimentation to the River Budhabalanga. The idol are been made up of clay, plaster of paris, cloth, paper wood, thermocol, jute, adhesive materials and synthetic paints etc. Out of the all material used in making the idol, thermocol is Non-biodegradable while paints contain heavy metals such as Chromium, Lead, Cadmium and Mercury. The present study was under taken to evaluate heavy metals. The findings of the increase heavy metal concentration after immersion may magnify in their concentrations at different tropic levels by food chain. On the basis of these changes it is concluded that the level of water pollution increases in Budhabalanga River due to these religious activities and cause adverse effect to the aquatic life or entire aquatic ecosystem. No one can change or stop these religious activities but awareness among the people and society can reduce the pollution.

Keywords: Budhabalanga River, Heavy metals, Religious activities, water quality, water pollution.

I. INTRODUCTION

“WATER” the elixir of life referred as nature, was worshiped since Vedic days. The Rig-Veda depicts that water functions as givers and sustainers of life. So, water is also called as “GOLDEN LIQUID”. But Now-A-Days water pollution is a major global problem. It occurs when pollutants are discharged directly or indirectly into water bodies without adequate treatment to remove harmful compound. Water pollution occurs due to the discharge of municipal sewage both domestic and industrial without any treatment which brings considerable changes in the river water quality in addition to many religious activities now became a threat to the ecosystem [1, 2]. The idols of Lord Viswakarma, Lord Ganesh, Goddess Durga etc. worshipped by Hindu are immersed in the month of August to October respectively every year. Similarly during the Moorum festival, tazias are being immersed by Muslims in the month of May every year [3]. The idol are been made up of clay, plaster of paris, cloth, paper wood, thermocol, jute, adhesive materials and synthetic paints etc. Out of the all

Material used in making the idol, thermocol is Non-biodegradable while paints contain

Heavy metals such as Chromium, Lead, Cadmium and Mercury. The chemical paints used to decorate the idols increases heavy metal concentration and acidity in the water [4]. Lead and Chromium, which also adds through SINDUR in the water bodies, are very toxic even in very small quantity for human being through the process known as Bioaccumulation and Biomagnifications [5]. When immersed, these colours and chemical dissolve slowly leading to significant alternation in the water quality [6].

Balasore is situated on the bank of Budhabalanga River that plays important and major role in its economic and social growth and development. Budhabalanga River is a river of Eastern India and North east Odisha with a length around 175 km. It originates from the Similipal Hill, Mayurbhanj district, Odisha and has a total catchment area of 4840 square kilometres. Its major tributaries are the Sono River, the Gangahar River and the Catra River. The flow of Budhabalanga covers Fuladi, Remuna, Balasore in Odisha and empty into the Bay of Bengal at Balighat. The confluence point of river Budhabalanga with Bay of Bengal is very near to the sampling station Balighat, when due to back water of sea the flow of water is almost nil. Therefore after emersion of idol the pollutant accumulated in the sampling site due to still water current of the river.

In India, a lot of religious activities take place all around the year. Most of the Temples and ritual places are located near the aquatic resources like pond, lakes, river etc. The people of Balasore are always excited for celebration of festivals. Ganesh Chaturthi and Durga puja are of the important festivals of them. In this festivals number of Ganesh and Durga idols in different sizes are immersed in Budhabalanga River. About 500 or more Ganesh idols and about 150 Durga idols were immersed during 2011 in Balighat immersion point. Ganesh idol increases pollution in Hussainsagar Lake, Hyderabad was observed [7]. Malik et al, 2010 reported deterioration in water quality of rivers due to idols immersion in South Gujarat. The floating materials released through idol in the river and lake after decomposition result in eutrophication of the river, lake etc [8]. The idol immersion is a religious activity which is responsible for adding pollution load in the water bodies.

The reservoir can serve as a model for studying heavy metal contamination through idol immersion.



Fig-1 Photo of Goddess Durga

II. MATERIAL AND METHODS

The water samples was collected from surface layer during morning hours from Balighat idol immersion point and the site of idol immersion at different intervals i.e. pre immersion, during immersion and post immersion in the period of period of Ganesh chaturthi, Viswakarma puja and Durga puja in month of August to October respectively. Pre idol immersion samples were collected a week before the commencement of the immersion activities. During idol immersion samples were collected during the immersion activities. Post idol immersion samples were collected ten day after the completion of immersion activities. The water samples collected for the heavy metals analysis like chromium and lead were analyzed according to standard methods prescribed in [9, 10]. The heavy metals were preserved by adding 5 ml of 1N HNO₃ and bringing down the pH to near about 4 and analyzed using AAS (Perkin Elmer A Analyst 100).



Fig-2 Lord Ganesh Bisarjan

III. RESULT AND DISSCUSSION

The results of this research work have been shown in table 1 and figure1. These data revealed that the water of River Budhabalanga is deteriorated due to the immersion of different idols. The concentration of calcium has increased significantly in the river water after the idol immersion and became came to normal after one to two month of the idol immersion; however it was below the limits of permissible limits. Magnesium, Chromium, Cadmium, Lead and Arsenic concentration has also increased significantly in the river water ten days after the idol immersion [11].

Magnesium is non-poisons, though it increases the hardness of water. Over the year the concentration of heavy metals, especially manganese, lead and mercury has also increased considerably in the river water compared to the specifications of highest desirable limits as set by BIS and ICMR [12]. The concentration of cadmium, mercury and lead, the potentially obnoxious heavy metals had increased many folds in the water due to idol immersion compared to highest desirable limits of BIS and ICMR standard. The heavy metal especially manganese, lead and mercury excess in water cause skin diseases [7]. The chromium concentration in the river water did not change much and was below the limits of standards. After the immersion of the idols, its concentration increased further and after about 45 days of immersion its concentration slightly decreases still it higher than before idol immersion. The heavy metals are known to be persistent and gradually accumulate and magnify through the process known as bioaccumulation and

biomagnifications, while they move up in the food chain [1]. Thus load Cadmium and Mercury may magnify in their concentrations at different tropic levels in the river ecosystem and finally reach the humans through food chain.

Organic compounds of Mercury, for example Methyl Mercury when it enters the human body, concentrates in the brain and destroy the brain cells, damaging the central nervous system and also cause Ulceration of the digestive facts [13]. Therefore, it is suggested that the authorities looking into the environmental protection of the river need to take necessary steps.

Fig-3 Concentration of Ca & Mg before, during, after 10days and after 45days of immersion in comparison to the BIS & ICMR standards.

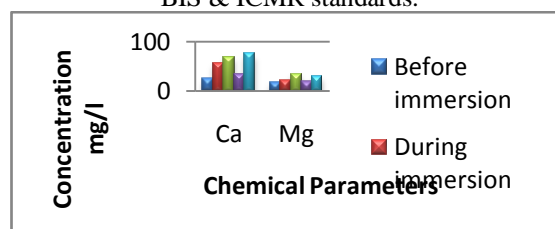


Fig-4 Concentration of Cd, Cr & Hg before, during, after 10days and after 45days of immersion in comparison to the BIS & ICMR standards

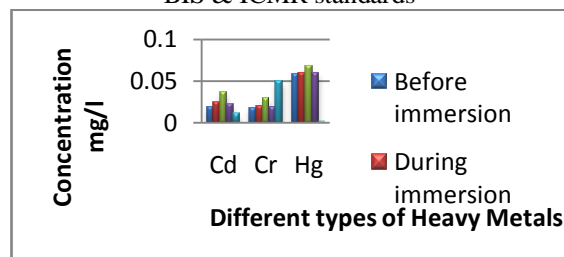
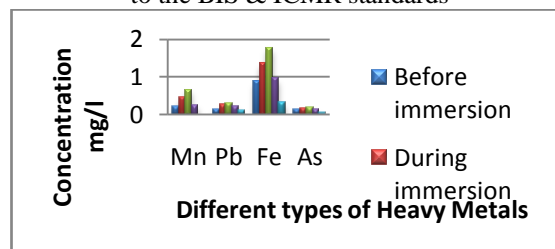


Fig-5 Concentration of Mn, Pb, Fe & As before, during, after 10days and after 45days of immersion in comparison to the BIS & ICMR standards



IV. CONCLUSION

From the mythological point of view, the water bodies are related to religious sentiments but from the scientific point of view, these water bodies like ponds, rivers and lakes are not suitable for human uses. The main cause of change in water quality in River Budhabalanga is various religious activities. The idol immersion like Lord Ganesh idol, Goddess Durga idol and Lord Viswakarma idol plays an important role because the plaster of paris, clothes, iron rods, chemical colours, varnish and paints used for making the idols deteriorate water quality of river Budhabalanga. No one can stop these religious activities but awareness among the problem.



Fig-6 Idol Immersion activities kill aquatic fauna

V. SUGGESTION

To make the idol an environmental friendly we should follow the following points

Table-1. Change in concentration (mg/l) of some chemical pollutants in Balighat Immersion Point of Budhabalanga River before immersion, during immersion and after immersion of idols in month of August 2011 to October 2011

Heavy Metals	Before immersion	During immersion	Immersion after 10days	Immersion after 45days	Standard as per BIS & ICMR
Ca	24.05	56.11	68.16	35.27	75
Mg	17.56	21.70	35.18	19.71	30
Cd	0.019	0.024	0.036	0.022	0.01
Cr	0.018	0.020	0.029	0.019	0.05
Hg	0.058	0.0592	0.067	0.059	0.001
Mn	0.2	0.44	0.65	0.23	-
Pb	0.13	0.25	0.291	0.205	0.1
Fe	0.87	1.35	1.75	0.94	0.3
As	0.124	0.169	0.173	0.134	-

REFERENCE

- [1] Bajpai, A., Pani, S., Jain, R.K. and Mishra, S.M. (2003) Heavy metal concentration through idol immersion in a tropical lake, *Eco. Env. And Cons.*, 8(2):157-159.
- [2] Ujjain, N.C. and Azhar, A.M. (2011) Impact of Ganesh Idol Immersion Activities on the Water Quality of Tapi River, Surat (Gujarat) India, *Research Journal of Biology*, Vol.01, Issue.01, pp. 11-15.
- [3] Mukerjee, A., (2003) Religious Activities and Management of Water Bodies. Case study of idol immersion in context of Urban lakes Management, *International Water History Association* (3) 325.
- [4] Vyas, A., Bajpai, A., Verma, N. and Dixit, S. (2007) Heavy Metal Contamination Causes of Idol Immersion Activities in Urban Lake, Bhopal, India, *J. Appl. Sci. Environ. Manage*, Vol.11 (4) 37-39.
- [5] Bibicz, M., (1982) Heavy metal in the aquatic environment of some water bodies of the Lublin basin *Actuatic Hydrobiology.*, 24, 125-138.
- [6] Dhote, S., Varghese, B., Mishra, S.M., (2001) Impact of idol immersion on water quality of Twin Lakes of Bhopal, *Indian Journal Environmental Protection*. Vol.21, 998-1005.
- [7] Reddy, V.M. and Kumar, V.A. (2001) Effect of Ganesh Idol Immersion on some water quality parameters of Hussain Sagar, *Current DScience*, Vol.18:1412.
- [8] Leland, H.V. (1991) Transport and distribution of trace elements in a watershed ecosystem in environment. Boggess, W.R., and Wixson, B.G. Eds. Castle House Publication, pp. 105-134.
- [9] APHA (1995), Standard methods for examination of water and waste water, American Public Health Association, Washington, D.C., 19th Edition.
- [10] Trivedy, P.K., Goel, R.K. (1986) Chemical and Biological methods water pollution studies. Karad, India, Environmental Publication.
- [11] Kulshrestha, S.K., George, M.P., and Khan, A.A. (1988) Preliminary Studies on the impact of certain religious activities on water quality of Upper Lake, Bhopal, *National. Symp. Past present and future of Bhopal lakes*, 253-257.
- [12] ICMR, (1975) Manual of standards of quality for drinking water supplies, Special report series No.44, 2nd Edition.
- [13] Bowen, H.J.M., (1966) Trace Element in Biochemical (New York: Academic Press Including)

- The idols should be made of traditional clay instead of baked clay.
- The paints of idols should be water soluble.
- Idols should be small as they would dissolve faster.
- Non-degradable chemical dyes are banned.
- Stress on natural colours used in food products.

VI. ACKNOWLEDGEMENT

The authors pay their deep sense of gratitude to the Vice-Chancellor of Fakir Mohan University. The authors also record their thanks to the person for kind co-operation in collecting the samples.

Image Denoising Using Non Linear Filter

Mr. Vijay R. Tripathi

Assistant Professor IN College of Engg & Technology, Akola-444004.

Abstract: Noise in an image is a serious problem. In this project, the various noise conditions are studied which are: Additive white Gaussian noise (AWGN), Bipolar fixed-valued impulse noise, also called salt and pepper noise (SPN), Random-valued impulse noise (RVIN), Mixed noise (MN). Digital images are often corrupted by impulse noise during the acquisition or transmission through communication channels the developed filters are meant for online and real-time applications. In this paper, the following activities are taken up to draw the results: Study of various impulse noise types and their effect on digital images; Study and implementation of various efficient nonlinear digital image filters available in the literature and their relative performance comparison;

I. Introduction

Today digital imaging is required in many applications e.g., object recognition, satellite imagery, biomedical instrumentation, digital entertainment media, internet etc. The quality of image degrades due to contamination of various types of noise. Noise corrupts the image during the process of acquisition, transmission, storage etc[1]. For a meaningful and useful processing such as image segmentation and object recognition, and to have very good visual display in applications like television, photo-phone, etc., the acquired image signal must be noise free and made deblurred. The noise suppression (filtering) and deblurring come under a common class of image processing tasks known as image restoration.

In common use the word noise means unwanted signal. In electronics noise can refer to the electronic signal corresponding to acoustic noise (in an audio system) or the electronic signal corresponding to the (visual) noise commonly seen as 'snow' on a degraded television or video image. In signal processing or computing it can be considered data without meaning; that is, data that is not being used to transmit a signal, but is simply produced as an unwanted by-product of other activities. In Information Theory, however, noise is still considered to be information. In a broader sense, film grain or even advertisements in web pages can be considered noise.

In early days, linear filters were the primary tools in signal and image processing. However; linear filters have poor performance in the presence of noise that is not additive as well as in systems where system nonlinearities or non-Gaussian statistics are encountered. Linear filters tend to blur edges, do not remove impulsive noise effectively, and do not perform well in the presence of signal dependent noise. To overcome these shortcomings, various types of nonlinear filters have been proposed in the literature.

II. Median Based Filters

In order to effectively remove impulse noise as described in while preserving image details, ideally the filtering should be applied only to the corrupted pixels, and

the noise-free pixels should be kept unchanged. This can be achieved by determining whether the current pixel is corrupted, prior to possibly replacing it with a new value. Decision-based filters correspond to a well-known class of filters that appear to be particularly efficient to reduced impulse noise. In this work, we propose an impulse detection scheme by successfully combining the SM filter with CWM filter.

PROGRESSIVE SWITCHING MEDIAN FILTER

A median-based filter, progressive switching median (PSM) filter, is implemented to restore images corrupted by salt-pepper impulse noise. The algorithm is developed by the following two main points: 1) switching scheme—an impulse detection algorithm is used before filtering, thus only a proportion of all the pixels will be filtered and 2) progressive methods—both the impulse detection and the noise filtering procedures are progressively applied through several iterations. The noise pixels processed in the current iteration are used to help the process of the other pixels in the subsequent iterations. A main advantage of such a method is that some impulse pixels located in the middle of large noise blotches can also be properly detected and filtered. Therefore, better restoration results are expected, especially for the cases where the images are highly corrupted.

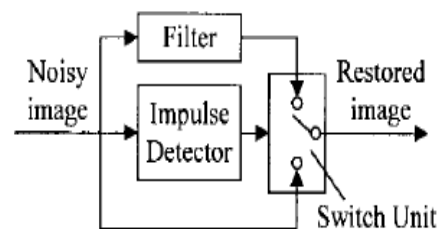


Fig. 1. A general framework of switching scheme-based image filters.

PSM Filter

1. Impulse Detection

Similar to other impulse detection algorithms, this impulse detector is implemented by prior information on natural images, i.e., a noise-free image should be locally smoothly varying, and is separated by edges [4]. The noise considered for this algorithm is only salt-pepper impulsive noise which means: 1) only a proportion of all the image pixels are corrupted while other pixels are noise-free and 2) a noise pixel takes either a very large value as a positive impulse or a very small value as a negative impulse. In this chapter, we use noise ratio $R(0 \leq R \leq 1)$ to represent how much an image is corrupted. For example, if an image is corrupted by $R = 30\%$ impulse noise, then 15% of the

pixels in the image are corrupted by positive impulses and 15% of the pixels by negative impulses.

Two image sequences are generated during the impulse detection procedure. The first is a sequence of gray scale images, $\{x_{(i,j)}^{(0)}, x_{(i,j)}^{(1)}, x_{(i,j)}^{(2)}, \dots, x_{(i,j)}^{(n)} \dots\}$, where the initial image $x_{(i,j)}^{(0)}$ is noisy image itself, (i, j) is position of pixel in image, it can be $1 \leq i \leq M, 1 \leq j \leq N$ where M and N are the number of the pixel in horizontal and vertical direction respectively, and $x_{(i,j)}^{(n)}$ is image after n^{th} iteration.

The second is a binary flag image sequence, $\{f_{(i,j)}^{(0)}, f_{(i,j)}^{(1)}, f_{(i,j)}^{(2)}, \dots, f_{(i,j)}^{(n)} \dots\}$ where the binary flag $f_{(i,j)}^{(n)}$ is used to indicate whether the pixel at (i, j) in noisy image detected as noisy or noise-free after n^{th} iteration. If $f_{(i,j)}^{(n)} = 0$ means pixel at (i, j) has been found as noise-free after n^{th} iteration and if $f_{(i,j)}^{(n)} = 1$ means pixel at (i, j) has been found as noisy after n^{th} iteration. Before the first iteration, we assume that all the image pixels are good, i.e. $f_{(i,j)}^{(0)} = 0$ for all (i, j) .

In the n^{th} iteration ($n = 1, 2, 3, \dots$) for each pixel $x_{(i,j)}^{(n-1)}$ we first find out the median value of the samples in a $W_D \times W_D$ (W_D is an odd integer not smaller than 3) window centered about it. To represent the set of the pixels within a $W_D \times W_D$ window centered about $x_{(i,j)}^{(n-1)}$ is $x_{(i+k,j+l)}^{(n-1)}$ where $-W \leq k \leq W, -W \leq l \leq W, k \leq W, -W \leq l \leq W$ and $W \geq 1$, then we have median value of this window $m_{(i,j)}^{(n-1)}$ is

$$m_{(i,j)}^{(n-1)} = \text{median} (x_{(i+k,j+l)}^{(n-1)})$$

The difference between $m_{(i,j)}^{(n-1)}$ and $x_{(i,j)}^{(n-1)}$ provides us with a simple measurement to detect impulses

$$f_{(i,j)}^{(n)} = \begin{cases} f_{(i,j)}^{(n-1)}, & \text{if } |x_{(i,j)}^{(n-1)} - m_{(i,j)}^{(n-1)}| < T \\ 1, & \text{otherwise} \end{cases}$$

Where T is a predefined threshold value. Once a pixel (i, j) is detected as an impulse, the value of

$x_{(i,j)}^{(n)}$ is subsequently modified

$$x_{(i,j)}^{(n)} = \begin{cases} m_{(i,j)}^{(n-1)}, & \text{if } f_{(i,j)}^{(n)} \neq f_{(i,j)}^{(n-1)} \\ x_{(i,j)}^{(n-1)}, & \text{if } f_{(i,j)}^{(n)} = f_{(i,j)}^{(n-1)} \end{cases}$$

(4.3)

Suppose the impulse detection procedure is stopped after the N_D th iteration, then two output images- $x_{(i,j)}^{(N_D)}$ and $f_{(i,j)}^{(N_D)}$ are obtained, but only $f_{(i,j)}^{(N_D)}$ is useful for our noise filtering algorithm.

2. Noise Filtering

Like the impulse detection procedure, the noise filtering procedure also generates a gray scale image sequence, $\{y_{(i,j)}^{(0)}, y_{(i,j)}^{(1)}, y_{(i,j)}^{(2)}, \dots, y_{(i,j)}^{(n)} \dots\}$ and a binary

flag image sequence $\{g_{(i,j)}^{(0)}, g_{(i,j)}^{(1)}, \dots, g_{(i,j)}^{(n)} \dots\}$. In the gray scale image sequence, we still use $y_{(i,j)}^{(0)}$ to denote the pixel value at position (i, j) in the noisy image to be filtered and use $y_{(i,j)}^{(n)}$ to represent the pixel value at position (i, j) in the image after the n^{th} iteration. In a binary flag image $g_{(i,j)}^{(n)}$, the value $g_{(i,j)}^{(n)} = 0$ means the pixel (i, j) is good and $g_{(i,j)}^{(n)} = 1$ means it is an impulse that should be filtered. A difference between the impulse detection and noise-filtering procedures is that the initial flag image $g_{(i,j)}^{(0)}$ of the noise-filtering procedure is not a blank image, but the impulse detection result $f_{(i,j)}^{(N_D)}$, i.e., $g_{(i,j)}^{(0)} = f_{(i,j)}^{(N_D)}$.

In the n^{th} iteration ($n = 1; 2; \dots$), for each pixel $y_{(i,j)}^{(n-1)}$, we also first find its median value $m_{(i,j)}^{(n-1)}$ of a $W_F \times W_F$ (W_F is an odd integer and not smaller than 3) window centered about it. However, unlike that in the impulse detection procedure, the median value here is selected from only good pixels with $g_{(i,j)}^{(n-1)} = 0$ in the window.

Let M denote the number of all the pixels with $g_{(i,j)}^{(n-1)} = 0$ in the $W_F \times W_F$ window. If M is odd, then

$$m_{(i,j)}^{(n-1)} = \text{median}\{y_{(i,j)}^{(n-1)} | g_{(i,j)}^{(n-1)} = 0, (i, j) \in W_F \times W_F\}$$

The value of $y_{(i,j)}^{(n)}$ is modified only when the pixel (i, j) is an impulse and M is greater than 0:

$$y_{(i,j)}^{(n)} = \begin{cases} m_{(i,j)}^{(n-1)}, & \text{if } g_{(i,j)}^{(n-1)} = 1; M > 0 \\ y_{(i,j)}^{(n-1)}, & \text{else} \end{cases}$$

Once an impulse pixel is modified, it is considered as a good pixel in the subsequent iterations

$$g_{(i,j)}^{(n)} = \begin{cases} g_{(i,j)}^{(n-1)}, & \text{if } y_{(i,j)}^{(n)} = y_{(i,j)}^{(n-1)} \\ 0, & \text{if } y_{(i,j)}^{(n)} = m_{(i,j)}^{(n-1)} \end{cases}$$

The procedure stops after the N_F th iteration when all of the impulse pixels have been modified, i.e.,

$$\sum_{(i,j)} g_{(i,j)}^{N_F} = 0$$

Then we obtain the image $\{y_{(i,j)}^{(N_F)}\}$ which is our restored output image.

Table 1. WF(3 * 3) Median Filter, CWM Filter & PWM Filter

Noise	PSNR With Noise	PSNR After Filtering		
		Median Filter	CWM Filter	PWM Filter
10%	15	12	13.5	29
20%	12	12	13	27
30%	11	12	13	26
40%	9.5	12	13	24

The Experimental results are shown in Table.2 for WF (5 * 5) PWM Filter

Table 2. WF (5 * 5) PWM Filter

Noise	PSNR with Noisy	PSNR after Filtering
10	15	21
20	12	19
30	11	19
40	9.5	19

The Experimental results are shown in Table.3 for WF (7 * 7) PWM Filter

Table 3. WF (7 * 7) PWM Filter

Noise	PSNR with Noisy	PSNR after Filtering
10	15	14
20	12	7.3
30	11	6
40	9.5	5.9



(d)



(e)



(f)



(a)



(b)



(c)



(g)



(h)



(i)

Figure 2. a, b, c, d are noisy images of Lena (512×512) corrupted by salt and pepper noise with noise density of 10%, 20%, 30%, 40% respectively and corresponding restored image by PWM are in e, f, g, h for WF (3 * 3)

III. Conclusion

In this entire dissertation work, two different non-linear filters are implemented and extensive experiments are performed to obtain the results with various parameters to assess the performance of each filter. The plot of PSNR for these two filters is given below. The Table.1, 2 & 3 below shows the PSNR value obtain using Lena Image of size 512 x 512.

From the PSNR value mention in the simulation result it is very clear that PWM Filter shows better performance in suppressing impulsive noise compare to above mention filter in suppressing impulse noise when noise exceeds from 10 % to 40 %.

& Secondly extensive experimental result show that if we increase window size i.e. 5 * 5 & 7 * 7, we find that by increasing the window size image get more & more corrupted & filter is not able to suppress impulsive noise effectively compare to when window size in filter was (3 * 3) in filter. Though simulation time required is less, which is given in table below.

Filter Used	PSM
Window Size	Time In Sec
WF (3 * 3)	16sec
WF (5 * 5)	13sec
WF (7 * 7)	10sec

Table4: Average Run Time in Sec

Therefore from the above table it is very cleared that as window size increases image get more & more blurred & distorted though it requires less simulation time compare to that when window size in filter was (3 * 3). So mostly window size of WF (3 * 3) is preferred compare to that of WF (5 * 5) & WF (7 * 7).

Reference

- [1] R.C. Gonzalez and R.E. Woods Digital Image Processing Second Edition.
- [2] A. C. Bovik, T. S. Huang, and D. C. Munson, "A generalization of median filtering using Linear combinations of order statistics," IEEE Tran Acoust., Speech, Signal Process., vol. ASSP-31, no.6, pp.1342–1350, Dec. 1983.
- [3] J. Astola and P. Kuosmanen, Fundamental of Nonlinear Filtering, Boca Raton, CRC Press, 1997.
- [4] T. Sun and Y. Neuvo, "Detail-preserving median based filters in image processing," *Pattern Recognit. Lett.*, vol. 15, pp. 341–347, Apr. 1994
- [5] I. Pitas and A. N. Venetsanopoulos, Nonlinear Digital Filters: Principles and Applications, Boston, Kluwer, 1990.
- [6] B. I. Justus son, "Median filtering: Statistical properties," "Two-Dimensional Digital Signal Processing II, T. S. Huang Ed., New York; Springer Verlag, 1981.
- [7] S-J. KO and Y. H. Lee, "Center-weighted median filters and their applications to image enhancement," IEEE Trans. Circuits and Syst., vol. 38, pp. 984-993, Sept. 1991.
- [8] J.-H. Wang, "Rescanned minmax center-weighted filters for image restoration," Proc. Inst. Elect. Eng., vol. 146, no. 2, pp. 101–107, 1999.
- [9] "Tri-State Median Filter for Image Image Denoising", T. Chen, K-K. Ma, and L-H. Chen IEEE TRANSACTIONS ON IMAGE PROCESSING, VOL. 8, NO. 12, DECEMBER 1999.
- [10] T. Kasparis, N. S. Tzannes, and Q., "Detail-preserving adaptive conditional median filters," J. Electron. Imag, vol. 1, no. 14, pp. 358–364, 1992.

An Overview of Clearance Optimization in Sheet Metal Blanking Process

Prof. T. Z. Quazi,¹ R.S.Shaikh²

^{1,2}Department of Mechanical Engineering, Mumbai University, India

Abstract: This document prescribes a model investigation the effect of potential parameters influencing the blanking process and their interaction. The blanking process optimization carried out by using Design of Experiment (DOE), Finite Element Method (FEM) with ANSYS Package, Simulation with ABAQUS-Explicit software, Blank soft Software and Neural Network Simulation in order to achieve the intended model objectives.

Keywords: Blanking Process, DOE, FEM, Optimum Clearance and Simulation.

I. INTRODUCTION

There are thousands of products manufactured with sheet metal parts. The first step in forming such a part involves cutting of the sheet into appropriate shapes by means of the physical process of shearing. A contoured part is cut between a punch and die in a press. Recent international market demands are that mechanical parts should be produced to net-shape or near net-shape with improved mechanical properties, a smooth surface finish, good dimensional accuracy and material savings, depending on service conditions. In practice, manufacturing engineers are faced with the problem of determining the proper design of dies to cut metal sheets without causing any surface or internal defects at a lower manufacturing cost, depending on the material, the part geometry, and the process.

1.1 The Blanking Process

Blanking is a manufacturing operation as old as the technology itself. Its applications range from components of very light to heavy appliances and machineries [1]. Blanking is defined as the cutting of a work piece between two die components to a predetermined contour [2]. During blanking, the part is subjected to complex solicitations such as deformation, hardening and crack initiation and propagation. The theoretical modeling of such processes is very difficult due to the complexity in describing the different stages of the whole shearing process starting with the elastic stage and ending with the total separation of the sheet metal [3].

The behavior of the blank material during the blanking process can be divided into five stages. During the start of the process, the sheet is pushed into the die and the blank material is deformed, first elastically. The process continues and the yield strength of the blank material is reached, first at the outer fibers and later at all the fibers in the zone between the punch and the die. Normally, the material underneath the punch is subjected to thinning. The plastic deformation causes rounding of the edge of the blank. During this stage, or possibly as early as during the plastic deformation stage, damage initiation followed by the nucleation and growth of cracks takes places. In most of the conventional blanking situations, ductile fracture occurs after shear deformation. This causes rough, dimpled rupture morphology on the fractured surface of the product. Finally, the work due to friction is dissipated when forcing (pushing) the slug through the die hole [4].

II. Literature Review

The process of identifying process influencing parameters of blanking process includes an exhaustive literature review of the factors that have been suggested by various authors. Literature review was performed by collecting articles from various journals, and various popular research related sites viz. Science Direct, IEEE, Emerald, Springer Link and various free articles from internet. Literature from journal papers and conference studied for various press tool works parameters optimization are reviewed.

S. K. Maiti, A. A. Ambekar, U. P. Singh, P.P. Date, K. Narasimhan, [1], they evaluate the influence of tool clearance, friction, sheet thickness, punch/die size and blanking layout on the sheet deformation for thin M. S. sheet. The punch load variation with tool travel and stress distribution in the sheet has been obtained. The results indicate that a reduction in the tool clearance increases the blanking load. The blanking load increases with an increase in the coefficient of friction. These observations are very similar to the case of blanking of component of large size. Further, these effects are very similar in the case of both single and double blanking. An inter blanking site distance of about twice the sheet thickness is good to reduce the thinning of sheet at the intermediate regions between the two blanking sites.

Ridha Hambli [3], presents industrial software called BLANKSOFT dedicated to sheet metal blanking processes optimization. The code allows for the prediction of the geometry of the sheared profile, the mechanical state of the sheared zone, the burr height, the force-penetration curve, and the wear evolution of the punch versus the number of the blanking cycles. The approach is based on an original theoretical investigation formulated from plasticity theories. This program is designed by considering several factors, such as material and geometry of product as well as the wear state of the tool. The numerical results obtained by the proposed programs were compared with experimental ones to verify the validity of the proposed software.

R. Hambli [5], presents an experimental investigation into the blanking process was carried out using tools with four different wear states (wear radius 0.01, 0.06, 0.012, 0.2 mm) and four different clearances (5%, 10%, 15%, 20%). The aim was to study the effects of the interaction between the clearance, the wear state of the tool and the sheet metal thickness on the evolution of the blanking force and the geometry of the sheared profile. He used designed of experiment method for

model and analysis the relationships that describe process variations. This investigation shows that, in order to minimize the blanking force, the clearance should be set at 10%, however, to minimize the fracture angle and the fracture depth, it is preferable to set the clearance at 5%. When the clearance is set at 10%, the process is slightly more robust to tool wear, as far as the blanking force response is concerned. Whether clearance should be set at 5% or 10% ultimately depends on the priorities of the practitioners.

F. Faura, A. Garcia, M. Estrems [6], they proposed a methodology to obtain optimum punch-die clearance values for a given sheet material and thickness to be blanked, using the finite-element technique. To determine the optimum clearance, the diagonal angle and the angle of the direction of crack propagation for different clearances were calculated. The influence of clearance on diagonal angle and angle of the direction of crack propagation, from which it is seen that as the clearance increases, diagonal angle increases proportionally while angle of the direction of crack propagation remains nearly constant. At the point of intersection, the direction of crack propagation coincides with the diagonal line, and so the cracks emanating from the punch and die meet, resulting in a cleanly blanked surface. Hence, this value of clearance is taken as the optimum clearance. The optimum clearance for the values of the parameters used in this work is between 11 and 12%. It is observed that punch penetration increases as the c/t ratio increases.

R. Hambli, S. Richir, P. Crubleau, B. Taravel [7] elaborates blanking process and structures of the blanked surfaces are influenced by both the tooling (clearance and tool geometry) and properties of the work piece material (blank thickness, mechanical properties, microstructure, etc.). Therefore, for a given material, the clearance and tool geometry are the most important parameters. They use simulation of an ax symmetric blanking operation with ABAQUS- explicit software for a given sheet material. A damage model of the Lemaitre type is used in order to describe crack initiation and propagation into the sheet. They use four materials for testing with four different elongation (30%, 47%, 58%, and 65%). They show that the optimum clearance decreases as the material elongation increases. The results of the proposed experimental investigation show that there is no universal optimal clearance value. Whether clearance should be set at 5% or 10% ultimately depends on the priorities of the practitioners.

Emad Al-Momani, Ibrahim Rawabdeh [8], Represents a model investigates the effect of potential parameters influencing the blanking process and their interactions. Finite Element Method (FEM) and Design of Experiments (DOE) approach are used in order to achieve the intended model objectives. They use Design of Experiments (DOE) technique by selecting the experimental levels for each selected factor, i.e. the clearance to be in five levels (5, 10, 15, 20, 25) % of the sheet metal thickness, blank holder force to be in two levels (0, 3000N) and sheet metal thickness to be in four levels (0.5, 0.6, 0.7, 0.8)mm. Perform a factorial experimental design in order to take high-level interactions. Develop a Finite Element Model (FEM) that represents the existing process in order to evaluate the quality of the inputs. Compare the two techniques (FEM and DOE) and analyze the results to get the proposed optimal set of parameters. Simulations are conducted on commercial FEM software package ABAQUS/Explicit. in their article , they show that, in order to minimize the burrs height, the clearance should be set at about 5 % with almost no blank holder force.

Ridha Hambli [9], describes a methodology using the finite element method and neural network simulation in order to predict the optimum punch-die clearance during sheet metal blanking processes. A damage model is used in order to describe crack initiation and propagation into the sheet. The proposed approach combines predictive finite element and neural network modeling of the leading blanking parameters.

Gang Fang*, Pan Zeng, Lulian Lou [10], in this paper, the punch-die clearance values for a given sheet material and thickness are optimized, using the finite element technique and Cockcroft and Latham fracture criterion. In the study, the shearing mechanism was studied by simulating the blanking operation of an aluminum alloy 2024. The results of the present paper agree with the previous experimental results.

III. FUNDAMENTALS OF THE THEORETICAL MODEL

The errors on blanks are influenced by material, the tool shape, process variations and the machine. The form errors represented in "Fig. (1)" are connected to the geometry of the sheared edge such as the roll-over depth, the fracture depth, the smooth-sheared depth, the burr formation and the fracture angle.

Various experimental studies [17–23] showed that the mechanical and geometrical aspect of the sheared edge during the blanking operation for a given material are affected by some parameters like the blanking clearance, the wear state of the tool and the thickness of the sheet.

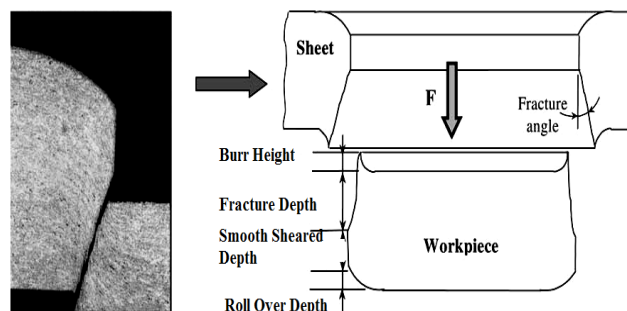


Figure. (1).Geometry of the sheared work piece

3.1. Deformation and rupture mechanism

During sheet metal shearing operation, the part is subjected to complex solicitations such as deformation, hardening and crack initiation and propagation. The theoretical modeling of such processes is very difficult due to the complexity of describing the different stages of the whole shearing process starting from the elastic stage and ending to the total separation of the sheet metal" Fig (2)".

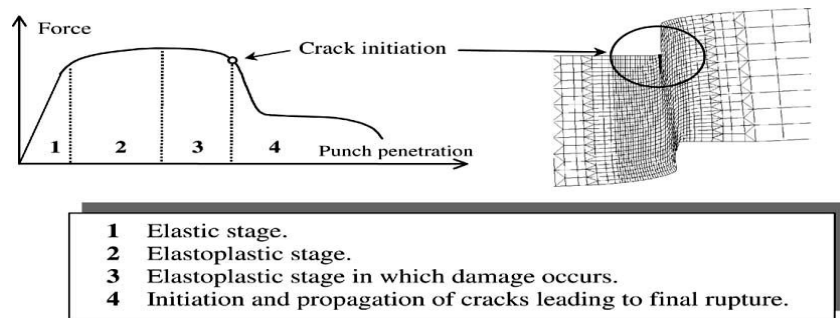


Figure. (2). Different stage of the blanking process.

Accurate knowledge of the failure process is essential for the selection of a suitable damage model. In the case of sheet blanking by shearing processes, numerous authors have studied the different physical mechanisms leading to the final rupture, and proposed their own models.

In their investigation dealing with a planar blanking process, Stegeman et al. [12] used a CCD camera records in order to quantify the displacement of material points at the sheared surface "Fig.(3)". One can observe the grid deformation in the

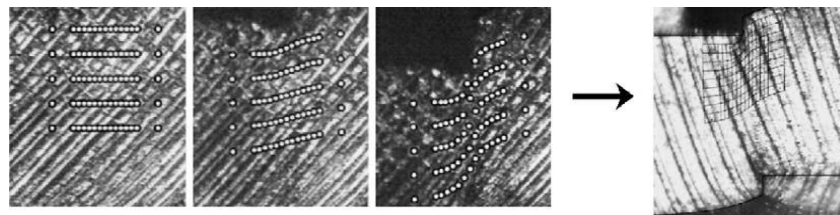


Figure. (3). Grid deformation of material points during blanking process.

Clearance zone of the tool. Recently, an analytical study and experimental tests [20, 21] showed that the physical mechanisms leading to the complete failure of the sheet material can be described as follows.

First, due to the penetration of the punch into the sheet, cracks initiate at the cutting edges 'A' and 'B' of the tools "Fig.(4)". Secondly, the cracks propagate when and where Rice & Tracey fracture criterion value exceeds a critical value, and thus progressively cut the material fibers one after the other.

The aforementioned rupture mechanism has been applied with success in a previous work [11] to numerically simulate the whole blanking process until the final separation of the sheet. In this investigation, the mechanism model based on the material cutting fibers has been applied to describe the deformation mechanism of the sheet metal during the shearing process. The main idea is to update incrementally the deformation mechanism in the clearance zone of the part for a given punch penetration increment. The equilibrium state of the part is then described using the concept of the continuum mechanics theory.

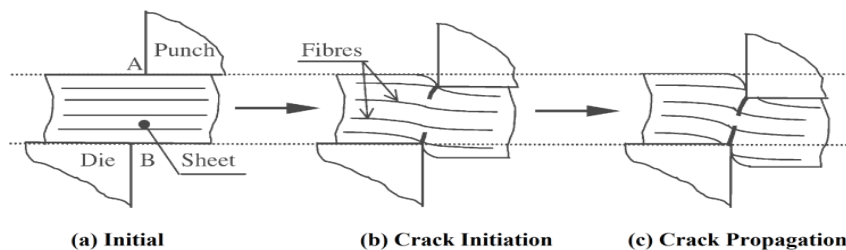


Figure. (4). Rupture of the sheet.

A set of formulae taking into account the material characteristics of the sheet, the geometry of the operation and the wear state of the tool has been developed allowing for the prediction of the characteristic zone heights of the blanked part such the heights of the burr the roll-over, the sheared and the fractured zones. The punch penetration curve can also be plotted which allows for the computation of the maximum blanking force and the blanking energy. The equivalent plastic strain and equivalent stress of the sheared zone can be also predicted which permits the computation of the hardening state of the sheared zone.

IV. OPTIMUM CLEARANCE

Various experimental studies [15,16,22,23,24,25,26] showed that the mechanical and geometrical aspect of the sheared edge during the blanking operation for a given material are affected by some parameters such as the blanking clearance, the wear state of the tool, and the thickness of the sheet. In blanking processes, the clearance is expressed in percentage of the sheet thickness and is defined by:

$$c = \frac{100(D_m - D_p)}{2t} \%$$

Where D_m , D_p and t are the die diameter, the punch diameter and the sheet thickness, respectively.

In the case of blanking processes, one seeks to generate cracks at the sharp edges of the punch and the die, then, through the choice of the parameters of cutting, attempt to make this crack propagate as soon as possible to obtain total rupture.

In this investigation, it is assumed that the clearance is optimum when the direction of crack propagation coincides with the line joining the points of crack initiation (A and B of "Fig.(5)" in the punch and die, giving cleanly blanked surfaces without secondary crack formation "Fig.(5)". In this case, the total separation of the sheet is obtained for a lower value of punch penetration. If the cracks generated by the punch and die (A and B of "Fig.(5b)" do not coincide, the formation of secondary cracks exists.

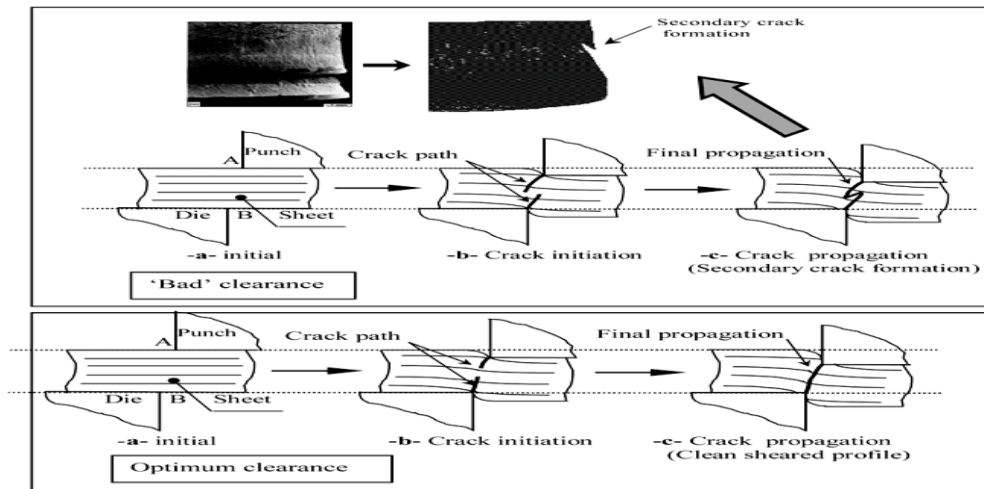


Figure. (5). Secondary crack formation during blanking process.

In order to obtain the optimum clearance value, the angle (θ) of the line joining the points of crack initiation in the punch and die (diagonal angle) and the angle (β) of the direction of crack propagation must coincide "Fig.(6)". This can be expressed by:

$$\theta = \beta$$

The diagonal angle can be expressed by:

$$\theta = \text{Arc tan}(c / t - u_p)$$

Where u_p is the punch penetration corresponding to the First crack initiation within the sheet.

4.1. Optimum Clearance Algorithm

The optimum clearance value can be obtained by performing a series of numerical analyses in order to pursue a minimum cost function between the angle of the line joining the points of crack initiation in the punch and die θ_d (diagonal angle) and the angle of the direction of crack propagation (DCP) β "Figure (6)".

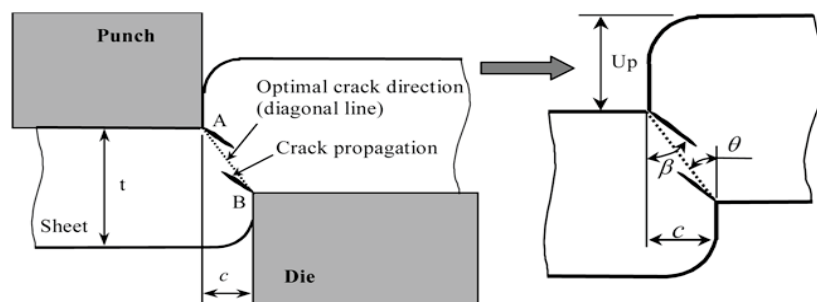


Figure. (6) Crack propagation angle and diagonal angle.

During the optimization process a multi-variable objective function was chosen in the following form:

$$\Phi = \beta^n - \theta_d^n$$

β^n is the direction of crack propagation angle at increment and θ_d^n is the diagonal angle at increment n .

The optimum clearance value can be obtained by performing a series of numerical analyses in order to pursue a minimum cost function between the angles θ_d and β .

The global criteria of convergence are such that the numerical results must satisfy the following conditions:

$$\frac{\text{Abs}(\beta^n - \theta_d^n)}{\theta_d^n} \leq \text{Tol}$$

Tol. Is tolerance convergence value given by the user?

Different simulations using different values of tolerance parameter showed that the final results are not sensitive to the selection of *Tol*.

In this investigation, *Tol.* is taken equal to 10E-05.

The iterative finite element program including the algorithm of the clearance optimization is schematically represented by the following flow chart of “Figure (7)”.

Incremental displacements are applied to the punch. At each increment, a fracture test is applied to each finite element of the mesh. When the damage reaches its critical value at fracture D_c , the programs compute the angles β^n and θ_d^n .

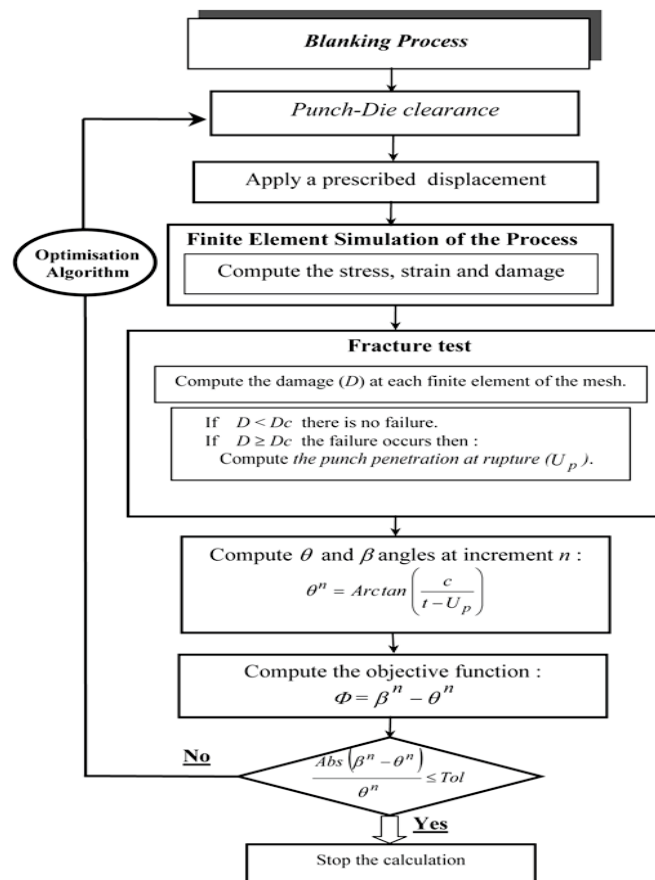


Figure. (7). Flow chart of calculation.

V. FINITE ELEMENT METHOD (FEM) AND DESIGN OF EXPERIMENTS (DOE)

Numerical methods provide a general tool to analyze arbitrary geometries and loading conditions. Among the numerical methods, Finite Element Analysis (FEA) has been extensively used with success; however, this kind of analysis requires the generation of a large set of data in order to obtain reasonably accurate results and consumes large investment in engineering time and computer resources [27]. FEM is a good choice for the analysis of sheet metal processes since it helps in eliminating the need for time-consuming experiments to optimize the process parameters [1]. The FEM simulations are increasingly used for investigating and optimizing the blanking processes. Many time-consuming experiments can be replaced by computer simulations. Therefore, highly accurate results of sheet metal forming may be obtained by using the FEM simulation [28]. The finite element method gives an approximate solution with an accuracy that depends mainly on the type of element and the fineness of the finite element mesh.

In the manufacturing area, Design of Experiments (DOE) is found to be an efficient statistical technique that can be used for various experimental investigations. The design of experiments is one of the powerful tools used to investigate deeply hidden causes of process variation [29]. It is a systematic, rigorous approach to engineering problem solving that applies principles and techniques at the data collection stage to ensure the generation of valid, defensible, and supportable conclusions. In the blanking process, experimental design is considered a powerful approach for product and process

development, and for improving the yield and stability of an ongoing process. Hambli *et al.*, [30] found that the design of experiments technique is an efficient and cost-effective way to model and analyze the relationships that describe process variations.

The sheet metal industry is highly interested in knowing if two identical products manufactured of two different materials, can be blanked with a reasonable quality without the need to build two separate setups. This will increase the efficiency of the production processes and reduce the level of wasted materials, time, cost, and effort involved in the production stages. In addition, the industry needs a suitable model to overcome the long cycle time in developing a particular blanking process. This can be achieved by combining the Finite Element Method and Design of Experiments techniques aiming at identifying opportunities to increase efficiency and productivity as well as eliminating waste and reducing production cost associated with the blanking process. The main objective of this paper is to construct a finite element model to predict the shape of the cut side of a blanked product, and to investigate the effect of potential parameters influencing the blanking process and their interactions using the design of experiments approach in order to choose the process leading parameters in an optimal way.

VI. SIMULATION OF THE PROCESS

6.1. FEM package

The FEM program used to simulate the blanking process is ANSYS v. 5.1 [31], which is capable of solving the non-linearity's of material behavior, large deformations, and contact between surfaces of different bodies.

For the simulation described here, which is merely to determine the stress and strain of each node during the process, the use of specific codes devoted to simulating metal forming processes is not necessary.

6.2. Model geometry

The following assumptions are made for the purposes of the present analysis:

- The process is simplified to a two-dimensional situation, under plane-strain conditions, since in a normal blanking operation the punch-die clearance is usually very small in relation to the blank diameter.
- The process is considered quasi-static, and hence the effects of strain rate are neglected.
- The sheet material is considered as a plastic object while the punch and die are defined as rigid bodies. Table I: summaries the geometric values used in the simulations.

The tool wear geometry has been simulated by rounding off of the cutting edge (P-D radius). The friction contact between sheet and tool follows Coulomb's law:

$$T_f = \mu s_n$$

Where T_f is friction shear stress, s_n is normal stress at interface, and μ is the friction coefficient.

"Fig. (8)". Shows the finite element model. The increasing deformation in the simulation shows that the regions beyond a distance t from the shear zone undergo very much smaller deformation than that in the clearance zone. Moreover, the strains at the punch-die cutting edges reach the crack initiation value well before any significant deformation can take place in the region beyond t . Thus, the blanking operation is modeled by two rigid blocks, which are separated by a distance c and which move in opposite directions.

Parameter	Value	Dimension
Shearing gap	$c = (D-d)/2$	M
Clearance	$Cl = [(D-d)/2t] \times 100$	%
P-D radius	$r = 10^{-4}$	M
Friction coefficient	$\mu = 0.05$	

Table I: Geometric parameter settings

D and d are punch and die diameters;
 t is thickness.

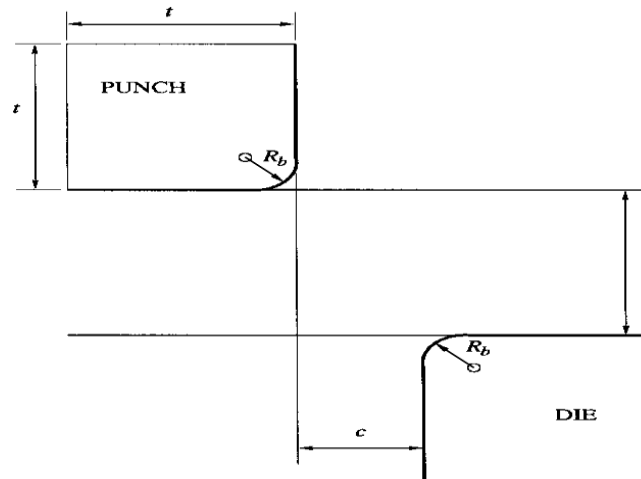


Figure. (8). Simulation model.

In the blanking operation, deformation is concentrated along the very narrow shear band. The width of the shear band is a few microns. Thus, the number of elements used is critical for every simulation since a large number of elements increases the accuracy of the result, but also substantially increases the calculation time. Therefore, a very dense mesh was defined in the shearing band and relatively large elements for the remainder. It should also be mentioned that the CPU-time for one simulation was about 10 h on an IBM RISC 6000 work station.

VII. CASE STUDY

Design of Experiment Based Analysis for Sheet Metal Blanking Processes Optimization

R. Hambli

ISTIA – LASQUO, Angers, France

7.1 Material model

In the present investigation, the optimum clearance was studied by simulating blanking of an AISI 304 sheet with the specifications as in Table:2.

It is assumed that the material is isotropic and that its yielding point follows the von Mises yield criterion. A bilinear representation of the stress-strain curve is used to model the behavior of the material, which is defined by two slopes: the elastic and the plastic slope.

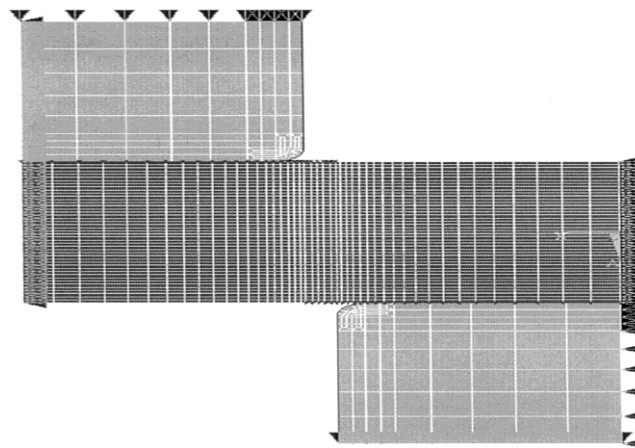


Figure. (9). Mesh in the shearing zone.

7.2 Ductile fracture criterion (crack initiation criterion)

Many experimental studies have been conducted to establish ductile fracture criteria in order to calculate the formability limits of different materials. Among the various fracture criteria proposed, it has been found that the criterion suggested by Cockcroft and Latham [10] predicts the most reasonable fracture strain in metal forming operations. This criterion states that fracture takes place when the following relation is satisfied:

$$\int_0^{\varepsilon^f} \left(\frac{\sigma^*}{\bar{\sigma}} \right) d\bar{\varepsilon} = C$$

Where σ^* is the maximum principal tensile stress, ε^f the fracture strain, and C the material constant. The effective stress and effective strain are represented by $\bar{\sigma}$ and $\bar{\varepsilon}$, respectively. In the shearing operation, deformation is concentrated along the shear band the stress ratio ($\sigma^*/\bar{\sigma}$) is not expected to change along the shear band.

Parameter	Value	Dimension
Thickness	$t=10^{-3}$	M
Yield Stress	$\sigma_y=2.45 \cdot 10^8$	Pa
Elastic modules	$E=1.225 \cdot 10^{11}$	Pa
Tangent plastic slope	$E_t=1.586 \cdot 10^9$	Pa

Table II: Material specifications

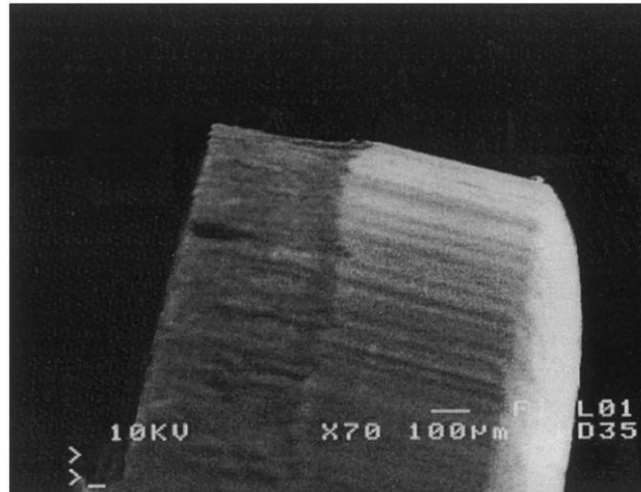


Figure. (10). Electron microscopic observation on sheared blank (11% Clearance, 8 mm punch diameter).

Therefore, Cockcroft and Latham's criterion may be approximated by $\varepsilon^f = C^*$ at the shear band [7]. Consequently, it may be assumed that fracture takes place at a given effective strain. (During the blanking operation it is observed that when the punch penetrates the sheet, the metal lying between the edges of the punch and the die (shearing gap) deforms severely, and finally cracks are initiated. Crack initiation is a local phenomenon and in this methodology it is postulated that a crack is initiated at the point of the sheet whose effective strain first reaches the fracture strain of the work material. In the present investigation, the material constant, C^* was obtained by measuring experimentally the punch penetration (Δ) that causes a crack to begin, and computing numerically the maximum effective deformation for the punch penetration value determined.

According to the studies with worn tools presented in [1, 2], the crack does not emanate from the cutting edge but from the free surface. We considered that a crack starts in the punch-die flank at or just before the beginning of the radius of the cutting edges. The following values were obtained: $\Delta=7.5 \cdot 10^{-4}$ m in the experimental "Fig. (10)", and $\varepsilon^f = 3.88$ in the numerical Simulation.

7.3 Optimum clearance

In this investigation it is assumed that clearance is optimum when the direction of crack propagation coincides with the line joining the points of crack initiation in the punch and die (diagonal line), giving cleanly blanked surfaces. To determine the optimum clearance, the diagonal angle (θ) and the angle of the direction of crack propagation (ϕ) for different clearances were

C l (%)	Δ (%)	φ ($^{\circ}$)	θ ($^{\circ}$)
5	64	14.38	5.10
8	69.3	15.34	8.97
11	75	14.49	13.74
14	81.5	14.12	19.18
17	88.5	14.57	28.35

Table III: Punch penetration, diagonal angle and direction of crack Propagation for different clearances Calculated. It is postulated that cracks propagate perpendicularly to the maximum principal tensile stress [8].

In order to obtain the diagonal angle it is also assumed that the crack is initiated at or just before the radius of the cutting edges. The process to determine the optimum clearance can be observed in the flow chart represented in “Fig. (11)”. Successive displacements are imposed on the punch until any node (i) fulfils the crack initiation criterion The values of the effective strains, principal stress directions and punch penetration at crack initiation were obtained from the output of each computer run. When the crack is initiated, the angle made by the diagonal with the y-axis was also calculated.

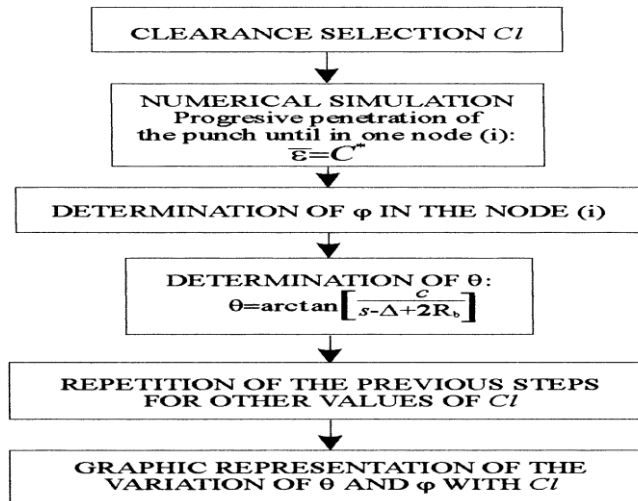


Figure. (11). Flow chart to applied to determining the optimum clearance.

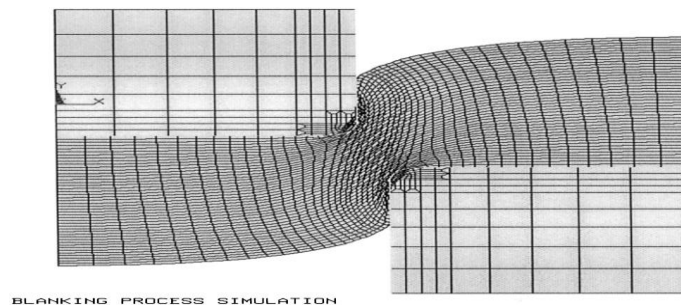


Figure. (12). Simulated part edge ($Cl=11\%$, $\Delta=75\%$).

“Fig. (12)” shows the final edge of a simulation carried out with an 11% punch-die clearance and 75% punch penetration (percentages refer to the thickness of the sheet).

7.4 Analysis of the results

The values of the angles θ and φ were calculated for different clearances using the results of the finite-element analysis. These results are tabulated in Table 3, in which the punch penetration values (Δ as % of the thickness of the work material) at crack initiation are also shown. “Fig. (13)” illustrates the influence of Cl on θ and φ , from which it is seen that as the clearance increases, angle θ increases proportionally while angle φ remains nearly constant: the plots thus intersect.

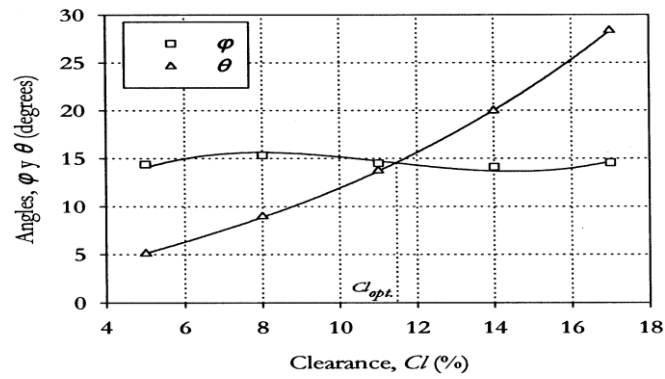


Figure. (13). Variation of the diagonal angle and the direction of crack Propagation with the clearance.

At the point of intersection, the direction of crack propagation coincides with the diagonal line, and so the cracks emanating from the punch and die meet, resulting in a cleanly blanked surface. Hence, this value of CI is taken as the optimum clearance.

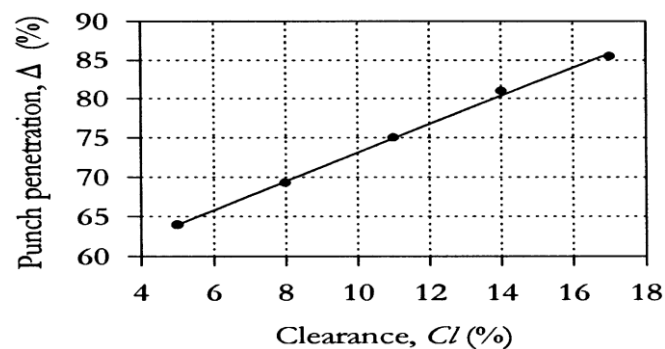


Figure. (14). Correlation between punch penetrations at crack initiation with Clearance.

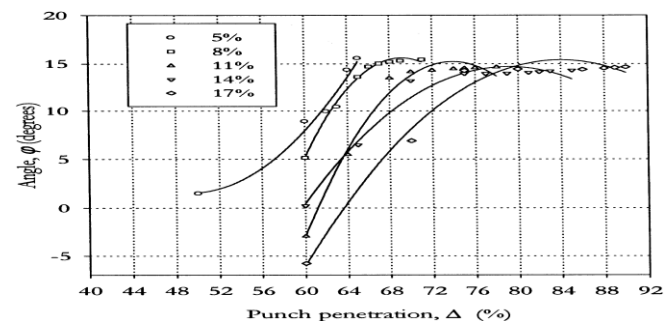


Figure. (15). Variation of angle of the direction perpendicular to the maximum principal tensile stress in node i , with punch penetration.

The optimum clearance for the values of the parameters used in this work is between 11 and 12%, which is in agreement with previous experimental results and theoretical work [11, 12]. “Fig.(14)” illustrates the influence of clearance on punch penetration at crack initiation, the results being similar to those of previous investigations [13]. It is observed that punch penetration increases as the c/t ratio increases. Consequently, with larger clearance, the severity of deformation decreases, i.e. the material can deform more easily, so that greater punch penetration is necessary before cracks are initiated. “Fig.(15)” shows variations in the angle of the direction perpendicular to the maximum principal tensile stress in node i with increasing punch penetration values, for different clearances. This figure shows how this angle reaches feasible values (in terms of material fracture) for a range of punch penetration values similar to those observed experimentally at crack initiation.

7.5 Conclusions

The methodology proposed makes it possible to predict optimum clearance using a general purpose FEM code for a given sheet material and thickness to be blanked. In the absence of such an analytical method, a large number of experiments would be required and their results would have to be analyzed carefully, for the optimum clearance to be calculated. The hypothesis proposed in the present work regarding the point of crack initiation in the punch and die, which is used to determine the values of C^* and diagonal angle, closely reflects previous experimental results concerning optimum clearance.

REFERENCES

- [1] F.W. Timmerbil, Werkstatt. Maschin. 46 (1956) 58–66.
- [2] K. Buchmann, Werkstatt. Maschin. 53 (1963) 128–134.
- [3] F. Faura, J. Lo´pez, C. Lu´is, M.A. Sebastia´n, and Blanking of stainless steel: tool life equation model, in: T. Altan (Ed.), Advanced Technology of Plasticity, vol. II, Columbus, OH, 1996, pp. 655–663.
- [4] F. Faura, J. Lo´pez, J. Sanes, Criterion for tool wears limitation on blanking 18-8 stainless steel strips, Rev. Metal. Madrid 33 (5) (1997) 304–310.
- [5] T. Altan, V. Vazquez, Numerical process simulation for tool and process design in bulk metal forming, Ann. CIRP 45 (1996) 599–615.
- [6] E. Taupin, J. Breitling, W.T. Wu, T. Altan, Material fracture and burr formation in blanking results of FEM simulations and comparison with experiments, J. Mater. Process. Technol. 59 (1996) 68–78.
- [7] S.H. Jeong, A study on shearing mechanism by FEM, MS Thesis, Seoul National University, Seoul, 1995.
- [8] D. Brokken, W.A.M. Brekelmans, F.P.T. Baaijens, Numerical analysis of the metal blanking process, in: T. Altan (Ed.), Advanced Technology of Plasticity, vol. II, Columbus, OH, 1996, pp. 665–668.
- [9] ANSYS User’s Guide, ANSYS Inc., Houston, PA, 1995.
- [10] M.G. Cockcroft, D.J. Latham, A Simple Criterion of Fracture for Ductile Fracture of Metals, National Engineering Laboratory, Report No. 240, 1966.
- [11] T. Maeda, I. Aoki, The study on wear of blanking tool for 18-8 stainless steel and bainite hardened steel strips, J. Fac. Eng. Univ. Tokyo XXXII (3) (1974) 443–475.
- [12] A. Garcí’a, Estudio te´orico-experimental Del proceso de conformado de chapa por punzonado: modelos de predicció’n Del juego de corte óptimo, Ph.D. Thesis, ETS Ingenieros Industriales, Univ. Murcia, Cartagena, 1997.
- [13] P.B. Popat, A. Ghosh, N.N. Kishore, Finite-element analysis of the blanking process, J. Mech. Work. Technol. 18 (1989) 269–282.

VIII. CONCLUSION

The experimental investigation of the sheet metal blanking process makes it possible to study the effects of process parameters such as the material type, the punch-die clearance, the thickness of the sheet and their interactions on the geometry of the sheared edge especially the burrs height. Various methods are used in order to obtain a better understanding of the blanking manufacturing response.

The investigation shows that, the blanking load increases with a reduction in the tool clearance in the case of both single and double blanking. It is observed that the diagonal angle (θ) increases linearly according to the clearance, the crack propagation angle (β) evolves nearly constant. One clear trend is that optimum clearance decreases as the material elongation increases.

There is no universal optimal clearance value in order to minimize the blanking force, the clearance should be set at 10% and however, to minimize the fracture angle, the fracture depth and the burrs height; it is preferable to set the clearance at 5%. When the clearance is set at 10%, the process is slightly more robust to tool wear, as far as the blanking force response is concerned. Whether clearance should be set at 5% or 10% ultimately depends on the priorities of the practitioners.

As a conclusion drawn from the proposed investigation, it is possible to optimize the sheet metal blanking process by a proper selection of the clearance.

IX. FUTURE WORK

Further investigation is needed to explore more parameters and operating conditions to develop a general model for more material types by using the combination of various techniques. A combination of techniques can be used in order to achieve a higher level of verification and to reduce the cost of the necessary experimental effort.

It is recommended to experimentally perform the blanking process that combines the optimal set of parameters and monitor its output quality.

X. NOMENCLATURE

Cl or c = Punch-Die Clearance
t = Sheet Thickness
D_m or D = Die Diameter
D_p or d = Punch Diameter
 θ = Diagonal Angle
B or ϕ = Direction of Crack Propagation Angle
Up = Punch Penetration
Tol = Tolerance Convergence Value
Tf = Friction Shear Stress,
S_n = Normal Stress at Interface
m = Friction Coefficient.
r = Punch-Die Radius
 μ = Friction Coefficient

Σ^* = the Maximum Principal Tensile Stress,
 $E-f$ = Fracture Strain
 C = Material Constant.
 σ^- = Effective Stress
 ε^- = Effective Strain
 Σ_y = Yield Stress
 E = Elastic Modules
 E_T = Tangent Plastic Slope
 Δ = Punch Penetration

REFERENCES

- [1] S. Maiti, A. Ambekar, U. Singh, P. Date, and K. Narasimhan, "Assessment of influence of some process parameters on sheet metal blanking". Journal of Materials Processing Technology, Vol. 102, 2000, 249-256.
- [2] R. Hambli, "Finite element simulation of fine blanking process using a pressure-dependent damage model". Journal of Materials Processing Technology, Vol. 116, 2001, 252-264.
- [3] R. Hambli, "BLANKSOFT: a code for sheet metal blanking processes optimization". Journal of Materials Processing Technology, Vol. 141, 2003, 234-242.
- [4] W. Klingenberg, and Using, "Comparison of two analytical models of blanking and proposal of a new model". International Journal of Machine Tools and Manufacture, Vol. 45, 2005, 519-527.
- [5] R. Hambli, (2002), "Design of Experiment Based Analysis for Sheet Metal Blanking Processes Optimization". The International Journal of Advanced Manufacturing Technology, Vol.19, Page No.403-410.
- [6] F.F aura, A. Garcia and M. Estrems, (1998), "Finite element analysis of optimum clearance in the blanking process". Journal of Materials Processing Technology, Vol.80-81, Page no.121-125.
- [7] R. Hambli, S. Richir, P. Crubleau, and B. Taravel, (2003), "Prediction of optimum clearance in sheet metal blanking processes". International Journal of Advanced Manufacturing Technology, Vol. 22, page no. 20-25.
- [8] Emad Al-Momani, Ibrahim Rawabdeh, (Mar. 2008), "An Application of Finite Element Method and Design of Experiments in the Optimization of Sheet Metal Blanking Process" Jordan Journal of Mechanical and Industrial Engineering. Volume 2, Number 1, Pages 53 -63.
- [9] Ridha Hambli, (June 2005), "Optimization of blanking process using neural network simulation", The Arabian Journal for Science and Engineering, Volume 30.
- [10] G. Fang, G., P. Zeng, and L. Lou, (2002), "Finite element simulation of the effect of clearance on the forming quality in the blanking process". Journal of Materials Processing Technology Vol.122 page no. 249-254.
- [11] R. Hambli, A. Potiron, Finite element modeling of sheet-metal blanking operations with experimental verification, J. Mater. Process. Technol. 102 (2000) 257-265.
- [12] Y.W. Stegeman, A.M. Goijaerts, D. Brokken, W.A.M. Brekelmans, L.E. Govaert, F.P.T. Baaijens, An experimental and numerical study of a planar blanking process, J. Mater. Process. Technol. 87(1-3, 15) (1999) 266-276.
- [13] A.G. Atkins, Surfaces produced by guillotining, Phil. Mag. 4 (1981) 627-641.
- [14] A.G. Atkins, Possible explanation for unexpected departures in hydrostatic tension-fracture strain relations, Metal Science, February 1981, pp. 81-83.
- [15] C.M. Choy, R. Balendra, Experimental analysis of parameters influencing sheared-edge profiles, in: Proceedings of the Fifth International Conference on Sheet Metal, University of Twente, The Netherlands, April 1-3, 1996, pp. 101-110.
- [16] T.M. Chang, Shearing of metal blanks, J. Inst. Met. 78 (1951) 393-414.
- [17] M. Cervenka, B. Bouchet, C. Gasc, Influence du mode de découpe sur le comportement en fatigue de tôles minces d'aciers dual phase, Mémoires d'études scientifiques Revue de métallurgie, March 1990, pp. 185-194.
- [18] Y. Kasuga, S. Tsutsumi, T. Mori, Investigation into shearing process of ductile sheet metals, Mem. Fac. Eng. Nagoya Univ., Japan, 1979, pp. 1-46.
- [19] S. Kalpakjian, Manufacturing Processes for Engineering Materials, 2nd ed., Addison-Wesley, Reading, MA, 1991.
- [20] R. Hambli, Numerical fracture prediction during sheet-metal blanking processes, Eng. Fract. Mech. 68 (3) (2000) 365-378.
- [21] R. Hambli, Etude expérimentale, numérique ET théorique du découpage des tôles en vue de l'optimisation du procédé, Thesis Dissertation, ENSAM d'Angers, 15 October 1996 (in French).
- [22] Atkins AG (1981) Surfaces produced by guillotining. Phil Mag 4:627-641
- [23] Kasuga Y, Tsutsumi S, Mori T (1979) Investigation into shearing process of ductile sheet metals. Mem Fac Eng Nagoya Univ, Japan, pp 1-46
- [24] Hambli R (1996) Etude expérimentale, numérique ET théorique du découpage des tôles en vue de l'optimisation du procédé (in French). Thesis dissertation, ENSAM, d'Angers
- [25] Crisped MA (1991) Non linear finite element analysis of solids and structures, vol 1. Wiley, New York
- [26] BAQUS-HKS, Theory manual, Version 5.8
- [27] H. Andruet, "Special 2-D and 3-D Geometrically Nonlinear Finite Elements for Analysis of Adhesively Bonded Joints," Unpublished Doctoral Dissertation, Virginia Polytechnic Institute, USA, 1998.
- [28] M. Samuel, "FEM simulations and experimental analysis of parameters of influence in the blanking process". Journal of Materials Processing Technology, Vol. 84, 1998, 97-106.
- [29] Rawabdeh, H. Hilwa, and M. Abu Hammed, "Minimizing Necking Defects in Aluminum beverage Cans Using Experimental Design Techniques". Dirasat, Engineering science, Vol. 30, No.1, 2003, 84-97.
- [30] R. Hambli, S. Richir, P. Crubleau, and B. Taravel, "Prediction of optimum clearance in sheet metal blanking processes". International Journal of Advanced Manufacturing Technology, Vol. 22, 2003, 20-25.
- [31] ANSYS User's Guide, ANSYS Inc., Houston, PA, 1995.

Efficient Bandwidth Recycling In Wireless Broadband Networks

Y.Tulasi Rami Reddy,¹ M.Jaya Babu,² B.J.Job Karuna Sagar,³
N.Suresh Babu⁴

1. M.Tech Student in CSE Department, Kottam College of Engineering, Kurnool (India) 518218,
2. Assistant Professor in CSE Department, Kottam College of Engineering, Kurnool (India) 518218,
3. Assistant Professor in CSE Department, KsrmCollege of Engineering, Kadapa (India) 516003,
4. M.Tech Student in CSE Department, Sphoorthy Engineering College, Hyderabad (India) 501510,

Abstract: Bandwidth recycling is proliferated in wireless broadband networks, in which IEEE 802.16 standard was designed to support the bandwidth demanding applications with quality of service (QoS). Bandwidth is reserved for each application to ensure the QoS. For variable bit rate (VBR) applications, however, it is difficult for the subscriber station (SS) to predict the amount of incoming data. To ensure the QoS guaranteed services, the SS may reserve more bandwidth than its demand. As a result, the reserved bandwidth may not be fully utilized all the time. In this paper, we propose a scheme, named Bandwidth Recycling, to recycle the unused bandwidth without changing the existing bandwidth reservation. The idea of the proposed scheme is to allow other SSs to utilize the unused bandwidth when it is available. Thus, the system throughput can be improved while maintaining the same QoS guaranteed services. Mathematical analysis and simulation are used to evaluate the proposed scheme. Simulation and analysis results confirm that the proposed scheme can recycle 55% of unused bandwidth on average. By analyzing factors affecting the recycling performance, three scheduling algorithms are proposed to improve the overall throughput. The simulation results show that our proposed algorithm improves the overall throughput by 60% in a steady network. to carry out research object at providing quality of network performance in Heterogeneous computing environment

Index Terms: QoS, WiMAX, IEEE 802.16, Bandwidth Recycling,

1. Introduction

THE WiMAX refers to interoperable implementations of the IEEE 802.16 family of wireless-networks standards ratified by the WiMAX Forum. Similarly, Wi-Fi, refers to interoperable implementations of the IEEE 802.11 Wireless LAN standards certified by the Wi-Fi Alliance. WiMAX Forum certification allows vendors to sell fixed or mobile products as WiMAX.

Certified, thus ensuring a level of interoperability with other certified products, as long as they fit the same profile. The Worldwide Interoperability for Microwave Access. (WiMAX), based on IEEE 802.16 standard standards [1], [2], is designed to facilitate services with high transmission Rates for data and multimedia applications in metropolitan areas.

The original IEEE 802.16 standard (now called "Fixed WiMAX") was published in 2001. WiMAX adopted some of its technology from WiBro, a service marketed in Korea.^[1] Mobile WiMAX (originally based on 802.16e-2005) is the revision that was deployed in many countries, and basis of future revisions such as 802.16m-2011. WiMAX is sometimes referred to as "Wi-Fi on steroids" and can be used for a number of applications including broadband connections, cellular backhaul, hotspots, etc. It is similar to Wi-Fi, but it can enable usage at much greater distances. IEEE 802.16 is a series of Wireless Broadband standards authored by the Institute of Electrical and Electronics Engineers (IEEE). The IEEE Standards Board established a working group in 1999 to develop standards for broadband for Wireless Metropolitan Area Networks. The Workgroup is a unit of the IEEE 802 local area network and metropolitan area network standards committee. Although the 802.16 family of standards is officially called Wireless MAN in IEEE, it has been commercialized under the name "WiMAX" (from "Worldwide Interoperability for Microwave Access") by the WiMAX Forum industry alliance. The Forum promotes and certifies compatibility and interoperability of products based on the IEEE 802.16 standards. QoS Quality of service (QoS) in 802.16e is supported by allocating each connection between the SS and the BS (called a *service flow* in 802.16 terminologies) to a specific *QoS class*. In 802.16e, there are 5 QoS classes:

The physical (PHY) and medium access control (MAC) layers of WiMAX have been specified in the IEEE 802.16 standard.

Many advanced communication technologies such as Orthogonal Frequency- Division Multiple Access (OFDMA) and multiple-input and multiple-output (MIMO) are embraced in the standards. Supported by these modern technologies, WiMAX is able to provide large service coverage, high data rates and QoS guaranteed services. Because of these features, WiMAX is considered as a promising alternative for last mile broadband wireless access (BWA).

802.16e-2005 QoS classes			
Service	Abbrev	Definition	Typical Applications
Unsolicited Grant Service	UGS	Real-time data streams comprising fixed-size data packets issued at periodic intervals	T1/E1 transport
Extended Real-time Polling Service	ertPS	Real-time service flows that generate variable-sized data packets on a periodic basis	VoIP

Real-time Polling Service	rtPS	Real-time data streams comprising variable-sized data packets that are issued at periodic intervals	MPEG Video
Non-real-time Polling Service	nrtPS	Delay-tolerant data streams comprising variable-sized data packets for which a minimum data rate is required	FTP with guaranteed minimum throughput
Best Effort	BE	Data streams for which no minimum service level is required and therefore may be handled on a space-available basis	HTTP

To improve the bandwidth utilization while maintaining the same QoS guaranteed services, our research objective is twofold: 1) the existing bandwidth reservation is not changed to maintain the same QoS guaranteed services. 2) our research work focuses on increasing the bandwidth utilization by utilizing the unused bandwidth. We propose a scheme, named *Bandwidth Recycling*, which recycles the unused bandwidth while keeping the same QoS guaranteed services without introducing extra delay. The general concept behind our scheme is to allow other SSs to utilize the unused bandwidth left by the current transmitting SS. Since the unused bandwidth is not supposed to occur regularly, our scheme allows SSs with non-real time applications, which have more flexibility of delay requirements, to recycle the unused bandwidth. Consequently, the unused bandwidth in the *current* frame can be utilized. It is different from the bandwidth adjustment in which the adjusted bandwidth is enforced as early as in the next coming frame. Moreover, the unused bandwidth is likely to be released temporarily (i.e., only in the current frame) and the existing bandwidth reservation does not change. Therefore, our scheme improves the overall throughput while providing the same QoS guaranteed services.

In computer networking and computer science, the words bandwidth, network bandwidth, data bandwidth, or digital bandwidth are terms used to refer to various bit-rate measures, representing the available or consumed data communication resources expressed in bits per second or multiples of it (bit/s, kbit/s, Mbit/s, Gbit/s, etc.).

1.1 Network bandwidth capacity

Bandwidth sometimes defines the net bit rate (aka. peak bit rate, information rate or physical layer useful bit rate), channel capacity, or the maximum throughput of a logical or physical communication path in a digital communication system. For example, bandwidth tests measure the maximum throughput of a computer network. The reason for this usage is that according to Hartley's law, the maximum data rate of a physical communication link is proportional to its bandwidth in hertz, which is sometimes called frequency bandwidth, spectral bandwidth, RF bandwidth, signal bandwidth or analog bandwidth.

1.2 Network bandwidth consumption

Bandwidth in bit/s may also refer to consumed bandwidth, corresponding to achieved throughput or good put, i.e., the average rate of successful data transfer through a communication path. This sense applies to concepts and technologies such as bandwidth shaping, bandwidth management, bandwidth throttling, bandwidth cap, bandwidth allocation (for example bandwidth allocation protocol and dynamic bandwidth allocation), etc. A bit stream's bandwidth is proportional to the average consumed signal bandwidth in Hertz (the average spectral bandwidth of the analog signal representing the bit stream) during a studied time interval.

Channel bandwidth may be confused with data throughput. A channel with x bps may not necessarily transmit data at x rate, since protocols, encryption, and other factors can add appreciable overhead. For instance, a lot of internet traffic uses the transmission control protocol (TCP) which requires a three-way handshake for each transaction, which, though in many modern implementations is efficient, does add significant overhead compared to simpler protocols. In general, for any effective digital communication, a framing protocol is needed; overhead and effective throughput depends on implementation. Actual throughput is less than or equal to the actual channel capacity plus implementation overhead.

1.3 Asymptotic bandwidth

The asymptotic bandwidth for a network is the measure of useful throughput, when the packet size approaches infinity.

Asymptotic bandwidths are usually estimated by sending a number of very large messages through the network, measuring the end-to-end throughput. As other bandwidths, the asymptotic bandwidth is measured in multiples of bits per second.

1.4 Multimedia bandwidth

Digital bandwidth may also refer to: multimedia bit rate or average bitrate after multimedia data compression (source coding), defined as the total amount of data divided by the playback time.

1.5 Bandwidth in web hosting

In website hosting, the term "bandwidth" is often ^[citation needed] incorrectly used to describe the amount of data transferred to or from the website or server within a prescribed period of time, for example bandwidth consumption accumulated over a month measured in gigabytes per month. The more accurate phrase used for this meaning of a maximum amount of data transfer each month or given period is monthly data transfer.

Variable bit rate (VBR) is a term used in telecommunications and computing that relates to the bit rate used in sound or video encoding. As opposed to constant bit rate (CBR), VBR files vary the amount of output data per time segment.

VBR allows a higher bit rate (and therefore more storage space) to be allocated to the more complex segments of media files while less space is allocated to less complex segments. The average of these rates can be calculated to produce an average bit rate for the file.

2.1 OVERVIEW OF WIMAX/IEEE 802.16 STANDARDS

Worldwide Interoperability for Microwave Access (WiMAX) is known as a metropolitan area network technology whose goal is to one day provides last-mile broadband wireless access to the general population. The WiMAX technology is based on the IEEE 802.16 standard and is capable of providing a platform to deliver the applications for the convergence of data, voice and video services. The WiMAX protocol is designed to accommodate several different methods of data transmission, one of which is Voice over Internet Protocol (VoIP). The use of VoIP could increase dramatically when WiMAX-compatible devices become common. WiMAX gives hope to millions of people to access the Internet cheaply and easily. The WiMAX forum was created by industry leaders in 2000 in order to promote deployment of broadband wireless access networks by using the IEEE 802.16 standard and certifying interoperability and standards compliance of products and technologies manufactured by member companies. The IEEE 802.16, which is called the Wireless Metropolitan Area Network (WMAN) standard, will enable a single base station to support both fixed and mobile Broadband Wireless Access (BWA). It aims to fill the gap between high data rate Wireless Local Area Networks (WLAN) and high mobility cellular Wide Area Networks (WAN). The IEEE 802.16 extends this coverage of WLAN, which is known as IEEE 802.11, while offering the features consistent with the stringent demands of operators in a wide variety of deployment scenarios.



Figure 2.1 WiMAX bridges the gap between LAN and WAN

2.2 WiMAX/IEEE 802.16 Architecture

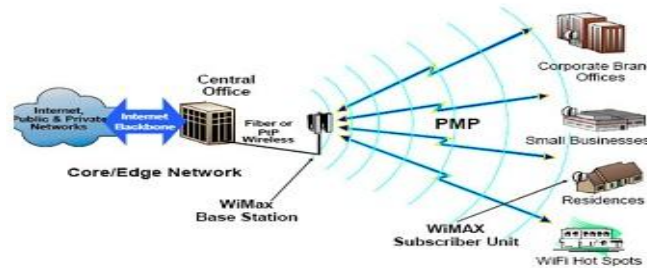


Figure 2.2 shows that a typical IEEE 802.16 network in PMP mode comprising of a BaseStation (BS) that communicates with one or more Subscriber Stations (SS) known as Customer Premises Equipment (CPE). IEEE 802.16 specifies the following modes of deployment architectures:

- **Point-to-point (PTP):** A connection between one BS and one SS. The PTP mode extends the range over the PMP mode.
- **Point-to-multipoint (PMP):** A connection between one BS and multiple SS nodes. The BS always coordinates the uplink and downlink transmission. This mode supports multicast communication.
- **Point-to-consecutive point (PTCM):** It involves the creation of a closed loop through multiple PTP connections.
- **Mesh:** SSs can communicate with each other without the coordination of a BS

2.3 WiMAX Advantages

- **Good standard:** IEEE Standard and WiMAX interoperability certification. WiMAX can support mobility, roaming and meshing.
- **Long range:** WiMAX forum points out that the most significant advantage of WiMAX is the range it provides compared to existing wireless technologies. WiMAX can provide a communication range of up to 30 miles.
- **Low cost:** WiMAX reduces the capital expenditures required for network expansion and reduces fixed broadband prices.
- **Quality of Service (QoS) support:** WiMAX MAC protocol supports high QoS and guaranteed service levels.

- **High number of simultaneous sessions:** WiMAX MAC is designed to support thousands of users.

The WiMAX/IEEE 802.16 standard specifies a system comprising of two core components: the Subscriber Station (SS) or Customer Premises Equipment (CPE), and the Base Station (BS). The 802.16 MAC protocol is designed to support different QoS requirements for different applications at the MAC layer. The mechanisms for supporting QoS in the IEEE 802.16 MAC layer are presented in this section. The overview of the WiMAX/IEEE 802.16 standard and MAC protocol aims to clarify the research background of this study.

III. BACKGROUND INFORMATION

The IEEE 802.16 standard specifies three types of transmission mediums supported as the physical layer (PHY): single channel (SC), orthogonal frequency-division multiplexing (OFDM) and Orthogonal Frequency-Division Multiple Access (OFDMA). We assume OFDMA as the PHY in our analytical model since it is employed to support mobility in IEEE 802.16e standard and the scheme working in OFDMA should also work in others. There are four types of modulations supported by OFDMA: BPSK, QPSK, 16-QAM and 64-QAM.

This paper is focused on the point-to-multipoint (PMP) mode in which the SS is not allowed to communicate with any other SSs but the BS directly. Based on the transmission direction, the transmissions between BS and SSs are classified into downlink (DL) and uplink (UL) transmissions. The former are the transmissions from the BS to SSs. Conversely, the latter are the transmissions in the opposite direction. There are two transmission modes: Time Division Duplex (TDD) and Frequency Division Duplex (FDD) supported in IEEE 802.16. Both UL and DL transmissions can not be operated simultaneously in TDD mode but in FDD mode. In this paper, our scheme is focused on the TDD mode. In WiMAX, the BS is responsible for scheduling both UL and DL transmissions. All scheduling behavior is expressed in a MAC frame.

There are two types of BRs defined in the IEEE 802.16 Standard: incremental and aggregate BRs. The former allow the SS to indicate the extra bandwidth required for a connection. Thus, the amount of reserved bandwidth can be only increased via incremental BRs. On the other hand, the SS specifies the current state of queue for the particular connection via a aggregate request. The BS resets its perception of that service's needs upon receiving the request. Consequently, the reserved bandwidth may be decreased.

IV. MOTIVATION AND RELATED WORK

Bandwidth reservation allows IEEE 802.16 networks to provide QoS guaranteed services. The SS reserves the required bandwidth before any data transmissions. Due to the nature of VBR applications, it is very difficult for the SS to make the optimal bandwidth reservation. It is possible that the amount of reserved bandwidth is more than the demand. Therefore, the reserved bandwidth cannot be fully utilized. Although the reserved bandwidth can be adjusted via BRs, however, the updated reserved bandwidth is applied as early as to the next coming frame and there is no way to utilize the unused bandwidth in the current frame. In our scheme, the SS releases its unused bandwidth in the current frame and another SS pre-assigned by the BS has opportunities to utilize this unused bandwidth. This improves IEEE TRANSACTIONS ON MOBILE COMPUTING VOLUME 9, ISSUE 10 (OCTOBER 2010)3 the bandwidth utilization. Moreover, since the existing bandwidth reservation is not changed, the same QoS guaranteed services are provided without introducing any extra delay. A dynamic bandwidth request-allocation algorithm for real-time services is proposed in [7]. The authors predict the amount of bandwidth to be requested based on the information of the backlogged amount of traffic in the queue and the rate mismatch between packet arrival and service rate to improve the bandwidth utilization. The research works listed above improve the performance by predicting the traffic coming in the future. Instead of prediction, our scheme can allow SSs to accurately identify the portion of unused bandwidth and provides a Method to recycle the unused bandwidth. It can improve the utilization of bandwidth while keeping the same QoS guaranteed services and introducing no extra delay.

4.1 Existing Scheme

Bandwidth transmitted data may be more than the amount of transmitted data and may not be fully utilized all the time. Before it is different from the bandwidth adjustment in which the adjusted bandwidth is enforced as early as in the next coming frame. Moreover, the unused bandwidth is likely to be released temporarily (i.e., only in the current frame) and the existing bandwidth reservation does not change. The ad hoc networking community assumes that the underlying wireless technology is the IEEE 802.11 standard due to the broad availability of interface cards and simulation models.

V. PROPOSED SCHEME

The IEEE 802.16 network is connection-oriented. It gives the advantage of having better control over network resource to provide QoS guaranteed services. To improve the bandwidth utilization while maintaining the same QoS guaranteed services, our research objective is two fold: 1) the same QoS guaranteed services are provided by maintaining the existing bandwidth reservation. 2) The bandwidth utilization is improved by recycling the unused bandwidth. To achieve these objectives, our scheme named Bandwidth Recycling is proposed.

The existing bandwidth reservation is not changed to maintain the same QoS guaranteed services. Our research work focuses on increasing the bandwidth utilization by utilizing the unused bandwidth we propose a scheme, named Bandwidth Recycling, which recycles the unused bandwidth while keeping the same QoS guaranteed services without introducing extra delay. The general concept behind

our scheme is to allow other SSs to utilize the unused bandwidth left by the current transmitting SS. Since the unused bandwidth is not supposed to occur regularly, our scheme allows SSs with non-realtime applications, which have more flexibility of delay requirements, to recycle the unused bandwidth. In this system they are using 802.11 MAC layer to evaluate the correct bandwidth. This method combines channel monitoring to estimate each node's medium occupancy. Synchronization between nodes, estimation of the collision probability between each couple of nodes, and variable overhead's impact estimation.

5.1 Module Design and Organization

5.1.1 Bandwidth utilization Module

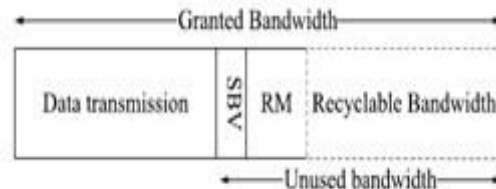


Figure 5.1.1 Bandwidth Utilization Module

Bandwidth utilization improvements have been proposed in the literature. In, a dynamic resource reservation mechanism is proposed. It can dynamically change the amount of reserved resource depending on the actual number of active connections. The investigation of dynamic bandwidth reservation for hybrid networks is presented in. Evaluated the performance and effectiveness for the hybrid network, and proposed efficient methods to ensure optimum reservation and utilization of bandwidth while minimizing signal blocking probability and signaling cost. In, the enhanced the system throughput by using concurrent transmission in mesh mode

5.1.2 Packet Creation Module

In this module we split the Data in to N number of fixed size packet with Maximum length of 48 Characters. As result of packet creation module, the splitting data can be easily transmitted to great extent with out interruption in network bandwidth across the different nodes.

5.1.3 Bandwidth Recycling

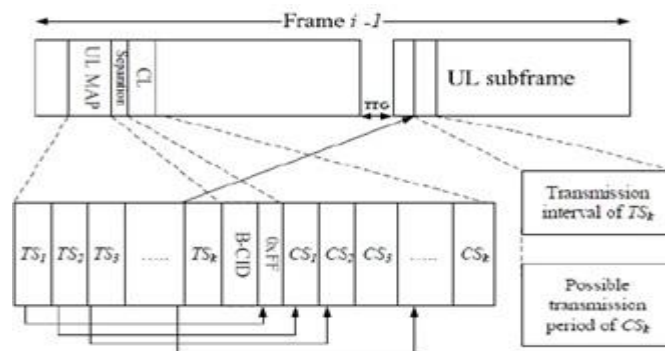


Figure 5.1.3 Bandwidth Recycling Module

The complementary station (CS). Waits for the possible opportunities to recycle the unused bandwidth of its corresponding TS in this frame. The CS information scheduled by the BS is resided in a list, called complementary list (CL). The CL includes the mapping relation between each pair of pre-assigned C and TS.

5.1.4 QoS Guaranteed Services:

It is different from the bandwidth adjustment in which the adjusted bandwidth is enforced as early as in the next coming frame. Moreover, the unused bandwidth is likely to be released temporarily (i.e., only in the current frame) and the existing bandwidth reservation does not change. Therefore, our scheme improves the overall throughput while providing the same QoS guaranteed services.

5.1.5 Traffic and Packet Performance

The Packet mean data rate of each application but make the mean packet size randomly selected from 512 to 1024 bytes. Thus, the mean packet arrive rate can be determined based on the corresponding mean packet size. As mentioned earlier, the size of each packet is modeled as Poisson distribution and the packet arrival rate is modeled as exponential distribution. The other factor that may affect the performance of bandwidth recycling is the probability of the RM to be received by the CS successfully.

5.2 Algorithms

❖ Dynamic bandwidth request-allocation algorithm and Priority-based Scheduling Algorithm

A dynamic bandwidth request-allocation algorithm for real-time services is proposed in. The authors predict the amount of bandwidth to be requested based on the information of the backlogged amount of traffic in the queue and the rate mismatch between packet arrival and service rate to improve the bandwidth utilization. The research works listed above improve the performance by predicting the traffic coming in the future. Instead of prediction, our scheme can allow SSs to accurately identify the portion of unused bandwidth and provides a method to recycle the unused bandwidth. It can improve the utilization of bandwidth while keeping the same QoS guaranteed services and introducing no extra delay

Algorithm 1 Priority-based Scheduling Algorithm

Input: T is the set of TSs scheduled on the UL map.

Q is the set of SSs running non-real time applications.

Output: Schedule CSs for all TSs in T.

For $i = 1$ to $\|T\|$ **do**

a. $St \leftarrow TS_i$.

b. $Qt \leftarrow Q - Ot$.

c. Calculate the SF for each SS in Qt .

d. **If** Any SS $\in Qt$ has zero granted bandwidth,

If Any SSs have nrtPS traffics and zero granted

Bandwidth,

Choose one running nrtPS traffics with the

Largest CR.

Else

Choose one with the largest CR.

Else

Choose one with largest SF and CR.

e. Schedule the SS as the corresponding CS of St .

End For

VI. ANALYSIS

The percentage of potentially unused bandwidth occupied in the reserved bandwidth is critical for the potential performance gain of our scheme. We investigate this percentage on VBR traffics which is popularly used today. Additionally, in our scheme, each T should transmit

A RM to inform its corresponding CS when it has unused bandwidth. However, the transmission range of the TS may not be able to cover the corresponding CS. It depends on the location and the transmission power of the TS. It is possible that the unused bandwidth cannot be recycled because the CS does not receive the RM. Therefore, the benefit of our scheme is reduced. In this section, we analyze mathematically the probability of a CS to receive a RM successfully. Obviously, this probability affects the bandwidth recycling rate BR. BBR stands for the percentage of the unused bandwidth which is recycled. Moreover, the performance analysis is presented in terms of throughput gain (TG). At the end, we evaluate the performance of our scheme under different traffic load.

6.1 Analysis of potential unused bandwidth

Based on the traffic generation rate, the applications can be classified into two types: constant bit rate (CBR) and variable bit rate (VBR). Since CBR applications generate data in a constant rate, SSs rarely adjust the reserved bandwidth. As long as the reasonable amount of bandwidth is reserved, it is hard to have unused bandwidth in this type of applications. Therefore, our scheme has very limited benefit on CBR traffic. However, VBR applications generate data in a variable rate. It is hard for a SS to predict the amount of incoming data precisely for making the appropriate bandwidth Reservation. Thus, in order to provide QoS guaranteed services, the SS tends to keep the amount of reserved bandwidth to serve the possible bursty data arrived in the future. The reserved bandwidth may not be fully utilized all the time. Our analysis focuses on investigating the percentage of potentially unused bandwidth of VBR traffics. The relation between W and B can be formulated as:

$$W = B Df \leq W_{max} \quad (1)$$

Suppose X_{i-1} represents the amount of data arriving in the frame $i-1$ (in terms of bytes), where $1 \leq i \leq N-1$ and N is the total number of frames we analyze. If we

Have unused bandwidth in frame i , then the amount of

Data in queue must be less than the number of assigned

Bandwidth. By considering the inter-frame dependence

(i.e., the number of data changed in the previous frame

Affects the number of data in queue in the current frame),

It can be represented as the the following condition:

$$X_{i-1} < W_i - \max \{0; Q_{i-1} - W_{i-1}\} \quad (2)$$

Where Q_{i-1} is the amount of data stored in queue before transmitting frame $i - 1$. W_i and W_{i-1} are the amount of bandwidth assigned in frame i and $i - 1$, respectively. Again, both W_i and W_{i-1} are at most W_{max} . $\max \{0; Q_{i-1} - W_{i-1}\}$ represents the amount of queued

Data arriving before frame $i - 1$.

As mentioned, X_{i-1} is the amount of data arriving in the frame $i - 1$. Thus, X_{i-1} must be nonnegative. Consequently, the probability of having unused bandwidth in frame i , $P_u(i)$, is derived as:

$$P_u(i) = \int_0^{X_{i-1}} p(X) dX. \quad (3)$$

Thus, the expected amount of unused bandwidth in Frame i , $E(i)$, can be derived as:

$$E(i) = \int_0^{X_{i-1}} X p(X) dX. \quad (4)$$

Finally, by summing the expected unused bandwidth

In all frames, the ratio of the total potentially unused bandwidth to total reserved bandwidth in N frames, R_u , can be presented as:

$$R_u = \frac{\sum_{i=0}^{N-1} E(i)}{\sum_{i=0}^{N-1} W_i} \quad (5)$$

VII. SIMULATION RESULTS

Our simulation is conducted by using Qualnet 4.5 [11].

In this section, we first present our simulation model followed by introducing the definition of performance Metrics used for measuring the network performance.

The simulation results are shown as the third part of this section. At the end, we provide the validation of Theoretical analysis and simulation results.

The simulation for evaluating the performance of the proposed scheme is based on the three metrics:

1) *Throughput gain (TG):*

It represents the percentage of throughput which Is improved by implementing our scheme. The Formal definition can be expressed as:

$$TG = \frac{T_{recycle} - T_{no recycle}}{T_{no recycle}}$$

Where $T_{recycle}$ and $T_{no recycle}$ represent the Throughput with and without implementing our Scheme, respectively. The higher TG achieved shows the higher performance that our scheme can make.

2) *Unused bandwidth rate (UBR):*

It is defined as the percentage of the unused bandwidth Occupied in the total granted bandwidth in the system without using bandwidth recycling. It can be defined formally as:

$$UBR = \frac{B_{unused BW}}{B_{total BW}}$$

Where $B_{unused BW}$ and $B_{total BW}$ are the unused Bandwidth and total allocated bandwidth, respectively.

The UBR shows the room which can be improved by our scheme. The higher UBR means The more recycling opportunities.

3) *Bandwidth recycling rate (BRR):*

It illustrates the percentage of bandwidth which is Recycled from the unused bandwidth. The percentage Can be demonstrated formally as:

$$BRR = \frac{B_{recycled}}{B_{unused BW}}$$

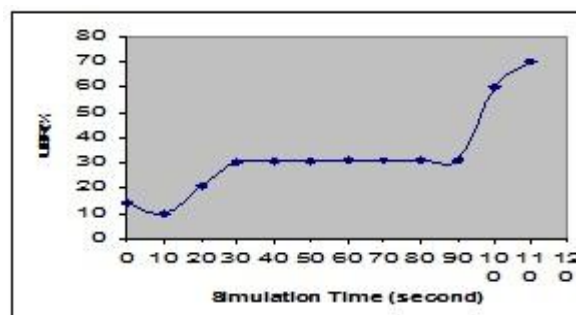


Fig 7.1 Simulation results of UBR

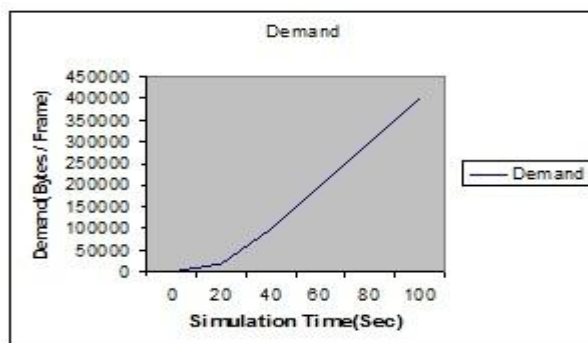


Fig 7.2 Total Bandwidth demand.

The simulation results of recycling rate are presented from the above figures we observe that the recycling rate is very close to zero at the beginning of the simulation. It is because that only a few connections transmit data during that time and the network has a light load. Therefore, only few connections need to recycle the unused bandwidth from others. As time goes on, many active connections join in the network. The available bandwidth may not be able to satisfy the needs of connections. Therefore, there is a high probability that the CS recycles the unused bandwidth. It leads a higher *BRR*. The total bandwidth demand requested by SSs during the simulation. In the figure, the dashed line indicates the system bandwidth capacity. During the simulation, the BS always allocates the bandwidth to satisfy the demand of real time connections due to the QoS requirement. Therefore, the amount of bandwidth allocated to non-real time connections may be shrunk. At the same time, the new non-real time data are generated. Therefore, the non-real time data are accumulated in the queue. It is the reason that the demand of bandwidth keeps increasing.

As our investigation, one of the factors causing recycling. Failures are that the CS does not have data to transmit while receiving a RM. The other factor that may affect the performance of bandwidth recycling is the probability of the RM to be received by the CS successfully. To increase this probability, a scheduling algorithm, named history-Based Scheduling Algorithm (HBA), is proposed. According to our protocol, the CS transmits data or pad the rest of transmission interval if a RM is received.

VIII. RESULTS

The results consists of the output screens for the given Transmission nodes and Complementary nodes in wireless broadband networks for recycling the bandwidth usage. The Home page for starting the application is as shown below.



Screen 1 for Bandwidth Recycling in IEEE802.16 Networks



Screen 2 for selecting the destination Node



Screen 3 for selecting the another destination Node



Screen 7 for Completing the Data Transmission.



Screen 4 for Sending the RREQ (recycling request) to Node2



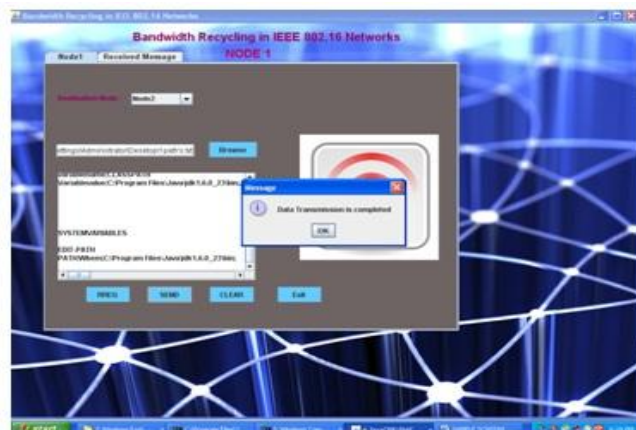
Screen 8 for Clear History about Recycling Bandwidth



Screen 5 for Receiving the Response (RREP) from Node2



Screen 9 for Transmission of packets from Node2



Screen 6 for Message send to Node2

IX. CONCLUSIONS

Variable bit rate applications generate data in variant rates. It is very challenging for SSs to predict the amount of arriving data precisely. Although the existing method allows the SS to adjust the reserved bandwidth via risk of failing to satisfy the QoS requirements. Moreover, the unused bandwidth occurs in the current frame cannot be utilized by the existing bandwidth adjustment since the adjusted amount of bandwidth can be applied as early as in the next coming frame. Variable bit rate applications generate data in variant rates. It is very challenging for SSs to predict the amount of arriving data precisely. Although the existing method allows the SS to adjust the reserved bandwidth via bandwidth requests in each frame, it cannot avoid the risk of failing to satisfy the QoS requirements. Moreover, the unused bandwidth occurs in the current frame cannot be utilized by the existing bandwidth adjustment since the adjusted amount of bandwidth can be applied as early as in the next coming frame. Our research does not change the existing bandwidth reservation to ensure that the same QoS guaranteed services are provided. We proposed *bandwidth recycling* to recycle the unused bandwidth once it occurs. It allows the BS to schedule a complementary station for each transmission stations. Each complementary station monitors the entire UL transmission interval of its corresponding TS and standby for any opportunities to recycle the unused bandwidth. Besides the naive priority-based scheduling algorithm, three additional algorithms have been proposed to improve the recycling effectiveness.

Our mathematical and simulation results confirm that our scheme can not only improve the throughput but also reduce the delay with negligible overhead and satisfy the QoS requirements.

We proposed bandwidth recycling to recycle the unused bandwidth once it occurs. It allows the BS to schedule a complementary station for each transmission stations. Each complementary station monitors the entire UL transmission interval of its corresponding TS and standby for any opportunities to recycle the unused bandwidth. Besides the naive priority-based scheduling algorithm, three additional algorithms have been proposed to improve the recycling effectiveness. Our mathematical and simulation results confirm that our scheme can not only improve the throughput but also reduce the delay with negligible overhead and satisfy the QoS

9.1 Future Enhancements

Our research does not change the existing bandwidth reservation to ensure that the same QoS guaranteed services are provided. We proposed bandwidth recycling to recycle the unused bandwidth once it occurs. It allows the BS to schedule a complementary station for each transmission stations. Each complementary station monitors the entire UL transmission interval of its corresponding TS and standby for any opportunities to recycle the unused bandwidth. Besides the naive priority-based scheduling algorithm, three additional algorithms have been proposed to improve the recycling effectiveness. Our mathematical and simulation results confirm that our scheme can not only improve the throughput but also reduce the delay with negligible overhead and satisfy the QoS requirements.

REFERENCES

- [1] Sri M.Jaya Babu, Sri K.Gopinath Y.Tulasi Rami Reddy, "Data Caching between Mobile nodes in wireless adhoc networks", International Journal of Modern Engineering Research, Vol.2, Issue.5, pp 3841-3849., ISSN: 2249-6645., Sep-Oct-2012.
- [2] Eun-Chan Park, Hwangnam Kim, Jae-Young Kim, Han-Seok Kim "Dynamic Bandwidth Request-Allocation Algorithm for Real-time Services in IEEE 802.16 Broadband Wireless Access Networks", INFOCOM 2008,p.852 - 860
- [3] IEEE 802.16 WG,"IEEE Standard for Local and Metropolitan Area Network Part 16: Air Interface for Fixed Broadband Wireless Access Systems" IEEE Std 802.16-2004 p.1 - p.857
- [4] IEEE 802.16WG,"IEEE standard for local and metropolitan area networks part 16: Air interface for fixed and mobile broadband wireless access systems, Amendment 2," IEEE 802.16 Standard, December 2005.
- [5] Jianhua He, Kun Yang and Ken Guild"A Dynamic Bandwidth Reservation Scheme for Hybrid IEEE 802.16 Wireless Networks" ICC'08 p.2571-2575.
- [6] J. Tao, F. Liu, Z. Zeng, and Z. Lin, Throughput enhancement in WiMax mesh networks using concurrent transmission, In Proc. IEEE Int. Conf. Wireless Commun., Netw. Mobile Comput. 2005, p. 871V874.
- [7] Kamal Gakhar, Mounir Achir and Annie Gravey,"Dynamic resource reservation in IEEE 802.16 broadband wireless networks", IWQoS, 2006. p.140-148
- [8] Thomas G. Robertazzi"Computer Networks and Systems: Theory and Performance Evaluation." Springer-Verlag 1990
- [9] Xiaofeng Bai, Abdullah Shami and Yinghua Ye"Robust QoS Control for Single Carrier PMP Mode IEEE 802.16 Systems", IEEE TRANSACTIONS ON MOBILE COMPUTING, VOL. 7, NO. 4, APRIL 2008, p.416-429

References Made From:

1. Professional Java Network Programming
2. Java Complete Reference
4. Data Communications and Networking, by Behrouz A Forouzan.
5. Computer Networking: A Top-Down Approach, by James F. Kurose.
6. Operating System Concepts, by Abraham Silberschatz.

AUTHORS LIST



Y.TULASI RAMI REDDY (M.Tech) pursuing M.Tech CSE final year Kottam College of Engineering, Affiliated to JNTU Anantapur, approved by AICTE, New Delhi. Chinnatekur, Kurnool, His research Areas of interest are Computer Networks and Data Mining.



M.JAYA BABU. M.Tech. Assistant Professor in CSE Department, Kottam College of Engineering, Kurnool. Received his M.Tech, in Computer Science from (JNTU, Kakinada) His area of interest include Computer Networks and Data Mining.



B.J.JOB KARUNA SAGAR. M.Tech, Assistant Professor in CSE Department, KSRM College of Engineering, Kadapa. Received his M.E, in C.S.E from SathyaBama University, Chennai. He is currently working towards the PhD Degree in C.S.E at Bharthiar University. His areas of interest include Wireless Networking and Resource Allocation.



N.SURESH BABU. (M.Tech.) Pursuing M.Tech CSE final year in Sphoorthy Engineering College, Affiliated to, JNTU, HYD, approved by AICTE, New Delhi. Vanasthalipuram, Hyd. His area of interest include Computer Networks and Data Mining.

A Novel Approach to Detect Mischief Activities (Fraud) In On-Line Transaction

Dr. K. Subramanian

Vice-Principal & Head IT, J J College of Arts and Science, Pudukkottai.

Abstract: Nowadays, Credit cards are used in E-Commerce and for other financial transactions. The Credit card fraud is widespread in the recent years. It leads to the financial loss, for the individuals and also to the merchants. Here, to find these mischief activities clustering and outlier detection techniques can be used. Using the Clustering the data sets are partitioned and outlier detection is used to find the fraudulent data.

Key words: Outlier detection, Clustering, Fraud Detection, Credit cards.

I. Introduction

In Modern world most of the people are using the Credit cards. It is the most popular payment mode. Detecting the frauds in these on-line transaction is a very difficult task. So, there is need to develop a model to detect these frauds, in the business area and also in the academics. Finding the mischief means identifying suspicious fraud cases. Clustering means grouping the similar data object into a single set or cluster. Outliers can be defined as an observation which appears to be inconsistent with the remainder of the data sets. Outlier is an object whose attribute value is significantly different from the values of its neighbor. Outlier detection is a data mining technique which identifies the abnormal values. In this paper, outlier detection algorithm is employed to find the fraudulent transactions.

II. Related Work

More research work has been carried out with special emphasis to prevent the credit card frauds. In the year 2002 M.J.Kim, Sam *et. al* .identified and suggested some approaches for the outlier data in the credit card transactions. They used the Bayesian and Neural networking concepts. Clustering based outlier detection techniques and grid based techniques are also devised to find the mischief data. Most of the outlier detection algorithms use the distance based approaches. In this paper, a system is developed to find the fraudulent data points and an algorithm is also conceived.

III. Fraud Detection System

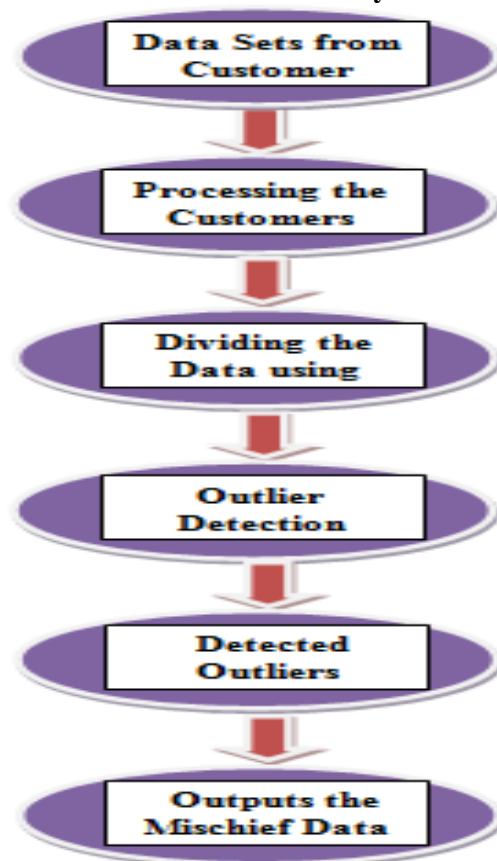


Figure 1: Fraud Detection System

Figure one shows the fraud detection system. Initially the data of the clients has been taken and split into group of similar data called clusters in second and third stage. From fourth stage onwards the standout data is find out using the outlier detection algorithm and if any listed.

IV. Methods for Detecting the Standout data

4.1 Clustering: Clustering helps the users to group the similar data into separate clusters or partitions. In this technique the data is broken down into related components. The goal of clustering is to find common patterns in the data or the similarity among the data. For clustering the customers data point can use the algorithms like k-means algorithm. This algorithm group the data as dense region and sparse region. This algorithm partitions 'n' observations into 'k' clusters. The cluster mean of $k_i = \{g_{i1}, g_{i2}, \dots, g_{im}\}$ is defined:

$$M_i = \frac{1}{m} \sum_{j=1}^m g_{ij}$$

The partitioned data region is shown in the following diagram Density Based Spatial Clustering Application with Noise (DBSCAN). This algorithm was designed to discover the clusters and noise in the data sets. Let us define, D be a data set of points a cluster with respect to EPS and MinPts is a non-empty subset of D satisfying the following conditions: 1. For all p,q: if p belongs to C and q is density-reachable from p with respect to EPS and MinPts then q belongs to C. 2. For all p, q belongs to C: p is density-connected to q with respect to with respect to EPS and MinPts.

4.2 Outlier Detection: Outliers are the data which deviate from the other observations. One has to use different mechanisms to detect outliers from the dense as well as from the sparse region. The data which deviates from the other data indicates the abnormal activity. It is based on the mean and standard deviation of the data observed. Outliers observed from the dense and sparse region is taken and it is ranked. The data with the severity is listed as fraudulent data.

V. OUDOLCCT Algorithms

This algorithm is used to find the outlier data points in on on-line credit card transactions.

```

REPEAT WHILE i <= n (in a sorted list)
  CHECK1 r(i) = r(i+1)
  CHECK2 r(i+1) = r(i+2)
  OUTPUT RESULT "Not an Outlier"
  (OR)
  OUTPUT RESULT "The Outlier is" r(i+2)
  END CHECK2
  (OR) OUTPUT RESULT "The Outlier is" r(i+1)
END of REPEAT.
(SORTED ON, DATE AND TIME IN ASENDING)

```

An arrangement of n objects in a given order is called a permutation of objects by taking all the objects at a time. An arrangements of any $r \leq n$ of these objects in a given order is called r-permutation. The permutations of n objects taken r at a time is denoted by $p(n,r)$, observes that the first element in an r-permutation of n objects can be chosen in n different ways, following. The second element in the permutation can be chosen in n-1 ways, then next element in n-2 ways, continues till the last element in n-r+1 ways. Then $p(n,r) = n(n-1)(n-2) \dots (n-r)$

VI. Discussions

Using this present system the unknown outliers are easily found. Supervised approach can found the anomalies and normal data easily; in contrast, unsupervised approach not uses the labeled records. It finds the mischief or strange data sets. To find the outliers, in this paper Clustering and outlier detection methods are used. Nearest neighbor in the data sets are clubbed using Clustering approaches, this present system extracts mischief transactions, if any, as outlier.

VII. Conclusions and Prospect

This paper presents a system to detect the mischief in online transactions. The clustering approaches are used to group the data sets and outlier detection algorithm presented is for finding the outliers. Finally the standout data is listed as outliers. In future, the algorithm presented in this paper is updated to find the stand out data in the real time.

Experimental Investigation of Flow Pattern on Rectangular Fin Arrays under Natural Convection

Vinod M. Wankar,¹ S.G. Taji²

¹(Student in Department of Mechanical, PES Modern College of Engineering, Pune, India)

²(Professor in Department of Mechanical PES Modern College of Engineering, Pune, India)

Abstract: In Natural convection heat transfer with the help of fin arrays, parameter are fin length to height ratio, spacing and orientation of geometry. In the longitudinally short fin array, where single chimney flow pattern is present hence heat transfer coefficient is high. In long rectangular fin arrays, air is stagnant at central zone hence it is not so much contributed in heat dissipation. In present study experimental setup is developed to studying the effect of natural convection over rectangular fin array. Fin spacing, height and heater input are the parameter study during experimentation. Lampblack coating is used to black fin surface. Flow patterns of various spacing's are investigated using smoke flow visualization techniques.

Keyword: Fin Arrays, Flow Visualization, Flow Pattern, Heat Transfer Coefficient, Natural convection.

NOMENCLATURE:

a = correlation constants

A_b = area of base

g = acceleration due to gravity

Gr = Grashoff's number

H = heat transfer coefficient

H = fin height

K = thermal conductivity

L = fin length

Nu_s = Nusselt number based on S

Nu_b = Nusselt number based on base

Ra = Rayleigh number

Q = heat transfer rate

S = fin spacing

T = temperature

Subscripts

a = Ambient

b = base

S = Fin spacing

I. INTRODUCTION

Natural convection cooling with the help of finned surfaces often offers an economical and trouble free solution in many situation. Fin arrays on horizontal and vertical surface are used in variety of engineering application to dissipate heat to surrounding. The main controlling variables generally available to the designer are the orientation and the geometry of the fin arrays. For effective dissipation of heat, plain horizontal surfaces facing upward are preferred since they provide relatively higher surface heat transfer coefficients than other orientations. Since the heat transfer coefficient strongly depends upon the mechanism of fluid flow, a thorough understanding of the resulting flow patterns from the fin array is also of much use to the designer. The problem of natural convection heat transfer from a rectangular fin array on a horizontal base surface has been studied experimentally by some investigators. In some of these investigations, flow visualization studies have been conducted aiming at the study of associated flow patterns.

II. LITERATURE REVIEW

Experimental work on horizontal fin arrays was studied by various authors. Starner and McManus [1] was the first one on the topic of natural convection heat transfer from rectangular fin arrays on horizontal surfaces. The purposed of investigation was to experimentally determined average heat transfer coefficients for rectangular fin arrays of various dimension. Harahap and McManus [2] extended the work of Starner and McManus with object of more fully investigating the other objectives of their study were to investigate flow field. The other objectives of their study were to investigate flow field. Jones and Smith [5] undertook their investigation with prime objective of establishing the optimum spacing of fins for maximum transfer from given base surface. They experimentally determined averaged heat transfer coefficient for horizontal arrays over a wide range of spacing. Mannan [4] studied the effect all pertinent geometrical parameter of fin array on its performance. His work covered wide range of length: 127mm to 508mm, height: 254mm to 1016mm and spacing: 4.8mm to 28.6mm with temperature difference varying from 39°C to 156°C. Sane and Sukhatme [6] considered the situation of an isothermal rectangular fin array on a horizontal surface.

III. EXPERIMENTAL SETUP

Experimental setup is constructed on the basis of simplicity and practicability. Fin flats are manufactured using 2 mm thick commercially available aluminum sheet cut to the size of 200 X 75 mm. Spacers are cut from same aluminum sheet. Some spacer of 2mm and 3mm thickness are also cut of required size and quantity. Basic dimension of fin array used

for experimentation are $L=200$ mm, $W=100$ mm, $H=40$ mm. These dimensions are decided by taking into account the convenience of measurement of surface temperature, input wattage as well as location of thermocouples so as to observe flow pattern by using simple smoke technique. This experiment deals with the study of natural convection, proper care is taken to avoid any effect of turbulent air flow around the fin array. An enclosure is fabricated in the form of cubical with a volume of approximately 1 m^3 . Three wall of cubical are enclosed with plywood sheets and front wall with acrylic sheet.

Top of the enclosure is kept open for undisturbed natural convection. The base plate of fin array was heated using cartridge type heater, which were given stabilized power input using dimmerstat. For realistic temperature measurement of the fin surface and ambient temperature, thirteen calibrated Cu-Constantan 36 gauge thermocouples, mounted at appropriate location are used. In order to account for heat dissipated by radiation black coating (using the black soot by burning camphor) is used. Symporex block placed at bottom and side of assembled array make provision four thermocouple to account the conduction loss through bottom and sides of the arrays. Two thermocouples are attached to the Bakelite plate to measure temperature. Schematic diagram of experimental setup showing electrical connection is shown in Fig 1. The fin array assembly is mounted inside the cavity of symporex block is as shown in Fig. 2.

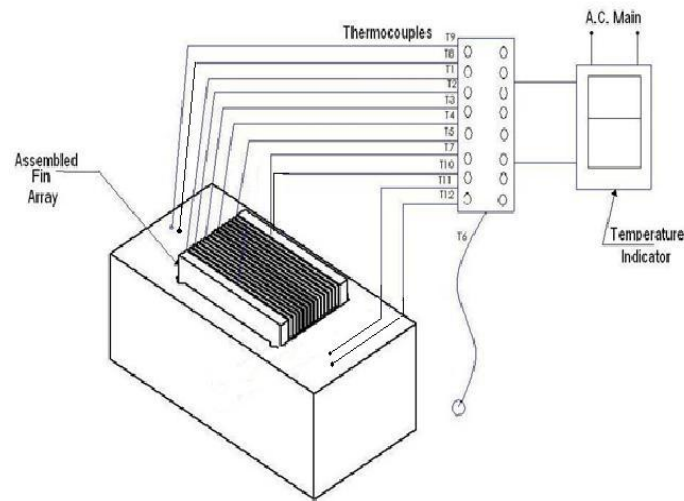


Fig. 1 Schematic diagram of experimental setup showing Electrical connection

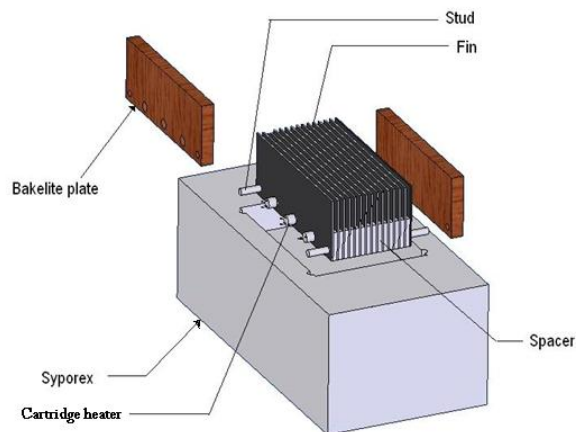


Fig. 2 Fin array assembly is mounted inside the cavity Of symporex block

IV. RESULT AND DISCUSSION

Fig. 3 shows the effect of fin spacing on h_a with heater input as the parameter. As the fin spacing increases the h_a increases for fin array, as expected. For 2-4 mm spacing h_a is very small i.e. in the range of 0.88 to $1.81 \text{ W/m}^2 \text{ K}$. The highest value of h_a is $5.7929 \text{ W/m}^2 \text{ K}$ at the spacing of 12 mm . The increasing trend is steep up to spacing about 9 mm after which there is a gradual rise. The percentage increase of h_a from 2 mm to optimum value is approximate 27% . Fig. 4 shows the effect of fin spacing on h_b with heater input as the parameter. From the Figure 4.2 it is clear that the values of h_b increases as fin spacing increases. It reaches to its maximum value ($h_b=40 \text{ W/m}^2 \text{ K}$) at fin spacing about 10 mm and again decreases ($h_b=18 \text{ W/m}^2 \text{ K}$). This trend can be attributed to restriction of entry of air in the channel at smaller fin spacing. The trend of increase in base heat transfer coefficient is observed from $S= 4$ to 10 mm and it is maximum at fin spacing 10 mm . At the

optimum spacing, h_b is nearly $40 \text{ W/m}^2 \text{ K}$ for the fin array. Fig. 5 shows variation of base Nusselt number with fin spacing to height ratio. It is observed that as the value of Nu_b increases as fin spacing increases from 4 to 8 mm. It reaches to its maximum value and again decreases. The reason for decrement in Nu_b may be due to the choking of fluid flow at smaller spacing for spacing 2 to 4 mm. Optimum fin spacing is decided by the highest value of base Nusselt number i.e. Nu_b is 53.35 at $S=10\text{mm}$. Nu_b is increased by 45% from spacing 2mm to 10mm. It is observed that the optimum fin spacing for the two arrays is in a band of 8 to 10 mm. Fig. 6 shows variation of h_a with ΔT . It is observed that as the value of ΔT increases with the value of h_a also increases. For spacing is 2 mm, h_a value is less than $0.884 \text{ W/m}^2 \text{ K}$ as spacing increases then it increases upto $5.7 \text{ W/m}^2 \text{ K}$ for spacing equal to 12 mm.

Fig. 7 shows a comprehensive plot of Nu_s vs Ra_s with previous investigators. On the same plot the present experimental data is superimposed. It is observed that the present data is confirming the trends obtained by previous investigators. Mannan shows a diversion from other investigator because of he has wide range of short fin arrays.

V. FLOW VISUALIZATION

In the present work flow visualization study is conducted by simple smoke technique using dhoop stick. Fig. 8 shows photographs of flow visualization by means of simple smoke studies using dhoop stick for heater input of 100W for the fin array under study. It is clear from the photographs that the single chimney flow pattern is obtained in higher spacing whereas fluctuating flow pattern found in 2mm to 4mm spacing. This confirms better performance of higher spacing fin array in terms of increase in the heat transfer coefficient.

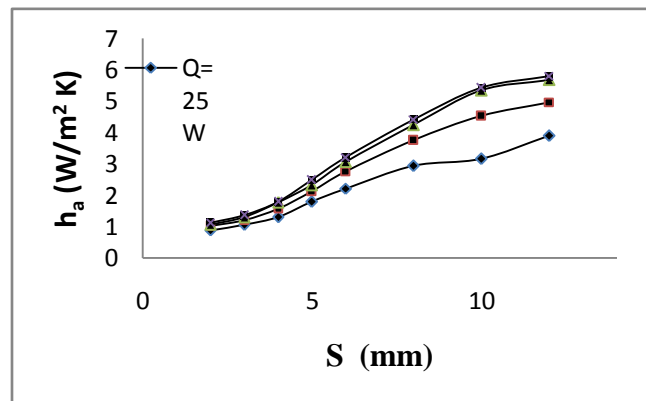


Fig 3: Variation of fin spacing 'S' with h_a

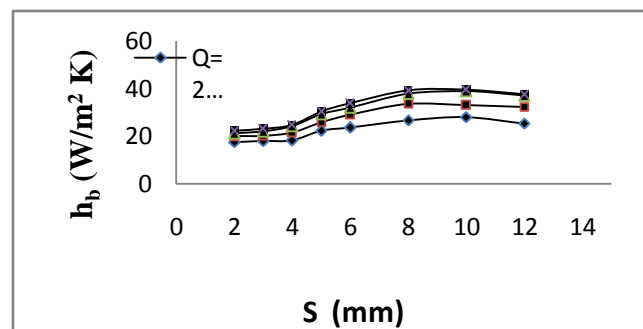


Fig 4: Variation of fin spacing 'S' with h_b

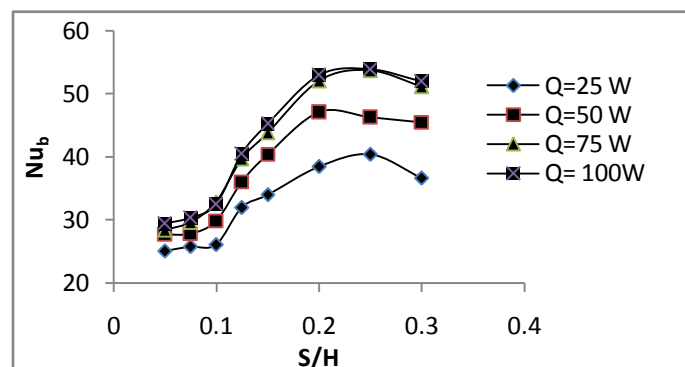


Fig. 5: Variation of 'S/H' with Nu_b

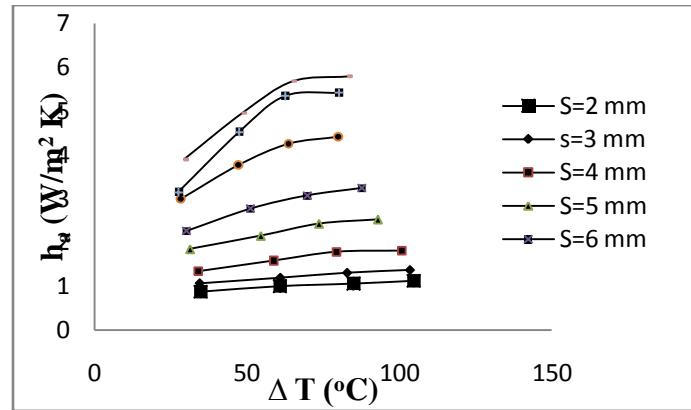


Fig. 6: Variation of ΔT with h_a

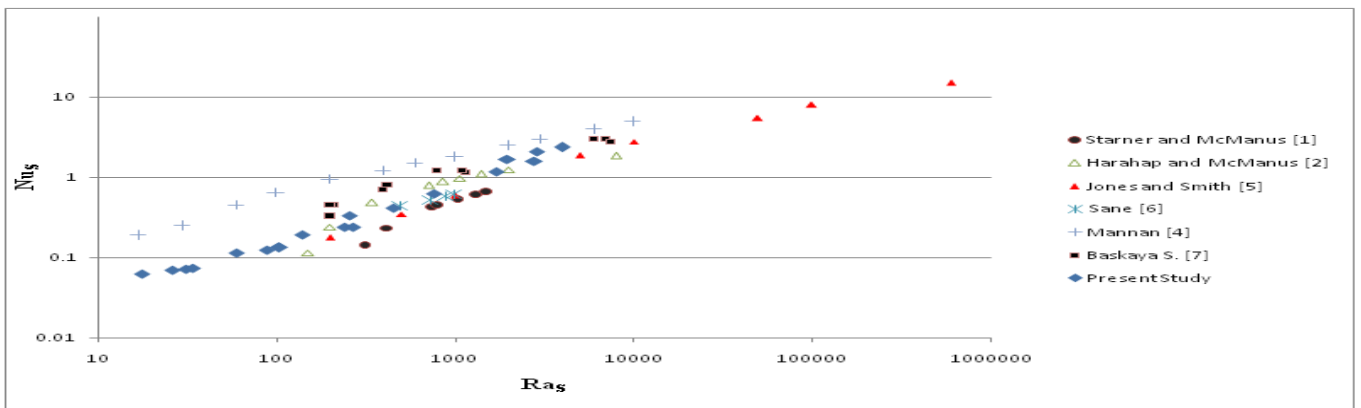


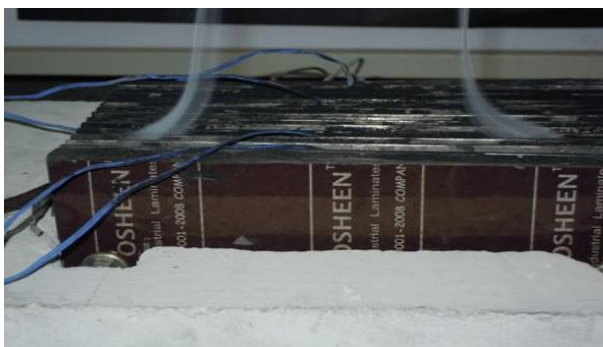
Fig. 7: variation of Ra_s with Nu_s



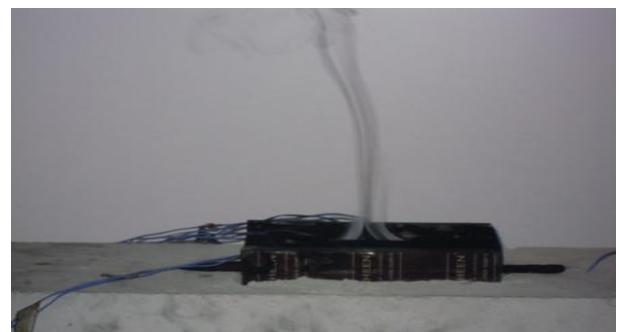
(a)



(b)



(c)



(d)

Fig.8: Flow pattern obtained with heater input of 100W

(a) 2mm (b) 4mm (c) 6mm (d) 12mm

VI. CONCLUSION

From the present study following conclusion are made:

- 1) Average heat transfer increase in optimum spacing 9-11 mm in Natural convection mode.
- 2) Fig. 7 shows experimental results also a good match with the previous experimental work reported on natural convection.
- 3) From experimental result it is observed that the heat transfer coefficient h_a is very small in case of spacing 2 mm to 4 mm (the range 0.88 W/m² K to 1.81 W/m² K) whereas h_a in case 6 to 12 mm (range of 1.9 W/m² K to 5.8 W/m² K). The percentages increased of h_a are 27% from 2mm to 12mm.
- 4) From experimental result it is observed that maximum value of Nu_a is 7.86 for 12mm spacing and maximum value of Nu_b is 58.35 for 10 mm spacing. Nu_a is increased by 81% from 2 to 12 mm spacing whereas Nu_b is increased by 27% from 2 to 10 mm spacing.
- 5) Base heat transfer coefficient values increase with optimum spacing and again decreases.
- 6) From flow visualization, it is observed that during spacing 2 mm to 4 mm the air entering from ends is not sufficient to cool the arrays and leaves before reaching central zone and single chimney flow pattern is not return.

REFERENCES

- [1] Starner K.E. and McManus Jr. 1963. An experimental investigation of free convection heat transfer from rectangular fin arrays. *Journal of Heat Transfer*. 85: 273-278.
- [2] F. Harahap, H.N. McManus Jr, Natural convection heat transfer from horizontal rectangular fin arrays, *Journal of Heat Transfer* 89 (1967) 32–38.
- [3] Dayan A., Kushnir R., Mittelman G. and Ullmann A. 2004. Laminar free convection underneath a downward facing hot fin array. *International Journal of Heat and Mass Transfer*. 47: 2849-2860.
- [4] Mannan K.D. 1970. An experimental investigation of rectangular fins on horizontal surfaces, Ph.D. Thesis, Ohio State University.
- [5] Charles D. Jones. And Lester. F. Smith. 1970. Optimum arrangement of rectangular fins on horizontal surfaces for free convection heat transfer. *ASME Journal of heat transfer*. 92: 6-10.
- [6] Sane N.K. and Sukhatme S.P. 1974. Natural convection heat transfer from rectangular fin arrays, 5th International heat Transfer conference, Tokyo, Japan, Vol. 3.
- [7] Baskaya S., Sivrioglu M., and Ozek M. "Parametric study of natural convection heat transfer from horizontal rectangular fin arrays", *International Journal of Thermal Science*, 39, 797–805 (2000).
- [8] Welling and Wooldridge. 1965. Free convection heat transfer coefficient from rectangular vertical fins. *Journal of Heat Transfer*, Trans ASME series C pp 438-444.
- [9] M. Mobedi and H. Yuncu 2003. A three dimensional numerical study on natural convection heat transfer from short horizontal rectangular fin arrays, *Heat Mass Transf.* 39 267–275.
- [10] Yuncu H. and Anbar G. 1998. An experimental investigation on performance of fins on a horizontal base in free convection heat transfer. *Sprigler-Verlag Heidelberg, Heat and Mass Transfer*. 33: 507-514.
- [11] Sobhan C.B., Venkateshan S.P and Seetharamu K.N. 1989. Experimental analysis of unsteady free convection heat transfer from horizontal fin arrays. *Warne-and Stoffubertragung, Springer-Verlag*. 24: 155-160.
- [12] Dharma Rao V., Naidu S.V., Govinda Rao B. and Sharma K.V. 2006. Heat transfer from horizontal fin array by natural convection and radiation-A conjugate analysis. *International Journal of Heat and Mass Transfer*. 49: 3379-3391.

Comprehensive Long-Run Incremental Cost (LRIC)-Voltage Network Pricing Approach to Support Network Voltages Given Contingencies

E. Matlotse,¹ E.T. Rakgati²

^{1,2}Edwin Matlotse is with the Department of Electrical Engineering, University of Botswana, Botswana,

Abstract: *most network charges are based on components' thermal limits providing correct economic signals to reinforcing network transformers and lines. However, less attention is drawn to the reinforcement cost driven by nodal voltage limits, particularly those resulting from contingencies. In this work, a new charging approach is proposed in which busbar power perturbation is linked to busbar voltage degradation rate which, in turn, is related to the incremental investment cost required to maintain voltage levels. The incremental cost results by employing the use of the nodal voltage spare capacity to gauge the time to invest in a reactive power compensation device for a defined load growth rate. The time to invest takes into account the network nodal voltage profiles under N-1 circuit contingencies (one line outage at a time). Further, the nodal MW and MVar perturbations are considered in this paper. This novel approach is demonstrated on the IEEE 14 bus network, illustrating the difference in charges when considering contingencies, therefore, providing correct forward-looking economic signals to potential network users. In turn, this will help them make informed decisions as to whether to invest in reactive power compensation assets or pay the network operators for reactive power provision. Most importantly, this new approach outperforms the currently used power factor (pf) penalty.*

Index Terms: *Base LRIC-voltage network charges, CF LRIC-voltage network charges, lower Nodal Voltage Limit, Upper Nodal Voltage Limit, Contingency Factors, Spare nodal voltage capacity and VAr compensation assets.*

I. INTRODUCTION

ONE of the fundamental requirements for network operators is to ensure that network nodal voltages are within prescribed limits. The natural way of achieving this is by having reactive power sources (static and dynamic devices) distributed through-out the entire network during its steady state operation and when its experiencing credible contingencies. The extent at which this can be achieved is sometimes limited by the availability of funds. In this regard, reasonable funding can be used to install just adequate reactive power sources and, then as a measure of enhancement, an appropriate economic model can be used to charge for the use of the network reactive power compensation assets to ensure that network voltages are within predetermined limits. Also, it should be noted that it is a requirement for network operators to operate their infrastructure subject to N-1 circuit contingencies (outage of each line at a time) to guarantee that it operates reliably and securely. This is even more important under the prevailing worldwide trend of privatization and

Restructuring of the respective power systems as voltage instability incidents

Have been experienced in a number of countries. These, at times, led to several major voltage collapse scenarios. The Aforementioned voltage instability is due to power systems operated tightly to their transmission capability limits against the backdrop of economic and environmental concerns. The problem is often compounded by delays in developing transmission lines resulting from lengthy and complex approval processes, particular regarding interconnected independent power systems. These aforementioned effects make it difficult to master the control of reactive power demand and, hence, difficult to retain network nodal voltages within prescribed limits.

Most research in reactive power pricing [1]-[12] reflects the operational cost related to reactive power due to new customers, i.e. how they might affect network losses. Also, network reactive power pricing has generated substantial research interests into methodologies to reflect investment costs incurred in network when supporting nodal real and reactive power injection/withdrawal [13], [14]-[33], however, the network investment costs are restricted to the circuits and transformers triggered by thermal limits. Further, this investment does not account for contingencies. The investment cost-related price (ICRP) charging model [34] used in the UK does not consider the network security requirement in the model, but it relies on post-processing through a full-contingency analysis to give an average security factor of 1.86 for all concerned network assets. Based upon those latter methodologies, particularly those in [20], [26] and [30], the first approach to charge for the cost of supporting network nodal voltages was developed [35], but does not consider the effect on the reinforcement cost from contingencies, hence, it does not consider the additional stress to the network when contingencies occur. Further, authors of [36] presented a study on the approach on [35] i.e. LRIC-voltage network charges given different network R/X ratios to demonstrate the practical reality of a network ranging from a transmission to distribution infrastructure. On the other hand, authors of [37]-[40] considered the N-1 contingency analysis into their charging principles and all of these were for pricing of network circuits and transformers based on the thermal use of the network. Paper [14] demonstrated a simplistic approach to account for N-1 contingencies based on the assumption that reinforcement is required when a branch thermal power flow reaches 50% of its capacity. Therefore, it is against this background that in this research an approach that factor in the effect of N-1 contingencies in the LRIC-voltage network charging model in proposed.

This paper is concerned with development of network charges that account for reinforcement cost triggered by busbar voltage limits under N-1 contingencies. Further, these are compared with those under normal conditions of the network. This charging principle employs the use of the unused nodal voltage capacity or headroom within an existing network to gauge time to invest in reactive power compensation device for each node in the system. A nodal withdrawal/injection of real/reactive power will impact on the nodal voltage, which in turn impact on the time to reinforce reactive power compensation devices. LRIC-V network charges are the difference in the present value of future Var compensation devices with and without the nodal perturbation, providing an economically efficient forward-looking pricing signal to influence the siting and/or reactive power consumption of demand and generation for bettering network voltage profile. It should be noted and emphasized that this paper demonstrates the charging model at nodes without VAr compensation assets (future VAr assets) and later (not part of this paper) this undertaking would be extended to nodes with compensation assets (existing VAr assets). Ultimately, the reactive power planning (RPP) problem (also, not part of this paper) would be integrated with the LRIC-voltage network pricing approach, to price for the future and the existing network VAr compensation assets as the most practical approach to employ. In this case, N-1 circuit contingencies should be considered.

This paper is organized as follows: Section II details the mathematical models of the LRIC-voltage network charging (base LRIC) principle under normal state and the impact to network voltages when considering N-1 contingencies and the resulting LRIC-voltage network charging formulation considering N-1 contingencies (CF LRIC). Section III provides comparison and analyses of LRIC-voltage charges with and without considering N-1 contingencies on an IEEE 14 bus network. The paper's conclusions are drawn in Section IV. Section V provides for Appendix which outlines the loading condition of the test system while References are depicted in Section VI...

II. MATHEMATICAL FORMULATION OF LONG-RUN INCREMENTAL COST PRICING BASED ON NODAL SPARE CAPACITY

The LRIC-V network charging principle is based upon the premise that for an assumed nodal generation/load growth rate there will be an associated rate of busbar voltage degradation. Given this assumption the time horizon for a busbar to reach its upper /lower voltage limit can be evaluated. Once the limit has been reached, a compensation device will be placed at the node as the future network reinforcement to support the network voltage profiles. A nodal demand/generation increment would affect the future investment horizon. The nodal voltage charge would then be the difference in the present value of the future reinforcement consequent to voltage with and without the nodal increment

In this section, the nodal base LRIC-V network charging principle formulation would be outlined. Thereafter, the formulation to reflect the nodal voltage impact on buses

resulting from N-1 contingencies would be shown. Finally, this effect of N-1 contingencies would be factored into the former charging principle to constitute CF (contingency factor) LRIC-voltage network charges.

A. Base LRIC-Voltage Network Charging Principle

The following steps outlined below can be utilized to implement this charging model:

1) Evaluating the future investment cost of network VAr compensation assets to support existing customers

If a network node b , has lower voltage limit, V_L and upper voltage limit V_H , and holds a voltage level of V_b , then the number of years for the voltage to grow from V_b to V_L/V_H for a given voltage degradation rate v_r can be evaluated from (1.a) or (1.b).

If V_L is critical, i.e, bus voltage is less than target voltage, 1 pu :

$$V_L = V_b \times (1 - v_r)^{n_{bL}}$$

(1.a)

On the other hand if V_H is critical, i.e, bus voltage is more than target voltage, 1 pu :

$$V_H = V_b \times (1 + v_r)^{n_{bH}}$$

(1.b)

Where: n_{bL} and n_{bH} are the respective numbers of years that takes V_b to reach V_L/V_H .

Reconfiguring equations (1.a) and (1.b) constitute:

$$(1 - v_r)^{n_{bL}} = \frac{V_L}{V_b}$$

(2.a)

$$(1 + v_r)^{n_{bH}} = \frac{V_H}{V_b}$$

(2.b)

Then the values of n_{bL}/n_{bH} are

$$n_{bL} = \frac{\log V_L - \log V_b}{\log(1 - v_r)}$$

(3.a)

$$n_{bH} = \frac{\log V_H - \log V_b}{\log(1 + v_r)}$$

(3.b)

The assumption is that when the node is fully loaded the reinforcement will take effect. This means that investment will be effected in n_{bL}/n_{bH} years when the node utilization reaches V_L/V_H , respectively. At this point an installation of a VAr compensation asset is regarded as the future investment that will be needed at the node to support the voltage.

2) Determining the present value of future investment cost

For a given discount rate of d , the present value of the future investment in n_{bL}/n_{bH} years will be:

$$PV_{bL} = \frac{Asset_{CbL}}{(1+d)^{n_{bL}}} \quad (4.a)$$

$$PV_{bH} = \frac{Asset_{CbH}}{(1+d)^{n_{bH}}} \quad (4.b)$$

Where $Asset_{CbL}$ and $Asset_{CbH}$ are the modern equivalent asset cost to cater for supporting voltage due to lower voltage limit and upper voltage limit violations, respectively.

3). Deriving the incremental cost as a result of an additional power injection or withdrawal at node N

If the nodal voltage change is $\Delta V_{bL}/\Delta V_{bH}$ consequent upon an additional ΔQ_{In} withdrawal/injection at node N, this will bring forward/delay the future investment from year n_{bL}/n_{bH} to n_{bnewL}/n_{bnewH} and when V_L is critical

$$\text{For withdrawal } V_L = (V_b - \Delta V_{bL}) \times (1 - v_r)^{n_{bnewL}} \quad (5.a)$$

or

$$\text{For injection } V_L = (V_b + \Delta V_{bH}) \times (1 - v_r)^{n_{bnewL}} \quad (5.b)$$

And when V_H is critical

$$\text{For withdrawal } V_H = (V_b - \Delta V_{bL}) \times (1 + v_r)^{n_{bnewH}} \quad (5.c)$$

or

$$\text{For injection } V_H = (V_b + \Delta V_{bH}) \times (1 + v_r)^{n_{bnewH}} \quad (5.d)$$

Equations (6.a), (6.b), (6.c) and (6.d) give the new investment horizons as

$$n_{bnewL} = \frac{\log V_L - \log(V_b - \Delta V_{bL})}{\log(1 - v_r)} \quad (6.a)$$

or

$$n_{bnewL} = \frac{\log V_L - \log(V_b + \Delta V_{bH})}{\log(1 - v_r)} \quad (6.b)$$

$$n_{bnewH} = \frac{\log V_H - \log(V_b - \Delta V_{bL})}{\log(1 + v_r)} \quad (6.c)$$

or

$$n_{bnewH} = \frac{\log V_H - \log(V_b + \Delta V_{bH})}{\log(1 + v_r)} \quad (6.d)$$

Then the new present values of the future investments are

$$PV_{bnewL} = \frac{Asset_{CbL}}{(1+d)^{n_{bnewL}}} \quad (7.a)$$

$$PV_{bnewH} = \frac{Asset_{CbH}}{(1+d)^{n_{bnewH}}} \quad (7.b)$$

The changes in the present values as consequent of the nodal withdrawal/injection ΔQ_{In} are given by (8.a) and (8.b)

$$\Delta PV_{bL} = PV_{bnewL} - PV_{bL} \quad (8.a)$$

$$\Delta PV_{bH} = PV_{bnewH} - PV_{bH} \quad (8.b)$$

The annualized incremental cost of the network items associated with component b is the difference in the present values of the future investment due to the reactive power magnitude change $\Delta Q_{In}/\Delta P_{In}$ at node N multiplied by an annuity factor

$$IV_{bL} = \Delta PV_{bL} * \text{annuityfactor} \quad (9.a)$$

$$IV_{bH} = \Delta PV_{bH} * \text{annuityfactor} \quad (9.b)$$

4) Evaluating the long-run incremental cost

If there are a total of bL busbars' lower limits and bH busbars' high limits that are affected by a nodal increment from N , then the LRIC-V network charges at node N will be the aggregation of the changes in present value of future incremental costs over all affected nodes:

$$LRIC_{-V_{N,L}} = \frac{\sum_{bL} IV_{bL}}{\Delta Q_{In} / \Delta P_{In}} \quad (10.a)$$

$$LRIC_{-V_{N,H}} = \frac{\sum_{bH} IV_{bH}}{\Delta Q_{In} / \Delta P_{In}} \quad (10.b)$$

B. Impact to Network Voltage When Considering N-1 Contingencies

If a network node b supports voltage V_b under the normal state and has to carry an additional voltage of ΔV_L due to the most severe N-1 contingency situation, then the contingency factor at that node can be determined by (11)

$$CF_L = \frac{V_b + \Delta V_L}{V_b} \quad (11)$$

Given the node has to withstand additional voltage disturbance, where the magnitude of the disturbance is indicated by contingency factor, CF_L , the system cannot be allowed to operate to its limits. Instead, the maximum

allowed voltage level at each busbar has to be modified to cater for potential contingencies. This new nodal voltage limit for the lower bus voltage limit can be determined by (12)

$$V_{b_{cf_L}} = \frac{V_L}{CF_L}$$

(12)

On the other hand, if a network node b supports voltage V_b under normal state and has to carry an additional voltage of ΔV_H due to the most severe N-1 contingency situation, then the contingency factor at that node can be determined by (13)

$$CF_H = \frac{V_b + \Delta V_H}{V_b}$$

(13)

Given the node has to withstand additional voltage disturbance, where the magnitude of the disturbance is indicated by contingency factor, CF_H , the system cannot be allowed to operate to its limits. Instead, the maximum allowed voltage level at each busbar has to be modified to cater for potential contingencies. This new nodal voltage $V_{b_{cf_H}}$ limit for the higher bus voltage limit can be determined by (14)

$$V_{b_{cf_H}} = \frac{V_H}{CF_H}$$

(14)

C. CF LRIC-Voltage Network Charges

Given the newly determined network lower bus limit, $V_{b_{cf_L}}$, and higher bus limit, $V_{b_{cf_H}}$, to support N-1 contingencies, these can be utilized in the LRIC-v charging principle to formulate the CF LRIC-voltage network charges by replacing V_L by the former new limit while replacing V_H by the latter new limit in the relevant equations above.

III. IMPLEMENTATION

1. Test System

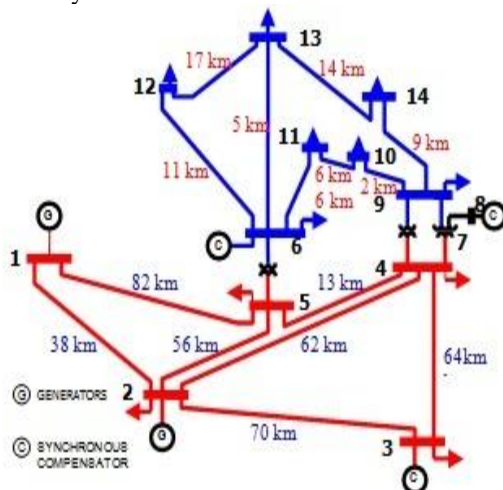


Fig. 1: IEEE 14 Bus System

The test system shown above in Fig. 1 is the IEEE 14 bus network, the load and generation data of this network are shown in the appendix section. This network consists of 275kV sub transmission voltage level shown in red and the 132kV distribution voltage level shown in blue. There are two generators and three synchronous compensators. The synchronous compensators boost the voltage at buses 3, 6, 8 since the subtransmission lines are fairly long. It is also worthwhile to note that, these synchronous compensators have reached their full capacities and, therefore, they cannot maintain their respective bus voltages at pre-set voltage levels and, as such, during withdrawals/injections, voltage changes are experienced at the buses where these are connected. The line distances between the buses are depicted in blue and red for the sub transmission and distribution levels, respectively. The compensation assets (SVCs) have the investment costs of £1, 452,000 and £696, 960 at the 275-kV and 132-kV voltage levels, respectively.

Bus 1 is the slack bus. The voltage limits are assumed to be $1 \pm 6\%$ pu. The use of power flow was employed to capture the nodal voltages while performing nodal withdrawals/injections on the system. The annual load growth for this test network is assumed to be 1.6% while the discount rate is assumed to be 6.9%.

A. Base LRIC-Voltage Network Charges

The base LRIC-v network charges are determined by injecting/withdrawing 1 MVar/1 MW at every node of the system without subjecting the system to N-1 contingencies.

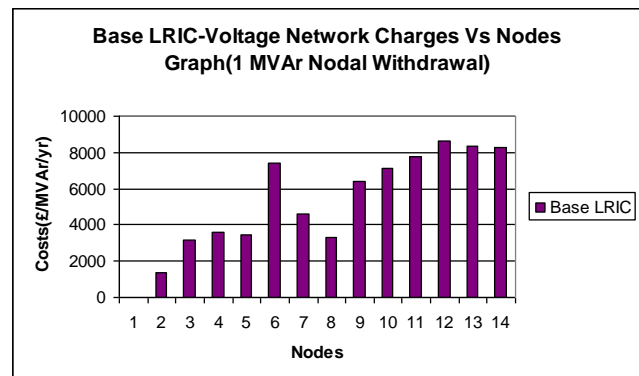


Fig. 2: Base Nodal LRIC-Voltage Network Charges per MVar withdrawal

Buses 2, 7 and 8 have their initial voltages greater than the target voltage of 1 pu while the rest of buses excluding the slack bus have their initial voltages below 1 pu.

Withdrawing reactive power would help buses 2, 7, and 8 to be closer to the target voltage, thus should be rewarded for increasing the margins of the already critical busbar upper voltage limits. Customers at these buses are incentivized to take reactive power from the network as the investment horizons of the VAr compensation assets at the respective bus are deferred. While the rest of the buses excluding the slack bus are penalized for reactive power withdrawal as it decrease the margins to the lower voltage limits since this action advance the investment horizons of the VAr compensation assets at the study bus. Although individual busbars may have charges or credits against the

same nodal withdrawal, the nodal LRIC-voltage network price in this system is a charge against each node, since the price accounts for the system wide effects from a nodal withdrawal, the credits from buses 2, 7 and 8 are far less than the accumulated charges from the rest of the busbars.

It can also be observed that the LRIC-voltage network charges generally increase with increasing distance. Bus 3 has the largest distance but the charge is comparably small, This is because the bus is connected with a synchronous Condenser which boosts the voltage at that bus. The same occurs at bus 6 and 8. The charge at bus 8 is smaller than at bus 7 since bus 8 has its voltage boosted. Even though Bus 14 has a larger distance than buses 12 and 13, as withdrawing from this node has a larger impact to buses 7 and 8 which earn larger credit contributing to reduced overall charge. The same applies to bus 13 since it is closer to buses 7 and 8 than bus 12. Bus 12 under the aforementioned circumstances attracts the most charge since it is further from buses 7 and 8 than buses 13 and 14 resulting in less credit at buses 7 and 8 in contribution to the overall higher charge at this bus. Bus 2 has the least charge since it is closer to the slack bus.

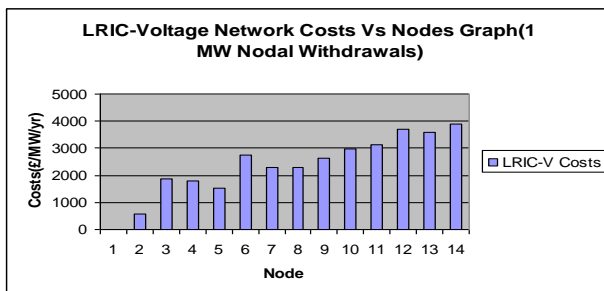


Fig. 3: Base LRIC-Voltage Network Charges due to 1MW nodal withdrawal

As it can be observed from **Fig. 3**, the LRIC-v charges follow the same pattern as those of MVar nodal withdrawals in **Fig. 2** since the conditions are the same as the latter case, in terms of, respective nodal distances from the slack bus and the initial voltages before nodal withdrawals. However, during the MW withdrawals, the nodal voltages are degraded less than in the case with MVar withdrawals and, hence, less resulting LRIC-v network costs. This owes to the fact that the resulting network circuit reactance (X) is more than the resulting network circuit resistance (R).

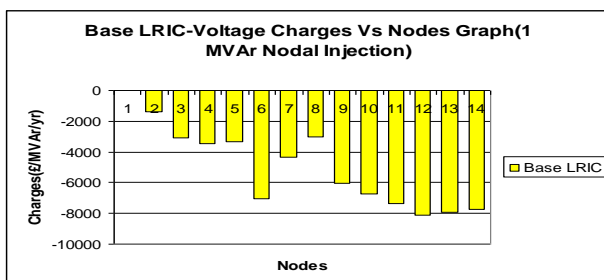


Fig. 4: Base LRIC-Voltage Network Charges due to 1MVar nodal injections

Fig. 4 shows benefits against buses given 1 MVar nodal injections.

During nodal injections, the buses (2, 7 & 8) having their initial voltages above 1 pu are penalized for degrading the already critical busbar upper voltage limits while the rest except the slack bus are credited for relieving the already critical busbar lower voltage limits. The same reasons as for nodal withdrawals hold as the overall result is that all buses earn credits. Also, observed is that the credits increase as distances increase. The conditions in this case are the same as for the previous case of **Fig.2**, therefore, the pattern remains the same, in that, Bus 12 attracts the most credit while Bus 2 attracts the least.

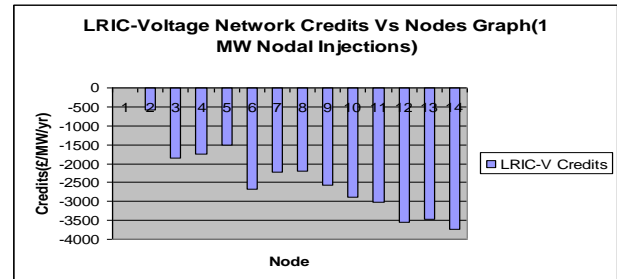


Fig. 5: Base LRIC-Voltage Network Charges due to 1MW nodal injections

It can also be observed from **Fig. 5**, that the LRIC-v charges follow the same pattern as those of MVar nodal injections, but with less LRIC-v credits for the same reasons relating to the differences depicted above for the MVar and MW withdrawals.

B. Contingency Factor Terms

The nodal contingency factors reflect additional voltage change that would be incurred following the worst contingency. Since every network bus has both the lower and upper limits, the contingency factors to cater for both of these limits on each bus were determined, subject to N-1 contingencies.

Fig. 6 and **TABLE 1** show lower voltage limit contingency factors against nodes. In addition, **TABLE 1** shows initial, and outage voltages and the resulting lower nodal voltage limits.

On the other hand, **Fig. 7** and **TABLE 2** show higher Voltage limits contingency factors against nodes. In addition, **TABLE 2** shows initial, and outage voltages and the Resulting higher nodal voltage limits.

1. Test System CF_L

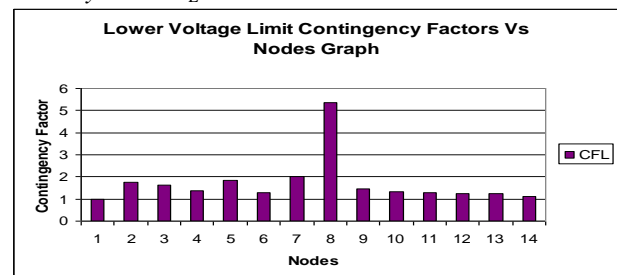


Fig. 6: IEEE 14 bus system lower voltage limit contingency factors at each node

TABLE 1

LOWER NODAL VOLTAGE LIMIT CONTINGENCY FACTORS
SUBJECT TO N-1 CONTINGENCIES

Bus	Initial Voltage (pu)	Outage Voltage (pu)	CF _L	Resulting VL (pu)
1	1.03	1.03	1	0.94
2	1.02	0.99	1.752	0.992
3	0.996	0.954	1.646	0.987
4	0.988	0.962	1.374	0.973
5	0.995	0.941	1.83	0.994
6	0.982	0.96	1.284	0.967
7	1.008	0.955	2.015	1.000
8	1.048	0.998	5.345	1.038
9	0.981	0.947	1.442	0.977
10	0.974	0.946	1.314	0.969
11	0.974	0.95	1.281	0.966
12	0.967	0.945	1.244	0.964
13	0.963	0.94	1.239	0.963
14	0.954	0.943	1.099	0.951

HIGHER NODAL VOLTAGE LIMIT CONTINGENCY FACTORS
SUBJECT TO N-1 CONTINGENCIES

Bus	Initial Voltage (pu)	Outage Voltage (u)	CF _H	Resulting VH (pu)
1	1.03	1.03	1	1.06
2	1.02	1.02	1.001	1.060
3	0.996	1	1.081	1.051
4	0.988	0.989	1.02	1.058
5	0.995	0.999	1.07	1.052
6	0.982	0.986	1.088	1.050
7	1.008	1.052	1.644	1.013
8	1.048	1.056	1.068	1.052
9	0.981	0.992	1.268	1.035
10	0.974	0.977	1.097	1.049
11	0.974	0.975	1.029	1.057
12	0.967	0.971	1.12	1.047
13	0.963	0.968	1.222	1.038
14	0.954	0.955	1.089	1.050

Fig. 6 shows a plot of CF_L values against nodes given the most severe N-1 contingency condition impacting on each lower voltage bus limit on the IEEE 14 bus test system. TABLE 1 also shows the CF_L values against nodes and in addition the initial voltages before the outages, the outage voltages and the resulting new lower voltage limits.

The largest CF_L is recorded at bus 8. The most severe outage on this bus was when the line between buses 2 and 3 is outaged. This particular line was critical in supplying the necessary apparent power to support the load at bus 3. During this outage, all the apparent power had to be re-routed along the line between buses 3 and 4. This caused the voltage at bus 8 to drop from 1.048 pu to 0.998 pu which corresponds to a bus loading variation from 9.73% to 52% with respect to the lower voltage limit. The CF_L value at bus 7 is the second largest since both aforementioned buses were severely affected by the same outage. The least CF_L value is at the slack bus since the voltage at this bus remains the same across all the outages.

The results generally show that the more the CF_L values the more reduced the resulting nodal lower voltage limits.

Fig. 7 shows a plot of CF_H values against nodes given the most severe N-1 contingency condition impacting on each higher voltage bus limit on the IEEE 14 bus test system. TABLE 2 also shows the CF_H values against nodes and in addition the initial voltages before the outages, the outage voltages and the resulting higher voltage limits.

The largest CF_H value is recorded at bus 7. The most Severe outage on this bus is when the line between buses 7 and 9 was taken out. This outage resulted in a large voltage rise at this bus since this line was critical in linking the sub Transmission and most of the distribution side of the network. Due to this outage the power was re-routed from the line connecting the slack bus to bus 5 and eventually from bus 5 through to bus 6 through the transformer to other buses. The voltage rised from 1.008 Pu to 1.052 Pu This constituted bus loading variation from 56.67% to 93.17% with reference to the higher voltage limit. The least CF_H value is also at the slack bus since the voltage at this bus remains the same across all the outages.

The results generally show that the more the CF_H values the more reduced the resulting nodal higher voltage limits.

2. Test System CF_H

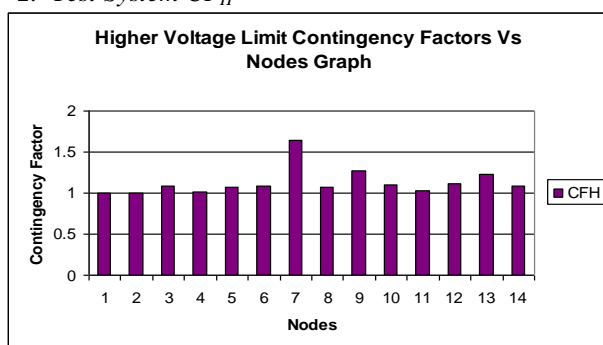


Fig. 7: IEEE 14 bus system higher voltage limit contingency factors at each node
TABLE 2`

C. CF LRIC-Voltage Network Charges

After calculating the contingency factors for the corresponding lower and higher nodal voltage limits then the CF LRIC-voltage network charges were determined based on those new limits.

Fig. 8 and **Fig. 9** show CF LRIC-voltage network charges due to 1 MVar and 1MW nodal withdrawals, respectively. On the other hand, **Fig. 10** and **Fig. 11** show CF LRIC-voltage network charges due to 1 MVar and MW nodal injections, respectively.

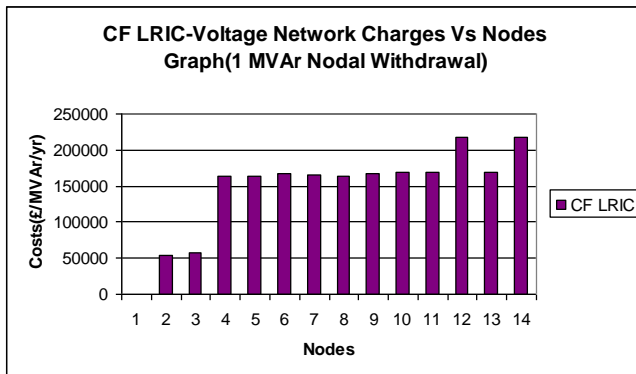


Fig. 8: CF LRIC-voltage network charges due to 1 MVar withdrawal at each node

Since the lower nodal voltage limit margins have been reduced to support N-1 contingencies, during nodal withdrawals, a number of lower voltage limits have been reached therefore reinforcements indications were as follows:

- 1) During withdrawals at buses 2 and 3, the lower voltage limit at bus 13 was reached; therefore, a reinforcement cost was attracted at this bus. At other buses during these respective withdrawals, some attracted credits (buses 2, 7 and 8) while the rest excluding the slack bus attracted costs for degrading the respective lower voltage limit margins. Since bus 3 has more distance from the slack bus it attracted more cost than bus 2.
- 2) During withdrawals at buses 4, 5, 6, 7, 8, 9, 10, 11 & 13 there were lower voltage limit violations at buses 5, and 13, as such, these attracted reinforcement costs.
- 3) During withdrawal at bus 12, buses 5, 12 and 13 had their lower voltage limits reached and, as such, attracted reinforcement costs.
- 4) Lastly, during withdrawal at bus 14, buses 5, 13 and 14 had their lower voltage limits reached; therefore, they attracted some reinforcement costs.

Since buses 12 and 14 attracted three reinforcement costs have their costs around £218,000.00 while buses 2 and 3 have the least costs around £55,000.00 and £58,000.00 respectively since they attracted only one reinforcement costs.

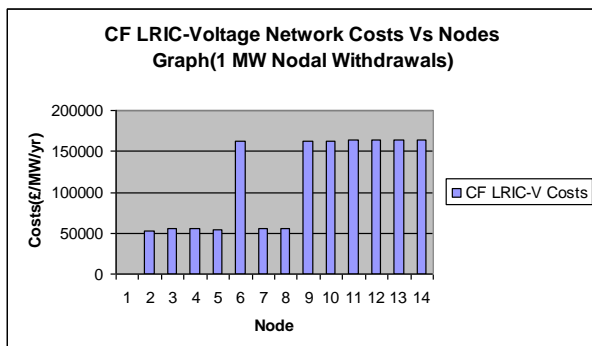


Fig. 9: CF LRIC-voltage network charges due to 1 MW withdrawal at each node

During 1 MW nodal withdrawals, the nodal voltage changes were relative smaller than in the MVar nodal withdrawals' case and, as such, the number of nodal lower voltage limits reached was few, hence, less comparable

nodal costs. The following number of nodal lower voltage limits has been reached, therefore, reinforcements indications were as follows:

- 1) During MW withdrawals at buses 2, 3, 4, 5, 7 and 8, reinforcements were triggered at bus 13.
- 2) MW withdrawals at buses 6, 9, 10, 11, 12, 13 and 14 triggered reinforcements at buses 5 and 13.

Given the above triggered reinforcements, buses 2, 3, 4, 5, 7 and 8 attract costs around the region of £52, 865.00 to £55, and 881.00 since they all triggered one reinforcement investment. On the other hand, the rest of the buses, excluding the slack bus, triggered two reinforcement investments, therefore, comparatively more costs ranging from £162, 645.00 to £163, and 955.00. However, the costs are relatively more during the 1 MVar withdrawals since up to three reinforcement investments were triggered.

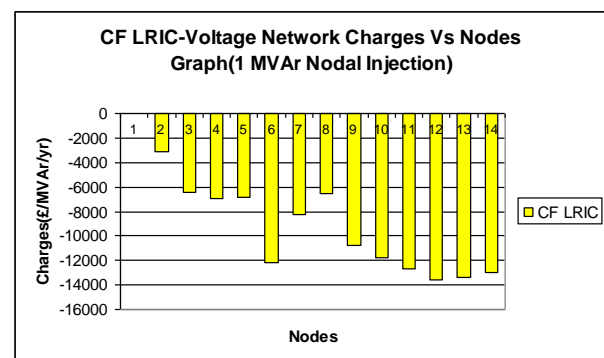


Fig. 10: CF LRIC-voltage network charges due to 1 MVar injection at each node

During nodal injections, there were not limits reached. It should be noted that the ranges of nodal voltage limits with contingency factors considered is less than that without contingency factors considered. This factor leads to more nodal credits for CF LRIC-voltage network charges than base LRIC-voltage network charges. It should also be noted that the nodal credits follow the same pattern as the case without considering the contingency factors but only increased credits, therefore bus 12 attracts the most credits while bus 2 the least.

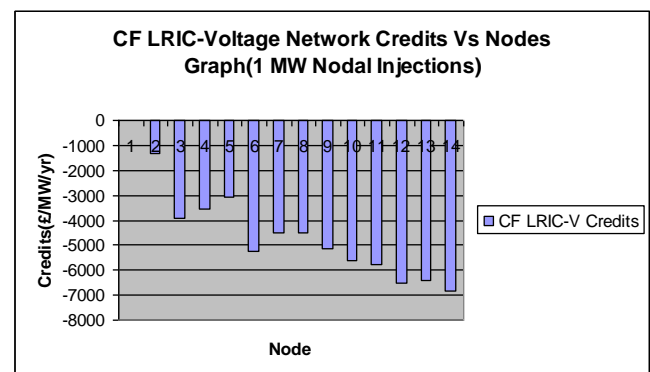


Fig. 11: CF LRIC-voltage network charges due to 1 MW injection at each node

It can be seen from **Fig. 11** that the results follow the same pattern as those of **Fig. 5**, but, the credits sought in the former case are small than in the latter one since the

network resulting reactance (X) is more than the corresponding resulting resistance (R) and, hence, less network nodal voltage increments.

IV. CONCLUSIONS

This paper presents a novel long-run incremental cost (LRIC) pricing principle to price the cost of network reactive power compensation for keeping the system voltages within statutory limits when subjected to N-1 contingencies. This principle is based on the spare nodal voltage capacity of an existing network to reflect the impact to the network wide voltage profile and the cost of future network VAr compensation consequent upon a nodal injection/withdrawal, i.e. whether they accelerate or delay the need for future network compensation devices. The model is thus cost-reflective and able to provide forward-looking economic signals to influence network users' behavior in order to minimize the cost of future investment in VAr compensation. Most importantly, these principles integrate the MW and MVar perturbations.

The separation of pricing the use of network for carrying reactive power (the use of circuits and transformers) and Generating reactive power (the use of VAr compensation Devices) also adds further clarity thus transparency to network users of their respective impact to the future network investment.

This study was carried-out on a 14-bus network. The major findings from the demonstrations are summarized as follows:

- 1) Both the Base and CF LRIC-V network charges increase as the nodal withdrawal/injection distances increase from the slack bus and the extent at which the buses are utilized.
- 2) the base LRIC-V network charges do not take into Account N-1 contingencies which are a statutory requirement for network operators to maintain security of supply, therefore, provide incorrect price signals.
- 3) The CF LRIC-V network charges consider N-1 contingencies, accounting for the additional cost brought to the network operator, therefore, provide more cost-reflective economic signals for network users to make informed decisions.
- 4) The CF LRIC-V network charges are more than base LRIC-V network charges since each network bus voltage Limit range (both the lower and higher limit margins are Reduced) used for determining the former is reduced to Accommodate the constraints of supporting N-1 Contingencies and, as such, each network bus headroom is Inherently reduced.

This paper demonstrated a very simplistic approach to determine the cost/benefit of LRIC-voltage network charges on a system subjected to N-1 contingencies (which is a statutory requirement for network operators) and, further, compared the charges when these contingencies are considered and when not considered. The charges with N-1 contingencies provide better economic signals to potential network users which, in turn, will help them to exercise an economic choice as to whether to invest in reactive power devices or pay the network operators for reactive power provision. Ultimately, this will guide towards an effective

and efficient usage of the network's reactive power resources.

Compared with the currently used power factor (pf) penalty, the proposed novel LRIC-voltage network charging principle is able to provide correct nodal forward-looking charges, incentivizing those network users who defer overall network investment in VAr compensation costs and, otherwise, penalize those who bring closer the network VAr compensation investment horizons. It should be noted that pf penalty approach only penalizes those network users who operate below the preset trigger threshold but fails to incentivize those that operate above the preset pf threshold. In addition, the pf penalty approach was used specifically to recover charges for generator operating costs, that is, ensuring that network losses are reduced. Furthermore, different network companies have different pf penalty trigger thresholds [42, 43, 44] and, for that reason, it can be concluded that there is no solid basis for determining such and, therefore, it is not cost reflective [45].

The next phase would be to price for the existing network compensation devices at the nodes where these exist and, ultimately, the reactive power planning (RPP) problem would be integrated with the LRIC-voltage network pricing approach, to price for the future and the aforementioned existing network VAr compensation assets as the most practical approach to employ. In this case, N-1 circuit contingencies should be considered.

V. APPENDIX

The used IEEE 14 bus network is described in detail in [46]. The loading and the generation conditions of this used network are shown below in TABLES, 3 and 4, respectively.

TABLE 3
IEEE 14 NETWORK LOAD DATA

Bus	MW	MVar
1	0	0
2	21.7	12.7
3	94.2	19
4	47.8	-3.9
5	7.6	1.6
6	11.2	7.5
7	0	0
8	0	0
9	29.5	16.6
10	9	5.8
11	3.5	1.8
12	6.1	1.6
13	13.5	5.8
14	14.9	5

TABLE 4
IEEE 14 GENERATOR DATA

Bus	Real Power(MW)	Max VAr(MVAr)	Min Var(MVAr)	Voltage pu
2	40	50	-40	1.045
3	0	40	0	1.01
6	0	24	-6	1.07
8	0	24	-6	1.09

VI. REFERENCES

- [1] S. Hao, A. Papalexopoulos, "Reactive power pricing and management", IEEE Transactions on Power Systems, Volume 12, no. 1, pp. 95-104, Feb. 1997.
- [2] D. Chattopadhyay, K. Bhattacharya, J. Parikh, "Optimal reactive power planning and its spot-pricing: an integrated approach", IEEE Transactions on Power Systems, Volume 10, no. 4, pp. 2014 – 2020, Nov.1995.
- [3] K.K. Mandal, B. Kar, D. Pal, M. Basu, N. Chakraborty, "Reactive Power Pricing in a Deregulated Electricity Industry", Power Engineering Conference-7th International, Volume 2, no. 9110484, pp. 853-858, Dec. 2005.
- [4] J. Zhong and K. Bhattacharya, "Toward a competitive market for reactive power", IEEE Trans. Power Systems, Vol.17, no.4, pp.1206–1215, Nov.2002.
- [5] V.M. Dona and A.N. Paredes, "Reactive power pricing in competitive electric markets using the transmission losses function", IEEE Porto Power Tech Proceedings, Vol. 1, pp. 6,10-13Sept.2001.
- [6] Y. Dai, Y.X. Ni, F.S. Wen and Z.X. Han, "Analysis of reactive power pricing under deregulation", IEEE Power Engineering Society Summer Meeting, Vol. 4, pp. 2162 – 2167, 16-20 July 2000.
- [7] V. Cataliotti, M.G. Ippolito, F. Massaro, G.Pecoraro and E.R. Sanseverino, "A New Method for the Price Determination of the Reactive Power Supply", UPEC '06. Proceedings of the 41st International Universities Power Engineering, Vol. 1, pp. 242 – 246, 6-8 Sept. 2006.
- [8] J.D. Weber, T.J. Overbye, P.W. Sauer and C.L. DeMarco, "A simulation based approach to pricing reactive power", Proceedings of the Thirty-First Hawaii International Conference System Sciences, Vol. 3, pp. 96 – 103, 6-9 Jan. 1998.
- [9] A.D. Papalexopoulos and G.A. Angelidis, "Reactive power management and pricing in the California market", IEEE Mediterranean MELECON Electrotechnical Conference, pp.902–905, 16-19May 2006.
- [10] K.L. Lo and Y.A. Alturki, "Towards reactive power markets. Part 1: reactive power allocation", IEE Proceedings, Generation, Transmission and Distribution, Vol. 153, no. 1, pp. 59 – 70, 12 Jan. 2006.
- [11] M.L. Baughman, S.N. Siddiqi, "Real-time pricing of reactive power: theory and case study results", IEEE Transactions on Power Systems, Volume 6, no. 1, pp.23-29, Feb.1991.
- [12] J.W. Lamont and J. Fu, "Cost analysis of reactive power support", IEEE Trans. Power Systems, Vol.14, no.3, pp.890–898, Aug.1999.
- [13] Furong Li, N.P. Padhy, Ji Wang and B. Kuri, "Cost-Benefit Reflective Distribution Charging Methodology", IEEE Trans. Power Systems, Vol. 23, no. 1, pp. 58 – 64, Feb. 2008.
- [14] Furong Li and D.L. Tolley, "Long-Run Incremental Cost Pricing Based on Unused Capacity", IEEE Trans. Power Systems, Vol. 22, no. 4, pp. 1683 – 1689, Nov. 2007.
- [15] Ji Wang and Furong Li, "LRMC pricing based MW + MVAR-miles methodology in open access distribution network", CIRED 19th International Conference on Electricity Distribution, page 0790, 21-24 May 2007.
- [16] P.M. Sotkiewicz and J.M.Vignolo, "Nodal pricing for distribution networks: efficient pricing for efficiency enhancing DG", IEEE Trans. Power Systems, Vol. 21, no. 2, pp. 1013–1014, May 2006.
- [17] B.S. Lecinq and M.D. Ilic, "Peak-load pricing for electric power transmission", Proceedings of the Thirtieth Hawaii International Conference System Sciences, Vol. 5, pp. 624-633, 7-10 Jan 1997.
- [18] Kovacs, R.R., Leverett, A.L., A load flow based method for calculating embedded, incremental and marginal cost of transmission capacity. Power Systems, IEEE Transaction on, 1994.9(1):pp. 272-278.
- [19] H. Rudnick, R. Palma and J.E. Fernandez, "Marginal pricing and supplement cost allocation in transmission open access", IEEE Trans. Power Systems, Vol. 10, no. 2, pp. 1125–1132, May 1995.
- [20] Hyi Yi Heng, Ji Wang and Furong Li, "Comparison between long-run incremental cost pricing and investment cost-related pricing for electricity distribution network", CIRED 19th International Conference on Electricity Distribution, page 0717, 21-24 May 2007.
- [21] Y.Z. Li and A.K. David, "Wheeling rates of reactive power flow under marginal cost pricing", IEEE Trans. Power Systems, Vol. 9, no. 3, pp. 1263 – 1269, Aug. 1994.
- [22] D. Tolley, F. Prashad and M. Veitch, "Charging transmission", Power Engineer, Vol. 17, no.2, pp.22–25, April/May 2003.
- [23] G. Strbac, D. Kirschen and S. Ahmed, "Allocating transmission system usage on the basis of traceable contributions of generators and loads to flows", IEEE Trans. Power Systems, Vol.13, no.2, pp.527–534, May 1998.
- [24] Park Young-Moon, Park Jong-Bae, Lim Jung-Uk and Won Jong-Ryul, "An analytical approach for transaction costs allocation in transmission system", IEEE Trans. Power Systems, Volume 13, no.4, pp. 1407 – 1412, Nov. 1998.
- [25] M. T. Ponce De Leao and J. T. Saraiva, "Solving the Revenue Reconciliation Problem of Distribution Network Providers Using Long-Term Marginal Prices", IEEE Power Engineering Review, Vol.22, no.11, pp.55–55, Nov.2002.
- [26] H.H. Happ, "Cost of wheeling methodologies", IEEE Trans. Power Systems, Vol. 9, no. 1, pp. 147 – 156, Feb. 1994.
- [27] D. Shirmohammadi, P.R. Gribik, E.T. K. Law, J. H. Malinowski and R.E. O'Donnell, "Evaluation of Transmission Network Capacity Use for Wheeling Transactions", IEEE Power Engineering Review, Vol. 9, no. 11, pp. 37 – 37, Nov. 1989.
- [28] J. Kabouris, S. Efstathiou, A. Koronides and A. Maissis, "Transmission charging for the Greek Electric Power System", PowerTech Budapest Electric Power Engineering, pp. 16, 9 Aug.-2 Sept. 1999.
- [29] P.M. Sotkiewicz and J.M. Vignolo, "Allocation of fixed costs in distribution networks with distributed generation", IEEE Trans. Power Systems, Vol. 21, no. 2, pp. 639 – 652, May 2006.
- [30] D. Shirmohammadi, X.V.Filho, B. Gorenstin, and M.V.P. Pereira, "Some fundamental technical concepts about cost based transmission pricing", IEEE Tran. On Power Systems, vol. 11 no. 2, pp 1001-1008, May, 1996.

- [31] J. Bialek, "Allocation of transmission supplementary charge to real and reactive loads", *IEEE Trans. Power Systems*, Vol. 13, no. 3, pp. 749 – 754, Aug. 1998.
- [32] P. Jiuping, Y. Teklu, S. Rahman and K. Jun, " Review of usage-based transmission cost allocation methods under open access", *IEEE Trans. Power Systems*, Vol. 15, no. 4, pp. 1218–1224, Nov.2000.
- [33] J.W. Marangon Lima, "Allocation of transmission fixed charges: an overview", *IEEE Trans. Power Systems*, Vol. 11, no. 3, pp. 1409 – 1418, Aug. 1996.
- [34] The Statement of the Use of System Charging Methodology, the Charging Team. National Grid, U.K.[Online]. [Http://www.nationalgrid.com/uk/indifo/charging/pdfs.UoSC_Apr_03_\(I3R0\).pdf](http://www.nationalgrid.com/uk/indifo/charging/pdfs.UoSC_Apr_03_(I3R0).pdf).
- [35] Furong Li and E. Matlotse, "Long-Run Incremental Cost Pricing Based on Nodal Voltage Spare Capacity", *IEEE Power and Energy Society General Meeting*, pp. 1 – 5, 20-24 July 2008.
- [36] Matlotse E. and Furong Li, "Long-run incremental cost pricing for the use of network reactive power compensation devices for systems with different R/X ratios", *IEEE PES General Meeting*, pp. 1-8, 26-30 July 2009.
- [37] Hui Yi Heng, Furong Li and Xifan Wang, "Charging for Network Security Based on Long-Run Incremental Cost Pricing", *IEEE Trans. Power Syst.*, vol. 24, no. 4, pp. 1686–1693, Nov. 2009.
- [38] Strbac G. and Jenkins N., *Network Security of the Future UK, PIU, U.K.*, 2001. [Online]. Available: http://www.tyndall.uea.ac.uk/research/theme2/Network_Security_UMIST.pdf.
- [39] Mutale J., Strbac G., and Pudjianto D., "Methodology for cost reflective pricing of distribution networks with distributed generation," in *Proc. IEEE Power Eng. Soc. General Meeting*, 2007.
- [40] Pudjianto D., Strbac G. and Mutale J., "Access and pricing of distribution network with distributed generation," in *Proc. IEEE Power Eng. Soc. General Meeting*, 2007.
- [41] Western Power Distribution (WPD), "The Statement of the Use of System Charging Methodology", April 2007.
- [42] Central Networks East, "Use of System Charging Methodology", http://www.eon-k.com/downloads/CN_East_UoS_methodology_statement_Apr08.pdf, 7th April 2008.
- [43] Scottish Hydro Electric Power Distribution plc, "Statement of charges for use of Scottish Hydro Electric Power Distribution PLC's Electricity Distribution Network", <http://www.ssepd.co.uk>, 1st April 2008.
- [44] Berg S.V., Adams J. and Niekum B., "Power factors and the efficient pricing and production of reactive power", *The Energy Journal*, Vol. 4, pp. 93-102.
- [45] "IEEE 14 Bus Test Data", Available:<http://www.ee.washington.edu>

Cost Analysis of Small Scale Solar and Wind Energy Systems

Yandra Shivrath

(Department of Electrical & Electronics Engineering, JNT University, Hyderabad, A.P, India)

Abstract: The recent dramatic increase in the use of renewable energy systems leading towards competitive markets within the various individual renewable energy systems. The aim of this paper is to prove the hypothesis i.e. in next few years, when the cost of the solar PV modules come down below 1\$ per Watt, small wind turbines become more costlier because of the cost of structures required to support the wind generator. And also if the threat from the market is not addressed both technically and commercially, small wind turbine manufactures will lose the competition to solar PV module manufactures in the near visible future. Objective of this paper is to do cost analysis on the industry data and prove hypothesis and to arrive at the cutoff point, where after the generating energy from the wind is not economically feasible. With this cost analysis, author here by alarm for the small scale wind turbine manufactures to take necessary measures to survive the competitive markets of small scale renewable energy systems.

Keywords: Renewable energy, Solar PV, Wind Turbine, Curve Fitting, Cost analysis.

I. INTRODUCTION

1.1 Renewable energy system

A Renewable energy system uses any sources of energy that can be used without depleting its reserves. These resources include Sunlight or Solar energy and any other sources such as wind, wave, biomass, hydro energy and geothermal energy. These are replenished by nature rather than by man. Renewable energy systems help protects the environment since they usually do not release harmful byproducts into the atmosphere.

1.2 Industry Scenario of Solar Energy systems

Author have visited few industries related to Solar Power Plant Equipment Manufacturers in Hyderabad, Complete process of fabrication of a solar Photovoltaic module along with merits and demerits of various solar cells and Process techniques and Q/A methodologies had been studied, It was observed that very soon cost of production of solar photovoltaic module per peak watt is going to be as low as 1\$/ watt. These are some of the factors responsible for the rapid down fall of solar panel costs.

- Shortage of silicon used in solar panels is almost over. Multi crystalline solar cells are being more efficient over mono crystalline solar cells which are considered to be at higher costs.
- Latest technologies in amorphous solar cells are also responsible for the reduction of solar PV module costs.

This rapid drop down of costs of solar panels became a problematic for small scale wind energy systems which may not be able to compete with small scale solar energy systems in the market.

1.3 Industry scenario of small scale wind Energy systems

As per the study conducted by author on small scale wind generator producer companies, in India, small scale wind turbines are installed by Nature lovers, self financing institutions, universities, government funded projects, energy parks etc. For any Renewable Energy System, presently there is 80% depreciation in first year, 20% in second year and results in 30% tax savings in India. Wind generator Customers are more worried about the work failure, quality of the product than on investment.

In 100% depreciation projects, industry gets direct benefits payback is 10 years. Supernova Technologies, Gujarat manufactures a patented design of small scale wind generator ranging from 700W to 5KW and had completed more than 100 installations for the past 10 years. Benefits of these designs are more service life, low noise level. SNT's nano model of Wind Turbine is claimed to be the world's smallest commercial Wind Turbine with cut in wind speed of 1.2 m/s.

II. Need for Cost Analysis

Solar and wind energy systems involve a significant initial investment, they can be competitive with conventional energy sources when accounted for a lifetime of reduced or avoided utility costs. The cost of the system itself—depends on the system chosen, resources on the site and electric costs in the area. So the entire solar and wind energy system is analyzed for subsystem costs. Objectively to get an optimized cost model for the best selection of the renewable energy system.

III. Methodology

The parameters required for the cost analysis of solar and wind energy systems are

Table1: Parameters of Evaluation for Solar Energy

1	Annual Average Daily Peak Sunshine Hours (h)
2	Daily solar Radiation Horizontal (KWh/m ² /day)

Table2: Parameters of Evaluation for Wind Energy

1	Mean Annual Hourly Wind Speed(m/sec)
2	Hub Height (m)

The cost analysis is done by evaluating the parameters for a Particular location. Example Hyderabad situated in Southern India, geographically located at Latitude 17° 22'31" North of the equator and 78°28'27" East of the Prime Meridian of the world map.

According to the Indian Metrological Department IMD, the daily solar radiation horizontal and Mean Annual Wind Speed at Hyderabad is shown in table3.

Table3

Parameter	Design Value
Annual Average Daily Peak Sunshine Hours (ADPS)	9.31
Daily solar Radiation Horizontal(KWh/m ² /day)	3.83
Mean Annual Hourly Wind Speed(m/sec)	3.277
Hub Height (m)	50

The above parameters of a particular location are used to compute and estimate the energy density.

IV. Description

The below graphs were developed to prove the hypothesis and to arrive at the cut-off point (Energy demand Vs. Cost of the system), where after generating energy from Wind is not economically feasible.

Graph #1 Energy demand (KWh) vs. Cost of the solar energy system (excluding structure costs).

Graph #2 Energy demand (KWh) vs. Cost of the Wind energy system (excluding structure costs).

Graph #3 Energy demand (KWh) vs. Cost of the solar energy system (including structure costs).

Graph #4 Energy demand (KWh) vs. Cost of the Wind energy system (including structure costs).

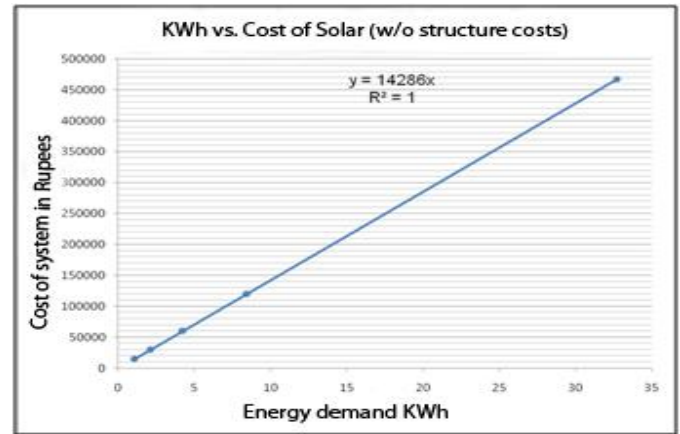
- The supporting structures are different for both the Solar PV modules and Wind turbine. Hence, their costs.
- Once, these graphs are developed on the same scale of Energy demand (KWh) vs. Cost of the energy system, and overlapped them to find the optimal region defined by the intersection of the curves.
- Assuming that without structure costs of the energy system, the slope of the graphs Cost/KWh does not vary much between solar and wind energies. But, there is a huge variation when structure costs are included.
- Building the graphs is to gather X, Y values (KWh vs. Cost) of Solar panels and Wind turbines with and without their respective structures.

Energy demand vs. Cost of system graph of solar and wind energy systems:

Graph #1: Energy demand (KWh) vs. Cost for solar energy system (excluding structure cost)

Data Points:

KWh	Cost
1.05	15000
2.1	30000
4.2	60000
8.4	120000
32.68	466866.5

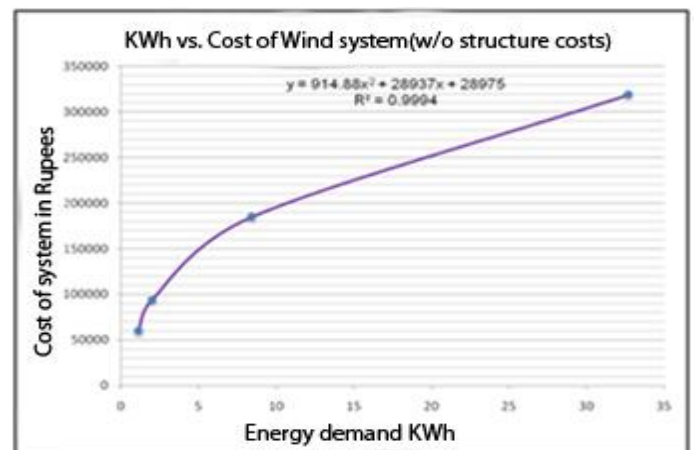


The graph shows a linear relationship between the energy demand and cost of the solar system (excluding the structure cost). Graph represented by the linear equation $y = 14286x$.

Graph #2 Energy demand (KWh) vs. Cost for wind energy system (excluding structure cost).

Data points:

KWh	System Cost
1.12	60000
1.99	94000
8.4	185000
32.68	319000

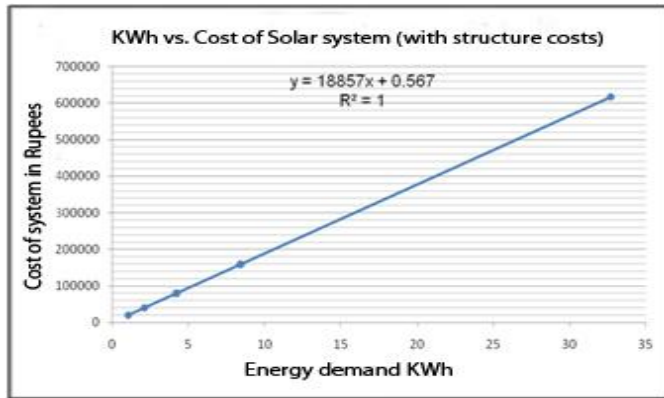


The above graph shows nonlinear relation between the energy demand and wind system cost (excluding the structure costs). Graph represented by the polynomial equation $y = 914.88x^2 + 28937x + 28975$ with a correlation coefficient of $R^2 = 0.9994$.

Graph #3 Energy demand (KWh) vs. Cost for solar energy system (including structure cost)

Data points:

KWh	System Cost
1.05	19800
2.1	39600
4.2	79200
8.4	158400
32.68	616246.8

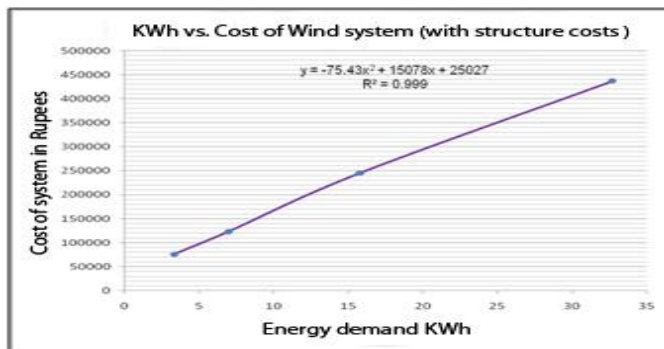


The above graph shows a linear relationship between the Energy demand and cost of the solar system (with structure cost). Graph represented by linear equation $y = 18857x + 0.567$

Graph #4 Energy demand (KWh) vs. Cost for Wind energy system (including structure cost)

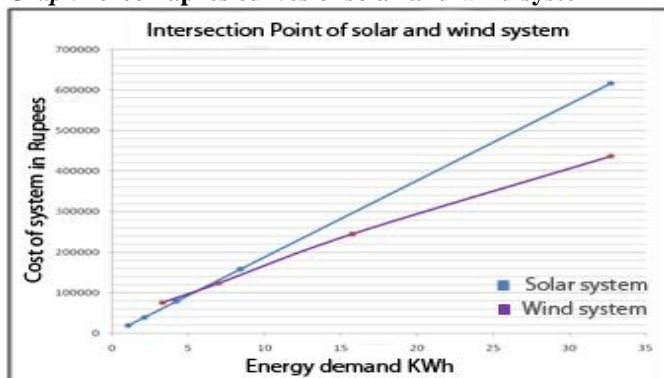
Data points:

KWh	System Cost
3.312	76000
6.96	123300
15.74	245000
32.68	437000



The graph shows a non linear relationship between the Energy demand and cost of the wind system (with structure cost). Graph represented by non linear equation $y = -75.43x^2 + 15078x + 25027$ with a Correlation coefficient of $R^2 = 0.999$

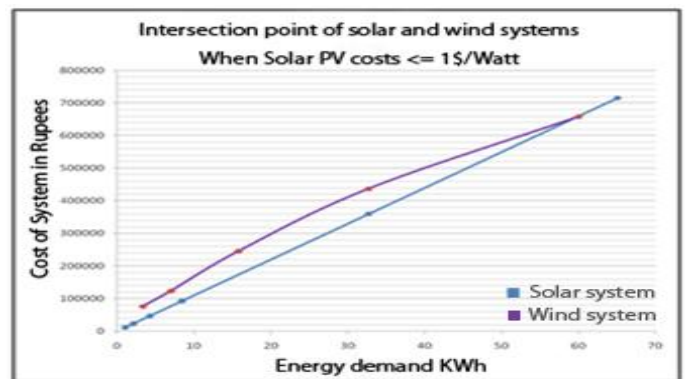
Graph #5 compares curves of solar and wind system



Graph #3 & Graph #4 were overlapped (i.e. energy demand vs. cost of solar system and wind system

including their structures) to get the cutoff point where after generating energy from the wind is not economically feasible. And obtained cutoff point from the above graph as (KWh, Cost) = (6.96, 123300).

Graph #6 shows intersection point of solar and wind system (assuming solar PV module costs < 1\$/peak watt)



When the graphs, Energy demand vs. Cost of solar and wind systems (including the structures costs and also assuming the solar PV module costs < 1\$/ peak watt) are compared and arrives at a cutoff point (KWh, Cost) = (59.604, 655643.734). From the graph generating energy from wind below this cutoff point is economically not feasible. This proves author's hypothesis i.e. when the cost of the solar PV modules comes down below 1\$ per Watt small wind turbines become uneconomical because of the structures cost required to support the wind turbine and wind generator. And also if the threat from the market is not addressed both technically and commercially, small wind turbine manufactures will lose the competition to solar panel manufactures in the near visible future.

V. Analysis

Graphs were developed between energy demands vs. the cost of renewable energy system. Projecting energy demand on x-axis and Cost on y-axis. For wind energy systems the data is acquired from the supernova technologies ltd. and the data for the solar photovoltaic modules is obtained from the Andromeda.

The following assumptions are made in the cost analysis of small scale solar and wind energy systems.

- The Mean Annual Hourly Wind Speed is 6.0m/s
- Annual Average Daily Peak Sunshine Hours is 9Hrs.

Graphs are developed using Microsoft Excel.

VI. Result and Discussions

From the above graphs it is clear that the cost of solar system follows a linear relation, whereas the cost for wind generators slightly varies at higher ratings. The comparison of the two curves in graph #5 gives an intersection point i.e. cost of both the systems at this point is same and the region below this point, solar is preferable and wind is preferable above the intersection point as per cost analysis. In a couple of years, we can expect cost of solar photovoltaic modules may bring down to less than 1\$/peak Watt, at this situation from graph #6 we can say

small scale wind generator manufacturers may lose their competition to solar market.

VII. Conclusion

Structure Costs are highly considered in case of total cost of the energy system either for solar or wind. Solar structure cost takes 20% to 25% of the total system cost while wind turbine structure cost is about the 40% to 60% of the total system cost.

So wind turbine structure cost is more than that of solar structure cost. Therefore some measures are to be taken in order to reduce the structure cost, so that small wind generators may survive in the market.

References

- [1] Science & Technology of Photovoltaic's- P. Jayarama Reddy, B.S. Publications
- [2] <http://www.supernovawindsolar.com/home.html>.
- [3] http://www.imd.gov.in/section/nhac/dynamic/allindia_main.htm
- [4] Renewable Energy Resources: Basic Principles and Applications. G. N. Tiwari, G. N. Tiwari M. K. Ghosal.
- [5] Photovoltaic Solar Energy Generation Volume 112 of Springer Series in Optical Sciences Authors Adolf Goetzberger, Volker Uwe Hoffmann
- [6] Re-considering the Economics of Photovoltaic Power
- [7] Morgan Baziliana,b, IjeomaOnyejia, Michael Liebreichc, Ian MacGilld, Jennifer Chassec, Jigar Shahe, Dolf Gielenf, Doug Arentg, Doug Landfearh, and Shi Zhengrong
- [8] Sezai Taskin*,Bahtiyar Dursun,Bora Alboyaci, Performance assessment of a combined solar and wind system, The Arabian Journal for Science and Engineering, Volume 34, Number 1B

Removal of Clutter by Using Wavelet Transform For Wind Profiler

P.Srilaxmi,¹ I. Kullayamma,² M. Durga Rao³

¹ Department of ECE, SVU College of Engineering, Tirupati, Andhra Pradesh, India

² Assistant Professor, Department of ECE, SVU College of Engineering, Tirupati, Andhra Pradesh, India.

³ Scientist Engineer SC-D, NARL, Gadanki

ABSTRACT: Removal of clutter in the radar wind profiler is the utmost important consideration in radar. Wavelet transform is very effective method to remove the clutter. This paper presents a technique based on the wavelet transform to remove the clutter. In this technique we used Fourier transform and discrete wavelet transform after that applied inverse discrete wavelet transform for signal. These techniques applied for inphase and quadrature phase, total spectrum and single range gate. Very encouraging results got with this technique that have shown practical possibilities for a real time implementation and for applications related to frequency domain.

Keywords: Wind profiler, wavelet transform, Fourier transform, clutter, signal processing.

I. INTRODUCTION

Wavelet analysis attracted much attention recently in signal processing. It has been successfully applied in many applications such as transient signal analysis, image analysis, communication systems and other signal processing applications. It is not a new theory in the sense that many of ideas and techniques involved in wavelets (subband coding, quadrature mirror filters etc.) were developed independently in various signal processing applications. Especially, it has turned out that the specific features of wavelets can also be efficiently used for certain problems in the context of radar signal analysis. The aim of this paper is to give an overview on the analysis of RWP data and to explain how wavelets can be utilized for clutter removal.

The goal of RWP systems is to gather information concerning the three dimensional atmospheric wind vectors. Radio frequency pulses are emitted and backscattered from small inhomogeneities in the atmosphere.

The reflected signal is sampled at certain rates corresponding to different heights. The Doppler shift of the atmospheric (clear-air) signal, which can assumed to be constant over the small measurement period (quasistationarity), generates a peak in the Fourier power spectrum.

II. FOURIER TRANSFORMS

The Fourier transform is as ubiquitous in radar signal processing as in most other signal processing fields. Frequency domain representations are often used to separate desired signals from interference; the Doppler shift is a frequency domain phenomenon of critical importance; and it will be seen that in some radar systems, especially imaging systems, the collected data are related to the desired end product by a Fourier transform. Both continuous and discrete signals are of interest, and therefore Fourier transforms are required for both. Consider a signal x

(u) that is a function of a continuous variable in one dimension called the *signal domain*.[†] Its Fourier transform, denoted as $X(\Omega)$, is given by

$$X(\Omega) = \int_{-\infty}^{+\infty} x(u) e^{-j\Omega u} du \quad \Omega \in (-\infty, \infty) \quad (1)$$

And is said to be a function in the *transform domain*. The inverse transform is

$$X(u) = \frac{1}{2\pi} \int_{-\infty}^{+\infty} X(\Omega) e^{+j\Omega u} d\Omega \quad u \in (-\infty, \infty) \quad (2)$$

In Eq. (1) And (2), the frequency variable Ω is in radians per unit of u . For example, if $u = t$, that is, u is in units of seconds, then Ω is the usual radian frequency in units of radians per second; if u is a spatial variable in meters, then Ω is spatial frequency in units of radians per meter. Equivalents transform pair using a cyclical frequency variable $F = \Omega / 2\pi$ is

$$X(F) = \int_{-\infty}^{+\infty} x(u) e^{-j2\pi Fu} du \quad F \in (-\infty, \infty)$$

$$X(u) = \frac{1}{2\pi} \int_{-\infty}^{+\infty} X(F) e^{+j2\pi Fu} dF \quad u \in (-\infty, \infty)$$

If the signal domain is time ($u = t$), then F is in cycles per second, or hertz. The various wavelet analysis methods are described in comparison to the widely known Fourier transform. The Fourier transform only retrieves the global frequency content of a signal, all time information is lost. To overcome this problem the short time Fourier transform is developed, however this method suffers from a limitation due to a fixed resolution in both time and frequency. A multiresolution analysis of the local frequency content of a signal is made possible by wavelet analysis.

III. WAVELET TRANSFORMS

The term wavelet means a small wave. The smallness refers to the condition that this (window) function is of finite length (compactly supported). The wave refers to the condition that this function is oscillatory. The term mother implies that the functions with different region of support that are used in the transformation process are derived from one main function, or the mother wavelet. In other words, the mother wavelet is a prototype for generating the other window functions.

Like Fourier analysis, wavelet analysis deals with expansion of functions in terms of a set of basis functions. Unlike Fourier analysis, wavelet analysis expands functions not in term of trigonometric polynomials but in terms of wavelets which are generated in the form of translations and dilations of a fixed function called the mother wavelet. The wavelets obtained in this way have special scaling properties. They are localized in time and frequency, permitting a closer connection between the function being

represented and their coefficients. Greater numerical stability in reconstruction and manipulation is ensured.

The objective of wavelet analysis is to define these powerful wavelet basis functions and find efficient methods for their computation. It can be shown that every application using the fast Fourier transform (FFT) can be formulated using wavelets to provide more localized temporal (or spatial) and frequency information. Thus, instead of a frequency spectrum, for example, one gets a wavelet spectrum. In signal processing, wavelets are very useful for processing nonstationary signals. A major advance in wavelet theory was the discovery of smooth mother wavelets whose set of discrete translations. Two different kinds of wavelet transform can be distinguished, a continuous and a discrete wavelet transform. The continuous wavelet transform is calculated by the convolution of the signal and a wavelet function. A wavelet function is a small oscillatory wave which contains both

The analysis and the window function. The discrete wavelet transform uses filter banks for the analysis and synthesis of a signal. The filter banks contain wavelet filters and extract the frequency content of the signal in various sub bands.

CONTINUOUS WAVELET TRANSFORM

At the most redundant end, one has the CWT. For CWT the parameters vary in a continuous fashion. This representation offers the maximum freedom in the choice of the analysis wavelet. The only requirement is that the wavelet satisfies an admissibility condition; in particular it must have zero mean. The condition is also crucial to be CWT invertible on its range.

DISCRETE WAVELET TRANSFORM

Here, we have discrete function $f(n)$ and the definition of discrete wavelet transform (DWT) is given by

$$C(a,b) = C(j,k) = \sum_{n \in \mathbb{Z}} f(n) \psi_{j,k}(n)$$

Where $\psi_{j,k}$ is a discrete wavelet defined as:

$$\psi_{j,k}(n) = 2^{-j/2} \psi(2^{-j}n - k)$$

The parameters a, b are defined in such a way that $a = 2^j, b = 2^j k$. Sometimes the analysis is called dyadic as well. One of the function of wavelet transform is Daubechies.

DAUBECHIES

The Daubechies familie is named after Ingrid Daubechies who invented the compactly supported orthonormal wavelet, making wavelet analysis in discrete time possible. The first order Daubechies wavelet is also known as the Haar wavelet, which wavelet function resembles a step function. Higher order Daubechies functions are not easy to describe with an analytical expression. The order of the Daubechies functions denotes the number of vanishing moments, or the number of zero moments of the wavelet function. This is weakly related to the number of oscillations of the wavelet function. The larger the number of vanishing moments, the better the frequency localization of the decomposition.

IV. WIND PROFILING RADARS

Conventional Doppler weather radars, which are designed to detect hydrometeor, are not sensitive enough because of their short wavelengths to detect the clear air,

except under unusual conditions. The development of modern wind profiler is an outgrowth of research work done with radars designed to probe the ionosphere, where longer wavelengths and extreme sensitivity was required.

BASIC PRINCIPLE OF WIND PROFILING RADARS

Wind profiling radars depend upon the scattering of electromagnetic energy by minor irregularities in the index of refraction of the air. The index of refraction is a measure of the speed at which electromagnetic waves propagate through a medium. For wind profiling, this medium is the atmosphere. A spatial variation in this index encountered by a propagating electromagnetic (radio wave) causes a minute amount of the energy to be scattered (or dispersed) in all directions. Most of the energy incident on the refractive irregularity propagates through it without being scattered.

V. SIGNAL PROCESSING

The purpose of radar signal processing is to extract desired data from radar backscattered echoes. The desired data usually concerns the detection of a target of interest, the location of the target in space.

The accuracy of the data available from radar is limited by thermal noise introduced by the radar receiver, echoes from targets of no interest (clutter), and externally generated interface.

Radar signal processing is used to enhance signals and to suppress clutter and externally generated signals. In the case of atmospheric radars the target generated by the process of refractive index fluctuations. These signals are very weak even for powerful radar systems. So, sophisticated signal processing technique is required to extract these signals.

An elementary form of radar consists of transmitter, antenna and an energy detecting device, which may be receiver. Single antenna is used for both transmission and reception. The signal transmitted by the transmitting antenna gets reflected by the target and is re-radiated in all directions. This energy re-radiated in the backward directions, is of prime interest to radar.

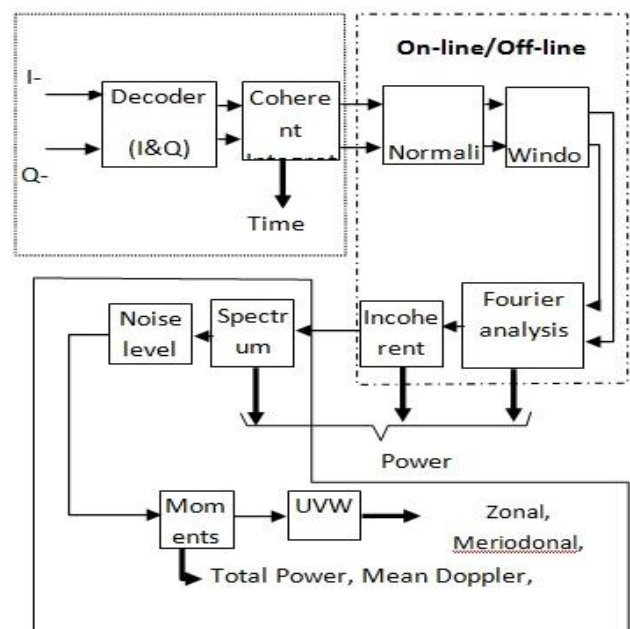


Fig (a): Processing steps for extraction of parameters

The receiving antenna captures the returned signals and channels it to the receiver, where it is processed to detect the presence of target and to extract its location and relative velocity. The distance of the target is determined by measuring the time taken for the radar signal to travel between target and radar the shift in carrier of the reflected wave is a measure of the target's relative velocity and may be used to distinguish moving objects from stationary objects. to the target and back. If relative motion exists

NARL LAWP

Most important feature or NARL LAWP is the simplified active array configuration. In this configuration, each element of the planar micro strip patch antenna array is fed directly by dedicated low power solid-state transceiver module consisting of a power amplifier (PA) and LNA connected to the common antenna port through a circulator. A transmit/receive (T/R) switch switches the input port between the PA and LNA. These transceiver modules are made with commercially available communication components, making them low cost and affordable. Signal-to-Noise Ratio (SNR), thereby the range performance is significantly improved as the feed loss is eliminated. This configuration reduces the antenna size significantly (at least by a factor of 4-6) when compared to a conventional passive array system for the given range performance and makes the wind profiler compact and transportable. The second important feature of this system is the utilization of a low power two-dimensional passive multi-beam forming network, which simplifies the beam formation.

IN-PHASE AND QUADRATURE COMPONENTS

Method and apparatus are disclosed for correcting amplitude and phase imbalances between the "in phase" and "quadrature" channels of a digital signal processor by determining a correction coefficient from a test signal periodically introduced into the quadrature phase detector of a radar system.

The frequency spectrum of the signal at the output of the phase detector in response to each such test signal is utilized to produce a correction coefficient for application to radar return signals passing through the phase detector during normal radar operation, thereby providing true quadrature radar return signals for digital processing.

The ground clutter signal characteristic with a 90-degree phase difference between I and Q components. The mountains through the radar beam causes a frequency sweep, and a localized appearance during the dwell period. This type of vibrating signal can be analyzed with the discrete wavelets. The frequency presentation of a discrete wavelet that covers a band of frequencies.

In the time-domain, the wavelet consists of real and imaginary sinusoidal wavelets that closely match with the mountain signal. The discrete wavelet transform can be calculated using a Fast Fourier Transform. To avoid frequency leakage, a strong radar return signal should first be removed with the wavelet method.

Figure1.shows the inphase signal in which we have both signals. which are before and after wavelets.

Figure2.shows the Quadrature phase signal in which we have both signals. which are before and after wavelets.

By using wavelet transform remove the clutter in inphase and quadrature signals.

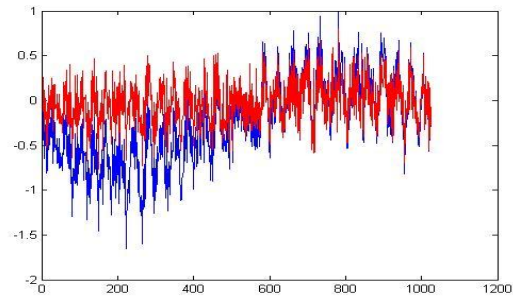


Figure 1. Time-series data from a 1280MHz wind profiler. The original inphase component is shown in blue, the wavelet re moved clutter component in red.

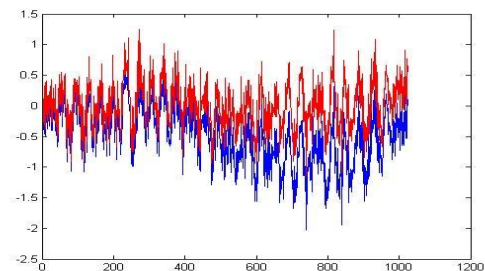


Figure 2. Time-series data from a 1280MHz wind profiler. The original quadrature component is shown in blue, the wavelet re moved clutter component in red.

Figure3. Shows the power spectrum compared to the after wavelet. This spectrum for single range gate. The discrete wavelet transform is used for to remove the clutter which is present in the range gate

Figure4. Shows the power spectrum before the wavelet transform. In which clutter is present.

Figure5. Shows the power spectrum after the wavelet. In which clutter is removed. We collect the LAWP data upto 7km.

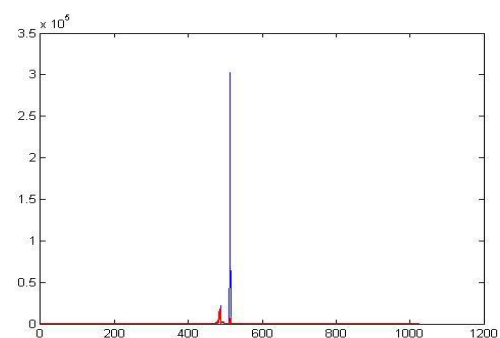


Figure 3. power spectrum (blue) is compared to the removed clutter power spectrum (red).

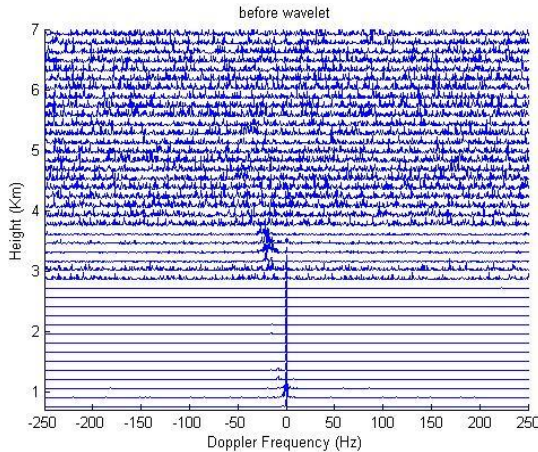


Figure4. Power spectra before wavelets.

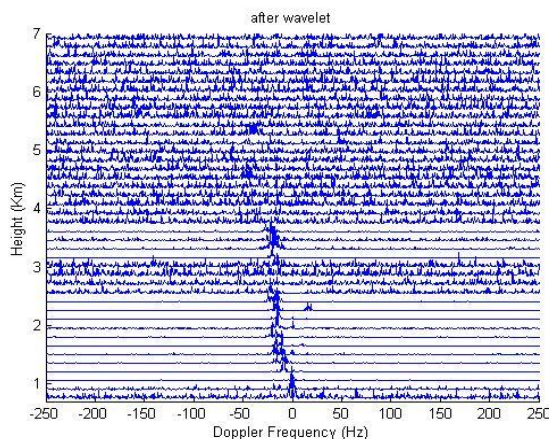


Figure5. Power spectra after wavelets.

VI. CONCLUSION

The wavelet transform method presented in this paper can efficiently remove clutter appearing in wind profiler. Signals represented in the time domain can be evaluated for their properties in the frequency Domain by applying signal analysis.

The most commonly known method to analyze a time signal for its frequency content is the Fourier transform. The wavelet transform is a relatively new technique which has some attractive characteristics. It has been found by the discrete wavelet transform. The raw data is stored in host processor first it converts into spectral data. Spectral data is also stored in digital receiver. The spectral data is processed by MATLAB programming. The clutter is removed from the inphase and quadrature phase signals and also from the total spectrum by using the discrete wavelet transform for LAWP radar which is used at NARL, Gadanki. By using different wavelet transform techniques the clutter is removed from the wind profiler.

VII. ACKNOWLEDGEMENTS

The Authors thank to M.Durga Rao, Scientist engineer, SC-D, National Atmospheric Research Laboratory Department of Space, Government of India Gadanki India and I.kullayamma, Assistant Professor, S.V.U. College Of Engineering, Tirupathi, India for their encouragement and infrastructure facilities to carry out this work.

REFERENCES

- [1] Newland, D. E., 1994: Wavelet analysis of vibration, Part 1: Theory. J. Vibration Acoust, **116**, 409–416.
- [2] Anandan, V. K., Atmospheric Data Processor – Technical and User reference manual, National Atmospheric Research Laboratory, Gdansk.
- [3] Liu, P. C., and G. S. Miller, 1996: Wavelet transforms and ocean current data analysis. J. Atmos. Oceanic Technol., **13**, 1090–1099.
- [4] BOISSE, J.-C., V. KLAUS, J.-P. AUBAGNAC, 1999: Wavelets transform technique for removing airplane echos from ST radar signals. – J. Atmos. Oceanic Technol. **16**, 334–346.
- [5] HLAWATSCH, F., G. BOUDREAUX- BARTELS, 1992: Linear and quadratic Time- frequency signal representations. –IEEE Sig. Proc. Magazine, 21–67.
- [6] FLANDRIN, P., 1999: Time-Frequency / Time- Scale Analysis. Wavelet Analysis and Its Applications. – Academi Press.
- [7] DAUBECHIES, I., 1992: Ten Lectures on Wavelets. – SIAM, Philadelphia.
- [8] COHEN, L., 1989: Time-frequency distributions – A review. –Proc. IEEE **77**(7), 941–981.
- [9] Riddle, A.C., and W.M. Angevine, 1992: Ground Clutter removal from profiler spectra. Proc. Fifth Workshop of Technical and Scientific Aspects of MST Radar, Aberystwyth, Wales, United Kingdom, URSI/SCOSTEP 418- 420.
- [10] Benjamin, Z. B., and D. S. Zrnica, 1991: Clutter Rejection for Doppler weather radars which use Staggered pulses. IEEE Trans. Geosci. Remote Sens., **29**, 610–620.
- [11] F. C. A. Fernandes, R. v. Spaendonck, M. J. Coates, and S. Burrus, "Directional Complex-Wavelet Processing," Proceedings of Society of Photo-Optical Instrumental Engineers/SPIE2000, Wavelet Applications in Signal Processing VIII, San Diego, , 2000.
- [12] Strang, G., and T. Nguyen, 1996: Wavelets and Filter Banks. Wellesley- Cambridge Press, 490pp.

Study the Situation of Housing Social Quantitative and Qualitative Indicators in Rural Areas of Ghachsaran Township, Iran

Dr. Saeed Maleki,¹ Atefeh Ahmadi,² Taha Rabbani³

¹Department of Geography and Urban Planning, Faculty of Earth Sciences and GIS, Shahid Chamran University of Ahvaz, Golestan St, Ahvaz, Iran.

²PhD Student of Geography and rural planning, Kharazmi University, Tehran, Iran

³PhD Student of Geography and Urban planning, University of Tarbiat Modares, Tehran, Iran

Abstract: Housing indicators are fundamental factor and determine in descriptive, analysis and making decision for housing which can lead to as outline in housing planning for maker decision and planner if housing indicators recognize and understanding, it's study and analysis of way a applied and fundamental or basic research and correctly done with in plans. Among housing indicators, social indicators are the most property fundamental factor of housing progress and goals.

The aim this article is to study the situation of the social quantitative and qualitative indicators of housing in rural areas of Ghachsaran Township.

The methodology used in this article is a combination of descriptive, analytical method and case study.

The results of this article in relation of housing social quantitative and qualitative indicators in rural areas of Ghachsaran township within the years of 1996 to 2006 shows there are problems in terms of social quantitative indicators of housing and unbelievable bad conditions (density of family per dwelling). But from view point of social qualitative indicators of housing (infrastructure facilities and basic services of housing units and construction materials) in rural areas have had a relative developing trend.

Therefore, one plan of housing is need of recognize, understanding and analysis of housing dimension and its effect. In the among is necessary study of this indicators as one of the most important housing indicators in housing quality update and their role in housing development planning and progress.

Keywords: Housing, Social Indicators, Quantitative and Qualitative Indicators, Rural Areas, Ghachsaran township.

I. Introduction

Housing as an actual phenomenon, the first things that man has always struggled with it and always trying to find the right response to change, it is reasonable to think. So housing is a necessary but not in any sedative, whitish ideal man to access appropriate housing (Azizi: 1996:108). This is what should be affordable housing. In general, the wider issue of housing is complex and is composed of various dimensions (Pour Mohammadi, 2001). Therefore we cannot provide a comprehensive definition of the obstacle. Housing as a physical place, each family is considered basic shelter, in the shelter of the family or individual needs such as sleep, rest, protection against environmental conditions and the nature of the summary is supplied (Khsrvnya, 2009). What is noteworthy is that in addition to the physical structure housing a family can be used as shelter, the total also includes residential environment (Ahari et al, 1998) which includes all the necessary facilities, services and installations needed for better social and family life and employment schemes, education and health of individuals. In other words, the physical pain is nothing more than a mere shelter and all public facilities and services necessary to better human life involves and use it to be sure it has a relatively long tenure (Mokhber, 1984).

Housing the urban area will be important as most private; the most important role in rural areas than in urban areas is weaker. Development of communication technology in various fields of physical presence in different parts of town lessen the image of his presence will add to the housing (Tamanna, 2010). In fact, it is possible that, unlike past resident of the clock to finish their homes his presence in the house and surroundings are far from inevitable and he was in the other parts of the township (Poor Mohammadi, 2010).

Housing and social housing and general development process is essential. That is why the United Nations (UN) in 1987 as the international year of shelter for the homeless announced (Gallent, 2009). Before that the 1976 United Nations Conference on Human Settlements (UNCHS) The emphasis was on the importance of affordable housing. Food, clothing, shelter and employment benefits to meet their basic needs in our life and for each of the major components are the basic needs approach (Tolon, 2011).

II. Methodology

Specific methods to achieve the goals and objectives need to be that we can follow to achieve the desired results, and we can deduce that no scientific conclusion is unlikely unless a specific method (Haryngand Lloyd, 1997). Therefore, the methodology used to reach rural housing is Gachsaran townshop. Since the control variables in the current study is not practical, so the standard method (description) is used to achieve desired goals). (Kazemi Pour, 2004). (With regard to control variables that affect human behavior, it is difficult and often impossible, so the most useful descriptive methods used in social geography matters.

In the beginning, we have tried as much as possible all the studies in this area of the township and is diagnosed Gachsaran in cases where additional information is needed to collect data from field studies and the preparation of the questionnaire data, the action is and then review and analyze any data taken from various references has been discussed. Finally, the issue of how the role and influence of various factors on each realtor is specified.

III. Social indicators of housing quality

3.1. Density of household in residential unit

In 1986, 7,227 families residing in rural areas of the township were Gachsaran while the number of housing units, about 7,178 units is listed and these data indicate that for every 100 households, there are 106 housing units in rural areas. Units in 1996 to over 7,285 in 7838 households in 100 housing units per 107 households reported finally, in 2011 the number of rural households in the township has increased from 8,740 households to 8,726 residential units.

Table 1-Density of household in residential unit in Gachsaran rural area 1986-2011

Year Title	1986	1996	2011
Household Number	7227	7838	8740
residential unit Number	7178	7285	8726
Density of household in residential unit	1/06	1/07	1/01

Reference: Census of Population and Housing Detailed results for the years 1986-2011.

3.2. Density of Person in Room

Research results indicate that it is the ideal housing for every person in the room is 2. Also, in 1986, 9/5 people in the room, and in 1996, while the sixth and reached in 2011 to 8/4 down.

Together these indicators in the rural township of Gachsaran can say that in 1986, 9/5 people in the room, and in 1996, while the sixth and reached in 2011 to 8/4 down.

Table 2- Density of person in room Gachsaran township rural area during 1986-2011

Year Title	1986	1996	2011
Room Number	8208	7285	8672
Population Number	48386	44494	41770
Density of Person in Room	5/9	6/1	4/8

Reference: Census of Population and Housing Detailed results for the years 1986-2011.

3.3. Density of person in residential Unit

The index for rural areas in 1986 vs. 75/6 housing units was people. In 1996, sixth in 2011 and reached the 3/5 is less than the density of housing units in rural households in the township.

Table 3- Density of person in residential unit Gachsaran township rural area during 1986-2011

Year Title	1986	1996	2011
Population Number	48386	44494	41770
Household Number	7227	7838	8740
Density of Person in Room	7/6	6/5	7/4
Household size rate	7178	7282	7826
Residential unit Number	6/75	6/1	5/3

Reference: Census of Population and Housing Detailed results for the years 1986-2011.

3.4. Density of Residential Unit in Household

Also shows the distribution of housing units by households living in rural areas Gachsaran township is a better way of living. In 1986, the proportion of single-family housing units in the rural township 5/88 percent ten years later, in 1996, more than 2/94 of a family who lived in residential areas, and in 2011, compared to 4/95% increase which reflects this time with a single nuclear family and the evolution of biological households tend to have a more residential units are independent of parent families, and increase the index of housing recovery will follow housing units than households in which there are two the following table Gachsaran township vs. Rural areas 2/9 percent in 1986 to 5/4 percent is reached in 1996. And finally in 2011 to 7/3 percent decline, and three-family residential units and more than in 1986, about 6/1 percent in the years 1996 and 2011 to less than 1 percent of all housing units in rural areas Gachsaran township.

Table 4- Density of residential unit in household in Gachsaran township rural area during 1986-2011

Year Household Number	1986		1996		2011	
	Number	Percent	Number	Percent	Number	Percent
1 Household	6398	88/5	6863	94/2	7847	95/4
2 Household	669	9/2	328	4/5	308	3/7
3 Household	121	1/6	61	0/8	40	0/4
4 Household and more	39	0/5	33	0/4	26	0/3
Residential unit Number	7227	100	7285	100	8221	100

Reference: Census of Population and Housing Detailed results for the years 1986-2011.

IV. Social indicators of housing quality

4.1. Average level of floor area Residential units

The following table Gachsaran largest township in the year 2011 in the rural areas of residential units from 101 to 150 square meters with a building area about 9/21 percent of the housing units are included and then to 101 residential units with area of 81 square meters, which is about 8/21 percent of the units are in residential units with area of 201 m² and more infrastructure from the most minimal housing units are included.

Table 5- Average level of floor area Residential units in Gachsaran township rural area 2011

Year Floor Area	Number	Percent
50 m ² and less	1336	16/25
51-75 m ²	1525	18/5
76-80 m ²	1192	14/5
81-100 m ²	1795	21/8
101-150 m ²	1800	21/9
151-200 m ²	455	5/5
200 m ² and more	118	1/4
Total	8221	100

Reference: Census of Population and Housing Detailed results for the years 1986-2011.

4.2. Residential units depending on the durability of building materials

Table 6. Distribution of residential units in Gachsaran township rural areas durability of building materials during 1986-2011

Year Building Material	1986		1996		2011	
	Number	Percent	Number	Percent	Number	Percent
Full- durability	3604	50/2	808	11/1	5457	66/4
Semi- durability	2197	30/6	761	10/5	2157	26/2
No -durability	212	3	280	3/8	204	2/5
miss	1165	16/2	5436	74/6	403	4/9
Total	7178	100	7285	100	8221	100

Reference: Census of Population and Housing Detailed results for the years 1986-2011.

4.3. Social indicators related to basic services

Studies conducted in the years 1986-2011 shows that residential facilities housing units in rural areas has improved Gachsaran township trend.

Table 7. Residential facilities of residential units in Gachsaran township rural areas during 1986-2011

Year Residential facilities	1986		1996		2011	
	Number	Percent	Number	Percent	Number	Percent
Water	5868	81/7	6495	89/1	7401	90
Power	5087	70/9	6621	90/9	7932	96/5
Gas	753	10/5	33	0/45	1679	20/4
Telephone	33	0/45	1093	15	5112	62/2
Bath	3123	43/5	4968	68/2	6395	77/8
Kitchen	2420	33/7	4649	63/8	7525	91/5

WC	6261	87/2	6711	92/1	8207	99/8
Cooler	2002	27/9	3969	84/5	—	—
Total of Residential Unit	7178	100	7285	100	8221	100

Reference: Census of Population and Housing Detailed results for the years 1986-2011.

4.4. Social indicators relating to ownership of property and housing

Table 8. Ownership of residential units in Gachsaran township rural areas during 1986-2011

Year	1986		1996		2011	
	Number	Percent	Number	Percent	Number	Percent
Ownership						
Private	7411	89/5	6618	84/4	7331	84/5
tenant	226	2/7	337	3/4	770	8/9
Housing Free	437	5/3	538	6/9	181	1/2
	125	1/5	154	1/9	282	3/2
Other	0	0	26	0/3	73	0/85
Miss	79	0/95	165	2/1	35	0/4
Total	8278	100	7838	100	8672	100

Reference: Census of Population and Housing Detailed results for the years 1986-2011.

According to the table above, in 1986, 5/89% of rural households in their housing units were owner Gachsaran township. In 1996 compared to 4/84 percent in 2011, to 5/84 dropped) (Taghavi, 1378: 88) (In the 1986 to 2011 added tenant that come in 2011, 8% of rural households are tenant township. also, the number of households that have free housing units in 1986 until 2011 has been upward, from 5/1 percent in 1986 to 9/1 percent in 1996 and finally to 2/3 percent increase in 2011.

The most appropriate indicators for measuring progress in social housing and housing are the general goal. The index can be used at all levels from national to individual and collective review and assess.

V. Conclusion

Index housing policy is an appropriate tool for assessment criteria. These indicators can be used to help the housing conditions gave a visual image. On the other hand, using the experience of countries that have been successful in their housing community, we can provide solutions for housing in urban and rural of Iran.

The most important indicators of housing applications, increasing the level of information available to understand the living conditions of residents. So that decision makers and planners can affect the lives of residents in the housing assessment and determine a more accurate and better.

In this paper, the role of social indicators in the housing development plan the introduction of social housing in rural areas and the township of Gachsaran the indicators in these areas have been studied.

-In terms of facilities and basic services in rural areas have improved Gachsaran town shop trend.

According to studies conducted in the years 2011 – 1986 shows that residential facilities housing units in rural areas are improving the township Gachsaran. For example, the number of rural households have piped water in 1986 the township had a 7/81 percent to 90 percent in 2011.

-The number of housing units, households living in rural areas does not meet Gachsaran township. In 1986, 7,227 families residing in rural areas were Gachsaran township while the number of housing units, about 7,178 units are listed these data indicate that for every 100 households, there are 106 housing units in rural areas. Units in 1996 to over 7,285 in 7838 households in 100 housing units per 107 households reported finally, in 2011 the number of rural households in the township has increased from 8,740 household to 8,726 residential units.

-Seems to be used in housing construction in rural areas Gachsaran Township is more durable construction materials.

According to the research materials used in rural housing Gachsaran township in 1986, about 2/50 of a durable material, and only 3% of it is kind of flimsy materials.

-In terms of social housing in rural areas Gachsaran township proper conditions are favorable.

According to investigations from 1986 to 2011, the index had a slightly downward trend of housing for example, the density of rural households Gachsaran Township in 1986 vs. 75/6 housing units was people. In 2011, the 3/5 is less than the density of rural households in the township's housing units and housing quality indicators have been rising, and the conditions are favorable.

References

- [1] Ahari, Z. et al., (1998), Minimum Housing, Building and Housing Research Centre, Publications Department of Housing and Urban Development, Tehran.
- [2] Azizi, Muhammad M. (1996) Analysis of the housing program, the National Land Agency.
- [3] Gallent, N., 2009, Housing Rural, Journal of International Encyclopedia of Human Geography, vol.7, pp.207-212.
- [4] Habibi, M et al (1991), Minimum Housing, Building and Housing Research Center, second edition.

- [5] Haryng, Lloyd (1997) Scientific research in Geography, translated by Mohammad Ali Mvlazadh, martyr Chamran University Press.
- [6] Mokhber, A. (1984) Social Dimensions of Housing, Planning and Budget Organization, Tehran.
- [7] Khsrvnya,M.,(2001), Formation evaluation of different approaches on rural housing, Journal of Housing and Rural Environment, Housing Foundation of Islamic Revolution, No. 127.
- [8] Pour Mohammadi, M. (2011), the housing planning, SAMT Press, third edition.
- [9] PourKazemi, SH (2004), Principles of Population–Tehran, Center for Population Studies and Research Asia Pacific,second edition.
- [10] Robert. (1998); cities in the developing world, the translators, publications, organizations, municipalities and Dhyaryhay country.
- [11] Sarookhani, B.(1994) Research Methods in the Social Sciences, Volume One, publisher, Institute for Humanities and Cultural Studies.
- [12] Taghavi, Nmtalh(1378),Principles of Population, Tabriz, Jamhpzhvhand Daniel, Fifth Edition.
- [13] Tamana, S. (2011), Principles of demography, first edition, publisher of Payam Noor University,Tehran.
- [14] Tolon, B.,(2011),Geography of Habitat, Rural Housing, Ankara University Press.Turkey.p.67.
- [15] Zabardast, Esfandiar(2000), indicators of housing and urban indicators, Lodging Magazine, Issue1.

Influence of Mineralogy and Fabric on the Engineering Properties of the Miango Granite Porphyry, North Central Nigeria

Stephen J. Mallo,¹ Sunday Daku Sani²

^{1,2}Department of Geology and Mining, University of Jos, Nigeria

Abstract: The major problem associated with the use of rock aggregates in engineering construction, is the difficulty of predicting their probable field performance. This is mainly due to the inadequate understanding of the decisive factors that control their engineering behavior. The mineralogy and fabric of the Miango granite porphyry was studied to assess their influence on engineering properties. The uniaxial compressive strength and aggregate crushing values show that the rocks are weak while other tests such as aggregate impact strength, water absorption, and absorption under saturation, soundness and specific gravity values are fairly good. However, thin section studies revealed three distinctive features which greatly influence the physico-mechanical properties: (a) abundant fractures of varying sizes (b) Sericitization of the orthoclase and or plagioclase feldspars (c) intergrowth of quartz and or orthoclase feldspars. The quartz grains shows extensive cracking which further reduces their mechanical strength. The strength loss of the granite porphyry could be attributed to the presence of the fractures on the quartz grains and the sericitization of the orthoclase and plagioclase feldspars. Geotechnical characterization of the rocks shows that they can be utilized as roadstone or could be polished and used as facing stones because of their non disintegration to sulphate attack and the large feldspar phenocrysts in the rock.

Key Words: Aggregate Impact Value Tests; Aggregate Crushing Value; Water Absorption; Crushing Load

I. Introduction

The study area is located in Bassa Local Government Area (L.G.A) of Plateau State North Central Nigeria. It is between latitudes 9° 49' 02''N and 9° 52' 36''N and longitudes 8° 39' 06''E and 8° 43' 18''E (Fig.1.1). The area falls under the basement complex of Nigeria (Wright, 1971; Jacobson, 1971) with some parts having relatively high relief while others have low relief and show extensive weathering and erosion thus, the ease with which the rocks are quarried for use as foundation stones and building.

The study on the influence of petrology and fabric on the Engineering properties of concretionary laterite aggregates and rocks in Nigeria have been carried out by Akpokodje and Hudec (1991), and Akpokodje (1992) and recommended that the mineralogy, petrology and fabric of commonly used laterite gravel aggregate in Nigeria should always be studied to assess their influence on engineering properties. Result of thin section studies by Akpokodje and Hudec revealed two characteristics feature which greatly influence the physico-mechanical properties: (a) abundant voids and fissures of varying sizes and (b) varying degree of iron oxide impregnation. For Akpokodje, the pyroclastic aggregates exhibited high expansions (greater than critical value of 0.07%) when immersed in hot IN NaOH due to alkali carbonate reactivity. This constitutes serious durability problem for concretes produced with pyroclastic aggregates. The granite and granite gneiss aggregates generally showed lower and permissible-expansion although, some varieties show values that are higher than the critical expansion, depending on geochemistry.

Ogunsanwo (1994) studied the significance of geochemistry and mineralogy on the optimum geotechnical utilization of some laterite sorts from four Basement Complex rocks and a Sedimentary formation from South-Western Nigeria. Some geotechnical properties of these soils namely compaction, consolidation, permeability and shear strength were investigated in addition to the classification test in the laboratory. The results obtained show that the soils generally possess very favorable geotechnical properties.

From these studies it follows that successful exploitation and use of any rock for engineering purpose requires proper understanding of the physical, structural, mineralogical and strength characteristics of the rock. This is important because rocks like other solids, fail when subjected to load beyond their strength. The failure takes place under compression, tension and shear forces at different values.

The Miango granite porphyry is underlain by Precambrian rocks of the Nigeria Basement Complex. Here, the rocks vary in mineralogical composition, texture, color and some other physico-mechanical properties (Macleod and Berridge 1971). Over the years, rocks have usually been quarried and used with or without the knowledge of their engineering properties, as only private construction companies always bother to test for the strength characteristics before they are used for civil engineering construction. Therefore, there is insufficient information on the engineering properties of the abundant rocks on the Plateau particularly the younger and older granites. The significance or influence of mineralogy and fabric (texture) on the Miango granite porphyry in relation to the engineering properties of the rocks has been studied by petrographically indentifying the constituent minerals of the rocks, their arrangement, texture and their role on the engineering properties of the rocks.

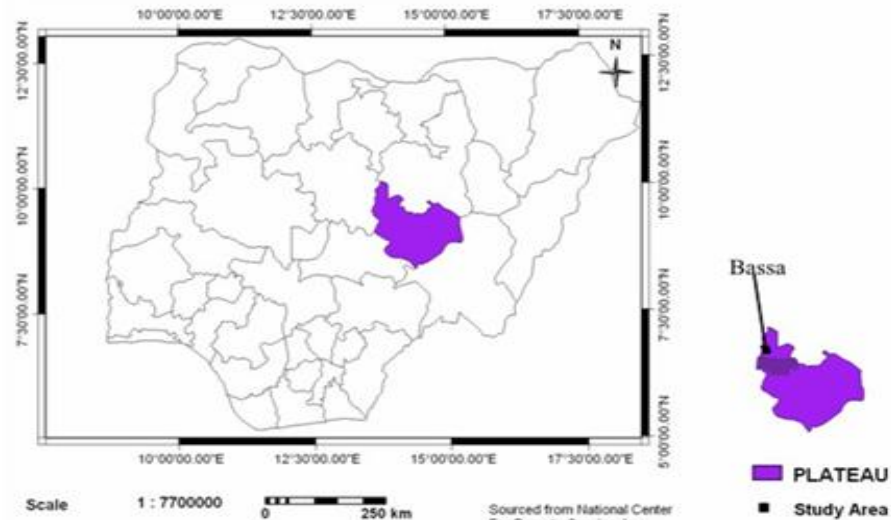


Figure 1.1: Location map of study area

II. Materials and Methods

The main thrust of the research is to determine the engineering properties of the Miango granite porphyry in relation to their mineralogy and fabric (texture). Geological data were gathered from secondary data. Primary data were generated through a systematic method of sampling from where twenty (20) representative samples (Fig.1.2) were collected and subjected to various geo-technical tests (Water Absorption, Specific gravity, Uniaxial Compressive Test, Aggregate Crushing Value Test (ACV), Aggregate Impact Value (AIV) Test, Thin Section Preparation and soundness test) as well as petrographic studies. Equipments and materials deployed for the study include the Global Positioning System (GPS), sampling equipments, digital cameras, and ILWIS 3.0 Academic, Surfer 8.0 and Grapher 5.0 Soft wares.

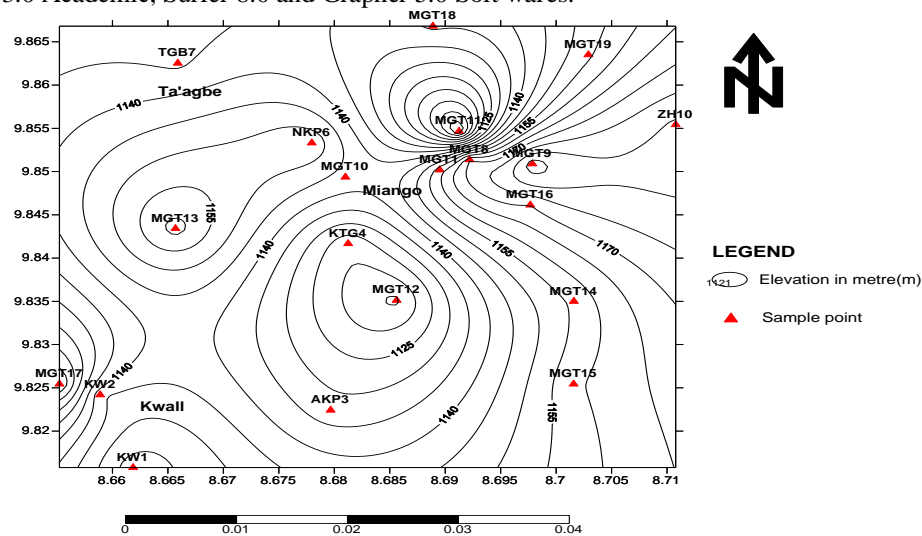


Fig. 1.2: Samples Location Map of the Study Area

III. Structural Geology

Structures of the Miango granite porphyry are the imprints of deformation on rocks which include joints, dykes, foliations, veins, folds etc. Such structural features exhibit variable trends in conformity with the general fracture pattern recorded in the Basement and Younger Granite province of Nigeria. These structures are believed to have resulted from intense regional tectonism that preceded and accompanied the emplacement of the Older Granites during the Pan-African Orogeny which produced a well defined and extensive N-S trend in North Central Nigeria including the Miango area (Macleod and Turner, 1971). The origin of these structures cannot be totally related to tectonism and accompanying deformations, but they may have been due to tensional forces set up as a result of cooling.

The structural setting in the study area has greatly controlled the geological setting, relief, drainage, geological boundaries and trend of younger rocks (Fig.1.3).

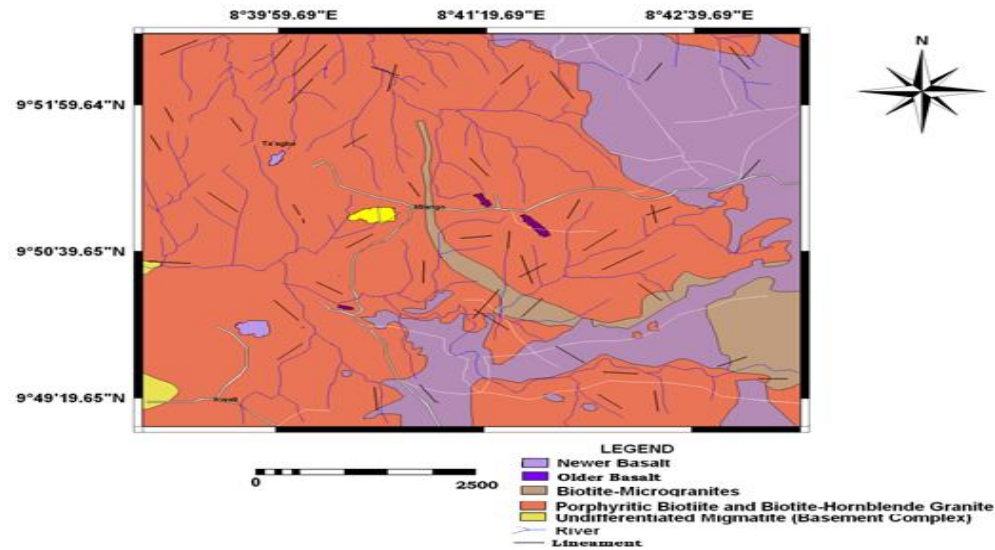


Fig. 1.3: Modified Geological Map of Study Area

Generally, the nature and extent of structures depends on the duration and intensity of deformation.

IV. Field Observation

Fractures and Joints: Fractures represent any break in a rock whether or not it causes displacement due to mechanical failure by stress. It includes cracks, joints and faults. Joints on the other hand are fractures on rocks in the study area in which there is no relative movement along the fracture planes. They are linear structural features resulting from the fracturing of brittle rocks. They are the most common structural features observed within the study area (Plate 1).



Plate1: Joints on the porphyritic biotite granite

Foliation: The term foliation is a general term sometimes used as essentially synonymous with cleavage, but it is applied most generally to mineral alignment in metamorphic rocks and sometimes in igneous rocks (older granites). Thus, salty "cleavage" and "schistosity" are special types of metamorphic foliation characterized by the types of fabric or mineral arrangement commonly found in slates and schists. Foliation is mostly used for metamorphic fabric like migmatite gneiss.

Foliation is formed as a result of static pressure that act on the pre-existing rock changing the platy mineral such as mica and amphiboles contained in the rock structurally to a new form. The presence and degree of foliation in a rock helps in knowing the rock type and condition under which the rock was formed.



Plate 2: Foliation on the Migmatite

Veins: These are tabular or sheet like bodies of mineralization which were introduced into fissures and joints within the study area. They are brought about by the infilling of fractures by mineral fluid before recrystallization. Most of the veins are quartz veins, although, some are fine grained felsic materials. In some places the size of the quartz vein is as thick as 17cm. Plate 3 shows a typical quartz vein within the study area.



Plate 3: Quartz Vein on porphyritic biotite granite

Sampling: Samples were collected using the systematic sampling method using the grid map at an average of 2km per sample. However, because of non total coverage of the study area by granite porphyry some samples were taken at intervals exceeding 2km.

V. Presentation Geotechnical Result

A summary of the geotechnical test carried out which include; soundness or durability test, water absorption, specific gravity, uniaxial compressive test. Aggregate crushing value and aggregate impact value tests are presented in Table 1. Individually the results are graphically presented in Figures. 1.4 to 1.9 below.

Table 1 Summary of Rock Test of the Representative Samples

S/No	Sample No	Specific Gravity	Water Absorption	Water Absorption Under Saturation	Crushing Load(KN)	Crushing Strength (N/mm ²)	Aggregate Crushing Value ACV(%)	Aggregate Impact Value AIV(%)	Soundness Test(%)
1	AKP3	2.46	0.98	1.00	50	21.83	23.44	20.60	5.00
2	KW2	2.59	0.88	0.92	55	24.01	22.69	20.00	4.50
3	MGT9	2.60	0.95	0.98	62	27.07	22.27	19.70	4.40
4	MGT8	2.48	0.98	1.00	51	22.26	22.87	20.80	4.70
5	NKP6	2.60	0.95	0.99	60	26.19	21.57	17.72	5.70
6	KW1	2.29	0.89	0.94	47	20.52	24.33	18.40	4.90
7	MGT1	2.62	0.90	0.93	64	27.94	19.18	20.00	4.20

8	KTG4	2.55	0.95	0.99	52	22.70	21.80	22.22	4.50
9	ZH10	2.49	0.95	0.97	49	21.39	23.20	20.00	4.10
10	TGB7	2.41	0.85	0.90	43	18.77	24.80	22.00	4.90
11	MGT10	2.54	0.91	0.94	48	20.96	24.50	22.80	5.00
12	MGT11	2.50	0.98	1.00	53	23.14	20.30	23.00	4.40
13	MGT12	2.53	0.98	1.00	43	18.77	25.40	18.00	5.35
14	MGT13	2.27	0.97	1.00	40	17.46	23.30	22.00	4.80
15	MGT14	2.31	0.89	0.93	45	19.65	23.81	21.30	5.50
16	MGT15	2.45	0.94	0.96	50	21.83	24.36	22.60	4.40
17	MGT16	2.48	0.93	0.95	50	21.83	22.86	20.00	3.90
18	MGT17	2.51	0.90	0.93	55	24.00	21.64	23.10	4.20
19	MGT18	2.52	0.89	0.93	55	24.00	23.00	22.20	4.20
20	MGT19	2.58	0.94	0.97	59	25.76	24.88	19.70	4.85

The Soundness Test is to simulate weathering characteristics of an aggregate, or more precisely its ability to resist weathering. The particular aggregate being tested is subject to a number of immersions (twelve) in an aggressive solution of magnesium or sodium sulphate to hasten the degrading process the environment has on the aggregate.

After the aggregate has been subjected to the testing regime the remaining weight of the aggregate is expressed as a percentage of the original weight. Aggregate soundness tends to be related to the water absorption of an aggregate i.e. an aggregate with a high moisture absorption value tends to have a low soundness value.

Although, all the twenty rock samples have a soundness value within the acceptable range, (BS 812, Part 2) which should be below 12%, some samples tend to have relatively high water absorption. This could be attributed to the coarse nature of the rock samples and the gradual sericitization of the orthoclase/plagioclase feldspars in some of the rock samples. Samples MGT17 and MGT18 have good soundness value while AKP3 (South western part of the study area) have the highest soundness value which by interpretation is least good particularly for road surface.

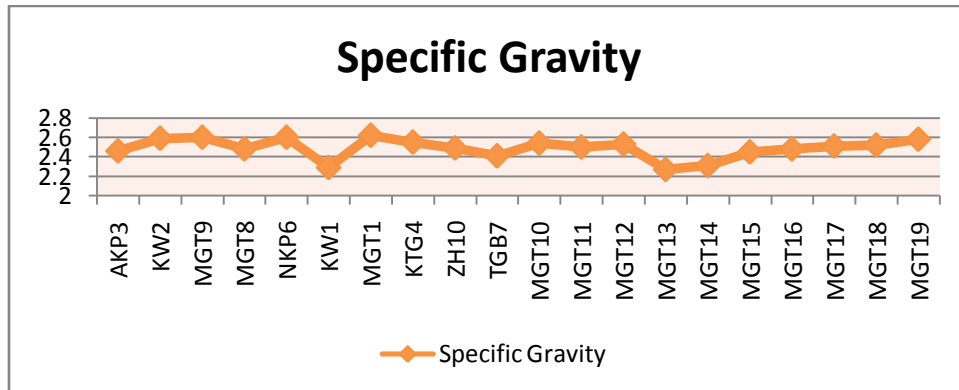


Fig.1.4 Specific Gravity of samples

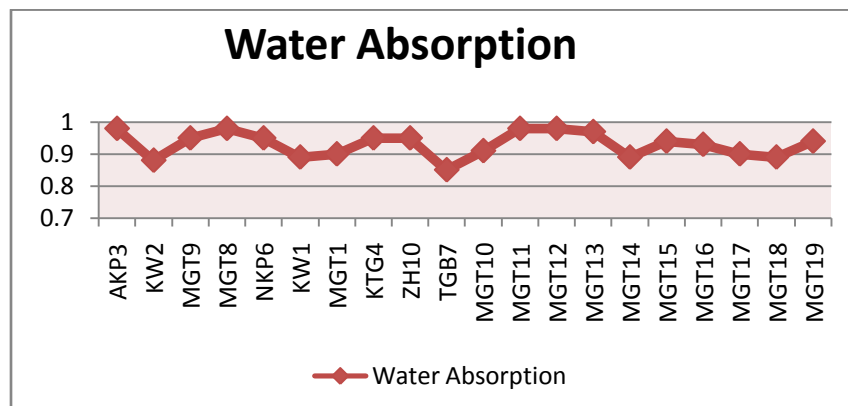
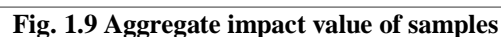


Fig. 1.5 Water Absorption of samples



Crushing Strength(N/mm2)



VI. Discussion

This is a test to simulate weathering characteristics of an aggregate, or more precisely its ability to resist weathering. The particular aggregate being tested is subject to a number of immersions (twelve) in an aggressive solution of magnesium or sodium sulphate to hasten the degrading process the environment has on the aggregate.

After the aggregate has been subjected to the testing regime the remaining weight of the aggregate is expressed as a percentage of the original weight. Aggregate soundness tends to be related to the water absorption of an aggregate i.e. an aggregate with a high moisture absorption value tends to have a low soundness value.

Although, all the twenty rock samples have a soundness value within the acceptable range, (BS 812, Part 2) which should be below 12%, some samples tend to have relatively high water absorption. This could be attributed to the coarse nature of the rock samples and the gradual sericitization of the orthoclase/plagioclase feldspars in some of the rock samples. Samples MGT17 and MGT18 have good soundness value while AKP3 (South western part of the study area) have the highest soundness value which by interpretation is least good particularly for road surface.

The specific gravity is defined as the weight per unit volume of a substance, in this case a rock. The unit weight of a rock depends on the constituent minerals of the rock, porosity and on the amount of water in the pores. It has been observed that of the three main categories of rocks (Igneous, metamorphic and sedimentary), sedimentary rocks usually have lower specific gravities, followed by metamorphic and igneous rocks. Rocks containing heavy metals possess high densities (4.5 and above) whereas the ranges of densities for sedimentary, metamorphic and igneous rocks vary from 2.63 to 2.86 (Mallo, 2010).

Almost all the rock samples analyzed have low to moderate specific gravities according to (Anon, 1979). This is attributable to the dominant constituent minerals in the rock. Sample number KW1 has the least specific gravity of 2.29 and is the coarsest of all samples in hand specimen while samples MGT1 has the highest specific gravity of 2.62 and is relatively fine in hand specimen. The implication of these is that the rocks have medium-low porosity whereas higher the porosity, the faster the weathering. Hence, their utilization for engineering construction is hampered (Mallo, 2011).

The rate of water absorption of any rock depends on its porosity. The porosity in turn depends on the mineral composition, grain size distribution, degree of packing and the cementing materials in case of sedimentary rocks. The utilization of highly porous construction materials is not advisable as a result of buoyancy effect, because the weight of porous materials decreases due to buoyancy, to the detriment of the carrying capacity (Mallo, 2010). Also, the samples analysed have water absorption of less than 1% which is good for most construction work.

Under normal conditions water fills only a certain portion of the total volume of pores. The degree of saturation is the ratio of the volume of pores filled with water to the total volume of pores. The degree of saturation and water absorption by rocks can affect the bearing capacities of foundation materials of civil engineering structures. Samples AKP3, MGT8, MGT11, MGT12 and MGT13 have a water absorption under saturation of 1% which means that they cannot be used in logged areas as foundation materials, while the other samples have water absorption under saturation of less than 1% which means that they can be considered as foundation materials. A reason could be advanced for the relatively high rate of water absorption under saturation of samples AKP3, MGT8, MGT11, MGT12 and MGT13 to the micro fractures in the samples and the high orthoclase quartz ratio in the sample.

Generally, the compressive strength of rocks is influenced by its texture. The compressive strength of igneous rocks depends on porosity. The more compact the porphyry, the higher the compressive strength. This argument is also true for metamorphic rocks (Mallo, 2010). The cementing materials and presence of fractures or fissures and the degree of saturation affects the compressive strength of most rocks. Consequently, as percentage sorption of rocks increases, the compressive strength decreases.

The classification of rocks based on compressive strength and field estimate of strength by Brown 1981 indicates that only samples MGT1, NKP 6, MGT9 and MGT19 have compressive strength of above 25 MPa while the remaining samples have compressive strength ranging from 18-24.04 MPa. This then implies that 80% of the samples are likely to yield ambiguous results in civil engineering construction in line with dry density and porosity (Anon, 1979).

The aggregate crushing value is a value which indicates the ability of an aggregate to resist crushing. The lower the crushing values the stronger the aggregate and the greater its ability to resist crushing. Crushing strength is related to porosity and grain size, the higher the porosity and the larger the grain size, the lower the crushing strength. On the other hand, with increasing content of altered minerals in a rock, the lower the crushing strength. Some of the samples which have their orthoclase/plagioclase feldspars sericitized have low crushing strength.

Based on the aggregate crushing value of some rocks given by Bell (2007) all the rock samples have low crushing strength as none have aggregate crushing strength of less than 20%. The implication of this is that the rock material cannot be used as wearing course in roads because of low crushing strength and altered form.

Aggregate impact value is a strength value that is determined by performing the aggregate impact test on a rock aggregate. Basically, the aggregate impact value is the percentage fines produced from the aggregate samples after subjecting it to a standard amount of impact. Aggregate impact values and aggregate crushing values are often numerically very similar and indicate similar aggregate strength properties.

The principal tests carried out in order to assess the value of a roadstone are aggregate crushing test, the aggregate impact test, the aggregate abrasion test and the test for the assessment of the polished stone value. Other tests of consequence are those of water absorption, specific gravity and density and the aggregate shape tests (Anon, 1975a).

Of the twenty rock samples analysed for aggregate impact strength, all are satisfactorily for road surfacing because their AIV ranges from 18%-23% for MGT12 which has the highest lowest value, by implication the strongest to 23.10% for MGT18 which is "weakest". Based on table 5.3 the rock samples are satisfactory for road surfacing. This is because most roads are more susceptible to crushing than to impact.

VII. Characterization Based on Geo-Technical Test.

Crushed rock is produced for a number of purposes, and principally for concrete and road aggregate. Most volume of concrete consist of aggregate, therefore its properties have significant influence on the engineering behavior of concrete. An attempt is made here to characterize the Miango Granite Porphyry with respect to their suitability and utilization for construction works based on the laboratory analyses carried out on them.

Aggregate with compressive strength below 25MPa are likely to yield ambiguous results in engineering construction (Brown, 1981). Those with aggregate crushing strength of more than 20% are considered weak. Conversely, aggregates with aggregate impact strength of 20%-30% are considered satisfactorily for road surfacing. The average compressive strength of the Miango Granite porphyry is 20MPa, aggregate crushing strength of 23% and aggregate impact strength of 22%.

Aggregates used for roads have to bear the main stresses imposed by traffic such as slow-crushing loads and rapid-impact loads have to resist wears (Bell, 2007). Based on the above, the aggregates produced from the Miango Granite porphyry can be utilized as road metal.

The unit weight of a rock depends on the constituent minerals of the rock, porosity and the amount of water in pores of the rock. The BS acceptance limits for water absorption is < 3%, bulk density of >2.60g/cm³ and aggregate impact of 30% (Akpokodje, 1992). The twenty rock samples analysed have water absorption and water absorption under saturation of < 3% and an average specific gravity of 2.45. Based on the results, the Miango Granite porphyry tends to be of high quality however, their compressive strength is low. Therefore, they can utilized as roadstone because are more prone to impact than to crushing loads.

Soundness also known as durability test, measures a rock resistance to weathering, freeze-thaw, sulphate and moisture attack. The acceptable standard for durability test according to BS 812 part 2 is < 12%. All the twenty samples analysed have soundness value of less than 6%. This implies that the rocks can withstand harsh climatic conditions but because of their low crushing and compressive strength, they can be polished and used as facing stone because of their beautiful large feldspar phenocrysts.

VIII. Summary

The influence of mineralogy and fabric of the Miango Granite porphyry, North- Central Nigeria was carried out. The study area lies within the Jos Plateau characterized by an undulating topography with a hybrid of drainage pattern and various rock types. The Miango area is underlain mainly by the Younger Granite suite which composed essentially of Granite, syenites, rhyolite and basalts, and localized occurrences of basement rocks which are mainly migmatites and granite gneiss.

Geological, geotechnical data were acquired and used to ascertain the engineering properties of the Granite porphyry. The geological mapping was mainly from existing geological maps and surface mapping which revealed most outcrops in the study area and of particular interest the Granite porphyry. The geotechnical laboratory analyses carried out include those of specific gravity, water absorption, water absorption under saturation, soundness test, aggregate crushing test, aggregate impact test and uniaxial compressive test of the twenty rock samples from different locations in the study area. Also, thin section and petrographic studies of the twenty samples was carried out to determine the mineral grain orientation and the extent of deformation of the rock samples.

The results of geotechnical analyses were interpreted with the aid of some standards. The results showed that based on (BS 812 part 2) all the twenty rock samples have a soundness value within the acceptable range which is below 12%, none of the rock samples have a soundness value of up to 6%. Almost all the rock samples analysed have low to moderate specific gravities according to (Anon, 1979). This is attributable to the dominant constituent minerals in the rock. Sample KW1 (Zarama Kwall) has the least specific gravity of 2.29 and is the coarsest of all in hand specimen and is the coarsest of all samples while MGT1 (Miango adjacent ECWA Goodnews) has the highest specific gravity of 2.62 and is relatively fine in hand specimen. The implication of this is that the rocks have medium-low porosity. The samples analysed have water absorption of less than 1% which is good for most construction. Samples AKP3, (Akpene Kwall road), MGT8 (Miango Town), MGT 11 (Miango environs) have a water absorption under saturation of 1% which means that they cannot be used in water logged areas as foundation materials while the other samples that have water absorption under salivation of less 1% can be considered as foundation materials. According to Brown, (1981) only samples MGT1, (Miango Adjacent ECWA Goodnews), NKP6 (Nkepru Miango), MGT16 (Miango and environs) have compressive strength of 25MPa while the remaining samples have compressive strength of 18-24 MPa. This means that 80% of the samples are likely to yield ambiguous results in civil engineering construction. Based on Bell, (2007) granites should have an aggregate crushing value of 17%, however, none of the rocks have aggregate crushing values of less than 20% which means that the rocks cannot be used as wearing course in roads because of low aggregate crushing

strength. According to IS 383 rocks with aggregate impact value of 20-30% are satisfactorily for road surfacing. Twenty of the rock samples analyzed for aggregate impact strength shows that they have AIV range of 18-23% which implies that they can be used satisfactorily for road surfacing that would not be subject to crushing load.

IX. Conclusion

The need for rock aggregates of high quality in engineering construction is of great importance as its demand is on the increases daily. As this study demonstrates however, it is possible to adopt a scientific approach to determine the quality of the rock aggregates for specific engineering works. This study has been able to show that the geotechnical competence of a rock depends more on the texture and spatial arrangement of the mineral grains than on the mineralogy of the rock (granite porphyry). The fine to medium- grained rocks tend to have more engineering strength than the coarse grained rocks with the same mineralogy therefore, the following conclusion can be drawn from the studies.

The rock samples analysed have poor values for uniaxial compressive strength and aggregate crushing strength which are tests of significance in aggregates for use in heavy engineering works. However, the soundness (durability), aggregate impact, specific gravity, water absorption under saturation values are good which implies that the rocks can be utilized as road surface course where wearing and crushing effects are less.

The orthoclase and or the plagioclase feldspars in 80% of the rock samples have been hydrothermally altered to sericite and also have intergrowth of quartz and orthoclase or plagioclase thereby reducing the strength of the rocks.

The presence of micro fractures on 80% of the rock samples analyzed can hampered their use for engineering construction.

References

- [1] Akpokodje, E.G. and Hudec, P.P (1991): The influence of petrology and fabric on the Engineering properties of concretionary Laterite Aggregates. Journal of The Nigerian Mining and Geosciences Society, abstract Vol. 29.
- [2] Akpokodje, E.G. (1992): Properties of Some Nigerian Rock Aggregates and Concretes. Jour Min. and Geol. Vol. 28 (2), Pp. 185-190.
- [3] Anon. (1975). Methods for Sampling and testing Mineral Aggregates, Sands and Fillers. British Standards Institutions, London.
- [4] Anon (1979): Classification of Rocks and Soils for Engineering Geological Mapping, Part 1- Rock and Soil Materials. Report of the Commission of Engineering Geological Mapping, Bulletin International Association of Engineering Geology Vol. 19, pp. 364-371.
- [5] Bell, F. G. (2007): Engineering Geology, 2nd Ed. Elsevier Ltd. India. pp 294-296.
- [6] Brown, S.F. (1981): Soil Mechanics in Pavement Engineering Geotechnique, Vol. 46 pp. 383-426.
- [7] Indian Standard Specification for Course and Fine Aggregates from Natural Sources, I.S. 383, Indian Standard Institution.
- [8] Jacobson, R.R. E., Macleod, M.N, and Black, R. (1964): Ring Complexes in the Younger Granite Province of Northern Nigeria. Memoir No. 1, Geological Society of London pp. 65-66.
- [9] Macleod, W.N, and Berridge, N.G. (1971): Geology of the Jos Plateau. Bulletin 32, Vol. 2, Geological Survey of Nigeria.
- [10] Macleod, W.N. and Turner, D.C. (1971): Geology of Jos Plateau. Geological Survey of Nigeria. Bulletin 32, Vol. 1, pp. 12-47.
- [11] Mallo, S. J. (2010): Unpublished M.Sc. Lecture Notes on Rock Mechanics.
- [12] Mallo S.J. (2011): Fundamentals of Geotechnical Engineering (unpublished).
- [13] Ogunsanwo, O. (1994): Influence of Schistosity on the Strength and Wave Velocity Characteristics of a Mica Schist Coprolite. Jour. Min. and Geol. Vol.27 (2) pp. 135-138.
- [14] Ogunsanwo, O. (1994): Influence of Geochemistry and Mineralogy on the Optimum Geotechnical Utilization of some Laterite Soils from S.W. Nigeria. Jour. Min. and Geol. Vol. 31 (2), pp. 183-188.
- [15] Turner, D.C. (1989): Structures and Petrology of the Younger Granite Ring Complexes. In Geology of Nigeria (Kogbe, C.A. ed), Rock View Nig. Ltd., Jos, Nigeria pp. 175-189.
- [16] Wright, E.P. (1971): The Basement Complex, Bulletin 32, Vol. 1, Geological Society of Nigeria pp. 12-41.

Need of Lapping Machine for Valve Component: A Case Study

S. M. Fulmali,¹ R.B.Chadge²

¹Student of M.Tech, Yeshwantrao Chavan College of Engineering, Nagpur

²Asst. Professor, Yeshwantrao Chavan College of Engineering, Nagpur

ABSTRACT: Lapping process is characterized by its low speed, low pressure, and low material removal rate. This process is used in achieving finer surfaces and closer fits, correction of minor imperfections, and maintaining close tolerances. During the process of lapping, the mechanisms of surface formation and removal rate are decisively influenced by the movement type of the individual grains within the lapping abrasive. A gate valve is used to start and stop the flow of fluid. So the wedge and seat ring of a valve are in continuous pressure of fluid flow and due to opening and closing of valve these component get wear and they need lapping during reconditioning. This paper will share the need, requirement and application of lapping during the reconditioning of valve.

This paper will explore the current working condition of lapping machine in valve industry. It will elaborate the effect of abrasive particals, working speed, surface roughness and other related parameters. What are the difficulties they are facing during the valve reconditioning related to lapping, will be discussed. Current set up and the changes required in this model are suggested with the proposed model.

Key words: Lapping process, wedge, seat ring, abrasive particles.

I. INTRODUCTION

Lapping is a micro finishing operation which is required to require getting a mirror like surface finish on the meting component. It provides a good strength to joint formed. Lapping has been used extensively in the manufacture of optical mirrors and lenses, ceramics, hard disk drive, semi-conductor wafers, valve seats, ball bearings, and, and many more parts[1]. Several factors need to be considered during the process of lapping. This includes factors such as type of machine, condition of the lap plate surface, speed of the lap plate, type of abrasive, type of carrier fluid, slurry concentration, slurry flow rate, size and shape of abrasive, material of the lap plate, rigidity of the lap plate, applied force on the work piece, time of operation and duration between the two consecutive instances of application of fresh abrasive slurry [1, 2].

II. LITERATURE RELATED TO LAPPING

Commonly used as a finishing operation, lapping has been used for achieving ultra-high finishes and close tolerances between mating pieces. This process is characterized by its low speed, low pressure, and low material removal. The lapping process is carried out by applying loose abrasive grains between two surfaces and causing a relative motion between the two surfaces resulting in a finish of multi-directional lay[1].

Lalit Suhas Deshpande [1] stated the procedure and testing on valve component. They performed the test on two materials stainless steel (S31600), and bronze (C86300). These materials were identified as commonly used materials in the manufacturing of relief valve seats and thus selected for the experiments. The most commonly used abrasive materials for lapping of valves seats are alumina and silicon carbide. Metal tubes were machined in the form of circular rings resembling valve seats. The papers explain the result of testing with respect to varying speed, size of abrasive particals, material removal rate etc.

C. J. Evans [3] stated the selection of related component used in the lapping and polishing operation. The paper explains the role of granules in the slurry used for the removal of material during the lapping process. It also explains the material that should be used for the lap, its hardness and what should be the material removal rate in the process of lapping.

The physical scale of material removal processes in polishing is such that it is difficult (practically impossible) to observe them directly. Much of what we know about the fundamental mechanisms involved in the process has been derived either by correlating macroscopic measurements of process outputs with models, or by extrapolation from experiments at scales which can conveniently be observed.

J. Kang[4] in this paper Two types of HIPed Si3 N4 bearing ball blanks with different surface hardness and fracture toughness were lapped under various loads, speeds, and lubricants using a novel eccentric lapping machine.

The lapped surfaces were examined by optical microscope and SEM. The experimental results show that the material removal rate for type 1 ball blanks were 3–4-fold of type 2 in most cases. Different lapping fluids affected the material removal rate at lower lapping loads, but they had much less influence on the material removal rate at higher lapping loads.

III. NEED OF LAPPING FOR VALVE COMPONENT

Valve lapping is a essential part of maintenance work that often interrupt production work. Repairing leaking valve in industry is a laborious operation involving extended downtime, production losses and substantial unwanted cost. The given figure shows different parts of a gate valve.

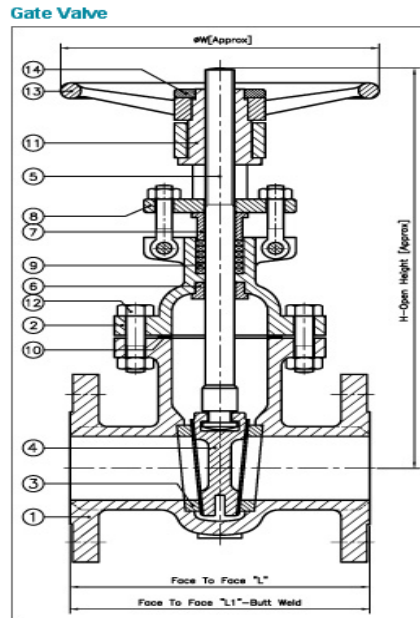


Fig.1. Gate Valve

Parts description:-

1.Body 2.Bonnet 3. Seat 4.Wedge 5. Stem 6. Back seat bush 7. Gland bush 8. Gland Flange 9. Gland packing 10. Gasket 11. Yoke sleeve 12. Bonnet Bolt and Nut 13. Hand wheel 14. Hand wheel Nut.

There are various reasons why repairing valves has many advantages, since:

- repair costs are only 5 – 35% of the procurement price of replacement valves
- maintaining stocks of all replacement valves ties up too much capital
- the delivery times of replacement valves can be extremely long, which can cause serious (and therefore expensive) production problems.

So we are trying to develop a set up for lapping operation which will be a portable one, available at cheaper cost and will perform lapping with minimum set up time.

IV. COMPONENT THAT REQUIRE LAPPING

4.1. Wedge of a valve:

This is a wedge of a valve which is under continuous pressure of fluid flow. The sizes of the wedge varies as per the size of valve for example 2", 4", 6" etc. valves. To close the valve these wedge meshes with the seat ring. These wedge requires lapping after 60-70 openings of valve. To get a leak proof component these portion requires lapping.



Fig. 1.Wedge of valve



Fig. 2.Wedge

4.2. Seat Ring

Wedge or disc meshes with the seat ring of valve. It is actually a ring made up of stainless steel, bronze etc. material. The shape of seat ring goes on changing with continuous use. It becomes tapered and gets leaked so it requires lapping. Size of seat ring also varies as per the size of valve. Small size seat rings are either press fitted or they may be welded to sustain fluid pressure.



Fig.3. Seat ring

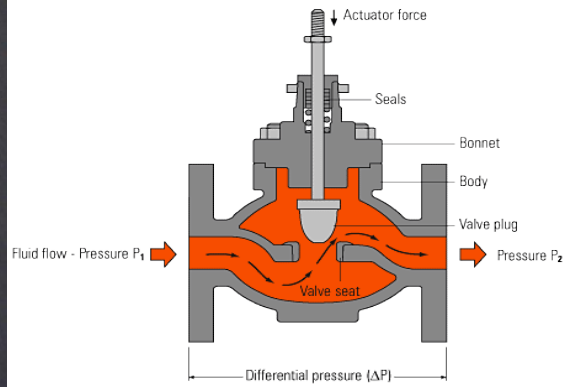


Fig.4. flow through valve

V. DEVELOPMENT OF LAPPING MACHINE

A visit to an industry it is being observed that they were performing lapping operation on a set up which was developed by them. They fixed the lapping tool to the conventional lapping machine which is fixed. They fixed the valve on a vice and perform lapping on the valves.

Observing the operation we are trying to propose on model which will be portable, can be handled by one person and it will reduce the set up time also.



Fig.5. Set up used in industry

VI. PROPOSED MODEL OF LAPPING MACHINE

A high torque drilling machine is used which will be generating a shaft speed of around 240 rpm. Through this shaft rpm is transferred to reduction gear box which will reduce it to 80-100 rpm. This speed is best for performing low speed lapping operation [1,3]. This gear box is mounted on holding plate which has holes on it. This plate will help us to hold the set up on frame for lapping wedge or hold the set up on body of valve.

Shaft through that gear box is connected with the lapping plate which is made up of cast iron [3]. A guide is provided at the centre to keep lap steady. The distance between seat ring and body of valve will vary according to the size of valve. So length of shaft will be according to the size of valve.

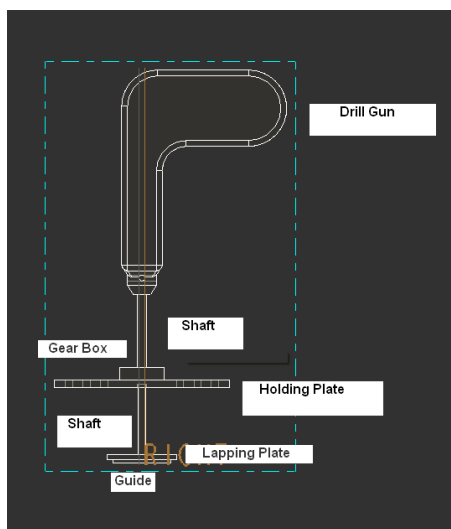


Fig.6. Drawing of proposed model

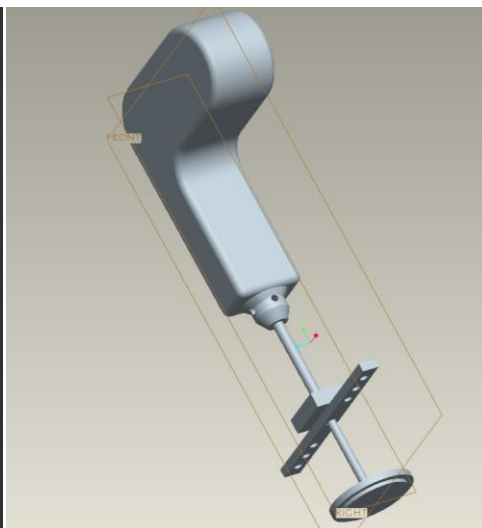


Fig.7. CAD model for lapping machine

VII. ABRASIVE MATERIAL USED FOR LAPPING

The most commonly used abrasive materials for lapping of valves seats are alumina and silicon carbide. It is the objective of this research to obtain sufficient data by lapping. Three types of abrasives: (1) garnet, (2) alun-dum (aluminum oxide), and (3) crystolon (silicon carbide) (4) CARBURANDM (silicon carbide) were used to lap the work pieces. Generally, the high peaks are abraded by coarse grains of average diameter about 80 mm (F80: coarse lapping), the average height s peak s by grain size between 40 and 20 mm (F40 and F20: average lapping) and the low height s peaks by fine grain size of 7 mm (F7: fine lapping) are available for lapping. We will perform coarse lapping and fine lapping on valve component.

The material removal rate is calculated by measuring the change in the height of the specimens before and after lapping with selected abrasives and dividing the height difference by the amount of time the process of lapping was performed (20 min period). Xiaobin and Peterson [1, 7] relationship was used for the calculation of MRR as:

$$MRR = dH/dt = \Delta H / \Delta t = (H_1 - H_2) / t$$

Where dH is the change in thickness, dt is the change in time, H1 is the average height of the specimen before lapping, H2 is the average height of the specimen after lapping and t is the time of lapping (a 20 min period).

VIII. CONCLUSION

The above research work and the proposed model can provide benefit in the lapping of valve component. Model will provide portability and reduce the set up time for lapping to some extent. The paper shows the importance of lapping operation in a valve industry. It show the size and type of abrasive used for valve lapping. As compared to the available machine for lapping, this proposed model will be the cheaper model. It will prove to be an economical model. The number of labors require to operate this machine is only one and less skilled labor can operate this model.

REFERENCES

- [1] Lalit Suhas Deshpande, Shivakumar Raman ,Owat Sunanta, Casmir Agbaraji "Observations in the flat lapping of stainless steel and bronze" Tribology International 40 (2007) 498 – 502,2007.
- [2] U. Heisel (I), J. Avroutine Institut fur Werkzeugmaschinen, "Process Analysis for the Evaluation of the Surface Formation and Removal Rate in Lapping" Wear 265 (2008) 105–116,2006.
- [3] C. J. Evans "Material Removal Mechanisms in Lapping and Polishing" peer reviewed 01-01-2003
- [4] J. Kang, M. Hadfield "Examination of the material removal mechanisms during the lapping process of advanced ceramic rolling elements". Wear 258 (2005) 2–12.
- [5] N. Belkhir D. Bouzid V. Herold "Correlation between the surface quality and the abrasive grains wear in optical glass lapping" Tribology International 40 (2007) 498 – 502
- [6] J.K.Wang,Desi Somogoi"Flow Loop Testing and Validation of Thermal Binding Model for Wedge Gate Valve".kalsi engineering
- [7] L. Xiaobin, M.L. Peterson, Material removal rate in flat lapping, J. Manuf.Process. 1 (1999) 71–78.

Analysis of Multicast Routing Protocols: Puma and Odmrp

S Sumathy,¹ Beegala Yuvaraj,² E Sri Harsha³

1, 2, 3 School of Information Technology and Engineering VIT University, Vellore, TN-632014, India.

ABSTRACT: In general, Wireless communication is defined as sharing of information between one or more systems through wireless links. Wireless networks can be categorized into two different modes as infrastructure based and infrastructure less. Infrastructure based mode is the most common use wireless mode for the end user loop. Infrastructure based networks are characterized by their use of access points (AP), or base stations. The most known example of infrastructure based wireless network is GSM and more recently, Wi-Fi. Ad Hoc networks introduce a new way of communication. An ad hoc network is a collection of wireless mobile nodes that dynamically functions as a network without the use of any existing infrastructure and centralized administration. Mobile Ad-hoc networking (MANET), an emerging field of wireless networking is an autonomous system of wireless mobile hosts, connected by wireless links that dynamically create a temporary network and establish an infrastructure less network. The topology of the network may change frequently and unpredictably. Multicast routing has been widely applied in mobile ad hoc networks (MANETs), to support different group oriented applications like video conferencing, interactions with Special interest groups etc., efficiently. This paper presents the comparative analysis of two multicast routing protocols, PUMA and ODMRP.

Keywords: MANET, PUMA, ODMRP, AODV, WMN's.

I. Introduction

1.1 Ad hoc

Mobile Ad-hoc Network (MANET) is an autonomous system of mobile hosts, connected by wireless links that dynamically create a temporary network and establish an infrastructure less network [1]. The topology of the network may change frequently and unpredictably. Each and every node in the MANET should be aware of its neighbour and act as a router to forward datagram's to the specified destination. If two mobile nodes are located within the forwarding range, they communicate with each other directly over the wireless radio frequencies. Otherwise, they need intermediate node(s) to forward their datagram's using a multi-point hopping method. MANETs are characterized by non-restricted mobility and easy deployment, which makes them very popular. Mobile wireless nodes will typically have limited transmission range, which means that packets might have to be forwarded by several nodes in order to ensure communication between one node in the network to another. Fig 1 below illustrates how node A uses a route through node B to send data to node C, as C is out of A's transmission range.

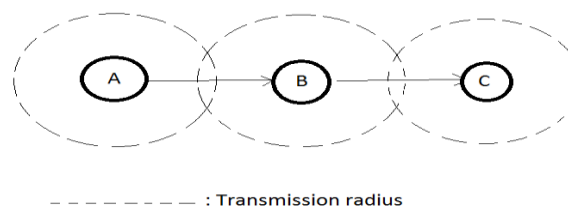


Fig 1. Routing in MANET

As a technology for dynamic wireless networks, ad hoc networking has been deployed in military since 1970s. Commercial interest in such networks has recently grown due to the advances in wireless communications. A new working group for MANET has been formed within the Internet Engineering Task Force (IETF), aiming to investigate and develop a framework for running IP based protocols in ad hoc networks. In recent years, many group oriented applications have gained a lot of importance. Multicast routing has been widely applied in mobile ad hoc networks (MANETs), to support different group oriented applications efficiently. Some of them are:

- Military applications used in the battlefield
- Search and rescue operations
- Temporary networks within meeting rooms and airports
- Personal Area Networks connecting mobile devices like mobile phones, laptops, smart watches, and other wearable computers
- Disaster recovery
- Video conferencing and multimedia streaming

The rest of the paper is organized as follows. Section 2 describes related work on unicast and multicast routing protocols for MANET. Section 3 describes PUMA routing protocol. Simulation setup and Performance analysis are described in section 4. Finally, section 5 follows with a conclusion and future enhancement.

II. Related Work

This section explains some of the most representative unicast and multicast routing protocols such as AODV, ODMRP and PUMA.

2.1 Routing Protocols

Routing protocol is a procedure used by router to determine the appropriate path onto which data should be forwarded. It also specifies how routers report changes and share information with the other routers in the network that they can reach. This decides whether the network should dynamically adjust to changing conditions, otherwise all routing decisions have to be predetermined and remain static. To achieve the preliminary objectives, several routing protocols in the area of mobile ad hoc networks should be examined. Routing Protocols can be classified based on message delivery semantics as unicast, multicast and broadcast showed in the Fig 2, Fig 3, and Fig 4.

- **Unicast** – to single specified node by the host
- **Broadcast** – to all nodes in the network
- **Multicast** – to a group of nodes that have expressed interest in receiving messages

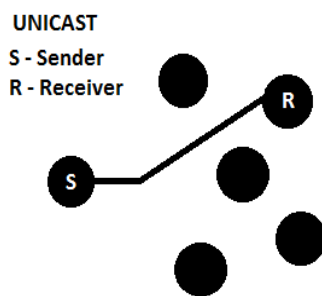


Fig 2. Unicast

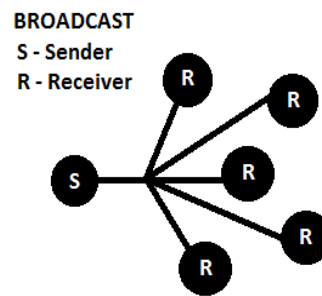


Fig 3. Broadcast

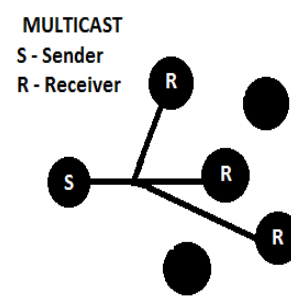


Fig 4. Multicast

2.2 Unicast Routing

Unicast routing refers to finding a feasible path between a single source and a single receiver. Unicast term is used to describe communication where a piece of information is sent from one point to another point. Some of the unicast protocols are AODV, DSDV and DSR

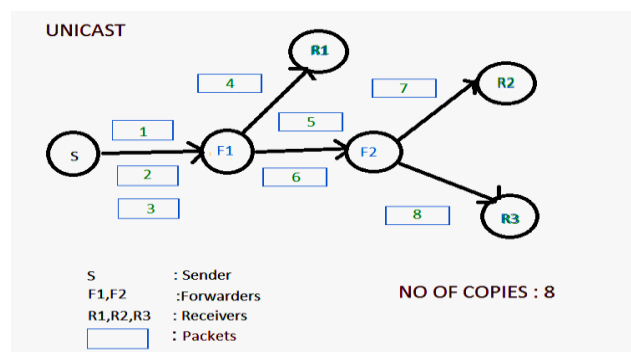


Fig 5. Packet Transmissions in Unicast

2.2.1 AODV

AODV [2] is a reactive distance vector routing protocol, which means routing decisions will be taken depending on the number of hops to destination on demand.

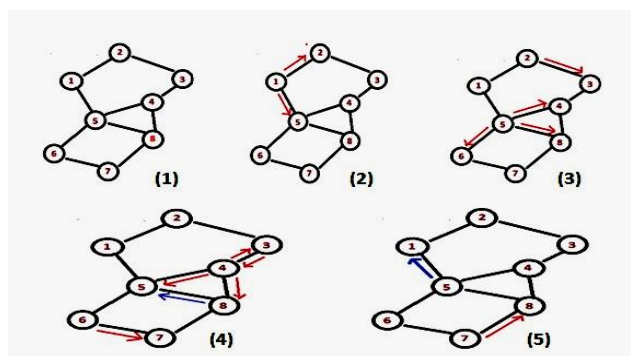


Fig 6. AODV Illustration

In the example illustrated by Fig 6, node 1 intends to send a packet to node 8.

“ROUTE REQUEST” packet will be generated by Node 1 and sent to node 2 and node 5. Node 2 and node 5 add node 1 in their routing table, as a reverse route, and forward the “ROUTE REQUEST” packet to their neighbors. The forwarding process continues while no route is known. Once node 8 receives the “ROUTE REQUEST” from node 5, it generates the “ROUTE REPLY” packet. Duplicate packets continue to be ignored while the “ROUTE REPLY” packet goes on the shortest way to node 1, using routing table of each node. The reverse routes created by the other nodes that have not been used for the “ROUTE REPLY” are deleted after a delay. Node 5 will add the route to node 8 once they receive the “ROUTE REPLY” packet.

2.2.2 Merits of AODV:

It does not need any central administrative system to control the routing process. It reacts relatively fast to the topological changes in the network and updates only the nodes affected by these changes. The HELLO messages supporting the routes maintenance are range-limited, so they do not cause unnecessary overhead in the network.

2.2.3 Drawbacks of AODV:

The performance of the AODV protocol is poor in larger networks. A long path is more vulnerable to link breakages and requires high control overhead for its maintenance. Furthermore, as a size of a network grows, various performance metrics begin decreasing because of increasing administrative work, so-called administrative load.

2.3 Multicast Routing

Multicast [3] is a bandwidth-conserving technology that reduces traffic by simultaneously delivering a single stream of information to thousands of recipients. Multicast routing refers to finding a feasible tree covering a single source and a set of receivers. Multicast transmission is a more effective mechanism when compared to unicasting in supporting group communication applications and hence is an important aspect of future network development. Multicast is used in videoconferencing, corporate communications, distance learning, and distribution of software, stock quotes, and news in real time.

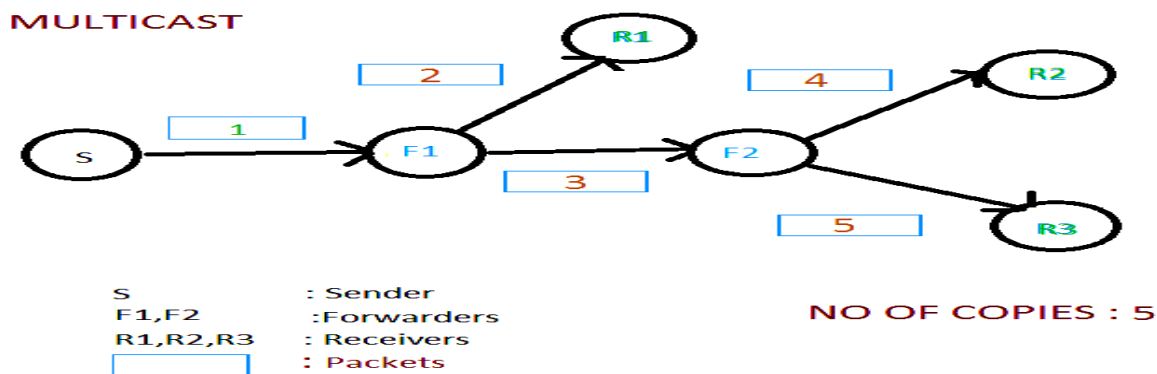


Fig 7. Packet Transmissions in Multicast

Since, MANETs have dynamic topology, the position of the nodes change with time resulting in wireless-link failure across nodes. If the mobile nodes in the MANET move too quickly, they have to repair the routes to achieve node to node communication to forward the packets. So, the multicast routing protocol should be capable of handling the link-breakages and find new optimal paths, if necessary. Several multicast routing protocols have been proposed to solve these problems. Every multicast routing protocol has its advantages and disadvantages, and aims at a specific application. Finally, the expected standard for multicast routing protocols in the Mobile Ad-Hoc Networks is very likely to minimize its energy consumption and control traffic overhead while at the same time, it should be capable of responding rapidly to link failure and addition caused by mobile node movements.

Existing protocols are either tree or mesh-based [4] or hybrid. Tree-based schemes establish a single path between any two nodes (generally sender and a receiver) in the multicast group. These schemes require minimum number of copies per packet to be sent along the branches of the multicast tree. Hence, they are bandwidth efficient. However, as mobility increases, link failures trigger the reconfiguration of entire tree. When there are many sources, network either has to maintain a shared tree, losing path optimality or maintain multiple trees resulting in storage and control overheads. Examples of tree-based schemes include: ad hoc multicast routing utilizing increasing ID-numbers protocol (AMRIS) [5], and multicast ad hoc on-demand distance vector routing protocol (MAODV)[6].

Mesh-based schemes establish a mesh of paths that connect the source and destinations. They are more resilient to link failures and also to various mobility conditions of ad hoc nodes. The disadvantage of a mesh based scheme is its increase in redundancy because multiple copies of the same packet are transmitted through the mesh, resulting in reduced packet delivery and increased control overhead under highly mobile conditions. Examples of mesh-based schemes include: on-demand multicast routing protocol (ODMRP) [7], Core Assisted Mesh Protocol (CAMP) [8].

2.3.1 On-Demand Multicast Routing protocol (ODMRP)

On-Demand Multicast Routing protocol (ODMRP) [8] is a mesh based source-initiated protocol, i.e., it uses forwarding group concept and multiple paths exist between sender and receiver. It applies on-demand procedures to build route and maintain multicast group membership dynamically. By maintaining a mesh, instead of a tree, the drawbacks of multicast trees in ad hoc networks like frequent tree reconfiguration and non-shortest path in a shared tree are avoided.

2.3.1.1 Algorithm

In ODMRP, group membership and multicast routes are established by the source on-demand. When a multicast source has packets to send but no route to the multicast group, it broadcasts a Join-Query control packet to the entire network. This control packet is periodically broadcast to refresh the membership information and updates routes. When the Join-Query packet reaches a multicast receiver, it creates and broadcasts Join-Reply to its neighbors. When it has been received by the node, it checks if the next hop id is its own id. If it matches, the node realizes that it is on the path to the source and becomes the part of the forwarding group by setting the FG_FLAG (Forwarding Group flag). When receiving a multicast data packet, a node forwards it only when it is not a duplicate, hence minimizing traffic overhead. Because the nodes maintain soft state, finding the optimal flooding interval is critical to ODMRP performance. ODMRP uses location and movement information to predict the duration of time that routes will remain valid. With the predicted time of route disconnection, a "join data" packet is flooded when route breaks or ongoing data sessions are imminent. It reveals that ODMRP is better suited for ad hoc networks in terms of bandwidth utilization.

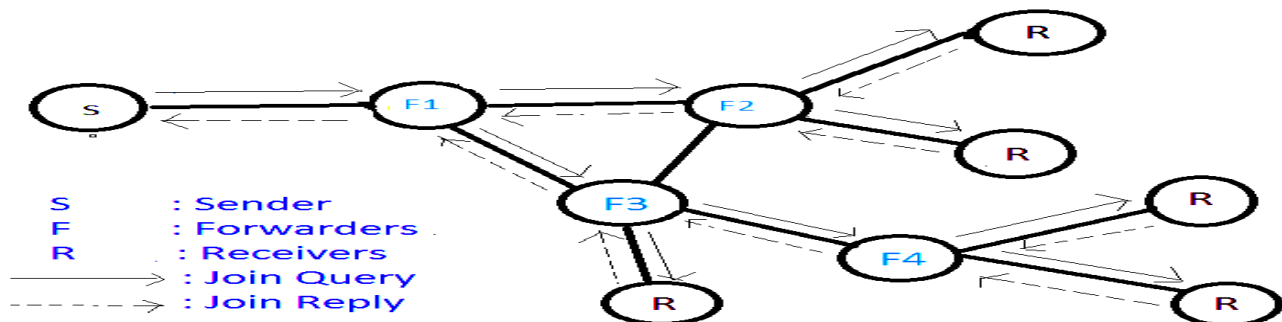


Fig 8. On-demand procedure for membership setup and maintenance

Fig 8, Fig 9 is an example to show the robustness of a mesh configuration. Sender 'S' send multicast data packets to three receivers (R1, R2, and R3) via three forwarding group nodes (F1, F2 and F3). In case the route from S to R1 is <S-F1-F2-R1>. In a tree configuration, if the link between nodes F1 and F2 breaks R1 cannot receive any packets from S until the tree is reconfigured but in ODMRP has a redundant route <S-F1-F3-F2-R1> to deliver packets without going through the broken link between nodes F1 and F2.

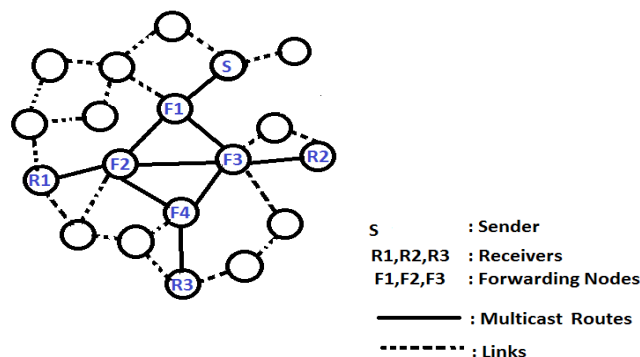


Fig 9. ODMRP Illustration

2.3.1.2 Merits of ODMRP

- Usage of up-to-date shortest routes
- Robustness in terms of host mobility
- Exploitation of the broadcast nature of the wireless environment
- Capability to perform Unicast Routing.
- multiple redundant paths are maintained and exploited

2.3.1.3 Drawbacks of ODMRP

- The main disadvantage of ODMRP is its excessive overhead, due to broadcasting of the reply packets to many nodes.
- As it is mesh based, topology is complex.

III. PUMA

Puma[9] is a receiver initiated routing protocol in which receivers join a multicast group using special address (core in CAMP protocol or group leader in Multicast AODV protocol).The flooding of data or control packets is reduced using special address (core of the group) by all sources.

Distributed algorithm is used to elect core among receivers of a multicast group. Election algorithm is same as the spanning tree algorithm to find loop-free shortest path between the core and group members. The elected core is connected to receivers in the network through all possible shortest paths. All intermediate nodes on shortest paths collectively form the mesh structure. Data packets are sent from sender to the group via core along any possible shortest path and flooded within the formed mesh whenever mesh member receives. All nodes in the network keep a packet ID cache to remove data packets that are duplicated [9]. Multicast announcement acts as a single control message to perform all tasks in PUMA.

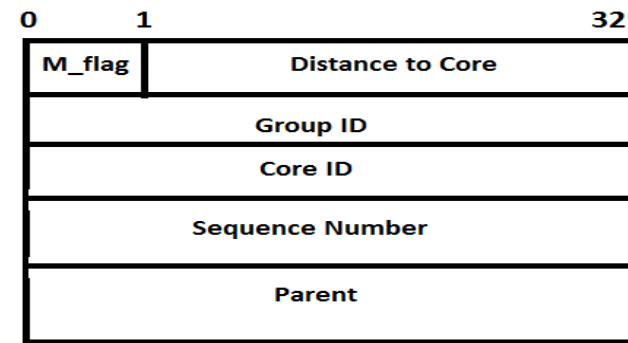


Fig 10. MAP Format

Each multicast announcement showed in Fig 10 specifies a sequence number, the address of the group(group ID), the address of the core (core ID), the distance to the core, a mesh member flag that is set when the sending node belongs to the mesh, and a parent that states the preferred neighbor to reach the core. With the information contained in such announcements, nodes elect cores, determine the routes for sources outside a multicast group to unicast multicast data packets towards the group, notify others about joining or leaving the mesh of a group, and maintain the mesh of the group. Connectivity list is established using multicast announcements at every node in the network. It is used to establish a mesh and keep track of multicast announcement received from neighbor by nodes. It also stores the receiving time and neighborhood details.

3.1 Establishment of Mesh

Initially mesh member flag of all receivers set to TRUE by considering themselves as mesh members in the multicast announcements they send. Non-receivers consider themselves mesh-members if they have at least one mesh child in their connectivity list. A neighbor in the connectivity list is a mesh child if : (a) its mesh member flag is set; (b) the distance to core of the neighbor is larger than the nodes own distance to core; and (c) the multicast announcement corresponding to this entry was received within a time period equal to two multicast announcement intervals. Condition (c) is used to ensure that a neighbor is still in the neighborhood. If a node has a mesh child and is hence a mesh member, then it means that it lies on a shortest path from a receiver to the core.

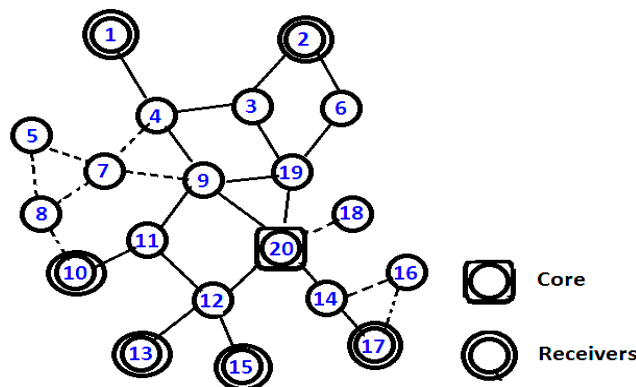


Fig 11.Mesh Establishment and Maintenance

As represented in Fig 11, node 20 is treated as core and other nodes in the group mark the connectivity list distance field by adding one to the finest entry. The receivers (nodes 1, 2, 10, 13, 15, 17 and 20 update the mesh member status to 1. node 3 and node 6 become mesh-members after receiving multicast announcement from qualified mesh child node2 as the distance to core is same. Similarly, nodes 4, 9, 12, 19 and 14 become the mesh members as the overall distance to the core node from mesh members is small. The procedure continues until the shortest paths are detected to the core from the receivers in the mesh. In this example, the route between the node 2 and core 20 of distance 3 exist through 2-3-19-20 and 2-6-19-20 and both paths are part of the mesh.

3.3 Core Election

If a node does not receive any multicast announcement for particular group, it assumes itself the core of the multicast group and transmits multicast announcements to its neighbors and set self-distance to 0. Nodes update their connectivity list based on multicast announcements with higher core ID. The receiver which joins the group first becomes the core of the multicast group. If two or more receivers join simultaneously, then the one with largest IP address becomes core [10].

3.4 Propagation of Data Packets

The best multicast announcement from neighbor is considered in order to fill the parent field of connectivity list. A node fills parent field with a node entry from which it receives a best announcement. This field allows nodes that are non-members to forward multicast packets towards the mesh of a group. A node forwards a multicast data packet it receives from its neighbor if the parent for the neighbor is the node itself.

Hence, multicast data packets move hop by hop, until they reach mesh members. The packets are then flooded within the mesh, and group members use a packet ID cache to detect and discard packet duplicates.

IV. Performance evaluation

4.1 Performance Metrics

Performance of MANET routing protocols can be evaluated using a number of quantitative metrics those are mentioned in RFC2501. We have used packet delivery ratio, throughput, end-to-end delay and normalized routing load for evaluating the performance of unicast routing protocol AODV and multicast routing protocols (PUMA & ODMRP).

4.1.1 Packet Delivery Ratio

It is defined as the ratio of number of data packets delivered to all the receivers to the number of data packets supposed to be delivered to the receivers. This ratio represents the routing effectiveness of the protocol:

$$PDR = \frac{\text{Packets delivered}}{\text{Packets sent}} \quad (1)$$

4.1.2 Average End-to-End Delay

It is the average time taken for a data packet to move from the source to the receivers:

$$\text{Avg. EED} = \frac{\text{Total EED}}{\text{No. of packets sent}} \quad (2)$$

4.1.3 Throughput

Throughput refers to how much data can be transferred from the source to the receiver(s) in a given amount of time:

$$\text{Throughput} = \frac{\text{Number of packets sent}}{\text{Time Taken}} \quad (3)$$

4.1.4 Normalized Routing Load (NRL)

It is defined as the ratio of total no. of data packets received to the total no. of routing packets received:

$$NRL = \frac{\text{No. of data packets received}}{\text{No. of routing packets received}} \quad (4)$$

4.2 Unicasting

4.2.1 AODV Simulation Setup

We compared the performance of AODV with two different transport layer traffic protocols TCP and CBR. We used NS-2 which is an event driven simulator targeted especially at network research. Experimental scenario considered with a network of 50 mobile nodes placed randomly within a 1500 x 300 m. Random waypoint is used as the mobility model. Radio propagation range for each node is 250 m and channel sensing threshold is set to 550 m. Packet size of each datagram is of 512 KB and maximum Queue length is set to 50 packets. Each simulation executes for 200 sec of simulation time. MAC_802.11 is used as medium access control protocol. Multiple runs by varying traffic and receivers are conducted for each scenario and the average of the collected data is obtained.

4.2.2 Results

TABLE I: AODV Metrics with TCP Traffic

Number of Receivers	PDR	Throughput (in kbps)	End to End Delay (in ms)	Network Routing Load
01	99.93	1072.53	37.18	0.003
05	98.92	666.79	231.18	0.060
10	97.24	732.17	216.70	0.472
15	95.73	745.25	225.27	0.578
20	95.29	748.90	234.29	0.580

TABLE II: AODV Metrics with CBR Traffic

Number of Receivers	PDR	Throughput (in kbps)	End to End Delay (in ms)	Network Routing Load
01	99.79	40.80	2.59	0.184
05	99.91	201.74	14.75	0.103
10	99.78	404.53	8.90	0.073
15	97.44	592.86	14.20	0.086
20	98.75	799.81	29.33	0.097

4.3 Multicasting

We compared the performance of PUMA and ODMRP using Network Simulator and Qualnet respectively. Experimental scenario considered with a network of 50 mobile nodes placed randomly within a 1500 x 300 m. Table III provides the details of the simulation setup.



Fig 12. NS-2 Simulation Scenario

4.3.1 Simulation Setup

TABLE III: Simulation Parameters

Simulator	Network Simulator (NS-2)	QualNet 5.0.2
Total Nodes	50	50
Simulation Time	200 sec	200 sec
Simulation Area	1500x300	1500x300
Propagation Model	Two Ray Ground Model	Two Ray Ground Model
Pause Time	0 - 10 sec	0 -10 sec
Mobility Model	Random Waypoint Model	Random Waypoint Model
Radio Range	250 m	250 m
MAC Protocol	MAC_802.11	MAC_802.11
Data Packet Size	512 bytes	512 bytes
Data Rate	11 Mbps	11 Mbps
Antenna	Omni Directional Antenna	Omni Directional Antenna
IFQ Length	50 packets	50 packets
Bandwidth of Physical Layer	11 Mbps	11 Mbps
No. of Receivers	10, 20, 30, 40	10, 20, 30, 40
Routing Protocol	PUMA	ODMRP
Destination Address	224.0.0.1	225.0.0.1
No. of Packets Per Sec	10	10
Mobility Speed	0 – 10 m/sec	0 – 10 m/sec
Traffic	CBR	MCBR

4.4 Results and analysis

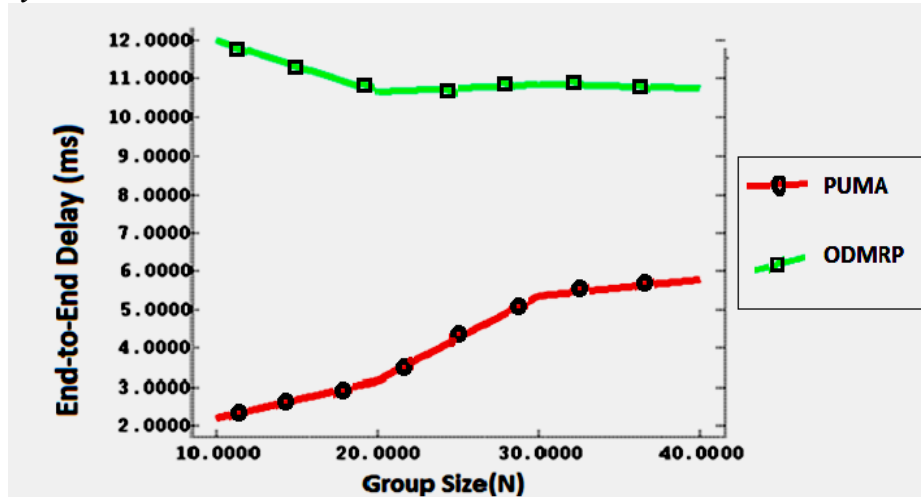


Fig 13. End-to-End Delay Vs Group Size [No. of nodes]

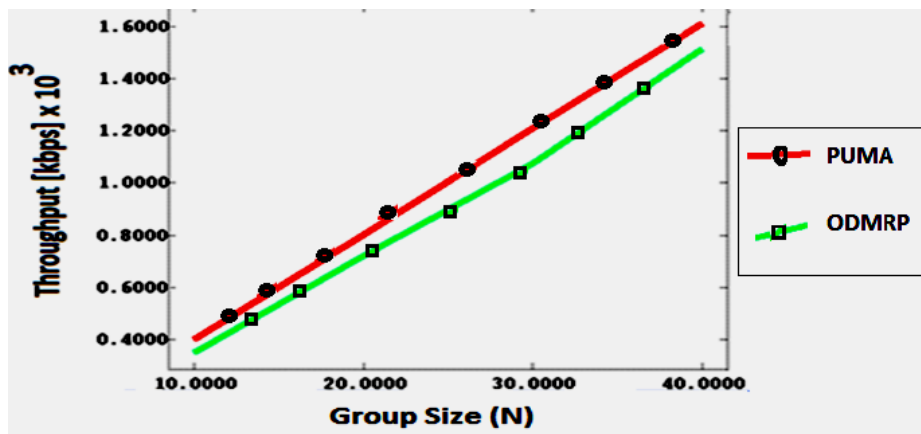


Fig 14. Throughput Vs Group Size [No. of Nodes]

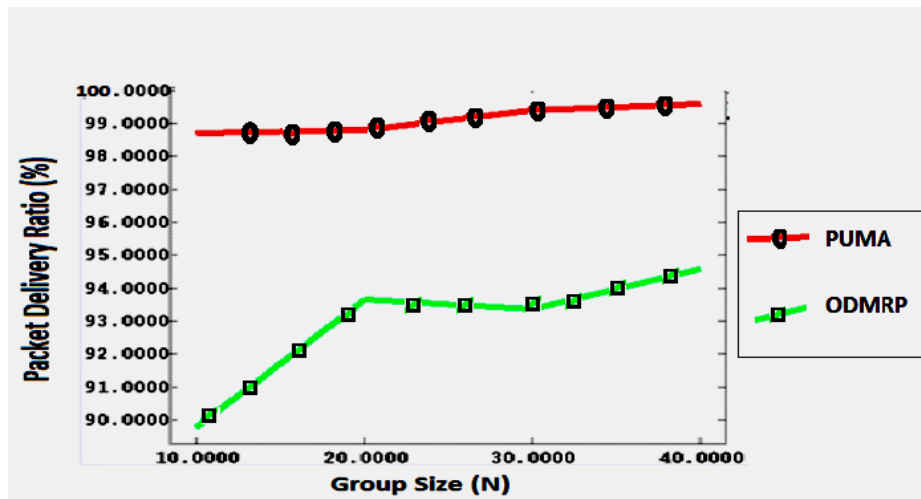


Fig 15. Packet Delivery Ratio Vs Group Size [No. of nodes]

4.5 Discussion

From the analysis of AODV, a unicast routing protocol, it can be observed that delay is high even though the group size is less. Hence, AODV cannot be used for group communications, specifically in the area of multimedia, where delay is considered to be an important metric. The same scenario is taken and simulated using multicast routing protocols, ODMRP and PUMA. For the chosen simulation parameters, it is observed that the average end to end delay is less in PUMA, compared to ODMRP and AODV. PUMA outperforms ODMRP with respect to the metrics like packet delivery ratio, average end-to-end delay and throughput. This is because the per-source flooding of ODMRP leads to significant number of packet drops due to congestion as the number of senders is increased beyond 10. On the other hand, the only node that floods the network in PUMA is the core. It is also observed that, when the number of multicast groups is increased, per source

flooding per group leads to congestion [11] and packet drops. Increasing the number of multicast groups does not have a significant effect in PUMA, because the multicast announcements for multiple groups are aggregated by every node.

Similarly, the higher signaling overhead of ODMRP due to per-source flooding and higher data packet overhead due to its mesh structure results in network saturation much earlier. As a result, when the traffic load is increased beyond 10 packets per sec, the packet delivery ratio of PUMA is higher than that of ODMRP, as shown in Fig 15. It is also found that, PUMA maintains almost constant EED with multiple sender scenarios also. This makes, PUMA as a more suitable protocol for video streaming applications. As PUMA is a mesh based scheme, even if there is a link failure, the packets are transmitted using the redundant path in mesh for efficient group communication.

V. Conclusion

In MANETs, both unicasting and multicasting can be used. But according to the performance analysis, specifically for group communications, multicast routing increases the efficiency and provides better performance when compared to unicast routing.

5.1 Future Enhancements:

In PUMA, core is responsible for creation and maintenance of mesh and forwarding the data packets. If the core node fails, core election takes place among the receivers. During the core election, energy of the receiver node is not considered. We can introduce an energy field in the Message Announcement packet, which can be used for electing a core node. Electing a node which possesses higher energy as core will serve better, as core takes all the responsibility of creating and maintaining mesh as well as forwarding the data packets.

WMNs have been widely accepted in the traditional application sectors of ad hoc network. With increasing demand for real-time services in the next generation wireless networks, quality-of-service (QoS)-based routing offers significant challenges in WMNs. The multi constrained QoS-multicast routing has been proved as NP-hard problem. Further, based on genetic algorithm approach, multiple QoS parameters can be optimized simultaneously.

References

- [1] S. Seas, Z. Yang, and J. He, (2004) 'A survey on mobile ad hoc wireless network', Information Technology Journal (3), pp.168–175.
- [2] C.E. Perkins, E.M. Royer, S.R. Das, Ad hoc on demand distance vector (AODV) routing, in: IEEE WMCSA, 1999.
- [3] S. Paul, Multicast on the Internet and Its Applications, Kluwer Academic Publishers, 1998.
- [4] Ian F. Akyildiz, Xudong Wang, Weilin Wang "Wireless Mesh Networks: a survey", Computer Networks, Vol.47, 2007, pp.445-487
- [5] C.W. Wu, Y.C. Tay, C.K. Toh, Ad hoc multicast routing protocol utilizing increasing id-numbers (AMRIS) functional specification, in: IEEE MILCOM, 1999, pp. 25–29.
- [6] E.M. Royer, C.E. Perkins, Multicast operation of the ad hoc ondemand distance vector routing protocol, in: ACM MobiCom, 1999.
- [7] Sung-Ju Lee, Mario Gerla, and Ching-Chuan Chiang, "On-Demand Multicast Routing Protocol" in proceedings of WCNC, September 1999.
- [8] J.J. Garcia-Luna-Aceves, E.L. Madruga, The core-assisted mesh protocol, IEEE Journal on Selected Areas in Communications 17 (8) (1999) 1380–1994.
- [9] R. Vaishampayan and J.J. Garcia-Luna-Aceves, "Efficient and Robust Multicast Routing in Mobile Ad Hoc Networks", Proc, IEEE MASS 2004, The First IEEE International Conference on Mobile Adhoc and Sensor Systems.
- [10] Sidney Santos Doria, Marco Aurélio Spohn, "A Multicast Approach for Peer-to-Peer Content Distribution in Mobile Ad Hoc Networks", WCNC 2009 proceedings.
- [11] H. Moustafa, "Unicast and Multicast Routing in Mobile Ad-hoc Networks," Ph.D. Thesis, (ENST) -Telecom, France, (2004).
- [12] <http://www.nsnam.isi.edu/nsnam/index.php>

Non Linear Finite Element Method of Analysis of Reinforced Concrete Deep Beam

Prof. S. S. Patil,¹ A. N. Shaikh,² Prof. Dr.B.R.Niranjan³

^{1,2}(Department of Civil Engineering, Walchand Institute of Technology, Sholapur, India)

³(Department of Civil Engineering, U.V.C.E Bangalore University, Bangalore, India)

ABSTRACT: This paper describes analysis of deep beams subjected to two point loading with three different L/D ratios (1.5, 1.6, 1.71) using Non-linear Finite element method (ANSYS 9.0 software) in order to investigate the stress and strain distribution pattern at mid-section of the beam. In ANSYS 9.0 software, SOLID 65 and LINK 8 element represent concrete and reinforcing steel bars. Non-linear material properties were defined for both elements. Using ANSYS software Flexural Strains and Stresses were determined at mid-section of the beam and shear stresses near the support of the beam. Also the failure crack-patterns were obtained. Variation of flexural stresses and strains, shear stresses were plotted. It was found that the smaller the span/depth ratio, the more pronounced is the deviation of strain pattern at mid-section of the beam.

Keywords: Deep Beam, Non-Linear Finite element method, ANSYS 9.0. L/D (Span to depth).

I. INTRODUCTION

Deep beam can be defined as a beam having a ratio of span to depth of about 2 or less. The deep beams were usually observed in case of transfer girder, pile cap, raft beam, wall of rectangular tank, hopper, shear wall [5]. Because of their proportions deep beams are likely to have strength controlled by shear rather than flexure. In IS-456 (2000) Clause 29, a simply supported beam is classified as deep when the ratio of its effective span L to overall depth D is less than 2. Continuous beams are considered as deep when the ratio L/D is less than 2.5. The effective span is defined as the centre-to-centre distance between the supports or 1.15 times the clear span whichever is less.

II. ANALYSIS USING ANSYS SOFTWARE

The finite element analysis calibration study included modeling a concrete beam with the dimensions and properties [1]. To create the finite element model in ANSYS 9.0 there are multiple tasks that have to be completed for the model to run properly. Models can be created using command prompt line input or the Graphical User Interface. For this model, the graphical user interface was utilized to create the model. This section describes the different tasks and entries to be used to create the finite element calibration model.

2.1. Element Types

The element type for this model is shown in Table 1.

Table1. Element Types for Working Model

Material Type Element	ANSYS
Concrete	Solid65
Steel Reinforcement	Link8

A Solid65 element was used to model the concrete [2]. This element has eight nodes with three degrees of freedom at each node translations in the nodal x, y, and z directions. The element is capable of plastic deformation, cracking in three orthogonal directions, and crushing. A schematic of the element was shown in Fig.1.

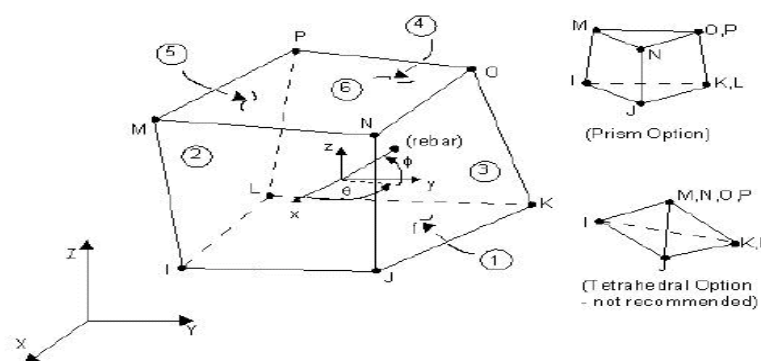


Figure1. Solid 65 elements

A Link8 element was used to model steel reinforcement [2]. This element is a 3D spar element and it has two nodes with three degrees of freedom translations in the nodal x, y, and z directions. This element is capable of plastic deformation and element was shown in the Fig.2.

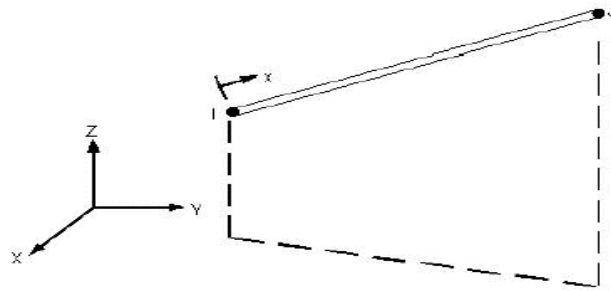


Figure 2. Link 8 element

2.2. Real Constants

Real Constant Set 1 was used for the Solid65 element [2]. It requires real constants for rebar assuming a smeared model. Values can be entered for Material Number, Volume Ratio, and Orientation Angles. The material number refers to the type of material for the reinforcement. The volume ratio refers to the ratio of steel to concrete in the element. The reinforcement has uniaxial stiffness and the directional orientations were defined by the user. In the present study the beam was modeled using discrete reinforcement. Therefore, a value of zero was entered for all real constants, which turned the smeared reinforcement capability of the Solid65 element of Real Constant Sets 2 and 3 were defined for the Link8 element. Values for cross-sectional area and initial strain were entered. Cross-sectional area in set 2 refers to the reinforcement of two numbers of 10mm diameter bars. Cross-sectional area in set 3 refers to the 8 mm diameter two legged stirrups. A value of zero was entered for the initial strain because there is no initial stress in the reinforcement. The real constants were given in Table 2.

Table 2. Real Constants

Real Constants Set	Element Type		Real constants for Rebar 1	Real constants for Rebar 2	Real constants for Rebar 3
1	Solid 65	Material no. V.R	0	0	0
2	LINK 8	Area (mm2) Initial strain	78.5 0	- 0	- 0
3	LINK 8	Area (mm2) Initial strain	50.24 0	- 0	- 0

2.3. Modeling

The beam was modeled as volume [2]. The model was 700 mm long with a cross section of 150 mm X 350 mm. The Finite Element beam model was shown in Fig.3. The dimensions for the concrete volume were shown in Table.3.

Table 3. Dimensions for Concrete

ANSYS	Concrete(mm)
X1,X2,X-coordinates	0, 700
Y1,Y2,Y-coordinates	0, 350
Z1,Z2,Z-coordinates	0, 150

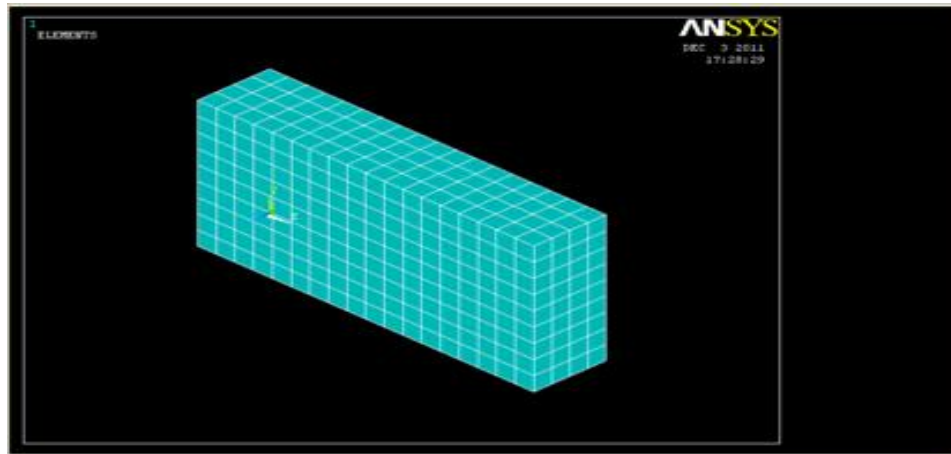


Figure 3. Finite element model & mesh of beam

2.4. Meshing

To obtain good results from the Solid65 element, the use of a rectangular mesh was recommended [2]. Therefore, the mesh was set up such that square or rectangular elements were created. The meshing of the reinforcement was a special case compared to the volumes. No mesh of the reinforcement was needed because individual elements were created in the modeling through the nodes created by the mesh of the concrete volume. The meshing and reinforcement configuration of the beam were shown in Fig.3 and Fig.4.

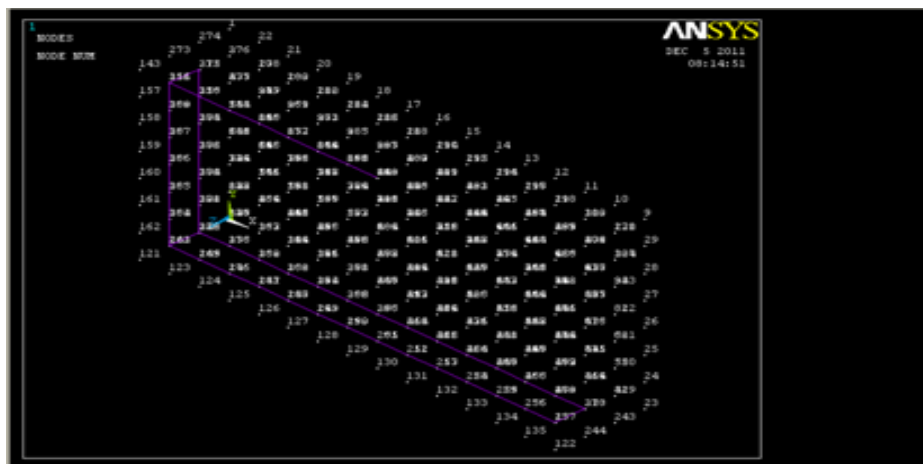


Figure 4. Reinforcement Configuration

2.5. Loads and Boundary Conditions

Displacement boundary conditions were needed to constraint the model to get a unique solution [2]. To ensure that the model acts the same way as the experimental beam boundary conditions need to be applied at points of symmetry, and where the supports and loading exist. The support was modeled as a hinged support at both ends. Nodes on the plate were given constraint in all directions, applied as constant values of zero. The loading and boundary conditions of the beam were shown in Fig.5.

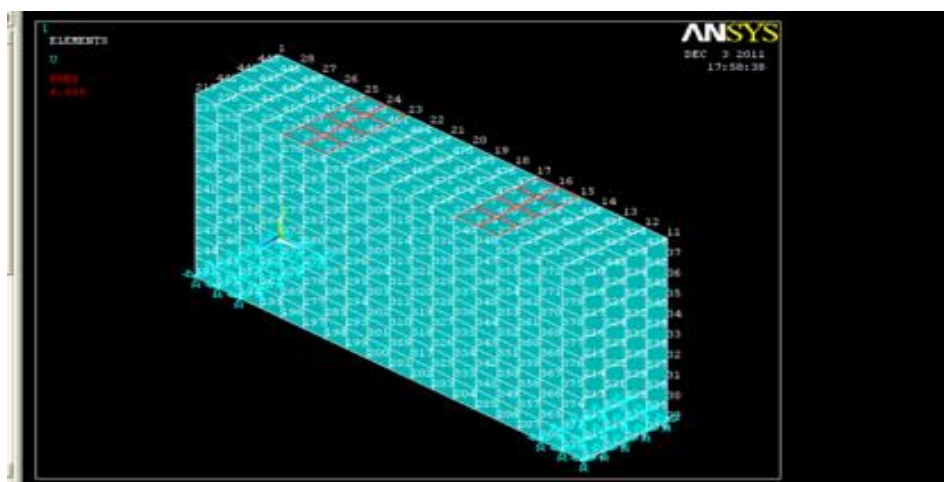


Figure 5. Loading and boundary conditions

III. RESULTS AND DISCUSSION

The variation of flexural stresses, strains at mid span and shear stresses near support were evaluated for various L/D ratios.

2.6. Variation of Flexural Strain

The variations of flexural strain were plotted at mid span of the beam for different L/D ratios. It was found that behaviour of flexural strain variation was non-linear. Also it was found that as the L/D ratio decreases the more pronounced was the deviation of strain pattern at mid-section of the beam. Fig.6.a to Fig.6.c were shown the variation of flexural strain at mid span for different L/D ratios.

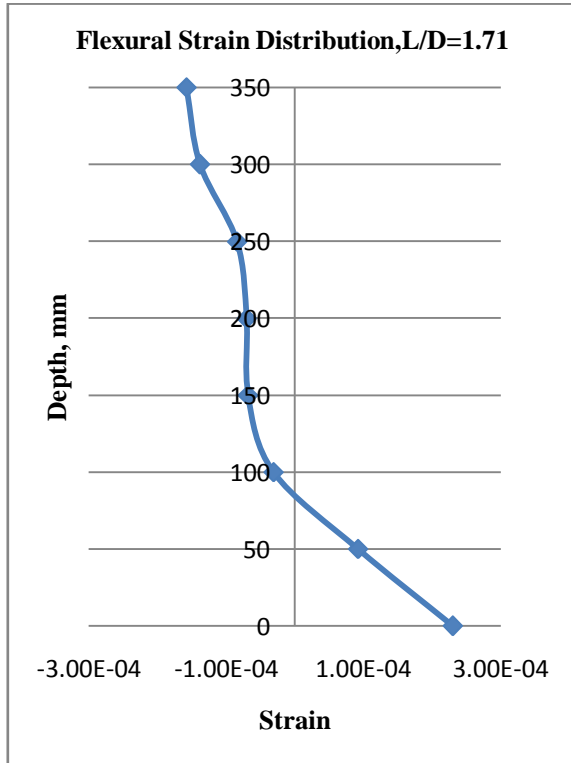


Figure 6.a. Flexural strain distribution for L/D = 1.71

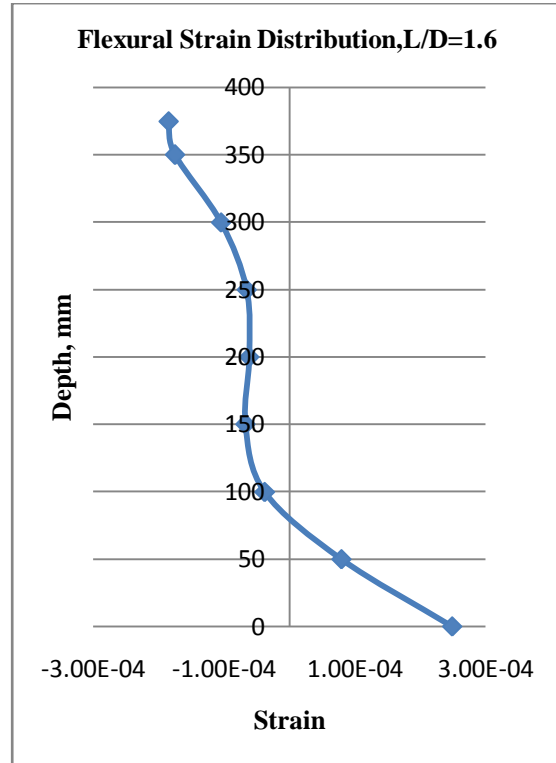


Figure 6.b. Flexural strain distribution for L/D = 1.6

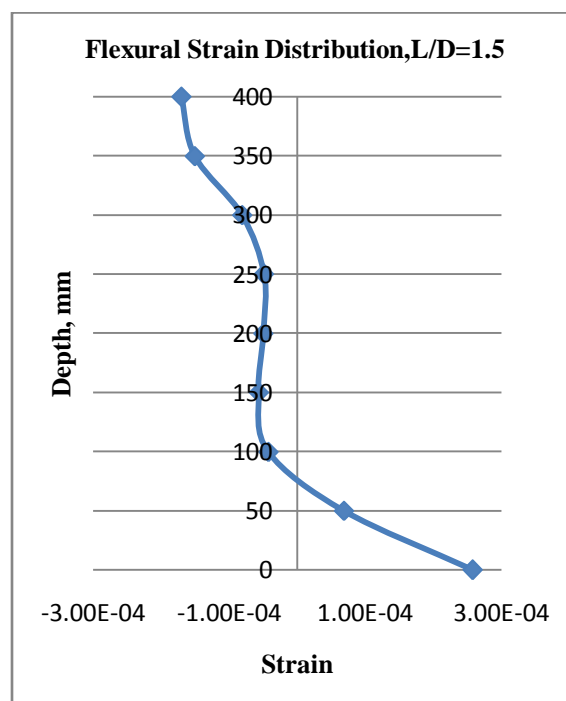


Figure 6.c. Flexural strain distribution for L/D = 1.5

2.7. Variation of Flexural stress

The variations of flexural stress were plotted at mid span of the beam for different L/D ratios. It was found that behaviour of flexural stress variation was non-linear. Fig.7.a to Fig.7.c were shown the variation of flexural stress at mid span for different L/D ratios.

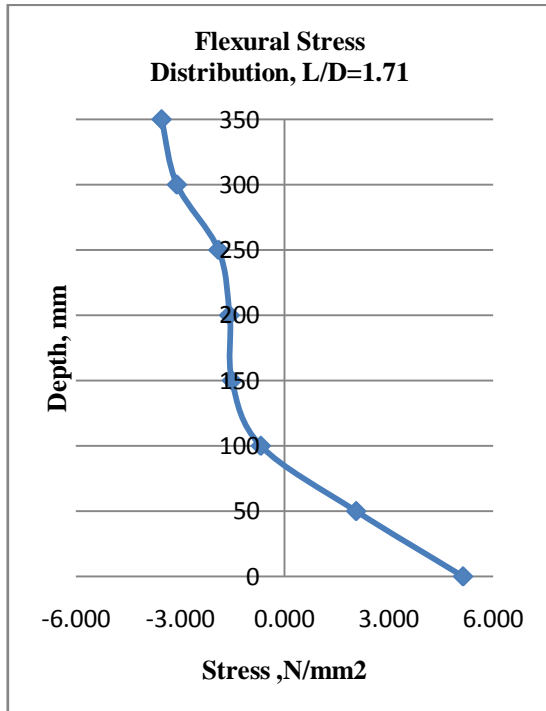


Figure 7.a. Flexural stress distribution for L/D=1.71

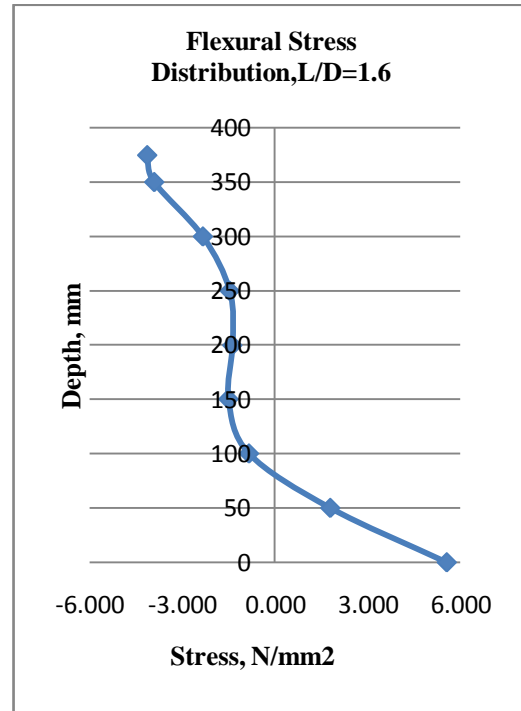


Figure 7.b. Flexural stress distribution for L/D=1.6

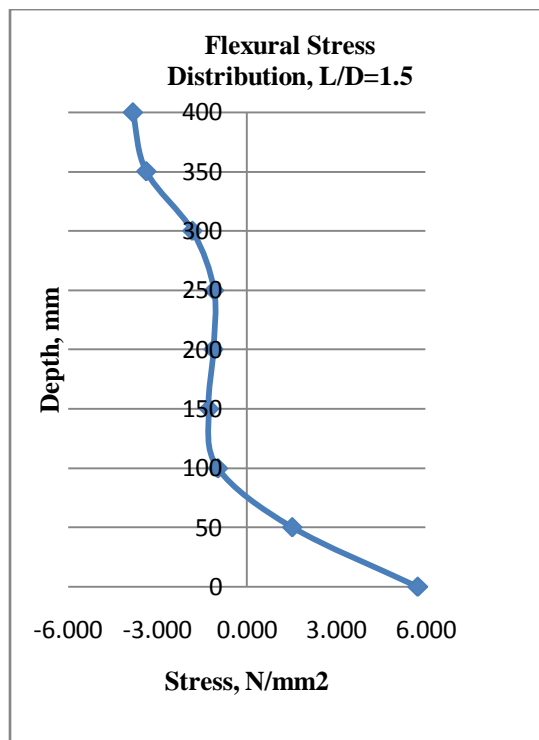


Figure 7.c. Flexural stress distribution for L/D=1.5

2.8. Variation of Shear Stress

Fig.8.a to Fig.8.c shows the shear stress near support of simply supported deep beam for different ratios of L/D. It was found that the smaller the span/depth ratio (i.e. less than 2.0), the more pronounced was the deviation of the shear stress distribution.

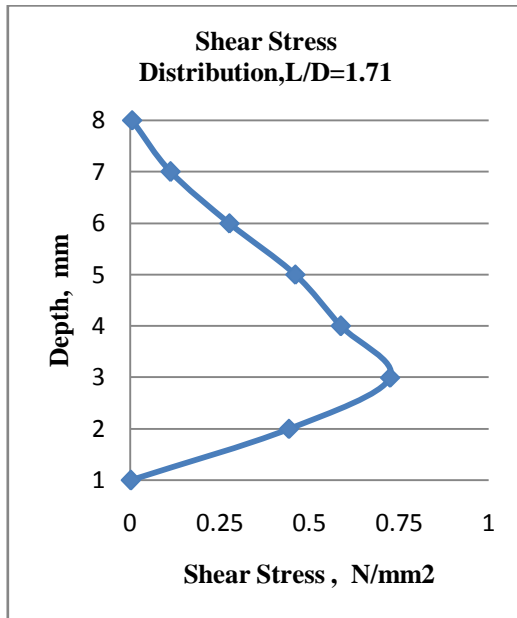


Figure 8.a. Shear stress distribution for L/D=1.71

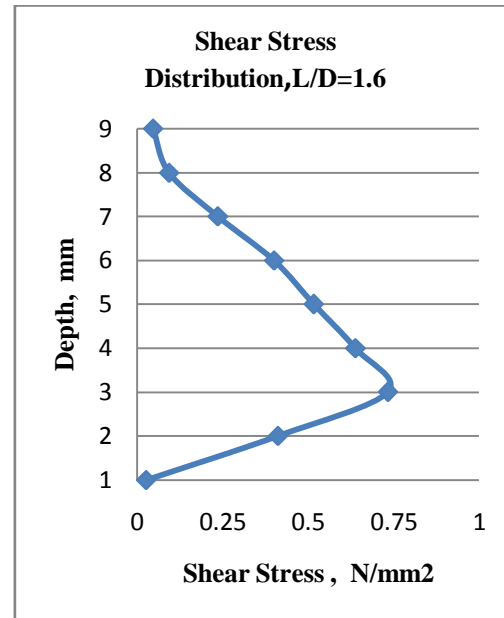


Figure 8.b. Shear stress distribution for L/D=1.6

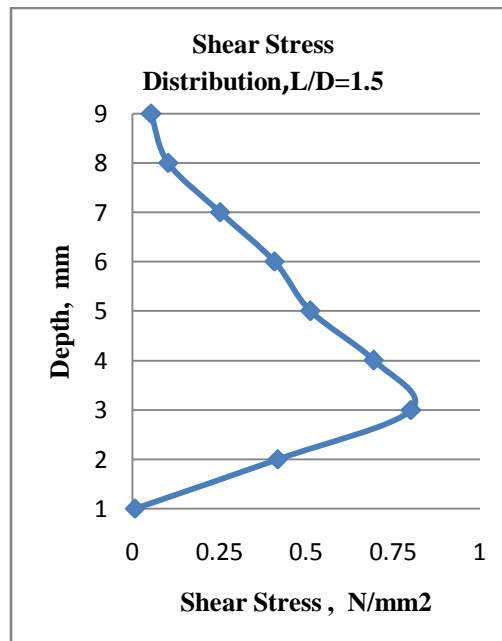


Figure 8.c. Shear stress distribution for L/D=1.5

IV. Conclusions

Deep beams having different L/D ratios were analyzed by using non-linear finite element method (by ANSYS 9.0) subjected to two points loading. Some prominent conclusions were summarized here.

1. From the flexural stress and strain graphs it was observed that smaller the span/depth ratio (i.e. less than or equal to 2.0), the more pronounced is the deviation of the stress-strain pattern i.e. the variation is not linear as in case of shallow beams.
2. Flexural stress and strain variation graphs indicate that the definition of simply supported deep beam as per IS 456:2000 i.e. when L/D ratio is less than or equal to 2.0 is reasonably accurate.
3. From the flexural strain and stress graphs it was observed that as L/D ratio of the beam decreases the neutral axis shifted towards soffit of the beam.
4. From the shear stress variation graph it was observed that as span/depth ratio decreases the shear stress increases.

REFERENCES

Journal Papers:

- [1] Anand Parande, P. Dhayalan, M. S. Karthikeyan, K. Kumar and N. Palaniswamy, Assessment of Structural Behavior of Non-corroded and Corroded RCC Beams Using Finite Element Method, Sensors & Transducers Journal, Vol. 96, Issue 9, pp.121-136(2008).
- [2] Mohammed Sh. Mahmood and Amer M. Ibrahim, Finite Element Modeling of Reinforced Concrete Beams Strengthened with FRP Laminates, European Journal of Scientific Research ISSN 1450-216X Vol.30 No.4 (2009), pp.526-541.
- [3] Muhammad Abdur Rashid And Ahsanul Kabir, Behaviour Of Reinforced Concrete Deep Beam Under Uniform Loading, Journal Of Civil Engineering, The Institution Of Engineers, Bangladesh, Vol CE 24,No-2,1996.

Books:

- [4] F. K. Kong Reinforced Concrete Deep Beams, (Van Nostrand Reinhold, New York 2011).
- [5] Varghese and Krishnamoorthy, Strength and Behavior of Deep Reinforced Concrete Beams. (Asoke K. Ghose, Prentice-Hall of India private Ltd. , 2006).
- [6] S. Ramamrutham, Design of Reinforced concrete structures.(Dhanpat Rai publishing company,2011).
- [7] S S. Bhavikatti, Finite Element Analysis, (New Age International (P) Ltd., Publishers, 2010).
- [8] R.D.Cook, D.S.Makus and M.F.Plesha, Concept and Applications of Finite Element Analysis, (John Wiley and Sons, 1989).

Use of LPG in A Dual Fuel Engine

A. Kumaraswamy¹ Dr. B. Durga Prasad²

¹(Mechatronics Engineering Department, Bharath University, Selaiyur, Chennai, Tamil Nadu- 600073, India)

² (Mechanical Engineering Department, JNTU College of Engineering, Anantapur, Andhra Pradesh-515002, India)

ABSTRACT: In this paper, the control scheme of a Liquefied Petroleum Gas (LPG)–diesel dual-fuel engine with electronic control is illustrated, the external characteristics and load characteristics of the LPG– diesel dual-fuel engine and the diesel engine are compared and analyzed. The experimental results show that, compared with diesel, the output performance of dual fuel is not reduced, while smoke emission of dual fuel is significantly reduced, NO_x emission of dual fuel is hardly changed, but HC emission and CO emission of dual fuel are increased and fuel consumption of dual fuel is reduced.

Keywords: LPG–Diesel dual fuel, electronic control, engine performance, pollutant emissions, fuel consumption

I. INTRODUCTION

Reducing the pollution of automobile emission and studying the application of an automobile alternate fuel are crucial subjects in the field of automobiles at present. With the constant increase in high-grade highway mileage and the significant improvement in production technology of the high-speed diesel engine and the increasing need for heavy-duty trucks for transportation, the number of diesel vehicles is increasing. Many cities in India have prohibited the running of diesel vehicles in urban areas because diesel automobiles have heavy smoke emission and loud noise and people feel that diesel automobiles are very harmful to the environment. Therefore, reducing the smoke emission of diesel automobiles, especially to used diesel automobiles, has become a problem that calls for an urgent solution. Smoke emission can be largely reduced if diesel vehicles are changed to fuel with liquefied petroleum gas (LPG)– diesel dual fuel, which is one of the efficient ways to reduce the smoke emission of diesel vehicles. The following list describes the potential health risks associated with these emissions:

- **Carbon Monoxide (CO):** An odorless and colorless gas which is highly poisonous. CO can reduce the blood's ability to carry oxygen and can aggravate lung and heart disease. Exposure to high concentrations can cause headaches, fatigue and dizziness.
- **Nitrogen Oxides (NO_x) and Nitrogen Dioxide (NO₂):** These chemicals form the yellowish-brown haze seen over dirty cities. When combined with oxygen from the atmosphere, NO becomes NO₂, a poisonous gas that can damage lung tissue.
- **Hydrocarbons (HC):** This is a group of pollutants containing hydrogen and carbon. Hydrocarbons can react to form ozone. Some are carcinogenic and other can irritate mucous membranes. Hydrocarbons include: Volatile organic compounds (VOC); Volatile organic gases (VOG); Reactive organic gases (ROG); Reactive organic compounds (ROC); Nonmethane hydrocarbons (NMHC); Non-methane organic gases (NMOG).
- **Ozone (O₃):** This is the white haze or smog seen over many cities. Ozone is formed in the lower atmosphere when NMOG and NO_x react with heat and sunlight. Ozone can irritate the respiratory system, decrease lung function and aggravate chronic lung disease such as asthma.

II. THE CONTROL SCHEME AND CONTROL DEVICE

The study on co-combustion characteristics of LPG– diesel dual fuel shows that, after co-burning LPG, the smoke emission of diesel engine at high loads can be significantly reduced, but at low loads, the specific fuel consumption is increased and the hydrocarbon (HC) emission and carbon monoxide (CO) emission are also increased. So, the way in which fuel consumption, HC emission and CO emission at middle and low loads can be reduced has become an urgent problem when dual fuel has to be adopted to reduce the smoke emission of diesel vehicles. To improve fuel economy, and to reduce HC emission and CO emission of dual-fuel engines at partial load, used the method of electronic control compressed natural gas (CNG) injection outside the cylinder and adopted the 'stopping-cylinder technique'. In other words, this method continues diesel supply of all cylinders and stops the CNG supply of some cylinders. It makes 'the working cylinders' operate at the optimum excess air ratio. This scheme is limited to the condition of applying electronically controlled gaseous-fuel injection. To ensure complete combustion and to reduce HC emission and CO emission of dual-fuel engines at partial load, used the intake-throttling method to increase the concentration of the gaseous-fuel pre-mixture. The performance of this kind of dual-fuel engine is close to that of a gasoline engine at partial load. Its fuel consumption increases because of the reduction in filling efficiency. This scheme has been tested only by the manual method. To reduce the HC emission of discharged dual-fuel engines due to the scavenging of the gaseous fuel premixture in the valves' overlap period used the gaseous-fuel mixer fixed in the intake manifold. The mixer is one kind of pipe system and uses the fluid dynamic effect to control the initial Timing of the gaseous-fuel intake. This scheme has poor adaptability to variable operating Conditions of engines.

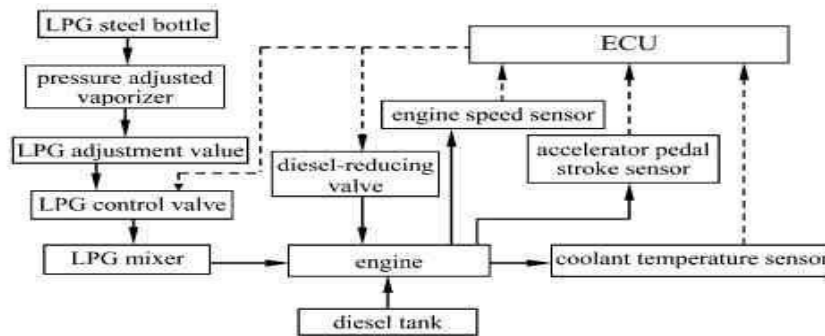


Fig. 1. The LPG-diesel dual-fuel, electronically controlled engine

This paper describes the development of an electronically controlled scheme, in which the engine is fuelled with diesel at low loads, and with LPG– diesel dual fuel after the engine load reaches a preset level. The advantage of this scheme is not only to adopt low-fuel consumption and emissions of HC and CO of diesel engines at low loads, but also to diminish heavy smoke emission at high loads and full load of diesel engines, by co-burning LPG. The LPG–diesel dual-fuel, electronically controlled engine is shown in Fig. 1. The electronic control unit (ECU) controls a diesel-reducing valve and an LPG control valve according to the signals from sensors, including engine speed, coolant temperature and accelerator pedal stroke, which indicate the engine's operating condition. The diesel-reducing valve, located on the high-pressure pump, is to reduce diesel supply when it is on. The LPG control valve, located between the pressure-adjusted vaporizer and LPG mixer, is to control the LPG supply. The engine resumes its operation with diesel when the ECU turns off the diesel-reducing valve to resume the diesel supply and shuts off the LPG control valve to stop the LPG supply. The electronic control device developed in this paper is shown in Fig. 2. The input signals of the control device are the accelerator pedal stroke, engine speed, and coolant temperature. The accelerator pedal stroke signal is supplied by a linear resistance installed at the speed-adjustment axle of the high-pressure pump. The engine speed signal, entering the single-chip computer system as a square wave after plastic handling and a wave filter, is supplied by an electromagnetic sensor. The frequency of the square wave signal is directly proportional to the engine speed. The coolant temperature signal, after electric-level transformation and comparison, is supplied as a switch signal to enter the single-chip computer system. No matter what the model of the speed governor of original diesel engine is, the device can complete the designed control characteristics of fuel supply by changing the read-only memory with a written relevant program.

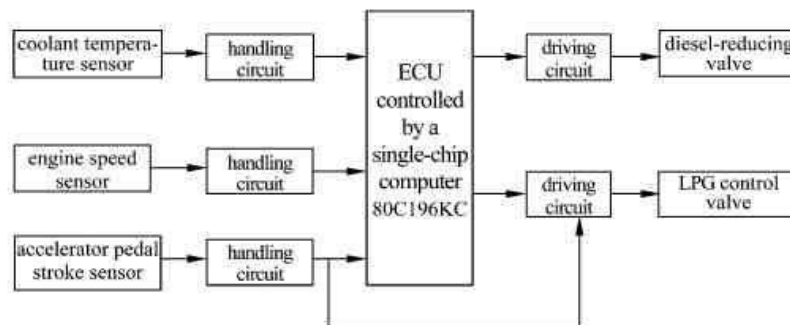


Fig. 2 The electronic control device

The single-chip computer program for the all-speed governor is illustrated below. After entering the subroutine, under the condition that the accelerator stroke is larger than the idle opening, as the coolant temperature is higher than 60°C, and the engine speed is higher than the idle speed and lower than the maximum speed, it is determined by the control table whether the diesel-reducing valve and LPG control valve works or not: under the condition when the engine speed is higher than the maximum value, the diesel supply is reduced and the LPG supply is shut off; under the condition when the coolant temperature is lower than 60°C, the LPG supply is shut off, and the engine is operated by diesel considering that LPG vaporizing condition is not good and control accuracy of the LPG control valve to LPG flow is reduce.

III. THE RESULTS AND ANALYSES OF ENGINE PERFORMANCES

Engine performance tests were completed on a four-cylinder supercharged direct injection diesel engine with electronic control. When the engine is fuelled with LPG–diesel dual-fuel, the brake specific fuel consumption (BSFC) is taken to be the LPG consumption which is commuted to diesel consumption according to their low calorific values, and the co-combustion ratio (CCR) is defined as the percentage ratio of LPG energy to the dual-fuel energy, given by

$$CCR = m_{LPG}H_{uLPG} \times 100 / (m_{LPG}H_{uLPG} + m_{diesel}H_{udiesel}) \quad \text{-----} (1)$$

Where m_{LPG} is the consumption of LPG, H_{uLPG} is the low calorific value of LPG (45.31 MJ/kg), m_{diesel} is the consumption of diesel, and $H_{u_{diesel}}$ is the low calorific value of diesel (42.50 MJ/kg).

3.1 The comparison and analysis of the engine external characteristics

3.1.1 Torque

The comparison between the torques of the external characteristics of LPG–diesel dual fuel and diesel is shown in Fig. 3. The torque of the dual fuel is slightly less than that of diesel, but the difference is very small; so the dynamic characteristic of the dual-fuel engine almost does not decline. To avoid knocking of the LPG mixture, CCRs are controlled in the range from 29.7 to 33.8 per cent when the compression ratio of the engine is not changed.

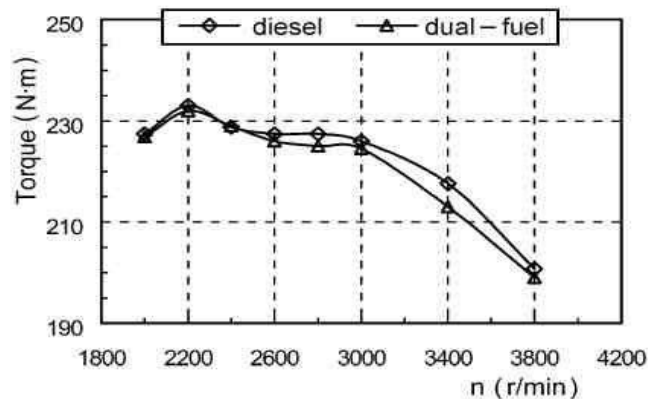


Fig. 3 The comparison of torques at full load

The air–fuel ratio of dual fuel is slightly smaller than that of diesel. Although the LPG pre-mixture causes a small decrease in the engine's intake air amount, the torque of dual fuel is almost equal to that of diesel because the reduction in air–fuel ratio of the LPG pre-mixture makes the heat value of the mixture in the cylinder recover, and dual fuel has a higher combustion efficiency than diesel.

3.1.2 Fuel Consumption

The comparison between the BSFCs of the external characteristics of LPG–diesel dual fuel and diesel is shown in Fig. 4. The BSFC of dual fuel is slightly less than that of diesel. Because of the good quality of the mixture and high combustion efficiency of dual fuel, the BSFC of dual fuel at full load is low.

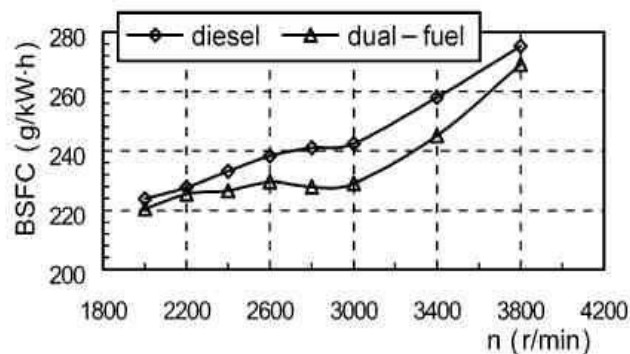


Fig. 4 The comparison of BSFCs at full load

3.1.3 Smoke Emission

The comparison between the smoke emissions, R_b , of the external characteristics of LPG–diesel dual fuel and diesel is shown in Fig. 5. Compared with the smoke emission of the diesel engine, that of the dual-fuel engine is reduced significantly, 59 per cent on average. When the engine is fuelled with dual fuel, consumption of diesel is reduced. The possibility of producing smoke is reduced due to the reduction in the possibility that oxygen is absent at high temperatures for diesel. The combustion velocity is increased and the burning duration is shortened, which also helps to restrain smoke production. Therefore, the LPG–diesel dual fuel engine's smoke emission is reduced.

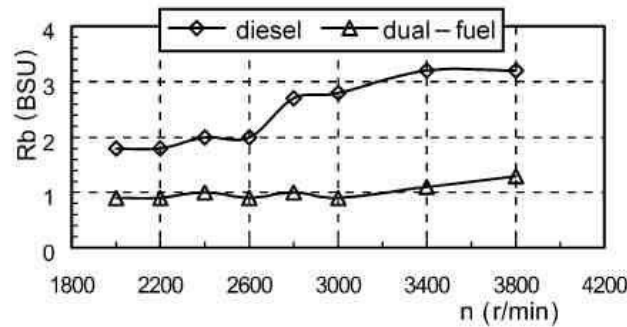


Fig. 5 The comparison of smoke emissions at full load

3.1.3 NO_x Emission

The comparison between the nitrogen oxides (NO_x) emissions of the external characteristics of LPG– diesel dual fuel and diesel is shown in Fig. 6.

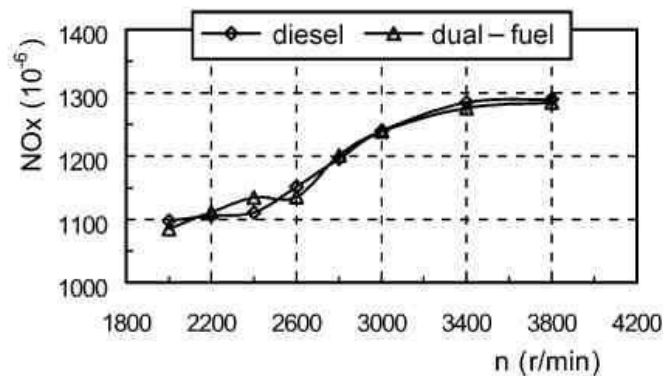


Fig. 6 The comparison of NO_x emissions at full load

The NO_x emission of dual fuel is almost equal to that of diesel. The change in the creation of NO_x is determined by factors such as the mixture concentration and the combustion temperature, which are slightly changed. Therefore, the NO_x emission is slightly changed.

3.1.5 HC Emission

The comparison between the HC emissions of the external characteristics of LPG – diesel dual fuel and diesel is shown in Fig. 7.

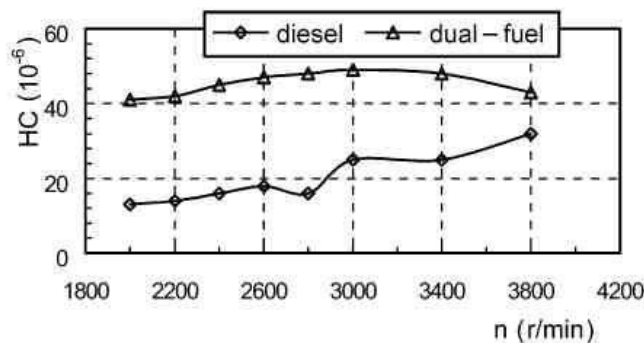


Fig. 7 The comparison of HC emissions at full load

At full load, the HC emission of dual fuel is higher than that of diesel, which is caused by two key factors; the first is that the LPG pre-mixture is scavenged to outside from the cylinder in the overlap period of the valves of the discharged dual-fuel engine, and the second is that the LPG pre-mixture that is pressed into the cooled crevices during compression stroke is difficult to burn.

3.1.6 CO Emission

The comparison between the CO emissions of the external characteristics of LPG– diesel dual fuel and diesel is shown in Fig. 8.

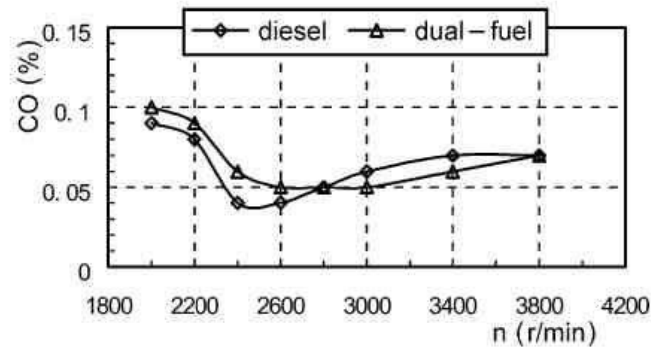


Fig. 8 The comparison of CO emissions at full load

At full load, the CO emission of dual fuel is almost equal to that of diesel. The formation of CO is related to the mixture concentration and fuel composition; the change in CO emission is the result of the two factors that exert effects at the same time.

IV. CONCLUSIONS

1. Smoke emission can be largely reduced by using dual-fuel operation. However, the problems remain of how the fuel consumption, HC emission and CO emission of the dual-fuel engine are reduced at middle loads and low loads; this needs urgent attention. The electronically controlled scheme developed by our research group is that the engine burns diesel fuel at low loads and the engine burns LPG–diesel dual fuel after the engine load reaches the preset limit. This measure not only utilizes the diesel engine's good economy and low emissions of HC and CO but also reduces the diesel engine's high smoke emission at high loads and full load, by co-burning LPG.
2. The electronically controlled LPG–diesel dual-fuel scheme takes the accelerator pedal stroke, coolant temperature and engine speed as input signals, and the results of stand tests show that, when the engine burns dual fuel, the power output does not reduce; the electronically controlled scheme overcomes the common dual-fuel controlled scheme disadvantage of poor fuel economy and high emissions of HC and CO at low loads, but the ratio of diesel alternated by LPG is reduced. Despite the increase in HC emission and CO emission resulting from the engine's co-burning LPG, the HC and CO emissions of the dualfuel engine are still generally lower than those of common gasoline engines.
3. Attempts may also be made to apply the electronically controlled scheme and the electronic control device, after a little modification, to CNG– diesel dual-fuel vehicles because CNG and LPG, as fuels, have many similar properties.

REFERENCES

- [1] CHETHAN RAO, G., CHIRU, A., – MOTORS AND AUTOMOBILE, SI TRACTOARCADE, VOLUME III, TEHNICAL-INFO, INDIA.
- [2] Cofaru, C. – LegislaŃia si Ingineria Mediului în Transportul Rutier, Editura UniversităŃii Transilvania, Brasov, 2002.
- [3] Cofaru, C., Ispas, N., Chiru, A. – Autovehiculul si mediul, Editura UniversităŃii Transilvania, Brasov 2000.
- [4] Daisho, Y., Yaeo, T., Koseki, T., Kihara, R., and Saito, T. Combustion and exhaust emissions in a direct injection diesel engine dual-fuelled with natural gas. SAE paper 950465, 1995.
- [5] Zhang, C., Bian, Y., Ma, Z., and Qi, D. An experimental study of the co-combustion characteristics on a supercharged diesel engine fuelled with LPG–diesel dual-fuel. Chin. Internal Combust. Engine Engng, 2002.

Steganography and Its Applications in Security

Ronak Doshi,¹ Pratik Jain,² Lalit Gupta³

1, 2,3Department of Electronics and telecommunication, Pune University, India

ABSTRACT: *Steganography is the dark cousin of cryptography, the use of codes. While cryptography provides privacy, steganography is intended to provide secrecy. Steganography is a method of covertly communicating. Steganography is a process that involves hiding a message in an appropriate carrier for example an image or an audio file. The carrier can then be sent to a receiver without anyone else knowing that it contains a hidden message. This is a process, which can be used for example by civil rights organizations in repressive states to communicate their message to the outside world without their own government being aware of it. In this article we have tried to elucidate the different approaches towards implementation of Steganography using 'multimedia' file (text, static image, audio and video). Steganalysis is a newly emerging branch of data processing that seeks the identification of steganographic covers, and if possible message extraction. It is similar to cryptanalysis in cryptography. The technique is ancient emerging monster that have gained immutable notice as it have newly penetrated the world of digital communication security. Objective is not only to prevent the message being read but also to hide its existence.*

Keywords: Carrier, Privacy, Secrecy, Steganalysis, Steganography

I. INTRODUCTION

The word steganography is of Greek origin and means "covered, or hidden writing". It is the science of hiding information. Whereas the goal of cryptography is to make data unreadable by a third party, the goal of steganography is to hide the data from a third party. In steganography information can be hidden in carriers such as images, audio files, text files, and video and data transmissions. When message is hidden in the carrier a stego carrier is formed for example a stego-image. It will be perceived to be as close as possible to the original carrier or cover image by the human senses. Steganography and cryptography are closely related. Cryptography scrambles messages so they cannot be understood. Steganography, on the other hand, will hide the message so that there is no knowledge of the existence of the message in the first place. Steganography includes the concealment of information within computer files. In digital steganography, electronic communications may include steganographic coding inside of a transport layer, such as a document file, image file, program or protocol.[1]

Steganography today, however, is significantly more sophisticated, allowing a user to hide large amounts of information within image and audio files. These forms of steganography often are used in conjunction with cryptography so that the information is doubly protected; first it is encrypted and then hidden so that an adversary has to first find the information (an often difficult task in and of itself) and *then* decrypt it.

In this paper, a security thesis is proposed which imposes the concept of secrecy over privacy for messages in various formats.

II. HISTORY

Steganographic techniques have been used for centuries. Steganography has been widely used in historical times, especially before cryptographic systems were developed.

The first known application dates back to the ancient Greek times, when messengers tattooed messages on their shaved heads and then let their hair grow so the message remained unseen.

A different method from that time used wax tables as a cover source. Text was written on the underlying wood and the message was covered with a new wax layer. The tablets appeared to be blank so they passed inspection without question.

During World War 2 invisible ink was used to write information on pieces of paper so that the paper appeared to the average person as just being blank pieces of paper. Liquids such as urine, milk, vinegar and fruit juices were used, because when each one of these substances is heated they darken and become visible to the human eye.

Another clever invention in *Steganographia* was the "Ave Maria" cipher. The book contains a series of tables, each of which has a list of words, one per letter. To code a message, the message letters are replaced by the corresponding words. If the tables are used in order, one table per letter, then the coded message will appear to be an innocent prayer.

All of these approaches to steganography have one thing in common -- they hide the secret message in the physical object which is sent. The cover message is merely a distraction, and could be anything. Of the innumerable variations on this theme, none will work for electronic communications because only the pure information of the cover message is transmitted. Nevertheless, there is plenty of room to hide secret information in a not-so-secret message. It just takes ingenuity.

III. IMPLEMENTATION OF STEGANOGRAPHY

Secrets can be hidden inside all sorts of cover information. The following formula provides a very generic description of the pieces of the steganographic process:

$$\text{cover_medium} + \text{hidden_data} + \text{stego_key} = \text{stego_medium} \quad (1)$$

In this context, the cover_medium is the file in which we will hide the hidden_data, which may also be encrypted using the stego_key. The resultant file is the stego_medium (which will, of course be the same type of file as the cover_medium).

There are four ways to implement steganography:

1. Using text.
2. Using images.
3. Using audio files.
4. Using video files.[2]

3.1 Text Steganography:

Text steganography can be classified in three basic categories - format-based, random and statistical generation and linguistic method. Format-based methods used physical text formatting of text as a place in which to hide information. Generally, this method modifies existing text in order to hide the steganographic text. Insertion of spaces, deliberate misspellings distributed throughout the text, resizing the fonts are some of the many format-based methods being used in text steganography. However, Bennett has stated that those format-based methods managed to trick most of the human eyes but it cannot trick once computer systems have been used. Random and statistical generation is generating cover text according to the statistical properties. This method is based on character sequences and words sequences. The hiding of information within character sequences is embedding the information to be appeared in random sequence of characters. This sequence must appear to be random to anyone who intercepts the message.[5]

A second approach for character generation is to take the statistical properties of word-length and letter frequency in order to create "words" (without lexical value) which will appear to have the same statistical properties as actual words in a given language. The hiding of information within word sequences, the actual dictionary items can be used to encode one or more bits of information per word using a codebook of mappings between lexical items and bit sequences, or words themselves can encode the hidden information.

The final category is linguistic method which specifically considers the linguistic properties of generated and modified text, frequently uses linguistic structure as a place for hidden messages. In fact, steganographic data can be hidden within the syntactic structure itself.

Example:

Sender sends a series of integer number (Key) to the recipient with a prior agreement that the secret message is hidden within the respective position of subsequent words of the cover text. For example the series is '1, 1, 2, 3, 4, 2, 4' and the cover text is "**A team of five men joined today**". So the hidden message is "**Attfova**". A "0" in the number series will indicate a blank space in the recovered message. The word in the received cover text will be skipped if the number of characters in that word is less than the respective number in the series (Key) which shall also be skipped during the process of message unhide.

3.2 Image Steganography:

The most widely used technique today is hiding of secret messages into a digital image. This steganography technique exploits the weakness of the human visual system (HVS). HVS cannot detect the variation in luminance of color vectors at collection of color pixels. The individual pixels can be represented by their optical higher frequency side of the visual spectrum. A picture can be represented by a characteristics like 'brightness', 'chroma' etc. Each of these characteristics can be digitally expressed in terms of 1s and 0s.

For example: a 24-bit bitmap will have 8 bits, representing each of the three color values (red, green, and blue) at each pixel. If we consider just the blue there will be 2 different values of blue. The difference between 11111111 and 11111110 in the value for blue intensity is likely to be undetectable by the human eye. Hence, if the terminal recipient of the data is nothing but human visual system (HVS) then the Least Significant Bit (LSB) can be used for something else other than color information.

3.2.1 LSB Coding

The simplest approach to hiding data within an image file is called least significant bit (LSB) insertion. In this method, we can take the binary representation of the hidden_data and overwrite the LSB of each byte within the cover_image. If we are using 24-bit color, the amount of change will be minimal and indiscernible to the human eye. As an example, suppose that we have three adjacent pixels (nine bytes) with the following RGB encoding:

10010101	00001101	11001001
10010110	00001111	11001010
10011111	00010000	11001011

Now suppose we want to "hide" the following 9 bits of data (the hidden data is usually compressed prior to being hidden): 101101101. If we overlay these 9 bits over the LSB of the 9 bytes above, we get the following (where bits in **bold** have been changed):

10010101	00001100	11001001
10010111	00001110	11001011
10011111	00010000	11001011

Note that we have successfully hidden 9 bits but at a cost of only changing 4, or roughly 50%, of the LSBs.



Fig. 1. Original image



Fig. 2. Embedded image

Example of still imagery steganography. Left hand side image is the original cover image, whereas right hand side does embedding a text file into the cover image make the stego image

3.2.2 Masking And Filtering:

Masking and filtering techniques are mostly used on 24 bit and grey scale images. They hide information in a way similar to watermarks on actual paper and are sometimes used as digital watermarks. Masking images entails changing the luminance of the masked area. The smaller the luminance change, the less of a chance that it can be detected.

Masking is more robust than LSB insertion with respect to compression, cropping, and some image processing. Masking techniques embed information in significant areas so that the hidden message is more integral to the cover image than just hiding it in the “noise” level. This makes it more suitable than LSB with, for instance, lossy JPEG images.

3.3 Audio Steganography:

Steganography, in general, relies on the imperfection of the human auditory and visual systems. Audio steganography takes advantage of the psychoacoustical masking phenomenon of the human auditory system [HAS]. Psychoacoustical or auditory masking property renders a weak tone imperceptible in the presence of a strong tone in its temporal or spectral neighborhood. This property arises because of the low differential range of the HAS even though the dynamic range covers 80 dB below ambient level. Frequency masking occurs when human ear cannot perceive frequencies at lower power level if these frequencies are present in the vicinity of tone- or noise-like frequencies at higher level.

Additionally, a weak pure tone is masked by wide-band noise if the tone occurs within a critical band. This property of inaudibility of weaker sounds is used in different ways for embedding information. Embedding of data by inserting inaudible tones in cover audio signal has been presented recently. [3]

In audio steganography, secret message is embedded into digitized audio signal which result slight altering of binary sequence of the corresponding audio file. The list of methods that are commonly used for audio steganography are listed and discussed below.

- LSB coding
- Parity coding
- Phase coding
- Spread spectrum
- Echo hiding

3.3.1 LSB Coding:

Sampling technique followed by Quantization converts analog audio signal to digital binary sequence.

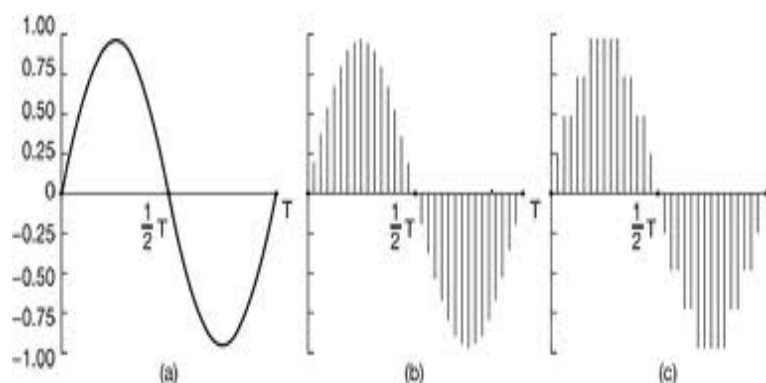


Fig. 3. Sampling of the Sine Wave followed by Quantization process.

In this technique LSB of binary sequence of each sample of digitized audio file is replaced with binary equivalent of secret message.

3.3.2 Parity Coding:

Instead of breaking a signal down into individual samples, the parity coding method breaks a signal down into separate regions of samples and encodes each bit from the secret message in a sample region's parity bit. If the parity bit of a selected region does not match the secret bit to be encoded, the process flips the LSB of one of the samples in the region. Thus, the sender has more of a choice in encoding the secret bit, and the signal can be changed in a more unobtrusive fashion.

3.3.3 Phase coding:

Human Auditory System (HAS) can't recognize the phase change in audio signal as easy it can recognize noise in the signal. The phase coding method exploits this fact. This technique encodes the secret message bits as phase shifts in the phase spectrum of a digital signal, achieving an inaudible encoding in terms of signal-to-noise ratio.

3.3.4 Spread spectrum:

In the context of audio steganography, the basic spread spectrum (SS) method attempts to spread secret information across the audio signal's frequency spectrum as much as possible. This is analogous to a system using an implementation of the LSB coding that randomly spreads the message bits over the entire sound file. However, unlike LSB coding, the SS method spreads the secret message over the sound file's frequency spectrum, using a code that is independent of the actual signal. As a result, the final signal occupies a bandwidth in excess of what is actually required for transmission.

3.3.5 Echo Hiding:

In echo hiding, information is embedded in a sound file by introducing an echo into the discrete signal. Like the spread spectrum method, it too provides advantages in that it allows for a high data transmission rate and provides superior robustness when compared to the noise inducing methods. If only one echo was produced from the original signal, only one bit of information could be encoded. Therefore, the original signal is broken down into blocks before the encoding process begins. Once the encoding process is completed, the blocks are concatenated back together to create the final signal.

3.4 Video Steganography:

Video files are generally a collection of images and sounds, so most of the presented techniques on images and audio can be applied to video files too. When information is hidden inside video the program or person hiding the information will usually use the DCT (Discrete Cosine Transform) method. DCT works by slightly changing each of the images in the video, only so much that it is not noticeable by the human eye. To be more precise about how DCT works, DCT alters values of certain parts of the images, it usually rounds them up. For example, if part of an image has a value of 6.667 it will round it up to 7. [6]

The great advantages of video are the large amount of data that can be hidden inside and the fact that it is a moving stream of images and sounds. Therefore, any small but otherwise noticeable distortions might go by unobserved by humans because of the continuous flow of information.

IV. STEGANALYSIS

The art of detecting Steganography is referred to as Steganalysis. Steganalysis is the process of identifying steganography by inspecting various parameter of a stego media. The primary step of this process is to identify a suspected stego media. After that steganalysis process determines whether that media contains hidden message or not and then try to recover the message from it. In cryptanalysis, it is clear that the intercepted message is encrypted and it certainly contains the hidden message because the message is scrambled. But in the case of steganalysis this may not be true. The suspected media may or may not be with hidden message. The steganalysis process starts with set of suspected information streams. Then the set is reduced with the help of advance statistical methods.[4]

In the case of Visual detection steganalysis technique, a set of stego images are compared with original cover images and note the visible difference. Signature of the hidden message can be derived by comparing numerous images. Cropping or padding of image also is a visual clue of hidden message because some stego tool is cropping or padding blank spaces to fit the stego image into fixed size. Difference in file size between cover image and stego images, increase or decrease of unique colors in stego images can also be used in the Visual Detection steganalysis technique.

Scientists and researchers are trying new methods to try and discover ways of detecting hidden files and rendering them useless. The U. S. Government has contracted Wetstone Technologies to work with the U.S. Air Force to research algorithms that can be used to discover embedded files in digital, audio and video format. Steganalysis is the technique to detect steganography or defeat steganography. The research to device strong steganographic and steganalysis technique is a continuous process.

V. APPLICATIONS

Steganography can be used anytime you want to hide data. There are many reasons to hide data but they all boil down to the desire to prevent unauthorized persons from becoming aware of the existence of a message. With these new techniques, a hidden message is indistinguishable from white noise. Even if the message is suspected, there is no proof of its existence. In the business world steganography can be used to hide a secret chemical formula or plans for a new invention.

Steganography can also be used for corporate espionage by sending out trade secrets without anyone at the company being any the wiser. [7]

Terrorists can also use steganography to keep their communications secret and to coordinate attacks. All of this sounds fairly nefarious, and in fact the obvious uses of steganography are for things like espionage. But there are a number of peaceful applications. The simplest and oldest are used in map making, where cartographers sometimes add a tiny fictional street to their maps, allowing them to prosecute copycats. A similar trick is to add fictional names to mailing lists as a check against unauthorized resellers.

Most of the newer applications use steganography like a watermark, to protect a copyright on information. Photo collections, sold on CD, often have hidden messages in the photos which allow detection of unauthorized use. The same technique applied to DVDs is even more effective, since the industry builds DVD recorders to detect and disallow copying of protected DVDs.

VI. FUTURE

In today's world, we often listen a popular term "Hacking". Hacking is nothing but an unauthorized access of data which can be collected at the time of data transmission. With respect to steganography this problem is often taken as Steganalysis.

Steganalysis is a process in which a steganalyzer cracks the cover object to get the hidden data. So, whatever be the technique will be developed in future, degree of security related with that has to be kept in mind. It is hoped that Dual Steganography, Steganography along with Cryptography may be some of the future solution for this above mentioned problem.

VII. CONCLUSION

Steganography is a fascinating and effective method of hiding data that has been used throughout history. Methods that can be employed to uncover such devious tactics, but the first step are awareness that such methods even exist. There are many good reasons as well to use this type of data hiding, including watermarking or a more secure central storage method for such things as passwords, or key processes. Regardless, the technology is easy to use and difficult to detect. The more that you know about its features and functionality, the more ahead you will be in the game.

In this paper, different techniques are discussed for embedding data in text, image, and audio/video signals as cover media. I have presented a brief overview of a very exciting and fast paced area of computer security. This technology has many in the security field worried as the possible harm that may be done to both government and private industries. As pc's become more powerful this technology will grow substantially and become much more main stream. There are already hundreds of steganography programs available that can be used on text, audio and graphic files. The government and many private companies are researching ways to best detect the use of steganography on files. As steganalysis becomes more mature it will be implemented as a standard security tool the way firewalls, virus detection software and intrusion detection programs currently are.

REFERENCES

Books:

- [1] Compression Algorithms for Real Programmers, Wayner Peter. 2000
- [2] Disappearing Cryptography: Being and Nothingness on the Net, Wayner Peter. 1996
- [3] Secure Steganography for Audio Signals

Journal Papers:

- [4] Steganography and steganalysis-Robert Krenn, Internet Publication, March 2004
<http://www.krenn.nl/univ/cry/steg/article.pdf>
- [5] Steganography, http://searchsecurity.techtarget.com/sDefinition/0,,sid14_gci213717,00.html
- [6] Johnson, Neil F., "Steganography", 2000 <http://www.jjtc.com/stegdoc/index2.html>
- [7] The WEPIN Store, "Steganography (Hidden Writing)", 1995, <http://www.wepin.com/pgp/stego.html>

User Interactive Color Transformation between Images

Miss. Aarti K. Masal,¹ Asst. Prof. R.R.Dube²

^{1,2}Dept. of Electronics Engineering, Walchand Institute of Technology, Solapur University, Solapur (Maharashtra).

Abstract: In this paper we present a process called color transfer which can borrow one image's color characteristics from another. Most current colorization algorithms either require a significant user effort or have large computational time. Here focus on orthogonal color space i.e. $l\alpha\beta$ color space without correlation between the axes is given. Here we have implemented two global color transfer algorithms in $l\alpha\beta$ color space using simple color statistical information such as mean, standard deviation and covariance between the pixels of image. Our approach is the extension of Reinhard's. Our local color transfer algorithm uses simple color statistical analysis to recolor the target image according to selected color range in source image. Target image's color influence mask is prepared. It is a mask that specifies what parts of target image will be affected according to selected color range.

After that target image is recolored in $l\alpha\beta$ color space according to prepared color influence map. In the $l\alpha\beta$ color space luminance and chrominance information is separate so it allows making image recoloring optional. The basic color transformation uses stored color statistics of source and target image. All the algorithms are implemented in JAVA object oriented language. The main advantage of proposed method over the existing one is it allows the user to recolor a part of the image in a simple & intuitive way, preserving other color intact & achieving natural look.

Index Terms: color transfer, local color statistics, color characteristics, orthogonal color space, color influence map.

I. INTRODUCTION

Color is one of the main image attributes used in many different areas, such as medical image analysis, video object extraction, image compression, tracking system, art, photography and visualization for relaying information, or for conveying a specific mood. Nowadays, digital cameras are very popular, and most people take many photos on their trips, reunions, etc. However, since most end users are not professional photographers, a user usually takes a lot of photos but eventually finds out that only a small portion of them are satisfactory. Indeed, with powerful commercial post-processing software, the experts could enhance these defect photos, but this task can be time-consuming. The direct enhancement of the photos by using some post processing tools may not be an easy task. For example, in the case of a backlight photo, one may think that the user can use the brightness/hue adjustment tools as contained in ordinary image processing software. However, such tools usually can only be used to adjust the brightness/hue

globally. If such tools are applied to achieve a brighter foreground, the background might be overexposed. Even if the foreground region in interest is carefully specified, the process is not only time-consuming but also may result in artifacts at the foreground and background border. On the other hand, if we can refer to the same object in other good quality photos, it would be much easier. Considering such users, color transfer forms a class of techniques that allow the color palette of an image to be altered using a second image as a reference. The task is then to select a reference image whose colors are preferred. Subsequently the algorithm will modify the original image such that it acquires the palette of that reference. In essence this operation can be seen as a function that, given two images,

produces a third that has maintained the semantic content of the one while acquiring the colors of the second. There are two types of color transfer between images, global color transfer and local color transfer. Most of the available algorithms either perform a global color transfer or local color transfer. In our work we have implemented both types of color transfer which are user interactive.



Figure 1: (a) Target Image, (b) Source image, (c) resulting image using proposed first global color transfer algorithm, (d) resulting image using proposed second global color transfer algorithm.



Figure 2: (a) Target Image, (b) Source image, (c) resulting image of local color transfer using proposed algorithm

Figure 1 shows the effect of global color transfer in which the whole image gets affected while figure 2 shows the partial image recoloring which is nothing but a local color transfer. Here the user just has to select a pair of corresponding regions in the source and target image for the color change. The data of the selected region is used to calculate its color statistics. We use them to estimate pixels of the target image belong, or rather are close enough, to the selected color range. Then color transformation is applied to the image, according to this estimation. In this paper we present color transfer algorithms which are user interactive and perform both types of color transfer global as well as local color transfer.

II. RELATED WORK

Most of the existing color transfer algorithm performs global color transfer. Reinhard et al presented a method for global color transfer. [1] Shifts and scales the pixel values of the source image to match the mean and standard deviation from the target. This is done in the lab opponent color space, which is on averaged correlated [2]. This allows the transfer to take place independently in each channel, turning a potentially complex 3D problem into three much simpler 1D problems. Although this technique can be successful for a large range of images, the quality of the results largely depend on the composition of the source and target images. While this algorithm is simple and efficient, it cannot distinguish the color statistics of local regions, which generate an unnatural or oversaturation in resulting image. Some authors try to solve this problem using complex image spatial or color characteristics, but these methods have other limitations. Method based on Basic Color Categories [3] is limited in variations of color changing, because any color can be replaced only by a color from the same color category. For example, we can't turn blue into red. Another method, described in [4], uses complex image color and spatial characteristics to determine image palette associations. Image color segmentation using Expectation Maximization method is offered in [6] to solve the problem of local color transfer, but segmentation and region color decision is performed fully automatically, and again for the whole image, which is not always desirable. Cellular automata is used successfully in [7] to select an object of interest, but only a single color can be used as color source and recoloring is very uniform, even when some variability of color shade is desired according to initial look and feel of the object.

Maslennikova designed a weighted mask of influence map for each pixel of the target image using a color influence map (CIM)[8] that specifies which part of the target image will be affected according to the selected color. Singular value decomposition algorithm used in [9] to decompose the covariance matrix which represents the covariance between source image's pixel and also between the pixels of target image. It gives a method for global color transfer but it only works with the images of similar composition.

III. GLOBAL COLOR TRANSFER (FIRST ALGORITHM)

Color transfer is carried out by a statistics-based method that can achieve the goal in $l\alpha\beta$ color space just utilizing the statistics -mean and covariance matrix. Here the covariance matrix can be deemed to the extension of standard deviation in decorrelated space. Data points of source image is scaled, rotated and translated to fit data points' cluster of target image in $l\alpha\beta$ color space.

First, calculate the mean of pixel data along the three axes and the covariance matrix between the three components in color space for both the source and target images. All of the statistics are denoted by ($lsrcmean$; $\alpha srcmean$; $\beta srcmean$), ($ltgtmean$; $\alpha tgtmean$; $\beta tgtmean$), $Covsrc$ and $Covtgt$, respectively.

Then decomposition of covariance matrices is carried out by Singular value decomposition algorithm. Singular value decomposition algorithm is factorization of a real or complex matrix [9].

$$Cov = U \Lambda V^T \quad (1)$$

Where U and V are orthogonal matrices and are composed of the eigenvectors of Cov , $\Lambda = diag(\lambda^l; \lambda^\alpha; \lambda^\beta)$ and λ^l , λ^α and λ^β are the eigenvalues of Cov . U is the used as rotation matrix.

Transformation is carried out as:

$$I = Tsrc.Rsrc.Ssrc.Stgt.Rtgt.Ttgt.Itgt \quad (2)$$

where $I = (l;\alpha;\beta;1)^T$ and $Itgt = (ltgt;\alpha tgt;\beta tgt;1)^T$ denote the homogeneous coordinates of pixel points in $l\alpha\beta$ space for the result and target images respectively; $Tsrc$, $Ttgt$, $Rsrc$, $Rtgt$, $Ssrc$ and $Stgt$ denote the matrices of translation, rotation and scaling derived from the source and target images separately. Here is their definition:

$$Tsrc = \begin{bmatrix} 1 & 0 & 0 & tsrc^l \\ 0 & 1 & 0 & tsrc^\alpha \\ 0 & 0 & 1 & tsrc^\beta \\ 0 & 0 & 0 & 1 \end{bmatrix}, \quad Ttgt = \begin{bmatrix} 1 & 0 & 0 & tgt^l \\ 0 & 1 & 0 & tgt^\alpha \\ 0 & 0 & 1 & tgt^\beta \\ 0 & 0 & 0 & 1 \end{bmatrix}$$

$$Rsrc = U_{src}, Rtgt = U_{tgt}^{-1} \quad (3)$$

$$Ssrc = \begin{bmatrix} Ssrc^l & 0 & 0 & 0 \\ 0 & Ssrc^\alpha & 0 & 0 \\ 0 & 0 & Ssrc^\beta & 0 \\ 0 & 0 & 0 & 1 \end{bmatrix}, \quad Stgt = \begin{bmatrix} Ssrc^l & 0 & 0 & 0 \\ 0 & Ssrc^\alpha & 0 & 0 \\ 0 & 0 & Ssrc^\beta & 0 \\ 0 & 0 & 0 & 1 \end{bmatrix}$$

Where, $tsrc^l = lsrcmean$, $tsrc^\alpha = \alpha srcmean$, $tsrc^\beta = \beta srcmean$; $tgt^l = ltgtmean$, $tgt^\alpha = \alpha tgtmean$, $tgt^\beta = \beta tgtmean$; $Ssrc^l = \lambda_{src}^l$, $Ssrc^\alpha = \lambda_{src}^\alpha$, $Ssrc^\beta = \lambda_{src}^\beta$; $Stgt^l = 1/\lambda_{tgt}^l$, $Stgt^\alpha = 1/\lambda_{tgt}^\alpha$, $Stgt^\beta = 1/\lambda_{tgt}^\beta$

The subscripts of src and tgt indicate source image and target image, respectively. Finally the result is converted back to RGB color space.

IV. GLOBAL COLOR TRANSFER (SECOND ALGORITHM)

In this algorithm some aspects of the distribution of data points in $l\alpha\beta$ space is transferred between images.

Mean and standard deviation along each of the three axes is computed for both source image & target image.

First the mean is subtracted from data points:

$$\begin{aligned} l^* &= l - \langle l \rangle \\ \alpha^* &= \alpha - \langle \alpha \rangle \\ \beta^* &= \beta - \langle \beta \rangle \end{aligned} \quad (4)$$

Data points of target image are scaled by factors determined by the respective standard deviations:

$$\begin{aligned} l' &= \frac{\sigma_l}{\sigma_s} l^* \\ \alpha' &= \frac{\sigma_\alpha}{\sigma_s} \alpha^* \\ \beta' &= \frac{\sigma_\beta}{\sigma_s} \beta^* \end{aligned} \quad (5)$$

After this transformation, the resulting data points have standard deviations that conform to the source image. Next, instead of adding the averages that previously subtracted, the averages computed for the source image is added. Finally the result is converted back to RGB color space.

V. LOCAL COLOR TRANSFER

Color transformation is carried out in $l\alpha\beta$ color space. At first user has to select an object to correct at the target image. This can be done by loosely selecting a rectangular region of the object that needs correction. There's no need to select the region precisely close to the edges of the area, that user wants to correct, because color range used. The only limitation is that the whole region must be inside this object.

After the user has selected the region at the target image, we calculate color statistics (mean and variation) for this region, for each channel of the working color space separately:

$$\mu_c^R = \frac{1}{N_R} \sum_{i=i_1}^{i_2} \sum_{j=j_1}^{j_2} c(i, j) \quad (6)$$

$$\sigma_c^R = \sqrt{\frac{1}{N_R - 1} \sum_{i=i_1}^{i_2} \sum_{j=j_1}^{j_2} (c(i, j) - E^R c)^2} \quad (7)$$

Where $N_R = (i_2 - i_1 + 1)(j_2 - j_1 + 1)$ is the number of pixels in the selected region R , $1 \leq i_1 < i_2 \leq H$ and $1 \leq j_1 < j_2 \leq W$ define the rectangular region R and $c(i, j)$ is a processed color channel of pixel (i, j) . Maximum distance from the mean is calculated in both source image and target image for the selected color range. After the information of the target color range is gathered, we prepare the target image's Color Influence Map (CIM). It is a mask that specifies what parts of the target image will be affected according to the selected color range. CIM contains weights for color transformation for each pixel of the target image.

Each pixel's weight is determined from its proximity to the color range, selected by user and stored in color

statistics information Data points of the selected color range in target image are scaled by a factor determined by maximum distance from the mean. After scaling the mean of the rectangular region in source image is added. Here we have three sliders to user to have better control over color transfer. First slider is used to decide the size of mask. Second slider is used to adjust the how much color should be transferred and third slider provides user exponential adjustment on color transfer. The formula used to calculate the final pixel's value is as follows:

$$\begin{aligned} nl &= \text{labColorMean}[0] + ((\text{labTarget}[0] - \text{labTargetMean}[0]) \\ &\quad * \text{totalMaxDistance1} / \text{totalMaxDistance}); \\ na &= \text{labColorMean}[1] + ((\text{labTarget}[1] - \text{labTargetMean}[1]) \\ &\quad * \text{totalMaxDistance1} / \text{totalMaxDistance}); \\ nb &= \text{labColorMean}[2] + ((\text{labTarget}[2] - \text{labTargetMean}[2]) \\ &\quad * \text{totalMaxDistance1} / \text{totalMaxDistance}); \dots\dots\dots(8) \end{aligned}$$

Here nl , na and nb are temporary variables whereas totalMaxDistance1 and totalMaxDistance indicates the maximum distance of pixel from the selected color range for source image and target image respectively.

Next step is to calculate the new pixel value according to the slider values.

$$\begin{aligned} \text{labTarget}[0] &= \text{labTarget}[0] + (nl - \text{labTarget}[0]) * \text{slider2} / 100 * \text{Math.pow}(\text{slider3}, (\text{Euclidian} / \text{totalMaxDistance})); \\ \text{labTarget}[1] &= \text{labTarget}[1] + (na - \text{labTarget}[1]) * \text{slider2} / 100 * \text{Math.pow}(\text{slider3}, (\text{Euclidian} / \text{totalMaxDistance})); \\ \text{labTarget}[2] &= \text{labTarget}[2] + (nb - \text{labTarget}[2]) * \text{slider2} / 100 * \text{Math.pow}(\text{slider3}, (\text{Euclidian} / \text{totalMaxDistance})); \end{aligned} \quad (9)$$

Equestion (9) shows the resulting pixel's value which can be obtained by adjusting the sliders value. Final step is to transfer the $l\alpha\beta$ color space into RGB color space.

VI. EXPERIMENTS

We have implemented the proposed algorithms in JAVA (object oriented language). The proposed algorithms are tested on the set of images downloaded from the internet. It is found that both global color transfer algorithms give best result for the source and target images which are similar in composition. The result of first global color transfer algorithm shows that not only the mood of source image is transferred to target image but the object's color of target image is recolored according to source image's object's color. The result of second global color transfer shows that it retains object's color in target image. It only transfers the appearance of source image to target image. The proposed local color transfer algorithm is tested on a set of images of different compositions. Our experiment included the cases of 1) using an image fragment or a single color as color source 2) correction of both luminance and chrominance or chrominance only; 3) using images of similar or different composition for the case of using an image fragment as color source. The time required for the local color transfer with the images of size 960×720 is 28seconds with core i3 processor. It preserves natural look of images and the color range which is selected by user modified rest of the image remains unaffected. The

proposed algorithm gives best result with any size of images.

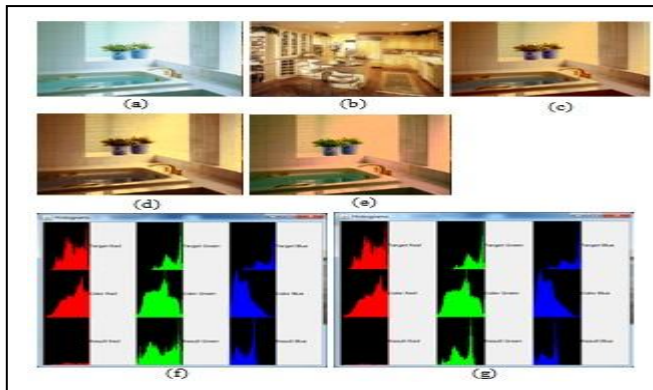


Figure 3. Comparison of resulting images; (a) target image, (b) source image, (c) resulting image of global color transfer[9], (d) resulting image of the global color transfer using algorithm first, (e) resulting image of the global color transfer using algorithm second, (f) Histogram comparison of images a,b and d, (g) Histogram comparison of images a,b and e.

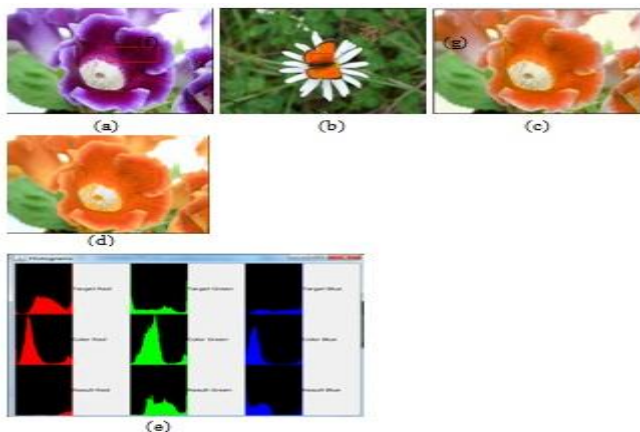


Figure 4. Comparison of resulting images; (a) target image, (b) source image, (c) resulting image of local color transfer[8], (d) resulting image of the local color transfer using proposed algorithm, (e) Histogram comparison of images a,b and d.

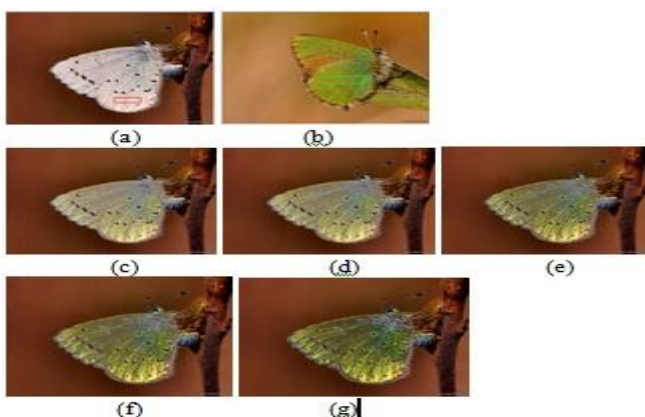


Figure 5. Result for local color transfer; (a) target image, (b) source image, (c)(d)(e)(f)(g) resulting images at various sliders values.

VII. LIMITATIONS

We have implemented both global as well as local color transfer algorithms. The main limitation of our work is our first global color transfer algorithm gives best result for monotonic images only & second global color transfer gives best result when source and target images are similar in composition. If images with multiple tones are used for global color transfer then our algorithm will not perform well.

VIII. CONCLUSION

Our global color transfer algorithms are the extension of Reinhard's. It is very hard to evaluate results objectively, the evaluation is really subjective. Our proposed global color transfer algorithms work well for the images with similar compositions. Our local color transfer algorithm allows user to correct an object of interest at an image saving one from the trouble of selecting it precisely. Also it allows user to obtain a desired color transfer just by adjusting the sliders. Only the selected object's color range is changed preserving other color intact and achieving natural look of the result for wide variety of input images. Our proposed algorithms work with all real size images.

REFERENCES

- [1] Eric Reinhard, Michael Ashikhmin, Bruce Gooch, Peter Shirley, "Color Transfer between Images", Computer Graphics and Applications, 2001, Vol.21, Issue 5, pp. 34-41.
- [2] Ruderman D, Cronin T, Chiao C. Statistics of cone responses to n natural images: implications for visual coding. Journal of the Optical Society of America A 1998; 15(8):2036-45.
- [3] Youngha Chang, Suguru Saito, Masayuki Nakajima, "Color transformation based on Basic Color Categories of a Painting", Proceedings of Computer Graphics International, 2003, pp. 176-181.
- [4] Donald H. House, Gary R. Greenfield, "Image Recoloring Induced by Palette Color Associations", Journal of WSCG, 2003, Vol.11, No.1, pp. 189-196.
- [5] Daniel L. Rudermann, Thomas W. Cronin, Chuan-Chin Chiao, "Statistics of cone responses to natural images: implications for visual coding", Journal of the Optical Society of America, 1998, Vol.15, Issue 8, pp. 2036-2045.
- [6] Jiaya Jia, Chi-Keung Tang, Yu-Wing Tai, "Local Color Transfer via Probabilistic Segmentation by Expectation-Maximization", IEEE Computer Society Conference on Computer Vision and Pattern Recognition, 2005, Vol.1, pp. 747-754.
- [7] V. Konushin, V. Vezhnevets, "Interactive Image Colorization and Recoloring Based on Coupled Map Lattices", Graphicon'2006 Conference Proceedings, 2006, pp.231-234.
- [8] Alla Maslennikova, Vladimir Vezhnevets "Interactive Color Transfer Between Images" Graphics and Media Lab., Department of Computational Mathematics and Cybernetics Lomonosov Moscow State University, Moscow, Russia.
- [9] Xuezhong Xiao and Lizhuang Ma, "Color Transfer in correlated color space", ACM International Conference on Virtual Reality Continuum and Its Applications VRCIA 2006.

Feature Level Fusion of Multibiometric Cryptosystem in Distributed System

N. Geethanjali¹, Assistant.Prof. K.Thamaraiselvi², R. Priyadharshini³
^{1, 2, 3} Department of Information Technology, SNS College of Technology, INDIA.

ABSTRACT: *Multibiometrics is the combination of one or more biometrics (e.g., Fingerprint, Iris, and Face). Researchers are focusing on how to provide security to the system, the template which was generated from the biometric need to be protected. The problems of unimodal biometrics are solved by multibiometrics. The main objective is to provide a security to the biometric template by generating a secure sketch by making use of multibiometric cryptosystem and which is stored in a database. Once the biometric template is stolen it becomes a serious issue for the security of the system and also for user privacy. In the existing approach, feature level fusion is used to combine the features securely with well-known biometric cryptosystems namely fuzzy vault and fuzzy commitment. The drawbacks of existing system include accuracy of the biometric need to be improved and the noises in the biometrics also need to be reduced. The proposed work is to enhance the security using multibiometric cryptosystem in distributed system applications like e-commerce transactions, e-banking and ATM.*

Keywords: *Biometric Cryptosystem, Error correcting code, Fingerprint, Iris, Multibiometrics, Unimodal biometrics.*

I. INTRODUCTION

The term “biometrics” is derived from the Greek words “Bio” (life) and “Metrics”(to measure). Biometrics refers to the physiological or behavioural characteristics of a person to authenticate his/her identity [1] [2]. Biometric system is essentially a pattern recognition system that recognizes a person by determining the authenticity of a specific physiological or/and behavioural characteristics possessed by the person. Physiological biometrics also known as physical biometrics or static biometrics is based on data derived from the measurement of a part of an individual’s anatomy. It includes fingerprint recognition, Iris scan, Retina scan, Hand Geometry; Palm print, Face recognition, DNA and Vascular Pattern Recognition. Among all fingerprint recognition is the olden technology.

Behavioural biometrics also known as dynamic biometrics is based on data derived from measurements of an action performed by an individual and distinctively incorporating time as a metric; the measures action has a beginning, middle and end. It includes Signature, Keystroke, Handwriting, Voice recognition and Gait. Soft biometrics is a human characteristic that provide some information about the individual, but lack the distinctiveness and permanence to sufficiently differentiate any two individuals. Examples of soft biometrics include scars, marks and tattoos, color of eyes and hair color [3]. Trustable authentication plays an important role in secure communication systems. Traditionally, passwords (knowledge-based security) and smartcards (token-based security) are used as the first step towards identity proof in the system. However, security can be breached since dynamic passwords are easily divulged and guessed by means of social engineering or by dictionary attacks. Token-based authentication may in part compensate the limitation of knowledge-based authentication; however, it is not reliable and easily stolen. If passwords and smartcards are shared or stolen form of an individual authentication based on the certain physiological or behavioural traits associated with the individual, overcomes the disadvantages of passwords and smartcards, but it is known that the sensed single biometric data is always noisy and distorted.

Multibiometrics overcomes the limitations imposed by unimodal biometrics by using multiple biometric modalities [4]. These systems are expected to be more reliable due to the presence of multiple, fairly independent pieces of evidence. Multibiometric systems address the problem of non-universality and provide anti-spoofing measures by making it difficult for an intruder to simultaneously spoof the multiple biometric traits of a legitimate user. The variety of factors should be considered when designing a multibiometric system. These include the choice and number of biometric traits; the level in the biometric system at which information provided by multiple traits should be integrated.

II. PROBLEM DEFINITION

If an attacker can hack into a biometric database, he can easily obtain the stored biometric information of a user. Biometric information can be used to gain unauthorized access to the system by either reverse engineering the template to create a physical spoof or replaying the stolen template. Biometric template information for unintended purposes (e.g., covertly track a user across different applications by cross-matching the templates from the associated databases) leading to violation of user privacy. The challenge in designing a biometric template protection scheme [15] is to overcome the large intra user variability among multiple acquisitions of the same biometric trait.

III. LITERATURE SURVEY

The earlier work in the fingerprint recognition was done by Moses and Ignatius [16]. They have used the fingerprint recognition in ATM for security purpose. Minutiae based technique was introduced by Jain et.al [17] presented among current fingerprint matching algorithms like minutiae based matching, correlation filters based matching, transform feature based matching, graph based matching and generic algorithm based matching; minutiae based fingerprint matching is

dominant. Abhishek and K.Jain provided security to the biometric template using biometric template using biometric cryptosystem and feature level fusion is used to combine multibiometrics [5]. To overcome the cancelable biometrics, by not storing the original template in the database is given by N.K.Ratna [6]. The biometrics authentication systems are done with two stages of enrollment and authentication. The problems of hacking a biometric template and usage of ECC (Error Correcting Code) and feature extraction of Iris biometrics is given by Emanuele and Chiara [7]. Multibiometrics can be applied to distributed system using biometric cryptosystem is given by Manish et.al [18].

IV. ENROLLMENT AND VERIFICATION OF UNIMODAL BIOMETRICS

Unimodal biometrics makes use of single source of biometrics for personal identification. The biometrics which is taken under consideration is fingerprint biometrics [14]. The biometric system operates in two modes namely, enrollment and authentication. The features are extracted using singular point detection and minutiae extraction. Singular point makes use of core and delta [15] and minutiae extraction is done with ridge endings and ridge bifurcations.

In the enrollment stage, the fingerprint images were collected using optical fingerprint sensor. Once fingerprint is acquired, next stage is to preprocess the fingerprint and to extract the feature using minutiae extraction and it is stored in the database. In authentication stage, the fingerprint query is given which undergoes image segmentation, image binarization and image minutiae shown in figure1, which either accepts or rejects the user's identity by matching against an existing fingerprint database.

1. Image Segmentation

The original image is given and the image undergoes image segmentation [13]. The fingerprint enhancement algorithm is image segmentation. Segmentation is the process of partitioning a digital image into multiple segments and typically used to locate objects and boundaries in images. In segmentation only a Region of Interest (ROI) is useful to be recognized for each fingerprint image. The image area without effective ridges and furrows is first discarded since it only holds background information.

2. Image Binarization

After performing segmentation the noisy area will be removed. In the image binarization, the gray scale image is transformed into a binary image by computing the mean value of each 32-by-32 input block matrix and transferring the pixel value to 1 if larger than the mean or to 0 if smaller. This improves the contrast between the ridges and valleys in a fingerprint image and consequently facilitates the extraction of minutiae.

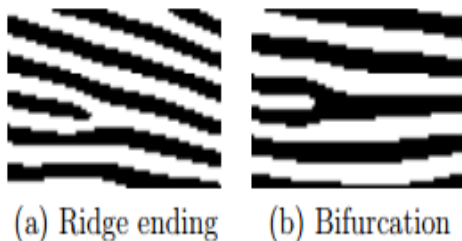


Fig.1 Ridge ending and bifurcation

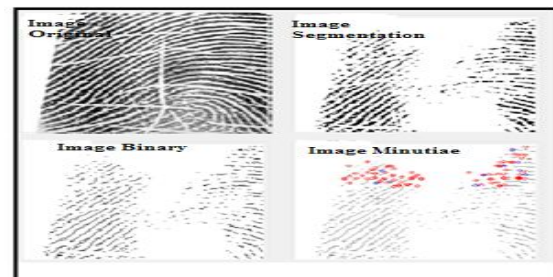


Fig.2 Fingerprint Feature Extraction

3. Image Minutiae

Most minutiae extraction algorithms operate on binary images where the black pixels that represent ridges, and the white pixels that represent valleys. Minutiae-based fingerprint representation [11] can also assist privacy issues since one cannot reconstruct the original image from using only minutiae information. The minutiae are relatively stable and robust to contrast; image resolutions and global distortion are compared to other fingerprint representations. Two fingerprint match if their minutiae points match. Most minutiae extraction algorithms operate on binary images where the black pixels that represent ridges, and the white pixels that represent valleys.

V. FEATURE LEVEL FUSION USING MULTIBIOMETRICS

Multibiometrics is a combination of one or more biometrics, which is taken into consideration in this paper are fingerprint and Iris. Using feature level fusion the features are extracted separately and combined into a single biometric feature set. Instead of storing the original template in the database, secure sketch is generated and stored in the database to provide protection to the template [8], which is achieved by two well known biometric cryptosystem fuzzy vault and fuzzy commitment.

The most important thing in an information fusion system is to determine the type of information that should be consolidated by the fusion module [19]. In feature level fusion which is shown in figure 3, the data or feature set originating from multiple sensors are first pre-processed and features are extracted separately from each sensor, form a feature vector. These features are then concatenated to form a single new vector. Feature level fusion can use same feature extraction algorithm or different feature extraction algorithm on different modalities whose feature has to be fused. The composite feature vector is then used for classification process. The fingerprint features are extracted using fingerprint minutiae and iris

features are extracted using binary strings. The fingerprint image will undergo processes of image segmentation, filtering of image using Gabor filter, noise removal and image binarization to extract the fingerprint features. Likewise the iris image will undergo processes of image segmentation, filtering of image using Gabor filter and at last the iris binary vector is obtained is shown in figure 5.

The templates which are extracted separately are fused with the random key which is given as input using ECC and stored in the database. In the verification stage, the fused single vector is compared with the vector which is stored in the database and key is regenerated. If the key which is not public matches, then the user is valid or it is decided that user is invalid.

Matching performance of a biometric system is measured with the help of false acceptance rate (FAR) and genuine acceptance rate (GAR). The biometric cryptosystem fuzzy vault and fuzzy commitment do not generate revocable templates. The step by step process followed to extract features from the biometrics is shown in figure 4, to achieve the goal of providing accuracy and security is given by:

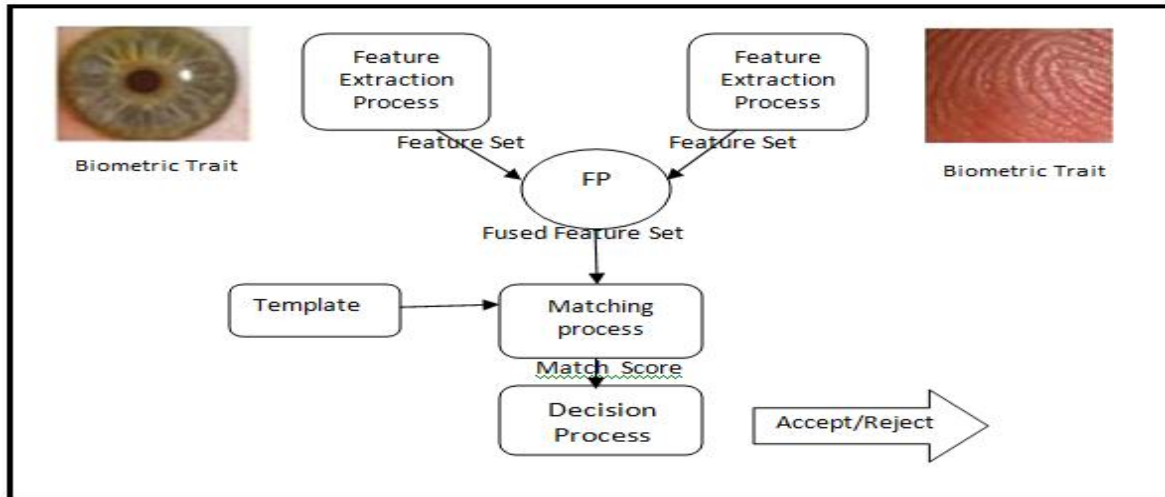


Fig.3 Feature Level Fusion

Data Acquisition – Images are collected using sensor. The optical sensors are most popular and are inexpensive.

Pre-processing - Tasks like image alignment or region of interest (ROI) identification take place in pre-processing.

Feature Extraction – To extract the features from the segmented image, resulting in a feature vector.

Feature Vector Binarization – To generate a binary string b of length T represents the feature vector. Additional information about interval boundaries is necessary.

ECC - In the enrollment stage, an error correcting code (ECC) is applied to b , to extract a set of parity-check bits. In the verification stage, the new binary feature vector b' is considered as a noisy version of the enrolled one. The stored parity-check bits are used to attempt the correction of b' .

XOR- In order to provide the system with revocable templates, this module computes bitwise exclusive OR between a binary feature vector and a randomly generated binary string b .

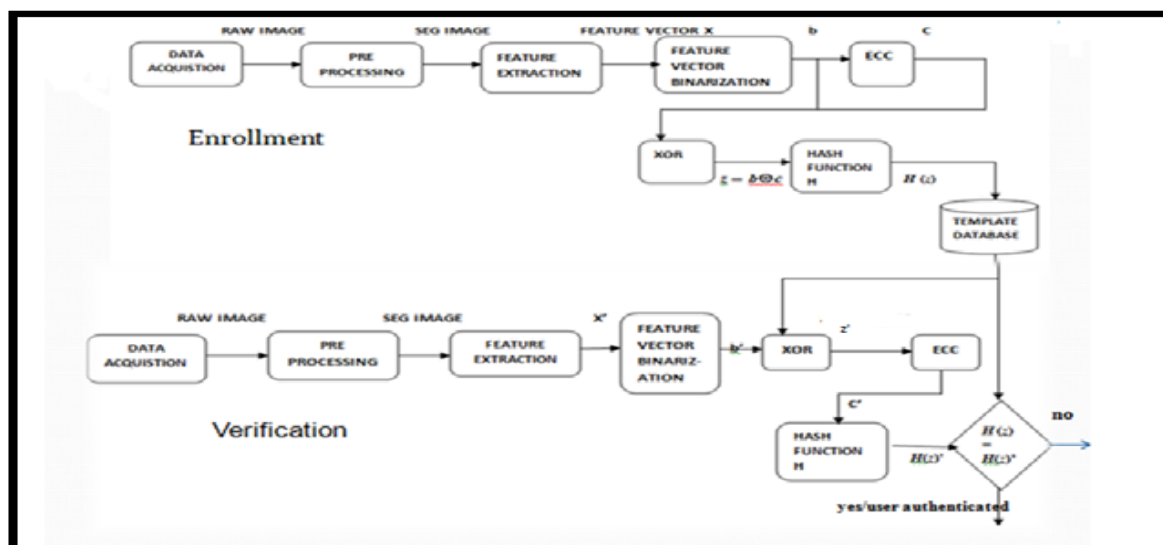
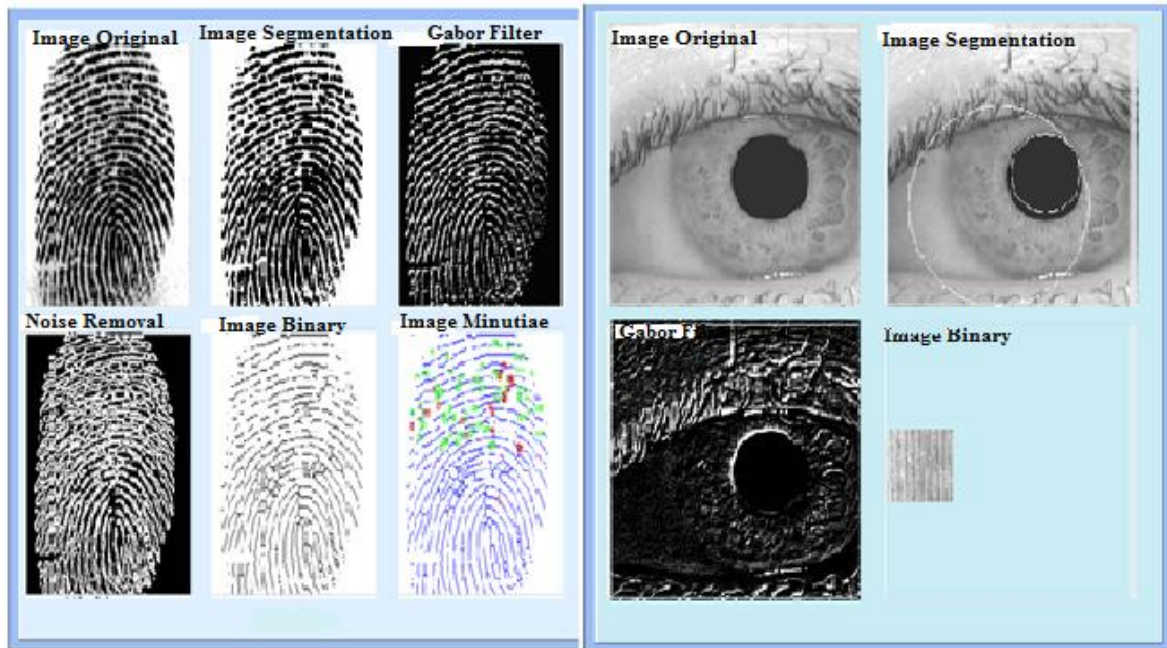


Fig.4 Block Diagram for Feature Level Fusion using Multibiometric Cryptosystem



a) Fingerprint Feature Extraction

b) Iris Feature Extraction

Fig.5 Level By Level Feature Extraction of Fingerprint and Iris

Hash Function – When an individual is enrolled in the system, a hash function H , is applied to $z = c \oplus b$. The output is stored in the system database, ensuring the privacy of b . In the verification stage, H is applied to corrected binary string $z' = c \oplus b''$, so that the output can be corrected to the stored hash.

Decision – If the stored hash $H(z)$ and $H(z')$ matches, then the user is successfully verified and the key will be regenerated, which is responsible for decision making.

VI. BIOMETRIC CRYPTOSYSTEM IN DISTRIBUTED SYSTEM

In distributed system, multibiometrics is used to provide security to the system and biometric cryptosystem for providing protection to the templates. ATM system is designed and users register their details and face image is captured and encrypted and stored in the binary format in the database and using feature level fusion fingerprint and iris templates are fused and stored in database. Fuzzy vault and fuzzy commitment build the biometric cryptosystem [10]. They do not generate revocable templates. Fuzzy Commitment is a biometric system that can be used to secure biometric traits represented in the form of binary vectors and fuzzy vault is represented in the form of point set.

1. Fuzzy Vault and Fuzzy Commitment

In fuzzy vault encoder, the biometric template will be given along with random secret key which is converted to a polynomial degree and polynomial is evaluated in a graph. The set of points is then secured by hiding them with chaff points [9]. The set of genuine points along with polynomial evaluations together with chaff points constitute the sketch or vault. In fuzzy vault decoder, the biometric will be given and then by using the filter the vault points and the query are compared. If the biometric query set is sufficiently close to many genuine points and it can be correctly identified and polynomial is reconstructed successfully and key is generated which is used for validity check. In multibiometric vault the feature level fusion is used to combine the biometrics and then fuzzy vault scheme is addressed.

Fuzzy commitment is represented in the form of binary vectors. The binary string is divided into a number of segments and each segment is separately secured using a fuzzy commitment scheme [12]. The keys associated with these segment wise fuzzy commitment schemes are then used as additional points in the fuzzy vault constructed using the point-set based features.

VII. CONCLUSION

Biometrics is not only a fascinating pattern recognition research problem but, if carefully used, could also be an embedding technology with the potential to make our society safer, reduce fraud and lead to user convenience. The proposed methodology presented here provides security to the distributed system and feature level fusion framework is provided. Likewise, it cannot be guessed it out how many biometrics is used and what type of biometrics are used. As secure sketch is generated from the template and stored in the database, the hackers cannot be able to use the template, unless and until they know the secret key. In future, the work is to overcome the failure of biometrics, which can be addressed by using multimodal model which gain the advantage of other biometrics in case of failure of one biometrics.

REFERENCES

- [1] A.Ross , K.Nandakumar and A.K. Jain, "Handbook of Multibiometrics", New York: Springer,2006.
- [2] Jain A.K, Ross A. and Prabhakar S, IEEE Transactions on Circuits and Systems for Video Technology,14, 4-20, 2009.
- [3] Jain A.K, Dass SC and Nandakumar K, "Soft Biometric Traits for Personal Recognition Systems". Proc of International Conference on Biometric Authentication, Hong Kong: 731-738, 2004.
- [4] Brunelli, R., and Falavigna, D. "Person Identification Using Multiple Cues", IEEE Trans. on Pattern Analysis and Machine Intelligence (Oct. 1995). IEEE, NY, 955-966.
- [5] Abhishek Nagar, Karthik Nandakumar and AnilK. Jain, "Multibiometric Cryptosystems Based on Feature-Level Fusion", IEEE transactions on information forensics and security, vol. 7, no. 1255-268, 2012
- [6] N. K. Ratha, S. Chikkerur, J. H. Connell, and R.M. Bolle, "Generating Cancelable Fingerprint Templates," IEEE Trans. Pattern Anal. Mach. Intell., vol. 29, no. 4, pp. 561-572, Apr. 2007.
- [7] Emanuele Maiorana, Chiara Ercole, "Secure Biometric Authentication System Architecture using Error Correcting Codes and Distributed Cryptography", 2007.
- [8] A. Jain, K. Nandakumar, and A. Nagar, "Biometric Template Security," *EURASIP J. Adv. Signal Process.*, 2008.
- [9] K. Nandakumar and A. K. Jain, "Multibiometric Template Security Using Fuzzy Vault," in Proc. IEEE 2nd Int. Conf. Biometrics: Theory, Applications, and Systems, Washington, DC, Sep. 2008.
- [10] A. Nagar, K. Nandakumar, and A. K. Jain, "Adapting Biometric Representations For Cryptosystems" Department of Computer Science and Engineering, Michigan State University,2011.
- [11] Raymond Thai, "Fingerprint Image Enhancement and Minutiae Extraction", 2003.
- [12] Juels and Wattenberg, "A Fuzzy Commitment Scheme", in proc, 6th ACM conf, Computer and Communication Security, 1999.
- [13] Sangram Bana and Dr.Davinder Kaur, "Fingerprint Recognition using Image Segmentation", IJAEST, Volume no.5, 012-023, 2011.
- [14] Ing. Martin Drahansky, "Biometric Security Systems Fingerprint Recognition Technology", 2005.
- [15] D. Maltoni, D. Maio, A.K.Jain and S.Prabhakar, "Handbook of Fingerprint Recognition" , Springer, Berlin, Germany,2003.
- [16] Moses Okechukwu Onyesolu and Ignatius Majesty Ezeani, " ATM Security Using Fingerprint Biometric Identifier: An Investigate Study", IJACSA Vol.3,No.4,2012.
- [17] Jain et.al. "On-line Fingerprint Verification", IEEE Transactions on Pattern Analysis.
- [18] Manish Manoria , Ajit Kumar, Satyendra Singh and Debu Sinha, " Secure Biometric Cryptosystem for Distributed System", IJCNS, Vol 1, 2011.
- [19] Mini Singh Ahuja and Sumit Chhabra, " A Survey of Multimodal Biometrics", IJCSA,2250-3765,2011.

Planning Strategy for Heritage Conservation of Campal Heritage Precinct in Panaji City

Shaikh Ali Ahmed,¹ Dr. B. Shankar²

¹(Planning Assistant, North Goa Planning Development Authority, Panaji)

² (Associate Professor, Institute of Development Studies, University of Mysore, Mysore)

ABSTRACT: Panaji was formally a Portuguese colony and it is well known for its rich cultural and built heritage. The city has been declared as heritage city to provide assistance under Jawaharlal Nehru Urban Renewal Mission (JNNURM) Scheme, which was launched by the central government in coordination with the state government. It is also one of the important tourist destinations and has one of the longest coastlines in India. The city has many heritage buildings and precincts. The Campal heritage precinct is one of the Conservation areas, which has been identified in the Outline Development Plan 2011. "The Goa Land Development and Building Construction Regulation 2010" has also identified two residential houses and a statue of Dr. Francisco Luis Gomes in the Campal garden. The heritage area has number architectural and heritage buildings of high significance, which requires identification and notification. These have come under tremendous threat due to new developmental pressures in the area and some of them are getting demolished due to non comprehensive approach to the heritage conservation by the agencies concerned including people at large. The paper focuses on the issues faced by the heritage precinct and proposes planning strategies and measures for harmonious development in the Campal heritage precinct.

Keywords: Heritage Precinct, Conservation Areas, Strategies.

I. Introduction

Panaji city is an historical and cultural capital of Goa State. The city had a population of 59,066 persons (as per census 2001) which spreads over an area of 8.12sq.kms, with a density of 7274 persons per sq.km. It was a small fishing village with lots of coconut trees, creeks and fields. The city is an Indo-Portuguese cultural heritage city and is situated on the bank of river Mandovi. It is famous for its natural scenic beauty, exuberant greenery, attractive beaches, temples, churches and distinctive neo-classic architecture. The city has been identified as heritage city by the Government of India for providing assistance under JNNURM project. It has many monuments, heritage buildings, precincts and sites of architectural and historical importance. There are many heritage areas/precincts namely Campal heritage precinct, the Massano do Amorim heritage precinct, the and Mala Fontainhas and these areas have come under great threat of new developments. The precinct has neither heritage management plan nor heritage inventory and significance assessment of buildings and areas for preparing the conservation plan for up-keeping of these monuments, heritage buildings and heritage precincts which need to be preserved, protected, and conserved in a professional manner.

The Campal Heritage area is one among the five declared areas for "Conservation" in the recently published development control regulation by the Government of Goa under the Goa Land Development and Building Construction Regulation 2010. This area has come under the threats of demolitions of old and dilapidated architectural buildings by replacing with the modern buildings due to increase in land value and high maintenance cost. There is no heritage management strategy or policy of the government for the area by which the heritage structures are to be repaired, maintained and restored in a cost effective manner, as it has been done in other countries. The paper addresses the issues of heritage area and proposes strategies for harmonious conservation of heritage precinct of Campal in the City of Panaji.

II. Characteristics of Campal Heritage Precinct

The City of Panaji has strong historical connotations, dating back to the 18th century, when it was officially made the capital of Goa and called Nova Goa. In the year 1830 the "Father of Panjim", Dom Manuel de Portugal-e-Castro developed a place by making it commercial from urban. This is a beautiful place situated approximately at a distance of 4 km from Panjim came to be known as "Campal" named after 'Campal-de-Dom Manuel'. The precinct's predominant land use is residential and commercial uses, which starts from the end of the medical college and the road that leads to Campal is now called 'Dayan and Bandodkar Marg'. Unlike other areas of Panaji, the Campal heritage area is unique in its nature and characteristics. The street pattern consists of a grid iron pattern and only residential houses fully self sufficient in their needs and demands. Every house is different in its character, accessible with well tarred roads, parking space and compound is housed with ornamental railings carved in stones, and a distinct construction technology used to construct these houses. Basically, a formal layout with a garden (Jardin de Francisco Luis Gomes) facing the river front as focal point. Campal lies along river Mandovi and predominantly a residential area, occupied by higher economic group of population. The area is serene and tranquil away from the main hub of activity.

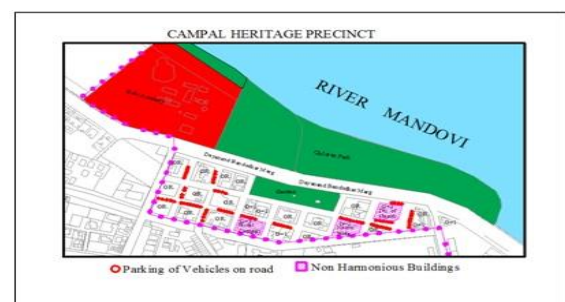


Fig. 1 Campal Heritage Area

Architectural elements such as verandahs, balconies, cornices, windows corners etc., play an important role in the appearance for conservation areas. Individual low stung bungalows oriented towards river Mandovi. Compound walls form a strong visual element and lend distinctive character. Green setting for built up areas adds to general ambience.

III. Historical Bridges in Campal

The Campal precinct had six bridges which were reclaimed between 1827 and 1835. The Viceroy D. Manoel Francisco de Portugal-e-Crasto undertook large scale reclamation of the western marshes of Panajim. The open area was called Campo de Manuel or Campal, which means an extensive open ground. The several measures initiated by the illustrious Viceroy included the construction of six

bridges leading towards and beyond the Campal area. These include:

- The Bridge connecting the mouth of St. Inez creek to the Mandovi,
- The bridge by name Ponte Minerva built in 1829 located on the west of the old Goa Medical College leading to the market,
- The bridge near the present sports complex,
- The bridge connecting the main road beyond Caculo circle to Campal,
- The bridge near the Military Hospital named Ponte Portugal built in 1832 and later was renamed Ponte Alexandre Herculano, and
- The bridge connecting St. Inez to Tonca.

With the construction of these bridges the Capital was poised for further expansion and growth.



Fig. 2. View of the Historical Bridges

IV. Listed Heritage Structures in Campal

The Goa Land Development and Building Construction Regulation 2010 has listed down as many as three heritage structures of importance in the area of Campal. They are: (a) Statue of Dr. Francisco Luis Gomes, (b) House of Mr. Paulo Mesquita, and (c) House of Professor Leao Fernandes. The names of the owners of these houses are

mentioned in the listed heritage structures but there are no identifications made for these houses. The listed houses are in dilapidated condition which needs urgent repairs for restoration. Due to high cost of maintenance the owners are unable to maintain these houses. Some of these structures are having high significance that are not listed are on the verge of demolition for promoting the new developments.



Fig.3 Statue of Dr. Francisco Luis Gomes in Campal Heritage Precinct garden



Fig. 4 House of Mr. Paulo Mesquita



Fig.5 House of Professor Leao Fernandes

Dr. Francisco Luis Gomes was born on 31st May 1829 and one of the intellectual figures of Goa. Graduated as a doctor from the Escola Medico-Cirurgica de nova Goa in 1850. Like his father he too was involved in civic matters and was elected as the Corte (Portuguese Parliament during the monarchical times in 1860. Wrote extensively but remained best known for his book "Os Brahmanes" and died at young age. The statue was inaugurated at Campal in 1932 in the garden known as Jardin de Campal further the

name was changed to Jardin de Francisco Luis Gomes in 1952 by the Ministro de Ultramar Sarmiento Rodriguez.

There are many Residential Buildings of high architectural significance in the Campal Heritage Precinct which needs identification. Some of the heritage buildings which are having architectural and cultural value with high significance in the heritage areas of Campal are depicted in the following figures.



Fig.6 House near Central Lodge (Paulo Mesquita)



Fig.7 House of Perigarine Da Costa



Fig.8 House of Wendell Rodrigues



Fig.9 Heritage House Facing the Garden



Fig.10 Heritage House Recently Restored



Fig.11 Restored Heritage House

VI. Issues of Campal Heritage Precinct

The Campal Heritage Precinct is facing many problems to be taken for the conservation and preservation by the Planning Authority and is as follows:

- a) Even though Campal heritage area is an old residential area and many architectural and heritage buildings only two heritage residential houses and a statue of Dr. Francisco Luis Gomes which is situated in the garden have been notified in the "Goa Land Development and Building Construction Regulation 2010".
- b) There is no comprehensive approach followed in identifying heritage buildings in the precinct area.
- c) New and tall buildings that were permitted by the local authority do not have the harmony with existing architecture and the area losing its significance.
- d) The heritage structures of high significant value are dilapidated in condition due to non provision of financial assistance from the Government or Local Authority in conserving and maintaining them.
- e) Original owners are disposing off their properties due to increase in land value and maintenance cost of these heritage structures.
- f) Poor quality of roads and gutters continued, although the area is unique in its character.
- g) The number of vehicles plying in this precinct has increased over the years. Campal being a very peaceful residential area gets disturbed due to the frequent movement of vehicles.
- h) Also, on-street parking of vehicles is allowed, thereby reducing the carriage width of road by the outsiders who visit market and Campal trade centre and park their vehicles due to non availability of parking space.
- i) Parking on roads blocks the visibility of these heritage structures of high significance.
- j) There is no Management Action Plan to improve the precinct with the support from the government for improvement and restoration of houses in the area.
- k) Streetscape and street furniture are not adequate.
- l) There is no proper signage in the area to control the hoardings.

VII. Planning Strategies for Conservation in Campal Heritage Precinct

The heritage precinct recognises that the whole is greater than the sum of the parts; that a collection of heritage buildings has a greater impact on the observer and has greater heritage value than the same number of buildings scattered throughout the city. The loss or the unsympathetic alteration to even a single building detracts from the whole precinct rather like a missing tooth from a smile. The precinct includes non-listed buildings form an integral part of the visual catchment. The aim is to achieve more

sympathetic development on non-listed sites as these are rebuilt or altered areas. The strategy or policy shall ensure that alterations of existing houses and new buildings are sensitive and enhance the existing visual qualities of the streetscape in the precinct. The proposed strategy for harmonious conservation of Campal heritage precinct to include:

- a) The area needs Heritage Conservation Management Plan to identify, develop, and maintain the heritage buildings or structures of high significant value.
- b) Campal precinct needs Heritage Inventory Assessment for identification of heritage buildings or structures of high significance.
- c) The character is to be preserved in all the identified and listed heritage buildings in the precinct.
- d) The streets which are having single storey buildings need to be preserved or conserved.
- e) Steps to be taken for maintaining the listed heritage buildings and encouraging the restoration of street frontages.
- f) Ensuring alterations and additions for maintaining the architectural integrity of listed heritage buildings and also enhancing the appearance of non-listed buildings in line with the general streetscape.
- g) The safety measures like gated community to be introduced in view of the area being small and protection for their invaluable heritage structures of high significance.
- h) Parking restrictions are to be imposed in the precinct.
- i) Abandoned and dilapidated structures shall be restored by providing financial assistance and incentives to the owners in form of tax rebate, concessions etc., by the Local Authority with the assistance of state government so that the structures of significant value could be restored or preserved and managed.
- j) Special Grants may be obtained from State and Central governments for getting finance for up-keeping of these buildings, developing streetscape and street furniture and landscaping by encouraging Public-Private-People-Partnerships joint ventures with a formula: Government-50% : owner -50%).
- k) Visitors' parking place, cafeteria, entry and exit is the need of the hour. And such works/activities to be allotted to the local residents of the place only.
- l) Entry tickets shall be made compulsory for the heritage tourism and revenue generated to be used for the maintenance of the area.
- m) Garden that facing the heritage precinct to be developed and maintained.
- n) Modern and non-harmonious buildings in the areas are to be discouraged by proper development control in the area. After proper assessment of building condition,

restoring, re-plastering, re-roofing and re-flooring to be allowed.

- o) Ensuring the design harmony which is sympathetic to the neighbouring houses and the streetscape so that the visual qualities of the Precinct are enhanced.

VIII. Conclusion

The Campal is one of the important heritage precincts in the City of Panaji. There are many residential buildings of high architectural significance in the Campal Heritage Precinct which needs identification. Some of the heritage buildings are having architectural and cultural value with high significance in the heritage areas of Campal. It has rich built heritage of Campal needs to be protected, managed and properly planned for the future generations in terms of sustainable development. As far as possible care need to be taken to protect these houses from demolition and the area getting spoiled with the new buildings of modern architecture which detracts the significance and the area gets developed in a non- harmonious manner. The heritage conservation strategies which are proposed in the previous paragraphs shall be adopted to safeguard this area from getting developed in unsympathetic manner. Maximum efforts are needed to manage, maintain and restore the heritage structures of high significant value to retain the character of the heritage precinct.

References

- [1]. Shaikh Ali Ahmed and Shankar B., "Challenges of Planning for Heritage Areas in Panaji City", International Journal of Modern Engineering Research (IJMER), Vol.2, Issue.1, Jan-Feb 2012 pp-446-450
- [2]. Shaikh Ali Ahmed and Shankar B., "Conservation of Heritage Areas in the City of Panaji: A Case Study of Fontainhas Area", International Journal of Modern Engineering Research (IJMER), Vol.2, Issue.2, Mar-Apr 2012 pp-442-446.
- [3]. Shaikh Ali Ahmed and Shankar B, "Planning for Conservation of Heritage Areas in Old Goa: Issues and Strategies", IDES_CPS, Civil Engineering Series-Advances in Civil Engineering ACE, Ed., pp-11-15, 2011, New York.
- [4]. Shaikh ali Ahmed and Shankar B, "Municipal Solid Waste in Heritage Conservation Areas- A Case Study of Panaji", 1st Edn. Vol. 1 and Vol.2, Sustainable Waste Management- Municipal, Industrial and Agricultural, by Sadhan K. Ghosh et al, Oxford Publishing House , Kolkataka (ISBN 81-86862-46-3 & ISBN 81-86862-74-1, July 2012, pp-59-63 Mysore.
- [5]. Report on Inner City Guide, Nelson City Council, 2004
- [6]. Joshi C., et al, World Heritage Series Old Goa, Archaeological Survey of India, Goa.
- [7]. Regional plan Goa, 2001 and 2021, Town & Country Planning Department, and Government of Goa.
- [8]. Report of the Sewri Consultants Pvt. Ltd., Mumbai, India and Sandhya Sawant, Director Bombay

- Collaborative Urban design and Conservation Pvt. Ltd., Mumbai, India. on restoration of Capela da Nossa Senhora do Monte, Old Goa by Managing Director,
- [9]. Government of Goa, the Ancient Monuments and Archaeological Sites and Remains Act, No. 24 of 1958, Government of India.
- [10]. Government of Goa, the Goa Ancient Monuments and Archaeological Sites and Remains Act, 1978 and Rules, 1980.
- [11]. Government of Goa, The Goa Town and Country Planning Act and Rules, Government of Goa, Planning and Development Authority (Development Plan), Regulations, 1989, Panjim Planning and Development Authority, Panjim.
- [12]. Report of the Tourism Master Plan: GOA- 2011 final report prepared by Consulting Engg. Services (I) Ltd. for Government of Goa, Department of Tourism.
- [13]. Walking in and Around Panaji-Goa, Published in January 2005 by Goa Heritage Action Group and The Corporation of City of Panaji.
- [14]. Govt. of Goa, The Goa (Regulation of Land Development and building) Act 2008 and the Goa Land Development and Building Construction Regulation 2010, second edition 2011.
- [15]. Government of Goa, Panaji, A Search for Identity, Oct. 1997, The North Goa Planning and Development Authority.
- [16]. Vasco Pinho, November 2009, Snapshots of Indo-Portuguese History-I, Panaji.
- [17]. The Story Behind the Panjim Creek, May 2012, (web publication; Goenchen.com).

Biographies



Shaikh Ali Ahmed received M.Tech in Urban and Regional Planning from the University of Mysore, Mysore. Presently, he is working as Planning Assistant in North Goa Planning Authority, Panaji. He is Associate Member of the Institute of Town Planners, India; He is presently pursuing his Ph.D in Urban and Regional Planning at the Institute of Development Studies, University of Mysore. His research interests to include heritage conservation, heritage legislation.



Dr. B. Shankar received the B.E. degree in Civil Engineering in 1984, M.U.R.P degree in Urban and Regional Planning in 1989 and Ph.D degree in Urban and Regional Planning in 1997 from the University of Mysore, Mysore. He is working as Associate Professor in Urban and Regional Planning at the Institute of Development Studies, University of Mysore, and Mysore. His research interests to include Urban Planning, Urban Poverty, Community Development, Heritage Conservation, and Planning Legislation.

Environmental Pollution Reduction in Cement Industry for Co Combustion of Waste Tyre and Coal as a Fuel

¹R.K.Patil, ²B.Garnaik, ³M.P.Khond, ⁴L.G.Nawale

¹TSSM'S Bhivarabai Sawant College of Engineering and Research, Mechanical Engineering Department, Pune 411 041, India.

²National Chemical Laboratory (Principal Scientist), Polymer Science and Engineering Division, Pune 411 008, India.

³College of Engineering, Mechanical Engineering Department, Pune 411 005, India

⁴MES College of Engineering, Mechanical Engineering Department, Pune 411 001, India

Abstract: In recent years, there are several problems encountered in waste management system particularly waste tyre as well as coals. The energy generation on incineration provides large amount of polycyclic aromatic hydrocarbon (PAH) emissions which is the cause of major environmental threat. Therefore, the combustion of coal and tyre were carried out in cement industry in order to generate heat energy at 1300°C and the only remaining residue (steel powder) to enhance the strength of the cement. At the outset, the particle size of coal and tyre was cut into 63-75 and 180-212 µm respectively. Combustion experiments were conducted using Nelson reactor under controlled conditions in presence of air and also in presence of nitrogen gas (INOX) atmosphere. The temperature range was varied from 300-1300°C and several fuel mass loading in the furnace, expressed in terms of bulk equivalence ratios in the range of 0.7-2.4. At fixed bulk equivalence ratios, as the furnace gas (Air) temperature increased the polycyclic aromatic hydrocarbon yields from both fuels decreased drastically, while the CO₂ yields increased. At the highest temperature around 1300°C, the effluent of combustion of both (coal and tyre) fuels was practically devoid of polycyclic aromatic hydrocarbon (PAH) (at a detection limit of 0.3 µg of a PAH component/g of fuel burnt). In order to understand the rate of thermal effect and morphology of co combustion material (coal and tyre), the preliminary results are very essential to explore. Therefore, the thermo gravimetric analysis (TGA) and environmental scanning electron microscopy (ESEM) were carried out and results of coal and tyre mixture at various temperature conditions will be highlighted.

Keywords: Environmental Emission, Cement Industry, Carbon dioxide, polycyclic aromatic hydrocarbon (PAH), Nelson reactor.

I. INTRODUCTION

Coal is the predominant fuel for power generation in the world. India alone produces 1.5 and consumes approximately 1.0 billion of coal yearly for power generation. Thus, a thorough study of the emissions of coal is warranted. Waste tyres, on the other hand, are generated by the billions every year, with India alone discarding an estimated quarter of a billion tyres, but they are not currently used for energy generation to any significant extent. Instead, they are either land filled or stored in tyre dumps, creating health problems and fire hazards. Because of their high heating value (29-37 MJ/kg, which is higher than most coals), however, waste tyres are being considered as an attractive potential fuel. With an average weight for tyres of 10 kg, a total of 2.5 million ton of tyre-derived fuel can be produced in India per year amounting to 0.5% of the coal consumption. In addition to this amount, more fuel can be deduced from existing tyre stockpiles, and the yearly electric energy production potential from tyres could reach 2% of that from coal.

While pulverized coal is widely used in most utility fired boilers, pulverized rubber from waste tyres is still a costly proposition, mainly because it is made desired smaller sizes using cryogenic processes that are currently used to produce it and the small scale of existing operations. According to certain sources, the current price of pulverized tyres is currently 3-5 times higher than that of coal (Rs. 9000-15000 vs Rs.3000/ton). This price difference can be bridged, however, if cost effective large scale tyre grinding processes

are invented and/ or if higher fees are implemented. First of all, the waste tyre will be grinded after dipping into liquid nitrogen (-196°C). This will avoid the high cost of building dedicated tyre-to-energy combustion facilities. Therefore the combustion and emissions of both fuels in pulverized form will be examined.

Six industries have been identified as energy intensive industries globally: Cement, Aluminum, Fertilizer, Iron and Steel, Glass and Paper [1]. Cement industry consumes about 4 GJ per tons energy of cement produced. Indian cement industry accounts for 10.3 % of total fuel consumption in the manufacturing sector [2]. Out of total, about 50% carbon dioxide is generated during calcinations and remaining during the combustion processes [3]. Cement industry had emitted 43 million tCO₂ in 1990 that has increased to 59 million tCO₂ in 1995. In 1995, energy use contributed 40% of total cement sector emissions while the remaining was due to calcinations process [4]. Worrell et al.,

[5] have carried out an in-depth analysis of the US cement industry. They found that the use of blended fuel is a key cost-effective strategy for energy efficiency improvement and CO₂ emission reductions. Xiang - Guo et al., [6] have performed experiment on combustion of waste tyre, high ash coal and tyre-coal blends with 10, 30 and 50% waste tyre were investigated by means of thermogravimetric analysis (TGA). They found that incorporation of waste tyre can improve the combustion characteristics of high ash coal, especially the ignition performance and the peak weight loss

compared with the separate burning of waste tyre and coal. This indicates that the co-combustion of waste tyre and low qualities coal as fuel is feasible. Giere et al., [7] have studied a mixture of 95 wt. % coal plus 5 wt. % Tyre-Derived Fuel (TDF) in the form of shredded automotive tyres by combusting it in a stoker boiler under plant conditions. They found that emissions of CO decreased slightly, whereas those of NO_x, SO₂, and total particulate matter remained virtually unchanged. Katsioti et al., [8] have stated the prerequisites for using of TDF as a supplement fuel for the clinker production.

The compressive strength of cement produced was measured. In this specific study 6% of the total fuel used was TDF. It was concluded that no apparent problems occurred from the use of TDF as a supplemental fuel in the clinker burning. Kemm et al., [9] describes a Health Impact Assessment (HIA) of a proposal to change the fuel used in a cement plant. It concludes that there is no change in emission of tyre burning. It was carried out to support a health authority, known as a Primary Care Trust (PCT), in preparing its response to consultation under the Integrated Pollution Prevention and Control (IPPC) process.

In this study, combustion of waste tyre, coal and tyre-coal blends of 1%, 3% and 6% were investigated by means of Thermogravimetric Analysis (TGA) which was carried out at 10⁰C/min in Thermogravimetric Analyzer and in the range from 50⁰C to 900⁰C i.e. Thermogravimetric Analysis (TG), Derived Thermogravimetric Analysis (DTG) and Differential Thermal Analysis (DTA). For blends of coal and waste tyre, no interactions between blend components are observed in TGs. However, for DTG, comparatively difference was seen that could be related to a certain degree of interaction between the components. The co-combustion of coal and waste tyre cannot be predicted from the weighted sum of the blend components. The incorporation of waste tyre can improve the combustion characteristics of coal, especially the ignition performance and the peak weight loss compared with the separate burning of waste tyre and coal. This indicates that the combustion of waste tyre and coal as fuel is feasible. With this in view, the study attempts to investigate the effect of percentage blending waste tyre with coal.

II. EXPERIMENTAL STUDY

Fine powder of tyres was prepared by shredding and grinding of waste tyres. Coal powder was prepared by crushing the coal pellets. The material whose thermal decomposition was studied consists of waste tyre, coal and tyre-coal blends of 1%, 3% and 6%. The percentage of waste tyre refers to weight of coal. Waste tyre and coal was mixed properly. The combustion characteristics of coal, waste tyre and tyre-coal blends were determined in Perkin Elmer TGA 7 Thermogravimetric Analyzer. Sensitivity variation was ± 0.1 μ g. The specimen size was approximately 1 to 100 mg. The temperature variation of furnace was from room temperature 25⁰C to 1000⁰C. The heating rate of sample was varied from 0.1 to 200⁰C. The furnace temperature was increased from 50⁰C to 900⁰C at 10⁰C min⁻¹ under Nitrogen atmosphere.

Then sample was cooled to room temperature under Nitrogen atmosphere. The weight of sample was monitored

continuously as function of temperature. The TG, DTG and DTA were performed.

III. RESULT AND DISCUSSION

The analysis results were obtained in the form of plot of temperature vs. weight loss with Heat Flow Endo Down. Figure 1 shows Thermo gravimetric Analysis (TG) of Coal, Tyre, and Tyre blended with coal. Figure (1a) shows the typical TG profile of coal with weight loss (~9%) and result of thermal decomposition and loss of volatiles as well as char gasification (hydrocarbon of low molecular weight up to C₆).

Figure (1b) shows the TG profile of waste tyre. It was found that tyre shows typical TG profile of waste tyre with maximum weight loss (~70%). Figure (1c) shows the TG profile of 1% tyre blended with coal. It shows typical TG profile with maximum weight loss (~8.5 %). Figure (1d) shows the TG profile of 3% tyre blended with coal. It was found that typical TG profile with maximum weight loss (~9%). Figure (1e) shows the TG profile of 6% tyre blended with coal. TG analysis curve showed weight loss was (~11%).

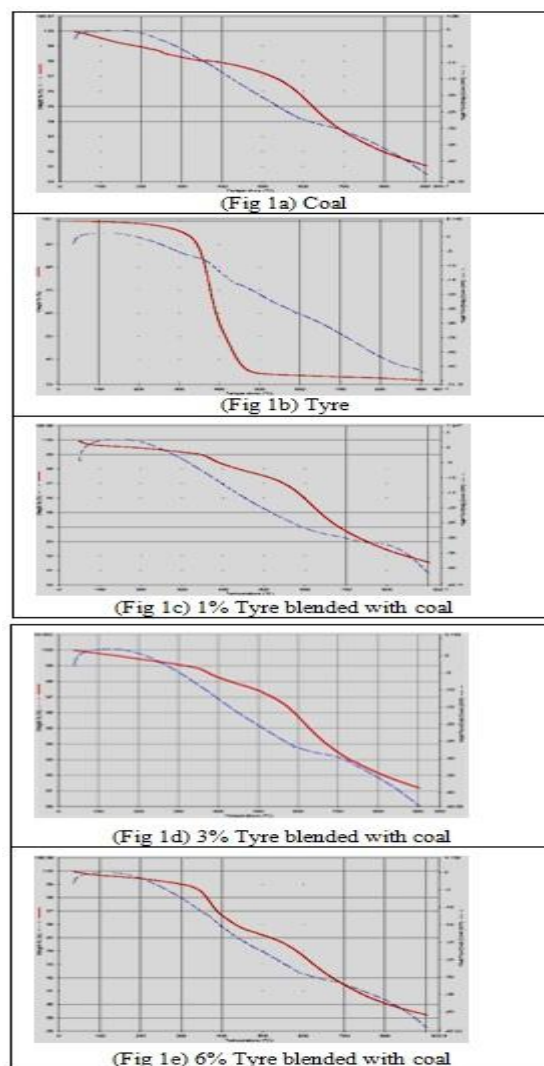


Figure 1 Thermo gravimetric Analysis (TG) of Coal, Tyre and Tyre blended with coal

Figure 2 shows Derived Thermo gravimetric Analysis (DTG) of Coal, Tyre, and Tyre blended with coal. Figure (2a) shows the DTG analysis of coal. Two distinct peaks were obtained at 250°C and 630°C respectively which may be attributed due to volatile product elimination. Figure (2b) shows the DTG analysis of tyre of two stages. The first peak is at 377.87°C due to the thermal decomposition of the mixture of oils, moisture, plasticizers and other additives. The second peak at 417.87°C may be attributed due to the thermal decomposition of natural rubber, polybutadiene and polybutadiene – styrene, the main constituents of tyres. Figure (2c) shows the DTG analysis of 1% tyre blended with coal.

The weight loss observed at two temperatures 380°C and 620°C respectively. Waste tyre at 380°C showed weight loss (~ 4.8%), where as the pure tyre showed (~ 70%) weight loss and the remaining (~ 30%) was steel. The second peak at 620°C is due to combustion of coal and (~ 8.5%) weight loss occurred. The weight loss of coal was (~ 7 %) in comparison with the result obtained in the blend (~ 8.5%). The disappearance of the peak at 250°C occurred in case of 1% blend sample. Figure (2d) shows the DTG analysis of 3% tyre blended with coal. There are two broad peaks appeared at 380°C and 620°C respectively. However, the nature of the peaks is broader in comparison with 1% blending. The weight loss was (~ 3.3 %) at 380°C and (~ 4.5%) at 620°C respectively. The disappearance of the peak at 250°C also observed in case of 3% blended sample. Figure (2e) shows the DTG analysis of 6% tyre blended with coal. There are two broad peaks. The peak appeared at 380°C showed (~ 11.2%) weight loss and the second peak at 620°C showed (~ 7%) weight loss.

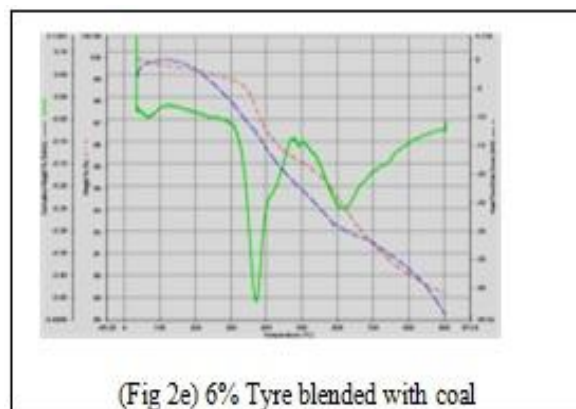
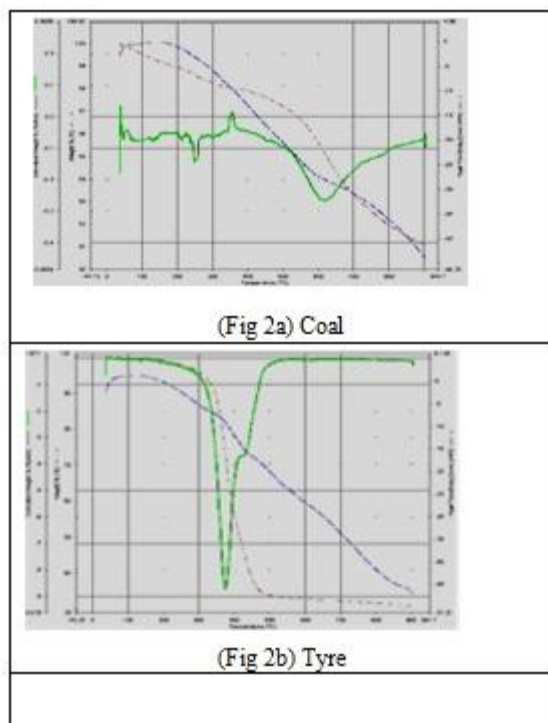
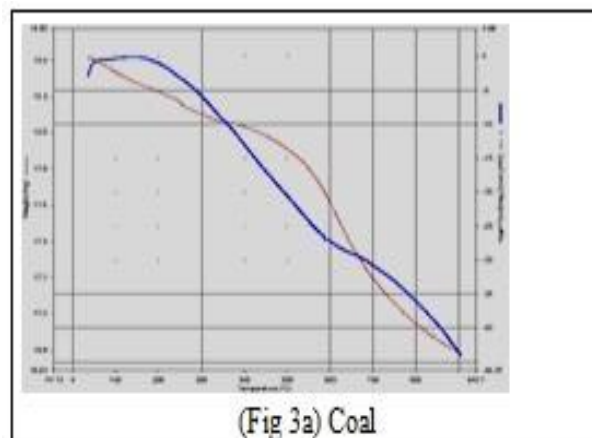
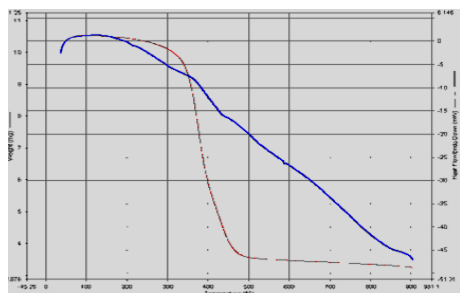


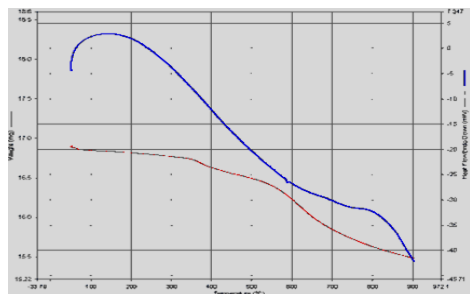
Figure 2 Derived Thermo gravimetric Analysis (DTG) of Coal, Tyre and Tyre blended with coal.

Figure 3 shows Differential Thermal Analysis (DTA) of Coal, Tyre and tyre blended with coal. Figure (3a) shows the DTA analysis of coal. The area under the DTA peak may be related to the heat produced in combustion process that is the high calorific value (HCV). This was the consequence of a greater process of volatile matter in the coal at 250°C and 630°C. Figure (3b) shows the DTA analysis of the waste tyre. The result derived from DTA analysis also showed two peaks at 377.87°C and 417.87°C respectively. Figure (3c) shows the DTA analysis of 1% tyre blended with coal. The result derived from DTA analysis also showed two peaks at 380°C and 620°C respectively. Figure (3d) shows the DTA analysis of 3% tyre blended with coal. The result derived from DTA analysis also showed two peaks at 380°C and 620°C respectively. Figure (3e) shows the DTA analysis of 6% tyre blended with coal. The result derived from DTA analysis also showed two peaks at 380°C and 620°C respectively. The low boiling point organic compounds present in the coal can mix with waste tyre and decomposes at 380°C which is a broader range from 300°C to 400°C.





(Fig 3b) Tyre



(Fig 3c) 1% Tyre blended with coal

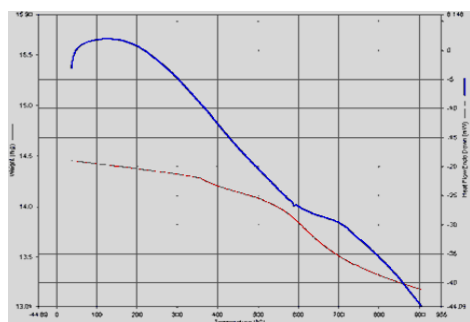


(Fig 3d) 3% Tyre blended with coal

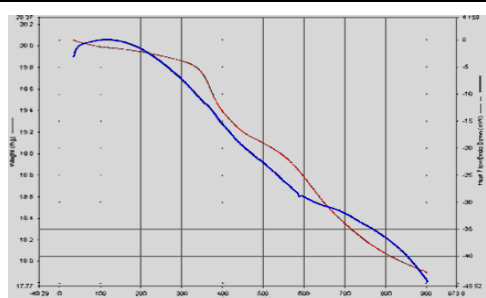


(Fig 3e) 6% Tyre blended with coal

Figure 3 Differential Thermal Analysis (DTA) of Coal, Tyre and Tyre blended with coal.

For blends of waste tyre and coal, no interactions between blend components are observed in TGs. However, DTGs indicated that a comparatively important difference can be seen that may be related to a certain degree of interaction between the components. The co-combustion of waste tyre and coal cannot be predicted from the weighted sum of the blend components. The incorporation of waste tyre can

improve the combustion efficiency of coal, especially the ignition and the peak weight loss compared with the separate burning of waste tyre and coal, which indicate that the combustion of waste tyre and coal as alternative fuel is feasible in industry.

IV. COMBUSTION BEHAVIOR

The combustion characteristics of pulverized coal have been extensively studied, but little has been reported on the combustion of waste tyres. A comparison on the combustion characteristics of single particles (80-200 μ m) of both fuels was recently conducted in this laboratory, under high heating rates (10⁵ °C/s). In this study, separate volatile and char combustion phases were detected for the coal particles examined. Tyre particles experienced an intense primary volatile combustion phase, followed by a phase of secondary evolution and burning of volatiles, of lesser intensity, and simultaneous char combustion. During the initial volatile phase combustion, the peak flame temperatures were comparable for both materials and were in the range of 2200-2400 K at a gas temperature of 1150°C (1423K). The secondary volatile/char combustion phase observed for the tyre particles was cooler i.e.1423K. The coal chars burned even cooler, with surface temperatures of 1850-2000K. Combustion was found to be diffusion ally controlled. Char burnout time were much shorter for tyre particles than for coal particles of the same size, which can be attributed to the secondary devolatilization and the lower density of the former.

COMBUSTION EMISSIONS-The most important emissions from the combustion of coal and tyres are the inorganic gases sulphur dioxide(SO₂) and nitrogen oxide (NO_x), submicron metal aerosols (fumes), and toxic organic emissions, such as polynuclear aromatic hydrocarbons (PAHs), soot, and carbon monoxide(CO). Of recent concern are also the emissions of carbon dioxide (CO₂).

The present study was undertaken to assess and compare PAH emissions and CO₂ emissions from pulverized coal and waste wire-in-tyre crumb burning under well-controlled conditions. The compositions of fuels were tabulated in Table 1.

Table.1Composition of Fuels

Property	Ground tyre (SBR)	Coal
Particle size (μ m)	180-212	63-75
Fixed carbon (%)	21.7	51.9
Volatiles (%)	52.3	34.4
Ash (%)	26.0	13.7
Carbon (%)	60.9	71.9
Hydrogen (%)	5.3	4.7
Sulfur (%)	2.46	1.36
Nitrogen (%)	0.28	1.36
Oxygen (%)	7.1	7.0
Heating value(MJ / kg)	29	29.2

The goal was to understand the influence of combustion parameters on toxic emissions. Combustion of clouds of particles (aerosols) of pulverized coal and tyres under steady-state/steady-flow conditions took place in Nelson reactor, in air, at a gas temperature of 1150°C. Emissions were monitored at various fuel mass flow rates that resulted in overall bulk equivalence ratios that differed widely. Experiments were also conducted under pyrolytic conditions (in an inert gas atmosphere i.e. argon) to simulate a worse-case scenario in a pulverized-fuel furnace, i.e. severe oxygen deficiency.

Polynuclear aromatic hydrocarbons (PAHs) were monitored at the exit of the furnace by trapping the particulate (condensed) and gas-phase compounds separately. The sampling stage was placed directly below the furnace to minimize losses. The products were characterized using GC/MS techniques. The further work is under progress.

V. CONCLUSION

Coal and waste tyre at various compositions were burnt in a Nelson Reactor in presence of N₂ gas as well O₂ gas. The amount of PAH generation were reduced in presence of O₂ gas in comparison with N₂ gas. For coal, a few of the PAHs, such as fluoranthene, pyrene and cyclopental pyrene showed an increase in concentration (by a factor 2) when oxygen was introduced, however most PAHs decreased and the total amount were 7.58 mg/(g of coal) in N₂ and 6.39 mg/(g of coal) in the presence of O₂. The combustion is predominantly dependent on sample size and mixing with gases for tyre, but much less so for coal. The total PAH emissions were 1.82 mg/g for tyre and 0.72 mg/g for coal.

When additional oxygen was introduced, the PAH emissions diminished. For coal, PAH emissions were rarely detected except of naphthalene. For tyre crumb, PAHs could not be detected. The major component CO₂ was thought to be reused in the Cement Industry. The small amount of mutagenic components should be adsorbed using polymeric hydrophobic nanofiber. The work is currently under progress. From the above study it is highlighted that combustion of waste tyre along with coal can be used as environmentally safe fuel in Cement Industry in future.

REFERENCES

- [1] Schumacher K. and Sathaye J., "Indian's Pulp & Paper Industry; Productivity & Energy Efficiency." J of Economic research, Vol. 4, 2001, pp. 1-46.
- [2] Banerjee R and Khurana S., "Energy Balance and Cogeneration for a Cement Plant." J. of Applied Thermal Engineering, Vol. 22, 2002, pp. 485-494.
- [3] Hendriks C., Worrell E., "Emission Reduction of Greenhouse Gases from the Cement Industry." "Greenhouse Gas R&D
a. Programme IEA, www.ieagreen.org.uk/prghgt 42. htm, 2004
- [4] Amit G. and Shukla P., "Emissions Inventory of India", Tata McGraw-Hill Publishing Company Ltd, New Delhi, 2002.
- [5] Worrell E., "Potentials for energy efficiency improvement in the US cement industry." J. of Energy, Vol. 25, 1999, pp. 1189-1214.
- [6] Asthana, S.R. and Patil, R.K., "Use of Alternative Fuels in Indian Cement Industry." Proceeding of National Conference on Advances in energy research, Indian Institute of Technology, Bombay, 2006.
- [7] Mokrzycki E., Uliasz-Bochericz A. "Alternative fuels for the cement industry." J. of Applied Energy, Vol. 74, 2003, pp. 95-100.
- [8] Kaantee U., Zevenhoven R., Backman R., Hupa M., "Cement Manufacturing Using Alternative Fuels and Advantages of Process Modelling." J. of Fuel Process Technology Vol. 85, 2004, pp. 293-301.
- [9] John Kemm., Andrew C., "Health impact assessment of proposal to burn tyres in a cement plant." J. of Environmental Impact Assessment Review, Vol. 24, 2004, pp. 207-216.
- [10] Flagan, R. C.; Seinfeld, J. H. "Fundamentals of Air Pollution Engineering"; Prentice Hall: Englewood Cliffs, NJ, 1988.
- [11] Leung, D. Y. C.; Lam, G. C. K. Presented at the 3rd Asian-Pacific International Conference on Coal and Energy Utilization, 1995.
- [12] Levendis, Y. A.; Atal, A.; Steciak, J. Presented at the Twentieth International Conference on Coal Utilization and Fuel Systems, Clearwater, FL, Mar 1995.

Data Mining: Future Trends and Applications

Annan Naidu Paidi

Asst.Prof of CSE Centurion University, Odisha, India.

Abstract: Knowledge has played a significant role on human activities since his development. Data mining is the process of knowledge discovery where knowledge is gained by analyzing the data store in very large repositories, which are analyzed from various perspectives and the result is summarized it into useful information. Due to the importance of extracting knowledge/information from the large data repositories, data mining has become a very important and guaranteed branch of engineering affecting human life in various spheres directly or indirectly. The purpose of this paper is to survey many of the future trends in the field of data mining, with a focus on those which are thought to have the most promise and applicability to future data mining applications.

Keywords: Current and Future of Data Mining, Data Mining, Data Mining Trends, Data mining Applications.

I. Introduction

Originated from knowledge discovery from databases (KDD), also known as data Mining (DM), Data Mining (DM) is the extraction of new knowledge from large databases. Many techniques are currently used in this fast emerging field, including statistical analysis and machine learning based approaches. With the rapid development of the World Wide Web and the fast increase of unstructured databases, new technologies and applications are continuously coming forth in this field. The main challenges in data mining are:

- Data mining to deal with huge amounts of data located at different sites. The amount of data can easily exceed the terabyte limit;
- Data mining is very computationally intensive process involving very large data sets. Usually, it is necessary to partition and distribute the data for parallel processing to achieve acceptable time and space performance;
- Input data change rapidly. In many application domain data to be mined either is produced with high rate or they actually come in streams. In those cases, knowledge has to be mined fast and efficiently in order to be usable and updated.

II. The Scope of Data Mining

Data mining derives its name from the similarities between searching for valuable business information in a large database — for example, finding linked products in gigabytes of store scanner data — and mining a mountain for a vein of valuable ore. Both processes require either sifting through an immense amount of material, or intelligently probing it to find exactly where the value resides. Given databases of sufficient size and quality, data mining technology can generate new business opportunities by providing these capabilities:

- **Automated prediction of trends and behaviours.** Data mining automates the process of finding predictive information in large databases. Questions that traditionally required extensive hands-on analysis can now be answered directly from the data — quickly. A typical example of a predictive problem is targeted marketing. Data mining uses data on past promotional mailings to identify the targets most likely to maximize return on investment in future mailings. Other predictive problems include forecasting bankruptcy and other forms of default, and identifying segments of a population likely to respond similarly to given events.
- **Automated discovery of previously unknown patterns.** Data mining tools sweep through databases and identify previously hidden patterns in one step. An example of pattern discovery is the analysis of retail sales data to identify seemingly unrelated products that are often purchased together. Other pattern discovery problems include detecting fraudulent credit card transactions and identifying anomalous data that could represent data entry keying errors.
The most commonly used techniques in data mining are:
- **Artificial neural networks:** Non-linear predictive models that learn through training and resemble biological neural networks in structure.
- **Decision trees:** Tree-shaped structures that represent sets of decisions. These decisions generate rules for the classification of a dataset. Specific decision tree methods include Classification and Regression Trees (CART) and Chi Square Automatic Interaction Detection (CHAID).
- **Genetic algorithms:** Optimization techniques that use process such as genetic combination, mutation, and natural selection in a design based on the concepts of evolution.
- **Nearest neighbour method:** A technique that classifies each record in a dataset based on a combination of the classes of the k record(s) most similar to it in a historical dataset (where $k \geq 1$). Sometimes called the k -nearest neighbour technique.
- **Rule induction:** The extraction of useful if-then rules from data based on statistical significance.

III. ROOTS OF DATA MINING

A. Statistics

The most important lines is statistics. Without statistics, there would be no data mining, as statistics are the foundation of most technologies on which data mining is built. Statistics embrace concepts such as regression analysis, standard distribution, standard deviation, standard variance, discriminate analysis, cluster analysis, and confidence intervals, all of which are used to study data and data relationships. These are the very building blocks with which more advanced statistical analyses are underpinned. Certainly, within the heart of today's data mining tools and techniques, classical statistical analysis plays a significant role.

B. Artificial Intelligence & Machine Learning

Data mining's second longest family line is artificial intelligence and machine learning. AI is built upon heuristics as opposed to statistics, and attempts to apply human-thought like processing to statistical problems. Because this approach requires vast computer processing power, it was not practical until the early 1980s, when computers began to offer useful power at reasonable prices. AI found a few applications at the very high end scientific/government markets, but the required supercomputers of the era priced AI out of the reach of virtually everyone else. Machine Learning could be considered as an evolution of AI, because it blends AI heuristics with advanced statistical methods. It let computer programs learn about the data they study and then apply learned knowledge to data.

C. Databases

Third family is Databases. Huge amount of data needs to be stored in a repository, and that too needs to be managed. So, comes in light the databases. Earlier data was managed in records and fields, then in various models like hierarchical, network etc. Relational model served the needs of data storage for long while. Other advanced system that emerged is object relational databases. But in data mining, volume of data is too high, so we need specialized servers for it. We call the term as Data Warehousing. Data warehousing also supports OLAP operations to be applied on it, to support decision making.

D. Other Technologies

Apart from these, data mining inculcates various other areas e.g. pattern discovery, visualization, business intelligence etc. The table summarizes the evolution data mining on the grounds of development in databases.

Evolutionary Step	Business Question	Enabling Technologies	Product Providers	Characteristics
Data Collection (1960s)	"What was my total revenue in the last five years?"	Computers, tapes, disks	IBM, CDC	Retrospective, static data delivery
Data Access (1980s)	"What were unit sales in New England last March?"	Relational databases (RDBMS), Structured Query Language (SQL), ODBC	Oracle, Sybase, Informix, IBM, Microsoft	Retrospective, dynamic data delivery at record level
Data Warehousing & Decision Support (1990s)	"What were unit sales in New England last March? Drill down to Boston."	On-line analytic processing (OLAP), multidimensional databases, data warehouses	Pilot, Comshare, Arbor, Cognos, Microstrategy	Retrospective, dynamic data delivery at multiple levels
Data Mining (Emerging Today)	"What's likely to happen to Boston unit sales next month? Why?"	Advanced algorithms, multiprocessor computers, massive databases	Pilot, Lockheed, IBM, SGI, numerous startups (nascent industry)	Prospective, proactive information delivery

Table 1. Steps in the Evolution of Data Mining.

IV. CURRENT TRENDS AND APPLICATIONS

Data mining is formally defined as the non-trivial process of identifying valid, novel, potentially useful, and ultimately understandable patterns in data [2]. The field of data mining has been growing rapidly due to its broad applicability, achievements and scientific progress, understanding. A number of data mining applications have been successfully implemented in various domains like fraud detection, retail, health care, finance, telecommunication, and risk analysis...etc. are few to name. The ever increasing complexities in various fields and improvements in technology have posed new challenges to data mining; the various challenges include different data formats, data from disparate locations, advances in computation and networking resources, research and scientific fields, ever growing business challenges etc. Advancements in data mining with various integrations and implications of methods and techniques have shaped the present data mining applications to handle the various challenges, the current trends of data mining applications are:

A. Fight against Terrorism

After 9-11 attacks, many countries imposed new laws against fighting terrorism. These laws allow intelligence agencies to effectively fight against terrorist organizations. USA launched Total Information Awareness program with the goal of creating a huge database of that consolidate all the information on population. Similar projects were also launched in European countries and rest of the world. This program faced several problems,

- a. The heterogeneity of database, the target database had to deal with text, audio, image and multimedia data.
- b. Second problem was scalability of algorithms. The execution time increases as size of data (which is huge). For example, 230 cameras were placed in London, to read number plates of vehicles. An estimated 40,000 vehicles pass camera every hour, in this way the camera must recognize 10 vehicles per second, which poses heavy loads on both hardware and software.

B. Bio-informatics and Cure for Diseases

The second most important application trend, deals with mining and interpretation of biological sequences and structures. Data mining tools are rapidly being used in finding genes regarding cure of diseases like Cancer and AIDS .

C. Web and Semantic Web

Web is the hottest trend now, but it is unstructured. Data mining is helping web to be organized, which is called Semantic web. The underlying technology is Resource Description Framework (RDF) which is used to describe resources. FOAF is also a supporting technology, heavily used in Face book and Orkut for tagging. But still there are issues like combining all RDF statements and dealing with erroneous RDF statements. Data mining technologies are serving a lot to make the web, a semantic web.

D. Business Trends

Today's business environment is more dynamic, so businesses must be able to react quicker, must be more profitable, and offer high quality services that ever before. Here, data mining serves as a fundamental technology in enabling customer's transactions more accurately, faster and meaningfully. Data mining techniques of classification, regression, and cluster analysis are used for in current business trends . Almost all of the current business data mining applications are based on the classification and prediction techniques for supporting business decisions, thus creating strong Business Intelligence (BI) system.

APPLICATIONS

As data mining matures, new and increasingly innovative applications for it emerge. Although a wide variety of data mining scenarios can be described. For the purpose of this paper the applications of data mining are divided in the following categories:

- Healthcare
- Finance
- Retail industry
- Telecommunication
- Text Mining & Web Mining
- Higher Education

Healthcare

The past decade has seen an explosive growth in biomedical research, ranging from the development of new pharmaceuticals and in cancer therapies to the identification and study of human genome by discovering large scale sequencing patterns and gene functions. Recent research in DNA analysis has led to the discovery of genetic causes for many diseases and disabilities as well as approaches for disease diagnosis, prevention and treatment.

Finance

Most banks and financial institutions offer a wide variety of banking services (such as checking, saving, and business and individual customer transactions), credit (such as business, mortgage, and automobile loans), and investment services (such as mutual funds). Some also offer insurance services and stock services. Financial data collected in the

banking and financial industry is often relatively complete, reliable and high quality, which facilitates systematic data analysis and data mining. For example it can also help in fraud detection by detecting a group of people who stage accidents to collect on insurance money.

Retail Industry

Retail industry collects huge amount of data on sales, customer shopping history, goods transportation and consumption and service records and so on. The quantity of data collected continues to expand rapidly, especially due to the increasing ease, availability and popularity of the business conducted on web, or e-commerce. Retail industry provides a rich source for data mining. Retail data mining can help identify customer behaviour, discover customer shopping patterns and trends, improve the quality of customer service, achieve better customer retention and satisfaction, enhance goods consumption ratios design more effective goods transportation and distribution policies and reduce the cost of business.

Telecommunication

The telecommunication industry has quickly evolved from offering local and long distance telephone services to provide many other comprehensive communication services including voice, fax, pager, cellular phone, images, e-mail, computer and web data transmission and other data traffic. The integration of telecommunication, computer network, Internet and numerous other means of communication and computing are underway. Moreover, with the deregulation of the telecommunication industry in many countries and the development of new computer and communication technologies, the telecommunication market is rapidly expanding and highly competitive. This creates a great demand from data mining in order to help understand business involved, identify telecommunication patterns, catch fraudulent activities, make better use of resources ,and improve the quality of service.

Text Mining and Web Mining

Text mining is the process of searching large volumes of documents from certain keywords or key phrases. By searching literally thousands of documents various relationships between the documents can be established. Using text mining however, we can easily derive certain patterns in the comments that may help identify a commonest of customer perceptions not captured by the other survey questions. An extension of text mining is web mining. Web mining is an exciting new field that integrates data and text mining within a website. It enhances the web site with intelligent behaviour, such as suggesting related links or recommending new products to the consumer. Web mining is especially exciting because it enables tasks that were previously difficult to implement. They can be configured to monitor and gather data from a wide variety of locations and can analyze the data across one or multiple sites. For example the search engines work on the principle of data mining.

Higher Education

An important challenge that higher education faces today is predicting paths of students and alumni. Which student will enrol in particular course programs? Who will need additional assistance in order to graduate? Meanwhile additional issues, enrolment management and time-to-degree, continue to exert pressure on colleges to search for new and faster solutions. Institutions can better address these students and alumni through the analysis and presentation of data. Data mining has quickly emerged as a highly desirable tool for using current reporting capabilities to uncover and understand hidden patterns in vast databases.

V. Future Trends and Applications

DISTRIBUTED/COLLECTIVE DATA MINING

One area of data mining which is attracting a good amount of attention is that of distributed and collective data mining. Much of the data mining which is being done currently focuses on a database or data warehouse of information which is physically located in one place. However, the situation arises where information may be located in different places, in different physical locations. This is known generally as distributed data mining (DDM). Therefore, the goal is to effectively mine distributed data which is located in heterogeneous sites. Examples of this include biological information located in different databases, data which comes from the databases of two different firms, or analysis of data from different branches of a corporation, the combining of which would be an expensive and time-consuming process.

Distributed data mining (DDM) is used to offer a different approach to traditional approaches analysis, by using a combination of localized data analysis, together with a "global data model. " In more specific terms, this is specified as:- performing local data analysis for generating partial data models, and-combining the local data models from different data sites in order to develop the global model. This global model combines the results of the separate analyses. Often the global model produced, especially if the data in different locations has different features or characteristics, may become incorrect or ambiguous. This problem is especially critical when the data in distributed sites is heterogeneous rather than homogeneous.

UBIQUITOUS DATA MINING (UDM)

The advent of laptops, palmtops, cell phones, and wearable computers is making ubiquitous access to large quantity of data possible. Advanced analysis of data for extracting useful knowledge is the next natural step in the world of ubiquitous computing. Accessing and analyzing data from a ubiquitous computing device offer many challenges. For

example, UDM introduces additional cost due to communication, computation, security, and other factors. So one of the objectives of UDM is to mine data while minimizing the cost of ubiquitous presence.

Human-computer interaction is another challenging aspect of UDM. Visualizing patterns like classifiers, clusters, associations and others, in portable devices are usually difficult. The small display areas offer serious challenges to interactive data mining environments. Data management in a mobile environment is also a challenging issue. Moreover, the sociological and psychological aspects of the integration between data mining technology and our lifestyle are yet to be explored. The key issues to consider include theories of UDM, advanced algorithms for mobile and distributed applications, data management issues, mark-up languages, and other data representation techniques; integration with database applications for mobile environments, architectural issues: (architecture, control, security, and communication issues), specialized mobile devices for UDM, software agents and UDM (Agent based approaches in UDM, agent interaction---cooperation, collaboration, negotiation, organizational behavior), applications of UDM (Application in business, science, engineering, medicine, and other disciplines), location management issues in UDM and technology for web-based applications of UDM.

HYPERTEXT AND HYPERMEDIA DATA MINING

Hypertext and hypermedia data mining can be characterized as mining data which includes text, hyperlinks, text mark-ups, and various other forms of hypermedia information. As such, it is closely related to both web mining, and multimedia mining, which are covered separately in this section, but in reality are quite close in terms of content and applications. While the World Wide Web is substantially composed of hypertext and hypermedia elements, there are other kinds of hypertext/hypermedia data sources which are not found on the web. Examples of these include the information found in online catalogues, digital libraries, online information databases, and the like.. Some of the important data mining techniques used for hypertext and hypermedia data mining include classification (supervised learning), clustering (unsupervised learning), semi-structured learning, and social network analysis.

In the case of classification, or supervised learning, the process starts off by reviewing training data in which items are marked as being part of a certain class or group. This data is the basis from which the algorithm is trained. One application of classification is in the area of web topic directories, which can group similar sounding or spelled terms into appropriate categories, so that searches will not bring up inappropriate sites and pages. The use of classification can also result in searches which are not only based on keywords, but also on category and classification attributes. Methods used for classification include naive Bayes classification, parameter smoothing, dependence modelling, and maximum entropy. Unsupervised learning, or clustering, differs from classification in that classification involved the use of training data, clustering is concerned with the creation of hierarchies of documents based on similarity, and organize the documents based on that hierarchy. Intuitively, this would result in more similar documents being placed on the leaf levels of the hierarchy, with less similar sets of document areas being placed higher up, closer to the root of the tree. Techniques which have been used for unsupervised learning include k-means clustering, agglomerative clustering, random projections, and latent semantic indexing.

Semi-supervised learning and social network analysis are other methods which are important to hypermediabased data mining. Semi-supervised learning is the case where there are both labelled and unlabeled documents, and there is a need to learn from both types of documents. Social network analysis is also applicable because the web is considered a social network, which examines networks formed through collaborative association, whether it be between friends, academics doing research or service on committees, and between papers through references and citations. Graph distances and various aspects of connectivity come into play when working in the area of social networks.

MULTIMEDIA DATA MINING

Multimedia Data Mining is the mining and analysis of various types of data, including images, video, audio, and animation. The idea of mining data which contains different kinds of information is the main objective of multimedia data mining. As multimedia data mining incorporates the areas of text mining, as well as hypertext/hypermedia mining, these fields are closely related. Much of the information describing these other areas also applies to multimedia data mining. This field is also rather new, but holds much promise for the future. Multimedia information, because its nature as a large collection of multimedia objects, must be represented differently from conventional forms of data. One approach is to create a multimedia data cube which can be used to convert multimedia-type data into a form which is suited to analysis using one of the main data mining techniques, but taking into account the unique characteristics of the data. This may include the use of measures and dimensions for texture, shape, colour, and related attributes. In essence, it is possible to create a multidimensional spatial database. Among the types of analyses which can be conducted on multimedia databases include associations, clustering, classification, and similarity search. Another developing area in multimedia data mining is that of audio data mining (mining music). The idea is basically to use audio signals to indicate the patterns of data or to represent the features of data mining results. The basic advantage of audio data mining is that while using a technique such as visual data mining may disclose interesting patterns from observing graphical displays, it does require users to concentrate on watching patterns, which can become monotonous. But when representing it as a stream of audio, it is possible to transform patterns into sound and music and listen top itches, rhythms, tune, and melody in order to identify anything interesting or unusual.

SPATIAL AND GEOGRAPHIC DATA MINING

The data types which come to mind when the term data mining is mentioned involves data as we know it—statistical, generally numerical data of varying kinds. However, it is also important to consider information which is of an entirely different kind—spatial and geographic data which could contain information about astronomical data, natural resources, or even orbiting satellites and spacecraft which transmit images of earth from out in space. Much of this data is image-oriented, and can represent a great deal of information if properly analyzed and mined.

A definition of spatial data mining is as follows: “the extraction of implicit knowledge, spatial relationships, or other patterns not explicitly stored in spatial databases.” Some of the components of spatial data which differentiate it from other kinds include distance and topological information, which can be indexed using multidimensional structures, and required special spatial data access methods, together with spatial knowledge representation and data access methods, along with the ability to handle geometric calculations. Analyzing spatial and geographic data include such tasks as understanding and browsing spatial data, uncovering relationships between spatial data items (and also between non-spatial and spatial items), and also analysis using spatial databases and spatial knowledge bases. The applications of these would be useful in such fields as remote sensing, medical imaging, navigation, and related uses. Some of the techniques and data structures which are used when analyzing spatial and related types of data include the use of spatial warehouses, spatial data cubes and spatial OLAP. Spatial data warehouses can be defined as those which are subject oriented, integrated, nonvolatile, and time-variant. Some of the challenges in constructing a spatial data warehouse include the difficulties of integration of data from heterogeneous sources, and also applying the use of on-line analytical processing which is not only relatively fast, but also offers some forms of flexibility. In general, spatial data cubes, which are components of spatial data warehouses, are designed with three types of dimensions and two types of measures. The three types of dimensions include the noncapital dimension (data which is noncapital in nature), the spatial to noncapital dimension (primitive level is spatial but higher level-generalization is noncapital), and the spatial-to-spatial dimension (both primitive and higher levels are all spatial). In terms of measures, there are both numerical (numbers only), and spatial (pointers to spatial object) measured used in spatial data cubes. A side from the implementation of data warehouses for spatial data, there is also the issue of analyses which can be done on the data. Some of the analyses which can be done include association analysis, clustering methods, and the mining of raster databases. There have been number of studies conducted on spatial data mining.

TIME SERIES/SEQUENCE DATA MINING

Another important area in data mining centres on the mining of time series and sequence-based data. Simply put, this involves the mining of a sequence of data, which can either be referenced by time (time-series, such as stock market and production process data), or is simply a sequence of data which is ordered in a sequence. In general, one aspect of mining time series data focuses on the goal of identifying movements or components which exist within the data (trend analysis). These can include long-term or trend movements, seasonal variations, cyclical variations, and random movements (Han and Kamber, 2001). Other techniques which can be used on these kinds of data include similarity search, sequential pattern mining, and periodicity analysis. *Similarity search* is concerned with the identification of a pattern sequence which is close or similar to a given pattern, and this form of analysis can be broken down into two subtypes: whole sequence matching and subsequence matching. Whole sequence matching attempts to find all sequences which bear a likeness to each other, while subsequence matching attempts to find those patterns which are similar to a specified, given sequence.

Sequential pattern mining has as its focus the identification of sequences which occur frequently in a time series or sequence of data. This is particularly useful in the analysis of customers, where certain buying patterns could be identified, such as what might be the likely follow-up purchase to purchasing a certain electronics item or computer, for example.

Periodicity analysis attempts to analyze the data from the perspective of identifying patterns which repeat or recur in a time series. This form of data mining analysis can be categorized as being full periodic, partial periodic or cyclic periodic. In general, full periodic is the situation where all of the data points in time contribute to the behaviour of the series. This is in contrast to partial periodicity, where only certain points in time contribute to series behaviour.

CONSTRAINT-BASED DATA MINING

Many of the data mining techniques which currently exist are very useful but lack the benefit of any guidance or user control. One method of implementing some form of human involvement into data mining is in the form of constraint-based data mining. This form of data mining incorporates the use of constraints which guides the process. Frequently this is combined with the benefits of multidimensional mining to add greater power to the process. There are several categories of constraints which can be used, each of which has its own characteristics and purpose. These are:

Knowledge-type constraints. This type of constraint specifies the “type of knowledge” which is to be mined, and is typically specified at the beginning of any data mining query. Some of the types of constraints which can be used include clustering, association, and classification.

Data constraints. This constraint identifies the data which is to be used in the specific data mining query. Since constraint-based mining is ideally conducted within the framework of an ad-hoc, query driven system, data constraints can be specified in a form similar to that of a SQL query.

Dimension/level constraints. Because much of the information being mined is in the form of a database or multidimensional data warehouse, it is possible to specify constraints which specify the levels or dimensions to be included in the current query.

Interestingness constraints. It would also be useful to determine what ranges of a particular variable or measures are considered to be particularly interesting and should be included in the query.

Rule constraints. It is also important to specify the specific rules which should be applied and used for a particular data mining query or application. One application of the constraint-based approach is in the Online Analytical Mining Architecture (OLAM) developed by Han, Lakshamanan, and Ng, 1999, and is designed to support the multidimensional and constraint based mining of databases and data warehouses.

PHENOMENAL DATA MINING

Phenomenal data mining is not a term for a data mining project that went extremely well. Instead, it focuses on the relationships between data and the phenomena which are inferred from the data. One example of this is that using receipts from cash supermarket purchases, it is possible to identify various aspects of the customers who are making these purchases. Some of these phenomena could include age, income, ethnicity, and purchasing habits. One aspect of phenomenal data mining, and in particular the goal to infer phenomena from data, is the need to have access to some facts about the relations between these data and their related phenomena. These could be included the program which examines data for phenomena, or also could be placed in a kind of knowledge base or database which can be drawn upon when doing the data mining. Part of the challenge in creating such a knowledge base involves the coding of common sense into a database, which has proved to be a difficult problem so far.

VI. Conclusions

In this paper I briefly reviewed the various data mining trends and applications from its inception to the future. This review puts focus on the hot and promising areas of data mining. Though very few areas are named here in this paper, yet they are those which are commonly forgotten. This paper provides a new perspective of a researcher regarding applications of data mining in social welfare.

References

- [1] Heikki, Mannila, "Data mining: machine learning, statistics, and databases", Statistics and Scientific Data Management, pp. 2-9. 1996.
- [2] Knowledge Discovery in Databases, AAAI Press / the MIT Press, Massachusetts Institute of Technology. ISBN 0-26256097-6. MIT 1996.
- [3] Chakrabarti, van den Berg, and Dom. "Distributed Hypertext Resource Discovery through Examples, "Proceedings of the 25th VLDB (International Conference on Very Large Data Bases), Edinburgh Scotland, 1999.
- [4] Han, J. and M. Kamber, Data Mining: Concepts and Techniques, Morgan Kaufmann, 2001.
- [5] Han, J., M. Kamber, and A. K. H. Tung, "Spatial Clustering Methods in Data Mining: A Survey", H. Miller and J. Han (eds.), Geographic Data Mining and Knowledge Discovery, Taylor and Francis, 2001.
- [6] Miller and J. Han (eds.), Geographic Data Mining and Knowledge Discovery, Taylor and Francis, 2001.
- [7] Kotsiantis, S., Kanellopoulos, D., Pintelas, P., "Multimedia mining", SEAS Transactions on Systems, No 3, s. 3263-3268, 2005.
- [8] Huysmans, Baesens, Martens, Denys and Vanthienen, "New Trends in Data Mining", Tijdschrift voor Economie en Management, vol. L, 4, 2005.
- [9] Olfa Nasraoui and Maha Soliman, "Market-Based Profile Infrastructure: Giving Back to the User", Next Generation of Data Mining, Taylor and Francis, 2008.
- [10] Salmin, Sultana et al., "Ubiquitous Secretary: A Ubiquitous Computing Application Based on Web Services Architecture", International Journal of Multimedia and Ubiquitous Engineering Vol. 4, No. 4, October, 2009.
- [11] Jing He, "Advances in Data Mining: History and Future", Third international Symposium on Information Technology Application, 978-0-7695-3859-4/09 IEEE 2009 DOI 10.1109/IITA.2009.204.
- [12] M.S. Chen, J. Han, and P.S. Yu. "Data mining: An overview from database perspective", IEEE Transactions on Knowledge and Data Eng., 8(6):866-883, December 1999
- [13] Venkatadari M., Dr. Lokanataha C. Reddy, "A Review on Data Mining From Past to Future", International Journal of Computer Applications, pp.19-22, vol. 15, No. 7, Feb 2011.

Analysis of R.C Deep Beam by Finite Element Method

B.R. Niranjan,¹ S.S.Patil²

¹ Professor, Civil Engineering Department, U.V.C.E. Bangalore University Bangalore. India.)

² Associate Professor, Civil Engineering Department, Walchand Institute of Technology. Solapur India

ABSTRACT : The analytical study of reinforced concrete simply supported deep beams subjected to two point loads was carried out using finite element method to study the behavior of deep beam by considering flexural stress, flexural strain, and shear stress variations at different sections for various effective lengths to depth ratio and compared with Euler-Bernoulli Theory. The effective span to depth ratios of the beams considered were 1.25, 1.375 and 1.5

Keywords: Finite Element Method (FEM), Reinforced Concrete (R.C) deep beam, Shear strength.

I. INTRODUCTION

The use of Reinforced deep beam has become more prevalent in recent years. In IS-456 (2000) clause 29, a simply supported beam is classified as deep when the ratio of its effective span L to overall depth D is less than 2. Continuous beam are consider as deep when the ratio L/D is less than 2.5. The effective span is defined as the center to center distance between the supports or 1.15 times the clear span whichever is less.

Deep beam often appear in form of transfer girders in high-rise building as well as pile caps, foundation walls, water tanks, bins, folded plate roof structures, floor diaphragms, shear walls & brackets or corbels. They are characterized as being relatively short & deep, having thickness that is small relative to their span or depth and being primarily loaded in the plane of the member. They are “two dimensional” members in a state of plane stress in which shear is dominant feature. The internal stresses cannot be determined by ordinary beam theory & ordinary design procedures for determining strength do not apply.

The behavior of deep beams is significantly different from that of beams of more normal proportions, requiring special consideration in analysis, design and detailing of reinforcement. A deep beam is in fact a vertical plate subjected to loading in its own plane. The strain or stress distribution across the depth is no longer a straight line, and the variation is mainly dependent on the aspect ratio of the beam.

Stresses in deep beams can be studied using the methods of two dimensional elasticity or Finite Element analysis. Plane sections before bending remaining plane after bending does not hold good for deep beams. Significantly warping of the cross-sections occurs because of high shear stresses consequently flexural stresses are not linearly distributed, even in the elastic range, and the usual methods for calculating section properties and stresses cannot be applied. Shear strength of deep beams may be as much as 2 to 3 times greater than that predicated using conventional equations developed for members of normal proportions.

The stresses in isotropic homogeneous deep beams before cracking can be determined using finite element analysis or photo elastic model studies. It is found that the smaller the span/depth ratio (i.e., less than 2.5), the more pronounced the deviation of the stress pattern from that of Bernoulli and Navier.

II. OBJECTIVES OF STUDIE

- To analyze the deep beam by using Finite Element Method. The finite element model consists of subdividing the Deep beam into small 2D rectangular elements. Each element has four noded plane stress Element to study the behavior of deep beam through flexural stresses, flexural strains, and shear stresses variation with various L/D Ratio.
- To compare the flexural steel requirement as per codal provisions with that calculated using the finite element method.

III. ANALYTICAL STUDY OF DEEP BEAMS

A deep beam having following data is analyzed for various L/D ratios. Beam is simply supported subjected to two points loading as shown in Figure 1.

Depth = 400 mm and Width of beam = 150 mm (constant for all cases);

L/D ratios is varied from 1.25, 1.375, 1.5 i.e. (Span = 500, 550, 600) mm

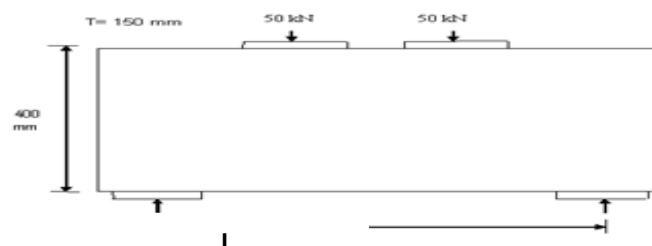


Fig. 1 Deep beam with two point loads

Deep beam is an example of plane stress conditions. It is assumed that no stress component varies across the thickness. The state of stress is then specified by σ_x, σ_y and τ_{xy} only.

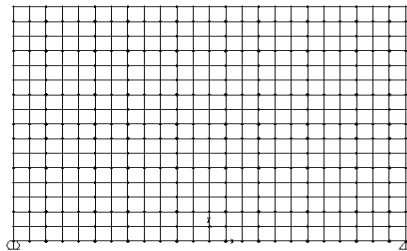


Fig.2a-Deep beam subdivided into rectangular element

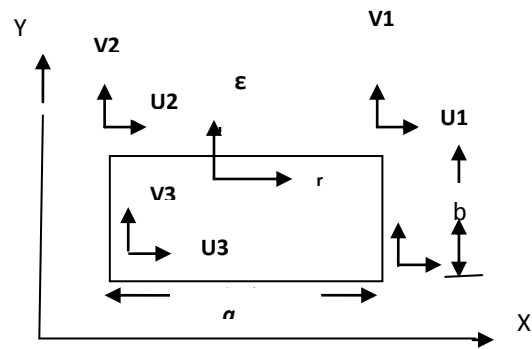


Fig.2b-Typical rectangular finite Element

Fig 2a shows Deep Beam which has been subdivided into small rectangular finite element for analysis purpose. The selection of mesh size for element depend on accuracy desired, the finer the mesh, the better the result but at the same time the larger the computation required. Rectangular elements are found to be very convenient due to simplicity in formulation,

The accuracy of FEM depends on the determination of stiffness matrix of Rectangular element. The two dimensional four noded Rectangular element is as shown in fig.2b. It has four nodes located at the corners and has two translational degrees of freedom at each node, displacement component in X and Y directions with constant σ_x, σ_y and τ_{xy} .

The analysis of Deep Beam is carried out with the Finite Element Method by using the SAP (Structural Analysis program me) software. The variation of flexural stresses, strains at mid span and shear stresses near support is valued for all these cases.

➤ (a) Variation of flexural strain

Fig.3a to Fig. 3c show that the flexural strain at mid span of simply supported deep beam for different span –to–depth ratios. The beams have disturbed region in flexural strain distribution. Deep beams behave differently from shallow beams. In these members, the distribution of strain across the depth of the cross section is nonlinear and a significant amount of load is carried to the supports by a compression strut joining the load and the reaction. It is found that the smaller the span/depth ratio (i.e., less than 2.0), the more pronounced the deviation of the strain pattern from that of Euler Bernoulli theory.

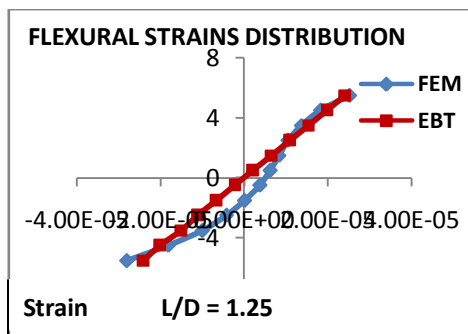


Fig. 3a Flexural Strain Distribution

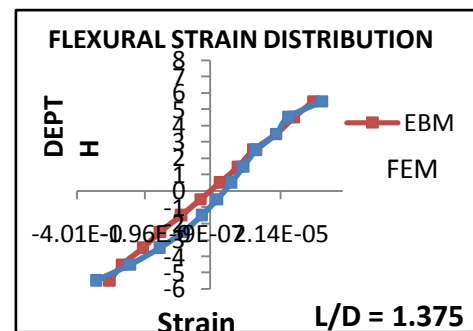


Fig. 3b Flexural Strain Distribution

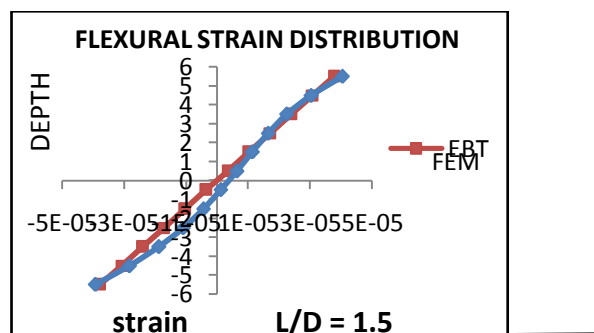


Fig.3c Flexural Strain Distribution

(b) Variation of flexural stress

Fig. 4a to Fig. 4c shows the flexural stress at mid span of simply supported deep beam for two different shear span-to-depth ratios. The compressive stresses increase rapidly at the top and neutral axis moves towards soffit of the beam. From the variation of flexural stress graphs the definition of simply supported deep beam as per IS 456:2000 i.e. when L/D ratio is less than or equal to 2.0 is reasonably accurate.

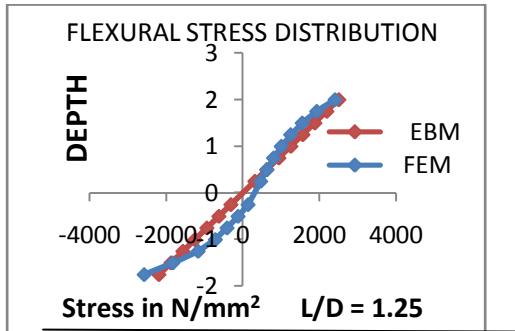


Fig.4a Flexural Stress Distribution

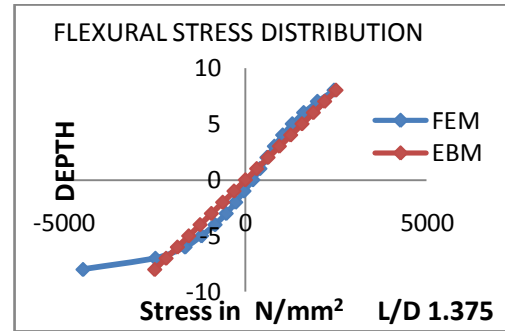


Fig.4b Flexural Stress Distribution

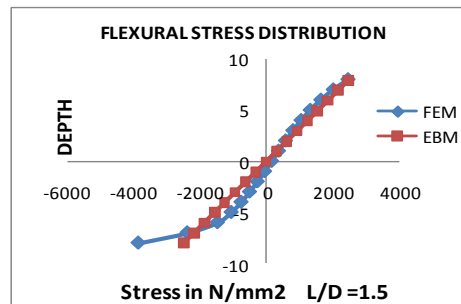


Fig.4c Flexural Stress Distribution

(c) Variation of shear stress

Fig.5a to Fig.5c shows the shear stress near support of simply supported deep beam for different shear span to depth ratios. The beams have drastic change in shear stress distribution. Deep beams behave differently from shallow beams. The shear stress patterns have also changed in case of deep beam. It is found that the smaller the span/depth ratio (i.e., less than 2.0), the more pronounced the deviation of the shear stress distribution from that of Euler Bernoulli theory

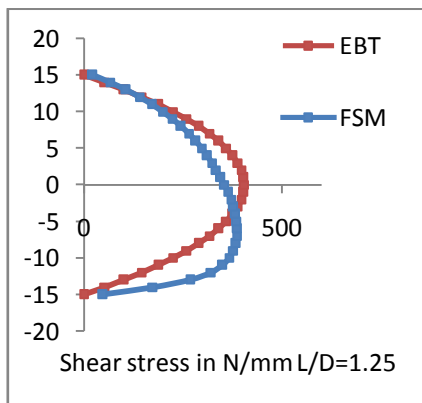


Fig.5a Shear Stress Distribution

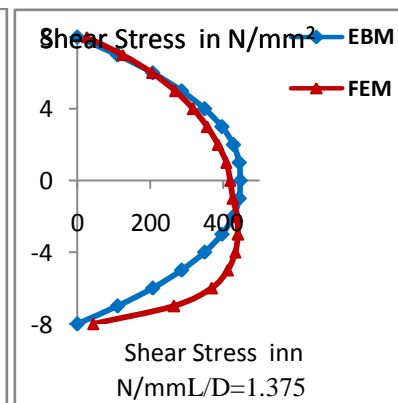


Fig.5b Shear Stress Distribution

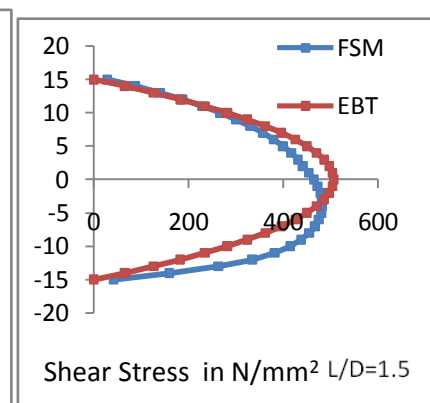


Fig. 5c Shear Stress Distribution

From the variation of shear stress graph it is clear that shear effect is predominant in beams having L/D ratio less than or equal to 2.0 which may lead to warping of the section.

The reinforcement required as per Finite Element Method based on flexural stress distribution graphs for various L/D ratios was presented in table1.

Table1. Reinforcement required as per FEM

Sr.No.	Depth from Center of Beam (mm)	Reinforcement required mm2		
	L / D Ratio	1.50	1.375	1.25
	200	39.23	46.56	56.73

	175	23.57	25.79	26.70
	150	15.59	17.24	18.97
	125	11.65	12.56	12.05
	100	6.39	8.692	7.36
	75	3.923	5.493	4.2
	50	1.987	2.77	1.205
	25	0.123	0.398	1.5
Total		102.45	119.503	128.75

TABLE 2: AREA OF FLEXURAL STEEL REQUIRED

Case No.	Case 1a	Case 1b	Case 2a	Case 2b	Case 3a	Case 3b
Design Method	I.S.456	ACI 318	I.S.456	ACI318	I.S.456	ACI318
Span L (mm)	500	500	550	550	600	600
Span to depth (L/D) ratio	1.25	1.25	1.375	1.375	1.50	1.50
Z (Lever Arm)	280	333	270	333	260	333
Flexure steel Required in mm ²	149.37	179.42	154.89	179.42	160.85	179.42
Flexural steel required in mm ²	102.45	102.45	119.5	119.5	128.72	128.72

IV. CONCLUSION

- Flexural stress and strain variation graphs indicate that the definition of simply supported deep beam as per IS 456:2000 i.e. when L/D ratio is less than or equal to 2.0 is reasonably accurate.
- With Finite element analysis, Flexural strain and stress of deep beams is not linear is confirmed.
- Shear effect is predominant in beams having L/D ratio less than or equal to 2.0 which may lead to warping of the section.
- The flexural steel requirements inversely proportionally to the Effective span to Depth Ratio of deep beam.
- The flexural steel required by finite element method is approximately 21 % less than I.S.456 and A.C.I.318.

REFERENCES

Journal Papers

- [1] Mohammed Reza Salamy, Hiroshi Kobayashi and Shigeki Unjoh, Experimental and Analytical Study on Deep Beams.
- [2] R.S. Londhe(2010-11), Experimental studies in RC Transfer(Deep) Beam for High rise building', The structural Engg. Vol.37No.5, pp.305-312
- [3] Mr. Varghese and Mr. Krishnamoorthy, (1966), Strength and Behaviour of Deep Reinforced Concrete Beams, Indian Concrete Journal, 104-108.

Books

- [4] N. Krishna Raju. Advanced reinforced concrete design, CBS Publications.
- [5] C. S. Krishnamoorthy(1995), 'The finite Element Analysis' Tata McGraw-Hill Education, 1995.
- [6] F. K. Kong. 'Reinforced Concrete Deep Beam', Van Nostrand Reinhold, New York.

Standard Codes

- [7] 'Indian Standard Code of Practice Plain and Reinforced Concrete' IS 456:2000-. Bureau of Indian Standards, Manak Bhavan, New Delhi, India.
- [8] ACI 318-05. 'Building Code Requirements for Structural Concrete and Commentary' American Concrete Institute, Detroit, USA.

Significance Assessment of Architectural Heritage Monuments in Old-Goa

B. Shankar,¹ Shaikh Ali Ahmed²

¹Associate Professor, Institute of Development Studies, University of Mysore, Mysore

²Planning Assistant, North Goa Planning and Development Authority, Panaji

Abstract: Old-Goa has been declared as a World Heritage site in 1986 for its rich culture, built heritage and includes many magnificent churches, monuments and temples. Most of these churches are world famous and constructed way back in the 16th century and are the best examples of Manueline and Gothic architecture. These churches have very intricate detailing and ornamentation reflecting the past and playing an important role in shaping the community to know about the ancient culture, way of life, architecture, level of development, building techniques, and use of material, art and other aspects of the society of a particular period. The rich heritage structures are on the verge of deterioration and alarms for effective management. The surrounding areas are getting developed in a non harmonious manner without any due respect to the fine existing architecture. The detracting and non-contributory buildings will deface the heritage area losing its identity due to non harmonious approach by the agencies and people. These heritage monuments and areas are to be made their significance assessment for undertaking the conservation and preservation. The paper deals with the significant assessment of the heritage monuments in the heritage area of Old Goa.

Keywords: Architectural Significance, Heritage, Conservation, Renaissance, Baroque.

I. Background of Goa

Old-Goa was founded in the 15th century as a port on the banks of river Mandovi by the rulers of Bijapur Sultanate and was the second capital of Bijapur under the rule of Adil Shah. The city was surrounded by a moat and contained the Shah's Palace, mosques and temples. The city was captured by the Portuguese in 1510 from the ruler of Bijapur. Old-Goa was thus a Portuguese colony and a principal city of Eastern Empire. Ruled by Portuguese ruler for almost four centuries, it has a number of Churches and convents which are date back to 16th Century and are the best examples of Manueline and Gothic architecture with intricate detailing and ornamentation.

The Monuments of Old-Goa are the blend of Hindu, Mughal and Portuguese styles of Architecture. Several churches and convents are constructed from 15th to 17th century A.D. These are constructed with laterite stones and lime plaster which displays the fusion of Renaissance and Baroque styles. These monuments include Se Cathedral, Basilica of Bom Jesus, Chapel of St. Catherine, Convent and Church of St. Francis Assissi and many others which are considered as the Architectural Heritage and come under the UNESCO World Heritage site.

II. Monuments in Old-Goa

There are about fifty heritage sites and monuments in the Heritage areas of Old-Goa. Few of these are identified and managed by the ASI and State Archaeology. Remaining is managed by the local authorities. The UNESCO has declared seven monuments as world heritage monuments and sites namely: (1) Chapel of St. Catherine, (2) Church of St. Francis of Assisi, (3) Church of Our Lady of the Rosary, (4) Basilica of Bom Jesus (5) Se- Cathedral, (6) Church of St. Cajetan and (7) Church and Convent of St. Augustine in the year 1986. There are many more structures of high significance needs identification, conservation, and management.

III. Styles of Architecture and Idioms of Neo-Roman

Till 11th Century Islamic style of Architecture prevailed in parts of Goa. Post 15th century the style extended and encompassed all the continents of globe, a style that recovered the glory of imperial Rome and identified as Neo-Roman. Idioms of Neo-Roman have five orders of architecture i.e. Doric, Tuscan, Ionic, Corinthian and Composite. An order is a unit consisting of a fixed sequence of structural and decorative elements, interrelated by a distinctive proportion.

Except for the *Doric*, each order is tripartite, formed of pedestal, column and entablature. The pedestal is composed of base, die and cap; column is of base, shaft and capital; and the entablature of architrave, frieze and cornice.

Above the cornice there may be an attic or pediment. The orders most used in Neo-Roman Goa are the Tuscan and the Corinthian, which is described as follows:

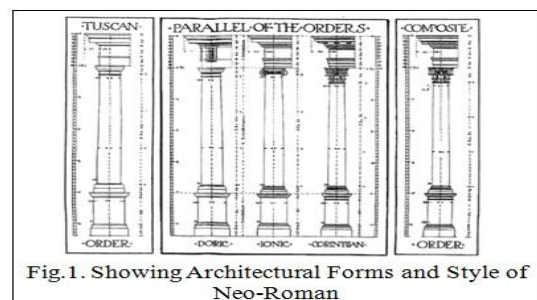


Fig.1. Showing Architectural Forms and Style of Neo-Roman

The Tuscan is an Italian order; its column has a simple base and is unfluted, while both capital and entablature are without adornments. The capital has a miniature torus (large convex moulding, also known as an astragal), a necking that is a short continuation of the shaft, and an echinus (or quarter circle moulding), with a fillet above carrying a square abacus.

The Corinthian was invented by the Greeks and completed by the Romans. Its column has base, shaft and capital. The capital intricately combines volutes and

acanthus leaves. The shaft is fluted, the flutes sometimes partly filled with cables. The entablature is elaborate; its cornice, in addition to dentils, displays small brackets or consoles (also known as modillions), supporting its upper projecting fascia, itself often topped by a cyma recta moulding.

Typically Baroque is common in Goa is the salomonic column, a variant of the Corinthian and Composite. It has base, shaft and capital; its shaft is spiralled, with broad coils of rounded edges. Convex projections curve into concave hollows (channels). The shaft is divisible into zones, some unscrolled and some scrolled.

One variety of the Gothic is the Manueline, which arose during the reign of the Portuguese King Joao II, but is named after his son under whose rule it flourished, Manuel I. The style persisted in Portugal till the mid-16th century and in Portuguese India till that century's end. One of its architects was Tomas Fernandes, who was in Goa from around 1505 to 1516, where the church was build in 1512 (Nossa Senhora da Serra, demolished).

IV. Monuments and Styles of Architecture

The Portuguese induced the western culture in Goa through their monuments during their four hundred years long imperial rule. Several monuments of Old-Goa like churches and convents are constructed during the period of 15th and 17th century A.D. These structures are constructed of laterite stones and lime plastered which displays the affluent Architectural fusion of Renaissance and Baroque styles. These monuments include Se Cathedral, Basilica of Bom Jesus, Chapel of St. Catherine, Convent and Church of St. Francis Assisi and many others which are considered as the Architectural Heritage and have been declared by UNESCO in 1986 as World Heritage site. Below are the few of the monuments showing the style of architecture in which order these are constructed



Fig. 2. Convent and Church of St. Francis Assisi



Fig. 3. Interiors of Church of St. Francis Assisi

The Church was built on the same spot in 1661 by retaining only the existence of the earlier church. Built with laterite blocks and lime plastered. The exteriors of the church are Tuscan order while the main entrance is in Manueline style. The main Altar is in Baroque with Corinthian features.



Fig. 5. Interiors of Church of St. Cajetan



Fig. 4. Church of St. Cajetan



Fig. 6. Convent of St. Cajetan

The Church of St. Cajetan was built with laterite blocks and lime plastered. Italian monks of the theatines order built this diminutive dome church on the lines of the Roman Basilica. It has Italian renaissance in baroque and external with Corinthian style.



Fig. 7. Interiors of Se Cathedral



Fig. 8. Church of Se Cathedral

The Church of Se Cathedral was built with mud and straws in 1514 with three naves at the site of battle giving thanks to God and owes the success of the battle to St. Catherine. Built on raised laterite structure, covered with lime plaster and Mixture of Tuscan and Doric style with Corinthian columns.



Fig. 9. Church of Basilica of Bom Jesus

Built with laterite, its exterior excluding the façade is without plaster, tiled roof and cruciform on plan. It has elements of five schools of Architecture, Roman, Ionic, Doric, Corinthian, and Composite style, built in Renaissance and baroque style.



Fig.10. Casket of Mortal Remains of St. Francis Xavier in the Church of Basilica of Bom Jesus

V. Need for Significance Assessment

The 'cultural significance' defined as 'aesthetic, historic, scientific and social value for past, present and future generations'. Significance is thus an expression of the cultural value afforded a place, site or item. Understanding the significance of an historic building complex or area (the 'asset') and the possible impact of the proposed scheme on this significance is the key to good conservation practice.

Monuments of different styles are scattered all over the heritage conservation area of Old-Goa. As per the Regional Plan, the Conservation area admeasures 801 hectares and contains a number of heritage monuments and sites of high architectural significance. The styles of architecture like, Romanesque, Gothic and Neo-Roman are originated by the Greeks, where the roof is covered exclusively by lintels. Some of these vestiges are found in Kerala. Gothic was flourished in Goa during the tenure of Portuguese rule as variety of Manueline.

Corinthian and Tuscan are the two varieties of architectural styles of high significance are rarely seen in the entire country. The styles of high architectural significance are getting vanished due to non comprehensive approach in protecting it. These architectural styles are rarely available in the globe and fortunately the part of the built heritage in Old-Goa needs to be identified, assessed its significance for protection and management these monuments to future generations.

VI. Criteria for Assessment of Architectural Significance

Architectural assessment is conceded based on the style of architecture used in construction of the monuments like, Doric Corinthian, Tuscan, Ionic and Composite styles. These orders of architecture of high significance value are seen very rarely all over the globe. Harold Kalman's Criteria for evaluation and assessment of Heritage monuments is an accepted criterion all over the world and is to be adopted in assessing the architectural significance of high importance in Old-Goa. Table below shows the criteria used for assessment.

Table 1: Criteria Used for Assessment

Date of construction and grading			
Excellent	Good	Fair	Poor
1500 to 1599	1600 to 1799	1800 to 1950	1951 and later
10	08	06	04

Architectural significance		
Indicators	Grading	Score
1. Architectural Design	Out standing	10
2. Architectural Style	Very good	06
3. Architectural Condition	Good	04
4. Architectural Elements		
5. Year of construction		

Evaluation of structures was conceded by incorporating proper indicators and the year of construction and proper ranking was done.

A) The date of construction plays an important role in measuring the heritage structure. The three indicators are used to assess for grading, namely (a) year of construction, (b) technology used for construction, and (c) present status of the structure. These indicators were applied to measure the heritage structures and grading. The scores are given after assessing the monuments and added to get the total score. The monuments are ranked based on the scores.

B) Architectural significance assessment was conceded as per the indicators mentioned in the (Architectural significance) table above. The significance grading and scoring are given based on their indicators and the details are depicted in the following table:

Name of the Monument	Architectural Significance				Year of construction			Total Score	Ranking
	Architectural Style	Architectural Design	Architectural Condition	Architectural Elements	Year of construction	Technology used	Present status		
Basilica of Bom Jesus	Roman, Ionic, Doric, Corinthian, and Composite style (10)	10	10	As per the style of Fig. 1 (10)	Built in 1585 and rebuilt in 1783 (8)	Carved laterite exposed stone masonry and lime plastered (10)	Very good condition (under the control of ASI) (10)	68	I
Se-Cathedral	Mixture of Tuscan and Doric style with Corinthian columns (8)	10	10	As per the style of Fig. 1 (10)	Built in 1631 (8)	Built on raised Carved laterite stone masonry and lime plastered (8)	Very good condition (under the control of ASI) (10)	58	II
Church of St. Cajetan	Italian renaissance in baroque and external with Corinthian style (6)	6	6	As per the style of Fig. 1 (10)	Built in 1661 (8)	Built with laterite blocks and lime plastered (8)	Very good condition (under the control of ASI) (10)	50	III

Basilica of Bom Jesus topped the rank followed by Se-Cathedral and Church of St. Cajetan and their individual total score are 68, 58 and 50 in the order of ranking respectively.

VII. Conclusion

The assessment of architectural significance of Monuments in Old-Goa includes Tuscan, Doric, Ionic, Corinthian, Composite and Manueline which are rare of its kind, seldom seen all over the globe. The historical monuments are treasures of architectural heritage and effort needs to be made to protect them through appropriate policies, laws, guidelines and regulations. As the buildings and monuments have their own life cycle and grow old with the ageing of their components and materials. Therefore, a systematic effort needs to be made for significance assessment of heritage monuments to ensure continuous and careful maintenance of the monuments and manage them without disturbing the original character otherwise there is likelihood of their damage. Although a lot has been

done to preserve the heritage of our built environment, a great deal more is required to be done in terms of developing the awareness among the people about the incredible architectural features of the monument which needs to be transferred to our future generation in terms of sustainable development.

References

- [1]. Shaikh Ali Ahmed and Shankar B., "Challenges of Planning for Heritage Areas in Panaji City", International Journal of Modern Engineering Research ,Vol.2, Issue.1, Jan-Feb 2012 pp-446-450
- [2]. Shaikh Ali Ahmed and Shankar B., "Conservation of Heritage Areas in the City of Panaji: A Case Study of Fontainhas Area", International Journal of Modern Engineering Research, Vol.2, Issue.2, Mar-Apr 2012 pp-442-446.
- [3]. Shaikh Ali Ahmed and Shankar B, "Planning for Conservation of Heritage Areas in Old Goa: Issues and Strategies", IDES_CPS, Civil Engineering Series-

- Advances in Civil Engineering ACE, Ed., pp-11-15, 2011, New York.
- [4]. Shaikh Ali Ahmed and Shankar B, "Municipal Solid Waste in Heritage Conservation Areas- A Case Study of Panaji", 1st Edn. Vol. 1 and Vol.2, Sustainable Waste Management- Municipal, Industrial and Agricultural, by Sadhan K. Ghosh et al, Oxford Publishing House , Kolkataka (ISBN 81-86862-46-3 & ISBN 81-86862-74-1, July 2012, pp-59-63 Mysore.
 - [5]. Hali, Prasanth(2006), Conservation of Heritage - The Kerala Experience, Institute of Town Planners India Journal, Vol.3 No.4 pp-55-60, New Delhi.
 - [6]. The Government of Goa, "Regional Plan of Goa 2021" Town & Country Planning Department, 2009.
 - [7]. Government of India, "The Ancient Monuments and Archaeological Sites and Remains Act" No. 24, 1958.
 - [8]. The Goa Ancient Monuments and Archaeological Sites and Remains Act, 1978 and Rules, 1980.
 - [9]. Government of Goa, "The Goa Town and Country Planning Act and Rules, 2000
 - [10]. Government of Goa, "Planning and Development Authority (Development Plan), Regulations", Panjim Planning and Development Authority, 1989, Panjim.
 - [11]. Government of Goa, "Tourism Master Plan: GOA-2011 Final Report" Consulting Engg. Services (I) Ltd., Department of Tourism.
 - [12]. Jain. A.K. (2008), Book Review of "Heritage and Environment: An Indian Diary" by Shyam Chainani, Journal of the Development and Research Organisation for Nature, Arts and Heritage, Vol5, Issue1, pp-187-188.
 - [13]. Armitage Lynne, and Yau, Yung (2003) Heritage Protection in the Built Environment in Hong Kong and Queensland, A Cross Cultural Comparison, in Australia and Hong Kong respectively.
 - [14]. Belind Yuen, on Strengthening Urban Heritage in Singapore: Building Economic Competitiveness and Civic Identity, Global Urban Development Magazine.
 - [15]. Built Heritage Policies of Winchester, (2006) Government of U.K.
 - [16]. Cork City Development Plan (Draft) (2009) 2015 Vol. 1, Written Statement, Built Heritage and Archaeology.
 - [17]. Culture and Tourism and Heritage, (2005) Core strategy Brighton and Hove.
 - [18]. City of Sydney Heritage Development Control Plan, (2006) prepared by City of Sydney, Architecture Sydney Pvt. Ltd.
 - [19]. Conservation of Buildings and Sites of Historical and Aesthetic importance,(1986) Government of Goa.
 - [20]. Government of U.K, East Hertz Local Plan (2005)
 - [21]. Fr. Moreno de Souza, S.J. (2000) A short History of the old City of Goa.
 - [22]. Shankar B. and Uma S., "Conservation Strategies for Srirangapatna Town: Evaluation of Heritage Buildings", International Journal of Modern Engineering Research, Vol.2, Issue.2, Mar-Apr 2012 pp-160-164.

BIOGRAPHIES



B. Shankar received the B.E. degree in Civil Engineering in 1984, M.U.R.P degree in Urban and Regional Planning in 1989 and Ph.D. degree in Urban and Regional Planning in 1997 from the University of Mysore, Mysore. He is working as Associate Professor in Urban and Regional Planning at the Institute of Development Studies, University of Mysore, Mysore. His research interests to include Urban Planning, Community Development, Heritage Conservation, and Planning Legislation.



Shaikh Ali Ahmed received M.Tech in Urban and Regional Planning from the University of Mysore, Mysore. He is working as Planning Assistant in North Goa Planning and Development Authority, Panaji. Presently, he is pursuing his Doctoral degree in the University of Mysore, Mysore. His research interests to include heritage conservation and heritage legislation.

Estimation of Manufacturing Costs in the Early Stages of Product Development Project

Esa Hietikko

Mechanical Engineering Department, Savonia University of Applied Sciences, Finland

ABSTRACT : *One of the crucial factors in increase of productivity of supply chains is the management of production costs. Since the number of methods and tools used to estimate the production costs in product development phase is limited, the designers often estimate the costs based on their experience. The designers can mainly affect the direct costs of a product, including material, labor and purchased parts. Direct costs vary greatly depending on the number of produced units. Indirect costs include for example the work in process, storage and internal transportations. The developed software prototype is based on the Lucas method. It will take a simple and ideal part, whose costs are known and then use factors to produce the final costs. The application calculates sophisticated estimates about how much it would cost to produce a single part. The developed software seems to work surprisingly well. It may not tell the final truth about the component costs but can be used to open the eyes of the designer when the costs of the component under design are growing too high. It can also be used to find the most suitable manufacturing method and when considering the make or buy decisions.*

Keywords: *Cost estimation, Manufacturing costs, Product Development*

I. INTRODUCTION

The strength and basis of competitiveness of the technology industry in many European countries will be a flexible, rapid and cost effective mass customized small batch production. The effective performance of supply chains has also a strong connection with the competitiveness. The know-how of modern solutions and new innovations in products and production as well as the agility of production are important aspects in the future.

One of the most crucial factors in the productivity increase of supply chains is the management of production costs. Since the number of methods and tools used to estimate production costs in product development phase is very limited, the designers often estimate the costs based on their experience. They have tacit knowledge of manufacturing feedback, work community and general design rules. However, when manufacturing is more often performed in the supply chains, the information flow from manufacturing to design is limited.

It is well known fact that 70–80 % of the product life cycle costs are defined at the product development stage. An experienced designer can estimate the costs of different alternatives quite reliably. However, for example big assemblies or machining large welded constructions (tolerances, fixtures etc.) may cause difficulties. Experience may also be a negative factor. Designers are not often easily willing to give up traditional manufacturing methods and modern and more effective methods are not considered.

The only accurate way to define the manufacturing costs is to calculate them afterwards. In many cases, however, the calculation methods are used by the accountants, who use generalizations and don't have engineering education or experience. These calculations are also performed when the product is ready and nothing can be done to reduce the costs.

The vision of the research presented in this paper is to find a simple and easy tool to be used to estimate the life cycle costs of a component in the early stages of product development process. This paper presents a cost estimate model based on so called Lucas-method and evaluates it preliminary by comparing the cost results with some values of literature and other cost estimate tools.

II. UNDERSTANDING THE MANUFACTURING COSTS

The ultimate goal of a company is to produce profit. Selling price is defined by markets so it is not easily changed by company actions. The only efficient way to increase profit is manufacturing cost reduction.

The costs can be lumped into two categories: direct and indirect costs. Direct costs can be traced to a specific component and are then potential target for cost reduction in product development phase. A major part of direct costs are based on material used to build the component. A good estimate for material costs of a large volume production would be about 50 % of total costs. For smaller lots it may be as low as 10 % of total costs. This includes the material of the final product but also the waste. The components that are purchased outside the company are also included in direct costs. Direct labor costs include the salaries and other expenses of the work force needed to manufacture and assemble the product. Also tooling costs can be seen to be direct costs. It is also good to remember the familiar 20/80 principle: 80% of costs are generated by 20 % of parts.

Indirect costs include for example work in process, storage and internal transportations. Work in process (WIP) inventory takes floor space and demands internal transportations. There may be thousands of work pieces in WIP inventories. Other types of inventories may be for raw materials and finished products. The common rule of thumb for estimating the costs of inventories is 25 % of the inventory value per year. If the value of inventories is for instant 1 million Euros, then the cost of it will be 250.000 Euros every year. Product development does not have much influence to these costs, but it is good to keep them in mind anyway.

Lot size has a significant meaning in production costs of a single component. The smaller the lot size, the higher are the costs per one piece of the product. This is mainly depending on the setup costs. Setup consists of those actions used to change the manufactured part, tools, programs, manufacturing instructions and fixtures and preparations for the part waiting to be manufactured. Fixed costs will also grow when the lot size is growing.

In order to reduce the manufacturing costs both the manufacturing and design must be developed. Fig. 1 is an example of how design and manufacturing affect the cost of a manufactured component [1]. Average part cost is considered as 100 % (or for example 100 Euros). If it is possible to improve both production and design, the cost can be lowered to 61 % of average. If both of them are instead worsen to poor level then the cost is increased to 175 %. It is worth realizing that improving only manufacturing efficiency, the cost is almost the same as average.

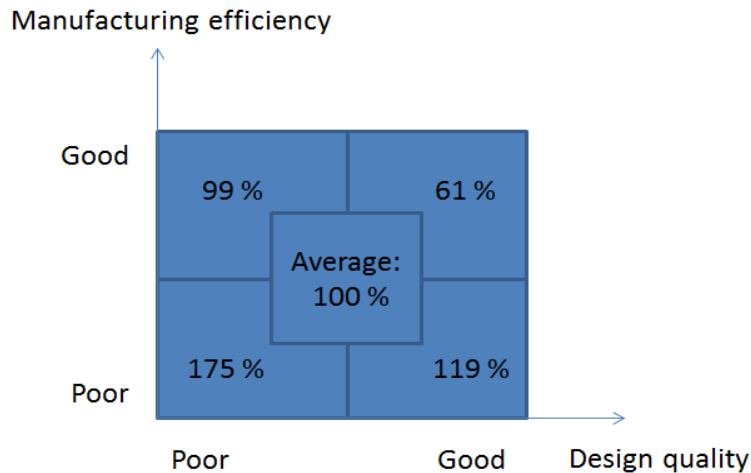


Figure 1. The effect of design and manufacturing quality on costs. Modified from [1].

III. ESTIMATING THE MANUFACTURING COSTS

Many of the DFMA-based solution are going hand in hand with manufacturing costs [2] [3]. It is important that the designer understands the meaning of manufacturability in the determination of product's cost structure. However there is still need for a simple and easy tool to estimate the costs. Examples of such research can be found from [4], [5] and [6].

The Lucas- method [7] [8] is developed to estimate production costs in concept phase of product development process. It will take a simple and ideal part, whose costs are known and then use factors to produce the final cost estimate. The method was developed at the early 80's and it includes estimate models for both the single parts and assemblies. This paper concentrates on the cost calculations of single parts only.

The cost is calculated by using the equation

$$M_i = VC_{mt} + R_c P_c$$

Where,

M_i = manufacturing cost

V = volume of the manufactured piece

C_{mt} = material cost including waste

R_c = factor based on the complexity of the piece

P_c = processing cost of ideal piece

Lucas calculation model requires the use of multipliers based on for example the material, manufacturing method, tolerances and roughness. The material cost is calculated using the volume (V) of a part multiplied with the cost of the specific material and the waste cost factor of the part. Another factor related to the material illustrates how well certain material is suited for a used work method. The Lucas method is explained in more detail in [7] and [8].

IV. COMPUTER APPLICATION

A prototype application that uses the Lucas method to calculate sophisticated estimates on how much it would cost to produce a single part was developed. It was created using the SolidWorks software and its VBA (Visual Basic for Applications) system. The screenshot of the software is presented in Fig. 2. The user simply needs to find suitable selections and the software will give the cost estimate. The user can also easily compare for example different materials, manufacturing methods and lot sizes in order to find an optimal solution.

Some modifications had to be done to make the method suitable for the used manufacturing machines and work force. Also the material prices vary depending on time and place.

Figure 2. The software user interface.

V. THE RESULTS ACHIEVED

Two machined parts (materials low carbon steel AISI 1020 and aluminum alloy 6061) represented in figures 3 and 4 were taken as test examples. Their costs were calculated for a lot of one by using the developed software. Reference cost information was taken from literature, asked from an expert (only in part number one) and by using the Solid Works costing solution included in the software version 2013. The results are presented in tables 1 and 2.

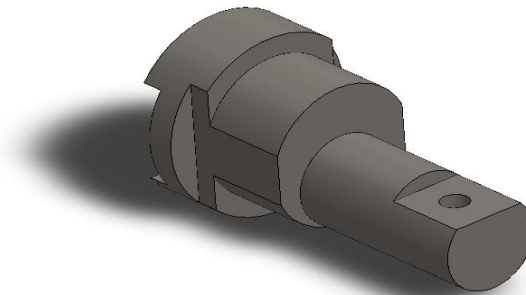


Figure 3. A test piece number one [1].

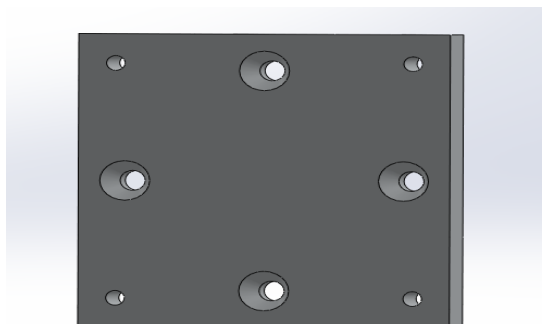


Figure 4. A test piece number two [9].

Table 1. Cost comparison for piece one.

Method	Material cost [€]	Processing cost [€]	Manufacturing cost [€]
SolidWorks macro	9	171	180
Litterature	N/A	N/A	130
Expert estimate	11	173	184
SolidWorks Costing	5	140	146

Table 2. Cost comparison for piece two.

Method	Material cost [€]	Processing cost [€]	Manufacturing cost [€]
SolidWorks macro	17	51	68
Litterature	7	52	59
SolidWorks Costing	12	39	51

VI. CONCLUSION

The developed software seems to work surprisingly well. It may not tell the final truth about the component costs but can be used to open the eyes of the designer when costs of the component under design are growing too high. It can also be used to find the most suitable manufacturing method and when considering the make or buy decisions.

The software is very simple and easy to use. The Solid Works costing application uses the feature structure of the part before it can be used. The Lucas-based solution works also without it and it has wider range of manufacturing methods. So the conclusion might be that the Lucas-based solution is useful in the early stages where the shape and manufacturing methods are unclear. Solid Works costing can be used to evaluate the piece whose shape and manufacturing methods are fixed.

REFERENCES

- [1] D. G. Ullman. The Mechanical Design Process. Fourth Ed. New York: Mc Graw Hill, 2010.
- [2] D. Anderson. Design for Manufacturability & Concurrent Engineering. CIM Press, 2006.
- [3] G. Boothroyd, P. Dewhurst, W. Knight. Product Design for Manufacture and Assembly. Marcel Dekker Inc., 2002.
- [4] P. Leibl. Cost Calculation with a Feature-based CAD System Using Modules for Calculation, Comparison and Forecast. Journal of Engineering Design 10, no. 1 (March 1999): 93–102.
- [5] K. Schreve, A. H. Basson. Small Volume Fabrication Cost Estimation Models for Embodiment Design. R&D Journal 2004 Vol 20, no. No 1 to 3 (n.d.): 10 – 15.
- [6] Y. Liu, A. H. Basson. Interfacing CAD and Manufacturing Cost Estimation Software Using COM/OLE. PROCEEDINGS OF THE INTERNATIONAL CIRP DESIGN SEMINAR SWEDEN, 6-8 JUNE 2001.
- [7] V. Chan, F. A. Salustri, DFA: The Lucas Method,. <http://deed.ryerson.ca/~fil/t/dfmlucas.html>.
- [8] K. G. Swift, J. D. Booker. Process selection: from design to manufacture. Oxford [England]; Boston: Butterworth-Heinemann, 2003.
- [9] K. T. Ulrich, S. D. Eppinger. Product design and development. Boston: McGraw-Hill Higher Education, 2008.

Signal Processing Algorithm of Space Time Coded Waveforms for Coherent MIMO Radar: Overview on Target Localization

Samiran Pramanik,¹ Nirmalendu Bikas Sinha,² C.K. Sarkar³

¹College of Engineering & Management, Kolaghat, K.T.P.P Township, Purba-Medinipur, W.B, 721171, India.

²Jadavpur University, Kolkata 700032, W.B, India.

ABSTRACT: Space-time coding (STC) has been shown to play a key role in the design of MIMO radars with closely spaced antennas. Multiple-input-multiple-output (MIMO) radar is emerging technology for target detection, parameter identification, and target classification due to diversity of waveform and perspective. First, it turns out that a joint waveform optimization problem can be decoupled into a set of individual waveform design problems. Second, a number of mono-static waveforms can be directly used in a MIMO radar system, which offers flexibility in waveform selection. We provide conditions for the elimination of waveform cross correlation. However, the mutual interference among the waveforms may lead to performance degradation in resolving spatially close returns. We consider the use of space-time coding (STC) to mitigate the waveform cross-correlation effects in MIMO radar. In addition, we also extend the model to partial waveform cross-correlation removal based on waveform set division. Numerical results demonstrate the effectiveness of STC in MIMO radar for waveform de-correlation. This paper introduces the signal processing issued for the coherent MIMO radar without and with STC waveforms and also studied signal processing algorithms of coherent MIMO radar with STC waveforms for improvement of target detection and recognition performance for real life scenario.

Keywords: STC, coherent, Probability detection, MIMO and SNR.

I. INTRODUCTION

Traditional MIMO radar [1]-[2] takes the opposite direction of the phased-array radar. The approach is to employ multiple uncorrelated waveforms that are radiated via omnidirectional transmission, in compare to phased-array radar [3], where a single probing waveform is sent via directional transmission. Inspired by several publications have advocated the concept of MIMO radar from the system implementation point of view, processing techniques for target detection and parameter estimation. Target parameters of interest in radar systems include target strength, location, and Doppler characteristics. MIMO radar systems employ multiple antennas to transmit multiple waveforms and engage in joint processing of the received echoes from the target. MIMO radar may be configured with its antennas co-located or widely [4] distributed over an area and able to provide independent diversity paths. The co-located MIMO [5], [6] radar where the transmitter and the receiver are close enough so that they share the same angle variable, i.e., coherent MIMO radar.

STC for waveform design has been introduced in [7] and [8] to cope with detection under possibly correlated clutter and, more generally, to introduce a further degree of freedom at the transmitter side. It is a revolutionary development for exploiting the MIMO channel by using antenna array processing technology, which is currently stimulating considerable interest across the wireless industry. The STC 'concept' builds on the significant work by Winter's in the mid-80's which highlighted the importance of antenna diversity on the capacity of wireless systems [9]. The use of multiple antennas at both the transmitter and receiver is essential for the STC concept to work effectively, since STC exploits both the temporal and spatial dimensions for the construction of coding designs which effectively mitigate fading (for improved power efficiency) and are able to capitalise upon parallel transmission paths within the propagation channel (for improved bandwidth, efficiency).

In this paper, the problem of target detection in co-located MIMO radars is considered. A pulse-train signalling [10] is assumed to be used in this system. STC [12] is a MIMO technique that is designed for use with multiple transmitter antennas. This technique introduces temporal and spatial correlation into signals transmitted from different antennas. The intention is to provide diversity at the receiver and coding gain over an uncoded system without sacrificing the bandwidth.

The other MIMO technique is spatial multiplexing in which different data streams are transmitted from multiple antennas. In [11], a pulse-train signalling for co-located MIMO radars has been proposed. The received signal modelling and problem formulation is presented. It is shown that due to unknown values of Doppler frequency and target Direction of Arrival (DOA), a compound hypothesis testing problem is confronted. The standard technique for compound hypothesis tests when the Probability Distribution Function (PDF) of the unknown parameters is not known is the Generalized Likelihood Ratio (GLR) detection.. Full exploitation of these potentials can result in significant improvement in target detection, parameter estimation, target tracking and recognition performance. This motivates the authors MIMO radar using pulse-train signalling. Thus, each orthogonal waveform carries independent information about the target; spatial diversity about the target is thus created. Exploiting the independence between signals at the array elements, MIMO radar achieves improved detection performance and increased radar sensitivity.

II. COHERENT MIMO RADAR

Coherent MIMO radar uses antenna arrays for transmitting and receiving signals. These arrays may be co-located and even transmit and receive functions can be performed by the same array or the arrays may be separated. The separation between the elements may be uniform or non-uniform. The arrays can be filled or sparse depending on the application type.

But the separation is always small compared to the range extent of the target. Whatever the separation between the array elements is, the important point in coherent MIMO radar is that the array elements are close enough so that every element sees the same aspect of the target i.e. the same RCS. As a result, point target assumption is generally used in coherent MIMO radar applications.

A. System Model

Consider a coherent MIMO radar system that has transmit and a receive array consisting of M and N elements respectively. Then the received signal can be written as

$$y(t) = \sqrt{\frac{E_t}{M}} Hx(t - \tau) + w(t) \dots \dots (1)$$

Where, $\sqrt{\frac{E_t}{M}} Hx(t - \tau)$ denote the discrete time baseband signal transmitted by the transmit antenna elements where $x(t - \tau)$ is the input message signal with delay time, E_t is the total average transmitted energy and $w(t)$ is the noise vector.

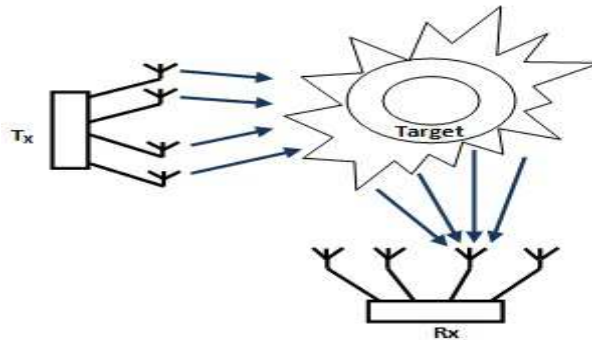


Fig.1. Coherent MIMO radar configuration.

B. Probability detection

The detection problem here can be formulated as binary hypothesis testing problem as follows:

$$\left. \begin{aligned} H_0: \bar{y} &= \bar{w} \\ H_1: \bar{y} &= \sqrt{\frac{E_t}{M}} \bar{\alpha} + \bar{w} \end{aligned} \right\} \dots \dots \dots (2)$$

Where H_0 indicates absence of signal and H_1 indicates presence of signal.

It is well known that the optimum solution to this hypothesis testing problem under Neyman-Pearson criterion is the Likelihood Ratio Test (LRT).

The likelihood ratio test becomes,

$$\|\bar{y}\|_{H_0}^2 \overset{H_1}{T'} \dots \dots \dots (3)$$

To see the performance limit of coherent MIMO radar, the vector α become identical and coherent integration of the received samples becomes possible before detection process. The modified binary hypothesis testing problem turns in the form,

$$\left. \begin{aligned} H_0: y &= w \\ H_1: y &= \sqrt{\frac{E_t}{M_t}} MN\alpha + w \end{aligned} \right\} \dots \dots \dots (4)$$

Where w is now a complex number.

The probability of false alarm rate, P_{fa} can be calculated as,

$$\begin{aligned} P_{fa} &= \text{Prob} \left\{ \exp \left(\frac{1}{MN\sigma_w^2} \right) > T' \right\} \\ &= \exp \left(\frac{T'}{MN\sigma_w^2} \right) \dots \dots \dots (5) \end{aligned}$$

Then P_d can be written in terms of SNR and probability of false alarm rate as,

$$P_d = \exp \left(\frac{\ln(P_{fa})}{(SNR)N + 1} \right) \dots \dots \dots (6)$$

So, the probability of detection does not depend on the number of transmit antennas but depends only on number of receive antennas and SNR.

C. Results and Observation

To compare with the detection performance of Coherent MIMO Radar, the detector in (6) is implemented. P_{fa} value is set to 10^{-6} . If the number of receive elements is held constant at the value of 5, and the number of transmit elements is increased, the P_d vs SNR curve in Fig. 2 is obtained.

The graphics in Fig. 2 show that the detection performance does not change with increasing M. This is because the transmitted power is normalized and it does not change with the number of transmit elements, and also because the noise power and the signal power in the received signal after coherent summation increase at the same rate.

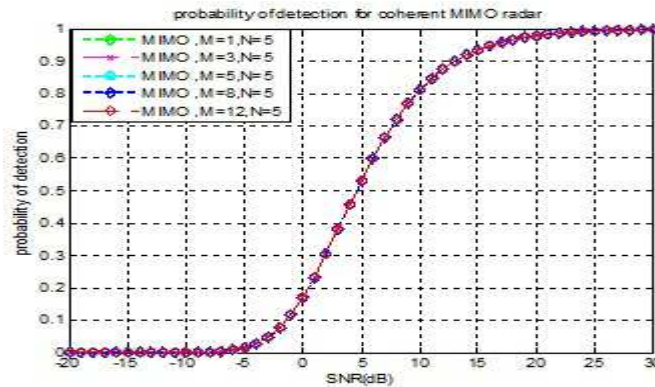


Fig. 2. Probability of detection for coherent MIMO radar, changing M

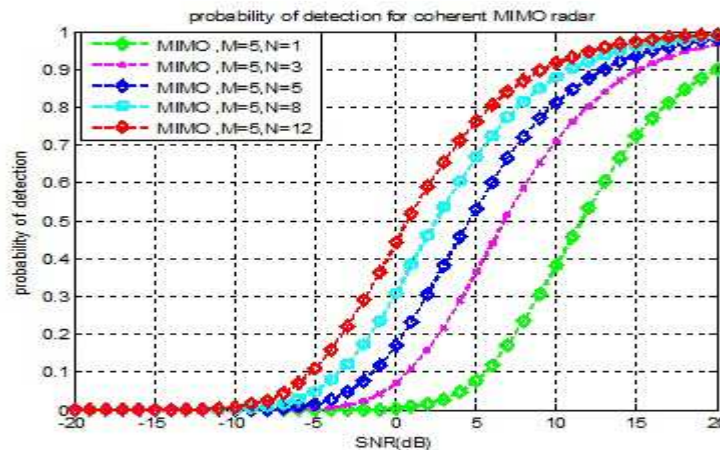


Fig. 3: Probability of detection for coherent MIMO radar, changing N.

If the number of transmit elements is held constant at the value of 5 and the number of receive elements is increased, the P_d vs SNR curve in Fig. 3 is obtained. We can see from the graph that as number of receiving antennas is increased the probability of detection increases, because the total received energy increases.

III. COHERENT MIMO RADAR WITH STC WAVEFORMS

In the detection problems studied so far for the coherent MIMO radar which employs antenna are close enough, are developed without including these space time coded (STC) signals explicitly. In the transmitted signals are modeled as a train of rectangular pulses whose amplitudes are modulated by space time codes and the corresponding detectors are developed. With this approach, the transmitted signals can be further optimized to better a given performance metric. The STC Coherent MIMO radar configuration is shown in Fig. 4.

A. System Model

Consider a coherent MIMO radar with STC waveforms system that has transmit and a receive array consisting of M and N elements respectively. The received signal is also scaled so that the total received signal increases directly proportional to rectangular pulses. The resultant signal model for the received signal can be written as

$$y_k(t) = \sqrt{\frac{nE_t}{M}} Hx(t - \tau) + w_k(t) \dots \dots (7)$$

Where, $\sqrt{E_t/M} Hx(t - \tau)$ denote the discrete time baseband signal transmitted by the transmit antenna elements where $x(t - \tau)$ is the input message signal with delay time, E_t is the total average transmitted energy and $w_k(t)$ is the noise vector.

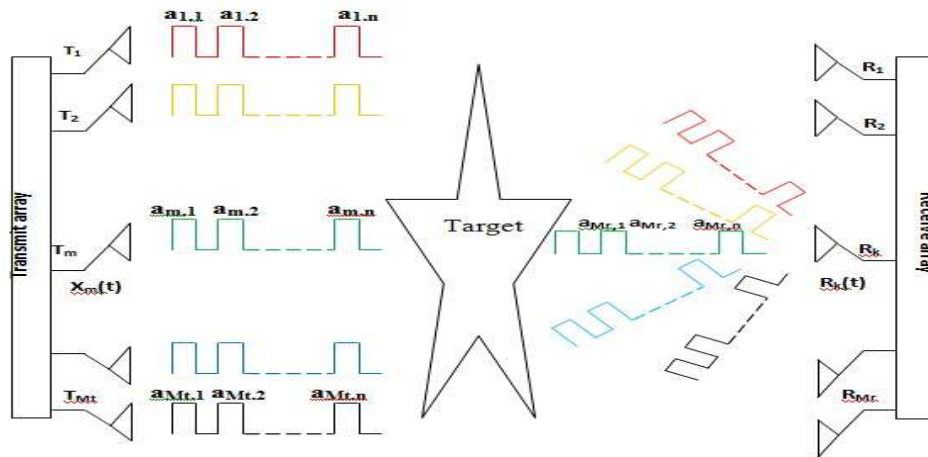


Fig.4. STC Coherent MIMO radar configuration.

B. Probability detection

The detection problem here can be formulated as binary hypothesis testing problem as follows:

$$\left. \begin{aligned} H_0: y_k &= w_k \\ H_1: y_k &= \sqrt{\frac{nE_t}{M}} \alpha_k + w_k \end{aligned} \right\} \dots \dots (8)$$

Where H_0 indicates absence of signal and H_1 indicates presence of signal.

To see the performance limit of coherent MIMO radar, the vector α become identical and coherent integration of the received samples becomes possible before detection process and w_k is now a complex number. For coherent MIMO radar with STC waveforms, from the definition of SNR for the radar system is

$$(SNR)_{STC} = \frac{nE_t}{\sigma_w^2} = n * SNR$$

Then P_d can be written in terms of SNR and probability of false alarm rate as,

$$P_d = \exp\left(\frac{\ln(P_{fa})}{(n * SNR)N + 1}\right) \dots \dots (9)$$

C. Results and Observation

To compare with the detection performance of coherent MIMO radar with STC waveforms, the probability detection in equation (9) is implemented for which P_{fa} value is set to 10^{-2} . If the number of receiving elements is held constant at the value of 5, and the number of transmitting elements is increased, the P_d vs. SNR curve in Fig. 5 is obtained. The graphics in Fig. 5 show that the detection performance does not change with increasing M.

But if the number of transmitting elements is held constant at the value of 5, and the number of receiving elements is increased, the p_d vs. SNR curve in Fig. 6 is obtained. It is interesting to see that the detection performance increases as the number of receiving antennas increases.

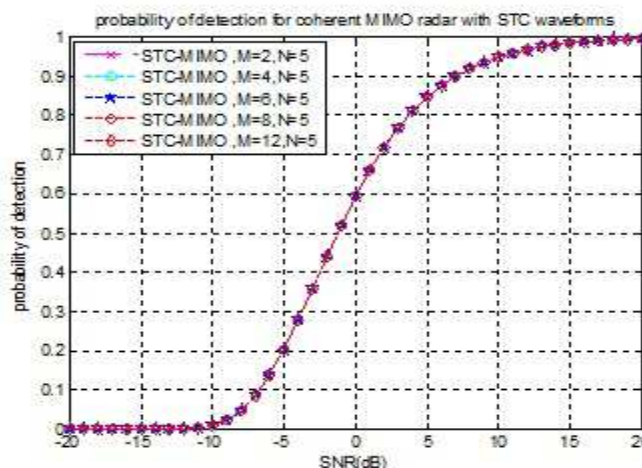


Fig. 5. Probability of detection for coherent MIMO radar with STC waveforms, changing M.

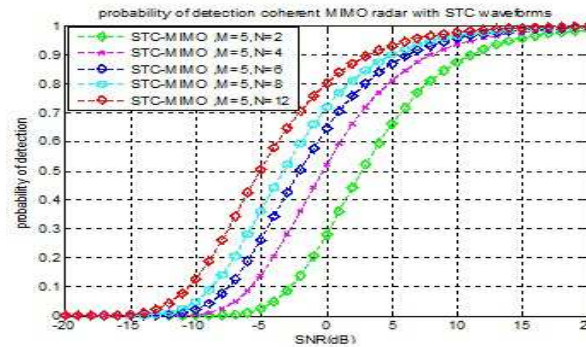


Fig. 6. Probability of detection for coherent MIMO radar with STC waveforms, changing N.

The ROC of coherent MIMO radar versus coherent MIMO radar with STC waveforms and also comparison of probability detection of both type of MIMO radar are is given in Fig. 7 and Fig. 8 respectively. These figures (Fig. 7 & Fig. 8) are obtained using the analytical expressions given in equations (6), (9) for $M = N = 5$. In the both figures, the blue lines belong to coherent MIMO radar with STC waveforms and the red lines belong to coherent MIMO radar.

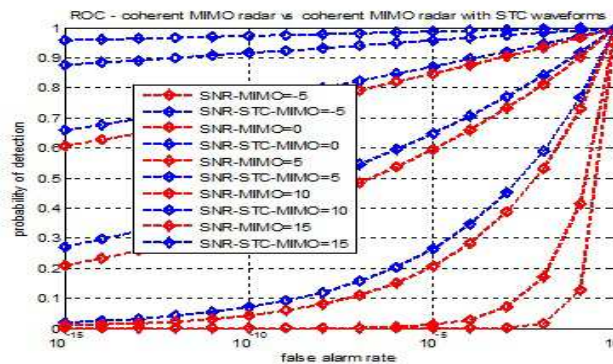


Fig. 7: ROC- Coherent MIMO vs. STC coherent MIMO radar.

The results in Fig.7 and 8 show that at high SNR values and at high detection probabilities, the detection performance of STC coherent MIMO radar is better than coherent MIMO radar.

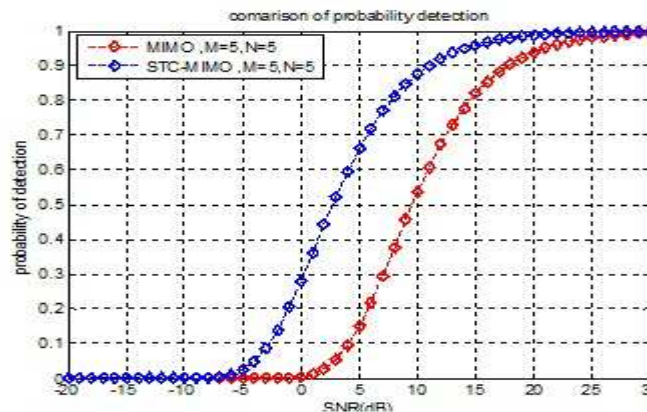


Fig. 8: Comparison of probability detection for coherent MIMO vs. STC coherent MIMO radar.

IV. CONCLUSION

In this paper, a wide variety of signal processing algorithms for coherent MIMO radar with and without STC waveforms have been presented. A novel algorithm on the space-time adaptive processing is proposed for improving the performance of coherent MIMO radar system. Derivations of the respective optimal detectors are shown when the target and noise level are either known or unknown. The coherent MIMO radar with pulse-train signalling outperforms the conventional MIMO radar at high detection rates which enables RCS fluctuation smoothing is demonstrated. The waveform design problem with information about the target and the clutter responses are being dealt. We have provided several numerical examples which show that the coherent MIMO radar with STC waveforms has much better performance than others. We also proposed a new metric to analyze the performance of these systems. Development of an adaptive optimal energy allocation mechanism is done to get significant improvement in performance. Finally we simulated a realistic scenario to analyze the performance of the proposed system. Using higher order modulations in MIMO systems with STC, we can achieve better detection rates, target localization and bandwidth efficiency.

REFERENCES

- [1] E. Fishler, A. Haimovich, R. Blum, D. Chizhik, L. Cimini, and R. Valenzuela, "MIMO Radar: An idea whose time has come", proceedings of IEEE radar Conference, pp.71-78, April 2004.
- [2] N. H. Lehmann, E. Fishler, A. M. Haimovich, et al., "Evaluation of transmit diversity in MIMO-radar direction finding, IEEE Transactions on Signal Processing, vol.55, no.5, pp. 2215-2225, May 2007.
- [3] A. Haimovich, R. Blum, and L. Cimini, "MIMO radar with widely separated antennas," IEEE Signal Processing Magaz., vol. 25, pp. 116–129, Jan. 2008.
- [4] J. Li and P. Stoica, "MIMO radar with colocated antennas," IEEE Signal Processing Magaz., vol. 24, no. 5, pp. 106–114, Sept. 2007.
- [5] Yang Yang and Rick S. Blum, "Phase Synchronization for Coherent MIMO Radar: Algorithms and Their Analysis" IEEE TRANSACTIONS ON SIGNAL PROCESSING, VOL. 59, NO. 11, pp. 5538-5557, NOVEMBER 2011.
- [6] Francesco Belfiori, Wim van Rossum, and Peter Hooiboom, "Coherent MIMO Array Design With Periodical Physical Element Structures", IEEE ANTENNAS AND WIRELESS PROPAGATION LETTERS, VOL. 10, pp. 1341-1344, 2011.
- [7] A. De Maio and M. Lops, "Design principles of MIMO radar detectors," IEEE Trans. Aerosp. Electron. Syst., vol. 43, no. 3, pp. 886–898, Jul. 2007.
- [8] A. De Maio, M. Lops, and L. Venturino, "Diversity-integration tradeoffs in MIMO detection," IEEE Trans. Signal Process. vol. 56, no. 10, pp. 5051–5061, Oct. 2008.
- [9] Winters J.H.: 'On the Capacity of Radio Communication Systems with Diversity in a Rayleigh Fading Environment' IEEE Journal on Sel. Areas in Comm., Vol. SAC-5, No. 5, June 1987.
- [10] A. De Maio and M. Lops, "Design Principles Of MIMO Radar Detectors", IEEE Transactions on Aerospace and Electronic Systems, vol. 43, no. 3, pp. 886-898, Jul. 2007.
- [11] Hatam, M., A. Sheikhi, and M. A. Masnadi-Shirazi, "A pulse-train mimo radar based on theory of independent component analysis," Submitted for Publication in the Iranian Journal of Science and Technology, Jun. 2011.
- [12] Alamouti S. M. 1998. A Simple Transmit Diversity Technique for Wireless Communications, IEEE Journal on Selected Areas in Communications, vol. 16, no. 8, pp. 1451 – 1458.



Prof. Samiran Pramanik received the B. Tech degrees in Electronics and Communication Engg. from W.B.U.T, West Bengal and M. Tech degrees in Electronic and communication Engg. (Specialization in microwave) Burdwan University, India, in 2007 and 2009 respectively. He is currently working towards the Ph.D. degree in Electronics and Telecommunication Engineering at Jadavpur University, W.B. Since 2010, he has been associated with the College of Engineering and Management, Kolaghat. W.B, India where he is currently an Asst. Professor is with the department of Electronics & Communication Engineering & Electronics & Instrumentation Engineering. His current research Interests are in the area of MIMO, multiuser communications, Wireless 4G communications and Digital Radar, RCS Imaging. He has published large number of papers in different International Conference and Journals.



Dr. Nirmalendu Bikas Sinha received the B.Sc (Honours in Physics), B. Tech, M. Tech degrees in Radio-Physics and Electronics from Calcutta University, Calcutta, India, in 1996, 1999 and 2001, respectively. He has received Ph.D (Engg.) degree in Electronics and Telecommunication Engineering from Bengal Engineering and Science University, Shibpur in 2012. Since 2003, he has been associated with the College of Engineering and Management, Kolaghat. W.B, India where he is currently an Associate Professor is with the department of Electronics & Communication Engineering & Electronics & Instrumentation Engineering. His current research Interests are in the area of signal processing for high-speed digital communications, signal detection, MIMO, Multiuser Communications, Microwave /Millimeter wave based Broadband Wireless Mobile Communication, semiconductor Devices, Remote Sensing, Digital Radar, RCS Imaging, and Wireless 4G communication. He has published more than fifty papers in different international Conference, Proceedings and Journals. He is presently the editor and reviewers in different International Journals.



Dr. Chandan Kumar Sarkar (SM'87) received the M.Sc. degree in physics from the Aligarh Muslim University, Aligarh, India, in 1975, the Ph.D. degree from Calcutta University, Kolkata, India, in 1979, and the D.Phil. degree from the University of Oxford, Oxford, U.K., in 1983. He was a Research Fellow of the Royal Commission for the Exhibition of 1851 at the Clarendon Laboratory, University of Oxford, from 1983 to 1985. He was also a Visiting Fellow with the Linköping University, Linköping, Sweden. He joined Jadavpur University, Kolkata, in 1987 as a Reader in electronics and telecommunication engineering and became a Professor and the Head of the Department of Physics, BESUS, India, in 1996. Since 1999, he has been a Professor with the Department of Electronics and Telecommunication Engineering, J.U. He has served as a Visiting Professor in many universities and has published around 100 papers in referred journals. Dr. Sarkar is the Chair of the IEEE Electron Devices Society (EDS), Calcutta Chapter. He serves as a Distinguished Lecturer of the IEEE EDS.

Cure Characteristics and Physico-Mechanical Properties of Carbonized Bamboo Fibre Filled Natural Rubber Vulcanizates

G.N.Onyeagoro

Department of Polymer and Textile Engineering Federal University of Technology, Owerri, Nigeria

ABSTRACT: *Bamboo fibres were carbonized at 600°C and used as particulate filler in natural rubber vulcanizates. Carbon black was used as the reference filler, while maleic anhydride-grafted-polyisoprene was used as a compatibilizer. The natural rubber vulcanizates were compounded on a two-roll mill, and test samples were prepared by compression moulding. The cure characteristics and physico-mechanical properties of the natural rubber vulcanizates were studied at filler loadings of 0, 2, 4, 6, 10, and 15 phr (parts per hundred parts rubber). The carbonized bamboo fibre was characterized for filler properties and sieved to 0.08µm and 0.35µm particle sizes. Results obtained showed that compatibilized carbonized bamboo fibre filled vulcanizates exhibited improvement in the cure properties investigated over the non-compatibilized vulcanizates. Carbon black exhibited higher tensile strength, modulus, hardness and elongation at break in the vulcanizates than carbonized bamboo fibre. However, at any given loading of carbonized bamboo fibre, these properties increased with a reduction in particle size of the filler. Specific gravity of the vulcanizates increased with increases in filler loading, and was found to be dependent on filler particle size. The smaller particle-sized carbonized bamboo fibre filled vulcanizates exhibited higher specific gravity than those vulcanizates containing the larger particle-sized filler.*

Keywords: *bamboo fibre, carbonization, cure characteristics, natural rubber, physico-mechanical properties.*

I. Introduction

Natural rubber (NR) is an interesting material with commercial success due to its excellent physical properties, especially high mechanical strength, low heat build-up, excellent flexibility, and resistance to impact and tear, and above all its renewability [1]. However, raw dry rubber is seldom used in its original state for any engineering and domestic application. Consequently, rubber manufacture involves the addition to rubber many ancilliary materials called additives to allow the rubber compounds to be satisfactorily processed and vulcanized in order to improve the application properties of the rubber compound. Additives used in rubber manufacture include vulcanizing agents, accelerators, activators and/or retarders, fillers, anti-degradants, among others.

Fillers represent one of the most important additives used in rubber compounding. Fillers are added to rubber formulation in order to optimize properties needed for service application [2]. Reinforcement of rubber polymers with particulate fillers is a subject that has captured the interest of a large number of researchers [3, 4, 5, 6, 7]. Property advantages obtainable from filler reinforced rubber vulcanizates include design flexibility, improved physico-mechanical properties such as tensile properties, hardness, and processing economy. Due to strong environmental regulations worldwide and increased interest in the proper utilization of renewable natural resources, efforts have been made to find alternative reinforcements that are environmentally friendly while providing the same performance as their synthetic counterparts [8].

With their low cost, easy availability, ease of chemical and mechanical modification, and high specific mechanical properties, natural fibres represent a good, renewable and biodegradable alternative to the most common synthetic reinforcement [9].

Carbon black is always considered the most commonly consumed reinforcing filler in the rubber industry [10]. Considering its problems such as its non-renewable petroleum origin, dark color, contamination and pollution, researchers are seeking an adequate alternative [11],[12]. Thus, the use of nano-fillers such as nano-ZnO, nano-Al₂O₃, and nano-CaCO₃ as substitutes for carbon black in rubber compounding has been suggested [13]. The authors reported that the use of these fillers exhibited superior physical and mechanical properties in the vulcanizates when compared to the conventional micro-composites. Excellent reports exist in the literature on the use of different fillers to reinforce natural/synthetic rubber and their blends. Osman et al. [14] studied the effect of maleic anhydride-grafted polypropylene (MAPP) on the properties of recycled newspaper (RNP) filled polypropylene (PP)/natural rubber (NR) composites. The authors found that the incorporation of MAPP reduced the water uptakes of the composites. In a study by Ansarifer et al. [15] on the properties of natural rubber reinforced with synthetic precipitated amorphous white silica nano-filler it was reported that compression set, tensile strength and harness were improved on addition of filler into the rubber, while elongation at break, tear strength and cyclic fatigue were adversely affected. Yang et al. [16] in their studies on the influence of graphite particle size, and shape on the properties of acrylonitrile butadiene rubber (NBR) found that graphite with the smallest particle size possessed the best reinforcing ability, while the largest graphite particles exhibited the lowest function coefficient of the composites among four fillers investigated.

The reinforcing effects of coal shale-based fillers on natural rubber on the basis of filler particle size have been investigated [17]. The authors reported that the ultra micro coal-shale powder exhibited excellent filler properties. In other reports, the use of renewable agro-based materials such as cocoa pod husk and rubber seed shells [18], palm kernel husk [19], short pineapple leaf fiber [20], and snail shell powder [4] as fillers in natural rubber were examined.

The present study reports the use of carbonized bamboo fibre as filler in natural rubber. One of the most important aspects of composite manufacture is to achieve adequate adhesion between filler and the rubber matrix. In this work, the cure

characteristics and physico-mechanical properties of carbonized bamboo fibre filled natural rubber vulcanizates using maleic anhydride-graft-polyisoprene (MAPI) as compatibilizer are reported. Bamboo fibre was selected as the reinforcement because bamboo is an abundant natural resource in Nigeria and its overall mechanical properties are comparable to those of wood [21]. The use of carbonized bamboo fibre in reinforcing natural/synthetic rubber had not been reported in the scientific literature to my knowledge. However, the effect of filler carbonization temperature on the tensile properties of natural rubber compounds filled with cassava (*Manihot esculenta*) peel carbon filler was reported by Stella et al. [22] who revealed that the physico-mechanical properties of the composites were greatly influenced by filler loading and filler carbonization temperature. Similarly, the influence of carbonized Dika (*Irivalgia Gabonensis*) nutshell powder on the vulcanizate properties of natural rubber/acrylonitrile-butadiene rubber blends was studied by Onyeagoro [23]. The author found that synchronous use of carbon black and carbonized Dika nutshell produced significant improvements in the vulcanizate properties of the blends at 10 phr filler loading, and suggested that carbonized Dika nutshell powder could serve as potential substitute filler for carbon black in the rubber industry, especially in the production of low-cost/high volume rubber products where strength is not critical.

II. Experimental

2.1. Materials

Natural rubber (Standard African Rubber, SAR 3) having the properties given in Table 1 was obtained from the Rubber Research Institute of Nigeria (RRIN), Iyanomo, Benin City. The rubber compounding ingredients such as carbon black (N330), sulphur, accelerator (MBT), zinc oxide, stearic acid, wax and anti-oxidant (TMQ) were of commercial grade and supplied by Dunlop Plc, Lagos, Nigeria. The bamboo used in this work belongs to the species of *Bambusa Paravariabilis* and was obtained from Forest Reserve Areas in Umuokanne in Imo State, Nigeria. Maleic anhydride-graft-Polyisoprene used as compatibilizer was purchased from Rovet Chemicals Ltd, Benin City, Nigeria.

Table 1: Properties of Standard African Rubber (SAR 3) [25]

Parameters	
Volatile matter	0.40
Dirt content retained on 45µm sieve (%)	0.02
Nitrogen (%)	0.23
Ash content (%)	0.32
Initial Plasticity (P^0)	36
Plasticity Retention Index (PRI)	67
Plasticity after aging for 30 min @ 140°C (P^{30})	24
Mooney Viscosity, ML (1+4), 100°C	70

2.2. Carbonization and Characterization of Bamboo Fibres

Bamboo chips were produced by means of a wood planar which were then air-dried to a constant weight. Portion of the dried bamboo chips was milled to fine powder, sieved through a mesh of 150µm, and collected as unmodified bamboo fibre in a dessicator until required. The unmodified bamboo fibre was weighed and carbonized at a temperature of 600°C for 3 hours [26] using a Muffle furnace. The carbonized bamboo fibre (CBF) portion was then milled to fine powder and sieved through a mesh size of 0.08, and 0.35µm. It was kept in a dessicator and allowed to cool to room temperature until required. CBF and carbon black (CB) were then characterized and used for compounding.

2.3. Characterization of Carbonized Bamboo Fibre and Carbon Black (N330)

Carbonized bamboo fibre (CBF) and Carbon black (CB) were characterized in terms of loss in ignition, P^H , bulk density and surface area. The loss on ignition was determined gravimetrically according to ASTM 1509 standard test method. The P^H and bulk density were determined by methods described by Ahmedna et al [27]. Iodine adsorption number method was used to measure the surface area as described by Ahmedna et al [28]. Moisture content and oil absorption were measured according to standard procedures described by ASTM D 1510, 1983 and BS 3483, Part B7, respectively. The results obtained are as presented in Table 2.

Table 2: Characterization of Carbonized Bamboo Fibre (CBF) and Carbon black (CB)

Parameter	CBF	CB (N330)
Loss on ignition	79.3	91.3
P^H of slurry @ 32°C	8.45	6.35
Iodine adsorption number (mg/g)	56.10	82.43
Bulk density (g/ml)	0.47	-
Moisture content (%)	5.13	2.72
Oil absorption (kg)	5.83 (0.35µm) 6.25 (0.08µm)	8.76

2.4. Preparation of Natural Rubber Vulcanizates

Table 3 gives the recipe used in the formulation of natural rubber compound. Mixing was carried out on a laboratory two-roll mill size (160 x 320 mm) in accordance with ASTM-D 3184-80. The nip gap, mill roll speed ratio, sequence of addition and time of mixing of the ingredients were kept the same for all the composite samples. The sheeted rubber compound was conditioned at room temperature, 32°C for 24 hours in a closed container and was further processed by curing. Curing was achieved by a method described by Igwe and Ejim [4]. The cured samples were coded accordingly for property testing.

Table 3: Compounding recipe for Filler reinforced Natural Rubber Composites

Ingredients (Phr)	Formulation			
	A	B	C	D
Natural Rubber (NR)	100	100	100	100
Stearic acid	2	2	2	2
Zinc Oxide	5	5	5	5
TMQ*	1	1	1	1
MBT ⁺	1	1	1	1
Sulphur	2	2	2	2
Processing aid	2	2	2	2
Maleic anhydride-graft-Polyisoprene (Compatibilizer)	3.5	3.5	3.5	3.5
Filler [#]	Variable (2, 4, 6, 10, 15)			

* TMQ = Trimethyl Quinoline

⁺ MBT = Mercaptobenzoylthiazole

[#] Filler = Bamboo fibres (CBF) and Carbon black (CB)

2.5. Cure Characteristics of Natural Rubber Vulcanizates

The cure characteristics were measured using a Monsanto Moving Die Rheometer (MDR Model). The scorch time, t_2 and cure time, t_{90} were obtained from the rheometer at 150°C. The Mooney viscosity was also determined at 120°C using a Monsanto automatic Mooney Viscometer (MV 2000 Model). The testing procedure was done according to the method described in ASTM D 1646 – 94.

2.6. Testing of Natural Rubber Vulcanizates

The following tests were conducted on the rubber samples using standard test methods [14, 16, 17, 22]: tensile strength, tensile modulus, elongation at break, hardness and specific gravity.

III. Results and Discussion

3.1 Characterization of bamboo fibre

Measurement of some characteristics of carbonized bamboo fibre (CBF) and those of carbon black (CB) which served as the reference filler in this study was carried out, and the results are presented in Table 4. The weight loss in ignition is a measure of the carbon content lost during combustion and measures the effectiveness of the filler. The higher the value, the greater the reinforcement effect of the filler [18, 20]. The higher value of loss in ignition recorded for CB when compared to CBF is an indication that CB is more resistant to heat effect. Table 4 shows that the iodine adsorption number of CB is greater than that of CBF. The iodine adsorption number is a measure of the surface area of the filler; the higher the value, the finer or smaller the particle sizes of the filler (larger surface area) and the greater the reinforcing ability.

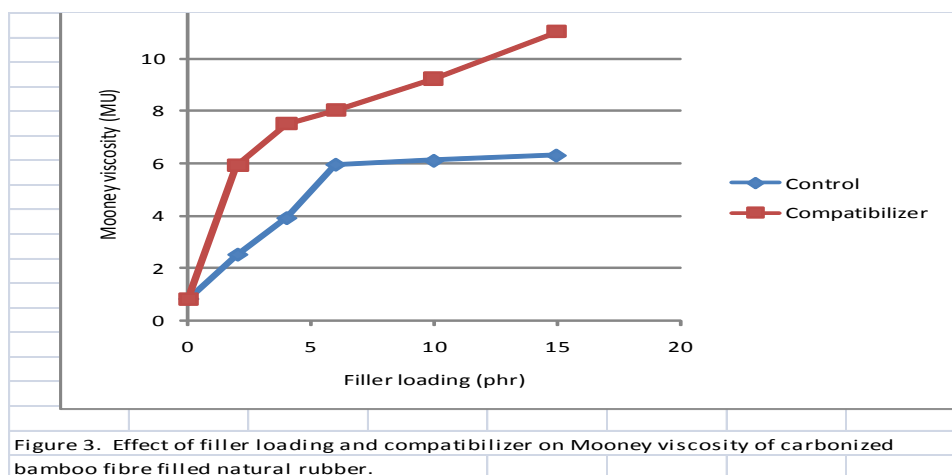
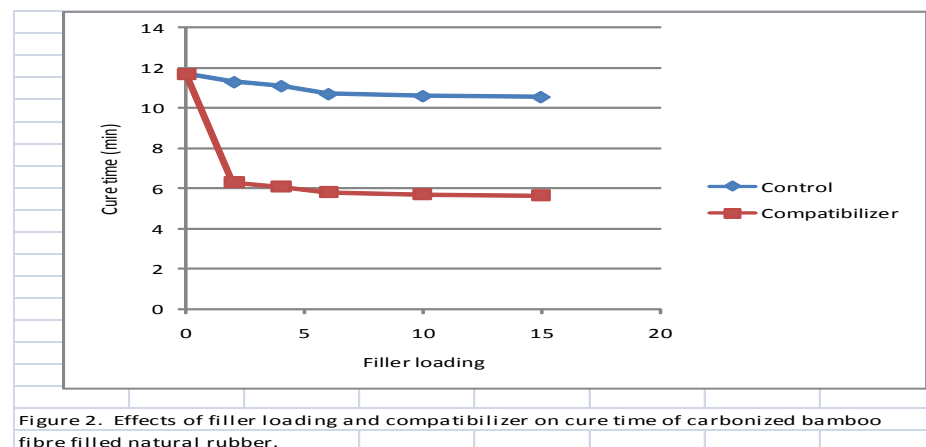
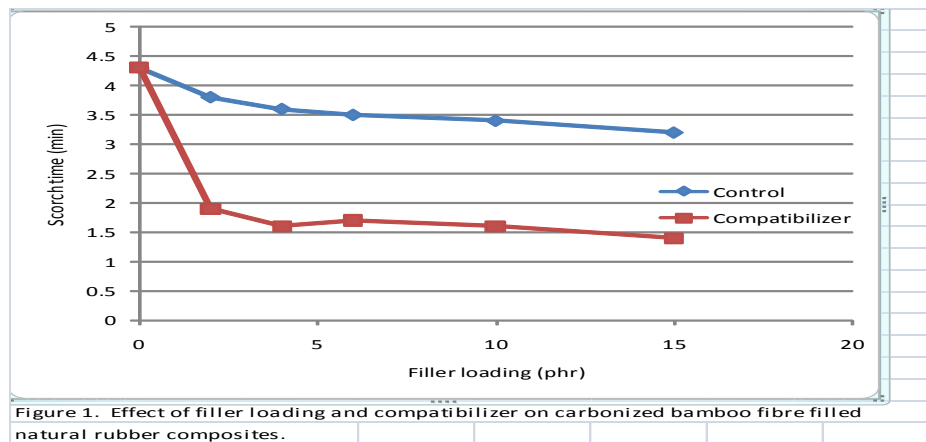
Table 4 also shows the oil absorption values for the fillers. The values indicate that the aggregate structure of carbon black is only greater than that of carbonized bamboo fibre particle size 0.08 and 0.35µm by about 2.51 and 2.93 kg, respectively. According to ASTM classification, CB consists of modular subunits called particles [18]. The similarity in the oil absorption values for the fillers may be an indication that CBF of particle sizes, 0.08 and 0.35µm have structures that may be closely related to CB, and therefore may produce similar effects in the vulcanizate [4].

3.2 Cure Characteristics of natural rubber vulcanizates

The effects of filler loading and compatibilizer on the scorch time, t_2 and cure time, t_{90} of carbonized bamboo fibre filled natural rubber vulcanizates are shown in Figs. 1 and 2. It can be seen that both properties decrease with increase in filler loading. This is attributed to longer residence time of the rubber vulcanizates in the mill during mixing. Similar observation was reported by Geethamma et al. [29]. According to the authors, the incorporation time of filler into rubber matrix increases as the filler loading increases and consequently generates more heat due to additional friction. However, at similar filler loading, the scorch and cure times of vulcanizates with compatibilizer are shorter than for the vulcanizates without compatibilizer, which is attributed to enhanced fibre-matrix adhesion and more energy required to incorporate the fibres due to increased viscosity.

The effect of filler loading and compatibilizer on Mooney viscosity of carbonized bamboo fibre filled natural rubber is shown in Fig. 3. The result shows that the Mooney viscosity increases with increase in filler loading and addition of compatibilizer. This indicates that the addition of both filler and compatibilizer increase the stiffness of the vulcanizates.

This observation is consistent with the report of Kumar et al. [30] for short sisal fibre filled styrene-butadiene rubber composites.



3.3 Mechanical properties of natural rubber vulcanizates

The effect of filler loading and particle size on tensile strength of filled natural rubber is presented in Fig. 4. It can be seen that tensile strength decreases with increasing filler loading. The decrease in tensile strength of rubber vulcanizates with increase in filler loading has been reported by Arumugam et al. [31] who worked on coconut fibre reinforced rubber composites and found that the tensile strength of rubber vulcanizates decreased with increases in coconut fibre content. Similarly, Ismail et al. [12] reported a decrease in tensile strength of rubber vulcanizates with increase in filler loading when working with oil palm wood flour reinforced epoxidized natural rubber. The authors attributed the decrease in tensile strength to poor filler dispersion with filler addition. This behavior can be related to the probable tendency of the filler to form agglomerates. However, other researchers [32, 33] reported increases in tensile strength with increase in filler loading.

The tensile strength of rubber vulcanizates filled with CBF, particle size, $0.08\mu\text{m}$ showed higher tensile strength than those filled with CBF, particle size, $0.35\mu\text{m}$. This observation is expected, and it is attributed to better filler dispersion and filler-matrix interaction. Generally, the smaller the particle sizes of filler, the greater the tensile strength of the vulcanizates [12]. Carbon black (CB), used as reference filler in this study steadily showed significant increases in the tensile strength of the vulcanizates, and produced higher tensile strengths than CBF filled NR. As earlier pointed out, the effectiveness of filler may be measured by its carbon content. Fillers with higher carbon content, provide greater reinforcement than those with lower carbon content because carbon itself is a very good reinforcing filler, Okieimen and Imanah [18]. It can be seen from the weight loss on ignition (Table 2) that CB has more carbon content than CBF and this partly explains the better reinforcing ability shown by CB over CBF. Tensile strength is affected by filler particle size, filler surface area and filler geometry. The filler geometry may be responsible for the poor strength property shown by carbonized bamboo fibre. Excellent reports by Mishra and Shimpi [32] have shown that irregularly shaped fillers could cause decreases in the strength of composites. The authors attributed this observation to the inability of the filler to support stresses transferred from the polymer matrix.

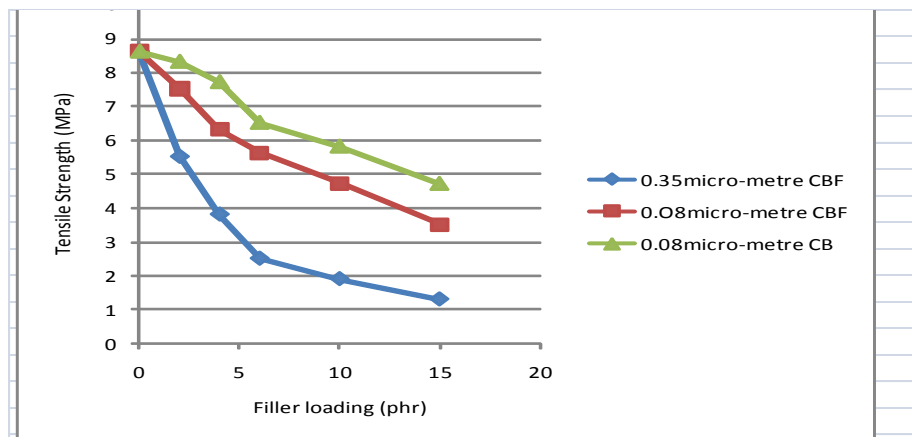


Figure 4. Effect of filler loading and particle size on tensile strength of filled natural rubber.

Figs. 5 and 6 show the effect of filler loading and particle size on tensile modulus and hardness of filled natural rubber, respectively. The results show that both properties increase with increasing filler loading, indicating increases in stiffness of the composites with the incorporation of filler into the rubber matrix. It is evident from the figure that the tensile moduli and hardness of carbonized bamboo fibre filled natural rubber are less than that of carbon black filled natural rubber, at all the filler loadings and particle sizes investigated. However, the carbonized bamboo fibre (CBF) with the smaller particle sizes ($0.08\mu\text{m}$) showed higher values in both properties in the vulcanizates than the CBF with larger particle sizes ($0.35\mu\text{m}$). This is because a reduction in particle size provides a greater surface area and reinforcement [36]. Carbon black has a very high surface activity, which provided greater reinforcement in comparison with carbonized bamboo fibre. Thus, the observed trends reveal that surface activity and polymer matrix-filler interaction are important factors controlling the tensile modulus and hardness. Ahmad et al. [3] reported that natural rubber forms a strong adsorptive bond with carbon black. In their independent studies, Kohjiya and Ikeda [34] and Poh et al. [35], reported that the modulus and hardness of filled vulcanizates can be enhanced by improving the surface and surface reactivity of fillers, filler dispersion and filler-polymer matrix interaction.

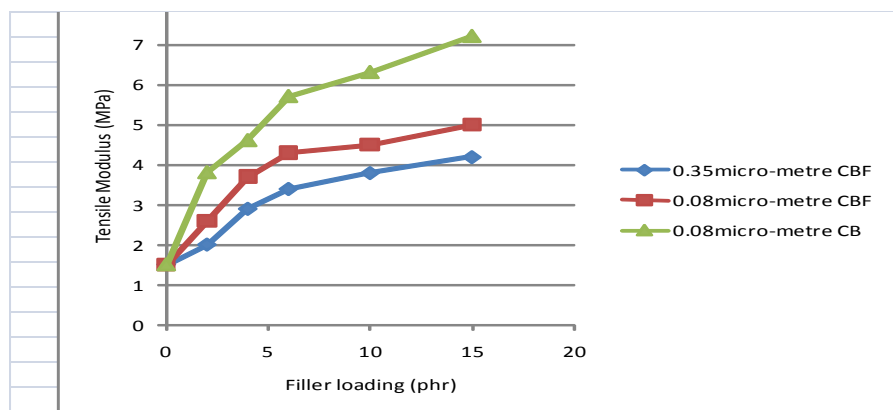


Figure 5. Effect of filler loading and particle size on tensile modulus of filled natural rubber.

Fig. 7 shows the effect of filler loading and particle size on elongation at break (EB) of vulcanized natural rubber. The result shows that the EB of carbon black filled natural rubber vulcanizate is higher than the EB of carbonized bamboo fibre filled natural rubber vulcanizate at the filler loadings studied. In general, the incorporation of reinforcing or non-reinforcing (inert) fillers into natural rubber produces decreases in elongation at break of rubber vulcanizates [18]. The decreasing trend in EB with increasing filler loading is attributed to increase in stiffness and brittleness, which decreased the resistance to stretch on application of strain.

However, at any given carbonized bamboo fibre loading investigated, the EB of the vulcanizates increases with decrease in the particle size of carbonized bamboo fibre. The increase in the EB with a reduction in the filler particle size can be attributed to more uniform dispersion of the smaller sized filler in the rubber matrix, which resulted in greater absorption and more efficient transfer of stresses to the matrix.

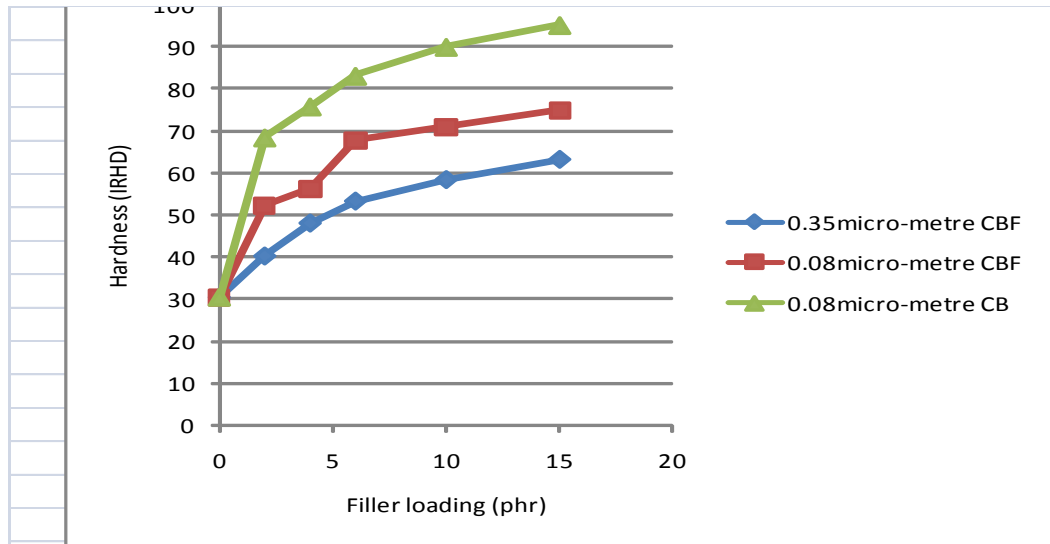


Figure 6. Effect of filler loading and particle size on the hardness of filled natural rubber.

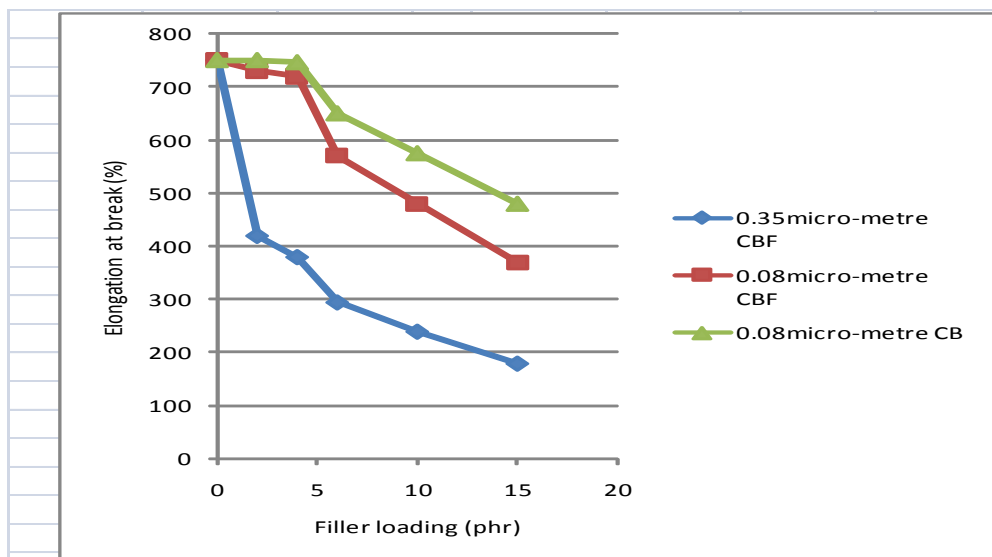


Figure 7. Effect of filler loading and particle size on the elongation at break of filled natural rubber.

Fig. 8 shows the effect of filler loading and particle size on the specific gravity of natural rubber vulcanizates. The figure shows a general increase in specific gravity with increases in filler loading, irrespective of the type of filler loading considered. This observation is consistent with the reports of Igwe and Ejim [4] and Mishra and Shimpi [32] who revealed a general increase in the specific gravity of rubber vulcanizates with increasing filler loading. However, at all particle sizes investigated, the specific gravity of the carbon black filled natural rubber vulcanizates was greater than those of rubber vulcanizates filled with carbonized bamboo fibre. This may be due to more uniform dispersion of carbon black in the matrix, with the resultant increase in filler-matrix interaction.

At any given loading of carbonized bamboo fibre considered, the specific gravity of the vulcanizates increases with a reduction in the particle size of the filler. The increasing trend in the specific gravity with decrease in the filler particle size may be due to the filler size effect, in which case the smaller sized filler became more uniformly dispersed in the rubber matrix to keep the rubber chain intact on crosslinking.

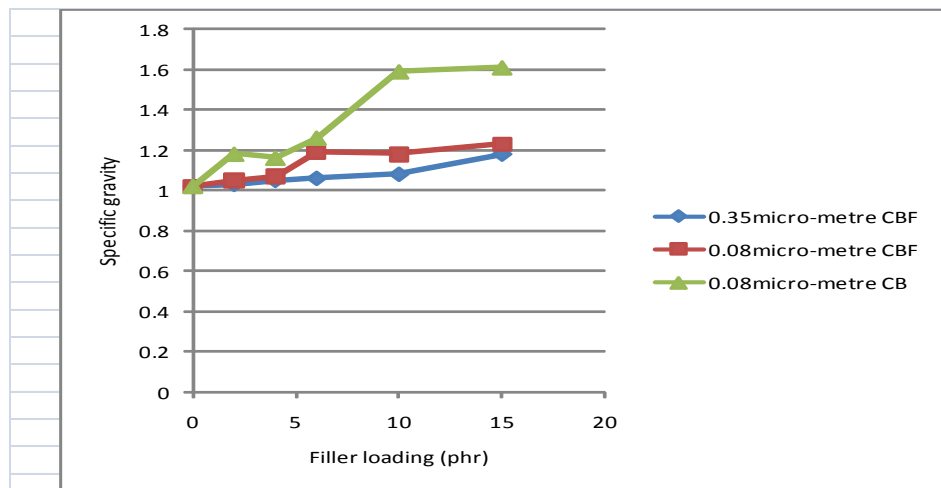


Figure 8. Effect of filler loading and particle size on specific gravity of filled natural rubber.

IV. CONCLUSION

The cure characteristics and physico-mechanical properties of carbonized bamboo fibre filled natural rubber vulcanizates were studied as a function of filler loading, filler particle size and compatibilizer. The scorch time, t_2 and cure time, t_{90} of carbonized bamboo fibre filled natural rubber vulcanizates decreased with increase in filler loading and the presence of compatibilizer.

Carbon black (CB), the reference filler, exhibited higher tensile strength, modulus and hardness in the vulcanizates than carbonized bamboo fibre (CBF). However, at any given loading of CBF considered, these properties increased with a reduction in particle size of the filler. An increasing trend in specific gravity with increases in filler loading was observed, irrespective of the type of filler considered. However, rubber vulcanizates containing smaller particle- sized CBF exhibited higher specific gravity than those containing the larger particle-sized filler.

REFERENCES

- [1] D Daniel, I. Punyanich, N.T Quang, G. Frederic, and N. Charoen, Graft copolymers of natural rubber and poly(dimethyl(acryloyloxymethyl)phosphate) (NR-g-PDMAMP) or poly(dimethyl (methacryloyloxyethyl)phosphate) (NR-g-PDMMEP) from photo-polymerization in latex medium, European Polymer Journal, 45, 2009, 820-836.
- [2] M.S Sobby, D.E El-Nashar, and N.A Maziad, Egypt. J. Sol. 26(2), 2003, 241.
- [3] A Ahmad, D.H Mohd, and I. Abdullah, Mechanical properties of filled NR/LLDPE blends, Iranian Polymer Journal, 13(3), 2004, 173-178.
- [4] I.O Igwe and A.A Ejim, Studies on mechanical and end-use properties of natural rubber filled with snail shell powder, Materials Sciences and Application, 2, 2011, 802-810.
- [5] E Osabohien and S.H.O Egbo, Cure characteristics and physico-mechanical properties of natural rubber filled with the seed shells o cherry (chrysophyllum albidum), J. Appl. Sci. Environ. Manage, 11(2), 2007, 43-48.
- [6] P Suwatthana and P. Cattaleeya, Compatibility improvement of rice husk and bagasse ashes with natural rubber by molten state maleation, European Journal of Scientific Research, 43(3), 2010, 411-416.
- [7] P. A Egwaikhide, E.E Akporhonor, and F.E Okieimen, Effect of coconut fibre filler on the cure characteristics, physico- mechanical and swelling properties of natural rubber vulcanizates, International Journal of Physical Sciences, 2(2), 2007, 39-46.
- [8] M Jacob, S. Thomas, and K.T Varghese, Comp. Sci. Technol., 64, 2004, 955.
- [9] M Lovely, K.U Joseph, and R. Joseph, swelling behavior of isora/natural rubber composites in oils used in automobiles, bull. Mater. Sci., 29(1), 2006, 91-99.
- [10] J.B Donnet, R.C Bansal, and M.J Wang, Carbon black: Science and Technology (Marcel Dekker, NY, 1993).
- [11] M Arroyo, M.A Lopez-Manchado, and B Herrera, Organo-montmorillonite as substitute for carbon black in natural rubber compounds, Polymer, 44(8), 2003, 2447-2453.
- [12] H Ismail, H.D Rozman, R.M Jaffri, and Z.A Ishak, Oil palm wood flour reinforced epoxidized natural rubber composites: Effects of filler content and size, European Polymer Journal, 33(10-11), 1997, 1627-1632.

- [13] H Zhang, Y Wang, L Zhang, and J Yang, Preparation and processing of novel polymer materials, *Journal of Applied Polymer Science*, 97(3), 2004, 844-849.
- [14] H Osman, H Ismail, and M Mustapha, Effects of maleic anhydride polypropylene on tensile, water absorption and morphological properties of recycled newspaper filled polypropylene/natural rubber composites, *Journal of Composite Materials*, 44(12), 2010, 1477-1491.
- [15] A Ansarifar, S.F Shiah, and M Bennett, Optimizing the chemical bonding between silanized silica nanofiller and natural rubber and assessing its effects on the properties of the rubber, *International Journal of Adhesion and Adhesives*, 26(6), 2005, 454-463.
- [16] J Yang, M Tian, Q Jia, L Zhang, and X Li, Influence of graphite particle size and shape on the properties of NBR, *Journal of Applied Polymer Science*, 102(4), 2006, 4007-4015.
- [17] M Zhao and Y Xiang, Natural rubber vulcanizate reinforced by modified coalshale-based fillers, *Journal of Applied Polymer Science*, 93(3), 2004, 1397-1400.
- [18] F.E Okieimen and J.E Imanah, Characterization of agricultural waste products as fillers in natural rubber formulation, *Nig. J. Polym. Technol.*, 3(1), 2003, 201-207.
- [19] P.A Egwaikhide, E.E Akporhonor, and F.E Okieimen, An investigation on the potential of palm kernel husk as fillers in rubber reinforcement, *Middle-East Journal of Scientific Research*, 2(1), 2007, 28-32.
- [20] N Lopattananon, K Panawarangkul, K Sahakaro, and B Ellis, Performance of pineapple leaf fibre-natural rubber composites: The effect of fibre surface treatments, *Journal of Applied Polymer Science*, 102, 2006, 1974-1984.
- [21] X Lakkad and J.M Patel, *Fibre Science and Technology* (Marcel Dekker, NY, 1980).
- [22] U Stella, O.E Lawrence, M.D Ayo, Effect of carbonization temperature of filler on the tensile properties of natural rubber compounds filled with cassava (*Manihot esculenta*) peel carbon, *The Pacific Journal of Science and Technology*, 12(1), 2011, 339-343.
- [23] G.N Onyeagoro, Influence of carbonized Dika (*Irvialgia Gabonensis*) nutshell powder on the vulcanizate properties of natural rubber/acrylonitrile-butadiene rubber blend, *Academic Research International*, 2(3), 2012, 218-229.
- [24] O.O John and I.A Samuel, Potential of carbonized bagasse filler in rubber products, *Journal of Emerging Trends in Engineering and Applied Sciences*, 1(2), 2010, 157-160.
- [25] Professional Association of Natural Rubber in Africa, *Standard African Rubber (SAR) Manual*, 2, Specification and Test Methods, 1998.
- [26] Z.A.M Ishak and A.A Bakar, Investigation on the potential of rice husk ash as fillers for epoxidized natural rubber (ENR), *European Polymer Journal*, 31(3), 1995, 259-269.
- [27] M Ahmedna, M Johnson, S.J Clarke, W.E Marshal, and R.M Rao, Potential of agricultural by-product based activated carbon for use in raw sugar delolonzation, *J. Sci. Food. Agric.*, 75, 1997, 117-124.
- [28] M Ahmedna, W.E Marshal, and R.M Rao, Granular activated carbons from agricultural by-products: Preparation, properties and application in cane sugar refining, *Bulletin of Lousiana State University Agricultural Centre, Bioresource Technol.*, 71, 2000, 113-123.
- [29] V.G Geethamma, R Joseph, and S Thomas, *Journal of Applied Polymer Science*, 55, 1995, 583.
- [30] R.P Kumar, M.L Geethakumari Amma, and S Thomas, *Journal of Applied Polymer Science*, 58, 1995, 597.
- [31] N Arumugam, K Tamare, K.V Rao, *Journal of Applied Polymer Science*, 25, 1980, 795.
- [32] S Mishra and N.G Shimpi, Mechanical properties of flame-retardant properties of styrene-butadiene rubber filled with CaCO_3 as a filler and Linseed oil as an extender, *Journal of Applied Polymer Science*, 98(6), 2005, 2563-2571.
- [33] D.K Setua and S.K De, *Rubber Chemistry and Technology*, 56, 1983, 808.
- [34] S Kohjiya and Y Ikeda, *Rubber Chem. Techno*, 73, 2000, 534.
- [35] B.T Poh, H Ismail, and K.S Tan, *Polymer Testing*, 21, 2002, 801.
- [36] L Zhang, Y Wang, V Way, Y Sin, and D Yu, Morphology and mechanical properties of clay/styrene-butadiene rubber nanocomposites, *Journal of Applied Polymer Science*, 78(11), 2000, 1873-1878.

Design and Implementation of Wireless Embedded Systems at 60 GHz Millimeter-Wave for Vehicular Communication

Samiran Pramanik,¹ Nirmalendu Bikas Sinha,² R. Bera,³ C.K. Sarkar⁴

¹College of Engineering & Management, Kolaghat, K.T.P.P Township, East Midnapur, W.B, 721171, India.

²Sikkim Manipal University, Majitar, Rangpo, East Sikkim, 73713, India.

³Jadavpur University, Kolkata 700032, W.B, India.

ABSTRACT: Globally, there is a burning desire for a communication system that provides high quality, high capacity and high speed information exchange and we need to develop an extremely spectrum-efficient transmission technology for the same. This paper describes a realistic capacity and BER comparison of a robust and secured multiple access schemes and develops a wireless embedded system at 60 GHz Millimeter-Wave using WiMAX waveform. The system is tested at the laboratory with multimedia transmission and reception but yet to be tested after mounting on the vehicles. Technical expertise are developed towards Simulink programming, methods of poring to VSG, IF and millimeter wave hardware, RTSA use, Data Acquisition and DSP. With proper deployment of this 60 GHz system on vehicles, the existing commercial products for 802.11P will be required to be replaced or updated soon. Simulation and implementation of the results will elucidate that a significant amelioration in the spectral efficiency parameter can be achieved using the proposed WiMAX at 60GHz which provides both frequency diversity and spectral efficiency to yield a powerful and affordable solution for super-high speed/4G transmission and ever-increasing requirement of high throughput in wideband multimedia communications and ITS in vehicular communication.

Keywords: AWG, C2C-CC, MC-CDMA, VSA, WiMAX and WMAN, 4G.

I. INTRODUCTION

The communication and remote sensing technology are the two most important specialized sectors for electronics research today. Important developments and commercial applications are exploring those technologies. Safety and security are very important in car-to-car communication. It is even more important when wireless systems are used because it is generally perceived that wireless systems are easier to attack than wire line systems. In search of best, secured and reliable communication technology towards next generation e-car safety application, IEEE 802.16, an emerging wireless technology for deploying broadband wireless metropolitan area network (WMAN), is one the most promising wireless technology for the next-generation ubiquitous network. Though IEEE802.11P WiFi based products are commercially available for same functionality. But, disadvantages incurred in the Wi-Fi security have been addressed into the IEEE 802.16 standard and also flexibility parameters are also addressed in WiMAX. WiMAX is designed to deliver next-generation, high-speed mobile voice and data services and wireless "last-mile" backhaul connections [1]. The University of Texas at Austin. IEEE 802.16e (Mobile WiMax) deals with the Data Link Layer security. The Data-Link Layer authentication and authorization makes sure that the network is only accessed by permitted users while the encryption ensures privacy and protects traffic data from hacking or spying by unauthorized users. The WiMAX 802.16e provides number of advanced security protections including: strong traffic encryption, mutual device/user authentication, flexible key management protocol, control/management message protection, and security protocol optimizations for fast handovers when users switch between different networks. Commercial products of vehicular networks exists viz. DENSO's Wireless Safety Unit (WSU), Hitachi-Renesas.

DENSO's Wireless Safety Unit (WSU) is the follow up envelopment to DENSO's first generation 802.11p communication module, the Wave Radio Module (WRM). The WSU is a feasibility test platform for communication protocol evaluation and application prototyping. It is specifically designed for automotive environments (temperatures, shock and vibration) and has its primary focus on safety related applications. During normal driving, the equipped vehicles anonymously share relevant information such as position, speed and heading. In a C2C environment message authorization is vital. The possibility to certify attributes and bind those to certain vehicles is particularly important for public safety.

Assuming no security, his attacker could generate valid messages for and consequently disturb the whole transportation system. While unlicensed spectrum around 2.5 GHz and 5 GHz is also available internationally; the amount of available 60G bandwidth is much higher than that around 2.5GHz and 5GHz. unlicensed spectrum surrounding the 60 GHz carrier frequency has the ability to accommodate high-throughput wireless communications. It is highly directive and can be used for long and directed link. 60GHz system enjoys the size reduction and cost reduction advantages. Additionally, due to availability of 5GHz bandwidth the data-rate for communication is more interesting. Many commercial products have been developed facing these challenges. The use of 60 GHz [2]-[8] MMW (millimeter wave) based communications for road safety is complementary to the DSRC and is currently under discussion in the C2C-CC (Car to Car Communication-Consortium manifesto). Since a vehicle can communicate with other vehicles both in front and behind it, the line-of-sight (LOS) condition is used to obtain the propagation path and able to reject multipath or jitter effects. In addition, it allows vehicle drivers and passengers several real time transactions while vehicles travel at highway cruising speed.

Thus, exploring the WiMAX 802.16e for its security, reliability and high throughput features, exploring 60 GHz millimeter wave as carrier for its size and cost reduction, wide bandwidth and highest throughput, the Car2Car communication system is required to be developed for the next generation Car for safety applications. The development of

60 GHz C2C communication system comprised of two step procedure discussed below. The MATLAB/SIMULINK is used for the design verification and simulation at the 1st stage. The final simulation result in the form of *.mdl file is ported to the ARB unit of one R&S VSG for the realization of the base band hardware. The transmit IF at 1 GHz and transmit RF at 60 GHz are realized through VSG and RTSA. The above system development efforts are discussed below. Section I will discuss the necessity of multiple antennas. Section III will discuss all about WiMAX simulation at the base band level. The successful development of section III will produce one *.mdl file which is ported to the VSG for base band hardware realization. Section III will discuss the efforts pertaining to hardware development.

II. CHANNEL CAPACITIES OF MIMO MULTIPLEXING AND MULTIPLE SIMO

The channel capacity of MC-CDMA and OFDM are compared in Fig. 1 as a function of the average E_s/N_0 with the number of transmitter or receiver antenna as a parameter. Fig. 1 shows that MC-CDMA always provides higher channel capacity as compared to OFDM systems irrespective of the number of transmitter or receiver antennas. As the number of antennas increases, capacities of MC-CDMA and OFDM increase. However, the capacity difference between MC-CDMA and OFDM for a fixed SNR becomes larger. From Figure 1, it is observed that MIMO multiplexing provides lower channel capacity than SIMO in a lower E_s/N_0 region. However, the channel capacity of MIMO multiplexing increases substantially in a large E_s/N_0 region owing to the spatial diversity and multiplexing. The capacity difference between MC-CDMA and OFDM is found to be smaller for SIMO and STBC than for MIMO multiplexing. The advantage of MC-CDMA over OFDM is the frequency diversity gain obtained from frequency domain spreading. However, the frequency diversity gain becomes relatively small compared to the spatial diversity gain when SIMO or STBC-MISO is used.

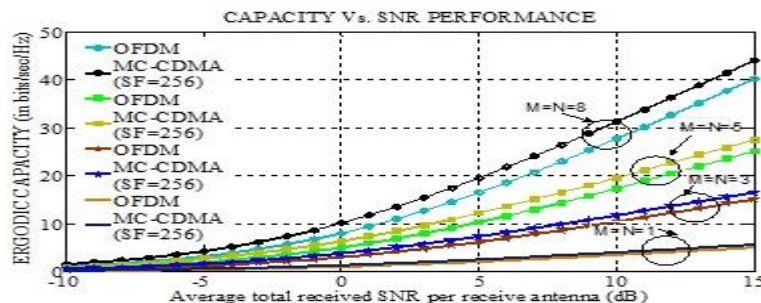


Fig. 1. Impact of number of antennas.

III. END-TO-END SIMULATION OF 60 GHZ WiMAX COMMUNICATION

The full WiMAX simulation is shown in the Fig. 2. The descriptions of some important blocks are as follows:

A. Data generator [MAC PDU] block under 'data' block:

The 802.16 standard is designed with the network and communication security keeping in considerations. Over the wireless link the robust security aspects are to be considered as the most important to control the confidentiality during data communication. In 802.16 standards, the security keys and encryption techniques are involved as shown in the Fig. 3. It has the similarity in concepts of adopting the security parameters as of IP sec. After the authorization from Security Association, the X.509 certificate, consists of an authorization key (AK), a key encryption key (KEK), and a hash message authentication code (HMAC) key, which are used for authorization, authentication, and key management [6] Here in the following model, we have 10 blocks utilized for message authentication and security management.

From the top to bottom, those blocks are: (i) HT: Header Type, (ii) EC: Encryption Control, (iii) Type: Payload Type, (iv) RSV: Reserved, (v) CI: CRC Identifier, (vi) EKS: Encryption Key Sequence, (vii) RSV: Reserved, (viii) LEN: Length of Packet, (ix) CID: Connection Identifier and (x) HCS: Header Check Sequence.

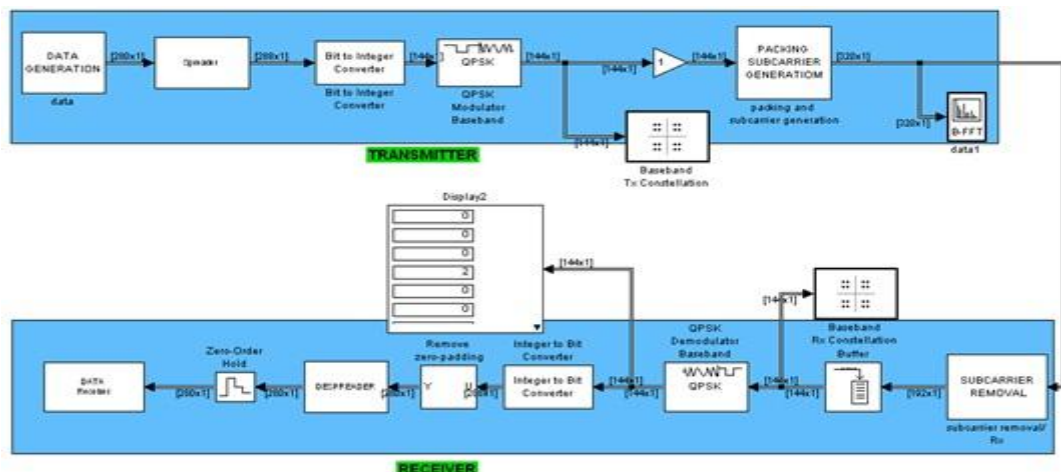


Fig. 2: The Simulink model of WiMAX transmitter and receiver.

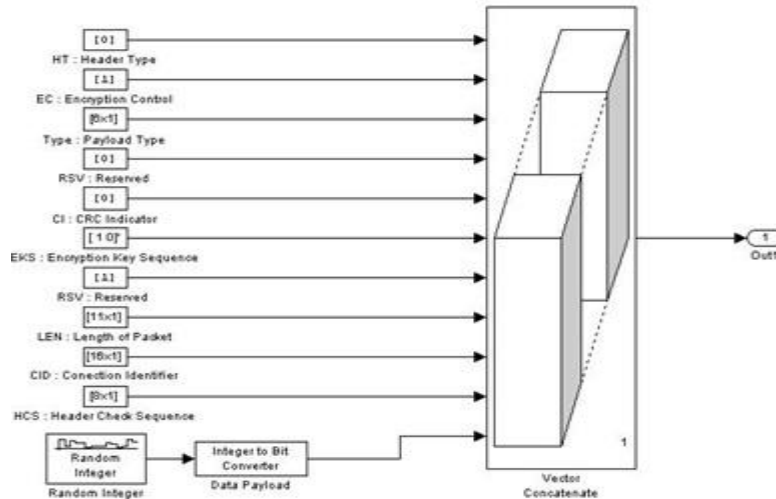


Fig. 3: The MAC PDU generator including header scheme and payload.

In terms of message authentication, there are some important shortcomings in IEEE 802.16 standard implemented at the MAC Layer. To avoid the serious threats arise from its authentication schemes, the WiMAX involves a two-way sequential transactions for controlling, authorization and authentication. During the basic and primary connection, MAC management messages are sent in plain text format which is not a robust type of authentication and so can be easily hijacked over the Air and this can be done by the attacker once again. So, as per the X.509 Certificate, the Public Key Infrastructure (PKI) defines a valid connection path to identify a genuine Security Systems. It uses RSA Encryption with SHA1 hashing. The certificate, as pre-configured by the specific manufacturer and embedded within the system must be kept secret so that it cannot be stolen by other users/vendors. A Security System that is certificated by a particular manufacturer is implemented in a Base Station (BS) and the particular BS cannot know the internal standards priory. Since, mutual authentication verifies the genuineness of a BS, it should be present in any wireless communication as it is virtually open to all. Extensible Authentication Protocol (EAP) is mostly utilized in any WiMAX Base Stations as to protect IEEE 802.16 / WiMAX against masquerading parties. Fig. 4 represents the base band spectrum. The incoming signal is XOR'd with the bit pattern generated by a PN sequence generator. This is further zero padded to increase the frame size to 288×1 . The Chip sample time is $1/1000$ S, so the chip rate is 1 KHz. The spectrum after spreading looks like as shown in the figure 8 below: The bit pattern generated after this is fed into a bit to integer converter and then to a QPSK modulator. Fig. 5 shows spectrum after spreading.

After the QPSK modulation, pilot is inserted which helps in channel estimation. Here 192×1 input stream is broken down into 10 different data pipes and pilots inserted in between them according to the above figure. All the rows of the resulting data are combined before feeding it to the IFFT block for sub carrier generation in time domain and then cyclic prefixing to add guard time.

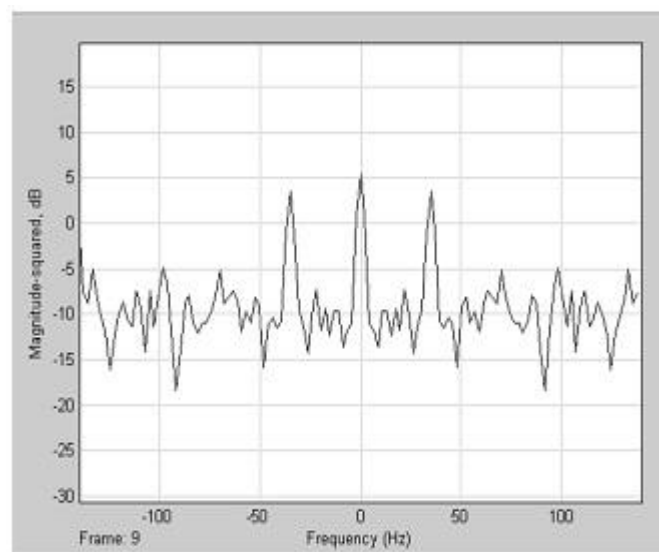


Fig. 4: Base band spectrum.

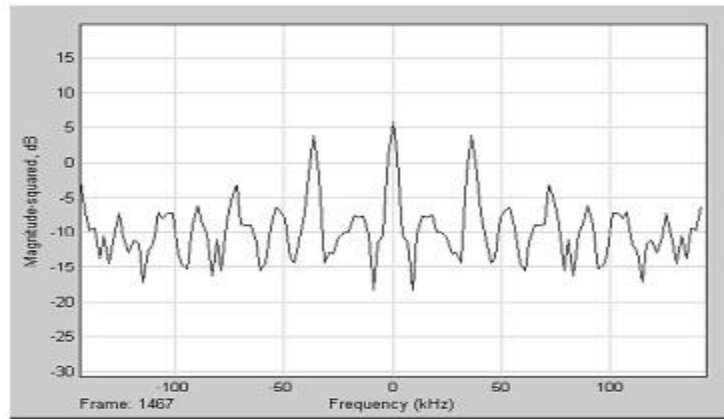


Fig. 5: Spectrum after spreading.

IV. HARDWARE IMPLEMENTATION OF THE 60 GHZ SYSTEM

The block diagram of a 60 GHz transmitter and receiver Sub System can be shown (Fig. 6) as follows.

A. Description of Transmitter Section

The prototype model of the 60 GHz transmitter is shown in Fig. 7 and Fig. 8 shows the final transmit spectrum. The PC is used to program the VSG using MATLAB/ SIMULINK for the generation of two orthogonal basis functions. In the base band section we programmed the ARB section of the VSG to generate the base band WiMAX signal and it is then up converted to IF level of 1 GHz and fed to the 60 GHz varactor tuned Gunn oscillator, which is supplied with 4.7-volt dc voltage obtained from a combination of regulated power supply and precision regulator. The basic block diagram is shown in the Fig. 9. The varactor terminal is connected with the signal to be transmitted so that the desired signal is up converted to millimeter wave by this process. The Gunn oscillator is followed by 60 GHz attenuator and frequency meter for the control and frequency measurement of 60 GHz transmitted signal respectively. The 2 feet parabolic disc antenna is connected at the output for radiation of 60 GHz signal.

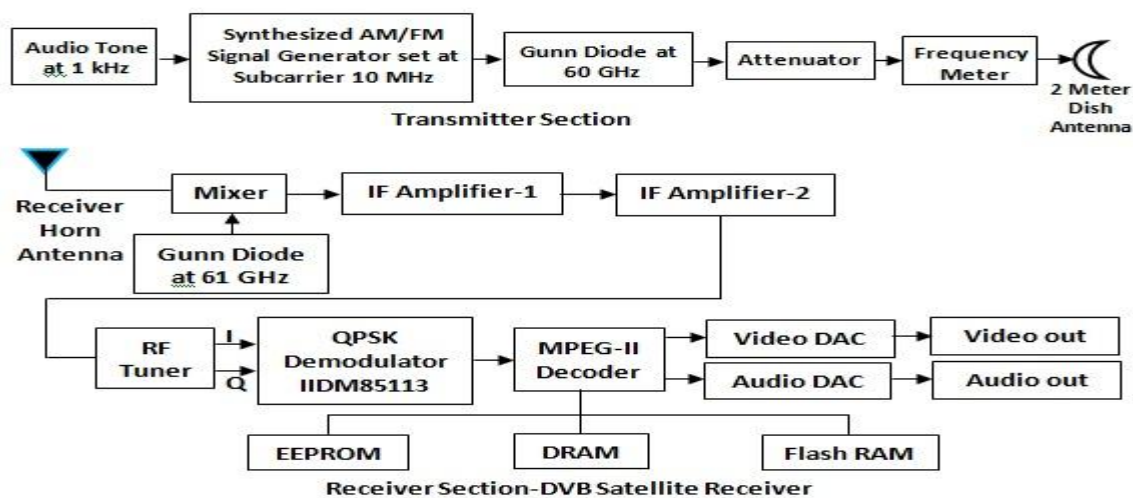


Fig. 6: Block Diagram of a 60 GHz TX-RX Sub System.



Fig. 7: The 60 GHz Transmitter.

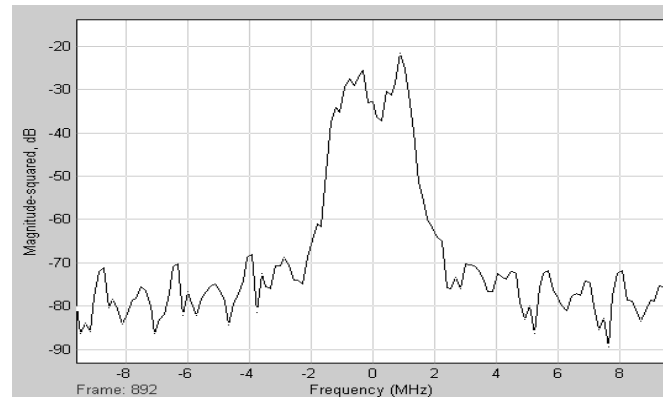


Fig. 8: The final transmit spectrum.

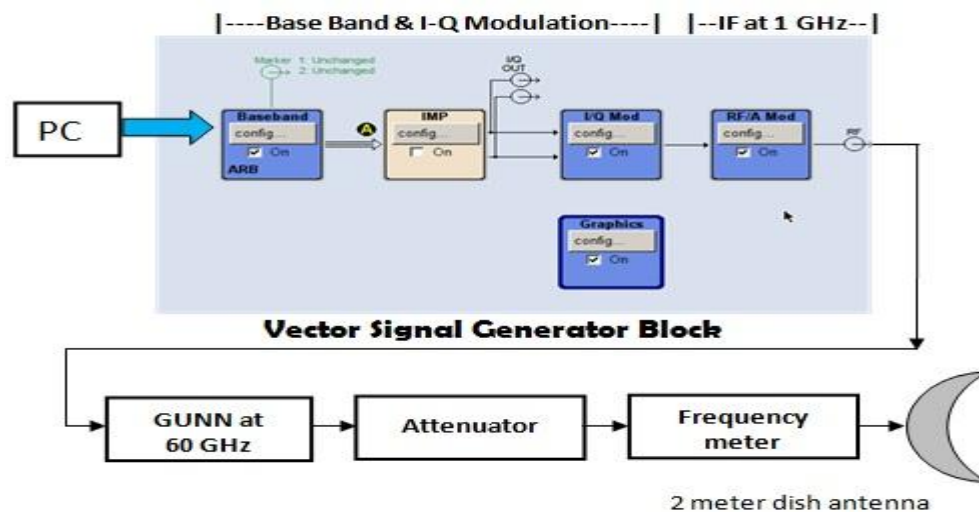


Fig. 9: Block diagram of the WiMAX Transmitter.

B. Performance Analysis of WiMAX Radio Sub System at 60 GHZ

The measurement of various parameters of the 60 GHz LOS link has been determined as follows.

C/N ratio measurement

The modulation source is switched off during this measurement and received IF spectrum having a C/N ratio of 51.89 dB is obtained as in Fig. 10. The obtained C/N ratio is greater than the (C/N) Threshold value which is around 8.4dB. The finer critical adjustment of the antenna is only possible by observing the spectrum and maximizing it and that should be at least the threshold level.

Received I/Q spectrum with/without carrier signal

The demodulated signal at the receiver is reshaped by means of a complementary square root raised cosine filter. In compliance to the filter at the transmitting end, the roll-off factor α is 0.35. This results in an acceptable level of interference with adjacent channels. The I channel spectrum at the output of the RF tuner is shown in Fig. 11. As measured, the one sided bandwidth of this spectrum is 50 MHz which dictates a maximum symbol rate per channel of 74 Ms/s. According to Nyquist criterion, the bandwidth (B) occupied by the pulse spectrum is $B = (r_s / 2)(1 + \alpha)$, in which r_s represents the symbol rate and α is the filter's roll off factor, where $\alpha = 0.35$. The data rate per channel is 148 Mbps.

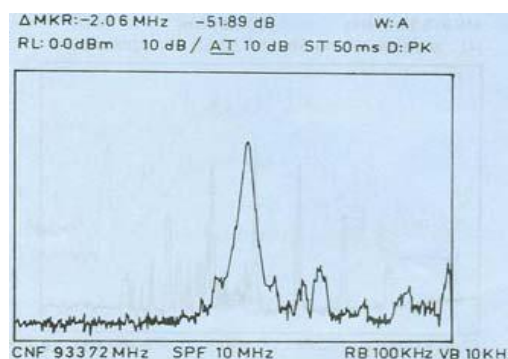


Fig. 10: C/N ratio measurement using spectrum analyzer.

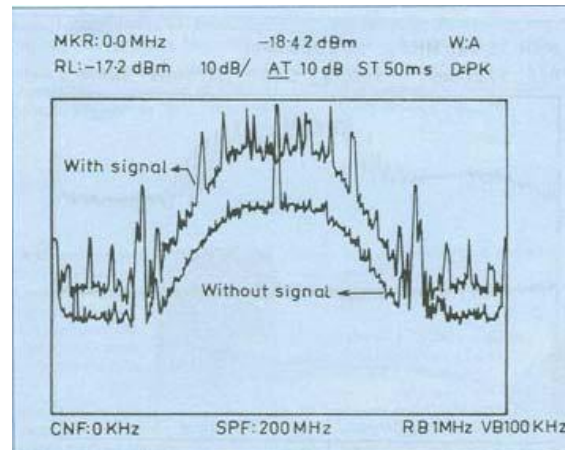


Fig. 11: Received I channel spectrum with/without signal in frequency domain.

Received I/Q waveform with/ without signal in time domain

The received I channel waveform with/without RF signal is shown in the Fig. 12.

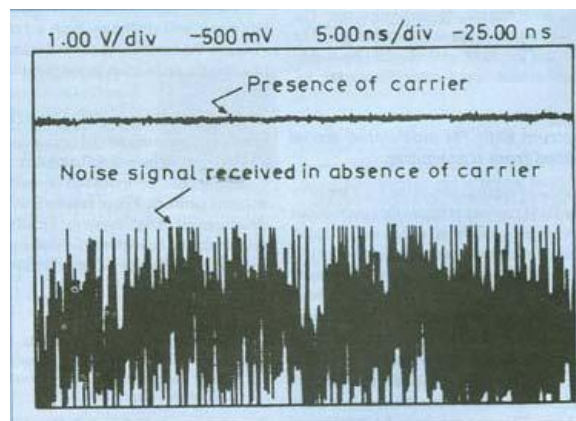


Fig. 12: Received I channel waveform with/without signal in time domain.

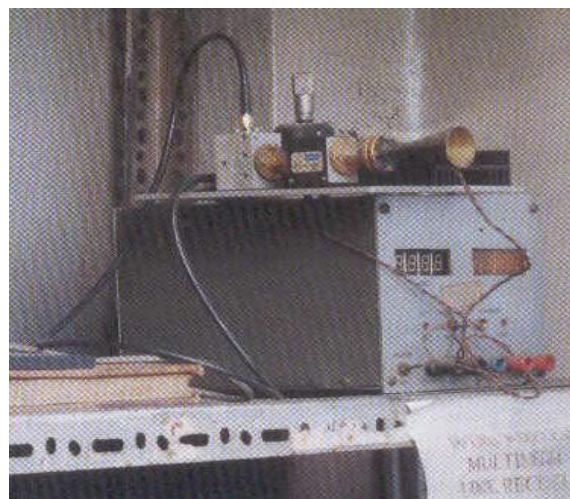


Fig. 13: The 60 GHz Received RF Front End.

C. Description of Receiver Section

The prototype model of the 60 GHz receiver is shown in Fig. 13. The block schematic diagram is shown in Figure 13 where the receiver consists of a front end, which receives signal through a horn antenna. There is another Gunn oscillator generating 61GHz frequency. These two frequencies are fed to a mixer and produces 1GHz signal at the output. This signal is further amplified by two IF amplifiers and is fed to input of the DVB satellite receiver tuner. The I-Q signal from the receiver tuner is connected to the RTSA as shown in Fig. 14. Received spectrum with bandwidth is 1.75 MHz is shown in Fig. 15. We store the received I-Q data in RTSA for further analysis, as shown in Fig. 16. The Received In-Phase and Quadrature-Phase Signals in Real Time Spectrum Analyzer is shown in Figure 16. Received WiMAX Sub-Carriers in RTSA is shown in Fig. 17.

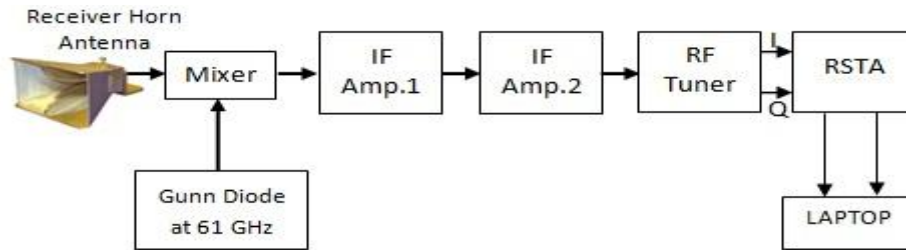


Fig. 14: Block diagram of the 60 GHz WiMAX receiver.

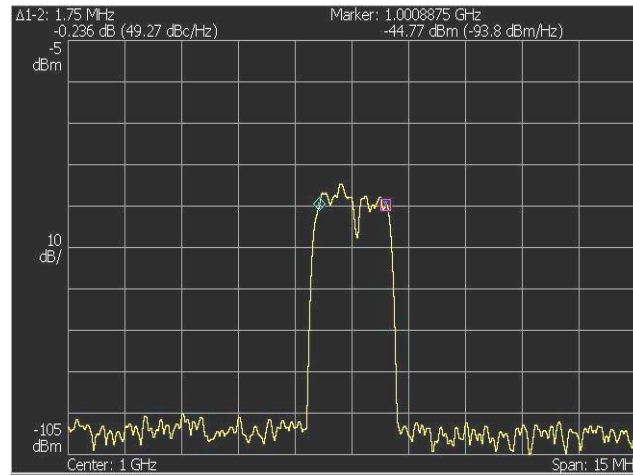


Fig. 15: Received spectrum with bandwidth is 1.75 MHz.

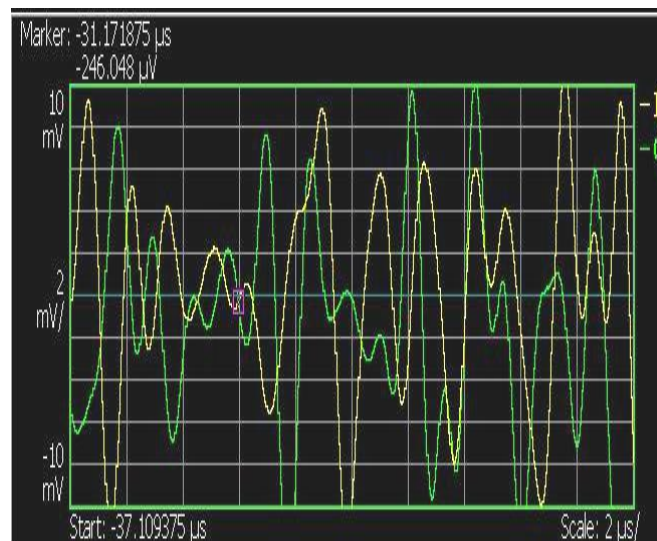


Fig. 16: Received I, Q Signals in RTSA.

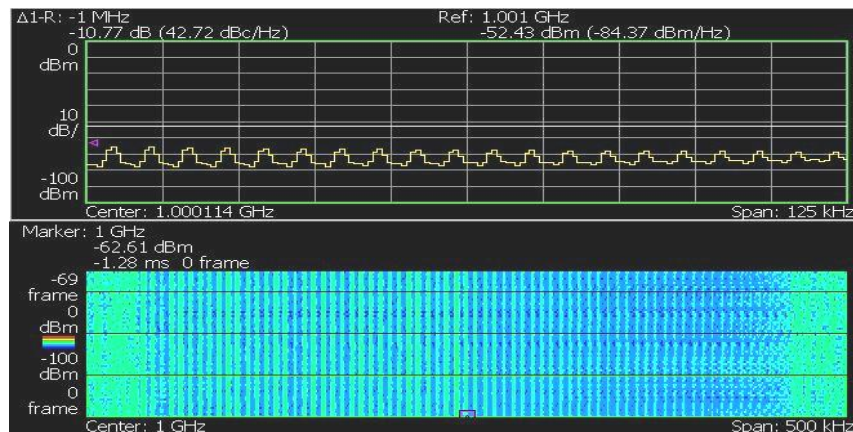


Fig. 17: Received WiMAX Sub-Carriers in RTSA.

V. CONCLUSION

In this study, we have investigated the effect of spectral efficiency of hybrid system with various traditional multiple-access communications schemes. It is then noticed that MC-CDMA - MIMO can approach the capacity of multiple SIMO while OFDM- MIMO cannot do so. Finally Wireless Embedded Systems using WiMAX waveform at 60 GHz Millimeter-Wave is being implemented using VSG and RTSA. Hardware was programmed from Work Station using MATLAB/SIMULINK for its vehicular realization. With proper deployment of this 60 GHz system on vehicles, the existing commercial products for 802.11P will be required to be replaced or updated soon and we look forward for the improved society with intelligent vehicles.

REFERENCES

- [1] Robert C. Daniels and Robert W. Heath, Jr., "60GHz Wireless Communications: Emerging Requirements and Design Recommendations", IEEE Vehicular Technology Magazine, pp.41-51, Sept.2007.
- [2] K. Mizutani and R. Kohno, "Inter-vehicle spread spectrum communication and ranging system with concatenated EOE sequence," IEEE Trans on Intelligent Transport. Syst., vol. 2, no. 4, pp. 180-191, Dec. 2001.
- [3] J. K. Hedrick, et al., "Control Issues in Automated Highway Systems", IEEE Control Systems, Vol.14, No. 6, pp.21-32, 1994.
- [4] K. Mizutani and R. Kohno, "Inter-vehicle spread spectrum communication and ranging system with concatenated EOE sequence," IEEE Trans. on Intelligent Transport System, Vol. 2, No. 4, pp. 180-191, Dec. 2001.
- [5] S. Nishikawa and H. Endo, "Application of millimeter-wave sensors in ITS," Furukawa Review, no. 18, pp.1-5, 1999.
- [6] S. Nishikawa and H. Endo, "Application of Millimeter-wave sensors in ITS," Furukawa Review, No. 18, pp. 1-5, 1999.
- [7] Bera,R. Sinha, N.B. Paul,B. Guchhait,A. Sil,S. and Dogra,S, "Wireless Embedded System for Multimedia Campus Network Utilizing IEEE 802.11N (draft) &WiMax radio", Proc. of International conference on Wireless and Optical Communication Networks (IEEE WOCN '07), Singapore, pp.1-5, 2-4 July 2007.
- [8] R. Bera, N.B.Sinha ,R. purandare,S. Sil and S. Dogra, "Wireless Multimedia Campus Networking Utilizing WiFi and WiMax Radio", International symposium of IEEE MOROCCO on Information and Communication Technologies(ICTIS-07), Fez, 3-5 April 2007.

Structural Formation & Seismicity of Kopili Fault Region in North-East India and Estimation of Its Crustal Velocity

Kashyap Mahanta,¹ Jyotirmoy Das Chowdhury,² Atowar-Ul Islam³

¹Cotton College, India,

²Jagiroad College, India

Abstract: In the North-East India region, Meghalaya plateau plays a distinct physical characteristic for its high rising granitic rocks and rocks of Gondwana character. The exposed portion of the Indian peninsular shield is evident in Meghalaya plateau and Mikir hills. Here in the plateau we mainly get Archaean gneissic complex, overlain by proterozoic intracratonic sediments of Shillong group. Upper Cretaceous and Carbonatite ultramafic complex are also evident in Kopili Fault region. The Kopili Fault, which extends from western part of Manipur up to the tri-junction of Bhutan, Arunachal Pradesh and Assam, covers a distance of about 400 km. The Kopili fault bisects the Meghalaya Plateau and isolated the Mishmi block from the main part of the plateau. The fault behaviour is studied using Global Positioning System (GPS) techniques to understand the velocity of twelve (12) different points selected on both bank of the Kopili river, since the fault is almost passing through the river. From a field study of four long years, it is observed that the Kopili Fault region is moving in North-East direction at an average velocity of 28.397N(± 1.167) mm/yr and 40.227E(± 1.184) mm/yr. This paper makes an attempt to understand the physical development or geological character of the region and its crustal velocity studied on various parts of the Kopili Fault area.

Key words: Kopili fault region, global positioning system, Meghalaya plateau, crustal velocity

I. INTRODUCTION

Studying the seismotectonic morphology of India, it evident that most of the high intensity seismic events occurred in North-Eastern part of India. North East India is one of the five most active seismic zones of the world. It lies between northern collision and eastern subduction margins of the Indian plate. Out of 5 great earthquakes experienced by India of magnitude greater than 8 in Richter Scale (R.S.), 2 occurred in this region. These are the 1897 Great Assam Earthquake and 1950 Assam Earthquake. Besides these, there are 7 events of large earthquakes of magnitude greater than 7 in R.S. occurred in this region till today. Two of them occurred in the Kopili Fault Zone making it seismically unstable. Moreover, there are hundreds of earthquake events occurring in this region signifying the tectonic importance of the fault zone (Das Chowdhury, J. 2005). These earthquakes give a clear picture of the instability of this region. Kopili Fault, which almost bisected the eastern part of massive Meghalaya plateau, also plays a dominant role in triggering earthquakes in this region.

II. THE KOPILI FAULT REGION

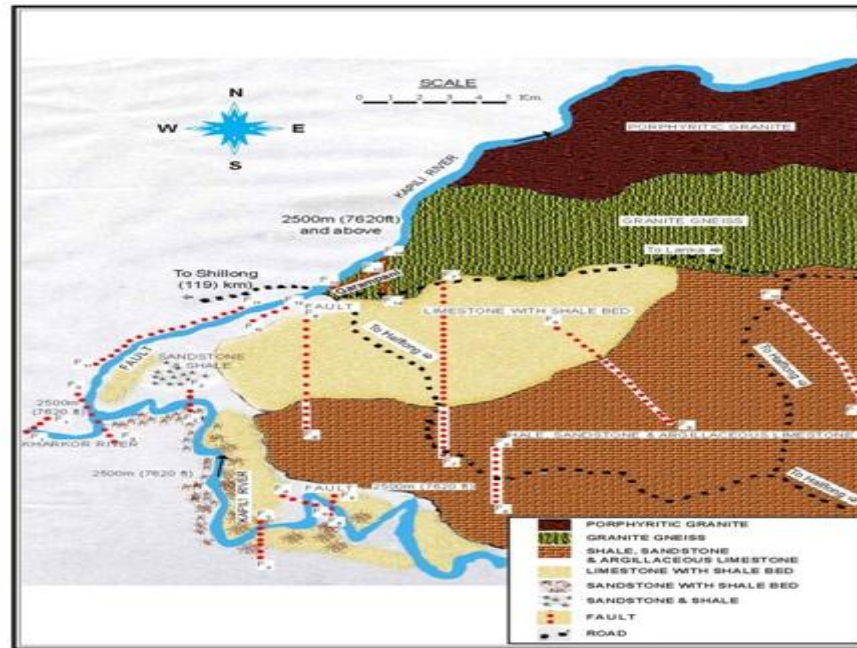
From the starting point, the Kopili River passes over various types of rocks, sands, granites in the hilly region, till it comes out into the plain. To the joining of the Kharkov River, it passes through sandstone with shale bed and argillaceous limestone. Then till Grampani, it passes through limestone with shale bed. From Grampani to Penumbra it passes through Granite gneiss and then through the porphyritic granite.

The river Kopili rises in the North Cachar Hills District in Borail Range at an altitude of 1525 meter. Then it passes through Kopili Ghat, Penumbra, Kheroni, Rajagoan, Kampur, Amsoi, Kumoi, Mayang. The river covers a vast area of North Cachar Hill, Karbi Anglong, Nagaon, and Morigaon District. It is the largest tributary of Brahmaputra on its south bank in Assam. Total length of the river from its source up to its outfall to the Kolong at Hatimukh, a spill channel of Brahmaputra, is 290 km. Total catchment area of the river up to the outfall is 16,420 sq.km. The river flows almost due north in the first 120 km through deep gorges passing over numerous rapids falls till it comes out into the plain of Nagaon district.

Along the course of the Kopili river, there are innumerable cataracts and rapids. The notable among them are the 18 meter fall (almost vertical) located nearly 200 m downstream of the Kopili - Kharkor confluence. Another major cascade with a total drop of 36 meter is visible near the downstream of the Khandong dam site across Kopili. In Panimura area also, one 12 meter notable rapid is visible.

There are many faults in the upper Kopili river region. The developments of the faults have been generally along NE-SW, NW-SE and N-S. In between the Kopili Kharkor confluence and the Garampani, two parallel faults (F_{11} - F_{11} , F_{12} - F_{12}) have been recognized. These are normal faults trending nearly NE-SW and the Kopili river is flowing on the down throw block of these two faults. The famous Garampani hot spring is located near these two faults. One km upstream of the Garampani, there is a NW-SE trending fault (F_0 - F_0) which is 18 meter long in the North-South direction crossing the confluence of the Kopili Kharkor. It gives rise to famous Yale Falls. At the upstream of the Kopili Kharkor confluences, five other normal faults (F_1 - F_1 to F_5 - F_5) trending NE-SW, N-S, NW-SE and traversing along the banks and also cutting these two rivers are recognised. Apart from these, there are many other faults recognized on the bank of the river Kopili. In Kopili Ghat (Sokra Pam) area, there are two small faults, one is N-S and other is NE-SW direction. From the right bank of the Kopili river to the East of the Halflong road there are another five big faults (F_6 - F_6 to F_{10} - F_{10}), out of which three are trending N-S, and two are NW-SE direction (Figure 1).

Figure 1: Geological map of upper Kopili Fault region



Submitted to MoES by Dr. J. Das Chowdhury on MoES Project

III. SEISMICITY IN KOPILI FAULT REGION

The Kopili Fault which extends from western part of Manipur upto the tri-junction of Bhutan, Arunachal Pradesh and Assam covers a distance of about 400km. The topography of the region is such that there is slope from SW to North and almost the whole of its higher altitude region is made up of granite and gneiss. Moreover, the Kopili fault bisects the Meghalaya Plateau and isolated the Mishmi block from the main part of the plateau.

If we analyze the history of major earthquakes in N-E India and its neighborhood we see that out of these, two major Earthquakes of magnitude more than 7 in (R.S.) were occurred in the Kopili Fault Zone. In 1869, January 10, the earthquake with magnitude 7.8 in R.S. occurred at a depth of 60 km along the Kopili Fault zone. This Earthquake has severely damaged the entire Nagaland region. In 1943, October 23, there was an earthquake with epicenter at 27.5° N 93.5° E originated along the Kopili Fault with magnitude 7.3 in R.S. It shook the whole North-East and damaged a lot. During the last 140 years, the Kopili fault has experienced 2 earthquakes of magnitude greater than 7 in R.S., three of magnitude 6 to 7 in R.S. and several of magnitude 4.5 to 6 in R.S (Das Chowdhury, J. 2002).

IV. METHODOLOGY

In this research, total number of twelve (12) campaign points in different locations of North-East India has been selected for campaign study. The first field study was initiated in October, 2006 and thereafter it was continued for four years up to February, 2011. These GPS campaign stations are studied with Trimble 5700 and Leica1200 receivers with choke ring and Zephyr geodetic antennae. The selection of twelve sites was based on hard and stable granite rocks. All the points were selected in an open area without having any disturbance to the antenna. The machines were installed in each campaign sites at least for continuous 72 hours. The machines were set to record its exact location and time in every 30 seconds. The GPS data so collected has been converted into RINEX observation files and quality check has been conducted using TEQC (Translations, Editing and Quality Checking) software. The error free data are analysed using GAMIT/GLOBK software developed by Massachusetts Institute of Technology (MIT), USA. In the processing the reference IGS (International GPS Service) stations KUNM, HYDE, IISC, POL2, and KIT3 are used.

V. RESULTS

After analysis of the data, we finally found out the East component and the North component of velocity plots in millimetre with error estimation. From the table 1, it is observed that the Kopili Fault region is moving in North-East direction at an average velocity of 28.39N (± 1.167) mm/yr and 40.22E (± 1.184) mm/yr (Table 1, figure 4). It is also observed that the North velocity component is more stable and all points are almost same except Sokra Pam (SOKR). But the East velocity is quite different. Umrangsho (UMRA), Panimuraa (PANI), Raja Gaon (RAJA) & Bura Mayang (BURA) shows less movement whereas Natun Bazar (NATU), Sokra Pam (SOKR) & Kumoi (KUMO) shows more movement. All points are moving almost parallel, except the point Sokra Pam (SOKR), Panimura (PANI) & Kumoi (KUMO) indicates something is happening in those points which force them to move in different way (figure 4). This may also take place due to the presence of local faults near those points or due to the different structural formation of the region.

Figure 2: East Component in mm

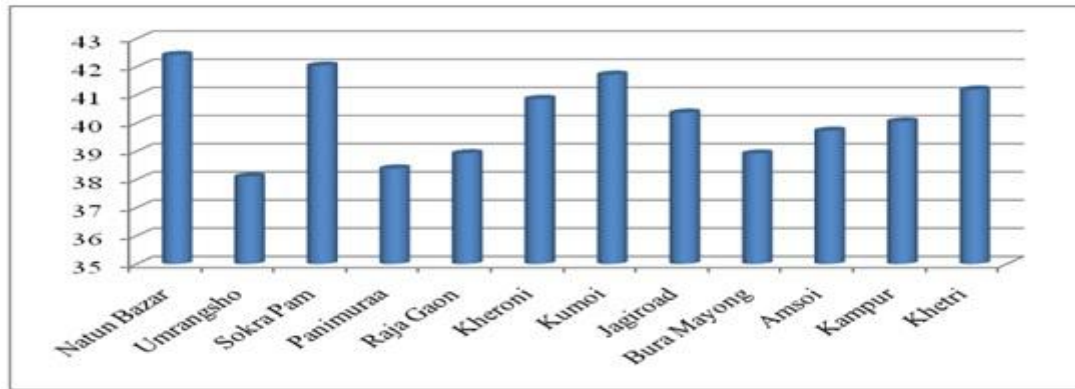
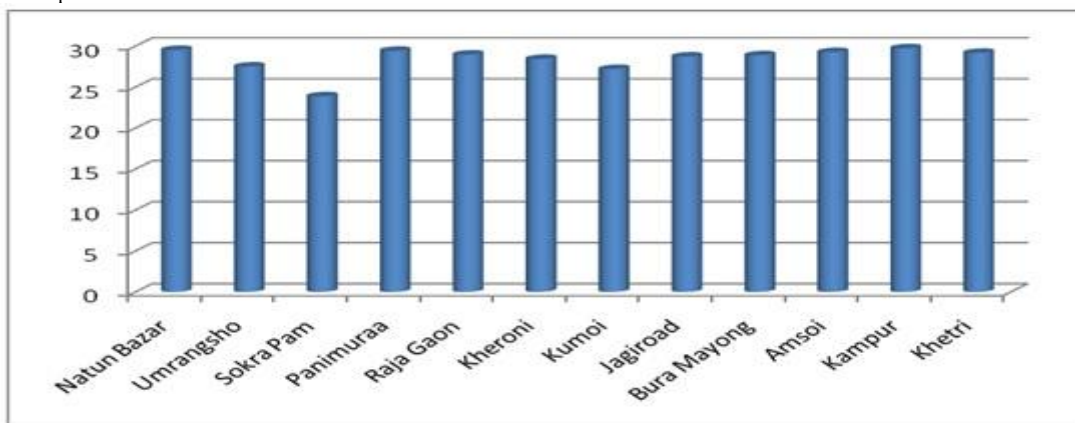


Table I: Estimated velocities of campaign sites of Kopili Fault region (using GLOBK Version 5.19)

Sl. No.	Name of the Stations	Station Code	Longitude (deg) (Final epoch)	Latitude (deg) (Final epoch)	Crustal Velocity	
					East (mm/yr)	North (mm/yr)
1	Natun Bazar	NATU	92.85725	25.81246	42.42(±1.06)	29.53(±1.06)
2	Umrangsho	UMRA	92.72512	25.52585	38.10(±.73)	27.51(±.77)
3	Sokra Pam	SOKR	92.73616	25.59636	42.04(±2.44)	23.88(±2.32)
4	Panimura	PANI	92.82508	25.71731	38.39(±.70)	29.43(±.75)
5	Raja Gaon	RAJA	92.62908	26.07280	38.93(±.73)	28.97(±.79)
6	Kheroni	KHER	92.85725	25.81246	40.86(±.67)	28.44(±.73)
7	Kumoi	KUMO	92.24822	26.19624	41.72(±.99)	27.21(±.97)
8	Jagiroad	JAGI	92.20407	26.11709	40.37(±1.04)	28.73(±1.03)
9	Bura Mayong	BURA	92.01294	26.24631	38.92(±1.30)	28.88(±1.25)
1	Amsoi	AMSO	92.48437	26.15559	39.73(±2.25)	29.27(±2.12)
1	Kampur	KAMP	92.64987	26.16261	40.06(±1.31)	29.74(±1.24)
1	Khetri	KHET	92.08036	26.12592	41.19(±.99)	29.18(±.98)
Average Velocity					40.22(±1.184)	28.39(±1.167)

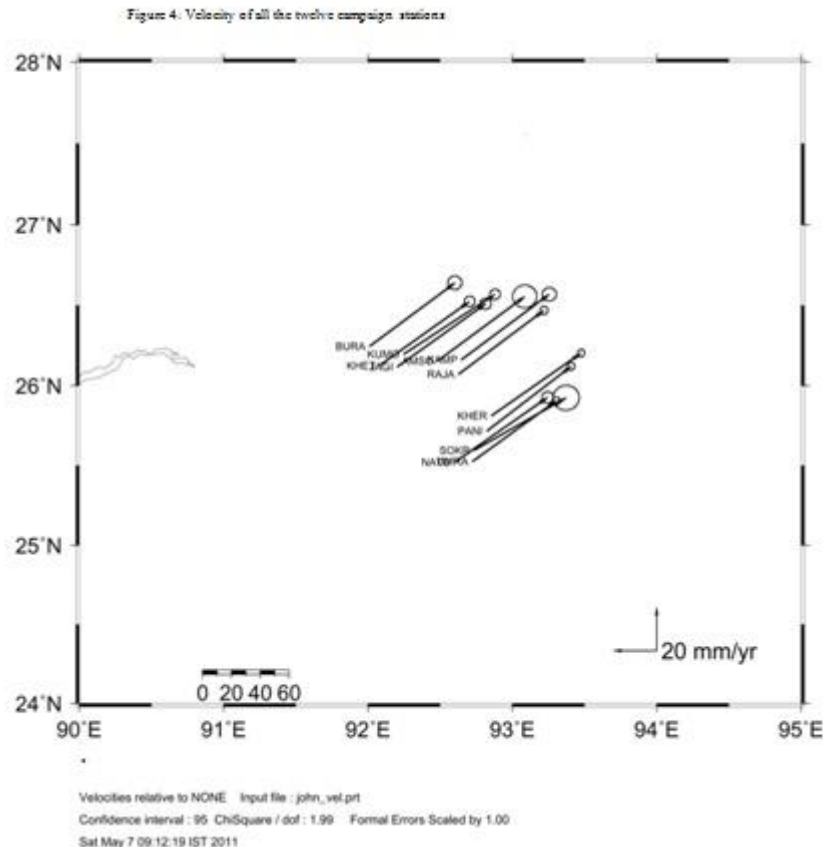
Figure 3: North Component in mm



VI. DISCUSSION AND CONCLUSION

Observing the continuous seismic activity in the Kopili Fault region, we undertook the Global Positioning System (GPS) study of that region covering the physically assumed Kopili Fault. The most scientific GPS study and its critical analysis reveal a number of unknown facts about the crustal behaviour of the selected points stretching along the bank of Kopili River.

As shown in the table above (Table 1), Natun Bazar (NATU) in Meghalaya and Sokra Pam (SOKR) in Karbi Anglong district of Assam, on the north bank of Kopili river shows highest eastward movement of 42.42 (±1.06) mm/yr and 42.04 (±2.44) mm/yr followed by Khetri (KHET) 41.72 (±0.99) mm/yr and Kumoi 41.72(±0.99) mm/yr. The result based on GAMIT/GLOBK software analysis is at par with all India velocity movement of the



Indian landmass of its average velocity of 35.28N (± 0.47) mm/yr and 41.125E (± 0.48) mm per/yr (Mahanta *et. al.*, 2012). the difference in various points of the Kopili Fault region, where occurs over 3000 mm rainfall per year is an area of extreme erosion, deposition and tectonic elevation and depression. The Kopili Fault region passes through numerous types of rocks, from new sedimentary to oldest igneous and metamorphic. The fault passes through sands and granites in the high rising areas. In some places sandstone and shale bed and argillaceous limestone formation is also evident. The granite base in the hilly region is mainly of poor pyritic granite and sedimentary layers in the Brahmaputra river valley region which extends towards the north bank of river Brahmaputra bisecting the river near Mayang in Morigaon district of Assam upto the middle Himalayan mountain. After thorough study, the paper comes to the conclusion that the North East region, more specially the Kopili Fault area is a geologically unstable region, surrounded by faults and lineaments and seduction zones in the east. The complex geo-tectonic character of the region compounded with complex geologic formation of old and new rocks play its distinct role in plate movement of the region. As no specific cause may be pin pointed for generating structural movement, the complexity in geologic formation, variations in topographic layers, severely volatile geo-dynamics and extremely high summer rainfall, all in combination played their distinct role in variations in crustal movement at various points of the Kopili Fault region.

VII. ACKNOWLEDGEMENT

We acknowledge Ministry of Earth Sciences (MoES) and Department of Science and Technology (DST), Government of India for providing funds vide project no. MoES/P.O.(Seismo)/GPS/48/2005 to Department of Geography, Jagiroad College for carrying out the GPS surveys in the North-East Region.

REFERENCES

- [1] Das Chowdhury, J.(2002): Plate Tectonics: The latest Findings, paper on National Seminar at Mongaldoi College, Assam Dt. 21st & 22nd Sept. 2002
- [2] Das Chowdhury, J.(2005): A feasibility report on "A delineation of the seismically active Kopili Fault Zone of North-East India" submitted to MoES
- [3] Mahanta, K., Das Chowdhury, J., Kumar,A., Kumar,A., Laskar,I., Singh, L.S., Barman,P. (2012): "Earthquakes and crustal deformation studies of the seismically active Kopili Fault as well as North East India: A scientific field study using Global Positioning System (GPS)"International Journal Vol. 1 No. 1, PP 127-132, February 2012, ISSN: 2277-1697
- [4] Nandy, D. R. (2001): Geodynamics of North East India and the adjoining region; abc publications, Kolkata

A Single Phase Eleven Level Cascaded H-Bridge Multilevel Inverter for Photovoltaic Systems Using Multicarrier Pwm

M.S.Sivagamasundari,¹ P.Melba Mary²

¹(Assistant Professor, Department of EEE, V V College of Engineering, Tamilnadu, INDIA)

² (Principal, Department of EEE, V V College of Engineering, Tamilnadu, INDIA)

Abstract: A Cascaded H-Bridge Multilevel Inverter is a power electronic converter built to synthesize a desired ac voltage from several levels of dc voltages with better harmonic spectrum. Such inverters are suitable for high voltage and high power applications and have been an important development in recent years. This paper presents the performance of a eleven level cascaded H-Bridge multilevel inverter topology with multicarrier pulse width modulation technique for photovoltaic cell. This inverter is capable of producing eleven levels of output voltage from the dc supply voltage. This topology magnifies the fundamental output voltage with reduction in total harmonic distortion. The output is drawn near the sine wave because of more levels. It can also be easily extended to an m-level inverter. The performance of the proposed PWM strategy in terms of output voltage and THD is shown using MATLAB/Simulink.

Keywords: Multilevel inverter, Cascaded H-Bridge multilevel inverter, Multicarrier pulse width modulation, PV cell, Total harmonic distortion.

I. INTRODUCTION

Renewable energy is a challenging aspect for now and future of the world's increasing energy demand. Since last three Decades, there is a growing effort to make renewable energy more feasible due to its particular characteristics and high costs.

Among renewable energy sources, photovoltaic energy is one of the most considerable sources because of its advantages like being widely available and cost free, clean and abundant.

Furthermore, being a semiconductor device it is free of moving parts which results little operation and maintenance costs [1]. PV cell is especially attractive for applications in where sunshine is available for most of the time. Such a system generates electricity by converting the Sun's energy directly into electricity. [2].

Power switches with the suitable switching frequency at ratings above 5kV are rare; hence it is difficult to achieve inverter output voltage which is compatible to the medium voltage grid. One approach is to utilize the MLI structure. Multilevel inverter is an array of power semiconductor switches and voltage sources which is switched in a manner that an output voltage of stepped waveform is generated. Several multilevel topologies have evolved: most common are the diode-clamped inverter (neutral-point clamped), capacitor-clamped(flying capacitor) requiring only one dc source and the cascaded bridge inverter requiring separate dc sources.[3]. The latter characteristic, which is a drawback when a single dc source is available, becomes a very attractive feature in the case of PV systems, because solar cells can be assembled in a number of separate generators. In this way, they satisfy the requirements of the Cascaded H-Bridge multilevel inverter, obtaining additional advantages such as a possible elimination of the dc/dc booster (needed in order to adapt voltage levels), a significant reduction of the power drops caused by sun darkening (usually, it influences only a fraction of the overall PV field), and, therefore, a potential increase of efficiency and reliability [4].

Performance of the multilevel inverter (such as switching loss and THD) is mainly decided by the modulation strategies. For the cascaded multilevel inverter there are several well known pulse width modulation strategies. [5].

Compared to the conventional method, the proposed method is subjected to a new modulation scheme adopting the multicarrier pulse width modulation concept which uses multiple modulating signals with a single carrier reduces the total harmonic distortion and switching losses. In this paper, a PV array is connected to eleven level cascaded H-bridge multilevel inverter to achieve sinusoidal output voltage waveforms and the simulation results are shown.

II. MATHEMATICAL MODEL OF THE PV ARRAY

2.1. Equivalent model

A Photovoltaic cell is a device used to convert solar radiation directly into electricity. It consists of two or more thin layers of semiconducting material, most commonly silicon. When the silicon is exposed to light, electrical charges are generated. A PV cell is usually represented by an electrical equivalent one-diode model shown in fig.1.

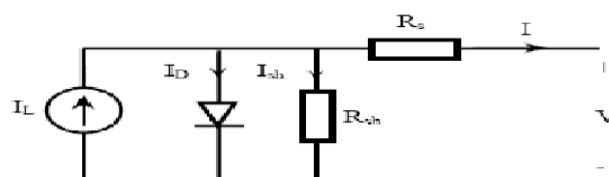


Fig. 1. Single PV cell model

The model contains a current source, one diode, internal shunt resistance and a series resistance which represents the resistance inside each cell. The net current is the difference between the photo current and the normal diode current which is given by the equation.

$$I_D = I_0 \left[e^{\frac{q(V+I R_s)}{K T}} - 1 \right] \quad \dots\dots\dots (1)$$

$$I = I_L - I_0 \left[e^{\frac{q(V+I R_s)}{K T}} - 1 \right] - \frac{V+I R_s}{R_{sh}} \quad \dots\dots\dots (2)$$

Where

I is the cell current (A).

q is the charge of electron (coul).

K is the Boltzmann's constant (j/K).

T is the cell temperature (K).

I_L is the photo current (A).

I_0 is the diode saturation current.(A)

R_s , R_{sh} are cell series and shunt resistances (ohms).

V is the cell output voltage (V).

2.2. Current – Voltage Curve for PV cell

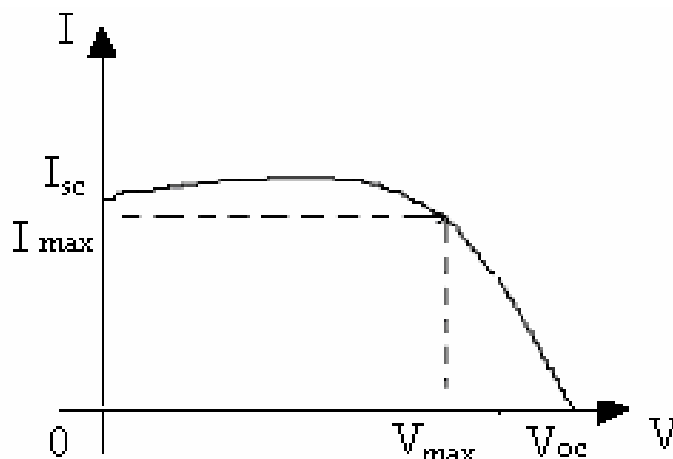


Fig.2.Current – Voltage curve

The Current – Voltage characteristic curve of a PV cell for a certain irradiance at a fixed cell temperature is shown in fig.2. The current from a PV cell depends on the external voltage applied and the amount of sunlight on the cell. When the PV cell circuit is short, the current is at maximum and the voltage across the cell is zero. When the PV cell circuit is open, the voltage is at maximum and the current is zero.

2.3. Power – Voltage Curve for PV cell

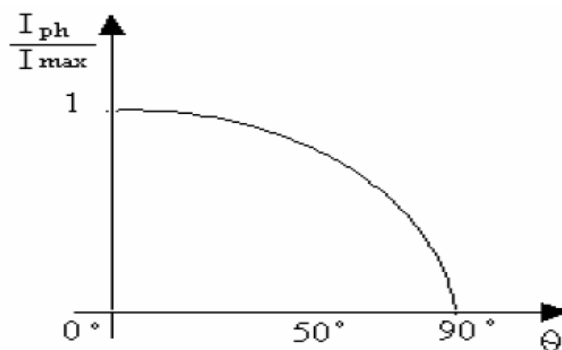


Fig.3.Power – Voltage curve

The Power – Voltage curve for PV cell is shown in fig.3. Here P is the power extracted from the PV array and V is the voltage across the terminals of the PV array. This curve varies due to the current insolation and temperature. When insolation increases, the power available from PV array increases whereas when temperature increases the power available from PV array decreases.[5].

2.3. Variation in Available Energy due to Sun's Incident Angle

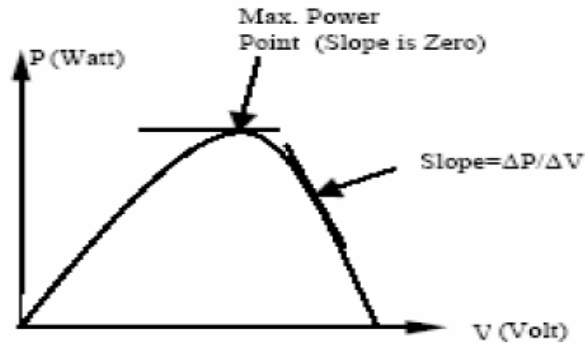


Fig.4. Variation in Available Energy due to Sun's

Incident Angle PV cell output with respect to sun's angle of incidence is approximated by cosines function at sun angles from 0° to 50°. Beyond the incident angle of 50° the available solar energy falls off rapidly as shown in the fig.4. Therefore it is convenient and sufficient within the normal operating range to model the fluctuations in photo current versus incident angle is given by Eq (3).[5].

$$I_{ph} = I_{max} \cos \theta$$

..... (3)

III. CASCADED H-BRIDGE MULTILEVEL INVERTER TOPOLOGY

A single-phase structure of an m-level cascaded inverter is illustrated in Figure.5. Each separate dc source is connected to a single-phase full bridge, or H-bridge, inverter. Each inverter level can generate three different voltage outputs, $+V_{dc}$, 0, and $-V_{dc}$ by connecting the dc source to the ac output by different combinations of the four switches, S_1 , S_2 , S_3 , and S_4 . To obtain $+V_{dc}$, switches S_1 and S_4 are turned on, whereas $-V_{dc}$ can be obtained by turning on switches S_2 and S_3 . By turning on S_1 and S_2 or S_3 and S_4 , the output voltage is 0. The ac outputs of each of the different full-bridge inverter levels are connected in series such that the synthesized voltage waveform is the sum of the inverter outputs. The number of output phase voltage levels m in a cascade inverter is defined by $m = 2s + 1$, where s is the number of separate dc sources.

An example phase voltage waveform for an 11-level cascaded H-bridge inverter with 5 SDCSs and 5 full bridges is shown in Figure.6. The phase voltage $v_{an} = v_{a1} + v_{a2} + v_{a3} + v_{a4} + v_{a5}$.

The Fourier Transform for a stepped waveform such as the one depicted in Figure 6 with s steps is as follows [6]:

$$V(\omega t) = \left(\frac{4V_{dc}}{\pi} \right) \sum [\cos(n\theta_1) + \cos(n\theta_2) + \dots] \quad \text{where } n = 1, 3, 5, 7, \dots (4)$$

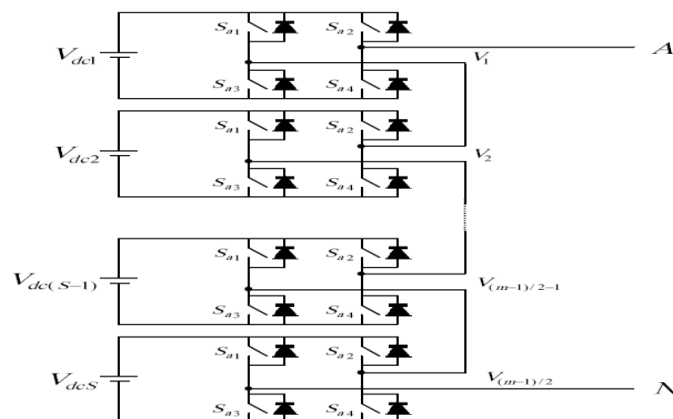


Fig.5.Single-phase structure of an m level cascaded H-bridge multilevel inverter

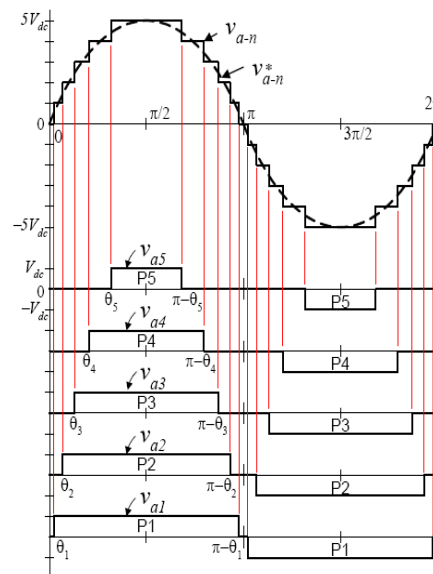


Fig.6.Output voltage waveform of an 11-level cascade inverter

The conducting angles, $\theta_1, \theta_2, \dots, \theta_5$, can be chosen such that the voltage total harmonic distortion is minimum. Generally, these angles are chosen such that predominant lower frequency harmonics 5th, 7th, 11th, and 13th harmonics are eliminated. [7].

IV. MULTICARRIER PWM TECHNIQUE

The Multicarrier PWM technique was introduced and uses several triangular carrier signals and only one modulating sinusoidal signal as reference wave to generate the PWM switching signals. If an 'n' level inverter is employed, 'n-1' carriers will be needed. At every instant each carrier is compared with the modulating signal. Each comparison gives one if the modulating signal is greater than the triangular carrier, zero otherwise. The results are added to give the voltage level, which is required at the output terminal of the inverter. [8].

Frequency modulation ratio is defined as the ratio of carrier frequency and modulating frequency.

$$M_f = f_c / f_m \quad \dots\dots\dots (5)$$

Amplitude modulation ratio is defined as the ratio of amplitude of modulating signal and amplitude of carrier signal.

$$M_a = \frac{A_m}{A_c} \quad \dots\dots\dots (6)$$

Using this technique THD value can be reduced.

V. PROPOSED TOPOLOGY

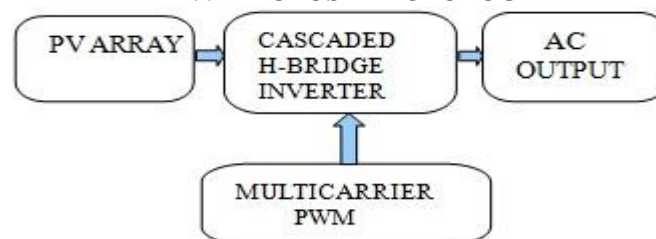


Fig.7.Block diagram of the proposed multilevel inverter

Fig.7. shows the block diagram of the proposed multilevel inverter. The PV array which is connected to the Cascaded H-Bridge Multilevel inverter converts sunlight directly into DC power. Cascaded H-Bridge multilevel inverter converts DC power into AC power for AC load and it is controlled by multicarrier PWM technique.

The Proposed Cascaded Multilevel Inverter is simply a number of conventional five-level bridges, whose AC terminals are simply connected in series to synthesize a five level square wave output voltage waveform. The circuit needs independent dc source which is supplied from photovoltaic cell. Fig.8. shows the power circuit for a single phase eleven level cascaded H-bridge inverter and the cascaded output is shown in fig.9.

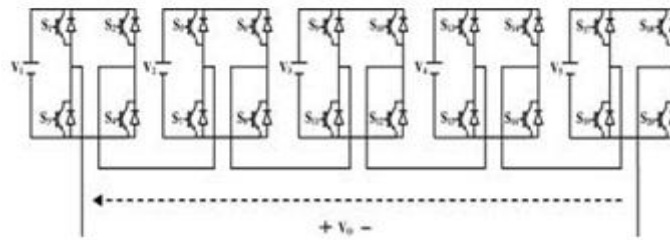


Fig.8. Proposed power circuit for an eleven-level inverter

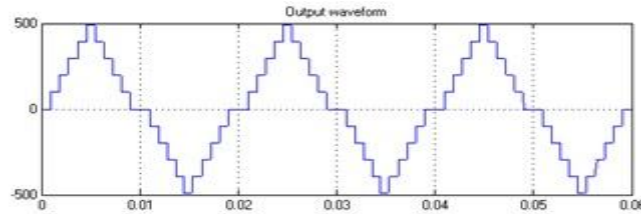


Fig.9. Output voltage waveform of an eleven level inverter

The switching angles of the waveform will be adjusted to obtain the lowest output voltage THD. Harmonics are disagreeable in current or voltage waveform. They exist at some fraction or multiple of the fundamental frequency. The harmonics order and magnitude are depending upon the type of inverter and the control techniques for example in single phase VSI, the output voltage waveform typically consists only of odd harmonics. The even harmonics are not existing due to the half wave symmetry of the output voltage harmonics. [9].

In this paper, the simulation model is developed using MATLAB/Simulink. The SIMULINK model for the power circuit is shown in figures.10.1, 10.2, 10.3 & 10.4.

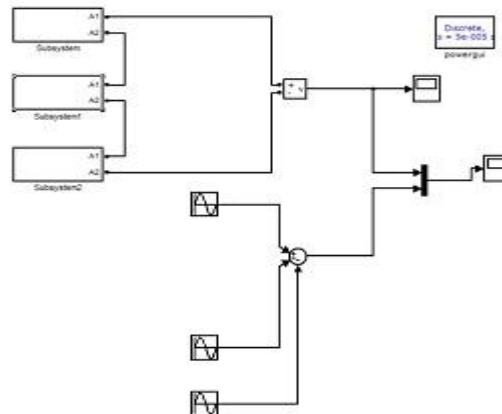


Fig.10.1. Simulation circuit of the proposed method

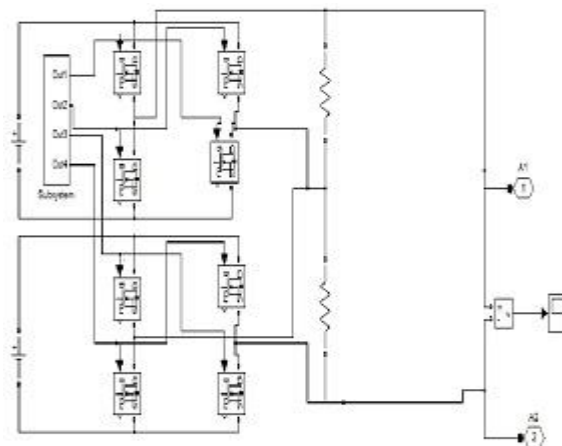


Fig.10.2. Sub circuit

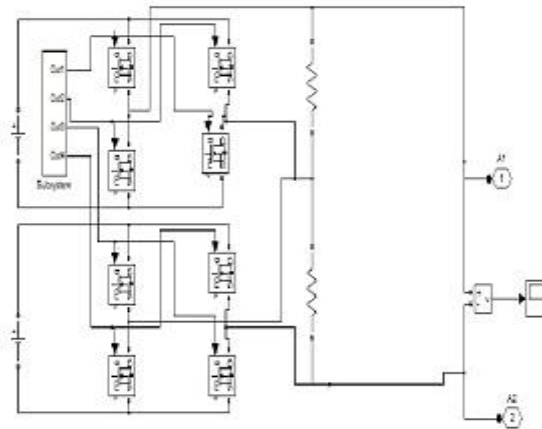


Fig.10.3.Sub circuit 1

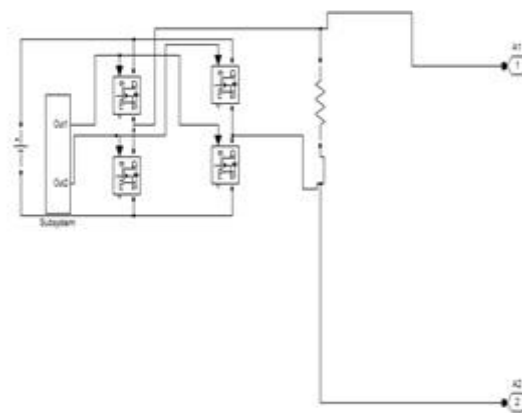


Fig.10.4.Sub circuit 2

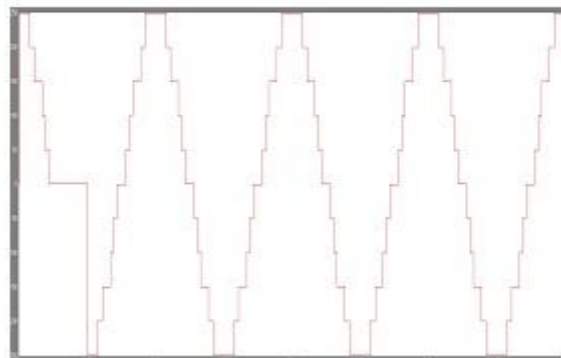


Fig.11.Output voltage waveform of the proposed method

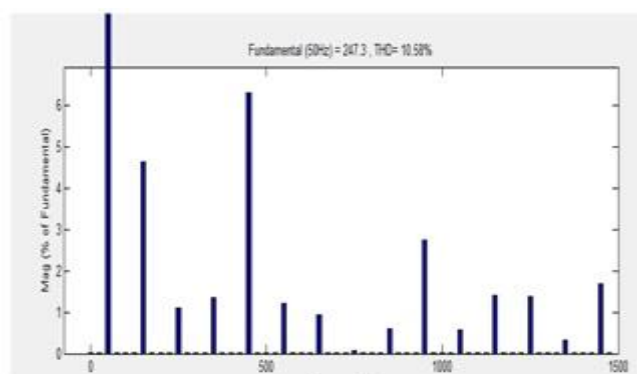


Fig.12.Harmonic spectrum

Fig.11.and Fig.12.shows the simulation results of output voltage and current harmonics spectrum waveforms respectively.

VI. CONCLUSION

In this work , a Photovoltaic cell based eleven level Cascaded H-bridge Inverter employing multicarrier pulse width modulation technique is developed which enhances the fundamental output voltage and hence reduces the total harmonic distortion to 10.58% compared to the conventional method .The operation and performance of the proposed multilevel inverter is verified through MATLAB/SIMULINK. It can be also shown for any number of phases or levels.

REFERENCES

- [1] H. L. Tsai, C. S. Tu, Y.J. Su, "Development of generalized photovoltaic model using MATLAB/SIMULINK", Proceedings of the World Congress on Engineering and Computer Science (WCECS), San Francisco, CA, 2008.
- [2] K.Surya Suresh, M.Vishnu Prasad,"PV Cell Based Five Level Inverter Using Multicarrier PWM "International Journal of Modern Engineering Research, Vol.1, Issue.2, pp-545-551.
- [3] Jae-hyun Jeon, Tae-Jin Kim, Dae-wook Kang, and Dong-seok Hyun, A Symmetric Carrier Technique of CRPWM for Voltage Balance Method of Flying Capacitor Multi-level Inverter, IEEE Transactions on Industrial Electronics, Vol.52 , No. 3, June 2005, pp. 2759-2763.
- [4] Elena Villanueva, Pablo Correa, José Rodriguez, and Mario Pacas, "Control of a Single-Phase Cascaded H- Bridge Multilevel Inverter for Grid-Connected Photovoltaic Systems",IEEE Transactions on Industrial Electronics, Vol. 56, No. 11, Nov. 2009.
- [5] L. M. Tolbert, F. Z. Peng, T. G. Habetler, "Multilevel converters for large electric drives," IEEE Transactions on Industry Applications, vol. 35, no. 1, Jan./Feb. 1999, pp. 36-44.
- [6] L. M. Tolbert, F. Z. Peng, T. G. Habetler, "Multilevel Inverters for Electric Vehicle Applications," IEEE Workshop on Power Electronics in Transportation, Oct 22-23, 1998, Dearborn, Michigan, pp. 1424-1431.
- [7] R.W.Menzies, Y. Zhuang, "Advanced Static Compensation Using a Multilevel GTO Thyristor Inverter," IEEE Transactions on Power Delivery, vol. 10, no. 2, April 1995, pp. 732-738.
- [8] R.Seyezhai, Dr.B.L.Mathur," Performance evaluation of inverted sine PWM technique for an asymmetric cascaded multilevel inverter" Journal of Theoretical and Applied Information Technology, 2009, pp.91-98.
- [9] M.Balachandran, P.Senthilkumar, and N.P. Subramaniam,"Performance Evaluation of a Cascaded Multilevel Inverter with a Single DC Source using ISCPWM"International Journal of Electrical Engineering, Volume 5, Number 1 (2012), pp. 49-60.
- [10] Nasr din A. Rahim, Krishnamadina Chaniagoand Jeyraj Selvaraj,"Single-Phase Seven-Level Grid-Connected Inverter for Photovoltaic System," IEEE Transactions on Industrial Electronics, June 2011.
- [11] Carlo Cecati, Fabrizio Cianetta, and Pierluigi Siano, "A Multilevel Inverter for Photovoltaic Systems with Fuzzy Logic Control" IEEE Transactions on Industrial Electronics, Vol. 57, No. 12,pp 4115-4124 Dec. 2010.
- [12] Thanuj Kumar. Jala, G. Srinivasa Rao, "A Novel Nine Level Grid-Connected Inverter for Photovoltaic System" International Journal of Modern Engineering Research, Vol.2, Issue.2, Mar-Apr 2012 pp-154-159.
- [13] Philip T.Krein ,Robert S.Balog and Xin Geng,"High-Frequency Link Inverter for fuel cells Based on Multiple Carrier PWM", IEEE Transactions on Power Electronics, Vol 19, NO.5, Sep 2004.
- [14] G.Carrara, S.Gardella, M.Marchesoni, R.salutari,and Gsciutto, "A New Multilevel PWM Method; A theoretical analysis", IEEE Trans. Power. Electron. vol.7, no.3, pp.497-505. Jul.1992.
- [15] A.M Hava, R.JKerman, and T.A Lipo, "Carrier-based PWM-VSI Over modulation Strategies: Analysis, Comparison, and Design," IEEE Trans. Power. Electron., vol.13, no.4, pp.674-689. Jul.1998.
- [16] B.P.McGrath and Holmes, "Multicarrier PWM strategies for multilevel inverter," IEEE Trans.Ind.Electron., vol.49, no.4, pp.858-867. Aug.2002.
- [17] Multilevel Power Converters book chapter by Surin Khomfoi and Leon M. Tolbert pp31.1-31.14

Design and Development of Turmeric Polishing Machine

S.M.Moghe,¹ K.S.Zakiuddin,² V.G.Arajpure³

^{1,3} (Department of Mechanical engineering, B.D.C.O.E.Sevagram RTMN University, Wardha, Maharastra, India)

² (Department of Mechanical engineering, PCE RTMN University, Nagpur, Maharastra, India)

Abstract: Polishing of harvested turmeric is a bigger problem for the turmeric producers in an India. The customer is in need of high quality polished turmeric for making turmeric powder. In this regard there is a need of polishing machine for washing turmeric to remove unwanted impurities and scales of harvested turmeric. The paper presents the new design of turmeric polishing machine which is based on designed for manufacturing, assembly and maintenance. The phenomenon of abrasion used in polishing, which is caused by the friction between expanded wired metal mesh and turmeric. The scale and unwanted impurities are fallen down on the base easily, which seems to be quite difficult in hand polishing. The designed machine is very simple in operation, efficient in polishing of harvested turmeric at a good speed of production. This machine seems very simple at same time very efficient in polishing about 50 kg of harvested turmeric at a speed about of 75 rpm for about 20 min.

Keywords: Turmeric polishing machine,

I. Introduction

India is a agriculture oriented country, agriculture is the prime business of India and so we aim to help the farmers by designing a mechanical device empowered width the capacity of polishing one of the important spice of India "The Turmeric". Turmeric is very important spice in India, which produces nearly entire whole world's crop and consumes 80% of it. India is by far the largest producer and exporter of turmeric in the world. Turmeric occupies about 6% of the total area under spices and condiments in India. As World scenario, Turmeric is also cultivated in China, Myanmar, Nigeria and Bangladesh. However, authentic figures about area and production are not available. Major area is in India which constitutes 82% followed by China (8%), Myanmar (4%), Nigeria (3%) and Bangladesh (3%).

Turmeric plays a very important role in increasing the taste of spicy Indian foods; also it is having a great role in medicinal product making. As the harvested turmeric product is surrounded by the mud and the other unexpected waste it was the prime need to polish the harvested turmeric and very there comes the idea of developing a machine which would meet such requirements. And that's because we thought of developing such a machine.

Table 1 Physical properties of turmeric

Physical property	Primary finger, raw		Primary finger, dried	
	Range	Average value	Range	Average value
Length, cm	8.94-9.55	9.25	5.15-7.50	6.3
Diameter, cm	1.47-1.69	1.58	1.0-1.4	1.2
Bulk density, kg/m ³	678-710	694	470-496	483
True density, kg/m ³	1,295-1,317	1,306	1,136-1,164	1,150
Porosity, %	46-47	46.5	57-58	57.5
Angle of repose, °	30-32	31	35-37	35-37

II. Need of Development of Machine

The need to develop such type of machine is raise due to the following reasons:-

Turmeric needs to be polished and cleaned before 48 hours after harvesting to avoid loss in its nutrient values since it is not every time possible to have this much man power to enable hand polishing ,machine polishing was required.

Machine polishing enables greater and furnished quality of turmeric which may or may not be possible in hand polishing.

There are some where drums are used but this development in the machine can provide simple and easier to operate whose working would be easily understood by the local farmers. This development tries to make machine smaller and compact so that space constrain should be satisfied also employ a gear pair to run the machine under power cut conditions which is being run by motor in normal conditions so that power cut would not hamper the production capacity.

III. Basic Concept of the Machine



Figure 2. Turmeric polishing machine

Turmeric rhizomes can be mechanically washed as well as polished in a portable, electric power operated, rotary drum type turmeric washing and polishing machine. The machine when operated at optimum rotational speed for optimum time can wash 50 kg of turmeric rhizomes. At optimum performance parameters, i.e. 75 rpm for 15-20 min. there is no bruising of turmeric rhizomes. The same machine can be used for polishing turmeric with some modification.

To increase the friction, three detachable perforated screens (0.91mm) of G.I. steels are attached along the inner periphery of the drum with abrasive surface on the inner side. The capacity of turmeric polishing machine is 50kg. The optimum performance parameters for polishing are 75 rpm for 15-20 min. at which the desirable olive yellow color is obtained and the surface becomes smooth. The microbiological quality of turmeric rhizomes is also improved by polishing because the surface microbial load is reduced to half.

IV. Mechanical Design of the Machine

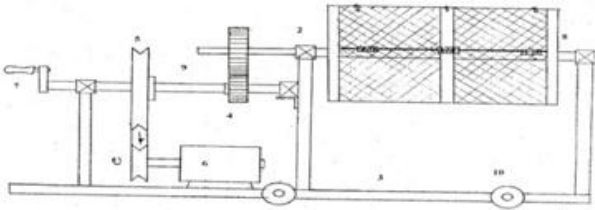


Figure 2 Conceptual design of turmeric polishing machine

Nomenclature:-

1 Drum (Expanded Metal Mesh) with door, 2 Bearing, 3 Base, 4 Gear Drive, 5 Pulley Arrangement, 6 Motor, Handle, 8, 9 Counter shaft, 10 Roller for movement.

4.1 Design of Shaft:-

The diameter of shaft was determined on the basis of formula proposed by Sharma and Aggrawal (1998)

$$\text{Maximum shear stress} = \frac{16 \times 103 / \pi \times d^3}{\sqrt{M^2 + Td^2}} \quad (1)$$

τ_{\max} allowable shear stress is 88.8 N/mm² as per ASME code, Maximum torque founded for the rated power 0.745 kw at a speed of 75rpm, there is gear mounted on the shaft 8 as in fig 2 which has 336 PCD and 30 N its weight. By considering gear weight and 50 Kg of turmeric i.e. 490 N. As shown in fig 5 Maximum bending moment obtained at point C. From equation (1) diameter of shaft was determined 20mm.

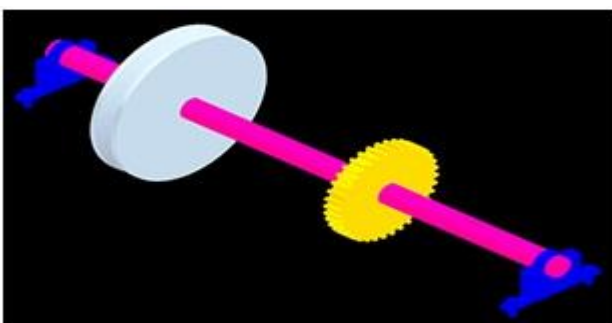


Figure 3. Main shaft (8)

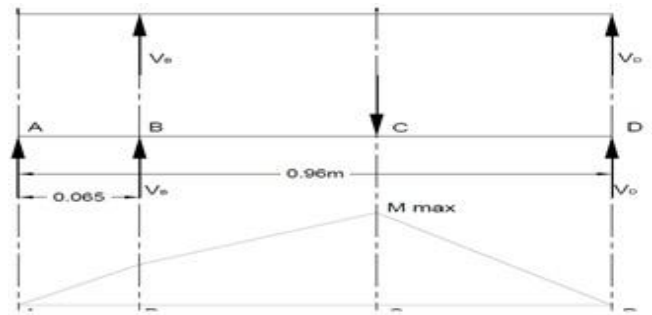


Figure 4. Bending Moment Diagram

Counter shaft diameter was determined 16mm by using equation (1), in fig. 1 the shaft is rotated by two bearing with speed of 300rpm, there is pinion 4 in fig.1 which meshes with gear which has 84mm PCD with 21 teeth. By considering pulley weight 119N and the tensions on pulley 9, T₁ Tension on tight side 179.4N, T₂ Tension on slack side 47.43N

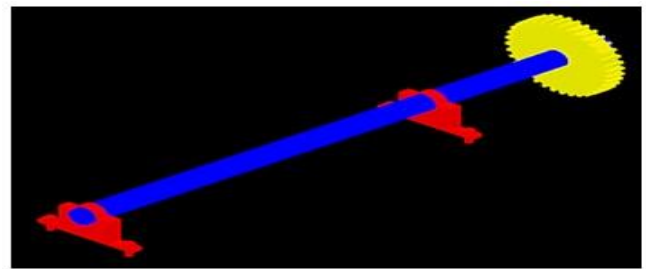


Figure 5. Counter Shaft (9)

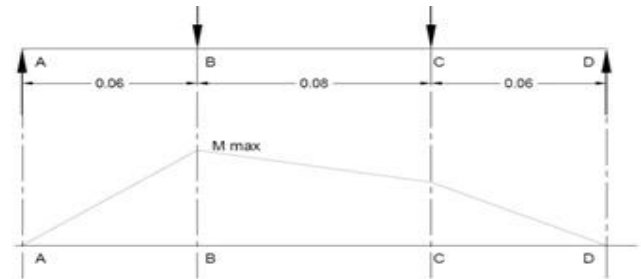


Figure 6. Bending Moment Diagram

4.2 Design of V-Belt Drive:-

Motor power is transmitted with the help of v-belt drive for which rated power was 0.745 kw, with 1440 rpm, and driven shaft was running at 300 rpm for electric motor. Calculated design power was 0.92 Kw, from design power selected belt designation is C, for which belt width 13mm, belt thickness 8mm, diameter of small pulley 75mm. The peripheral velocity (Vp) of the driving pulley and the diameter of driven pulley D₂, were obtained from Equations (3) and (4) given respectively by Joshi (1981) and Sahay (2006).

$$V_p = \frac{\pi \times D \times N}{60 \times 1000} \text{ m/s} \quad (3)$$

$$\pi \times D_1 \times N_1 = \pi \times D_2 \times N_2 \quad (4)$$

No. of belt required 1, length of belt is calculated from equations (7) and (8) given respectively by Joshi (1981) and Sahay (2006): in which θ angle of lap on larger

pulley is 2.8 rad., power/belt 863.18W ,working load F_w , centrifugal tension F_c , calculated from

$$\text{Power/belt} = F_w - F_c \quad (5)$$

$$F_w = W^2, F_c = K_c \left(\frac{V_p}{5} \right)^2 \quad (6)$$

$$\text{No. of belt} = \frac{P_d}{(\text{power /belt})} \quad (7)$$

$$\text{Length of belt} = \frac{\pi(D1+D2)+2 \times C+(D1-D2)^2}{4 \times C}$$

4.2 Design of Bearing:-

The bearing were designed using the loads resulting from the belt tension as well as from gear drives, rotating drum, and the appropriate size and strength of bearing to withstand such a load selected from calculation by assuming 40 hours per week for three years, equivalent load on the bearing calculated from

$$F_e = (X \times F_r + Y \times F_a) \times k_s \times k_p \times k_o \times k_r \quad (9)$$

K_s = Service factor, K_o = Oscillation factor, K_r = Preloading Rotational factor, and $X = 0.65$ $Y = 2.8$ selected for Self aligning ball bearings,

$$C = (L_{10})^{1/3} \times F_e \quad (10)$$

$$\text{Avg. life} = L_{10} \times K_{ref}, \quad (11)$$

$$L = \left(\frac{C}{F_e} \right)^n \times K_{ref} \quad (12)$$

A ball bearing that will withstand the load was selected for C = dynamic load capacity, $n = 3$ for ball bearing., $K_{ref} = 5$ for 50% reliability, from the code is 0201 with outside diameter 24mm and 13mm. width.

V. Cost Estimation

Table 1 Cost estimation for different machine component

Sr. No	Component	Material	Qty.	Wt. Kg	Per unit Price in Rs	Amount
1	Shaft	M.S.	2	12	45	538
2	Angle	M.S.	16	38	45	1710
3	Flat plate	M.S.	9	6	33	198
4	Nut & Bolt	M.S.	-	1.5	60	90
5	Bush	M.S.	5	0.5	70	350
6	Circular disk	M.S.	2	3	50	150
7	Wire mesh1	G.I.	1	-	-	250
8	Wire mesh2	G.I.	1	-	-	95
9	Gear	C.I.	1	3	-	531
10	Pulleys	C.I.	2	5	-	150
11	V belt	Rubber	1	-	-	122
12	Motor 1hp	-	1	18	-	1200
13	Bearing	-	4	-	225	900
14	Pinion	C.I.	1	0.5	-	126
15	Pedestal	C.I.	4	2	125	300

5.1 Miscellaneous Cost:-

Labour cost = 500Rs

Fabrication charges = 1000 Rs

Oil paint charges = 100 Rs.

Total Cost:-

Material cost +Miscellaneous cost

Total cost= 6710+1600 = 8310 Rs

6 Result and Discussion

It took 20 minutes to polished a batch of 50 kg turmeric in the polisher to achieve 8% polishing. The field test data of the turmeric polisher are given in Table 5.

Table 5 Field performance data

Parameters	Turmeric polishing machine
Material processed	Dried turmeric
Amount processed	100 kg
Operating time	60 min
Capacity	100 kg/h
Power consumption	0.3 kWh/q
Labour requirement	1 man.h
Breakdown of equipment	Breakage of Vbelt,sliping
Test result	8% polishing achieved
Overall performance	Satisfactory
Remark	Useful for on-farm polishing job

Fig. 11. And fig.12, shows result on the turmeric before polishing and after polishing the



Fig.11. before Polishing



Fig.12. after Polishing

Machine is being fabricated according to our design and seems to satisfy the required condition as mentioned below

1. It can clean 50 Kg of turmeric with good result in terms of quality as well as quantity

2. It can be easily operated at 75 rpm at optimum load and 65 rpm for maximum load.
3. It can clean turmeric minimum time 20 min. at 70 rpm.

VI. Conclusion

The turmeric polishing machine is simple in operation and easily accessible to farmer because of its simple design. All parts are easily available in the market, and machine is easily assembled and dissembled in case of breakdown as well as for replacement of any part. The machine is easy to operate and maintenance, and requires only one operator to operate. This machine is very efficient in polishing and 50kg of harvested turmeric has been polished at a time. The 50kg of turmeric could be easily washed at an optimum speed of about 75rpm for about 20 min using this machine. The developed machine uses simple mechanism which found to be a simple and cost effective solution to the turmeric producers. Performance of the equipment was found quite satisfactory and therefore, can be used for carrying out tedious post harvested polishing operation.

References

- [1] U. S. Pal, K. Khan, N. R. Sahoo, G. Sahoo, 2008. Development and Evaluation of Farm Level Turmeric Processing Equipment. AGRICULTURAL MECHANIZATION IN ASIA, AFRICA AND LATIN AMERICA. VOL.39, No.4, AUTUMN 2008.
- [2] Varshney, A. K., S. N. Garala, and S. H. Akbari. 2004. Status of postharvest technology of turmeric. Agricultural Engineering Today, 28(1-2): 13-19.
- [3] Ms.K.S.Priyenka Devi.. . Ms. A.Sangamithra. march 2004. Article in the science tech Entrepreneur .Department of Chemical Engineering, School of Chemical and Food Sciences , Kongu Engineering College, Perundurai -638052. Department of Food Technology, Tamil Nadu.
- [4] Purseglove, J. M., E. G. Brown, C. L. Green, and Robbin, S. R. J. 1981 Spices, Vol. 2. Longman group Ltd., London, New York.
- [5] Anne Plotto. Edited by François Mazaud, Alexandra Rottger, Katja Steffel. 22/04/2004. TURMERIC: Post-Production Management Organisation. Food and Agriculture Organization of the United Nations (FAO). AGST.
- [6] Sharma, P. C. and Aggarwal, D. K. 1998. Machine Design. I. S. K. Kataria and Sons Publishers, Delhi.

Mitigating the Activities of Artisanal and Small-Scale Miners in Africa: Challenges for Engineering and Technological Institutions

Stephen J. Mallo

Department of Geology and Mining, University of Jos, PMB 2084 Jos, Nigeria.

Abstract: *The urgent demand for appropriate mitigation of the activities of Artisanal and Small-scale Miners in Africa has become necessary in view of the immense contribution of the mining activities to poverty alleviation in the continent. The concept of appropriate social contract for artisanal and small-scale mining (ASM) emerged amid calls for more humane working conditions for this cadre of miners, whose contribution to the alleviation of poverty especially in the developing nations of the world has been recognized by the United Nations. The sector which is a form of subsistence mining provides a direct or indirect livelihood for over 100 million people in the developing world out of which about 5 million are from Africa. Of particular note is the contribution of this sector to the world supply of strategic minerals for industrial growth and advancement. The presence of ASM is very often associated with challenges, including poor environmental, health and safety practices, the spread of communicable disease, heightened security risks to neighboring communities and operations, child and forced labour, inequitable distribution of benefits in communities and an illegal trade in minerals such as gold, coltan, diamonds, construction materials etc. There is overwhelming consensus that the current worldwide natural resource constraints and the high rising cost of mineral investment and ecosystem pressures require new economic and social contract trajectories which should protect the interests of the Artisanal and Small-scale Miners. These trajectories should address alternatives exploration, mining/processing methods and marketing of vital minerals in an environmentally safe manner while improving the economic status of the miners. It is already the mainstream economy of the future, which is desirable to particularly support the rising African population within the context of sustainable consumption and production patterns. The opportunity exists to make better use of the ASM personnel towards the exploitation of natural resources and use mitigation and adaptation actions as a tool towards a more inclusive development path for the developing countries of Africa. It is in this regard that the contributions of engineering and Technological Institutions are pertinent in terms of training, design and fabrication of appropriate mining and processing equipments that are affordable are adaptable to the African condition and / or geological environment. Although concerted effort is being made particularly by some organs of the United Nations, the paper examines how such mitigations can be further enhanced and accomplished using the expertise and knowledge available in Engineering and Technological Institutions of Africa.*

Key Words: *Artisanal Mining; Small-Scale Mining; Sustainable Development; Mineral Investors; Social Contract.*

I. Introduction

The Africa continent harbours the largest concentration of minerals and presently is the world's largest producer of mineral commodities. The most important issue lacking is the systematic geological mapping which could unveil its vast mineral resources endowments. The countries of Europe are heavily or fully reliant on imports with regard to many critical metals and minerals which African countries are endowed with. At a time when the minerals industry is becoming more and more diversified, there is nevertheless an increased vulnerability to regulatory changes in access to resources, to obstacles in trade and commerce and to major fluctuations in commodity prices (Mallo, 2012). The disheartening trend is that most of Africa's minerals are exported as ores, concentrates or metals, without significant value-addition to the products.

Furthermore, there exist significant resources of fossil fuels (oil, gas and coal) in addition to large potentials for biomass and bio-fuels potential (ethanol, bio-diesel), especially in the tropics. The mineral industry in Africa if adequately harnessed can constitute a formidable source of socio-economic alternative for growth and development. African mineral reserves rank 1st or 2nd for bauxite, cobalt, diamonds, phosphate rocks, platinum-group metals (PGM), vermiculite, and zirconium. More minerals also occur in economic quantity as evidenced by the 2005 share of world production from African soil which showed the following statistics: bauxite 9%; aluminium 5%; chromite 44%; cobalt 57%; copper 5%; gold 21%; iron ore 4%; steel 2%; lead (Pb) 3%; manganese 39%; zinc 2%; cement 4%; natural diamond 46%; graphite 2%; phosphate rock 31%; coal 5%; mineral fuels (including coal) & petroleum 13%; uranium 16% (Mineral Industry of Africa-Wikipedia). Artisanal and small-scale mining takes place throughout the world, but is particularly widespread in developing countries in Africa, Asia, Oceania, and Central and South America. Mining Minerals and Sustainable Development (MMSD) country research studies have been elaborated in the most important ASM countries as Burkina Faso, Ghana, Malawi, Mali, Mozambique, South Africa, Tanzania, Zambia, Zimbabwe, China, India, Indonesia, Papua New Guinea, Philippines, Bolivia, Brazil, Ecuador and Peru. Other relevant ASM countries are Central African Republic, Congo, Ethiopia, Guinea, Kenya, Madagascar, Namibia, Nigeria, Niger, Sierra Leone, Uganda in Africa, Laos, Malaysia, Myanmar, Thailand and Viet Nam in Asia and Chile, Colombia, Dominican Republic, French Guyana, Guyana, Mexico, Nicaragua, Surinam and Venezuela in Latin America and the Caribbean (Thomas Herschel et al, 2002).

The present study however centres on such minerals that attract the participation of the subsistent miners which fall into the category of artisanal and small-scale miners. An array of such minerals is shown in Table 1.

Table 1: Some Leading African Mineral Resources (2005)

Mineral	Production	Rank	Reserves	Rank
PGMs*	54%	1	60+%	1
Phosphate	27%	1	66%	1
Gold	20%	1	42%	1
Chromium	40%	1	44%	1
Manganese	28%	2	82%	1
Vanadium	51%	1	95%	1
Cobalt	18%	1	55+%	1
Diamonds	78%	1	88%	1
Aluminium	4%	7	45%	1

Also Ti (20%), U (20%), Fe (17%), Cu (13%), etc.

PGMs: Platinum Group Minerals Africa's dire need to industrialise is universally acknowledged. The structural transformation of our economies must be an essential component of any long-term strategy to ensure the achievement of the Millennium Development Goals (MDGs) in Africa, eradicate poverty and underpin sustainable growth and development across our continent. The key issue, however, is in the formulation and implementation of workable industrialisation strategies based on our continent's unique strengths, rather than the emulation of strategies that may have been effective in other contexts. A resource-based African industrialization and development strategy must be rooted in the utilisation of Africa's significant resource assets to catalyse diversified industrial development, as was successfully implemented by several erstwhile resource-based economies in the developed world such as in Finland, Sweden, Germany (especially in the Ruhr region), and the US over a century ago and to some extent in more recently in middle income countries Malaysia, Brazil and South Africa (York, 2012).

The artisanal and small-scale mining provides a substantial percentage of the afore-mentioned production. An estimated 13 - 20 million men, women, and children from over 50 developing countries are directly engaged in the artisanal mining sector (<http://en.wikipedia.org/wiki/Artisanal>). As many as 650,000 women in 12 of the world's poorest countries are engaged in artisanal mining, and between 1 and 1.5 million children are also involved in this activity. This explains why artisanal and small-scale mining is exclusively practiced by individuals, groups, families or cooperatives with minimal expertise and technical know-how to exploit the minerals while often depending on the informal (illegal) mineral market which is substantially exploitative. The range of commodities exploited by artisanal and small-scale miners is diverse, including gemstones, gold, copper, cobalt, coltan, coal, construction materials and other industrial minerals.

The term 'Small-Scale Mining' according to Seydou (2001) is the subject of a great debate in the sub-region. Generally, the main criteria commonly used in the attempts to define the precise content of this expression are:

- The physical size of the deposit and the continuity or not of mining activities.
- The organizational structure of the activity and the management system.
- The importance of investment required and turnover generated.
- The number and level of qualifications of the workers involved in the production unit.
- The kind of equipment, degree of mechanization and the level of technology used.

Artisanal mining can include activities as simple as panning for gold in rivers, to as complex as development of sub-surface workings and small-scale processing plants. In any of these circumstances, issues can stem from difficulties in achieving regulatory oversight of a large number of small operations (including issues such as security of land tenure for artisanal miners, to enforcement of environment, safety standards, and labour standards). An artisanal miner or small-scale miner is, in effect, a subsistence miner. They are not officially employed by a mining company, but rather work independently, mining or panning for gold using their own resources. Small-scale mining includes enterprises or individuals that employ workers for mining, but generally working with hand tools. Artisanal miners often undertake the activity of mining seasonally – for example crops are planted in the rainy season, and mining is pursued in the dry season. However, they also frequently travel to mining areas and work year round. Apart from gold and diamonds, other small-scale activities serving for employment for a lot of people center on the extraction of salt, kaolin, silica, sand, brown clay, aggregates and crushed rocks, etc.

The mineral industry is an important source of export earnings for many African nations. In realization of its importance and order to promote exports for these economically vital commodities, groups of African countries have formed numerous trade blocs, which included the Economic Community of West African States, the West African Economic and Monetary Union, Common Market for Eastern and Southern Africa, the Economic and Monetary Community of Central Africa, the Economic Community of Central African States, the Mano River Union, and the Southern African Development Community. In view of their participation in oil production, Algeria, Libya, and Nigeria were members of the Organization of the Petroleum Exporting Countries (OPEC). Furthermore, the African Union was formally launched as a successor to the Organization of African Unity in 2002 with the sole aim of accelerating socio-economic integration and promotion of peace, security, and stability on the continent (en.wikipedia.org/wiki/Mining_in_Africa).

National governments are becoming increasingly aware of the sector's importance as a means of poverty alleviation and a generator of national income. In recent years, a number of governments have formally recognised the sector and attempted to provide facilitating enabling environments. Despite these changes, the implementation of legislation remains

problematic at a local level and many miners do not have faith in the ability or commitment of their governments to provide assistance (Hentschel et al, 2002).

The international development community has been concerned with the artisanal and small-scale mining sector for the past 30 years having identified the sector as a formidable source of ameliorating hunger. As understanding of ASM has increased, the approaches taken have changed. Table 2 summarizes this evolution:

Table2. Historical Evolution of ASM

Period	Approaches for dealing with ASM
1970's	Definitional issues
1980's	Technical issues
Early 1990's	Towards integration of technical, environmental, legal, social and economic Issues
1990's	Special attention on legalisation of ASM sectors
Mid to late 1990's	Relation between large mining companies and ASM
2000's	Community related issues and sustainable livelihoods

Source: Hentschel et al, 2002

II. Methodology

The methodology included two components: analysis of secondary information, and primary research on the activities of artisanal tin mining on the Jos Plateau, Nigeria.

Artisanal Mining in Africa- Country Specifics

The African continent can be described as the hub of major strategic and industrial minerals which the developing countries of the world largely depend on for their industrial growth and development. The contribution of artisanal mining in the production of gold, diamond and tin/tantalum/Columbite and other minerals is provided in Table 3. While this sector contributes to poverty alleviation, it is by no means associated with socio-economic misgivings. Some country specifics on artisanal and small-scale mining are given, thus:

Botswana: Gold has been mined in Botswana for several hundred years, with many old mine workings identified in north-east Botswana. Botswana's gold deposits were relatively small and difficult to mine, and attention soon turned to the much richer South African gold deposits on the Witwatersrand. Exploration and mining in Botswana is governed primarily by the Mines and Minerals Act, 1999 (Cap 66:01). Botswana's policy towards dealing with investors in extractive industries is generally considered to be amongst the best in the world. The legislation governs the ownership of minerals and mineral rights, applications for prospecting licenses, retention licenses, mining licenses and environmental obligations. The Act also addresses the issue of royalties to be paid, license fees and penalties. Other relevant legislation include: the Precious and Semi-Precious Stones (Protection) Act, which provides for the protection of the precious stones industry and regulates dealing in precious and semi-precious stones; the Mines, Quarries, Works and Machinery Act. Botswana's policy provides a stable macroeconomic framework is important, including low inflation and a stable real effective exchange rate. The general policy framework is market-oriented, and supportive of the private sector with focus on revenue sharing/appropriation of mineral rents.

According to Keith Jefferis, 2012, the policy has encouraged the participation of multinational mining companies. For most of this period, De Beers was a public company, listed on the Johannesburg and London Stock Exchanges, although with a major block of shares held by Anglo American. In 2001, De Beers was restructured, and became a privately owned company. As a result, the ownership of De Beers changed to: Anglo American (45%); Central Holdings (Oppenheimer Family) (40%); and Government of Botswana (15%). The restructuring gave the Government an even greater say in the operations of De Beers, and access to significant dividends from De Beers' profits. This success story of Botswana notwithstanding, artisanal and small-scale mining exists in Botswana for the mining of gold, diamond, nickel cobalt etc.

Burkina Faso: According to article 1 of law no. 23-07/II-AN related to mining legislation in Burkina Faso, traditional mining is defined as 'any operation, which consists in extracting and concentrating mineral substances to recover merchant products, using traditional and manual methods and procedures'. Small-scale mining is defined as 'a small size mining having a minimum of fixed facilities, using state of the art semi-industrial and industrial procedures and which is based on prior revealing of a deposit.

Cameroon: In the East Province of Cameroon, an estimated 100 kg of gold is now produced per month by some 10,000 small-scale miners, mostly channeled through informal circuits (Sale 2003). Official figures by the Department of Mines and Geological Research are much lower: approximately 500 kg of gold produced annually by ASM throughout the entire country (Lang 2007). With regard to diamonds, the 700- km border between Cameroon and the Central African Republic has significant diamond production evaluated at 800 carats per month in 1993, despite the inadequate experience of Cameroonians in diamond exploitation (Gweth 2003). In most countries in central Africa, gold and diamond mining remain

artisanal, albeit significant revenue contributors to local and national economies. This informal system can still yield significant socio- economic impact on the Cameroonian economy.

Central African Republic: Artisanal mining of diamonds and gold in the CAR occurs mostly in the regions of Berberati, Upper Kotto, and Sangha. Since 1962, 98% of diamonds and 100% of gold production came from ASM in these regions. The new code includes more attractive fiscal policies and other flexibility that are geared towards deregulating the mining sector and encouraging its development by attracting foreign investors. The Codes are classified into 'Quarry' (construction minerals including sand, gravel and stone) and 'Mine' (all other mineral substances) with permits for exploration and mining falling under six categories: artisanal mine, prospecting, exploration type A, exploration type B, mining, and mine concession (Tieguhong, 2009).

Democratic Republic of the Congo: Conservative estimates are that 2 million people are actively involved in mining and are responsible for producing 90% of the minerals exported from the country. With their dependents, this means 15-20% of the population is directly dependent on this dangerous, illegal activity. ASM, as it is practiced in the country today, is unregulated, hazardous, controlled by illegal traders and security forces, and increasingly marginalized with the advent of new investment in formal mining.

It is not possible to estimate how many people depend on the cascade of economic activity that the miners generate but it is clear that this is the backbone of the trading economy in the DRC today. Twenty percent of the artisanal mining community, or 400,000 miners, sorters, transporters and suppliers, are women. Twice that many are children. The principal mineral being mined is the coltan which is in very high demand by the developed nations especially in the electronic sub-sector.

Ghana: Artisanal and Small scale mining of gold is traced to the 15th Century. □ Prior to 1989, SSM activities, especially gold, was regarded as illegal because of non-existence of legislations to control the activity. □ Thus proceeds from their operations were smuggled to neighbouring countries for sale. Estimated US\$15 million worth of gold from illegal mining was smuggled out in 1985 to neighbouring the activities of artisanal and small scale miners. In Ghana, the regulation of artisanal gold mining is set countries. In a bid to mainstream this activity, Government made a policy decision in 1989 to regularise forth in the Small-Scale Gold Mining Law, 1989 (PNDCL 218). The Precious Minerals Marketing Corporation Law, 1989 (PNDCL 219), was set to promote the development of small-scale gold and diamond mining in Ghana and to purchase the output of such mining, either directly or through licensed buyers. In Ghana the concept of 'small-scale mining' is defined in Mineral and Mining Law 1989

PNDCL 153 as mineral resources mining using methods that do not require heavy investment or the use of sophisticated technologies. In the provisions of 'the small-scale Gold Mining Law', this is defined as gold mining by a group of persons fewer than nine or by a cooperative of more than ten people using methods that do not require neither heavy investment nor sophisticated technologies. The other criteria set by the law are: small-scale mining can be done only by Ghanaians; the maximum period for the licence is five year, renewable; the maximum area for the licence is 10 hectares; the use of explosives is forbidden (Keita 2001).

In 2006, the legal regime of SSM was integrated into the new Minerals and Mining Act 2006, (Act 703). The positive impact of these reforms was that SSM Contributed 23% of total gold production in 2010. By the end of 2010 – ASM sold 776,000 oz of gold, valued at US\$ 797.60 million and 308.679carrats of Diamond valued at US\$ 11.13 million to official agents (Tetteh, 2011). In Ghana, there are about 300 registered small-scale mining groups and they constitute a major source of employment especially for small-scale gold and diamond miners, and contribute some foreign exchange to Ghana's economy. However, there are a lot more of such groups that are not registered, and cannot access any meaningful form of support to boost their business (Adu-Gyamfi, 2011). In all, an estimated 1,000,000 people are directly or indirectly involved in artisanal and small scale mining in Ghana.

Niger: Exploitable deposits of gold have long been known to exist in Niger in the region between the Niger River and the border with Burkina Faso and artisanal gold mining has previously taken place in the area (<http://en.wikipedia.org/wiki/Samira>). The Koma Bangou gold deposit was discovered by ONAREM (l'Office National des Ressources Minières, the Nigerien government's mining company) in 1985. According to articles 43 and 44 of ordinance no. 93-16 related to the mining law in Niger, traditional mining is extracting and concentrating mine stones to recover the useful substance(s) using traditional methods and procedures. Traditional methods apply to mineralization profiles of some substances which have been mined traditionally, or to deposits for which there is evidence that industrial working would not be economically profitable. The Namaga concession upon which the Mine was built is hoped to be the first mine to produce gold from the Tera greenstone belt which surrounds Koma Bangou, the country's largest artisanal mining site.

Mali: Traditional mining has been practiced in Mali and West Africa for a very long time. This is exemplified in the part the Kingdom of Mali in supplying Europe and the Middle East with traditionally extracted gold. Oral and written documents suggest that 12,000 camels loaded with salt would arrive in Timbuktu and when they leave, they are loaded with gold (Keita, 2001). The traditional exploitation concerns mainly auriferous minerals, diamonds and semi-precious stones. As an indication, Kéniéba gold washers have found nice stones and among the most recent discoveries that can be quoted: a diamond jewel of about 299 carats in 1985; a 230-carat diamond in 1990; and a diamond of about 299 carats in 1998.

Concerning the exploitation of semi-precious stones, there was a rush in the Diakon zone in the western part of Mali

between 1994 and 1995. Three thousand people there extracted more than 15 tons of garnet. This uncontrolled production saturated the international market and eventually miners abandoned the sites.

On a regional scale, one can cite the example of the Siguiri Basin in High Guinea where almost 50,000 gold washers produce annually between three and five tons of gold. In 1999, his activity injected \$22 million into the local economy.

The main auriferous deposits, which are the focus of traditional mining, are located mostly in volcano-sedimentary formations (green rocks) of the Birrimian age which are found in two main zones. The first is in the western Bambouck auriferous district with the Sadiola deposit (about 150 tons exploited by Anglo-American Mining Co since 1997, the Yétala deposit (40 tons exploited since September 2001). Additionally, there are the Loulo deposit (40 tons proved), Médinandi (evidence of four tons of gold), Tabakoto (43 tons), Ségala (40 tons) in various phases of certification and development. The second main zone is in the southern auriferous district of Bouré with deposits in Bagoé, Yanfolila, Kangaba and Syama (with 150 tons of gold) worked since 1990. The gold deposit of Morila located in the same district with reserves estimated at 150 tons of gold started production in February 2001.

Mali mining legislation is based on simplicity of equipment used, technologies implemented on the one hand, and on the other hand, the low level of investment required for the operation and non-qualification of workers. Following the recommendation of the national seminar on gold washing, held in Bamako in 1989, where the profession of gold washer was regulated by a special legislation namely ordinance no. 90-09/P-RM of 13 April and its enforcement decree no. 90-186/P-RM of 2 May 1990. The objectives of these texts were on the one hand to legalize gold-washing activities, and on the other to promote small-scale mining of auriferous lodes which are impossible to exploit with large-scale industrial methods and heavy investment. Between 1991 and 1999, traditional mining activities and small exploitations were regulated in several ways. Ordinance no. 91-065/P-CTSP of 19 September 1991 and its enforcement rules included legal provisions related to small-scale mining. Through this regulation, the legislator wanted to correct the weaknesses of former texts and give some importance to small-scale mining. The legislator also specified the parameters to be taken into consideration in classifications. Decree no. 96-214/PM-RM of 16 August 1996 was promulgated for purpose of regulating the collection, processing and marketing of gold.

Nigeria: The artisanal and small-scale mining of gold, tin/ Columbite, lead/Zinc, coal etc has strived in Nigeria at the advent of colonial mining around 1902. In Nigeria artisanal mining practices are unguided and unregulated. Over 95% of mining activities in Nigeria are artisanal and another 95% of these are illegal (this includes minerals such as Tourmaline, Galena, Limestone, Feldspar, Tantalite, Coal, etc Policies in place are inadequate, and miners are untrained and contribute hugely to environmental degradation, and poor quality operational techniques and the loss of minerals. Most activities have proceeded undocumented, resulting in loss of minerals and precious stones. This has caused substantial losses in revenue to the country by way of exports, as well as through royalties and taxes (Mallo 2011). Long before this however, there has been pre-colonial mining of iron ore, gold, tin and construction materials amongst various communities which made them self-sufficient in terms of production of war armaments, jewelry etc. This activity however burgeoned as a result of commerce introduced by the colonial masters where illegal mining strived along commercial mining of these commodities. This activity reached its peak in the late 1970s the when price of metallic minerals at the international market nose-dived to an all time low prices. The nationalization decree of 1972 further encouraged the activity as major multinational companies exited.

Although there has been a significant leap in terms of mineral reforms in Nigeria, as regards to the new Minerals act of 2007, attention has not been adequately given to the recognition of this informal sector as a formidable source of revenue for government. This notwithstanding, some palliative monetary measures have been extended to small-scale miners through the release of some investment fund in both cash and kind through a World Bank loan. The activities of artisanal miners in Nigeria have caused the lives of people, the Zamfara lead poisoning being the freshest in mind. According to Mallo et al, 2011 and 2012, artisanal mining has contributed to poverty alleviation for tin miners on the Jos Plateau. This has however, not been without corresponding socio-economic consequences to the environment as studied by the Author recently (Fig.1 and Table 3), health of the workers and loss of revenue to the country.

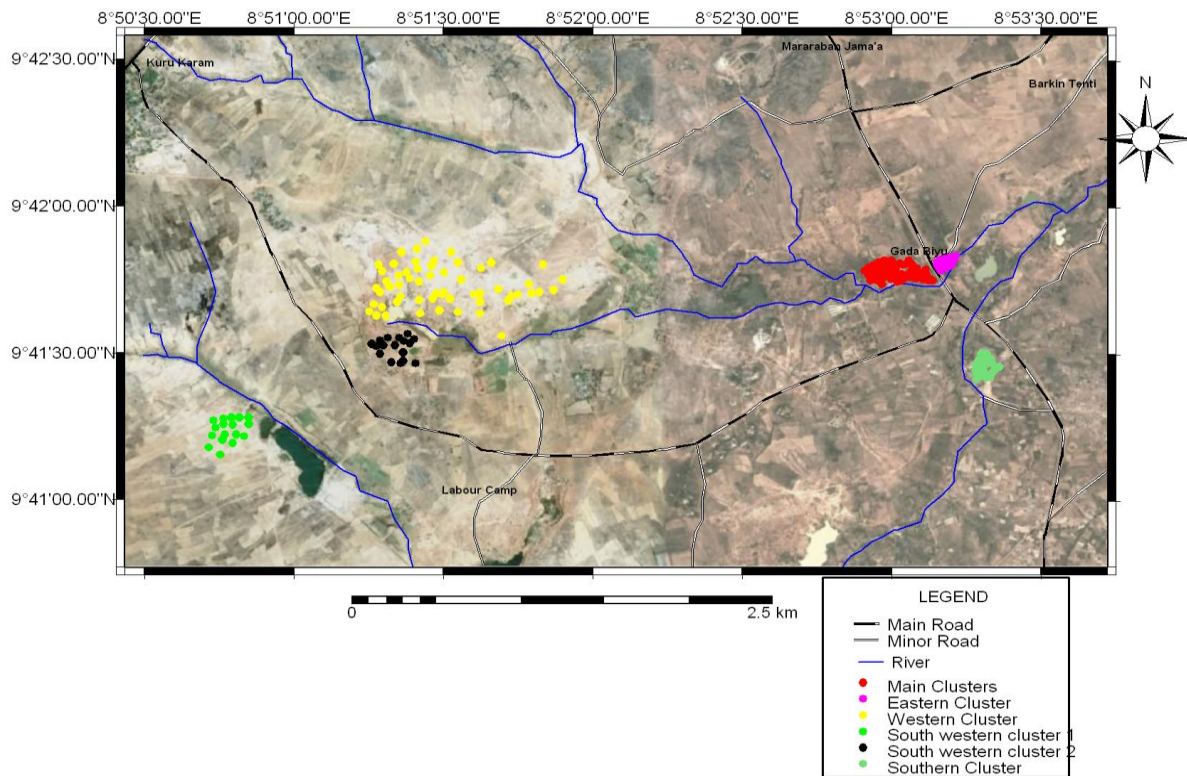


Fig.1. Satellite image showing mining clusters within Kuru and environs: Source Mallo, 2012

Table 3. Locations of Mining Clusters

S/No.	Clusters	GPS Coordinates	Area of Devastation
1	Main Cluster	9041'46.91"N 8053'00.55"E	0.334 km ²
2	Eastern Cluster	9041'49.37"N 8053'11.62"E	0.075 km ²
3	Western (Primary Deposit) Cluster	9041'43.69"N 8051'30.40"E	0.600 km ²
4.	Southern Cluster	9041'26.37"N 8053'18.76"E	0.194 km ²
5	South-western cluster 1	9041'13.93"N 8053'18.76"E	0.064 km ²
6	South-western cluster 2	9041'31.11"N 8051'20.03"E	0.074 km ²

Source: Mallo, 2012

Tanzania: The activities of artisanal mining of gold and diamond in Tanzania has been extensible studied by Rosemarie Mwaipopo, Wilson Mutagwaba, David Nyange, Eleanor Fisher (2004) and Heschel et al, 2002. Artisanal mining in Tanzania dates back to the early 20th century. Since then, this activity has provided a livelihood for thousands of people. It was difficult work, using dangerous explosives and toxic chemicals. But for 1.5 million Tanzanians, this primitive form of artisanal mining is a daily reality. Yet over time, small-scale miners have adopted harmful environmental practices, with little regard for their own safety. Organized crime has also traditionally been involved in the industry, indenturing countless artisanal miners who have few alternatives. Mining of diamonds is carried out through excavation of shallow pits down to the layer of gravels that contain diamonds. The overburden material covering the diamond bearing gravels contains of consolidated black cotton soils. As such, excavation is usually carried out using picks and shovels.

Most pits are shallow and their depth range between 3 – 5m. Once the gravels have been reached, they are scooped using shovels and loaded into buckets that are then hoisted to surface ready for processing. The processing of diamonds is less sophisticated than that used to process gold. At Mabuki, the diamond bearing gravel is panned and thus allowing the heavy diamonds to collect at the bottom of the pan from where it is collected through sorting. As such the processing equipments needed are less sophisticated and include pans and sieves. During the rainy season miners process ore mined during the dry season by using the water that has filled their pits. During the dry season, the shortage of water drives most miners to other activities. However, there are a few deep wells from which processing water is fetched.

These miners rely on knowledge passed down from their parents, and use outdated technology. Most are unaware of fluctuations in the market value of gold, and often sell their gold for a pittance, perpetuating a cycle of poverty.

The mining sector is one of the new pacemakers for growth of the Tanzanian economy. This is evidenced by an increase in its contribution to the GDP from 0.8 percent in 1987 to 2.3 percent in 2000. The target is to raise the contribution of the sector to 10 percent of GDP as new investments come into full operation. However, information on the share of ASM to the mining sector GDP is lacking although it is known that legitimate ASM companies pay 3% of their revenues as royalty to the government hence contributing to the national GDP (Mwaipopo et al 2004). In a study carried out by Heschel et al 2003, for Tanzania, the implementation of a mineral trade liberalization policy in the late 1980s created a more formalized ASM sector. This increased legally traded gold production from US\$0.55m in 1985 to US\$38.78m in 1992.

Zambia: In Zambia ASM is explicitly mentioned in the PRS. As a result key policy objectives regarding the sector are prioritised, allocated and regularly monitored. As a result ASM becomes the interest of a wide range of influential stakeholders; monitored at a national level (Zambia, MFNP, 2003). Possibly as a consequence of its inclusion in the PRS the sector is supported by significant EU and World Bank interventions running into millions of dollars.

Table 4 Artisanal Mining in Africa

Country	Locations	Commodity
Angola	Luali River Area	Gold
Burundi	Murehe	Tin, Tungsten
Cameroon	Various Locations	Diamond ,Gold
Central African Republic	Bandas Greenstone Belt, Bangana Area, Bogoin-Boali Greenstone Belt , Bria Area, Carnot Area , Kotto Area Quadda Area,	Gold Diamond, Gold, Diamond, Diamond, Diamond and Diamond respectively
Chad	Mayo Dala Department	Gold
Congo – Brazzaville	KellÃ©, Covette-Ouest Department, Likouala Department and Yangadou, Sangha DepartmentÃ	Diamond Diamond, Diamond,
Congo – Kinshasa KasaÃ	Occidental Provinces, in Bandundu Province, at Bafwansende and Kisangani in Haut-Congo Province, at Lubutu in Maniema Province, at Kota-Koli, Yakoma, and Gbadolite in Equateur Province), in Nord Kivu Province, and at Luozi in Bas-Congo Province	Diamond
Equatorial Guinea	Aconibe, Coro, and Mongomo	Gold
Ghana	Birim Valley	Diamond
Madagascar	Mananjary, Andilamena and Vatomandry, Ilakaka and Sakara	Emerald, Ruby, Sapphire
Morocco	Errachidia, Figuig, and OuarzazateÃ	Barite
Niger	Liptako Region	Gold
Nigeria	Dutse Nkura, Jos Region , Zamfara,Nasarawa,Birnin Gwari	Tin, Tantulum, Lead. Barite, Gold,
Rwanda	Cyangugu ,Nyungwe Forest	Sapphire, Gold,
Zambia	Eastern ProvinceÃ, Iteshi Teshi; Mumbwa Kalunga Wbeba, HofmeyerÃ , Katete, Kitwe , Siavunga.	Beryl, Citrine, Tourmaline, Aquamarine, Garnet, Emerald
Zimbabwe	Gwanda, Kamativi	Gold Tin,

Source: Mallo, 2011

Socio-Economic Impact of Artisanal and Small-scale Mining

Activities of artisanal and small scale miners have substantially increased over the last years, in particular in many Asian countries following the financial crises that drove many poor, in particular women and children, into artisanal mining. Today, an estimated 13 million people in about 30 countries across the world are small scale/artisanal miners, with about 80 million to 100 million people depending on such mining for their livelihood. Miners and their families expose themselves to harsh working conditions for minimal income in a high risk context, endangering their health as well as often the surrounding environment. In areas where miners are invading the lands of indigenous or tribal peoples, there can be very serious cultural conflicts, bordering on cultural warfare, also given environmental degradation and diseases brought to these regions by the miners. Meanwhile, much of the actual economic potential is lost due to the absence of a legal or fiscal framework for Small-Scale Mining and due to rudimentary production, processing and marketing techniques. Public or private services to provide essential health care and education typically do not exist. As many as 650,000 women in 12 of the world's poorest countries are engaged in artisanal mining, and between 1 and 1.5 million children are also involved in this

activity. The range of commodities exploited by artisan miners is diverse, including gemstones, gold, copper, cobalt, coltan, coal, and other industrial minerals.

The activities of artisanal mining which is mainly clandestine lack statistics on income generated by activities associated with mining. The activity attracts miners and many people like traders, merchants, blacksmiths, cooks and canvassers. The jobs created by artisanal mining operations are important and constitute an important source of income for poor families in mining vicinity and beyond. These jobs are more significant when seen from the social impact standpoint, because they integrate the village's spirit of solidarity with the traditional extended family.

However these gems and minerals that make lives so much easier in the developed world, exact a heavy toll on the people who extract them and on the environment. As the world becomes more aware of the sources of these minerals, the need for a group such as Communities and Small-Scale Mining (CASM) becomes self-evident (<http://www.artisanalmining.org/casm/>) Women working in artisanal and small-scale mining in most African countries face a huge array of issues, challenges and threats. ASM, as it is practiced in the continent today, is unregulated, hazardous, controlled by illegal traders and security forces, and increasingly marginalized with the advent of new investment in formal mining. The men, women and children who carry out this work are indebted, exploited and manipulated for political and financial purposes.

Whilst everyone in the sector faces challenges, the security, health, and social risks posed to women are particularly acute and include:

1. Sexual violence and abuse in the mines, particularly in remote areas where mines are still controlled by military forces. Eastern DRC has the worst rate of rape and sexual abuse in the world, much of which is perpetrated by security forces and militia,
2. Family break-up, polygamy, and abandonment due to the highly migratory nature of ASM,
3. Health risks due to lack of sanitation in camps, malnutrition, and physical trauma from the difficulty of the manual labour. Women in mining camps suffer a high rate of miscarriages due to injury and stress,
4. Exposure to, and involvement in, disruptive and damaging behaviour due to the high levels of alcohol and drug abuse in camps,
5. The risk of HIV/AIDS and other STDs due to prostitution and the risk profile of ASM activities (large concentrations of migratory young men, family separation for prolonged periods, high levels of military presence, lack of awareness, no condom use) and
6. Gender discrimination whereby women do not receive equal pay or opportunities, and are often required surrendering high value products.

Women are frequently obliged to bring their children with them to the mines, and live with them in mining camps. That United Nations agency launched a campaign against children working in mining in 2005, calling it one of the world's worst forms of labour (York 2012). Although some countries like the DRC has ratified the UN Convention on the Worst Forms of Child Labor, and it is illegal for children under 18 to work in mines; however, between 800,000 to 1 million are engaged in artisanal mining. In Mali, an estimated 20,000 children toil in artisanal gold mines, and injury is common. Of 33 child workers interviewed by Human Rights Watch last year, 21 suffered from regular pain in their limbs, back, head or neck, while others were plagued by coughing and respiratory disease. In the Zamfara region of northern Nigeria, about 400 children have died of lead poisoning from the lead-laden rock that they pulverize in search of gold, and thousands of other children need urgent medical care, according to reports by Human Rights Watch and *Médecins sans frontières* (Doctors without Borders). Globally, the number of child miners is probably more than a million. Hazardous underage labour is banned in most countries, yet groups such as the International Labour Organization have struggled in vain to prohibit it.

This exposes them to hazards and health risks, and frequently prevents them from going to school, thereby limiting their future options and the hope for transition to a better life. The activity of artisanal mining in the DRC symbolizes general the conditions such miners are subjected to in most African countries. This is in addition to the tribulations of war.

Artisanal miners exploit over 40 different minerals but gold and diamond typically occupy about 60% of their mining. In DRC and Sierra Leone, artisanal gold and diamond mining make up 75% of national mining production (CASM 2008). Small-scale mines are testimonies for the existence of mineral resources, often pioneering alluvial production close to primary sources that later become industrial discoveries. The small-scale mining operations are also appropriate activities for marginal deposits, where industrial exploitation might not be economically feasible (Gweth 2003).

The social and economic characteristics of small-scale mining fully reflect the challenges of the Millennium Development Goals (MDGs), including: health, environment, gender, education, child labor, and poverty eradication. Small-scale mining communities, for instance, are highly vulnerable to communicable diseases including malaria, tuberculosis, influenza, cholera, yellow fever, sexually transmitted diseases, and HIV/AIDS. HIV/AIDS is not just a public health problem; it is a major development crisis. Because it kills so many adults in the prime of their working and parenting lives, it decimates the workforce, fractures and impoverishes families, orphans millions, and shreds the fabric of communities. Further, large scale mining often comes to areas of traditional artisanal and small-scale mining, which creates potential conflicts around issues of ownership rights and alternative livelihoods, particularly in post-conflict and fragile states which already experience high levels of social and economic stress.

Initiatives for the Promotion of Artisanal Mining in Africa

In an attempt to ensure that Artisanal and Small-scale mining takes place in a sustainable manner Regional and international initiatives have been advanced in order to promote the mining sector, Regional initiatives to promote the small-scale mining sector are more pronounced in the western, eastern and southern parts of Africa. A plethora of international

organizations exist in the mining sector, mostly tackling issues governing large- scale mining rather than dispersed small-scale mining. Some of these major initiatives are presented below:

1. The International Labour Organization (ILO)'s Convention on Safety and Health in Mines, 1995 (No. 176) provides minimum safety standards against which all changes to mine operations should be measured (Walle and Jennings 2001).
2. The International Council on Mining and Metals (ICMM): is a multi-partnership organization that commits corporate members to implement its principles under a sustainable development framework, including global standards, public reporting, independent assurance and sharing best practices. (http://www.icmm.com/sd_framework.php).
3. The World Gold Council (WGC) is a global advocate for gold committed to playing a key role in the development of responsible gold mining. As a member of the ICMM, the WGC seeks to improve sustainable development (http://www.icmm.com/icmm_principles.php). The World Diamond Council (WDC) has a mandate similar to the WGC.
4. The Council for Responsible Jewellery Practices (CRJP) promotes ethical, social and environmental practices throughout the diamond and gold jewellery supply chain, from mine to retail shop (<http://www.responsiblejewellery.com/what.html>).
5. The Kimberley Process was initiated by African diamond-producing countries in May 2000 to develop an international certification scheme for rough diamonds to prevent "conflict diamonds" from entering legitimate markets (Kimberly Process 2004).
 This process was supported by the World Diamond Council and the United Nations, and implemented by a UN General Assembly vote in 2003. The certification process follows each diamond from mine through every transfer of ownership to retail sale. The process is supported by a broad range of international stakeholders in the diamond trade, including government officials, industry representatives and non-governmental organisations. Participants officially launched the Kimberley Process Certification The CAR, DRC, Gabon and Republic of Congo are currently participants in the KPCS and in 2007 Cameroon affirmed its intention to join.
6. Extractive Industries Transparency International (EITI): Founded in 2002 encourages governments to disclose their revenues from oil, gas and mining operations, verified by reports of company payments to governments. EITI starts by gaining consent from host governments for reporting their revenues and the payments by companies. Most of the consenting countries have called for disclosure of aggregate company payments across all reporting companies (EITI Fact sheet, 2008).
7. Collaborative group on Artisanal and Small-Scale Mining (CASM): The Communities and Small-scale Mining (CASM) initiative was launched in 2001, in response to a critical need for integrated, multi-disciplinary solutions to the complex social and environmental challenges facing ASM communities, and improved coordination between those working in this sector. CASM is a global networking and coordination facility with a stated mission to "to reduce poverty by improving the environmental, social and economic performance of artisanal and small-scale mining in developing countries." CASM is currently chaired by the UK's Department for International Development and is housed at the World Bank headquarters in Washington, D.C. Resourced by a multi-donor trust fund, CASM currently receives its core funding from the UK and the World Bank, supplemented by program support from Japan, amongst others, Canada, France and the US. Several companies, trade associations and charitable funds, such as Tiffany & Co Foundation, also contribute finances to CASM's work program. CASM funding has leveraged significant additional funding for work in the ASM sector.
8. International Program on the Elimination of Child Labour (IPEC): IPEC, a program of the ILO, includes a sector of activity in "Mining and Quarrying". It notes that child labour "can still be seen in small-scale mines of Asia, Africa, Latin America, and even parts of Europe". The IPEC approach focuses particularly on the development of a solid knowledge base and assessment, and working with partners for delivery of programs.
9. The International Council on Mining and Metals (ICMM). A significant issue in artisanal and small-scale arises when larger mining companies gain rights to develop deposits that are currently worked by artisanal mining. The International Council on Mining and Metals (ICMM) has produced a guidance note for companies engaging with the artisanal and small-scale mining (ASM) sector. As is noted in the introduction to this document "The fact that much of ASM activity occurs In 2009, ICMM collaborated with the Ghana Chamber of Mines and the Ghana Minerals Commission to host a workshop on interactions between companies and ASM in Ghana. This resulted in a report that outlines pragmatic actions for the government, companies and other relevant stakeholders.
10. The Global Mercury Project (GMP): This project was initiated in 2002 when the United Nations Industrial Organization (UNIDO) received \$6.8 million US in financial support from the Global Environment Facility (GEF) and UN Development Programme (UNDP) to initiate the Global Mercury Project (GMP). It was a six-country project (at ASGM sites in Brazil, Indonesia, Laos, Sudan, Tanzania and Zimbabwe), assisting communities along key trans-boundary rivers and lakes in assessing the pollution from current activities to reduce health hazards, introducing cleaner gold mining and extraction technologies to minimize or eliminate mercury releases and develop the capacity and regulatory mechanisms that will enable the sector to minimize negative environmental aspects. Mercury amalgamation is the easiest, cheapest and quickest way to extract gold, but not the most efficient or safest method. When mercury is used in artisanal mining, it escapes into bodies of water as droplets, or is emitted to the atmosphere when the amalgams are heated inadequately. If a retort or fume hood is not used, miners are exposed directly to mercury vapours, which poses an immediate health threat. For the majority of miners, the small income that results from Artisanal and Small-scale Gold Mine (ASGM) outweighs the health risks of using mercury (Sandra Garcia, 2010).

The project aims as well at increasing the knowledge and awareness of miners, government institutions and the public at large on the environmental impacts associated with the application of current technologies. This has been enhanced through introduction of cleaner and efficient technology that apart from minimizing negative environmental impacts will improve earnings, health and safety. (Sandra Garcia, 2010).

11. The UN Department for Economic and Social Affairs: has developed an interesting sustainable livelihood approach for artisanal mining communities, which is currently under pilot implementation in Mali, Ethiopia, Ghana, and Guinea. The main policy recommendations for this approach, according to Labonne and Gilman (1999) are: Mainstreaming poverty eradication into national policymaking in all sectors including minerals; Promoting small-scale mining as a catalyst and anchor for other productive activities to stimulate the development of complementary and alternative productive ventures necessary for sustainable poverty alleviation. Placing people first through both pro-poor strategies and participatory strategies aimed at strengthening the organizational capability of grassroots communities, thereby favouring a bottom-up approach. Reversing the focus from 'hands-on state intervention' (which has rarely been successful) to the creation of private enterprises, particularly microenterprises or cooperatives (Adu-Gyamfi Kwaku (20011); Small scale mining Business in Ghana: challenges and Prospects GhanaWeb)
12. Barrick Mining Company: When large-scale mining came to Tanzania in the 1990s, companies such as Barrick purchased mineral rights from their legal owners. As a consequence, so-called artisanal miners were often displaced from land they held no legal title to. Today, many of them now search for gold in and around the country's large mines, posing numerous safety and environmental risks. In consultation with the community, Barrick has identified key steps that are being implemented in sequence to arrive at regulated, productive and sustainable small-scale mining operations. A mobilization campaign involves educating and informing artisanal communities to build a desire to transform the industry. The aim is to impart a sense of ownership, civic responsibility and entrepreneurial skills to ensure there is a common sense of purpose within the community.

Challenges for Engineering and Technological Institutions

Mining is an engineering discipline that involves the practice, the theory, the science, the technology, and application of extracting and processing minerals from a naturally occurring environment. Mining engineering also includes processing minerals for additional value. Mineral extraction is essential to modern society. Mining activities by their nature cause a disturbance of the environment in and around which the minerals are located. Mining engineers must therefore be concerned not only with the production and processing of mineral commodities, but also with the mitigation of damage to the environment as a result of that production and processing (<http://en.wikipedia.org/wiki/Mining>)

Mining engineers play a key role in the planning, exploitation and excavation of mineral resources. Mining also requires the skills and technology of several other branches of engineering, which is why most of the curriculum for years one and two is common to all branches of engineering such as mechanical, electrical, etc. The third and fourth years focus on mining engineering and include technical valuation, ventilation and environmental engineering, mine transport and rock mechanics. Engineering and technological programme are designed to provide the graduate with the engineering/technological expertise that he or she will require as a mining engineer or a technologist. These institutions can work, in conjunction with one another and in with mining industry, developed a programme designed to cater for the needs of the artisanal and small-scale miners. These include technical subjects for specialist skills in mining, mineral resource management and evaluation, and rock engineering, as well as management skills in evaluation techniques and fundamental mineral economic principles.

The challenges before African Engineering and Technological Institutions is to accept that beside their primary responsibility of the production of high and middle manpower, they are also to consider themselves as agents of positive change within their immediate and remote environment. The institutions must strive to positively bring about changes in the informal sector of the economy by engaging in capacity building of artisans. The institutions must come to terms with the reality that all modern exploration, mining and mineral processing equipments in use in the mineral industry today are the results of centuries of constant improvement and modification from their initial rudimentary stages. The ASM operators will require not very complicated implements/ equipments to improve on their mineral productivity and value addition. The major problems of the ASM are acquisition of mining equipment and basic materials that can enhance their work. The Engineering Institutions can engage in copy technology where simple mining and mineral processing equipment can easily be developed.

Exploration: Mining engineers are involved in the mineral discovery stage by working with geologists to identify a mineral reserve. The discovery can be made from research of mineral maps, academic geological reports or local, state, and national geological reports. Other sources of information include property assays, well drilling logs, and local word of mouth. Mineral research may also include satellite and airborne photographs. Mineral exploration is capital intensive and is capable of writing off millions of dollars without any returns on investments. Engineering and Technological institutions can liaise with Organizations such as those listed above to provide mineral exploration services to artisanal miners. Mining companies can assist the artisanal miners by conceding parts of their mining leases with lower or space concentration of minerals for mining. In doing so the artisanal and small-scale miners can benefit from the mineral data already established by the companies. Large mining companies should acknowledge the important role that ASM plays in the mining sector and provide support where possible, particularly through fostering partnership approaches.

Mining: The act of mining required different methods of extraction depending on the mineralogy, geology, and location of the resources. Characteristics such as mineral hardness, the mineral stratification, and access to that mineral will determine

the method of extraction. Generally, mining is either done from the surface or underground. Mining can also occur with both surface and underground operations taking place on the same reserve. Mining activity varies as to what method is employed to remove the mineral. The artisanal miners lack the technical know-how to scientifically extract minerals either by surface or underground methods. Mining is accomplished in a haphazard manner without recourse to safety standards and environmental sustainability. The result is loss of lives due to roof and bench collapses. Furthermore, the sub-surface openings are often very poorly ventilated and lighted leading to mine disasters through suffocation etc. The technological Institutions can embark in the fabrications of underground supports, ventilation networks and effective lightening of sub-surface mine openings in addition to dewatering, mine Haulage, Mine Dewatering, design of Pit Slopes/benches, detection of Rock Failures amongst.

Mineral Processing: Mineral processing methods are critical to the profitability of a mine operation, particularly as customers demand higher production, reliability, efficiency and new features from processing equipment. Some of the most advanced technology in the world for crushing, grinding, washing and separating ores have been developed over a very long time and outside the financial reaches of artisanal and small-scale miners. The institutions are in a position to fabricate affordable crushing, grinding/washing and separation machines. Artisanal and small-scale miners can be trained as lapidarists and empowered with lapidary machines. A *lapidarist* is an artist or artisan who forms stone, mineral, gemstones into decorative items such as engraved gems, including cameos, or cabochons, and faceted designs, or who is an expert in precious stones; and can be a collector of or dealer in gems. Diamond cutters are generally *not* referred to as lapidaries, due to the specialized techniques which are required to work diamond. There are also many other forms of lapidary, not just cutting and polishing stones and gemstones. These include: casting, faceting, carving, jewellery and mosaics. Most lapidary work is done using motorized equipment and resin or metal bonded diamond tooling in successively decreasing particle sizes until a polish is achieved. The development of amalgam retorts should be encouraged to assist the gold miners in effective recovery and minimize the mercury pollution. The essence of mineral processing is value addition and consequently higher selling prices of commodities.

Marketing: Artisanal and small-scale miners are generally poor people whose daily living is dependent on mined commodities. The marketing of minerals by the artisanal miners is generally through the middle-men who stake in trade is maximum exploitation taking advantage of the financial vulnerability of the miners. Fair-trade initiatives for giving small-scale producers in developing countries the opportunity of trading their products under better selling terms and conditions should be developed where possible. The establishment of Marketing Boards for the purchase of minerals by the government can enhance the marketing value of mineral commodities. Alternatively, collaborative relationships between Mining companies and artisanal and small-scale miners can ensure that minerals mined are purchased at higher value by the companies.

III. Conclusion

Artisanal and small-scale mining is one of the world's fastest-growing industries which trigger the conclusion that for the ASM sector to make the expected contribution to poverty alleviation; serious efforts must be made to break the vicious circle of resource-dependence and poverty. Artisanal mining by its mode of operation which is unscientific is neither legalized nor organized. Artisanal mining in Africa whether is at the tin fields Jos, Goldfields of Zamfara, coltan-fields of the rebel-controlled region of north-eastern Congo, the goldfields of Mali, the Karajipopo cobalt mine in Congo, the goldfields of the East Province of Cameroon, the of Tanzania, the copper-fields of Zambia etc, the Artisanal and small-scale mining (ASM) is a form of subsistence mining, which provides a direct or indirect livelihood for some 60 million people in Africa.

The sector has traditionally received a low proportion of aid relative to its contribution to livelihoods. However, in the last 10 years recognition of the sector's close connection to poverty has increased, and as a consequence and in line with a global shift in concern towards poverty alleviation ASM is gaining more attention. With the exception of few countries like Ghana, Botswana, Mali and Zambia who have made concerted efforts at legislation of the ASM sector, other countries merely pay lip-service to the plight of the miners. Lack of legislation and non-registration with the government deprive these people access to social services. Mindful of the contribution of Artisanal and small-scale mining to poverty eradication, the United Nations has recognized the contribution of this sector. World Bank projects in Bolivia, Burkina Faso, Ecuador, Ghana, Guinea, Madagascar, Mali, Mozambique, Papua New Guinea and Tanzania has attested to this assertion. Furthermore, UN-Organizations as UNDESA, UNDP, ECA, CEPAL, ESCAP, UNCTAD, UNEP, UNIDO and ILO are important multilateral donor agencies that can advance the cause ASM in line with best-practices. By the fastest contributions to the plight of the artisanal miners shall be the contributions of local Engineering and technological Institutions of African nations in ensuring that affordable equipment for exploration, mining and mineral processing are developed and/or fabricated to meet the local needs of the ASMs. The ASM sector must be recognized by Engineering and Technological Institutions as a significant generator of rural livelihoods that has the potential to alleviate Poverty and be a tool for sustainable development. An enhanced fiscal and regulatory frameworks by governments will ensure sustainable environmental and occupational health management to mitigate risks to the poor within Stabilized macroeconomic/fiscal regimes of African Nations.

References

- [1] Adu-Gyamfi Kwaku (2011): Small scale mining Business in Ghana: challenges and Prospects GhanaWeb
- [2] Geoffrey York (2012): Young and Dying: The scandal of Artisanal Mining. The Global Mail.
- [3] Keith Jefferis (2009): The Role of TNCs in the Extractive Industry of Botswana. Transnational Corporation; Vol. 18 no 1.
- [4] Kofi Tetteh (2011): An Overview of Ghana's Artisanal and Small Scale Mining (ASM) Sector. minerals commission
- [5] Mallo Stephen J. (2007): Mineral and Mining on the Jos Plateau, First Edition: ISBN 978-978-082-823-3 (ACON Publishers, Jos, Nigeria)
- [6] Mallo Stephen J. (2012): The Nigerian Mining Sector: An Overview. Continental J. Applied Sciences 7 (1): 34 – 45.
- [7] Mallo Stephen J. (2011): Capacity Building for Engineers and Geoscientists: As Essential Tool Toward the Realization of Nigeria's Vision 20:2020. *Continental Journal of Engineering Sciences*: Vol. 6 (3): 38 - 45, 2011 ISSN: 2141 – 4068.
- [8] Mallo Stephen J. (2011): Wazoh H.N. Aluwong K.C Elam EA. Artisanal Mining of Cassiterite: The Subsurface (Loto) Approach, Sheet 390, Rayfield Jos, Nigeria. *Continental Journal of Environmental Sciences*: Vol.5 (2): 38 - 50, 2011 ISSN: 2141 – 4246.
- [9] Mallo Stephen J. (2012): The Re-Emerging Mining Industry in Nigeria: Issues for appropriate Manpower Training. Continental Journal of Sustainable Development. 3(2):15-25, 2012. ISSN: 2251-0486.
- [10] Mallo Stephen J. ; Wazoh H.N. Aluwong K.C Elam EA. Artisanal Mining of Cassiterite: The Sub-surface (Loto) Approach, Sheet 390, Rayfield Jos, Nigeria. Continental Journal of Environmental Science: Vol.5 (2): 38 - 50, 2011 ISSN: 2141 – 4246.
- [11] Mallo S.J. The Socio-Economic Impact of Artisanal Mining in Kuru (Naraguta Sheet168) Plateau State, North Central Nigeria. Continental J. Engineering Sciences 7 (3): 27 - 32, 2012 ISSN: 2141 – 4068.
- [12] Rosemarie Mwaipopo, Wilson Mutagwaba, David Nyange, Eleanor Fisher (2004):
- [13] Increasing the contribution of artisanal and small-scale mining to poverty reduction in Tanzania. Based on an analysis of mining livelihoods in Misungwi and Geita Districts, Mwanza Region. A report prepared for the Department for International Development (UK).
- [14] Sandra Garcia (2010): Artisanal Gold Mining: Unglamorous Practices at High Prices. MINING.COM.
- [15] Seydou Keita 2001): Study on Artisanal and Small-Scale Mining in Mali. Mining Minerals and Sustainable Development (MMSD).
- [16] Thomas Hentschel, Felix Hruscka, Michael Priester (2002): Global report on Artisanal & Small-Scale Mining. MMSD project of IIED.
- [17] Tieguhong Julius Chupezi (2009): Impacts of artisanal gold and diamond mining on livelihoods and the environment in the Sangha tri-National Park Landscape. Center for International Forestry Research).
- [18] Thomas Hentschel, Felix Hruscka, Michael Priester (2003): Artisanal and small-scale Mining: Opportunities and challenges. Projekt-Consult GmbH.
- [19] Thomas R. Yager, Omayra Bermúdez-Lugo, Philip M. Mobbs, Harold R. Newman, and David Wilburn R. (2007): "The Mineral Industries of Africa". 2005 Minerals Yearbook. U.S. Geological Survey, PD license (U.S. government source, public domain).
- [20] Background Note: Niger, United States State Department, Bureau of Public Affairs: Electronic Information and Publications Office. Bureau of African Affairs; September 2008. <http://en.wikipedia.org/wiki/Samira>
- [21] <http://minerals.usgs.gov/minerals/pubs/country/2005/myb3-sum-2005-africa.pdf>
- [22] Mining- www.un.org/esa/dsd/dsd_aofw_ni/ni_pdfs/.../fiji/Mining.pdf
- [23] http://www.mmsd.gov.ng/solid_minerals_sector/bitumen2.asp
- [24] Minerals Planning Policies and supply practices in Europe (2004), Commissioned by the European commission, enterprise Directorate under contract No ETD/FIF 2003 0781.
- [25] www.unido.org/index. Global Mercury Project.
- [26] Finland's Mineral Strategy, 2012
- [27] Center for Development studies University of Wales Swansea (2004): Livelihoods and Policy in the Artisanal and Small-scale mining Sector-An
- [28] "The Mineral Industries of Africa". 1994 Minerals Yearbook. U.S. Geological Survey (August 2007)

Ku Band Annular Ring Antenna on Different PBG Substrates

Shatabdi Chakraborty,¹ Shweta Srivastava²

^{1,2}Department of Electronics and communication, Birla Institute of Technology, India

ABSTRACT: In this paper, two types of PBG structures, one is the periodic lattice of air holes on the substrate and the other is a periodic lattice of air holes through the substrate and the ground plane, have been incorporated on the FR4 substrate to improve the performance of a simple annular ring antenna operating in the TM_{31} mode. For Ku band FR4 has higher loss which is reduced by integrating the air holes on the substrates. The effective dielectric constant of the substrates with two PBG structures are calculated theoretically using the Wheeler's Transform. There is a considerable increase in gain of annular ring antenna with these two different forms of PBG structures. The designed antenna structures are compared to find out an optimum design.

Keywords: Annular ring antenna, higher order mode, Ku band, Photonic Bandgap, Surface wave,

I. INTRODUCTION

The Antenna technology for satellite applications is an interesting commercial market for the mobile satellite terminals. Ku band is very popular for different satellite communication services, because of small component size and less interference at higher frequencies [1]. The effective size of the antenna is less which is very useful for satellite communication where small size is a great requirement. Therefore, the frequency of 14.5 GHz (Ku band) is selected for an optimum antenna design for applications in satellite communications.

In general it has been found that the FR4 substrate has high loss tangent in higher communication frequencies, and hence it is supposed to be unsuitable for Ku band. But conversely, FR4 is a low cost substrate and is very easily available. Also, the FR4 substrate has a higher dielectric constant which results in a smaller antenna size. To design a Ku band antenna on FR4, the losses due to the substrate have to be minimized. To reduce the losses, PBG structures can be integrated with the antenna. In the present endeavor, the structures selected are having air holes in the substrate resulting in reduction of dielectric constant and hence reducing the dielectric losses.

The objective of the present paper is to design, simulate, fabricate and test an enhanced gain Ku band patch antenna on FR4 substrate using Photonic Bandgap technology.

Photonic Band-gap structures (PBG) are periodic structures in which propagation of certain bands of frequencies is prohibited [2]. PBG structures are readily scalable and applicable to wide range of frequencies, including microwaves and millimeter waves. Several types of PBG structures have been developed previously for wide range of applications [3]-[8]. Two different forms of PBG structures have been used in this paper. One is a periodic lattice of air holes drilled on the substrate with the ground plane intact and the other is periodic lattice of air holes drilled through the substrate and ground plane [9]. Simulations have been carried out using the an soft HFSS software.

In section II, antenna design will be discussed. The simulated and experimental results of gain and power pattern will be discussed in section III. The last section will be conclusion that will summarize the entire research findings.

II. ANTENNA DESIGN

1.1 Theoretical Considerations: A simple annular ring antenna is designed for operation in the TM_{31} mode. An annular ring antenna has an advantage over the rectangular or circular patch antenna of having higher radiation efficiency because of two radiating edges. The selection of higher order mode is done to obtain good matching so that the antenna could be fed directly using coaxial cables [10]. The antenna is designed on FR4 substrate of height 1.6mm, $\epsilon_r = 4.4$ and loss tangent 0.03 [11-12]. The dimensions 'a' and 'b' are the inner and outer radii of the ring and are calculated as 3.9 mm. and 5.85 mm. for a design frequency of 14.5 GHz. Feed point is optimized for best matching at (x,y,z) = (28, 22, 1.6). Antenna with PBG structure has slightly different dimensions than the reference antenna, so that annular ring antenna with PBG structure resonates at the operating frequency f_0 of reference antenna. Period of the PBG structure is obtained using the following relation [13].

$$f_0 = \frac{c}{2S\sqrt{\epsilon_{ef}}} \quad (1)$$

Where f_0 operating frequency of the antenna, S = period of the structure, c= speed of the light in free space and ϵ_{ef} = effective dielectric constant [14]. Radius of the air holes of Figure 1 and Figure 2 are calculated as 0.25S, such that an optimized PBG structure is obtained [15].

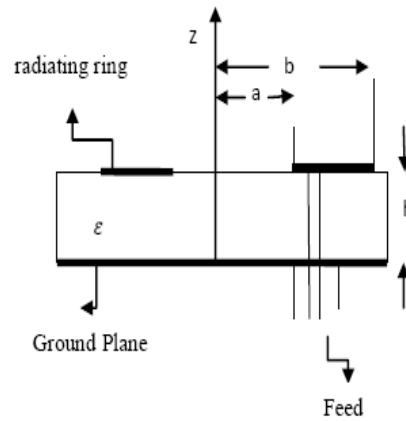


Fig.1 Geometry of annular ring antenna without PBG

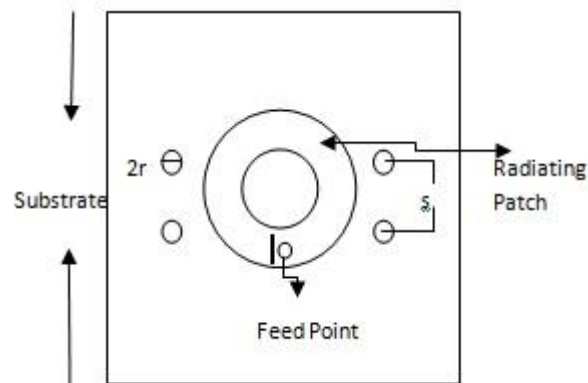


Fig.2 Annular ring antenna with periodic lattice of air holes drilled only on substrate (antenna1)

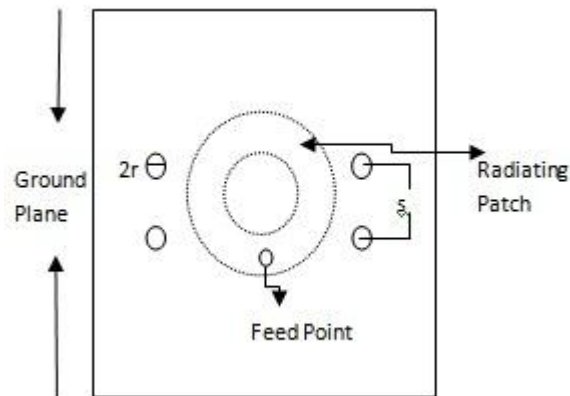


Fig.3 Annular ring antenna with periodic lattice of air holes drilled through substrate and ground plane (antenna2)

III. FABRICATED ANTENNA

The antennas are fabricated using photolithography and chemical etching. For antenna 1, the ground plane is added after the holes are drilled (Fig.4) and for antenna 2 the holes are drilled through the substrate and the ground plane (Fig.5).

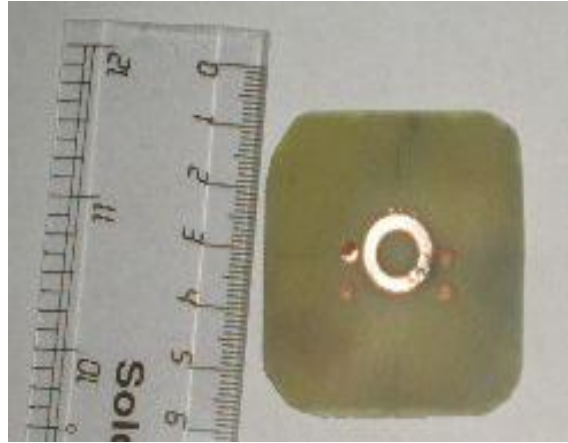


Fig.4. Top view of the fabricated annular ring antenna with periodic lattice of air holes drilled only on substrate (antenna1).

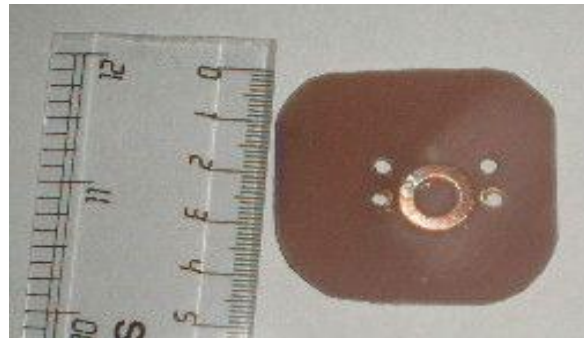


Fig.5 Top view of the annular ring antenna with periodic lattice of air holes drilled through substrate and ground plane (antenna2).

IV. THEORETICAL CALCULATION OF EFFECTIVE DIELECTRIC CONSTANT

Effective dielectric constant of the substrate plays an important role in PBG concept. In antenna1 and antenna 2 due to introduction of air holes effective dielectric constant of the substrate reduces and hence increases the gain of antenna. Using Wheeler transform effective dielectric constant is calculated [16, 17]. The effective dielectric constant, ϵ_{ef} is calculated from the following equation [18].

$$\epsilon_{ef} = \frac{\epsilon_0 \epsilon_1}{\epsilon_0(1 - q) + q\epsilon_1} \quad (2)$$

Where q is the filling factor and is calculated as

$$q = \frac{\text{area of the four air hole cylinders}}{\text{Total area of the rectangle}} \quad (3)$$

ϵ_0 and ϵ_1 are dielectric constants of air and substrate respectively.

V. EXPERIMENTAL AND SIMULATION RESULTS

The reflection loss, S_{11} of the fabricated antenna is measured with the help of the Vector Network Analyzer and Radiation patterns are obtained using Spectrum Analyzer and Signal Generator. Reference patch antenna resonates at 14.5 GHz showing good agreement between experimental and simulated results. Figure 6 shows comparative experimental and simulated reflection loss of the reference antenna and antenna 1, Figure 7 shows the comparative experimental and simulated reflection loss of reference antenna and antenna 2, and Figure 8 shows the comparative experimental and simulated results of antenna 1 and antenna 2 for comparison.

Figure 10 and figure 11 shows experimental and simulated Power Pattern (dB10 normalized) at resonance for the antenna 1 and antenna 2.

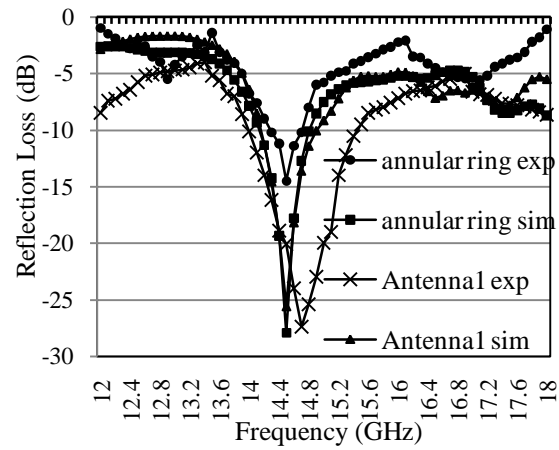


Fig. 6 Experimental and simulated reflection loss for the reference antenna and antenna 1.

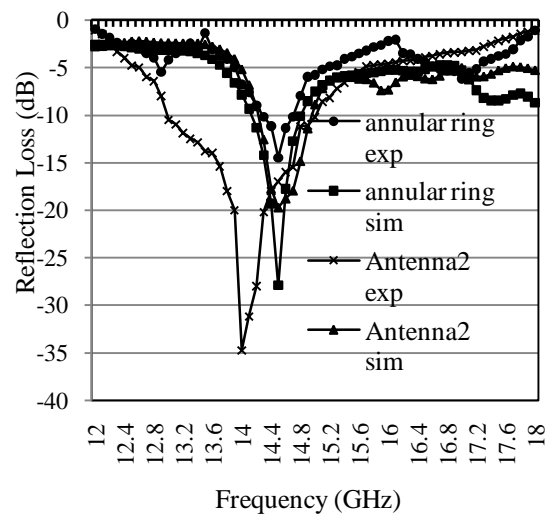


Fig.7 Experimental and simulated reflection loss for the reference antenna and antenna 2.

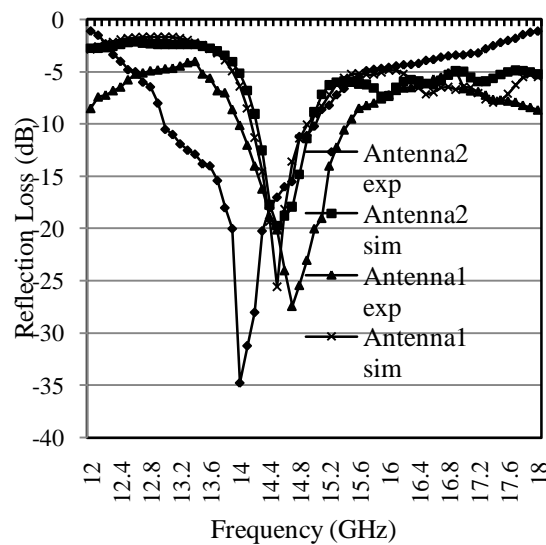


Fig. 8 Experimental and simulated reflection loss for the antenna 1 and antenna 2.

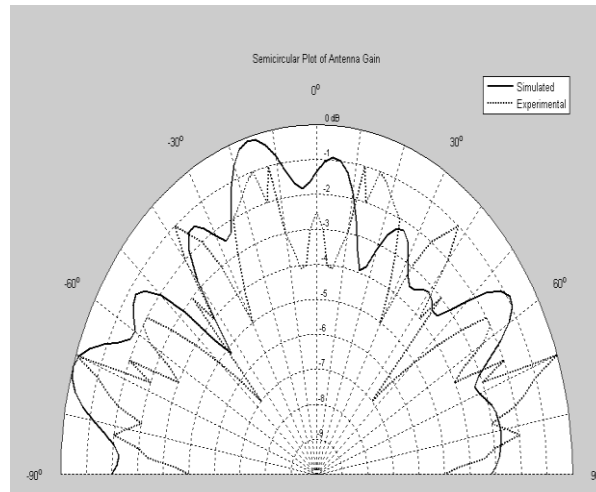


Fig.9 Experimental and simulated Radiation Pattern for reference antenna

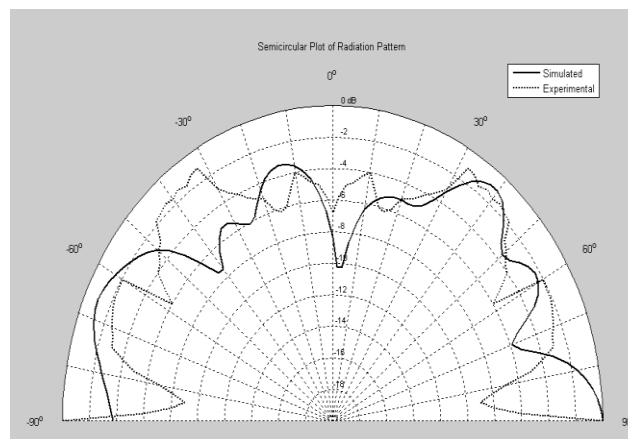


Fig. 10 Experimental and simulated Radiation Pattern for antenna1

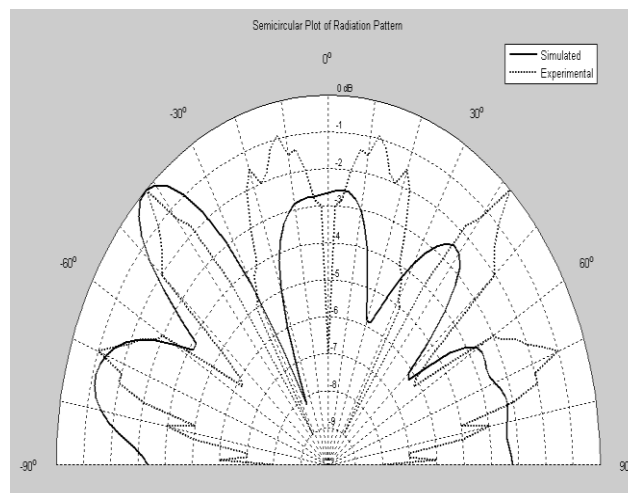


Fig. 11 Experimental and simulated Radiation Pattern for antenna2

VI. DISCUSSIONS

Figure 6 shows comparative experimental and simulated reflection loss of reference antenna and annular ring antenna with periodic lattice of air holes on the substrate (antenna1). From this figure it is clear that antenna1 resonates at the operating frequency of reference antenna. Reference antenna resonates at 14.5 GHz with experimental and simulated reflection loss of -14.4 dB and -27.9dB respectively and antenna1 resonates at 14.5 GHz with simulated reflection loss of -25.5 dB and experimentally resonates at 14.7 GHz with reflection loss of -27.41 dB. The Matching improves with the PBG structure but there is a slight shift in the resonant frequency. Bandwidth of antenna1 has increased by three times of the reference antenna. Bandwidth of reference antenna is 2.75% and bandwidth of antenna1 is 9.52%. Figure 7 shows comparative experimental and simulated reflection loss for antenna 2 which resonates at 14.5 GHz with simulated reflection loss of -19 dB and experimentally it resonates at 14.0 GHz with reflection loss of -34.75 dB. The slight shift in the resonance frequency of experimental results of both the antennas can be attributed to little bit of fabrication inaccuracy.

Bandwidth is also increased in antenna 2, it again increases more than three times than the reference antenna. Bandwidth of antenna 2 is 10%. Figure 8 shows comparative experimental and simulated reflection loss for antenna1 and antenna 2 which emphasizes on the fact that antenna 2 gives the best value of S_{11} . The reference annular ring antenna has experimental and simulated maximum gain of 5.105 dB and 8.81 dB respectively. Antenna1 has experimental and simulated gain 9.168 dB and 13.48 dB respectively. Antenna2 has experimental and simulated gain 10.45 dB and 14.37dB respectively. The normalized power pattern of the antennas is shown in Fig. 9-11. The experimental and simulated results of the radiated power with angle are in good agreement for all the three antennas. The shift in radiation maxima is seen in all the cases which are a result of higher mode excitation [19]. Table 1 shows the comparative results of all fabricated antennas.

VII. CONCLUSION

In this research article annular ring antenna with two different forms of PBG structures is presented. From the Theoretical calculation of effective dielectric constant, simulated and experimental results it is observed that the annular ring antenna with PBG structures have the advantage of gain enhancement. Annular ring antenna with periodic lattice of air holes drilled through the substrate and ground plane exhibits better gain enhancement than annular ring antenna with periodic lattice of air hole drilled only on the substrate. Objective of my research work is also fulfilled as gain of antenna2 is just doubled than simple annular ring antenna on FR4 and using Photonic Bandgap technology, a high gain, highly cost effective Ku band annular ring antenna is successfully designed. Improved antenna performances with this design make it useful for wide range of applications for higher frequencies.

TABLE I
COMPARISON TABLE

Para-meter		Simple annular ring antenna (Reference Patch antenna)	Antenna1	Antenna2
S11 dB	Simulated	-27.9dB (14.5 GHz)	-25.5 dB (14.5 GHz)	-19dB (14.5 GHz)
	Experimental	-14.4dB(14.5 GHz)	-27.41 dB(14.7GHz)	-34.75 dB(14.0 GHz)
Gain dB	Simulated	8.81 dB	13.48 dB	14.37 dB
	Experimental	5.105 dB	9.168 dB	B

REFERENCES

- [1] M. Habibullah and M. T. Islam, Design of a modified W shaped patch antenna on AL₂O₃ ceramic material substrate for Ku band,” Chalcogenide Letters, vol. 9, no. 2, pp. 61–66, February 2012.
- [2] Shun-Yun Lin and Kin-Lu Wong A Conical-Pattern Annular-Ring Microstrip Antenna With A Photonic Bandgap Ground Plane Microwave and optical technology letters Vol. 30, No. 3, August 5 2001 pp 159-161
- [3] T.H. Liu, W.X.zhang, and K.F.Tsang, Low profile spiral antennas with PBG substrate, Electronic Lett 36 (2000),779-780
- [4] Y.Qian,R.Coccioli D.Sievenpiper,V.Radisic,E.Yablonvitch and T.itoh, A microstrip patch antenna using Photonic bandgap structures” Microwave J 42 (1999),66-76
- [5] R.Coccioli, W.R. Deal and T.itoh ,Radiation characteristic of patch antenna on a thin PBG substrate,1998 IEEE Antenna and Propagation Soc Int symp Dig, pp 650-659
- [6] R. Coccioli, F.R. Yang, K.P. Ma, and T. Itoh, Aperture-coupled patch antenna on UC-PBG substrate, IEEE Trans Microwave Theory Tech 47(1999), 2123_2130
- [7] Ramon Gonzalo, Beatriz Martínez, Peter de Maagt, and Mario Sorolla Improved patch antenna performance using Photonic bandgap substrate,Microwave and optical technology letters Vol. 24, No. 4, February 20 2000 pp 213-214
- [8] Shun-Yun Lin and Kin-Lu Wong ,Effects of slotted and Photonic Bandgap ground planes on the characteristics of an air substrate annular ring patch antenna in the TM₂₁ mode, Microwave and optical technology letters Vol. 31, No. 1, October 5 2001 pp 1-3
- [9] R. Gonzalo, B. Martinez, P. Maagt, and M. Sorolla, Improved patch antenna performance by using photonic bandgap substrates, Microwave Opt Technol Lett 24(2000), 213_215.
- [10] Microstrip Antenna Design Handbook, Artech House, Garg R., et.al 2001, pp.366-367
- [11] Dipl.-Ing ,Manfred Huschka and Mullingar ,New Base Materials for Multilayer Applications in High-Speed Digital and RF Technology, PLUS 4(2002)3
- [12] Maria Roo Ons, S.V. Shynuy, M Seredynskiz, Max Ammann, Sarah McCormack and Brian Nortonzz ,Influence of Solar Heating on the Performance of Integrated Solar Cell Microstrip Patch Antennas, Antenna & High Frequency Research Centre Articles 2009
- [13] Y.Horii and M.Tsutsumi ,Harmonic control by photonic bandgap on microstrip patch antenna, IEEE Microwave Guided Wave Lett 9 (1999), 13-15
- [14] Microstrip Antenna Design Handbook, Artech House, Garg R., et.al 2001, pp.772
- [15] V.Radisic, Y Qian, R. Cockily and T. Itoh ,Novel 2D Photonic Bandgap Structure for microstrip Lines, IEEE Microwave Guided Wave Lett 8 (1998), 69-71
- [16] Harold A. Wheeler ,Transmission Line Properties of Parallel Strips Separated by a Dielectric Sheet, IEEE Transactions on Microwave Theory and Techniques March 1965 pp 172-185

Guidelines for Regulating the Heritage Monuments and Areas in Old-Goa

Shaikh Ali Ahmed,¹ Dr. B. Shankar²

¹(Planning Assistant, North Goa Planning Development Authority, Panaji)

²(Associate Professor, Institute of Development Studies, University of Mysore, Mysore)

ABSTRACT: Old-Goa is a world Heritage site declared by UNESCO, and well known for its rich built Heritage and culture having more than 50 monuments and sites of high significance. The area consists of a number of churches, convents and monuments way back from 16th century of innovative construction technology and architecture of significant value. The area surrounding the monuments with the surrounding architecture, height and bulk of the buildings has come under the threat of new developments without maintaining the harmony. These buildings are non contributory and also detracting the surrounding area. If the surrounding area development continues in a non-harmonious way, then the visibility of the heritage structures will be lost and the very purpose of protecting the monuments will be defeated. This paper brings out the issues of regulations around monuments and areas and suggests guidelines for the development of heritage monuments and areas of special zones.

Key words: Heritage structures, special zone, harmony, significant value,

I. Background

Old Goa is located on the East of Panaji about a distance of 10 kms in Tiswadi Taluka. It was the capital of new Portuguese colony and thus a principal city of Portuguese Eastern Empire. It is famous for its rich culture, built heritage, imposing churches and convents. The area around the Church of Basilica of Bom Jesus has been declared as a preservation area and admeasures approximately 801 hectares. This area includes about fifty sites, buildings and Monuments. The churches and monuments located in Old-Goa are already been declared as World Heritage Monuments by UNESCO in 1986. Old-Goa was founded by Adil Shah, the Sultan of Bijapur as port during the 15th Century on the banks of river Mandovi and was the second capital of the Bijapur Kingdom. It was a port city during the regime of Vijayanagar and Kadamba kings and conquered by the Portuguese ruler Alfonso de Albuquerque in 1510 from the Sultan of Bijapur. The city served as Portuguese India's administrative seat. The Portuguese constructed Churches and convents during their tenure and Old-Goa was a flourished city. During the 17th century, epidemics of plaque destroyed the city and it was left abandoned. The capital then shifted to Panaji, it was then the city earned the name "Velha Goa" which means "Old-Goa" in Portuguese. Ruled by Portuguese ruler, Old-Goa has a number of Monuments, churches and convents.

Most of these churches date back to the 16th century and are best examples of Manueline and Gothic architecture having very intricate detailing and ornamentation.

II. Importance Of Old-Goa

Old-Goa is gifted with scenic beauty, and is an important heritage city in terms of its historical back ground, rich built monuments and churches in unique Architecture i.e., in Manueline, Gothic, Tuscan, Ionic, Corinthian and Baroque which are rarely seen all over the globe. The innovative construction technology used for building the monuments in laterite blocks and lime plastered. Old Goa, the burial place of St. Francis Xavier, known for its unique cultural atmosphere, which is the result of the influences absorbed after 450 years long Portuguese rule. The influence has left a deep impact on the local traditions in all spheres and has formed a distinct cultural identity of the people of Goa. St. Francis Xavier had come to Goa to bless this land and its people. His mortal remains and spirit still resided at the imposing Church of Basilica of Bom Jesus. He was an instrumental to carry out with him the gospel of Jesus but more than that he also carried a way of life of people, their ethos and a rich culture in which perhaps dance, music, arts, crafts, architecture, festivals, fun and frolic were all entwined with each other. Old-Goa, therefore, has become "A symbol of religious coexistence, tolerance, and a unique example of cross fertilization of cultures in our vast, multi-racial, multi-lingual, multidimensional complex society". It has developed a strong identity of being "nature's own beautiful gift" that combines all the three aspects of heritage namely natural heritage, built heritage and cultural heritage.

It is now an important tourist destination for national and international tourist.

III. Heritage Conservation Area



Fig. 1: Map of trail area of Old-Goa

As per the Regional Plan of Goa 2021, the total heritage conservation area admeasures 801 hectares. There are more than 50 monuments and sites in the area declared as conservation area by the State Government. UNESCO has already declared the monuments of high significance as world heritage in 1986 and is under the control of ASI (Archaeological Survey of India) within the radius of 300

metres, but has no control over the areas beyond 300 metres. Some of the monuments are under the control of state Archaeology, and few are managed by the local government. There are many more heritage structures need identification for the purpose conservation and management.

IV. Heritage Resources



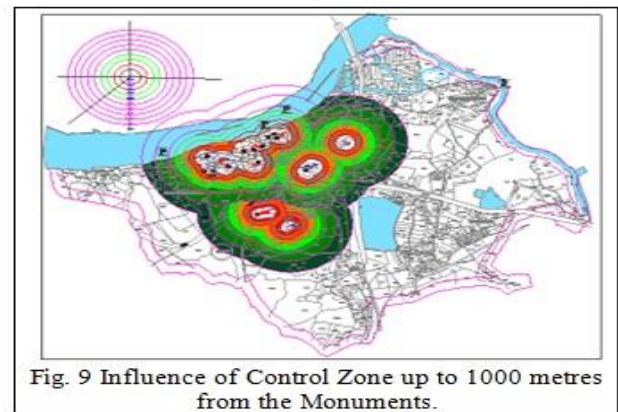
Monuments under the control of State Archaeology are: (a) Gate of the Palace of Adil Shah, (b) Chapel of St. Anthony, (c) Monastery of St. Monica and Chapel, (d) Chapel of St. Xavier, (e) Gate of the College of St. Papulo, (f) The Chapel of our Lady of Monte, (g) The Church of Our Lady of Rosary, (h) Ruins of Brahammapuri etc. The structures managed by the local authorities are: (i) Church and Convent of Miraculous Cross, (ii) Convent and Church of St. John of God, (iii) Chapel of St. Anthony, (iv) The Arch of Immaculate Conception etc. Many more heritage structures require identification for conservation and management so that the same can be transferred to the future generation in terms of sustainable development.

V. Influence Of Control Zone

An assessment for the heritage area was conceded by correctly mapping the heritage resources and existing structures on the plan. 100 to 1000 metres circles were drawn (as shown in fig. 9) from the heritage resources to know the impact of the existing structures within the control area of 300 metres, illegal construction and the new buildings cropping up in the vicinity on the heritage buildings and monuments controlled by the Archaeological Survey of India and State Archaeology. Red colour circle is drawn from 300 to 400 metres from the monuments indicates the high risk area of development. Orange colour circle is drawn from 400 to 500 metres indicates the medium risk and light green colour circle from 500 to 600 indicates low risk for monuments to allow the development. Last two circles of

Old-Goa has a number of heritage resources in the Heritage Conservation area. Few are listed below which are under the control of ASI viz. (a) Church of Basilica of Bom Jesus, (b) Tower and ruins of St. Augustine (c) Chapel of St. Catherine (d) Church of St. Cajetan. (e) Church of Se Cathedral (f) Church of St. Francis Assissi and (g) the Arch of Vice Roys.

Leaf green and dark green of 600 to 800 and 800 to 1000 metres, the area is suitable for imposing restrictions the development (fig. 10). The findings are noted below:



There are old existing structures within the radius of 300 metres from the monuments. Illegal and unauthorised constructions have cropped up near the Chapel of St. Francis Xavier and Se-Cathedral. The Conservation boundary demarcated on Regional Plan touches the radius of 300 metres at some places and 500 metres at the remaining areas.

The new development in the vicinity of the demarcated conservation area starts from 600 metres onwards without due respect to the architectural significance and in a non harmonious manner.

- The taller buildings in the area will hide the visibility of the monuments within a distance of 700 metres radius.
- The increase in coverage will develop the area in a congested manner.

- The aesthetic look of the area will be lost due to modern buildings coming up in the 600 metres radius from the monuments.
- Non-compatible commercial use within the radius of 300 metres is spoiling the environment of the area (Near the Arch of Viceroy's and Se-Cathedral).
- Vehicles are parked on the drive way of the roads reducing the carriage width of the road within the radius of 400 metres from the monuments.
- Disposal of solid waste is noticed within the 400 metres from the monuments (near the church of St. Francis Assisi)

VI. Proposed Heritage Guidelines

The area around the protected monuments is to be kept open upto 300 mts. from the protected monuments and no development of what so ever nature shall be allowed within this area. No Person including the owner or the occupier of a protected area shall construct any building within the protected area or carryout any type of activities without the permission of the Authority responsible.

The planned development will not arrest the vision of the world Heritage Monuments in the area and will have control over the skyline/roofscares so that the monuments will be seen at a distance of 1000 mts. without any obstructions. The present conservation line differs from a distance of 300 metres, to 700 metres from the Heritage monuments as it is analysed during the assessment. A further distance of 300 mts shall be provided so as to have a planned development within the trail area of Old-Goa.

A) Maintaining Skyline/ Roof-scape:

Buildings included in the listed Heritage Precincts or heritage conservation zone shall maintain their skyline or roof-scapes in the precincts. No high rise development shall be detrimental to the skyline or roof-scape or landscapes in the heritage precincts or conservation zone shall be allowed as may exist in the surrounding areas, so as not to diminish or destroy the value and beauty of the listed heritage buildings in the heritage conservation zone.

B) Existing structures within "No Development Zone"

The existing structures within the radius of 300 mts from the monuments near the church of St. Cajetan, shall be allowed for minor repairs to the existing structures, any type of major repairs like re-roofing, re-construction of walls, extensions and additions be discouraged. No new developments shall be allowed in this area.

C) Parking

The area near the church of St. Francis Assisi and Basilica of Bom Jesus can be acquired for the purpose of an organized pay parking lot to be charged every hourly, initially to accommodate 200 vehicles and further Extendable to accommodate 500 vehicles. The scheme will generate funds that can be utilised for maintenance and upkeep of the heritage structures.

D) Disposal of Solid waste

Portable litter bin at every (50mts to 100mts) be erected to facilitate the visitors and tourist in the areas for disposal of litter, and plastic articles like, carry bags, bottles, packets tea and coffee cups be banned in the area.

VII. Model For Development Of Monuments In Old Goa

"It shall be the duty of every citizen of India to value and preserve the rich heritage of our composite culture" -Article 51 A (F) of the Constitution of India. The necessity to preserve and conserve the cultural and built heritage was recognised by the state. The Government of Goa has recently notified and published "The Goa Land Development and Building Construction Regulation 2010" to preserve, conserve and manage the Heritage monuments and structures of Old-Goa. However, a lot more needs to be done for the planned development of heritage areas by enforcing effective regulation that will give a new vision for the heritage areas of Old-Goa. Keeping the vision for Old-Goa, a model for effective planned development of the area has been developed so that the vision of the monuments is not lost up till the distance of 1000 metres from the monuments protected by Archaeological Survey of India and State Archaeology. Below fig. shows the type of development to be allowed from 300 metres to 1000 metres from monuments for effective development of the area.

Table No. 1 Showing the Guidelines in tabulated form							
Sr. No.	Distance from monuments	Set back		Maximum floors allowed	Permissible height in meters	Maximum, per. coverage	Max. per. FAR
		front	Side and rear				
1.	Within 300 metres	---	---	No development of whatsoever nature be allowed			
2.	300 to 500 metres	3.0	3.0	Ground + First Floor only	7.60 mts.	30%	60 %
3.	300 to 500 metres	3.0	3.0	Ground + First Floor, and second floor recessed	9.00 mts.	30%	80 %
4.	1000 and above	3.0	3.0	General regulation apply			

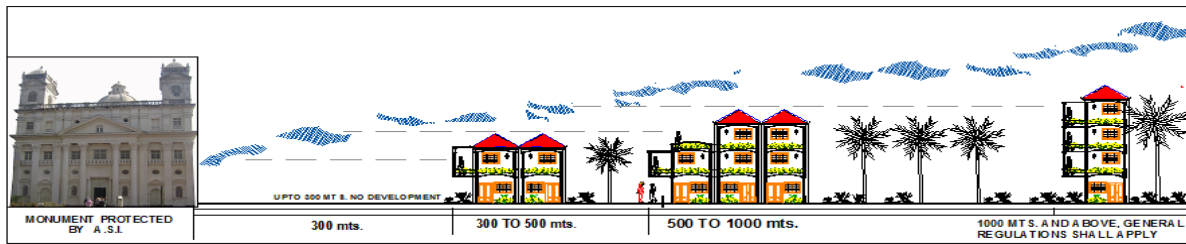


Fig. 10 Suggested Development Model for Monuments of Old-Goa

VIII. Conclusion

Old-Goa is known for its rich culture and built heritage in unique Manueline and Gothic Architecture and innovative construction technology which needs to be managed properly. The heritage areas are facing threats of losing its vision due to new developments that are taking place in the immediate vicinity of heritage monuments and areas. The new buildings that are coming are taller in height, bulk in size, less in setbacks, more in coverage and Floor Area Ratio (FAR). If this development trend continues without proper guidelines for regulating the control zone and around the monuments, in harmonious developments mushrooms in the built areas and the image of city will also be lost. The guidelines are required to regulate the control zone and around the monuments and also to ensure the planned development in the control zone and monuments thereby maintaining its vision for the monuments from a distance of 1000 metres. The rich Manueline and Gothic styled built heritage will be focused and will gain its value for its high significance.

The area will be developed in planned manner retaining its significant value. The heritage guideline serves as legal tool for regulating the heritage areas and monuments in the City of Old Goa.

References

- [1]. Shaikh Ali Ahmed and Shankar B., "Challenges of Planning for Heritage Areas in Panaji City", International Journal of Modern Engineering Research (IJMER), Vol.2, Issue.1, Jan-Feb 2012 pp-446-450
- [2]. Shaikh Ali Ahmed and Shankar B., "Conservation of Heritage Areas in the City of Panaji: A Case Study of Fontainhas Area", International Journal of Modern Engineering Research (IJMER), Vol.2, Issue.2, Mar-Apr 2012 pp-442-446.
- [3]. Shaikh Ali Ahmed and Shankar B., "Planning for Conservation of Heritage Areas in Old Goa: Issues and Strategies", IDES_CPS, Civil Engineering Series-Advances in Civil Engineering ACE, Ed., pp-11-15, 2011, New York.
- [4]. Shaikh ali Ahmed and Shankar B., "Municipal Solid Waste in Heritage Conservation Areas- A Case Study of Panaji", 1st Edn. Vol. 1 and Vol.2, Sustainable Waste Management- Municipal, Industrial and Agricultural, by Sadhan K. Ghosh et al, Oxford Publishing House , Kolkata (ISBN 81-86862-46-3 & ISBN 81-86862-74-1, July 2012, pp-59-63 Mysore.
- [5]. Report on Inner City Guide, Nelson City Council, 2004
- [6]. Joshi C., et al, World Heritage Series Old Goa, Archaeological Survey of India, Goa.
- [7]. Regional plan Goa, 2001 and 2021, Town & Country Planning Department, and Government of Goa.
- [8]. Report of the Sewri Consultants Pvt. Ltd., Mumbai, India and Sandhya Sawant, Director Bombay Collaborative Urban design and Conservation Pvt. Ltd., Mumbai, India.

on restoration of Capela da Nossa Senhora do Monte, Old Goa by Managing Director,

- [9]. Government of Goa, The Ancient Monuments and Archaeological Sites and Remains Act, No. 24 of 1958, Government of India.
- [10]. Government of Goa, The Goa Ancient Monuments and Archaeological Sites and Remains Act, 1978 and Rules, 1980.
- [11]. Government of Goa, The Goa Town and Country Planning Act and Rules, Government of Goa, Planning and Development Authority (Development Plan), Regulations, 1989, Panjim Planning and Development Authority, Panjim.
- [12]. Report of the Tourism Master Plan: GOA- 2011 final report prepared by Consulting Engg. Services (I) Ltd. for Government of Goa, Department of Tourism.
- [13]. Walking in and Around Panaji-Goa, Published in January 2005 by Goa Heritage Action Group and The Corporation of City of Panaji.
- [14]. Govt. of Goa, The Goa (Regulation of Land Development and building) Act 2008 and the Goa Land Development and Building Construction Regulation 2010, second edition 2011.
- [15]. Government of Goa, Panaji, a Search for Identity, Oct. 1997, The North Goa Planning and Development Authority.
- [16]. Vasco Pinho, November 2009, Snapshots of Indo-Portuguese History-I, Panaji.
- [17]. The Story Behind the Panjim Creek, May 2012, (web publication; Goenchen.com).

BIOGRAPHIES



Shaikh Ali Ahmed received M.Tech in Urban and Regional Planning from the University of Mysore, Mysore. Presently, he is working as Planning Assistant in North Goa Planning Authority, Panaji. He is Associate Member of the Institute of Town Planners, India; He is presently pursuing his Ph.D in Urban and Regional Planning at the Institute of Development Studies, University of Mysore. His research interests to include heritage conservation, heritage legislation.



Dr. B. Shankar received the B.E. degree in Civil Engineering in 1984, M.U.R.P degree in Urban and Regional Planning in 1989 and Ph.D degree in Urban and Regional Planning in 1997 from the University of Mysore, Mysore. He is working as Associate Professor in Urban and Regional Planning at the Institute of Development Studies, University of Mysore, Mysore.. His research interests to include Urban Planning, Urban Poverty, Community Development, Heritage Conservation, and Planning Legislation.

Design and Implementation of Truncated Multipliers for Precision Improvement and Its Application to a Filter Structure

R. Devarani,¹ Mr. C.S. Manikanda Babu,²

1, 2(ECE-PG, Sri Ramakrishna Engineering College/ Anna University, Chennai, India)

ABSTRACT: Truncated multipliers offers significant improvements in area, delay, and power. The proposed method finally reduces the number of full adders and half adders during the tree reduction. While using this proposed method experimentally, area can be saved. The output is in the form of LSB and MSB. Finally the LSB part is compressed by using operations such as deletion, reduction, truncation, rounding and final addition. In previous related papers, to reduce the truncation error by adding error compensation circuits. In this project truncation error is not more than 1 ulp (unit of least position). So there is no need of error compensation circuits, and the final output will be précised. To further extend the work the design is realized in a FIR filter.

Keywords: Computer arithmetic, faithful rounding, fixed- width multiplier, tree reduction, and truncated multiplier.

I. INTRODUCTION

MULTIPLICATION is one of the most area consuming arithmetic operations in high-performance circuits. As a consequence many research works deal with low power design of high speed multipliers. Multiplication involves two basic operations, the generation of the partial products and their sum, performed using two kinds of multiplication algorithms, serial and parallel.

Serial multiplication algorithms use sequential circuits with feedbacks: inner products are sequentially produced and computed. Parallel multiplication algorithms often use combinational circuits and do not contain feedback structures. Multiplication of two bits produces an output which is twice that of the original bit.

It is usually needed to truncate the partial product bits to the required precision to reduce area cost. Fixed-width multipliers, a subset of truncated multipliers, compute only n most significant bits (MSBs) of the $2n$ -bit product for $n \times n$ multiplication and use extra correction/compensation circuits to reduce truncation errors. In previous related papers, to reduce the truncation error by adding error compensation circuits. So that the output will be précised.

In this approach jointly considers the tree reduction, truncation, and rounding of the PP bits during the design of fast parallel truncated multipliers so that the final truncated product satisfies the precision requirement. In our approach truncation error is not more than 1ulp (unit of least position), so there is no need of error compensation circuits, and the final output will be précised.

II. REDUCTION SCHEMES OF PARALLEL MULTIPLIERS

PP (partial product) generation produces partial product bits from the multiplicand and multiplier. PP reduction is used to compress the partial product bits to two. Finally the partial products bits are summed by using carry propagate addition.

1. Dadda tree
2. Wallace tree

Dadda reduction performs the compression operation whenever it required. Wallace tree reduction always compresses the partial product bits. In the proposed method, uses RA reduction method. So that the final bit will be reduced. In the proposed truncated multiplier design, introduces column-by-column reduction. Here two reduction schemes are used, to minimize the half adders in each column because the full adder has high compression rate when compared to HA.

2.1 Scheme1 and Scheme2

Fig. 1 shows the reduction procedure of Scheme 1, reduction starting from the least significant column. Column height is h , including the carry bits from least significant columns, are also shown on the top row where the columns that need HAs are highlighted by square boxes. Fig. 2 shows the RTL schematic of scheme 1 using Mentor Graphics.

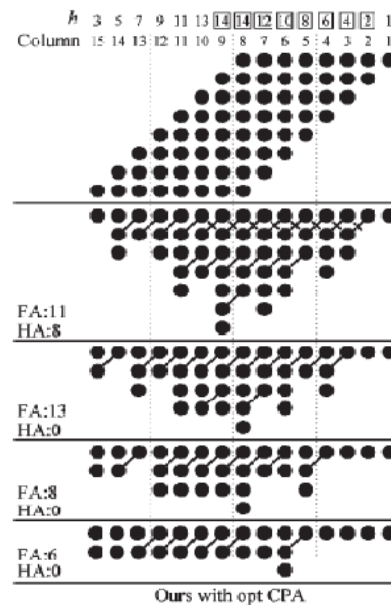


Fig. 1 Shows reduction procedure of scheme1 (38 FAs and 8 HAs).



Fig. 2 RTL schematic of scheme 1 using Mentor Graphics.

Scheme 1 having minimum CPA (carry propagate addition) bit width as twice reduction efficiency when compared to the Wallace method which produces the same result as that of RA method. Fig. 3 Shows reduction procedure of scheme 2. Scheme 1 is only used to determine whether an HA is needed and how many FAs are required in the per-column reduction that does not exceed the maximum number of Carry Save Additions in reduction levels.

The scheme1, scheme2 and proposed multiplier architecture has been simulated and synthesized using XILINX ISE Design Suite 8.1. From the synthesized results, the scheme 1 and scheme 2 has 1056 and 822 number of gates. The proposed multiplier has only 582 gates. Area utilization by the proposed method is less when compared to scheme 1 and scheme 2. Fig. 4 RTL schematic of scheme 2 using Mentor Graphics.

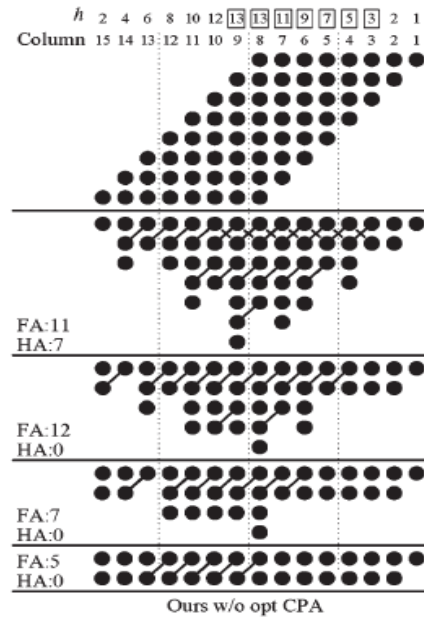


Fig. 3 Shows reduction procedure of scheme 2(35 FAs and 7 HAs).

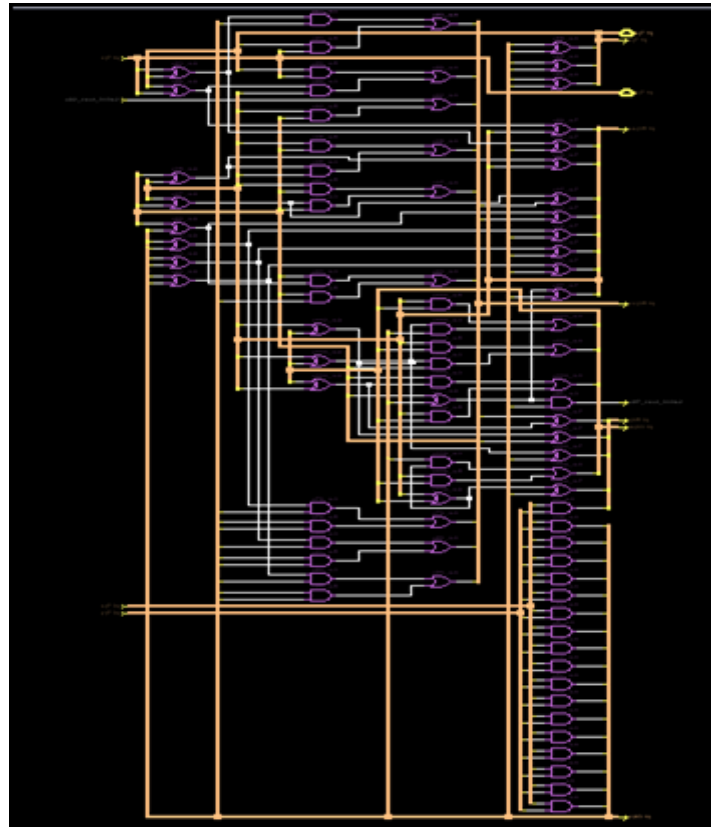


Fig. 4 RTL schematic of scheme 2 using Mentor Graphics.

III. PROPOSED PRECISION TRUNCATED MULTIPLIER DESIGN

The objective of a good multiplier is to provide a physically compact, good speed and low power consuming chip. To save significant power consumption of a VLSI design. In a truncated multiplier, several of the least significant columns of bits in the partial product matrix are not formed. This reduces the area and power consumption of the multiplier. It also reduces the delay of the multiplier in many cases, because the carry propagate adder producing the product can be shorter.

3.1 Deletion, Reduction, and Truncation of partial product bits

In the first step deletion operation is performed, that removes all the avoidable partial product bits which are shown by the light gray dots (fig 5). In this deletion operation, delete as many partial product bits as possible. Deletion error E_D should be in the range $-1/2 \text{ ulp} \leq E_D \leq 0$. Hereafter, the injection correction bias constant of $1/4 \text{ ulp}$.

The deletion error after the bias adjustment $-1/4 \text{ ulp} \leq E_D \leq 1/4 \text{ ulp}$. In Fig. 5, the deletion of partial product bits starts from column 3 by skipping the first two of partial product bits. After the deletion of partial product bits, perform column-by-column reduction of scheme 2.

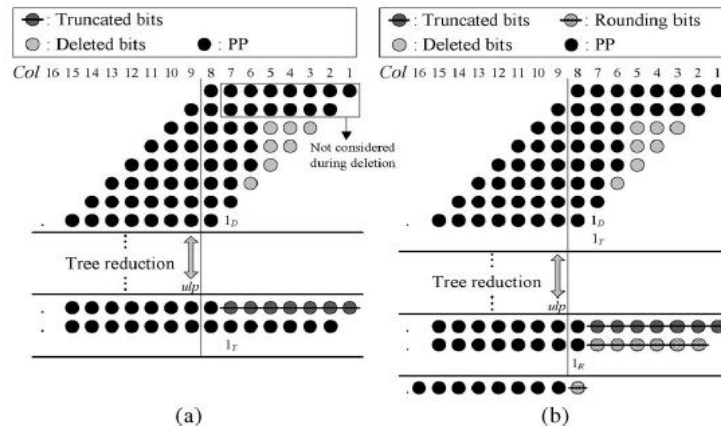


Fig. 5 8x8 truncated multiplication.(a) deletion, reduction and truncation. (b)deletion, reduction, truncation, and final addition.

After the reduction, perform the truncation, which will further removes the first row of (n-1) bits from column 1 to column (n-1). It will produces the truncation error which is in the range of $-1/2 \text{ ulp} \leq E_T \leq 0$. Hence introduction of another bias constant of $1/4 \text{ ulp}$ in truncation part. So the adjusted truncation error is $-1/4 \text{ ulp} \leq E_T \leq 1/4 \text{ ulp}$.

3.2 Rounding and Final Addition

All the operations (deletion, reduction, and truncation) are done, finally the PP bits are added by using CPA (carry propagate addition) to generate final product of P bits. Before the final CPA, add a bias constant of $1/2 \text{ ulp}$ for rounding. Rounding error is in the form of $-1/2 \text{ ulp} \leq E_R \leq 1/2 \text{ ulp}$. The faithfully truncated multiplier has the total error in the form of $-\text{ulp} < E = (E_D + E_T + E_R) \leq \text{ulp}$.

3.3 Proposed Algorithm

In proposed architecture we can multiply 8x8 bits, and the bits are reduced in step by step manner. Deletion is the first operation performed in Stage 1 to remove the PP bits, as long as the magnitude of the total deletion error is no more than 2^{-P-1} . Then number of stages to reduce the final bit width without increasing the error.

In normal truncated multiplier design, the architecture produces the output with some truncation error. But in the proposed design of truncated multiplier the truncation error is not more than 1 ulp, so the precision of the final result is improved. Fig. 6 shows proposed truncated multiplier.

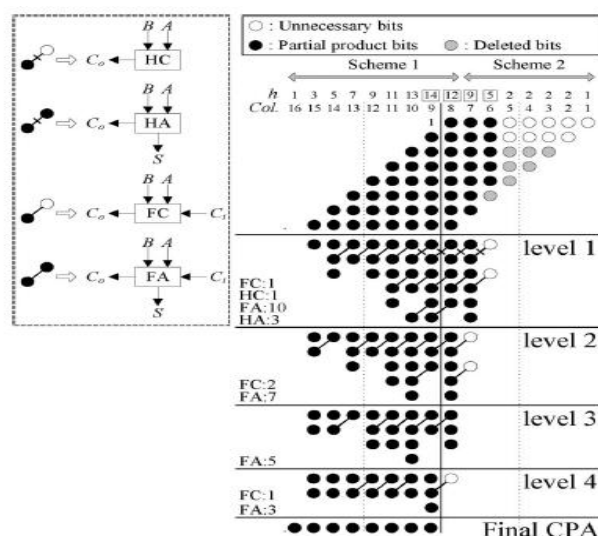


Fig. 6 Shows Proposed Truncated Multiplier.

IV. EXPERIMENTAL RESULTS

By using the Synthesis tool is Modelsim. The proposed system is implemented by using FPGA-Spartan 3E. This methods are mainly applicable in DSP systems.

4.1 Power and Area Analysis

TABLE 1 Power and Area analysis of the scheme 1, 2 & proposed

Parameter	Scheme 1	Scheme 2	Proposed
Power(W)	0.185	0.176	0.088
No. of Gate counts	1056	822	582

The scheme1, scheme2 and proposed multiplier architecture has been simulated and synthesized using XILINX ISE Design Suite 8.1. From the synthesized results, it is found that the scheme 1 consumes 185mW, scheme 2 consumes 176mW. The proposed multiplier consumes low power of 88mW when compared to scheme 1 and scheme 2.

The table 1 & 2 shows that the proposed method reduces the power and area than the previous methods. When compared to previous methods the precision is improved.

V. REALIZATION OF PROPOSED WORK IN FIR FILTER

Truncated multiplier can be effectively implemented in FIR filter structure. Conventional FIR filter performs ordinary multiplication of co-efficient and input without considers the length. Thus the structure can be made effective by replacing the existing multiplier with the proposed fixed width truncated multiplier for visible area reduction. Fig. 7 shows the architecture of FIR Filter.

5.1 General FIR filter

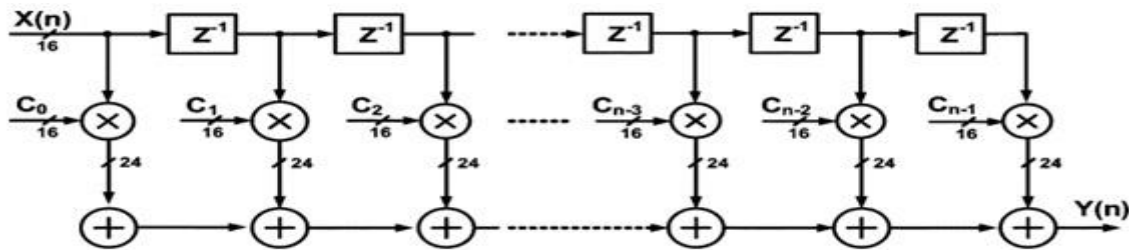


Fig. 7 Architecture of FIR Filter.

Fig. 7 FIR filtering operation performs the weighted summations of input sequences, called as convolution sum, which are frequently used to implement the frequency selective—low-pass, high-pass, or band-pass filters. Generally, since

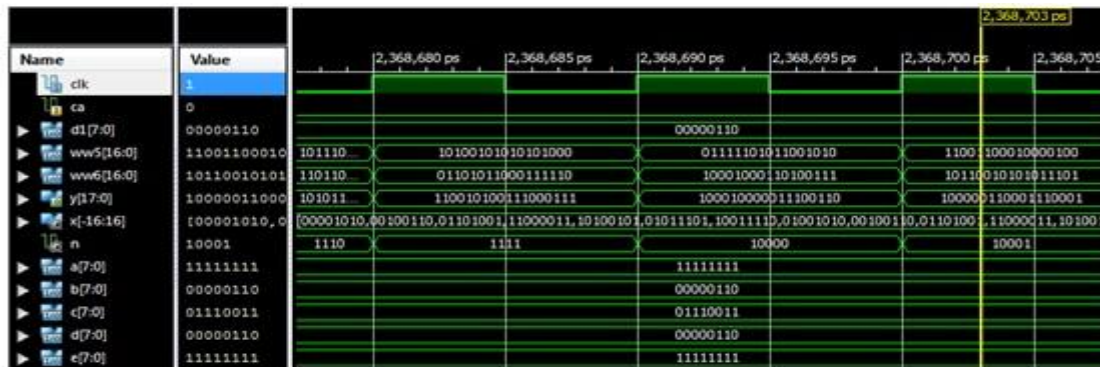


Fig. 8 Simulation Result of Conventional FIR Filter.

The amount of computation and the corresponding power consumption of FIR filter are directly proportional to the filter order, if we can dynamically change the filter order by turning off some of multipliers, significant power savings can be achieved.

However, performance degradation should be carefully considered when we change the filter order. The simulation result of conventional digital filter is shown in Fig. 8. The CLK represents the clock signal. The output is represented as the y. The coefficients are stored in the ROM as they are fixed. The n represents the tap of the filter. The output y changes with respect to the CLK signal.

The power of the conventional FIR filter is analyzed by using XILINX power analyzer . The power calculated with respect to the CLK.

TABLE 2 Area analysis of conventional FIR filter

Parameter	Conventional
No. of Gate counts	22,362

VI. CONCLUSION

There are many works proposed to reduce the truncation error by adding error compensation circuits so as to produce a précised output. This approach jointly considers the tree reduction, truncation, and rounding of the PP bits during the design of fast parallel truncated multipliers, so that the final truncated product satisfies the precision requirement.

In this approach truncation error is not more than lulp, so there is no need of error compensation circuits, and the final output will be précised. The scheme1, scheme2 and proposed multiplier architecture has been simulated and synthesized using XILINX ISE Design Suite 8.1.

From the synthesized results, it is found that the scheme 1 consumes 185mW, scheme 2 consumes 176mW. The proposed multiplier consumes low power of 88mW when compared to scheme 1 and scheme 2. The scheme 1 and scheme 2 has 1056 and 822 number of gates. The proposed multiplier has only 582 gates. Area utilization by the proposed method is less when compared to scheme 1 and scheme 2.

The proposed work is implemented in FIR filter structure, where the results of the FIR structure with fixed width multipliers show considerable area reduction. The power is also reduced due to the effectiveness of the design.

VII. ACKNOWLEDGEMENTS

The authors thank the Management and Principal of Sri Ramakrishna Engineering College, Coimbatore for providing excellent computing facility and encouragement.

REFERENCES

- [1] J. E. Stine and O. M. Duverne, "Variations on truncated multiplication," in Proc. Euromicro Symp. Digit. Syst. Des., 2003, pp. 112–119.
- [2] J. M. Jou, S. R. Kuang, and R. D. Chen, "Design of low-error fixed-width multipliers for DSP applications," IEEE Trans. Circuits Syst. II, s Analog Digit. Signal Process., vol. 46, no. 6, pp. 836–842, Jun. 1999.
- [3] L.-D. Van and C.-C. Yang, "Generalized low-error area-efficient fixed width multipliers," IEEE Trans. Circuits Syst. I, Reg. Papers, vol. 52, no. 8, pp. 1608–1619, Aug. 2005.
- [4] M. J. Schulte and E. E. Swartzlander, Jr., "Truncated multiplication with correction constant," in VLSI Signal Processing VI. Piscataway, NJ:IEEE Press, 1993, pp. 388–396.
- [5] E. J. King and E. E. Swartzlander, Jr., "Data-dependent truncation scheme for parallel multipliers," in Proc. 31st Asilomar Conf. Signals, Syst. Comput., 1997, pp. 1178–1182.
- [6] M. J. Schulte, J. G. Hansen, and J. E. Stine, "Reduced power dissipation through truncated multiplication," in Proc. IEEE Alessandro Volta Memorial Int. Workshop Low Power Des., 1999, pp. 61–69.
- [7] T.-B. Juang and S.-F. Hsiao, "Low-error carry-free fixed-width multipliers with low-cost compensation circuits," IEEE Trans. Circuits Syst. I, Reg. Papers, vol. 52, no. 6, pp. 299–303, Jun. 2005.
- [8] A.G.M. Strollo, N. Petra, and D. De Caro, "Dual-tree error compensation for high-performance fixed-width multipliers," IEEE Trans. Circuits Syst. II, Exp. Briefs, vol. 52, no. 8, pp. 501–507, Aug. 2005.
- [9] E. G. Walters and M. J. Schulte, "Efficient function approximation using truncated multipliers and squarers," in Proc. 17th IEEE Symp. ARITH, 2005, pp. 232–239.
- [10] C. S. Wallace, "A suggestion for a fast multiplier," IEEE Trans. Electron. Comput., vol. EC-13, no. 1, pp. 14–17, Feb. 1964.
- [11] L. Dadda, "Some schemes for parallel multipliers," Alta Frequenza, vol. 34, pp. 349–356, 1965.
- [12] N. Petra, D. De Caro, V. Garofalo, E. Napoli, and A. G.M. Strollo, "Truncated binary multipliers with variable correction and minimum mean square error," IEEE Trans. Circuits Syst. I, Reg. Papers, vol. 57, no. 6, pp. 1312–1325, Jun. 2010.
- [13] J.-P. Wang, S.-R. Kuang, and S.-C. Liang, "High-accuracy fixed-width modified booth multipliers for lossy applications," in IEEE Trans. Very Large Scale Integr. (VLSI) Syst., Jan. 2011, vol. 19, no. 1, pp. 52–60.
- [14] J.-A. Pineiro, S. F. Oberman, J. M. Muller, and J. D. Bruguera, "Highspeed function approximation using a minimax quadratic interpolator," IEEE Trans. Comput., vol. 54, no. 3, pp. 304–318, Mar. 2005.
- [15] K. C. Bickerstaff, M. Schulte, and E. E. Swartzlander, Jr., "Parallel reduced area multipliers," J. VLSI Signal Process., vol. 9, no. 3, pp. 181–191, 1995.
- [16] Hou-Jen Ko and Shen-Fu Hsiao (2011) 'Design and Application of Faithfully Rounded and Truncated Multipliers With Combined Deletion, Reduction, Truncation, and Rounding,' IEEE Trans. Circuits Syst. II, vol. 58, no. 5, pp. 304–308.

Evaluation and Comparison of the Meaning and Concepts of Contemporary Urban Parks and Historic Gardens

Mohammadjavad Mahdavinejad,¹ Mahmoud Abedi²

¹ Assistant Professor, Faculty of Art and Architecture, Tarbiat Modares University, Tehran 1411713116, IRAN

² M. A. In Architecture, Faculty of Art and Architecture, Tarbiat Modares University, Tehran (1411713116), IRAN.

Abstract: The meaning of the built environment has always attracted architects and landscape designers. This study is aimed to study meaning and concepts of urban parks in comparison with historic gardens. The literature review of the research emphasizes on impacts of environment on the addressees because of environmental elements and design. To address the issue the study have been done in two categories i.e. urban parks and historic gardens. Theoretical framework of the paper shows that there are three primary emotional responses - i.e. pleasure, excitation and dominance, in perception of meaning. Ten of the bipolar pairs emotions extracted from library state of the art of the paper were classified in these three primary emotional responses. Then a questionnaire was given to randomly selected samples of the research - fifty undergraduate students of the Architecture Departments of Sama Islamic Azad University in Saveh. These students were asked to rate a total of twenty photographs from four sites (Gardens: Arbab Mahdi and Akbarieh - Parks: Amirieh and Shahr) with the help of seven-point semantic differential scales under three headings; namely: pleasure, excitation and dominance. The results show that there are differences in perception of meaning between urban parks and historic gardens. In addition some invaluable aspects of historic gardens are missing in contemporary urban parks.

Keywords: concept, semantic differential, urban parks, historic gardens

I. INTRODUCTION

Looking from the theoretical point of view, the necessity of the protection and enhance of landscape visual quality is one of the environmental design fundamentals, which is essential while creating the ecologically stable, ergonomically comfortable, aesthetically attractive, and semantically meaningful landscape (Kamičaitytė-Virbašienė & Janušaitis, 2004). The idea that some places possess more pronounced character than others has been an underlying premise of many geomantic traditions in both eastern and western cultures since antiquity. More recently, humanistic geographers, environmental psychologists, and planners have revived this notion in concepts such as place, sense of place, place character, and genius loci (Altman & Low, 1992) (Seamon & Mugerauer, 1985). In addition it can be used to determine the relationship between perceived use and urban design characteristics. Many studies have been made to the physical characteristics of the communication and integration between the built environments and find a reaction of participants. Researches are related with the tourism development and Sustainable design as the recreational resource (Ansari, Mahdavinejad, & Abedi, 2012) (Mahdavinejad & Abedi, 2011). The results of public opinion analysis in 1972 showed that vicinity is beautiful when there is water (71%), forest (64%), expressive relief (27%), and structures (13%). According to the results of the research performed in 1986, the natural landscape visual type is beautiful considering its structure when there is 52% of water, 47% of relief, 32% of vegetation, 4% of architecture of buildings. A townscape is beautiful when the architecture of buildings consists 58%, vegetation – 50%, water – 13%, and relief – 10% (Kavaliauskas & Kurševičius, 1977). Although these studies analyze specific physical attributes, they do not include an in-depth analysis of the structure of observer emotional image reactions and how that relates to their overall evaluation (Llinares & Page, 2007). The conception of the visual environment includes an object i.e. the material environment, and a subject, i.e. the society, according to which the environment is analyzed.

Therefore, seeking to create landscape of a particular visual quality by means of environmental design, there is a need to know not only objective indicators of landscape visual quality but also the evaluation of these objective indicators by society – preferences of experts and laity (Kamičaitytė-Virbašienė & Janušaitis, 2004).

It is important to emphasize on participants conceptions and needs to meet sustainability in architecture and planning (Mahdavinejad & Abedi, 2011: 337-344). It is in need of architectural design criteria of socio-behavioral approach (Mahdavinejad & Mansoori, 2012: 475 – 482). Community-led method in art education and learning (Mahdavinejad & Moradchelleh, 2011a: 554-560) as well as community and social class (Mahdavinejad & Moradchelleh, 2012: 1068-1077) has a lot to do with Traditional architecture of developing countries especially in Iran (Mahdavinejad & Moradchelleh, 2011b: 677-682). It seems that the role of vernacular architecture in design of green areas e.g. urban parks has a lot to do with comfort and satisfaction of participants (Mahdavinejad et al., 2012: 65-68). Regarding to the literature review of the research, the purpose of this study is three fold: (1) describe characteristics of historic gardens and urban parks, (2) examine how these characteristics might differ between historic gardens and urban parks, and (3) describe how different types of landscape changes are liked and perceived, so we tested three hypotheses:

(H1): there is no difference in the perception of emotional concepts in the field of "pleasure" between urban park and garden audiences.

(H2): there is no difference in the perception of emotional concepts in the field of "excitation" between contemporary urban park and garden audiences.

(H3): there is no difference in the perception of emotional concepts in the field of "dominance" between contemporary urban park and garden audiences.

II. Literature Review

2.1. Importance of Meaning

The conception of the visual environment includes an object as the material environment, and the subject, according to which the environment is analyzed. The problems of the evaluation and creation of the visual environment cannot be solved considering only the environment without a subject –the society. The society is miscellaneous and there are a lot of attitudes to the landscape as a visual environment. Those attitudes differ according to the social position, education, profession, etc. These factors determine evaluation purposes and priorities (Kamičaitytė-Virbašienė & Janušaitis, 2004). The model explains landscape perception as a function of two latent variables: making sense (understanding) and involvement.

Humans, for adaptive reasons, prefer environments that are easy to comprehend, or easy to make sense of, but that are also simultaneously challenging or involving. Furthermore, environments that are easy to understand possess coherence and legibility; whereas, environments that are involving contain complexity/diversity and mystery (N.Singh, Donavan, Mishra, & Todd D., 2008). When we try to describe the meaning of a cultural symbol, we sometimes have difficulties to find the right words. The reason for this seems to be that cultural symbols often have very complex meanings (Schaefer & Rotte, 2010). Of several approaches to assessing landscape perception, one dominant approach (the cognitive paradigm) attempts to identify the meanings and values associated with landscapes with the objective of building predictive models of landscape preference (Zube, 1991).

2.2. Persian Garden

Persian garden is a place surrounded with mystery and restricted by codes and secrets, a place and position of memory and fantasy which does not remain within its boundaries, its scope expands beyond its walls and limitations, including the natural and cultural basis and the potentials of the environment that is around it. It means more than its tangible and objective characteristics and also associates and recalls its relations with universal order. Garden, this tame nature, enjoys the aesthetic, high, transcendent and utility values all at the same time (Irani behbahnai & khosravi).

2.3. Semantic Differential

The technique of semantic differentials has been introduced by Osgood et al. (1957). It was designed to measure the connotative meaning of concepts, personalities, or symbols. In this method subjects are asked to rate a concept or term on a scale with the poles described by two contrary adjectives (e.g. 'healthy' and 'sick'). The results provide information about the connotations of the term by revealing its relationships to a number of adjectives in a semantic space (Osgood, Suci, & Tannenbaum, 1957); for a German sample: Hofsta'tter, (1957). For example, the term 'safety' may be close to the adjectives 'peaceful' and 'cooperative', but far away from the adjective 'wild'. Based on a large collection of semantic differential scales, Osgood et al. (1957) performed factorial analyses and found three underlying determinants of semantic space that people use to assess concepts or phrases. Subsequent studies revealed that these three underlying dimensions are used by all subjects to evaluate concepts, values, or terms of their social environment, irrespective of language or culture. The first of these three factors are referred to 'evaluation' and loaded high on the adjective pair 'good-bad'. A second factor was related to 'strong-weak' adjectives. This factor was named 'potency'. Finally, the third factor described an 'active-passive' dimension and was labeled 'activity'.

Experimental studies have showed three primary emotional responses: pleasure, excitement and dominance. Pleasure deal with like and dislike sense; Exciting related to environment interesting features and Dominance is related to the sense of personal freedom (Lang, 1987). Ten of the bipolar pairs emotions extracted from library sources were classified in three primary emotional responses on a 7-point scale (It shows in Table 1).

Table 1: Definitions of the landscape descriptor variables and their attributes

Variables	Semantic differential bipolar pairs (1-7)	Definitions
Pleasure	Pleasant - Unpleasant	Pleasure deal with like and dislike sense
	Friendly - Unfriendly	
	Happy - Unhappy	
Excitation	Fictional - Realistic	Exciting related to environment interesting features
	Beautiful-Ugly	
	Glorious- Trivial	
	Hectic - Peaceful	
Dominance	Safe - Unsafe	Dominance is related to the sense of personal freedom
	Closed - Open	
	Comfortable - Uncomfortable	

III. Methodology

3.1. Environmental Setting and Procedure

The Kaplan's preference model views humans as information- seeking, information-using organisms. Because efficient gathering, processing, and storage of environmental information (in the form of cognitive maps) have survival and adaptive significance, humans have become extremely proficient at gathering and processing information from their environment. People react to visual environments, including landscapes, in two ways: as a visual array or two dimensional patterns, similar to a flat picture (e.g., the photograph of a given landscape), and as a three- dimensional pattern of the space that unfolds before them. That is, in perceiving a setting, scene, or landscape, apart from considering the immediate, two-dimensional qualities of the scene, people also imagine themselves in the scene and make projections about how they would function if they were to enter into the scene (Kaplan, 1992). Semantic Differential was developed by Charles Egerton Osgood and is designed to measure the connotative meaning of concepts. Firstly, after widely surveying a great amount of landscape resources, the method sets up landscape visual influence factors. Secondly, by showing photos, public feelings towards the visual elements can be measured and quantificational data considering public feelings can be produced. Lastly, it utilizes factor analysis to measure the quantificational data. Many surveys proved that using photographs as landscape evaluation intermediary is almost as same as site landscape evaluation (Weimin, 1996). The technique of altering the sets of items from positive to negative, as previously done by (Yildirim, Akalin-Baskaya, & Hidayetog`lu, 2007) (Akalin-Baskaya & Yildirim, 2007) (Kavaliauskas & Kurševičius, 1977) (Natori & Chenoweth, 2008) (Schaefer & Rotte, 2010) (Weimin, 1996).

In this study historic garden and urban park was represented by photographic prints. Photographs have been shown to serve as a good representation of real scenes. To reduce the seasonality bias, all Photographs were taken in early autumn approximately the same season in which the study was conducted. Photographs were chosen projection for the presentation media for logic reasons. The projection method has the advantage of enabling the survey of a large number of subjects, but we chose Photographs because we assumed it difficult to gather a large number of participants in one location. Slide projection would also limit the locations where the survey could be conducted, and pose difficulties in controlling for the brightness and contrast of showed Photographs.

3.2. Participants and Samples

The participants in this study were selected randomly among the students who study in department of architecture at Sama Islamic Azad University in Saveh, Iran and who were selected from those who had not seen the materials prepared for the experiment. In total there were fifty students involved. In order to achieve a more robust statistical result, the distribution of class years and gender of the participants were equally apportioned: 50% of the participants were in their first year and 50% second; additionally, 50% of the participants were female and 50% were male. The ages of all the participants range from 19 to 26.

3.3. Questionnaire

The questionnaire form consisted of two parts: the first part asked for general information about the participants i.e. department, age, gender, degree, years of education etc.; the second part consisted of seven-point semantic differential scales about their perception of meaning and concept between historic garden and urban park. The participants had to evaluate each of the bipolar adjective pairs on a 1–7 semantic differential scale. A total of ten bipolar adjective pairs were evaluated by the participants after familiarizing themselves with the items, three of which dealt with pleasure, four of which with Excitation, while the remaining items measured Dominance. Related bipolar adjective pairs were designated for each category; for pleasure: Pleasant – Unpleasant, Friendly – Unfriendly, Happy – Unhappy; for Excitation: Fictional - Realistic, Beautiful – Ugly, Glorious- trivial, Hectic – Peaceful; and for Dominance: Safe – Unsafe, Closed – Open, Comfortable – Uncomfortable.

3.4. Survey Administration

Participants were familiarized with the survey instrument using a sample Photographs at the beginning of the study. Participants were instructed to assume being present in the landscapes depicted by the Photographs not to evaluate the Photographs themselves and to describe their perceptions of those scenes on the Semantic Differential scales on the questionnaire. Having been familiarized with the survey instrument, the participants evaluated the photographs one at a time.

The set of Photographs were sorted in a random order. Two identical sets of Photographs were prepared, so that up to two persons could simultaneously complete the survey with their own set. When there were more than two persons participating simultaneously, Photographs were passed around the participants until everyone had evaluated all the Photographs. Students were surveyed in groups in their classrooms during their normal class hours, and all completed the survey within 20 min.

IV. Results and Discussions

The dependent variables (Pleasure, Excitation and Dominance) were separately computed for each of the historic garden and urban park. There were a total of five Photographs for each site. Preparation for testing ten scales conducted with SPSS software. Cronbach's alpha to assess the validity and reliability of the items in each scale was used. If the coefficient alpha for the factor was less than 0.7, the hypothesis test was dropped. The survey is a valid and reliable measure of the

construct because its validity and reliability coefficient confirmed by Cronbach alpha (0.7) and a pilot study with 32 respondents was undertaken to assess the validity and reliability of a questionnaire. Factor analysis of each scale was developed and Sample items for each scale in historic garden and urban park are showed that ten scale (Table2). The Cronbach alpha coefficient estimate of internal consistency for the scale, including the average scores for ten bipolar Semantic Differential scales grouped together in Table 2, was 0.91. The coefficient of all items was above 0.70, representing good reliability.

Table 2: Scale reliability of Semantic Differential used in the survey

Semantic differential bipolar pairs (1-7)	Factor loading	Scale reliability
Pleasant - unpleasant	0.86	0.91
Friendly - unfriendly	0.94	
Happy - unhappy	0.93	
Fictional - realistic	0.92	
Beautiful-ugly	0.83	
Glorious- trivial	0.88	
Hectic – peaceful	0.92	
Safe – unsafe	0.93	
Closed – open	0.88	
Comfortable - uncomfortable	0.82	

In this part, the statistical differences between meaning and implications for the dependent variables were analyzed. The results are given (in Table 3) as the mean, standard deviation and homogeneous group for three groups of scale items (Pleasure, Excitation and Dominance). The results (Table 3) indicate that perceptions of the meaning and implications for the dependent variables were statistically different and the ordering of meaning and concepts from the most positive to the most negative value is given as follows:

Table 3: The mean and standard deviation for ten bipolar Semantic Differential scales

Semantic differential bipolar pairs (1-7)	M	SD
Pleasant - unpleasant	5.02	1.53
Friendly - unfriendly	5.16	1.68
Happy - unhappy	4.94	1.97
Fictional - realistic	4.92	1.42
Beautiful-ugly	4.8	1.45
Glorious- trivial	5.1	1.72
Hectic – peaceful	4.64	1.21
Safe – unsafe	4.88	1.66
Closed – open	5	1.34
Comfortable - uncomfortable	5.06	1.36

The differences among the dependent variables including between historic garden and urban park were tested with one-way analysis of variance (ANOVA). According to these results, the differences among the dependent variables were found to be statistically significant for all Semantic differential bipolar pairs. The further steps of the analysis addressed the effect of the kind of landscape on the emotional responses of participants. For this purpose, in the first step of the analysis, mean values of the factors were compared across the experimental conditions. The comparison of the mean values of the observed variables between the different conditions of the experimental factor revealed significant differences as a result of the type of landscape. Subjects showed a clear preference for Initial emotional reactions representing historic site imagery, as compared to the visual representations of historic garden or urban park, with respect to attitude toward the initial emotional reactions and positive emotional responses evoked by the stimuli. Results of the descriptive analysis of the attitude toward the Initial emotional reactions scale and the semantic differential scales on emotional responses are shown in Table 4. One

way ANOVA analyses were performed for initial emotional reactions and each of the emotional response measures. Differences in the preference scores are appreciable and overall significant ($p < 0.001$).

Table 4: NOVA results of the dependent variables in terms of Initial emotional reactions

Variables	Semantic differential bipolar pairs (1-7)		Sum of squares	df	Mean squares	F
Pleasure	Pleasant – unpleasant	Between groups	0.18	1	0.18	0.11
		Within groups	74.8	48	1.56	
		Total	74.98	49		
	Friendly – unfriendly	Between groups	0.32	1	0.32	0.19
		Within groups	82.4	48	1.72	
		Total	82.72	49		
	Happy – unhappy	Between groups	2.42	1	2.42	1.23
		Within groups	94.4	48	1.96	
		Total	96.82	49		
Excitation	Fictional - realistic	Between groups	8	1	8	6.22
		Within groups	61.68	48	1.28	
		Total	69.68	49		
	Beautiful-ugly	Between groups	2	1	2	1.45
		Within groups	66	48	1.37	
		Total	68	49		
	Glorious- trivial	Between groups	7.22	1	7.22	4.48
		Within groups	77.28	48	1.61	
		Total	84.5	49		
	Hectic – peaceful	Between groups	5.12	1	5.12	4.51
		Within groups	54.4	48	1.13	
		Total	59.52	49		
Dominance	Safe – unsafe	Between groups	9.68	1	9.68	6.48
		Within groups	71.6	48	1.49	
		Total	81.28	49		
	Closed – open	Between groups	2.88	1	2.88	2.19
		Within groups	63.12	48	1.31	
		Total	66	49		
	Comfortable - uncomfortable	Between groups	0.02	1	0.02	0.014
		Within groups	66.8	48	1.39	
		Total	66.82	49		

With regard to the emotional responses, the initial emotional responses showing the conqueror setting rated lowest on comfortable- uncomfortable a feeling of dominance and second lowest in pleasant – unpleasant a feeling of pleasure. Conversely, conqueror elicited safe – unsafe most feelings of dominance, while rating second fictional - realistic most on excitation. Strongest positive responses were evoked by the semantic differential depicting the historic garden.

For the analyses of inferred landscape, paired t-test was performed to test for significant difference in ratings (by the same observers) between two similar historic gardens and two similar urban parks ($p = 0.05$). The differences among ten factors in the study (for each observer type, two kinds of landscape) were tested. Analysis of the variables was conducted by using SPSS software. If the direction of the response categories does not make a difference, then the means for the ten factors should all be statistically equivalent. Differences were considered significant at $P < 0.05$, indicating that the vectors of means for the two groups were equivalent.

V. Conclusion

In terms of ecological psychology, environment aesthetics shaped by the enjoyable environment. The findings confirm the theory of ecological perception on the importance of systems, the perceptual senses and creating an environment rich in sensory highlights. The sensory richness can increase the reliability and quality of the call action.

The research shows that the perception of emotional meaning and concepts of pleasure Variable, pleasantness, friendliness and happiness, between historic garden and urban park visitors, there is no difference. Test results of one-way analysis of variance (ANOVA) showed that the differences observed is in arousal of interest in the Excitation variable of the environment that includes “Fictional – realistic”, “Glorious- trivial” and “Hectic – peaceful”. Thus, a set of environmental capabilities and potentials, make a unique position for human behavior in the environment. In other words, the difference in the emotional responses, the interaction between features of a historic garden or urban park, and the needs of its audience.

Also in Dominance variable in scale of security among historic gardens and parks in urban contemporary audiences, major differences were observed.

Persian Gardens have a lot of apparent and latent values that many of these values are missing. This study has shown that most of these values are probably related to excitement variables of Persian Garden. In other words, fictional, majesty and excitement scales of Persian gardens are same missing values. The research shows that urban parks design are far from their original, so it is not the extension of the principles of Persian garden.

References

- [1] Akalin-Baskaya, A., Yildirim, K., 2007. Design of circulation axes in densely-used polyclinic waiting halls. *Building and Environment*. 42, 1743-1751.
- [2] Altman, I., Low, S., 1992. *Place Attachment*. New York: Plenum Press.
- [3] Ansari, M., Mahdavinejad, M., Abedi, M., 2012. THE ROLE OF HISTORIC AND HERITAGE WEALTH IN SUSTAINABLE TOURISM DEVELOPMENT. *ASIAN JOURNAL OF SOCIAL SCIENCES & HUMANITIES*. 1(3), 70-77.
- [4] Hofstadter, P., 1957. *Gruppendynamik*. Reinbek: Rowohlt.
- [5] Irani behbahani, H., Khosravi, F. Persian Garden between Permanence and Innovation from .Retrieved 9 18, 2012, from icomos: <http://www.icomos.org/landscapes/english-text-final%20-%20RESIZE.pdf>
- [6] Kamičaitytė-Virbašienė, J., Janušaitis, R., 2004. Some Methodical Aspects of Landscape Visual Quality Preferences Analysis. *Environmental Research, Engineering and Management*. 3(29), 51-60.
- [7] Kaplan, S., 1992. *Environmental preference in knowledge-seeking, knowledge using organism*. New York: Oxford University Press.
- [8] Kavaliauskas, P., Kurševičius, K., 1997. Landscape and recreational needs of Lithuanian inhabitants. *Geography and geology* 13, 93-109.
- [9] Lang, J., 1987. *Creating Architectural Theory: The Role of the Behavioral Sciences in Environmental Design*. New York: Van Nostrand Reinhold Company.
- [10] Llinas, C., Page, A., 2007. Application of product differential semantic to quantify purchaser perceptions in housing assessment. *Building and Environment* 42(7), 2488-2497.
- [11] Mahdavinejad, M., Abedi, M. 2011. Community-Oriented Landscape Design for Sustainability in Architecture and Planning. *Procedia Engineering*. 21, 337-344.
- [12] Mahdavinejad, M., Mansoori, S., 2012. Architectural Design Criteria of Socio-Behavioral Approach toward Healthy Model. *Procedia - Social and Behavioral Sciences* 35(1), 475-482.
- [13] Mahdavinejad, M., Moradchelleh, A., 2011a. Family-Led Method in Art Education and Learning, Case: Tehran, Iran. *Middle-East Journal of Scientific Research*. 9(4), 554-560.
- [14] Mahdavinejad, M., Moradchelleh, A., 2011b. Problems and Tendencies of the Development of the Architectural Sciences: Culture Research Aspect. *Middle-East Journal of Scientific Research*. 10(6), 677-682.
- [15] Mahdavinejad, M., Moradchelleh, A., 2012. The Impact of Family and Social Class on Efficiency of Arts Education and Learning. *Middle-East Journal of Scientific Research*. 11(8), 1068-1077.
- [16] N. Singh, S., Donovan, D., Mishra, S., Todd D., L., 2008. The latent structure of landscape perception: A mean and covariance structure modeling approach. *Journal of Environmental Psychology*. 28, 339-352.
- [17] Nassauer, J., 1983. Framing the landscape in photographic simulation. *Journal of Environmental Management*. 17, 1-16.
- [18] Natori, Y., Chenoweth, R., 2008. Differences in rural landscape perceptions and preferences between farmers and naturalists. *Journal of Environmental Psychology*. 28, 250-267.
- [19] Osgood, C., Suci, G., Tannenbaum, P., 1957. *The Measurement of Meaning*. Urbana, IL: University of Illinois Press.
- [20] Schaefer, M., Rotte, M., 2010. Combining a semantic differential with fMRI to investigate brands as cultural symbols. *SCAN*. 5, 274-281.
- [21] Seamon, D., Mugerauer, R., 1985. *Dwelling, Place and Environment: Towards a Phenomenology of Person and World*. Dordrecht: Martinus Nijhoff Publishers.
- [22] Stewart, T., Middleton, P., Downton, M., Ely, D. 1984. Judgments of photographs vs. field observations in studies of perception and judgment of the visual environment. *Journal of Environmental Psychology*. 4, 283-302.
- [23] Weimin, Z., 1996. SD in environmental evaluation of Architectural space. *Tsinghua Science and Technology*. 4, 42-45.
- [24] Yildirim, K., Akalin-Baskaya, A., Hidayetoglu, M., 2007. Effects of indoor color on mood and cognitive performance. *Building and Environment*. 42, 3233-3240.
- [25] Zube, E., 1991. Environmental psychology, global issues, and local landscape research. *Journal of Environmental Psychology*. 11, 321-334.

Innovative Ideas in Requirements Engineering For E-Commerce Applications

Dr. VENKATA SURYANARAYANA T, ¹ M. AMBICA²

¹Associate Prof. ECM Dept, K L UNIVERSITY, GUNTUR.

²Associate Prof. CSE Dept, LAKSHYA College of Engineering, Khammam

ABSTRACT: Innovative ideas are characterized by commercial products yet unknown to the market, enabled by information technology. How to develop such products is hardly known. We propose a interdisciplinary approach, e3-value, to explore an innovative Ideas with the aim to understand such an idea thoroughly and to evaluate it for potential Profitability. Our methodology exploits a requirements engineering's way of working, but employs concepts and terminology from business science, marketing and axiology. It shows how to model business requirements and improve Business-IT alignment, in sophisticated multi-actor value constellations that are common in electronic commerce.

I. INTRODUCTION

A challenge in putting e-commerce ideas into operation, in addition to satisfying a profitability requirement, is that business and technology closely interlock. This greatly expands the e-commerce 'design space'. A new technological feature enables more than one business idea, while new business ideas are only possible if technological constraints are satisfied.

This close interaction between on the one hand designing a sound value proposition and on the other hand designing an information system enabling this proposition is very typical for e-commerce projects, and results in more than only an information system or business design problem. Moreover, Innovative e-commerce ideas tend to be formulated very vaguely initially. Such an idea is a statement about a combination of an innovative value proposition utilizing a new technological possibility, but it often lacks a precise description. As a result, many innovative e-commerce ideas are somewhat unfocused and inaccurate. This makes it different to put the idea into operation, and to develop a supporting information system. What is needed is an in-depth exploration process of an e-commerce idea, to understand the idea better as well as to formulate it more precisely, and to focus the idea into a direction that is feasible from an economical and technical perspective.

This paper, discusses how such an innovative e-commerce idea can be explored taking into account business and technological perspectives. Our e3-value approach to do so is on the one hand based on the analysis of economic value creation, distribution, and consumption in a multi-actor network. On the other hand, e3-value is founded on requirements engineering and underlying conceptual modeling techniques, borrowed from the information systems community.

Requirements engineering is the process of developing requirements through an iterative co-operative process of analyzing the problem, documenting the resulting observations in a variety of representation formats, and checking the accuracy of the understanding gained. In this thesis, we focus on the use of a requirements engineering and conceptual modeling approach to articulate, analyze and validate a value proposition more thoroughly. One of the observations we have made during e-commerce idea exploration tracks is that initially these tracks are about finding an Internet enabled value reposition. Therefore, in this thesis much attention is paid to finding, representing, analyzing and evaluating such a value proposition. We describe a value proposition using a conceptual value model that shows how actors create, distribute, and consume objects of economic value.

The motivation to use a more formal, conceptual approach for exploring a value proposition is two fold. First, modeling a value proposition explicitly, may contribute to a common understanding of the proposition by all stakeholders involved. While doing so, special attention should be paid to stakeholders with an information technology interest. Such stakeholders should understand the proposition well, because they have to design and implement an information system that puts the proposition into operation. Moreover, these stakeholders often have in-depth technological knowledge and thus can provide valuable input for designing an Internet enabled value proposition. Because this stakeholder group is used to more formal conceptual models, we hope that a conceptual value proposition model may help their understanding of the e-commerce idea. Second, a more formal model of the e-commerce idea allows for evaluation of the idea, which is in our case biased towards assessment of potential profitability of the idea. In addition, e3 value is a lightweight approach. In our experience, e-commerce idea exploration tracks typically may take a few weeks to a month, so an approach supporting idea exploration should facilitate a relatively short exploration track.

II. Innovative Ideas for Requirements engineering

Values for requirements engineering exploits the concept of economic value during the requirements engineering process and is especially useful when doing requirements engineering for innovative e-commerce information systems. Such systems have in common that they presuppose a new, hardly understood, e-commerce idea with which actors potentially can make a profit, or when put into operation, produces something of economic value for actors. In fact, a new and profitable information technology intensive value proposition has to be invented, and stakeholders have to agree on this. In this paper, i concentrate on the very first phase of developing innovative e-commerce information systems. Typically, such a track starts with one or more, often vaguely articulated, innovative ideas, utilizing new technological possibilities.

III. Requirements engineering

Requirements engineering stands for an approach, often used by information technologists, to develop information system requirements, which can be used as a Starting point for system design and implementation. We think that requirements engineering as an approach can be of help in finding, formulating and assessing e-commerce requirements. Requirements engineering is the process of developing requirements through an iterative co-operative process of analyzing the problem, documenting the resulting observations in a variety of representation formats, and checking the accuracy of the understanding gained. Figure1 shows the process of requirements engineering in general.

IV. E-Commerce idea exploration observations

Observation 1: Exploration of innovative e-commerce ideas is initially about finding a value proposition. Explanation. As defined before, innovative e-commerce information systems have in common that they exploit a new value proposition. Consequently, e-commerce development tracks start with a new e-commerce idea, which is often articulated vaguely and is subject to change and refinement. Compare this to the development of more traditional systems, which can rely on a known enterprise mission and enterprise goals to derive system requirements.

Observation 2: Knowledge of information technology plays a crucial role in e-commerce idea exploration.

Observation 3: A concern of stakeholders regarding an e-commerce idea can sometimes be addressed on the business level and on the technical level. Explanation. If a concern comes up during the exploration of the e-commerce idea, it may be possible to address this issue by technical measures, but sometimes it is possible to solve this issue by changing the value proposition slightly. This results in an explosion of the design space: in traditional system development tracks it is difficult enough to make system design decisions in a systematic way; in an e-commerce development track even more design options become available because we can easily change the value proposition.

Observation 4: e-Commerce models are created rather than elicited. Explanation. Elicitation of e-commerce models supposes that stakeholders have dormant knowledge of an innovative e-commerce idea. It is our experience that in most cases, such an idea has to be invented rather than that such an idea can be elicited. It requires a paradigm shift of stakeholders. The paradigm shift theory recognizes that people think within an accepted frame of reference and that to be able to find new ideas, people have to step out of that frame of reference.

Observation 5: A wide range of stakeholders is involved, thereby mixing up discussions. Explanation. In a typical innovative e-commerce exploration track stakeholders range from CxO's (e.g. Chief Executive/Financial/Operation Officers) to information technology persons. The first group of stakeholders is involved because innovative e-commerce projects are about new value propositions which touch the core of companies: how they are making money. The information technology oriented stakeholders play a role to ensure that the enabling or enforcing role of information technology is accounted for.

These stakeholder groups have very different foci, which result in mixed-up and inefficient discussions between those stakeholders.

Observation 6: An e-commerce model is often specified very informally, thereby leading to different interpretations by stakeholders, and hindering analysis and evaluation. Explanation. Specification of an e-commerce model, if done at all, tends to be very informal. Often, especially for the value proposition perspective, natural language is used. Such a specification leads to different interpretations by various stakeholder groups. Also, it makes a specification more difficult to analyze and to evaluate. Moreover, information technology oriented stakeholders require a more precise specification to develop e-commerce information systems.

Observation 7: A model-based specification mechanism for the value proposition is lacking. Explanation. Model-based specification techniques, such as the Unified Modeling Language (UML) exist to represent various information technology requirements from different angles, but there is no technique available for representing a value proposition in such a way. Modeling a value proposition is needed, amongst others to reach common understanding, to be able to evaluate the e-commerce idea more thoroughly, and to allow for a more detailed system requirement elicitation track.

Observation 8: Innovative e-commerce idea exploration is to be carried out in a limited timeframe; typically a few weeks. Explanation. To bring an initial e-commerce idea into execution a limited timeframe (typically three to six months) is available. Consequently, the exploration of the idea can take only a fraction of this timeframe. This limitation is caused by rapidly increasing technological possibilities, which cause ideas to become obsolete fast. Moreover companies want to create a high volume operation fast, before a competitor takes market share by developing a similar idea. Therefore, companies typically demand a quick, first execution of the e-commerce idea comprising the essentials of the idea, rather than a long-term implementation track, which delivers a full blown operation.

Observation 9: Validation of an e-commerce model initially focuses on feasibility. Explanation. The main concern of stakeholders is the issue whether the e-commerce idea is feasible from an economical, but also from a technical perspective. Feasibility study can also mean an investigation of other major concerns, e.g. security.

V. Requirements engineering for e- commerce applications

The key question to be answered in the early phases of requirements engineering for innovative e-commerce applications is the feasibility of the e-commerce idea. This question must be answered for new and fuzzy e-commerce ideas, with many different types of stakeholders involved, and in a short timeframe. Also, stakeholders must have a common understanding of the e-commerce idea, before they can start a more detailed requirements engineering track. In this section we discuss how we address these issues in this thesis. Elements of our solution are:

- A lightweight approach to carry out the exploration track in a limited timeframe;
- A graphical conceptual modeling approach to create a common understanding of an e-commerce idea, and to allow for evaluation of an e-commerce idea;
- A multi-viewpoint approach to deal with a wide range of stakeholders;
- A scenario approach to create a more common understanding of an e-commerce idea, to capture a value proposition, and to evaluate such an e-commerce idea;
- An economic value aware approach to capture a value proposition and to evaluate a value proposition.

VI. A lightweight approach

E-Commerce tracks are characterized by short development times. A typical timeframe is three to six months: from idea to a first implementation. Only a portion of this timeframe is available for exploration of e-commerce ideas. So, within a certain timeframe, only limited manpower is available. Consequently, the first phase of e-commerce requirements engineering should be a lightweight approach.

VII. A graphical conceptual modeling approach

A conceptual modeling approach comprises the activity of formally defining aspects of the physical and social world around us for the purpose of understanding and communication. Formal in this context means the abstraction, structure, and representation of knowledge. The activity of modeling is well known and accepted in the requirements engineering community for describing information system requirements, but it is our experience that business-oriented stakeholders are often unaware of this approach. Such stakeholders use natural language requirement representations. There are a number of drawbacks with such representations, such as noise (irrelevant information), silence (omission of important information), over-specification, contradictions, ambiguity, forward references.

Conceptual modeling approach can be useful for the exploration of e-commerce ideas, provided that models can be easily communicated to business-oriented stakeholders. Goals to exploit a conceptual modeling approach are:

- To enhance the common understanding of an e-commerce idea amongst stakeholders (compared to informal, textual outlines of the e-commerce idea)
- To be able to evaluate an e-commerce idea with respect to economic feasibility. For both purposes, it is necessary to have a language, which can be used to express conceptual models, specifically for the value viewpoint. The semantics of this language should be well and commonly understood by stakeholders to facilitate a common understanding of models expressed in the language.

Moreover, to facilitate a common understanding, we choose our language constructs in such a way, that they closely resemble the perspective stakeholders have on the e-commerce idea. To allow for evaluation of the e-commerce idea, semantics should be chosen in such a way that assessment of economic feasibility is possible. In doing so, we use a semi-formal conceptual approach rather than a strictly logical approach because many stakeholders involved in this phase of idea exploration do not understand very formal models well. To allow for easy communication with stakeholders, we opt for a lightweight approach, but also a language with a graphical syntax. Many approaches used in the realm of information systems employ a graphical approach for representing requirements to contribute to an easy communication with stakeholders.

VIII. A multi-viewpoint approach

It is widely accepted that the exploration of requirements can be very complex, amongst others caused by a wide range of perspectives taken by various stakeholders. These perspectives are grounded in differences in skills, responsibilities, knowledge and expertise of stakeholders. This holds even more for the development of innovative e-commerce information systems, where besides stakeholders with a technical or traditional business background, also value proposition oriented stakeholders like marketers and Chief x Officers (where x=Executive, Financial, Operational, Information, Technical) are involved. It is our experience that during innovative e-commerce projects.

The development of an IT-intensive value proposition requires the involvement of amongst others strategic decision makers, Requirement engineers deal with such a unfocused group stakeholders by developing multiple viewpoints.

Viewpoints deal with the aforementioned multi-perspective problem by decomposing complicated requirement issues into self-contained perspectives, which can be addressed and decided on relatively independent from each other, According to them, a viewpoint is a loosely coupled, locally managed object which representation scheme, and partial knowledge of the process of design. One of the problems with viewpoint approaches is to find suitable viewpoints in the first place, because we want to use viewpoints as a way to clarify and organize stakeholder discussions, we use the various kinds of stakeholders as an important driver for viewpoint identification.

The value viewpoint: The top-level viewpoint of our electronic commerce framework concerns the value viewpoint. The value viewpoint focus is the (new) way of economic value creation, distribution and consumption. The contribution of this viewpoint to the evaluation of an e-commerce idea is a statement of revenues and expenses, caused by the exchange of valuable objects between actors.

The business process viewpoint: The business process viewpoint focuses on business processes, which are needed to put into practice, a new value proposition, and focuses on ownership of these processes, to be able to contribute operational and capital expenses to the performing actor.

The information system viewpoint: The information system viewpoint focuses on constituting components of an information system to be developed at course granularity. Techniques are available to represent this viewpoint, such as the UML.

A scenario approach: A scenario approach distinguishes in to 2 types:

- Operational scenarios
- Evolutionary scenarios.

By describing system behavior, operational scenarios may contribute to a better understanding of such a system by stakeholders. Evolutionary scenarios are used to envision events in the life of a system that may cause the system to change. The notion of system should be interpreted in a broad sense; we see a network of actors exchanging things of value with each other as a system also. The e3-value methodology utilizes both types of scenarios.

IX. An economic value aware approach

In most cases, requirements engineering focuses on information system requirements. Over the past few years it has been understood that is also important to know the business goals an information system should contribute to. This is reflected in the realm of goal-oriented requirements engineering. In goal-oriented requirements engineering approaches.

X. Conclusions

This paper is about the exploration of innovative e-commerce ideas, which utilizes principles from both requirements engineering and conceptual modeling, and focuses on the exploration of an information technology intensive value proposition. We call such an exploration track value-based requirements engineering. Based on observations made during e-commerce idea exploration tracks, we motivate the need for an e-commerce model, rather than a vaguely described idea. Development of such a model serves two goals: (1) Enhancing agreement and a common understanding of an e-commerce idea amongst a wide group of stakeholders, and (2) Enabling validation of the e-commerce idea in terms of evaluating economic feasibility. Additionally, an e-commerce model can be used as a starting point for a more detailed requirements engineering process. Based on experiences in exploring e-commerce ideas, such a model-based approach should be:

1. A lightweight approach to address the only limited time-span available for doing exploration tracks;
2. A graphical conceptual modeling approach to enhance a common, more precise understanding of the idea amongst stakeholders, and to allow for validation by evaluation of the e-commerce idea;
3. A multi-viewpoint approach to deal efficiently with the different interests of a multi-stakeholder group. We distinguish three viewpoints, being (1) the business value viewpoint, (2) the business process viewpoint, and (3) the information system viewpoint.
4. A scenario approach, which can be subdivided in an operational scenario approach and an evolutionary scenario approach. Operational scenarios are used to relate stakeholder viewpoints, and to express viewpoint specific semantics. We employ evolutionary scenarios to do a what-if assessment for an e-commerce idea.
5. An economic value aware approach, to explicitly account for the financial effects of the execution of an e-commerce idea, thereby gaining insight and confidence into the feasibility of an e-commerce idea. To present the model in such a way that stakeholders reasonably can understand the model; we have also developed a way to visualize value models. Furthermore, based on economic value-based modeling approach is sometimes confused with business process modeling approaches. A value model is about who is creating something of value for whom, in a profitable way, while a business process model shows the activities, the sequential ordering of these, and resources needed to put a value model into practice.

References

- [1] Amyot, D. & Mussbacher, G. Vol. 1939 of LNCS, Springer Verlag, Berlin pp. 16–31.
- [2] Ant 'on, A. I. & Potts, C. (1998), 'A representational framework for Requirements Engineering.
- [3] Baida, Z., de Bruin, H. & Gordijn, J Baskerville, R. L. (1999), 'Investigating information systems with action research', Communications of the AIS 2(3), 436
- [4] Borst, W. N., Akkermans, J. M. & Top, J. L. (1997), 'Engineering ontologies', International Journal of Human-Computer Studies 46, 365–406.

- [5] De Bruin, H. & van Vliet, J. C, Scenario based generation and evaluation of software architectures, in J. Bosch Buhr, R. J. A. (1998), 'Use case maps as architectural entities for complex systems', IEEE Transactions on Software Engineering 24(12), 1131–1155.
- [6] BusMod consortium (2001), BusMod Project NNE5-2001-00256: Business Models in a World Characterised. Checkland, P. & Holwell, S. Business Processes - Modelling and Analysis for Re-engineering
- [7] Choi, S.-Y., Stahl, D. O. & Whinston, A. B. The Economics of Doing Business in the Electronic Marketplace, MACMillan Technical Publishing, Indianapolis, IN.
- [8] Davenport, T. H. (2003), Process Innovation Reengineering Work through Information Technology, Harvard Business School Press, Boston, MA.
- [9] Fowler, M. & Scott, K. UML Distilled - Applying the Standard Object Modelling Language, Addison Wesley Longmann, Inc., Reading, MA.
- [10] Fowler, M. Analysis Patterns, Addison Wesley Longmann, Inc., Reading, MA. Fox, M. S. & Gruninger, M.
- [11] Gamma, E., Helm, R., Johnson, R. & Vlissides, J. Design patterns: Elements of Reusable Object-oriented Software, Addison Wesley Longmann, Inc., Reading, MA.
- [12] Gordijn, J., Akkermans, J. M. & van Vliet, J. C. (2000c), Business modelling is not process modelling, in S. W. Liddle & H. C. Mayr, eds, 'Conceptual Modeling for E-Business and the Web', Vol. 1921 of LNCS, Springer Verlag, Berlin
- [13] Gordijn, J., Akkermans, J. M., van Vliet, J. C. & Paalvast, E. R. M. R. (2000d), Selling bits: A matter of creating consumer value, in K. Bauknecht, S. K. Madria & G. Pernul, eds, 'First International Conference on Electronic Commerce and Web Technologies (EC-Web 2000)', Vol. 1875 of LNCS, Springer Verlag, Berlin, D,
- [14] Gordijn, J., de Bruin, H. & Akkermans, J. M. (2001), Scenario methods for viewpoint integration in e-business requirements engineering, in R. H. Sprague
- [15] Gordijn, J. & Akkermans, J. M. (2001), 'Designing and evaluating e-Business models', IEEE Intelligent Systems - Intelligent e-Business 16(4), 11–17.
- [16] Holbrook, M. B. Consumer Value: A Framework for Analysis and Research, Routledge, New York, NY.
- [17] McCarthy, W. E. 'The REA accounting model: A generalized framework for accounting systems in a shared data environment', The Accounting Review pp. 554–78.
- [18] Meyer, B. 'On formalism in specifications', IEEE Software 2(1), 6–26.
- [19] Motschnig-Pitrig, R., Nissen, H. W. & Jarke, M. (1997), View-directed requirements engineering: A framework and metamodel, in 'Proceedings of the 9th Mylopoulos, J. (2007), Conceptual modeling and telos, in 'Conceptual Modelling, Databases and CASE: An Integrated View of Information Systems Development', Wiley, New York, NY, pp. 49–68.

Analysis of Microstrip Antenna Array

Shruti Vashist,¹ M.K Soni,² P.K.Singhal³

¹Research Scholar, Department Of Electronics & Communication Engineering, Faculty of Engineering and Technology, Manav Rachna International University Faridabad-121004, Haryana, India

Abstract: Antenna exhibits a specific radiation pattern. The overall radiation pattern changes when several antenna elements are combined in an array. Arrays of antennas are generally used to direct radiated power towards a desired direction. This is due to array factor. It is this factor which quantifies the effect of combining radiating elements in an array without the element specific radiation pattern taken into account. This paper presents a design approach for four element antenna array. Simulation results show that the antenna array shows good performance in the operating frequency band of (1-1.89GHz) in L-band with return loss of -13db.

Keywords: Antenna array, Microstrip patch antenna, radiation pattern, Array factor.

I. INTRODUCTION

The overall radiation pattern of an array is determined by array factor combined with the radiation pattern of the antenna element. The overall radiation pattern results in a certain directivity and gain. Directivity and gain are equal if the efficiency is 100%. The number of antenna elements, geometrical arrangement, relative amplitudes and phases of the array elements depend on the angular pattern that must be achieved. Once an array [2] has been designed to focus towards desired direction, it becomes easier to steer it in some other direction by simply changing the relative phases of the array elements—a process called steering or scanning. Figure 1. shows an example of one- and two-dimensional arrays consisting of identical linear antennas.

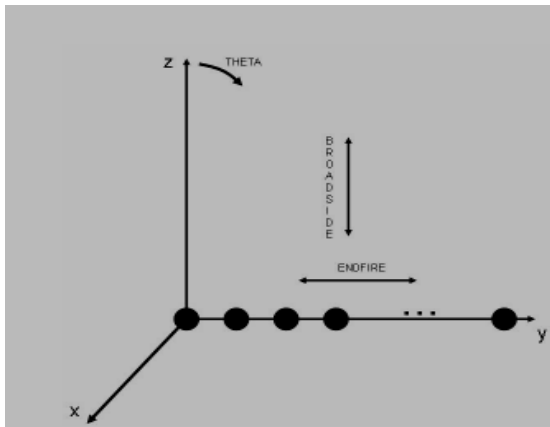


Fig1.Topology of linear array

Broadside vs. end fire arrays

Arrays can be designed to radiate in a direction perpendicular to array orientation (the z axis in figure 1) are called **Broadfire** or if the radiation is in the same direction as the array orientation (the y axis in figure 1) are called **End fire**. Generally broadside arrays are used and radiation in the z direction is considered. This allows an easy transformation to 2dimensional planar arrays with the elements in the xy plane. There are several applications in this above mentioned L-band. The L band is held by the military for telemetry, thereby forcing digital radio to in-

band on-channel (IBOC) solutions. Digital Audio Broadcasting (DAB) is typically done in the 1452–1492-MHz range as in most of the world, but other countries also use VHF and UHF bands [2].

In this paper four element microstrip patch antenna array is proposed which is capable of operating at a frequency of 1.89GHz which lies in L-band. The design of the array is adapted from the formulas found in [1] and [4]. Simulations were carried out using IE3D software and various performance analysis parameters such as S-parameters, gain, directivity; radiation pattern was analyzed to prove the effectiveness of the proposed design at such a high frequency.

This paper is organized as follows: Section II presents design approach of four element microstrip patch antenna in which its design equations and design parameters are discussed. Section III shows simulation results of the antenna array and finally in section IV conclusions are drawn.

II. DESIGN APPROACH

Fig.2 shows a schematic layout of a four element microstrip patch antenna array. Four ports are used to provide maximum coupling between all the four elements which in turn provides good return loss and radiation pattern.

Generally for the Rectangular Patch length of the element [1]

is kept as $\frac{\lambda_o}{3} \leq L \leq \frac{\lambda_o}{2}$ where λ_o is the wavelength of wave.

Because of fringing fields the actual effective length becomes $L_{eff} = L + 2\Delta l$

Where $\Delta l = \frac{0.412h(\epsilon_{reff} + 0.03)(w + 0.2644h)}{(\epsilon_{reff} - 0.258)(w + 0.8h)}$, it

depends on width to height ratio and effective dielectric. Effective dielectric is taken into consideration as there is board dielectric on one end and on top is usually air, it is given by

$$\epsilon_{reff} = \frac{\epsilon_r + 1}{2} + \frac{\epsilon_r - 1}{2} \frac{1}{\sqrt{1 + \left(\frac{12h}{w}\right)^2}}$$

There are numerous substrates that can be used for designing of the microstrip antenna. Their dielectric constants are generally in the range $2.2 \leq \epsilon_r \leq 12$. Antenna performance is most desirable with thick substrate whose dielectric constant is low as they provide better efficiency and larger bandwidth. But by doing so the element size will increase. If we use thin substrate with high dielectric constant no doubt the element size will reduce but gain, efficiency and bandwidth will be affected and so a compromise has to be made between the antenna performance and the circuit design.

Width is calculated as

$$W = \frac{1}{2f_r \sqrt{\mu_o \epsilon_o}} \sqrt{\frac{2}{\epsilon_{r+1}}}$$

Or

$$W = \frac{v_o}{2f_r} \sqrt{\frac{2}{\epsilon_{r+1}}}$$

$$\text{Characteristic impedance is } Z_0 = \frac{60 \ln \left(\frac{8h}{w} + \frac{w}{4h} \right)}{\sqrt{\epsilon_{\text{eff}}}}$$

III. Simulation

The specifications mentioned in section II is designed and simulated using IE3D software. The return loss is shown in Fig.3 and from this it is quite clear that good results are obtained as the loss is well below -10db and a sharp frequency is obtained at 1.89GHz. Smith chart obtained in Fig 4 shows that most of the points are located at the bottom of the circle, means impedance is capacitive in nature. Fig 5.shows that VSWR is less than 2 at about 1.8GHz.VSWR of the antenna can be considered desirable as it is less than 2. Various other parameters like Magnitude Vs. Frequency, 3D-geometry, Radiation pattern, Current distribution pattern and Gain Vs. Frequency are given below.

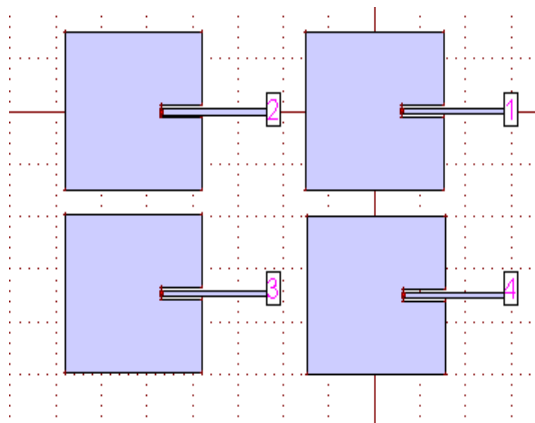


Fig 2.Design of 4- element Microstrip patch array

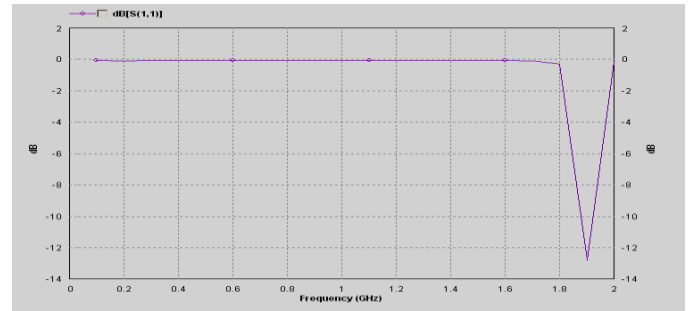


Fig 3.Return Loss

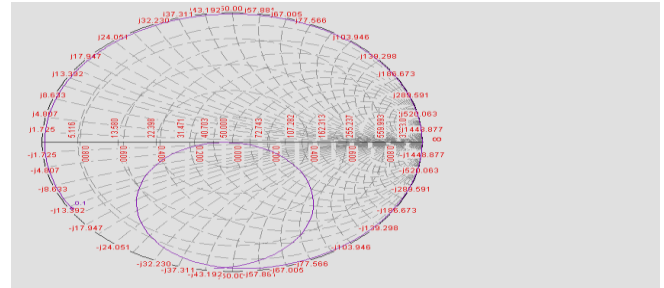


Fig 4.Smith Chart

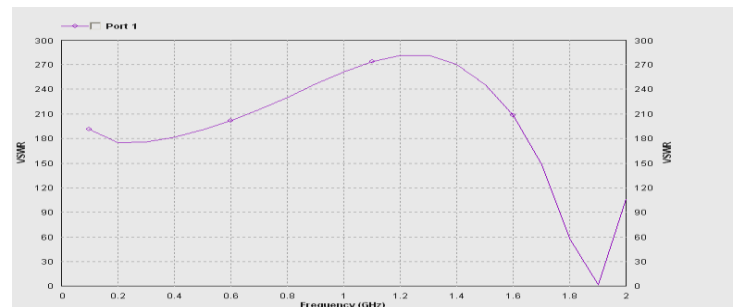


Fig 5.VSWR

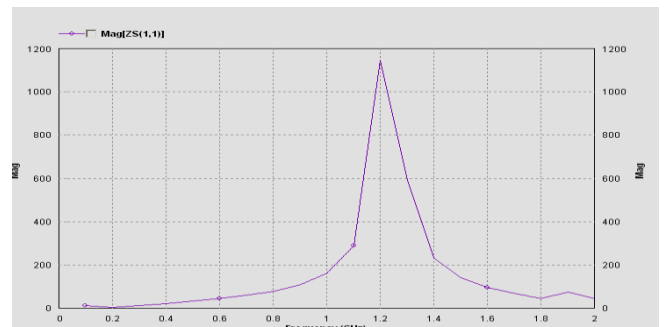


Fig 6.Magnitude Vs. Frequency

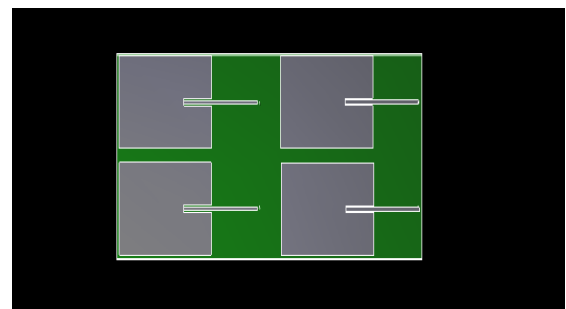


Fig 7.3D-geometry

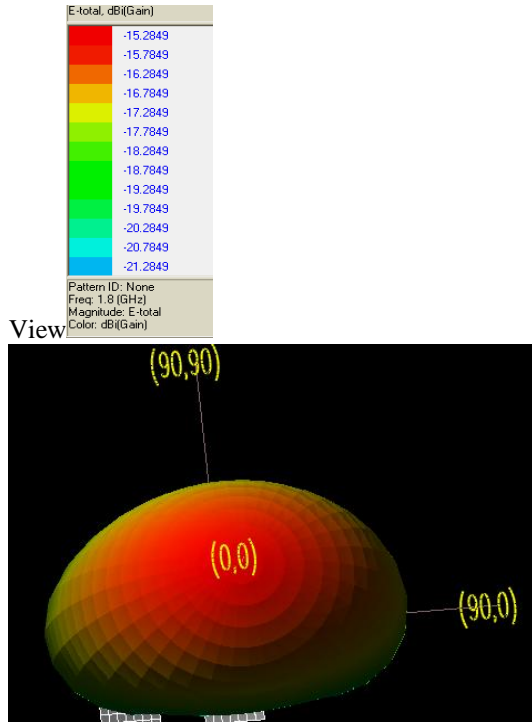


Fig 7.3D Radiation pattern

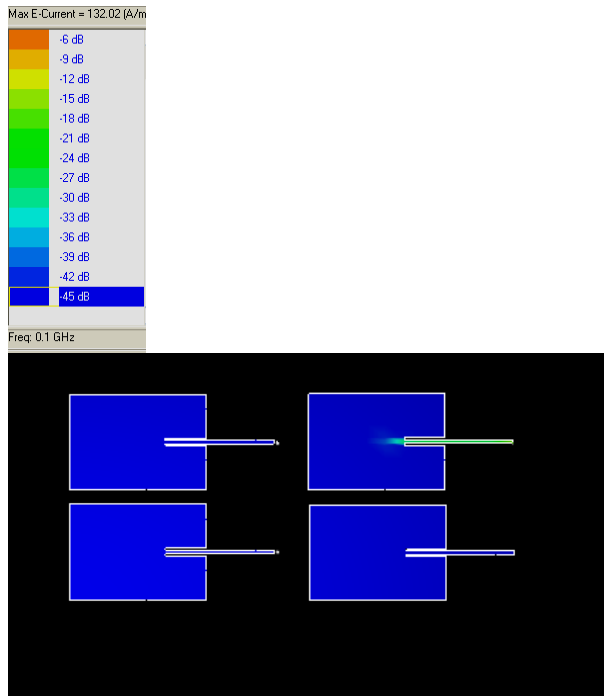


Fig .8 .3D Current distributions

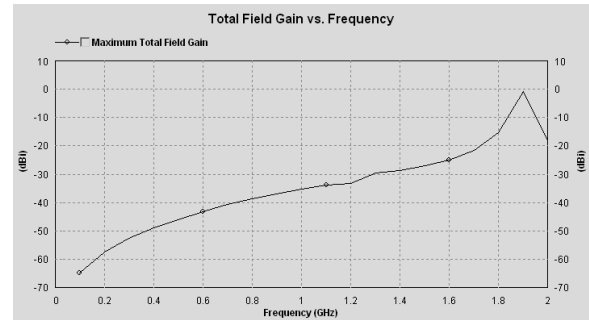


Fig.9.Gain Vs.Frequency

IV. CONCLUSIONS

A design approach for four element antenna array has been presented. L-band four-element array has been simulated. The simulated array has shown very good performance in terms of radiation pattern and S-parameter values.

References

- [1] T. C. Edwards, "Foundations for Microstrip Circuit Design," John Wiley & Sons, USA, 1981.
- [2] C.A. Balanis, "Antenna Theory: Analysis and Design," 2nd ed., John Wiley & Sons, New York, 1997.
- [3] Wentworth M. Stuart (2005), "Fundamentals of Electromagnetics with Engineering Applications", pp 442-445, John Wiley & Sons, NJ, USA.
- [4] Ramesh Garg, Prakash Bartia, Inder Bahl, Apisak Ittipiboon, "Microstrip Antenna Design Handbook", 2001, pp 1-68, 253-316 Artech House Inc. Norwood, MA.
- [5] Alla I. Abunjaileh, Ian C. Hunter, Andrew H. Kemp, "Multi-Band Matching Technique for Microstrip Patch Antenna Receivers", School of electronic and electrical engineering, The University of Leeds" IEEE, EUMC.2007.4405174.
- [6] Yasir Ahmed, Yang Hao and Clive Parini, "A 31.5 GHz Patch Antenna Design for Medical Implants", University of London, International Journal of Antennas & Propagation", volume 2008, (2008), article ID 167980.
- [7] S. Satthamsakul, N. Anantrasirichai, C. Benjangkrapaset, and T. Wakabayashi, "Rectangular Patch Antenna with inset feed and modifier ground plane for wide band antennas", IEEE, Aug. 2008.
- [8] "Theory of a single Microstrip Square Patch" internet source: <http://surf.syr.edu/projects/SamirArrayAntenna/theory.doc>. As on 2009/01/10. as on 2009/01/10
- [9] 30. E. O. Hammers tad, "Equations for Microstrip Circuit Design", Proc. Fifth European Microwave Conf., pp 268-272, September 1975.